



IN THE UNITED STATES PATENT AND TRADEMARK OFFICE

Applicant: McDonald *et al.* Group Art Unit: 1647
Serial No.: 09/360,242 Examiner: Landsman, R.
Filed: July 22, 1999
For: *METHODS AND COMPOSITIONS FOR TREATING SECONDARY TISSUE
DAMAGE AND OTHER INFLAMMATORY CONDITIONS AND DISORDERS*

DECLARATION PURSUANT TO 37 C.F.R. §1.132

Commissioner for Patents
Alexandria, VA 22313-1450

Sir:

I, JOHN R. McDONALD, declare as follows:

1. I am an inventor of and am familiar with the subject matter of the above-captioned application.
2. I received B.Sc. and Ph.D. degrees at Napier College, Edinburgh, completed successful postdoctoral appointments in Canada and The United States before leaving academia for the biotechnology industry (Boulder CO, and San Diego CA). I have been involved in all aspects of the Research and Development process from project planning through IND filing. My research has focused upon growth factor signal transduction, multiple sclerosis, and the purification and characterization of neurotrophic factors and growth factor-mitotoxin fusion proteins. I have received several peer-reviewed awards and grants, including a US National Institutes of Health Small Business Innovation Research Grant. I am co-author of over fifty publications, and a named inventor on nine patent applications.

CERTIFICATE OF MAILING BY "EXPRESS MAIL"
"Express Mail" Mailing Label Number EV738975037US
Date of Deposit: February 10, 2006
I hereby certify that this paper is being deposited with the United States Postal "Express Mail Post Office to Addressee" Service under 37 CFR §1.10 on the date indicated above and is addressed to: Commissioner for Patents, U.S. Patent and Trademark Office, P.O. Box 1450, Alexandria, VA, 22313-1450.

Stephanie Seidman

BEST AVAILABLE COPY

Applicant : John R. McDonald et al.
Serial No. : 09/360,242
Filed : July 22, 1999
DECLARATION PURUSANT TO 37 C.F.R. §1.132

Attorney's Docket No.: 17080-002002/601B

3. I am a founder of Osprey Pharmaceuticals Limited, Canada. I was Vice-President of Research & Development and a Director at the company from its founding in 1997 to 2002. Since 2005, I have held the position of Director of Science and Intellectual Property at the company.

4. As described in previous DECLARATIONS of record in this application, the conjugates described in the above-captioned application and encoded by the described nucleic acid molecules, are broad-based, widely applicable anti-immunoinflammatory drugs for inhibiting activation, proliferation and/or migration of immune effector cells. As a result of such activity, these conjugates can be used in methods for such inhibition. Activation, proliferation, and/or migration of immune effector cells are known to play a role in the etiology and/or pathology of a variety of diseases and conditions. Numerous such diseases and conditions and the role of immune effector cells in each are described in the application. These diseases and conditions, include secondary tissue damage-associated disorders such as those that accompany central nervous system trauma and disease, including spinal cord injury and head injury, auto immune diseases, including multiple sclerosis, amongst others, and other inflammation-driven diseases as divergent as asthma, arthritis, HIV and cancer.

5. In my capacity as a Director, I directed the experiments described below (**Section B**). These experiments demonstrate the effectiveness of conjugates of chemokine receptor-targeting agents for treatment of diseases that are characterized or caused by a pathophysiological inflammatory response. These data are in addition to data already of record. These data and the data of record further demonstrate that these conjugates provide a more selective and targeted delivery than previous ligand-directed delivery conjugates. The data indicate that the chemokine-toxin conjugates target cells with specificity and a certain degree of predictability. In addition, the data indicates that these agents distinguish between activated and quiescent cells and that potential toxic side effects may be a non-issue or at most, minimal.

6. This DECLARATION also provides a discussion of the inflammatory disease process and provides citations to numerous articles published before the July 21, 1998, priority date of this application (**Section A**). This discussion is provided to describe and establish that the role of immune effector cells in the inflammatory response was well known at the time of filing of this application, to establish that treatments targeting immune effector cells are known to be effective, and to rebut scientifically unsound or incorrect assertions in the Office Action. Attention also is directed to the application, which also includes such

Applicant : John R. McDonald et al.
Serial No. : 09/360,242
Filed : July 22, 1999
DECLARATION PURUSANT TO 37 C.F.R. §1.132

Attorney's Docket No.: 17080-002002/601B

disclosure. As described at length in the application and discussed at length in previous responses of record, the instant application provides is a new modality for targeting immune effector cells. As established during the lengthy prosecution of this application, there is no disclosure, teaching or suggestion in the art for the preparation of conjugates that target chemokine receptors. Inhibiting and depleting immune effector cells for treatment of diverse diseases, however, has been used for at least more than 50 years; the instant application provides a new way to achieve this result. Examples of such treatments to demonstrate that inhibiting and/or depleting immune cells are effective and are discussed below in **SECTION C**.

7. Also, provided in this DECLARATION is a summary of recent developments in the field that support the operability of the methods in this application and validate the approach as it was described in the instant application and its parent applications (**SECTION C**). Any literature published after the priority date of the application is cited in order to provide such evidence of operability and validation of the generic approach provided by the application.

Section A. The Inflammatory Response

1. The immune system

The immune system can be divided into the innate and adaptive arms that together confer a host defense system comprised of different immune effector cells. The innate immune system relies on cells immediately reactive toward invading entities, such as microbes, and includes phagocytosing macrophages, neutrophils (polymorphonuclear neutrophils, PMN) and natural killer T cells (NK). The adaptive immune system includes T and B cells, which require activation by antigen presenting cells of the innate immune system in order to target specific host invaders. Cells of the innate and adaptive immune responses work in concert with tissue residential cells (TRC) in order to maintain a homeostatic balance in many organ specific processes including embryogenesis, angiogenesis, lymphocyte trafficking, wound healing, tissue repair, removal of cellular debris and other unwanted agents such as microbes, viruses or cancer cell clones. Macrophages, monocytes, and microglia (collectively referred to as mononuclear phagocytes, MNP), PMN, eosinophils, subtypes of the T-lymphocyte family and other immune cells are responsible for these homeostatic processes and for the maintenance of an intact surveillance and host defense system.

The generic inflammatory response is a multi-factorial biochemical process that is orchestrated and perpetuated by cells of immune effector cell lineage. Soluble factors released from injured and dying cells, immune complexes or complex charged antigens like bacterial lipopolysaccharides (LPS) and viral envelope proteins working via the complement and toll receptor system are common triggers of leukocyte activation and recruitment. In response leukocytes undergo profound phenotypic changes including the upregulation of cell adhesion molecules (CAM) and proinflammatory cytokines and chemokines for trafficking and communication with other leukocyte groups.

The recruitment of leukocytes from the blood to specific tissues in homeostatic or inflammatory environments is highly regulated and orchestrated by chemokines, a variety

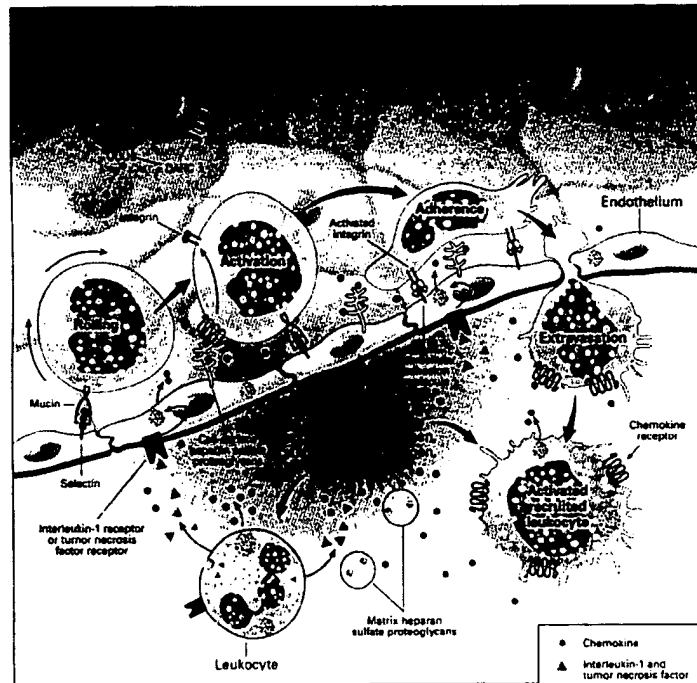


Diagram 1. Trafficking of Leukocytes: In response to chemokine gradients leukocytes traffic to selected tissues in the body and carry out homeostatic (e.g., immunosurveillance) or become involved in disease pathology. Rolling, activation, adherence and extravasation (movement from blood vessels in to tissue) occur in a sequential manner. Rolling occurs in response to chemokines and therefore the receptors are expressed. Thus delivery of a claimed chemokine-toxin will kill cells prior to pathological activation and thereafter. (see, e.g., Tanaka *et al.* (1996) *J. Exp. Med.* 184:1987-1997; Carlos *et al.*, (1994) *Blood* 84:2068-210; Alon *et al.* (1994) *The J. Cell Biol.* 127:1485-1495)

of CAM, immunoglobulin CAM, and glycosaminoglycans (GAG). The detailed nature of specific molecular migratory patterns differs among leukocyte subtypes, the tissue of destination and the type of migratory stimuli. In general, leukocytes migrate toward a gradient of adherent chemokines along the endothelial cell walls. The gradient is formed by

chemokine attachment to GAG (e.g., heparin sulfate) and promotes presentation of the ligand(s) to receptors on the traveling leukocytes. The extravasation of cells into the tissues occurs in several steps; tethering, rolling, activation, firm adhesion and extravasation (Diagram 1; Tanaka *et al.* (1996) *J. Exp. Med.* 184:1987-1997; Carlos *et al.*, (1994) *Blood* 84:2068-210; Alon *et al.* (1994) *The J. Cell Biol.* 127:1485-1495). All steps involve the binding of leukocytes to the endothelium by families of CAM expressed on both sets of cells. Tethering begins with weak interaction of leukocytes to the endothelium promoted by selectins. Migratory cells begin to roll and adhesion to other selectins enhances the tethering strength and stabilizes cell rolling. Activation and adherence is mediated by leukocyte expression of integrins and immunoglobulin CAM. The integrins bind firmly to their ligands on the endothelial cell, selectin is shed by leukocytes and rolling ceases. Chemokines and integrin binding activate the cells and leukocytes are ready to traverse the endothelium into the tissue.

The cells also produce and secrete proteases that degrade basement membrane and extracellular matrix (ECM) components, thus aiding entry into and migration within the tissue. The expression of specific chemokines, receptors and CAM contribute to the selective locomotion and tissue specificity of leukocyte subgroups. Once at the site of injury (or disease) leukocytes produce an armament of cytotoxic mediators (see, *e.g.*, Benveniste (1997) *J. Mol. Med.* 75:165-173; Stout *et al.* (1997) *Frontiers in Bioscience* 2:197-206). Reactive oxygen and nitrogen species, proteolytic enzymes and eicosanoids kill off invading microbes and fungi which are phagocytosed principally by MNP and PMN. Leukocyte (especially macrophage) derived growth factors (GF) including vascular endothelial growth factor (VEGF) and fibroblast GF (FGF) facilitates angiogenesis. Angiogenesis helps in tissue repair but can also contribute to pathological conditions.

2. Immune effector cells leukocytes underlie or are involved in the pathogenesis of a variety of diseases and disorders

As described in the application immune effector cells are involved in the pathogenesis of a variety of diseases and disorders. As described in the application immune effector cells refer to all cells involved in innate and adaptive immunity and include leukocytes and lymphocytes both which can be broken down again into antigen presenting cells and granulocytes (e.g., neutrophils, eosinophils and mast cells). The descriptions and classifications of cell types overlap greatly. In any pathology a mixture of these cell types are involved. As described in the application, an over-zealous infiltration (migration), (chronic)

activation and proliferation (increased numbers) of relatively disease-specific subtypes of leukocytes are responsible the inflammatory response that leads to tissue destruction in the pathology of a wide range diseases. Numerous diseases and conditions and disorders, such as secondary tissue damage including spinal cord injury (SCI), autoimmune diseases including multiple sclerosis, inflammatory disease, such as inflammatory bowel diseases and inflammatory joint diseases, allergic diseases, inflammatory lung diseases, CNS diseases including Alzheimer's Disease, traumatic brain injury, stroke, and other neurodegenerative diseases, inflammation after gene therapy, and cancers, and the role of the inflammatory response and the chemokine system are described in the application. The application describes, as exemplary, the role of leukocytes in each such disease and chemokines and receptors therefore in each such disease.

Table 1, below, lists only some of about 200 diseases in which immune effector cells, including, activated leukocytes play a role. This Table was compiled from about 150 review articles; with the focus to provide information known at the time of the filing of earliest priority application. References that provide such information include art cited throughout the specification and made of record in the application. Other references include: Makita *et al.* (1998) *Am. J. Respir. Crit. Care Med.* 158:573-579; Kaartinen *et al.* (1995) *Arterioscler. Thromb. Vasc. Biology* 15:2047-2054; Kaartinen *et al.* (1996) *Circulation* 94:2787-2792; Barnes *et al.* (1998) *J. Clin. Invest.* 101:2910-2919; Qin *et al.* (1997) *J. Clin. Invest.* 101:746-754; Ogata *et al.* (1997) *J. Pathology* 182:106-114; Ying *et al.* (1997) *Eur. J. Immunol.* 27:3507-3516; Gauvreau *et al.* (1997) *Am. J. Respir. Crit. Care Med.* 156:1738-1745; Ponath *et al.* (1996) *J. Clin. Invest.* 97:604-612; Gonazalo *et al.* (1996) *J. Clin. Invest.* 98:2332-2345; Desbaillets *et al.* (1997) *J. Exp. Med.* 186:1201-1212; Youngs *et al.* (1997) *Int. J. Cancer* 71:257-266; Leek *et al.* (1997) *Cancer Res.* 56:4625-4629; Pantoni *et al.* (1998) *Arterioscler. Thromb. Vasc. Biology* 18:503-513; Sansores *et al.* (1997) *Ches.* 112:214-219 ; Pawluczyk *et al.* (1997) *J. Am. Soc. Nephrology* 8 :1525-1536; Zoja *et al.* (1997) *J. Am. Soc. Nephrology* 8:720-729; Lavaud *et al.* (1996) *J. Am. Soc. Nephrology* 7:2604-2615; Rastaldi *et al.* (1996) *J. Am. Soc. Nephrology* 7:2419-2427; Wada *et al.* (1996) *FASEB J.* 10:1418-1425; Hvas *et al.* (1997) *Scand. J. Immunol.* 46:195-203 ; Huitinga *et al.* (1995) *Clin Exp Immunol* 100: 344-51; Gerriste *et al.* (1996) *Proc Natl Acad Sci* 93: 2499-504; Chiang *et al.* (1996) *J. Clin. Invest.* 97:1512-1524; Matsumura *et al.* (1996) *J. Clin. Invest.* 97:2192-2203; Zwacka *et al.* (1997) *J. Clin. Invest.* 100:279-289; and Teixeira *et al.* (1997) *J. Clin. Invest.* 100:1657-1666). These references describe leukocyte-mediated

diseases such as acute lung injury; arthritis; asthma; atherosclerosis; cancers; cerebral ischemia; chronic kidney diseases; chronic obstructive pulmonary disease (COPD); dermatitis; emphysema, encephalomyelitis; HIV-associated diseases (HAD), ischemic/reperfusion injury (e.g., liver and myocardium) and multiple sclerosis. Researchers had shown, for example, that, with the use of fairly limited leukocyte-depleting reagents, the pathologies of experimental allergic encephalomyelitis (an multiple sclerosis model) and a colitis model can be ameliorated (see, e.g., Giulian, D.(1987) *J. Neurosci. Res.* 18:155-171; Giulian *et al.* (1993) *J. Neurosci.* 13:29-37; Giulian *et al.* (1990) *Ann. Neurol.* 27:33-42; Giulian *et al.* (1995) *Neurochem, Int.* 27:119-137; Giulian *et al.* (1989) *J. Neurosci.* 9:4416-429; Giulian *et al.* (1988) *J. Neurosci.* 8:4707-4717; Giulian *et al.* (1988) *J. Neurosci.* 8:2485-2490; Giulian *et al.* (1988) *J. Neurosci.* 8:709-714; Giulian *et al.* (1996) *J. Neurosci.* 16:3139-3153; Giulian *et al.* (1995) *J. Neurosci.* 15:7712-7726; Giulian *et al.* (1994) *Dev. Neurosci.* 16:128-136; Giulian *et al.* (1993) *J. Neurosci. Res.* 36:681-693, which are of record in this application). In each case amelioration of the pathological signs were correlated with the decreased numbers of leukocytes (see, e.g. Bauer *et al.* (1995) *Glia* 15: 437-46; Huitinga *et al.* (1995) *Clin Exp Immunol* 100: 344-51; Natsui *et al.* (1997) *J Gastroenterol Hepatol.* 12: 801-8). For the diseases, conditions or disorders involving an inflammatory response leading to secondary tissue damage, the secondary tissue damaging response increases the zone and severity of an initial injury.

In pathological situations, TRC including glial cells of the CNS, mesangial cells (MC) of the kidney, endothelial cells of many organs and leukocytes can be activated by a great number of stimuli including viruses, bacteria, parasites, proinflammatory cytokines and chemokines, hypoxia, ischemia, proteinuria (protein in the urine), autoantibodies, systemic nucleotides, complement, immune complexes, immunoglobulins and environmental pollutants such as cigarette smoke. These can be the initiating factor(s) of disease, but TRC and inflammatory leukocytes are the soldiers of disease pathology. Activated TRC and resident leukocytes express among other things members of the cytokine superfamily and several powerful leukocyte chemoattractants of the chemokine superfamily, which facilitate leukocyte activation, infiltration and proliferation at the site of inflammation. Many investigators and clinicians had shown that there is a correlation between numbers and increased activity of leukocytes with the severity of disease and measured pathological parameters (e.g., Wada *et al.* (1996) *FASEB J.* 10:1418-1425; Zoja *et al.* (1997) *J. Am. Soc. Nephrology* 8:720-729; and Chiang *et al.* (1996) *J. Clin. Invest.* 97:1512-1524).

As described in previously and discussed again in **Section C**, killing (depletion) of leukocytes and other immune effector cells or inhibition thereof is an established approach for treatment of such diseases. As discussed previously, the role of activated leukocytes in disease was known; using the chemokine receptor system for targeting such cells for depletion and/or inhibition of proliferation, migration or activation was not known. As described in the application and in previous Declarations of record, we have identified the chemokine system, via targeting of cells that express receptors therefor, as a target for intervention in the inflammatory response.

Table 1. Immune Effector Cell Types in Diverse Human Diseases

DISEASE/TRAUMA	MAJOR LEUKOCYTE SUBTYPES
Cancers (all organs)	
General Growth, Angiogenesis & Metastasis	TAM, T, Eosinophils, B, MaC, PMN, DC, Basophils
Breast Cancer	TAM, CD, T, PMN, B
Glioma	TAM, PMN, DC
Kidney Cancer	TAM, PMN
Ovarian Cancer	MNP, T, NK, MaC
Cardiovascular Diseases	
Atherosclerosis	MNP, T, PMN
Myocardial Infarction	MNP, PMN, T, MaC
Restenosis	MNP, T, Eosinophils
Chronic Kidney Diseases	
Diabetic Nephropathy	MNP, T, PMN, MaC
Glomerulonephritides	MNP, PMN, T, MaC, DC
IgA Nephropathy	MNP, T, PMN, MaC, DC, B
Lupus Nephritis	MNP, T, PMN, B, DC, MaC
CNS Diseases and Trauma	
Alzheimer's Disease	MNP, T, PMN
Multiple Sclerosis	MNP, T, Th1, PMN, B
Traumatic Brain Injury	MNP, T, PMN
Spinal Cord Injury	MNP, T, PMN
Spongiform Encephalopathies	MNP, T, B, DC
Stroke	MNP, T, PMN, DC, MaC
Eye Diseases	
Conjunctivitis	MNP, T, MaC, Eosinophils, B
Proliferative Vitreoretinopathy	MNP, PMN, T
Retinitis and Iritis	MNP, PMN, B, T
Uveitis	MNP, T, PMN, DC
HIV and AIDS	MNP, T, MaC, DC
Inflammatory Bowel Diseases	
Crohn's Disease	DC, T, MNP, B, MaC, Eosinophils, PMN
Ulcerative Colitis	MNP, T, B, DC, Eosinophils, MaC, PMN
Eosinophilic Gastroenteritis	Eosinophils, Th2, MaC, B, PMN
Joint Diseases	
Gout	MNP, PMN, T, Eosinophils
Osteoarthritis	MNP, B, T, PMN, DC
Osteoporosis	MNP, T

Applicant : John R. McDonald et al.

Attorney's Docket No.: 17080-002002/601B

Serial No. : 09/360,242

Filed : July 22, 1999

DECLARATION PURUSANT TO 37 C.F.R. §1.132

Rheumatoid Arthritis	MNP, DC, PMN, B, T
Liver Diseases	MNP, Th1, K, NK, MaC, B, GC
Pulmonary Diseases	
Acute Lung Injury	PMN, MNP, T, MaC
Acute Respiratory Distress Syndrome	PMN, MNP, T, GC, MaC
Asthma	Eosinophils, MNP, B, Th2, MaC, NK
Chronic Obstructive Pulmonary Disease	MNP, T, PMN, DC, MaC, Eosinophils
Cystic Fibrosis	PMN, MNP, Eosinophils, MaC, T, B
Emphysema	MNP, PMN, T, MaC, Eosinophils
Eosinophilic Pneumonia	Eosinophils, MNP, MNP, T, GC
Pulmonary Fibrosis	PMN, T, Eosinophils, MNP, MaC
Skin Diseases	
Dermatitis	MNP, DC, T, MaC, Eosinophils, B, PMN
Eczema	MNP, T, DC, MaC, Basophils T, MNP, DC, MaC, Basophils, Eosinophils, PMN
Psoriasis	
Systemic Diseases	
Behcet's Disease	PMN, T, B, MNP, Basophils, MaC
Sarcoidosis	MNP, PMN, T, Eosinophils, NK, GC MNP, T, Eosinophils, MNP, DC, B, Basophils, NK
Scleroderma	
Sepsis	PMN, MNP, T
Sjogren's Syndrome	T, B, MNP, DC, MaC, PMN
Systemic Lupus Erythematosus	PMN, T, MaC, B, MNP, DC, Basophils
Obesity	MNP, T, MaC, Adipocytes
Transplantation	
Graft Versus Host Disease	MNP, T, DC, MaC, Eosinophils, PMN, B
Graft/Organ Rejection	MNP, T, DC, MaC, Eosinophils, NK, B
Vascular Diseases	
Giant Cell Arteritis	GC, MNP, T, DC
Hypertension	MNP, PMN, T, Basophils
Varicose Veins	MaC, MNP, DC, T
Vasculitides	T, PMN, MNP, Eosinophils, GC

Key: B, B cells; DC, dendritic cells; GC, giant cells (multinucleated fused macrophages); MaC, mast cells; MNP, mononuclear phagocytes (monocytes, macrophages and microglia); PMN, polymononuclear neutrophils; T, various subtypes of T cells; Th2, type 2 helper T cells. N.B. Many disease categories listed here include several distinct diseases. It is important to note that the composition of the microenvironmental milieu of inflammatory factors etc has effects on the phenotypes of different cells. For example, PMN are known to express CXC receptors but in certain cases like septic acute lung injury and reperfusion injury they express CC receptors including CCR2. Under pulmonary diseases above OPL-CCL2-LPM can be used to treat ALI, ARDS, COPD and sepsis as all cell types listed express CCR2.

For selection of a conjugate drug provided in the application, the chemokine receptor targeting agent selected depends upon the immune effector cell(s) involved, the tissue in question and the stage of injury or disease. *But as is evident from above, and as described in the application*, particular cells and tissues involved in a particular disease with an underlying inflammatory pathology were known to those of skill in the art at the time of filing and/or can be determined using known methods (see papers cited herein and in the application; see Table 1). The application describes what cells and chemokines are involved in large number of

diseases and also identifies chemokine receptor targeting agents for use to treat such diseases. As shown in Table 1 and the cited references, cell types involved in particular diseases that result from or involve inflammatory responses were known at the time of filing of the priority application. As described in the application, chemokine receptor expression profiles also were known.

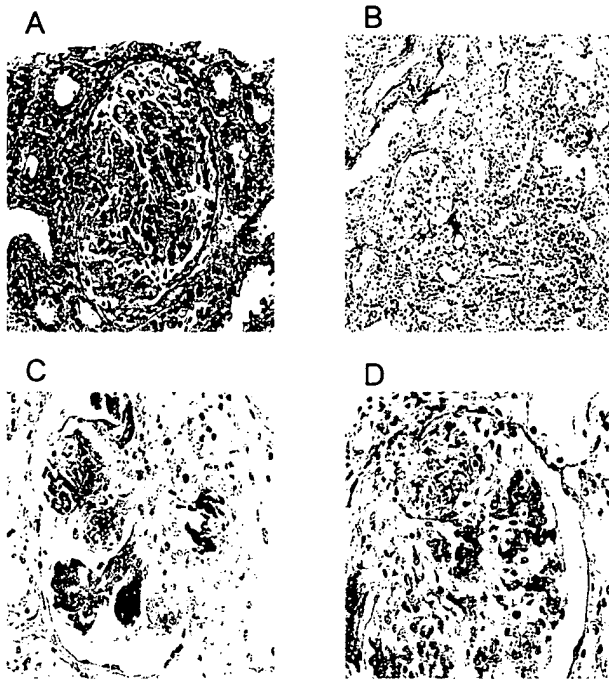
Chemokines perpetuate their own production and are released from immune effector cells, including leukocytes, via autocrine and paracrine mechanisms. They also induce the synthesis and release of cytotoxic compounds from the cells that they target. Resident and infiltrating leukocytes release the very same molecules to mediate tissue damage as used for homeostatic purposes mentioned above (Benveniste (1997) *J. Mol. Med.* 75:165-173; Stout *et al.* (1997) *Frontiers in Bioscience* 2:197-206). Chemokines induce expression of CAM and cell surface antigens (including cytokine and chemokine receptors) on various cell types including leukocytes, endothelial, glomerular mesangial cells and CNS glial cells, thus upregulating the expression of proinflammatory mediators. Therefore, the vicious cycle continues with secondary tissue damage leading to diseased states. This culminates in the destruction of (organ) tissue resident cells, a decrease in organ function and eventually organ shut down. Chronic kidney disease (CKD) is an example of such a disease. CKD patients are routinely treated with immunosuppressive drugs and research has shown that interference with principally macrophage activity slows the progression of disease as measured by the pathology scoring systems (Slide 1) for the specific disease including proteinuria, albuminuria and degree of crescent formation (fibrosis). Figure 1 shows stained slides of human lupus nephritis tissue and the secondary tissue damage that inflammation can orchestrate.

Slide 1

Renal pathology scoring system in lupus nephritis	
Activity index	Chronicity index
<u>Glomerular abnormalities</u>	
1. Cellular proliferation	1. Glomerular sclerosis
2. Fibrinoid necrosis, karyorrhexis	2. Fibrous crescents
3. Cellular crescents	
4. Hyaline thrombi, wire loops	
5. Leucocyte infiltration	
<u>Tubulointerstitial abnormalities</u>	
1. Mononuclear cell infiltration	1. Interstitial fibrosis
	2. Tubular atrophy
Austin HA, et al. Am J Med 1983, 75: 329-391	

Immune cell infiltration and contribution to fibrosis was appreciated well before 1983.

Figure 1. Histological findings of (A) glomerular crescents/fibrosis (B) interstitial inflammation (mixed groups of immune cells) and (C) immune deposits and (D) PMN infiltration and fibrinoid necrosis. Renal biopsy tissue taken from a 40 year old woman in June 1998 (Ponticelli C. and Moroni G. Division of Nephrology and Dialysis, Maggiore Hospital IRCCS, Milan; http://www.sin-italy.org/jnonline/forum/quattro/case_2.htm).



The references and discussion herein, as well as the application, establish that prior to the filing date of the priority application, it was well established that different dominant immune effector cells are pivotal in the pathogenesis of a variety of diseases. For example, eosinophils, Th2 (CD4+) cells and mast cells (MaC) in asthma; PMN, macrophages and Th1 (CD8+) cells in COPD; MNP and PMN in spinal cord and brain injury; PMN and macrophages in acute lung injury; MNP and Th1 cells in multiple sclerosis; macrophages, Th1 cells and MaC in several CKD; macrophages and T cells in atherosclerosis and granulomatous lung disease; T cells and macrophages in arthritis and several leucocyte types in different cancers were known..

Hence, as described in the instant application, chemokine-regulated leukocyte actions are part of in the immunopathology of diseases in diverse areas of study including: oncology, neurology, nephrology, rheumatology, virology, cardiology, pulmonology, gastroenterology, hepatology, gynecology, dermatology, endocrinology, mycology and transplantology (see Table 1 for examples of diseases that are leukocyte-mediated and the principal leukocyte groups involved; see also, the application Tables 1 and 2, the Examples and sections E and G of the application).

Conclusions

The activities of leukocytes are most exquisitely regulated by the chemokine family of ligands and receptors. Targeting the chemokine system is an elegant way to exploit this exquisite regulation to inhibit migration, activation and/or proliferation of such cells to thereby alter disease progression. There are several levels of regulation that are targeted. The most apparent regulation occurs at the level of the ligands and their receptors; both typically are significantly elevated in response to proinflammatory stimuli. The next area of regulation derives from the distribution of receptors across different cells (leukocytes). Each cell type has a chemokine receptor profile that is akin to a fingerprint or "chemoprint" except that it changes with the specific cell type, tissue type, disease type, function type and is time dependent. Quiescent cells will quickly change and upregulate receptor expression once activated and /or undergoes differentiation. Many chemoprints were known at the time of filing of the priority application.

The identity of a chemoprint also depends on the types and abundance of inflammatory and non-inflammatory mediators in the milieu. Most receptors are inducible in that they are not expressed unless there are inflammatory stimuli. For example, the inducible CCR2 is expressed on macrophages, monocytes, T cells, and basophils and can be targeted by MCP-1/CCL2. Leukocyte subtypes that do not express the prerequisite chemokine receptor or are not physiologically close to areas of inflammation areas are *not activated* and consequently do not participate in inflammatory processes. The eotaxin/CCL11 and CCR3; MCP-1/CCL2 and CCR2; SDF-1/CXCL12 and CXCR4; IP-10/CXCL10 and CXCR3 and IL-8/CXCL8 and CCL3/CCR1 ligand – receptor axes offer good therapeutic targets because of the fidelity of the ligands for their receptors and the fact that they are implicated in several specific diseases.

Therefore, as described in the application, a chemokine receptor targeting agent, and hence a conjugate, can be selected based upon the type of immune effector cell(s) present at a site of inflammation in a particular disease. For example, as described in the application and further demonstrated herein, Eotaxin targets CCR3 expressing eosinophils and Th2 cells in allergic asthma and skin diseases. MCP-1 targets macrophages and Th1 cells in CKD, atherosclerosis, multiple sclerosis and SCI. SDF-1 and MCP-1 target CXCR4 and CCR2 respectively, on specific tumor cells, leukocytes and activated (proliferating) endothelial cells, which are responsible for neovascularization/angiogenesis and tumor nourishment, to

eradicate or slow down the progress of the disease. The experimental results provided herein (see **Section B**) and in previous DECLARATIONS evidence this.

Furthermore, sets of diseases have certain leukocyte profiles *e.g.*, eosinophilic diseases and Th1/macrophage diseases. As a result, the LPMs, as described in the application, can be used in seemingly diverse diseases. These diverse diseases, share the common underlying pathological activation of leukocytes. In addition certain diseases are linked to co-morbidities that have the same pathology. Multiple sclerosis patients have a good chance of developing uveitis (inflammation of the anterior chamber of the eye). There is an old adage for CKD patients stating that they are more likely to die of heart disease than reach end stage kidney failure. Macrophages are pivotal in the disease pathologies in both cases. Obesity begets diabetes begets CKD (due to hyperglycemia). Indeed 40% of all CKD cases are diabetics. Hence these drugs are beneficial by virtue of their activity in targeting chemokine receptors, which express in different pathologies of the same disease condition.

Section B: Studies and results

The conjugates of the instant application, referred to herein as Leukocyte Population Modulators (LPMs), are named using current chemokine nomenclature, which identifies ligands (L) and receptors (R) by their chemokine sub-division followed by a number. For example the ligands monocyte chemoattractant protein (MCP)-1 and stromal-derived cell factor (SDF-1) are referred to as CCL2 and CXCL12, respectively. Their receptors are referred to as CCR2 and CXCR4, respectively. Data demonstrating activity as taught in the application for the following four LPMs is discussed in this DECLARATION:

1. OPL-CCL2-LPM (MCP-1-AM-ShigaHIS ; formerly designated OPL98110 in Table 6 of the application was used for *in vitro* data and OPL98102 MCP-1-AM-Shiga was used for the *in vivo* data;
2. OPL-CCL11-LPM (Eotaxin –AM-ShigaHIS; formerly designated OPL98112 in Table 6 of the application);
3. OPL-CCL7-LPM (MCP-3-AM-ShigaHIS; formerly designated OPL98109 in Table 6 of the application or *in vitro* data and OPL98103 for the *in vivo* data); and
4. OPL-CXCL12-LPM (SDF-1 β -AM-Shiga; formerly designated OPL98103 in Table 6 of the application).

In some cases in the former nomenclature is employed. All were prepared as described in the application.

1. **IN VIVO OPL-CXCL12-LPM STUDIES**

Toxicity Study

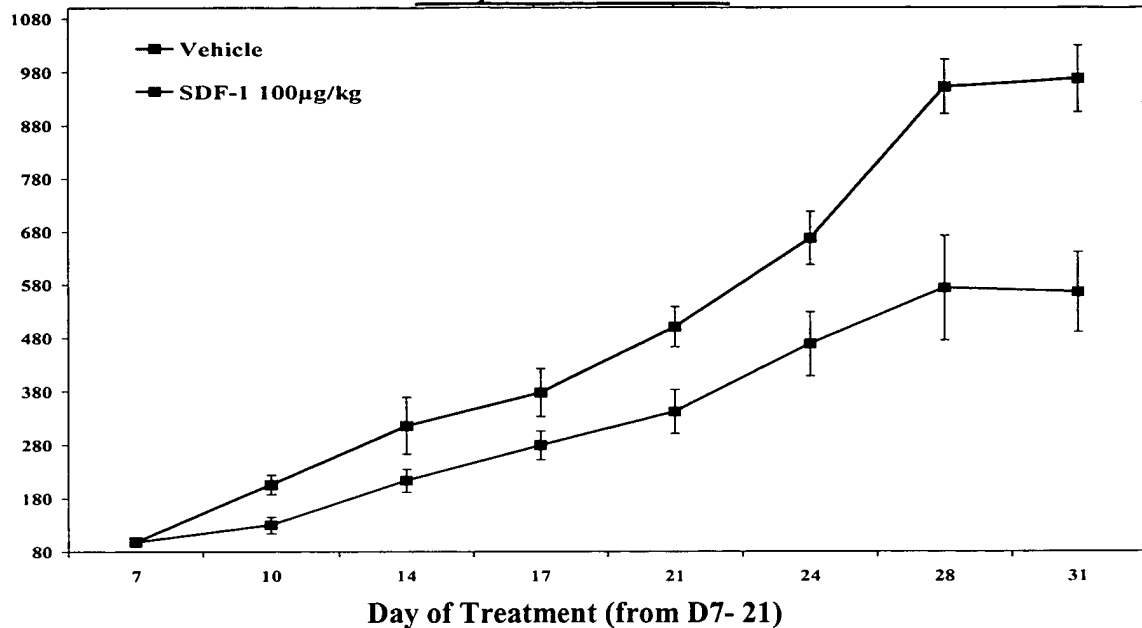
A 2mg/kg bolus of OPL-CXCL12-LPM was given to 5 Female and 5 Male Athymic Nude (nu/nu) mice (25 g) which were observed for 14 days. Gross necropsy examination revealed no organ damage and both control and test mice gained weight and were healthy. A previous experiment revealed no toxicity after examining the histopathology of stained tissue from several organs from control and test mice. Organs from this experiment have been stored with histopathology examination eminent. A previous toxicity study was reviewed elsewhere (McDonald, 2001; P435, Paragraph 2). In a total of 4 Xenograft 30 days plus studies with this molecule no animals have died due to test compounds toxicity.

MCF-7 Breast Cancer Cell Xenograft Model

A study was performed to evaluate the effects of OPL-CXCL12-LPM compared to Vehicle in an established tumor xenograft model. Female nude mice (nu/nu) were injected with 2.5 million cells (0.2 ml of PBS/Matrigel) of the estrogen dependent breast carcinoma cell line MCF-7. Intraperitoneal dosing began on day 7 and continued every day through day 21. Tumors were allowed to continue to grow until Day 31. Figure 2 shows a statistically significant decrease in the rate of MCF-7 tumor growth as measured by tumor volume with 100 μ g/kg of OPL-CXCL12-LPM. The final tumor weights from test animals decreased by an average of 35% and final tumor volumes by 41.5% that of control (significant using $p < 0.05$ two tail t-test).

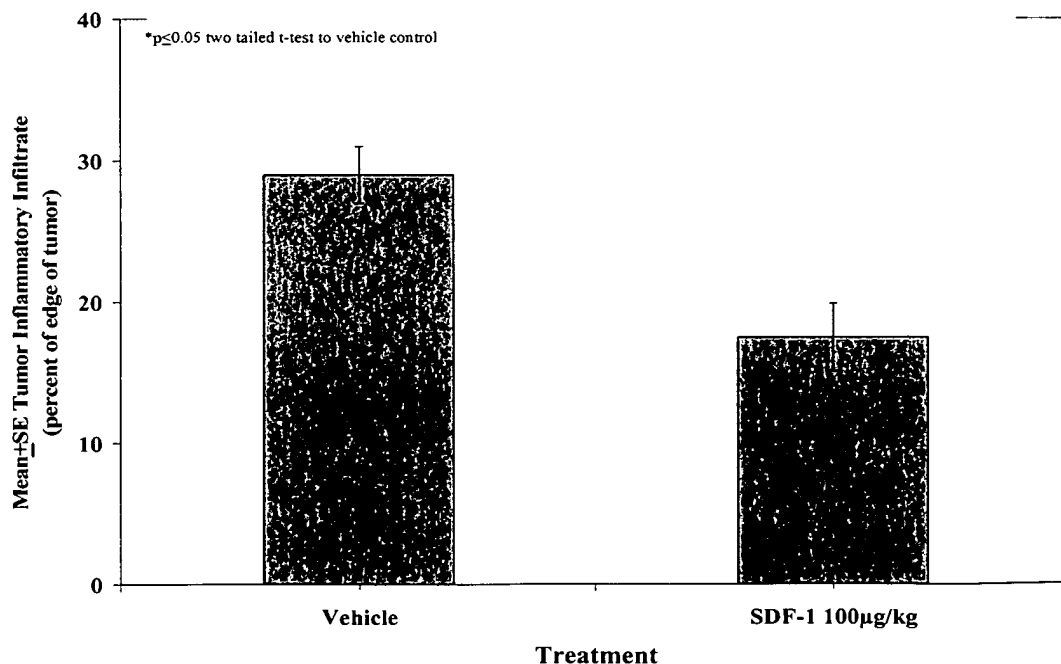
A clearer picture emerges upon histological examination, which allows visualization the extent of intratumoral necrosis and vacuolization (see Figure 4 below, anti-Ki-67 staining, Figure 4 and page 435 of McDonald, 2001). Apoptotic staining can be done to judge the numbers of dying cells.

Figure 2. Effects of Intraperitoneal OPL-CXCL12-LPM on MCF-7 Tumor Growth Compared with Vehicle.



The X axis is the measured volume of tumors(mm3). Here SDF-1 refers to OPL-CXCL12-LPM.

Figure 3. Effects of Intraperitoneal OPL-CXCL12-LPM on Inflammatory Infiltrate Around MCF-7 Tumors Compared with Vehicle



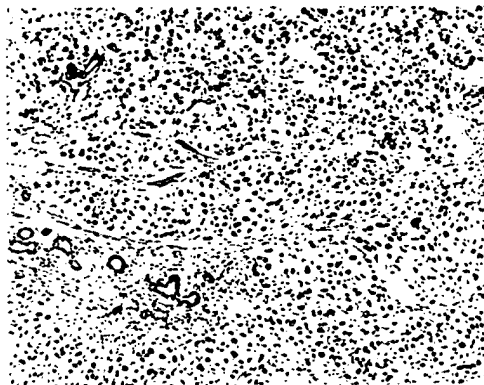
Here SDF-1 refers to OPL-CXCL12-LPM.

Applicant : John R. McDonald et al.
Serial No. : 09/360,242
Filed : July 22, 1999
DECLARATION PURUSANT TO 37 C.F.R. §1.132

Attorney's Docket No.: 17080-002002/601B

Figure 4. Histological Staining of Representative Tumors

Anti-CD31



CONTROL

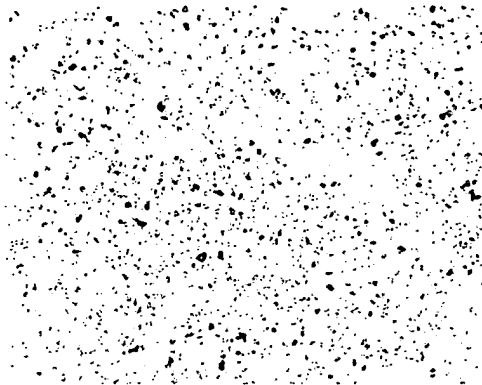


TEST

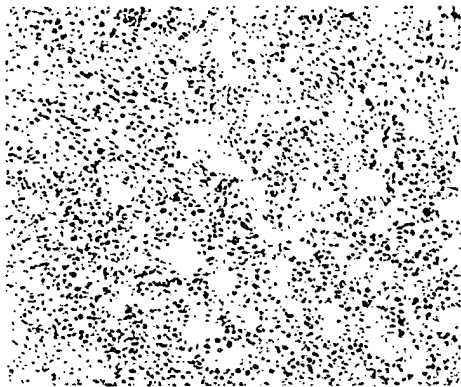
ANTI-Ki-67

Applicant : John R. McDonald et al.
Serial No. : 09/360,242
Filed : July 22, 1999
DECLARATION PURSUANT TO 37 C.F.R. §1.132

Attorney's Docket No.: 17080-002002/601B



CONTROL



TEST

Tumors were excised and exposed (along with peripheral tissue) to histological and microscopic examination as shown in Figure 3 and 4. Microscopic evaluation of leukocyte infiltrate around the periphery of the tumors showed that there was 36% less cells in the tissue of treated animals and was statistically significant (Figure 3). The tissue was processed 10 days after the last dose given to the mice. This suggests that most TAMs and infiltrating (migrating) leukocytes were destroyed by the drug during dosing.

CD-31 (PECAM-1) is a cell adhesion molecule from a family of closely related cell surface glycoproteins involved in cell-cell interactions during growth that are thought to play an important role in embryogenesis and development. CD31 is a glycoprotein expressed on the cell surfaces of monocytes, neutrophils, platelets and a subpopulation of T cells. It is also expressed on the surface of adult and embryonic endothelial cells. The CD-31 staining suggests that some leukocytes (circular staining) and angiogenesis (endothelial cells – elongated shaped staining) are present in the growing control tumors. Conversely there is no staining in the treated tumors suggesting the absence of macrophages (athymic mice have no T cells) and the absence of intratumoral endothelial cell blood vessels. This is consistent with

the mode of action of the compound which eradicates these activated cell types. These data support the conclusion that OPL-CXCL12-LPM eradicates intratumoral newly forming blood vessels as evidenced by the lack of cross sectioned (round white circles) vessels in treated tumors versus control tumors witnessed in a HT29 colon carcinoma xenograft study (McDonald, 2001; Figure 4, P 435).

The Ki-67 antigen is preferentially expressed during all active phase of the cell cycle (G_1 , S, G_2 and M phases), but is absent in resting cells (G_0 -phase). During interphase, the antigen can be exclusively detected within the nucleus, whereas in mitosis most of the protein is relocated to the surface of the chromosomes. This antigen is rapidly degraded as the cell enters the non-proliferative state, and there appears to be no expression of Ki-67 during DNA repair processes. A large number of cells appear to be proliferating in the non-treated tumors as shown by Ki-67 staining. In contrast treated tumors show little staining due to decreased tumor progression and it appears that many of the cancer cells have necrosed as evidenced by the clear vacuoles in the field.

This is the second MCF-7 breast cancer study showing efficacy and adds to the data set of two prior HT29 colon carcinoma cell xenograft studies with OPL-CXCL12-LPM. This compound has shown efficacy in 4 xenograft studies. Collectively, the data supports the view that the drug targets CXCR4 expressing tumor, endothelial and leukocyte cells as predicted and is proof of concept of specificity (no observed toxicity upon i.p. delivery) and efficacy *in vivo*. Additionally, there was no evidence of toxicity upon i.p. delivery.

2. IN VITRO OPL-CXCL12-LPM STUDIES

Tissue culture was performed using cell lines obtained from the ATCC or specific human cells enriched by gradient centrifugation from fresh blood obtained from human donors. Cell culture conditions were determined from the ATCC insert instructions and standard conditions for donated blood. Control and test conditions were carried out in quadruplicate and results shown as the Mean \pm SEM. In general cells were left for 24 h prior to treatment and the cell viability determined by the MTT color-dye assay or by Trypan Blue exclusion. This was the methodology for all compounds tested on such cells.

The compound routinely shows dose responsive toxicity to MCF-7 carcinoma cells used in the *in vivo* studies. In an earlier Declaration of record, *in vitro* dose response data on human U251 glioma, HT29 colon cancer and THP-1 (monocyte cell line) cells were provided. The data presented in Figures 5 and 6, below show OPL-CXCL12-LPM dose responses on freshly isolated human monocytes and T cells, respectively. The compound did

not show any toxicity toward human astrocytes (maximum of 40% cell death) or human foreskin fibroblasts until the dose reached 10 μ g/ml and above. The compound showed non-dose response toxicity to human neurons with a maximum effect of 75 % killing at 10 μ g/ml.

Figure 5.

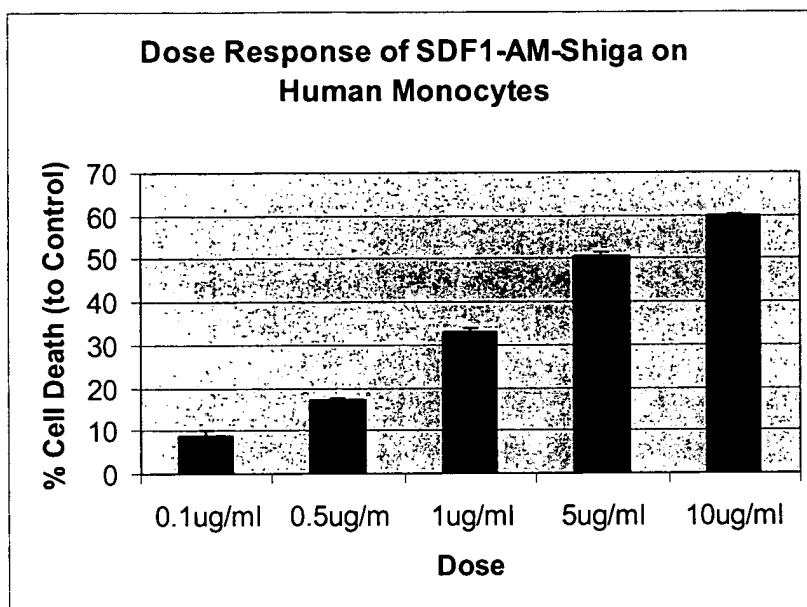
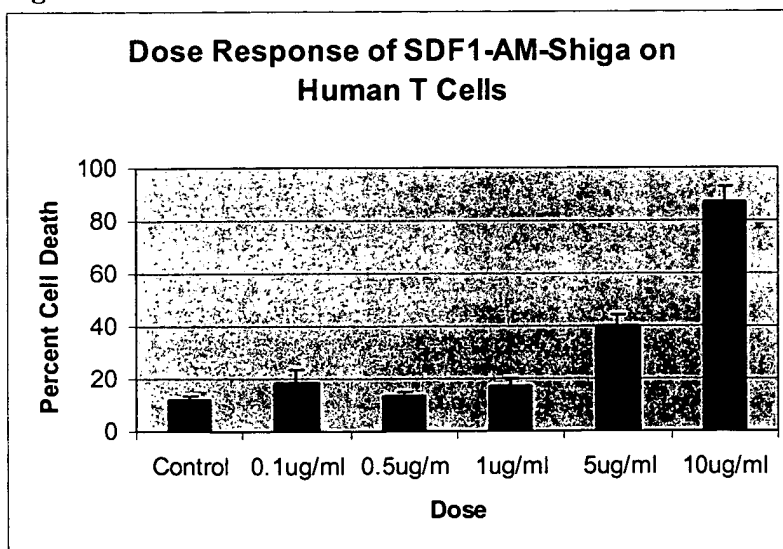


Figure 6.



One hundred percent killing is not observed on these freshly isolated cells, which could be explained if a saturating dose was not achieved. On the other hand, non-activated (non- targeted receptor expressing cells) are likely present and they would not succumb to the

drug. I have observed less than 100% killing using freshly isolated human cells on several occasions with the CCL2 and CXCL12 LPM variants. When using proliferating cells rather than freshly isolated cells, CCL2, CCL7 and CXCL12 have consistently shown 100% killing of highly activated proliferating THP-1 monocytes (cell line) at doses of approximately 20 µg/ml. Monocytes appear less susceptible to OPL-CXCL12-LPM than T cells, which is consistent with their lower expression of the targeted receptor CXCR4.

3. IN VIVO OPL-CCL2-LPM STUDIES

Toxicity Study

A 2mg/kg bolus of OPL-CCL2-LPM was given to 5 Female and 5 Male Athymic Nude (nu/nu) mice (25 g) which were observed for 14 days. Gross necropsy revealed no organ damage and test mice variations mirrored that of controls. Organs were retrieved and stored prior to ongoing histological examination. No animals died during the 31 day study due to toxicity of the compound. Activity of drug lots are routinely tested using MCF-7 breast carcinoma cells.

MCF-7 Breast Cancer Cell Xenograft Model

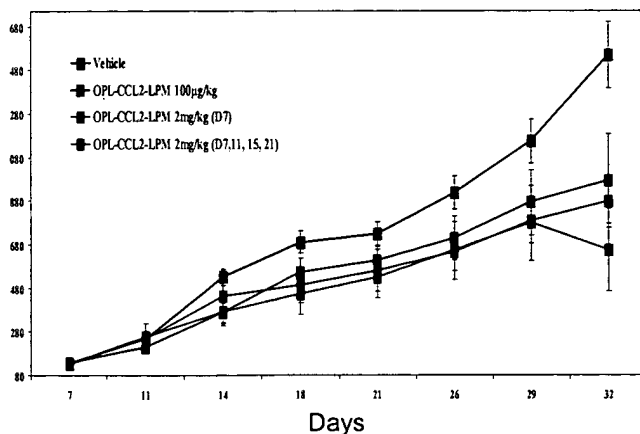
A study was performed to evaluate the effects of OPL-CCL2-LPM compared to vehicle in an established tumor xenograft model. Female nude mice (nu/nu) were injected with 2.5 million cells (0.2 ml of PBS/Matrigel) of the estrogen dependent breast carcinoma cell line MCF-7. Intraperitoneal dosing began on day 7 and cohorts received either vehicle; (1) one dose of 2 mg/Kg on day 7; (2) 2mg/Kg on days 7, 11, 15 and 21 or (3) 100 µg/Kg every day from day 7 through day 21. Tumors were allowed to continue to grow until Day 32 (Figure 7). The percent change in body between different cohorts including the control did not exceed 0.5%. Treatment induced a statistically significant decrease in the MCF-7 tumor growth as measured by tumor volume and weight. The final tumor weights from groups 1-3 decreased by 41, 58.6 and 36% that of control (significant using $p < 0.05$ two tail t-test). The final tumor volumes from groups 1-3 decreased by 47, 63 and 40.4% that of control (significant using $p < 0.05$ two tail t-test). Organs and tumors have been collected for histopathology (data not shown). This study indicates that a single or minimal repeated dosing is enough to at significantly decrease the rate of tumor growth. MCP-1 is known to target receptors on these cancer cells and infiltrating macrophages (see, *e.g.*, Youngs *et al.* (1997) *Int. J. Cancer* 71:257-266) and OPL-CCL2-LPM is a conjugate that contains **MCP-1**. In the light of the *in vitro* data with this compound and the OPL-CXCL12 –LPM histological

data indicating macrophage eradication, OPL-CCL2-LPM appears to exhibit similar effects.

4. IN VITRO OPL-CCL2-LPM STUDIES

OPL-CCL2-LPM/ MCP-1-AM-Shiga dose responsive cytotoxic activity has been demonstrated on THP-1 human monocytes and human MCF-7 breast carcinoma cells. A dose response of cytotoxicity on THP-1 cells in tissue culture is shown in Figure 8. The compound has been shown to kill freshly isolated T cells and monocytes from human healthy donors (data not shown) and human U937 monocytes (Figure 8, bottom row) in a dose responsive manner. OPL-CCL2-LPM shows no activity on murine P388D1 monocytes which do not express the mCCR2 receptor (Boring, 1996) or human U251 glioma (astrocytes) cells. In one set of experiments no activity was detected on primary human neurons and human astrocytes or in W1095HF and W1093NMA, two human astrocytes cell lines.

Figure 7. Effects of Intraperitoneal OPL-CCL2-LPM on MCF-7 Tumor Growth Compared with Vehicle.



The X axis is the measured volume of tumors (mm³).

The above *in vitro* and *in vivo* studies confirm the targeting activity of OPL-CCL2-LPM on CCR2 receptor-bearing cells. As known in the literature, see above discussion, MCF-7, endothelial cells and macrophages all express this receptor.

5. IN VITRO OPL-CCL11-LPM STUDIES

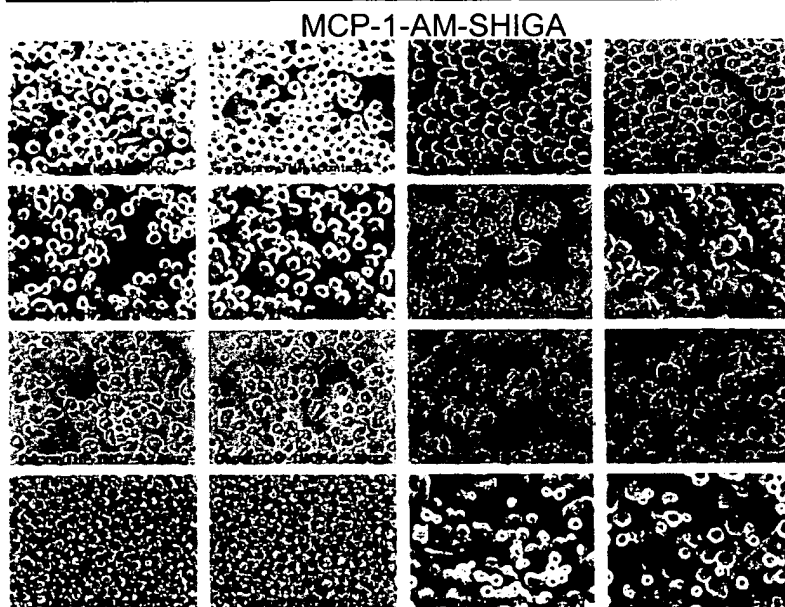
The cell isolation and culture conditions were the same as for the CXCL12 variant studies. The activity of freshly purified OPL-CCL11-LPM/Eotaxin-AM-Shiga conjugate, which targets the CCR3 receptor (see, *e.g.*, Table 1 in the application) was studied. Serial dilutions of the product were made and added to human T cells and monocytes (Figures 9 and

10). Both these cell types are known to express the targeted CCR3 receptor. Significant cell killing was achieved at high dilutions and there was a demonstrated dose response.

6. **IN VITRO OPL-CCL7-LPM STUDIES**

THP-1 monocytes were cultured as described above. A small batch of the MCP-3-AM-Shiga conjugate was made and 10 $\mu\text{g/ml}$ was added to wells in quadruplicate (see Figure 12). The second and third frames of Figure 11 show different fields of a representative culture well containing THP-1 cell survivors in suspension. As described in the application MCP-3 binds to CCR1, 2, 3 and 5, which occur on these cells. The results show that there are many necrotic cells, sick cells and cellular debris. At this concentration 100% cell death was achieved.

Figure 8. Activity of OPL-CCL2-LPM on THP-1 and U937 Monocyte Cell Lines.



Reading left to right from the top there are duplicates of THP-1 control wells followed by increasing doses of compound to a maximum of 22.5 (last 2 wells third row). On the fourth row there are 2 wells of U937 monocyte controls and then 2 wells of 22.5 $\mu\text{g/ml}$ of compound added. Quite clearly OPL-CCL2-LPM has a dramatic killing effect on both these cell isolates.

Figure 9.

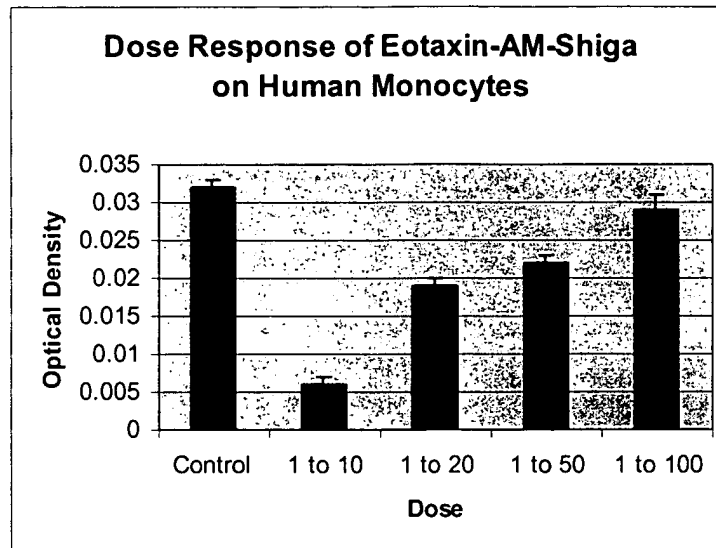


Figure 10.

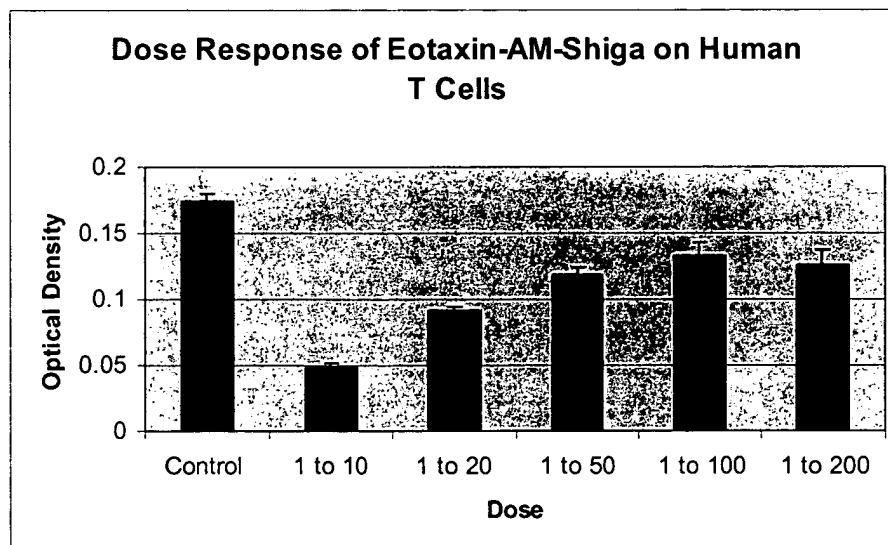
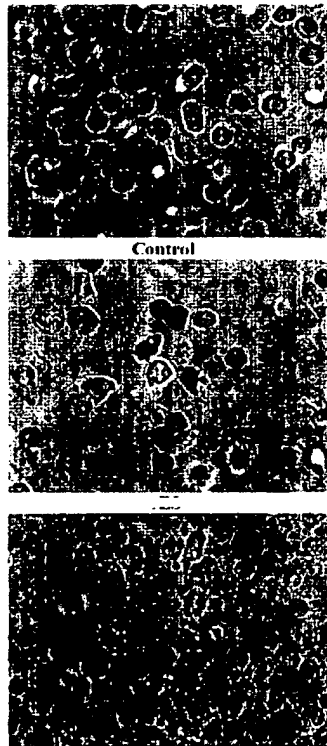


Figure 11. Activity of OPL-CCL7-LPM of THP-1 cells

Activity of MCP-3-AM-Shiga on THP-1 Monocytes



7. SUMMARY AND CONCLUSION

In this DECLARATION data is provided for conjugates containing SDF-1 β , Eotaxin, MCP-3 and MCP-1. *In vitro* and *in vivo* data are provided and show that each conjugate targets receptors on cells as described in the application. The results show that the LMPs prepared and described in the application exhibit toxicity toward targeted cells. The results also evidence cell selectivity. The *in vivo* studies clearly show that there is little, if any, toxicity. This is as expected and as described in the application as LPMs are designed to target activated chemokine receptor expressing target cells involved in inflammatory processes. We have shown that four different LPMs can target leukocytes in accord with the

Applicant : John R. McDonald et al.
Serial No. : 09/360,242
Filed : July 22, 1999
DECLARATION PURUSANT TO 37 C.F.R. §1.132

Attorney's Docket No.: 17080-002002/601B

specificities of the chemokine targeting portion and that the LPMs can deplete and/or inhibit proliferation of targeted cells.

C. Evidence that targeting leukocytes is an effective modality

This section lists the mechanisms of action and other properties of FDA approved Immunosuppressive and Cell-Depleting drugs. This evidences that there are numerous approved drugs that target leukocytes; reduction in their amounts is a recognized mode of treatment of numerous diseases.

1. Immunosuppressives

Immunosuppressive drugs for the treatment of leukocyte-mediated inflammatory diseases which have been around for at least 30 years and longer . Some drugs have superseded these immunosuppressives, but in serious cases or where there are no alternatives they are still used. A problem with these drugs is that they are too pleiotropic, can have serious side effects and are non-selective. This led researchers in the quest for more selective therapeutics. Some examples of immunosuppressives, their mechanism of action and side effects are given below.

a. Corticosteroids

- **Action:** Wide range of immunosuppressive effects including, lymphocytopenia, monocytopenia (including eosinophils), reduction in monocytic proteases, and blockage of chemotactic factors.
- **Indications:** Transplant Rejection, CNS trauma, Pulmonary, Kidney and Dermatological Diseases, Acute MS.
- **Side Effects:** Cushing's syndrome Hypothyroidism, Hypertension, Lymphocytopenia, Gastrointestinal ulcers, Infections, Dermatological diseases, Cataracts, Osteoporosis.

b. Cyclophosphamide and Chlorambucil

- **Action:** These alkylating agents cross link DNA and RNA and therefore inhibit leukocyte proliferation.
- **Indications:** Various Cancers, Rheumatic and Kidney diseases, SLE, Interstitial Lung diseases, Vasculitides.
- **Side Effects:** Teratogenic, Gonadal, Hematologic, Pulmonary, Kidney and Bladder toxicity, Malignancies.

c. Cyclosporine

- **Action:** Inhibits cytokine production including IL-2 (a T cell activator and mitogen) by activated T cells via calcineurin phosphatase inhibition.
- **Indications:** Transplant Rejection, Arthritic, Kidney and Dermatological diseases, IBD.
- **Side Effects:** Hepatotoxic, Neurotoxic, Nephrotoxic, Hypertension, Infection, Malignancies, Osteoporosis.

d. Novantrone

- **Action:** A DNA-reactive agent that intercalates into and crosslinks with DNA and RNA. It is also a potent inhibitor of topoisomerase II, an enzyme responsible for uncoiling and repairing damaged DNA. It has a cytocidal effect on both proliferating and nonproliferating cultured human cells, suggesting lack of cell cycle phase specificity. It also inhibits B cell, T cell, and macrophage proliferation and impairs antigen presentation, as well as the secretion of IFN- γ , TNF- α , and IL-2.
- **Indications:** Cancers, Secondary Progressive MS.
- **Side Effects:** Malignancies, Leukopenia, Myelosuppression, Renal Failure, Congestive Heart Failure, Interstitial Pneumonitis, Dermatological reactions.

2. Cell-Depleting Agents

Depletion of macrophages with chloroquine, colchicine and diphosphonates in models of spinal cord injury and multiple sclerosis showed efficacy and thus proof of that macrophages are the culprits of secondary tissue damage and ultimately the presentation of disease/trauma (Guilian papers). Unfortunately these agents cannot be used in the clinic for these purposes. Other targeting agents are in the clinic or are FDA approved. These cell targeting agents, especially lytic antibodies have been used to eliminate mostly cancerous leukocytes or cancers themselves. Most have proven to be too pleiotropic and can have severe side effects or have shown to be effective for a small percentage of patients. Ligand-fusion toxin proteins usually possess cell-targeting antibodies or pleiotropic cytokines (e.g., IL-2, IL-3, and IL-4) and have toxicity issues. These compounds are mostly used in the cancer field since toxicity is weighed against life extension for the patient. Using these particular classes of ligand to target cells has by enlarge been disappointing because of the side effects. As demonstrated previously, targeting the chemokine system, as described in the instant application, is far less toxic.

Cell-depleting agents, which the instantly claimed conjugates are, are known to be effective for treatment of diseases with an inflammatory component. Examples of cell-depleting agents include:

a. Campath

- **Action:** Alemtuzumab is an anti-CD52 recombinant humanized monoclonal antibody, which targets a CD52, which occurs on the surface of many normal and cancerous leukocyte subtypes. Cell lysis occurs via complement-dependent cytotoxicity (CDC) and antibody-dependent cell mediated cytotoxicity (ADCC).
- **Indications:** B-cell Chronic Lymphocytic Leukemia (B-CLL)...
- **Side Effects:** Pancytopenia/Marrow Hypoplasia, Autoimmune Idiopathic Thrombocytopenia, Autoimmune Hemolytic Anemia, Severe Infusion Reactions and Infections affecting several organs. Fatalities have occurred from these listed effects. Although Campath showed efficacy in MS trials, its high toxicity recently caused cases of idiopathic thrombocytopenic purpura with one fatality and three other deaths from other side effects (Reuters, Sept. 16th 2005).

b. Mylotarg

- **Action:** Gemtuzumab-ozogamicin is a ligand-toxin fusion protein composed of a humanized monoclonal antibody against CD33 fused to a calicheamicin derivative. Once endocytosed by target cells the toxin (an enediyne) causes DNA breakage and the cells die apoptotically.
- **Indications:** Acute Myeloid Leukemia.
- **Side Effects:** Anemia, Neutropenia, Thrombocytopenia, Myelosuppression, Infections, Bleeding, Hepatotoxicity, Mucositis.

c. Ontak

- **Action:** Denileukin diftitox is a ligand-toxin fusion protein composed of the human IL-2 ligand fused to a genetically modified version of diphtheria toxin. IL2 receptor bearing cells including T cells take up the protein and are killed by the ADP ribosylation of elongation factor 2 which terminates cellular protein synthesis.
- **Indications:** Cutaneous T Cell Lymphoma. In clinical trials for GVDH, Psoriasis, non-Hodgkin's Lymphoma, Chronic Lymphocytic Leukemia.
- **Side Effects:** Hypersensitivity Reactions, Immunogenicity, Vascular Leak Syndrome.

d. Rituxan

- **Action:** Rituximab is a chimeric (mouse/human) anti-CD20 antibody. The Fab domain of Rituximab binds to the CD20 antigen on B lymphocytes, and the Fc domain recruits immune effector functions to mediate B-cell lysis in vitro. Possible mechanisms of cell lysis include CDC and ADCC.
- **Indications:** Relapsing, Refractory and Follicular B cell NHL.

- **Side Effects:** Cytopenias similar to Bexxar, Severe Infusion and Hypersensitivity reactions (Pulmonary and Cardiovascular effects). Renal toxicity, Infections. Female gender, Pulmonary infiltrates, Chronic Lymphocytic Leukemia and Mantle Cell Lymphoma were more frequently associated with fatal outcomes than other reported side effects.

e. Zenapax

- **Action:** Daclizumab is an immunosuppressive humanized monoclonal antibody which specifically binds the CD25 alpha subunit of the human IL-2 receptor. This receptor is blocked on human activated T cells and causes their deactivation. The antibody inhibits cell cycle progression and induces T cell apoptosis.
- **Indications:** Transplant rejection, Cancer.
- **Side Effects:** Severe Infections, Death (4 drugs co-treatment), Cardiovascular, Gastrointestinal and Hematologic reactions, Hypersensitivity, Anaphylaxis.

f. Zevalin

- **Action:** Ibritumomab-tiuxetan- Y^{90} is a ligand-toxin fusion protein comprised of a murine monoclonal antibody (ibritumomab) bound to a radioactive isotope (yttrium-90) by a strong linking agent (tiuxetan). The antibody targets the CD20 antigen on the surface of mature B cells and B-cell tumors, (and not CD20-negative progenitor cells). The radioactivity kills the cells.
- **Indications:** Relapsed or Refractory low-grade, Follicular or Transformed B-cell NHL.
- **Side Effects:** Severe Cytopenias and Infusion Reactions, Hypersensitivity (Cardiovascular and Pulmonary systems can be fatal), Severe Mucocutaneous reactions (some fatal), Myeloid Malignancies.

Applicant : John R. McDonald et al.

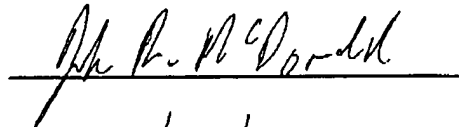
Attorney's Docket No.: 17080-002002/601B

Serial No. : 09/360,242

Filed : July 22, 1999

DECLARATION PURSUANT TO 37 C.F.R. §1.132

I further declare that all statements made herein of my own knowledge are true and that all statements made on information and belief are believed to be true; and further, that these statements were made with knowledge that willful false statements and the like so made are punishable by fine or imprisonment, or both, under Section 1001 of Title 18 of the United States Code, and that such willful false statements may jeopardize the validity of the application or any patent resulting therefrom.



JOHN R. McDONALD

Date: 02/09/06

17080-002002/601B

Distinct Cell Surface Ligands Mediate T Lymphocyte Attachment and Rolling on P and E Selectin Under Physiological Flow

Ronen Alon,* Heidemarie Rossiter,† Xiaohong Wang,§ Timothy A. Springer,* and Thomas S. Kupper†

*Center for Blood Research, Department of Pathology; and †Harvard Skin Disease Research Center, Division of Dermatology, Brigham and Women's Hospital, Harvard Medical School, Boston, Massachusetts 02115; and §Division of Dermatology, University of California, Los Angeles, California 90024

Abstract. Memory T lymphocytes extravasate at sites of inflammation, but the mechanisms employed by these cells to initiate contact and tethering with endothelium are incompletely understood. An important part of leukocyte extravasation is the initiation of rolling adhesions on endothelial selectins; such events have been studied in monocytes and neutrophils but not lymphocytes. In this study, the potential of T lymphocytes to adhere and roll on endothelial selectins in vitro was investigated. We demonstrate that T cells can form tethers and rolling adhesions on P selectin and E selectin under physiologic flow conditions. Tethering and rolling on P selectin was independent of cell-surface cutaneous lymphocyte antigen (CLA) expression, which correlated strictly with the capacity of T cells to form rolling adhesions under flow on E

selectin. T cell tethering to P selectin was abolished by selective removal of cell surface sialomucins by a *P. haemolytica* O-glycoprotease, while cutaneous lymphocyte antigen expression was unaffected. A sialomucin molecule identical or closely related to P selectin glycoprotein ligand-1 (PSGL-1), the major P selectin ligand on neutrophils and HL-60 cells, appears to be a major T cell ligand for P selectin. P selectin glycoprotein ligand-1 does not appear to support T cell rolling on E selectin. In turn, E selectin ligands do not appear to be associated with sialomucins. These data demonstrate the presence of structurally distinct ligands for P or E selectins on T cells, provide evidence that both ligands can be coexpressed on a single T cell, and mediate tethering and rolling on the respective selectins in a mutually exclusive fashion.

THE mechanism used by circulating leukocytes to initiate contact with the luminal aspect of inflamed endothelium lining vessel walls requires transient interactions (tethers) mediated by selectins (Lawrence and Springer, 1991; Ley et al., 1991; Mayadas et al., 1993; von Andrian et al., 1993). It has been proposed that tethered leukocytes, unlike cells flowing freely in vessels, can be selectively activated at the level of the endothelial cell membrane by chemokines or related molecules; these events appear to be essential for activation of integrin adhesiveness and trans-endothelial migration (Butcher, 1991; Bargatze and Butcher, 1993; Taub et al., 1993; Springer, 1994). The latter process depends on interactions between leukocyte integrins and endothelial ligands (e.g., VLA-4/VCAM, LFA-1/ICAM). The available in vitro data indicate that these integrins cannot efficiently initiate attachment of a freely flowing leukocyte to an endothelial cell lining the vessel wall (Butcher, 1991; Springer, 1994).

Several immunologically mediated human diseases are characterized by the pathophysiologic extravasation of memory T cells into peripheral tissue (Zhang, 1992; Kupper, 1994; Picker, 1994), yet there is no compelling evidence that the paradigm developed to explain neutrophil trans-endothelial migration can also apply to T cell extravasation into peripheral tissues. However, binding of memory T cell subsets to E selectin in static binding assays has been reported (Picker et al., 1991, 1993; Shimizu et al., 1992), and more recently, evidence that subsets of T lymphocytes bind to P selectin has been presented (Damle et al., 1992; Moore and Thompson, 1992; Rossiter et al., 1994). There is also evidence that chemokines (e.g., MIP-1 β , RANTES, MCP-1) and other T cell-triggering molecules can be trapped on the luminal aspect of the vessel wall by proteoglycans, thus setting the stage for antigen independent memory T cell activation in situ (Tanaka et al., 1993). Analogous multi-step mechanisms are postulated for T cell homing to peripheral lymph nodes and emigration through high endothelial venules (Shimizu et al., 1992), though in this case primary rolling interactions are mediated by lymphocyte surface L selectin and carbohydrate ligands expressed on the specialized endothelial walls (Imai et al., 1991; Lasky, 1992).

Address all correspondence to Dr. Thomas S. Kupper, Harvard Skin Disease Research Center, Division of Dermatology, Brigham and Women's Hospital, Harvard Medical School, 75 Francis St., Boston, MA 02115. Tel: (617) 278-0993. Fax: (617) 278-0305.

Recently, specific carbohydrate ligands for the endothelial selectins, E and P selectin, have been identified on neutrophils and myelomonocytic cell lines (Moore et al., 1992; Levinovitz et al., 1993; Norgard et al., 1993). Leukocyte binding to P selectin is mediated by a newly described sialomucin glycoprotein, termed P selectin glycoprotein ligand-1 (PSGL-1)¹ (Sako et al., 1993), while E selectin binding appears to be mediated by multiple glycoconjugate ligands sharing lactosamine motifs related to the sialyl Lewis x/a (SLe^{x/a}) antigen (Lowe et al., 1990; Picker et al., 1991; Polley et al., 1991; Rosen, 1993). We have shown previously (Rossiter et al., 1994) that T cell clones derived from peripheral blood and skin of atopic dermatitis patients differ in their levels of CLA (Berg et al., 1991), a SLe^x containing ligand for E selectin defined by mAbs HECA-452 and CSLEX-1 (Fukushima et al., 1984; Duijvestijn et al., 1988; Picker et al., 1990; Munro et al., 1992; van Reijssen et al., 1992). Binding of T cell clones to P selectin in this study did not correlate with either E selectin binding or CLA expression, raising the intriguing possibility that T cells express distinct ligands for E and P selectins (Rossiter et al., 1994).

In the present study, we report that T lymphocytes can indeed form rolling adhesions on purified endothelial selectins under conditions simulating physiological flow. Through the study of both normal peripheral blood T cells and specific CD4⁺ T cell clones, we conclude that distinct ligands appear to mediate T cell interactions with P and E selectins. We used a novel O-glycoprotease derived from *Pasteurella haemolytica* that is highly specific for O-sialo mucin-like glycoproteins (Abdullah et al., 1992; Sutherland et al., 1992) to characterize their contribution to rolling adhesions on P and E selectins. We have identified PSGL-1 (or a closely related molecule) as the major ligand for P selectin on T cells, and found it does not contribute to T cell rolling adhesions on E selectin. The physiological significance of distinct ligands on T lymphocytes for P and E selectin is discussed.

Materials and Methods

Antibodies

HECA-452 (Rat IgM), a gift of Dr. L. Picker (University of Texas/Southwestern, Dallas, TX) was produced and FITC labeled as previously described (Duijvestijn et al., 1988; Picker et al., 1990). FITC-conjugated Rat IgM was used to control for nonspecific binding. The anti-human P selectin murine mAbs used in this study as purified Igs were gifts of Dr. R. McEver (University of Oklahoma, Oklahoma City, OK); mAb G1 was used for blocking P selectin function; mAb S12, a non-function-blocking mAb, was used for site density determinations of P selectin in the planar membranes (Geng et al., 1990). mAb BB11(IgG2b), a function-blocking anti-E selectin mAb (Lobb et al., 1991) was obtained from Dr. R. Lobb (Biogen, Cambridge, MA). Rb 3026, a well-characterized polyclonal antibody to the fucosylated extracellular portion of PSGL-1 (Sako et al., 1993), was a gift of Dr. G. Larsen (Genetics Institute, Cambridge, MA). FITC- and phycoerythrin (PE)-conjugated secondary antibodies were obtained (Southern Biotechnology, Birmingham, AL), and used according to manufacturer's instructions.

Flow Cytometry

FACS analysis: flow cytometry was performed on a Becton-Dickinson FACSCAN: 10⁵ cells were analyzed per test, using FITC-labeled HECA

452. FITC-conjugated Rat IgM was used as a control. Cells were also stained with anti-PSGL-1 polyclonal antiserum (Rb 3026) (1:100 dilution), or control rabbit serum, washed, and labeled with a secondary FITC for single color or PE conjugated goat anti-rabbit antibody for two color analysis.

Isolation of Peripheral Blood T Cells and Generation of T Cell Clones

CFTS 4:3.1 and CFT 4:1.7 were derived from a patient known to develop atopic dermatitis after exposure to the house dust mite *Dermatophagoides pteronyssinus*. CFTS 4:3.1 was obtained from a biopsy of an epicutaneous patch test to *Dermatophagoides pteronyssinus* 24 h after challenge as previously described (van Reijssen, 1992). Clone CFT 4:1.7 was obtained from peripheral blood and was derived in an identical fashion; these cells are not antigen specific for Der.p. 1. Both clones are CD4⁺ and express the α/β TCR. Clone C4B5 was the generous gift of Dr. R. Modlin (UCLA, Los Angeles, CA) and was derived from a patient with leprosy. It is CD4⁺, produces a TH0 profile of cytokines, and is antigen specific for M. leprae. Clones were maintained as previously described (Rossiter, 1994).

Peripheral blood T lymphocytes were isolated by Ficoll Hypaque density gradient centrifugation, followed by depletion of monocytes, B lymphocytes, and NK cells using mAbs to selective surface markers followed by magnetic bead-mediated negative selection, as described (Carr et al., 1994). CD3 immunoreactivity was greater than 90% as determined by flow cytometry.

Cell Adhesion Assays

⁵¹Cr-labeled lymphocytes were preincubated at 4°C with various dilutions of PSGL-1-specific antiserum or normal rabbit serum (NRb) in binding medium (HBSS/Hepes/10 mM Ca²⁺/10 mM Mg²⁺/2% BSA). The cell suspension was added to multiwell plates precoated with anti-human IgG Fc Ab followed by P-selectin Rg, E-selectin Rg, or control CD4-Rg chimera absorption (Zettlmeissl et al., 1990), as previously described (Rossiter et al., 1994). The plates were gently rotated at room temperature for 30 min in order to maintain shear conditions. Unbound cells were separated from bound cells by inverting the plates, as described previously (Rossiter et al., 1994).

Preparation of Selectin Containing Planar Bilayers

Recombinant full length human E selectin was purified from a CHO cell line transfected with E selectin cDNA, (a generous gift of Dr. R. Lobb), by immunoaffinity chromatography using anti-E selectin mAb BB11 coupled to Sepharose. P selectin, purified from human platelets, was a gift of Dr. R. McEver. Liposomes containing the reconstituted selectins, were prepared as previously described (Lawrence and Springer, 1991) by the method of octyl-glucoside (OG; Sigma Chem. Co., St. Louis, MO) dialysis.

Determination of Selectin Site Densities

Liposomes were reconstituted with different quantities of a purified selectin and planar membranes were formed as described (Lawrence and Springer, 1991). Radiolabeled mAbs S12 or BB11 were used at 20 μ g/ml for site density determination of P or E selectin-containing membranes, respectively. The purified antibodies were iodinated to a known specific activity and site densities of each planar bilayer were determined by saturation binding as previously described (Dustin and Springer, 1989). Site densities were determined in triplicate.

Cell Treatments

To remove terminal cell-surface sialic acids, cells were incubated with 0.1 U/ml *Vibrio Cholera* neuraminidase (Calbiochem, San Diego, CA) for 30 min at 25°C in HBSS supplemented with 10 mM Hepes and 2 mM Ca²⁺ (H/H Ca²⁺ medium). To assess the role of O-sialo mucin-like ligands for selectins in leukocyte rolling adhesions to each selectin, lymphocytes or HL-60 cells (10⁷/ml) were incubated for 40 min at 37°C in binding medium: H/H Ca²⁺ medium supplemented with 2 mg/ml HSA (Calbiochem, San Diego, CA) in the presence of 50 μ g/ml of *P. haemolytica* O-glycoprotease (a generous gift of Dr. A. Mellors, University of Guelph, Ontario). Control cells were incubated at 37°C in this medium in absence of enzymes. Reactions were terminated by washing the cells twice with H/H medium + 5 mM EDTA. Cells were kept at 4°C up to 2 h in binding medium.

1. Abbreviation used in this paper: CLA, cutaneous lymphocyte antigen; Der.p.1, Dermatophagoides pteronyssinus antigen; NRb, normal rabbit serum; OG, octyl-glucoside; PE, phycoerythrin; PSGL-1, P-selectin glycoprotein ligand-1; SLe^x, Sialyl Lewis x.

Laminar Flow Assays

A glass slide containing a planar bilayer was assembled in a parallel flow chamber (260- μ m gap thickness) and mounted on the stage of an inverted phase-contrast microscope (Diaphot-TMD; Nikon Inc., Garden City, NY), as previously described (Lawrence and Springer, 1991). Cells were resuspended at a concentration of 1×10^6 /ml in binding medium and attachment during flow was assayed. The number of adherent cells per field of view (0.43 ± 0.01 mm²) which attached during initial periods of continuous flow was quantitated by a visual count of the fields videotaped while scanning the lower plate of the flow chamber. Cell attachment events were expressed in rate of attachment. The wall shear stress was calculated assuming a viscosity of assay buffer equal to the viscosity of water at room temperature (1.0 centipoise, 24°C). T clones or HL-60 failed to attach to the selectin containing membranes at shear stresses higher than 1.8 dynes/cm². PMN attached to identical selectin containing bilayers at shears as high as 3.6 dynes/cm².

For detachment assays, cells were infused into the chamber at a shear of 0.73 dynes/cm², allowed to adhere until equilibration was reached and the shear force was then increased every 20 s to a maximum of 36 dynes/cm². A given batch of cells, pretreated with the different enzymes, was compared for attachment rate to a given field of the selectin-containing membrane.

Analysis of Cell Rolling

All cells were bound during shear flow (0.73 dyne/cm²) for 1–2 min and the shear force was increased every 20 s. Images were recorded on a time-lapse video cassette recorder and analyzed as previously described (Lawrence and Springer, 1991) except that cell displacements were measured over 5–10-s intervals. Rolling was assessed only for cells which remained adherent for at least 20 s at the shear applied. Rolling of a given group of cells, differently pretreated with the various reagents, was measured in identical fields of view in order to directly assess the effects of these treatments. In each experiment, under the highest shear applied, at least 20% of the cells originally attached remained adherent and rolling.

Results

Normal Peripheral Blood T Lymphocytes Tether to P and E Selectin

We wished to determine the relative percentages of normal peripheral blood T cells that tethered to P and E selectin, respectively, under shear stress. At saturable selectin densities coated on the substrate, ~15% of T cells bound to P selectin, and a similar percentage of T cells bound to E selectin (Fig. 1). Tethering under these conditions was always followed by rolling of all cells on both selectins (not shown). Subsequent experiments to determine whether these ligands were distinct, and whether they were present on the same or different T cells, yielded equivocal results. While these data and our prior results (Rossiter et al., 1994) suggested that different ligands might mediate these interactions on peripheral blood T cells, such an analysis of a heterogeneous population of T cells could not shed further light on the expression and function of each type of putative selectin ligand on individual T cells. Subsequent analyses focused on homogeneous populations of cloned human T cells.

CLA is not Required for Tethering and Rolling of T Cells on P Selectin Under Physiological Flow

We characterized the properties of three representative T cell clones with regards to attachment and rolling under physiological flow conditions on artificial membranes containing P or E selectin (Lawrence and Springer, 1991). HL-60, a promyelocytic cell line that exhibits well-characterized binding to both E and P selectins, served as a positive control. All three T clones are CD4+, express $\alpha\beta$ T cell receptors, and are CD45RO positive and RA negative (Rossiter et

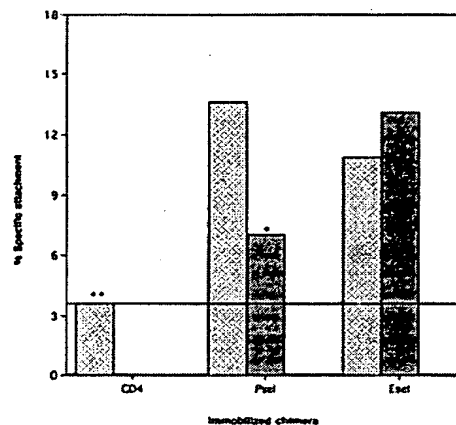


Figure 1. Attachment of peripheral blood T lymphocytes to P and E selectin under shear conditions. Purified ⁵¹Cr labeled T cells (5×10^4 /well) in binding medium (HBSS/Hepes/10 mM Ca²⁺/10 mM Mg²⁺/2% BSA) were allowed to attach to either P or E selectin chimeras, immobilized in multiwell plates. A CD4 chimera served as a control. Plates were gently rotated to maintain shear conditions under which selectin-mediated tethering predominates. In the presence of EDTA or EGTA all cell binding was abolished. E selectin function-blocking mAb (BB1) reduced T cell binding to background levels (not shown). Results are the means of triplicates. A representative of three experiments is shown. * $p < 0.05$ and ** $p < 0.001$ with respect to cell attachment to P selectin. □, No antibody; ■, a P selectin blocking antibody.

al., 1994; R. Modlin, unpublished data). These clones were selected because they expressed high, low, or absent levels of CLA, as defined by HECA-452 reactivity. This monoclonal antibody is an IgM that defines a sialylated carbohydrate antigen associated with multiple leukocyte glycoconjugates terminating with SLe^x-related carbohydrates (Berg et al., 1991). Clone C4B5 is a TH0 clone that lacks detectable CLA, while clone CFTS 4:3.1 expresses high levels of CLA (Fig. 2). Clone CFT 4:1.7 expresses low but detectable levels of CLA (Fig. 2).

Despite lacking any carbohydrate structures recognized by HECA-452, C4B5 lymphocytes attached and rolled on P selectin under flow. In fact, they did so more readily than HL-60 cells, which express high HECA-452 levels (Fig. 3 a). This attachment could be fully blocked by the anti-P selectin function-blocking antibody mAb G1 (data not shown). In contrast, C4B5 cells did not attach to E selectin under the flow conditions of the assay, while HL-60 cells did so readily (Fig. 3 a). We conclude that the T clone C4B5 expresses a functional P selectin ligand(s) that is not recognized by HECA-452 antibody and is thus distinct from CLA.

P Selectin Ligands on T Cells Are O-glycoprotease-sensitive Sialomucins

A novel endopeptidase that selectively degrades O-sialomucins (Abdullah et al., 1992) was recently shown to selectively abolish binding of HL-60 and PMN to P selectin (Steininger et al., 1992). Treatment of C4B5 cells or HL-60 cells with O-glycoprotease completely abolished their tethering to P selectin, but did not influence HL-60 attachment to E selectin (Fig. 3 a). Similar elimination of C4B5 attachments to P selectin was observed after neuraminidase treat-

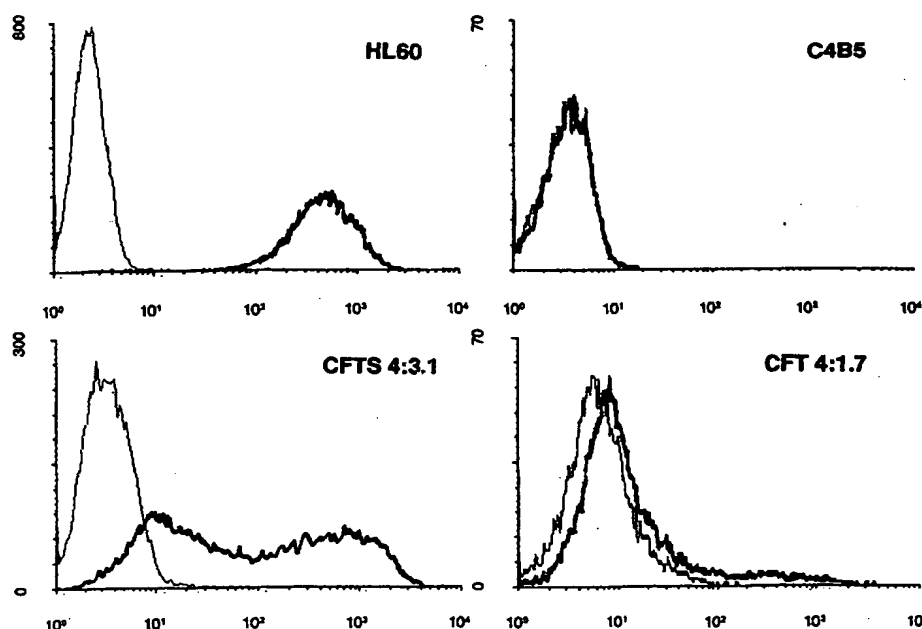


Figure 2. HECA-452 FACS analysis of HL-60 and T lymphocyte clones. Cells were stained with FITC-labeled HECA 452 or control IgM.

ment. The P selectin ligand on HL-60 cells was partially susceptible to neuraminidase treatment at 24°C (Fig. 3 a), and neuraminidase treatment at 37°C completely abolished the P selectin ligand (not shown). Collectively, the effects of these different enzyme treatments suggest that the predominant P selectin ligand on the C4B5 T cell clone is a sialomucin, just as in neutrophils and HL-60 cells (Steininger et al., 1992). This P selectin ligand does not appear to support the clone tethering and rolling on E selectin. It is notable that adherent C4B5 cells exhibited an extremely high resistance to increasing shear stresses applied on cells tethered to P selectin. The majority of C4B5 cells continued to roll on this selectin at shear stresses equivalent to the highest measured in post capillary venules (35 dynes/cm²) (Fig. 3 b). In contrast, the few T cells or HL-60 which tethered to P selectin after *O*-glycoprotease treatment, had transient rolling and readily detached from the selectin at low shear stresses, indicating near complete removal of P selectin ligands.

Binding of T Cells to E Selectin Is Not Mediated by *O*-glycoprotease Sensitive Sialomucins

The T cell clone CFTS 4:3.1, which expresses high levels of cell surface CLA (Fig. 2), attached and rolled on E selectin-containing membrane in a manner comparable to HL-60 cells (Fig. 4, a and b). These rolling adhesions were completely abolished by neuraminidase treatment (Fig. 4 b). CFTS 4:3.1 T cells had considerable resistance to increasing shear on E selectin, with a significant proportion of cells exhibiting persistent rolling at shear stresses as high as 15 dynes/cm² (Fig. 4 b). *O*-glycoprotease treatment of CFTS 4:3.1 had a negligible effect on E-selectin-mediated adhesions (Fig. 4 b). CFTS 4:3.1 T cells also express ligand(s) for P selectin. In contrast to interactions with E selectin, both attachment under flow (Fig. 4 a) and rolling on P selectin (Fig. 4 c) were eliminated by *O*-glycoprotease treatment,

indicating that the P selectin ligand on these cells is a sialomucin. *O*-glycoprotease-treated 4:3.1 cells appear to retain completely their functional E selectin ligands, despite having lost virtually all cell surface sialomucins to this endopeptidase (including their P selectin ligand(s)). Identical results were obtained with HL-60 cells (Fig. 4, a and b); after loss of their entire P selectin binding capacity, these cells could still attach (Fig. 4 a) and roll (Fig. 4 b) normally on E selectin. Taken together, these data suggest that CLA, or other sialylated E selectin ligands on T cells resistant to *O*-glycoprotease treatment, do not support rolling attachments to P selectin. This is consistent with previous studies on myeloid cell lines (Larsen et al., 1992).

CFT 4:1.7, a T cell clone derived from peripheral blood, expresses low but detectable levels of CLA (Fig. 2). Attachment rates of this clone to P selectin were comparable to those observed with HL-60 (Figs. 3 a and 5 a), and as always, attachment was followed by rolling (Fig. 5 b). All interactions of this clone with P selectin were completely abolished by *O*-glycoprotease treatment (Fig. 5, a and b). FACS analysis indicated that virtually complete removal of P selectin-binding activity by *O*-glycoprotease treatment did not result in any decrease in the cell surface expression of CLA or other HECA-452 reactive molecules, even on cells where the baseline expression of such epitopes was low (not shown).

Another parameter that assesses the average number of tethers being formed by a rolling cell is resistance to detachment of forces continuously applied on it (Lawrence and Springer, 1993). We compared the three T clones, all preattached under low flow conditions to P selectin, for their relative shear resistance on this selectin. The CLA^{low} C4B5 clone had the highest shear resistance on P selectin, whereas the CLA^{high} T clone 4:3.1 had the lowest value (Fig. 6). Based on this assay, and its highest cell attachment rates to

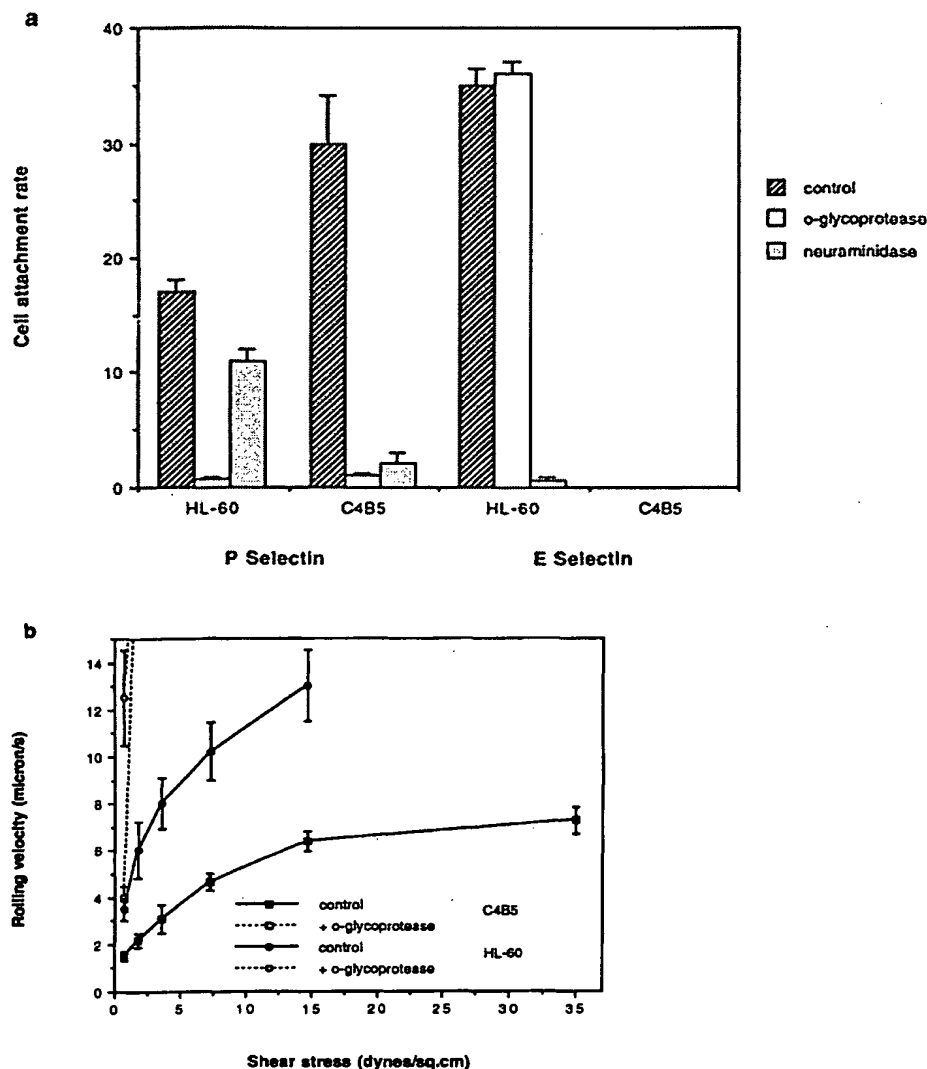


Figure 3. Attachment of C4B5 and HL-60 cells under flow conditions to purified P and E selectins reconstituted in lipid bilayers. (a) Effect of enzymatic pretreatments of the flowing cells. Cells (10^7 /ml) were preincubated with control binding medium alone or with *O*-glycoprotease (at 50 μ g/ml; 20) or 0.1 U/ml *Vibrio cholera* neuraminidase (Calbiochem, San Diego, CA) at 37 or 25°C, respectively, for 30 min. Reactions were terminated by washing the cells twice with H/H medium + 5 mM EDTA. Cells (1×10^6 /ml) were infused in binding medium (HBSS/Hepes/2 mM Ca^{2+} supplemented with 2 mg/ml HSA) at 0.73 dyne/cm² wall shear stress through a parallel plate flow chamber (Lawrence and Springer, 1991, 1993). Rates of cell attachment to the artificial planar bilayer containing P or E selectin at 650 and 500 sites/ μ m², respectively, were calculated from the numbers of cells adhered to a given field of view (0.43 ± 0.01 mm²) per minute. All cells started to roll upon adherence to the selectin-containing membrane. Bars show the standard error of the mean. Results are representative of two independent experiments. At 37°C, neuraminidase completely blocked attachment of both HL-60 and C4B5 cells to P selectin. (b) Effect of *O*-glycoprotease pretreatment on C4B5 and HL-60 rolling on P selectin. Cells, attached at

flow to the P selectin membranes as described in a were exposed to increasing shear stresses and their rolling velocities at each stress were determined. Each point represents the mean \pm SEM of 20–30 rolling cells. Velocity values of cells observed to roll at the given shear stress in a transient manner (mean velocities greater than 50 μ m/s) and eventually detach from the membrane are not shown but are indicated by connecting dashed lines. \blacksquare , Control; \square , *O*-glycoprotease; \blacksquare , neuraminidase.

P selectin (Fig. 3 a), C4B5 appears to express the highest P selectin ligand level.

These observations suggest that the P selectin ligands on all three T cells are sialomucin structures that do not react with an antibody specific for common SLe^x related structures. In contrast, rolling adhesions of T cells on E selectin are closely associated with the presence of SLe^x bearing glycoproteins (e.g., CLA). Since C4B5, the T cell clone negative for HECA-452 reactivity (Fig. 2), attached very poorly to E selectin under flow, it would appear that HECA-452 reactivity is indeed closely correlated with functional E selectin ligand activity. This was true for all lymphocyte clones thus far tested, a result consistent with data previously obtained on these T cells in static binding assays (Ros-

siter et al., 1994). The role of CLA in the binding of these cells has been difficult to confirm by antibody blocking experiments, since HECA-452 is an inefficient blocking antibody (L. Picker, personal communication; and Berg et al., 1992).

PSGL-1 or a Closely Related Molecule Is the Major P Selectin Ligand on T Cells

The P selectin ligand, PSGL-1, recently cloned from a cDNA library of HL-60, appears to be the sole P selectin ligand on myeloid cells and neutrophils (Sako et al., 1993). We asked whether the sialomucin ligand(s) for P selectin on T cells is homologous to PSGL-1, using a polyclonal anti-

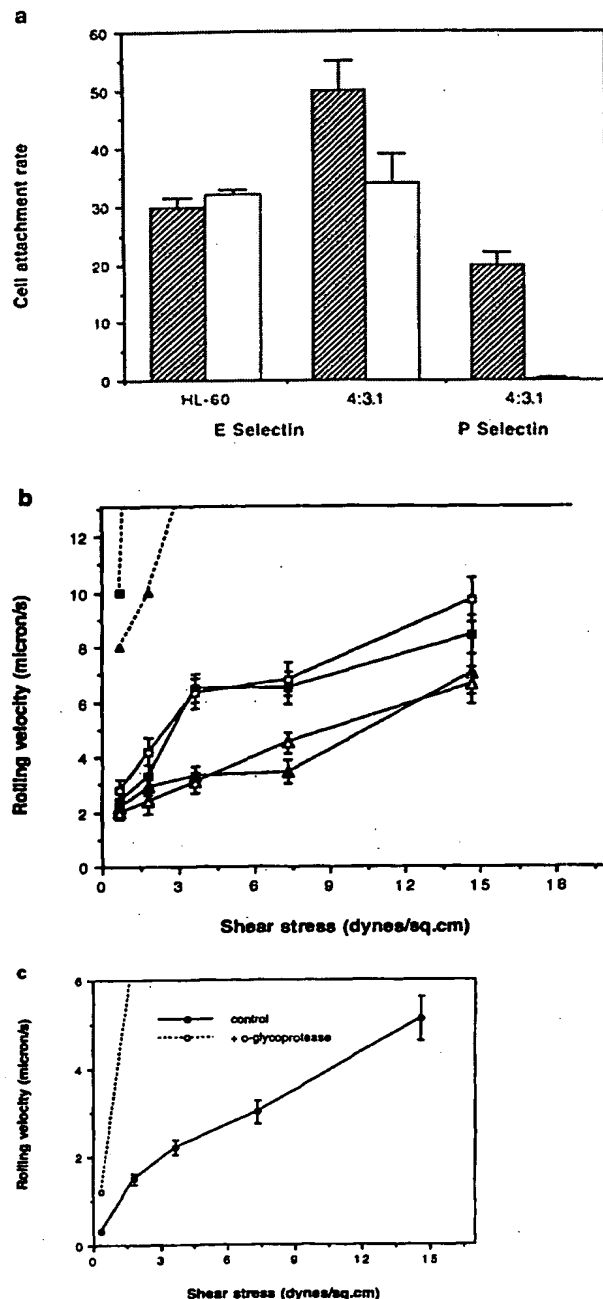


Figure 4. Attachment and rolling of CFTS 4:3.1 T clone on P but not on E selectin are mediated by sialomucins. (a) Effect of *O*-glycoprotease induced removal of surface mucin-like sialoglycoproteins on attachment of CFTS 4:3.1 under flow to E selectin and P selectin. HL-60 cell attachment to E selectin is shown for comparison. Cells (1×10^6 /ml) were infused at 0.73 dyne/cm^2 and attachment rates to P selectin at $650 \text{ sites}/\mu\text{m}^2$ or E selectin at $250 \text{ sites}/\mu\text{m}^2$ were determined as in Fig. 3. Bars show the standard error of the mean. \square , Control; \square , *O*-glycoprotease. (b) Effect of *O*-glycoprotease treatments and neuraminidase on rolling velocities of 4:3.1 clone at different shear stresses on E selectin (coated at $250 \text{ sites}/\mu\text{m}^2$). Effect of enzyme treatments on HL-60 rolling on E

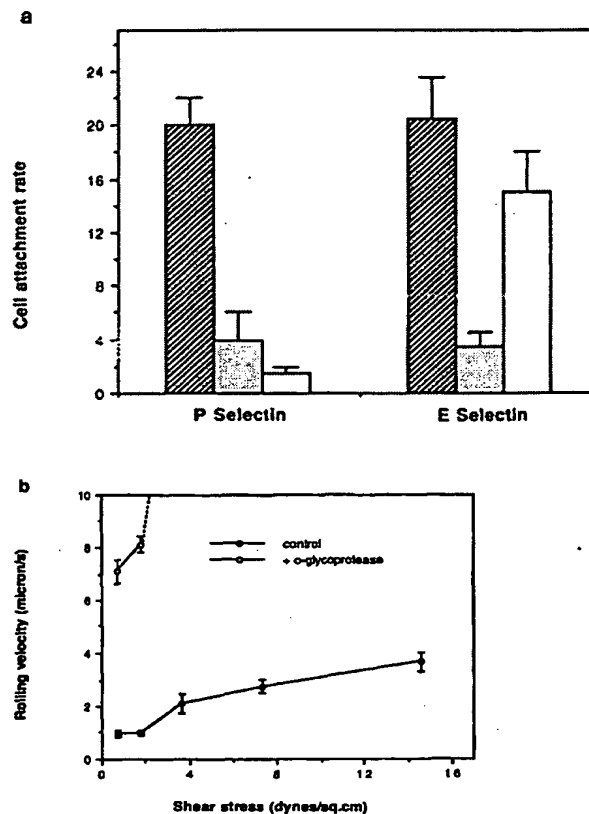


Figure 5. Different contribution of sialomucin and CLA ligands to CFT 4:1.7 T cell clone rolling adhesions on P and E selectins. (a) Attachment of 4:1.7 T clone to selectins under flow conditions following enzymatic treatments. Cells (1×10^6 /ml) were infused at 0.73 dyne/cm^2 and rates of attachment to P selectin (at $650 \text{ sites}/\mu\text{m}^2$) or to E selectin (at $500 \text{ sites}/\mu\text{m}^2$) were determined. The T clone attachment rate to the P selectin containing membrane was reduced two-fold at elevated shear (1.8 dynes/cm^2). Enzymatic pretreatments were as described above. Error bars show the standard error of the mean. Results are representative of three experiments. \square , control; \square , + neuraminidase; \square , + *O*-glycoprotease. (b) Rolling of 4:1.7 T cells on P selectin at different wall shear stress. Effect of *O*-glycoprotease treatment on rolling velocity. Cells attached during flow were exposed to increasing shear stresses and their rolling velocities were calculated as described in previous figures. Each point represents the mean \pm SEM of 20–30 cells.

selectin (coated at $500 \text{ sites}/\mu\text{m}^2$) is shown for comparison. \blacktriangle , HL-60 control; \triangle , HL-60 + *O*-glycoprotease; \blacktriangle , HL-60 + neuraminidase; \blacksquare , 4:3.1 control; \square , 4:3.1 + *O*-glycoprotease; \square , 4:3.1 + neuraminidase. (c) Effect of *O*-glycoprotease treatment on rolling of 4:3.1 clone on P selectin coated at $650 \text{ sites}/\mu\text{m}^2$. Velocities of cells which rolled transiently at the higher shear are indicated by dashed lines. *O*-glycoprotease treatments and rolling velocity analysis were performed as described in Fig. 2. Results are representative of two and four different sets of experiments, for 4:3.1 T clone and HL-60 cells, respectively.

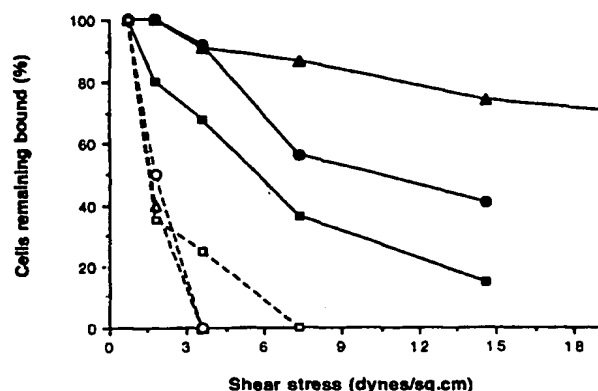


Figure 6. Relative resistance of T cells attached to P selectin to detaching shear stresses. Effect of *O*-glycoprotease pretreatment. Cells were infused through the chamber at 0.73 dynes/cm² for 2 min and then the flow rate was increased in stage increments every 20 s. The number of cells which attached to the P selectin-containing membrane after *O*-glycoprotease treatment was significantly lower than untreated cells. The percentage of cells that remained bound and rolling was determined after 10 s at each shear stress. Control (untreated) samples of each clone are shown in bold; *O*-glycoprotease treated cells are shown in open symbols. \blacktriangle , C4B5; \triangle , + *O*-glycoprotease; \bullet , 4:1.7; \circ , + *O*-glycoprotease, \blacksquare , 4:3.1; \square , + *O*-glycoprotease.

body (Rb 3026) specific for a functional selectin-binding glycoform of the recombinant PSGL-1 protein expressed in COS cells cotransfected with fucosyltransferase III (Sako et al., 1993). All T cell clones and lines thus far tested are positive by flow cytometry for PSGL-1 expression (not shown). Treatment of T cell clones and HL-60 cells with *O*-glycoprotease significantly reduced PSGL-1-specific staining (Fig. 7 a).

We next assessed the specific role of PSGL-1 in T cell binding to P selectin in a binding assay shown in Fig. 7 b. A significant, specific, and dose-dependent blocking of T cell binding to P selectin in the presence of Rb 3026 was reproducibly observed. The adhesion inhibition by this antiserum was not a result of cell agglutination by the polyclonal antibody, as judged by visual inspection. Rb 3026 did not influence T cell binding to E selectin (not shown). Collectively, these data demonstrate that T cell PSGL-1, or a closely related sialomucin, can function as a major P selectin ligand.

Finally, we turned our attention back to peripheral blood T cells. Two color flow cytometry analysis of peripheral blood T cells indicated that, surprisingly, the majority of T cells express immunoreactive PSGL-1 (judged by Rb 3026 binding), while only a small subset express CLA (Fig. 8). Treatment of T cells with *O*-glycoprotease completely abolishes Rb 3026 reactivity while not affecting HECA-452 reactivity. This indicates that all Rb 3026 immunoreactivity is associated with the *O*-glycoprotease sensitive sialomucin(s). The tethering of peripheral blood T cells to P selectin shown in Fig. 1 can be blocked by *O*-glycoprotease, while E selectin tethering cannot (not shown). These data indicate that peripheral blood T cells and the clones characterized in this study behave in a similar fashion with regards to selectin tethering.

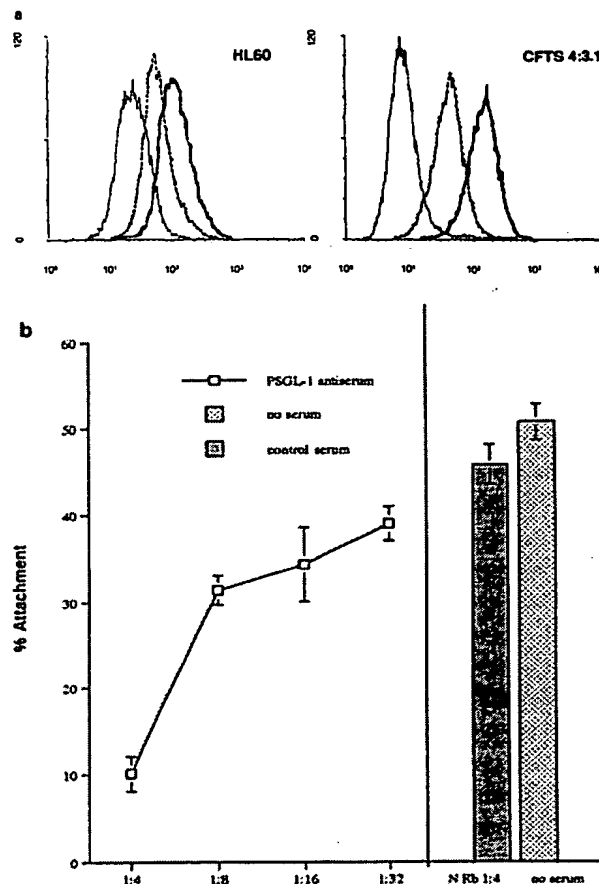


Figure 7. PSGL-1 is a major P selectin ligand in T cells. (a) PSGL-1 staining of CFTS 4:3.1 clone and HL-60 cells before and after treatment with *O*-glycoprotease. Cells were stained with anti-PSGL-1 rabbit antiserum (Sako et al., 1993) or control rabbit serum (1:100 dilution) washed and labeled with a secondary FITC-goat anti-rabbit antibody. Heavy line, before treatment; dotted line, after treatment; pole line, control Ab. (b) A dose-response blocking of CFTS 4:3.1 T cell adhesion to P selectin substrate in the presence of anti-PSGL-1 antiserum. ⁵¹Cr-labeled lymphocytes were preincubated at 4°C with various dilutions of PSGL-1-specific antiserum (Rb 3026) or NRb in binding medium. The cell suspension was added to multiwell plates precoated with P selectin or control BSA and the plates were gently rotated at room temperature for 30 min. Unbound cells were separated from bound cells by inverting the plates, as described previously (Rossiter et al., 1994). Adhesion is expressed as percentage of radioactivity bound. Background adhesion to human IgG was 4%.

It is clear that only a subset of PSGL-1 positive T cells bind to P selectin. It is likely that only specific glycoforms of PSGL-1 mediate binding to P selectin, and that glycosylation patterns, rather than surface-expression of PSGL-1 per se correlate with ligand binding activity. These results are consistent with the observation that transfection of COS cells with PSGL-1 cDNA alone did not result in P selectin binding. Cotransfection with fucosyltransferase was required for the acquisition of binding activity. The PSGL-1 sialomucin appears to be restricted to leukocytes, however, since fibro-

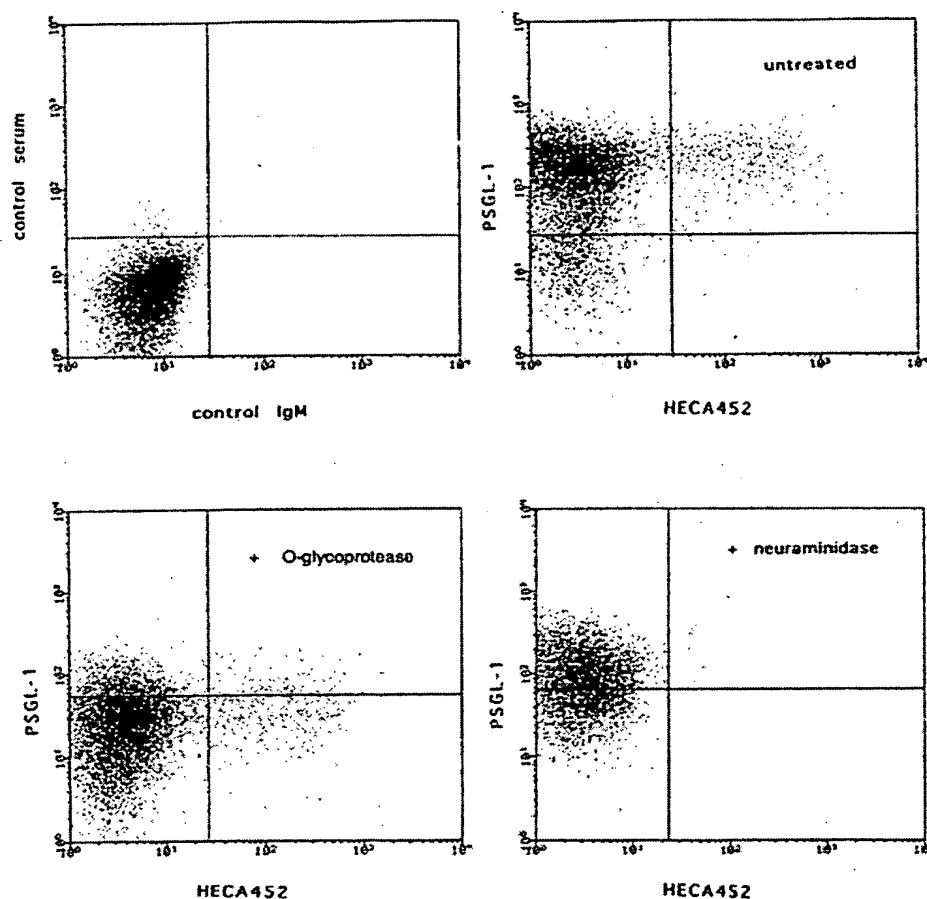


Figure 8. Distinct subsets of T lymphocytes express CLA and PSGL-1. Two color FACS analysis of cells stained with FITC-labeled HECA 452 and anti-PSGL-1 antiserum followed by PE-conjugated secondary antibody was performed before and after enzyme treatments with either *O*-glycoprotease or neuraminidase as described in Materials and Methods.

blasts and keratinocytes are not Rb 3026 positive (not shown). It should be noted that these latter cells do express multiple sialomucins that do not react with Rb 3026.

Discussion

The present study provides the first evidence that subsets of T cells tether and roll on P and E selectins. Our use of cloned T cells in addition to peripheral blood T cells in this study enabled us to analyze interactions of homogeneous populations with purified selectins in well defined flow conditions, using a parallel plate flow chamber system (Lawrence and Springer, 1991, 1993). We show that, under continuous flow conditions using P or E selectin reconstituted at physiological site densities in artificial membranes, all T cells that tethered to these selectins remained attached and rolled on the selectins at high shear stresses.

Three main observations made in this study indicate that CLA, previously implicated in E selectin binding (Picker et al., 1991; Shimizu et al., 1992), does not serve as a P selectin ligand. First, high levels of CLA as measured by FACS analysis on a subset of peripheral blood T cells, the 4:3.1 T clone, and HL-60 remained intact after *O*-glycoprotease treatments which remove surface sialomucins, but were not

sufficient to support rolling adhesions on P selectin. Second, attachment and rolling on E selectin was not significantly influenced on any cell treated with the *O*-glycoprotease, suggesting (at best) only a minor contribution of mucin-like ligands to E selectin binding. Finally, HECA-452 reactivity, the working definition of CLA expression on different T clones, did not correlate with the level of P selectin binding activity; in fact, T cells that lacked any CLA reactivity or E selectin binding expressed the highest levels of P selectin ligand as assessed by function (C4B5).

We did not find any CLA-related carbohydrates to be associated with the *O*-glycoprotease-sensitive sialomucins on T cells or HL-60, because even the most exhaustive *O*-glycoprotease treatments did not alter their level by FACS analysis. The insensitivity of CLA expression to *O*-glycoprotease digestion was confirmed both with the 4:1.7 clone (not shown), which expresses very low levels of CLA, and with peripheral blood T cells (Fig. 8). Although a previous report indicated that HL-60-derived PSGL-1 decorated with SLE^a can support cell adhesion of cells transfected with either P or E selectin (Sako et al., 1993), we could not demonstrate any contribution of cell surface PSGL-1 or any other sialomucin to leukocyte rolling adhesions of E selectin.

All T cells tested were positive for PSGL-1 immunoreac-

tivity, as judged by a polyclonal antibody Rb 3026 specific for the recombinantly expressed sialoglycoprotein. PSGL-1 immunoreactivity was abrogated by *O*-glycoprotease treatment, both on peripheral blood T cells, T cell clones, and HL-60 cells, indicating that the RB 3026 immunoreactivity is sialomucin associated. Furthermore, the anti-PSGL-1 antibody blocked binding of T cells to P selectin in a dose dependent fashion. This blocking was highly reproducible, though it required relatively high concentrations of antibody. While it is likely that T cells express authentic PSGL-1, it should be pointed out that this molecule was defined in HL-60 cells and neutrophils, and we cannot rule out the possibility that a closely related but distinct molecule on T cells is the authentic P selectin ligand. If so, this T cell P selectin ligand must be a sialomucin (based on the sensitivity of immunoreactivity to *O*-glycoprotease) and must share P selectin binding epitopes with HL-60-derived PSGL-1, based on the blocking ability of Rb 3026. The future cDNA cloning of the P selectin ligand from one of our T cell clones should resolve the question of structural differences between myeloid and lymphoid PSGL-1 glycoforms.

We were initially surprised that virtually all peripheral blood T cells reacted with Rb 3062 by FACS analysis. It now appears that the protein backbone of PSGL-1 is nearly ubiquitous on all leukocytes, although it is not found on fibroblasts and keratinocytes. It appears that PSGL-1 immunoreactivity is necessary but not sufficient for P selectin binding function. Precedence exists for this dichotomy, in that immunoreactivity of CD34, the sialomucin endothelial ligand of L selectin is also widespread, while only a small subset of cells that express CD34 also have the potential to glycosylate this molecule appropriately to express L selectin carbohydrate ligand (Baumhueter et al., 1993). There is also good evidence that fucosylation of PSGL-1 is necessary for function, based on the requirement that PSGL-1 cDNA must be co-transfected with α 1-3/4 fucosyltransferase cDNA into COS cells to confer a P selectin binding phenotype (Sako et al., 1993). Fucosyltransferases are also required for the biosynthesis of E selectin carbohydrate ligands (Lowe, 1990), but the finding that T cells lacking E selectin ligands express functional ligands for P selectin suggests the possibility that different types of glycosyltransferases are required for the generation of E and P selectin ligands on T lymphocytes.

Taken together, these results indicate that a subset of human T cells express a functional P-selectin sialomucin ligand which mediate their rolling adhesions on this selectin under conditions of physiologic flow, and that the major T cell P selectin ligand is similar or identical to PSGL-1. Cell associated PSGL-1 does not appear to be either necessary or sufficient for T cell or HL-60 cell binding to E selectin (Figs. 3 a and 4 a), which strictly correlates with the expression of the SLe^x-containing molecule, CLA. Conversely, the presence of this putative E selectin ligand on a subset of T cells is not sufficient for their rolling adhesions on P selectin. The presence of two structurally distinct ligands, specific for different endothelial selectins and subject to differential regulation on different subsets of T cells, that support rolling adhesions of T cells under physiological flow conditions is novel and has not been reported previously. This observation suggests that there is heterogeneity among T cells with regards to their preferential interaction with one endothelial

selectin over another. The analysis of peripheral blood T cells, as well as the clones, indicates that T cells can express either one or both of these selectin ligands.

It would appear that recruitment of circulating lymphocytes to endothelial sites of inflammation (as opposed to secondary lymphoid tissues) is primarily regulated by endothelial selectins recognizing counter-receptors on memory T cells, rather than by L selectin, since at least some of the memory T cells which recirculate through these sites lack L selectin (Picker et al., 1994). L selectin on C4B5 and on peripheral blood T cells was resistant to *O*-glycoprotease, under conditions which removed all P selectin ligands on these cells (data not shown), suggesting it has no direct contribution to P selectin binding. To the extent that some memory T cells bearing L selectin could interact with putative L selectin ligands on non-lymphoid endothelial sites of inflammation (von Andrian et al., 1991), this may represent yet a third potential adhesion pathway that can be used by T cells to initiate tethering to these peripheral endothelial sites. Coexpression of L selectin and endothelial selectin ligands (e.g., CLA, active PSGL-1) may permit memory T cells to recirculate between peripheral tissue, blood, and lymph nodes (Picker et al., 1994).

The potential of circulating peripheral blood T cells to interact with activated endothelial cells by adhering and rolling on E and P selectins, both of which in turn are subject to specific regulation in many pathophysiologic states of inflammation (Weller et al., 1992; Hahne, et al., 1993; Mulligan et al., 1993), points out a novel mechanism by which T cells may recirculate through peripheral tissues. It suggests that like monocytes and granulocytes (Lawrence and Springer, 1993), T lymphocytes may also use rolling adhesions on endothelial selectins at peripheral sites of inflammation as the antigen independent primary event that is prerequisite for subsequent multi-step activation, stable adhesion, and *trans*endothelial migration (Shimizu et al., 1992; Bevilacqua and Nelson, 1993; Springer, 1994).

While P selectin expression has been identified with immediate inflammatory events (e.g., platelet degranulation, endothelial cell Weibel-Palade body membrane fusion), evidence is accumulating that it can be expressed on endothelial cells at sites where inflammation is prolonged or chronic (Weller et al., 1992; Grober et al., 1993). It is therefore possible that different subsets of T cells home to different anatomical sites based in part upon their selectin ligand surface profile. Just as CLA positive T cells may preferentially home to skin or to chronic sites where E selectin expression is up-regulated, P selectin ligand-expressing T cells may home more efficiently (for example) to inflamed synovium (where P selectin expression is chronically elevated) or preferentially recirculate through any anatomical sites where endothelial P selectin expression is transiently induced. It is furthermore likely that differential expression of specific P and E selectin ligands would add to the diversity of potential adhesive interactions that regulate memory T cell recirculation through peripheral tissues. It is these memory T cells that have been activated by environmental antigens in the immediate or remote past, and are most likely to find their antigen in the context of tissue specific inflammation induced by injury or microbial infection, rather than in peripheral lymph nodes. Tethering of memory T cells mediated by en-

dothelial selectins, followed by integrin-mediated firm adhesions and cytoskeletal mobilization, culminates in successful extravasation.

The following individuals generously contributed reagents: Glen Larsen, Alan Mellors, Brian Seed, Geert Mudde, Frank Kalthoff, Louis Picker, Roy Lobb, and Rodger McKeever. We are particularly grateful to Dr. Xiaohong Wang and Dr. Robert Modlin (UCLA) for allowing us to use their C4B5 T cell clone, which has not been previously described elsewhere.

This work was supported by National Institutes of Health grants AI25082, AR40124, and AR42124, (T. S. Kupper), the Harvard Skin Disease Research Center at Brigham and Women's Hospital (AR42689, T. S. Kupper), and National Institutes of Health HL-48675 (T. A. Springer).

Received for publication 1 June 1994 and in revised form 23 August 1994.

References

- Abdullah, K. M., E. A. Udoh, P. E. Shewen, and A. Mellors. 1992. A neutral glycoproteinase of *Pasteurella haemolytica* A1 specifically cleaves O-sialoglycoproteins. *Infect. Immun.* 60:56-62.
- Bargatze, R. F., and E. C. Butcher. 1993. Rapid G protein-regulated activation event involved in lymphocyte binding to high endothelial venules. *J. Exp. Med.* 178:367-372.
- Baumhueter, S., M. S. Singer, W. Henzel, S. Hemmerich, M. Renz, S. D. Rosen, and L. A. Lasky. 1993. Binding of L selectin to the vascular sialomucin, CD34. *Science (Wash. DC)*. 262:436-438.
- Berg, E. L., M. K. Robinson, O. Mansson, E. C. Butcher, and J. L. Magnani. 1991. A carbohydrate domain common to both sialyl Le^x and sialyl Le^a is recognized by the endothelial cell leukocyte adhesion molecule ELAM-1. *J. Biol. Chem.* 266:14869-14872.
- Berg, E. L., J. Magnani, R. A. Warnock, M. K. Robinson, and E. C. Butcher. 1992. Comparison of L-selectin and E-selectin ligand specificities: the L-selectin can bind the E-selectin ligands sialyl Le^x and sialyl Le^a. *Biochem. Biophys. Res. Commun.* 184:1048-1055.
- Bevilacqua, M. P., and R. M. Nelson. 1993. Selectins. *J. Clin. Invest.* 91:379-387.
- Butcher, E. C. 1991. Leukocyte-endothelial cell recognition: three (or more) steps to specificity and diversity. *Cell*. 67:1033-1036.
- Carr, M. W., S. J. Roth, E. Luther, S. S. Rose, and T. A. Springer. 1994. Monocyte chemoattractant protein 1 acts as a T-lymphocyte chemoattractant. *Proc. Natl. Acad. Sci. USA*. 91:3652-3656.
- Damle, N. K., K. Klussman, M. T. Dietsch, N. Mohagheghpour, and A. Aruffo. 1992. GMP-140 (P-selectin/CD62) binds to chronically stimulated but not resting CD4⁺ T lymphocytes and regulates their production of proinflammatory cytokines. *Eur. J. Immunol.* 22:1789-1793.
- Duijvestijn, A. M., E. Horst, S. T. Pals, B. N. Rouse, A. C. Steere, L. J. Picker, C. J. Meijer, and E. C. Butcher. 1988. High endothelial differentiation in human lymphoid and inflammatory tissues defined by monoclonal antibody HECA-452. *Am. J. Pathol.* 130:147-155.
- Dustin, M. L., and T. A. Springer. 1989. T-cell receptor cross-linking transiently stimulates adhesiveness through LFA-1. *Nature (Lond.)*. 341:619-624.
- Fukushima, K., M. Hirota, P. I. Terasaki, A. Wakisaka, H. Togashi, D. Chia, N. Suyama, Y. Fukushi, E. Nudelmann, and S. Hakomori. 1984. Characterization of sialosylated Lewis-x as a new tumor-associated antigen. *Cancer Res.* 44:5279-5285.
- Geng, J. G., M. P. Bevilacqua, K. L. Moore, T. M. McIntyre, S. M. Prescott, J. Kim, G. A. Bliss, G. A. Zimmerman, and R. P. McEver. 1990. Rapid neutrophil adhesion to activated endothelium mediated by GMP-10. *Nature (Lond.)*. 343:757-760.
- Grober, J. S., B. L. Bowen, H. Ebling, B. Athey, C. B. Thompson, D. A. Fox, and L. M. Stoolman. 1993. Monocyte-endothelial adhesion in chronic rheumatoid arthritis. In situ detection of selectin and integrin-dependent interactions. *J. Clin. Invest.* 91:2609-2619.
- Hahne, M., U. Jager, S. Isenmann, R. Hallmann, and D. Vestweber. 1993. Five tumor necrosis factor-inducible cell adhesion mechanisms on the surface of mouse endothelioma cells mediate the binding of leukocytes. *J. Cell Biol.* 121:655-664.
- Imai, Y., M. S. Singer, C. Fennie, L. A. Lasky, and S. D. Rosen. 1991. Identification of a carbohydrate-based endothelial ligand for a lymphocyte homing receptor. *J. Cell Biol.* 113:1213-1221.
- Kupper, T. S. 1995. Immunity and inflammation in cutaneous tissues. In *Santers Immunologic Disease*. Vol. 1. M. Frank, K. F. Austen, H. Claman, and E. Unanue, editors. Little Brown and Co., Boston, MA. 353-362.
- Larsen, G. R., D. Sako, T. J. Ahern, M. Shaffer, J. Erban, S. A. Sajer, R. M. Gibson, D. D. Wagner, B. C. Furie, and B. Furie. 1992. P-selectin and E-selectin. Distinct but overlapping leukocyte ligand specificities. *J. Biol. Chem.* 267:11104-11110.
- Lasky, L. A. 1992. Selectins: interpreters of cell-specific carbohydrate information during inflammation. *Science (Wash. DC)*. 258:964-969.
- Lasky, L. A., M. S. Singer, D. Dowbenko, Y. Imai, W. J. Henzel, C. Grimley, C. Fennie, N. Gillett, S. R. Watson, and S. D. Rosen. 1992. An endothelial ligand for L-selectin is a novel mucin-like molecule. *Cell*. 69:927-938.
- Lawrence, M. B., and T. A. Springer. 1991. Leukocytes roll on a selectin at physiologic flow rates: distinction from and prerequisite for adhesion through integrins. *Cell*. 65:859-873.
- Lawrence, M. B., and T. A. Springer. 1993. Neutrophils roll on E-selectin. *J. Immunol.* 151:6338-6346.
- Levinovitz, A., J. Muhlhoff, S. Isenmann, and D. Vestweber. 1993. Identification of a glycoprotein ligand for E-selectin on mouse myeloid cells. *J. Cell Biol.* 121:449-459.
- Ley, K., P. Gaetgens, C. Fennie, M. S. Singer, L. A. Lasky, and S. D. Rosen. 1991. Lectin-like cell adhesion molecule 1 mediates leukocyte rolling in mesenteric venules in vivo. *Blood*. 77:2553-2555.
- Lobb, R. R., G. Chi-Rosso, D. R. Leone, M. D. Rosa, S. Bixler, B. M. Newman, S. Lohowskyj, C. D. Benjamin, I. G. Douglas, and S. E. Geolts. 1991. Expression and functional characterization of a soluble form of endothelial-leukocyte adhesion molecule 1. *J. Immunol.* 147:124-129.
- Lowe, J. B., L. M. Stoolman, R. P. Nair, R. D. Larsen, T. L. Berhand, and R. M. Marks. 1990. ELAM-1-dependent cell adhesion to vascular endothelium determined by a transfected human fucosyltransferase cDNA. *Cell*. 63:475-484.
- Mayadas, T. N., R. C. Johnson, H. Rayburn, R. O. Hynes, and D. D. Wagner. 1993. Leukocyte rolling and extravasation are severely compromised in P-selectin-deficient mice. *Cell*. 74:541-554.
- Moore, K. L., N. L. Stults, S. Diaz, D. F. Smith, R. D. Cummings, A. Varki, and R. P. McEver. 1992. Identification of a specific glycoprotein ligand for P-selectin (CD62) on myeloid cells. *J. Cell Biol.* 118:445-456.
- Moore, K. L., and L. F. Thompson. 1992. P-selectin (CD62) binds to subpopulations of human memory T lymphocytes and natural killer cells. *Biochem. Biophys. Res. Commun.* 186:173-181.
- Mulligan, M. S., J. C. Paulson, S. De Frees, Z. L. Zheng, J. B. Lowe, and P. A. Ward. 1993. Protective effects of oligosaccharides in P-selectin-dependent lung injury. *Nature (Lond.)*. 364:149-151.
- Munro, J. M., S. K. Lo, C. Corless, M. J. Robertson, N. C. Lee, R. L. Barnhill, D. S. Weinberg, and M. P. Bevilacqua. 1992. Expression of sialyl-Lewis x, an E-selectin ligand, in inflammation, immune processes, and lymphoid tissues. *Am. J. Pathol.* 141:1397-1408.
- Norgard, K. E., K. L. Moore, S. Diaz, N. L. Stults, S. Ushiyama, R. P. McEver, R. D. Cummings, and A. Varki. 1993. Characterization of a specific ligand for P-selectin on myeloid cells. A minor glycoprotein with sialylated O-linked oligosaccharides. *J. Biol. Chem.* 268:12764-12774.
- Picker, L. J., S. A. Michie, L. S. Roti, and E. C. Butcher. 1990. A unique phenotype of skin-associated lymphocytes in humans. Preferential expression of the HECA-452 epitope by benign and malignant T cells at cutaneous sites. *Am. J. Pathol.* 136:1053-1068.
- Picker, L. J., R. A. Warnock, A. R. Burns, C. M. Doerschuk, E. L. Berg, and E. C. Butcher. 1991. The neutrophil selectin LECAM-1 presents carbohydrate ligands to the vascular selectins ELAM-1 and GMP-140. *Cell*. 66:921-933.
- Picker, L. J., J. R. Treer, B. Ferguson-Darnell, P. A. Collins, P. R. Bergstresser, and L. W. Terstappen. 1993. Control of lymphocyte recirculation in man. II. Differential regulation of the cutaneous lymphocyte-associated antigen, a tissue-selective homing receptor for skin-homing T cells. *J. Immunol.* 150:1122-1136.
- Picker, L. J., R. J. Martin, A. Trumble, L. S. Newman, P. A. Collins, P. R. Bergstresser, and D. Y. Leung. 1994. Differential expression of lymphocyte homing receptors by human memory/effector T cells in pulmonary versus cutaneous immune effector sites. *Eur. J. Immunol.* 24:1269-1277.
- Polley, M. J., M. L. Phillips, E. Wayner, E. Nudelmann, A. K. Singhal, S. Hakomori, and J. C. Paulson. 1991. CD62 and endothelial cell leukocyte adhesion molecule 1 (ELAM-1) recognize the same carbohydrate ligand, sialyl-Lewis x. *Proc. Natl. Acad. Sci. USA*. 88:6224-6228.
- Rosen, S. D. 1993. Cell surface lectins in the immune system. *Semin. Immunol.* 5:237-247.
- Rossiter, H., F. C. van Reijssen, F. S. Kalthoff, G. C. Mudde, C. A. Bruijnzeel-Koomen, L. J. Picker, and T. S. Kupper. 1994. Skin disease-related T cells bind to endothelial selectins: expression of cutaneous lymphocyte antigen (CLA) predicts E-selectin but not P-selectin binding. *Eur. J. Immunol.* 24:205-210.
- Sako, D., X. J. Chang, K. M. Barone, G. Vachino, H. M. White, G. Shaw, G. M. Veldman, K. M. Bean, T. J. Ahern, and B. Furie. 1993. Expression cloning of a functional glycoprotein ligand for P-selectin. *Cell*. 75:1179-1186.
- Shimizu, Y., W. Newman, Y. Tanaka, and S. Shaw. 1992. Lymphocyte interactions with endothelial cells. *Immunol. Today*. 13:106-112.
- Springer, T. A. 1994. Traffic signals for lymphocyte recirculation and leukocyte emigration: the multistep paradigm. *Cell*. 76:301-314.
- Steininger, C. N., C. A. Eddy, R. M. Leimgruber, A. Mellors, and J. K. Welby. 1992. The glycoproteinase of *Pasteurella haemolytica* A1 eliminates binding of myeloid cells to P-selectin but not the E-selectin. *Biochem. Biophys.*

- Res. Comm.* 188:760-766.
- Sutherland, D. R., K. M. Abdullah, P. Cyopick, and A. Mellors. 1992. Cleavage of the cell-surface O-sialoglycoproteins CD34, CD43, CD44, and CD45 by a novel glycoprotease from *Pasteurella haemolytica*. *J. Immunol.* 148:1458-1464.
- Tanaka, Y., D. H. Adams, S. Hubscher, H. Hirano, U. Siebenlist, and S. Shaw. 1993. T-cell adhesion induced by proteoglycan-immobilized cytokine MIP-1 beta. *Nature (Lond.)*. 361:79-82.
- Taub, D. D., K. Conlon, A. R. Lloyd, J. J. Oppenheim, and D. J. Kelvin. 1993. Preferential migration of activated CD4+ and CD8+ T cells in response to MIP-1 alpha and MIP-1 beta. *Science (Wash. DC)*. 260:355-358.
- van Reijssen, F. C., C. A. Bruinzeel-Koomen, F. S. Kalthoff, E. Maggi, S. Romagnani, J. K. Westland, and G. C. Mudde. 1992. Skin-derived aeroallergen-specific T-cell clones of Th2 phenotype in patients with atopic dermatitis. *J. Allergy Clin. Immunol.* 90:184-193.
- von Andrian, U. H., J. D. Chambers, E. L. Berg, S. A. Michie, D. A. Brown, D. Karolak, L. Ramezani, E. M. Berger, K. E. Arfors, and E. C. Butcher. 1993. L-selectin mediates neutrophil rolling in inflamed venules through sialyl LewisX-dependent and -independent recognition pathways. *Blood*. 82:182-191.
- von Andrian, U. H., J. D. Chambers, L. M. McEvoy, R. F. Bargatze, K. E. Arfors, and E. C. Butcher. 1991. Two-step model of leukocyte-endothelial cell interaction in inflammation: distinct roles for LECAM-1 and the leukocyte beta 2 integrins in vivo. *Proc. Natl. Acad. Sci. USA*. 88:7538-7542.
- Weller, A., S. Isenmann, and D. Vestweber. 1992. Cloning of the mouse endothelial selectins. Expression of both E- and P-selectin is inducible by tumor necrosis factor alpha. *J. Biol. Chem.* 267:15176-15183.
- Zettlmeissl, G., J. P. Gregersen, J. M. Duport, S. Mehdli, G. Reiner, and B. Seed. 1990. Expression and characterization of human CD4: immunoglobulin fusion proteins. *DNA Cell Biol.* 9:347-353.
- Zhang, J., H. L. Weiner, and D. A. Hafler. 1992. Autoreactive T cells in multiple sclerosis. *Int. Rev. Immunol.* 9:183-201.

REVIEW ARTICLE

Leukocyte-Endothelial Adhesion Molecules

By Timothy M. Carlos and John M. Harlan

IN 1985, a review article appeared in this journal that examined the interactions of leukocytes with vascular endothelium during an immune or inflammatory response.¹ The basic physiology of leukocyte emigration as well as disease states in which alterations of leukocyte-endothelial interactions may contribute to pathology were discussed. Since then there has been an explosion of interest in this topic. This explosion has been fueled by remarkable advances in the elucidation of the molecular basis of leukocyte adherence to endothelium and the potential for new therapies directed at these adhesion molecules.²

Before 1985 only a single protein involved in leukocyte adherence to endothelium had clearly been identified immunologically—the murine lymphocyte homing receptor gp^{90-Mel}.³ In the subsequent years nine endothelial and nine leukocyte surface proteins involved in this heterotypic adhesion have been molecularly cloned (Fig 1, A and B). In addition, several other distinct leukocyte and endothelial molecules have been identified functionally or immunologically (Fig 1C).

In this review, we focus on the expression, regulation, and function of the endothelial proteins known to be involved in the adhesion of leukocytes. We also consider the leukocyte counter-receptors for these proteins, and examine the current model of the sequential steps involved in leukocyte emigration to sites of inflammation. Finally, the use of “anti-adhesion” therapy in animal models of several diseases is reviewed.

To provide a detailed review we have focused solely on the role of these adhesion proteins in leukocyte-endothelial interactions. We do not address the many additional functions subserved by these molecules such as binding of parasites (eg, malaria^{4,5}), viruses (eg, rhinovirus^{6,7}), tumor cells,⁸ and hematopoietic precursors,⁹⁻¹² or their participation in signal transduction.¹³⁻¹⁵

Finally, although we have attempted to be comprehensive with respect to several aspects of leukocyte-endothelial adhesive interactions, we have undoubtedly overlooked some important contributions in these areas, and we apologize for these oversights. The interested reader may wish to consider other recent reviews on this topic,¹⁶⁻²³ particularly those relating to altered expression of adhesion molecules in human

disease^{24,25} because this important aspect is not addressed in this review.

HOMING RECEPTORS AND VASCULAR ADDRESSINS

Lymphocytes recirculate between blood and lymphatics, gaining entrance into the latter at specialized endothelium on postcapillary venules in lymphoid tissue.²⁶ These high endothelial venules (HEVs) express specific surface proteins that have been designated as vascular addressins. Vascular addressins selectively bind subsets of circulating lymphocytes that express complementary (homing) receptors.^{17,27}

The specificity of this interaction has been shown in vitro with binding studies examining lymphocyte or leukemic cell line adhesion to HEV in frozen sections of lymphoid tissue.²⁸ Currently, four vascular addressins have been identified functionally: peripheral lymph node (PNAd),²⁹ mucosal lymph node (ie, Peyer's patches or appendix) (MAd),³⁰ synovium,³¹ and skin.³² Peripheral node addressins include GlyCAM-1 and CD34 (see “Counter-structures for selectins”); an MAd is designated MAdCAM-1 (see “Endothelial Immunoglobulin-like Proteins”). The complementary leukocyte homing receptors for these vascular addressins are L-selectin for GlyCAM-1, CD34, and MAdCAM-1 (see “Selectins”) and $\alpha_4\beta_1$ for MAdCAM-1 (see “Leukocyte Integrins”).

The tissue distribution and function of some of these vascular addressins have been characterized by monoclonal antibodies (MoAbs). The MoAb MECA-79 identifies 50-kD and 90-kD sulfated glycoproteins expressed by HEV in murine and human peripheral lymph nodes and blocks lymphocyte binding to peripheral, but not mucosal, lymph nodes in vitro and in vivo.²⁹ MoAb MECA-79 also reacts with venules at cutaneous sites of chronic, but not acute, inflammation in humans, suggesting that PNAd is expressed in other, non-HEV sites.²⁷ The MoAb MECA-367 identifies the MAd expressed by HEV in mucosa-associated lymphoid tissues.³⁰ MoAb MECA-367 immunoprecipitates an ~60-65-kD protein from labeled mesenteric lymph node stroma and inhibits lymphocyte homing to mucosal, but not peripheral, lymph nodes in vitro and in vivo.³⁰

MoAbs directed against the lymphocyte homing receptors for PNAd and MAd have also been shown to inhibit binding of lymphoid cells to HEV. Antibodies that react with L-selectin prevent the binding of lymphocytes to PNAd,³³ whereas MoAbs directed against an integrin (LPAM-1, $\alpha_4\beta_1$) inhibit the adhesion of lymphocytes to MAd.^{34,35}

SELECTINS

The selectin family is comprised of three proteins designated by the prefixes E (endothelial), P (platelet), and L (leukocyte).^{36,37} E-selectin (CD62E) and P-selectin (CD62P) are expressed by endothelial cells, and L-selectin (CD62L) is expressed only on leukocytes (Fig 1A). Structural features common to the selectins are the presence of an NH₂-terminal C-type (Ca²⁺-dependent) lectinlike binding domain, an epi-

From the Department of Medicine (Hematology/BMT), University of Pittsburgh Medical Center, Pittsburgh, PA; and the Department of Medicine (Hematology), University of Washington, Seattle.

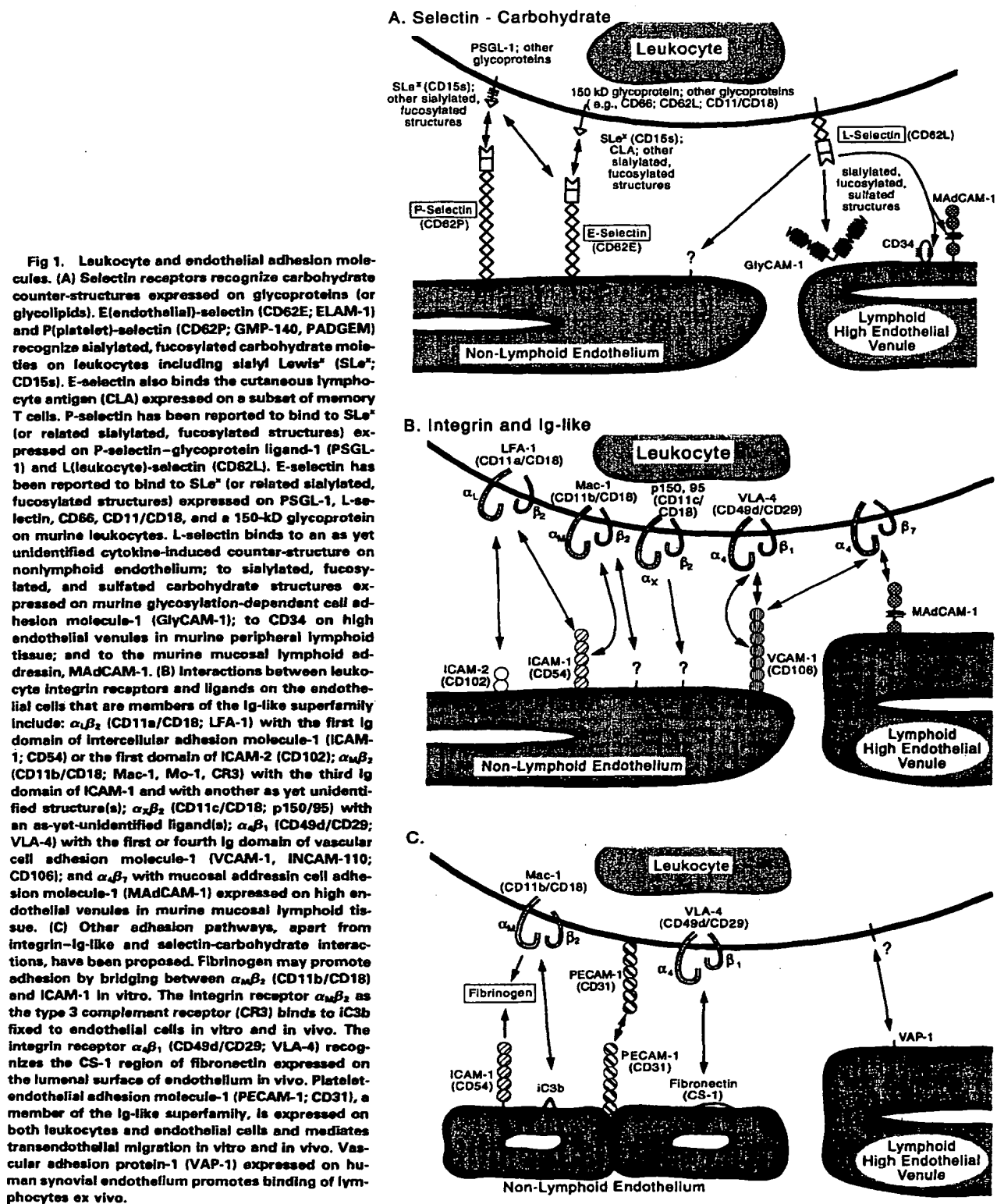
Submitted November 9, 1993; accepted June 20, 1994.

Supported in part by US Public Health Service Grants No. HL18645, HL30542, and HL47151. T.M.C. is the recipient of a Clinician-Scientist Award of the American Heart Association.

Address reprint requests to Timothy M. Carlos, MD, N811 MUH, Division of Hematology/BMT, University of Pittsburgh Medical Center, 200 Lothrop St, Pittsburgh, PA 15213-2582.

© 1994 by The American Society of Hematology.

0006-4971/94/8407-0038\$3.00/0



dermal growth factor (EGF)-like region, a variable number of consensus repeats of sequences similar to those appearing in complement-regulatory proteins, a membrane-spanning region, and a short cytoplasmic region.³⁶ The selectins share an overall identity of 40% to 60% at the nucleotide and protein levels whereas the lectin and EGF domains are 60% to 70% homologous.³⁷ The genes for the selectin family are closely linked on chromosome 1 (q21-24).^{38,39} Genes for other complement-binding proteins (C4 binding protein and decay accelerating factor) and factor V are also located in this region in both humans and mice, suggesting that the selectin family may have arisen by gene duplication.³⁸

E-selectin

E-selectin (CD62E) was initially described as a 115-kD antigen that was induced on cultured human umbilical vein endothelium after stimulation by interleukin-1 (IL-1) and that was involved in the adhesion of neutrophils and several leukemic cell lines.⁴⁰ The subsequent molecular cloning of E-selectin showed the C-type lectinlike binding domain, the EGF-like domain, and six complement-regulatory protein regions.⁴¹⁻⁴³ Translation of E-selectin yields a core protein of 64 kD with 11 potential N-glycosylation sites. The 32-amino acid cytoplasmic domain contains tyrosine residues that have been suggested to mediate the internalization of other transmembrane proteins,⁴⁴ and may account for the short half-life of E-selectin at the cell surface.⁴⁵ Murine^{46,47} and rabbit⁴⁸ E-selectin have been molecularly cloned, and show a high degree (>70%) of homology with human E-selectin.

Mapping of E-selectin domains by MoAbs has shown that the NH₂-terminal nine amino acids of the lectin domain and an epitope within the EGF-like region are important for ligand binding.^{49,50} Computer modeling and generation of site-specific mutants of the lectin domain of human E-selectin showed that three positively charged amino acids (arginine 97, lysine 111, and lysine 113) are critical for ligand binding.⁵⁰ Lysines in positions 111 and 113 have been conserved in all selectins.⁵¹ Additional evidence indicates that a region within the consensus repeats of E- and L-selectin may also be important in ligand binding.⁵²

P-selectin

P-selectin (CD62P) is an adhesion protein that was initially characterized in platelets where it was termed PADGEM (platelet activation-dependent granule-external membrane protein)⁵³ or GMP-140 (granule membrane protein-140).⁵⁴ Subsequently, P-selectin was shown to be present also in endothelial cells.^{55,56} In both cell types P-selectin is synthesized and stored in cytoplasmic granules; in platelets P-selectin is contained in α -granules,^{57,58} whereas in endothelial cells it is found in Weibel-Palade bodies.^{55,56} With appropriate activation P-selectin is mobilized to the external plasma membrane.

The cloning of P-selectin showed an organization of domains common to selectins, but with nine consensus repeats of the complement-regulatory protein regions.⁵⁹ The core protein has a predicted molecular weight of 86 kD. There

are 12 potential N-linked glycosylation sites which, if fully used, would yield a protein of 122 kD. Prior characterization of P-selectin has shown that there are no O-linked sugars in the mature protein.⁶⁰ There are 65 cysteine residues (8% of the total amino acid content) that are involved in organizing disulfide bridges. A 35-residue cytoplasmic tail contains serine, tyrosine, and threonine residues as sites of phosphorylation.^{61,62}

Two variant forms of P-selectin that arise by alternative splicing of mRNA have been described.⁶³ In one variant there is deletion of the seventh consensus repeat, whereas in the other variant the transmembrane region is deleted. Hydrophobicity plots of the latter suggest that this variant would be a soluble protein. Consistent with this possibility, soluble P-selectin has been detected in the plasma of normal individuals (0.15 to 0.30 $\mu\text{g/mL}$). However, it has not been shown that this is the secreted form rather than protein shed from platelets or endothelial cells. At this concentration in plasma, 20% to 40% of the binding sites for P-selectin on neutrophils would be saturated, raising the possibility that soluble plasma P-selectin may modulate leukocyte adhesion to P-selectin expressed on endothelium.^{25,64}

Murine^{47,65} and bovine⁶⁶ P-selectin have been cloned. There is greater than 80% homology between these species and human P-selectin lectin, EGF, transmembrane, and cytoplasmic domains. Murine P-selectin contains eight whereas bovine P-selectin contains six consensus repeats that are ~70% homologous to human P-selectin.

Computer modeling and generation of site-specific mutants of the lectin domain of human P-selectin have indicated that two residues (tyrosine 48 and lysine 111) are critical for ligand binding.^{67,68} Two other amino acids (tyrosine 94⁶⁸ and lysine 113⁶⁷) may also be important for function.

L-selectin

Although both E- and P-selectin are expressed by endothelial cells, L-selectin (CD62L) is found only on leukocytes. L-selectin is the human homologue of the murine peripheral lymph node homing receptor that was originally identified by the MoAb MEL-14.³ Although originally described as a lymphocyte homing receptor, it was subsequently shown to be expressed on most other peripheral blood leukocytes, and is involved in leukocyte traffic in the systemic microcirculation.⁶⁹

The cloning of human L-selectin demonstrated that it shares the organization of extracellular domains found in P- and E-selectins.⁷⁰⁻⁷³ L-selectin has two consensus repeats of the complement-regulatory protein domains. The sequence of human L-selectin encodes a core protein of 37 kD that has eight possible sites for N-linked glycosylation. There are no serine- or threonine-rich regions, which agrees with the lack of O-linked sugars.⁷² The molecular weight of L-selectin differs among lymphocytes (~75 kD), neutrophils (~95 to 105 kD), and monocytes (~110 kD). This variability is thought to result from differences in posttranslational glycosylation among these subsets of leukocytes. L-selectin has 22 cysteine residues, 19 of which are in the consensus repeat and EGF domains, suggesting a role for disulfide bond for-

mation in providing proper spatial conformation for the lectin region that is the proposed site of ligand binding.

Murine,^{74,75} rat,⁷⁶ and bovine⁷⁷ L-selectins have also been molecularly cloned. There is approximately 80% homology between human L-selectin and these other species with the highest degree of conservation in the lectin, EGF, transmembrane, and cytoplasmic regions.

Mapping of L-selectin domains by MoAbs has determined that the NH₂-terminal nine amino acids are critical for ligand binding.^{78,79} Maintenance of spatial conformation by the EGF and consensus repeat units of L-selectin is also important for ligand binding because MoAbs that interact with these domains affected binding in the lectin domain.^{52,80,81}

One group has reported that two forms of human L-selectin are generated by alternative splicing.⁷¹ One form retains a transmembrane region, whereas a second form is attached to the cellular membrane by a phosphatidylinositol linkage.

There is abundant evidence that L-selectin is shed with activation of leukocytes⁸²⁻⁸⁵ with the loss of L-selectin because of proteolytic cleavage near the membrane insertion.^{82,85} Soluble circulating L-selectin was measured in the plasma of normal individuals (normal plasma level = 1.6 $\mu\text{g/mL}$), and this concentration of soluble L-selectin was able to partially inhibit leukocyte adhesion to cytokine-stimulated endothelium.⁸⁶ Thus, circulating L-selectin, like soluble circulating P-selectin, may modulate leukocyte adhesion to endothelium during inflammation.²⁵

COUNTER-STRUCTURES FOR SELECTINS

As noted previously, L-selectin was initially characterized as the murine homing receptor that mediated lymphocyte binding to HEV in peripheral lymph nodes.³ Using the Stamper-Woodruff assay of leukocyte binding to HEVs of frozen sections of lymphoid tissue, it was shown that lymphocyte binding was observed at 4°C, was sensitive to sialidase treatment of the HEV, and was inhibited by phosphorylated oligosaccharides.⁸⁷ These characteristics suggested that the counter-structure in HEV recognized by this homing receptor was a carbohydrate moiety.⁸⁷ This proposal was validated by the molecular cloning of L-selectin that showed an NH₂-terminal C-type lectin domain.⁷⁰⁻⁷⁷ The presence of lectinlike domains in E- and P-selectin suggested that leukocyte binding to these receptors would also involve recognition of carbohydrates. In the past several years multiple studies have examined the characteristics of carbohydrate ligands for the three selectin receptors. Additionally, several proteins have been shown to participate in selectin binding (Fig 1A).

Carbohydrate Ligands

The carbohydrate determinants recognized by the selectins have recently been reviewed in detail^{36,37,88} and will be considered here only briefly.

E-selectin. In 1990 and 1991 several groups identified the fucosylated tetrasaccharide, sialyl Lewis X (SLe^x: NeuAc, α 2,3Gal β 1,4(Fuc α 1,3)GlcNAc) (CD15s) or closely related structures, as a ligand for E-selectin.⁸⁹⁻⁹³ Both the sialic acid and the fucose linkages were shown to be critical for efficient binding.⁹⁴⁻⁹⁶ Sialyl Lewis X and other fucosylated lactos-

amines are heavily expressed on neutrophils and monocytes^{91,97} and are also found on natural killer (NK) cells.^{98,99} Peripheral blood T and B lymphocytes do not normally express SLe^x, but do when activated *ex vivo*.¹⁰⁰ A subset of skin-homing lymphocytes expresses the cutaneous lymphocyte antigen (CLA) recognized by the HECA-452 MoAb,^{101,102} and these cells bind to E-selectin.^{32,101} The CLA-positive cells do not express SLe^x, but exhibit the Lewis X antigen (Le^x) after treatment with neuraminidase.¹⁰¹ Thus, the CLA antigen appears to be a sialylated, fucosylated structure closely related to SLe^x.

E-selectin also recognizes an isomer of SLe^x, sialyl Lewis A (SLe^a: NeuNAc α 2,3Gal β 1,3(Fuc α 1,4)GlcNAc).^{94,95,102} The HECA 452 MoAb recognizing CLA binds to SLe^a as well as SLe^x.¹⁰² Because SLe^a is expressed on some tumor cells but is not usually found on leukocytes, this interaction is more relevant to tumor metastases than to leukocyte trafficking.³⁶

P-selectin. Initial studies showed that P-selectin recognized the Lewis X (Le^x) trisaccharide (CD15), Gal β 1,4(Fuc α 1,3)GlcNAc,¹⁰³ although subsequently the sialylated tetrasaccharide, SLe^x, was shown to be a higher affinity ligand.¹⁰⁴⁻¹⁰⁷ Like E-selectin, P-selectin also binds to SLe^x.¹⁰⁴ However, both SLe^x and SLe^a fail to compete for binding to activated platelets, suggesting that P-selectin may use other structural modifications.¹⁰⁴ In this regard, P-selectin was also demonstrated to bind to sulfated glycolipids^{104,108-110} and certain sulfated polysaccharides such as heparin.¹¹¹

The physiologic importance of fucose in carbohydrate ligands for E- and P-selectin was shown recently by studies in two patients with an inherited defect in neutrophil adhesion resulting from a generalized abnormality in fucose metabolism.¹¹² Because the patients exhibited neutrophilia and recurrent infections such as the classic leukocyte adhesion deficiency (LAD) syndrome,¹¹³ but had normal levels of β_2 integrins, the syndrome was designated LAD type II. In the initial report it was shown that neutrophils from both LAD type II patients did not express SLe^x and failed to bind to E-selectin or cytokine-activated endothelium. Subsequent studies showed that neutrophils from an LAD type II patient did not bind to recombinant E-selectin, to purified P-selectin, or to P-selectin expressed on histamine-activated human umbilical vein endothelial cells (M.L. Phillips, B. Schwartz, A. Etzioni, R. Bryer, H. Ochs, J.C. Paulson, J.M. Harlan, manuscript submitted). From these investigations it is clear that SLe^x or other fucose-containing carbohydrate structures are critical for neutrophil binding to E- and P-selectin. Consequently, selectin interactions with potential protein, sulfated glycolipid, or polysaccharide ligands alone are not sufficient for neutrophil adherence under static assay conditions.

L-selectin. L-selectin is involved in leukocyte adherence to nonlymphoid microvasculature as well as to PNA⁺ HEV.⁶⁹ Like E- and P-selectin, murine L-selectin has been shown to bind to SLe^x (and SLe^a).^{94,107,114} Although MoAbs to SLe^x react minimally with nonlymphoid endothelium *in vivo* or *in vitro*, an SLe^x antigen was recently found to be expressed on human HEV, suggesting that it may serve as a ligand for L-selectin.^{97,115} In the murine system, L-selectin ligands in HEV are sialylated and fucosylated like SLe^x, but are also sulfated.¹¹⁶

L-selectin and P-selectin (but not E-selectin) also recognize sulfatides^{104,108-111,116-118} and sulfated-polysaccharides such as fucoidan and heparin.^{104,111} Recently, heparinlike ligands for L-selectin were identified in cultured nonlymphoid endothelial cells, and these structures are candidates for L-selectin ligands in the systemic microvasculature.¹¹⁹

Protein Ligands

Although lectin-carbohydrate binding is critical to selectin-mediated adhesion, certain proteins may also participate in the adhesive interaction. Many lectin-carbohydrate interactions, probably including selectin binding to various ligands in vitro, are of low affinity.³⁶ Appropriate presentation of specific carbohydrate moieties to lectin domains by membrane protein components may contribute to higher affinity binding of selectins to cellular ligands.³⁷

E-selectin. Several leukocyte surface structures modified by SLe^x, Le^x, or related structures have been reported to bind to E-selectin, including L-selectin,^{120,121} CD66,¹²² and β_2 integrins.¹²³ Other studies have characterized the human myeloid ligand of E-selectin to be resistant to a variety of proteases¹²⁴ and to O-glycoprotease.^{125,126}

Using an E-selectin-IgG chimeric protein as a probe, a protein ligand with a molecular weight of 150 kD reduced and 130 kD nonreduced was recently identified on murine neutrophils and the HL60 leukemic cell line.^{127,128} E-selectin binding to this glycoprotein was calcium-dependent and sensitive to neuraminidase pretreatment of the cell lysate, characteristics of E-selectin-dependent leukocyte adhesion.¹²⁷ Interestingly, adhesion to E-selectin also was reduced by pretreatment of leukocytes with N-glycosidase, but not O-sialoglycosidase.¹²⁸

P-selectin. In contrast to E-selectin, P-selectin-dependent adhesion was shown to be abolished by pretreatment of human myeloid cells with various proteases.¹²⁴ Pretreatment of neutrophils with an O-glycoprotease that selectively removes proteins that are heavily glycosylated also inhibited neutrophil binding to P-selectin.^{125,126,129} Interestingly, the O-glycoprotease did not dramatically alter surface SLe^x expression. Furthermore, only a small portion of the SLe^x-positive material bound to a P-selectin affinity column.¹²⁹ These observations suggest that the high-affinity ligand for P-selectin is only a minor component of SLe^x-modified glycoproteins on the neutrophil surface.¹²⁹

These results strongly implicate a specific glycoprotein ligand for P-selectin. Neutrophil L-selectin-bearing SLe^x has been reported to bind to P-selectin as well as to E-selectin.¹²⁰ However, candidate high-affinity glycoprotein ligands for P-selectin, distinct from L-selectin, have been described.¹²⁸⁻¹³² Affinity purification of neutrophil membrane extracts with P-selectin showed a glycoprotein of molecular weight 240 kD nonreduced and 120 kD reduced, suggesting that it may be a disulfide-linked heterodimer. Binding of P-selectin to this glycoprotein was calcium-dependent, and was specifically inhibited by a blocking anti-P-selectin MoAb.¹³¹

One P-selectin ligand, a mucinlike protein designated P-selectin glycoprotein ligand (PSGL-1), was recently molecularly cloned.¹³² After cotransfection of both a specific fucosyltransferase and a cDNA library from HL60 cells, a 220-

kD glycoprotein was expressed in COS cells that conferred adhesion to P-selectin (and, interestingly, E-selectin as well) that was abolished by EDTA or by inhibitory selectin-specific MoAbs. Analysis of cell lysates by sodium dodecyl sulfate-polyacrylamide gel electrophoresis (SDS-PAGE) demonstrated that this protein migrated as a single band of 110 kD after reduction, suggesting that it is a disulfide-linked dimer. Whether PSGL-1 is the dimeric glycoprotein identified in earlier studies¹²⁹⁻¹³¹ awaits further studies.

Another P-selectin-specific leukocyte ligand was recently identified.¹²⁸ A glycoprotein (160 kD nonreduced, 80 kD reduced) was found on mouse neutrophils and HL60 cells that mediated adhesion to P-selectin but not E-selectin. This binding was sensitive to EDTA and sialidase pretreatment of leukocytes. Adhesion to P-selectin was abolished by preincubation of leukocyte with either N-glycosidase and O-sialoglycosidase. In contrast, the 150-kD E-selectin ligand was resistant to the latter enzyme.

Additional glycoprotein ligands (230 kD and 130 kD) were identified that mediate adhesion to both E- and P-selectin and that are sensitive to O-sialoglycosidase but not N-glycosidase.¹²⁸

L-selectin. Using an L-selectin-IgG chimeric protein to precipitate ³⁵S-labeled proteins from murine peripheral lymph node organ culture, two glycoproteins, a predominant one of 50 kD and a minor one of 90 kD, were identified.¹³³ Sequence data derived from the lower molecular weight sulfated glycoprotein (sgp⁵⁰) were used to develop probes to screen a murine lymph node cDNA library.¹³³ A cDNA was cloned predicting a mature protein of 132 amino acids with a core protein molecular weight of 14 kD. This protein was shown to contain 29% of its amino acids as either serine or threonine that are clustered in two regions in which ~50% of the core protein structure is composed of these amino acids. Because there is only one possible site for N-linked glycosylation and because the molecular weight of the mature protein is ~50 kD, 70% of the mass is apparently caused by O-linked glycosylation. The sequence of this L-selectin ligand is similar to other heavily glycosylated proteins such as CD34 and MUC-1,¹³⁴ and these sialomucins have been proposed as a new family of adhesion proteins¹³⁵ (vide infra). The regions of O-linked glycosylation are thought to provide a scaffold for the presentation of the polyvalent carbohydrates that have been demonstrated to be involved in ligand binding. Because of its dependence on glycosylation, the 50 kD L-selectin ligand was designated GlyCAM-1 (glycosylation-dependent cell adhesion molecule-1). Interestingly, the structure of GlyCAM-1 does not contain a transmembrane region; hence, the mechanism by which GlyCAM-1 attaches to the cell surface is unclear. Indeed, it may function primarily as a circulating soluble protein.¹³⁶

Recently, the cloning of rat GlyCAM-1 was reported.¹³⁷ The rat protein was highly homologous to murine GlyCAM-1 with ~70% of the residues being identical. Rat GlyCAM-1 contains the serine/threonine-rich clusters that are ~68% and ~48% homologous to the murine sequence.

Additional studies have identified sgp⁵⁰ as the sialomucin, CD34, that is expressed on hematopoietic progenitors and endothelium.¹³⁸ Partial amino acid sequencing of sgp⁵⁰

showed a protein core identical to murine CD34. Moreover, a rabbit polyclonal antibody to recombinant murine CD34 was shown to react with HEV of peripheral lymph nodes and with sgp⁹⁰ on analysis by immunoprecipitation. Thus, CD34 is a PNAd.

ENDOTHELIAL Ig-LIKE PROTEINS

The Ig gene superfamily consists of cell-surface proteins that are involved in antigen recognition (C1-type) or complement-binding or cellular adhesion (C2-type). Common features of C2-type proteins include a variable number of extracellular Ig-like domains with conserved cysteine sequences that form disulfide bonds to stabilize β -sheets of the tertiary structure.¹³⁹ Members of the C2-type Ig gene superfamily include CD2, CD58 (LFA-3), and CD56 (NCAM). Five members of this family expressed by endothelial cells are involved in leukocyte adhesion: intercellular adhesion molecule-1 (ICAM-1; CD54), ICAM-2 (CD102), vascular cell adhesion molecule-1 (VCAM-1; CD106), platelet-endothelial cell adhesion molecule-1 (PECAM-1; CD31), and the mucosal addressin (MAdCAM-1) (Fig 1B).

ICAM-1

Human ICAM-1 is a single-copy gene located on chromosome 19.¹⁴⁰ Molecular cloning showed that ICAM-1 has a core protein of 55 kD with five extracellular Ig-like domains.^{141,142} Amino acid substitutions in the extracellular domains have indicated that the primary binding site for leukocyte CD11a/CD18 (LFA-1) is located in the NH₂-terminal first domain of ICAM-1.¹⁴³ Initial electron microscopy of soluble ICAM-1 suggested a hinge between the second and third domains of the extracellular region¹⁴³; however, a recent report has shown that the hinge in ICAM-1 occurs between the third and fourth Ig-like domains.¹⁴⁴ The location of this hinge may be germane for leukocyte adhesion to endothelium, because a second ligand-binding site for a leukocyte integrin (CD11b/CD18, Mac-1) was localized to the third Ig-like domain.¹⁴⁵

Leukocyte adhesion to the second ligand-binding site of ICAM-1 also is affected by the degree of glycosylation of ICAM-1.¹⁴⁵ There are eight possible sites for N-linked glycosylation in the five Ig-like extracellular domains of ICAM-1. ICAM-1 is expressed on leukocytes, fibroblasts, epithelial cells, as well as endothelial cells. The molecular weights of ICAM-1 extracted from these tissues varied between 76 and 114 kD, suggesting that there is variable posttranslational modification of ICAM-1.¹⁴⁶⁻¹⁴⁸ Affinity of leukocytes for the binding site within the third Ig-like region of ICAM-1 was found to increase as the degree of glycosylation decreased.¹⁴⁵ This observation suggested that selectivity of leukocyte adhesion via CD11b/CD18 may be dictated in part by the posttranslational glycosylation of ICAM-1 at the tissue level.

The cytoplasmic domain of ICAM-1 consists of a 28-residue, highly charged sequence rich in lysine and arginine residues.^{141,142} The cytoplasmic domain, or an 8-amino acid portion of the cytoplasmic region of ICAM-1 (RQRKIKKR), has been shown to bind to the cytoskeleton of COS cells transfected with the cDNA of human ICAM-1 and to the

cytoskeleton of Epstein-Barr virus (EBV)-transformed B cells.¹⁴⁹ The binding of ICAM-1 to the cytoskeleton was found to occur through linkage with α -actinin, a cytoskeleton protein that may serve to anchor actin filaments to the cell membrane.¹⁵⁰ When expressed as a glycosylphosphatidylinositol-linked membrane protein ICAM-1 was expressed diffusely on the cell surface.¹⁴⁹ Therefore, linkage with the cytoskeleton may localize ICAM-1 within regions of the endothelial cell membrane to facilitate leukocyte adherence and transmigration.

Murine¹⁵¹ and rat¹⁵² ICAM-1 have been molecularly cloned, and both have five extracellular Ig-like domains like human ICAM-1. However, in comparison with human ICAM-1, there is limited homology at the nucleotide (mouse = 65%, rat = 56%) or at the protein levels (mouse = 50%, rat = 51%) among these species. However, a partial cDNA sequence of canine ICAM-1 prepared by polymerase chain reaction (PCR) amplification of conserved sequences in domains 2 through 5 of human and murine ICAM-1 was slightly more homologous to human ICAM-1 (nucleotide = 74%, protein = 61%).¹⁵³

Mice deficient in ICAM-1 have recently been produced by targeted-gene disruption, and studies in this model should provide important information on the specific contribution of this adhesion molecule to leukocyte recruitment during inflammatory and immune reactions.¹⁵⁴

ICAM-2

Intercellular adhesion molecule-2 is another member of the Ig gene superfamily that is expressed on endothelium and is involved in leukocyte adherence. Human ICAM-2 is a single-copy gene located on chromosome 17.¹⁵⁵ Molecular cloning of ICAM-2 showed a core protein of 29 kD with six residues for possible N-linked glycosylation which, if fully used, would yield a mature protein of 46 kD.¹⁵⁶ ICAM-2 has only two extracellular Ig-like domains. However, these domains are 34% homologous to the two NH₂-terminal Ig-like domains of ICAM-1.¹⁵⁶ The ligand-binding site for CD11a/CD18 (LFA-1) is located in these domains of ICAM-1; hence, ICAM-2 is a second endothelial ligand for this leukocyte integrin.¹⁵⁶ However, the observation that CD11b/CD18 (Mac-1) binds to the third Ig-like domain of ICAM-1¹⁴⁵ suggests that ICAM-2 does not serve as an endothelial ligand for this leukocyte integrin.

Murine ICAM-2 has been molecularly cloned and shares ~60% homology to human ICAM-2 at the protein level.¹⁵⁷ However, the transmembrane and cytoplasmic regions of murine ICAM-2 are more highly conserved (75% protein homology). In contrast to human ICAM-2, murine ICAM-2 has five potential residues for N-linked glycosylation.

VCAM-1

The third member of the Ig gene superfamily that serves as an endothelial adhesion molecule for leukocytes is VCAM-1. The initial molecular cloning of VCAM-1 reported six extracellular Ig-like domains (6D VCAM-1).¹⁵⁸ However, 6D VCAM-1 arises due to alternative splicing of a seven-domain form of VCAM-1 (7D VCAM-1) that is the dominant form

expressed by cultured human endothelial cells.¹⁵⁹⁻¹⁶¹ The VCAM-1 cDNA initially cloned lacked a domain (designated domain 4) that is homologous to the NH₂-terminal domain of VCAM-1.¹⁵⁸ Indeed, domains 1 through 3 are highly homologous to domains 4 through 6, suggesting that 7D VCAM-1 arose by gene duplication.^{160,161} The cloning of 7D VCAM-1 predicted a core protein of ~81 kD with seven potential sites of N-linked glycosylation in 7D VCAM-1 which, if fully used, would yield a mature protein of ~102 kD. This observation is in general agreement with immunoprecipitation studies that showed a surface protein of ~110 kD on cytokine-activated endothelium.^{162,163}

The additional domain in 7D VCAM-1 may have a functional role in leukocyte adhesion to endothelium. One ligand-binding site for leukocytes on both 6D and 7D VCAM-1 was shown to be located within the NH₂-terminal first domain.¹⁶⁴ Similar to the presence of two ligand-binding sites for leukocytes on ICAM-1 (CD11a/CD18/domain 1-2 and CD11b/CD18/domain 3), leukocytes have also been shown to bind to domain 4 of 7D VCAM-1.¹⁶⁵

Murine¹⁶⁶ and rat^{166,167} VCAM-1 have been molecularly cloned. In contrast to ICAM-1, VCAM-1 appears to have been highly conserved through evolution. Both rat and mouse VCAM-1 are highly homologous at the protein level to the 7D form of human VCAM-1 (77% and 76%, respectively).¹⁶⁶

A glycosylphosphatidylinositol-linked form of murine VCAM-1, generated by alternative splicing of VCAM-1 mRNA and able to support VLA-4-dependent leukocyte adhesion after cleavage by phosphatidylinositol-specific phospholipase C, has been reported.¹⁶⁸⁻¹⁷⁰ Whether alternative splicing of human VCAM-1 occurs remains to be determined.

MAdCAM-1

The most recent member of endothelial adhesion proteins in the Ig gene superfamily to be molecularly cloned is the mucosal addressin, MAdCAM-1.¹⁷¹ MAdCAM-1 was initially characterized by MoAb MECA-367 as a 58- to 66-kD antigen that was present on high endothelial venules in murine mucosal lymph nodes (eg, Peyer's patches) and that was involved in lymphocyte emigration.^{30,172} Monoclonal and polyclonal antibodies against murine mucosal addressin were used to screen a cDNA library prepared from a tumor necrosis factor α (TNF α)-stimulated murine endothelioma cell line.¹⁷¹ A novel protein was cloned that has structural homology to two other endothelial Ig-like proteins involved in leukocyte adhesion, ICAM-1 and VCAM-1. The NH₂-terminal Ig domain of MAdCAM-1 is 30% homologous to the first Ig domain of rat ICAM-1 and human VCAM-1, whereas the second Ig domain has an equal degree of homology to the fifth Ig domain of VCAM-1. However, there are two novel aspects of MAdCAM-1. First, the third Ig-like domain of MAdCAM-1 is 30% homologous with another Ig involved in mucosal immunity, the C α 2 constant region of the Ig loop of human IgA₁. Second, between the second and third Ig domains is a 37-amino acid region rich in serine and threonine. These two amino acids constitute 41% of the structure of this region and are possible sites for O-linked

glycosylation. A subset of MAdCAM-1 isolated from mesenteric lymph nodes was found to express the MECA-79 carbohydrate antigen and to support L-selectin-dependent rolling.^{35,173} Thus, MAdCAM-1 is unique in being able to bind both $\alpha_4\beta_1$ integrin and L-selectin.^{35,173}

PECAM-1

Recent reports have suggested that another member of the endothelial Ig-superfamily, PECAM-1 (CD31), may have a role in leukocyte adhesion and, particularly, in transmigration. CD31 is a widely distributed ~130 kD glycoprotein found on endothelial cells, platelets and some leukocytes.¹⁷⁴⁻¹⁷⁷ CD31 is constitutively expressed on endothelial cells, and surface expression of CD31 is not increased by treatment with TNF α , IL-1, or the combination of TNF α and interferon γ (IFN γ).¹⁷⁴ Greater than 95% of monocytes and neutrophils, but only ~50% of peripheral blood lymphocytes, express CD31.^{174,176} Among T lymphocyte subsets 100% of naive and 50% of memory CD8⁺ T lymphocytes are CD31⁺, but only 20% of CD4⁺ T cells and few memory CD4⁺ lymphocytes express CD31⁺.¹⁷⁸

The cloning of CD31 showed six, C2-like extracellular Ig-like domains.¹⁷⁵⁻¹⁷⁷ The core protein has a molecular weight of ~80 kD with nine possible residues for N-linked glycosylation.¹⁷⁵⁻¹⁷⁷ With a molecular weight of ~130 kD for the mature protein, glycosylation may account for 40% of the mass of CD31.¹⁷⁵

Several observations suggested that CD31 might be involved in leukocyte adhesion. The molecular structure of CD31 is homologous to both carcinoembryonic antigen and ICAM-1, proteins that have been shown to be involved in homotypic and heterotypic cell adhesion, respectively.^{145,146,179} In contrast to ICAM-1 that is expressed over the entire surface of resting endothelial cells, CD31 was found to be localized at intercellular junctions.^{174,177} CD31 was shown to play a key role in homotypic adhesion of endothelial cells¹⁷⁷ as well as in the binding of platelets to myeloid cells.¹⁸⁰

Because of the molecular similarity to Fc γ R, a role for CD31 in leukocyte activation was proposed.¹⁷⁶ The binding of a CD31 MoAb increased CD8⁺ T-cell adhesion to fibronectin and VCAM-1, but not fibrinogen or collagen, consistent with activation of integrins containing α_4 subunits (eg, $\alpha_4\beta_1$ or $\alpha_4\beta_7$).¹⁷⁸ The binding of CD31 MoAbs to monocytes (but not neutrophils) induced a respiratory burst.¹⁷⁶ Thus, in addition to a role for CD31 in adhesion, binding to CD31 may also transduce activating signals to leukocytes.

Finally, treatment of leukocytes or endothelial cells with either soluble CD31 or blocking CD31 MoAbs was recently shown to prevent monocyte or neutrophil¹⁸¹ but not lymphocyte¹⁸² transmigration in vitro (see "Transmigration"). Treatment of either the leukocytes or the endothelium separately was effective, suggesting that a homophilic adhesive interaction, ie, leukocyte CD31 binding to endothelial CD31, was involved in neutrophil and monocyte transmigration.¹⁸¹ Similarly, in vivo administration of blocking CD31 polyclonal antibodies prevented the recruitment of neutrophils during acute peritoneal inflammation or skin allograft rejection.¹⁸³

LEUKOCYTE INTEGRINS

Integrins are transmembrane cell surface proteins that bind to cytoskeletal proteins and communicate extracellular signals.¹⁴ Each integrin consists of a noncovalently linked, heterodimeric α and β chains. To date, 8 known β chain subunits and 12 of 15 reported α subunits have been molecularly cloned.^{14,184} Integrins have been arranged in subfamilies according to the β subunits and each β subunit may have from one to eight different α subunits associated with it. However, in recent years it has also become apparent that individual α subunits may be associated with several different β subunits (eg, the α_v chain of the classic vitronectin receptor ($\alpha_v\beta_3$) can also associate with β_1 , β_3 , β_6 , and β_8 chains with changes in its ligand-binding capability.¹⁴ Thus, as many as 21 different integrin combinations have been reported.¹⁸⁴

Integrin α chains have several common structural characteristics.¹⁸⁵ First, there are ~ 7 tandem repeats of ~ 60 amino acids that share homology with EF-hand structures of the calcium-binding proteins calmodulin and troponin. Three or four of these regions are thought to contribute to a divalent cation-binding domain. However, divalent cation specificity differs among the various α chains with $\alpha_1\beta_2$ (CD11a/CD18) and $\alpha_2\beta_1$ (very late activation antigen-2 [VLA-2]) requiring magnesium, whereas calcium is necessary for $\alpha_5\beta_1$ (VLA-5) function.¹⁸⁶ Second, a region of ~ 180 amino acids similar to domains found in cartilage matrix protein, von Willebrand factor, and complement factor B is inserted between the divalent cation binding tandem repeats in several integrins ($\alpha_1\beta_1$ and $\alpha_2\beta_1$ (VLA-1 and -2, respectively) and $\alpha_1\beta_2$, $\alpha_M\beta_2$, and $\alpha_X\beta_2$ (CD11a or LFA-1, CD11b or Mac-1 and CD11c or p150,95, respectively). There are few cysteine-rich regions or sites for N-linked glycosylation in this area, suggesting that it may be important for ligand binding.¹⁸⁷ Several MoAbs that inhibited or activated β_2 leukocyte integrin function were shown to bind to this I (inserted) domain of their respective α chains.^{188,189} Recently, a novel, divalent cation-binding site that is required for metal-dependent ligand binding was identified within the A (I) domain of CD11b.¹⁹⁰ Third, several α chains ($\alpha_3\beta_1$, $\alpha_5\beta_1$, $\alpha_6\beta_1$ (VLA-3, -5, and -6 respectively), $\alpha_{IIb}\beta_3$, and $\alpha_v\beta_3$) have a site in the extracellular region near the membrane insertion domain that is proteolytically cleaved yet remains attached to the α chain by disulfide linkage.¹⁹¹ The cytoplasmic domains of several α chains are constitutively phosphorylated.¹⁸⁴ A conserved sequence—KXGFFKR—in the cytoplasmic domain of the α -subunits has been shown to bind to calreticulin¹⁹² and to be critical for the modulation of integrin avidity.¹⁹³

Integrin β chains also have characteristic features. Tandem repeats of four cysteine-rich regions that are thought to be essential for tertiary structure are conserved among the various β chains. Approximately 100 amino acids from the NH₂-terminus are additional conserved units that are critical for maintenance of the α/β heterodimer. Disruption by point mutations in either of these regions leads to absence of expression of the β_2 leukocyte integrins (leukocyte adhesion deficiency type I).¹⁹⁴ The cytoplasmic domain of the β -subunit, in concert with the α -subunit, is also necessary for avidity modulation.

Within the integrin family of adhesion receptors only five members have so far been shown to be involved in leukocyte adhesion to endothelium: the β_2 leukocyte integrins (CD11a/CD18, CD11b/CD18 and CD11c/CD18),¹⁹⁴ the β_1 integrin VLA-4 ($\alpha_4\beta_1$, CD49d/CD29),¹⁹⁵ and $\alpha_4\beta_7$ ³⁵ (Fig 1B).

 β_2 Integrins

The β_2 leukocyte integrins share a common β chain (CD18) that has the typical structure described above.¹⁹⁴ Three α subunits are noncovalently associated with CD18: CD11a (lymphocyte function-associated-1 or LFA-1), CD11b (Mac-1, Mo-1) and CD11c (p150,95). The CD11 subunits contain an I domain but are not proteolytically cleaved. The expression of the β_2 integrins is restricted to leukocytes, but among subtypes of leukocytes the distribution of CD11/CD18 differs. Peripheral blood lymphocytes express primarily CD11a/CD18 whereas neutrophils, monocytes, and NK cells express all three β_2 integrins.^{185,194} Intracellular storage pools of CD11b/CD18 and CD11c/CD18 are present in neutrophils and monocytes whereas there is no storage pool of CD11a/CD18. Surface expression of CD11b/CD18 and CD11c/CD18 is increased by a variety of agonists: calcium ionophore, phorbol esters, FMLP, GM-CSF, C5a, TNF- α , and LTB₄.¹⁹⁶ Increased expression of CD11b/CD18 also has been noted after neutrophil adhesion to E-selectin.¹⁹⁷

Ligands for the β_2 leukocyte integrins include proteins expressed by cells (ICAM-1 for CD11a/CD18, CD11b/CD18; ICAM-2 for CD11a/CD18; and ICAM-3 for CD11a/CD18¹⁹⁸) as well as soluble proteins (fibrinogen and factor X for CD11b/CD18 and complement fragments for CD11b/CD18 and CD11c/CD18).^{185,194} Neutrophil and monocyte adhesion to endothelium relies primarily on the CD11a/CD18 and CD11b/CD18 leukocyte integrins with only a minor role for CD11c/CD18.¹⁹⁹⁻²⁰⁵ Lymphocyte adhesion involves the interaction of CD11a/CD18 with the endothelial ligands ICAM-1 and ICAM-2.^{206,207}

The significance of the β_2 leukocyte integrins has been demonstrated by the LAD Type I syndrome.^{113,185} In this autosomal recessive disorder there is partial or total absence of expression of the β_2 leukocyte integrins on all leukocytes leading to a defect in the recruitment of neutrophils to sites of inflammation.²⁰⁸ Although neutrophils are absent in inflamed tissues, other leukocytes (mononuclear leukocytes and eosinophils) are able to emigrate to sites of inflammation,^{113,185} presumably via VLA-4.²⁰⁹ Absent or deficient β_2 integrin expression results from heterogeneous mutations in the β subunit that impairs synthesis or prevents association with the α chain.^{185,194} A CD18-mutant mouse with 2% to 16% normal CD18 expression was recently produced by gene targeting,²¹⁰ thus providing a model of partial deficiency for the study of inflammation.

 β_1 Integrins

The β_1 integrins share CD29 as their common β subunit.²¹¹ This widely distributed family of integrins contains a series of cellular receptors for extracellular matrix proteins including fibronectin, collagen, laminin, and vitronectin. One member of the β_1 integrins, $\alpha_4\beta_1$ (VLA-4, CD49d/CD29), has

been shown to be involved in lymphocyte,^{195,212-216} monocyte,^{217,218} eosinophil,²¹⁹⁻²²¹ basophil,^{220,221} and NK cell²²² adhesion to cytokine-activated endothelial cells. Because neutrophils do not express VLA-4,²¹¹ they cannot use this pathway to adhere to stimulated endothelium. The unique absence of VLA-4 on neutrophils likely accounts for the phenotype of LAD type I syndrome, ie, defective neutrophil emigration and recurrent infections with intact mononuclear leukocyte traffic and cell-mediated immunity.

The expression of $\alpha_4\beta_1$ is most prominent on cells of the hematopoietic system, being expressed only at low levels or absent on most adherent cells.²¹¹ Among leukocytes there is differential expression of $\alpha_4\beta_1$. On resting B and T lymphocytes $\alpha_4\beta_1$ is the major β_1 integrin expressed. Resting B cells also have small amounts of α_2 and α_3 on their cell surface, but do not express α_1 , α_5 , or α_6 . The amount of α_4 on the surface of B cells is twice the amount of β_1 , suggesting that a second β subunit (probably β_2)²²³ is associated with α_4 on B cells. On resting T lymphocyte there is also expression of α_6 and α_5 , but no α_1 or α_2 unless T cells are activated.²¹¹ The β_1 subunit also is expressed on T cells because the association of $\alpha_4\beta_1$ marks a subset of memory T lymphocytes with tropism for the intestinal tract.^{224,225} Monocytes express α_2 , α_4 , α_5 , and α_6 , but little α_1 or α_3 .^{211,226}

Ligands for $\alpha_4\beta_1$ include VCAM-1,¹⁹⁵ the extracellular matrix proteins fibronectin²²⁷⁻²³⁰ and thrombospondin,²³¹ and the bacterial outer membrane protein invasins.²³² In contrast to $\alpha_5\beta_1$, high-affinity binding of $\alpha_4\beta_1$ to fibronectin occurs at a non-RDG sequence in the connecting segment-1 (CS-1) of fibronectin.²²⁷⁻²²⁹ The HepII fragment of fibronectin has also been reported to contain a low-affinity binding site for $\alpha_4\beta_1$.²³⁰ The tripeptide LDV is the minimal sequence within the CS-1 region of fibronectin that is capable of supporting adherence of $\alpha_4\beta_1$.²³³

VCAM-1 expressed on cytokine-stimulated endothelial cells is a cellular ligand for $\alpha_4\beta_1$ (vide supra).¹⁹⁵ Other endothelial cell ligands for $\alpha_4\beta_1$ have been proposed (vide infra).²¹⁵ Finally, because some α_4 ^{234,235} or β_1 ²³⁶ MoAbs induce aggregation of lymphocyte cell lines, and because these cells do not express VCAM-1, another cellular ligand for $\alpha_4\beta_1$ may also exist on leukocytes.

β_7 Integrin

Initial reports showed that the murine mucosal homing receptors (LPAM-1 and -2) were the same as $\alpha_4\beta_1$ (LPAM-2) or closely related to $\alpha_4\beta_1$ (LPAM-1, $\alpha_4\beta_p$). Most recently, β_7 was shown to be identical to β_p ,^{237,238} and MoAbs to α_4 or β_7 were shown to inhibit binding to purified MAdCAM-1 or MAdCAM-1 transfectants.³⁵ The integrin $\alpha_4\beta_7$ can also bind to fibronectin and VCAM-1 (although requiring activation),^{223,239,240} but $\alpha_4\beta_1$ cannot bind to MAdCAM-1 (even with activation).³⁵ Thus, $\alpha_4\beta_7$ is one of the mucosal homing receptors that bind to the mucosal vascular addressin MAdCAM-1.

SIALOMUCINS

With the recent molecular cloning of GlyCAM-1,¹³³ MAdCAM-1,¹⁷¹ and PSGL-1,¹³² and the identification of

CD34 as a ligand for L-selectin,¹³⁸ a fourth family of adhesion molecules, the sialomucins, has been proposed.^{135,138} The common structural elements of this family of adhesion molecules are regions rich in O-linked sugars that provide an extended structure for the exposure of multiple terminal sugars. In addition, one of these sialomucins—MAdCAM-1—also contains Ig-like regions, thus providing a binding site for an integrin receptor.^{35,173} Therefore, the characterization of additional members of this family may identify molecules that subserve multiple adhesive functions.

EVIDENCE FOR OTHER ADHESION PATHWAYS

In addition to the defined integrin/Ig-like and selectin/carbohydrate interactions described above, a number of other adhesion pathways have been described (Fig 1, A through C).

A Second CD11b/CD18 Ligand on Vascular Endothelium

Two reports have suggested that leukocyte CD11b/CD18 (Mac-1) binds to a second ligand on endothelial cells distinct from ICAM-1.^{202,241} One study showed that the adhesion of phorbol dibutyrate-activated neutrophils to unstimulated endothelium was partially inhibited by pretreatment of neutrophils with blocking CD11a or CD11b MoAbs or by pretreatment of endothelial cells with ICAM-1 MoAbs that inhibited CD11a:ICAM-1-dependent adhesion.²⁰² The combination of the CD11b with either the CD11a or the ICAM-1 MoAbs totally inhibited the binding of activated neutrophils to resting endothelial cell, whereas pretreatment with CD11a and ICAM-1 MoAbs was no better than each MoAb alone. These results suggested that a separate endothelial ligand for CD11b/CD18 existed.

A second study reported that activated endothelial cells adhered to plastic coated with purified CD11b and that this binding was totally inhibited by blocking CD11b MoAbs.²⁴¹ A combination of blocking ICAM-1 MoAbs (RR1/1 and R6.5) only partially inhibited the adhesion of activated endothelial cells to purified CD11b. Pretreatment of FMLP-activated neutrophils with the CD11b MoAb alone prevented 73% of heterotypic conjugates formed with lipopolysaccharide (LPS)-stimulated endothelial cells whereas the combination of CD11b and CD11a MoAbs inhibited conjugate formation by 98%. The combination of ICAM-1 MoAbs again only partially inhibited aggregation (48%). The observation that the ICAM-1 MoAb R6.5, which was shown to prevent CD11b-dependent binding to the alternate binding domain (D3) on ICAM-1, was ineffective in totally preventing endothelial adhesion to purified CD11b or in blocking the binding of activated neutrophils to endothelium stimulated for 24 hours with LPS (a time chosen to avoid E-selectin-dependent neutrophil adhesion), again indicated that there was another ligand for CD11b on endothelium. Most importantly, the observation that neutrophils still emigrate into inflamed peritoneum in ICAM-1-null mice also indicates the existence of a second ligand.¹⁵⁴

An Induced Endothelial Ligand for CD11c

Endothelial cells stimulated for 24 hours with IL-1 or LPS, but not unactivated endothelial cells, were shown to

bind to purified CD11c/CD18.²⁴² This adhesion was inhibited specifically by a blocking CD11c MoAb or by EDTA-induced chelation of divalent cations. Binding of activated endothelial cells to purified CD11c/CD18 required a higher density of soluble protein, suggesting that the affinity of this β_2 leukocyte integrin for its endothelial ligand may be low, or that leukocyte capping of CD11c/CD18 may be required for binding.²⁴²

An Alternate Endothelial Ligand for VLA-4 (CD49d/CD29)

Two studies have reported that the binding of lymphoid cell lines or peripheral blood lymphocytes to TNF- α -stimulated endothelial cells was more potently inhibited by CD49d than by VCAM-1 blocking MoAbs.^{212,215} The CD49d-dependent, VCAM-1-independent lymphocyte adhesion was reported to increase with time after TNF- α treatment of endothelium and the majority of adhesion 7 hours poststimulation was VCAM-1-independent.²¹⁵ The CS-1 fragment of fibronectin has been shown to function as an alternate pathway of VLA-4 binding to stimulated endothelium in vivo²⁴³ (vide infra); however, cocubation of lymphocytes with a polyclonal, antifibronectin antisera did not affect binding to TNF- α -activated endothelium in vitro.²¹⁵

A Ligand on Nonlymphoid Endothelium for L-Selectin

Although the PNA α d is the original ligand described for L-selectin, the observation that a blocking L-selectin MoAb inhibited phagocyte emigration into nonlymphoid tissue showed that there are also counter-receptors on nonlymphoid endothelium for L-selectin.^{69,244} L-selectin was shown to be involved in the adhesion of neutrophils, lymphocytes, and monocytes to cytokine-activated endothelium in vitro.^{245,246} The induction of this ligand required de novo protein synthesis because cycloheximide prevented its expression. TNF- α , IL-1, and LPS were shown to induce this ligand whereas IL-4 and IFN- γ were less effective. Increased leukocyte adhesion was observed within 2 to 4 hours of endothelial activation and activity persisted for ~24 hours. An L-selectin-Ig fusion protein was shown to bind to activated, but not unstimulated, endothelium in vitro.²⁴⁵ In another study using a similar probe to screen tissue samples, no reactivity with endothelium other than HEV in peripheral lymph nodes was observed,²⁴⁷ indicating that this L-selectin ligand is not constitutively expressed by nonlymphoid endothelium in vivo.

Although the L-selectin-Ig probe failed to identify a ligand for L-selectin in normal rat tissues, a L-selectin-Ig affinity column was found to bind a heparin- or glycosaminoglycan-like substance from lysates of metabolically labeled calf pulmonary artery and human umbilical vein endothelial cells.¹¹⁹ This substance was insensitive to sialidase and O-sialoglycosidases that affect PNA α d activity, but was degraded by heparinases or chondroitinases, indicating that the metabolic label was present in glycosaminoglycans. Interestingly, an intracellular storage form of this L-selectin ligand was detected when examining permeated endothelial cells in culture. Whether this intracellular structure(s) represents the inducible ligand remains to be determined.

Finally, the sialomucin CD34 has recently been identified as a ligand for L-selectin in HEV.¹³⁸ CD34 is expressed on endothelium in diverse vascular beds, and, when appropriately glycosylated by endothelial activation, it could potentially serve as a ligand for L-selectin on nonlymphoid vasculature.¹³⁸

VAP-1: A Novel, Synovial Adhesion Protein That Binds Lymphocytes

Vascular adhesion protein-1 (VAP-1) is a recently described 90-kD endothelial adhesion protein that was identified by an MoAb (1B2) generated by immunizing mice with human synovium.²⁴⁸ Immunocytochemistry studies using MoAb 1B2 showed that VAP-1 was expressed on mucosal, peripheral lymph node, and synovial HEV, but was absent on endothelium from large vessels. In contrast to E- and P-selectin, ICAM-1, ICAM-2, and VCAM-1, VAP-1 was not expressed on unstimulated or LPS- or cytokine-treated human umbilical vein endothelium. Partial amino acid sequence of VAP-1 also indicated that it is a novel adhesion molecule. MoAb 1B2 inhibited the adhesion of lymphocytes to tonsil, peripheral lymph node, and synovial HEV as well as the binding of peripheral blood lymphocytes to immunoaffinity-purified VAP-1, thereby confirming VAP-1 as an endothelial adhesion molecule for lymphocytes. Whether VAP-1 is the proposed synovial vascular addressin has yet to be established.³¹

L-VAP-2

An additional putative endothelial adhesion molecule for lymphocytes that is expressed on venules in lymphoid and nonlymphoid tissues has been identified.²⁴⁹ This 70-kD protein, designated lymphocyte-vascular adhesion protein-2 (L-VAP-2), is constitutively expressed on human umbilical vein endothelial cells, and its expression is not upregulated by cytokines. L-VAP-2 is also expressed on B lymphocytes and CD8⁺ T cells. A MoAb to L-VAP-2 partially reduced lymphocyte adhesion to cultured endothelial cells. By molecular weight and tissue distribution, it is proposed that L-VAP-2 is a novel adhesion molecule involved in lymphocyte adherence to endothelium.

CD14: A Monocyte-Specific Adhesion Pathway?

Several MoAbs directed to CD14 were reported to inhibit binding of monocytes, but not neutrophils, to cytokine-activated human endothelial cells in vitro.²⁵⁰ CD14 is a glycosylphosphatidylinositol lipid-anchored surface protein that is highly expressed on monocytes, and, to a much lesser extent, on neutrophils. It functions as a receptor for LPS complexed with LPS-binding protein, an acute-phase protein.²⁵¹ The nature of the induced endothelial counter-structure for CD14 is unknown. Interestingly, cross-linking of monocyte CD14 by MoAbs has been shown to activate CD11/CD18-dependent adherence,²⁵² raising the possibility that binding of monocyte CD14 by its endothelial ligand may trigger subsequent β_2 integrin-mediated adherence.

CD18-Independent Neutrophil Emigration

In studies in a rabbit model, a CD18 MoAb was observed to inhibit completely neutrophil emigration in response to multiple inflammatory stimuli in the abdominal wall of rabbits, but failed to inhibit emigration after instillation of certain stimuli in the lung.²⁵³ These studies demonstrating a CD18-independent pathway of neutrophil emigration in the rabbit lung were supported by the finding of extravasated neutrophils at foci of bronchopneumonia in a patient with severe LAD type I syndrome, although no neutrophils were present at sites of infection elsewhere in the body.²⁵⁴ Subsequently, it was shown that the CD18-independent neutrophil emigration could also be induced in rabbit peritoneum in response to certain stimuli, if mononuclear phagocytes had previously been recruited to the peritoneum.²⁵⁵ These results suggest that a product of mononuclear phagocytes may be responsible for the induction of the CD18-independent pathway of neutrophil emigration. The adhesion molecules involved in β_2 integrin-independent neutrophil emigration have not been identified.

iC3b

CD11b/CD18 was initially identified as a receptor for iC3b and was defined as CR3.¹⁹⁴ CD11b/CD18-dependent neutrophil adhesion to endothelium was shown to be rapidly induced by fixation of complement on the endothelial surface in vivo.²⁵⁶ Similarly, neutrophil adhesion to xenogenic endothelium in vitro was shown to be mediated by CD11b/CD18 binding to iC3b deposited on endothelium after activation of complement by naturally occurring antibodies against endothelial cells.²⁵⁷ These pathways of adhesion may be particularly relevant to phagocyte-mediated vascular injury in vasculitides as well as in acute xenograft rejection.

Fibrinogen

Fibrinogen is a soluble ligand for CD11b/CD18.^{258,259} Recently, fibrinogen was shown to promote leukocyte adherence to endothelium by binding both leukocytes and endothelial cells.²⁶⁰ Purified fibrinogen or plasma fibrinogen increased leukocyte adherence by binding to CD11b/CD18 on the leukocyte and ICAM-1 on the endothelial cell. The physiologic relevance of this novel "bridging" mechanism remains to be determined.

CS-1

As discussed previously, the β_1 integrin VLA-4 recognizes the extracellular matrix protein fibronectin as well as VCAM-1. A major binding site for VLA-4 in fibronectin is found within the CS-1 segment, a 25-amino acid sequence present within the alternatively spliced III CS region. Analysis of rheumatoid synovium showed that CS-1-containing fibronectin isoforms were expressed exclusively on endothelium and in extracellular matrix.²⁴³ Luminal expression of CS-1 was confirmed by electron microscopy, and binding of T-lymphoblastoid cells to frozen sections of synovial tissues was inhibited by a blocking VLA-4 MoAb and CS-1 peptides. These studies show that CS-1-containing fibronectin

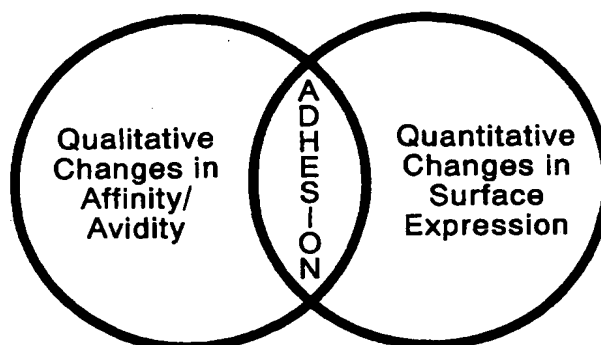


Fig 2. Regulation of leukocyte and endothelial adhesive interactions. Leukocyte adherence to endothelium is determined by qualitative and quantitative alterations in adhesion proteins. For leukocytes modulation of integrin avidity is most important. Endothelial adhesion proteins are regulated primarily by changes in surface expression.

may serve as an endothelial ligand for VLA-4-expressing leukocytes.

REGULATION OF ENDOTHELIAL ADHESION PROTEINS

The regulation of endothelial and leukocyte adhesion molecules involves both quantitative changes in surface expression and qualitative changes in avidity (Fig 2). For the endothelial adhesion molecules quantitative alterations in surface expression predominate, although qualitative changes affecting adhesion have been reported.¹⁴⁵

Among the endothelial adhesion proteins there are both similarities and differences regarding the agents that induce them and the kinetics of their expression. For example, a triad of agents—IL-1, TNF- α , and LPS—stimulate the expression of ICAM-1, VCAM-1, and E-selectin, but the kinetics of the induced surface expression in vitro differ with E-selectin having a shorter half-life than ICAM-1 or VCAM-1. Stimulated surface expression of ICAM-1, E-selectin, and VCAM-1 appears to result in large part from increased transcriptional regulation. However, surface expression of P-selectin may also involve a rapid mobilization of cytoplasmic granules induced by noncytokine agents, and surface expression of E-selectin is in part regulated by rapid internalization. Therefore, important differences in regulatory mechanisms exist among these proteins that may help to explain the recruitment of subsets of leukocytes to specific sites of endothelium during an inflammatory or immune response.

A detailed consideration of the signaling pathways, promoter elements, and transcriptional factors involved in regulation of endothelial adhesion protein gene expression is beyond the scope of this review. Instead we will focus on the modulation of surface expression by various inflammatory stimuli.

ICAM-2

ICAM-2 was found to be expressed constitutively on vascular endothelium both in vivo and in vitro, and was not subject to upregulation by cytokines (TNF- α , IL-1, or IFN-

γ) or LPS.^{156,261-263} However, surface expression of ICAM-2 has been reported to be increased on HEV and small vessel endothelium in malignant versus nonmalignant lymph nodes,²⁶⁴ suggesting that endothelial expression of ICAM-2 may be inducible under some circumstances.

P-selectin

P-selectin is constitutively synthesized by endothelial cells and platelets, and is stored in Weibel-Palade bodies or α -granules, respectively.^{55,56} With endothelial activation by thrombin, histamine, phorbol esters, calcium ionophores, or complement proteins, cytoplasmic storage granules fuse with the cell membrane externalizing their contents.^{55,265-267} Initial reports showed that surface expression of P-selectin was rapid and transient, peaking by 10 minutes and returning to baseline within 20 to 30 minutes.²⁶⁵ Rapid loss of surface P-selectin was believed to be secondary to internalization of the protein.

However, recent studies have shown that surface expression of P-selectin can last several hours. Stimulation of endothelial cells by thrombin²⁶⁸ or oxygen radicals²⁶⁹ led to P-selectin-dependent neutrophil adhesion lasting 1.5 to 4 hours, respectively. Whether this effect to prolong surface expression of P-selectin is secondary to new protein synthesis or to decreased internalization of the protein was not determined. Endothelial P-selectin mRNA and protein were shown to decrease 2 and 24 hours, respectively, after endothelial activation by phorbol esters.²⁷⁰ However, the mRNA of murine P-selectin was reported to be maximally increased 4 hours after administration of LPS with highest levels being found in the liver, lung, kidney, and heart.⁶⁵ Similarly, treatment of a murine endothelioma cell line with TNF- α -induced maximal P-selectin mRNA and protein 2 hours and 3 hours, respectively, after cytokine treatment.⁴⁷ Consistent with the murine studies, P-selectin was demonstrated to mediate adhesion of neutrophils to LPS-stimulated human endothelium that had been pretreated for 4 hours.²⁷¹ Further studies are needed to address the kinetics of human P-selectin synthesis after agonist-induced activation of endothelium.

E-selectin, ICAM-1, and VCAM-1

In contrast to ICAM-2 and P-selectin, there is abundant evidence that E-selectin, ICAM-1, and VCAM-1 are transcriptionally regulated by cytokines, LPS, or other mediators of inflammation. Recent reports have shown that combinations of cytokines can differentially modulate the induction of these endothelial adhesion proteins. Furthermore, there appear to be differences between endothelium in large vessels versus the microcirculation in the ability to express these proteins. Again, all of these factors may contribute to the selective recruitment of subsets of leukocytes during an inflammatory or immune response.

Several agonists induce the de novo expression of E-selectin and VCAM-1 and the upregulation of ICAM-1, whereas other agents are specific for one protein. TNF- α , IL-1, LPS, and polyinosinic acid, which binds to the scavenger receptor for low-density lipoprotein (LDL), stimulate the expression all three endothelial adhesion proteins.^{40,147,272-281} Thrombin

has also been reported to induce E-selectin, ICAM-1, and VCAM-1.²⁸²⁻²⁸⁴ In other studies phorbol esters induced E-selectin and upregulated ICAM-1, but were only weak inducers of VCAM-1.^{281,285} Hypoxia/reoxygenation,²⁸⁶ the generation of oxygen radicals,^{287,288} and TNF- β ²⁷⁵ have been shown to induce the endothelial expression of ICAM-1 and E-selectin. Lysophosphatidylcholine treatment of endothelium derived from rabbit aorta or human iliac artery stimulated the expression of ICAM-1 and VCAM-1, but not E-selectin.²⁸⁹ IFN- γ stimulated the upregulation of endothelial expression of ICAM-1, but not E-selectin or VCAM-1, whereas neither IFN- α nor IFN- β were active in inducing any of the three endothelial adhesion proteins *in vitro*.^{163,275} Several reports have shown that IL-4 stimulated the expression of VCAM-1 but not E-selectin or ICAM-1,^{277,290} whereas IL-3 induced the expression of E-selectin.²⁹¹

From these observations there appear to be both common and specific pathways of induction of the endothelial adhesion proteins. Gram-negative sepsis, for example, may be associated with circulating endotoxin leading to the generation of monokines (IL-1 and TNF- α) that could induce the expression of E-selectin, ICAM-1, VCAM-1, and P-selectin on vascular endothelium. However, certain chronic inflammatory disorders may be associated with the generation of lymphokines (IFN- γ or IL-4) that would favor recruitment of mononuclear leukocytes because they do not induce major neutrophil ligands, E- or P-selectin. Similarly, the generation of lysophosphatidylcholine during hyperlipidemia may induce endothelial ligands ICAM-1 and VCAM-1 that would preferentially recruit mononuclear leukocytes to sites of atherogenesis. Thus, the various patterns of cytokines or inflammatory mediators may lead to the differential induction of endothelial adhesions proteins.

Differences in the kinetics of endothelial expression of E-selectin, VCAM-1, and ICAM-1 may also contribute to the selective recruitment of leukocyte subtypes to sites of inflammation. *In vitro* the surface expression of E-selectin has been reported to peak 4 hours poststimulation with a return to basal levels of expression within 24 hours.^{40,148,272,292} However, studies *in vivo* have shown that E-selectin persists beyond 24 hours,^{293,294} indicating that additional factors may determine the duration of E-selectin expression. Endothelial expression of VCAM-1 and ICAM-1 *in vitro* peaks by ~6 hours and 12 hours, respectively, and both proteins persist for at least 72 hours after induction by TNF- α .^{148,163,276-279}

The induced expression of E-selectin, VCAM-1, and ICAM-1 is largely dependent on synthesis of new mRNA and protein because, in contrast to P-selectin, there are apparently no storage forms of these endothelial adhesion proteins. The de novo endothelial surface expression of E-selectin on cultured human endothelial cells requires the synthesis on new protein and mRNA because cycloheximide and actinomycin D were shown to inhibit the generation of E-selectin.^{272,292} In pulse-chase experiments it was found that treatment of endothelial cells with IL-1 or TNF- α induced E-selectin transcription within 1 hour. Maximal mRNA levels were attained within 2 to 4 hours with basal levels of expression occurring within 24 hours.^{274,295} Other studies indicated that there is little, if any, VCAM-1 or ICAM-1

mRNA detected in unstimulated endothelial cells.^{158,296,297} TNF- α -induced VCAM-1 mRNA peaked 2 hours post-stimulation and persisted for at least 72 hours,¹⁵⁸ whereas TNF- α -induced ICAM-1 mRNA peaked at 2 hours and then rapidly decreased over the next 24 hours.^{296,297} However, phorbol-ester-induced ICAM-1 mRNA was shown to peak later (4 hours) and to decline more slowly,²⁹⁷ demonstrating that agonist-induced expression of ICAM-1 may involve several pathways.

Reports using combinations of cytokines have provided further information regarding the regulation of E-selectin, ICAM-1, and VCAM-1 gene expression. Treatment of endothelial cells in vitro with the combination of IFN γ plus TNF- α or LPS prolonged the surface expression of E-selectin, whereas the combination of IL-1 and IFN γ had minimal effect.^{298,299} IFN γ increased early E-selectin mRNA accumulation induced by TNF- α , perhaps by preventing degradation of mRNA. However, the synergistic effect of the combination of TNF- α and IFN γ on E-selectin surface expression was not associated with marked changes in mRNA accumulation.²⁹⁹ Previous studies have shown that endocytosis of E-selectin accounts in large part for the short half-life of surface E-selectin.⁴⁵ Whether IFN γ or other cytokines modulate this internalization process remains to be determined.

In contrast to the prolongation of E-selectin mRNA and surface protein expression produced by IFN γ , both TGF- β and IL-4 have been shown to inhibit cytokine-induced expression of E-selectin.^{290,300} Pretreatment of endothelial cells in vitro with TGF- β partially inhibited the expression of E-selectin induced by both TNF- α and IL-1, but did not affect the TNF- α -induced expression of ICAM-1 or VCAM-1.^{300,301} Concurrent treatment of endothelial cells with IL-4 also inhibited TNF- α -induced expression of E-selectin, and the combination of TGF- β and IL-4 produced additive inhibition.²⁹⁰ Whereas IL-4 antagonized the cytokine-induced expression of E-selectin, it augmented the induction of VCAM-1 by IL-1.^{277,290,302} These studies show that combinations of cytokines may increase (TNF- α + IFN γ for E-selectin and TNF- α + IL-4 for VCAM-1) or reduce (TNF- α + IL-4 for E-selectin and ICAM-1) the expression of endothelial adhesion proteins.

Finally, endothelial cells in different vascular beds may vary in their capacity to express adhesion proteins. As mentioned earlier, lysophosphatidylcholine induced the expression of ICAM-1 and VCAM-1 on endothelium derived from human iliac arteries but not umbilical veins.²⁸⁹ Other studies have shown that ICAM-1 was induced on cultured dermal microvessel endothelium by either TNF- α and IL-1, whereas VCAM-1 was induced only by TNF- α .³⁰³ In contrast to responses observed with human umbilical vein endothelium, treatment of cultured human synovial microvascular endothelium with IL-1 or TNF- α led to minimal induction of ICAM-1.³⁰⁴ The basis for this differential response to agonists between endothelial cells derived from different vascular sites has not been defined.

In summary, expression of endothelial adhesion proteins is regulated at multiple levels. Some agonists are more selective for certain adhesion proteins (eg, IFN γ for ICAM-1, or IL-4 for VCAM-1); others (eg, IL-1, TNF- α , and LPS) are

less specific, inducing several proteins. Combinations of cytokines may produce additive or synergistic (eg, IL-4 and TNF- α for VCAM-1) or antagonistic (eg, IL-4 and TNF- α for E-selectin) effects. These multiple levels of regulation provide for precise modulation of the expression of endothelial adhesion proteins that are involved in recruitment of leukocytes to sites of inflammation or immune reaction.

REGULATION OF LEUKOCYTE ADHESION PROTEINS

In contrast to endothelium, quantitative changes in leukocyte adhesion molecule expression may be less important than qualitative alterations in function (Fig 2). Activation of phagocytes provokes rapid translocation of CD11b/CD18 and CD11c/CD18 from intracellular granules to the plasma membrane.¹⁹⁶ However, upregulation of CD11b/CD18 surface expression was not necessary for stimulated neutrophil adherence to endothelium in vitro.³⁰⁵ The functional importance of quantitative changes in CD11b/CD18 in neutrophil emigration has not yet been established. However, recent studies in vitro indicate that newly mobilized CD11b/CD18 receptors play an important role in subsequent adherence-dependent functions.³⁰⁶

Most stimuli that produce upregulation of neutrophil CD11b/CD18 also induce a rapid, concomitant decrease in surface L-selectin.⁸²⁻⁸⁵ With appropriate activation, there is also a decrease in lymphocyte L-selectin. The downregulation of L-selectin is a result of shedding of surface L-selectin that is produced by cleavage of the extracellular portion of L-selectin by an unidentified endogenous protease. The functional significance of L-selectin shedding in leukocyte emigration is uncertain, but it may serve to limit leukocyte recruitment. Finally, in addition to these rapid (minutes) changes in cell-surface expression of adhesion molecules, quantitative alteration in integrin receptors have also been reported to occur with longer stimulation (hours to days).¹⁸⁴

Qualitative changes in adhesion receptor avidity (binding to multivalent ligands) play a critical role in leukocyte adhesion to endothelium or matrix components. Integrin receptors on circulating leukocytes are normally in an inactive or low-avidity state in that they do not bind, or bind only minimally, to their endothelial ligands. With appropriate activation of the leukocyte, the integrin receptors are transformed to an active state in which they bind avidly to surface ligand. Recent studies showed that increased leukocyte avidity may result from two distinct mechanisms—an increase affinity (as measured by binding to soluble monovalent ligands) or postreceptor events (eg, cytoskeletal associations).³⁰⁷⁻³¹⁰ This avidity modulation or “inside-out” signaling³⁰⁷ can be triggered by a variety of mechanisms that range from the binding of peptide and lipid chemoattractants to membrane receptors to the cross-linking of other surface molecules (eg, T-cell receptor, PECAM-1). The ability of integrin receptor to transform rapidly from a low-avidity to a high-avidity state allows leukocytes to circulate freely, but then stick firmly at sites of inflammation. It is equally important for leukocytes to modulate integrin receptors from the high to the low-avidity states as “freezing” receptors in a high-avidity state prevents migration.³¹¹ This topic of avidity modulation of leukocyte β_1 and β_2 integrin receptors has recently been reviewed

in detail in this journal¹⁸⁴ and elsewhere,^{14,15,18,307-309} and will not be considered further in this review article except to emphasize that it is a major determinant of integrin-mediated leukocyte adhesion to endothelium.

Similar to avidity modulation of leukocyte integrins, activation of neutrophils and lymphocytes was shown to produce a transient high-avidity state of L-selectin before shedding.³¹² Whether changes in avidity also occur with E- and P-selectin remains to be determined.

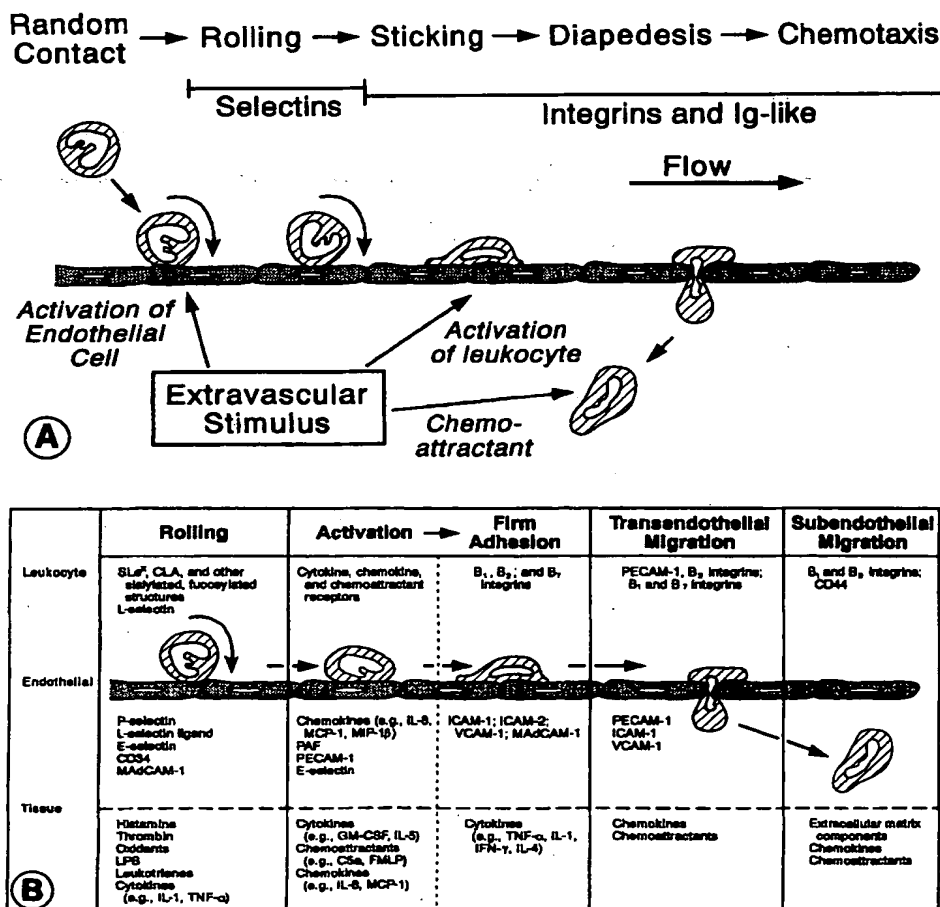
ADHESION CASCADE

Elegant studies by intravital microscopy, some dating back more than 100 years, have identified a sequence of adhesive interactions involved in leukocyte emigration from the bloodstream to extravascular sites of inflammation³¹³ (Fig 3A). Because leukocytes do not have cilia, they cannot "swim" to the vessel wall in response to extravascular chemotactic stimuli. Initial contact with the vessel wall then is in large part a random event, perhaps enhanced by local alterations in flow characteristics. After initial contact some of the leukocytes are observed to "roll" along the vessel wall adjacent to the site of injury. Rolling is a phenomenon

that is observed only under conditions of flow, and is the resultant of shear forces acting on the individual leukocyte and an adhesive interaction between the leukocyte and endothelium.³¹⁴ Whether rolling is observed in normal vessels is a matter of controversy,³¹⁵ but it has clearly been shown to be rapidly induced by only minimal perturbation of tissue.^{316,317}

Atherton and Born³¹⁴ calculated that the adhesive force to which each neutrophil is subjected is ~ 5 dynes/cm², and in vitro studies examining leukocyte adhesion to endothelium during shear force have used this estimate.³¹⁸ However, others have suggested that adhesive forces of 17 to 29 dynes/cm² may be better estimates of shear forces in vivo.^{319,320} Interestingly, a consistent in vivo observation has been that leukocyte rolling seldom occurs along endothelium of arterioles.^{317,320-322} Although 39% of leukocytes were observed to roll along the endothelium of rat mesenteric venules, only 0.6% rolled along the endothelium of arterioles.³¹⁷ It was initially reported that the mean velocity of rolling was directly proportional to mean blood velocity at flow rates less than 1 mm/s, but at higher rates was relatively constant.³¹⁴ Hence, higher flow rates in the arteriolar circulation may be one explanation of this difference. However, with reduction

Fig 3. Adhesive interactions during leukocyte emigration. (A) Studies using intravital microscopy have identified a series of events involved in leukocyte emigration from bloodstream to extravascular tissue. Under conditions of flow, leukocytes are first observed to roll along endothelium of postcapillary venules adjacent to the extravascular site of inflammation. Subsequently, some of the rolling leukocytes adhere firmly, diapedese between endothelial cells, and then migrate into subendothelial tissue. Recent studies in vitro and in vivo indicate that rolling is mediated by multiple low-affinity interactions between selectin receptors and carbohydrate counter-structures, and firm adhesion and diapedesis are largely dependent on integrin and Ig-like adhesion proteins. (B) The adhesive interactions involved in leukocyte emigration involve several distinct phases: initial transient adhesion, activation and firm adhesion, transendothelial migration, and subendothelial migration. Particular leukocyte, endothelial, and tissue components participate in each phase. (Adapted and reprinted with permission.³⁷ Copyright 1992 by the AAAS.)



of flow rates in arterioles to that of venules, the frequency of leukocyte rolling on venular endothelium remained higher.^{317,320} These studies suggest that there may be an intrinsic difference in the expression of endothelial adhesive components involved in leukocyte rolling, ie, the selectins and their counter-structures (vide supra) on venular versus arteriolar endothelium.

With sufficient tissue trauma or inflammation, a portion of the rolling leukocytes are observed to flatten and spread on the endothelium and then to 'stick' firmly. Occasionally, other leukocytes will stick to the leukocyte adherent to the vessel wall forming small aggregates of leukocytes attached to the endothelium. Some of the adherent leukocytes crawl over the endothelial surface, seeming to probe for an opening, and then diapedese or crawl between endothelial cells. Once in subendothelial tissue the extravasated leukocytes continue to migrate toward the inflammatory site.

In the past decade *in vitro* and *in vivo* studies have identified many of the adhesion molecules and locally generated inflammatory mediators that are involved in the adhesive interactions observed by intravital microscopy.³²³ The current model of leukocyte emigration proposes a cascade of adherence events analogous to the complement and coagulation cascades^{23,37,197,323-325} (Fig 3B). The initial step involves local generation of mediators and initial activation of endothelium juxtaposed to the inflammatory site. This results in increased leukocyte rolling along the postcapillary endothelium, thereby 'tethering' the leukocyte to the vessel wall.¹⁶

The next event in this cascade is continued activation of endothelium and now leukocytes by cytokines, chemokines, and chemoattractants that are produced locally. These agents may be specific for a particular endothelial adhesion protein (eg, IL-4 for VCAM-1) or a leukocyte subtype (eg, monocyte chemotactic protein-1 (MCP-1) for monocytes or IL-5 for eosinophils), thus promoting selective recruitment, or they may act nonspecifically to induce expression of several endothelial adhesion proteins (eg, TNF- α or IL-1 for E-selectin, ICAM-1, and VCAM-1) or activation of several leukocyte subtypes (eg, platelet-activating factor [PAF] for neutrophils, monocytes, and eosinophils). Endothelial cells may further augment leukocyte activation by secretion (eg, IL-8, MCP-1, or GM-CSF) or surface expression (eg, PAF, MIP-1 β , or IL-8) of proadhesive molecules. Additionally, endothelial adhesion proteins (eg, E-selectin, P-selectin, or PECAM-1) themselves may directly activate leukocytes. Events that occur during this phase of leukocyte activation strengthen adhesion and lead to firm sticking.

In the final steps of the cascade, some of the adherent leukocytes migrate between the inter-endothelial cell junctions, and then through the subendothelial extracellular matrix to accumulate finally at the site of inflammatory or immune reaction.

In general, the selectin family of adhesion proteins is primarily involved in the initial adhesive event manifested by rolling under conditions of flow, the binding of leukocyte integrins to endothelial Ig-like proteins mediates firm adhesion, and transendothelial migration involves leukocyte and endothelial PECAM-1 as well as leukocyte integrin and endothelial Ig-like proteins. Migration through subendothelial

tissue is mediated in large part by interaction of integrins with components of extracellular matrix. We will consider leukocyte-endothelial adhesive interactions during rolling, activation-firm adherence, and transendothelial migration in greater detail.

Rolling

Convincing evidence from both *in vitro* and *in vivo* studies indicates that selectins are involved in the leukocyte rolling that is observed immediately after tissue injury. Models examining leukocyte adhesion to endothelium *in vitro* have shown that CD11/CD18-dependent adhesion, stimulated either by leukocyte activation with increased expression/avidity of the β_2 integrins or with increased expression of ICAM-1 on activated endothelium, is seen only at low shear rates (<0.5 dynes/cm²) or in static adhesion systems.^{246,326-329} In contrast, with shear flow rates ~ 2 dynes/cm², either pretreatment of neutrophils or monocytes with anti-L-selectin MoAbs or with agonists that cause activation-induced shedding of L-selectin decreases neutrophil and monocyte adhesion to cytokine-stimulated endothelium.^{246,327-329} Agents previously shown to inhibit the adhesive function of L-selectin *in vitro*, including sulfated polysaccharides (fucoidan and dextran), were found to inhibit leukocyte rolling *in vivo*.^{319,330-332} The administration of MoAb^{323,333} or polyclonal sera³³⁴ against L-selectin or a soluble, recombinant Ig-chimera of L-selectin³³⁵ significantly inhibited leukocyte rolling *in vivo*. By preventing leukocyte rolling, treatment with blocking antibodies or L-selectin-Ig chimera decreased leukocyte recruitment *in vivo*.^{69,244,323,335} Activation-induced L-selectin shedding³³⁶ or removal of glycosylated L-selectin by chymotrypsin-treatment of neutrophils *ex vivo* also abrogated rolling *in vivo*.³³⁷ Finally, transfection of a SLe^x-negative murine lymphocyte line with human cDNA for L-selectin conferred the capacity to roll on inflamed rabbit venules.³³⁷

The participation of P-selectin in leukocyte rolling and adhesion with higher shear forces was first shown *in vitro*.³³⁸ P-selectin in lipid bilayers mediated rolling of neutrophils at shear forces <4 dynes/cm², but ICAM-1 was unable to support adhesion at these shear forces.³³⁸ However, neutrophil binding to P-selectin was sensitive to greater shear forces. If neutrophil adhesion to ICAM-1 was first allowed to occur at low shear forces, subsequent increases in shear forces did not disrupt ICAM-1-dependent binding. These studies indicate that selectin-mediated adhesion remains sensitive to shear forces, whereas, once activated, integrin-mediated binding to ICAM-1 is resistant to increasing shear forces. Consistent with the *in vitro* studies, administration of a blocking anti-P-selectin MoAb was shown to decrease leukocyte rolling *in vivo*.³³⁹ Most importantly, 'spontaneous' rolling was reported to be virtually absent in mesenteric venules of P-selectin-deficient mice generated by gene targeting.³⁴⁰

Evidence that E-selectin is also involved in leukocyte rolling *in vitro* has recently been reported.^{341,342} After binding to E-selectin, neutrophils do not undergo shape change and do not migrate under endothelial monolayers.³⁴¹ A portion of this adhesion to E-selectin can be inhibited by treatment

of neutrophils with blocking L-selectin antibodies, again suggesting E-selectin binding to SLe^x expressed on L-selectin. In contrast to leukocyte rolling on P-selectin *in vitro*, adhesive binding to E-selectin was stronger.³⁴² Because E-selectin is expressed only after several hours, it likely contributes to the later recruitment of leukocytes. In this regard, late neutrophil accumulation in inflamed peritoneum was not markedly reduced by treatment of normal animals with L-selectin Ig-chimeric protein or in the P-selectin-deficient mice, whereas an MoAb to E-selectin effectively inhibited neutrophil accumulation in the inflamed peritoneum and lungs of normal animals at 4 hours.³⁴³

Thus, both L- and P-selectin have been shown to mediate rolling and recruitment of leukocytes *in vivo*, and all three selectins have been shown to support leukocyte rolling *in vitro*. The fact that both functional L-selectin and P-selectin are necessary for efficient rolling raises the question of whether they interact directly. L-selectin present on microvilli of neutrophils has been shown to present SLe^x for recognition by P-selectin under conditions of shear forces *in vitro*.¹²⁰ However, P-selectin has also been shown to bind with high affinity to a 120-kD protein distinct from L-selectin¹³¹ and to PSGL-1.¹³² Also, a SLe^x-negative lymphocyte cell line transfected with human L-selectin cDNA was observed to roll *in vivo*,³³⁷ indicating that L-selectin (lacking carbohydrate ligands for P- or E-selectin) is able to mediate rolling, presumably by recognition of a rapidly induced carbohydrate counter-structure expressed on inflamed venules.³³⁷ Most likely then, both L-selectin and P-selectin are necessary for efficient rolling with each selectin interacting with a distinct counter-structure on the opposing cell (*vide supra*).

Activation-Firm Adherence

In the second phase of leukocyte recruitment, activation of leukocyte integrins and *de novo* expression of endothelial adhesion proteins occurs.^{16,78,323,324} As discussed previously, activation of leukocytes triggers an increase in avidity caused by a conformational change in the integrin heterodimer, resulting in greater affinity for ligands and/or to postreceptor events.^{14,184,307-309} In the setting of leukocyte-endothelial interactions there are diverse mechanisms to modulate leukocyte integrin avidity. Binding of chemokines (eg, IL-8, MCP-1, MIP-1 β), cytokines (eg, GM-CSF, IL-5), or chemoattractants (eg, C5a, FMLP) to leukocytes expressing complementary receptors transduces signals that can augment β_1 or β_2 integrin-dependent adhesion. These activating agents may be derived from local tissue cells, infiltrating leukocytes, microorganisms, or, importantly, from the endothelium itself. Endothelial-derived IL-8 secreted into subendothelial matrix³⁴⁴ or bound to the surface³⁴⁵ was shown to promote neutrophil adherence and transmigration. Surface-expressed endothelial PAF also augmented neutrophil adhesion by activating β_2 integrins.^{267,346} The chemokine MIP-1 β , bound to endothelial surface proteoglycans similarly augmented VLA-4-dependent T-cell adhesion to VCAM-1.³⁴⁷

Activation of leukocyte integrins can also occur after the engagement of counter-structures by other leukocyte surface

receptors. Cross-linking of several lymphocyte surface proteins, including CD2, CD3, CD43, and CD44, has been shown to induce high avidity binding of leukocyte CD11a/CD18.¹⁹ Moreover, the binding of leukocytes to endothelial adhesion proteins may also transduce activating signals. Cross-linking of the E- and P-selectin counter-structures, CD15 or its sialylated form, on neutrophils caused activation or upregulation of β_2 integrins.³⁴⁸⁻³⁵¹ Binding of neutrophils to E-selectin increased expression of CD11b/CD18 *in vitro* and augmented CD11/CD18-dependent adhesion to cultured endothelium.¹⁹⁷ Binding of T cells to endothelial CD31 (PECAM-1) increased the function of β_1 integrins.¹⁷⁸ Lymphocyte adhesion to ICAM-1, ICAM-2, and VCAM-1 was shown to provide costimulatory signals for T-cell proliferation and IL-2 secretion,³⁵²⁻³⁵⁶ whereas adhesion to E-selectin did not.³⁵⁴ Whether P-selectin also is involved in transmitting signals to leukocytes that bind to this selectin is unclear. In some studies neutrophil binding to P-selectin inhibited several neutrophil functions,^{357,358} whereas monocyte adhesion to P-selectin increased expression of tissue factor.³⁵⁹ Others have reported that neutrophil binding to P-selectin alone failed to provoke intracellular calcium transients, polarization, upregulation of β_2 integrins, or priming of neutrophils.³⁶⁰

Endogenous mediators may also function to reduce leukocyte-endothelial interactions. Although generally considered to be a proadhesive molecule promoting neutrophil emigration,^{344,345} under different assay conditions IL-8 reduced neutrophil adherence to endothelium *in vitro*,³⁶¹ and high concentrations of intravascular IL-8 inhibited neutrophil emigration.³⁶² Nitric oxide, presumably derived from endothelium, was shown to be an endogenous modulator of leukocyte adhesion because treatment with an inhibitor of endogenous nitric oxide synthesis resulted in neutrophil sticking to cat mesenteric venules observed by intravital microscopy.³⁶³ Also, the pleiotropic cytokine, TGF- β , which is likely elaborated in an active form in the perivascular space,^{364,365} has been reported to decrease neutrophil³⁶⁶ and lymphocyte³⁰¹ binding to basal and cytokine-stimulated endothelium, and to inhibit E-selectin expression on endothelial cells *in vitro*.³⁰⁰ Consistent with these *in vitro* studies, TGF- β was reported to suppress inflammatory responses in arthritis³⁶⁷ and in myocardial infarction,³⁶⁸ and mice that are deficient in TGF- β develop multifocal inflammatory disease with leukocyte infiltration.³⁶⁹

If proadhesive factors predominate, the net result of the activation processes is to promote firm adhesion via integrin interactions with endothelial Ig-like ligands. Shear-sensitive, selectin-mediated tethering is replaced by shear-resistant, activated integrin-mediated adhesion. Recently, this scenario of activation-dependent adhesion was confirmed by intravital microscopy of lymphocyte binding to HEV of mouse Peyer's patches.³⁷⁰ In this model pertussis toxin, an inhibitor of G-protein-mediated signal transduction from a number of membrane receptors was found to inhibit activation-dependent sticking of lymphocytes to HEV without affecting rolling along HEV. Interestingly, lymphocyte sticking was observed to occur within 1 to 3 seconds of rolling, illustrating the rapidity with which activation events can occur.

The importance of β_2 integrins in the firm adhesion of phagocytes, and, hence, in phagocyte emigration is established by LAD type I syndrome. As discussed previously, patients with this disorder have deficient or absent expression of CD11/CD18 because of heterogeneous mutations in the β_2 (CD18) subunit.¹⁸⁵ Neutrophils and monocytes from these patients fail to migrate to skin windows or skin chambers and surgical biopsies of inflammatory sites are devoid of neutrophils.^{185,208} Studies in vitro initially demonstrated that stimulated neutrophil adhesion to endothelium under static conditions was dependent on CD11/CD18,¹⁹⁹ and observations by intravital microscopy showed that administration of CD18 MoAbs prevented neutrophil sticking without affecting rolling.^{323,371}

Although neutrophil and, to some extent, monocyte emigration is defective in LAD type I, lymphocytes, eosinophils, and plasma cells are able to emigrate to tissue.¹⁸⁵ Moreover, cell-mediated immunity appears to remain relatively intact. From these observations it was apparent that an alternative adhesion pathway(s) existed. Studies in vitro^{158,162,163,195,212} identified the β_1 integrin VLA-4 and its endothelial ligand VCAM-1 as a candidate pathway of CD11/CD18-independent firm adherence. More recently, blocking VLA-4 or VCAM-1 MoAbs have been shown to inhibit lymphocyte,³⁷²⁻³⁷⁵ monocyte,²⁰⁹ and eosinophil³⁷⁶ emigration in vivo. Although intravital microscopy studies have not been reported, it seems likely that inhibition of leukocyte emigration observed with the blocking VLA-4 or VCAM-1 MoAbs is caused in large part by a reduction in leukocyte adhesion.

Finally, $\alpha_4\beta_7$ binding to MAdCAM-1 has recently been identified as an adhesion pathway involved in lymphocyte homing to mucosal lymphoid tissue. By analogy to other integrin-Ig-like ligand interactions, it is presumed that activated $\alpha_4\beta_7$ will promote firm adhesion to MAdCAM-1 on mucosal HEV.

Recent studies provide compelling evidence in support of the current paradigm in which selectin-carbohydrate interactions initiate low-affinity adhesion, and subsequent activation-induced engagement of integrins with endothelial Ig-like ligands promotes firm adhesion.³⁷⁷ In these studies, the relative contribution of selectin and β_2 integrin was determined by intravital microscopy using fluorescein-labeled neutrophils from a normal donor, an LAD type I patient, and an LAD type II patient. Labeled cells were observed during interactions with venules in the peritoneum of rabbits treated with IL-1 to induce E-selectin (and likely the L-selectin ligand and perhaps P-selectin as well). Neutrophils from the LAD type I patient showed normal rolling, but were unable to stick and emigrate upon chemotactic stimulation. Neutrophils from the LAD type II patient rolled poorly, and failed to stick and emigrate under the shear forces provided by flow. The minimal residual rolling observed with LAD type II cells may have resulted from interaction of normal L-selectin protein with a normally fucosylated ligand on rabbit endothelium. However, when flow was reduced LAD type II cells adhered and emigrated in response to a chemoattractant. Thus, under conditions of flow (ie, with shear force) selectin binding to SLe^x or related fucosylated carbohydrate structures is essential for rolling, and is prerequisite for subsequent integrin-mediated sticking and emigration.³⁷⁷

Leukocyte Transmigration

Many of the leukocytes that are tightly bound to endothelium next crawl over the luminal surface, a process that requires reversible adhesion, ie, cyclic modulation of integrin receptor avidity.^{378,379} Upon encountering an intercellular junction some of the migratory leukocytes then squeeze between endothelial cells to enter extravascular tissue. The term "transmigration" has been used broadly to describe the process of leukocyte migration *across* endothelium from the luminal to the abluminal surface, or, more narrowly, to specify the actual penetration or diapedesis of leukocytes *between* endothelial cells. Migration *across* endothelial monolayers involves adherence to endothelium, movement over the endothelial luminal surface, and often some component of migration through subendothelial matrix in addition to penetration between endothelial cells. The distinction between the broad and narrow use of the term is important because many more adhesion molecules are involved in migration *across* endothelium than in diapedesis *between* endothelial cells.

Transendothelial migration has been studied in a number of in vitro models using endothelial cells grown on nitrocellulose or polycarbonate filters, glass coverslips, collagen gels, or amniotic membranes.³⁸⁰ It is important to note that most of these assays assess transmigration in the broader sense of net movement across endothelium rather than specific penetration between endothelial cells. Migration across endothelium has been assessed in these assays under basal, unactivated conditions (spontaneous) or in response to a chemotactic gradient or cytokine-treatment of the endothelium. Generally, there is little spontaneous migration of neutrophils or eosinophils, but monocytes,³⁸¹ lymphocytes,³⁸²⁻³⁸⁴ and NK cells³⁸⁵ exhibit significant migration across unstimulated monolayers. With chemotactic stimulation, there is a marked increase in neutrophil^{199,344,386,387} and eosinophil^{311,388} transmigration. Pretreatment of endothelial monolayers with IL-1 or TNF- α also promotes neutrophil,³⁸⁹⁻³⁹³ monocyte,^{392,394} and eosinophil³⁹⁵⁻³⁹⁷ transmigration. For neutrophils, endothelial-associated PAF³⁹⁸ and endothelial-derived IL-8^{344,398} have been reported to play an important role in promoting diapedesis by activating (PAF) and guiding (IL-8) the neutrophil. Interestingly, endothelial cytosolic-free calcium was shown to regulate neutrophil transmigration in that clamping of endothelial intracellular calcium with a cell-permeant calcium buffer inhibited neutrophil migration across endothelium without affecting adherence.³⁹⁹

Numerous studies have examined the adhesion molecules involved in transmigration. The profound defect in neutrophil emigration observed in LAD type I syndrome suggested that CD11/CD18 may be involved in neutrophil transmigration as well as adherence. Early studies showed that neutrophils from LAD type I patients or normal neutrophils treated with a blocking CD18 MoAb were unable to migrate across endothelial monolayers in response to a chemotactic stimulus.¹⁹⁹ Subsequently, both CD11a/CD18 and CD11b/CD18 subunits were shown to be involved in transmigration in response to a chemotactic gradient.⁴⁰⁰ Chemoattractant-stimulated eosinophil migration across endothelial monolayers

was also found to be largely CD11/CD18-dependent.³¹¹ CD11/CD18 also was reported to contribute significantly to spontaneous migration of monocytes,³⁸¹ lymphocytes,³⁸³ and NK cells.³⁸⁵

Several studies have established that CD11/CD18 and, to a lesser extent, ICAM-1 are important determinants of neutrophil transmigration across cytokine-activated endothelium. Pretreatment of neutrophils with a blocking MoAb against CD18 inhibited the majority (~75% to 95%) of transendothelial migration by neutrophils on 4-hour IL-1-treated endothelium.^{201,392,400-402} Whether CD11a/CD18 or CD11b/CD18 predominates in the interaction of the β_2 leukocyte integrins with ICAM-1 during neutrophil migration is uncertain.^{201,391,400,401} However, MoAbs against ICAM-1 alone were noted to inhibit only a portion of neutrophil migration.^{391,400} The combination of E-selectin and ICAM-1 MoAbs was observed to be additive in their inhibition of neutrophil transendothelial migration on activated endothelium.^{391,392} Additive inhibition was also observed when MoAbs against CD11b/CD18 and ICAM-1 were combined.⁴⁰⁰ It has been suggested that these findings may be explained by upregulation of CD11b on initial binding of neutrophils to E-selectin on IL-1-activated endothelium at 4 hours (but not 24 hours).^{391,403,404} Because there is likely an unidentified endothelial ligand for CD11b/CD18^{202,241} that could circumvent ICAM-1-dependent migration, the combination of E-selectin (blocking upregulation of CD11b/CD18) and ICAM-1 (inhibiting CD11a-dependent migration) MoAbs would thus totally inhibit CD18-dependent migration.

As discussed previously, eosinophils, mononuclear phagocytes, and lymphocytes are present in surgical biopsies from LAD type I patients.¹⁸⁵ Studies of monocyte^{392,394} and eosinophil^{395,405} transmigration in vitro have shown that both E-selectin and VCAM-1 are involved. Treatment of endothelium with IL-1, IL-4, or TNF- α increased eosinophil migration for greater than 24 to 48 hours.⁴⁰⁵ Although an anti-ICAM-1 MoAb alone inhibited 24% of IL-1 or TNF- α -induced eosinophil migration, the combination of anti-E-selectin, anti-VCAM-1, and anti-ICAM-1 MoAbs produced additive inhibition of transmigration.³⁹⁵ Similar results were obtained for monocyte migration across IL-1-activated endothelium³⁹² where the combination of a CD18 MoAb with MoAbs against VLA-4 (CD49d) and E-selectin prevented 68% of monocyte migration, whereas the CD18 MoAb alone inhibited by only 51%.

The involvement of VCAM-1 in lymphocyte transendothelial migration remains to be shown definitively. Studies of lymphocyte migration on IL-1-activated endothelium have shown that a CD18 MoAb alone inhibited the majority of migration.⁴⁰⁶ Studies using an anti-VCAM-1 MoAb alone³⁸² or a CD49d MoAb alone found little or no inhibition in lymphocyte transmigration.³⁸³ However, in view of the additive inhibition of transendothelial migration produced by blocking eosinophil and monocyte binding to both VCAM-1 and E-selectin in vitro and the synergistic inhibition of mononuclear leukocyte emigration produced by combined treatment with CD18 and CD49d MoAbs in vivo,²⁰⁹ the role of VCAM-1 in lymphocyte migration remains to be clarified

in studies using combinations of MoAbs. Also, because VLA-4 binds to the CS-1 fragment of fibronectin that can be expressed on vascular lumen,²⁴³ it will be necessary to use MoAbs directed to VCAM-1 rather than CD49d, the α chain of VLA-4, to define the role of VCAM-1 in lymphocyte transmigration.

As noted previously, most transmigration assays assess some component of leukocyte migration through matrix components deposited by endothelium as well as adherence to and diapedesis between endothelial cells. Accordingly, in some studies transmigration was inhibited by MoAbs to the fibronectin receptor VLA-5 ($\alpha_5\beta_1$, CD49e/CD29) and the laminin receptor VLA-6 ($\alpha_6\beta_1$, CD49f/CD29)³⁹² and to the CS-1 fragment of fibronectin.³¹¹

In most assays it is difficult to distinguish between the contribution of a particular adhesion protein to adherence to endothelium versus diapedesis between endothelial cells during the process of transmigration. Because adherence to endothelium is prerequisite for subsequent diapedesis and transmigration, agents that inhibit adherence will also reduce diapedesis between endothelial cells and transmigration. However, studies have shown that only about half of neutrophils contacting the apical surface of endothelium eventually transmigrate under maximal stimulation.³⁸⁰ Thus, adherence alone is necessary, but not sufficient, for subsequent diapedesis between endothelial cells. The fact that neutrophil transmigration was inhibited by CD18 and ICAM-1 MoAbs, even when adherence was presumably dependent upon E-selectin,³⁸⁹ suggests that the interaction of CD11/CD18 with

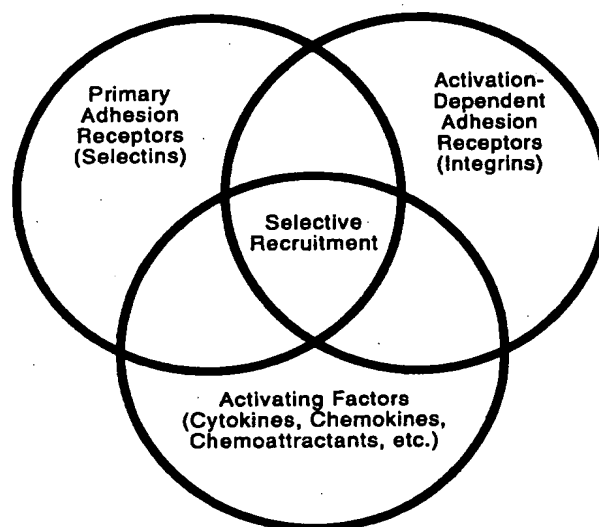


Fig 4. Selective recruitment of leukocyte subtypes. The selective recruitment of subpopulations of circulating leukocytes to sites of inflammation or immune reaction (eg, eosinophils to the lung in asthma) is a combinatorial process involving the coordinated interaction of various primary (selectin) and activation-dependent (integrin) adhesion receptors with different inflammatory stimuli (cytokines, chemokines, and chemoattractants) that activate leukocyte subtypes and/or endothelial cells.

Table 1. Animal Models of Anti-Adhesion Therapy. Models in Which Neutrophils Mediate Inflammation

MoAb Used	Observation
1. Ischemia/reperfusion	
ICAM-1	Reduced neurologic deficit with pretreatment in spinal cord ischemia/reperfusion but not irreversible ischemia ⁴²¹
ICAM-1	Reduced neurologic deficit with pretreatment in stroke model ⁴²²
ICAM-1	Pretreatment or posttreatment in burn model improved microvascular perfusion in zone of stasis ⁴²³
ICAM-1	Pretreatment of pulmonary artery occlusion decreased neutrophil accumulation in reperfused lung ⁴²⁴
ICAM-1	Pretreatment in myocardial ischemia-reperfusion decreased neutrophil accumulation in ischemic area ^{425,426}
ICAM-1	Partial inhibition of human neutrophil recruitment in perfused lung model ⁴²⁷
ICAM-1	Decreased neutrophilic infiltration, pulmonary hemorrhage and increased capillary permeability following limb ischemia/reperfusion injury ⁴²⁸
P-selectin	Prevented vascular leak and tissue injury following partial ear transection ⁴²⁹
P-selectin	Decreased myocardial necrosis ⁴³⁰
L-selectin	Decreased myocardial necrosis and neutrophilic infiltration ⁴³¹
2. Acute inflammation	
ICAM-1	Prevention of Shwartzman response ^{432,433}
ICAM-1	No inhibition of neutrophil recruitment in antigen-induced acute pulmonary inflammation ⁴³⁴
ICAM-1	Decreased neutrophil recruitment in a model of phorbol ester-induced inflammation ⁴³⁵
ICAM-1	Partial inhibition of neutrophil recruitment in complement-mediated acute lung injury ^{436,437}
ICAM-1	Decreased leukocyte recruitment in models of IgG- and IgA-immune complex-induced acute pulmonary inflammation ⁴³⁷
P-selectin	Decreased neutrophil recruitment in model of complement-mediated acute lung injury ⁴³⁸
E-selectin	Decreased accumulation of neutrophils in model of IgG immune complex-mediated lung injury ⁴³⁹
E-selectin	Decreased accumulation of total leukocytes and neutrophils in model of antigen-induced acute pulmonary inflammation ⁴³⁴
E-selectin	Failed to decrease leukocytic infiltration in model of colitis ⁴⁴⁰
L-selectin	Decreased neutrophil migration into inflamed peritoneum ^{244,336}
L-selectin	Decreased neutrophil migration into inflamed skin ⁴⁴¹
L-selectin	Decreased neutrophil migration into inflamed lung ⁴⁴¹
PECAM-1	Decreased neutrophil migration into inflamed lung, peritoneum and skin xenograft ¹⁸³

For reviews of anti-adhesion therapy directed to CD11/CD18, see refs 185, 196, and 313.

ICAM-1 may also play a role in neutrophil diapedesis between endothelial cells.

Recent studies *in vitro* indicate that both leukocyte and endothelial PECAM-1 (CD31) are directly involved in the process of neutrophil and monocyte diapedesis between endothelial cells.¹⁸¹ In these studies an anti-PECAM-1 MoAb or recombinant soluble PECAM-1 blocked neutrophil and monocyte migration across cytokine-activated endothelial monolayers. Most importantly, light and electron microscopy showed that leukocytes blocked in transmigration by the anti-PECAM-1 MoAb remained bound to the endothelial surface over the intercellular junction, thus clearly defining the role of PECAM-1 in diapedesis between endothelial cells versus adherence to endothelial cells. The fact that pretreatment of either the neutrophil or the endothelial cell was effective suggested that there was a homophilic interaction between leukocyte and endothelial PECAM-1 molecules, although other mechanisms (eg, bridging via binding to a soluble molecule, heterophilic binding to a shared ligand on both cells, or an indirect signaling) were not excluded.¹⁸¹

Consistent with the *in vitro* findings, polyclonal antibodies to PECAM-1 were shown to inhibit neutrophil emigration to inflammatory sites *in vivo*.¹⁸³ Proposed roles of PECAM-1 in transmigration between endothelial cells include possible function as a direct adhesion molecule, establishment of a haptotactic gradient to direct migration through the junction, activation of CD11/CD18 by signaling, and maintenance of

a permeability barrier.¹⁸¹ Because PECAM-1 is expressed only on a subpopulation of T cells,¹⁷⁸ the molecules involved in the penetration of other lymphocytes between endothelial cells remain to be defined.^{181,182}

SELECTIVE LEUKOCYTE RECRUITMENT

Experimental models of inflammation have shown that the recruitment of leukocyte subtypes follows a characteristic temporal sequence. Intradermal injection of chemotaxins or LPS induces an influx of neutrophils that peaks within 4 hours with minimal additional accumulation of neutrophils at 24 hours postinjection.^{407,408} In contrast, mononuclear leukocytes become the predominant leukocyte subtype by 12 hours postinjection, and continue to be recruited for at least 24 hours.^{408,409} By 48 hours postinjection the inflammatory infiltrate consists almost entirely of mononuclear leukocytes.⁴⁰⁸

In addition to the pattern of early emigration of neutrophils versus the late accumulation of mononuclear leukocytes in inflammation, there is often selective recruitment of a leukocyte subtype in inflammatory or immune reactions. The most striking example is the marked accumulation of eosinophils at extravascular sites of allergic reactions, eg, the nasal mucosa in allergic rhinitis or alveolar spaces in asthma, although eosinophils represent only a small percentage of circulating leukocytes. Also, in synovial tissue in rheumatoid arthritis⁴¹⁰ and in skin involved with inflammatory dermatoses⁴¹¹ there

Table 2. Animal Models of Anti-Adhesion Therapy. Models In Which Mononuclear Leukocytes Mediate Inflammation

MoAb Used	Observation
1. Organ transplantation	
ICAM-1	Partial prevention of rejection in cardiac allograft ⁴⁴²⁻⁴⁴⁵
ICAM-1	Partial prevention of renal allograft rejection ⁴⁴⁶
VCAM-1	Prevention of graft rejection in cardiac allograft ^{447,448}
VLA-4	Slight prolongation of cardiac allograft survival ^{449,450}
VLA-4	Decreased leukocyte infiltration and vasculitis in cardiac allograft ⁴⁴⁹
2. Autoimmune/chronic inflammatory disorder	
ICAM-1	Partial inhibition of leukocyte recruitment in collagen- or adjuvant-induced arthritis ^{451,452}
ICAM-1	Partial inhibition of mononuclear leukocyte recruitment in antiglomerular basement membrane form of glomerulonephritis ⁴⁵³
ICAM-1	Decreased leukocytic infiltration and suppressed the development of experimental autoimmune encephalitis (EAE) ⁴⁵⁴
ICAM-1	Decreased the development of active, but not passively transferred, EAE ⁴⁵⁵
ICAM-1	When administered with CD11a MoAb, prevented progression of crescentic glomerulonephritis ⁴⁵⁶
ICAM-1	Reduced leukocytic infiltration and proteinuria in model of autoimmune nephritis ⁴⁵⁷
ICAM-1	Partial reduction in number of mononuclear leukocytes at site of delayed-type hypersensitivity (DTH) reaction ⁴⁵⁸
VCAM-1	Decreased leukocyte entry into CNS in EAE model ³⁷⁴
VLA-4	Decreased migration to sites of DTH reaction ^{372,459,460}
VLA-4	Decreased lymphocyte accumulation into arthritic joints ³⁷²
VLA-4	Decreased leukocytic infiltration in model of colitis ⁴⁴⁰
VLA-4	Decreased accumulation of leukocytes in model of EAE ³⁷⁵
L-selectin	Decreased lymphocyte migration to sites of DTH reaction ⁴⁶¹
Models in Which Eosinophils Mediate Inflammation	
ICAM-1	Decreased accumulation of eosinophils in model of antigen-induced asthma ⁴⁶²
ICAM-1	No inhibition of eosinophil recruitment in primate model of asthma unless animals were withdrawn from dexamethasone ⁴⁶³
VLA-4	Decreased late phase airway hyperresponsiveness after antigen challenge ⁴⁶⁴
VLA-4	Decreased eosinophilic infiltration in passive cutaneous anaphylaxis reaction ³⁷⁶

For reviews of anti-adhesion therapy directed to CD11/CD18, see refs 185, 196, and 313.

is a preponderance of memory T cells that do not reflect their frequency in peripheral blood.

One possible mechanism to account for the selective recruitment of leukocyte subtypes is the expression of a specific combination of endothelial adhesion molecules that will preferentially bind certain leukocyte, ie, an endothelial 'area code' in the inflamed systemic vasculature analogous to an addressin in lymphoid tissue. This possibility is supported by the observation that endothelial adhesion proteins exhibit some specificity, eg, VCAM-1 binds mononuclear leukocytes but not neutrophils, E-selectin binds phagocytes but only a subset of memory T cells, and P-selectin binds phagocytes, NK cells, and some memory T but not B lymphocytes. However, the repertoire of known endothelial adhesion proteins in the systemic vasculature is somewhat limited, and analysis of tissue shows that several or all of the endothelial proteins may be expressed at sites of inflammation. More likely, additional levels of control are required to produce selective recruitment.

A model of leukocyte-endothelial cell recognition has been proposed that emphasizes combinatorial strategies to achieve diversity and specificity.^{23,324,325} There are three key components in this model as first proposed by Butcher³²⁴: primary adhesion receptors (selectins), activating factors or triggers, and activation-dependent adhesion receptors (integrins) (Fig 4). Given the limited number of known selectin-carbohydrate and integrin-Ig-like ligand interactions avail-

able and the redundancy of their expression in vivo, the major increment in the specificity and diversity in this model arises from the plethora of potential triggering molecules. Activating factors include the following: (1) cytokines and inflammatory mediators that induce expression of selectins and their ligands (eg, IL-1 and TNF- α for E-selectin, L-selectin ligand, and P-selectin); (2) cytokines that induce expression of endothelial ligands for leukocyte integrins (eg, TNF- α and IL-1 for ICAM-1 and VCAM-1; IFN- γ for ICAM-1; IL-4 for VCAM-1); and (3) chemoattractants, lipid mediators, and cytokines that activate integrin receptors. Chemoattractants include peptides such as C5a and formyl peptides that activate phagocytes, and, particularly, the expanding chemokine family of chemoattractant proteins⁴¹² that are able to attract leukocyte subtypes preferentially (eg, IL-8 for neutrophils and lymphocytes, RANTES for monocytes, eosinophils and memory T cells, and MCP-1 for monocytes). Lipid mediators that act as trigger molecules include leukotrienes and PAF for phagocytes. Among the cytokines are many that modulate leukocyte adhesive function including TNF- α ,^{413,414} GM-CSF,^{402,415-417} MCP-1,⁴¹⁸ IL-3,⁴¹⁷ and IL-5.^{396,419}

The three selectins and their multiple carbohydrate ligands and the five integrins and their Ig-like ligands, together with the dozen or more triggering molecules, provide for sufficient combinatorial diversity to allow selective recruitment of leukocyte subclasses.^{324,325} For example, both neutrophils

and monocytes bind to the induced L-selectin ligand, P-selectin, E-selectin, and ICAM-1. Even when all of these endothelial adhesion molecules are expressed, selective recruitment of neutrophils should occur if IL-8 is the major local chemoattractant. Similarly, monocytes should accumulate preferentially when MCP-1 predominates. The traffic of eosinophils to sites of allergic reaction might result from the generation of IL-3, IL-4, IL-5, and GM-CSF by T_H2 cells.⁴²⁰ As discussed previously, IL-4 induces VCAM-1 but not E-selectin, and would therefore augment the emigration of eosinophils and mononuclear leukocytes but not neutrophils that lack VLA-4. Selective activation of eosinophil integrins by IL-5 or other cytokines or chemokines would promote their adherence and transmigration, leading to eosinophil accumulation.

Experimental support for this combinatorial model will come from in vivo studies correlating the recruitment of leukocyte subclasses with the local expression of endothelial adhesion molecules, cytokines, and chemokines.

ANTI-ADHESION THERAPY IN ANIMAL MODELS OF HUMAN DISEASE STATES

In the past several years there have been numerous reports describing the systemic administration of MoAbs to inhibit leukocyte adhesion to endothelium in models of inflammation or immune reaction. The majority of these "anti-adhesion" studies have involved the use of MoAbs directed against CD11a, CD11b, or CD18 because these were some of the first reagents to be developed. Prior reviews have listed the results of these studies,^{18,185,196,313} and they will not be reiterated in this article. Instead, Tables 1 and 2 focus on animal models involving anti-adhesion therapy directed to endothelial adhesion proteins and leukocyte adhesion proteins other than CD11/CD18.

Animal models of human diseases in which neutrophils play a dominant role include models of ischemia/reperfusion and acute inflammation (Table 1). In the former, vascular occlusion initiates endothelial damage that is subsequently exacerbated after reperfusion by activation of the inflammatory system and the adherence of neutrophils.

Animal models of disorders in which mononuclear leukocytes play a dominant role include organ transplantation with allograft rejection and chronic inflammatory disorders (eg, models of rheumatoid arthritis and demyelinating diseases) (Table 2).

Although most studies have used MoAbs to block leukocyte adherence to endothelium, other specific approaches have been tested in vivo. An L-selectin-Ig chimera was shown to inhibit early neutrophil accumulation in inflamed mouse peritoneum.³³⁵ More recently, an SLe^x-oligosaccharide was shown to inhibit cobra venom factor- and IgG-induced acute lung injury in rat models and myocardial reperfusion injury in the cat.⁴⁶⁶⁻⁴⁶⁸ Other potential approaches to specific "anti-adhesion" therapy that will likely soon be tested in in vivo models include blocking peptides (eg,⁴⁶⁹⁻⁴⁷⁶), soluble integrin receptors, antisense oligonucleotides,^{477,478} and drugs that selectively block the signaling pathways involved in the induction of endothelial adhesion proteins or the modulation of

integrin avidity. Given the therapeutic potential, additional strategies will undoubtedly emerge.

SUMMARY

In the 9 years since the last review on leukocyte and endothelial interactions was published in this journal many of the critical structures involved in leukocyte adherence to and migration across endothelium have been elucidated. With the advent of cell and molecular biology approaches, investigations have progressed from the early descriptions by intravital microscopy and histology, to functional and immunologic characterization of adhesion molecules, and now to the development of genetically deficient animals^{154,210,340,479} and the first phase I trial of "anti-adhesion" therapy in humans.⁴⁶⁵ The molecular cloning and definition of the adhesive functions of the leukocyte integrins, endothelial members of the Ig gene superfamily, and the selectins has already provided sufficient information to construct an operative paradigm of the molecular basis of leukocyte emigration. The regulation of these adhesion molecules by chemoattractants, cytokines, or chemokines, and the interrelationships of adhesion pathways need to be examined in vitro and, particularly, in vivo. Additional studies are required to dissect the contribution of the individual adhesion molecules to leukocyte emigration in various models of inflammation or immune reaction. Certainly, new adhesion structures will be identified, and the current paradigm of leukocyte emigration will be refined. The promise of new insights into the biology and pathology of the inflammatory and immune response, and the potential for new therapies for a wide variety of diseases assures that this will continue to be an exciting area of investigation.

NOTE ADDED IN PROOF

Since the submission and revision of this manuscript the crystal structure of E-selectin has been reported (Graves et al: *Nature* 367:532, 1994). Mutagenesis studies of the lectin region confirmed the importance of arginine 97 and lysine 113 in ligand binding.

ACKNOWLEDGMENT

We gratefully acknowledge the numerous investigators who contributed to the studies cited in this review. We thank Barbara Schwartz for critically reviewing this manuscript and Andrew Blair for preparation of the figures.

REFERENCES

1. Harlan JM: Leukocyte-endothelial interactions. *Blood* 65:513, 1985
2. Travis J: Biotech gets a grip on cell adhesion. *Science* 260:906, 1993
3. Gallatin WM, Weissman IL, Butcher EC: A cell-surface molecule involved in organ-specific homing of lymphocytes. *Nature* 304:30, 1983
4. Berendt AR, Simmons DL, Tansey J, Newbold CI, Marsh K: Intercellular adhesion molecule-1 is an endothelial cell adhesion receptor for *Plasmodium falciparum*. *Nature* 341:57, 1989
5. Ockenhouse CF, Tegoshi T, Maeno Y, Benjamin C, Ho M, Kan KE, Thway Y, Win K, Aikawa M, Lobb RR: Human vascular endothelial cell adhesion receptors for *Plasmodium falciparum*-infected erythrocytes: Roles for endothelial leukocyte adhesion mole-

cule 1 and vascular cell adhesion molecule 1. *J Exp Med* 176:1183, 1992

6. Staunton DE, Merluzzi VJ, Rothlein R, Barton R, Marlin SD, Springer TA: A cell adhesion molecule, ICAM-1, is the major surface receptor for rhinoviruses. *Cell* 56:849, 1989

7. Greve JM, Davis G, Meyer AM, Forte CP, Connolly-Yost S, Marlor CW, Kamarck ME, McClelland A: The major human rhinovirus receptor is ICAM-1. *Cell* 56:839, 1989

8. Albelda SM: Biology of disease: Role of integrins and other cell adhesion molecules in tumor progression and metastasis. *Lab Invest* 68:4, 1993

9. Miyake K, Weissman IL, Greenberger JS, Kincade PW: Evidence for a role of the integrin VLA-4 in lymphopoiesis. *J Exp Med* 173:599, 1991

10. Miyake K, Medina K, Ishihara K, Kimoto M, Auerbach R, Kincade PW: A VCAM-1-like adhesion molecule on murine bone marrow stromal cells mediates binding of lymphoid precursors in culture. *J Cell Biol* 114:557, 1991

11. Simmons PJ, Masinovsky B, Longnecker BM, Berenson R, Torok-Storb B, Gallatin WM: Vascular cell adhesion molecule-1 expressed by bone marrow stromal cells mediates the binding of hematopoietic progenitor cells. *Blood* 80:388, 1992

12. Teixeira J, Hemler ME, Greenberger JS, Anklesaria P: Role of β_1 and β_2 integrins in the adhesion of human CD34⁺ stem cells to bone marrow stroma. *J Clin Invest* 90:358, 1992

13. Schwartz MA: Transmembrane signalling by integrins. *Trends Cell Biol* 2:304, 1992

14. Hynes RO: Integrins: Versatility, modulation, and signaling in cell adhesion. *Cell* 69:11, 1992

15. Damsky CH, Werb Z: Signal transduction by integrin receptors for extracellular matrix: Cooperative processing of extracellular information. *Curr Opin Cell Biol* 4:772, 1992

16. Zimmerman GA, Prescott SM, McIntyre TM: Endothelial cell interactions with granulocytes: Tethering and signaling molecules. *Immunol Today* 13:93, 1992

17. Picker LJ: Mechanisms of lymphocyte homing. *Curr Opin Immunol* 4:277, 1992

18. Makgoba MW, Bernard A, Sanders ME: Cell adhesion/signaling: Biology and clinical applications. *Eur J Clin Invest* 22:443, 1992

19. Shimizu Y, Newman W, Tanaka Y, Shaw S: Lymphocyte interactions with endothelial cells. *Immunol Today* 13:106, 1992

20. Hogg N, Landis RC: Adhesion molecules in cell interactions. *Curr Opin Immunol* 5:383, 1993

21. Cronstein BN, Weissmann G: The adhesion molecules of inflammation. *Arthritis Rheum* 36:147, 1993

22. Arnaout MA: Cell adhesion molecules in inflammation and thrombosis: Status and prospects. *Am J Kidney Dis* 21:72, 1993

23. Springer TA: Traffic signals for lymphocyte recirculation and leukocyte emigration: The multistep paradigm. *Cell* 76:301, 1994

24. Bevilacqua MP, Nelson RM, Mannori G, Cecconi O: Endothelial-leukocyte adhesion molecules in human disease. *Annu Rev Med* 45:361, 1994

25. Gearing AJH, Newman W: Circulating adhesion molecules in disease. *Immunol Today* 14:506, 1993

26. Gowans JL, Knight EJ: The route of recirculation of lymphocytes in the rat. *Proc R Soc Lond (Biol)* 159:257, 1964

27. Berg EL, Goldstein LA, Jutila MA, Nakache M, Picker LJ, Streeter PR, Wu NW, Zhou D, Butcher EC: Homing receptors and vascular addressins: Cell adhesion molecules that direct lymphocyte traffic. *Immunol Rev* 108:5, 1989

28. Stamper HB Jr, Woodruff JJ: Lymphocyte homing into lymph nodes: In vitro demonstration of the selective affinity of recirculating lymphocytes for high endothelial venules. *J Exp Med* 144:828, 1976

29. Streeter PR, Rouse BTN, Butcher EC: Immunohistologic and

functional characterization of a vascular addressin involved in lymphocyte homing into peripheral lymph nodes. *J Cell Biol* 107:1853, 1988

30. Streeter PR, Berg EL, Rouse BTN, Bargatze RF, Butcher EC: A tissue-specific endothelial cell molecule involved in lymphocyte homing. *Nature* 331:41, 1988

31. Jalkanen S, Steere A, Fox R, Butcher EC: A distinct endothelial cell recognition system that controls lymphocyte traffic into inflamed synovium. *Science* 233:556, 1986

32. Picker LJ, Kishimoto TK, Smith CW, Warnock RA, Butcher EC: ELAM-1 is an adhesion molecule for skin-homing T cells. *Nature* 349:796, 1991

33. Berg EL, Robinson MK, Warnock RA, Butcher EC: The human peripheral lymph node vascular addressin is a ligand for LECAM-1, the peripheral lymph node homing receptor. *J Cell Biol* 114:343, 1991

34. Holzmann B, McIntyre BW, Weissman IL: Identification of a murine Peyer's patch-specific lymphocyte homing receptor as an integrin molecule with an α chain homologous to human VLA-4 α . *Cell* 56:37, 1989

35. Berlin C, Berg EL, Briskin MJ, Andrew DP, Kilshaw PJ, Holzmann B, Weissman IL, Hamann A, Butcher EC: $\alpha_4\beta_1$ integrin mediates lymphocyte binding to the mucosal vascular addressin MAdCAM-1. *Cell* 74:185, 1993

36. Bevilacqua MP, Nelson RM: Selectins. *J Clin Invest* 91:379, 1993

37. Lasky LA: Selectins: Interpreters of cell-specific carbohydrate information during inflammation. *Science* 258:964, 1992

38. Watson ML, Kingsmore SF, Johnston GI, Siegelman MH, Le Beau MM, Lemons RS, Bora NS, Howard TA, Weissman IL, McEver RP, Seldin MF: Genomic organization of the selectin family of leukocyte adhesion molecules on human and mouse chromosome 1. *J Exp Med* 172:263, 1990

39. Collins T, Williams A, Johnston GI, Kim J, Eddy R, Shows T, Gimbrone MA, J Bevilacqua MP: Structure and chromosomal location of the gene for endothelial-leukocyte adhesion molecule 1. *J Biol Chem* 266:2466, 1991

40. Bevilacqua MP, Pober JS, Mendrick DL, Cotran RS, Gimbrone MA Jr: Identification of an inducible endothelial-leukocyte adhesion molecule. *Proc Natl Acad Sci USA* 84:9238, 1987

41. Bevilacqua MP, Stengelin S, Gimbrone MA Jr, Seed B: Endothelial leukocyte adhesion molecule 1: An inducible receptor for neutrophils related to complement regulatory proteins and lectins. *Science* 243:1160, 1989

42. Hession C, Osborn L, Goff D, Chi-Rosso G, Vassallo C, Pask M, Pittack C, Tizard R, Goelz S, McCarthy K, Hopple S, Lobb R: Endothelial leukocyte adhesion molecule 1: Direct expression cloning and functional interactions. *Proc Natl Acad Sci USA* 87:1673, 1990

43. Polte T, Newman W, Gopal TV: cDNA for endothelial leukocyte adhesion molecule 1 (ELAM-1): Sequence differences. *Nucleic Acids Res* 18:1083, 1990

44. Pearse BMF: Receptors compete for adaptors found in plasma membrane coated pits. *EMBO J* 7:3331, 1988

45. von Asmuth EJU, Smeets EF, Ginsel LA, Onderwater JJM, Leeuwenberg JFM, Buurman WA: Evidence for endocytosis of E-selectin in human endothelial cells. *Eur J Immunol* 22:2519, 1992

46. Becker-Andre M, van Huijsduijnen RH, Losberger C, Whelan J, Delamarier JF: Murine endothelial leukocyte-adhesion molecule-1 is a close structural and functional homologue of the human protein. *Eur J Biochem* 206:401, 1992

47. Weller A, Isenmann S, Vestweber D: Cloning of the mouse endothelial selectins: Expression of both E- and P-selectin is inducible by tumor necrosis factor. *J Biol Chem* 267:15176, 1992

48. Larigan JD, Tsang TC, Rumberger JM, Burns DK: Character-

ization of cDNA and genomic sequences encoding rabbit ELAM-1: Conservation of structure and functional interactions with leukocytes. *DNA Cell Biol* 11:149, 1992

49. Pigott R, Needham LA, Edwards RM, Walker C, Power C: Structural and functional studies of the endothelial activation antigen endothelial leukocyte adhesion molecule-1 using a panel of monoclonal antibodies. *J Immunol* 147:130, 1991

50. Erbe DV, Wolitzky BA, Presta LG, Norton CR, Ramos RJ, Burns DK, Rumberger JM, Narasinga Rao BN, Foxall C, Brandley BK, Lasky LA: Identification of an E-selectin region critical for carbohydrate recognition and cell adhesion. *J Cell Biol* 119:215, 1992

51. Lasky LA: Lectin cell adhesion molecules (LEC-CAMS): A new family of cell adhesion proteins involved with inflammation. *J Cell Biochem* 45:139, 1991

52. Jutila MA, Watts G, Walcheck B, Kansas GS: Characterization of a functionally important and evolutionarily well-conserved epitope mapped to the short consensus repeats of E-selectin and L-selectin. *J Exp Med* 175:1565, 1992

53. Hsu-Lin SC, Berman CL, Furie BC, August D, Furie B: A platelet membrane protein expressed during platelet activation and secretion. *J Biol Chem* 259:9121, 1984

54. McEver RP, Martins MN: A monoclonal antibody to a membrane glycoprotein binds only to activated platelets. *J Biol Chem* 259:9799, 1984

55. McEver RP, Beckstead JH, Moore KL, Marshall-Carlson L, Bainton DF: GMP-140, a platelet α -granule membrane protein, is also synthesized by vascular endothelial cells and is localized in Weibel-Palade bodies. *J Clin Invest* 84:92, 1989

56. Bonfanti R, Furie BC, Furie B, Wagner DD: PADGEM (GMP-140) is a component of Weibel-Palade bodies of human endothelial cells. *Blood* 73:1109, 1989

57. Stenberg PE, McEver RP, Shuman MA, Jacques YV, Bainton DF: A platelet α -granule membrane protein (GMP-140) is expressed on the plasma membrane after activation. *J Cell Biol* 101:880, 1985

58. Berman CL, Yeo EL, Wencel-Drake JD, Furie BC, Ginsberg MH, Furie B: A platelet α granule membrane protein that is associated with the plasma membrane after activation. *J Clin Invest* 78:130, 1986

59. Johnston GI, Cook RG, McEver RP: Cloning of GMP-140, a granule membrane protein of platelets and endothelium: Sequence similarity to proteins involved in cell adhesion and inflammation. *Cell* 56:1033, 1989

60. Johnston GI, Kurosky A, McEver RP: Structural and biosynthetic studies of the granule membrane protein, GMP-140, from human platelets and endothelial cells. *J Biol Chem* 264:1816, 1989

61. Crovello CS, Furie BC, Furie B: Rapid phosphorylation and selective dephosphorylation of P-selectin accompanies platelet activation. *J Biol Chem* 268:14590, 1993

62. Fujimoto T, McEver RP: The cytoplasmic domain of P-selectin is phosphorylated on serine and threonine residues. *Blood* 82:1758, 1993

63. Johnston GI, Bliss GA, Newman PJ, McEver RP: Structure of the human gene encoding granule membrane protein-140, a member of the selectin family of adhesion receptors for leukocytes. *J Biol Chem* 265:21381, 1990

64. Dunlop LC, Skinner MP, Bendall LJ, Favalaro EJ, Castaldi PA, Gorman JJ, Gamble JR, Vadas MA, Berndt MC: Characterization of GMP-140 (P-selectin) as a circulating plasma protein. *J Exp Med* 175:1147, 1992

65. Sanders WE, Wilson RW, Ballantyne CM, Beaudet AL: Molecular cloning and analysis of in vivo expression of murine P-selectin. *Blood* 80:795, 1992

66. Strubel NA, Nguyen M, Kansas GS, Tedder TF, Bischoff J: Isolation and characterization of a bovine cDNA encoding a func-

tional homolog of human P-selectin. *Biochem Biophys Res Commun* 192:338, 1993

67. Erbe DV, Watson SR, Presta LG, Wolitzky BA, Foxall C, Brandley BK, Lasky LA: P- and E-selectin use common sites for carbohydrate ligand recognition and cell adhesion. *J Cell Biol* 120:1227, 1993

68. Hollenbaugh D, Bajorath J, Stenkamp R, Aruffo A: Interaction of P-selectin and its cellular ligand: Analysis of critical residues. *Biochemistry* 32:2960, 1993

69. Lewisohn DM, Bargatze RF, Butcher EC: Leukocyte-endothelial cell recognition: Evidence of a common molecular mechanism shared by neutrophils, lymphocytes, and other leukocytes. *J Immunol* 138:4313, 1987

70. Tedder TF, Isaacs CM, Ernst TJ, Demetri GD, Adler DA, Distech CM: Isolation and chromosomal localization of cDNAs encoding a novel human lymphocyte cell surface molecule, LAM-1. Homology with the mouse lymphocyte homing receptor and other human adhesion proteins. *J Exp Med* 170:123, 1989

71. Camerini D, James SP, Stamenkovic I, Seed B: Leu-8/TQ 1 is the human equivalent of the Mel-14 lymph node homing receptor. *Nature* 342:78, 1989

72. Siegelman MH, Weissman IL: Human homologue of mouse lymph node homing receptor: Evolutionary conservation at tandem cell interaction domains. *Proc Natl Acad Sci USA* 86:5562, 1989

73. Bowen BR, Nguyen T, Lasky LA: Characterization of a human homologue of the murine peripheral lymph node homing receptor. *J Cell Biol* 109:421, 1989

74. Siegelman MH, van de Rijn M, Weissman IL: Mouse lymph node homing receptor cDNA clone encodes a glycoprotein revealing tandem interaction domains. *Science* 243:1165, 1989

75. Lasky LA, Singer MS, Yednock TA, Dowbenko D, Fennie C, Rodriguez H, Nguyen T, Stachel S, Rosen SD: Cloning of a lymphocyte homing receptor reveals a lectin domain. *Cell* 56:1045, 1989

76. Watanabe T, Song Y, Hirayama Y, Tamatani T, Kuida K, Miyasaka M: Sequence and expression of a rat cDNA for LECAM-1. *Biochim Biophys Acta* 1131:321, 1992

77. Walcheck B, White M, Kurk S, Kishimoto TK, Jutila MA: Characterization of the bovine peripheral lymph node homing receptor: A lectin cell adhesion molecule (LECAM). *Eur J Immunol* 22:469, 1992

78. Kishimoto TK, Jutila MA, Butcher EC: Identification of a human peripheral lymph node homing receptor: A rapidly down-regulated adhesion molecule. *Proc Natl Acad Sci USA* 87:2244, 1990

79. Kansas GS, Spertini O, Stoolman LM, Tedder TF: Molecular mapping of functional domains of the leukocyte receptor for endothelium, LAM-1. *J Cell Biol* 114:351, 1991

80. Siegelman MH, Cheng IC, Weissman IL, Wakeland EK: The mouse lymph node homing receptor is identical with the lymphocyte cell surface marker Ly-22: Role of the EGF domain in endothelial binding. *Cell* 61:611, 1990

81. Watson SR, Imai Y, Fennie C, Geoffrey J, Singer M, Rosen SD, Lasky LA: The complement binding-like domains of the murine homing receptor facilitate lectin activity. *J Cell Biol* 115:235, 1991

82. Kishimoto TK, Jutila MA, Berg EL, Butcher EC: Neutrophil Mac-1 and MEL-14 adhesion proteins inversely regulated by chemotactic factors. *Science* 245:1238, 1989

83. Jutila MA, Rott L, Berg EL, Butcher EC: Function and regulation of the neutrophil MEL-14 antigen *in vivo*: Comparison with LFA-1 and MAC-1. *J Immunol* 143:3318, 1989

84. Griffin JD, Spertini O, Ernst TJ, Belvin MP, Levine HB, Kanakura Y, Tedder TF: Granulocyte-macrophage colony-stimulating factor and other cytokines regulate surface expression of the

leukocyte adhesion molecule-1 on human neutrophils, monocytes, and their precursors. *J Immunol* 145:576, 1990

85. Jung TM, Dailey MO: Rapid modulation of homing receptors (gp90^{MEL-14}) induced by activators of protein kinase C: Receptor shedding due to accelerated proteolytic cleavage at the cell surface. *J Immunol* 144:3130, 1990

86. Schleiffenbaum B, Spertini O, Tedder TF: Soluble L-selectin is present in human plasma at high levels and retains functional activity. *J Cell Biol* 119:229, 1992

87. Yednock TA, Rosen SD: Lymphocyte homing. *Adv Immunol* 44:313, 1989

88. Kuijpers TW: Terminal glycosyltransferase activity: A selective role in cell adhesion. *Blood* 81:873, 1993

89. Lowe JB, Stoolman LM, Nair RP, Larsen RD, Berhend TL, Marks RM: ELAM-1-dependent cell adhesion to vascular endothelium determined by a transfected human fucosyltransferase. *Cell* 63:475, 1990

90. Phillips ML, Nudelman E, Gaeta FCA, Perez M, Singhal AK, Hakomori SI, Paulson JC: ELAM-1 mediates cell adhesion by recognition of a carbohydrate ligand, sialyl-Le^x. *Science* 250:1130, 1990

91. Walz G, Aruffo A, Kolanus W, Bevilacqua M, Seed B: Recognition by ELAM-1 of the sialyl-Le^x determinant on myeloid and tumor cells. *Science* 250:1132, 1990

92. Goelz SE, Hession C, Goff D, Griffiths B, Tizard R, Newman B, Chi-Rosso G, Lobb R: ELFT: A gene that directs the expression of an ELAM-1 ligand. *Cell* 63:1349, 1990

93. Tiemeyer M, Swiedler SJ, Ishihara M, Moreland M, Schwein-gruber H, Hirtzer P, Brandley BK: Carbohydrate ligands for endothelial-leukocyte adhesion molecule-1. *Proc Natl Acad Sci USA* 88:1138, 1991

94. Berg EL, Magnani J, Warnock RA, Robinson MK, Butcher EC: Comparison of L-selectin and E-selectin ligand specificities: The L-selectin can bind the E-selectin ligands sialyl Le^x and sialyl Le^a. *Biochem Biophys Res Commun* 184:1048, 1992

95. Tyrell D, James P, Rao N, Foxall C, Abbas S, Dasgupta F, Nashed M, Hasegawa A, Kiso M, Asa D, Kidd J, Brandley BK: Structural requirements for the carbohydrate ligand of E-selectin. *Proc Natl Acad Sci USA* 88:10372, 1991

96. Nelson RM, Dolich S, Aruffo A, Cecconi O, Bevilacqua MP: Higher affinity oligosaccharide ligands for E-selectin. *J Clin Invest* 91:1157, 1993

97. Munro JM, Lo SK, Corless C, Robertson MJ, Lee NC, Barnhill RL, Weinberg DS, Bevilacqua MP: Expression of sialyl-Lewis^x, an E-selectin ligand, in inflammation, immune processes, and lymphoid tissues. *Am J Pathol* 141:1397, 1992

98. Ohmori K, Yoneda T, Ishihara G, Shigeta K, Hirashima K, Kanai M, Itai S, Sasaki T, Aril S, Arita H, Kannagi R: Sialyl SSEA-1 antigen as a carbohydrate marker on human natural killer cells and immature lymphoid cells. *Blood* 74:255, 1989

99. Pinola M, Renkonen R, Majuri M-L, Tiisala S, Saksela E: Characterization of the E-selectin ligand on NK cells. *J Immunol* 152:3586, 1994

100. Ohmori K, Takada A, Yoneda T, Buma Y, Hirashima K, Tsuyuka K, Hasegawa A, Kannagi R: Differentiation-dependent expression of sialyl stage-specific embryonic antigen-1 and I-antigens on human lymphoid cells and its implications for carbohydrate-mediated adhesion to vascular endothelium. *Blood* 81:101, 1993

101. Berg EL, Yoshino T, Rott LS, Robinson MK, Warnock RA, Kishimoto TK, Picker LJ, Butcher EC: The cutaneous lymphocyte antigen is a skin lymphocyte homing receptor for the vascular lectin endothelial cell-leukocyte adhesion molecule-1. *J Exp Med* 174:1461, 1991

102. Berg EL, Robinson MK, Mansson O, Butcher EC, Magnani JL: A carbohydrate domain common to both sialyl Le^x and sialyl

Le^a is recognized by the endothelial cell leukocyte adhesion molecule ELAM-1. *J Biol Chem* 266:14869, 1991

103. Larsen E, Palabrica T, Sajer S, Gilbert GE, Wagner DD, Furie BC, Furie B: PADGEM-dependent adhesion of platelets to monocytes and neutrophils is mediated by a lineage-specific carbohydrate, LNF III (CD15). *Cell* 63:467, 1990

104. Handa K, Neudelman ED, Stroud MR, Shiozawa T, Hakomori S: Selectin GMP-140 (CD62; PADGEM) binds to sialosyl-Le^x and sialosyl-Le^a, and sulfated glycans modulate this binding. *Biochem Biophys Res Commun* 181:1223, 1991

105. Polley MJ, Phillips ML, Wayner E, Nudelman E, Singhal AK, Hakomori SI, Paulson JC: CD62 and endothelial cell-leukocyte adhesion molecule-1 (ELAM-1) recognize the same carbohydrate ligand, sialyl Lewis^x. *Proc Natl Acad Sci USA* 88:6224, 1991

106. Zhou Q, Moore KL, Smith DF, Varki A, McEver R, Cummings RD: The selectin GMP-140 binds to sialylated, fucosylated lactosaminoglycans on both myeloid and non-myeloid cells. *J Cell Biol* 115:557, 1991

107. Foxall C, Watson SR, Dowbenko D, Fennie C, Lasky LA, Kiso M, Hasegawa A, Asa D, Brandley BK: The three members of the selectin receptor family recognize a common carbohydrate epitope, the sialyl Lewis^x oligosaccharide. *J Cell Biol* 117:895, 1992

108. Aruffo A, Kolanus W, Walz G, Freedman P, Seed B: CD62/P-selectin recognition of myeloid and tumor sulfatides. *Cell* 67:35, 1991

109. Todderud G, Alford J, Millsap KA, Aruffo A, Trampusch KM: PMN binding to P-selectin is inhibited by sulfatide. *J Leukoc Biol* 52:85, 1992

110. Needham LK, Schnaar RL: The HNK-1 reactive sulfoglucuronidyl glycolipids are ligands for L-selectin and P-selectin but not E-selectin. *Proc Natl Acad Sci USA* 90:1359, 1993

111. Skinner MP, Fournier DJ, Andrews RK, Gorman JJ, Chesterman CN, Berndt MC: Characterization of human platelet GMP-140 as a heparin-binding protein. *Biochem Biophys Res Commun* 164:1373, 1989

112. Etzioni A, Frydman M, Pollack S, Avidor I, Phillips ML, Paulson JC, Gershon-Baruch R: Brief report: Recurrent severe infections caused by a novel leukocyte adhesion deficiency. *N Engl J Med* 327:1789, 1992

113. Anderson DC, Schmalstieg FC, Finegold MJ, Hughes BJ, Rothlein R, Miller LJ, Kohl S, Tosi MF, Jacobs RL, Waldrop TC, Goldman AS, Shearer WT, Springer TA: The severe and moderate phenotypes of heritable Mac-1, LFA-1 deficiency: Their quantitative definition and relation to leukocyte dysfunction and clinical features. *J Inf Dis* 152:668, 1985

114. Green PJ, Tamatani T, Watanabe T, Miyasaka M, Hasegawa A, Kiso M, Yuen CT, Stoll MS, Feizi T: High affinity binding of the leukocyte adhesion molecule L-selectin to 3'-sulphated-Le^x and -Le^a oligosaccharides and the predominance of sulphate in this interaction demonstrated by binding studies with a series of lipid-linked oligosaccharides. *Biochem Biophys Res Commun* 188:244, 1992

115. Sawada M, Takada A, Ohwaki I, Takahashi N, Tateno H, Sakamoto J, Kannagi R: Specific expression of a complex sialyl Lewis X antigen on high endothelial venules of human lymph nodes: Possible candidate for L-selectin ligand. *Biochem Biophys Res Commun* 193:337, 1993

116. Imai Y, Lasky LA, Rosen SD: Sulphation requirement for Glycam-1, an endothelial ligand for L-selectin. *Nature* 361:555, 1993

117. Yednock TA, Butcher EC, Stoolman LM, Rosen SD: Receptors involved in lymphocyte homing: Relationship between a carbohydrate-binding receptor and the MEL-14 antigen. *J Cell Biol* 104:725, 1987

118. Imai Y, True DD, Singer MS, Rosen SD: Direct demonstration of the lectin activity of gp^{90mel}, a lymphocyte homing receptor. *J Cell Biol* 11:1225, 1990

119. Norgard-Sumnicht KE, Varki NM, Varki A: Calcium-dependent heparin-like ligands for L-selectin in non-lymphoid endothelial cells. *Science* 261:480, 1993
120. Picker LJ, Warnock RA, Burns AR, Doerschuk CM, Berg EL, Butcher EC: The neutrophil selectin LECAM-1 presents carbohydrate ligands to the vascular selectins ELAM-1 and GMP-140. *Cell* 66:921, 1991
121. Kishimoto TK, Warnock RA, Jutila MA, Butcher EC, Lane C, Anderson DC, Smith CW: Antibodies against human neutrophil LECAM-1 (LAM-1/Leu-8/Dreg-56 antigen) and endothelial cell ELAM-1 inhibit a common CD18-independent adhesion pathway in vitro. *Blood* 78:805, 1991
122. Kuijpers TW, Hoogerwerf M, van der Laan LJW, Nagel G, van der Schoot CE, Grunert F, Roos D: CD66 nonspecific cross-reacting antigens are involved in neutrophil adherence to cytokine-activated endothelial cells. *J Cell Biol* 118:457, 1992
123. Kotovuroi P, Tontti E, Pigott R, Sheperd M, Kiso M, Hasegawa A, Renkonen R, Nortamo P, Altieri DC, Gahmberg CG: The vascular E-selectin binds to the leukocyte integrins CD11/CD18. *Glycobiology* 3:131, 1993
124. Larsen GR, Sako D, Ahern TJ, Shaffer M, Erban J, Sajer SA, Gibson RM, Wagner DD, Furie BC, Furie B: P-selectin and E-selectin: distinct but overlapping leukocyte ligand specificities. *J Biol Chem* 267:11104, 1992
125. Steininger CN, Eddy CA, Leimgruber RM, Mellors A, Welly JK: The glycoprotease of *Pasturella haemolytica* A1 eliminates binding of myeloid cells to P-selectin but not E-selectin. *Biochem Biophys Res Commun* 188:760, 1992
126. Ushiyama S, Laue TM, Moore KL, Erickson HP, McEver RP: Structural and functional characterization of monomeric soluble P-selectin and comparison with membrane P-selectin. *J Biol Chem* 268:15229, 1993
127. Levinovitz A, Muhlhoff J, Isenmann S, Vestweber D: Identification of a glycoprotein ligand for E-selectin on mouse myeloid cells. *J Cell Biol* 121:449, 1993
128. Lenter M, Levinovitz A, Isenmann S, Vestweber D: Monospecific and common glycoprotein ligands for E- and P-selectin on myeloid cells. *J Cell Biol* 125:471, 1994
129. Norgard KE, Moore KL, Diaz S, Stults NL, Ushiyama S, McEver RP, Cummings RD, Varki A: Characterization of a specific ligand for P-selectin on myeloid cells: A minor glycoprotein with sialylated O-linked oligosaccharides. *J Biol Chem* 268:12764, 1993
130. Moore KL, Varki A, McEver RP: GMP-140 binds to a glycoprotein receptor on human neutrophils: Evidence for a lectin-like interaction. *J Cell Biol* 112:491, 1991
131. Moore KL, Stults NL, Diaz S, Smith DF, Cummings RD, Varki A, McEver RP: Identification of a specific glycoprotein ligand for P-selectin (CD62) on myeloid cells. *J Cell Biol* 118:445, 1992
132. Sako D, Chang X-J, Barone KM, Vachino G, White HM, Shaw G, Veldman GM, Bean KM, Ahern TJ, Furie B, Cumming DA, Larsen GR: Expression cloning of a functional glycoprotein ligand for P-selectin. *Cell* 75:1179, 1993
133. Lasky LA, Singer MS, Dowbenko D, Imai Y, Henzel WJ, Grimley C, Fennie C, Gillet N, Watson SR, Rosen SD: An endothelial ligand for L-selectin is a novel mucin-like molecule. *Cell* 69:927, 1992
134. Dowbenko D, Andalibi A, Young PE, Lusic AJ, Lasky LA: Structure and chromosomal localization of the murine gene encoding glycamin-1: A mucin-like endothelial ligand for L-selectin. *J Biol Chem* 268:4525, 1993
135. Shimizu Y, Shaw S: Mucins in the mainstream. *Nature* 366:630, 1993
136. Brusteim M, Kraal G, Mebius RE, Watson SR: Identification of a soluble form of a ligand for the lymphocyte homing receptor. *J Exp Med* 176:1415, 1992
137. Dowbenko D, Watson SR, Lasky LA: Cloning of a rat homologue of mouse Glycam-1 reveals conservation of structural domains. *J Biol Chem* 268:14399, 1993
138. Baumhueter S, Singer MS, Henzel W, Hemmerich S, Renz M, Rosen SD, Lasky LA: Binding of L-selectin to the vascular sialomucin, CD34. *Science* 262:436, 1993
139. Williams AF, Barclay AN: The immunoglobulin superfamily. *Annu Rev Immunol* 6:381, 1988
140. Katz FE, Parkar M, Stanley K, Murray LJ, Clark EA, Greaves MF: Chromosome mapping of cell membrane antigens expressed on activated B cells. *Eur J Immunol* 15:103, 1985
141. Staunton DE, Marlin SD, Stratowa C, Dustin ML, Springer TA: Primary structure of ICAM-1 demonstrates interaction between members of the immunoglobulin and integrin supergene families. *Cell* 52:925, 1988
142. Simmons D, Makgoba MW, Seed B: ICAM, an adhesion ligand of LFA-1, is homologous to the neural cell adhesion molecule NCAM. *Nature* 331:624, 1988
143. Staunton DE, Dustin ML, Erickson HP, Springer TA: The arrangement of the immunoglobulin-like domains of ICAM-1 and the binding sites for LFA-1 and rhinovirus. *Cell* 61:243, 1990
144. Kirchhausen T, Staunton DE, Springer TA: Location of the domains of ICAM-1 by immunolabeling and single-molecule electron microscopy. *J Leukoc Biol* 53:342, 1993
145. Diamond MS, Staunton DE, Marlin SD, Springer TA: Binding of the integrin Mac-1 (CD11b/CD18) to the third immunoglobulin-like domain of ICAM-1 (CD54) and its regulation by glycosylation. *Cell* 65:961, 1991
146. Rothlein R, Dustin ML, Marlin SD, Springer TA: A human intercellular adhesion molecule (ICAM-1) distinct from LFA-1. *J Immunol* 137:1270, 1986
147. Dustin ML, Rothlein R, Bhan AF, Dinarello CA, Springer TA: A natural adherence molecule (ICAM-1): induction by IL-1 and IFN- γ , tissue distribution, biochemistry, and function. *J Immunol* 137:245, 1986
148. Pober JSM, Gimbrone MA, Jr., Lapierre LA, Mendrick DL, Fiers W, Rothlein R, Springer TA: Overlapping patterns of human endothelial cells by interleukin 1, tumor necrosis factor, and immune interferon. *J Immunol* 137:1893, 1986
149. Carpen O, Pallai P, Staunton DE, Springer TA: Association of intercellular adhesion molecule-1 (ICAM-1) with actin-containing cytoskeleton and α -actinin. *J Cell Biol* 118:1223, 1992
150. Mimura N, Asano A: Further characterization of a conserved actin-binding 27-kDa fragment of actinogelin and alpha-actinins and mapping of their binding sites on the actin molecule by chemical crosslinking. *J Biol Chem* 262:4717, 1987
151. Siu G, Hedrick SM, Brian AA: Isolation of the murine intercellular adhesion molecule-1 (ICAM-1) gene: ICAM-1 enhances antigen-specific T cell activation. *J Immunol* 143:3813, 1989
152. Kita Y, Takashi T, Iigo Y, Tamatani T, Miyasaka M, Horiuchi T: Sequence and expression of rat ICAM-1. *Biochim Biophys Acta* 1131:108, 1992
153. Smith WC, Entman ML, Lane CL, Beaudet AL, Ty TI, Youker K, Hawkins HK, Anderson DC: Adherence of neutrophils to canine cardiac myocytes in vitro is dependent on intercellular adhesion molecule-1. *J Clin Invest* 88:1216, 1991
154. Sligh JE, Ballantyne CM, Rich SS, Hawkins HK, Smith CW, Bradley A, Beaudet AL: Inflammatory and immune responses are impaired in mice deficient in intercellular adhesion molecule 1. *Proc Natl Acad Sci USA* 90:8529, 1993
155. Hogg N, Bates PA, Harvey J: Structure and function of intercellular adhesion molecule-1. *Chem Immunol* 50:98, 1991
156. Staunton DE, Dustin ML, Springer TA: Functional cloning of ICAM-2, a cell adhesion ligand for LFA-1 homologous to ICAM-1. *Nature* 339:61, 1989

157. Xu H, Tong IL, de Fougerolles A, Springer TA: Isolation, characterization, and expression of mouse ICAM-2 complementary and genomic DNA. *J Immunol* 149:2650, 1992
158. Osborn L, Hession C, Tizard R, Vassallo C, Luhowsky S, Chi-Rosso G, Lobb R: Direct expression cloning of vascular cell adhesion molecule 1, a cytokine-induced endothelial protein that binds to lymphocytes. *Cell* 59:1203, 1989
159. Polte T, Newman W, Gopal TV: Full length vascular cell adhesion molecule 1 (VCAM-1). *Nucleic Acids Res* 18:5901, 1990
160. Hession C, Tizard R, Vassallo C, Schiffer SB, Goff D, Moy P, Chi-Rosso G, Luhowsky S, Lobb R, Osborn L: Cloning of an alternate form of vascular cell adhesion molecule-1 (VCAM-1). *J Biol Chem* 266:6682, 1991
161. Cybulsky MI, Fries JW, Williams AJ, Sultan P, Davis VM, Gimbrone MA Jr, Collins T: Alternative splicing of human VCAM-1 in activated vascular endothelium. *Am J Pathol* 138:815, 1991
162. Rice GE, Munro JM, Bevilacqua MP: Inducible cell adhesion molecule 110 (INCAM-110) is an endothelial receptor for lymphocytes: A CD11/CD18-independent adhesion mechanism. *J Exp Med* 171:1369, 1990
163. Carlos TM, Schwartz BR, Kovach NL, Yee E, Rosa M, Osborn L, Chi-Rosso G, Newman B, Lobb R, Harlan JM: Vascular cell adhesion molecule-1 (VCAM-1) mediates lymphocyte adherence to cytokine-activated cultured human endothelial cells. *Blood* 76:965, 1990
164. Pepinsky B, Hession C, Chen L-L, Moy P, Burkly L, Jakubowski A, Chow EP, Benjamin C, Chi-Rosso G, Luhowsky S, Lobb R: Structure/function studies on vascular cell adhesion molecule-1. *J Biol Chem* 267:17820, 1992
165. Osborn L, Vassallo C, Benjamin CD: Activated endothelium binds lymphocytes through a novel binding site in the alternatively spliced domain of vascular cell adhesion molecule-1. *J Exp Med* 176:99, 1992
166. Hession C, Moy P, Tizard R, Chisholm P, Williams C, Wisk M, Burkly L, Miyake K, Kincade P, Lobb R: Cloning of murine and rat vascular cell adhesion molecule-1. *Biochem Biophys Res Commun* 183:163, 1992
167. Williams AJ, Atkins RC, Fries JW, Gimbrone MA Jr, Cybulsky MI, Collins T: Nucleotide sequence of rat vascular cell adhesion molecule-1 cDNA. *Biochim Biophys Acta* 1131:214, 1992
168. Terry RW, Kwee L, Levine JF, Labow MA: Cytokine induction of an alternatively spliced murine vascular cell adhesion molecule (VCAM) mRNA encoding a glycosylphosphoinositol-anchored VCAM protein. *Proc Natl Acad Sci USA* 90:5919, 1993
169. Moy P, Lobb R, Tizard R, Olson D, Hession C: Cloning of an inflammation-specific phosphatidyl inositol-linked form of murine vascular cell adhesion molecule-1. *J Biol Chem* 268:8835, 1993
170. Hahne M, Lenter M, Jager U, Vestweber D: A novel soluble form of mouse VCAM-1 is generated from a glycolipid-anchored splicing variant. *Eur J Immunol* 24:421, 1994
171. Briskin MJ, McEvoy LM, Butcher EC: MAdCAM-1 has homology to immunoglobulin and mucin-like adhesion receptors and to IgA1. *Nature* 363:461, 1993
172. Nakache M, Berg EL, Streeter PR, Butcher EC: The mucosal vascular addressin is a tissue-specific endothelial cell adhesion molecule for circulating lymphocytes. *Nature* 337:179, 1989
173. Berg EL, McEvoy LM, Berlin C, Bargatze RF, Butcher EC: L-selectin-mediated lymphocyte rolling on MAdCAM-1. *Nature* 366:695, 1993
174. Simmons DL, Walker C, Power C, Pigott R: Molecular cloning of CD31, a putative intercellular adhesion molecule closely related to carcinoembryonic antigen. *J Exp Med* 171:2147, 1990
175. Newman PJ, Berndt MC, Gorski J, White GC II, Lyman S, Paddock C, Muller WA: PECAM-1 (CD31) cloning and relation to adhesion molecules of the immunoglobulin gene superfamily. *Science* 247:1219, 1990
176. Stockinger H, Gadd SJ, Eher R, Majdic O, Schreiber W, Kasinrek W, Strass B, Schnabl E, Knapp W: Molecular characterization and functional analysis of the leukocyte surface protein CD31. *J Immunol* 145:3889, 1990
177. Albelda SM, Muller WA, Buck CA, Newman PJ: Molecular and cellular properties of PECAM-1 (EndoCAM/CD31): A novel vascular cell-cell adhesion molecule. *J Cell Biol* 114:1059, 1991
178. Tanaka Y, Albelda SM, Horgan KJ, van Seventer GA, Shimizu Y, Newman W, Hallam J, Newman PJ, Buck CA, Shaw S: CD31 expressed on distinctive T cell subsets is a preferential amplifier of $\beta 1$ integrin-mediated adhesion. *J Exp Med* 176:245, 1992
179. Benichou S, Fuks A, Jothy S, Beauchemin N, Shirota K, Stanners CP: Carcinoembryonic antigen, a human tumor marker, functions as an intercellular adhesion molecule. *Cell* 57:327, 1989
180. Muller WA, Berman ME, Newman PJ, DeLisser HM, Albelda SM: A heterophilic adhesion molecule for platelet/endothelial cell adhesion molecule-1 (CD31). *J Exp Med* 175:1401, 1992
181. Muller WA, Weigl SA, Deng X, Phillips DM: PECAM-1 is required for transendothelial migration of leukocytes. *J Exp Med* 178:449, 1993
182. Bird IN, Spragg JH, Ager A, Mathews N: Studies of lymphocyte transendothelial migration: analysis of migrated cell phenotypes with regard to CD31 (PECAM-1), CD45RA and CD45RO. *Immunology* 80:553, 1993
183. Vaporciyan AA, DeLisser HM, Yan H-C, Mendiguren II, Thom SR, Jones ML, Ward PA, Albelda SM: Involvement of platelet-endothelial cell adhesion molecule-1 in neutrophil recruitment in vivo. *Science* 262:1580, 1993
184. Smyth SS, Joneckis CC, Parise LV: Regulation of vascular integrins. *Blood* 81:2827, 1993
185. Kishimoto TK, Anderson DC: The role of integrins in inflammation, in Gallin JI, Goldstein IM, Snyderman R (eds): *Inflammation: Basic Principles and Clinical Correlates*, (ed 2). New York, NY, Raven, 1992, p 353
186. Hogg N: An integrin overview. *Chem Immunol* 50:1, 1991
187. Dransfield I: Leukocyte integrins, in Horton MA (ed): *Blood Cell Biochemistry*, vol. 5: Macrophages and Related Cells. New York, NY, Plenum, 1993, p 307
188. Diamond MS, Garcia-Aguilar J, Bickford JK, Corbi AL, Springer TA: The I domain is a major recognition site on the leukocyte integrin Mac-1 (CD11b/CD18) for four distinct adhesion ligands. *J Cell Biol* 120:1031, 1993
189. Landis RC, Bennett RI, Hogg N: A novel LFA-1 activation epitope maps to the I domain. *J Cell Biol* 120:1519, 1993
190. Michishita M, Videm V, Arnaout MA: A novel divalent cation-binding site in the A domain of the $\beta 2$ integrin CR3 (CD11b/CD18) is essential for ligand binding. *Cell* 72:857, 1993
191. Tuckwell DS, Humphries MJ: Molecular and cellular biology of integrins. *Crit Rev Oncol Hematol* 15:149, 1993
192. Leung-Hagesteijn CY, Milankov K, Michalak M, Wilkins J, Dedhar S: Cell attachment to extracellular matrix substrates is inhibited upon downregulation of expression of calreticulin, an intracellular integrin α -subunit-binding protein. *J Cell Sci* 107:589, 1994
193. O'Toole TE, Katagiri Y, Faull RJ, Peter K, Tamura R, Quaranta V, Loftus JC, Shattil SJ, Ginsberg MH: Integrin cytoplasmic domains mediate inside-out signal transduction. *J Cell Biol* 124:1047, 1994
194. Arnaout MA: Structure and function of the leukocyte adhesion molecule CD11/CD18. *Blood* 75:1037, 1990
195. Elices MJ, Osborn L, Takada Y, Crouse C, Luhowsky S, Hemler M, Lobb RR: VCAM-1 on activated endothelium interacts with the leukocyte integrin VLA-4 at a site distinct from the VLA-4/fibronectin binding site. *Cell* 60:577, 1990

196. Carlos TM, Harlan JM: Membrane proteins involved in phagocyte adherence to endothelium. *Immunol Rev* 114:5, 1990
197. Lo SK, Lee SL, Ramos RA, Lobb R, Rosa M, Chi-Rosso G, Wright SD: Endothelial-leukocyte adhesion molecule 1 stimulates the adhesive activity of leukocyte integrin CR3 (CD11b/CD18, Mac-1, $\alpha_M\beta_2$) on human neutrophils. *J Exp Med* 173:1493, 1991
198. de Fougerolles AR, Springer TA: Intercellular adhesion molecule 3, a third counter-receptor for lymphocyte function-associated molecule 1 on resting lymphocytes. *J Exp Med* 175:185, 1992
199. Harlan JM, Killen PD, Senecal FM, Schwartz BR, Yee EK, Taylor RF, Beatty PG, Price TH, Ochs HD: The role of neutrophil membrane glycoprotein GPI50 in neutrophil adherence to endothelium in vitro. *Blood* 66:167, 1985
200. Forsyth KD, Levinsky RJ: Role of the LFA-1 adhesion glycoprotein in neutrophil adhesion to endothelium and plastic surfaces. *Clin Exp Immunol* 75:265, 1989
201. Smith CW, Marlin SD, Rothlein R, Toman C, Anderson DA: Cooperative interactions of LFA-1 and Mac-1 with intercellular adhesion molecule-1 in facilitating adherence and transendothelial migration of human neutrophils in vitro. *J Clin Invest* 83:2008, 1989
202. Lo SK, van Seventer GA, Levin SM, Wright SD: Two leukocyte receptors (CD11a/CD18 and CD11b/CD18) mediate transient adhesion to endothelium by binding to different ligands. *J Immunol* 143:3325, 1989
203. Arnaout MA, Lanier LL, Faller DV: Relative contribution of the leukocyte molecules Mo1, LFA-1, and p150/95 (LeuM5) in adhesion of granulocytes and monocytes to vascular endothelium is tissue- and stimulus-specific. *J Cell Physiol* 137:305, 1988
204. Mentzer SJ, Crimmins MAV, Burakoff SJ, Faller DV: Alpha and beta subunits of the LFA-1 membrane molecule are involved in human monocyte-endothelial cell adhesion. *J Cell Physiol* 130:410, 1987
205. Te Velde AA, Keizer GD, Figdor CG: Differential function of LFA-1 family molecules (CD11 and CD18) in adhesion of human monocytes to melanoma and endothelial cells. *Immunology* 61:261, 1987
206. Dustin ML, Springer TA: Lymphocyte function-associated antigen-1 (LFA-1) interaction with intercellular adhesion molecule-1 (ICAM-1) is one of at least three mechanisms for lymphocyte adhesion to cultured endothelial cells. *J Cell Biol* 107:321, 1988
207. Shimizu Y, Newman W, Gopal TV, Horgan KJ, Graber N, Beall LD, van Seventer GA, Shaw S: Four molecular pathways of T cell adhesion to endothelial cells: Roles of LFA-1, VCAM-1, and ELAM-1 and changes in pathway hierarchy under different activation conditions. *J Cell Biol* 113:1203, 1991
208. Harlan JM: Leukocyte adhesion deficiency syndrome: insights into the molecular basis of leukocyte emigration. *Clin Immunol Immunopath* 67:S16, 1993
209. Winn RK, Harlan JM: CD18-independent neutrophil and mononuclear leukocyte emigration into the peritoneum of rabbits. *J Clin Invest* 92:1168, 1993
210. Wilson RW, Ballantyne CM, Smith CW, Montgomery C, Bradley A, O'Brien WE, Beaudet AL: Gene targeting yields a CD18-mutant mouse for study of inflammation. *J Immunol* 151:1571, 1993
211. Hemler ME: VLA proteins in the integrin family: Structures, functions, and their role on leukocytes. *Annu Rev Immunol* 8:365, 1990
212. Schwartz BR, Wayner EA, Carlos TM, Ochs HD, Harlan JM: Identification of surface proteins mediating adherence of CD11/CD18-deficient lymphoblastoid cells to cultured human endothelium. *J Clin Invest* 85:2019, 1990
213. Shimizu Y, Shaw S: Lymphocyte adhesion mediated by VLA (beta 1) integrins. *Chem Immunol* 50:34, 1991
214. Vennegoor CJGM, van de Wiel-van Kemenade E, Huijbens RJF, Sanchez-Madrid F, Melief CJM, Figdor CG: Role of LFA-1 and VLA-4 in the adhesion of cloned normal and LFA-1 (CD11/CD18)-deficient T cells to cultured endothelial cells: Indication for a new adhesion pathway. *J Immunol* 148:1093, 1992
215. Vonderheide RH, Springer TA: Lymphocyte adhesion through very late antigen 4: Evidence for a novel binding site in the alternatively spliced domain of vascular cell adhesion molecule 1 and an additional α_4 integrin counter-receptor on stimulated endothelium. *J Exp Med* 175:1433, 1992
216. van Kooyk Y, van de Wiel-van Kemenade E, Weder P, Huijbens RJF, Figdor CG: Lymphocyte function-associated antigen 1 dominates very late antigen 4 in binding of activated T cells to endothelium. *J Exp Med* 177:185, 1993
217. Carlos T, Kovach N, Schwartz B, Rosa M, Newman B, Wayner E, Benjamin C, Osborn L, Lobb R, Harlan J: Human monocytes bind to two cytokine-induced adhesive ligands on cultured human endothelial cells: endothelial-leukocyte adhesion molecule-1 and vascular cell adhesion molecule-1. *Blood* 77:2266, 1991
218. Jonjic N, Jilek P, Bernasconi S, Peri G, Martin-Padura I, Cenzuales S, Dejana E, Mantovani A: Molecules involved in the adhesion and cytotoxicity of activated monocytes on endothelial cells. *J Immunol* 148:2080, 1992
219. Dobrina A, Menegazzi R, Carlos TM, Nardon E, Cramer R, Zacchi T, Harlan JM, Patriarca P: Mechanisms of eosinophil adherence to cultured vascular endothelial cells: Eosinophils bind to the cytokine-induced endothelial ligand vascular cell adhesion molecule-1 via the very late activation antigen-4 integrin receptor. *J Clin Invest* 88:20, 1991
220. Bochner BS, Luscinskas FW, Gimbrone MA Jr, Newman W, Sterbinsky SA, Derse-Anthony CP, Klunk D, Schleimer RP: Adhesion of human basophils, eosinophils, and neutrophils to interleukin-1-activated human vascular endothelial cells: Contributions of endothelial cell adhesion molecules. *J Exp Med* 173:1553, 1991
221. Schleimer RP, Sterbinsky SA, Kaiser J, Bickel CA, Klunk DA, Tomioka K, Newman W, Luscinskas FW, Gimbrone MA, Jr, McIntyre BW, Bochner BS: IL-4 induces adherence of human eosinophils and basophils but not neutrophils to endothelium: Association with expression of VCAM-1. *J Immunol* 148:1086, 1992
222. Allavena P, Paganin C, Martin-Padura I, Peri G, Gaboli M, Dejana E, Marchisio PC, Mantovani A: Molecules and structures involved in the adhesion of natural killer cells to vascular endothelium. *J Exp Med* 173:439, 1991
223. Chan BMC, Elices MJ, Murphy E, Hemler ME: Adhesion to vascular cell adhesion molecule 1 and fibronectin: comparison of $\alpha_4\beta_1$ (VLA-4) and $\alpha_4\beta_7$ on the human B cell line JY. *J Biol Chem* 267:8366, 1992
224. Horgan KJ, Ginther Luce GE, Tanaka Y, Schweighoffer T, Shimizu Y, Sharrow SO, Shaw S: Differential expression of VLA- α_4 and VLA- β_1 discriminates multiple subsets of CD4⁺CD45RO⁺ "memory" T cells. *J Immunol* 149:4082, 1992
225. Schweighoffer T, Tanaka Y, Tidswell M, Erle DJ, Horgan KJ, Ginther Luce GE, Lazarovits AI, Buck D, Shaw S: Selective expression of integrin $\alpha_4\beta_7$ on a subset of human CD4⁺ memory T cells with hallmarks of gut-tropism. *J Immunol* 151:717, 1993
226. Klingemann H-G, Dedhar S: Distribution of integrins on human peripheral blood mononuclear cells. *Blood* 74:1348, 1989
227. Wayner EA, Garcia-Pardo A, Humphries MJ, McDonald JA, Carter WG: Identification and characterization of the T lymphocyte adhesion receptor for an alternative cell attachment domain (CS-1) in plasma fibronectin. *J Cell Biol* 109:1321, 1989
228. Garcia-Pardo A, Wayner EA, Carter WG, Ferreira OC Jr: Human B lymphocytes define an alternative mechanism of adhesion to fibronectin: the interaction of the $\alpha_4\beta_1$ integrin with LHGPEDLVPT sequence of the type III connecting segment is sufficient to promote cell attachment. *J Immunol* 144:3361, 1990
229. Guan J-L, Hynes RO: Lymphoid cells recognize an alterna-

tively spliced segment of fibronectin via the integrin receptor $\alpha_4\beta_1$. *Cell* 60:53, 1990

230. Sanchez-Aparicio P, Ferreira OC, Jr, Garcia-Pardo A: $\alpha_4\beta_1$ recognition of the Hep II domain of fibronectin is constitutive on some hemopoietic cells but requires activation on others. *J Immunol* 150:3506, 1993

231. Yabkowitz R, Dixit VM, Guo N, Roberts DD, Shimizu Y: Activated T-cell adhesion to thrombospondin is mediated by the $\alpha_4\beta_1$ (VLA-4) and $\alpha_5\beta_1$ (VLA-5) integrins. *J Immunol* 151:149, 1993

232. Ennis E, Isberg RR, Shimizu Y: Very late antigen 4-dependent adhesion and costimulation of resting human T cells by the bacterial β_1 integrin ligand invasins. *J Exp Med* 177:207, 1993

233. Wayner EA, Kovach NL: Activation-dependent recognition by hematopoietic cells of the LDV sequence in the V region of fibronectin. *J Cell Biol* 116:489, 1992

234. Bednarczyk JL, McIntyre BW: A monoclonal antibody to VLA-4 α -chain (CDw49d) induces homotypic lymphocyte aggregation. *J Immunol* 144:777, 1990

235. Campanero MR, Pulido R, Ursula MA, Rodriguez-Moya M, de Landazuri MO, Sanchez-Madrid F: An alternative leukocyte homotypic adhesion mechanism, LFA-1/ICAM-1-independent, triggered through the human VLA-4 integrin. *J Cell Biol* 110:2157, 1990

236. Bednarczyk JL, Wygant JN, Szabo MC, Molinari-Storey L, Renz M, Fong S, McIntyre BW: Homotypic leukocyte aggregation triggered by a monoclonal antibody specific for a novel epitope expressed by the integrin β_1 subunit: Conversion of nonresponsive cells by transfecting human integrin α_4 subunit cDNA. *J Cell Biochem* 51:465, 1993

237. Erle DJ, Ruegg C, Sheppard D, Pytela R: Complete amino acid sequence of an integrin β subunit (β_7) identified in leukocytes. *J Biol Chem* 266:11009, 1991

238. Jiang WM, Jenkins D, Yuan Q, Leung E, Choo KHA, Watson JD, Krissansen GW: The gene organization of the human β_7 subunit, the common β subunit of the leukocyte integrins HML-1 and LPAM-1. *Int Immunol* 4:1031, 1992

239. Ruegg C, Postigo AA, Sikorski EE, Butcher EC, Pytela R, Erle DJ: Role of integrin $\alpha_4\beta_1/\alpha_5\beta_1$ in lymphocyte adherence to fibronectin and VCAM-1 and in homotypic cell clustering. *J Cell Biol* 117:179, 1992

240. Postigo AA, Sanchez-Mateos P, Lazarovits AI, Sanchez-Madrid F, de Landazuri MO: $\alpha_4\beta_1$ integrin mediates B cell adhesion to fibronectin and vascular cell adhesion molecule-1. *J Immunol* 151:2471, 1993

241. Diamond MS, Staunton DE, de Fougères AR, Stacker SA, Garcia-Aguilar J, Hibbs ML, Springer TA: ICAM-1 (CD54): A counter-receptor for Mac-1 (CD11b/CD18). *J Cell Biol* 111:3129, 1990

242. Stacker SA, Springer TA: Leukocyte integrin p150,95 (CD11c/CD18) functions as an adhesion molecule binding to a counter-receptor on stimulated endothelium. *J Immunol* 146:648, 1991

243. Elices MJ, Tsai V, Strahl D, Goel AS, Tollefson V, Arrhenius T, Wayner EA, Gaeta FCA, Fikes JD, Firestein GS: Expression and functional significance of alternatively spliced CS1 fibronectin in rheumatoid arthritis microvasculature. *J Clin Invest* 93:405, 1994

244. Jutila MA, Berg EL, Kishimoto TK, Picker LJ, Bargatze RF, Bishop DK, Orosz CG, Wu NW, Butcher EC: Inflammation-induced endothelial cell adhesion to lymphocytes, neutrophils, and monocytes: Role of homing receptors and other adhesion molecules. *Transplantation* 48:727, 1989

245. Spertini O, Luscinskas FW, Kansas GS, Munro JM, Griffin JD, Gimbrone MA Jr, Tedder TF: Leukocyte adhesion molecule-1

(LAM-1, L-selectin) interacts with an inducible endothelial cell ligand to support leukocyte adhesion. *J Immunol* 147:2565, 1991

246. Spertini O, Luscinskas FW, Gimbrone MA, Jr, Tedder TF: Monocyte attachment to activated human vascular endothelium in vitro is mediated by leukocyte adhesion molecule-1 (L-selectin) under non-static conditions. *J Exp Med* 175:1789, 1992

247. Watson SR, Imai Y, Fennie C, Geoffroy JS, Rosen SD, Lasky LA: A homing receptor-IgG chimera as a probe for adhesive ligands of lymph node high endothelial venules. *J Cell Biol* 110:221, 1990

248. Salmi M, Jalkanen S: A 90-kilodalton endothelial cell molecule mediating lymphocyte binding in humans. *Science* 257:1407, 1992

249. Airas L, Salmi M, Jalkanen S: Lymphocyte-vascular adhesion protein-2 is a novel 70-kDa molecule involved in lymphocyte adhesion to vascular endothelium. *J Immunol* 151:4228, 1993

250. Beekhuizen H, Blokland I, Corseel-van Tilburg J, Koning F, van Furth R: CD14 contributes to the adherence of human monocytes to cytokine-stimulated endothelial cells. *J Immunol* 147:3761, 1991

251. Wright SD, Ramos RA, Tobias PS, Ulevitch RJ, Mathison JC: CD14, a receptor for complexes of lipopolysaccharide (LPS) and LPS binding protein. *Science* 249:1431, 1990

252. Beekhuizen H, Blokland I, van Furth R: Cross-linking of CD14 molecules on monocytes results in a CD11/CD18- and ICAM-1-dependent adherence to cytokine-stimulated human endothelial cells. *J Immunol* 150:950, 1993

253. Doerschuk CM, Winn RK, Coxson HO, Harlan JM: CD18-dependent and -independent mechanisms of neutrophil emigration in the pulmonary and systemic microcirculation of rabbits. *J Immunol* 144:2327, 1990

254. Hawkins HK, Heffelfinger SC, Anderson DC: Leukocyte adhesion deficiency: Clinical and post-mortem observations. *Pediatr Pathol* 12:119, 1992

255. Mileski W, Harlan J, Rice C, Winn R: Streptococcus pneumoniae-stimulated macrophages induce neutrophils to emigrate by a CD18-independent mechanism of adherence. *Circ Shock* 31:259, 1990

256. Marks R, Todd RF III, Ward PA: Rapid induction of neutrophil-endothelial adhesion by endothelial complement fixation. *Nature* 339:314, 1989

257. Vercellotti GM, Platt JL, Bach FH, Dalmasso AP: Neutrophil adhesion to xenogeneic endothelium via iC3b. *J Immunol* 146:730, 1991

258. Altieri DC, Bader R, Mannucci PM, Edgington TS: Oligospecificity of the cellular adhesion receptor Mac-1 encompasses an inducible recognition specificity for fibrinogen. *J Cell Biol* 107:1893, 1988

259. Wright SD, Weitz JI, Huang AJ, Levin SM, Silverstein SC, Loike JD: Complement receptor type 3 (CD11b/CD18) of human polymorphonuclear leukocytes recognizes fibrinogen. *Proc Natl Acad Sci USA* 85:7734, 1988

260. Languino LR, Plescia J, Duperray A, Brian AA, Plow EF, Geltosky JE, Altieri DC: Fibrinogen mediates leukocyte adhesion to vascular endothelium through an ICAM-1-dependent pathway. *Cell* 73:1423, 1993

261. Nortamo P, Li R, Renkonen R, Timonen T, Prieto J, Patarroyo M, Gahmberg CG: The expression of human intercellular adhesion molecule-2 is refractory to inflammatory cytokines. *Eur J Immunol* 21:2629, 1991

262. de Fougères AR, Stacker SA, Schwarting R, Springer TA: Characterization of ICAM-2 and evidence for a third counter-receptor for LFA-1. *J Exp Med* 174:253, 1991

263. Nortamo P, Salcedo R, Timonen T, Patarroyo M, Gahmberg CG: A monoclonal antibody to the human leukocyte adhesion mole-

- cule intercellular adhesion molecule-2: Cellular distribution and molecular characterization of the antigen. *J Immunol* 146:2530, 1991
264. Renkonen R, Paavonen T, Nortamo P, Gahmberg CG: Expression of endothelial adhesion molecules in vivo: Increased endothelial ICAM-2 expression in lymphoid malignancies. *Am J Pathol* 140:763, 1992
 265. Hattori R, Hamilton KK, Fugates RD, McEver RP, Sims PJ: Stimulated secretion of endothelial von Willebrand factor is accompanied by rapid redistribution to the cell surface of the intracellular granule membrane protein GMP-140. *J Biol Chem* 264:7768, 1989
 266. Hattori R, Hamilton KK, McEver RP, Sims PJ: Complement proteins C5b-9 induce secretion of high molecular weight multimers of endothelial von Willebrand factor and translocation of granule membrane protein GMP-140 to the cell surface. *J Biol Chem* 264:9053, 1989
 267. Lorant DE, Patel KD, McIntyre TM, McEver RP, Prescott SM, Zimmerman GA: Coexpression of GMP-140 and PAF by endothelium stimulated by histamine or thrombin: A juxtacrine system for adhesion and activation of neutrophils. *J Cell Biol* 115:223, 1991
 268. Sugama Y, Tirupathi C, Janakidevi K, Anderson TT, Fenton JW II, Malik AB: Thrombin-induced expression of endothelial P-selectin and intercellular adhesion molecule-1: A mechanism for stabilizing neutrophil adhesion. *J Cell Biol* 119:935, 1992
 269. Patel KD, Zimmerman GA, Prescott SM, McEver RP, McIntyre TM: Oxygen radicals induce human endothelial cells to express GMP-140 and bind neutrophils. *J Cell Biol* 112:749, 1991
 270. Vadas MA, Gamble JR, Khew-Goodall Y: Regulation of GMP-140 expression in endothelial cells. *J Cell Biochem* 16A:44, 1992 (abstr)
 271. Toothill VJ, van Mourik JA, Niewenhuys HK, Metzelaar MJ, Pearson JD: Characterization of the enhanced adhesion of neutrophil leukocytes to thrombin-stimulated endothelial cells. *J Immunol* 145:283, 1990
 272. Pober JS, Bevilacqua MP, Mendrick DL, LaPiere LA, Fiers W, Gimbrone MA Jr: Two distinct monokines, interleukin 1 and tumor necrosis factor, independently induce biosynthesis and transient expression of the same antigen on the surface of cultured human vascular endothelial cells. *J Immunol* 136:1680, 1986
 273. Leeuwenberg JFM, Jeunhomme TMAA, Buurman WA: Induction of an activation antigen on human endothelial cells in vitro. *Eur J Immunol* 19:715, 1989
 274. Montgomery KF, Osborn L, Hession C, Tizard R, Goff D, Vassallo C, Tarr PI, Bomszyk K, Lobb R, Harlan JM, Pohlman TH: Activation of endothelial-leukocyte adhesion molecule 1 (ELAM-1) gene transcription. *Proc Natl Acad Sci USA* 88:6523, 1991
 275. Pober JS, LaPierre LA, Stolpen AH, Brock TA, Springer TA, Fiers W, Bevilacqua MP, Mendrick DL, Gimbrone MA Jr: Activation of cultured human endothelial cells by recombinant lymphotoxin: Comparison with tumor necrosis factor and interleukin 1 species. *J Immunol* 138:3319, 1987
 276. Rice GE, Bevilacqua MP: An inducible endothelial cell surface glycoprotein mediates melanoma adhesion. *Science* 246:1303, 1989
 277. Masinovsky B, Urdal D, Gallatin WM: IL-4 acts synergistically with IL-1 β to promote lymphocyte adhesion to microvascular endothelium by induction of vascular cell adhesion molecule-1. *J Immunol* 145:2886, 1990
 278. Graber N, Gopal TV, Wilson D, Beall LD, Polte T, Newman W: T cells bind to cytokine-activated endothelial cells via a novel, inducible sialoglycoprotein and endothelial adhesion molecule-1. *J Immunol* 145:819, 1990
 279. Wellicome SM, Thornhill MH, Pitzalis C, Thomas DS, Lanchbury JSS, Panayi GS, Haskard DO: A monoclonal antibody that detects a novel antigen on endothelial cells that is induced by tumor necrosis factor, IL-1, or lipopolysaccharide. *J Immunol* 144:2558, 1990
 280. Palkama T, Majuri ML, Mattila P, Hurme M, Renkonen R: Regulation of endothelial adhesion molecules by ligands binding to the scavenger receptor. *Clin Exp Immunol* 92:353, 1993
 281. Lane TA, Lamkin GE, Wancewicz E: Modulation of endothelial cell expression of intercellular adhesion molecule-1 by protein kinase C activation. *Biochem Biophys Res Commun* 161:945, 1989
 282. Bender JR, Sadeghi MMM, Mills LK, Pardi R, Watson C: Endothelial cell adhesion molecule introduction by α -thrombin. *J Cell Biochem* 16A:15, 1992 (abstr)
 283. Shankar R, de la Motte CA, DiCorleto PE: 3-Deazaadenosine inhibits thrombin-stimulated platelet-derived growth factor production and endothelial-leukocyte adhesion molecule-1-mediated monocyte adhesion in human aortic endothelial cells. *J Biol Chem* 267:9376, 1992
 284. Huber AR, Schall TJ, Ellis SE: Thrombin induction of VCAM-1 and Rantes/Sis expression and monocyte invasion in an in vitro model of the vessel wall through a specific endothelial thrombin-receptor, G-protein coupled pathway. *Blood* 80:251a, 1992 (abstr, suppl 1)
 285. Deisher TA, Haddix TL, Montgomery KF, Pohlman TH, Harlan JM: Differential regulation of ELAM-1 and VCAM-1 expression in human umbilical vein endothelial cells by protein kinase C. *Circulation* 84:404, 1991
 286. Palluy O, Morliere L, Gris JC, Bonne C, Moda G: Hypoxia/reoxygenation stimulates endothelium to promote neutrophil adhesion. *Free Radic Biol Med* 13:21, 1992
 287. Suzuki Y, Wang W, Vu TH, Raffin TA: Effect of NADPH oxidase inhibition on endothelial cell ELAM-1 mRNA expression. *Biochem Biophys Res Commun* 184:1339, 1992
 288. Lo SK, Janakidevi K, Lai L, Malik AB: Hydrogen peroxide-induced increase in endothelial adhesiveness is dependent on ICAM-1 activation. *Am J Physiol* 264:L406, 1993
 289. Kume N, Cybulsky MI, Gimbrone MA Jr: Lysophosphatidylcholine, a component of atherogenic lipoproteins, induces mononuclear leukocyte adhesion molecules in cultured human and rabbit arterial endothelial cells. *J Clin Invest* 90:1138, 1992
 290. Thornhill MH, Haskard DO: IL-4 regulates endothelial cell activation by IL-1, tumor necrosis factor, or IFN- γ . *J Immunol* 145:865, 1990
 291. Brizzi MF, Garbarino G, Rossi PR, Pagliardi GL, Arduino C, Avanzi GC, Pegoraro L: Interleukin 3 stimulates proliferation and triggers endothelial-leukocyte adhesion molecule 1 gene activation of human endothelial cells. *J Clin Invest* 91:2887, 1993
 292. Bevilacqua MP, Pober JS, Wheeler ME, Cotran RS, Gimbrone MA Jr: Interleukin 1 acts on cultured human vascular endothelium to increase the adhesion of polymorphonuclear leukocytes, monocytes, and related leukocyte cell lines. *J Clin Invest* 76:2003, 1985
 293. Cotran RS, Gimbrone MA, Bevilacqua MP, Mendrick DL, Pober JS: Induction and detection of a human endothelial activation antigen in vivo. *J Exp Med* 164:661, 1986
 294. Munro JM, Pober JS, Cotran RS: Tumor necrosis factor and interferon- γ induce distinct patterns of endothelial activation and associated leukocyte accumulation in skin of *Papio anubis*. *Am J Pathol* 135:121, 1989
 295. Whelan J, Ghersa P, van Huijsduijnen RH, Gray J, Chandra G, Talbot F, DeLamarier JF: An NF- κ B-like factor is essential but not sufficient for cytokine induction of endothelial leukocyte adhesion molecule 1 (ELAM-1) gene transcription. *Nucleic Acids Res* 19:2645, 1991
 296. Lane TA, Wancewicz E: Transcriptional regulation of ICAM-1 expression in activated endothelial cells. *Blood* 78:107a, 1991 (abstr, suppl 1)

297. Wertheimer SJ, Myers CL, Wallace RW, Parks TP: Intercellular adhesion molecule-1 gene expression in human endothelial cells. *J Biol Chem* 267:12030, 1992
298. Leeuwenberg JFM, von Asmuth EJU, Jeunhomme TMAA, Buurman WA: IFN- γ regulates the expression of the adhesion molecule ELAM-1 and IL-6 production by human endothelial cells in vitro. *J Immunol* 145:2110, 1990
299. Doukas J, Pober JS: IFN- γ enhances endothelial activation induced by tumor necrosis factor but not by IL-1. *J Immunol* 145:1727, 1990
300. Gamble JR, Khew-Goodall Y, Vadas MA: Transforming growth factor- β inhibits E-selectin expression on human endothelial cells. *J Immunol* 150:4494, 1993
301. Gamble JR, Vadas MA: Endothelial cell adhesiveness for human T lymphocytes is inhibited by transforming growth factor- β . *J Immunol* 146:1149, 1991
302. Kapiotis S, Quehenberger P, Partan C, Eher R, Strobl H, Schwarzwinger I, Mannhalter C, Gabl F, Lechner K, Speiser W: IL-4 differentially modulates upregulation of endothelial adhesion molecules induced by IL-1, TNF and LPS. *Blood* 78:323a, 1991 (abstr, suppl 1)
303. Swerlick RA, Lee KH, Li L-J, Seep NT, Caughman SW, Lawley TJ: Regulation of vascular cell adhesion molecule 1 on human microvascular endothelial cells. *J Immunol* 149:698, 1992
304. Gerritsen ME, Kelley KA, Ligon G, Perry CA, Shen C-P, Szczepanski A, Carley WW: Regulation of the expression of intercellular adhesion molecule 1 in cultured human endothelial cells derived from rheumatoid synovium. *Arthritis Rheum* 36:593, 1993
305. Vedder NB, Harlan JM: Increased surface expression of CD11b/CD18 (Mac-1) is not required for stimulated neutrophil adherence to cultured endothelium. *J Clin Invest* 81:676, 1988
306. Hughes BJ, Hollers JC, Crockett-Torabi E, Smith CW: Recruitment of CD11b/CD18 to the neutrophil surface and adherence-dependent cell locomotion. *J Clin Invest* 90:1687, 1992
307. Ginsberg MH, Du X, Plow EF: Inside-out integrin signalling. *Curr Opin Cell Biol* 4:766, 1992
308. Sastry SK, Horwitz AF: Integrin cytoplasmic domains: mediators of cytoskeletal linkages and extra- and intracellular initiated transmembrane signaling. *Curr Opin Cell Biol* 5:819, 1993
309. Hogg N, Harvey J, Cabanas C, Landis RC: Control of leukocyte integrin activation. *Am Rev Respir Dis* 148:S55, 1993 (suppl)
310. Faull RJ, Kovach NL, Harlan JM, Ginsberg MH: Stimulation of integrin-mediated adhesion of T lymphocytes and monocytes: Two mechanisms with divergent biological consequences. *J Exp Med* 179:1307, 1994
311. Kuijpers TW, Mul EP, Blom M, Kovach NL, Gaeta FCA, Tollefson V, Elices MJ, Harlan JM: Freezing adhesion molecules in a state of high-avidity binding blocks eosinophil migration. *J Exp Med* 178:279, 1993
312. Spertini O, Kansas GS, Munro JM, Griffin JD, Tedder TF: Regulation of leukocyte migration by activation of the leukocyte adhesion molecule-1 (LAM-1) selectin. *Nature* 349:691, 1991
313. Harlan JM, Winn RK, Vedder NB, Doerschuk CM, Rice CL: In vivo models of leukocyte adherence to endothelium, in Harlan JM, Liu DY (eds): *Adhesion: Its Role in Inflammatory Disease*, New York, NY, Freeman, 1992, p 117
314. Atherton A, Born GVR: Relationship between the velocity of rolling granulocytes and that of the blood flow in venules. *J Physiol* 233:157, 1973
315. Mayrovitz HN: Leukocyte rolling: A prominent feature of venules in intact skin of anesthetized hairless mice. *Am J Physiol* 262:H157, 1992
316. Fiebig E, Ley G, Arfors K-E: Rapid leukocyte accumulation by "spontaneous" rolling and adhesion in the exteriorized rabbit mesentery. *J Microcirc Clin Exp* 10:127, 1991
317. Ley K, Gaehtgens P: Endothelial, not hemodynamic, differences are responsible for preferential leukocyte rolling in rat mesenteric venules. *Circ Res* 69:1034, 1991
318. Smith CW: Endothelial adhesion molecules and their role in inflammation. *Can J Physiol Pharmacol* 71:76, 1993
319. Tangelder GJ, Arfors KE: Inhibition of leukocyte rolling in venules by protamine and sulfated polysaccharides. *Blood* 77:1565, 1991
320. Perry MA, Granger DN: Role of CD11/CD18 in shear rate-dependent leukocyte-endothelial cell interactions in cat mesenteric venules. *J Clin Invest* 87:1798, 1991
321. Allison F Jr, Smith MR, Wood WB: Studies on the pathogenesis of acute inflammation: I. The inflammatory reaction to thermal injury as observed in the rabbit ear chamber. *J Exp Med* 102:655, 1955
322. Mayrovitz HN, Tuma RF, Wiedeman MP: Leukocyte adherence in arterioles following extravascular tissue trauma. *Microvasc Res* 20:264, 1980
323. von Andrian UH, Chambers JD, McEvoy LM, Bargatze RF, Arfors KE, Butcher EC: Two-step model of leukocyte-endothelial interaction in inflammation: distinct roles for LECAM-1 and the leukocyte β 2 integrins in vivo. *Proc Natl Acad Sci USA* 88:7538, 1991
324. Butcher EC: Leukocyte-endothelial cell recognition: three (or more) steps to specificity and diversity. *Cell* 67:1033, 1991
325. Schweighoffer T, Shaw S: Adhesion cascades: Diversity through combinatorial strategies. *Curr Opin Cell Biol* 4:824, 1992
326. Smith CW, Kishimoto TK, Abbass O, Hughes B, Rothlien R, McIntire LV, Butcher EC, Anderson DC: Chemotactic factors regulate lectin adhesion molecule 1 (LECAM-1)-dependent neutrophil adhesion to cytokine-stimulated endothelial cells in vitro. *J Clin Invest* 87:609, 1991
327. Lawrence MB, Smith CW, Eskin SG, McIntire LV: Effect of venous shear stress on CD18-mediated neutrophil adhesion to cultured endothelium. *Blood* 75:227, 1990
328. Abassi O, Lane CL, Krater S, Kishimoto TK, Anderson DC, McIntire LV, Smith CW: Canine neutrophil margination mediated by lectin adhesion molecule-1 in vitro. *J Immunol* 147:2107, 1991
329. Hallman R, Jutila MA, Smith CW, Anderson DC, Kishimoto TK, Butcher EC: The peripheral lymph node homing receptor, LECAM-1, is involved in CD-18-independent adhesion of human neutrophils to endothelium. *Biochem Biophys Res Commun* 174:236, 1991
330. Ley K, Cerrito M, Arfors K-E: Sulfated polysaccharides inhibit leukocyte rolling in rabbit mesentery venules. *Am J Physiol* 260:H1667, 1991
331. Ley K, Linnemann G, Meinen M, Stoolman LM, Gaehtgens P: Fucoidan, but not yeast polyphosphomannan PPME, inhibits leukocyte rolling in venules of the rat mesentery. *Blood* 81:177, 1993
332. Lindbom L, Xie X, Raud J, Hedqvist P: Chemoattractant-induced firm adhesion of leukocytes to vascular endothelium in vivo is critically dependent on initial leukocyte rolling. *Acta Physiol Scand* 146:415, 1992
333. Ley K, Tedder TF, Kansas GS: L-selectin can mediate leukocyte rolling in untreated mesenteric venules in vivo independent of E- and P-selectin. *Blood* 82:1632, 1993
334. Ley K, Gaehtgens P, Fennie C, Singer MS, Lasky LA, Rosen SD: Lectin-like cell adhesion molecule 1 mediates leukocyte rolling in mesenteric venules in vivo. *Blood* 77:2553, 1991
335. Watson SR, Fennie C, Lasky LA: Neutrophil influx into an inflammatory site inhibited by a soluble homing receptor-IgG chimera. *Nature* 349:164, 1991
336. von Andrian UH, Hansell P, Chambers JD, Berger EM, Filho IT, Butcher EC, Arfors K-E: L-selectin function is required for β 2-

integrin-mediated neutrophil adhesion at physiological shear rates in vivo. *Am J Physiol* 263:H1034, 1992

337. von Andrian UH, Chambers JD, Berg EL, Michie SA, Brown DA, Karolak D, Ramezani L, Berger EM, Arfors KE, Butcher EC: L-selectin mediates neutrophil rolling in inflamed venules through sialyl Lewis^x-dependent and -independent recognition pathways. *Blood* 82:182, 1993

338. Lawrence MB, Springer TA: Leukocytes roll on a selectin at physiologic flow rates: Distinction from and prerequisite for adhesion through integrins. *Cell* 65:859, 1991

339. Bienvenu K, Granger DN: Molecular determinants of shear rate-dependent leukocyte adhesion in postcapillary venules. *Am J Physiol* 266:H1504, 1993

340. Mayadas TN, Johnson RC, Rayburn H, Hynes RO, Wagner DD: Leukocyte rolling and extravasation are severely compromised in P-selectin-deficient mice. *Cell* 74:541, 1993

341. Abassi O, Kishimoto TK, McIntire LV, Anderson DC, Smith CW: E-selectin supports neutrophil rolling under conditions of flow. *J Clin Invest* 92:2719, 1993

342. Lawrence MB, Springer TA: Neutrophils roll on E-selectin. *J Immunol* 151:6338, 1993

343. Mulligan MS, Varani J, Dame MK, Lane CL, Smith CW, Anderson DC, Ward PA: Role of endothelial-leukocyte adhesion molecule 1 (ELAM-1) in neutrophil-mediated lung injury in rats. *J Clin Invest* 88:1396, 1991

344. Huber AR, Kunkel SL, Todd RF III, Weiss SJ: Regulation of transendothelial migration by endogenous interleukin-8. *Science* 254:99, 1991

345. Rot A: Endothelial cell binding of NAP-1/IL-8 role in neutrophil emigration. *Immunol Today* 13:291, 1992

346. Zimmerman GA, McIntyre TM, Mehra M, Prescott SM: Endothelial cell-associated platelet-activating factor: A novel mechanism for signaling intercellular adhesion. *J Cell Biol* 110:529, 1990

347. Tanaka Y, Adams DH, Hubscher S, Hirano H, Siebenlist U, Shaw S: T-cell adhesion induced by proteoglycan-immobilized cytokine MIP-1 β . *Nature* 361:79, 1993

348. Lund-Johansen F, Olweus J, Horejsi V, Skubitz KM, Thompson JS, Vilella R, Symington FW: Activation of human phagocytes through carbohydrate antigens (CD15, sialyl-CD15, CDw17, and CDw65). *J Immunol* 148:3221, 1992

349. Stocks SC, Kerr MA: Stimulation of neutrophil adhesion by antibodies recognizing CD15 (Le^x) and CD15-expressing carcinoembryonic antigen-related glycoprotein NCA-160. *Biochem J* 288:23, 1992

350. Forsyth KD, Simpson AC, Levinsky RJ: CD15 antibodies increase neutrophil adhesion to endothelium by an LFA-1-dependent mechanism. *Eur J Immunol* 19:1331, 1989

351. Stockl J, Majdic O, Rosenkranz A, Fiebiger E, Kniep B, Stockinger H, Knapp W: Monoclonal antibodies to the carbohydrate structure Lewis^x stimulate the adhesive activity of leukocyte integrin CD11b/CD18 (CR3, Mac-1, $\alpha_{M}\beta_2$) on human granulocytes. *J Leukoc Biol* 53:541, 1993

352. Burkly LC, Jakubowski A, Newman BM, Rosa MD, Chi-Rosso G, Lobb RR: Signaling by vascular cell adhesion molecule-1 (VCAM-1) through VLA-4 promotes CD3-dependent T cell proliferation. *Eur J Immunol* 21:2871, 1991

353. Damle NK, Aruffo A: Vascular cell adhesion molecule 1 induces T-cell antigen receptor-dependent activation of CD4⁺ T lymphocytes. *Proc Natl Acad Sci USA* 88:6403, 1991

354. van Seventer GA, Newman W, Shimizu Y, Nutman TB, Tanaka Y, Horgan KJ, Gopal TV, Ennis E, O'Sullivan D, Grey H, Shaw S: Analysis of T cell stimulation by superantigen plus major histocompatibility complex II molecules or by CD3 monoclonal antibody: Costimulation by purified adhesion ligands VCAM-1, ICAM-1, but not ELAM-1. *J Exp Med* 174:901, 1991

355. Damle NK, Klussman K, Linsley PS, Aruffo A: Differential costimulatory effects of adhesion molecules B7, ICAM-1, LFA-3, and VCAM-1 on resting and antigen-primed CD4⁺ T lymphocytes. *J Immunol* 148:1985, 1992

356. Damle NK, Klussman K, Aruffo A: Intercellular adhesion molecule-2, a counter-receptor for CD11a/CD18 (leukocyte function-associated antigen-1) provides a costimulatory signal for T-cell receptor-initiated activation of human T cells. *J Immunol* 148:665, 1992

357. Wong CS, Gamble JR, Skinner MP, Lucas CM, Berndt MC, Vadas MA: Adhesion protein GMP-140 inhibits superoxide anion release by human neutrophils. *Proc Natl Acad Sci USA* 88:2397, 1991

358. May GL, Dunlop LC, Sztelma K, Berndt MC, Sorrell TC: GMP-140 (P-selectin) inhibits human neutrophil activation by lipopolysaccharide: Analysis by proton magnetic resonance spectroscopy. *Biochem Biophys Res Commun* 183:1062, 1992

359. Catlett R, Moore K, McEver RP: GMP-140 (CD62) induces tissue factor expression in monocytes. *Blood* 78:72a, 1991 (abstr, suppl 1)

360. Lorant DE, Tophan MK, Whatley RE, McEver RP, McIntyre TM, Prescott SM, Zimmerman GA: Inflammatory roles of P-selectin. *J Clin Invest* 92:559, 1993

361. Gimbrone MA Jr, Obin MS, Brock AF, Luis EA, Hass PE, Hebert CA, Kip YK, Leung DW, Lowe DG, Kohr WJ, Darbonne WC, Bechtol DB, Baker JB: Endothelial interleukin-8: A novel inhibitor of leukocyte-endothelial interactions. *Science* 246:1601, 1989

362. Hechtman DH, Cybulsky MI, Fuchs HJ, Baker JB, Gimbrone MA Jr: Intravascular IL-8: Inhibitor of polymorphonuclear leukocyte accumulation at sites of acute inflammation. *J Immunol* 147:883, 1991

363. Kubes P, Suzuki M, Granger DN: Nitric oxide: An endogenous modulator of leukocyte adhesion. *Proc Natl Acad Sci USA* 88:4651, 1991

364. Antonelli-Orlidge A, Saunders KB, Smith SR, D'Amore PA: An activated form of transforming growth factor β is produced by cocultures of endothelial cells and pericytes. *Proc Natl Acad Sci USA* 86:4544, 1989

365. Sato Y, Rifkin DB: Inhibition of endothelial cell movement by pericytes and smooth muscle cells: Activation of a latent transforming growth factor- β 1-like molecule by plasmin during co-culture. *J Cell Biol* 109:309, 1991

366. Gamble JR, Vadas MA: Endothelial adhesiveness for blood neutrophils is inhibited by transforming growth factor- β . *Science* 242:97, 1988

367. Brandes ME, Allen JB, Ogawa Y, Wahl SM: Transforming growth factor beta 1 suppresses acute and chronic arthritis in experimental animals. *J Clin Invest* 87:1108, 1991

368. Lefler AM, Tsao P, Aoki N, Palladino MA Jr: Mediation of cardioprotection by transforming growth factor-beta. *Science* 249:61, 1990

369. Shull MM, Ormsby I, Kier AB, Pawlowski S, Diebold RJ, Yin M, Allen R, Proetzel G, Calvin D, Annunziata N, Doetschman T: Targeted disruption of the mouse transforming growth factor- β 1 gene results in multifocal inflammatory disease. *Nature* 359:693, 1992

370. Bargatze RF, Butcher EC: Rapid G protein-regulated activation event involved in lymphocyte binding to high endothelial venules. *J Exp Med* 178:367, 1993

371. Arfors K-E, Lundberg C, Lindbom L, Lundberg K, Beatty PG, Harlan JM: A monoclonal antibody to the membrane glycoprotein complex CD18 inhibits polymorphonuclear leukocyte accumulation and plasma leakage in vivo. *Blood* 69:338, 1987

372. Issekutz TB, Issekutz AC: T lymphocyte migration to arthritic joints and dermal inflammation in the rat: Differing migration

patterns and the involvement of VLA-4. *Clin Immunol Immunopathol* 61:436, 1991

373. Issekutz TB: Effect of antigen challenge on lymph node lymphocyte adhesion to vascular endothelial cells and the role of VLA-4 in the rat. *Cell Immunol* 138:300, 1991

374. Yednock TA, Cannon C, Fritz LC, Sanchez-Madrid F, Steinman L, Karin N: Prevention of experimental autoimmune encephalitis by antibodies against $\alpha_4\beta_1$ integrin. *Nature* 356:63, 1992

375. Baron JL, Madri JA, Ruddle NH, Hashim G, Janeway CA Jr: Surface expression of α_4 integrin by CD4 T cells is required for their entry into brain parenchyma. *J Exp Med* 177:57, 1993

376. Weg VB, Williams TJ, Lobb RR, Nourshargh S: A monoclonal antibody recognizing very late activation antigen-4 inhibits eosinophil accumulation in vivo. *J Exp Med* 177:561, 1993

377. von Andrian UH, Berger EM, Ramezani L, Chambers JD, Ochs HD, Harlan JM, Paulson JC, Etziono A, Arfors K-E: In vivo behavior of neutrophils from two patients with distinct inherited leukocyte adhesion deficiency syndromes. *J Clin Invest* 91:2893, 1993

378. Dustin ML, Springer TA: T-cell receptor cross-linking transiently stimulates adhesiveness through LFA-1. *Nature* 341:619, 1989

379. Stossel TP: On the crawling of animal cells. *Science* 260:1086, 1993

380. Smith CW: Transendothelial migration, in Harlan JM, Liu DY (eds): *Adhesion: Its Role in Inflammatory Disease*, New York, NY, Freeman, 1992, p 83

381. Muller WA, Weigl SA: Monocyte-selective transendothelial migration: Dissection of the binding and transmigration phases by an in vitro assay. *J Exp Med* 176:819, 1992

382. Kavanaugh AF, Lightfoot E, Lipsky PE, Oppenheimer-Marks N: Role of CD11/CD18 in adhesion and transendothelial migration of T cells: Analysis utilizing CD18-deficient T cell clones. *J Immunol* 146:4149, 1991

383. Oppenheimer-Marks N, Davis LS, Bogue DT, Ramberg J, Lipsky PE: Differential utilization of ICAM-1 and VCAM-1 during the adhesion and transendothelial migration of human T lymphocytes. *J Immunol* 147:2913, 1991

384. Hourihan H, Allen TD, Ager A: Lymphocyte migration across high endothelium is associated with increases in $\alpha_4\beta_1$ integrin (VLA-4) affinity. *J Cell Sci* 104:1049, 1993

385. Bianchi G, Sironi M, Ghibaudi E, Selvaggini C, Elices M, Allavena P, Mantovani A: Migration of natural killer cells across endothelial cell monolayers. *J Immunol* 151:5135, 1993

386. Furie MB, Naprstek BL, Silverstein SC: Migration of neutrophils across monolayers of cultured microvascular endothelial cells: An in vitro model of leukocyte extravasation. *J Cell Sci* 88:161, 1987

387. Taylor RF, Price TH, Schwartz SM, Dale DC: Neutrophil-endothelial cell interactions on endothelial monolayers grown on micropore filters. *J Clin Invest* 67:584, 1981

388. Morland CM, Wilson SJ, Holgate ST, Roche WR: Selective eosinophil leukocyte recruitment by transendothelial migration and not by leukocyte-endothelial cell adhesion. *Am J Respir Cell Mol Biol* 6:557, 1993

389. Smith CW, Rothlein R, Hughes BJ, Mariscalco MM, Rudloff HE, Schmalstieg FC, Anderson DC: Recognition of an endothelial determinant for CD18-dependent human neutrophil adherence and transendothelial migration. *J Clin Invest* 82:1746, 1988

390. Moser R, Schleiffenbaum B, Groscurth P, Fehr J: Interleukin 1 and tumor necrosis factor stimulate human vascular endothelial cells to promote transendothelial neutrophil passage. *J Clin Invest* 83:444, 1989

391. Lusinkas FW, Cybulsky MI, Kiely JM, Peckins CS, Davis VM, Gimbrone MA Jr: Cytokine-activated human endothelial mono-

layers support enhanced neutrophil transmigration via a mechanism involving both endothelial-leukocyte adhesion molecule-1 and intercellular adhesion molecule-1. *J Immunol* 146:1617, 1991

392. Hakkert BC, Kuijpers TW, Leeuwenberg JFM, van Mourik JA, Roos D: Neutrophil and monocyte adherence to and migration across monolayers of cytokine-activated endothelial cells: The contribution of CD18, ELAM-1 and VLA-4. *Blood* 78:2721, 1991

393. Furie MB, Burns MJ, Tancinco MCA, Benjamin CD, Lobb RR: E-selectin (endothelial-leukocyte adhesion molecule-1) is not required for the migration of neutrophils across IL-1-stimulated endothelium in vitro. *J Immunol* 148:2395, 1992

394. Meerschaert J, Furie MB: Monocytes use either CD11/CD18 or VLA-4 to migrate across endothelium in vitro. *J Immunol* 152:1915, 1994

395. Ebisawa M, Bochner BS, Georas SN, Schleimer RP: Eosinophil transendothelial migration induced by cytokines: role of endothelial and eosinophil adhesion molecules in IL-1 β -induced transendothelial migration. *J Immunol* 149:4021, 1992

396. Moser R, Fehr J, Olgiate L, Bruijnzeel PLB: Migration of primed human eosinophils across cytokine-activated endothelial cell monolayers. *Blood* 79:2937, 1992

397. Walker C, Rihs S, Braun RK, Betz S, Bruijnzeel PLB: Increased expression of CD11b and functional changes in eosinophils after migration across endothelial cell monolayers. *J Immunol* 150:4061, 1993

398. Kuijpers TW, Hakkert BC, Hart MHL, Roos D: Neutrophil migration across monolayers of cytokine-prestimulated endothelial cells: A role for platelet-activating factor and IL-8. *J Cell Biol* 117:565, 1992

399. Huang AJ, Manning JE, Bandak TM, Ratau MC, Hanser KR, Silverstein SC: Endothelial cell cytosolic free calcium regulates neutrophil migration across monolayers of endothelial cells. *J Cell Biol* 120:1371, 1993

400. Furie MB, Tancinco MCA, Smith CW: Monoclonal antibodies to leukocyte integrins CD11a/CD18 and CD11b/CD18 or intercellular adhesion molecule-1 inhibit chemoattractant-stimulated neutrophil transendothelial migration in vitro. *Blood* 78:2089, 1991

401. Anderson DC, Rothlein R, Martin SD, Krater SS, Smith CW: Impaired transendothelial migration by neonatal neutrophils: Abnormalities of Mac-1 (CD11b/CD18)-dependent adherence reactions. *Blood* 76:2613, 1990

402. Yong KL, Lynch DC: Granulocyte-macrophage-colony-stimulating factor differentially regulates neutrophil migration across IL-1-activated and nonactivated human endothelium. *J Immunol* 150:2449, 1993

403. Kuijpers TW, Hoogerwerf M, Roos D: Neutrophil migration across monolayers of resting or cytokine-activated endothelial cells: Role of intracellular calcium changes and fusion of specific granules with the plasma membrane. *J Immunol* 148:72, 1992

404. Hakkert BC, Rentenaar JM, van Aken WG, Roos D, van Mourik JA: A three dimensional model system to study the interactions between human leukocytes and endothelial cells. *Eur J Immunol* 20:2775, 1990

405. Moser R, Fehr J, Bruijnzeel PLB: IL-4 controls the selective endothelium-driven transmigration of eosinophils from allergic individuals. *J Immunol* 149:1432, 1992

406. van Epps DE, Potter J, Vachula M, Smith CW, Anderson DC: Suppression of human lymphocyte chemotaxis and transendothelial migration by anti-LFA-1 antibody. *J Immunol* 143:3207, 1989

407. Issekutz AC, Movat HZ: The in vivo quantitation and kinetics of rabbit neutrophil leukocyte accumulation in the skin in response to chemotactic agents and *Escherichia coli*. *Lab Invest* 42:310, 1980

408. Paz RA, Spector WG: The mononuclear-cell response to injury. *J Pathol Bact* 84:85, 1962

409. Issekutz TB, Issekutz AC, Movat HZ: The in vivo quantitation and kinetics of monocyte migration into acute inflammatory tissue. *Am J Pathol* 103:47, 1981
410. Pitzalis C, Kingsley G, Murphy J, Panayi G: Abnormal distribution of the helper-inducer and suppressor-inducer T-lymphocyte subsets in the rheumatoid joint. *Clin Immunol Immunopathol* 45:252, 1987
411. Markey AC, Allen MH, Pitzalis C, MacDonald DM: T-cell inducer populations in cutaneous inflammation: a predominance of T helper-inducer lymphocytes (T_H) in the inflammatory dermatoses. *Br J Dermatol* 122:325, 1990
412. Miller MD, Krangel MS: Biology and biochemistry of the chemokines: A family of chemotactic and inflammatory cytokines. *Crit Rev Immunol* 12:17, 1992
413. Gamble JR, Harlan JM, Klebanoff SJ, Vadas MA: Stimulation of the adherence of neutrophils to umbilical vein endothelium by human recombinant tumor necrosis factor. *Proc Natl Acad Sci USA* 82:8667, 1985
414. Klebanoff SJ, Vadas MA, Harlan JM, Sparks LH, Gamble JR, Agosti JM, Waltersdorff AM: Stimulation of neutrophils by tumor necrosis factor. *J Immunol* 136:4220, 1986
415. Socinski MA, Cannistra SA, Sullivan R, Elias A, Antman K, Schnipper L, Griffins JD: Granulocyte-macrophage colony-stimulating factor induces the expression of the CD11b surface adhesion molecule on human granulocytes in vivo. *Blood* 72:691, 1988
416. Yong KL, Rowles PM, Patterson KG, Linch DC: Granulocyte-macrophage colony-stimulating factor induces neutrophil adhesion to pulmonary vascular endothelium in vivo: role of β 2 integrins. *Blood* 80:1565, 1992
417. Elliot MJ, Vadas MA, Cleland LG, Gamble JR, Lopez AF: IL-3 and granulocyte-macrophage colony-stimulating factor stimulate two distinct phases of adhesion in human monocytes. *J Immunol* 145:167, 1990
418. Jiang Y, Beller DI, Frendl G, Graves DT: Monocyte chemoattractant protein-1 regulates adhesion molecule expression and cytokine production in human monocytes. *J Immunol* 148:2423, 1992
419. Walsh GM, Wardlaw AJ, Hartnell A, Sanderson CJ, Kay AB: Interleukin-5 enhances the in vitro adhesion of human eosinophils, but not neutrophils, in a leukocyte integrin (CD11/CD18)-dependent manner. *Int Arch Allergy Immunol* 94:174, 1991
420. Robinson DS, Hamid Q, Ying S, Tsicopoulos A, Barkans J, Bentley AM, Corrigan C, Durham SR, Kay AB: Predominant T_H -like bronchoalveolar T-lymphocyte population in atopic asthma. *N Engl J Med* 326:298, 1992
421. Clark WM, Madden KP, Rothlein R, Zivin JA: Reduction of central nervous system ischemic injury by monoclonal antibody to intercellular adhesion molecule. *J Neurosurg* 75:623, 1991
422. Bowes MP, Zivin JA, Rothlein R: Monoclonal antibody to the ICAM-1 adhesion site reduces neurological damage in a rabbit cerebral embolism model. *Exp Neurol* 119:215, 1993
423. Mileski W, Borgstrom D, Lightfoot E, Rothlein R, Faanes R, Lipsky P, Baxter C: Inhibition of leukocyte-endothelial adherence following thermal injury. *J Surg Res* 52:334, 1992
424. Horgan MJ, Ge M, Gu J, Rothlein R, Malik AB: Role of ICAM-1 in neutrophil-mediated lung vascular injury after occlusion and reperfusion. *Am J Physiol* 261:H1578, 1991
425. Ma X-L, Lefer DJ, Lefer AM, Rothlein R: Coronary endothelial and cardiac protective effects of a monoclonal antibody to intercellular adhesion molecule-1 in myocardial ischemia and reperfusion. *Circulation* 86:937, 1992
426. Yamazaki T, Seko Y, Tamatani T, Miyasaka M, Yagita H, Okumura K, Nagai R, Yazaki Y: Expression of intercellular adhesion molecule-1 in rat heart with ischemia/reperfusion and limitation of infarct size by treatment with antibodies against cell adhesion molecules. *Am J Pathol* 143:410, 1993
427. Mulligan MS, Wilson GP, Todd RF, Smith CW, Anderson DC, Varani J, Issekutz TB, Miyasaka M, Tamatani T, Rusche JR, Vaporciyan AA, Ward PA: Role of β 1, β 2 integrins and ICAM-1 in lung injury after deposition of IgG and IgA immune complexes. *J Immunol* 150:2407, 1993
428. Seekamp A, Mulligan MS, Till GO, Smith CW, Miyasaka M, Tamatani T, Todd RF III, Ward PA: Role of β 2 integrins and ICAM-1 in lung injury following ischemia-reperfusion of rat hind limbs. *Am J Pathol* 143:464, 1993
429. Winn RK, Liggitt D, Vedder NB, Paulson JC, Harlan JM: Anti-P-selectin monoclonal antibody attenuates reperfusion injury to the rabbit ear. *J Clin Invest* 92:2042, 1993
430. Weyrich AS, Ma X-L, Lefer DJ, Albertine KH, Lefer AM: In vivo neutralization of P-selectin protects feline heart and endothelium in myocardial ischemia and reperfusion injury. *J Clin Invest* 91:2620, 1993
431. Ma X-L, Weyrich AS, Lefer DJ, Buerke M, Albertine KH, Kishimoto TK, Lefer AM: Monoclonal antibody to L-selectin attenuates neutrophil accumulation and protects ischemic reperfused cat myocardium. *Circulation* 88:649, 1993
432. Argenbright LW, Barton RW: The Schwartzman response: A model of ICAM-1 dependent vasculitis. *Agents Actions* 34:208, 1991
433. Argenbright LW, Barton RW: Interactions of leukocyte integrins with intercellular adhesion molecule-1 in the production of inflammatory vascular injury in vivo: the Schwartzman reaction revisited. *J Clin Invest* 89:259, 1992
434. Gundel RH, Wegner CD, Torcellini CA, Clarke CC, Haynes N, Rothlein R, Smith CW, Letts LG: Endothelial leukocyte adhesion molecule-1 mediates antigen-induced acute airway inflammation and late-phase airway obstruction in monkeys. *J Clin Invest* 88:1407, 1991
435. Barton RW, Rothlein R, Ksiazek J, Kennedy C: The effect of anti-intercellular adhesion molecule-1 on phorbol-ester-induced rabbit lung inflammation. *J Immunol* 143:1278, 1989
436. Mulligan MS, Varani J, Warren JS, Till GO, Smith CW, Anderson DC, Todd RF III, Ward PA: Roles of β 2 integrins of rat neutrophils in complement- and oxygen radical-mediated acute inflammatory injury. *J Immunol* 148:1847, 1992
437. Mulligan MS, Smith CW, Anderson DC, Todd RF III, Miyasaka M, Tamatani T, Issekutz TB, Ward PA: Role of leukocyte adhesion molecules in complement-induced lung injury. *J Immunol* 150:2401, 1993
438. Mulligan MS, Polley MJ, Bayer RJ, Nunn MF, Paulson JC, Ward PA: Neutrophil-dependent acute lung injury: Requirement for P-selectin (GMP-140). *J Clin Invest* 90:1600, 1992
439. Mulligan MS, Warren JS, Smith CW, Anderson DC, Yeh CG, Rudolph AR, Ward PA: Lung injury after deposition of IgA immune complexes: Requirements for CD18 and L-arginine. *J Immunol* 148:3086, 1992
440. Podolsky DK, Lobb R, King N, Benjamin CD, Pepinsky B, Sehgal P, de Beaumont M: Attenuation of colitis in the cotton-top tamarin by anti- α 4 integrin monoclonal antibody. *J Clin Invest* 92:372, 1993
441. Mulligan MS, Miyasaka M, Tamatani T, Jones MJ, Ward PA: Requirements for L-selectin in neutrophil-mediated lung injury in rats. *J Immunol* 152:832, 1994
442. Isobe M, Yagita H, Okumura K, Ihara A: Specific acceptance of cardiac allograft after treatment with antibodies to ICAM-1 and LFA-1. *Science* 255:1125, 1992
443. Isobe M, Ihara A: Tolerance induction against cardiac allograft by anti-ICAM-1 and anti-LFA-1 treatment: T cells respond to in vitro allostimulation. *Transplant Proc* 25:1079, 1993

444. Komori A, Nagata M, Ochiai T, Nakajima K, Hori S, Asano T, Isono K, Tamatani T, Miyasaka M: Role of ICAM-1 and LFA-1 in cardiac allograft rejection of the rat. *Transplant Proc* 25:831, 1993
445. Flavin T, Ivens K, Rothlein R, Faanes R, Clayberger C, Billingham M, Starnes VA: Monoclonal antibodies against intercellular adhesion molecule 1 prolong cardiac allograft survival in cynomolgous monkeys. *Transplant Proc* 23:533, 1991
446. Cosimi AB, Conti D, Delmonico FL, Preffer FI, Wee S-L, Rothlein R, Faanes R, Colvin RB: In vivo effects of monoclonal antibody to ICAM-1 (CD54) in nonhuman primates with renal allografts. *J Immunol* 144:4604, 1990
447. Pelletier R, Ohye R, Kincade P, Ferguson R, Orosz C: Monoclonal antibody to anti-VCAM-1 interferes with murine cardiac allograft rejection. *Transplant Proc* 25:839, 1993
448. Orosz CG, Ohye RG, Pelletier RP, van Buskirk AM, Huang E, Morgan C, Kincade PW, Ferguson RM: Treatment with anti-vascular cell adhesion molecule 1 monoclonal antibody induces long-term murine cardiac allograft acceptance. *Transplantation* 56:453, 1993
449. Paul LC, Davidoff A, Paul DW, Benediktsson J, Issekutz TB: Monoclonal antibodies against LFA-1 and VLA-4 inhibit graft vasculitis in rat cardiac allografts. *Transplant Proc* 25:813, 1993
450. Paul LC, Davidoff A, Benediktsson H, Issekutz TB: The efficacy of LFA-1 and VLA-4 antibody treatment in rat vascularized cardiac allograft rejection. *Transplantation* 55:1196, 1993
451. Iigo Y, Takashi T, Tamatani T, Miyasaka M, Higashida T, Yagita H, Okumura K, Tsukada W: ICAM-1-dependent pathway is critically involved in the pathogenesis of adjuvant arthritis in rats. *J Immunol* 147:4167, 1991
452. Kakimoto K, Nakamura T, Ishii K, Takashi T, Iigo H, Yagita H, Okumura K, Onoue K: The effect of anti-adhesion molecule antibody on the development of collagen-induced arthritis. *Cell Immunol* 142:326, 1992
453. Kawasaki K, Yaoita E, Yamamoto T, Tamatani T, Miyasaka M, Kihara T: Antibodies against intercellular adhesion molecule-1 and lymphocyte function-associated antigen-1 prevent glomerular injury in experimental crescentic glomerulonephritis. *J Immunol* 150:1074, 1993
454. Archelos JJ, Jung S, Maurer M, Schmied M, Lassman H, Tamatani T, Miyasaka M, Toyka K, Hartung H-P: Inhibition of experimental autoimmune encephalomyelitis by an antibody to the intercellular adhesion molecule ICAM-1. *Ann Neurol* 34:145, 1993
455. Willenborg DO, Simmons RD, Tamatani T, Miyasaka M: ICAM-1-dependent pathway is not critically involved in the inflammatory process of autoimmune encephalomyelitis or in cytokine-induced inflammation of the central nervous system. *J Neuroimmunol* 45:147, 1993
456. Nishikawa K, Guo Y-J, Miyasaka M, Tamatani T, Collins AB, Sy M-S, McCluskey RT, Andres G: Antibodies to intercellular adhesion molecule 1/lymphocyte function-associated antigen 1 prevent crescent formation in rat autoimmune glomerulonephritis. *J Exp Med* 177:667, 1993
457. Haring R, Pelletier J, Van G, Takei F, Merluzzi VJ: Monoclonal antibody to MALA-2 (ICAM-1) reduces acute autoimmune nephritis in kdkd mice. *Clin Immunol Immunopathol* 64:129, 1992
458. Scheynius A, Camp RL, Pure E: Reduced contact sensitivity reactions in mice treated with monoclonal antibodies to leukocyte functional-associated molecule-1 and intercellular adhesion molecule-1. *J Immunol* 150:655, 1993
459. Chisholm PL, Williams CA, Lobb RR: Monoclonal antibodies to the integrin α_4 subunit inhibit the murine contact hypersensitivity response. *Eur J Immunol* 23:682, 1993
460. Elices MJ, Tamraz S, Tollefson V, Vollger LW: The integrin VLA-4 mediates leukocyte recruitment to skin inflammatory sites in vivo. *Clin Exp Rheumatol* 11:577, 1993 (suppl 8)
461. Dawson J, Sedgwick AD, Edwards JCW, Lees P: The monoclonal antibody MEL-14 can block lymphocyte migration into a site of chronic inflammation. *Eur J Immunol* 22:1647, 1992
462. Wegner CD, Gundel RH, Reilly P, Haynes N, Letts LG, Rothlein R: Intercellular adhesion molecule-1 (ICAM-1) in the pathogenesis of asthma. *Science* 247:456, 1990
463. Gundel RH, Wegner CD, Torcellini CA, Letts LG: The role of intercellular adhesion molecule-1 in chronic airway inflammation. *Clin Exp Allergy* 22:569, 1992
464. Abraham WM, Sielczak MW, Ahmed A, Cortes A, Lauro IT, Barrett T, Pepinsky B, Benjamin CD, Leone DR, Lobb RR, Weller PF: α_4 integrins mediate antigen-induced late bronchial responses and prolonged airway hyperresponsiveness in sheep. *J Clin Invest* 93:776, 1994
465. Haug CE, Colvin RB, Delmonico FL, Auchincloss H Jr, Tolkooff-Rubin N, Preffer FI, Rothlein R, Norris S, Scharschmidt L, Cosimi AB: A phase I trial of immunosuppression with anti-ICAM-1 (CD54) mAb in renal allograft recipients. *Transplantation* 55:766, 1993
466. Mulligan MS, Paulson JC, De Frees S, Zheng Z-L, Lowe JB, Ward PA: Protective effects of oligosaccharides in P-selectin-dependent lung injury. *Nature* 364:149, 1993
467. Mulligan MS, Lowe JB, Larsen RD, Paulson J, Zheng Z-L, De Frees S, Maemura K, Fukuda M, Ward PA: Protective effects of sialylated oligosaccharides in immune complex-induced acute lung injury. *J Exp Med* 178:623, 1993
468. Buerke M, Weyrich AS, Zheng Z, Gaeta FCA, Forrest MJ, Lefer AM: Sialyl Lewis^x-containing oligosaccharide attenuates myocardial reperfusion injury in cats. *J Clin Invest* 93:1140, 1994
469. Fecondo JV, Kent SBH, Boyd AW: Inhibition of intercellular adhesion molecule-1-dependent biological activities by a synthetic peptide analog. *Proc Natl Acad Sci USA* 88:2879, 1991
470. Ross L, Hassman F, Molony L: Inhibition of Molt-4-endothelial adherence by synthetic peptides from the sequence of ICAM-1. *J Biol Chem* 267:8537, 1992
471. Li R, Nortamo P, Valmuri L, Tolvanen M, Huuskonen J, Kantor C, Gahmberg CG: A peptide from ICAM-2 binds to the leukocyte integrin CD11a/CD18 and inhibits endothelial cell adhesion. *J Biol Chem* 268:17513, 1993
472. Nowlin DM, Gorcsan F, Moscinski M, Chiang S-L, Lobl TJ, Cardarelli PM: A novel cyclic pentapeptide inhibits $\alpha_4\beta_1$ and $\alpha_3\beta_1$ integrin-mediated cell adhesion. *J Biol Chem* 268:20352, 1993
473. Rozdzinski E, Jones T, Burnette WN, Burroughs M, Tuomanen E: Antiinflammatory effects in experimental meningitis of prokaryotic peptides that mimic selectins. *J Infect Dis* 168:1422, 1993
474. Heavner GA, Falcone M, Kruszynski M, Epps L, Mervic M, Riexinger D, McEver RP: Peptides from multiple regions of the lectin domain of P-selectin inhibiting neutrophil adhesion. *Int J Peptide Protein Res* 42:484, 1993
475. Nelson RM, Cecconi O, Roberts WG, Aruffo A, Linhardt RJ, Bevilacqua MP: Heparin oligosaccharides bind L- and P-selectin and inhibit acute inflammation. *Blood* 82:3253, 1993
476. Granert C, Raud J, Xie X, Lindquist L, Lindbom L: Inhibition of leukocyte rolling with polysaccharide fucoidin prevents pleocytosis in experimental meningitis in the rabbit. *J Clin Invest* 93:929, 1994
477. Chiang M-Y, Chan H, Zounes MA, Freier SM, Lima WF, Bennett CF: Antisense oligonucleotides inhibit intercellular adhesion molecule 1 expression by two distinct mechanisms. *J Biol Chem* 266:18162, 1991
478. Bennett CF: Regulation of leukocyte-endothelial cell adhesion molecule expression with synthetic oligonucleotides. *J Cell Biochem* 18A:E021, 1994 (abstr)
479. Wolitzky B, Kwee L, Terry R, Kontgen F, Stewart C, Rumberger JM, Burns DK, Labow MA: Targeted disruption of the murine E-selectin and VCAM-1 genes. *J Cell Biochem* 18A:E523, 1994 (abstr)

Heparan Sulfate Proteoglycan on Leukemic Cells is Primarily Involved in Integrin Triggering and Its Mediated Adhesion to Endothelial Cells

By Yoshiya Tanaka,* Koji Kimata,[‡] Atsushi Wake,* Shinichiro Mine,* Isao Morimoto,* Naomi Yamakawa,[‡] Hiroko Habuchi,[‡] Satoko Ashikari,[‡] Hisao Yamamoto,[§] Katsukiyo Sakurai,[§] Keiichi Yoshida,[§] Sakaru Suzuki,[‡] and Sumiya Eto*

From the *First Department of Internal Medicine, University of Occupational and Environmental Health, Japan, School of Medicine, Kitakyushu 807 Japan; [‡]Institute for Molecular Science of Medicine, Aichi Medical University, Nagakute 480-11 Japan; and the [§]Tokyo Research Institute, Seikagaku Kogyo Company Limited, Higashi-Yamato 207 Japan

Summary

Leukocyte migration from circulation into tissue depends on leukocyte integrin-mediated adhesion to endothelium, but integrins cannot function until activated. However, it remains to be understood how tumor cells adhere to endothelium and infiltrate into underlying tissue. We studied mechanisms of extravasation of leukemic cells using adult T cell leukemia (ATL) cells and report the following novel features of cell surface heparan sulfate proteoglycan on ATL cells in ATL cell adhesion to endothelium: ATL cells adhere to endothelial cells through already activated integrins without exogenous stimulation; different from any other hematopoietic cells, ATL cells express a characteristic heparan sulfate capable of immobilizing heparin-binding chemokine macrophage inflammatory protein (MIP)-1 β , a potent T cell integrin trigger, produced by the cells themselves; competitive interruption of endogenous heparan sulfate proteoglycan synthesis reduces cell surface MIP-1 β and prevents ATL cells from integrin-mediated adhesion to endothelial cells or intercellular adhesion molecule-1 triggered through G-protein. We propose that leukemic cells adhere to endothelial cells through the adhesion cascade, similar to normal leukocyte, and that the cell surface heparan sulfate, particularly on ATL cells, is pivotally involved in chemokine-dependent autocrine stimulation of integrin triggering by immobilizing the chemokine on them.

Leukocyte migration from circulation into tissue is understood to involve, in a coordinated sequence of events, stabilizing adhesion molecules both on the leukocyte and on the endothelium (1-4). The adhesion is mediated by leukocyte integrin binding to endothelial ligands (5). However, leukocyte integrins cannot function until they are activated and integrin triggers are essential to the integrin-mediated adhesion in which a signal transduced to the leukocyte converts the functionally inactive integrin to an active adhesive configuration (1, 3). We have reported that the chemokine macrophage inflammatory protein-1 β (MIP-1 β)¹ triggers integrin and induces adhesion of T cell

subsets to endothelial integrin ligands (6). Recent papers and reviews have supported the potential importance of chemokines in inflammatory responses that various other chemokines, as well as MIP-1 β , produced in large amounts from inflamed tissues trigger integrins on leukocytes and monocytes which leads to their accumulation in the tissues (4, 7). Furthermore, we and others have proposed that chemokines MIP-1 β and IL-8 recruit leukocytes most efficiently when immobilized on the luminal surface of endothelium and that heparan sulfate proteoglycan on the endothelium immobilize the chemokines in this process without being washed away by the blood flow (6, 8-10).

Heparan sulfate proteoglycan is posttranslationally modified by the addition of heparan sulfate glycosaminoglycan side chains made up of long and linear disaccharide subunits at serine residues of core protein, some of which are in the extracellular matrix, while others are integral membrane proteins (11, 12). Various cytokines and growth factors such as all the chemokines, IL-7, GM-CSF, fibroblast growth

¹Abbreviations used in this paper: ATL, adult T cell leukemia; FGF, fibroblast growth factor; HEX- α -xyloside, hexyl- β -D-xyloside; HUVEC, human umbilical vein endothelial cells; ICAM, intercellular adhesion molecule; MIP-1 β , macrophage inflammatory protein-1 β ; NAP-D-xyloside, (6-hydroxyl)-2-naphthyl- β -D-xyloside, NAP-L-xyloside, (6-hydroxyl)-2-naphthyl- β -L-xyloside.

factor (FGF), TGF, and hepatocyte growth factor possess heparan-binding sites, which allow these proteins to bind to heparan sulfate proteoglycan (13–17). These factors interact in functionally important ways with heparan sulfate in several contexts: (a) extracellular matrix heparan sulfate proteoglycan binds these factors such as FGF as a reservoir (18, 19); (b) cell surface heparan sulfate interacts with these factors, e.g., FGF, to facilitate their binding with the primary high affinity receptor on the same cells; and (c) we and others have proposed that cell surface heparan sulfate immobilize the factors such as GM-CSF and MIP-1 β and present them to their primary receptor on another cell (6, 17). Furthermore, heparan sulfate enhances formation of cytokine multimers, which facilitates cross-linking of the cytokine receptors.

The extravasation of tumor cells which is one important step of tumor metastasis is mediated by tumor cell adhesion to endothelial cells (20, 21). However, it remains to be understood how tumor cells adhere to endothelium and subsequently infiltrate into underlying tissue. We have addressed the mechanism of extravasation of leukemic cells using adult T cell leukemia (ATL) cells. ATL is a unique and useful model to assess the extravasation, since ATL is a peripheral CD4⁺ T cell malignancy caused by infection with HTLV-I and since ATL shows a marked increase of peripheral ATL cells with monoclonal growth and severe infiltration into multiple organs in an acute phase (22–24). The present report demonstrates that heparan sulfate proteoglycans are abundantly expressed on the surface of ATL cells and ATL cell lines, whereas any other hematopoietic cells and cell lines which we have screened do not express them, and proposes that the heparan sulfate proteoglycans on ATL cells which immobilize integrin-triggering chemokine in an autocrine mechanism play a pivotal role in the continuous triggering of integrin and facilitation of ATL cell adhesion to endothelial cells.

Materials and Methods

ATL Cells and ATL Cell Lines. 18 patients with ATL and one case of chronic T cell leukemia which is not infected with HTLV-I as a control, four established HTLV-I-infected T cell lines, MT-1, MT-2, HUT-102, and SALT-3 (from K. Sagawa, University of Kurume, Kurume, Japan, and I. Miyoshi, Kochi Medical University, Kochi, Japan) were used. ATL was diagnosed according to the clinical features, hematological findings, serum antibodies against HTLV-I, and monoclonal integration of HTLV-I proviral genome (22, 23). Highly purified CD4⁺ T cells and ATL cells were prepared by exhaustive negative selection (3) from PBMC of normal donors and ATL patients using magnetic beads (Dynal, Oslo, Norway) and multiple-antibody cocktail consisting of CD19 mAb FMC63, CD16 mAb 3G8, CD11b mAb NIH11b-1, and CD14 mAb 63D3.

Antibodies and Other Reagents. The following mAbs were used as purified Ig in preparation of T cells and ATL cells, staining and analysis of cell surface molecules, blocking of cellular adhesion; anti-heparan sulfate mAb HK249 which was locally established

(25) and 10E4 (Seikagaku Kogyo, Tokyo, Japan), activated LFA-1 mAb NKI-L16 (C. Figdor, University Hospital, Nijmegen, Netherlands) (26), CD19 mAb FMC63 (H. Zola, Flinders Medical Center, Bedford Park, Australia), CD11b mAb NIH11b-1, CD49d (very late antigen [VLA]-4) mAb NIH49d-1, CD54 (intracellular adhesion molecule [ICAM]-1) mAb 84H10 (S. Shaw, National Institutes of Health [NIH], Bethesda, MD), CD49d mAb HP2/1 (F. Sanchez-Madrid, The Princess Hospital, Madrid, Spain) (27, 28), CD16 mAb 3G8 (D. Siegel, Bethesda, MD), CD2 mAb MAR206 (A. Moretta, University of Genova, Genova, Italy), CD62L (L-selectin) mAb Leu-8 (Becton Dickinson Japan, Tokyo, Japan), CD14 mAb 63D3, CD11a (LFA-1 α) mAb TS1/22, MHC class I mAb W6/32, control mAb Thy1.2 (ATCC, Rockville, MD). ICAM-1 was purified by affinity column chromatography from the Reed-Sternberg cell line L428 as previously described (3, 29). (6-hydroxyl)-2-naphthyl- β -D-xyloside (NAP-D-xyloside) which is a competitive inhibitor capable of interrupting endogenous heparan sulfate- and chondroitin sulfate-proteoglycan biosynthesis, its nonfunctional isomer (6-hydroxyl)-2-naphthyl- β -L-xyloside (NAP-L-xyloside), and hexyl- β -D-xyloside (HEX-D-xyloside) which competitively interrupts endogenous chondroitin sulfate- but not heparan sulfate-proteoglycan synthesis were developed as previously described (30, 31, and manuscript in preparation).

Adhesion Assay. Adhesion assay of ATL cells and cell lines to human umbilical vein-derived endothelial cells (HUVEC) or purified ICAM-1 glycoproteins was performed as previously described (3, 29). HUVEC were applied to 48-well culture plates (Costar Corp., Cambridge, MA) coated with 2% gelatin and were cultured to confluence in DMEM (Nissui, Tokyo, Japan) containing 100 U/ml penicillin G, 100 U/ml streptomycin, 20% heat-inactivated FCS, endothelial mitogen 20 μ g/ml (Biomedical Technologies, Stoughton, MA) and heparin (10 U/ml). After washing with PBS, HUVEC were stimulated with 1 ng/ml IL-1 β (Otsuka, Tokyo, Japan) for 4 h at 37°C. Purified ICAM-1 (50 ng/well) was applied to the 48-well plates in Ca/Mg-free PBS at 4°C overnight. Binding sites on the plastic were subsequently blocked with Ca/Mg-free PBS/3% HSA (Green-Cross, Osaka, Japan) for 2 h at 37°C to reduce nonspecific attachment. The plates were washed three times with PBS before the addition of T cells. 2×10^5 T cells, ATL cells, and ATL cell lines, which were labeled with ⁵¹Cr (DuPont NEN, Wilmington, DE) in RPMI 1640 (Nissui) with 1% HSA, were added to the culture with or without relevant adhesion-blocking mAb in the presence or absence of PMA (10 ng/ml, Sigma Chemical Co., St. Louis, MO) which is a pharmacologically relevant trigger for integrin adhesiveness. All mAbs were used at a saturating concentration of 10 μ g/ml, which was shown in previous studies to maximally inhibit the relevant adhesive interaction (3). After a settling phase of 30 min at 4°C, which also allowed mAb binding, plates were rapidly warmed to 37°C for 30 min. Then, the plates were gently washed twice with RPMI 1640 at room temperature to remove nonadherent T cells and ATL cells completely. Contents of each well containing adherent T cells or ATL cells were lysed with 250 μ l of 1% Triton X-100 (Sigma), and γ emissions of well contents were determined. Data are expressed as mean percentage of binding of indicated cells from a representative experiment.

Flow Microfluorometry. Staining and flow cytometric analyses of freshly obtained ATL cells or normal T cells were carried out by standard procedures as already described using a FACScan[®] (Becton Dickinson and Co., Mountain View, CA) (3). Briefly, cells (2×10^5) were incubated with negative control mAb thy1.2,

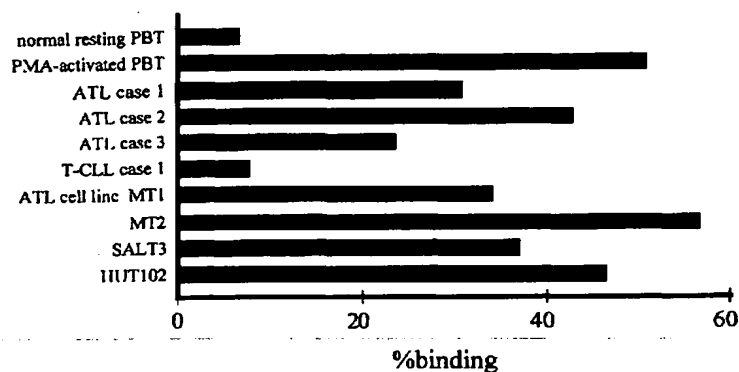


Figure 1. Spontaneous adhesion of ATL cells to IL-1 β -activated HUVEC. Adhesion of resting or PMA-activated peripheral normal CD4 $^{+}$ T cells, ATL cells freshly obtained from periphery of three representative ATL patients, CD4-positive leukemic cells from a patient with HTLV-I-negative T cell leukemia and four ATL cell lines, MT1, MT2, SALT-3, and HUT-102 which were labeled with ^{51}Cr to IL-1 β -activated HUVEC, was assessed after the 30-min incubation at 37°C. γ Emissions of the lysates of only adherent cells were determined. Data are expressed as mean percentage of binding of indicated cells from a representative experiment.

L-selectin (CD62L) mAb Leu-8, LFA-1 (CD11a) mAb TS1/22, VLA-4 (CD49d) mAb NIH49d-1, CD2 mAb MAR206, activated LFA-1 mAb NK1-L16, anti-heparan sulfate mAb HK249 (25), or 10E4 in FACS $^{\circ}$ media consisting of HBSS (Nissui, Tokyo, Japan), 0.5% HSA, and 0.2% NaN $_3$ (Sigma) for 30 min at 4°C. After washing the cells with FACS $^{\circ}$ media three times, the cells were further incubated with FITC-conjugated goat anti-mouse IgG Ab for 30 min at 4°C. After washing and incubating with irrelevant mAbs, the cells were further incubated with CD4-PE (Fujisawa, Osaka, Japan) for 30 min at 4°C. The staining of cells with the mAbs was detected by the gating on CD4-positive cells using a FACScan $^{\circ}$. Amplification of the mAb binding was provided by a three-decade logarithmic amplifier.

Northern Blot Analysis. For Northern blot analysis, total cellular RNA was isolated from freshly obtained normal T cells, ATL cells, and ATL cell lines by using single-step isolation procedure (32). The RNA (10 μg) was electrophoresed on 1% agarose gel and was blotted onto nylon membrane filters (Amersham Corp., Arlington Heights, IL). EcoRI fragment of pAT 744 MIP-1 β cDNA (U. Siebenlist, NIH, Bethesda, MD) (33) and β -actin cDNA (P.E. Auron, Harvard Medical School, Boston, MA) were labeled with [^{32}P]dCTP and subsequent Northern blot analysis was performed.

ELISA Assay of MIP-1 β in Supernatant or Cytosol of ATL Cells. Freshly obtained normal T cells and ATL cells (10 6) were washed in PBS and lysed with 250 μl of PBS containing 2% *N*-octyl- β -D-glucopyranoside (Sigma). The culture supernatants were collected from normal T cells (10 6) and ATL cells (10 6) after the 24-h incubation in RPMI 1640 with 5% FCS at 37°C without any stimulation. The MIP-1 β protein levels in each sample were measured by MIP-1 β ELISA system (R&D Systems, Minneapolis, MN). The sensitivity of the assay is 4.0 pg/ml of MIP-1 β and it was not affected by the presence of *N*-octyl- β -D-glucopyranoside at the concentration used to lyse cells. Results were expressed in nanograms per milliliter per 10 5 cells.

Immunofluorescence Staining of Cell Surface Heparan Sulfate and MIP-1 β . Freshly obtained ATL cells and ATL cell line MT1 were cultured with or without 1 mM NAP-D-xyloside for 5 h at 37°C or were treated with the mixture of 100 mU/ml heparinase I and II for 2 h at 37°C. After putting the cells on glass slides by cytopsin, indirect immunofluorescence was performed with anti-heparan sulfate mAb HK249 and PE-conjugated anti-rat IgG (Fujisawa) or anti-MIP-1 β Ab (U. Siebenlist) (33) and FITC-conjugated anti-rabbit IgG (Fujisawa). The staining was analyzed

with a fluorescence microscope (Epi-fluorescence Condense IV FI; Zeiss, Oberkochen, Germany).

Results

ATL Cells and Cell Lines Spontaneously Adhered to HUVEC. ATL is a characteristic leukemia which shows a marked increase of peripheral ATL cells and their severe infiltration into multiple organs in an acute phase (22–24). Leukocyte migration from circulation into tissue depends on leukocyte integrin-mediated adhesion to endothelial cells. Because leukocyte integrins cannot function until activated, the regulation of integrin-dependent adhesion is critical to the migration of virtually all the hematopoietic cells (1, 3). For instance, as shown in Fig. 1, resting peripheral T cells did not bind to IL-1-activated HUVEC, whereas T cells activated with PMA, which is one potent integrin trigger, adhered to them well. CD4-positive leukemic cells from a patient with HTLV-I-negative T cell leukemia also did not bind to HUVEC. However, both ATL cells freshly obtained from three representative ATL patients and four ATL cell lines, MT1, MT2, SALT-3, and HUT-102, spontaneously bound to HUVEC without any exogenous stimuli after the 30-min incubation.

ATL Cells and Cell Lines Expressed Activated LFA-1 and Heparan Sulfate on the Cell Surface. Leukocyte selectins and integrins mediate its adhesion to endothelial cells (1). Next, we assessed the expression of these adhesion molecules on freshly obtained ATL cells using a flow cytometer (Fig. 2). Although it was assumed that ATL cells (Fig. 2, group B) might express these adhesion molecules more than normal T cells (Fig. 2, group A), integrin LFA-1 and CD2 were equally expressed on ATL cells with normal CD4 $^{+}$ T cells (Fig. 2, b and d) and L-selectin and VLA-4 were rather decreased on ATL cells compared with CD4 $^{+}$ T cells (Fig. 2, a and c). However, it is of interest that NK1-L16 mAb which binds to functionally activated LFA-1 (26, 34) reacted significantly highly with most of the freshly obtained ATL cells, compared with resting CD4 $^{+}$ normal T cells (Fig. 2 e). The mean fluorescence intensity for NK1-L16

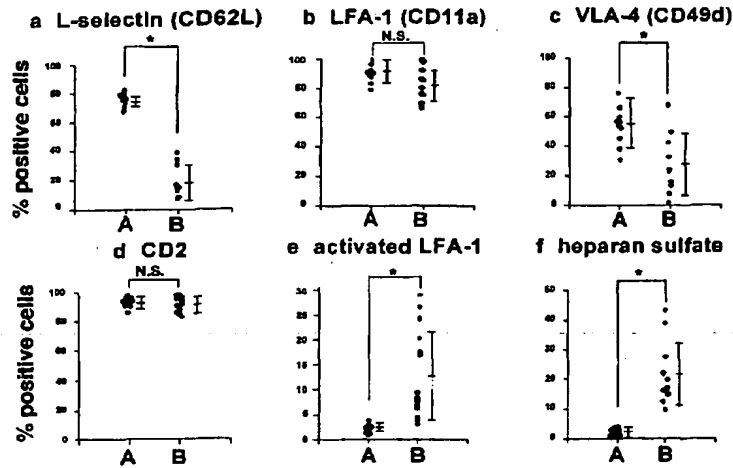


Figure 2. Phenotypic analysis of fresh ATL cells by flow cytometer. Staining and flow cytometric analyses of 10 resting peripheral normal CD4⁺ T cells (group A) and ATL cells freshly obtained from periphery of 18 ATL patients (group B) were carried out with (a) L-selectin (CD62L) mAb Leu-8, (b) LFA-1 (CD11a) mAb TS1/22, (c) VLA-4 (CD49d) mAb NIH49d-1, (d) CD2 mAb MAR206, (e) antiactivated form of LFA-1 mAb NK1-L16, (f) anti-heparan sulfate mAb HK249 using FACSscan®. Each point shows the percent positivity of the binding of indicated mAbs compared with control mAb Thy1.2 from individual persons. The bars indicate mean \pm SD of each group and the asterisks show an overall statistical significance of $P < 0.01$ (Student's *t* test).

staining was also higher in ATL cells than that in normal CD4⁺ T cells (285 ± 79 vs. 146 ± 31 , $P < 0.01$ by Student's *t* test). All the ATL cells also expressed MHC class II antigens, CD25 and CD69, regarded as activation markers (data not shown). The results suggest that spontaneous adhesion of ATL cells to endothelium depends on already triggered/activated integrins rather than the quantity of the integrins expressed on ATL cells.

Furthermore, it is worthy of note that all the ATL cells and cell lines expressed heparan sulfate proteoglycan on the cell surface detected by HK249 mAb, which possesses sharp

specificity for tumor type (O-sulfate deficient) heparan sulfate chains (25), but resting T cells did not at all (Fig. 2f). As far as we have done, none of both resting and cytokine or lectin-activated cells from hematopoietic origin expressed the heparan sulfate (data not shown). The heparan sulfate on one representative ATL patient and ATL cell line MT1 was also detected by another anti-heparan sulfate mAb 10E4 (Fig. 3, B and E). The expression was reduced by the pretreatment of ATL cells or MT1 with the mixture of 100 mU/ml heparitinase I and II for 2 h at 37°C (Fig. 3, C and F), whereas the expression of LFA-1 on ATL cells

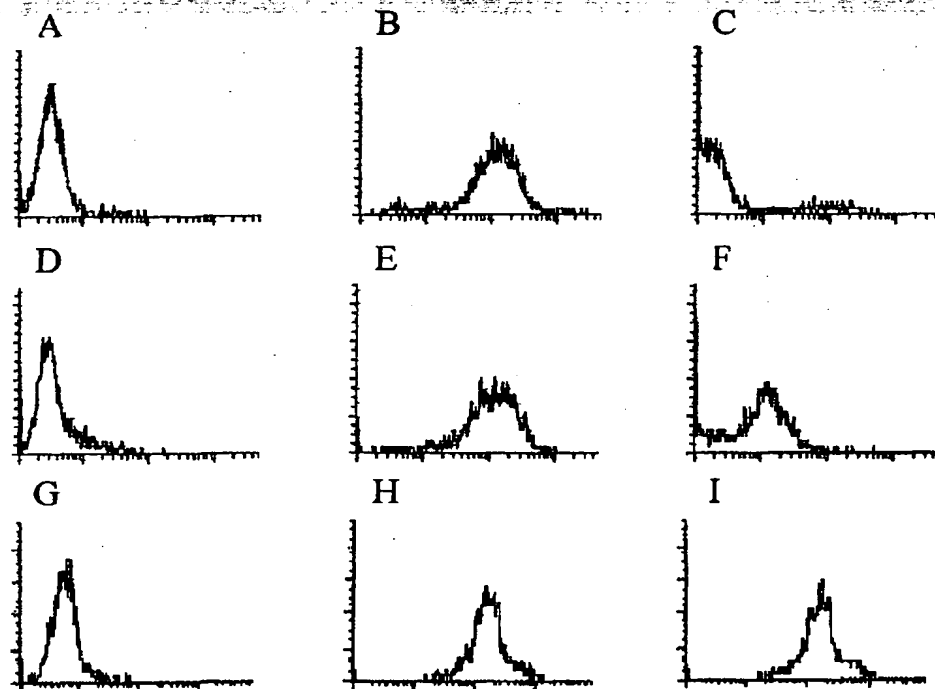


Figure 3. Expression of heparan sulfate on ATL cells and ATL cell line MT1. The expression of heparan sulfate on ATL cell line MT1 (A, B, C, G, H, and I) and one representative ATL patient (D-F) which were pretreated with (C, F, and I) or without (B, E, and H) the mixture of 100 mU/ml heparitinase I and II for 2 h at 37°C was detected by anti-heparan sulfate mAb 10E4 (B, C, E, and F) or anti-LFA-1 (CD11a) mAb TS1/22 (H, I) using FACSscan®. y-axis represents the histogram of cell number stained with mAbs in each logarithmic scale of fluorescence amplifier. Thy1.2 mAb was used as a negative control of the staining (A, D, and G).

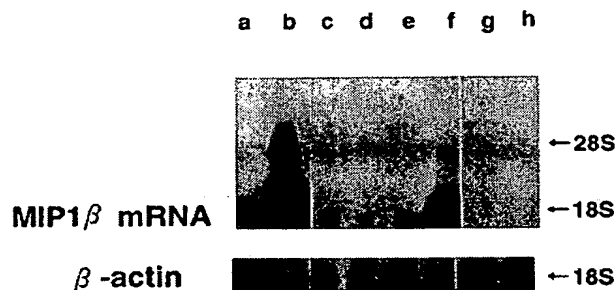


Figure 4. Spontaneous MIP-1 β mRNA transcription on ATL cells and cell lines. For the Northern blot analysis, total cellular RNA was isolated from HUT-102 (lane a) and MT2 (lane b), three representative ATL patients (lanes c-f), and normal CD4 $^{+}$ T cells (lanes g and h) and Northern blot analysis was performed using pAT 744 MIP-1 β cDNA and β -actin cDNA.

was not affected by the treatment (Fig. 3, H and I). Thus, different from any hematopoietic cells which we have examined, ATL cells characteristically and specifically expressed heparan sulfate proteoglycan on their surface.

ATL Cells and Cell Lines Spontaneously Produced Chemokine MIP-1 β . We and others have reported that ATL cells produce multiple cytokines including IL-1, IL-6, and TNF- α (35-37). ATL cell lines MT2 and HUT-102 and four representative freshly obtained ATL cells spontaneously synthesized large amounts of MIP-1 β mRNA by Northern blot analysis, whereas normal T cells did not (Fig. 4). Furthermore, freshly obtained ATL cells from periphery of the patients produced significantly high amounts of MIP-1 β protein in the culture supernatant as well as in the cytosol without any stimulation, compared with normal T cells (Fig. 5). MIP-1 β is a member of chemokine family which is now understood to trigger leukocyte integrin and to induce its adhesion, e.g., MIP-1 β and MIP-1 α for T cell subsets and IL-8 for neutrophils (6, 9, 38), all of which

were also produced by ATL cells (data not shown). Thus, ATL cells spontaneously produced multiple proadhesive chemokines.

MIP-1 β Was Expressed on the Surface of ATL Cells and Its Expression Was Reduced by the Interruption of Heparan Sulfate-Proteoglycan Synthesis. As shown in Fig. 6 A, heparan sulfate was strongly detected on ATL cell line MT1, by immunofluorescence staining using anti-heparan sulfate mAb HK249. Of note is that MIP-1 β was also comparably stained with anti-MIP-1 β Ab on the surface of not only MT1 (Fig. 6 D) but also freshly obtained ATL cells (Fig. 6 G). Chemokines including MIP-1 β possess heparin-binding sites (39) and we and others have proposed that cell surface heparan sulfate proteoglycan immobilizes chemokine (6, 8-10). Interestingly, when MT1 or ATL cells were pretreated with the mixture of 100 mU/ml heparitinase I and II for 2 h, the expression of MIP-1 β as well as heparan sulfate on the surface was markedly reduced (Fig. 6, B, E, and H). Furthermore, pretreatment of MT1 and ATL cells with 1 mM NAP-d-xyloside for 5 h which interrupts endogenous heparan sulfate proteoglycan biosynthesis (30, 31, and manuscript in preparation), resulted in suppression of cell surface MIP-1 β (Fig. 6, F and I). These results indicate that ATL cell-derived MIP-1 β appeared to be retained on the ATL cell surface through binding to heparan sulfate chains of proteoglycan expressed on ATL cells.

Heparan Sulfate Was Involved in the Spontaneous Adhesion of ATL Cells. Finally, we assessed if the heparan sulfate is involved in the spontaneous adhesion of ATL cells and MT1 to HUVEC. MT1 (Fig. 7 A) and freshly obtained ATL cells (Fig. 7 B) without stimulation and PMA-activated peripheral normal T cells (Fig. 7 C) adhered to IL-1-activated HUVEC well. However, when MT1 and ATL cells were pretreated with NAP-d-xyloside, the adhesion was inhibited in a concentration-dependent manner, whereas its nonfunctional isomer NAP-L-xyloside did not affect the adhesion (Fig. 7, A and B). Neither NAP-d-xyloside nor

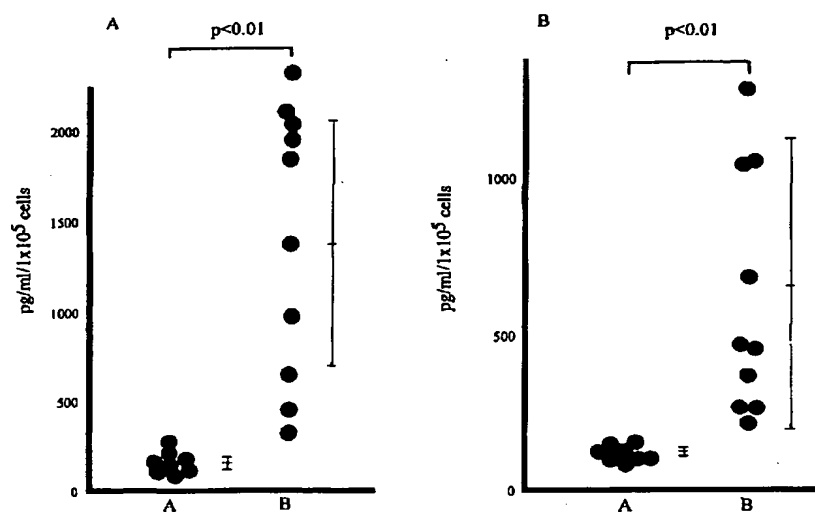


Figure 5. Spontaneous MIP-1 β production from ATL cells. The cytokine levels in cytosol (A) of normal CD4 $^{+}$ T cells (group A) and ATL cells freshly obtained from periphery of ATL patients (group B) or culture supernatants (B) collected from the normal CD4 $^{+}$ T cells (group A) or the ATL cells (group B) after the 24-h incubation at 37°C without any stimulation were determined by MIP-1 β ELISA system. Each point shows the quantity of MIP-1 β in the lysate or the supernatant derived from 10 5 cells of individual persons. The bars indicate mean \pm SD of each group and the asterisks show an overall statistical significance of $P < 0.01$ (Student's t test).

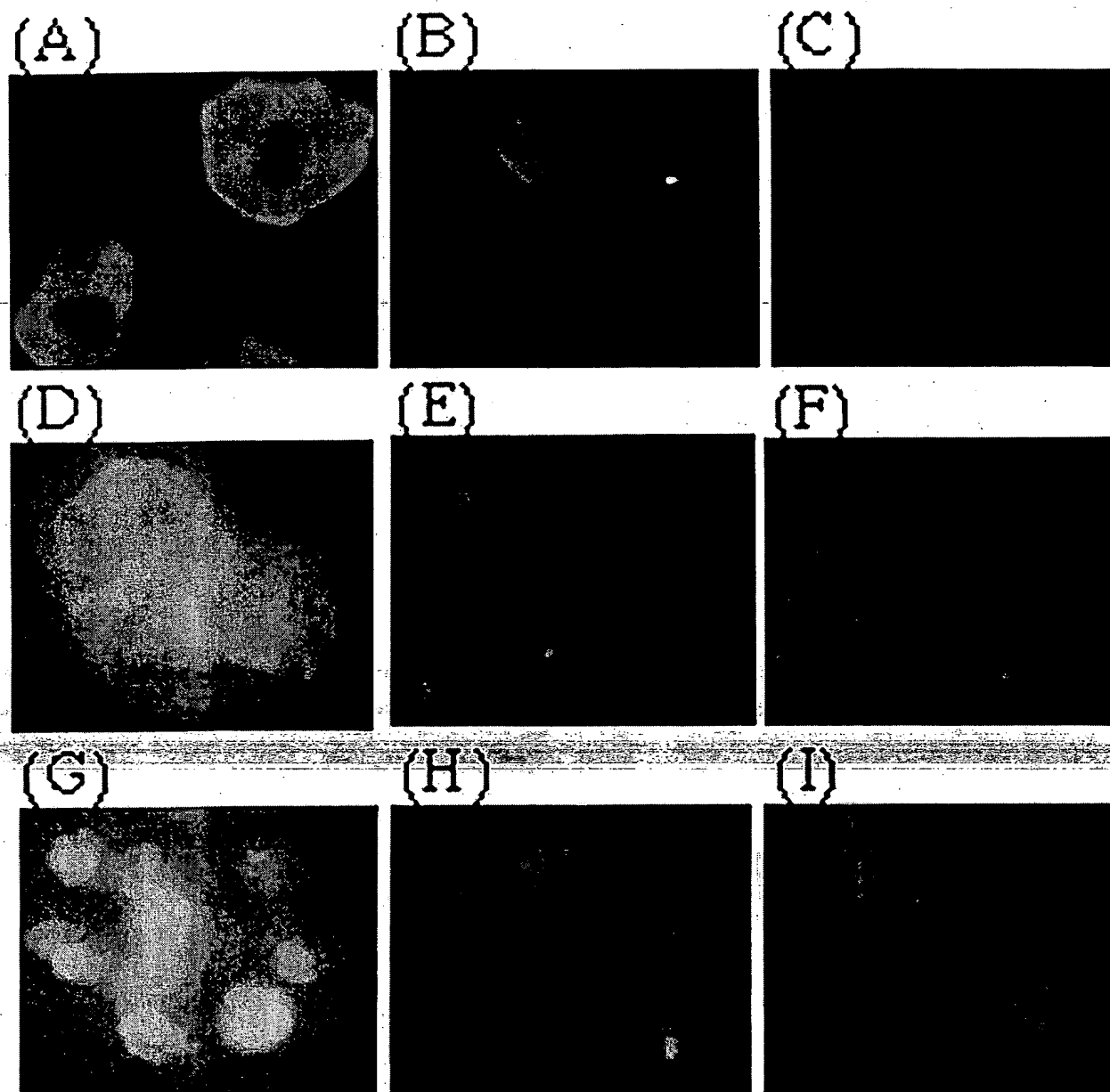


Figure 6. Expression of heparan sulfate and MIP-1 β on ATL cells and MT1 subjected to xyloside interruption of heparan sulfate proteoglycan biosynthesis and enzymatic digestion of heparan sulfate chains. MT1 (A-F) and fresh ATL cells from one representative patient (G-I) were cultured without (A, D, and G) or with 1 mM NAP-n-xyloside for 5 h at 37°C (B, E, and H) or were treated with the mixture of 100 mU/ml heparitinase I and II for 2 h at 37°C (C, F, and I). Indirect immunofluorescence was performed with anti-heparan sulfate mAb HK249 and PE-conjugated anti-rat IgG (A-C) or anti-MIP-1 β Ab and FITC-conjugated anti-rabbit IgG (D-I) and the expression was observed by fluorescence microscopy ($\times 1,000$).

NAP-l-xyloside affected the adhesion of PMA-activated normal T cells, which did not express heparan sulfate to HUVEC (Fig. 7 C).

MT-1 also spontaneously adhered to purified ICAM-1, an endothelial ligand for the integrin LFA-1 and it was in-

hibited by the pretreatment with NAP-n-xyloside, whereas neither NAP-l-xyloside nor HEX-D-xyloside did affect the adhesion (Fig. 8). Furthermore, both the adhesion of MT1 to purified ICAM-1 (Fig. 8 A) and to IL-1-activated HUVEC (Fig. 8 B) was reduced by the pretreatment of MT1 with

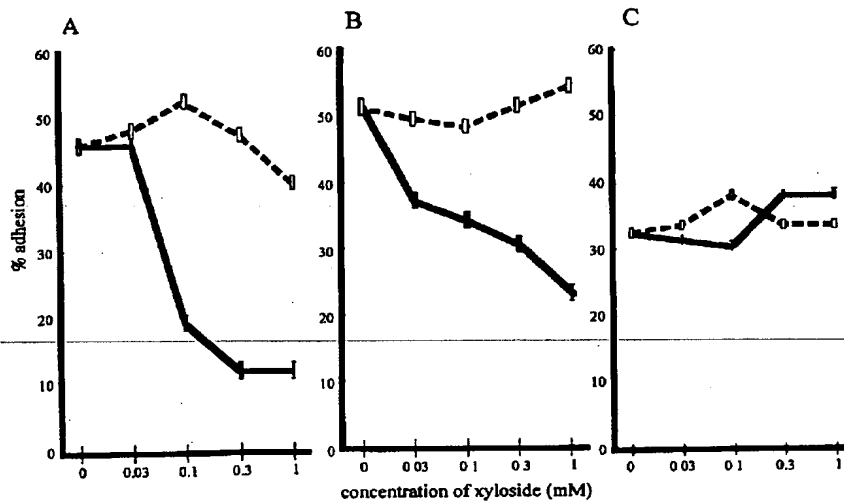


Figure 7. The effect of particular xyloside on the adhesion of ATL cells and MT1 to IL-1-activated HUVEC. (A) MT1, (B) fresh ATL cells, and (C) PMA-activated normal T cells were preincubated with or without indicated concentration of NAP-D-xyloside (dense line) or NAP-L-xyloside (dotted line) for 5 h at 37°C and adhesion assay of obtained cells to IL-1-activated HUVEC was performed as in Fig. 1. Data are expressed as mean percentage of binding of indicated cells from a representative experiment.

1 µg/ml pertussis toxin, ADP ribosylates which uncouple certain G-protein from its complex. mAb-blocking studies, in which MT1-adhesion to ICAM-1 or activated HUVEC was inhibited by anti-LFA-1/VLA-4 mAbs or anti-LFA-1 mAb (10 µg/ml), respectively, indicated that the adhesion was mediated by ATL cell integrins and their endothelial ligands. Thus, the results suggested that heparan sulfate was involved in integrin-mediated adhesion of ATL cells to endothelial integrin ligands, which might be activated through G-protein.

Discussion

The cell surface heparan sulfate in the form of proteoglycan is known to immobilize heparin-binding cytokines or growth factors, affecting cell growth/adhesion and modu-

lating clinically relevant events such as inflammation and tumor metastasis (11, 14, 18). Here we demonstrate three pivotal points for the mechanisms of how heparan sulfate amplifies leukemic cell adhesion to endothelium, using ATL cells, which show a spontaneous adhesion to HUVEC in vitro and a tendency of severe infiltration into tissue in vivo: (a) suitable heparan sulfate is expressed on ATL cells, whereas none of resting and activated cells from hematopoietic origin do express heparan sulfate; (b) cell surface heparan sulfate immobilizes integrin-triggering chemokine on ATL cells, since the expression of cell surface chemokine is abolished by xyloside-induced interruption of heparan sulfate-proteoglycan biosynthesis or by heparitinase digestion of cell surface-associated heparan sulfate chains; and (c) the artificially decreased cell surface heparan sulfate results in the integrin-mediated adhesion of ATL cells to en-

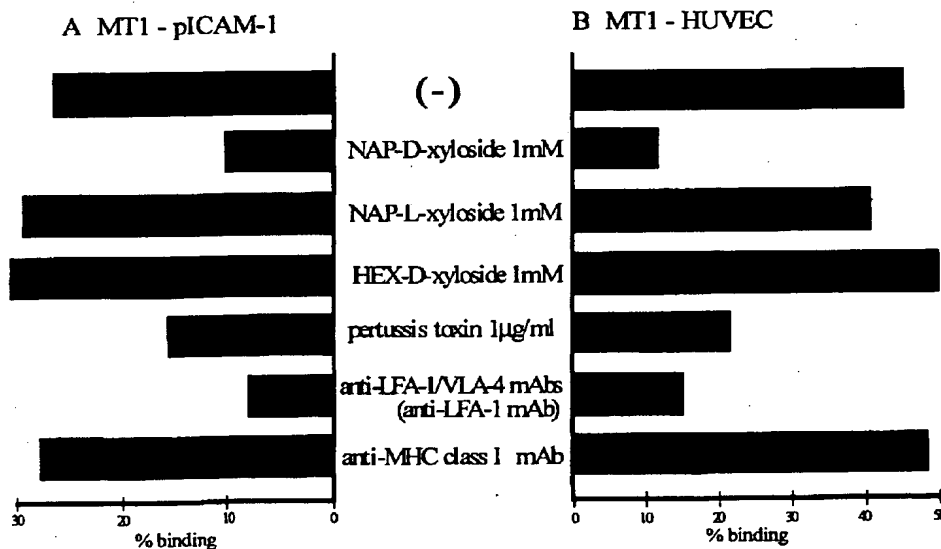


Figure 8. The adhesion of MT1 to IL-1-activated HUVEC and purified ICAM-1. The adhesion assay of MT1 which were pretreated with or without 1 mM NAP-D-xyloside, NAP-L-xyloside, HEX-D-xyloside or 1 µg/ml pertussis toxin to (A) purified ICAM-1 or (B) IL-1-activated HUVEC was carried out in the presence or absence of indicated adhesion-blocking mAbs (10 µg/ml). Data are expressed as mean percentage of binding of indicated cells from a representative experiment.

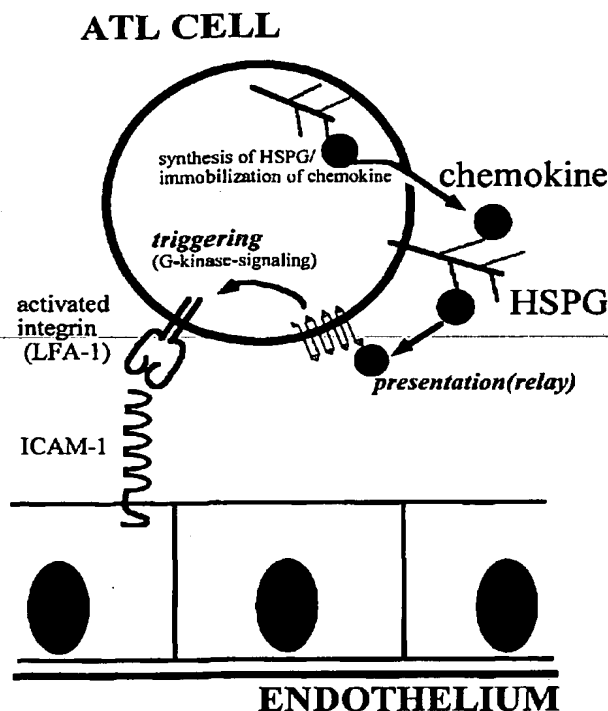


Figure 9. Diagram showing the significance of heparan sulfate in ATL cell infiltration. We propose that heparan sulfate on ATL cells immobilizes heparin-binding chemokine MIP-1 β derived from ATL cells, by which ATL cell integrins are efficiently triggered to adhere to ligands on endothelium.

endothelial cells and purified ICAM-1. Thus, we propose that heparan sulfate proteoglycan on the surface of ATL cells can be involved in integrin triggering and the cellular adhesion to endothelial ligands through immobilizing chemokines (Fig. 9).

Although the relevance of cell surface heparan sulfate proteoglycan to heparin-binding cytokines is emerging (13–17), it was difficult to investigate the involvement of heparan sulfate in cellular functions. It has been considered that suitable xylosides as well as heparitinases should be useful to perform these studies. We newly developed NAP-D-xyloside, which appears to be appropriate for functional assessments of heparan sulfate proteoglycan, since this compound, but not its L-isomer, is capable of interrupting endogenous heparan sulfate- and chondroitin sulfate-proteoglycan biosynthesis in cytoplasmic organelle such as Golgi bodies and also can inhibit the immobilization of heparin-binding cytokines there in advance to posting and transferring them to the cell surface (16, 40). Actually, NAP-D-xyloside inhibited not only the chemokine expression on the ATL cell surface but also the integrin-mediated adhesion through triggering by the posting chemokines. Furthermore, the control, NAP-L-xyloside, and HEX-D-xyloside, which selectively interrupts chondroitin sulfate-pro-

teoglycan synthesis, did not affect the chemokine expression and integrin-mediated adhesion of ATL cells. Thus, the newly established xyloside would allow us to execute precise functional investigations in the contexts with heparan sulfate on cellular functions.

It is becoming clearer that the heparan sulfate proteoglycan expressed on cellular surface is connected to cytokine network by their own bioactive functions as indicated by the following: (a) cell surface heparan sulfate interacts with basic FGF to facilitate their interaction with high affinity receptors on fibroblasts in an autocrine mechanism (41); (b) heparan sulfate on stromal cells in the bone marrow presents IL-3 and GM-CSF to myeloid progenitors in a paracrine mechanism (17); (c) heparan sulfate on vessels binds and presents not only chemokines such as MIP-1 β and IL-8 but also hepatocyte growth factor to passing (tethering) leukocytes without being washed away by the blood flow in a juxtacrine system as proposed by us and others (6, 8, 9, 38, 43). The concept that heparan sulfate proteoglycan can bind/hold and present/relay cytokines to the specific receptors and can induce cellular function have come into the involvement of heparan sulfate on ATL cells in chemokine-mediated integrin triggering. ATL cells produced a high quantity of chemokine MIP-1 β and the chemokine induced the integrin-mediated adhesion. The chemokine receptor is known to be a "serpentine" receptor with seven transmembrane domains and is a GTP-binding protein which is involved in integrin triggering (43–45). The results that pertussis toxin inhibited the integrin-mediated adhesion of ATL cells, but not PMA-activated T cell adhesion, and decreased the expression of the activated form of LFA-1 on ATL cells recognized by the NK1-L16 mAb (manuscript in preparation) suggest that MIP-1 β transduced signaling through certain G-protein by the binding to its serpentine receptor in an autocrine mechanism. The autocrine mechanism of the chemokine mediated by heparan sulfate proteoglycan would be emphasized in circulating leukocytes or leukemia cells. Heparan sulfate proteoglycan is known to be synthesized and to bind any heparin-binding cytokines in the cytoplasmic organelles such as Golgi bodies and to be transferred to the cell surface holding the cytokines (16, 40). Once "free" chemokines are secreted into the circulation, they would be washed away by the blood flow. However, by the binding to the heparan sulfate, chemokine could be practically accumulated on the cellular surface and be presented to the particular chemokine receptor in an autocrine mechanism efficaciously. Alternatively, it can be interpreted that the competitive interruption of heparan sulfate-proteoglycan synthesis by NAP-D-xyloside might reduce the binding of leukemic heparan sulfate to endothelial heparin-binding molecules such as CD31. However, the adhesion of ATL cells to purified ICAM-1 which does not have heparin-binding sites was also inhibited by the reduction of heparan sulfate synthesis equally to the adhesion of ATL cells to HUVEC. Thus, we propose here that heparan sulfate proteoglycan can be involved in chemokine-mediated autocrine mechanisms in the circulating leukemia cells.

The spontaneous production of MIP-1 β might be a characteristic feature of ATL cells, since the HTLV-I viral product tax induces MIP-1 β (46). However, as described, ATL cells produce multiple cytokines including heparin-binding chemokines in addition to MIP-1 β , and anti-MIP-1 β Ab only slightly inhibited the adhesion of ATL cells (data not shown), suggesting that MIP-1 β is one representative chemokine and the involvement of heparan sulfate proteoglycan in ATL cellular adhesion would be generalized to the adhesion mediated by multiple chemokines.

An adhesion cascade consisting of tethering, triggering, and adhesion, has been proposed to explain the mechanism of normal-leukocyte adhesion-to-endothelium (1-4, 7, 25). The present communication also suggests that this concept can be expanded to leukemic cell migration. Circulating ATL cells first tether to endothelium through the loose tethering of selectin to its ligand such as sialyl Lewis^x, since ATL cells express a high density of sialyl Lewis^x (47), which can effectively lead to the second step of triggering. The trigger appears to be essential for the adhesion of ATL cells similarly to leukocytes, in which signal transduction converts the functionally inactive integrin to an active adhesive configuration through the G-protein by the heparan sulfate-immobilized chemokine. The efficient triggering brings high affinity adhesion of ATL cells to endothelium and subsequent infiltration into underlying tissues (Fig. 9). The densities of heparan sulfate on ATL cells varied among patients who had different clinical features and activation

status. Several reports suggest that expression of heparan sulfate depends on the type of tumor cells and that the accumulation of cell surface heparan sulfate is correlated with metastatic properties of some tumor cells (11, 48). It has also been reported that the heparin-binding cytokines such as GM-CSF and IL-8 determine the metastatic potential of various tumor cells (49, 50). Structural diversity of cell surface proteoglycan in regard to protein core and heparan sulfate chains may provide additional specificity for cytokine immobilization (39), and differential production of heparin-binding cytokines from tumor cells might prescribe ability of integrin triggering, adhesion to endothelium, and metastasis.

Taken together, we propose that cell surface heparan sulfate on circulating leukemic cells can induce integrin-mediated adhesion through chemokine-mediated autocrine mechanisms by posting and relaying chemokine to the receptor on the cells. Heparan sulfate appears to have a junctional role between cytokines and adhesion molecules, the two greatest mediators of cellular communication. This is the first report to explore the significance of interaction among heparan sulfate proteoglycan and heparin-binding cytokine for circulating tumor adhesion. Our findings warrant further studies, to see whether different proteoglycans and cytokines might bring enormous flexibility to the process of leukemic cell infiltration and tumor metastasis, and would introduce new pharmacological approaches to control them.

We thank S. Shaw and D.H. Adams for critical review of the manuscript and Ms. T. Adachi for excellent technical assistance. We also thank the following investigators for providing mAbs, cDNA and cell lines: P.E. Auron for β -actin cDNA, C.G. Figdor for NKI-L16 mAb, I. Miyoshi and K. Sagawa for MT1, MT2, HUT-102, and SALT-3 cell line, A. Moretta for MAR206, F. Sanchez-Madrid for HP2/1 mAb, S. Shaw for NIH11b-1 and NIH49d-1 mAbs and L428 cell line, U. Siebenlist for anti-MIP-1 β Ab and MIP-1 β cDNA, D. Siegel for 3G8 mAb, and H. Zola for FMC63 mAb.

This work was supported in part by a Grant-in-Aid for Scientific Research from the Ministry of Education, Science and Culture of Japan and Seikagaku Kogyo Ltd. Co., Tokyo, Japan.

Address correspondence to Yoshiya Tanaka, The First Department of Internal Medicine, University of Occupational and Environmental Health, Japan, School of Medicine, 1-1 Iseigaoka, Yahatanishi-ku, Kitakyushu 807, Japan.

Received for publication 10 April 1996 and in revised form 23 July 1996.

References

1. Shimizu, Y., W. Newman, Y. Tanaka, and S. Shaw. 1992. Lymphocyte interactions with endothelial cells. *Immunol. Today*. 13:106-112.
2. Butcher, E.C. 1991. Leukocyte-endothelial cell recognition: three (or more) steps to specificity and diversity. *Cell*. 67: 1033-1036.
3. Tanaka, Y., S.M. Albelda, K.J. Horgan, G.A. van Seventer, Y. Shimizu, W. Newman, J. Hallam, P.J. Newman, C.A. Buck, and S. Shaw. 1992. CD31 expressed on distinctive T cell subsets is a preferential amplifier of β 1 integrin-mediated adhesion. *J. Exp. Med.* 176:245-253.
4. Adams, D.H., and S. Shaw. 1994. Leukocyte-endothelial interactions and regulation of leukocyte migration. *Lancet*. 343: 831-836.
5. Shimizu, Y., W. Newman, T.V. Gopal, K.J. Horgan, N. Graber, L.D. Beall, G.A. van Seventer, and S. Shaw. 1991. Four molecular pathways of T cell adhesion to endothelial cells: roles of LFA-1, VCAM-1, and ELAM-1 and changes in pathway hierarchy under different activation conditions. *J. Cell Biol.* 113:1203-1212.

6. Tanaka, Y., D.H. Adams, S. Hubscher, H. Hirano, U. Siebenlist, and S. Shaw. 1993. T-cell adhesion induced by proteoglycan-immobilized cytokine MIP-1 β . *Nature (Lond.)*. 361:79-82.
7. Springer, T.A. 1994. Traffic signals for lymphocyte recirculation and leukocyte emigration: the multistep paradigm. *Cell*. 76:301-314.
8. Tanaka, Y., D.H. Adams, and S. Shaw. 1993. Proteoglycans on endothelial cells present adhesion-inducing cytokines to leukocytes. *Immunol. Today*. 14:111-115.
9. Webb, L.M.C., M.U. Ehrenguber, I. Clark-Lewis, and M. Baggiolini. 1993. Binding to heparan sulfate or heparin enhances neutrophil responses to interleukin 8. *Proc. Natl. Acad. Sci. USA*. 90:7158-7162.
10. Rot, A. 1992. Endothelial cell binding of NAP-1/IL-8: role in neutrophil emigration. *Immunol. Today*. 13:291-294.
11. Jackson, R.L., S.J. Busch, and A.D. Cardin. 1991. Glycosaminoglycans: molecular properties, protein interactions, and role in physiological processes. *Physiol. Rev.* 71:481-539.
12. Hardingham, T.E., and A.J. Fosang. 1992. Proteoglycans: many forms and many functions. *FASEB J.* 6:861-870.
13. Thiery, J.P., and B. Boyer. 1992. The junction between cytokines and cell adhesion. *Curr. Opin. Cell Biol.* 4:782-792.
14. Wight, T.N., M.G. Kinsella, and E.E. Qvarnstrom. 1992. The role of proteoglycans in cell adhesion, migration and proliferation. *Curr. Opin. Cell Biol.* 4:793-801.
15. Gilat, D., I. Cahalon, R. HersHKoviz, and O. Lider. 1996. Interplay of T cells and cytokines in the context of enzymatically modified extracellular matrix. *Immunol. Today*. 17:16-20.
16. Templeton, D.M. 1992. Proteoglycans in cell regulation. *Crit. Rev. Clin. Lab. Sci.* 29:141-184.
17. Roberts, R., J. Gallagher, E. Spooner, T.D. Allen, F. Bloomfield, and T.M. Dexter. 1988. Heparan sulphate bound growth factors: a mechanism for stromal cell mediated haemopoiesis. *Nature (Lond.)*. 332:376-378.
18. Ruoslahti, E., and Y. Yamaguchi. 1991. Proteoglycans as modulator of growth factor activities. *Cell*. 64:867-869.
19. Nathan, C., and M. Sporn. 1991. Cytokines in context. *J. Cell Biol.* 113:981-986.
20. Poggi, A., M. Stella, and M.B. Donati. 1993. The importance of blood cell-vessel wall interactions in tumor metastasis. *Baillieres. Clin. Haematol.* 6:731-752.
21. Timens, W. 1995. Cell adhesion molecule expression and homing of hematologic malignancies. *Crit. Rev. Oncol. Hematol.* 19:111-129.
22. Hinuma, Y., K. Nagata, M. Hanaoka, M. Nakai, T. Matsumoto, K. Kinoshita, S. Shirakawa, and I. Miyoshi. 1981. Adult T-cell leukemia: antigen in an ATL cell line and detection of antibodies to the antigen in human sera. *Proc. Natl. Acad. Sci. USA*. 78:6476-6480.
23. Uchiyama, H., B.A. Barut, A.F. Mohrbacher, D. Chauhan, and K.C. Anderson. 1993. Adhesion of human myeloma-derived cell lines to bone marrow stroma cells stimulates interleukin-6. *Blood*. 82:3712-3718.
24. Utsunomiyama, A., S. Harada, A. Terada, M. Kodama, T. Uematsu, S. Tsukasa, S. Hashimoto, and M. Tokunaga. 1988. Adult T-cell leukemia with leukemia cell infiltration into the gastrointestinal tract. *Cancer*. 61:824-828.
25. Suzuki, S., A. Mizutani, Y. Koike, M. Kato, K. Yoshida, and K. Kimata. 1991. Glycosaminoglycan chains of proteoglycans: approaches to the study of their structure and function. *Pure Appl. Chem.* 63:545-554.
26. Lub, M., Y. van Kooyk, and C.G. Figdor. 1995. Ins and outs of LFA-1. *Immunol. Today*. 16:479-483.
27. Pulido, R., M.R. Campanero, A. Garcia-Pardo, and F. Sanchez-Madrid. 1991. Structure-function analysis of the human integrin VLA-4 ($\alpha 4/\beta 1$): correlation of proteolytic $\alpha 4$ peptides with $\alpha 4$ epitopes and sites of ligand interaction. *FEBS (Fed. Eur. Biochem. Soc.) Lett.* 294:121-124.
28. Postigo, A.A., P. Sanchez-Mateos, A.I. Lazarovits, F. Sanchez-Madrid, and M.O.D. Landazuri. 1994. $\alpha 4\beta 7$ Integrin mediates B cell binding to fibronectin and vascular cell adhesion molecule-1: expression and function of $\alpha 4$ integrins on human B lymphocytes. *J. Immunol.* 151:2471-2483.
29. van Seventer, G.A., W. Newman, Y. Shimizu, Y. Tanaka, K.J. Horgan, T. Nutman, and S. Shaw. 1991. Functional analysis of three activation-regulated endothelial adhesion molecules ICAM-1, VCAM-1 and ELAM-1. *J. Exp. Med.* 174:901-914.
30. Sobue, M., H. Habuchi, K. Ito, H. Yonekura, K. Oguri, K. Sakurai, S. Kamohar, Y. Ueno, R. Noyon, and S. Suzuki. 1987. β -D-xylosides and their analogues as artificial initiators of glycosaminoglycan chain synthesis: a glycone-related variation in their effectiveness in vitro and in vivo. *Biochem. J.* 241:591-601.
31. Kolset, S.O., K. Sakurai, I. Ivhed, A. Overatn, and S. Suzuki. 1990. The effect of β -D-xylosides on the proliferation and proteoglycan synthesis. *Biochem. J.* 265:637-645.
32. Chomczynski, P., and N. Sacchi. 1987. Single-step method of RNA isolation by acid guanidinium thiocyanate-phenol-chloroform extraction. *Anal. Biochem.* 162:156-159.
33. Zipfel, E.F., J. Balke, S.G. Irving, K. Kelly, and U. Siebenlist. 1989. Mitogenic activation of human T cells induces two closely related genes which share structural similarities with a new family of secreted factors. *J. Immunol.* 142:1582-1590.
34. van Kooyk, Y., P. Weder, K. Heije, and C.G. Figdor. 1994. Extracellular Ca^{2+} modulates leukocyte function-associated antigen-1 cell surface distribution on T lymphocytes and consequently affects cell adhesion. *J. Cell Biol.* 124:1061-1070.
35. Shirakawa, F., Y. Tanaka, S. Oda, S. Eto, and U. Yamashita. 1989. Autocrine stimulation of interleukin 1 alpha in the growth of adult human T-cell leukemia cells. *Cancer Res.* 49:1143-1147.
36. Wake, A., Y. Tanaka, K. Nakatsuka, M. Misagao, S. Oda, I. Morimoto, and S. Eto. 1995. Calcium-dependent homotypic adhesion through leukocyte function-associated antigen-1/intercellular adhesion molecule-1 induces interleukin-1 and parathyroid hormone-related protein production on adult T-cell leukemia cells in vitro. *Blood*. 86:2257-2267.
37. Lal, R.B., and D.L. Rudolph. 1991. Constitutive production of interleukin-6 and tumor necrosis factor-alpha from spontaneously proliferating T cells in patients with human T-cell lymphotropic virus type-I/II. *Blood*. 78:571-574.
38. Adams, D.H., L. Harvath, D.P. Bottaro, R. Interrante, G. Catalano, Y. Tanaka, A. Strain, S.G. Hubscher, and S. Shaw. 1994. Hepatocyte growth factor and macrophage inflammatory protein-1 β : structurally distinct cytokines that induce rapid cytoskeletal changes and subset-preferential migration in T cells. *Proc. Natl. Acad. Sci. USA*. 91:7144-7148.
39. Witt, D.P., and A.D. Lander. 1994. Differential binding of chemokines to glycosaminoglycan subpopulations. *Curr. Biol.* 4:394-400.
40. Lindahl, U., K. Lidholt, D. Spillmann, and L. Kjellen. 1994. More to "heparin" than anticoagulation. *Thromb. Res.* 75:1-32.
41. Klagsbrun, M., and A. Baird. 1991. A dual receptor system is

- required for basic fibroblast growth factor activity. *Cell*. 67: 229-231.
42. Zimmerman, G.A., D.E. Lorant, T.M. McIntyre, and S.M. Prescott. 1993. Juxtacrine intercellular signaling: another way to do it. *Am. J. Respir. Cell Mol. Biol.* 9:573-577.
 43. Neote, K., D. DiGregorio, J.Y. Mak, R. Horuk, and T.J. Schall. 1993. Molecular cloning, functional expression, and signaling characteristics of a C-C chemokine receptor. *Cell*. 72:415-425.
 44. Bargatze, R.F., and E.C. Butcher. 1993. Rapid G protein-regulated activation event involved in lymphocyte binding to high endothelial venules. *J. Exp. Med.* 187:367-372.
 45. Clark, E.A., and J.S. Brugge. 1995. Integrins and signal transduction pathway: the road taken. *Science (Wash. DC)*. 268: 233-239.
 46. Napolitano, M., K.B. Seamon, and W.J. Leonard. 1990. Identification of cell surface receptors for the Act-2 cytokine. *J. Exp. Med.* 172:285-289.
 47. Ishikawa, T., A. Imura, K. Tanaka, H. Shirane, M. Okuma, and T. Uchiyama. 1993. E-selectin and vascular cell adhesion molecule-1 mediate adult T-cell leukemia cell adhesion to endothelial cells. *Blood*. 82:1590-1598.
 48. Timar, J., A. Ladanyi, K. Lapis, and M. Moczar. 1992. Differential expression of proteoglycans on the surface of human melanoma cells characterized by altered experimental metastatic potential. *Am. J. Pathol.* 141:467-474.
 49. Singh, R.K., M. Gutman, R. Radinsky, C.D. Bucana, and I.J. Fidler. 1994. Expression of interleukin 8 correlates with the metastatic potential of human melanoma cells in nude mice. *Cancer Res.* 54:3242-3247.
 50. Young, M.R., Y. Lozano, A. Djordjevic, S. Devata, J. Matthews, M.E. Young, and M.A. Wright. 1993. Granulocyte-macrophage colony-stimulating factor stimulates the metastatic properties of Lewis lung carcinoma cells through a protein kinase A signal-transduction pathway. *Int. J. Cancer*. 53:667-671.

T CELL SIGNALING OF MACROPHAGE FUNCTION IN INFLAMMATORY DISEASE

Robert D. Stout¹ and Jill Suttles²

Program in Immunology, Departments of Microbiology¹ and Biochemistry², James H. Quillen College of Medicine at East Tennessee State University, Johnson City, TN, USA

TABLE OF CONTENTS

1. Abstract
2. Introduction
3. Multiple roles of macrophages in inflammatory disease
4. Mechanisms of T cell-mediated induction of macrophage function
5. Contact-dependent signaling of macrophage activation
6. Role of contact-dependent signaling in autoimmune disease
7. Perspective
8. Acknowledgments
9. References

1. ABSTRACT

Macrophages play diverse roles in episodic T cell-mediated inflammatory diseases such as multiple sclerosis and rheumatoid arthritis, function as accessory cells for T cell activation, as pro-inflammatory cells, as effector cells which mediate tissue damage, and as anti-inflammatory cells which promote wound healing. In addition to the many roles of T cell-derived cytokines in differentially modulating these diverse macrophage activities, research over the last few years has demonstrated that contact-dependent signaling which occurs during T cell-macrophage adhesion is a critical triggering event in the activation of macrophage function. Substantial research emphasis has been placed on CD40 as a mediator of contact-dependent signaling. However, other membrane-anchored receptor:ligand pairs may also contribute to the stimulation of macrophage function. This is a brief review of the rapidly expanding, but still incomplete, knowledge of how T cells, through both contact-dependent and cytokine signals, regulate macrophage function during inflammatory disease.

2. INTRODUCTION

Research over the past decade has only begun to unravel the complex interactions between T cells and macrophages that are involved in the

pathogenesis of cell-mediated inflammatory diseases such as multiple sclerosis. The cellular infiltrates of active sclerotic lesions include CD4+ T cells (Th1 with some Th0 and Th2), CD8+ T cells, and macrophages (microglia and monocytes) (1-8). The types of cells present reflect the state of progression of the inflammatory lesion. Macrophages play critical accessory, inflammatory, and effector roles in this non-septic T cell-mediated inflammatory disease (5-9) and tend to be present throughout the inflammatory process. The development of a cell-mediated response is currently hypothesized to depend on the differentiation of interferon (IFN)-gamma producing Th1 cells from activated Th0 precursors (10,11). The production of interleukin (IL)-12 by macrophages clearly plays an important role in the maturation of Th1 cells (10). Upon maturation, these Th1 cells, as well as inflammatory CD8+ cells, both of which produce IFN-gamma and tumor necrosis factor (TNF)-alpha/beta, play a dominant role in macrophage activation and pathogenesis of the inflammatory lesion (1,3,12-15). In contrast, IL4/IL10-producing T cells are hypothesized to play a role in down-regulation of the inflammatory response (1,3,16). It is these "type 2" CD8+ cells that appear to be active in the cellular infiltrate of sclerotic lesions that are in remission (1,3).

In addition to the many roles of T cell-derived cytokines in stimulation and inhibition of macrophage function (13), research over the last few years has demonstrated that the critical triggering event in activation of macrophage cytokine production and effector function is contact-dependent signaling during T cell-macrophage adhesion (17-24). Substantial research emphasis was placed on CD40 as a mediator of contact-dependent

Received 4/15/97; Accepted 4/18/97

To whom correspondence should be addressed at: Department of Microbiology, James H. Quillen College of Medicine, Box 70579, East Tennessee State University, Johnson City, TN 37614-0579, Tel: 423 439 6299, Fax: 423 439 5847, E-mail: stout@access.etsu-tn.edu

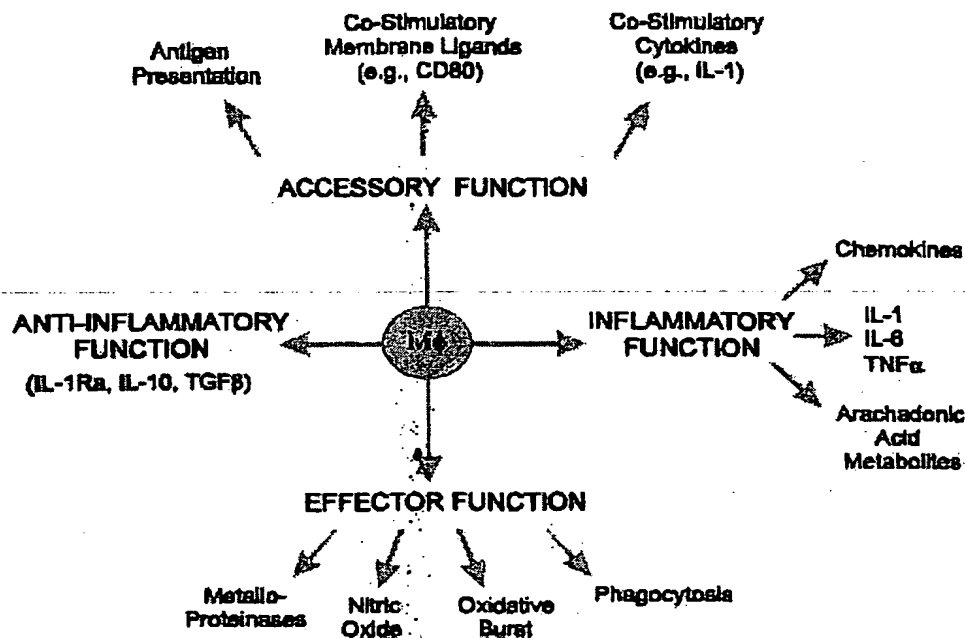


Figure 1. The diverse functions of macrophages: Macrophages are capable of many functional activities and contribute both to the initiation of cell-mediated immune response and to the effector limb of those responses. During the course of the response, macrophages can display, at different times, both inflammatory and anti-inflammatory activities.

signaling of macrophages. CD40 ligation has been reported to contribute to the induction of accessory molecules such as CD80 and CD86 (25-27), to the induction of inflammatory cytokines and chemokines (27-29), and to the induction of nitric oxide generation (24) and metalloproteinase secretion (30). However, the observation that T cells from CD40L-deficient mice are capable of contact-dependent signaling of macrophages (31) establishes that membrane-anchored receptor:ligand pairs other than CD40:CD40L can be involved in T cell signaling of macrophages. In the following sections, we try to provide a succinct account of T cell signaling of macrophages which, although brief and simplified for the sake of clarity, emphasizes the complexity of the cascading cell-cell interactions involved in a relapsing inflammatory autoimmune disease.

3. MULTIPLE ROLES OF MACROPHAGES IN INFLAMMATORY DISEASES.

The cellular infiltrates of active sclerotic lesions are dominated by cells of the monocytic lineage (macrophages and microglial cells) (6-8). These macrophages can display very diverse functions in sclerotic lesions (Fig. 1). They can function as accessory cells, presenting antigen and providing co-stimulatory ligands (e.g., CD80, CD86, and CD48) and co-stimulatory cytokines (e.g., IL-1 and IL-12) to the infiltrating T cells (10,13,32-36). Macrophages

can be activated to produce prodigious amounts of pro-inflammatory cytokines such as TNF- α , IL-1, and IL-6, chemoattractant cytokines such as IL-8 and macrophage inflammatory protein (MIP)-1 α/β (13,37), and pro-inflammatory products of arachidonic acid metabolism (13,38).

TNF- α , in particular, appears to play a critical role in the pathogenesis of experimental allergic encephalomyelitis, the murine model of multiple sclerosis, insofar as administration of anti-TNF- α antibodies *in vivo* inhibits the development of experimental allergic encephalomyelitis (39).

Interestingly, in addition to the inflammatory and destructive activities listed above, macrophages have the potential to contribute to the remission of the inflammatory episode, although the degree to which they participate in remission has not yet been directly assessed. Macrophages can be induced to generate toxic reactive oxygen and nitrogen intermediates (13,40-45) and to secrete "tissue restructuring" metalloproteinases (13,46-48), each of which have been hypothesized to directly contribute to the demyelination process (49-51). Macrophages also can be induced to secrete cytokines which inhibit macrophage accessory, inflammatory, and effector functions. IL-10, which is produced by both macrophages and T cells, down-regulates

T Cell:Macrophage interactions

expression of costimulatory molecules such as CD86 (52,53), inhibits the production of IL-1 and TNF-alpha and reduces generation of reactive oxygen and nitrogen intermediates (54-57). Transforming growth factor-beta (TGF-beta), which is produced by many cell types including macrophages and T cells, also inhibits generation of reactive oxygen and nitrogen intermediates (58,59), especially in synergy with IL-10 (43,57,60), and is hypothesized to play a critical role in resolution of inflammatory lesions in experimental allergic encephalomyelitis (61-63).

4. MECHANISMS OF T CELL-MEDIATED INDUCTION OF MACROPHAGE FUNCTIONS.

The induction of these diverse macrophage functions is complex, differentially regulated, and poorly understood. Cytokines can stimulate or inhibit many of the macrophage functions described above but the modulating effect of many of the cytokines depends on the state of activation of the target macrophage population, the triggering signal, and timing (13,64,65). Although some exceptions have been noted, T cell cytokines such as IFN-gamma, IL-4, GM-CSF, and IL-3 generally can enhance accessory and co-stimulatory activity (13,29,66-69) and IFN-gamma, GM-CSF, and IL-3 can augment oxidative burst capacity (70-73). The combination of IL-2 plus IFN-gamma has been shown to induce TNF-alpha production and the combination of TNF-alpha and IFN-gamma have been shown to induce nitric oxide production (74-79). Thus, cytokines, especially the Th1 cytokines (IL2, TNF-alpha, IFN-gamma), can stimulate inflammatory and tissue destructive activities in macrophages.

In contrast, IL-10, TGF-beta, and, to a lesser degree, IL-4 (Th2 cytokines) inhibit the induction of oxidative burst and nitric oxide generation (54,57-59,80) and inhibit inflammatory cytokine production by macrophages (54-56,61,81), but do not affect (or enhance) IL-1Ra (IL-1 Receptor antagonist), IL-10 and TGF-beta production (61,82,83). Thus activated macrophages modulated by TGF-beta may display predominantly anti-inflammatory activities, such as secretion of IL-1Ra, IL-10, and TGF-beta.

Although these cytokines play an important role in modulating macrophage function, it is now clear that a critical mechanism by which T cells trigger these macrophage functions involves engagement of membrane-anchored receptor:ligand pairs during heterotypic adhesion between T cells and macrophages. Macrophage accessory, inflammatory, effector, and inhibitory functions have all been shown to be stimulated by paraformaldehyde fixed activated T cells or plasma membranes isolated from activated T cells (13,17-24,44,45,47). In each of these systems, pre-activation of the T cells is a requirement for cell

contact-dependent signaling, suggesting the involvement of activation-induced membrane-anchored ligands on the T cells.

5. CONTACT-DEPENDENT SIGNALING OF MACROPHAGE ACTIVATION.

CD40:CD40L is the receptor:ligand pair that has received the most attention in the context of contact-dependent signaling of B cells and macrophages (34,84-87). CD40L is expressed transiently upon activation of T cells, with maximum expression usually observed at 5-10 hrs (88,89). Anti-CD40L antibody interferes with T cell signaling of macrophage accessory function, cytokine production and nitric oxide generation (24,25,28). Conversely, anti-CD40 antibody (28), CD40L-transfected cells (29), or soluble trimeric CD40L (27) induce expression of accessory molecules and production of a full array of cytokines (IL-1, TNF-alpha, IL-6, IL-10, IL-12) by macrophages. However, although anti-CD40L antibody nearly completely blocks induction of IL-1 release and CD80 expression by isolated T cell membranes or fixed T cells (25,28), it only partially blocks nitric oxide generation and CD86 expression (24,25). These observations suggested that CD40 ligation is not solely responsible for T cell contact-dependent signaling. This was confirmed by the observation that T cells from CD40L-deficient mice can activate macrophage nitric oxide generation via contact-dependent signaling (31). Although CD40L-deficient T cells, paraformaldehyde-fixed after being activated for 5 hrs on anti-CD3, lacked the ability to signal macrophage nitric oxide production, CD40L-deficient T cells, fixed after being activated for 24 hrs on anti-CD3, were able to signal macrophage nitric oxide production as effectively as similarly activated normal T cells (31). This indicates that CD40 ligation may dominate signaling early in T cell-macrophage interaction but that other receptors may become involved later in the interaction.

Receptors other than CD40 that have been reported to signal macrophage function include CD23 (90,91), CD31 (92), CD38 (93), CD44 (94), CD45 (45,94), CD69 (95,96), and LFA-3 (94). The most abundant data is on CD23. CD23 is the low affinity Fc RII and thus is capable of binding complexes of antigen and IgE antibody. In addition, CD23 binds CD21 (97) and, according to one report, also binds CD11b and CD11c (98). Ligation of membrane CD23 on macrophages induces production of TNF-alpha, IL-6, and nitric oxide (97,99,100). Interestingly, ligation of CD21 on the macrophage membrane by soluble CD23 also has been reported to induce the production of TNF-alpha and IL-1 by macrophages (101,102). CD21 (90) and, under more restricted conditions, CD23 (103) have been reported to be expressed by activated but not by resting T cells. It is therefore possible that the CD23:CD21 receptor:ligand pair is

T Cell:Macrophage interactions

Table 1
The Roles of CD40:CD40L Interactions in Cell-Mediated Inflammatory Disease

Interacting Cell	Functions Induced	Role in Inflammatory Response
Dendritic Cells	CD80 Expression IL-1 Production	Stimulation of Immune Response
Histiocytes, Monocytes	IL-12 Production	Development of Th1 Cells
Histiocytes, Monocytes	Inflammatory Cytokine Production	Enhancement of Inflammatory Response
Vascular Endothelial Cells	Homing/Adhesion Molecule Expression (e.g., VCAM)	Enhanced Recruitment of T Cells into Inflamed Tissue
Monocytes/Macrophages	Production of NO, O ₂ ⁻ , and metalloproteinases	Tissue Destruction
Macrophages/fibroblasts	Production of TGF-beta/Proliferation	Tissue Repair/Remission

Ligation of CD40 on myeloid cells, endothelial cells, and fibroblasts can induce a wide range of functional activities which could contribute to essentially every aspect of cell-mediated inflammatory responses.

involved in T cell-mediated signaling of some inflammatory macrophage functions.

6. ROLE OF CONTACT-DEPENDENT SIGNALING IN AUTOIMMUNE DISEASE.

The role of contact-dependent signaling in the development of experimental allergic encephalomyelitis has been shown dramatically using transgenic B10.PL mice expressing the T cell receptor reactive with the encephalitogenic peptide (A₁-11) of myelin basic protein. Transgenic CD40L-deficient mice, unlike +/- transgenic mice, do not develop acute experimental allergic encephalomyelitis upon immunization with A₁-11 (104). This nonresponsiveness was ascribed to the inability of CD40L-deficient T cells to induce CD80 expression on dendritic cells. The adoptive transfer of CD80-positive accessory cells into CD40L-deficient mice restored their ability to respond to antigen and to develop experimental allergic encephalomyelitis. This indicates that, unless an undiscovered second ligand for CD40 exists, T cells are capable of driving the inflammatory process by CD40-independent receptor:ligand and/or cytokine signaling.

Although the above studies with transgenic CD40L-deficient mice suggest that CD40 ligation is not required for the development of sclerotic lesions once the CD80 costimulus is provided, studies with normal animals indicate that CD40:CD40L interactions play a significant role throughout the inflammatory process. Administration of anti-CD40L antibody as late as 7-9 days after immunization of SJL mice with encephalitogenic peptide reduced the extent and severity of lesions by more than 50% (6). This is not surprising because CD40:CD40L interactions are known to play many roles in cell-mediated inflammatory responses, including stimulation of expression of adhesion and homing molecules on vascular endothelium, stimulation of

chemokine and inflammatory cytokine production, stimulation of the production of IL-12, which is critical for maturation of the inflammatory Th1 subset, and stimulation of fibroblasts (105) (Table 1). Several of the above activities are critical for the development of experimental allergic encephalomyelitis. VCAM-1 plays a critical role in the inflammatory process of experimental allergic encephalomyelitis (106); ligation of CD40 on endothelial cells induces VCAM-1 expression (107). Blockade of CD80 expression has been shown to prevent clinical relapses and chronicity of experimental allergic encephalomyelitis (108-110); antibody blockade of CD40:CD40L interactions completely blocks T cell contact-induction of CD80 expression (25). Since neither IL-10 nor TGF-beta appear to down-regulate CD80 expression (52,53), the down-regulation of CD40L, and hence CD40L stimulation of CD80 expression, may therefore be a pivotal event in the shift from inflammatory to anti-inflammatory activities in the sclerotic lesion.

7. PERSPECTIVE.

The studies on experimental allergic encephalomyelitis to date strongly support critical roles for CD40 and TNF-alpha (CD40-induced?) in the pathogenesis of sclerotic lesions and for TGF-beta in remission of the inflammatory episode. Although receptors other than CD40 (e.g., CD23 and CD69) have been shown to stimulate macrophage production of inflammatory cytokines *in vitro*, their role in the pathogenesis of inflammatory disease is still unexplored. The studies on T cell receptor transgenic and CD40L-deficient mice (105) indicate that CD40-independent receptor:ligand pairs and/or cytokines are sufficient to drive the development of disease once the T cells are activated. This is supported by the observation that administration of anti-CD40L antibodies after immunization with encephalitogenic peptide only partially interferes with the development

T Cell:Macrophage interactions

of disease. The identification of these CD40-independent receptors and of their role in the pathogenesis of inflammatory disease will be a major area of research interest throughout the next decade.

8. ACKNOWLEDGMENTS

This work was supported by grants from the National Institutes of Health (R01 AI34875) and from the Arthritis Foundation (Biomedical Sciences).

9. REFERENCES

- 1 A. O'Garra, & K. Murphy: T-cell subsets in autoimmunity. *Curr Opin Immunol* 5,880-6 (1993)
- 2 H. Wekerle: Immunopathogenesis of multiple sclerosis. *Acta Neurol* 13,197-204 (1991)
- 3 D. Mason, & D. Fowell: T-cell subsets in autoimmunity. *Curr Opin Immunol* 4,728-32 (1992)
- 4 C.S. Raine, U. Traugott, & S.H. Stone: Suppression of chronic allergic encephalomyelitis: relevance to multiple sclerosis. *Science* 201,445-8 (1978)
- 5 R. Martin, H.F. McFarland, & D.E. McFarlin: Immunological aspects of demyelinating diseases. *Ann Rev Immunol* 10,153-87 (1992)
- 6 K. Gerritse, R.J. Noelle, A. Aruffo, J. Ledbetter, J.D. Laman, W.J.A. Boersma, & E. Claassen: CD40:CD40 ligand interactions in experimental allergic encephalomyelitis and multiple sclerosis. *Proc Natl Acad Sci USA* 93,2499-504 (1996)
- 7 I. Huitanga, S.R. Ruuls, S. Jung, N. Van Rooijen, H.-P. Hartung, & C.D. Dijkstra: Macrophages in T cell line-mediated demyelinating and chronic relapsing experimental autoimmune encephalitis in Lewis rats. *Clin Exp Immunol* 100,344-51 (1995)
- 8 J. Bauer, T. Sminia, F.G. Wouterlood, & C.D. Dijkstra: Phagocytic activity of macrophages and microglial cells during the course of acute and chronic relapsing experimental autoimmune encephalomyelitis. *J Neurosci Res* 38,365-75 (1994)
- 9 S.D. Miller, & W.J. Karpus: The immunopathogenesis and regulation of T cell-mediated demyelinating diseases. *Immunol Today* 15,356-61 (1994)
- 10 R. Manetti, P. Parronchi, M.-G. Giudizi, M.-P. Piccinni, E. Maggi, G. Trinchieri, & S. Romagnani: Natural killer cell stimulatory factor (interleukin, 12) induces T helper type 1-specific immune responses and inhibits the development of IL-4-producing Th cells. *J Exp Med* 177,1199-204 (1993)
- 11 F.W. Fitch, M.D. McKisic, D.W. Lancki, & T.F. Gajewski: Differential regulation of murine T lymphocyte subsets. *Annu Rev Immunol* 11,29-48 (1993)
- 12 T.R. Mosmann, & R.L. Coffman: Heterogeneity of cytokine secretion patterns and functions of helper T cells. *Adv Immunol* 46,111-48 (1989)
- 13 R.D. Stout, & J. Suttles: T cell signaling of macrophage activation. Cell contact-dependent and cytokine signals. R. G. Landes Company; Springer-Verlag, Austin, (1995)
- 14 E. De Maeyer, & J. De Maeyer-Guignard: Interferon-gamma. *Curr Opin Immunol* 4,321-6 (1992)
- 15 M.A. Farrar, & R.D. Schreiber: The molecular cell biology of interferon-gamma and its receptor. *Annu Rev Immunol* 11,571-611 (1993)
- 16 P. Salgame, J.S. Abrams, C. Clayberger, H. Goldstein, J. Convit, R.L. Modlin, & B.R. Bloom: Differing lymphokine profiles of functional subsets of human CD4 and CD8 T cell clones. *Science* 254,279-82 (1991)
- 17 R.D. Stout, & K. Bottomly: Antigen specific activation of effector macrophages by interferon-gamma producing (Th1) T cell clones. Failure of IL-4 producing (Th2) T cell clones to activate effector function in macrophages. *J Immunol* 142,760-5 (1989)
- 18 R.D. Stout, & J. Suttles: T cell-macrophage cognate interaction in the activation of macrophage effector function by Th2 cells. *J Immunol* 150,5330-7 (1993)
- 19 X. Tao, & R.D. Stout: T cell-mediated cognate signaling of nitric oxide production by macrophages. Requirements for activation of macrophages by plasma membranes isolated from T cells. *Eur J Immunol* 23,2916-21 (1993)
- 20 J. Suttles, R.W. Miller, X. Tao, & R.D. Stout: T cells which do not express membrane tumor necrosis factor-alpha activate macrophage effector function by cell contact-dependent signaling of macrophage tumor necrosis factor-alpha production. *Eur J Immunol* 24,1736-42 (1994)
- 21 J.P. Sypek, M.M. Matzilevich, & D.J. Wyler: Th2 lymphocyte clone can activate macrophage antileishmanial defense by a lymphokine-independent mechanism *in vitro* and can augment parasite attrition *in vivo*. *Cell Immunol* 133,178-86 (1991)

T Cell:Macrophage interactions

- 22 J.-M. Li, P. Isler, J.-M. Dayer, & D. Burger: Contact-dependent stimulation of monocytic cells and neutrophils by stimulated human T cell clones. *Immunology* 84,571-6 (1995)
- 23 U. Shu, M. Kiniwa, C.Y. Wu, C. Maliszewski, N. Vezzio, J. Hakimi, M. Gately, & G. Delespesse: Activated T cells induce interleukin-12 production by monocytes via CD40-CD40 ligand interaction. *Eur J Immunol* 25,1125-8 (1995)
- 24 L. Tian, R.J. Noelle, & D.A. Lawrence: Activated T cells enhance nitric oxide production by murine splenic macrophages through gp39 and LFA-1. *Eur J Immunol* 25,306-9 (1995)
- 25 M. Roy, A. Aruffo, J. Ledbetter, P. Linsley, M. Kehry, & R.J. Noelle: Studies on the interdependence of gp39 and B7 expression and function during antigen-specific immune responses. *Eur J Immunol* 25,596-603 (1995)
- 26 M.K. Kennedy, K.M. Mohler, K.D. Shanebeck, P.R. Baum, K.S. Picha, C.A. Otten-Evans, C.A. Janeway, & K.H. Grabstein: Induction of B cell costimulatory function by recombinant murine CD40 ligand. *Eur J Immunol* 24,116-23 (1994)
- 27 P.A. Kiener, P. Moran-Davis, B.M. Rankin, A.F. Wahl, A. Aruffo, & D. Hollenbaugh: Stimulation of CD40 with purified soluble gp39 induces proinflammatory responses in human monocytes. *J Immunol* 155,4917-25 (1995)
- 28 D.H. Wagner, R.D. Stout, & J. Suttles: Role of the CD40-CD40 ligand interaction in CD4⁺ T cell contact-dependent activation of monocyte IL-1 synthesis. *Eur J Immunol* 24,3148-54 (1994)
- 29 M.R. Alderson, R.J. Armitage, T.W. Tough, L. Strockbine, W.C. Fanslow, & M.K. Spriggs: CD40 expression by human monocytes: regulation by cytokines and activation of monocytes by the ligand for CD40. *J Exp Med* 178,669-74 (1993)
- 30 N. Malik, B.W. Greenfield, A.F. Wahl, & P.A. Kiener: Activation of human monocytes through CD40 induces matrix metalloproteinases. *J Immunol* 156,3952-60 (1996)
- 31 R.D. Stout, J. Suttles, J. Xu, I.S. Grewal, & R.A. Flavell: Impaired T cell-mediated macrophage activation in CD40 ligand-deficient mice. *J Immunol* 156,8-12 (1996)
- 32 C.D. Gimmi, G.J. Freeman, J.G. Gribben, K. Sugita, A.S. Freedman, C. Morimoto, & L.M. Nadler: B-cell surface antigen B7 provides a costimulatory signal that induces T cells to proliferate and secrete interleukin 2. *Proc Natl Acad Sci USA* 88,6575-9 (1991)
- 33 G.J. Freeman, F. Borriello, R.J. Hodes, H. Reiser, J.G. Gribben, J.W. Ng, J. Kim, J.M. Goldberg, K. Hathcock, G. Laszlo, L.A. Lombard, S. Wang, G.S. Gray, L.M. Nadler, & A.H. Sharpe: Murine B7-2, an alternative CTLA-4 counter-receptor that costimulates T cell proliferation and interleukin 2 production. *J Exp Med* 178,2185-92 (1993)
- 34 E.A. Clark, & J.A. Ledbetter: How B and T cells talk to each other. *Nature* 367,425-8 (1994)
- 35 A.J. Kaplan, K.D. Chavin, H. Yagita, M.S. Sandrin, L.-H. Qin, J. Lin, G. Lindenmayer, & J.S. Bromberg: Production and characterization of soluble and transmembrane murine CD2. Demonstration that CD48 is a ligand for CD2 and that CD48 adhesion is regulated by CD2. *J Immunol* 151,4022-32 (1993)
- 36 S.B. Mizel: Interleukin 1 and T cell activation. *Immunol Today* 8,330 (1987)
- 37 J.J. Oppenheim, C.O.C. Zachariae, N. Mukaida, & K. Matsushima: Properties of the novel proinflammatory supergene "intercrine" cytokine family. *Ann Rev Immunol* 9,617-48 (1991)
- 38 P. Davies, P.J. Bailey, & M.M. Goldenberg: The role of arachidonic acid oxygenation products in pain and inflammation. *Ann Rev Immunol* 2,335-57 (1984)
- 39 N.H. Ruddle, C.M. Bergman, K.M. McGrath, E.G. Lingenheld, M.L. Grunnet, S.J. Padula, & R.B. Clark: An antibody to lymphotoxin and tumor necrosis factor prevents transfer of experimental allergic encephalomyelitis. *J Exp Med* 172,1193-9 (1990)
- 40 S.J. Green, M.S. Meltzer, J.B. Hibbs, & C.A. Nacy: Activated macrophages destroy intracellular *Leishmania* major amastigotes by an L-arginine-dependent killing mechanism. *J Immunol* 144,278 (1990)
- 41 D.J. Stuehr, & O.W. Griffith: Mammalian nitric oxide synthases. *Adv Enzymol Molec Biol* 65,287-364 (1992)
- 42 R.B. Johnston, Jr., S. Kitagawa, C.K. Edwards, III, J.Y. Channon, H. Suzuki, & M.J. Pabst: The respiratory burst in activated macrophages: Studies of its molecular basis and evidence for downregulation in chronic infection. *Adv Exp Med Biol* 239,63-72 (1988)
- 43 R.T. Gazzinelli, I.P. Oswald, S. Hieny, S.L. James, & A. Sher: The microbicidal activity of interferon-gamma-treated macrophages against *Trypanosoma cruzi* involves an L-arginine-dependent, nitrogen oxide-mediated mechanism inhibitable by

T Cell:Macrophage interactions

interleukin-10 and transforming growth factor-beta. *Eur J Immunol* 22,2501-6 (1992)

44 R. Rothlein, T.K. Kishimoto, & E. Mainolfi: Crosslinking of ICAM-1 induces co-signaling of an oxidative burst from mononuclear leukocytes. *J Immunol* 152,2488-95 (1994)

45 W.C. Liles, J.A. Ledbetter, A.W. Waltersdorff, & S.J. Klebanoff: Cross-linking of CD45 enhances activation of the respiratory burst in response to specific stimuli in human phagocytes. *J Immunol* 155,2175-84 (1995)

46 L.M. Wahl, C.E. Olsen, A.L. Sandberg, & S.E. Mergenhagen: Prostaglandin regulation of macrophage collagenase production. *Proc Natl Acad Sci USA* 74,4955-8 (1977)

47 S. Lacraz, P. Isler, E. Vey, H.G. Welgus, & J.-M. Dayer: Direct contact between T lymphocytes and monocytes is a major pathway for induction of metalloproteinase expression. *J Biol Chem* 269,22027-33 (1994)

48 A.M.M. Miltenburg, S. Lacraz, H.G. Welgus, & J.-M. Dayer: Immobilized anti-CD3 antibody activates T cell clones to induce the production of interstitial collagenase, but not tissue inhibitor of metalloproteinases, in monocytic THP-1 cells and dermal fibroblasts. *J Immunol* 154,2655-67 (1995)

49 A.K. Hewson, T. Smith, J.P. Leonard, & M.L. Cuzner: Suppression of experimental allergic encephalomyelitis in the Lewis rat by the matrix metalloproteinase inhibitor Ro31-9790. *Inflamm Res* 44,345-9 (1995)

50 T.P. Misko, J.L. Trotter, & A.H. Cross: Mediation of inflammation by encephalitogenic cells: interferon gamma induction of nitric oxide synthase and cyclooxygenase 2. *J Neuroimmunol* 61,195-204 (1995)

51 Y. Okuda, Y. Nakatsuji, H. Fujimura, H. Esumi, T. Ogura, T. Yanagihara, & S. Sakoda: Expression of the inducible isoform of nitric oxide synthase in the central nervous system of mice correlates with the severity of actively induced experimental allergic encephalomyelitis. *J Neuroimmunol* 62,103-12 (1995)

52 L. Ding, P.S. Linsley, L.Y. Huang, R.N. Germain, & E.M. Shevach: IL-10 inhibits macrophage costimulatory activity by selectively inhibiting the up-regulation of B7 expression. *J Immunol* 151,1224-34 (1993)

53 C. Buelens, F. Willems, A. Delvaux, G. Peirard, J.-P. Delville, T. Velu, & M. Goldman: Interleukin-10 differentially regulates B7-1 (CD80)

and B7-2 (CD86) expression on human peripheral blood dendritic cells. *Eur J Immunol* 25,2668-72 (1995)

54 C. Bogdan, Y. Vodovotz, & C. Nathan: Macrophage deactivation by interleukin 10. *J Exp Med* 174,1549-55 (1991)

55 I.P. Oswald, T.A. Wynn, A. Sher, & S.L. James: Interleukin 10 inhibits macrophage microbicidal activity by blocking the endogenous production of tumor necrosis factor alpha required as a costimulatory factor for interferon gamma-induced activation. *Proc Natl Acad Sci USA* 89,8676-80 (1992)

56 C. Bogdan, J. Paik, Y. Vodovotz, & C. Nathan: Contrasting mechanisms for suppression of macrophage cytokine release by transforming growth factor-beta and interleukin-10. *J Biol Chem* 267,23301-8 (1992)

57 R.T. Gazzinelli, I.P. Oswald, S.L. James, & A. Sher: IL-10 inhibits parasite killing and nitrogen oxide production by IFN-gamma-activated macrophages. *J Immunol* 148,1792-6 (1992)

58 S. Tsunawaki, M. Sporn, A. Ding, & C. Nathan: Deactivation of macrophages by transforming growth factor-beta. *Nature* 334,260-2 (1988)

59 A. Ding, C.F. Nathan, J. Graycar, R. Derynck, D.J. Stuehr, & S. Srinall: Macrophage deactivating factor and transforming growth factors-beta₁, -beta₂, and -beta₃ inhibit induction of macrophage nitrogen oxide synthesis by IFN-gamma. *J Immunol* 145,940-4 (1990)

60 I.P. Oswald, R.T. Gazzinelli, A. Sher, & S.L. James: IL-10 synergizes with IL-4 and transforming growth factor-beta to inhibit macrophage cytotoxic activity. *J Immunol* 148,3578-82 (1992)

61 J. Link, B. He, V. Navikas, W. Palasik, S. Fredrikson, M. Soderstrom, & H. Link: Transforming growth factor-beta 1 suppresses autoantigen-induced expression of pro-inflammatory cytokines but not of interleukin-10 in multiple sclerosis and myasthenia gravis. *J Neuroimmunol* 58,21-35 (1995)

62 D.B. Stevens, K.E. Gould, & R.H. Swanborg: Transforming growth factor-beta 1 inhibits tumor necrosis factor-alpha/lymphotoxin production and adoptive transfer of disease by effector cells of autoimmune encephalomyelitis. *J Neuroimmunol* 51,77-83 (1994)

63 L. Santambrogio, G.M. Hochwald, B. Saxena, C.H. Leu, J.E. Martz, J.A. Carlino, N.H. Ruddle, M.A. Palladino, L.I. Gold, & G.J. Thorbecke: Studies

T Cell:Macrophage interactions

- on the mechanisms by which transforming growth factor-beta (TGF-beta) protects against allergic encephalomyelitis. Antagonism between TGF-beta and tumor necrosis factor. *J Immunol* 151,1116-27 (1993)
- 64 D.M. Paulnock: Macrophage activation by T cells. *Curr Opin Immunol* 4,344-9 (1992)
- 65 C. Bogdan, & C. Nathan: Modulation of macrophage function by transforming growth factor beta, interleukin-4, and interleukin-10. *Ann N Y Acad Sci* 685,713-39 (1993)
- 66 F. Figueiredo, T.J. Koerner, & D.O. Adams: Molecular mechanisms regulating the expression of class II histocompatibility molecules on macrophages. Effects of inductive and suppressive signals on gene transcription. *J Immunol* 143,3781-6 (1989)
- 67 G. Frendl, & D.I. Beller: Regulation of macrophage activation by IL-3. I. IL-3 functions as a macrophage-activating factor with unique properties, inducing Ia and lymphocyte function-associated antigen-1 but not cytotoxicity. *J Immunol* 144,3392-9 (1990)
- 68 M.R. Alderson, T.W. Tough, S.F. Ziegler, & R.J. Armitage: Regulation of human monocyte cell surface and soluble CD23 (Fc RII) by granulocyte-macrophage colony stimulating factor and interleukin 3. *J Immunol* 149,1252-7 (1992)
- 69 A.S. Freedman, G.J. Freeman, K. Rhynhart, & L.M. Nadler: Selective induction of B7/BB-1 on interferon-gamma stimulated monocytes: A potential mechanism for amplification of T cell activation through the CD28 pathway. *Cell Immunol* 137,429-37 (1991)
- 70 J.L. Ho, S.H. He, M.J. Rios, & E.A. Wick: Interleukin-4 inhibits human macrophage activation by tumor necrosis factor, granulocyte-macrophage colony-stimulating factor, and interleukin-3 for antileishmanial activity and oxidative burst capacity. *J Infect Dis* 165,344-51 (1992)
- 71 J.L. Ho, S.G. Reed, J. Sobel, S. Arruda, S.H. He, E.A. Wick, & K.H. Grabstein: Interleukin-3 induces antimicrobial activity against *Leishmania amazonensis* and *Trypanosoma cruzi* and tumoricidal activity in human peripheral blood-derived macrophages. *Infect Immun* 60,2331-7 (1992)
- 72 W.A. Phillips, & J.A. Hamilton: Phorbol ester-stimulated superoxide production by murine bone marrow-derived macrophages requires preexposure to cytokines. *J Immunol* 142,2445-9 (1989)
- 73 S.L. Abramson, & J.I. Gallin: IL-4 inhibits superoxide production by human mononuclear phagocytes. *J Immunol* 144,625-30 (1990)
- 74 S. Gautam, J.M. Tebo, & T.A. Hamilton: IL-4 suppresses cytokine gene expression induced by IFN-gamma and/or IL-2 in murine peritoneal macrophages. *J Immunol* 148,1725-30 (1992)
- 75 S. Narumi, J.H. Finke, & T.A. Hamilton: Interferon gamma and interleukin 2 synergize to induce selective monokine expression in murine peritoneal macrophages. *J Biol Chem* 265,7036-41 (1990)
- 76 R.D. Stout: Macrophage activation by T cells: Cognate and noncognate signals. *Curr Opin Immunol* 5,398-403 (1993)
- 77 W. Deng, B. Thiel, C.S. Tannenbaum, T.A. Hamilton, & D.J. Stuehr: Synergistic cooperation between T cell lymphokines for induction of the nitric oxide synthase gene in murine peritoneal macrophages. *J Immunol* 151,322-9 (1993)
- 78 S.J. Green, R.M. Crawford, J.T. Hockmeyer, M.S. Meltzer, & C.A. Nacy: Leishmania major amastigotes initiate the L-arginine dependent killing mechanism in IFN-stimulated macrophages by induction of TNF-alpha. *J Immunol* 145,4290 (1990)
- 79 G.W. Cox, G. Melillo, U. Chattopadhyay, D. Mullet, R.H. Fertel, & L. Varesio: Tumor necrosis factor-alpha-dependent production of reactive nitrogen intermediates mediates IFN-gamma plus IL-2-induced murine macrophage tumoricidal activity. *J Immunol* 149,3290-6 (1992)
- 80 R. Appelberg, I.M. Orme, M.I. Pinto de Sousa, & M.T. Silva: In vitro effects of interleukin-4 on interferon-gamma-induced macrophage activation. *Immunology* 76,553-9 (1992)
- 81 D. Chantry, M. ATurner, E. Abney, & M. Feldmann: Modulation of cytokine production by transforming growth factor-beta. *J Immunol* 142,4295-300 (1989)
- 82 P. Chomarat, E. Vannier, J. Dechanet, M.C. Rissoan, J. Banchereau, C.A. Dinarello, & P. Miossec: Balance of IL-1 receptor antagonist/IL-1 beta in rheumatoid synovium and its regulation by IL-4 and IL-10. *J Immunol* 154,1432-9 (1995)
- 83 M. Turner, D. Chantry, P. Katsikis, A. Berger, F.M. Brennan, & M. Feldmann: Induction of the interleukin 1 receptor antagonist protein by transforming growth factor-beta. *Eur J Immunol* 21,1635-9 (1991)

T Cell:Macrophage interactions

- 84 R.J. Armitage, C.R. Maliszewski, M.R. Alderson, K.H. Grabstein, M.K. Spriggs, & W.C. Fanslow: CD40L: a multi-functional ligand. *Semin Immunol* 5,401-12 (1993)
- 85 R.A. Kroccek, D. Graf, D. Brugnoli, S. Giliani, U. Korthuer, A. Ugazio, G. Senger, H.W. Mages, A. Villa, & L.D. Notarangelo: Defective expression of CD40 ligand on T cells causes "X-linked immunodeficiency with hyper-IgM (HIGM1)". *Immunol Rev* 138,39-59 (1994)
- 86 F.H. Durie, T.M. Foy, S.R. Masters, J.D. Lamian, & R.J. Noelle: The role of CD40 in the regulation of humoral and cell-mediated immunity. *Immunol Today* 15,406-11 (1994)
- 87 J.E. Buhlmann, T.M. Foy, A. Aruffo, K.M. Crassi, J.A. Ledbetter, W.R. Green, J.C. Xu, L.D. Shultz, D. Roopesian, R.A. Flavell, & et al: In the absence of a CD40 signal, B cells are tolerogenic. *Immunity* 2,645-53 (1995)
- 88 M. Roy, T. Waldschmidt, A. Aruffo, J.A. Ledbetter, & R.J. Noelle: The regulation of the expression of gp39, the CD40 ligand, on normal and cloned CD4+ T cells. *J Immunol* 151,2497-510 (1993)
- 89 B.E. Castle, K. Kishimoto, C. Stearns, M.L. Brown, & M.R. Kehry: Regulation of expression of the ligand for CD40 on T helper lymphocytes. *J Immunol* 151,1777-88 (1993)
- 90 E. Fischer, C. Delibrias, & M.D. Kazatchkine: Expression of CR2 (the C3dg/EBV receptor, CD21) on normal human peripheral blood T lymphocytes. *J Immunol* 146,865-9 (1991)
- 91 L. Flores-Romo, J. Shields, Y. Humbert, P. Graber, J.-P. Aubry, J.-F. Gauchat, G. Ayala, B. Allet, M. Chavez, H. Bazin, M. Capron, & J.-Y. Bonnefoy: Inhibition of an in vivo antigen-specific IgE response by antibodies to CD23. *Science* 261,1038-41 (1993)
- 92 W. Chen, W. Knapp, O. Majdic, H. Stockinger, G.A. Bohmig, & G.J. Zlabinger: Co-ligation of CD31 and Fc RII induces cytokine production in human monocytes. *J Immunol* 152,3991-7 (1994)
- 93 F. Lund, N. Solvason, J.C. Grimaldi, R.M.E. Parkhouse, & M. Howard: Murine CD38: an immunoregulatory ectoenzyme. *Immunol Today* 16,469-73 (1995)
- 94 D.S.A. Webb, Y. Shimizu, G.A. Van Seventer, S. Shaw, & T.L. Gerrard: LFA-3, CD44, and CD45: Physiologic triggers of human monocyte TNF- α and IL-1 release. *Science* 249,1295-7 (1990)
- 95 P. Isler, E. Vey, J.H. Zhang, & J.M. Dayer: Cell surface glycoproteins expressed on activated human T cells induce production of interleukin-1 beta by monocytic cells: a possible role of CD69. *Eur Cytokine Netw* 4,15-23 (1993)
- 96 R. De Maria, M.G. Cifone, R. Trotta, M.R. Rippo, C. Festuccia, A. Santoni, & R. Testi: Triggering of human monocyte activation through CD69, a member of the natural killer cell gene complex family of signal transducing receptors. *J Exp Med* 180,1999-2004 (1994)
- 97 B. Dugas, M.D. Mossalayi, C. Damais, & J.-P. Kolb: Nitric oxide production by human monocytes: evidence for a role of CD23. *Immunol Today* 16,574-80 (1995)
- 98 S. Lecoanet Henchoz, J.F. Gauchat, J.P. Aubry, P. Graber, P. Life, N. Paul Eugene, B. Ferrua, A.L. Corbi, B. Dugas, C. Plater Zyberk, & et al: CD23 regulates monocyte activation through a novel interaction with the adhesion molecules CD11b-CD18 and CD11c-CD18. *Immunity* 3,119-25 (1995)
- 99 I. Vouldoukis, V. Riveros-Moreno, B. Dugas, F. Quaaaz, P. Becherel, P. Debre, S. Moncada, & M.D. Mossalayi: The killing of *Leishmania major* by human macrophages is mediated by nitric oxide induced after ligation of the Fc RII/CD23 surface antigen. *Proc Natl Acad Sci USA* 92,7804-8 (1995)
- 100 N. Paul Eugene, J.P. Kolb, A. Abadie, J. Gordon, G. Delespesse, M. Sarfati, J.M. Mencia Huerta, P. Braquet, & B. Dugas: Ligation of CD23 triggers cAMP generation and release of inflammatory mediators in human monocytes. *J Immunol* 149,3066-71 (1992)
- 101 A. Herbelin, S. Elhadad, F. Ouaz, D. deGroote, & B. Descamps-Latscha: Soluble CD23 potentiates interleukin-1 induced secretion of interleukin-6 and interleukin-1 receptor antagonist by human monocytes. *Eur J Immunol* 24,1869-73 (1994)
- 102 M. Armant, H. Ishihara, M. Rubio, G. Delespesse, & M. Sarfati: Regulation of cytokine production by soluble CD23: costimulation of interferon-gamma secretion and triggering of tumor necrosis factor-alpha release. *J Exp Med* 180,1005-11 (1994)
- 103 J.C. Prinz, X. Baur, G. Mazur, & E.B. Rieber: Allergen-directed expressin of Fc receptors for IgE (CD23) on human T lymphocytes is modulated by interleukin 4 and interferon-gamma. *Eur J Immunol* 20,1259-64 (1990)

T Cell:Macrophage interactions

104 I.S. Grewal, H.G. Foellmer, D.P. Grewal, J. Xu, F. Hardardottir, J.L. Baron, C.A. Janeway, Jr., & R.A. Flavell: Requirement for CD40 ligand in costimulation induction, T cell activation, and experimental allergic encephalomyelitis. *Science* 273,1864-7 (1996)

105 R.D. Stout, & J. Suttles: The many roles of CD40 in cell-mediated inflammatory responses. *Immunol Today* 17,487-92 (1996)

106 T.A. Yednock, C. Cannon, L.C. Fritz, F. Sanchez-Madrid, L. Steinman, & N. Karin: Prevention of experimental autoimmune encephalomyelitis by antibodies against 4 1 integrin. *Nature* 356,63-6 (1992)

107 M.J. Yellin, J. Brett, D. Baum, A. Matsushima, M. Szabolcs, D. Stern, & L. Chess: Functional interactions of T cells with endothelial cells: the role of CD40L-CD40-mediated signals. *J Exp Med* 182,1857-64 (1995)

108 J.A. Bluestone: New perspectives of CD28-B7-mediated T cell costimulation. *Immunity* 2,555-9 (1995)

109 S.D. Miller, C.L. Vanderlugt, D.J. Lenischow, J.G. Pope, N.J. Karandikar, M.C. Dal Canto, & J.A. Bluestone: Blockade of CD28/B7-1 interaction prevents epitope spreading and clinical relapses of murine EAE. *Immunity* 3,739-45 (1995)

110 M.K. Racke, D.E. Scott, L. Quigley, G.S. Gray, R. Abe, C.H. June, & P.J. Perrin: Distinct roles for B7-1 (CD-80) and B7-2 (CD-86) in the initiation of experimental allergic encephalomyelitis. *J Clin Invest* 96,2195-203 (1995)

REVIEW

Elly N. Benveniste

Role of macrophages/microglia in multiple sclerosis and experimental allergic encephalomyelitis

Received: 6 June 1996 / Accepted: 4 October 1996

Abstract One of the characteristic features of microglia is their rapid activation in response to injury, inflammation, neurodegeneration, infection, and brain tumors. This review focuses on the role of the microglia in multiple sclerosis (MS), a chronic inflammatory demyelinating disease of the central nervous system (CNS), and in the animal model of MS, experimental allergic encephalomyelitis (EAE). Microglial activation in MS and EAE is thought to contribute directly to CNS damage through several mechanisms, including production of proinflammatory cytokines, matrix metalloproteinases, and free radicals. In addition, activated microglia serve as the major antigen-presenting cell in the CNS, likely contributing to aberrant immune reactivity at this site. A mechanistic understanding of the way in which microglia are activated and ultimately inhibited is crucial for the formulation of therapeutic modalities to treat MS and other CNS autoimmune diseases.

Key words Glial cells · Neuroimmunology · Cytokines · Demyelination

Abbreviations APC Antigen-presenting cell · BBB Blood-brain barrier · Cl_2MDP Dichloromethylene diphosphonate · CNS Central nervous system · EAE Experimental allergic encephalomyelitis · ICAM-1 Interleukin · LFA Lymphocyte function associated antigen · LT Lymphotoxin · MBP Myelin basic protein · MCP Monocyte chemoattractant peptide · MHC Major histocompatibility complex · MIP Macrophage inflammatory protein · MMP Matrix metalloproteinases · MS Multiple sclerosis · PLP Proteolipid protein · TGF Transforming growth factor · TNF Tumor necrosis factor

Introduction

This review on the involvement of macrophages/microglia in multiple sclerosis (MS) and its animal model, experimental allergic encephalomyelitis (EAE), highlights the ability of these cells to contribute to inflammatory and immune responses in the central nervous system (CNS). We emphasize the ability of macrophages/microglia both to produce and to respond to a wide variety of cytokines, impair blood-brain barrier (BBB) function, act as an antigen-presenting cell (APC) within the CNS, mediate phagocytic events, and damage oligodendrocytes (the myelin-producing cells within the CNS). The phenotypic and functional characteristics of microglia are described initially, followed by a discussion of the involvement of macrophages/microglia in neurological diseases such as MS and EAE.

Microglia

There are two major subgroups of glial cells: the macroglia, which consist of astrocytes, oligodendrocytes, and ependymal cells, and microglia. This review focuses on microglia, the resident macrophage of the brain, which comprise 10–20% of all glial cells. Microglia were originally described by del Rio-Hortega [1]; he hypothesized that microglia are of mesodermal origin, have phagocytic functions, and exhibit changes in morphology following insult to the CNS. Most current evidence strongly suggests that microglia are derived from a bone marrow precursor of monocytic lineage [2, 3] and populate the CNS early in fetal development. In addition, there is immigration during the postnatal period. Microglia are a class of brain mononuclear phagocytes and are thought to be the principal immune cell resident to the CNS. Microglia have functions similar to those of other tissue macrophages, including phagocytosis, antigen presentation, and production of cytokines, eicosanoids, complement components, excitatory amino acids (glutamate), proteinases, oxidative radicals, and nitric oxide (for review see

E.N. Benveniste
Department of Cell Biology, University of Alabama at Birmingham,
Birmingham, AL 35294-0005, USA

Communicated by: H.D. Perez and G. Stock

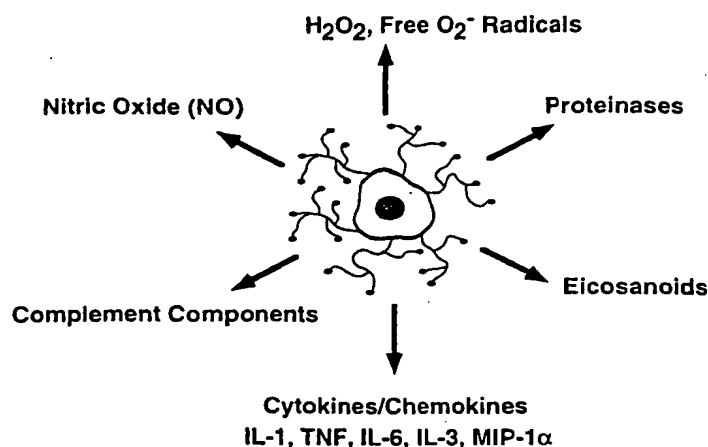


Fig. 1 Microglial mediators of CNS inflammation and damage. Upon activation microglia are induced to produce proinflammatory cytokines, complement components, eicosanoids, nitric oxide, and free radicals, all of which are involved in initiating and amplifying inflammation within the CNS

[4–6]; see Fig. 1). Production of these mediators is thought to contribute to CNS damage through a variety of mechanisms, some of which are discussed in detail below. Microglia also have specialized functions not related to inflammation or immunity that are not described in this article; readers are referred to excellent review articles on this topic [7, 8].

Parenchymal microglia represent a stable pool of cells having little or no turnover with bone marrow derived cells (for review see [6]). At least three clearly identifiable states of parenchymal microglia have been defined based on developmental and pathophysiological studies: (a) the ramified, resting microglia present in the normal, nonpathological adult CNS, (b) the activated, nonphagocytic microglia found in areas of secondary reaction due to nerve transection and CNS inflammation, and (c) the reactive, phagocytic microglia found in areas of trauma, infection, or neuronal degeneration. These different forms of parenchymal microglia are not independent of each other but likely represent transformations of a single cell type. Microglia exhibit plasticity in their morphology and appearance, particularly during injury and disease. Rest-

ing microglia are highly branched (ramified) cells with a small amount of perinuclear cytoplasm; however, upon pathological insult, these cells become hypertrophied with short processes and exhibit a “bushy” appearance (for review see [9]). The term “perivascular microglia” has been used to describe parenchymal microglia cells located in the vicinity of blood vessels. These perivascular microglia are found within the CNS parenchyma proper and form part of the perivascular glia limitans (for review see [6]). These cells are often confused with “perivascular cells” which are not part of the CNS parenchyma since they are separated from the brain tissue proper by a basal lamina. Perivascular cells have been shown to possess antigen-presenting and phagocytic functions and are thought to exist predominantly in an activated state [10].

There is a large amount of literature on the antigenic markers that microglia can express. These include class I and II major histocompatibility complex (MHC) antigens, Fc receptors (I–III), complement receptors (CR1, CR3, CR4), β_2 -integrins [lymphocyte function associated antigen (LFA) 1, 3], intercellular adhesion molecule (ICAM) 1, and the costimulatory molecules B7-1 and B7-2 [11–20] (see Table 1). Some of these markers are expressed constitutively by microglia while others are inducible following injury, infection, or inflammation of the nervous system. Currently there are no unique histochemical markers that distinguish resting or activated microglia from monocytes/macrophages in the circulation or peripheral tissues, or from macrophages which invade the brain [18].

Multiple sclerosis

MS is a chronic demyelinating disease of the CNS that generally afflicts persons between 20 and 50 years old, affecting more women than men. The cause of MS is unknown, although viral infections, genetic predisposition, environmental factors, and autoimmunity are all considered as contributing factors in the etiology of MS (for review see [21]). The major pathological hallmark of MS is the presence of sclerotic plaques in the CNS that are characterized by demyelination, while axonal processes are generally unaffected. During active disease demy-

Table 1 Functional properties of microglia

Molecules	Function	References
IL-1	Proinflammatory cytokine	53, 55
IL-3	Hematopoietic growth factor	50, 104
TNF- α	Proinflammatory cytokine, apoptosis	49, 57, 60, 61
LT	Apoptosis	50
IL-6	Pro-/anti-inflammatory cytokine	55, 59
IL-1 receptor antagonist	Anti-inflammatory molecule	11
TGF- β	Anti-inflammatory cytokine	11, 58
MIP-1 α	Chemoattractant	52
ClqB, C3, C4	Complement components	11, 19
MMP-2, 9	Proteinases	56, 62
Class II MHC	Antigen presentation	13, 14, 15, 64
B7-1, B7-2	Costimulation of antigen presentation	16, 17, 64, 66
ICAM-1	Antigen presentation/adhesion	12

elination is associated with an inflammatory reaction that is orchestrated by activated lymphocytes, macrophages, and endogenous glial cells (astrocytes and microglia). Early MS lesions are characterized by the local accumulation of activated CD4⁺ and CD8⁺ T-cells around small venules, with CD4⁺ cells predominating [22]. Later there is myelin degeneration associated with perivascular inflammation consisting of T-cells, B-cells, plasma cells and activated macrophages [23, 24]. The primary demyelination observed in MS results from damage to the myelin sheath and/or oligodendrocytes. Macrophage/microglia are active participants in myelin breakdown; phagocytosis of myelin proteins in the lesions by these cells is a reliable indicator of ongoing demyelinating activity [25]. In addition, microglia become activated during MS to express molecules critical for antigen presentation, including class II MHC and B7-1 [26, 27]. Another immunologically relevant antigen expressed by macrophages/microglia in MS brain is CD40, a member of the tumor necrosis factor (TNF) receptor family of cell surface proteins [28]. These CD40 positive macrophages/microglia co-localize with CD40 ligand (CD40L) positive T-helper cells. CD40-CD40L interactions are thought to play a role in activation of cells of the monocytic lineage [29], which is discussed below. Gliosis is also a prominent feature of MS, and is characterized by astrocyte proliferation, hypertrophy, and increased synthesis of glial fibrillary acidic protein, an astrocyte-specific protein [30]. This reaction is thought to contribute to the formation of dense glial scars in the CNS, leading to motor and sensory impairment. Recent findings with magnetic resonance imaging indicate that considerable subclinical disease occurs, and that early in lesion development there is breakdown of the BBB [31, 32], which may be a crucial event in the pathogenesis of new lesions in MS.

A wide range of cytokines have been detected in MS lesions. These include interleukins (ILs) 1, 2, 3, 4, 6, 10, and 12, TNF- α , lymphotoxin (LT), interferons (IFNs) α , β , and γ , transforming growth factor (TGF) β , and chemokines (for review see [33, 34]). IFN- γ is secreted by infiltrating activated T-cells, while all the other cytokines can be produced either by infiltrating leukocytes or by endogenous astrocytes and microglia. In particular, IL-1, IL-6, LT, and TNF- α have been localized to macrophages/microglia (see Table 1). TNF- α and LT have been implicated in the disease process of MS due to their ability to mediate myelin and oligodendrocyte damage, leading to the demyelination process observed in MS [35-37]. TNF- α and IL-1 β induce astrocyte proliferation [38, 39], which could elicit the astrogliosis associated with MS and contribute to impairment of the BBB (see Fig. 2). Cytokine networks are involved in MS; the cytokines implicated in disease progression include the TH1 cytokines IL-2, TNF- α , LT, and IFN- γ as well as IL-1, while TH2 cytokines such as IL-4 and IL-10 as well as IFN- β and TGF- β appear to mediate disease remission (for review see [33]). Thus macrophages/microglia in MS tissue express gene products that contribute to im-

mune reactivity, inflammation, and demyelination within the CNS.

Experimental allergic encephalomyelitis

EAE is an experimentally induced autoimmune disease of the CNS, and serves as an animal model for MS. EAE can be actively induced by the injection of whole spinal cord preparations, proteins derived from myelin [commonly myelin basic protein (MBP) or proteolipid protein (PLP)], or MBP or PLP peptides (for review see [40]). Activated T-cells isolated from the spleen and lymph nodes of actively immunized animals can be used to transfer disease to naive recipients; the T-cells must be activated *in vitro* by the encephalitogenic antigen in the presence of APCs prior to transfer. Additionally, transfer of encephalitogenic MBP or PLP-specific T-cell lines can be utilized to induce disease. In all described models of EAE, disease is characterized by perivascular infiltrates within the CNS and paralysis. Typically the BBB becomes disrupted. The cells which initiate disease are predominantly myelin-reactive CD4⁺ T helper cells that are class II MHC restricted and of a TH1 phenotype (secretion of IFN- γ , IL-2, TNF- α , LT; for review see [40]). These antigen-specific autoimmune T-cells first contact a naive intact BBB and are able to extravasate through the BBB due to their activational status. These cells are re-

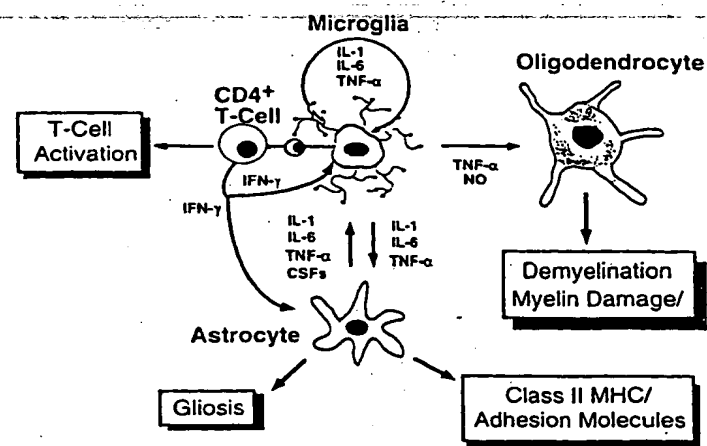


Fig. 2 Potential interactions between microglia/macrophages and T-cells, astrocytes, and oligodendrocytes. Activated microglia/macrophages can present foreign antigen in conjunction with class II MHC molecules to CD4⁺ T-helper cells. The T-cells then become activated and secrete cytokines such as IFN- γ which further contributes to the activation of microglia/macrophages. Microglia/macrophage products such as TNF- α and nitric oxide (NO) can damage oligodendrocytes, leading to interference with myelination and myelin gene expression. Astrocytes and microglia/macrophages also communicate via soluble mediators such as cytokines. IL-1, IL-6, and TNF- α produced by microglia/macrophages can induce astrogliosis and can regulate expression of adhesion molecules such as ICAM-1, vascular cell adhesion molecule 1, and E-selectin on astrocytes. Astrocytes in turn produce colony stimulating factors (CSFs) that are critical for sustaining the growth of microglia/macrophages

tained in the CNS due to presentation of appropriate antigen (most likely by endogenous microglia) and undergo further activation. This is followed by the recruitment of non-antigen-specific lymphocytes and activated macrophages from the blood into this site, accompanied by further disruption of the BBB. Infiltrating macrophages and intrinsic microglia take part in the inflammatory process by phagocytosis of myelin, leading to demyelination [25, 41]. In addition, class II MHC and CD40 expression is detected on both macrophages and microglia during EAE [28, 42]. Glial cells such as astrocytes and microglia become activated to produce proinflammatory cytokines such as TNF- α , IL-1, and IL-6 as well as chemokines, further contributing to inflammation and myelin damage within the CNS. Similar to MS, the cytokines TNF- α , IL-1, IL-2, and IFN- γ are implicated in disease progression due to their ability to activate T-cells and macrophages, while IL-4, IL-10, and TGF- β are thought to regulate recovery from EAE [43–47].

Involvement of macrophages/microglia in EAE and MS

Within the context of immune-mediated brain injury microglia are considered as the main intrinsic immune effector cell of the CNS. This section describes some of the effector functions ascribed to microglia as determined by *in vitro* studies to set the stage for discussing the involvement of microglia in EAE and, by extrapolation, MS.

Microglia can be activated to express a broad range of cytokines, including IL-1, IL-3, IL-6, TNF- α , LT, macrophage inflammatory protein (MIP) 1 α and TGF- β [11, 14, 48–59] (see Table 1). Many of these cytokines (IL-1, IL-6, TNF- α , LT, MIP-1 α) have proinflammatory properties that can mediate inflammation and demyelination within the CNS. As mentioned above, TNF- α has been documented to contribute to the demyelination process in the CNS, and activated microglia are involved in this event by production of both secreted and membrane bound TNF- α [60] or through induction of nitric oxide [61]. Interestingly, secreted TNF- α produced by microglia is capable of killing oligodendrocytes, but the membrane-bound form of TNF- α is more effective in this process [60], indicating a requirement for cell-cell contact between microglia and oligodendrocytes.

Activated microglia also have the capacity to secrete serine proteinases (elastase and urokinase-type plasminogen activators) and the matrix metalloproteinases (MMP) 2 and 9 [6, 56, 62, 63] (see Table 1). Some of these enzymes are capable of degrading MBP within the encephalitogenic region of the protein and thus can contribute both to immune reactivity against MBP epitopes within the CNS and to demyelination. In the CNS MMPs have been implicated in the pathogenesis of inflammatory/demyelinating diseases, particularly in the breakdown of the BBB.

Another aspect of microglial biology that can contribute to immune reactivity within the CNS is their ability

to function as an APC [64]. At least two distinct signals are provided by APCs that leads to the generation of activated effector CD4⁺ T-cells; an antigen-specific signal mediated through TCR ligation by antigen/class II and a second non-antigen-specific costimulatory signal (for review see [65]). Interactions between CD28 cells and its counterreceptors B7-1 (CD80) and CD86 on APCs are most important for providing costimulatory signals. Microglia can be induced *in vitro* by the cytokine IFN- γ to express class II MHC and B7-1 and other molecules critical for effective antigen presentation such as LFA-3 and ICAM-1 [12–16, 66]. *In vitro* experiments document that IFN- γ stimulated microglia are able to initiate and perpetuate CD4⁺ activation [14, 16, 67]. Thus microglia are poised to participate in T-cell activation within the CNS (see Fig. 1). IL-4, a TH2 cytokine, has no effect alone on class II MHC expression but inhibits IFN- γ induced class II expression by microglia [68]. As mentioned above, this has been implicated in contributing to suppression of recovery in EAE [45, 69]. This beneficial effect may in part be due to inhibition of class II MHC expression by microglia.

Macrophage depletion

EAE has proven to be a valuable model for studying immunological reactions involved in the pathogenesis of demyelinating diseases, in particular MS. The importance of T-cells in EAE has been extensively documented particularly by their ability to *initiate* disease, and an autoimmune specificity for myelin components is provided by these cells (for review see [40]). However, the actual effector mechanisms leading to inflammatory demyelination within the CNS are likely to be provided by other cell types, including infiltrating macrophages and endogenous microglia. A number of studies have documented an important role for macrophages/microglia as effector cells in EAE. Early studies by Brosnan et al. [70] demonstrated that macrophage depletion by treatment with silica dust can delay the onset of clinical signs and reduce the severity of disease in a Lewis rat model of EAE. A later study utilized liposomes containing the drug dichloromethylene diphosphonate (Cl₂MDP) to eliminate macrophages, and such treatment was shown to completely prevent the clinical manifestations of EAE [71]. This study assumed that the effect of Cl₂MDP liposome treatment is on *infiltrating* macrophages. More recently this same group demonstrated that the use of Cl₂MDP liposomes eliminates only peripheral blood-borne macrophages and not resident parenchymal microglia [72]; however, clinical signs of EAE are not suppressed by such treatment. Thus, although macrophages have the capacity to acquire many of the same functional properties as macrophages, it appears that in the absence of blood-borne macrophages, microglia are not adequately activated. The concomitant loss of blood-borne macrophages and the impaired activation of endogenous

microglia suggests that *infiltrating* macrophages are responsible for the subsequent activation of microglia, possibly through their interactions with T-cells and subsequent release of proinflammatory cytokines.

Blockade of macrophage entry into the CNS

MS and EAE are characterized by the migration of lymphocytes and monocytes from blood into the brain and by the subsequent invasion of the extravascular tissue. A number of strategies have been employed to block the entry and/or function of macrophages/microglia in the CNS. The mechanism by which macrophages traffic through the BBB is not completely understood but is likely to involve a variety of adhesion molecules and chemokines. Adhesion molecules involved in monocyte adherence to endothelium include the β_2 -integrins MAC-1 (CD11b/CD18) and LFA-1 (CD11a/CD18) which are expressed on monocytes, and ICAM-1 (CD54), the counterreceptor for both MAC-1 and LFA-1 that is expressed by activated endothelial cells (for review see [73]). Intravenous administration of antibodies against MAC-1 during the early effector phase of EAE significantly suppressed disease severity [74]; this suppression has been proposed to be due in part to the blockade of infiltration of macrophages into the CNS lesions. Another recent study utilizing antibodies to both MAC-1 and LFA-1 demonstrated suppression of EAE clinical severity [75]. Thus inhibition of the adhesion molecules involved in macrophage adherence to endothelium prevents entry of macrophages into the CNS and subsequent neurological disease.

Modulation of chemokine expression

Chemokines are low molecular weight (7- to 10-kDa) secreted proteins that mediate the recruitment and activation of leukocytes and other cells to sites of inflammation during an immune response. The two chemokine families involved in EAE include the CXC (α) chemokines that are chemotactic for neutrophils and T-cells, and the CC (β) chemokines that are chemotactic for monocyte/macrophage lineage cells (for review see [76, 77]). In particular there is strong evidence that members of the CC family of chemokines [MIP-1 α , MIP-1 β , monocyte chemoattractant peptide (MCP)-1, and RANTES] are involved in recruiting macrophages into the CNS. In the Lewis rat model of EAE, levels of MCP-1 mRNA were elevated immediately before the onset of clinical signs, peaked with the height of disease, and declined with resolution of disease [78]. The marked elevation of MCP-1 at the height of clinical disease was also correlated with extensive perivascular accumulation of monocytes. MCP-1 expression was localized to T-cells, endothelial cells, and astrocytes, and diminished concomitantly with a decrease in disease activity [79]. Ransohoff et al. [80] have also investigated chemokine

production in the CNS during EAE in SJL/J mice. Astrocytes were the only cells in the CNS which expressed mRNA transcripts for MCP-1, and expression was correlated with the appearance of clinical and histological EAE.

A different approach to examining the role of MCP-1 was taken by Fuentes et al. [81] who generated transgenic mice overexpressing MCP-1 in the brain. There was a pronounced mononuclear cell infiltrate in the CNS of these animals, with the majority of cells identified as monocytes and macrophages. These cells were localized in a perivascular orientation with little infiltration into the parenchyma, which may reflect the accumulation of MCP-1 protein around blood vessels. These MCP-1 transgenic mice did not display any significant neurological systems despite high transgene expression and the mononuclear cell infiltrate, indicating that the *presence* of monocytes/macrophages per se in the CNS is not sufficient to induce disease. This may reflect the need for activated T-cells to *initiate* CNS disease, which are lacking in this transgenic model.

Another CC chemokine implicated in EAE is MIP-1 α . Reverse-transcriptase polymerase chain reaction analysis of spinal cord from animals with both actively induced and adoptively transferred EAE demonstrates that MIP-1 α mRNA is induced 1-2 days prior to clinical signs and achieves highest levels at disease onset [82]. The importance of MIP-1 α was demonstrated in studies utilizing anti-MIP-1 α antibodies, in which such treatment prevented the development of both acute and relapsing paralytic disease as well as infiltration of mononuclear cells in the CNS [83]. Incubation of encephalitogenic T-cells with anti-MIP-1 α in vitro did not inhibit the ability of these cells to adoptively transfer EAE or produce inflammatory cytokines, suggesting that the beneficial effect of anti-MIP-1 α is by inhibiting recruitment of inflammatory mononuclear cells (macrophages) into the CNS.

Inhibition of matrix metalloproteinase activity: involvement of macrophages/microglia

As mentioned above, MMPs are thought to contribute to tissue destruction in diseases such as MS and EAE by their ability to degrade extracellular matrix components [84, 85]. In MS brain both macrophages and microglia express a variety of MMPs (1, 2, 3, and 9) [86], and in vitro, activated microglia and macrophages produce a number of MMPs [56, 62, 87, 88]. A MMP inhibitor (GM 6001) induced a partial inhibition of MMP activity in the cerebrospinal fluid of mice with actively induced EAE, suppressed the development of EAE, and reversed clinical signs of EAE [89]. The beneficial action of GM 6001 appears to be through restoration of the damaged BBB, i.e., animals treated with GM 6001 have normal permeability of the BBB compared to the enhanced permeability in nontreated animals. Whether macrophage and/or microglia MMP production is specifically

affected by GM 6001 was not examined; however, these cells would be likely targets for MMP inhibitors.

A recent study has demonstrated that monocytes can be activated to produce MMP-9 upon interaction with T-cells [90]. Specifically, this activation occurs through interaction of CD40L on T-cells and CD40 on monocytes, as a neutralizing antibody against CD40L inhibited MMP expression by monocytes. This finding is of particular interest in light of the paper by Gerritse et al. [28] in which treatment with anti-CD40L monoclonal antibody completely prevented EAE in SJL/J mice. Whether this inhibitory effect of anti-CD40L antibody is due to decreased MMP production by macrophages/microglia is not known; however, these cells express CD40 in EAE and MS brain, and their activation is likely blocked by anti-CD40L antibody. Other macrophage/microglia effector mechanisms can be activated through CD40 triggering, including tumoricidal activity, cytokine production (IL-1, TNF- α , IL-6, IL-8), and nitric oxide production [29, 91–93]. Inhibition of any of the above functions by anti-CD40L antibody would be of benefit in treating EAE.

Inhibition of TNF- α activity

The involvement of TNF- α in demyelinating diseases such as EAE and MS has been extensively documented (for review see [33]). Numerous studies indicate that there is aberrantly high expression of TNF- α by immune cells from MS patients during acute phases of disease [94–97]. In EAE TNF- α protein is expressed in the CNS of animals during the peak of clinical disease and declines upon remission [98, 99]. One study identified macrophages/microglia as the source of TNF- α in the CNS of animals with disease [99].

Studies have been conducted to neutralize TNF- α activity, including the use of anti-TNF antibodies and soluble TNF receptors. Antibodies to TNF- α prevented adoptive transfer of EAE by MBP encephalitogenic T-cells, and the CNS tissue from protected animals was devoid of inflammation or demyelination compared to control animals [37, 100, 101]. Preincubation of MBP-sensitized T-cells with anti-TNF- α antibody in vitro prior to injection did not affect their ability to transfer EAE, suggesting that the effect of the antibody is by interfering with the effector phase of disease (possibly depleting TNF- α secreted by macrophages/microglia). Another approach has been the administration of soluble TNF receptors in EAE. Baker et al. [102] demonstrated that treatment with bivalent human sTNF-R1 and sTNF-R2

immunoglobulin fusion proteins inhibits the development of actively induced EAE. Intracranial injection of sTNFR-Ig was more potent than systemic administration in inhibiting disease, suggesting that most TNF- α production occurs in the CNS [102]. These results have been confirmed by Selmaj et al. [101]. Thus both anti-TNF antibodies and sTNF-Rs are potent inhibitors of EAE and appear to function at steps subsequent to the activation of encephalitogenic T-cells.

The importance of TNF- α in demyelinating diseases was recently highlighted by the generation of transgenic mice constitutively expressing TNF- α in the CNS. These animals spontaneously developed a chronic inflammatory demyelinating disease with 100% penetrance from about 3–8 weeks of age [103]. Histopathological analysis revealed infiltration of the meninges and CNS parenchyma by CD4⁺ and CD8⁺ T-cells, widespread astrogliosis and microgliosis, and focal demyelination. The direct effect of TNF- α in this disease was documented by administration of a neutralizing antibody against TNF- α , which prevented the development of neurological symptoms, T-cell infiltration, astrogliosis, microgliosis, and demyelination. These results strongly support the hypothesis that in the CNS TNF- α functions as a potent proinflammatory cytokine and a major effector of immune-mediated demyelination.

Direct activation of macrophages/microglia in the CNS

Microglia have been shown to both produce and respond to the cytokine IL-3 [50, 104]. In the brain expression of the signal transducing subunit of the IL-3 receptor shows restricted distribution, being expressed only by macrophages and/or microglia [105]. IL-3 has numerous effects on microglia in vitro, including induction of proliferation and multinucleated giant cell formation [106]. Chiang et al. [107] developed transgenic mice in which the expression of IL-3 was targeted to astrocytes using a glial fibrillary acidic protein fusion gene. In symptomatic transgenic mice multifocal plaque-like lesions were detected in the cerebellum and brainstem. These lesions showed extensive primary demyelination and remyelination in association with the accumulation of large numbers of proliferating and activated macrophage/microglia. Lymphocytes were rarely present. This transgenic model exhibits many of the pathological features of MS and demonstrates that activation of macrophages/microglia in a T-cell independent manner is sufficient to induce demyelinating disease.

Table 2 Potential inhibitors of CNS disease

Anti-inflammatory cytokines	Anti-cytokine antibodies	Soluble receptors	Receptor antagonists	Anti-adhesion molecule antibodies
IFN- β	Anti-TNF	TNF RI and II	IL-1RA	Anti-VLA-4
IL-4	Anti-IFN- γ	IL-1R type I		Anti-VCAM-1
IL-10	Anti-IL-1	IFN- γ R		Anti-LFA-1
IL-13	Anti-MIP-1 α			Anti-ICAM-1
TGF- β	Anti-MCP-1			Anti-MAC-1

Conclusion

A number of therapeutic strategies for MS are directed towards the selective inhibition of autoreactive T-cells. Another complementary approach is to target the "non-antigen" specific aspects of MS, including the effector functions of macrophages/microglia. These include strategies to obtain a reduction in proinflammatory cytokine expression by the use of (a) anti-inflammatory cytokines, (b) neutralizing anti-proinflammatory cytokine antibodies, (c) soluble cytokine receptors, (d) receptor antagonists, and (e) neutralizing anti-adhesion molecule antibodies (see Table 2). Many of these reagents would target cytokines being produced by macrophages/microglia as well as adhesion molecules expressed by these cells. Clearly, inhibition of macrophage/microglia effector functions would be beneficial in reducing inflammation and demyelination within the CNS.

Acknowledgements I thank Sue Wade for superb secretarial and editorial assistance in preparing this manuscript. Work referenced in this article from the author's laboratory was supported in part by National Multiple Sclerosis Society grants 2269-B-5 and 2205-B-5, and National Institutes of Health grants NS-29719 and MH-55795.

References

- del Rio-Hortega P (1932) Microglia. In: Penfield W (ed) *Cytology and cellular pathology of the nervous system*. Hoeber, New York, pp 481-584
- Hickey WF, Kimura H (1988) Perivascular microglial cells of the CNS are bone marrow-derived and present antigen in vivo. *Science* 239:290-292
- Perry VH, Gordon S (1988) Macrophages and microglia in the nervous system. *Trends Neurosci* 11:273-277
- Banati RB, Gehrmann J, Schubert P, Kreutzberg GW (1993) Cytotoxicity of microglia. *Glia* 7:111-118
- Gordon S (1995) The macrophage. *Bioessays* 17:977-986
- Gehrmann J, Matsumoto Y, Kreutzberg GW (1995) Microglia: intrinsic immunoeffector cell of the brain. *Brain Res Rev* 20:269-287
- Moore S, Thanos S (1996) The concept of microglia in relation to central nervous system disease and regeneration. *Prog Neurobiol* 48:441-460
- Streit WJ (1995) Microglial cells. In: Ransom BR, Kettenmann H (eds) *Neuroglia*. Oxford University Press, pp 85-96
- Kreutzberg GW (1996) Microglia: a sensor for pathological events in the CNS. *Trends Neurosci* 19:312-318
- Graeber MB, Streit WJ, Kreutzberg GW (1989) Identity of ED2-positive perivascular cells in rat brain. *J Neurosci Res* 22:103-106
- Walker DG, Kim SU, McGeer PL (1995) Complement and cytokine gene expression in cultured microglia derived from postmortem human brains. *J Neurosci Res* 40:478-493
- Shrikant P, Weber E, Jilling T, Benveniste EN (1995) ICAM-1 gene expression by glial cells: differential mechanisms of inhibition by interleukin-10 and interleukin-6. *J Immunol* 155:1489-1501
- Panek RB, Benveniste EN (1995) Class II MHC gene expression in microglia: regulation by the cytokines IFN- γ , TNF- α and TGF- β . *J Immunol* 154:2846-2854
- Frei K, Siepl C, Groscurth P, Bodmer S, Schwerdel C, Fontana A (1987) Antigen presentation and tumor cytotoxicity by interferon- γ -treated microglial cells. *Eur J Immunol* 17:1271-1278
- Suzumura A, Mezitis SGE, Gonatas NK, Silberberg DH (1987) MHC antigen expression on bulk isolated macrophage-microglia from newborn mouse brain: induction of Ia antigen expression by γ -interferon. *J Neuroimmunol* 15:263-278
- Williams K, Ulvestad E, Antel JP (1994) B7/BB-1 antigen expression on adult human microglia studied in vitro and in situ. *Eur J Immunol* 24:3031-3037
- De Simone R, Giampaolo A, Giometto B, Gallo P, Levi G, Peschle C, Aloisi F (1995) The costimulatory molecule B7 is expressed on human microglia in culture and in multiple sclerosis acute lesions. *J Neuropath. Exp Neurol* 54:175-187
- Ulvestad E, Williams K, Bjerkvig R, Tiekotter K, Antel J, Matre R (1994) Human microglial cells have phenotypic and functional characteristics in common with both macrophages and dendritic antigen-presenting cells. *J Leukoc Biol* 56:732-740
- Korotzer AR, Watt J, Cribbs D, Tenner AJ, Burdick D, Glabe C, Cotman CW (1995) Cultured rat microglia express C1q and receptor for C1q: implications for amyloid effects on microglia. *Exp Neurology* 134:214-221
- Williams K, Bar-Or A, Ulvestad E, Olivier A, Antel JP, Yong VW (1992) Biology of adult human microglia in culture: comparisons with peripheral blood monocytes and astrocytes. *J Neuropathol Exp Neurol* 51:538-549
- Martin R, McFarland HF, McFarlin DE (1992) Immunological aspects of demyelinating diseases. *Annu Rev Immunol* 10:153-187
- Hauser SL, Bhan AK, Gilles FH, Hoban CJ, Reinherz EL, Schlossman SF, Weiner HL (1983) Immunohistochemical staining of human brain with monoclonal antibodies that identify lymphocytes, monocytes and the Ia antigen. *J Neuroimmunol* 5:197-205
- Prineas JW (1975) Pathology of the early lesion in multiple sclerosis. *Human Pathol* 6:531-554
- Prineas JW, Wright RG (1978) Macrophages, lymphocytes and plasma cells in the perivascular compartment in chronic multiple sclerosis. *Lab Invest* 38:409-421
- Bauer J, Sminia T, Wouterlood FG, Dijkstra CD (1994) Phagocytic activity of macrophages and microglial cells during the course of acute and chronic relapsing experimental autoimmune encephalomyelitis. *J Neurosci Res* 38:365-375
- Hofman FM, VonHanwher R, Dinarello C, Mizel S, Hinton D, Merrill JE (1986) Immunoregulatory molecules and IL-2 receptors identified in multiple sclerosis brain. *J Immunol* 136:3239-3245
- Winghagen A, Newcombe J, Dangond F, Strand C, Woodroffe MN, Cuzner ML, Hafler DA (1995) Expression of costimulatory molecules B7-1 (CD80), B7-2 (CD86), and interleukin 12 cytokine in multiple sclerosis lesions. *J Exp Med* 182:1985-1996
- Gerritse K, Laman JD, Noelle RJ, Aruffo A, Ledbetter JA, Boersma WJA, Claassen E (1996) CD40-CD40 ligand interactions in experimental allergic encephalomyelitis and multiple sclerosis. *Proc Natl Acad Sci USA* 93:2499-2504
- Alderson MR, Armitage RJ, Tough TW, Strockbine L, Fanslow WC, Spriggs MK (1993) CD40 expression by human monocytes: regulation by cytokines and activation of monocytes by the ligand for CD40. *J Exp Med* 178:669-674
- Bignami A, Eng LF, Dahl D, Uyeda CT (1972) Localization of the glial fibrillary acidic protein in astrocytes by immunofluorescence. *Brain Res* 43:429-435
- Thompson AJ, Miller D, Youl B, MacManus D, Moore S, Kingsley D, Kendall B, Feinstein A, McDonald WI (1992) Serial gadolinium-enhanced MRI in relapsing/remitting multiple sclerosis of varying disease duration. *Neurology* 42:60-63
- Gay D, Esiri M (1991) Blood-brain barrier damage in acute multiple sclerosis plaques: an immunocytological study. *Brain* 114:557-572
- Benveniste EN (1995) Role of cytokines in multiple sclerosis, autoimmune encephalitis, and other neurological disorders. In: Aggarawal B, Puri R (eds) *Human cytokines: Their role in research and therapy*. Blackwell, Boston, pp 195-216

34. Merrill JE, Benveniste EN (1996) Cytokines in inflammatory brain lesions: Helpful and harmful. *Trends Neurosci* 19: 331-338
35. Selmaj KW, Raine CS (1988) Tumor necrosis factor mediates myelin and oligodendrocyte damage in vitro. *Ann Neurol* 23: 339-346
36. Robbins DS, Shirazi Y, Drysdale BE, Lieberman A, Shin HS, Shin ML (1987) Production of cytotoxic factor for oligodendrocytes by stimulated astrocytes. *J Immunol* 139:2593-2597
37. Selmaj K, Raine CS, Cross AH (1991) Anti-tumor necrosis factor therapy abrogates autoimmune demyelination. *Ann Neurol* 30:694-700
38. Selmaj KW, Farooq M, Norton WT, Raine CS, Brosnan CF (1990) Proliferation of astrocytes in vitro in response to cytokines. A primary role for tumor necrosis factor. *J Immunol* 144:129-135
39. Giuliani D, Lachman LB (1985) Interleukin-1 stimulation of astroglial proliferation after brain injury. *Science* 228:497-499
40. Swanborg RH (1995) Experimental autoimmune encephalomyelitis in rodents as a model for human demyelinating disease. *Clin Immunol Immunopathol* 77:4-13
41. Gehrman J, Gold R, Linington C, Lannes-Vieira J, Wekerle H, Kreutzberg GW (1993) Microglial involvement in autoimmune inflammation of the central and peripheral nervous system. *Glia* 7:50-59
42. McCombe PA, de Jersey J, Pender MP (1994) Inflammatory cells, microglia and MHC class II antigen-positive cells in the spinal cord of Lewis rats with acute and chronic relapsing experimental autoimmune encephalomyelitis. *J Neuroimmunol* 51:153-167
43. Ando DG, Clayton J, Kono D, Urban JL, Sercarz EE (1989) Encephalitogenic T cells in the B10.PL model of experimental allergic encephalomyelitis (EAE) are of the Th-1 lymphokine subtype. *Cell Immunol* 124:132-143
44. Mustafa M, Vingsbo C, Olsson T, Ljungdahl A, Hsjeberg B, Holmdahl R (1993) The major histocompatibility complex influences myelin basic protein 63-88-induced T cell cytokine profile and experimental autoimmune encephalomyelitis. *Eur J Immunol* 23:3089-3095
45. Karpus WJ, Gould KE, Swanborg RH (1992) CD4+ suppressor cells of autoimmune encephalomyelitis respond to T cell receptor-associated determinants on effector cells by interleukin-4 secretion. *Eur J Immunol* 22:1757-1763
46. Racke MK, Burnett D, Pak S-H, Albert PS, Cannella B, Raine CS, McFarlin DE, Scott DE (1995) Retinoid treatment of experimental allergic encephalomyelitis. *J Immunol* 154: 450-458
47. Stevens DB, Gould KE, Swanborg RH (1994) Transforming growth factor- β 1 inhibits tumor necrosis factor- α /lymphotoxin production and adoptive transfer of disease by effector cells of autoimmune encephalomyelitis. *J Neuroimmunol* 51: 77-83
48. Lee SC, Liu W, Roth P, Dickson DW, Berman JW, Brosnan CF (1993) Macrophage colony-stimulating factor in human fetal astrocytes and microglia: Differential regulation by cytokines and lipopolysaccharide, and modulation of class II MHC on microglia. *J Immunol* 150:594-604
49. Lee SC, Liu W, Dickson DW, Brosnan CF, Berman JW (1993) Cytokine production by human fetal microglia and astrocytes: Differential induction by lipopolysaccharide and IL-1 β . *J Immunol* 150:2659-2667
50. Appel K, Honegger P, Gebicke-Haerter PJ (1995) Expression of interleukin-3 and tumor necrosis factor- β mRNAs in cultured microglia. *J Neuroimmunol* 60:83-91
51. Briers TW, Desmaretz C, Vanmechelen E (1994) Generation and characterization of mouse microglial cell lines. *J Neuroimmunol* 52:153-164
52. Murphy GM Jr, Jia X-C, Song Y, Ong E, Shrivastava R, Bocchini V, Lee YL, Eng LF (1995) Macrophage inflammatory protein 1- α mRNA expression in an immortalized microglial cell line and cortical astrocyte cultures. *J Neurosci Res* 40: 755-763
53. Giuliani D, Baker TJ, Shih LC, Lachman LB (1986) Kin-1 of the central nervous system is produced by microglia. *J Exp Med* 164:594-604
54. Giuliani D, Baker TJ (1986) Characterization of microglia isolated from developing mammalian brain. *Neurosci Lett* 62:163-167
55. Righi M, Mori L, De Libero G, Sironi M, Bianchi A, Donini SD, Ricciardi-Castagnoli P (1991) Production by microglial cell clones. *Eur J Immunol* 21:1443-1448
56. Gottschall PE, Yu X, Bing B (1995) Increased gelatinase B (matrix metalloproteinase-9) and by activated rat microglia in culture. *J Neurosci Res* 335-342
57. Chao CC, Hu S, Sheng WS, Peterson PK (1995) Tumor necrosis factor- α production by human fetal cells: regulation by other cytokines. *Dev Neurosci* 17: 358-365
58. Chao CC, Hu S, Sheng WS, Tsang M, Peterson PK (1995) Tumor necrosis factor- α mediates the release of transforming growth factor- β in murine microglia. *Clin Immunol Immunopathol* 77:358-365
59. Norris JG, Benveniste EN (1993) Interleukin-6 induces astrocytes: induction by the neurotransmitter acetylcholine. *J Neuroimmunol* 45:137-146
60. Zajicek JP, Wing M, Scolding NJ, Compston D (1995) Interactions between oligodendrocytes and microglia. *J Neurosci Res* 41:1611-1631
61. Merrill JE, Ignarro LJ, Sherman MP, Melinelli J (1993) Microglial cell cytotoxicity of oligodendrocytes mediated through nitric oxide. *J Immunol* 151:2 1611-1631
62. Colton CA, Keri JE, Chen W-T, Monsky WL (1993) Production by cultured microglia: substrate gelatinolytic activity and matrix degradation. *J Neurosci Res* 35: 1554-1558
63. Cammer W, Bloom BR, Norton WT, Gordon S (1981) Induction of basic protein in myelin by neutral proteases released by stimulated macrophages: a possible mechanism for inflammatory demyelination. *Proc Natl Acad Sci USA* 78:1554-1558
64. Shrikant P, Benveniste EN (1996) The central nervous system as an immunocompetent organ: role of glial cell presentation. *J Immunol* 157:1819-1822
65. June CH, Bluestone JA, Nadler LM, Thompson CB (1993) The B7 and CD28 receptor families. *Immunol Rev* 131:321-331
66. Satoh J-I, Lee YB, Kim SU (1995) T-cell costimulatory molecules B7-1 (CD80) and B7-2 (CD86) are expressed by human microglia but not in astrocytes in culture. *J Neurosci Res* 704:92-96
67. Woodroffe MN, Hayes GM, Cuzner ML (1989) MHC antigen expression and superoxide production are increased in interferon- γ -treated microglia from adult rat brain. *Immunol* 68:421-426
68. Suzumura A, Sawada M, Itoh Y, Marunouchi T (1993) Interleukin-4 induces proliferation and activation of microglia and suppresses their induction of class II major histocompatibility complex antigen expression. *J Neuroimmunol* 51: 77-83
69. Racke MK, Bonomo A, Scott DE, Cannella B, Raine CS, Shevach EM, Röcken M (1994) Cytokine deviation as a therapy for inflammatory disease. *J Exp Med* 180:1961-1966
70. Brosnan CF, Bornstein MB, Bloom BR (1981) Macrophage depletion on the clinical and pathogenesis of experimental allergic encephalomyelitis. *J Exp Med* 153:614-620
71. Huitinga I, van Rooijen N, de Groot CJA, Ulfhake H, Dijkstra CD (1990) Suppression of experimental allergic encephalomyelitis in Lewis rats after elimination of microglia. *J Exp Med* 172:1025-1033
72. Bauer J, Huitinga I, Zhao W, Lassmann H, Dijkstra CD (1995) The role of macrophages, pericytes and microglial cells in the pathogenesis of experimental allergic encephalomyelitis. *Glia* 15:437-446

- Springer TA (1994) Traffic signals for lymphocyte recirculation and leukocyte emigration: the multistep paradigm. *Cell* 76:301-314
74. Huitinga I, Damoiseaux JGMC, Döpp EA, Dijkstra CD (1993) Treatment with anti-CD3 antibodies ED7 and ED8 suppresses experimental allergic encephalomyelitis in Lewis rats. *Eur J Immunol* 23:709-715
75. Gordon EJ, Myers KJ, Dougherty JP, Rosen H, Ron Y (1995) Both anti-CD11a (LFA-1) and anti-CD11b (MAC-1) therapy delay the onset and diminish the severity of experimental autoimmune encephalomyelitis. *J Neuroimmunol* 62:153-160
76. Baggiolini M, Dewald B, Moser B (1994) Interleukin-8 and related chemotactic cytokines - CXC and CC chemokines. *Adv Immunol* 55:97-178
77. Strieter RM, Standiford TJ, Huffnagle GB, Colletti LM, Lukacs NW, Kunkel SL (1996) "The good, the bad, and the ugly" the role of chemokines in models of human disease. *J Immunol* 156:3583-3586
78. Hunkeler K, Brosnan CF, Aquino DA, Cammer W, Kulshrestha S, Guida MP, Rapoport DA, Berman JW (1993) Expression of CSF-1, c-fms, and MCP-1 in the central nervous system of rats with experimental allergic encephalomyelitis. *J Immunol* 150:2525-2533
79. Berman JW, Guida MP, Warren J, Amat J, Brosnan CF (1996) Localization of monocyte chemoattractant peptide-1 expression in the central nervous system in experimental autoimmune encephalomyelitis and trauma in the rat. *J Immunol* 156:3017-3023
80. Ransohoff RM, Hamilton TA, Tani M, Stoler MH, Shick HE, Major JA, Estes ML, Thomas DM, Tuohy VK (1993) Astrocyte expression of mRNA encoding cytokines IP-10 and JE/MCP-1 in experimental autoimmune encephalomyelitis. *FASEB J* 7:592-600
81. Fuentes ME, Durham SK, Swerdel MR, Lewin AC, Barton DS, McGill JR, Bravo R, Lira SA (1995) Controlled recruitment of monocytes and macrophages to specific organs through transgenic expression of monocyte chemoattractant protein-1. *J Immunol* 155:5769-5776
82. Godiska R, Chanry D, Dietsch GN, Gray PW (1995) Chemokine expression in murine experimental allergic encephalomyelitis. *J Neuroimmunol* 58:167-176
83. Karpus WJ, Lukacs NW, McRae BL, Strieter RM, Kunkel SL, Miller SD (1995) An important role for the chemokine macrophage inflammatory protein-1 α in the pathogenesis of the T cell-mediated autoimmune disease, experimental autoimmune encephalomyelitis. *J Immunol* 155:5003-5010
84. Gijbels K, Masure S, Carton H, Opdenakker G (1992) Gelatinase in the cerebrospinal fluid of patients with multiple sclerosis and other inflammatory neurological disorders. *J Neuroimmunol* 41:29-34
85. Gijbels K, Proost P, Masure S, Carton H, Billiau A, Opdenakker G (1993) Gelatinase B is present in the cerebrospinal fluid during experimental autoimmune encephalomyelitis and cleaves myelin basic protein. *J Neurosci Res* 36:432-440
86. Maeda A, Sobel RA (1996) Matrix metalloproteinases in the normal human central nervous system, microglial nodules, and multiple sclerosis lesions. *J Neuropath. Exp Neurol* 55:300-309
87. Welgus HG, Campbell EJ, Cury JD, Eisen AZ, Senior RM, Wilhelm SM, Goldberg GI (1990) Neutral metalloproteinases produced by human mononuclear phagocytes: enzyme profile, regulation, and expression during cellular development. *J Clin Invest* 86:1496-1502
88. Beezhold DH, Personius C (1992) Fibronectin fragments stimulate tumor necrosis factor secretion by human monocytes. *J Leukoc. Biol* 51:59-64
89. Gijbels K, Galaray RE, Steinman L (1994) Reversal of experimental autoimmune encephalomyelitis with a hydroxamate inhibitor of matrix metalloproteinases. *J Clin Invest* 94:2177-2182
90. Malik N, Greenfield BW, Wahl AF, Kiener PA (1996) Activation of human monocytes through CD40 induces matrix metalloproteinases. *J Immunol* 156:3952-3960
91. Wagner DH Jr, Stout RD, Suttles J (1994) Role of the CD40-CD40 ligand interaction in CD4+ T cell contact-dependent activation of monocyte interleukin-1 synthesis. *Eur J Immunol* 24:1348-1354
92. Shu U, Kuniwa M, Wu CY, Maliszewski C, Vezzio N, Hakimi J, Gately M, Delespesse G (1995) Activated T cells induce interleukin-12 production by monocytes via CD40-CD40 ligand interaction. *Eur J Immunol* 25:1125-1128
93. Tian L, Noelle RJ, Lawrence DA (1995) Activated T cells enhance nitric oxide production by murine splenic macrophages through gp39 and LFA-1. *Eur J Immunol* 25:306-309
94. Beck J, Rondot P, Catinot L, Falcoff E, Kirchner H, Wietzerbin J (1988) Increased production of interferon gamma and tumor necrosis factor precedes clinical manifestation in multiple sclerosis: do cytokines trigger off exacerbations? *Acta Neurol Scand* 78:318-323
95. Merrill JE, Strom SR, Ellison GW, Myers LW (1989) In vitro study of mediators of inflammation in multiple sclerosis. *J Clin Immunol* 9:84-96
96. Rieckmann P, Albrecht M, Kitze B, Weber T, Tumani H, Broocks A, Lür W, Helwig A, Poser S (1995) Tumor necrosis factor- α messenger RNA expression in patients with relapsing-remitting multiple sclerosis is associated with disease activity. *Ann Neurol* 37:82-88
97. Correale J, Gilmore W, McMillan M, Li S, McCarthy K, Le T, Weiner LP (1995) Patterns of cytokine secretion by autoreactive proteolipid protein-specific T cell clones during the course of multiple sclerosis. *J Immunol* 154:2959-2968
98. Khoury SJ, Hancock WW, Weiner HL (1992) Oral tolerance to myelin basic protein and natural recovery from experimental autoimmune encephalomyelitis are associated with down-regulation of inflammatory cytokines and differential upregulation of transforming growth factor β , interleukin 4, and prostaglandin E expression in the brain. *J Exp Med* 176:1355-1364
99. Renno T, Krakowski M, Piccirillo C, Lin J-Y, Owens T (1995) TNF- α expression by resident microglia and infiltrating leukocytes in the central nervous system of mice with experimental allergic encephalomyelitis. *J Immunol* 154:944-953
100. Ruddle NH, Bergman CM, McGrath KM, Lingenheld EG, Grunnet ML, Padula SJ, Clark RB (1990) An antibody to lymphotoxin and tumor necrosis factor prevents transfer of experimental allergic encephalomyelitis. *J Exp Med* 172:1193-1200
101. Selmaj K, Papierz W, Glabinski A, Kohno T (1995) Prevention of chronic relapsing experimental autoimmune encephalomyelitis by soluble tumor necrosis factor receptor 1. *J Neuroimmunol* 56:135-141
102. Baker D, Butler D, Scallon BJ, O'Neill JK, Turk JL, Feldmann M (1994) Control of established experimental allergic encephalomyelitis by inhibition of tumor necrosis factor (TNF) activity within the central nervous system using monoclonal antibodies and TNF receptor-immunoglobulin fusion proteins. *Eur J Immunol* 24:2040-2048
103. Probert L, Akassoglou K, Pasparakis M, Kontogeorgos G, Kollias G (1995) Spontaneous inflammatory demyelinating disease in transgenic mice showing central nervous system-specific expression of tumor necrosis factor α . *Proc Natl Acad Sci USA* 92:11294-11298
104. Gebicke-Haerter PJ, Appel K, Taylor GD, Schobert A, Rich IN, Northoff H, Berger M (1994) Rat microglial interleukin-3. *J Neuroimmunol* 50:203-214
105. Appel K, Buttini M, Sauter A, Gebicke-Haerter PJ (1995) Cloning of rat interleukin-3 receptor β -subunit from cultured microglia and its mRNA expression in vivo. *J Neurosci* 15:5800-5809
106. Lee TT, Martin FC, Merrill JE (1993) Lymphokine induction of rat microglia multinucleated giant cell formation. *Glia* 8:51-61
107. Chiang C-S, Powell HC, Gold LH, Samimi A, Campbell IL (1996) Macrophage/microglial-mediated primary demyelination and motor disease induced by the central nervous system production of interleukin-3 in transgenic mice. *J Clin Invest* 97:1512-1524

Effect of Anti-Macrophage Migration Inhibitory Factor Antibody on Lipopolysaccharide-induced Pulmonary Neutrophil Accumulation

HIRONI MAKITA, MASAHARU NISHIMURA, KENJI MIYAMOTO, TSUYOSHI NAKANO, YOSHINORI TANINO, JUNICHI HIROKAWA, JUN NISHIHARA, and YOSHIKAZU KAWAKAMI

First Department of Medicine and Central Research Institute, Hokkaido University School of Medicine, Sapporo, Japan

Macrophage migration inhibitory factor (MIF) is a recently rediscovered pro-inflammatory cytokine that has the unique potential to override the anti-inflammatory action of glucocorticoids. Since recent reports suggest the pivotal role of MIF in acute lung injury, we examined the protective effect of anti-MIF antibody on lipopolysaccharide (LPS)-induced acute lung injury in rats. Rats were injected with LPS (7 mg/kg) intraperitoneally with or without pretreatment with anti-MIF antibody. The anti-MIF antibody significantly attenuated LPS-induced migration of neutrophils to the lungs at 4 and 24 h as demonstrated by observation of the number of neutrophils per alveolus, the activity of myeloperoxidase of the lung tissue, and cell differentiation of neutrophils in bronchoalveolar lavage (BAL) fluid. The increased level of macrophage inflammatory protein-2, a powerful neutrophil chemokine, in BAL fluid was also significantly attenuated by pretreatment with the anti-MIF antibody as compared with the control group. Additionally, positive immunostaining for MIF was observed in bronchial epithelial cells and alveolar macrophages, and Northern blot analysis of lung tissues demonstrated increased MIF mRNA 24 h after LPS injection. These data suggest that the anti-MIF antibody has therapeutic potential for the treatment of acute lung injury by suppressing the level of neutrophil chemokine in the lungs. **Makita H, Nishimura M, Miyamoto K, Nakano T, Tanino Y, Hirokawa J, Nishihara J, Kawakami Y. Effect of anti-macrophage migration inhibitory factor antibody on lipopolysaccharide-induced pulmonary neutrophil accumulation.**

AM J RESPIR CRIT CARE MED 1998;158:573-579.

Macrophage migration inhibitory factor (MIF) was first described in 1966 as a cytokine "activity," derived from activated T lymphocytes, preventing random macrophage migration at the site of inflammation (1, 2). After the cloning of human MIF complementary DNA (cDNA) in 1989 (3), MIF "protein" was re-evaluated as an important pro-inflammatory cytokine (4, 5). In a series of recent studies using rodents, MIF was found to be a secretory product of anterior pituitary cells and activated macrophages that antagonizes the suppressive effects of glucocorticoids on cytokine production and potentiates effects of endotoxin in experimentally induced septic shock (6). Furthermore, administration of an anti-MIF antibody improves the survival rate in the case of lethal endotoxemia in mice (4, 5). Since then, a few laboratories, including ours, have reported that MIF can be detected in a variety of cells, tissues, and organs in humans as well as in rodents (7-10), and that MIF production is upregulated in gram-negative sepsis (11). More recently, Donnelly and colleagues (12) demonstrated that in patients with acute respiratory distress syndrome (ARDS),

MIF is present in the affected lungs, and that alveolar macrophages are one cellular source of MIF. They also showed that MIF augments, and the anti-MIF antibody attenuates, pro-inflammatory cytokine secretions, such as tumor necrosis factor alpha (TNF- α) and interleukin-8 (IL-8) from alveolar macrophages.

This background prompted us to examine the protective effect of an anti-MIF antibody on lipopolysaccharide (LPS)-induced acute lung injury in rats. We anticipated that pretreatment with the anti-MIF antibody could attenuate or abolish such lung injury. Additionally, we investigated the localization of MIF in the lungs of rats by immunohistochemical analysis, and the expression of MIF mRNA before and after the LPS-induced lung injury by northern blot analysis. Furthermore, in an attempt to gain insight into the mechanism by which the anti-MIF antibody attenuates LPS-induced neutrophil accumulation in the lungs, we measured macrophage inflammatory protein-2/cytokine-induced neutrophil chemoattractant (MIP-2/CINC-3), an important neutrophil chemokine, in bronchoalveolar lavage (BAL) fluid of the rats.

METHODS

Animals

Studies were performed on male Sprague-Dawley rats ($n = 69$) (224 ± 52 g [mean \pm SD]). They were allowed free access to water and commercial chow. This research adhered to the Declaration of Helsinki and was approved by the Animal Experiment Ethics Committee of Hokkaido University School of Medicine.

(Received in original form July 18, 1997 and in revised form February 24, 1998)

Supported by Science Research Grant 09877113 from the Ministry of Education, Science, Sports, and Culture of Japan, and Research Grant for the Intractable Diseases from the Ministry of Health and Welfare of Japan.

Correspondence and requests for reprints should be addressed to Hironi Makita, M.D., First Department of Medicine, Hokkaido University School of Medicine, North 15 West 7 Kita-ku Sapporo 060, Japan. E-mail: maki@sa2.so-net.ne.jp

Am J Respir Crit Care Med Vol 158, pp 573-579, 1998
Internet address: www.atsjournals.org

Materials

The following materials were obtained from commercial sources: LPS from *Escherichia coli* 0111:B4 was purchased from Sigma Chemical Company (St. Louis, MO) and dissolved in pyrogen-free physiologic saline just before each experiment; biodyne transfer membranes from Pall Biosupport Division (Glen Cove, NY); Isogen RNA extraction kit from Nippon Gene Chemical Company (Tokyo, Japan); [α - 32 P] dCTP from Dupont-NEN (Boston, MA); complete Freund's adjuvant (CFA) and incomplete Freund's adjuvant (IFA) from Wako Pure Chemical Industries (Osaka, Japan); Vector ABC Kit from Vector Laboratory (Burlingame, CA); horseradish peroxidase (HRP)-conjugated goat anti-rabbit antibody from Pierce (Rockford, IL); specific rat MIP-2/CINC-3 ELISA kit from Immunobiological Laboratory (Fujisawa, Japan). All other chemicals were of analytical grade.

Preparation of Rabbit Polyclonal Antibody against Rat MIF

Polyclonal anti-rat MIF serum was generated by immunizing New Zealand White rabbits with purified recombinant rat MIF. Rat MIF was expressed in *E. coli* and purified to homogeneity as described in our previous publications (13, 14). In brief, the rabbits were inoculated intradermally with 100 μ g of MIF emulsified in CFA at Weeks 1 and 2, and with 50 μ g of MIF diluted in IFA at Week 4. The immunoglobulin G (IgG) fraction was prepared using Protein A-Sepharose according to the manufacturer's protocol.

Experimental Design

Experiments were designed to evaluate the effects of the anti-MIF antibody on LPS-induced acute lung injury by comparing an LPS group (nonimmunized rabbit IgG + LPS) and an anti-MIF Ab group (anti-MIF antibody + LPS) 4 and 24 h after LPS administration. LPS was administered intraperitoneally (7 mg/kg of 2 mg/ml LPS in 0.9% NaCl). As a negative control, physiologic saline, instead of LPS, was given to rats intraperitoneally. Two hours before administration of LPS, the rats were intraperitoneally injected with either the anti-MIF antibody (IgG fraction; 3.9 ~ 8.6 mg/kg) or the same dose of nonimmunized rabbit IgG. The rats were then returned to their cages and allowed free access to food and water. Four and 24 h later, blood samples were taken by puncturing the abdominal aorta under anesthesia with 1.5% inhalant halothane. Then the lungs were excised by opening the chest, and free blood was removed by blotting the hilus onto paper towels. The left lung was fixed in buffered (pH 7.4) 10% formalin for at least 48 h and then embedded in paraffin for later histopathologic examination. The upper part of the right lung was used for the measurement of tissue myeloperoxidase (MPO) activity, and the lower part of the right lung was used for obtaining the lung tissue wet to dry (W/D) weight ratio.

Histologic examination. A 5- μ m section was cut from the mid-portion of paraffin-embedded whole lung tissue and stained with hematoxylin and eosin. An observer who was blinded to the animals' group assignment assessed more than 50 alveoli at $\times 400$ magnification and determined the average number of neutrophils per alveolus.

Measurement of the lung tissue MPO activity. The lung was homogenized and sonicated in 100 mM potassium phosphate-buffered solution (PBS), pH 6.0, with 0.5% hexadecyl-trimethylammonium bromide (HTAB) and 5 mM EDTA. After centrifugation (40,000 \times g, 15 min), the supernatant fluids were reacted with H_2O_2 (0.0005%) in the presence of orthodianisidine (0.167 mg/ml). The change in optical density (OD) (at 460 nm) per minute was determined (15).

Measurement of the lung tissue W/D weight ratio. The lung was weighed soon after excision, and then dried in an oven at 60°C for 72 h. The dried lung tissue was weighed again, and the lung tissue W/D weight ratio was obtained.

Neutrophil counts and albumin concentration in BAL fluid. Another set of animals was used for evaluation of cell differentiation and the albumin concentration in BAL fluid. BAL was performed under anesthesia with intraperitoneally administered sodium pentobarbital (50 mg/kg) 4 and 24 h after the administration of LPS. Each time, 8 ml of 37°C sterile physiologic saline was instilled through a tracheal cannula at a hydrostatic pressure of 15 cm and withdrawn by gravity while using a vibrator. The procedure was repeated five times, and all BAL fluid was collected. The recovery rate was over 90%. Then we centrifuged the BAL fluid (700 \times g for 5 min, 4°C) and counted the total

number of cells using a standard hemocytometer method. We stained the cells by the Dif-Quik method and determined the cell differentiation.

Immunohistochemistry

The lungs of rats that had received either LPS or physiologic saline ($n = 3$ for each) 24 h earlier were used for the immunohistochemical study. The lungs were fixed overnight in formaldehyde, after which 5- μ m thick paraffin sections were mounted on poly-L-lysine-coated slides. The BAL cells were collected as described above ($n = 3$ for each), and mounted on poly-L-lysine-coated glass slides. After centrifugation for mounting, the BAL cells were fixed in 95% ethanol at 4°C for 5 min. The tissue samples were immersed in 100% methanol containing hydrogen peroxide (0.3%) for 30 min to quench endogenous peroxidase reactivity. Subsequently, they were stained with the avidin-biotin-peroxidase complex procedure using a Vector ABC Kit according to the manufacturer's protocol. Nonspecific staining was blocked by incubation for 30 min with normal goat serum (10%). The sections were further incubated overnight at 4°C with the anti-rat MIF polyclonal antibody. After three washes with PBS, the samples were reacted with biotinylated goat anti-rabbit IgG and avidin-biotin complex at room temperature for 30 min. The reaction was developed in 3,3'-diaminobenzidine tetrahydrochloride containing hydrogen peroxide (0.01%), and the tissue samples were mounted with alkylacrylates.

Northern Blot Analysis

Lung tissues were collected under anesthesia before and 24 h after LPS administration ($n = 3$ for each). Northern blot analysis was carried out as previously described (7). In brief, RNA from these lung tissues was extracted and separated into 20- μ g units by electrophoresis on 1% agarose gel containing 0.6 M formaldehyde, and blotted on nylon membrane filters. The hybridization was carried out using a full-length rat MIF cDNA probe radiolabeled with [α - 32 P]dCTP at 42°C for 48 h. The MIF cDNA used in this study had been isolated from a rat liver cDNA library in this laboratory (7). After hybridization the filters were washed with 0.1 \times standard saline citrate (SSC)/0.1% SDS for 30 min at 65°C and exposed at -80°C for 2 d to X-OMAT film from Eastman Kodak Company (Rochester, NY). Relative intensities of the radioactive bands were quantitated by Bio-image analyzer (Fuji Film Ltd., Tokyo).

Enzyme-linked Immunosorbent Assay (ELISA) of MIF

The anti-rat MIF IgG polyclonal antibody dissolved in PBS (50 μ l) was added to each well of a 96-well microtiter plate, which was then left for 30 min at room temperature. The plate was washed three times with distilled water. All wells were filled with PBS containing 0.5% BSA for blocking and left for 20 min at room temperature. After removal of the blocking solution, the samples were added in duplicate to individual wells and incubated for 1 h at room temperature. After the plate was washed three times with PBS containing 0.05% Tween 20 (washing buffer), 50 μ l of biotin-conjugated anti-MIF antibody was added to each well. After incubation for 1 h at room temperature, the plate was again washed three times with the washing buffer. Avidin-conjugated horseradish peroxidase was added to each well, and the microtiter plate was again incubated for 15 min at room temperature. After washing three times, the substrate solution (10 ml) contained 8 mg of o-phenylenediamine and 4 μ l of 30% H_2O_2 in citrate phosphate buffer (pH 5.0). Finally, the substrate solution (50 μ l) was added to each well. After incubation for 20 min at room temperature, the reaction was terminated with 25 μ l of 4 N sulfuric acid. The absorbance was measured at 492 nm by an ELISA plate reader (Model 3550; Bio-Rad). The detection limit in this system was 1.5 ng/ml.

ELISA of MIP-2/CINC-3

The level of MIP-2/CINC-3 in BAL fluids was measured and the LPS group and anti-MIF Ab group were compared with a specific rat MIP-2 ELISA kit using recombinant rat MIP-2/CINC-3 as a standard. Although three other subtypes of CINC have been identified, such as CINC-1, CINC-2 α , and CINC-2 β , this system has no cross-reactivity for those (16). The detection limit in this system is reportedly 50 pg/ml.

TABLE 1
RESULTS OF MEASUREMENTS*

	Control	LPS	Anti-MIF + LPS
BAL			
Total no. of cells, $\times 10^5$ cells	12.87 \pm 1.38	15.97 \pm 3.62	6.80 \pm 0.37
Neutrophils, %	1.2 \pm 0.4	10.0 \pm 2.7 [†]	2.0 \pm 0.4 [‡]
Albumin, μ g/ml	1.89 \pm 0.76	1.57 \pm 0.36	1.62 \pm 0.09
Blood			
WBC, cells/ μ l	8,675 \pm 2,112	7,620 \pm 1,717	5,300 \pm 1,550
Platelets, $\times 10^4$ cells/ μ l	116.2 \pm 10.5	13.9 \pm 5.2 [†]	41.8 \pm 6.4 [‡]
Wet/dry weight ratio	5.14 \pm 0.12	5.12 \pm 0.08	5.07 \pm 0.04

Definition of abbreviations: BAL = bronchoalveolar lavage; WBC = white blood cells.

* Mean \pm SEM.

[†] $p < 0.05$ versus control group.

[‡] $p < 0.05$ versus LPS group.

Statistics

Data were analyzed by one-way analysis of variance (ANOVA), and individual group means were then compared with Student's *t* test. All values are expressed as mean \pm SEM unless otherwise specified.

RESULTS

Effect of Anti-MIF Antibody on Lung Inflammation

Histology and MPO activity. No rats died in any treatment groups throughout the experimental period. There was a significant decrease in the counts of circulating blood thrombocytes at 24 h in the LPS group, but the leukocyte numbers did not decline (Table 1). This LPS-induced thrombocytopenia was significantly attenuated by pretreatment with the anti-MIF antibody. Light microscopic examination revealed a slight but significant degree of neutrophil accumulation in and around alveoli only in the rats that had received the nonimmunized rabbit IgG + LPS (Figures 1A and 1B). However, there were no serious lung injuries, such as pulmonary edema or hemorrhage, even in the LPS group, so that no significant difference was found in the W/D weight ratio between the control group and the LPS group (Table 1). The numbers of neutrophils observed in the lung tissues 4 and 24 h after administration of LPS were significantly larger than those of the control group (Figure 2A). When rats were pretreated with the anti-MIF antibody, the number of neutrophils significantly decreased compared with the LPS group (2.67 \pm 0.33 versus 1.20 \pm 0.09

cells/alveolus at 4 h, 2.45 \pm 0.40 versus 1.38 \pm 0.29 cells/alveolus at 24 h, $p < 0.05$). The MPO activity of lung tissue in the anti-MIF Ab group was also markedly lower than that of the LPS group at 4 and 24 h after administration of LPS (2.04 \pm 0.27 versus 1.34 \pm 0.11 Δ OD/min at 4 h, 1.39 \pm 0.15 versus 0.66 \pm 0.24 Δ OD/min at 24 h, $p < 0.05$) (Figure 2B). There was a significant and close correlation between the number of neutrophils observed and the activity of MPO in the lung tissues ($r = 0.85$ at 4 h, $r = 0.93$ at 24 h), indicating that two independent evaluations provided exactly the same results on neutrophil migration.

BAL findings. Although there were no significant differences among all groups either in the total cell number or in the albumin concentration in BAL fluid, the neutrophil differentiation ratio was significantly increased again only in the LPS group at 24 h after LPS injection (10.0 \pm 2.7%) compared either with the control group (1.2 \pm 0.4%, $p < 0.05$) or with the anti-MIF Ab group (2.0 \pm 0.4%, $p < 0.05$) (Table 1, Figure 2C).

MIP-2/CINC-3 in BAL fluids. As is shown in Figure 3, the level of MIP-2 in BAL fluid was significantly lower in the anti-MIF Ab group than in the LPS group (253 \pm 62 pg/ml versus 759 \pm 101 pg/ml, $n = 5$ for each, $p < 0.01$).

MIF in serum and BAL fluids. The level of MIF in serum was 14 \pm 3 ng/ml in the control rats ($n = 5$). The serum level significantly and markedly increased at 4 h (121 \pm 25 ng/ml, $n = 8$, $p < 0.05$) and also at 24 h (38 \pm 9 ng/ml, $n = 5$, $p < 0.05$) in the rats that had been given LPS. However, we found

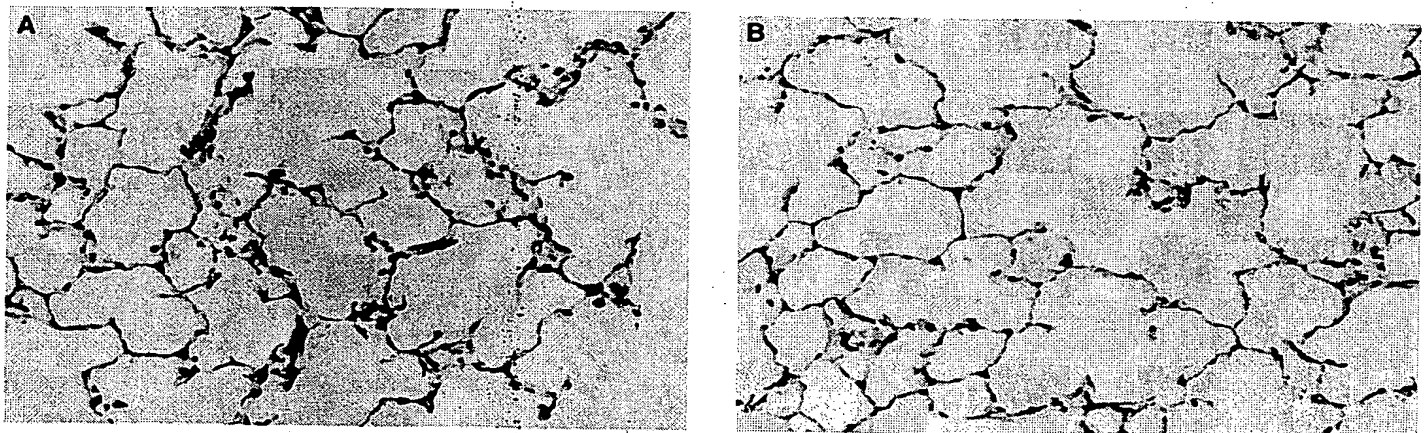


Figure 1. Light microscopic examination. (A) Neutrophils significantly accumulated in and around alveoli in the LPS group; however, there were no serious lung injuries such as pulmonary edema and hemorrhage. (B) Pretreatment with anti-MIF antibody attenuated LPS-induced neutrophil accumulation.

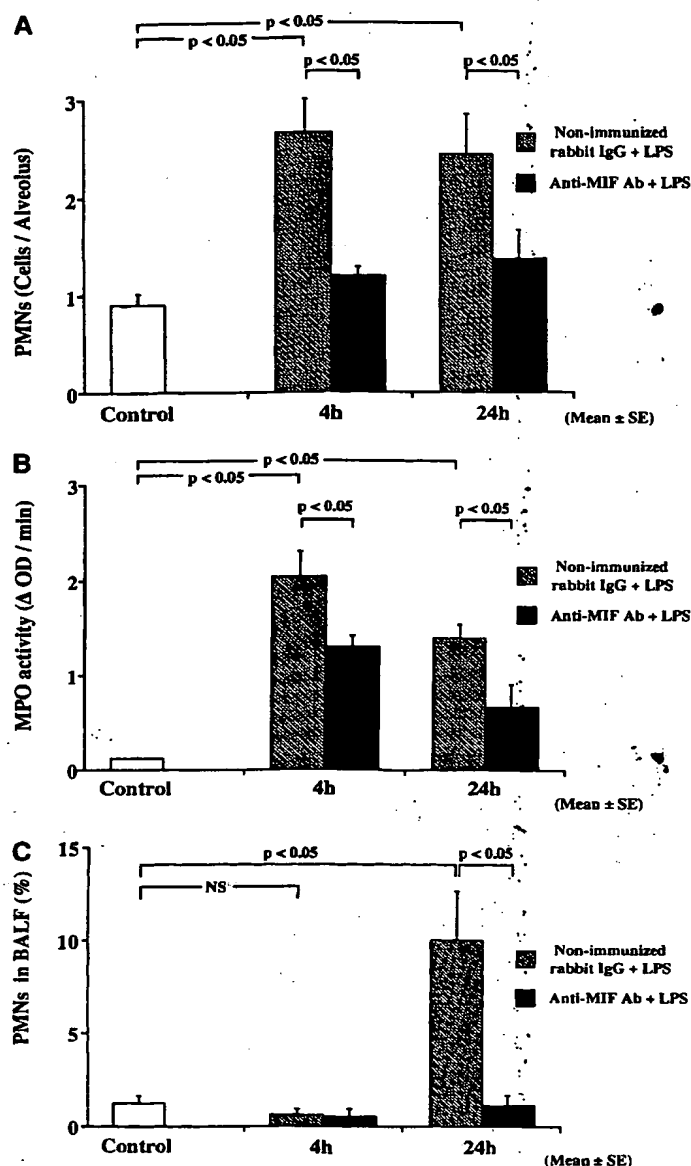


Figure 2. Accumulation of neutrophils in LPS-injured lungs. Negative control rats received saline instead of LPS ($n = 8$). The significant attenuation of neutrophil migration by the anti-MIF antibody was proved by three independent examinations at 4 and 24 h after administration of LPS: nonimmunized rabbit IgG + LPS ($n = 20$), anti-MIF antibody + LPS ($n = 20$). (A) The number of neutrophils per alveolus, (B) activity of MPO in the lung, and (C) the number of neutrophils in BAL fluid.

no significant increases in the level of MIF in BAL fluids at the same periods (2.17 ± 0.48 ng/ml at 0 h, 3.20 ± 1.18 ng/ml at 4 h, and 3.08 ± 0.74 ng/ml at 24 h, respectively, not significant).

Immunohistochemical Localization and Identification of MIF in Lungs of Rats

Positive immunostaining for MIF was observed even in the control animals within the bronchial epithelial cells and in almost all alveolar macrophages (Figures 4A and 4B). There was a moderate increase in immunostaining in both cell types in the LPS-treated rats (Figures 4C and 4D). Northern blot analysis demonstrated prominent MIF expression in the lung

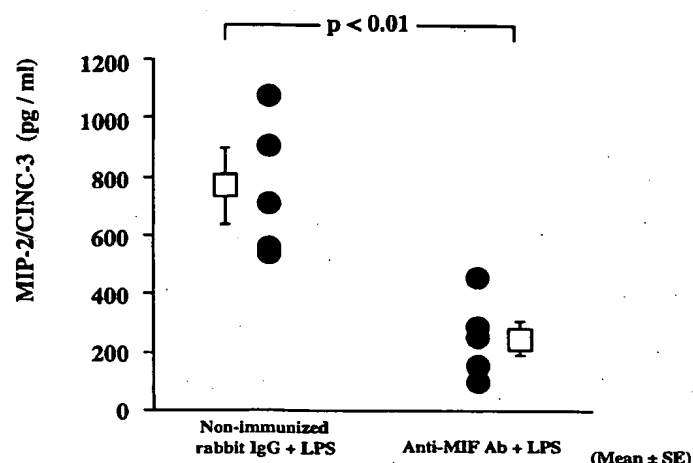


Figure 3. MIP-2/CINC-3 in BAL fluid. The MIP-2 levels in BAL fluids from the rats pretreated with anti-MIF antibody were significantly decreased at 4 h after commencement of injury (from 759 ± 101 pg/ml to 253 ± 62 pg/ml, $p < 0.01$). All values are expressed as mean \pm SEM, with $n = 5$ in each group.

tissue, and its mRNA levels clearly increased 24 h after LPS administration (Figure 5).

DISCUSSION

In this study, we demonstrated that pretreatment of rats with an anti-MIF antibody clearly attenuated the accumulation of neutrophils in the lungs 4 and 24 h after the administration of LPS. The significant attenuation of neutrophil accumulation caused by the anti-MIF antibody in this experiment was proved by three independent methods: histological examination of neutrophils in and around the alveoli, MPO activity of lung tissues, and quantification of neutrophils in BAL fluids. We also showed that MIF was present in bronchial epithelial cells and alveolar macrophages in the lungs and that MIF mRNA from lung tissues was certainly increased 24 h after the administration of LPS, although we could find increased levels of MIF only in serum, not in BAL fluids, in the rats that had been given LPS. Furthermore, we demonstrated that an increase in the level of MIP-2/CINC-3, a powerful neutrophil chemokine, in BAL fluids observed in the rats of the LPS group was significantly suppressed by pretreatment with the anti-MIF antibody. All these data indicate that MIF is implicated in the pathogenesis of LPS-induced neutrophil accumulation in the lungs and that the anti-MIF antibody has therapeutic potential for the treatment of acute lung injury, at least in part, by suppressing the level of a neutrophil chemokine in the lungs.

MIF was first described in 1966 as a lymphokine or a cytokine activity derived from activated T lymphocytes that had the ability to prevent the random migration of macrophages (1, 2). Since then, expression of MIF or MIF-like activity has been found at a variety of inflamed loci. However, the precise role of MIF in the immunologic response remained undefined until human MIF cDNA was cloned in 1989 (3). In a series of recent experiments using mice by Bucala and colleagues, MIF has been rediscovered as a pro-inflammatory cytokine that has the potential to override the anti-inflammatory action of glucocorticoids (5, 6). In sepsis, the level of MIF in blood increases, and administration of recombinant MIF enhances lethality. Conversely, pre-injection of an anti-MIF antibody could fully protect mice from lethal endotoxemia (4). Although it

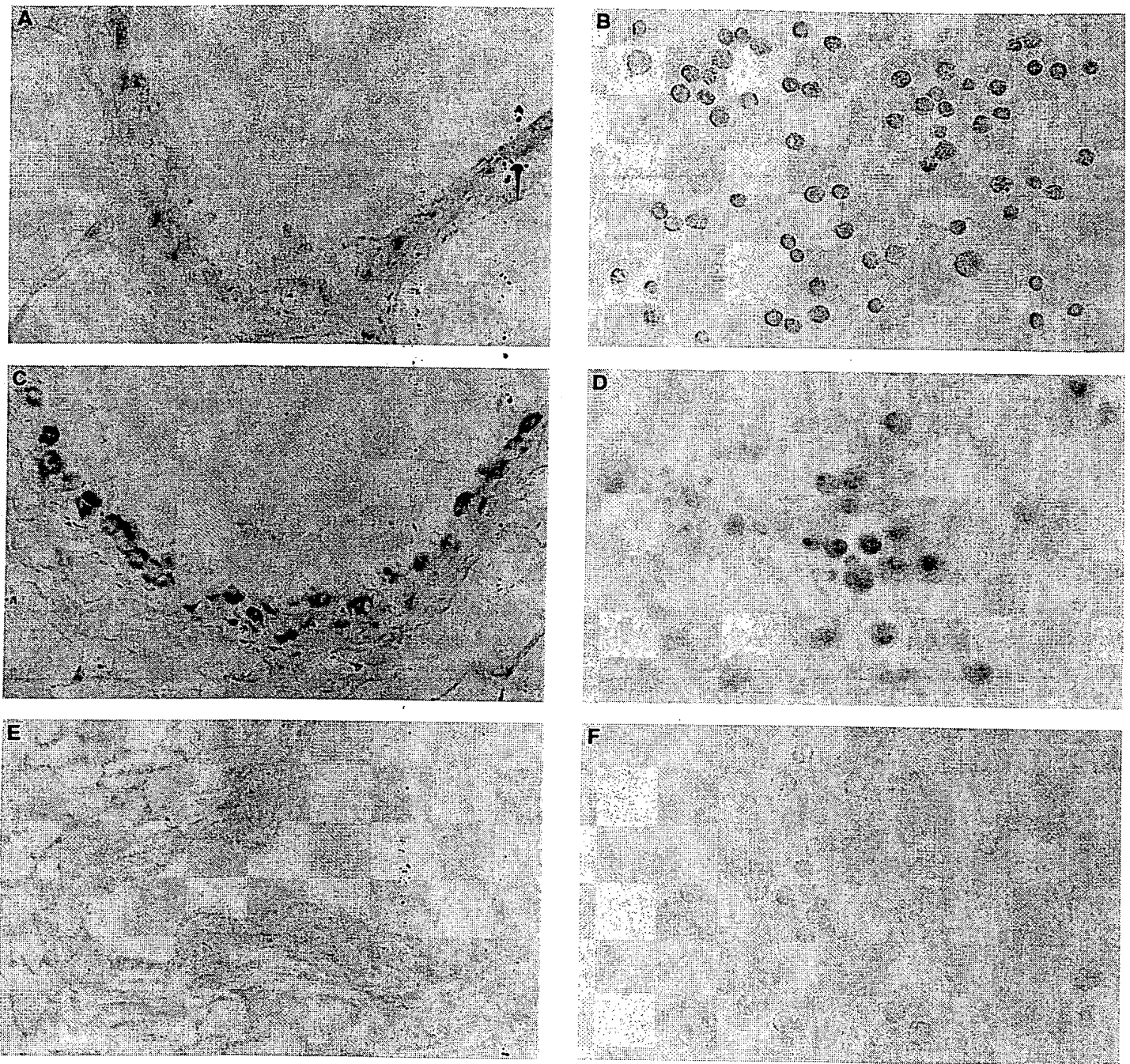


Figure 4. Immunostaining for MIF in the lungs of rats (original magnification: $\times 200$). Positive immunostaining for MIF was demonstrated even in the control rats within the bronchial epithelial cells (A) and alveolar macrophages (B). There was a moderate increase in immunostaining of bronchial epithelial cells (C) and alveolar macrophages (D) at 24 h after LPS injection. The tissue specimen reacted with pre-immune rabbit IgG as a negative control; bronchial epithelial cells (E), and alveolar macrophages (F).

has been reported that the major sources of MIF secretion are the pituitary glands and macrophages as well as T lymphocytes (4, 6, 17), it is now known that the MIF gene is expressed in a wide variety of cells, tissues, and organs, including the brain, spleen, liver, muscle, and kidney (7, 11). We previously reported for the first time the crystal structure of MIF (18), and provided evidence that MIF is also present in the differentiating cells of the cornea and the skin (8, 9).

There has been, to our knowledge, only one report examining the presence of MIF in the lungs in experimentally induced endotoxemia (11). In this study, positive immunostaining for MIF was observed in untreated animals within the bronchial epithelium and in alveolar macrophages. The level of MIF mRNA increased markedly 24 h after LPS administration. These findings on the localization of MIF in the lungs agree with those previously reported in animals as well as in

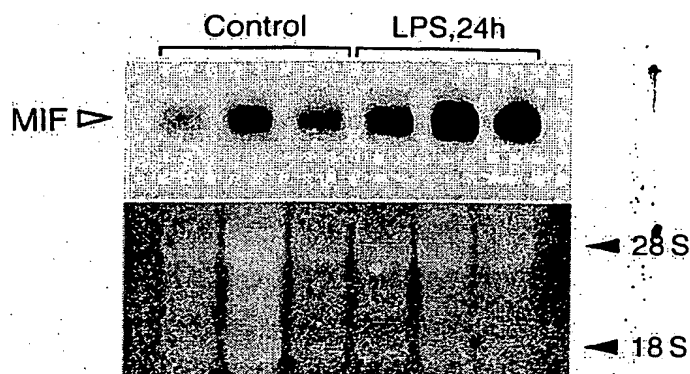


Figure 5. Northern blot analysis. Prominent expression of MIF was demonstrated in the lung tissues from control rats. Its mRNA level increased to 24 h after LPS administration.

humans (11, 12). In this study, however, we could not detect a significant increase in the immunologic level of MIF in BAL fluids in the rats that had been given LPS, although marked elevations in the serum level were seen 4 and 24 h after LPS administration. Failure to recognize increased levels of MIF in BAL fluids in those rats may have occurred because the lung injury caused by LPS was not severe enough in this experiment. The model of LPS-induced acute lung injury in rats resembles ARDS in patients, and intraperitoneal administration of LPS generally results in neutrophil recruitment in the lungs and increased vascular permeability (19, 20). It is not clear why the dose of LPS used in this study did not cause severe lung damage, leading to a significant increase in the W/D weight ratio in the LPS-treated rats. In this study, we gave 7 mg/kg LPS to each rat, which is not considered to be a small quantity.

The mechanism by which the anti-MIF antibody attenuated neutrophil accumulation in the lungs was thought to be, at least in part, due to its suppressive effect on a putative neutrophil chemokine, MIP-2/CINC-3. In this experiment, the level of MIP-2/CINC-3 in BAL fluids was significantly lower in the anti-MIF Ab group than in the LPS group 4 h after LPS administration. It was recently reported that MIP-2/CINC-3 plays a significant role in the LPS-induced inflammatory response in rat lungs and is required for the full recruitment of neutrophils (21, 22). The peak level of MIP-2/CINC-3 in BAL fluids was observed 4 h after intratracheal instillation of LPS in these studies. It remains to be elucidated whether this suppressive effect of the anti-MIF antibody on a neutrophil chemokine is a direct action of the antibody itself on MIF as a pro-inflammatory cytokine, or an indirect effect potentiating the action of endogenous glucocorticoids, which MIF is reported to counter-regulate.

Despite long-term intensive research efforts, the etiology of ARDS remains uncertain and no specific therapy has proven effective in either preventing or reversing the underlying injury (23). A number of trials using antibodies or inhibitors against various stages of the inflammatory process have been experimentally attempted. They included neutrophil elastase inhibitor (24), antibodies to E- and L-selectin (25), an antibody to IL-8 (26), and an antibody to endotoxin (27). However, none of them has demonstrated any significant improvement in clinical trials. As an endogenous inhibitor of glucocorticoid action, MIF may modulate the delicate balance between the proinflammatory cytokines, such as TNF- α and IL-8, and the anti-inflammatory effect of endogenous steroids in an early phase of ARDS. Since MIF is considered to be not

merely one more cytokine because of its potential for overriding the actions of endogenous steroids, the findings of this study may lead to new anti-inflammatory therapy for ARDS. Further studies will be required to determine the effect of the anti-MIF antibody on severe lung injuries and, moreover, its possible beneficial effect when the antibody is given after the initiation of lung injury.

Acknowledgment: The writers thank Dr. Shinji Sakaue for helpful discussions and his excellent technical assistance.

References

- Bloom, B. R., and B. Bennett. 1966. Mechanism of a reaction in vitro associated with delayed-type hypersensitivity. *Science* 153:80-82.
- David, J. R. 1966. Delayed hypersensitivity in vitro: its mediation by cell free substances formed by lymphoid cell-antigen interaction. *Proc. Natl. Acad. Sci. U.S.A.* 56:72-77.
- Weiser, W. Y., P. A. Temple, J. S. Witek-Giannotti, H. G. Remold, S. C. Clark, and J. R. David. 1989. Molecular cloning of a cDNA encoding a human macrophage migration inhibitory factor. *Proc. Natl. Acad. Sci. U.S.A.* 86:7522-7526.
- Bernhagen, J., T. Calandra, R. A. Mitchell, S. B. Martin, and R. Bucala. 1993. MIF is a pituitary-derived cytokine that potentiates lethal endotoxaemia. *Nature* 365:756-759.
- Bucala, R. 1996. MIF rediscovered: cytokine, pituitary hormone, and glucocorticoid-induced regulator of the immune response. *FASEB J.* 10:1607-1613.
- Calandra, T., J. Bernhagen, and R. Bucala. 1995. MIF as a glucocorticoid-induced modulator of cytokine production. *Nature* 377:68-71.
- Sakai, M., J. Nishihira, Y. Hibiy, Y. Koyama, and S. Nishi. 1994. Glutathione binding rat liver 13k protein is the homologue of the macrophage migration inhibitory factor. *Biochem. Mol. Int.* 33:439-446.
- Matsuda, A., Y. Tagawa, H. Matsuda, and J. Nishihira. 1996. Identification and immunohistochemical localization of macrophage migration inhibitory factor in human cornea. *FEBS Lett.* 385:225-228.
- Shimizu, T., A. Ohkawara, J. Nishihira, and W. Sakamoto. 1996. Identification of macrophage migration inhibitory factor (MIF) in human skin and its immunohistochemical localization. *FEBS Lett.* 381:199-202.
- Wistow, G. J., M. P. Shaughnessy, D. C. Lee, J. Hodin, and P. S. Zelenka. 1993. A macrophage migration inhibitory factor is expressed in the differentiating cells of the eye lens. *Proc. Natl. Acad. Sci. U.S.A.* 90:1272-1275.
- Bacher, M., A. Meinhardt, H. Y. Lan, W. Mu, C. N. Metz, J. A. Chesney, T. Calandra, D. Gerns, T. Donnelly, R. C. Atkins, and R. Bucala. 1997. Migration inhibitory factor expression in experimentally induced endotoxemia. *Am. J. Pathol.* 150:235-246.
- Donnelly, S. C., C. Haslett, P. T. Reid, I. S. Grant, W. A. H. Wallace, C. N. Metz, L. J. Bruce, and R. Bucala. 1997. Regulatory role for macrophage migration inhibitory factor in acute respiratory distress syndrome. *Nature Med.* 3:320-323.
- Nishihira, J., T. Kuriyama, H. Nishino, T. Ishibashi, M. Sakai, and S. Nishi. 1993. Purification and characterization of human macrophage migration inhibitory factor: evidence for specific binding to glutathione and formation of subunit structure. *Biochem. Mol. Biol. Int.* 31:841-850.
- Nishihira, J., T. Kuriyama, M. Sakai, S. Nishi, S. Ohki, and K. Hikichi. 1995. The structure and physicochemical properties of rat liver macrophage migration inhibitory factor. *Biochem. Biophys. Acta* 1247:159-162.
- Goldblum, S. E., K.-M. Wu, and M. Jay. 1985. Lung myeloperoxidase as a measure of pulmonary leukostasis in rabbit. *J. Appl. Physiol.* 59:1978-1985.
- Nakagawa, H., S. Shiota, K. Takano, F. Shibata, and H. Kato. 1996. Cytokine-induced neutrophil chemoattractant (CINC)-2, a novel member of rat GRO/CINC, is a predominant chemokine produced by lipopolysaccharide-stimulated rat macrophages in culture. *Biochem. Biophys. Res. Commun.* 220:945-948.
- Bacher, M., C. N. Metz, T. Calandra, K. Mayer, J. Chesney, M. Lohoff, D. Gerns, T. Donnelly, and R. Bucala. 1996. An essential regulatory role for macrophage migration inhibitory factor in T-cell activation. *Proc. Natl. Acad. Sci. U.S.A.* 93:7849-7854.
- Suzuki, M., H. Sugimoto, A. Nakagawa, I. Tanaka, J. Nishihira, and M. Sakai. 1996. Crystal structure of the macrophage migration inhibitory factor from rat liver. *Nature Struct. Biol.* 3:259-266.
- Hirano, S. 1996. Migratory responses of PMN after intraperitoneal and

- intratracheal administration of lipopolysaccharide. *Am. J. Physiol.* 270: L836-L845.
20. Strieter, R. M., and S. L. Kunkel. 1994. Acute lung injury: the role of cytokines in the elicitation of neutrophils. *J. Invest. Med.* 42:640-651.
 21. Schmal, H., T. P. Shanley, M. L. Jones, H. P. Friedl, and P. A. Ward. 1996. Role for macrophage inflammatory protein-2 in lipopolysaccharide-induced lung injury in rats. *J. Immunol.* 156:1963-1972.
 22. Shanley, T. P., H. Schmal, R. L. Warner, E. Schmid, H. P. Friedl, and P. A. Ward. 1997. Requirement for C-X-C chemokines (macrophage inflammatory protein-2 and cytokine-induced neutrophil chemoattractant) in IgG immune complex-induced lung injury. *J. Immunol.* 158:3439-3448.
 23. Pittet, J. F., R. C. Mackersie, T. R. Martin, and M. A. Matthay. 1997. Biological markers of acute lung injury: prognostic and pathogenic significance. *Am. J. Respir. Crit. Care Med.* 155:1187-1205.
 24. Sakamaki, F., A. Ishizaka, T. Urano, K. Sayama, H. Nakamura, T. Terasima, Y. Waki, S. Tasaka, N. Hasegawa, K. Sato, N. Nakagawa, T. Obata, and M. Kanazawa. 1996. Effect of a specific neutrophil elastase inhibitor, ONO-5046, on endotoxin-induced acute lung injury. *Am. J. Respir. Crit. Care Med.* 153:391-397.
 25. Ridings, P. C., G. L. Bloomfield, S. Holloway, A. C. J. Windsor, M. A. Jutila, A. A. Fowler, and H. J. Sugerman. 1995. Sepsis-induced acute lung injury is attenuated by selectin blockade following the onset of sepsis. *Arch. Surg.* 130:1199-1208.
 26. Sekido, N., N. Mukaida, A. Harada, I. Nakanishi, Y. Watanabe, and K. Matsushima. 1993. Prevention of lung reperfusion injury in rabbits by a monoclonal antibody against interleukin-8. *Nature* 365:654-657.
 27. Bone, R. C., R. A. Balk, A. M. Fein, T. M. Perl, R. P. Wenzel, H. D. Reines, R. W. Quenzer, T. J. Iberl, N. Macintyre, and R. M. H. Schein. 1995. A second large controlled clinical study of E5, a monoclonal antibody to endotoxin: results of a prospective, multicenter, randomized, controlled trial. *Crit. Care Med.* 23:994-1005.

(Circulation. 1996;94:2787-2792.)
© 1996 American Heart Association, Inc.

Articles

Mast Cells in Rupture-Prone Areas of Human Coronary Atheromas Produce and Store TNF- α

Maija Kaartinen, MD; Antti Penttilä, MD, PhD; Petri T. Kovanen, MD, PhD

the Wihuri Research Institute (M.K., P.T.K.) and the Department of Forensic Medicine, University of Helsinki (A.P.), Helsinki, Finland.

Correspondence to Petri T. Kovanen, MD, Wihuri Research Institute, Kallioliinantie 4, 00140 Helsinki, Finland.

▲ [Top](#)
• [Abstract](#)
▼ [Introduction](#)
▼ [Methods](#)
▼ [Results](#)
▼ [Discussion](#)
▼ [References](#)

► Abstract

Background Mast cells, a cell type involved in inflammatory reactions, are present in coronary atheromas and localize to the erosion or rupture site of atheromas in myocardial infarction. Here we report the presence of TNF- α , a proinflammatory cytokine, in mast cells of human coronary atheromas.

Methods and Results From samples of 37 coronary arteries from subjects autopsied for medicolegal reasons, sections of the bifurcation area of the left coronary artery were stained immunohistochemically for mast cells and TNF- α . In addition, macrophages, T

lymphocytes, smooth muscle cells, and endothelial cells were investigated for their content of TNF- α . In normal intimas and fatty streaks, none of the cell types studied were TNF- α -positive. In 14 of the 24 atheromas found, TNF- α -positive cells were present. Of the total number of mast cells, 23% stained for TNF- α ; of the macrophages, 1.3%; and of the smooth muscle cells, 0.4%. The majority (55%) of TNF- α -positive mast cells in the atheromas were located in the shoulder region and the remaining 35% in the cap and 10% in the core regions. Immunoelectron microscopy showed that the TNF- α in mast cells resided within their cytoplasmic secretory granules, demonstrating that these cells contain stores of TNF- α that will be released on degranulation.

Conclusions This study demonstrates the presence of mast cells with TNF- α -containing secretory granules, particularly in the shoulder region of human coronary atheromas. By releasing their TNF- α , mast cells may play an active role in the inflammatory reactions of these rupture-prone areas of atheromas.

Key Words: atherosclerosis • coronary disease • cells • cytokines

▲ [Top](#)
▲ [Abstract](#)
• [Introduction](#)
▼ [Methods](#)
▼ [Results](#)
▼ [Discussion](#)
▼ [References](#)

► Introduction

Activated mast cells are present in human coronary atheromas. They accumulate especially in the shoulder region of atheromas, the predilection sites of atheromatous rupture.¹ Indeed, infiltrates of activated mast cells are present at the sites of coronary atheromatous erosion or rupture in myocardial infarction.² It was recently shown that the sites of atheromatous rupture contain a strong inflammatory component.³ TNF- α , an important mediator of inflammatory reactions,^{4,5} has been found in several cell types (SMCs, macrophages, and endothelial cells) present in human atheromas,^{6,7} and this cytokine is also found in skin mast cells⁸ and in lung mast cells.^{9,10} Indeed, mast cells have been found to be unique in that they both synthesize and store TNF- α ,¹¹ and they often participate in inflammatory reactions.¹² For these reasons, we searched for evidence of the presence of TNF- α in the mast cells in human coronary atheromas.

▲ Top
▲ Abstract
▲ Introduction
• Methods
▼ Results
▼ Discussion
▼ References

► Methods

Autopsy Material and Tissue Preparation

The autopsy series comprised 37 subjects, their ages ranging from 13 to 73 years. The causes of death were cardiovascular disease (n=12) and violent deaths (n=19), ie, accidents, homicides, suicides, and poisonings (n=6). From each cadaver, the unopened left coronary artery was removed from the heart, and three successive tubelike specimens were cut from the bifurcation area of the artery. For light microscopy, the specimens were fixed in Carnoy's fluid (60% ethanol, 30% chloroform, and 10% glacial acetic acid) for 24 hours and embedded in paraffin. The mean interval between death and the start of fixation was 13 hours (range, 2 to 24 hours). Light microscopy was used to evaluate the atherosclerotic involvement of the coronary arteries. For this purpose, the sections (2 to 4 μ m) were stained with hematoxylin-eosin or elastica-van Gieson's stain (Weigert's hematoxylin, metanil yellow, acid fuchsin, and picric acid). The normal intima demonstrated variable thickness and moderate overall cellularity. Fatty streaks were recognizable as subendothelial and/or deep intimal collections of foam cells (containing numerous vacuoles). Atheromas appeared as intimal areas in which, in addition to foam cells, there were accumulations of extracellular lipid (large nonstaining areas interspersed with typical cholesterol clefts). These areas contained very few cells or were acellular, a sign of cell loss (necrotic lipid core), and covered by fibrotic tissue of various thicknesses (cap). Using these criteria, we found areas in which the intima appeared normal in all 37 subjects; 30 subjects also had fatty streaks, and 24 subjects, in addition to fatty streaks, had atheromas. In the atheroma, the various cell types to be studied were counted separately in the cap, core, and shoulder regions. Fig 1A* shows a light microscopic view of a segment of a ring from the bifurcation area of the left coronary artery displaying an atheroma. Also shown are the various regions of the atheroma (cap, core, and shoulder) (Fig 1B*). For immunoelectron microscopy, specimens were fixed for 3 hours in 3% paraformaldehyde, dehydrated, and embedded in LR white resin. Sections (1 μ m) of these specimens were stained with toluidine blue and observed with light microscopy for orientation of the site and for evaluation of the atherosclerotic involvement of each specimen.

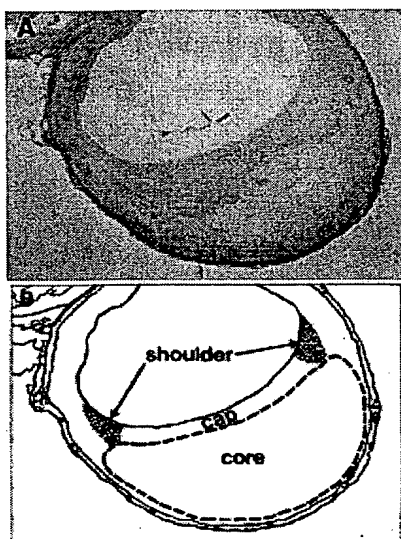


Figure 1. A, Light microscopic view of a ring from the bifurcation area of the left coronary artery displaying an atheroma in which there are foam cells, extracellular lipid, and an acellular area covered with a fibrous cap. The section was stained with elastica-van Gieson's stain. The specimen was from a 51-year-old man who died of an accident. Magnification x20. B, Schematic showing the various regions of the atheroma: shoulder, cap, and core.

[View larger version \(165K\):](#)

[\[in this window\]](#)

[\[in a new window\]](#)

Immunocytochemistry

For immunocytochemistry, fixed serial sections (2 to 4 μm) were dewaxed in xylene and rehydrated in a graded series of ethanol solutions, and endogenous peroxide activity was inhibited by incubation in 0.6% H_2O_2 in methanol. The sections were then incubated with one of the following: anti-tryptase monoclonal antibodies G3 (1.5 $\mu\text{g}/\text{mL}$) and B7 (4 $\mu\text{g}/\text{mL}$) (kind gifts from Dr L.B. Schwartz, Medical College of Virginia, Richmond) for mast cells¹³; HAM 56, a monoclonal antibody for macrophages (1:50); UCHL 1, a monoclonal antibody for T lymphocytes (1:50); and a polyclonal antibody for von Willebrand factor for endothelial cells (1:2000) (all from Dakopatts); a monoclonal antibody for α -smooth muscle actin for SMCs (1:12 000) (from Sigma Chemical Co); and a monoclonal antibody for $\text{TNF-}\alpha$ (1 $\mu\text{g}/\text{mL}$) (from Boehringer Mannheim). Mast cells and SMCs were stained according to the indirect immunoperoxidase method, and T lymphocytes, macrophages, and endothelial cells were stained by the avidin-biotin complex method, as recently described.^{1,2} $\text{TNF-}\alpha$ was stained by a modified avidin-biotin complex method to enhance the reaction, as follows: the sections were first incubated with normal horse serum for 10 minutes and with anti- $\text{TNF-}\alpha$ for 75 minutes, then with bridge antibody for 10 minutes, with avidin-biotin complex for 10 minutes, and again with bridge antibody for 10 minutes and with avidin-biotin complex for 10 minutes. The sections were then incubated overnight with anti- $\text{TNF-}\alpha$, 10 minutes with the bridge antibody, 10 minutes with avidin-biotin complex, and 15 minutes in diaminobenzidine-peroxidase substrate solution. Finally, the samples were incubated with avidin-biotin complex for 10 minutes, stained again with diaminobenzidine-peroxidase substrate, and counterstained with Mayer's hematoxylin. All staining steps were carried out in a humidified chamber at 37°C except the overnight $\text{TNF-}\alpha$ incubation, which was carried out at room temperature. Indirect evidence that the antibody against $\text{TNF-}\alpha$ was

recognizing this cytokine (positive controls) was obtained by staining one skin specimen and two colon cancer specimens.⁶ As expected, HAM 56-positive cells (macrophages) stained positively for TNF- α . Similarly, in skin, several tryptase-positive cells stained positively for TNF- α . Moreover, some basal keratinocytes stained positively, as also previously demonstrated by Walsh et al.⁸ As negative controls, we used sections from one brain⁶ stained for TNF- α as described above and coronary sections in which the primary antibody was omitted or replaced with normal serum (irrelevant antibody). In these sections, no positive staining was observed. Immunopositive mast cells, T lymphocytes, macrophages, SMCs, and endothelial cells were counted at x100 magnification. Magnification x1000 was used to observe degranulation of mast cells.

Immunoelectron Microscopy

The ultramicrotome sections of LR white resin-embedded samples on nickel grids were incubated at room temperature with buffer (PBS containing 3% BSA) for 10 minutes and then overnight with anti-TNF- α (10 μ g/mL). After two rinses in the buffer, the sections were incubated for 2 hours in 10 nm gold-labeled anti-mouse IgG+IgM (1:25) (Amersham) and finally stained with uranyl acetate and lead citrate. As negative controls, we used coronary sections in which the primary antibody was omitted or replaced with normal serum (irrelevant antibody). In these sections, no TNF- α staining was observed. The ultramicrotome sections were viewed with a Jeol JEM-1200EX transmission electron microscope at the Department of Electron Microscopy, University of Helsinki.

Statistical Analysis

The proportion of TNF- α -positive cells was analyzed by logistic regression with a cell type (mast cells, macrophages, or SMCs) and a region of an atheroma (shoulder, cap, or core) used as explanatory variables. Endothelial cells and T lymphocytes were excluded from the analysis, because no TNF- α positivity was found in these cells. Differences were considered statistically significant when $P < .05$.

▲ [Top](#)
▲ [Abstract](#)
▲ [Introduction](#)
▲ [Methods](#)
• [Results](#)
▼ [Discussion](#)
▼ [References](#)

Results

To demonstrate the presence of mast cells containing TNF- α in coronary atheromas, serial sections of atheromatous coronary specimens from the bifurcation areas of left coronary arteries were stained with monoclonal antibody against mast cell tryptase and against

TNF- α . Fig 2A* shows a typical example of mast cells in the shoulder region of a coronary atheroma; the five tryptase-containing mast cells are stained red-brown. When the same area was stained with anti-TNF- α antibody, four cells stained positively (Fig 2B*, brown). Comparison of the two adjacent sections revealed that, of the four TNF- α -positive cells, in this particular field, three were mast cells.

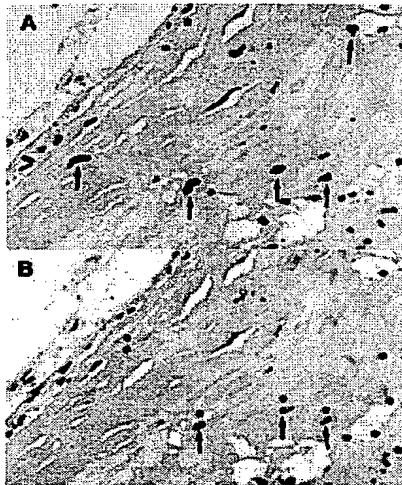


Figure 2. Photomicrographs showing that the mast cells in human coronary atheroma contain TNF- α . A, Five mast cells in the shoulder region of a coronary atheroma staining red-brown (arrows). The section was stained immunohistochemically for tryptase. B, Same area (adjacent section) as in A was stained for TNF- α . Four cells stained positively for TNF- α (brown; asterisks). Comparison of the two panels shows that in B, of the four TNF- α -positive cells (asterisks), three were mast cells (arrows). Specimen was from a 67-year-old man who died of myocardial infarction. Magnification x200 in A and B.

View larger version (290K):

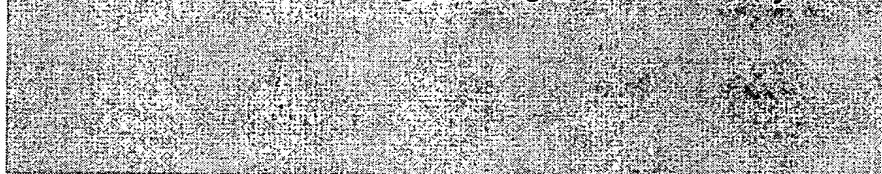
[\[in this window\]](#)

[\[in a new window\]](#)

We also stained the serial sections with antibodies against macrophages, T lymphocytes, SMCs, and endothelial cells. The frequency of TNF- α positivity in normal and atherosclerotic lesions as a function of histological classification is shown in Table 1*. All 37 subjects studied had normal intima, 30 had fatty streaks, and 24 had not only fatty streaks but also atheromas. The total number of mast cells counted in the normal intimas was 106; in the fatty streaks, 350; and in the atheromas, 542. In the areas classified as normal or as fatty streaks, there were no detectable TNF- α -positive cells. In 14 of 24 atheromas, TNF- α -positive cells were visible. TNF- α -positive staining was found in three cell types: mast cells (in 8 atheromas), macrophages (in 8 atheromas), and SMCs (in 7 atheromas). In these samples, T lymphocytes and endothelial cells did not stain for TNF- α . In 4 of 14 atheromas, TNF- α -positive mast cells, macrophages, and SMCs were found. In the remaining 10 of 14 atheromas, only one or two of the above cell types were TNF- α positive (see Table 1*).

**View this
table:
[\[in this
window\]](#)
[\[in a new
window\]](#)**

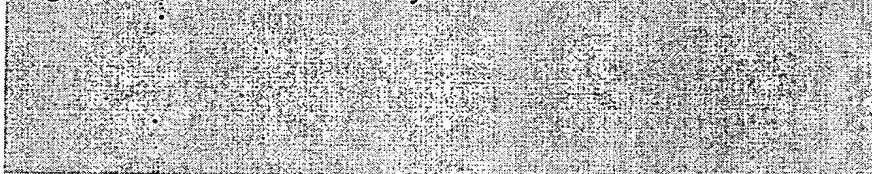
Table 1. Distribution of TNF- α Positivity in Five Different Cell Types as a Function of Histological Categories of a Coronary Intima



We next made a separate study of the three regions of atheromas: shoulder, cap, and core (Table 2+). Of the total number ($n=542$) of mast cells found, 23% ($n=124$) stained for TNF- α , whereas only 1.3% of the macrophages and 0.4% of the SMCs stained for TNF- α . The frequencies of TNF- α -positive mast cells in the various regions of the atheromas were as follows: 31% (68/219) in the shoulder, 26% (43/165) in the cap, and 8% (13/158) in the core region. It appeared that most (55%; 68/124) of the TNF- α -positive mast cells were located in the shoulder region, 35% (43/124) in the cap region, and the remaining 10% (13/124) in the core region. In contrast to the mast cells, the TNF- α -positive macrophages and SMCs were evenly distributed among the three regions of the atheromas.

**View this
table:
[\[in this
window\]](#)
[\[in a new
window\]](#)**

Table 2. Frequency of TNF- α Positive Cells in the Various Regions of the Human Coronary Atheromas



To search for evidence of TNF- α storage in mast cell granules, we turned to immunoelectron microscopy. Ultramicrotome sections obtained from coronary atheromas were stained with anti-TNF- α , and 10-nm gold IgG+IgM were used as secondary antibodies. Fig 3+ shows a typical mast cell in the shoulder region of a coronary atheroma staining positively for TNF- α . TNF- α (gold particles) can be clearly seen within the cytoplasmic secretory granules of mast cells. Furthermore, in agreement with the light-microscopic results, we failed to observe TNF- α positivity in any cells in normal intima or in fatty streaks when examined by immunoelectron microscopic techniques.

The present study shows that mast cells in human coronary atheromas contain TNF- α . As in earlier studies, we also found mast cells in normal intima and in fatty streaks.^{1,2} However, in contrast to the mast cells in atheromas, the mast cells in normal intima and in fatty streaks did not contain detectable amounts of TNF- α . Thus, as the atherosclerotic process advances (fatty streak→atheroma), the phenotype of a fraction of the intimal mast cells changes into an inflammatory one, as reflected by their TNF- α positivity. This finding is in accord with the observation that other intimal cell types, such as macrophages and SMCs, also began to express TNF- α as the atherosclerotic process advanced, an observation made by Barath et al.^{6,7} Similar disease-related upregulation of TNF- α has been observed in lung mast cells in patients suffering from atopic asthma.²

▲ Top
▲ Abstract
▲ Introduction
▲ Methods
▲ Results
• Discussion
▼ References

In the atheromatous lesions, the mast cells were shown to store TNF- α in their cytoplasmic secretory granules. Earlier studies with mouse peritoneal mast cells and with human dermal and lung mast cells have demonstrated that mast cells are capable of synthesizing TNF- α for storage in their granules.^{8,9,10} Thus, in all these experimental systems, IgE-dependent mast cell stimulation with ensuing degranulation resulted in significant increases in mRNA for TNF- α in the degranulated cells. What factors might have triggered the generation of TNF- α stores in mast cells in the atheromas? In other cell types, both IFN- γ and TNF- α have been documented to stimulate TNF- α synthesis.^{4,14} Recent findings that human coronary and aortic atheromas contain greatly increased (10- to 20-fold) numbers of T lymphocytes,^{1,2} a known source of IFN- γ ,^{15,16} and macrophages,^{1,2} a known source of TNF- α ,¹⁵ point to these two cell types as potential stimulators of TNF- α production in mast cells. In addition, the intimal SMCs, also a source of TNF- α ,^{6,7} could stimulate the mast cells to synthesize TNF- α . Although the percentages of TNF- α -positive macrophages and SMCs were lower than that of mast cells, the absolute numbers of these cells were higher, making them potentially important sources of TNF- α . Because vascular lesions can exhibit enhanced expression of TNF- α ,⁶ cytokine regulation of TNF- α synthesis and storage by mast cells in the atheromatous lesions may bear in vivo relevance.

The observation that TNF- α is localized to the cytoplasmic granules in mast cells demonstrates that these cells are able to store TNF- α and suggests that, once the mast cells have been stimulated to degranulate, TNF- α can be released rapidly in sizable amounts. Indeed, we recently found that the majority of the mast cells in the eroded or ruptured shoulder and cap regions have extracellular granules in their vicinity, a sign of their degranulation.² In the present study also, signs of mast cell degranulation were found in the atheromas. What factors might trigger mast cells to degranulate? The best-understood immunological stimulus leading to degranulation of human mast cells is their activation on binding of a relevant antigen (allergen) to the IgE molecules present on the mast cells.¹⁷ A second, and perhaps even more likely, pathway leading to mast cell degranulation is their stimulation by other immunologically activated cells, such as T lymphocytes¹⁸ and macrophages,¹⁹ two cell types also present in the shoulder and cap regions of coronary atheromas.² Moreover, atheromatous plaques activate complement

and produce C5a,²⁰ a powerful activator of mast cells.²¹ Admittedly, we cannot exclude the possibility that some coronary mast cells degranulate after death.

The mast cell-derived TNF- α may have several proinflammatory actions in coronary atheromas. It is known that TNF- α upregulates the leukocyte-endothelial adhesion molecules vascular cell adhesion molecule-1 and intercellular adhesion molecule-1.²² Interestingly, stimulation of human dermal mast cells results in release of TNF- α , which induces expression of endothelial-leukocyte adhesion molecule-1 on dermal endothelium.⁸ Therefore, the observation that TNF- α is expressed in the subendothelial mast cells of atheromas (ie, in the shoulder and cap regions) suggests that the mast cells are involved in recruitment of macrophages and T lymphocytes into the lesions. Moreover, TNF- α may enhance the growth of T lymphocytes⁴ and, by this means, may also contribute to the strongly increased (10-fold) number of T lymphocytes in atheromas compared with normal coronary intima.^{1,2} TNF- α is also known to enhance the number of IL-2 receptors on T lymphocytes and to induce production of IL-1, PGE₂, and hydrogen peroxide in macrophages.⁴ Thus, one important function of the TNF- α -containing mast cells of atheromas could be amplification of the immune response in these lesions.

Finally, an important concept is emerging that increased activity of enzymes required for extracellular matrix digestion (MMPs) are causing coronary atheromas to rupture.^{23, 24, 25} The MMPs are synthesized and secreted by SMCs and macrophages of the atherosclerotic lesions.^{23, 24, 25} In vitro studies have shown that both TNF- α and IL-1 stimulate SMCs to synthesize de novo 92-kD gelatinase, interstitial collagenase, and stromelysin, the three major MMPs found in atherosclerotic lesions.²⁶ Moreover, we have observed that TNF- α stimulates production of 92-kD gelatinase by human monocytes-macrophages in vitro.²⁷ Thus, activation of TNF- α -containing mast cells in human coronary atheromas, with ensuing degranulation and TNF- α release, could locally weaken the atheroma and lead to atheromatous erosion or rupture.²

In conclusion, the present study reveals that a fraction of the mast cells in human coronary atheromas contain a potent proinflammatory cytokine, TNF- α . This observation strengthens the notion that mast cells play a role in the initiation and maintenance of the inflammatory process found in advanced human coronary atheromas.

Limitations of the Study

In this autopsy study, in which TNF- α -positive mast cells in human coronary atheromas are described for the first time, the specimens were examined 2 to 24 hours after death. These conditions are suboptimal for detection of cytokine-positive cells by immunohistochemistry. Accordingly, the number of atheromas with TNF- α -positive cells is likely to represent an underestimate of the actual proportion of the atheromas in which cells were TNF- α -positive. Despite these problems, comparison between normal intima, fatty streaks, and atheromas was of interest, since it revealed that TNF- α -positive cells are found only in the most advanced lesions, which contain a strong inflammatory component and are prone to rupture.

► Selected Abbreviations and Acronyms

IFN	=	interferon
IL	=	interleukin
MMP	=	matrix metalloproteinase
PG	=	prostaglandin
SMC	=	smooth muscle cell
TNF	=	tumor necrosis factor

► Acknowledgments

This study was supported in part by the Aarne Koskelo Foundation. The authors thank the staff of the Department of Forensic Medicine and Electron Microscopy, University of Helsinki, for their excellent technical assistance, and Jari Haukka for advice in statistical analysis of the data.

Received May 6, 1996; revision received June 27, 1996; accepted July 1, 1996.

▲ [Top](#)
▲ [Abstract](#)
▲ [Introduction](#)
▲ [Methods](#)
▲ [Results](#)
▲ [Discussion](#)
• [References](#)

► References


1. Kaartinen M, Penttilä A, Kovanen PT. Accumulation of activated mast cells in the shoulder region of human coronary atheroma, the predilection site of atheromatous rupture. *Circulation*. 1994;90:1669-1678.[\[Abstract\]](#)
2. Kovanen PT, Kaartinen M, Paavonen T. Infiltrates of activated mast cells at the site of coronary atheromatous erosion or rupture in myocardial infarction. *Circulation*. 1995;92:1084-1088.[\[Abstract/Free Full Text\]](#)
3. van der Wal AC, Becker AE, van der Loos CM, Das PK. Site of intimal rupture or erosion of thrombosed coronary atherosclerotic plaques is characterized by an inflammatory process irrespective of the dominant plaque morphology. *Circulation*. 1994;89:36-44.[\[Abstract\]](#)
4. Wong GHW, Goeddel DV. Tumor necrosis factor. In: Zembala M, Asherson GL, eds. *Human Monocytes*. San Diego, Calif: Academic Press; 1989:195-215.
5. Tracey KJ, Cerami A. Tumor necrosis factor, other cytokines and disease. *Annu Rev Cell Biol*. 1993;9:317-343.
6. Barath P, Fishbein MC, Cao J, Berenson J, Helfant RH, Forrester JS. Detection and localization of tumor necrosis factor in human atheroma. *Am J Cardiol*. 1990;65:297-302.[\[Medline\]](#) [\[Order article via Infotrieve\]](#)
7. Barath P, Fishbein MC, Cao J, Berenson J, Helfant RH, Forrester JS. Tumor necrosis factor gene expression in human vascular intimal smooth muscle cells detected by in situ hybridization. *Am J Pathol*. 1990;137:503-509.[\[Abstract\]](#)
8. Walsh LJ, Trichieri G, Waldorf HA, Whitaker D, Murphy GF. Human dermal mast cells contain and release tumor necrosis factor α , which induces endothelial leukocyte adhesion molecule 1. *Proc Natl Acad Sci U S A*. 1991;88:4220-4224.[\[Abstract/Free Full Text\]](#)
9. Bradding P, Roberts JA, Britten KM, Montefort S, Djukanovic R, Mueller R, Heusser CH, Hoehar PH, Holgate ST. Interleukin-4, -5, and -6 and tumor necrosis factor- α in normal and asthmatic airways: evidence for the human mast cell as a source of these cytokines. *Am J Respir Cell Mol Biol*. 1994;10:471-480.[\[Abstract\]](#)

10. Ohkavara Y, Yamauchi K, Tanno Y, Tamura G, Ohtari H, Nugura H, Ohkuda K, Takishima T. Human lung mast cells and pulmonary macrophages produce tumor necrosis factor- α in sensitized lung tissue after IgE receptor triggering. *Am J Respir Cell Mol Biol.* 1992;7:385-392.[[Medline](#)] [[Order article via Infotrieve](#)]
11. Gordon JR, Galli SJ. Mast cells as a source of both preformed and immunologically inducible TNF- α /cachectin. *Nature.* 1990;346:274-276.[[Medline](#)] [[Order article via Infotrieve](#)]
12. Galli SJ. New concepts about the mast cell. *N Engl J Med.* 1993;328:257-265.[[Free Full Text](#)]
13. Irani A-M, Bradford TR, Kepley CL, Schechter NM, Schwartz LB. Detection of MC_T and MC_{TC} types of human mast cells by immunohistochemistry using new monoclonal anti-tryptase and anti-chymase antibodies. *J Histochem Cytochem.* 1989;37:1509-1515.[[Abstract](#)]
14. Kunkel SL, Remick DG, Strieter RM, Larrick JW. Mechanisms that regulate the production and effects of tumor necrosis factor- α . *Crit Rev Immunol.* 1989;9:93-117.[[Medline](#)] [[Order article via Infotrieve](#)]
15. Libby P, Hansson GK. Involvement of the human immune system in human atherogenesis: current knowledge and unanswered questions. *Lab Invest.* 1991;64:5-15.[[Medline](#)] [[Order article via Infotrieve](#)]
16. Stemme S, Hansson GK. Immune mechanisms in atherosclerosis. *Coron Artery Dis.* 1994;5:216-222.[[Medline](#)] [[Order article via Infotrieve](#)]
17. Ishizaka T, Ishizaka K. Activation of mast cells for mediator release through IgE receptors. *Prog Allergy.* 1984;34:188-235.[[Medline](#)] [[Order article via Infotrieve](#)]
18. Sedgwick JD, Holt PG, Turner KJ. Production of a histamine-releasing lymphokine by antigen- or mitogen-stimulated human peripheral T cells. *Clin Exp Immunol.* 1981;45:409-418.[[Medline](#)] [[Order article via Infotrieve](#)]
19. Liu MC, Proud D, Lichtenstein LM, MacGlashan DW, Schleimer RP, Adkinson NF, Kagey-Sobotka A, Schulman ES, Plaut M. Human lung macrophage-derived

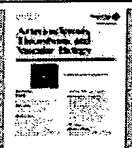
histamine-releasing activity is due to IgE-dependent factors. *J Immunol.* 1986;136:2588-2595.[\[Abstract/Free Full Text\]](#)

20. Rus HG, Niculescu F, Constantinescu E, Cristea A, Vlaicu R. Immunoelectron-microscopic localization of the terminal C5b-9 complement complex in human atherosclerotic fibrous plaque. *Atherosclerosis.* 1986;61:35-42.[\[Medline\]](#) [\[Order article via Infotrieve\]](#)
21. Metcalfe DD, Kaliner M, Donlon DA. The mast cell. In: *CRC Critical Reviews in Immunology.* Boca Raton, Fla.:CRC Press; 1981:23-74.
22. Collins T. Endothelial nuclear factor- κ B and the initiation of the atherosclerotic lesion. *Lab Invest.* 1993;68:499-508.[\[Medline\]](#) [\[Order article via Infotrieve\]](#)
23. Henney AM, Wakeley PR, Davies MJ, Foster K, Hembry R, Murphy G, Humphries S. Localization of stromelysin gene expression in atherosclerotic plaques by in situ hybridization. *Proc Natl Acad Sci U S A.* 1991;88:8154-8158.[\[Abstract/Free Full Text\]](#)
24. Galis ZS, Sukhova GK, Lark MW, Libby P. Increased expression of matrix metalloproteinases and matrix degrading activity in vulnerable regions of human atherosclerotic plaques. *J Clin Invest.* 1994;94:2493-2503.[\[Medline\]](#) [\[Order article via Infotrieve\]](#)
25. Brown DL, Hibbs MS, Kearney M, Loushin C, Isner JM. Identification of 92-kD gelatinase in human coronary atherosclerotic lesions: association of active enzyme synthesis with unstable angina. *Circulation.* 1995;91:2125-2131.[\[Abstract/Free Full Text\]](#)
26. Galis ZS, Muszynski M, Sukhova GK, Simon-Morrissey E, Unemori EN, Lark MW, Amento E, Libby P. Cytokine-stimulated human vascular smooth muscle cells synthesize a complement of enzymes required for extracellular matrix digestion. *Circ Res.* 1994;75:181-189.[\[Abstract\]](#)
27. Saren P, Welgus HG, Kovanen PT. Tumor necrosis factor- α and interleukin-1 β selectively induce expression of 92-kDa gelatinase by human macrophages. *J Immunol.* 1996;157:4159-4165.[\[Abstract\]](#)

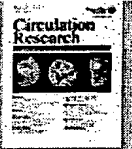
This article has been cited by other articles: ([Search Google Scholar for Other Citing Articles](#))



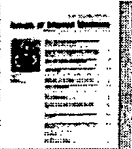
JOURNAL OF LIPID RESEARCH [HOME](#)
P. A. Vanderlaan and C. A. Reardon
**Thematic review series: The Immune System and Atherogenesis.
The unusual suspects: an overview of the minor leukocyte
populations in atherosclerosis**
J Lipid Res, May 1, 2005; 46(5): 829 - 838.
[\[Abstract\]](#) [\[Full Text\]](#) [\[PDF\]](#)




Arteriosclerosis, Thrombosis, and Vascular Biology [HOME](#)
K. A. Lindstedt, M. J. Leskinen, and P. T. Kovanen
**Proteolysis of the Pericellular Matrix: A Novel Element
Determining Cell Survival and Death in the Pathogenesis of
Plaque Erosion and Rupture**
Arterioscler. Thromb. Vasc. Biol., August 1, 2004; 24(8): 1350 - 1358.
[\[Abstract\]](#) [\[Full Text\]](#) [\[PDF\]](#)



Circulation Research [HOME](#)
R. Kishore, C. Luedemann, E. Bord, D. Goukassian, and D. W. Losordo
**Tumor Necrosis Factor-Mediated E2F1 Suppression in Endothelial
Cells: Differential Requirement of c-Jun N-Terminal Kinase and
p38 Mitogen-Activated Protein Kinase Signal Transduction
Pathways**
Circ. Res., November 14, 2003; 93(10): 932 - 940.
[\[Abstract\]](#) [\[Full Text\]](#) [\[PDF\]](#)



Annals of Internal Medicine [HOME](#)
G. Krishnaswamy, D. S. Chl, and J. Kelley
Vulnerable Plaque
Ann Intern Med, September 7, 1999; 131(5): 392 - 393.
[\[Full Text\]](#) [\[PDF\]](#)



Annals of Internal Medicine [HOME](#)
J. S. Forrester
Prevention of Plaque Rupture: A New Paradigm of Therapy
Ann Intern Med, November 19, 2002; 137(10): 823 - 833.
[\[Abstract\]](#) [\[Full Text\]](#) [\[PDF\]](#)



ENDOCRINE REVIEWS

[HOME](#)

J. M. Fernández-Real and W. Ricart

Insulin Resistance and Chronic Cardiovascular Inflammatory Syndrome

Endocr. Rev., June 1, 2003; 24(3): 278 - 301

[\[Abstract\]](#) [\[Full Text\]](#) [\[PDF\]](#)



PHARMACOLOGICAL REVIEWS

[HOME](#)

J. H. Von der Thüsen, J. Kuiper, T. J. C. Van Berkel, and E. A. L. Biessen

Interleukins in Atherosclerosis: Molecular Pathways and Therapeutic Potential

Pharmacol. Rev., March 1, 2003; 55(1): 133 - 166

[\[Abstract\]](#) [\[Full Text\]](#) [\[PDF\]](#)



ARCHIVES OF INTERNAL MEDICINE

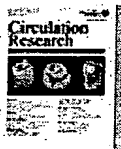
[HOME](#)

P. T. Kovanen, M. Manttari, T. Palosuo, V. Manninen, and K. Aho

Prediction of Myocardial Infarction in Dyslipidemic Men by Elevated Levels of Immunoglobulin Classes A, E, and G, but Not M

Archives of Internal Medicine, July 13, 1998; 158(13): 1434 - 1439

[\[Abstract\]](#) [\[Full Text\]](#)



Circulation Research

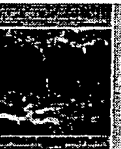
[HOME](#)

R. Kishore, I. Spyridopoulos, C. Luedemann, and D. W. Losordo

Functionally Novel Tumor Necrosis Factor- α -Modulated CHR-Binding Protein Mediates Cyclin A Transcriptional Repression in Vascular Endothelial Cells

Circ. Res., August 23, 2002; 91(4): 307 - 314

[\[Abstract\]](#) [\[Full Text\]](#) [\[PDF\]](#)



Am. J. Physiol.: Heart and Circulatory Physiology

[HOME](#)

G. L. Brower, A. L. Chancey, S. Thanigaraj, B. B. Matsubara, and J. S. Janicki

Cause and effect relationship between myocardial mast cell number and matrix metalloproteinase activity

Am J Physiol Heart Circ Physiol, August 1, 2002; 283(2): H518 - 525

[\[Abstract\]](#) [\[Full Text\]](#) [\[PDF\]](#)



JBC Online

[HOME](#)

S. A. Schreyer, C. M. Vick, and R. C. LeBoeuf

Loss of Lymphotoxin- α but Not Tumor Necrosis Factor- α Reduces Atherosclerosis in Mice

J. Biol. Chem., April 5, 2002; 277(14): 12364 - 12368

[\[Abstract\]](#) [\[Full Text\]](#) [\[PDF\]](#)



Arteriosclerosis, Thrombosis, and Vascular Biology

HOME

V. L. King, S. J. Szilvassy, and A. Daugherty

Interleukin-4 Deficiency Decreases Atherosclerotic Lesion Formation in a Site-Specific Manner in Female LDL Receptor-/- Mice

Arterioscler. Thromb. Vasc. Biol., March 1, 2002; 22(3): 456 - 461

[Abstract] [Full Text] [PDF]



Arteriosclerosis, Thrombosis, and Vascular Biology

HOME

K. P. Metsarinne, P. Vehmaan-Kreula, P. T. Kovanen, O. Salonen, M. Baumann, Y. Wang, T. Nyman, F. Y. Fyhrquist, and K. K. Eklund

Activated Mast Cells Increase the Level of Endothelin-1 mRNA in Cocultured Endothelial Cells and Degrade the Secreted Peptide

Arterioscler. Thromb. Vasc. Biol., February 1, 2002; 22(2): 268 - 273

[Abstract] [Full Text] [PDF]



Stroke

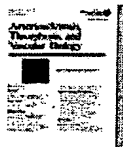
HOME

M. S. Elkind, J. Cheng, B. Boden-Albala, T. Rundek, J. Thomas, H. Chen, L. E. Rabbani, R. L. Sacco, and A. G. Thrift

Tumor Necrosis Factor Receptor Levels Are Associated With Carotid Atherosclerosis * Editorial Comment

Stroke, January 1, 2002; 33(1): 31 - 38

[Abstract] [Full Text] [PDF]



Arteriosclerosis, Thrombosis, and Vascular Biology

HOME

W.-H. Lee, S.-H. Kim, Y. Lee, B. B. Lee, B. Kwon, H. Song, B. S. Kwon, and J.-E. Park

Tumor Necrosis Factor Receptor Superfamily 14 Is Involved in Atherogenesis by Inducing Proinflammatory Cytokines and Matrix Metalloproteinases

Arterioscler. Thromb. Vasc. Biol., December 1, 2001; 21(12): 2004 - 2010

[Abstract] [Full Text] [PDF]



Arteriosclerosis, Thrombosis, and Vascular Biology

HOME

M. Leskinen, Y. Wang, D. Leszczynski, K. A. Lindstedt, and P. T. Kovanen

Mast Cell Chymase Induces Apoptosis of Vascular Smooth Muscle Cells

Arterioscler. Thromb. Vasc. Biol., April 1, 2001; 21(4): 516 - 522

[Abstract] [Full Text] [PDF]



Journal of the American College of Cardiology

[HOME](#)

M. Kaartinen, A. C. van der Wal, G. M. van der Loos, J. J. Piek, K. T. Koch, A. E. Becker, and P. T. Kovanen

Mast cell infiltration in acute coronary syndromes: implications for plaque rupture

J. Am. Coll. Cardiol., September 1, 1998; 32(3): 606 - 612.

[\[Abstract\]](#) [\[Full Text\]](#) [\[PDF\]](#)



Circulation

[HOME](#)

Y. Tintut, J. Patel, F. Parhami, and L. L. Demer

Tumor Necrosis Factor- α Promotes In Vitro Calcification of Vascular Cells via the cAMP Pathway

Circulation, November 21, 2000; 102(21): 2636 - 2642.

[\[Abstract\]](#) [\[Full Text\]](#) [\[PDF\]](#)



The Journal of Immunology

[HOME](#)

A. de Paulis, G. Minopoli, E. Arbustini, G. de Crescenzo, F. Dal Piaz, P. Pucci, T. Russo, and G. Marone

Stem Cell Factor Is Localized in, Released from, and Cleaved by Human Mast Cells

J. Immunol., September 1, 1999; 163(5): 2799 - 2808.

[\[Abstract\]](#) [\[Full Text\]](#) [\[PDF\]](#)



Infection and Immunity

[HOME](#)

A. Genovese, J.-P. Bouvet, G. Florio, B. Lamparter-Schummert, L. Björck, and G. Marone

Bacterial Immunoglobulin Superantigen Proteins A and L Activate Human Heart Mast Cells by Interacting with Immunoglobulin E

Infect. Immun., October 1, 2000; 68(10): 5517 - 5524.

[\[Abstract\]](#) [\[Full Text\]](#) [\[PDF\]](#)



Circulation

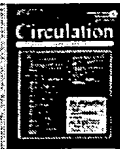
[HOME](#)

B. Schieffer, E. Schieffer, D. Hilfiker-Kleiner, A. Hilfiker, P. T. Kovanen, M. Kaartinen, J. Nussberger, W. Harringer, and H. Drexler

Expression of Angiotensin II and Interleukin 6 in Human Coronary Atherosclerotic Plaques: Potential Implications for Inflammation and Plaque Instability

Circulation, March 28, 2000; 101(12): 1372 - 1378.

[\[Abstract\]](#) [\[Full Text\]](#) [\[PDF\]](#)



Circulation

[HOME](#)

I. Spyridopoulos, N. Principe, K. L. Krasinski, S.-h. Xu, M. Kearney, M. Magner, J. M. Isner, and D. W. Losordo

Restoration of E2F Expression Rescues Vascular Endothelial Cells From Tumor Necrosis Factor- α -Induced Apoptosis

Circulation, December 22, 1998; 98(25): 2883 - 2890.

[\[Abstract\]](#) [\[Full Text\]](#) [\[PDF\]](#)



Arteriosclerosis, Thrombosis, and Vascular Biology

[HOME](#)

J. L. Johnson, C. L. Jackson, G. D. Angelini, and S. J. George

Activation of Matrix-Degrading Metalloproteinases by Mast Cell Proteases in Atherosclerotic Plaques

Arterioscler. Thromb. Vasc. Biol., November 1, 1998; 18(11): 1707-1715

[\[Abstract\]](#) [\[Full Text\]](#) [\[PDF\]](#)



Stroke

[HOME](#)

S. Jander, M. Sitzer, R. Schumann, M. Schroeter, M. Siebler, H. Steinmetz, and G. Stoll

Inflammation in High-Grade Carotid Stenosis: A Possible Role for Macrophages and T Cells in Plaque Destabilization

Stroke, August 1, 1998; 29(8): 1625-1630

[\[Abstract\]](#) [\[Full Text\]](#) [\[PDF\]](#)

This Article

- › [Abstract](#) **FREE**
- › [Alert me when this article is cited](#)
- › [Alert me if a correction is posted](#)
- › [Citation Map](#)

Services

- › [Email this article to a friend](#)
- › [Similar articles in this journal](#)
- › [Similar articles in PubMed](#)
- › [Alert me to new issues of the journal](#)
- › [Download to citation manager](#)
- › [Request Permissions](#)

Google Scholar

- › [Articles by Kaartinen, M.](#)
- › [Articles by Kovanen, P. T.](#)
- › [Articles citing this Article](#)

PubMed

- ▶ [PubMed Citation](#)
- ▶ [Articles by Kaartinen, M.](#)
- ▶ [Articles by Kovanen, P. T.](#)

HOME	HELP	FEEDBACK	SUBSCRIPTIONS	ARCHIVE	SEARCH	TABLE OF CONTENTS
CIRCULATION			ART, THRO, VASC BIO		ALL AHA JOURNALS	
CIRCULATION RESEARCH			HYPERTENSION		STROKE	

Extracellular Mast Cell Granules Carry Apolipoprotein B-100-Containing Lipoproteins Into Phagocytes in Human Arterial Intima

Functional Coupling of Exocytosis and Phagocytosis in Neighboring Cells

Maija Kaartinen; Antti Penttilä; Petri T. Kovanen

From the Wihuri Research Institute (M.K., P.T.K) and the Department of Forensic Medicine, University of Helsinki (A.P.), Helsinki, Finland.

Correspondence to Petri T. Kovanen, MD, Wihuri Research Institute, Kallioliinantie 4, 00140 Helsinki, Finland.

Abstract

Abstract In experimental studies in vitro, mast cells have induced uptake of apolipoprotein B-100 (apoB-100)-containing low-density lipoproteins by macrophages, with the subsequent formation of foam cells, the hallmarks of atherosclerosis. Recently, increased numbers of activated, ie, degranulated, mast cells were found to be present in human coronary fatty streaks and atheromas. We therefore sought evidence of a connection between mast cells and foam cell formation in vivo. In electron microscopic studies of human aortic and coronary fatty streaks and atheromas, exocytosed cytoplasmic secretory granules of mast cells were detected in the vicinity of their parent cells. These exocytosed granules had bound apoB-100-containing lipoproteins, as indicated by their positive staining with MB 47, a monoclonal antibody against apoB-100. A smooth muscle cell was observed to be in the process of phagocytosing one such exocytosed granule, and in the vicinity of a degranulated mast cell a foam cell contained an ingested mast cell granule. Therefore, the micrographs show that exocytosed granules of intimal mast cells may contribute to intimal foam cell formation and suggest a role for mast cells in human atherogenesis. More generally, the findings provide evidence that phagocytosis

of apoB-100-carrying particles is one mechanism by which lipoproteins enter human arterial intimal cells.

Key Words: atherosclerosis • exocytosis • mast cells • low-density lipoproteins • phagocytosis

► Introduction

The earliest recognizable gross lesion in atherogenesis, the fatty streak, is characterized by accumulation of LDL-derived cholesteryl esters in the cells of the arterial intima, with formation of foam cells.^{1,2} Foam cells are also present in the growing edges, the shoulder regions of late atherosclerotic lesions referred to as atheromas. Most foam cells have been shown to arise from macrophages that originally migrated from the circulation,³ and a variable fraction of them are derived from smooth muscle cells that have migrated to the intima from the medial layer of the artery.⁴ Mast cells are also present in the arterial intima, and the number of activated, ie, degranulated, mast cells is increased in human aortic and coronary fatty streaks and in the shoulder regions of atheromas.^{5,6} Moreover, mast cells are an integral part of aortic fatty streaks in cholesterol-fed African green monkeys.⁷

Since uptake of LDL through the classical LDL receptor pathway does not lead to cholesterol accumulation in cells,⁸ foam cell formation must depend on other mechanisms. Indeed, a specific chemical modification of the apoB-100 component of LDL is followed by massive uptake of LDL by another receptor-mediated mechanism, called the "scavenger receptor" pathway.⁹ In addition, foam cells may be generated by phagocytic uptake of LDL aggregates or of LDL bound to other macromolecules or to their aggregates.¹⁰ It is generally held that modifications of LDL and formation of complexes between LDL and macromolecules or their aggregates occur locally in the arterial intima by the action of the intimal cells.¹¹

In previous studies in vitro with rat serosal mast cells, we found that stimulated mast cells induced uptake of LDL by cocultured mouse peritoneal macrophages.¹² In rat serosal mast cells, the model used in our studies, the cytoplasm is filled with secretory granules, which upon stimulation of the mast cells are expelled into the extracellular fluid.^{13,14} There the soluble components of the granules, ie, histamine and a fraction of their proteoglycans, are released and diffuse away. In contrast, the major granule components, two neutral proteases (a chymotryptic endopeptidase chymase and an exopeptidase carboxypeptidase A), and the major fraction of the heparin proteoglycans remain tightly

bound to each other, forming extracellular "granule remnants."¹² When rat serosal mast cells were cocultured with mouse peritoneal macrophages and stimulated in the presence of LDL, the apoB-100 component of the LDL particles was bound by the heparin component of the granule remnants, and these LDL-coated granule remnants were phagocytosed by the macrophages, the result being massive uptake of LDL by the macrophages.¹⁵

On stimulation of rat serosal mast cells, most of the granules exposed to the extracellular fluid remain in the degranulation channels, and, like the granule remnants expelled into the extracellular space, these remnants too bind LDL.¹⁶ Such LDL is rapidly (within minutes) internalized by the mast cells, along with the remnants. The mast cells recover rapidly from stimulation and are soon (within hours) ready for a second stimulation. On restimulation, the already-LDL-loaded granule remnants may be expelled and then carry their cholesterol load to macrophages. However, some of these LDL-loaded remnants remain in the channels and bind more LDL. Thus, a mechanism was discovered by which LDL cholesterol can accumulate in mast cells.¹⁶

The presence of activated mast cells in the human arterial intima, where high LDL concentrations prevail and where foam cells are formed, prompted us to search for evidence of mast cell-dependent foam cell formation in this tissue site. The availability of monoclonal antibodies against apoB-100 and against tryptase, a neutral protease specific to human mast cells,¹⁷ allowed us to test this possibility with the aid of immunoelectron microscopic studies. The results revealed a novel extracellular carrier system of LDL in vivo, in which exocytosis and phagocytosis of mast cell granules are coupled. This pathway leads to transcellular transfer of mast cell granule remnants, which thus, when carrying LDL, contributes to the initiation of human atherogenesis.

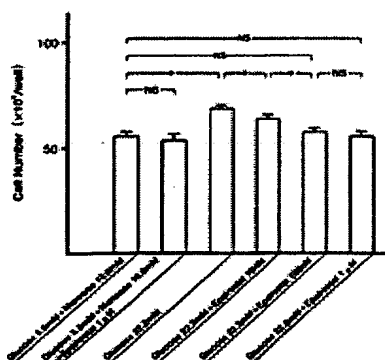
► Methods

An autopsy series comprising 19 subjects (15 males, 4 females) 24 to 84 years old was used for this study. The causes of death were cardiovascular disease (n=5), violent deaths, ie, accidents and suicides (n=8), and poisoning with self-administered alcohol and drugs (n=6). The autopsy material (abdominal aorta and left coronary artery) was obtained within 24 hours of death (range 2.5 to 24 hours; mean 10 hours). The aortic samples (n=19) included macroscopically identifiable fatty streaks (n=18) and raised atheromatous lesions (n=15), and the coronary samples included the (unopened) bifurcation area of the left coronary artery (n=10). Specimens for electron microscopy (11 aortic and 5 coronary) were fixed for 3 hours in a solution containing 2% glutaraldehyde and 1.5% paraformaldehyde and postfixed in osmium tetroxide. The samples were then

dehydrated, embedded in Epon, sectioned with an ultramicrotome, and finally stained with uranyl acetate and lead citrate. For immunoelectron microscopy, specimens (8 aortic and 5 coronary) were fixed for 3 hours in 3% paraformaldehyde, dehydrated, and embedded in LR white resin. The ultramicrotome sections on nickel grids were incubated at room temperature with buffer (PBS containing 3% BSA) for 10 minutes and then for 4 hours with anti-tryptase G3 monoclonal antibody (kindly provided by Dr L. B. Schwartz, Medical College of Virginia, Richmond) or with anti-apoB-100 MB 47 (1:100) (kindly provided by Dr J. L. Witztum, University of California, San Diego, La Jolla SCOR). After two rinses in the buffer, the sections were incubated for 2 hours in 10 nm gold-labeled anti-mouse IgG+IgM (1:50) (Amersham) and finally stained with uranyl acetate and lead citrate. In sections serving as negative controls, the primary antibody was omitted or replaced with normal serum (irrelevant antibody). In these sections no apoB-100 staining was observed. The sections (1 μ m) were stained with toluidine blue and observed with light microscopy for orientation of the site and for evaluation of the atherosclerotic involvement of the arteries.^{5,6} The ultramicrotome sections were viewed with a Jeol JEM-1200EX transmission electron microscope at the Department of Electron Microscopy, University of Helsinki.

► Results

Fig 1• shows a light micrograph of a section of an atherosclerotic human left coronary artery stained with toluidine blue. The lesion was classified as a fatty streak because it contained foam cells. This lesion also contained typical mast cells, which could be identified by their contents of metachromatic cytoplasmic granules. We could identify mast cells in all coronary fatty streaks examined (number of subjects, 10).



View larger version (28K):

[\[in this window\]](#)

[\[in a new window\]](#)

Figure 1. Light microscopic view of a section of an atherosclerotic human left coronary artery. The lesion is classified as a fatty streak because it contains foam cells (a typical foam cell is indicated by the arrowhead). The lesion also contains mast cells (arrows) with typical metachromatic cytoplasmic granules. The specimen was from a 41-year-old man who died of aortic dissection. The section is stained with toluidine blue; magnification x200.

To search for evidence of the granule carrier mechanism in which apoB-100-containing lipoproteins are bound to exocytosed mast cell granules, we turned to immunoelectron microscopy. For this purpose, coronary fatty streaks from five subjects were studied. First, mast cell granules were identified with anti-tryptase antibody. Fig 2+ shows an immunoelectron micrograph of a mast cell present in a fatty streak lesion of the coronary intima. Several intracellular tryptase-positive granules and four tryptase-positive extracellularly located mast cell granule remnants are visible. Indeed, 138 (71%) of the total of 194 mast cells that were identified and photographed had extracellular granule remnants in their vicinity. Therefore, in the atherosclerotic lesion shown (as in the other lesions studied), mast cells were degranulated, signifying their stimulation. Most important, the necessary condition for the granule carrier mechanism to operate, ie, the presence of granule remnants in the extracellular space, was fulfilled.



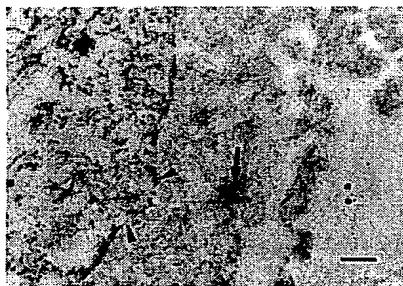
View larger version (185K):

[\[in this window\]](#)

[\[in a new window\]](#)

Figure 2. Electron micrograph showing an activated mast cell in a coronary fatty streak lesion. The section is stained with anti-tryptase antibody, which is detected with 10-nm gold-labeled IgG+IgM as secondary antibodies. Several tryptase-positive cytoplasmic secretory granules within the cell and four extracellularly located granule remnants (arrows) are visible. The specimen was from a 42-year-old man who died of poisoning with self-administered alcohol. Bar=0.2 μm.

We next searched for evidence of apoB-100 binding to mast cell granule remnants and stained the sections with monoclonal antibody MB 47 against the apoB-100 component of lipoproteins. Fig 3• shows an immunoelectron micrograph of a stimulated mast cell with one exocytosed granule. This extracellularly located granule remnant stained for MB 47, an observation made in three of the five samples studied. In sharp contrast, the extracellular matrix seen in this specimen is totally devoid of apoB-100, as evidenced by failure to stain for MB 47. In the other samples studied, occasional gold particles could be observed in the extracellular matrix; in each case, however, the density of the gold particles was smaller in the matrix than in the extracellular mast cell granules.



View larger version (146K):

[\[in this window\]](#)

[\[in a new window\]](#)

Figure 3. Demonstration of apoB-100 binding to mast cell granules. The sections were stained with MB 47, a monoclonal antibody against apolipoprotein B-100 (apoB-100). The primary antibody is detected with 10-nm gold-labeled IgG+IgM as secondary antibodies. A degranulated mast cell (left) with an exocytosed granule (arrow) that stains positively for MB 47 is shown. Note the opening of a degranulation channel into the extracellular space (between arrowheads) and some apoB-100 in the path of the exocytosed granule. The rest of the extracellular area is totally devoid of apoB-100. The specimen was from a 66-year-old man who died of myocardial infarction. Bar=0.2 μ m.

As described above, the granule remnants remaining in the degranulation channels of rat serosal mast cells bind LDL particles and internalize them. Similarly, in the mast cells of the coronary lesions we regularly found apoB-100-positive granule remnants (ie, the granules had bound LDL or other apoB-100-containing lipoproteins), whereas the cytoplasm of such cells was practically devoid of apoB-100. Fig 4• shows an immunoelectron micrograph of a mast cell with several intracellular granules that stain positively for MB 47. Notably, the MB 47-positive granules are electron transparent and the MB 47-negative granules are electron dense. Electron transparency of a granule reveals that the particular granule has been in contact with the extracellular fluid and has lost some of its contents.^{16 18} The above finding was made in four of the five samples studied and corroborates the idea that any apoB-100 bound to intracellular granule remnants has an extracellular origin.



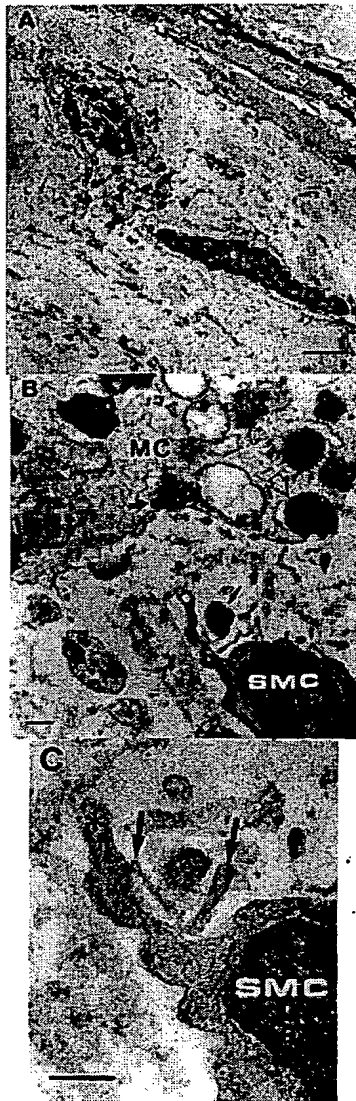
View larger version (153K):

[\[in this window\]](#)

[\[in a new window\]](#)

Figure 4. Demonstration of apolipoprotein B-100 (apoB-100) inside a mast cell. The sections were stained with MB 47, a monoclonal antibody against apoB-100. The primary antibody is detected with 10-nm gold-labeled IgG+IgM as secondary antibodies. A mast cell (top) contains several intracellular granules (arrows) that stain positively for MB 47. Notably, the MB 47-positive granules are electron transparent and the MB 47-negative granules (arrowheads) are electron dense. The specimen was from a 66-year-old man who died of myocardial infarction. Bar=1 μ m.

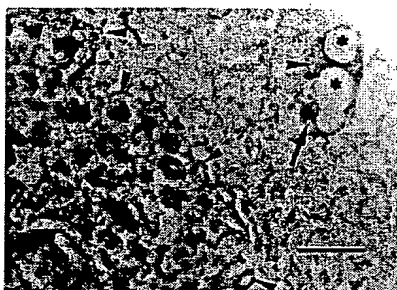
Fig 5A• shows an electron micrograph of a mast cell and a smooth muscle cell in an aortic fatty streak. In addition to the electron-dense cytoplasmic granules, electron-transparent granules and also empty membrane-bound vacuoles can be seen inside the mast cell, revealing that this particular cell has previously been stimulated to degranulate. At higher magnification (Fig 5B•), one exocytosed mast cell granule (arrow) can be detected. At this magnification, the heterogeneous morphology of the mast cell granules can be discerned: Several intracellular granules contain the scrolls¹⁸ typical of human mast cells (seen in both cross and longitudinal sections). The single extracellularly located granule also displayed the typical structural pattern of mast cell granules, ie, several sets of parallel stripes (scrolls in longitudinal view) and one set of concentric circles (scroll in cross section; arrow). This panel also shows a large cytoplasmic cell projection (pseudopod) extending from the smooth muscle cell at the site where the granule remnant is located. Fig 5C• shows the next section cut from this area, in which the remnant is surrounded by two smaller pseudopods, one on each side. Thus, the smooth muscle cell appears to be in the process of engulfing the granule remnant. This set of micrographs displayed all the necessary components to perform the steps of the granule-mediated carrier pathway (ie, the parent mast cell, the exocytosed granule remnant, and the phagocytosing cell with pseudopods directed toward the granule remnant) visualized together. This finding was observed in 2 of 18 aortic samples.



View larger version
(542K):
[\[in this window\]](#)
[\[in a new window\]](#)

Figure 5. (This page and previous page). An exocytosed mast cell granule about to be engulfed by a smooth muscle cell. A, A mast cell (left) containing several granules of varying appearance (electron dense and electron lucent) is located near a smooth muscle cell (right). Bar=2 μ m. B, Detailed view of the mast cell (MC), the smooth muscle cell (SMC), and the extracellular space between the mast cell and the smooth muscle cell. Inside the mast cell secretory granules of varying morphology (scrolls in cross section [arrow], scrolls in longitudinal section [arrowhead], and dense granular contents [open arrow]) are seen. Note that the smooth muscle cell has extended a large pseudopod (*) next to the extracellular granule remnant (arrow). Bar=0.2 μ m. C, Section adjacent to A and B (at 60 nm distance) showing two small cytoplasmic projections (arrows), one on each side of the granule remnant, extending from the larger pseudopod (*). The smooth muscle cell appears to be in the process of engulfing the granule remnant. Bar=0.2 μ m. The specimen was from a 63-year-old man who died of myocardial infarction.

Fig 6+ shows an immunoelectron micrograph of an aortic fatty streak in which mast cell granules were identified with the anti-tryptase antibody. Adjacent to a mast cell, a small section of a typical foam cell with large empty vacuoles is seen. The foam cell contains one tryptase-positive particle that is thus identified as a granule remnant. In three of eight aortic samples studied, a granule remnant-containing foam cell could be observed.



View larger version (163K):
[\[in this window\]](#)
[\[in a new window\]](#)

Figure 6. Demonstration of a mast cell granule inside a foam cell. A foam cell (right) can be identified near a mast cell (left) (cell boundaries are marked with arrowheads). The foam cell (with two cytoplasmic vacuoles [•]) contains a small cytoplasmic inclusion, which, being tryptase-positive, can be identified as a mast cell granule (arrow). The section was stained with anti-tryptase antibody, which is detected with 10-nm gold-labeled IgG+IgM as secondary antibodies. The specimen was from a 51-year-old man who died of poisoning with self-administered alcohol. Bar=1 μ m.

- ▲ [Top](#)
- ▲ [Abstract](#)
- ▲ [Introduction](#)
- ▲ [Methods](#)
- ▲ [Results](#)
- [Discussion](#)
- ▼ [References](#)

Discussion

The current study demonstrates that exocytosed mast cell granules, ie, granule remnants, bind apoB-100-containing lipoproteins present in the intimal fluid of human aortic and coronary vessels. Indeed, we regularly observed binding of apoB-100 to the exocytosed granules. Since some of the apoB-100-containing lipoproteins are lost during tissue processing (fixation, dehydration, and staining), the above observation shows that the apoB-100-containing lipoproteins are bound to the exocytosed granules rather than to the extracellular matrix. This suggestion is supported by the fact that, among the glycosaminoglycans present in the intima, heparin, the component of mast cell granules responsible for binding apoB-100, has the highest density of negative charges.¹⁹ Heparin can therefore interact most extensively with the positively charged amino acid residues of the apoB-100.²⁰ Another reason for the more intense reaction of MB 47 with LDL bound to the heparin proteoglycans of granule remnants than with LDL bound to (chondroitin sulfate) proteoglycans of the arterial extracellular matrix could be differences in binding of apoB-100 to these two types of proteoglycans,^{21 22 23} thus leading to differential

exposure (or steric hindrance) of the epitope responsible for binding MB 47.²⁴ Moreover, a specific mechanism that increases the strength of binding between LDL particles and mast cell granule remnants was recently discovered.²⁵ When the apoB-100 component of granule-bound LDL is proteolyzed by granule chymase, the LDL particles become unstable and fuse, and the fused particles bind more tightly to the granule remnant heparin proteoglycans.

The present study also describes a mechanism by which exocytosed mast cell granules carry apoB-100-containing lipoproteins into intimal cells. The electron microscopic studies do not allow us to conclude which of the apoB-100-containing lipoproteins present in the intimal fluid [VLDL remnant-like particles, LDL, or LP(a)]^{26 27 28} had actually bound to the granules. Since, of the total immunoreactive apoB-100 in lipoproteins isolated from atherosclerotic intima, most (>95%) is present in LDL-like particles, it is likely that the majority of granule-associated apoB-100 also represents binding of LDL.^{26 29}

The efficiency of the granule-remnant carrier system in the intima must depend on the number of carriers available and their binding capacity. In atherosclerotic lesions the number of degranulated mast cells is increased,⁶ indicating that during atherogenesis more granules are available for lipoprotein binding. The binding capacity of exocytosed rat mast cell granules has been studied in detail.³⁰ Thus, each exocytosed granule has the capacity, depending on its size, to bind maximally 5000 to 10 000 LDL particles. We have also observed that the proteolytic activity of a granule remnant increases its maximal capacity to bind LDL.³¹ Degradation of the apoB-100 moiety of the granule-remnant-bound LDL by the also granule-remnant-bound chymase is followed by fusion of LDL particles, whereupon the capacity of the remnants to carry LDL increases fivefold. Accordingly, the human granule remnants containing chymase in addition to tryptase have the potential to bind extra LDL and thus become even more efficient carriers. Since the concentration of LDL usually found in the intimal fluid²⁷ (1500 µg/mL of apoB-100) is far higher than that required to saturate granule-remnant binding sites (25 µg/mL), the exocytosed granules in the intimal fluid are likely to be maximally loaded with LDL. However, the current morphological studies do not allow any conclusions about the quantitative significance of the granule carrier mechanism in foam cell formation in human arterial intima. Neither have other mechanisms of foam cell formation been quantified in human atherogenesis. Thus, it remains to be shown how important the newly described mechanism is in comparison with all of the other mechanisms of intimal foam cell formation.

The natural fate of an exocytosed mast cell granule is to be phagocytosed by the cells present in the vicinity of the degranulated mast cell.^{32 33} Hence, the factors responsible for granule-remnant traffic in the intimal space are the rates of granule exocytosis and granule phagocytosis. The mast cells in the atherosclerotic areas reside in an inflamed area where many potential mast cell activators are present. Among these are activated T lymphocytes, activated macrophages, and activated complement.³⁴ Indeed, in human coronary fatty streaks the degree of mast cell degranulation was recently found to be markedly increased (from 18% in normal intima to 52% in fatty streaks).⁶ Similarly, in

the present study 71% of the mast cells in the arterial (coronary or aortic) intima showed signs of degranulation. Thus, we can infer that the majority of the mast cells actively participated in the granule-remnant carrier system. In contrast to degranulation (ie, granule exocytosis), no quantitative data are available on granule phagocytosis in the various intimal lesions. However, it appears that, in the intima, mast cells reside in a tissue composed of many cells capable of phagocytosis. Thus, as the smooth muscle cells leave the medial layer and enter the intima, their phenotype is switched from contractile to synthetic, and this change in phenotype is accompanied by an apparent increase in phagocytotic capacity.³⁵ Indeed, we recently found that smooth muscle cells of synthetic phenotype actively phagocytose exocytosed mast cell granules, and that, in vitro, the granule remnants can carry LDL into the cells and induce their conversion into foam cells.³⁶ Similarly, as the blood monocytes enter the atherosclerotic intima, they differentiate into tissue macrophages and become activated, and their phagocytic capacity increases.³⁷ Accordingly, the necessary conditions for the two events in the granule carrier pathway, granule exocytosis and phagocytosis, prevail in the atherosclerosis-prone areas of human arterial intima.

A carrier mechanism for cellular uptake of LDL was originally described in a cell culture system in which formation of LDL-dextran sulfate complexes in the incubation medium was associated with uptake of cholesteryl esters by mouse macrophages ("piggyback system").³⁸ Later, uptake of complexes between LDL and proteoglycans obtained from the arterial wall was also described.^{39 40 41} However, phagosomal uptake of such complexes in human atherosclerotic lesions has eluded direct observation so far. The current observations provide the first visual evidence that an exocytosis-phagocytosis-coupled carrier mechanism leads to uptake of apoB-100-containing lipoproteins by phagocytes in the human arterial intima. Unraveling the factors that regulate this novel pathway in the arterial intima is a challenge for the future.

Acknowledgments

This study was supported in part by the Aarne Koskelo Foundation and the Meilahti Foundation. The authors thank the staff of the Department of Forensic Medicine and Electron Microscopy, University of Helsinki, for their excellent technical assistance.

Received March 2, 1995; accepted August 14, 1995.

References

▲ Top
▲ Abstract
▲ Introduction
▲ Methods
▲ Results
▲ Discussion
• References

1. Smith E, Slater RS. Relationship between low density lipoprotein in aortic intima and serum lipid levels. *Lancet*. 1972;1:463-469. [\[Medline\]](#) [\[Order article via Infotrieve\]](#)
2. Haust, MD. The natural history of human atherosclerotic lesions. In: Moore S, ed. *Vascular Injury and Atherosclerosis*. New York, NY: Marcel Dekker Inc; 1981:1-23.
3. Mitchinson MJ, Ball RY. Macrophages and atherogenesis. *Lancet*. 1987;2:146-149.
4. Katsuda S, Boyd HC, Flinger C, Ross R, Gown AM. Human atherosclerosis, III: immunocytochemical analysis of the cell composition of lesions of young adults. *Am J Pathol*. 1992;140:907-914. [\[Abstract\]](#)
5. Kaartinen M, Penttilä A, Kovanen PT. Mast cells of two types differing in neutral protease composition in the human aortic intima. *Arterioscler Thromb*. 1994;14:966-972. [\[Abstract\]](#)
6. Kaartinen M, Penttilä A, Kovanen PT. Accumulation of activated mast cells in the shoulder region of human coronary atheroma, the predilection site of atheromatous rupture. *Circulation*. 1994;90:1669-1678. [\[Abstract\]](#)
7. Trillo AA. The cell population of aortic fatty streaks in African green monkeys with special reference to granulocytic cells: an ultrastructural study. *Atherosclerosis*. 1982;43:259-275. [\[Medline\]](#) [\[Order article via Infotrieve\]](#)
8. Brown MS, Goldstein JL. A receptor-mediated pathway for cholesterol homeostasis. *Science*. 1986;232:34-47. [\[Medline\]](#) [\[Order article via Infotrieve\]](#)
9. Goldstein JL, Ho YK, Basu SK, Brown MS. Binding site on macrophages that mediates uptake and degradation of acetylated low density lipoproteins, producing massive cholesterol deposition. *Proc Natl Acad Sci U S A*. 1979;76:333-337. [\[Abstract\]](#)
10. Fogelman AM, Van Lenten BJ, Warden C, Haberland ME, Edwards PA. Macrophage lipoprotein receptors. *J Cell Sci*. 1988;9(suppl):135-149.
11. Steinberg D, Parthasarathy S, Carew TE, Khoo JC, Witztum JL. Beyond cholesterol: modifications of low-density lipoprotein that increase its atherogenicity. *N Engl J Med*. 1989;320:915-924. [\[Medline\]](#) [\[Order article via Infotrieve\]](#)

12. Kovanen PT. The mast cell—a potential link between inflammation and cellular cholesterol deposition in atherogenesis. *Eur Heart J.* 1993;14(suppl K):105-117.
13. Helander HF, Bloom GD. Quantitative analysis of mast cell structure. *J Microsc.* 1974;100:315-321. [[Medline](#)] [[Order article via Infotrieve](#)]
14. Metcalfe DD, Kaliner M, Donlon DA. The mast cell. In: *CRC Critical Reviews in Immunology*. Boca Raton, Fla: CRC Press; 1981:23-74.
15. Kokkonen JO, Kovanen PT. Stimulation of mast cells leads to cholesterol accumulation in macrophages in vitro by a mast cell granule-mediated uptake of low density lipoprotein. *Proc Natl Acad Sci U S A.* 1987;84:2287-2291. [[Abstract](#)]
16. Kokkonen JO, Lindstedt KA, Kovanen PT. Metabolism of LDL in mast cells recovering from degranulation: description of a novel intracellular pathway leading to proteolytic modification of the lipoprotein. *Arterioscler Thromb.* 1993;13:276-285. [[Abstract](#)]
17. Irani AM, Bradford TR, Kepley CL, Schechter NM, Schwartz LB. Detection of MC_T and MC_{TC} types of human mast cells by immunohistochemistry using new monoclonal anti-tryptase and anti-chymase antibodies. *J Histochem Cytochem.* 1989;37:1509-1515. [[Abstract](#)]
18. Dvorak AM. *Basophil and Mast Cell Degranulation and Recovery*. In: Harris JR, ed. *Blood Cell Biochemistry 4*. New York, NY: Plenum Press; 1991:1-415.
19. Nieduszyński I. General physical properties of heparin. In: Lane DA, Lindahl U, eds. *Heparin: Chemical and Biological Properties, Clinical Applications*. London, England: Edward Arnold; 1989:51-63.
20. Kokkonen JO, Kovanen PT. Low-density-lipoprotein binding by mast-cell granules: demonstration of binding of apolipoprotein B to heparin proteoglycan of exocytosed granules. *Biochem.J.* 1987;241:583-589. [[Medline](#)] [[Order article via Infotrieve](#)]
21. Hirose N, Blankenship DT, Krivanek M, Jackson RL, Cardin AD. Isolation and characterization of four heparin-binding cyanogen bromide peptides of human plasma apolipoprotein B. *Biochemistry.* 1987;26:5505-5512. [[Medline](#)] [[Order article via Infotrieve](#)]
22. Weisgraber KH, Rall SC. Human apolipoprotein B-100 heparin-binding sites. *J Biol Chem.* 1987;262:11097-11103. [[Abstract/Free Full Text](#)]
23. Camejo G, Olofsson S-O, Lopez F, Carlsson P, Bondjers G. Identification of apoB-100 segments mediating the interaction of low density lipoproteins with arterial proteoglycans. *Arteriosclerosis.* 1988;8:368-377. [[Abstract](#)]

24. Young SG, Koduri RK, Austin RK, Bonnet DJ, Smith RS, Curtiss LK. Definition of a nonlinear conformational epitope for the apolipoprotein B-100-specific monoclonal antibody, MB 47. *J Lipid Res.* 1994;35:399-407. [[Abstract](#)]
25. Paananen K, Kovanen PT. Proteolysis and fusion of low density lipoprotein particles independently strengthen their binding to exocytosed mast cell granules. *J Biol Chem.* 1994;269:2023-2031. [[Abstract/Free Full Text](#)]
26. Ylä-Herttuala S, Palinski W, Rosenfeld ME, Steinberg D, Witztum JL. Lipoproteins in normal and atherosclerotic aorta. *Eur Heart J.* 1990;11(suppl E):88-99.
27. Smith EB. Transport, interactions and retention of plasma proteins in the intima: the barrier function of the internal elastic lamina. *Eur Heart J.* 1990;11(suppl E):72-81.
28. Beisiegel U, Niendorf A, Wolf K, Reblin T, Rath M. Lipoprotein(a) in the arterial wall. *Eur Heart J.* 1990;11(suppl E):174-183.
29. Ylä-Herttuala S, Palinski W, Rosenfeld M, Parthasarathy S, Carew TE, Butler S, Witztum JL, Steinberg D. Evidence for presence of oxidative modified low density lipoproteins in atherosclerotic lesions of rabbit and man. *J Clin Invest.* 1989;84:1086-1095. [[Medline](#)] [[Order article via Infotrieve](#)]
30. Kovanen PT. Mast cell granule-mediated uptake of low density lipoproteins by macrophages: a novel carrier mechanism leading to the formation of foam cells. *Ann Med.* 1991;23:551-559. [[Medline](#)] [[Order article via Infotrieve](#)]
31. Kokkonen JO, Kovanen PT. Proteolytic enzymes of mast cell granules degrade low density lipoproteins and promote their granule-mediated uptake by macrophages in vitro. *J Biol Chem.* 1989;264:10749-10755. [[Abstract/Free Full Text](#)]
32. Lindahl U, Pertoft H, Seljelid R. Uptake and degradation of mast-cell granules by mouse peritoneal macrophages. *Biochem J.* 1979;182:189-193. [[Medline](#)] [[Order article via Infotrieve](#)]
33. Baggiolini M, Horisberger U, Martin U. Phagocytosis of mast cell granules by mononuclear phagocytes, neutrophils and eosinophils during anaphylaxis. *Int Arch Allergy Appl Immunol.* 1982;67:219-226. [[Medline](#)] [[Order article via Infotrieve](#)]
34. Libby P, Hansson GK. Involvement of the human immune system in human atherogenesis: current knowledge and unanswered questions. *Lab Invest.* 1991;64:5-15. [[Medline](#)] [[Order article via Infotrieve](#)]

35. Inaba T, Gotoda T, Shimano H, Shimada M, Harada K, Kozaki K, Watanabe Y, Hoh E, Motoyoshi K, Yazaki Y, Yamada N. Platelet-derived growth factor induces c-fms and scavenger receptor genes in vascular smooth muscle cells. *J Biol Chem.* 1992;267:13107-13112. [[Abstract/Free Full Text](#)]
36. Wang Y, Lindstedt KA, Kovanen PT. Mast cell granule remnants carry LDL into smooth muscle cells of the synthetic phenotype and induce their conversion into foam cells. *Arterioscler Thromb Vasc Biol.* 1995;15:801-810. [[Abstract/Free Full Text](#)]
37. Adams DO, Hamilton TA. The cell biology of macrophage activation. *Annu Rev Immunol.* 1984;2:283-318. [[Medline](#)] [[Order article via Infotrieve](#)]
38. Basu SK, Brown MS, Ho YK, Goldstein JL. Degradation of low density lipoprotein dextran sulfate complexes associated with deposition of cholesteryl esters in mouse macrophages. *J Biol Chem.* 1979;254:7141-7146. [[Medline](#)] [[Order article via Infotrieve](#)]
39. Vijayagopal P, Srinivasan SR, Jones KM, Radhakrishnamurthy B, Berenson GS. Complexes of low density lipoproteins and arterial proteoglycan aggregates promote cholesteryl ester accumulation in mouse macrophages. *Biochim Biophys Acta.* 1985;837:251-261. [[Medline](#)] [[Order article via Infotrieve](#)]
40. Salisbyry BGJ, Falcone DJ, Minick CR. Insoluble low-density lipoprotein-proteoglycan complexes enhance cholesteryl ester accumulation in macrophages. *Am J Pathol.* 1985;120:6-11. [[Abstract](#)]
41. Hurt E, Bondjers G, Camejo G. Interaction of LDL with human arterial proteoglycans stimulates its uptake by human monocyte-derived macrophages. *J Lipid Res.* 1990;31:443-454. [[Abstract](#)]

Polyclonal Antibody Directed Against Human RANTES Ameliorates Disease in the Lewis Rat Adjuvant-induced Arthritis Model

Debra A. Barnes,* Jenny Tse,[†] Margaret Kaufhold,[‡] Matt Owen,[‡] Joe Hesselgesser,* Robert Strieter,[§] Richard Horuk,* and H. Daniel Perez*

*Department of Immunology and [†]Department of Pharmacology, Berlex Biosciences, Richmond, California 94804; and [‡]Department of Internal Medicine, University of Michigan Medical School, Ann Arbor, Michigan 48109

Abstract

Adjuvant-induced arthritis (AIA) is one of many animal models of rheumatoid arthritis, a disease characterized by a T-lymphocyte and macrophage cellular infiltrate. We have characterized the development of this disease model with respect to chemokine expression. Increased levels of two chemokines, RANTES, a T-lymphocyte and monocyte chemo-attractant, and KC a chemoattractant for neutrophils, were found in whole blood and in the joint. Surprisingly, levels of MIP-1 α , another T-lymphocyte and monocyte chemoattractant, were unchanged throughout the course of the disease in whole blood and only slightly elevated in the joint. RANTES expression plays an important role in the disease since a polyclonal antibody to RANTES greatly ameliorated symptoms in animals induced for AIA and was found to be as efficacious as treatment with indomethacin, a non-steroidal anti inflammatory. Polyclonal antibodies to either MIP-1 α or KC were ineffective. This is the first report to show the importance of RANTES in the development of AIA. (*J. Clin. Invest.* 1998. 101:2910–2919.) Key words: RANTES • MIP-1 α • KC • arthritis • chemokine

Introduction

Rheumatoid arthritis (RA)¹ is a chronic inflammatory disease characterized by infiltration of the synovial membrane with T lymphocytes and macrophages and pannus formation over the

underlying cartilage and bone (1). The pannus is rich in activated macrophages secreting proteases and other inflammatory mediators resulting in destruction of these tissues. In comparison with normal synovial fluid, which is essentially acellular, RA synovial fluid is abundant in neutrophils, macrophages, T lymphocytes, and dendritic cells. It is thought that both humoral immunity and cellular immunity operating at the same time may contribute to the pathology of the disease.

A role for humoral immunity has been proposed based on the presence of rheumatoid factors in the sera of most RA patients (2). Rheumatoid factors are autoantibodies that are directed against the Fc fragment of IgG. Cellular immunity is also thought to be important because of the linkage of RA to certain MHC-encoded T cell restriction elements (e.g., DR4 and DR1 [3, 4]). Examination of RA synovial tissue shows high levels of proinflammatory cytokines IL-1 (5), TNF- α (6–8), IL-6 (6) and growth factors such as GM-CSF (7) and M-CSF (8), but the T cell-derived mediators IL-2 (8), IL-3 (8), IL-4 (9), and TNF- β (10) are either absent or present at low levels. These results have led some researchers to conclude that RA is not T cell driven (11) during the chronic phase of the disease.

While the proinflammatory cytokines are thought to play a role in inflammation, there is also a role for those cytokines that are negative immunoregulators and that are inhibitors of inflammation. IL-10 is presumed to repress expression of TNF- α and IL-1 in RA since it was found that a monoclonal antibody that neutralized IL-10 resulted in elevated levels of these proinflammatory cytokines from RA synovial cell cultures (12). More importantly, treatment of mice with anti-IL-10 antibody resulted in a worsening of the clinical score and raised the levels of the chemokines macrophage inflammatory protein-1 α (MIP-1 α) and MIP-2 in the joints of animals induced for type II collagen arthritis (13).

The inflammatory process observed in RA is mediated, in part, by chemotactic factors released by inflamed tissues. The proinflammatory cytokines IL-1 β and TNF- α are known to induce expression of small chemotactic proteins (i.e., chemokines) in a number of different cell types. Chemokines are subdivided into two major classes, C-X-C and C-C, depending on the position of the first two cysteines (14). Regulated upon activation, normal T cell expressed and secreted (RANTES; reference 15) and MIP-1 α (16, 17) are both members of the C-C chemokine family and have overlapping activities. Both of these chemokines can chemoattract T lymphocytes, although MIP-1 α preferentially attracts CD8⁺ cells (18, 19) while RANTES preferentially attracts CD4⁺ T lymphocytes (20). Both chemokines also attract monocytes (20, 21). Recently, MIP-1 α , and especially RANTES, have been shown to be able to activate T lymphocytes and promote T cell proliferation (21, 22). These data suggest that RANTES may be involved in

D.A. Barnes and J. Tse contributed equally to this work.

Address correspondence to Dr. Debra A. Barnes, Department of Immunology, Berlex Biosciences, 15049 San Pablo Avenue, Richmond, CA 94804-0099. Phone: 510-660-4075; FAX: 510-669-4244; E-mail: debra_barnes@berlex.com J. Tse's current address is Pharmaceutical Division, Bayer Corporation, Berkeley, CA 94701.

Received for publication 3 November 1997 and accepted in revised form 15 April 1998.

1. Abbreviations used in this paper: AIA, adjuvant-induced arthritis; CIA, collagen type II-induced arthritis; DARC, Duffy antigen receptor for chemokines; MIP-1 α , macrophage inflammatory protein-1 α ; RA, rheumatoid arthritis; RANTES, regulated upon activation, normal T cell expressed and secreted.

J. Clin. Invest.

© The American Society for Clinical Investigation, Inc.
0021-9738/98/06/2910/10 \$2.00

Volume 101, Number 12, June 1998, 2910–2919

<http://www.jci.org>

the clonal amplification of activated T cells indicating that RANTES can not only attract activated T cells but also induce the expansion of the activated population at local sites of RANTES production. RANTES and MIP-1 α mediate their effects through specific binding to high affinity receptors expressed on the surface of target cells (23). One of the receptors for these ligands, CCR1, is a member of a growing family of seven transmembrane domain, G protein-linked receptors (24).

Recently, it was found that rheumatoid synovial fibroblasts upregulate RANTES mRNA in response to IL-1 β , TNF- α , and γ IFN. Rathanswami et al. (25) demonstrated, by Northern hybridization analysis and ELISA, that cultured synovial fibroblasts isolated from rheumatoid patients were capable of expressing and producing RANTES and other chemokines in response to IL-1 β . Snowden et al. (26) have used reverse transcriptase-PCR to detect RANTES mRNA in four out of seven synovial tissue samples from rheumatoid arthritis patients. By contrast, osteoarthritis tissue does not express RANTES mRNA (26). These data constitute indirect evidence that RANTES may play a role in RA. The purpose of this study was to determine the role of RANTES in the development of the inflammatory process present in RA. This is only possible with the use of animal models and we have used an adjuvant-induced arthritis (AIA) model in Lewis rats. We also assessed the importance of other chemokines, including MIP-1 α and KC, in the AIA model by comparing control serum-treated animals to those in which chemokine production was blocked by treatment with polyclonal antibody. Our data indicates a specific role for RANTES in the mediation of the inflammatory and destructive aspects of AIA.

Methods

Antibody. Polyclonal antibody to recombinant human RANTES was prepared by injecting New Zealand white rabbits with purified RANTES (250 μ g per injection) subcutaneously in incomplete Freund's adjuvant followed by subsequent boosts in incomplete Freund's. The serum was collected and titered against immunogen. Titer of the antibody used in this study was 1/500,000 against human RANTES and 1/50,000 for rat RANTES. It did not react with any other chemokine tested including: MIP-1 α , MIP-1 β , MCP-1, KC, MIP-2, IL-1 β , TNF- α , or IL-6. Polyclonal antibody to mouse MIP-1 α was described previously (27) and had a titer of 1/1,000,000 for mouse MIP-1 α and cross reacted with rat MIP-1 α with a titer of 1/200,000. Polyclonal antibody to rat KC was obtained from PeproTech, Inc. (Rocky Hill, NJ) and had a titer of 1/200,000.

Adjuvant-induced arthritis. All animal studies were approved by the Berlex Biosciences Institutional Review Board. Adult male Lewis rats (160–170 g) were injected with 0.1 ml of CFA containing 10 mg/ml of *Mycobacterium butyricum* subcutaneously in the proximal quarter of the tail essentially as described previously (28). The day of injection is designated day 0. On days 3, 5, and 7, animals in a given study group were injected with the appropriate antibody or with normal rabbit serum (0.5 ml/injection per rat) i.p. Animals receiving indomethacin received i.p. injections of 0.5 mg/kg per day in sterile saline. Vehicle controls for these animals were i.p. injections of sterile saline solution alone. Animals were monitored periodically for body weight, measurement of swelling of each hind paw, degree of redness and flexibility of the rear ankle joints. Each characteristic was then assigned a subjective score of zero to four. The sum of these scores for each animal was determined and the total is designated as the clinical score, as described previously (29).

Radiological score. Whole body radiographs were taken on day

22 after induction and at the end of the study (day 34). Animals were anesthetized with sodium pentobarbital, 20 mg/kg. All radiographs were taken by a Raymax imager (Raymax Medical Corp., Ontario, Canada) at 25 mA, 50 kV for anteroposterior or 56 kV for lateral projections with Kodak Memmo Ready Pack film with a 3 s exposure (Eastman Kodak Co., Rochester, NY). A zero to three subjective grading system was then used to evaluate five different parameters including: degree of swelling, osteoporosis, cartilage loss, erosion, heterotopic ossification, and periosteal new bone formation all as described (29). The radiological score refers to the sum of the subjective scores for each of the above parameters.

Histopathological evaluation. After death, rat paws were resected above the ankle joint and fixed in buffered 10% formalin. After decalcification in 10% formic acid, the paws were sectioned longitudinally between digits one and two, and between three and four. These tissue blocks were embedded in paraffin and sectioned longitudinally until the tarsal, metatarsal, and phalangeal joints with adjacent bones and soft tissue were in view. Tissue sections 5- μ m thick were picked up on glass slides and stained with hematoxylin-eosin and evaluated for morphological changes and cellular infiltrate.

Chemokine determination. Blood was drawn into heparin-containing tubes (50 U/ml of blood). An aliquot of 100 μ l was removed and treated with 100 μ l of 1% Triton X-100 in PBS (1.0 mM NaH₂PO₄, 8.1 mM Na₂HPO₄, 154 mM NaCl, pH 7.2). Chemokines from ankle joints were assayed by first removing the hind feet and distal portion of the leg. The skin was removed and the tissue surrounding the ankle joint was dissected away from the bone. This tissue was placed in a tube containing lysis buffer (20 mM imidazole-HCl, pH 6.8, 100 mM KCl, 1 mM MgCl₂, 10 mM EGTA, 1.0% Triton X-100, 10 mM NaF, 1 mM sodium molybdate, 1 mM EDTA, 1 μ g/ml of leupeptin, aprotinin, and PEFA block) and frozen at -80°C. Samples were then thawed and allowed to sit at 4°C overnight. An aliquot of the lysate supernatant was removed and spun in a microfuge at 10,000 g for 5 min to remove insoluble material. The supernatant was assayed for presence of chemokines. The lysates were also assayed for presence of hemoglobin by measuring the absorbance at 450 nm compared with whole blood lysate using the method described previously (30).

Chemokines were assayed by the use of ELISA kits (R & D Systems, Inc., Minneapolis, MN). Because of the high degree of similarity maintained in chemokines across species, kits that used polyclonal antibodies for the detection of either mouse or human chemokines could also be used to detect the rat cognate provided that a standard curve was obtained using known concentrations of rat chemokine. Thus, rat RANTES was assayed using a kit to detect human RANTES except that the standard curve was obtained using rat RANTES (PeproTech, Inc.). MIP-1 α and KC levels were determined using kits that detect mouse chemokines and, in this case, standard curves were prepared using rat MIP-1 α and rat KC (both from PeproTech, Inc.). Optical densities were read at 450 nm using a V_{\max} kinetic microplate reader (Molecular Devices, Sunnyvale, CA).

Results

Chemokine production in AIA. Our initial question was aimed at determining whether there was any correlation with the inflammatory and destructive elements of AIA and the appearance of various chemokines in whole blood or joint. A number of different cells make up the cellular infiltrate of the pannus in RA, but the T lymphocytes and monocytes are postulated to play the most important roles. Therefore, it seemed reasonable to examine the role of chemokines such as RANTES and MIP-1 α that would be expected to attract these cell subsets. In addition we asked whether KC, a chemoattractant for neutrophils that have been postulated to play a role in RA (for review see reference 31) was involved in mediating the disease.

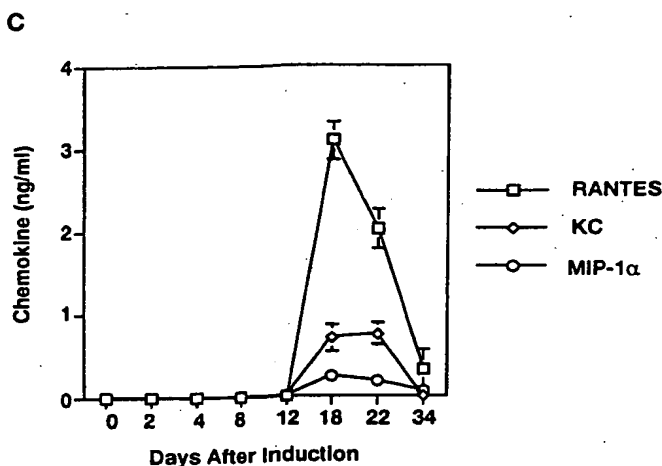
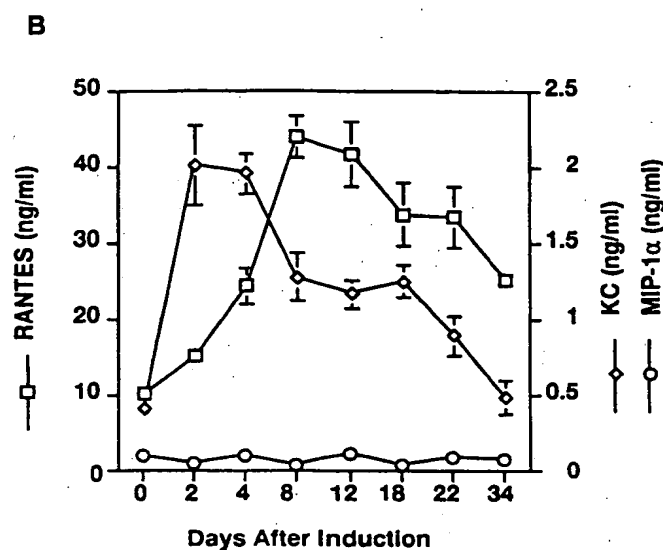
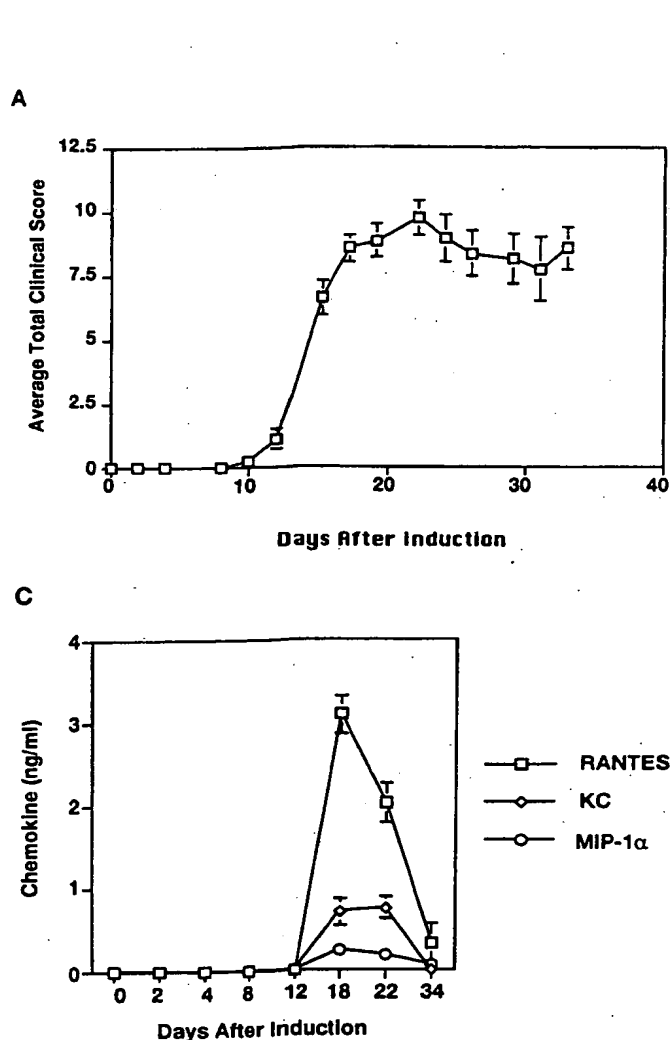


Figure 1. Chemokines and development of AIA. (A) The clinical score during the progression of AIA. Day 0 represents the time of induction. Each time point represents an average of five animals. The SEM is also given for each point. (B) Graph depicting the level of chemokines in whole blood as determined by ELISA. RANTES levels are represented by squares and concentrations are given on the left y axis, MIP-1α by circles and concentrations are given on the right y axis, KC by diamonds and their concentrations are given on the right y axis. Each point represents the average of five animals and the SEM is given. (C) Graph depicting the level of chemokines in the ankle joint. Graph designations are as in B. Each point represents the average of five animals and the SEM is given.

To determine the role of chemokines during the development of AIA, 35 Lewis rats were induced and a simple time course study was performed. In addition, as a control, three age-matched uninduced naive animals were included. Animals were induced on day 0 and five animals each were killed at each time point on days 2, 4, 8, 12, 18, 22, and 34. At the time of death, each animal was assessed for the clinical score. At that time blood samples were collected, x rays were taken, and joints were prepared. Blood and joint samples were frozen away at -80°C until all samples could be analyzed at the same time at the end of the study. X rays for all animals were also assessed at the end of the study. As shown in Fig. 1 A, animals do not show any signs of disease until day 12. From days 12 to 20, there is a steep increase in clinical score which then plateaus after day 20. The course of AIA is monophasic given that animals, once they become ill, maintain high clinical scores.

The degree of bone destruction with time was also followed using radiographic analysis. Data from the x rays were analyzed and scored with respect to swelling, osteoporosis, cartilage loss, erosion, heterotopic ossification, and periosteal new

bone formation. Addition of each of these individual numbers gives the radiological score. A study of the radiological score reveals that the bone destruction characteristic of AIA is just detectable at day 22, but the most deleterious symptoms are not seen until day 34 after induction (data not shown).

As shown in Fig. 1 B, KC in whole blood rises immediately after induction and then gradually declines until by the end of the study it has decreased to preinduction levels. MIP-1α, however, never increases and remains at very low levels in the blood (between 50–100 pg/ml) throughout the entire study. RANTES is found in normal animals in whole blood at very high levels (10 ng/ml) probably because of its presence in platelet granules. Whole blood was assayed rather than plasma as it was easier to maintain uniform treatment of samples and bypass the possibility of variable platelet activation. The RANTES levels rise and peak by days 8–12 and then fall. The rise in RANTES levels in the blood just precedes the onset of clinical signs of disease.

Because induction of chemokines in the blood was observed, we were interested to determine whether there would

also be an increase observed in the ankle joint of the affected animals. As shown in Fig. 1 C, there is no detectable chemokine in the joint through day 12. Maximal levels were detected at days 18–22, depending on the chemokine. At this point, there is a rise in RANTES as well as KC levels with RANTES being the greater of the two. Both RANTES and KC levels return to undetectable levels by day 34. There is also a very slight increase in the MIP-1 α levels as compared with those observed in whole blood. The MIP-1 α in the joint is between 200–250 pg/ml. It is unlikely that these increases are due to the leakiness of the vasculature surrounding the joint, otherwise one would expect to observe continued high levels of RANTES in the joint on day 34 because blood levels remained high (Fig. 1 B). However, to rule out this possibility, we measured the absorbance of the joint extract at 450 nm against a standard curve of whole blood. Absorbance at this wavelength gives an indication of the amount of hemoglobin present and allowed us to estimate the degree of contamination in the joint extract. With this approach we calculated that there was < 3% whole blood contamination of our cell extracts (data not shown). Therefore, at days 18–22 when RANTES is at its peak in the joint, the maximum amount of RANTES present in the joint due to contamination can be no more than 3% of the value in whole blood (35 ng/ml at days 18–22) and could account for 1 ng/ml. Since the actual measurement is 3 ng/ml, at least 2 ng/ml must be produced by those cells in the joint. Since MIP-1 α levels are higher in the joint than in the circulation this must be due to production of MIP-1 α in the local environment by resident cells. The fact that by day 34 all chemokine levels return to 0 suggests that RANTES, MIP-1 α , and KC may be downregulated in the cells making up the inflammatory response once the destructive process has been initiated.

RANTES is involved in the development of AIA. To determine whether RANTES played any role in the development of AIA, 30 Lewis rats were induced for disease and 5 age-matched naive control animals remained uninduced. Animals were induced on day 0. On days 3, 5, and 7, 10 animals received normal rabbit serum and ten received a polyclonal antibody directed against recombinant human RANTES. As a positive control, five animals that were induced on day 0 were given indomethacin (0.5 mg/kg per day in saline, i.p.) a nonsteroidal anti-inflammatory drug known to ameliorate the clinical effects of AIA through the inhibition of cyclooxygenase (32). These animals received indomethacin on day 0 and throughout the course of the study. Finally, five animals induced on day 0 were given a vehicle control (saline, i.p.) starting on day 0 and continuing through the course of the study. The negative control animals treated with either normal rabbit serum (control for the anti-RANTES-treated group) or with vehicle (control for the indomethacin-treated group) were necessary so that each group of animals would be handled in the same manner. It is well known that differential handling of the animals can lead to ambiguous results. All animals were assessed periodically for clinical score. On days 24 and 34, all animals were x rayed. On day 34, all of the anti-RANTES, serum control animals and naive animals were killed and joints were prepared for histopathological examination. Indomethacin and vehicle control animals were killed on day 42.

Clinical scores for this study are shown in Fig. 2. Animals which were treated with control serum or with vehicle had very high cumulative clinical scores. As with the study depicted in Fig. 1 A, clinical scores begin to rise on day 12 and

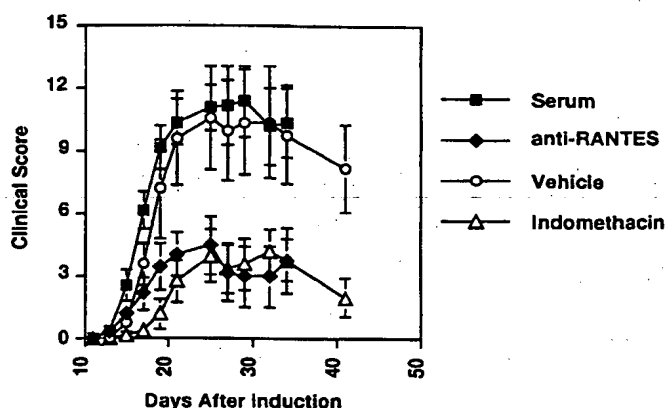


Figure 2. Anti-RANTES and indomethacin treatment ameliorate AIA. There were six animals in each study group. Study groups consisted of anti-RANTES-treated animals (black diamonds), animals given normal rabbit serum (black squares), animals treated with indomethacin (open triangles), and finally animals treated with a vehicle control for indomethacin (open circles). Each point represents the average and the SEM is shown.

peak by day 20–22. Animals which were treated with either the anti-RANTES antibody or with indomethacin never showed the high clinical scores associated with the disease.

Because the clinical score is associated with the inflammatory response we wanted to determine what effects anti-RANTES treatment had on histopathology. Fig. 3 shows the representative histopathological changes in these animals at day 34. First, examination of the synovial joint of naive animals at low magnification reveals that the space between the bones is completely clear (Fig. 3 A). Animals treated with normal rabbit serum have lost the integrity of the joint. This space now shows severe leukocyte infiltration and interstitial edema (Fig. 3 B). There is also significant bone erosion and periosteal new bone formation. By comparison the anti-RANTES-treated animals show relatively little infiltration (Fig. 3 C). The synovial lining is discerned at higher magnification (Figs. 3, D–F). In naive animals (Fig. 3 D) the synovial cells form a single layer and are flat and quiescent. No leukocyte infiltration is observed. In animals treated with control serum (Fig. 3 E) the synovial lining cells are round to cuboidal, suggesting active proliferation and form a layer two to three cells deep. The underlying connective tissues show infiltration by large numbers of lymphocytes. Irregularly-shaped mesenchymal cells (Fig. 3 E, arrowhead) are indicative of active differentiation. In the synovial tissues of anti-RANTES-treated rats (Fig. 3 F), fewer leukocytes are present and no active mesenchymal cells are seen. The synovial lining cells, however, are reactive with rounded somata and oval nuclei. Their cytoplasm is often pale and vacuolated. In some areas, these cells appear to be dissociating from the underlying connective tissue.

One of the hallmarks of the AIA model is that it results in severe destruction of the ankle joint with characteristic bone proliferation in soft tissue and concurrent erosion of pre-existing bony structures. This destruction can be assayed by radiographic analysis. An example of representative joints from each of the study groups is shown in Fig. 4, A–H. An animal that received the preimmune serum (Fig. 4, B and F) clearly

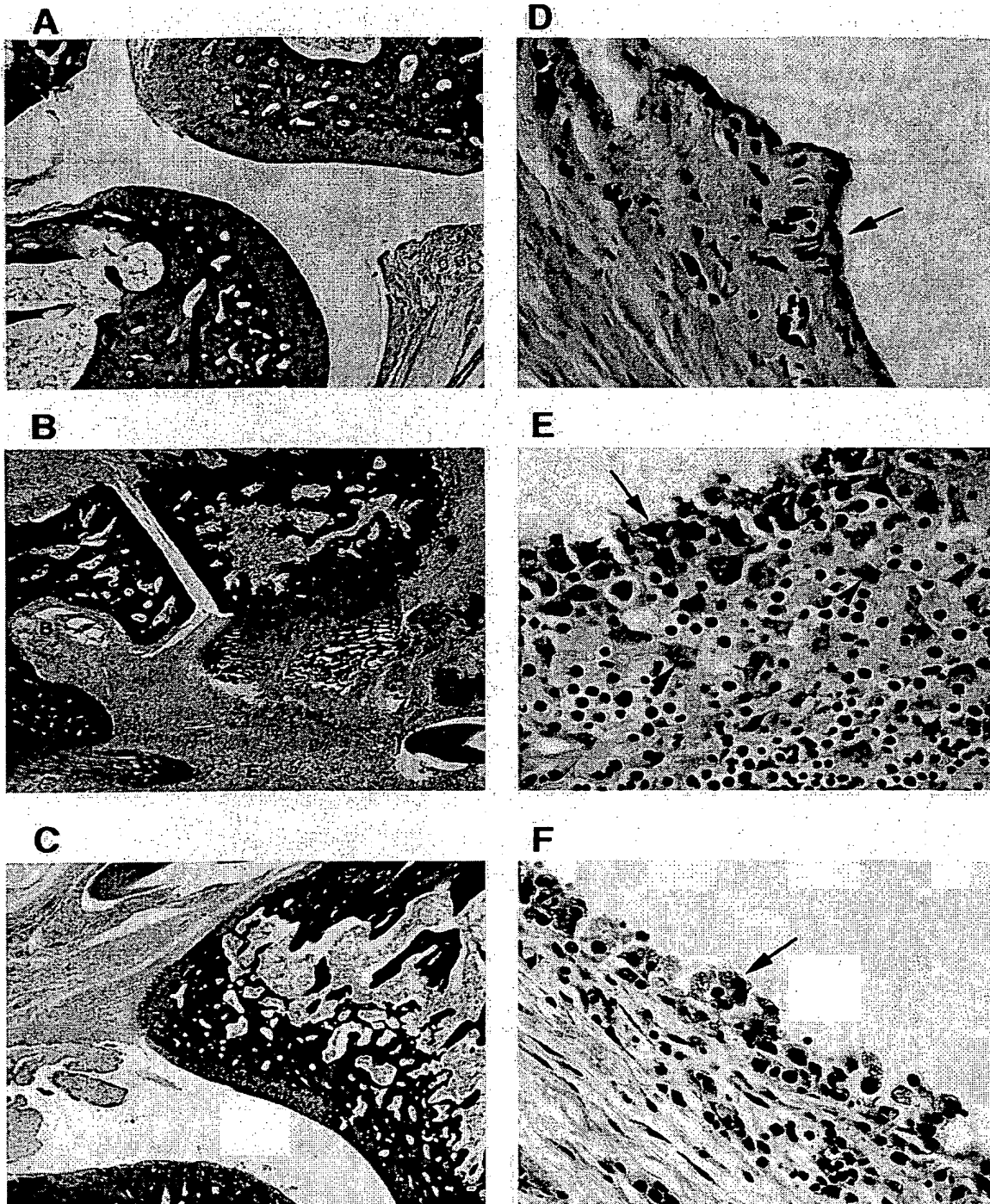


Figure 3. Anti-RANTES treatment reduces the severity of histopathological changes in AIA. *A, B, and C* show a synovial joint at a magnification of 5. *D, E, and F* show synovial tissues at a magnification of 40. *A* and *D* show naive rat joint; *B* and *E* show an arthritic joint from a rat treated with control serum; *C* and *F* show effects of treatment with anti-RANTES antibodies. *B* shows severe leukocyte infiltration (*L*), interstitial edema (*E*), periosteal new bone formation (*P*), and bone erosion (*B*). By comparison, the anti-RANTES-treated sample (*C*) shows very little infiltration. The arrows in *D, E, and F* point to the synovial lining. The arrowheads point to mesenchymal cells.

shows the destruction typically seen using this model. No significant destruction is seen in the naive animals (Fig. 4, *A* and *E*), the anti-RANTES-treated animals (Fig. 4, *C* and *G*), or in the indomethacin control animals (Fig. 4, *D* and *H*).

All of the animals killed in the study were evaluated for bone destruction using x-ray analysis. The summary of the radiological scores are graphed in Fig. 5. At 24 d there is no significant statistical difference between any of the study groups

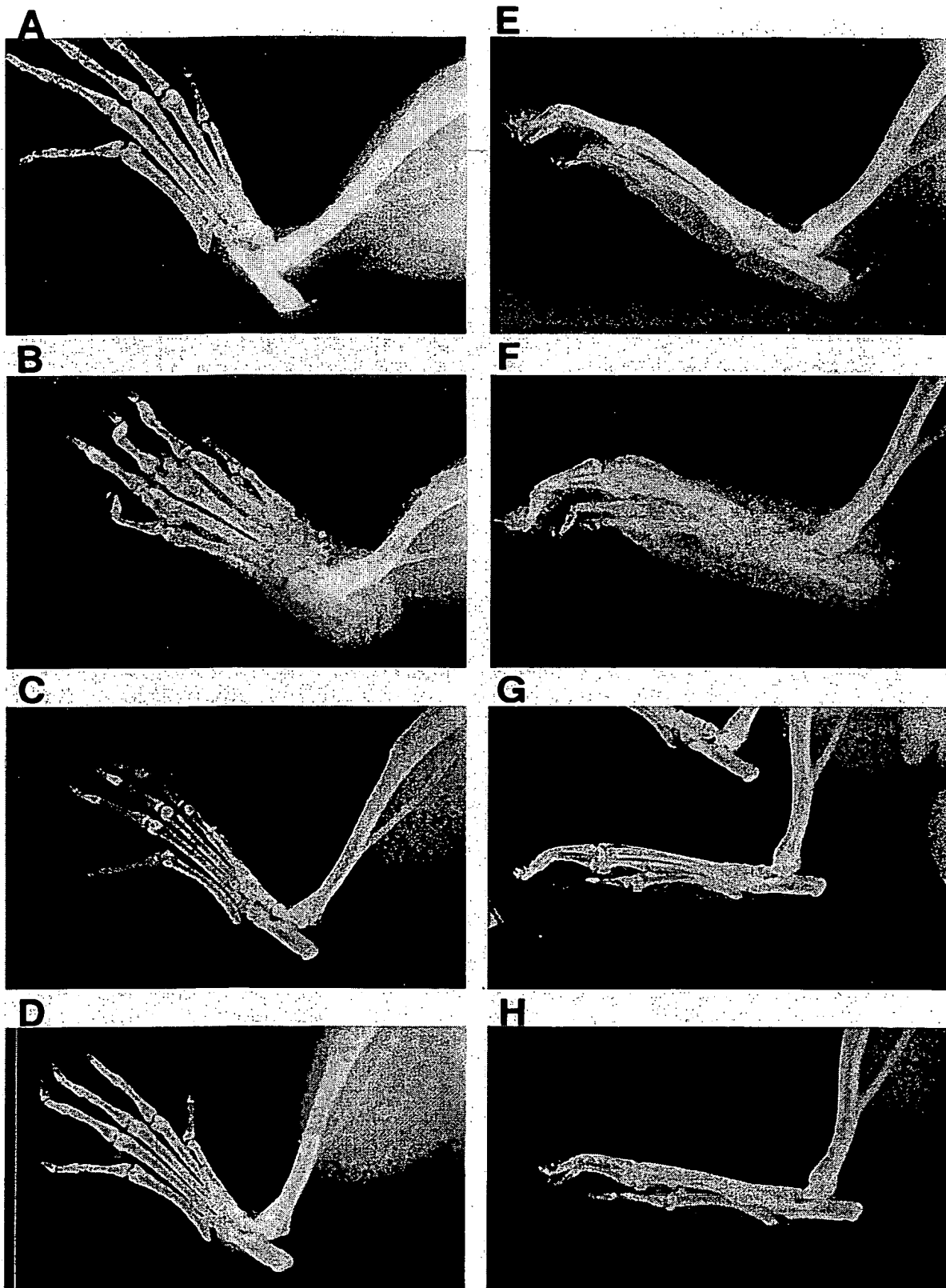


Figure 4. Anti-RANTES treatment reduces the level of bone destruction in A1A. *A, B, C, and D* represent anteroposterior radiographs and *E, F, G, and H* represent lateral radiographs. *A* and *E* are from naive animal, *B* and *F* are from serum control animal, *C* and *G* are from anti-RANTES treated animal, panel *D* and *H* are from an indomethacin-treated animal. Of particular note is the soft tissue swelling and heterotopic ossification.

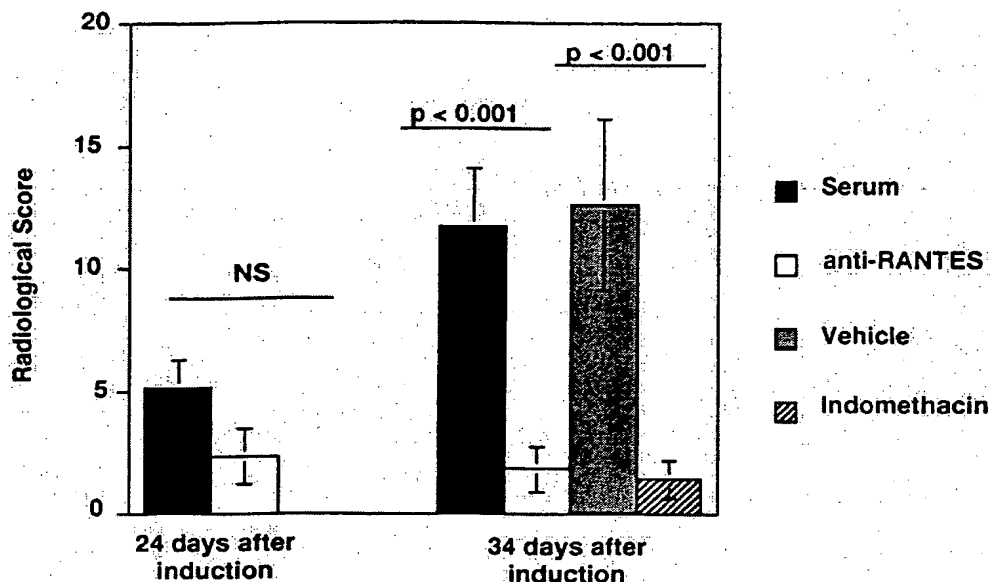


Figure 5. Anti-RANTES and indomethacin treatment reduce the radiographic score. Animals were scored on day 24 and day 34 using a subjective grading system described (29). Each graph represents the average of 6 animals and the SEM is given. Differences between study groups were evaluated using Fisher's test (41). The *P* values for the serum control and anti-RANTES-treated animals, however, have much reduced levels of RANTES in the joints. These data correlate with the lower clinical scores (Fig. 6 B) and with a reduced radiological score (data not shown) observed in the anti-RANTES animals and is a result of the prevention of the cellular infiltrate from reaching the target joint in the first place.

(Fig. 5, only anti-RANTES and serum control group are shown). By day 34, however, destruction has reached very high levels for those animals in the serum control and vehicle control groups. Radiological scores for animals treated with anti-RANTES or indomethacin have significantly lower scores. There is no statistical difference between the anti-RANTES-treated group and those given indomethacin.

These data strongly suggest that RANTES is important in the development of AIA and that pretreatment of the animals before onset of disease with an antibody directed against RANTES prevents the inflammation and destruction associated as efficiently as a known nonsteroidal anti-inflammatory, indomethacin.

Specific chemokine involvement in AIA. Because we had shown a role for RANTES in the development of AIA, and because RANTES and MIP-1 α are ligands for the chemokine receptor CCR1 (24), we wanted to determine whether MIP-1 α was involved in the pathophysiology of the disease. To answer this question various animal study groups were treated with polyclonal antibodies directed against either RANTES or MIP-1 α . Two groups of 16 animals were injected either with anti-RANTES, or with anti-MIP-1 α all as described in the previous study. In addition, 16 animals were injected with normal rabbit serum. 3 animals out of the 16 in both the anti-MIP-1 α and serum control group did not develop disease and were not included in the study. To maintain consistency, three animals from the anti-RANTES group that did not develop disease were also excluded from the study. Clinical scores were determined periodically. Half of the animals from each group were killed on day 22 and the remaining half were killed on day 34. At those times they were subjected to radiography.

Clinical scores from this study are given in Fig. 6A. Again, anti-RANTES is found to ameliorate the symptoms of AIA. Polyclonal antibody to MIP-1 α had no effect on amelioration of disease. This is interesting given the overlapping activities of these two chemokines. Polyclonal antibody to KC was also tested in this manner and had no effect on the course of the disease (data not shown).

The fact that anti-RANTES treatment before appearance of clinical symptoms has an effect on disease progress is shown most clearly by examining the level of this chemokine in the ankle joint itself. As shown in Fig. 6 B, RANTES levels in the serum control joint are high as expected at day 22 and drop back down again at day 34, the end of the study. The anti-RANTES-treated animals, however, have much reduced levels of RANTES in the joints. These data correlate with the lower clinical scores (Fig. 6 B) and with a reduced radiological score (data not shown) observed in the anti-RANTES animals and is a result of the prevention of the cellular infiltrate from reaching the target joint in the first place.

Discussion

The availability of animal models of human diseases makes possible the identification and analysis of factors involved in pathogenesis. The usefulness of a model is determined by its relative similarity to human disease, its reproducibility and its predictability with respect to responsiveness to therapeutic agents in comparison to human disease. Two widely used animal models of rheumatoid arthritis are collagen type II-induced arthritis (CIA) and AIA.

We have used the AIA model of RA in the Lewis rat to examine the role RANTES plays in the development of this disease. Unfortunately, there is no animal model available that perfectly mimics the course and features of human rheumatoid arthritis. Both AIA and CIA, however, show peripheral joint involvement, erosion, pannus formation, and T cell dependence (for review see reference 33) similar to that observed in human disease.

In this study, we determined the levels of the chemokines RANTES, MIP-1 α , and KC in AIA animals. We found very little change in the MIP-1 α levels in either whole blood or in the joint. The levels of KC in whole blood were elevated immediately after induction through day 4 and then were found to slowly decrease until they resumed preinduction levels by day 34. These data measure the total amount of KC in blood.

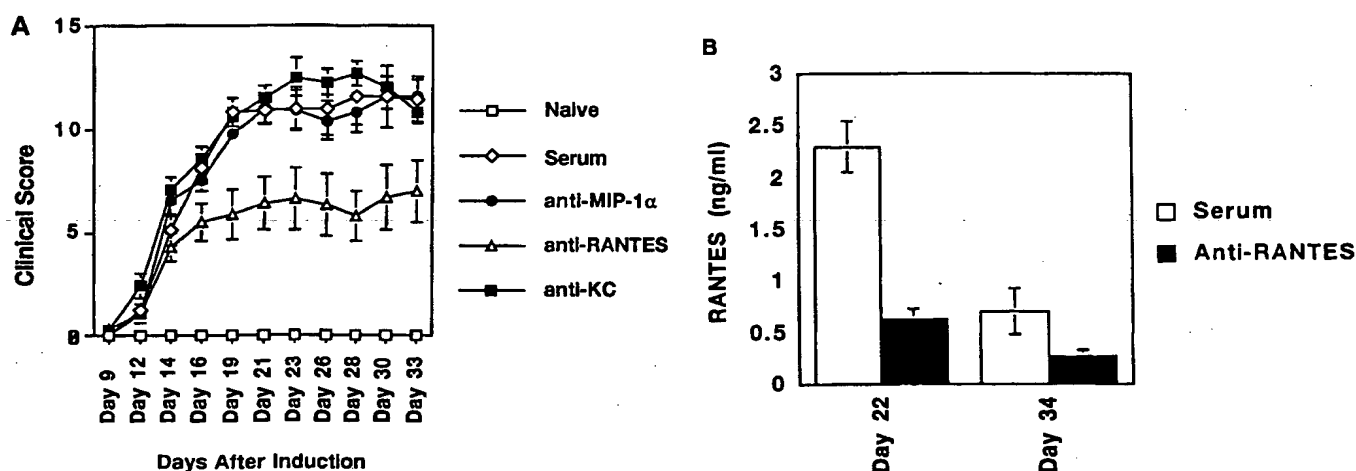


Figure 6. Development of AIA is chemokine specific. (A) Lewis rats were induced for AIA and injected on days 3, 5, and 7 with polyclonal antibody to RANTES (open triangles), MIP-1 α (black circles), KC (black squares), or normal rabbit serum (open diamonds). Each point represents the mean average. The SEM is also given. (B) RANTES levels in the joint of anti-RANTES-treated animals and serum-treated animals.

The circulating levels of KC in plasma are undetectable (Barnes, D.A., unpublished observation). This discrepancy may be due to the binding of KC to the Duffy antigen receptor for chemokines (DARC) which is found in abundance on the surface of red blood cells and binds this chemokine (34). It has been suggested that DARC serves as a receptor sink for a number of chemokines, including RANTES, and may be involved in clearing of these potent peptides (35). If this receptor plays a role in the modulation of RA, by clearing chemokines from the blood, one might expect that individuals that are Duffy negative would have more devastating disease. In fact, African Americans who are in large part Duffy negative have a much lower incidence of RA than the Caucasian population (36). This is primarily a result of the fact that African Americans do not generally carry the DR1 or DR4 markers. DR1 and DR4 are variants of the HLA-D locus and are highly correlated with appearance of rheumatoid factors in patients with RA. It would be interesting to determine whether Duffy negative individuals that are diagnosed with RA have more severe disease than those that are Duffy positive.

RANTES has an entirely different profile than KC and levels of this chemokine are not elevated until days 8–12, the time just before the onset of inflammation as measured by the clinical score. While the cellular source of this circulating RANTES is still unclear, the levels in circulation must be higher than can be removed by DARC, otherwise one would predict that an antibody that binds RANTES would have no effect since RANTES would be bound to DARC and unavailable to the antibody. Furthermore, because antibody was given in only three injections (days 3, 5, and 7) and would be predicted to be cleared from the animal after 3 d, it suggests that the RANTES generated in the circulation during the day 8–12 time period is critical to disease development.

Previously, it was shown that when mice were induced for CIA and passively immunized with antibodies directed against MIP-1 α or MIP-2 they had significantly decreased severity of disease (13). Unlike Kasama et al. (13), we did not find that

treatment with antibody to MIP-1 α had any ameliorating effect on disease. However, we used a different animal model in this study. The CIA model has a much longer time course (> 60 d) than the AIA model and the rise in clinical score is much more gradual. In addition, anti-MIP-1 α treatments in the form of F(ab)₂ fragments were provided throughout the study whereas in the AIA model, anti-RANTES treatment was limited to three injections before onset. Nevertheless, the actual amount of MIP-1 α detected at peak levels in the joints of afflicted CIA animals was quite low (200 pg/ml) and there appeared to be a very low level constitutive expression of MIP-1 α (100 pg/ml). These data agree well with our findings in the AIA model in the rat. The induction of MIP-2 observed in the CIA model was much greater, from < 100 pg/ml in naive animals to 800 pg/ml in CIA induced animals.

Our finding that antibodies to RANTES but not to MIP-1 α ameliorate disease in this RA model are interesting, particularly since both of these CC chemokines bind to similar receptors, CCR1 and CCR5 (23). How, then, can we explain our data? Interestingly, Cook et al. (37) have examined the *in vivo* biologic role of MIP-1 α in mice in which the gene encoding the chemokine has been disrupted. They showed that mice homozygous for MIP-1 α mutant (–/–) were resistant to Coxsackie virus-induced myocarditis but wild-type (+/+) mice were not. Obviously in this case MIP-1 α and RANTES have entirely separate effects. Further evidence that these two chemokines have distinct biological effects comes from findings by Karpus et al. (27) who have shown that antibodies to MIP-1 α ameliorate an EAE model of multiple sclerosis in the mouse. We have repeated these studies and not only confirm their data but show that antibodies to RANTES have no effect in this model (Barnes, D., and J. Tse, data not shown). Thus, it is possible that our data can be explained by assuming that RANTES effects in the AIA model of RA are produced by action through an as yet uncloned chemokine receptor or through a distinct signaling pathway, that MIP-1 α cannot trigger, through an existing receptor. In line with these specula-

tions, it is interesting that at least one group of investigators (21) has reported that T cells stimulated with RANTES and with MIP-1 α produce an increase in intracellular Ca at low nM concentrations. However, at higher concentrations RANTES but not MIP-1 α produces a second Ca²⁺ transient that is more sustained than the first and is not desensitized by pretreatment with MIP-1 α . These data show that RANTES can activate a novel chemokine receptor that is not sensitive to MIP-1 α and that activation of this receptor may play a role in this model of RA.

There is clear evidence that RANTES and MIP-1 α have distinctly different effects on T cells and monocytes, the major cell types involved in RA. For example a number of reports have demonstrated that RANTES affects the directed migration of CD4⁺ T cells and upregulates integrin expression, all effects that would culminate in the extravasation of T cells to sites of inflammation (18, 21). In contrast, it appears that MIP-1 α is mainly effective in inducing the directed migration of CD8⁺, but not CD4⁺, T cells. In addition to these cell-specific effects, RANTES is also about 10 times more potent than MIP-1 α in inducing T cell migration (18). Taken together, these data provide a partial explanation for the effects of RANTES on the RA model that we have investigated here and may speak for a specific effect of this chemokine in the human disease.

It has recently been shown that a human monocyte chemoattractant protein-1 (MCP-1) antagonist greatly ameliorated adjuvant arthritis-induced disease in a mouse MRL-lpr genetic background (38). MCP-1 is a chemokine with the ability to attract monocytes (39), the precursors of macrophages. The MRL-lpr disease model has an earlier onset than that observed in the rat AIA model, although, as with the AIA model, onset is rapid and the development from no detectable symptoms to peak clinical score occurs within a matter of days (generally from day 5–10). In these experiments, an MCP-1 peptide (amino acids 9–76) was synthesized and found to compete with MCP-1 for binding to monocytes. This antagonist, when given continually throughout the course of disease, resulted in decreased inflammation. However, the MCP-1 antagonist was given only through day 15 (after inflammation had already peaked) and then withdrawn. After withdrawal the disease progressed until swelling reached the same level as that observed in the untreated animals.

This is a very different pattern from what we observed with the RANTES antibody treatment. In our study anti-RANTES treatment ended on day 7. By day 11 one would predict that all of the rabbit polyclonal antibody had disappeared. Since peak inflammation is observed by day 18, the data suggest that early expression of RANTES in circulation is one of the critical steps involved in development of AIA. RANTES may be involved in initiating the inflammatory response because this chemokine has the potential to play key roles as both a chemoattractant and as an immunomodulator, since it also serves to activate and expand clonal T cell populations. It should also be noted that studies by Plater-Zyberk et al. (40) using an altered form of RANTES, met-RANTES, which acts as a CCR1 antagonist were also able to show efficacy in an animal model of RA. In their studies, delivery of the antagonist i.p. three times per week through day 21 resulted in the delay of onset and amelioration of CIA in DBA/1 mice. These data constitute additional proof for the role of RANTES in the development of disease.

If RANTES directs the initial response, what roles do other chemokines play in the development of AIA? It may be that the chemokines MIP-1 α and MCP-1 are expressed later in the course of disease and are involved in the destructive process of arthritis by their actions on the appropriate cell types once the initial inflammatory signal has been given.

We show here that RANTES is expressed in whole blood and in the joint of AIA animals and that antibody to RANTES can prevent development of disease. Thus, these data strongly support the concept that RANTES plays a pivotal role in the pathogenesis of RA. These potent proinflammatory effects and chemoattraction for T lymphocytes and monocytes makes RANTES an attractive candidate for therapeutic intervention. Furthermore, since RANTES binds to and mediates its biologic effects through the CCR1 receptor, this makes this receptor an important target for intervention therapy in RA and provides evidence in support of the notion that CCR1 antagonists will be useful therapeutics in the treatment of RA. Other useful therapeutic approaches could, for example, take the form of inhibitors of the cellular expression of RANTES. Finally, an anti-RANTES treatment regimen has the potential to serve not only as an anti-inflammatory agent, but also as a disease modifying antirheumatic drug.

Acknowledgments

The authors would like to thank Ms. Baby Martin-McNulty, Mr. Cornell Mallari and Ms. Wendy Fraser for technical assistance and Dr. Jean Merrill for a critical reading of this manuscript.

References

1. Harrison's Principles of Internal Medicine, 13th Ed. 1994. K.J. Isselbacher, E. Braunwald, J.D. Wilson, J.B. Martin, A.S. Fauci, and D.L. Kasper, editors. McGraw-Hill Inc., New York. 1437–1443.
2. Waller, M. 1969. Methods of measurement of rheumatoid factor. *Ann. NY Acad. Sci.* 168:5–16.
3. Stasny, P. 1978. HLA-D and Ia antigens in rheumatoid arthritis and systemic lupus erythematosus. *Arthritis Rheum.* 21:S139–S143.
4. Woodrow, T.C., F.E. Nichol, and G. Zaphiropoulos. 1981. DR antigens and rheumatoid arthritis: a study of two populations. *Br. Med. J.* 283:1287–1288.
5. Fontana, A., H. Hentgartner, K. Fehr, P.J. Grob, and G. Cohen. 1982. Interleukin-1 activity in the synovial fluid of patients with rheumatoid arthritis. *Rheumatol. Int.* 2:49–56.
6. Houssiau, F.A., J.-P. Devogelaer, J. van Damme, C. Nagant de Deuxchaisnes, and J. van Snick. 1988. Interleukin-6 in synovial fluid and serum of patients with rheumatoid arthritis and other inflammatory arthritides. *Arthritis Rheum.* 31:784–788.
7. Xu, W.D., G.S. Firestein, R. Taetle, K. Kaushansky, and N.J. Avallier. 1989. Cytokines in chronic inflammatory arthritis. II. Granulocyte-macrophage colony-stimulating factor in rheumatoid synovial effusions. *J. Clin. Invest.* 83:876–882.
8. Firestein, G.S., W.-D. Xu, K. Townsend, D. Broide, J. Alvaro-Gracia, A. Glasebrook, and N.J. Zvaifler. 1988. Cytokines in chronic inflammatory arthritis. I. Failure to detect T cell lymphokines (interleukin-2 and interleukin-3) and presence of macrophage colony-stimulating factor in rheumatoid synovitis. *J. Exp. Med.* 168:1573–1586.
9. Miossec, P., M. Naviliat, A.D. D'Angeac, J. Sany, and J. Bancherau. 1990. Low levels of interleukin-4 and high levels of transforming growth factor b in rheumatoid synovitis. *Arthritis Rheum.* 33:1180–1187.
10. Saxne, T., M.A. Palladino, D. Heinegard, N. Talal, and F.A. Wollheim. 1988. Detection of tumor necrosis factor as but not tumor necrosis factor b in rheumatoid arthritis synovial fluid and serum. *Arthritis Rheum.* 31:1041–1045.
11. Firestein, G.S., and N.J. Zvaifler. 1990. How important are T cells in chronic rheumatoid synovitis? *Arthritis Rheum.* 33:768–773.
12. Katsikis, P., C. Chu, F.M. Brennan, R.N. Maini, and M. Feldmann. 1994. Immunoregulatory role of interleukin 10 (IL-10) in rheumatoid arthritis. *J. Exp. Med.* 179:1517–1527.
13. Kasama, T., R.M. Strieter, N.W. Lukacs, P.M. Lincoln, M.D. Burdick, and S.L. Kunkel. 1995. Interleukin-10 expression and chemokine regulation during the evolution of murine type II collagen-induced arthritis. *J. Clin. Invest.* 95:2868–2876.

14. Oppenheim, J.J., C.O.C. Zachariae, N. Mukaida, and K. Matsushima. 1991. Properties of the novel proinflammatory supergene "intercrine" cytokine family. *Annu. Rev. Immunol.* 9:617-648.
15. Schall, T.J., J. Jongstra, B.J. Bradley, J. Dyer, J. Jorgensen, C. Clayberger, M. Davis, and A.M. Krensky. 1988. A human T cell-specific molecule is a member of a new gene family. *J. Immunol.* 141:1018-1025.
16. Brown, K.D., S.M. Zurawski, T.R. Mosmann, and G. Zurawski. 1989. A family of small inducible proteins secreted by leukocytes are members of a new superfamily that includes leukocytes and fibroblast-derived inflammatory agents, growth factors and indicators of various activation processes. *J. Immunol.* 142:679-687.
17. Zipfel, P.F., J. Balke, S.G. Irving, K. Kelly, and U. Siebenlist. 1989. Mitogenic activation of human T-cells induces two closely related genes which share structural similarities with a new family of secreted factors. *J. Immunol.* 142:1582-1590.
18. Taub, D.T., K. Conlon, A.R. Lloyd, J.J. Oppenheim, and D.J. Kelvin. 1993. Preferential migration of activated CD4⁺ and CD8⁺ T cells in response to MIP-1 α and MIP-1 β . *Science*. 260:355-358.
19. Schall, T.J., K. Bacon, D.R. Camp, J.W. Kaspari, and D.V. Goeddel. 1993. Human macrophage inflammatory protein α (MIP-1 α) and MIP-1 β chemokines attract distinct populations of lymphocytes. *J. Exp. Med.* 177:1821-1826.
20. Schall, T.J., K.B. Bacon, K.J. Toy, and D.V. Goeddel. 1990. Selective attraction of monocytes and T lymphocytes of the memory phenotype by cytokine RANTES. *Nature*. 347:669-671.
21. Bacon, K.B., B.A. Premack, P. Gardner, and T.J. Schall. 1995. Activation of dual T cell signaling pathways by the chemokine RANTES. *Science*. 269:1727-1730.
22. Taub, D.D., S.M. Turcovski-Corrales, M.L. Key, D.L. Longo, and W.J. Murphy. 1996. Chemokines and T lymphocyte activation. I. β chemokines co-stimulate human T lymphocyte activation in vitro. *J. Immunol.* 156:2095-2103.
23. Horuk, R. 1994. Molecular properties of the chemokine receptor family. *Trends Pharmacol. Sci.* 15:159-165.
24. Neote, K., D. DiGregorio, J.Y. Mak, R. Horuk, and T.J. Schall. 1993. Molecular cloning, functional expression, and signaling characteristics of a C-C chemokine receptor. *Cell*. 72:415-425.
25. Rathanaswami, P., M. Hachicha, M. Sadick, T.J. Schall, and S.R. McColl. 1993. Expression of the cytokine RANTES in human rheumatoid synovial fibroblasts. *J. Biol. Chem.* 268:5834-5839.
26. Snowden, N., A. Hajeer, W. Thomson, and B. Ollier. 1994. RANTES role in rheumatoid arthritis. *Lancet*. 343:547-548.
27. Karpus, W.J., N.W. Lukacs, B.L. McRae, R.M. Strieter, S.L. Kunkel, and S.D. Miller. 1995. An important role for the chemokine macrophage inflammatory protein-1 α in the pathogenesis of the T cell-mediated autoimmune disease, experimental autoimmune encephalomyelitis. *J. Immunol.* 155:5003-5010.
28. Pearson, C.M. 1956. Development of arthritis, peri-arthritis and periostitis in rats given adjuvants. *Proc. Soc. Exp. Biol. Med.* 91:95-101.
29. Ackerman, N.R., W.H. Rooks, L. Shott, H. Genant, P. Maloney, and E. West. 1979. Effects of Naproxen on connective tissue changes in the adjuvant arthritic rat. *Arthritis Rheum.* 22:1365-1374.
30. Horuk, R., A.W. Martin, W.Z.L. Schweitzer, A. Gerassimides, H. Guo, Z. Lu, J. Hesselgesser, H.D. Perez, J. Kim, J. Parker, et al. 1997. Expression of chemokine receptors by subsets of neurons in the central nervous system. *J. Immunol.* 158:2882-2890.
31. Edwards, S.W., and M.B. Hallett. 1997. Seeing the wood for the trees: the forgotten role of neutrophils in rheumatoid arthritis. *Immunol. Today*. 18:320-324.
32. Meade, E.A., W.L. Smith, and D.L. DeWitt. 1993. Differential inhibition of prostaglandin endoperoxide synthase (cyclooxygenase) isozymes by aspirin and other nonsteroidal antiinflammatory drugs. *J. Biol. Chem.* 268:6610-6614.
33. Oliver, S.J., and E. Brahn. 1996. Combination therapy in rheumatoid arthritis: the animal model perspective. *J. Rheumatol.* 23(Suppl. 44):56-60.
34. Horuk, R., A. Martin, J. Hesselgesser, T. Hadley, Z.-H. Lu, Z.-X. Wang, S.C. Peiper. 1996. The Duffy antigen receptor for chemokines: structural analysis and expression in the brain. *J. Leukocyte Biol.* 59:29-38.
35. Darbonne, W.C., G.C. Rice, M.A. Mohler, T. Apple, C.A. Hebert, A.J. Valente, and J.B. Baker. 1991. Red blood cells are a sink for Interleukin-8, a leukocyte chemotaxin. *J. Clin. Invest.* 88:1362-1369.
36. Marsh, W.L. 1975. Present status of the Duffy blood group system. *CRC Crit. Rev. Clin. Lab. Sci.* 5:387-412.
37. Cook, D.N., M.A. Beck, T.M. Coffman, S.L. Kirby, J.F. Sheridan, I.B. Pragnell, O. Smithies. 1995. Requirement of MIP-1 α for an inflammatory response to viral infection. *Science*. 269:1583-1585.
38. Gong, J.-H., L.G. Ratkay, J.D. Waterfield, and I. Clark-Lewis. 1997. An antagonist of monocyte chemoattractant Protein 1 (MCP-1) inhibits arthritis in the MRL-lpr mouse model. *J. Exp. Med.* 186:131-137.
39. Yoshimura, T., E.A. Robinson, S. Tanaka, E. Appella, J.-I. Kuratsu, and E.J. Leonard. 1989. Purification and amino acid analysis of two human glioma-derived monocyte chemoattractants. *J. Exp. Med.* 169:1449-1459.
40. Plater-Zyberk, C., A.J. Hoogwerf, A.E.I. Proudfoot, C.A. Power, and T.N.C. Wells. 1997. Effect of a CC chemokine receptor antagonist on collagen induced arthritis in DBA/1 mice. *Immunol. Lett.* 57:117-120.
41. Finney, D.J. 1964. Statistical methods in biological assay. Hafner Publishing Company, Inc., New York, NY. 25-30.

The Chemokine Receptors CXCR3 and CCR5 Mark Subsets of T Cells Associated with Certain Inflammatory Reactions

Shixin Qin,* James B. Rottman,* Paul Myers,* Nasim Kassam,* Michael Weinblatt,[‡] Marcel Loetscher,[‡] Alisa E. Koch,[§] Bernhard Moser,[‡] and Charles R. Mackay*

*LeukoSite, Inc., Cambridge, Massachusetts 02142; [‡]Brigham and Women's Hospital, Boston, Massachusetts 02150; [§]Northwestern University Medical School and Veterans' Administration Chicago Healthcare System, Lakeside Division, Chicago, Illinois 60611; [‡]Theodor-Kocher Institute, University of Bern, CH-3000-Bern-9, Switzerland

Abstract

T cells infiltrating inflammatory sites are usually of the activated/memory type. The precise mechanism for the positioning of these cells within tissues is unclear. Adhesion molecules certainly play a role; however, the intricate control of cell migration appears to be mediated by numerous chemokines and their receptors. Particularly important chemokines for activated/memory T cells are the CXCR3 ligands IP-10 and Mig and the CCR5 ligands RANTES, macrophage inflammatory protein-1 α , and macrophage inflammatory protein-1 β . We raised anti-CXCR3 mAbs and were able to detect high levels of CXCR3 expression on activated T cells. Surprisingly, a proportion of circulating blood T cells, B cells, and natural killer cells also expressed CXCR3. CCR5 showed a similar expression pattern as CXCR3, but was expressed on fewer circulating T cells. Blood T cells expressing CXCR3 (and CCR5) were mostly CD45RO⁺, and generally expressed high levels of β 1 integrins. This phenotype resembled that of T cells infiltrating inflammatory lesions. Immunostaining of T cells in rheumatoid arthritis synovial fluid confirmed that virtually all such T cells expressed CXCR3 and ~80% expressed CCR5, representing high enrichment over levels of CXCR3⁺ and CCR5⁺ T cells in blood, 35 and 15%, respectively. Analysis by immunohistochemistry of various inflamed tissues gave comparable findings in that virtually all T cells within the lesions expressed CXCR3, particularly in perivascular regions, whereas far fewer T cells within normal lymph nodes expressed CXCR3 or CCR5. These results demonstrate that the chemokine receptor CXCR3 and CCR5 are markers for T cells associated with certain inflammatory reactions, particularly TH-1 type

reactions. Moreover, CXCR3 and CCR5 appear to identify subsets of T cells in blood with a predilection for homing to these sites. (*J. Clin. Invest.* 1998. 101:746-754.) Key words: chemokines • inflammation • cell migration • antibodies • monoclonal • lymphocytes

Introduction

Leukocyte migration is essential for immune surveillance of the body's tissues, and for focusing immune cells to sites of antigenic challenge. The control of leukocyte migration depends on the combined actions of various adhesion molecules, as well as a vast array of chemotactic cytokines (chemokines) and their receptors. The role of adhesion molecules in leukocyte migration is well appreciated (1, 2), whereas that of different chemokines and their receptors is less certain. The chemokine receptors comprise two groups, the CC receptors 1-8 (CCR1-8)¹ that bind CC chemokines, and the CXC receptors 1-4 (CXCR1-4), which bind CXC chemokines (3-5). In general, the CC chemokines and their receptors effect the migration of monocytes, eosinophils, basophils, and T cells (6-8), whereas CXCR1 and CXCR2, which are the two IL-8 receptors, effect the migration of neutrophils (3).

The notion that CXC chemokines are generally poor chemoattractants for T cells has been challenged recently. Thus the CXC chemokine SDF-1 is a potent chemoattractant for blood T cells (9), and binds to CXCR4 (10, 11), a broadly expressed chemokine receptor (12). The CXC chemokines IP-10 and Mig, both inducible by interferon- γ during inflammation, also are effective T cell chemoattractants (13-15). IP-10 and Mig attract activated T cells, but not resting T cells. These two chemokines induce an increase in intracellular calcium by cells transfected with the cDNA for the chemokine receptor CXCR3, indicating that this is the likely IP-10/Mig receptor on T cells (14). By Northern blot analysis, CXCR3 is highly restricted to activated T cells and natural killer (NK) cells, and not to other leukocytes (14). Therefore IP-10 or Mig signaling appears to be an important mechanism for selective homing of activated/effector cells, which are known to accumulate preferentially at inflammatory sites (16), as well as in many tumors. IP-10 is expressed abundantly in various inflammatory lesions,

S. Qin and J.B. Rottman contributed equally to this work.

Address correspondence to Dr. Shixin Qin, LeukoSite, Inc., 215 First Street, Cambridge, MA 02142. Phone: 617-621-9350; FAX: 617-621-9349; E-mail: shixin_qin@leukosite.com Charles R. Mackay's current address is Millennium Biotherapeutics, Cambridge, MA 02139.

Received for publication 6 August 1997 and accepted in revised form 5 December 1997.

J. Clin. Invest.

© The American Society for Clinical Investigation, Inc.
0021-9738/98/02/0746/09 \$2.00

Volume 101, Number 4, February 1998, 746-754

http://www.jci.org

1. Abbreviations used in this paper: CCR, CC chemokine receptor; CXCR, CXC chemokine receptor; MCP, monocyte chemotactic protein; MIP, macrophage inflammatory protein; NK, natural killer; [Ca²⁺]_i, intracellular calcium concentration.

particularly those characterized by T cell infiltration, such as delayed type hypersensitivity responses in skin (17), in EAE (18), and in transplants undergoing rejection (19).

Another chemokine receptor expressed by T cells is CCR5, the receptor for RANTES, macrophage inflammatory protein-1 α (MIP-1 α), and MIP-1 β . CCR5 is expressed on activated and memory (CD45RO⁺) T cells (12, 20), which correlates with the finding that memory and activated T cells, but not naive T cells, respond to RANTES, MIP-1 α , and MIP-1 β in chemotaxis assays (21, 22). In addition, RANTES, MIP-1 α , and MIP-1 β are expressed in many inflammatory lesions (23). The assumption has been that different chemokines will attract particular types of leukocytes based on the ligand specificity and expression patterns of the relevant receptors. For instance, CCR5 and CXCR4 are expressed on T cells in a largely reciprocal fashion (12), and probably facilitate the positioning of two types of T cells in different tissues.

We now report on the distribution of CXCR3 and CCR5, particularly their association with inflammation. A striking finding was the high proportion of CXCR3⁺ and CCR5⁺ T cells in certain inflammatory lesions, compared with relatively low levels of CXCR3⁺ and CCR5⁺ T cells in blood or lymph node. In the blood, CXCR3, as well as CCR5, was expressed on a subset of circulating CD45RO⁺ and β 1 integrin^{hi} T cells, a phenotype consistent with previous activation. Moreover, the CCR5⁺ subset was contained entirely within the CXCR3⁺ subset. We conclude that these two chemokine receptors mark the majority of T cells within inflamed tissues, as well as peripheral blood T cells with a predilection for homing to these sites.

Methods

Cells, cell lines, and tissue culture. Normal human blood leukocytes were isolated as described (24). To generate CD3 blasts, 2×10^6 PBMC/ml in RPMI 1640 plus 10% FCS were added to tissue culture plates first coated with the anti-CD3 antibody TR66. After 4–6 d, blasts were removed to fresh media and supplemented with IL-2 (kindly provided by Antonio Lanzavecchia, Basel Institute for Immunology, Basel, Switzerland) at 50 U/ml. Other cell lines used included transfectants of the L1.2 murine pre B cell lymphoma, expressing high levels of either CXCR3 (this report), CXCR1 (25), CXCR2 (25), CCR2b, CCR4, CCR5 (26), or CCR1 (27). CXCR3 cDNA was obtained by PCR using a 5'-oligonucleotide primer and 3'-oligonucleotide primer which contained flanking XhoI and XbaI sites respectively. The PCR fragment was subcloned into the XhoI–XbaI sites of pCDNA3 (Invitrogen Corp., San Diego, CA), and the inserted gene was driven by a CMV promoter. Stable transfection of the DNA into a murine pre B lymphoma cell line (L1.2) was obtained as described (24). The cell surface expression of CXCR3 was monitored by ligand binding and Scatchard analysis. Transfectants were maintained in RPMI 1640 supplemented with 10% bovine serum and 800 μ g/ml G418.

mAb production and flow cytometry. mAbs reactive with CXCR3 were generated by immunizing BALB/C mice with 10 μ g of a 37-mer synthetic peptide corresponding to the first 37 NH₂-terminal amino acids of CXCR3 (14), five times over a period of 10 wk. This peptide was synthesized and coupled to purified protein derivative of tuberculin by the manufacturer (Severn Biotech Ltd., Kidderminster, United Kingdom). The first immunization was intraperitoneal with CFA, the second, third, and fourth were intraperitoneal with IFA, and the final immunization was intravenous with protein alone. 4 d after the last immunization, the spleen was taken and cell fusion performed using the cell line SP2/O, as described (28). Specific mAbs reactive with CXCR3 were identified using untransfected and CXCR3 transfected L1.2 cells, and immunofluorescent staining and analysis

using a FACScan[®] (Becton Dickinson, Mountain View, CA). The main mAb used in this study termed 1C6, is of isotype IgG1. Anti-CXCR3 mAbs were also generated by immunizing mice with CXCR3/L1-2 transfectant, in a similar manner to that described for anti-CCR3 and anti-CCR5 (20, 29).

mAbs to CCR5 have been described (20). PE-conjugated mAbs to CD4, CD8, CD14, CD19, CD25, CD26, CD29, CD69, CD45RO, CD45RA, and CD95 were supplied by PharMingen (San Diego, CA). To assess reactivity of mAbs against transfected cells or leukocytes, indirect immunofluorescence and flow cytometry were used. Cells were washed once with PBS, and resuspended in 100 μ l PBS containing 2% human serum and 0.1% sodium azide (staining buffer), 5 μ g/ml purified antibody, 5 μ g/ml isotype matched control mAb (Sigma Chemical Co., St. Louis, MO) or 50 μ l hybridoma culture supernatant. After 20 min at 4°C, cells were washed twice with staining buffer, and resuspended in 50 μ l FITC-conjugated affinity purified F(ab')₂ goat anti-mouse IgG (Jackson ImmunoResearch Labs., Inc., West Grove, PA). After 20 min, cells were washed twice in staining buffer and analyzed on the FACScan[®] to determine the level of surface expression. Propidium iodide was used to exclude dead cells. For multicolor analysis, PE- or FITC-conjugated mAbs were used together with biotinylated anti-CXCR3 mAb 1C6 to stain cells. After washing, the cells were incubated with Streptavidin-Red 670 (GIBCO BRL, Gaithersburg, MD). The results were analyzed by FACScan[®] using electronic gating and compensation.

Chemokines, chemotaxis assays, and ligand-binding assay. Recombinant human chemokines were obtained from PeproTech, Inc. (Rocky Hill, NJ). Chemotaxis of CD3 blasts was assessed using a modification of a transendothelial assay (7), using the cell line ECV304 as described (24). Cells that had migrated to the bottom chamber were placed in a tube, and relative cell counts were obtained using the FACScan[®].

¹²⁵I-labeled chemokines were obtained from DuPont-NEN (Boston, MA). The functional activity of radiolabeled IP-10 was tested in chemotaxis assays and was found to have 80% activity of unlabeled IP-10 (data not shown). Chemokine binding to target cells was carried out as described previously (24). Briefly, cells were resuspended in binding buffer (50 mM Hepes, 1 mM CaCl₂, 5 mM MgCl₂, 0.5% BSA) and incubated with radiolabeled ligand in the presence or absence of inhibitors. After 60 min at 37°C, cells were washed three times in binding buffer supplemented with 0.5 N NaCl and pellets were counted. All experiments were repeated at least three times. Curve fit and concentrations that inhibit 50% specific binding (IC₅₀) were calculated by Kaleidagraph software (Synergy Software, Inc., Reading, PA). Scatchard Plot analysis was carried out using Microsoft Excel.

Tissues and immunohistochemistry. Human tissues (normal and inflamed colon and vagina) were obtained from the National Disease Research Institute, a service organization funded by the National Institutes of Health. Synovial fluid was obtained from patients with rheumatoid arthritis.

Immunohistochemical analysis for CXCR3 was performed on frozen tissue samples. Briefly, tissue was sectioned at a thickness of 4 μ m, desiccated, and then fixed in 2% paraformaldehyde/0.5 X PBS for 10 min at 4°C. After PBS washing, nonspecific antibody binding sites were blocked with 10% normal goat serum/5% human AB serum/PBS for 30 min at room temperature. Next, the purified CXCR3 monoclonal antibody 1C6 was diluted to a concentration of 1 μ g/ml in 0.3% Triton X-100/0.2% Tween 20/1% FCS/5% human AB serum/0.1% sodium azide and applied to tissue sections overnight at 4°C. An isotype-matched irrelevant monoclonal antibody was used as a negative control on step sections of tissues (IgG1, MOPC21; Sigma Chemical Co.). Subsequently, biotinylated goat anti-mouse IgG (Vector Laboratories, Inc., Burlingame, CA) and avidin-biotin-alkaline phosphatase complexes (BioGenex Labs, San Ramon, CA) were added in sequence. Fast Red (BioGenex Labs), containing 2% levamisole to block endogenous alkaline phosphatase activity, was used as the chromogen and Mayers hematoxylin as the counterstain.

Results

CXCR3 is expressed by lymphocytes but not by other leukocyte types. mAbs have proven to be powerful tools for assessing the biology of various chemokine receptors (6, 25, 29), particularly CCR5 (12, 20). To study the functions of one of the important T cell chemokine receptors, CXCR3, specific mAbs were generated by immunizing mice either with synthetic peptides or with CXCR3 transfected cells (see Methods). These mAbs reacted specifically with CXCR3, as judged by FACS[®] staining of CXCR3 transfected L1.2 cells, and not wild-type L1.2 cells or L1.2 cells transfected with numerous other receptors. (Fig. 1 A). In peripheral blood, anti-CXCR3 mAbs were unreactive on neutrophils, monocytes, and eosinophils (not shown), as expected from previous analyses of CXCR3 expression by Northern blot, as well as functional responsiveness of cells to IP-10 (14). However the phenotypic analysis did reveal the expression of CXCR3 on a proportion of circulating lymphocytes (Fig. 1 B, day 0), observed in all (> 20) normal individuals examined. A feature of CXCR3, determined from previous studies on mRNA expression, is its expression on activated T cells (14). Staining of T cells activated by anti-CD3 confirmed that CXCR3 was expressed at high levels on these cells, but only after 5–8 d of activation, and in fact CXCR3 expression was downregulated immediately after activation (Fig. 1 B, day 3). This pattern of expression and regulation was similar to that observed for CCR5 (Fig. 1 B). Both CCR5 and CXCR3 were upregulated on long-term-activated IL-2-stimulated cells, and usually required 2–3 wk for peak expression (Fig. 1 B, day 21).

CXCR3 expression is skewed to previously activated/memory lymphocytes, but shows a broader pattern of expression than CCR5. A two color immunofluorescence analysis of peripheral blood lymphocytes showed that it was mostly CD3⁺ cells that expressed CXCR3, although a small proportion of B cells (CD19⁺) and NK cells (CD56⁺) also expressed this receptor (Fig. 2 A). A three color analysis of T cells, performed using anti-CD3-FITC to label T cells, showed that a

subset of both CD4⁺ cells and CD8⁺ cells expressed CXCR3. An analysis using markers of acute activation, such as CD25 and CD69, revealed that acutely activated T cells generally expressed this receptor, in contrast to CCR5 which is absent from such cells (12). CXCR3⁺ T cells were CD95⁺, CD45RO⁺, and CD45RA^{low}, a phenotype consistent with previous activation. We next compared the expression of CXCR3 with that of CCR5, since in peripheral blood, CCR5 is also expressed predominantly on previously activated T cells (20). In all instances, CCR5⁺ cells were contained entirely within the CXCR3⁺ subset, with CXCR3 being always expressed on more cells than CCR5 (Fig. 2 B). The subset of B cells expressing CXCR3 was assessed by gating on CD19⁺ lymphocytes. In general, CXCR3⁺ B cells expressed higher levels of β 1 integrins, however there was no strong correlation with IgD or CD11a expression (Fig. 2 C).

Activated T cell binding of IP-10 and chemotaxis is blocked by anti-CXCR3 mAb. In a previous study, IP-10 and Mig were found to signal through the chemokine receptor CXCR3 (14). To confirm that these two chemokines did in fact bind to CXCR3, and to gather information on the binding affinity and expression of CXCR3, studies were performed using radiolabeled IP-10. Fig. 3 A shows that ¹²⁵I-labeled IP-10 bound to anti-CD3-activated, IL-2-stimulated T cells, and this binding could be inhibited with increasing concentrations of unlabeled IP-10. Scatchard analysis revealed a K_d of 69 pM, and 11,000 receptors per cell (Fig. 3 A, insert). ¹²⁵I-labeled IP-10 binding to activated T cells could also be totally inhibited by unlabeled Mig, with a K_d of 90 pM (Fig. 3 A). To verify IP-10 indeed binds CXCR3, we carried out ligand binding assays using receptor transfectants. Only the CXCR3 transfected, but not parental L1.2 cells or other chemokine receptor transfected cells demonstrated significant binding activity to ¹²⁵I-labeled IP-10, with a similar affinity to that observed on activated T cells (data not shown). Another evidence to support IP-10 binding specifically to CXCR3 was obtained by blocking IP-10 binding with anti-CXCR3 mAbs. The ability of mAb 1C6 to inhibit ¹²⁵I-labeled IP-10 binding to activated T cells is shown in Fig. 3 B.

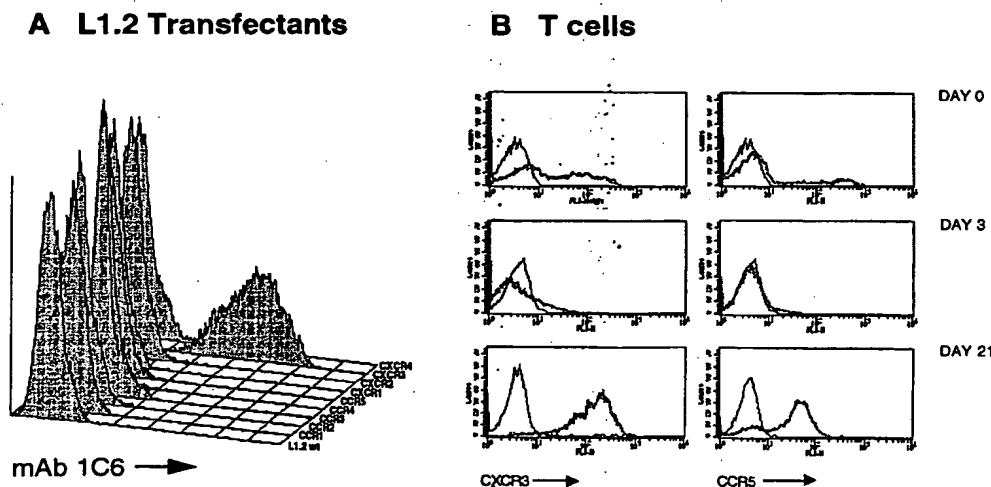
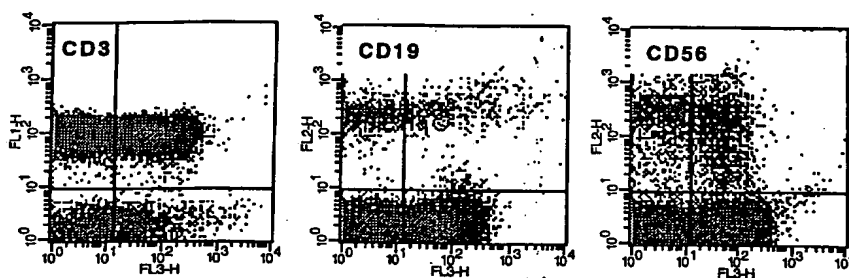


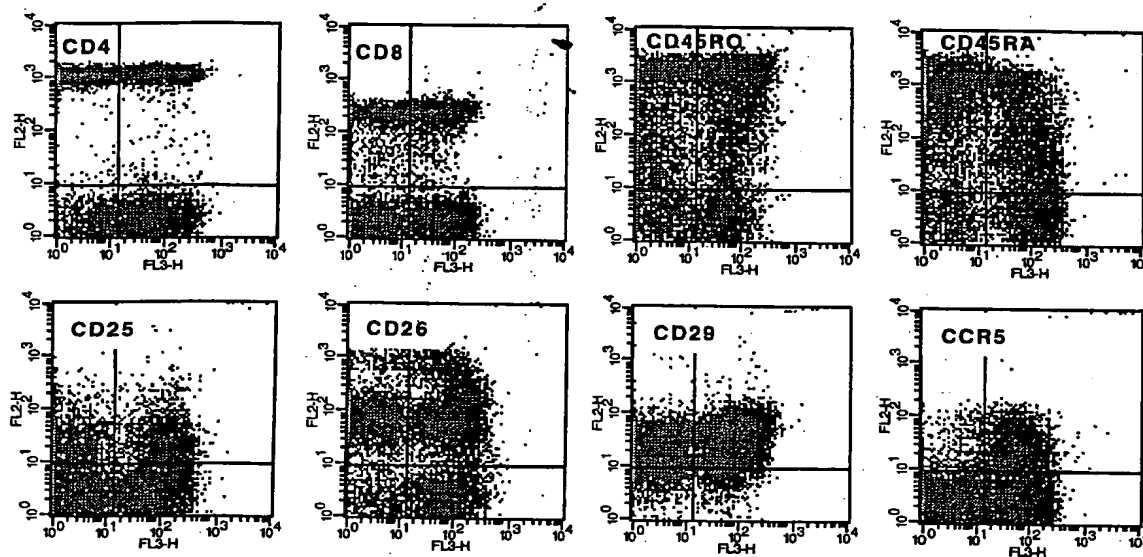
Figure 1. Identification of a CXCR3-specific mAb, expression of CXCR3 on activated T cells, and comparison with expression of CCR5. (A) mAb 1C6 staining of various L1.2 transfectants. Stable L1.2 transfectants expressing either CCR1, CCR2b, CCR3, CCR4, CCR5, CXCR1, CXCR2, CXCR3, and CXCR4 were stained with the anti-CXCR3 mAb 1C6. Negative control staining for all the L1.2 transfectants (not shown) resembled the staining shown for 1C6 on wt L1.2 cells. (B) Expression of CXCR3 and CCR5 on resting and activated T cells. Leukocyte subsets were identified in whole blood, by their forward angle and side scatter, and were gated accordingly. To gener-

erate CD3 blasts, PBMC were activated with anti-CD3 mAb, and were then maintained in media containing IL-2 for the indicated time periods. In each plot, the fainter profile represents staining with the anti-CXCR3 mAb 1C6, and the sharper profile staining with an isotype matched control mAb.

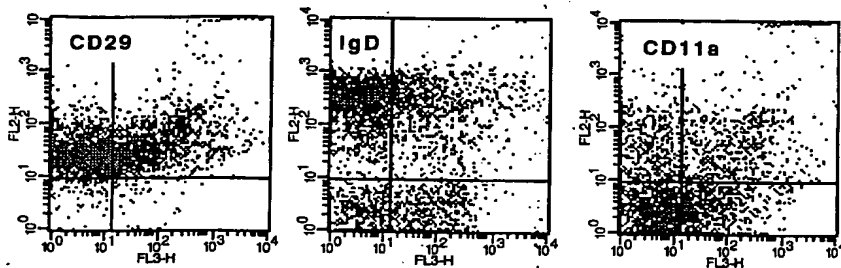
A blood lymphocytes



B CD3 gated



C CD19 gated



CXCR3 expression →

Figure 2. CXCR3 expression on various populations of blood lymphocytes. (A) Two color staining protocol was used to assess for expression of CXCR3 (horizontal axis) on T cells ($CD3^+$), B cells ($CD19^+$), and NK cells ($CD56^+$) as displayed on the vertical axis. (B) CXCR3 expression (horizontal axis) versus various markers (vertical axis), on the $CD3^+$ subset of blood lymphocytes, analyzed by three color immunofluorescence. Anti-CD3 FITC was used to stain T cells, and these cells were gated electronically for analysis. (C) CXCR3 expression on B cells ($CD19^+$). Quadrants were set according to the staining of control mAbs. The staining shown was representative of five donors analyzed.

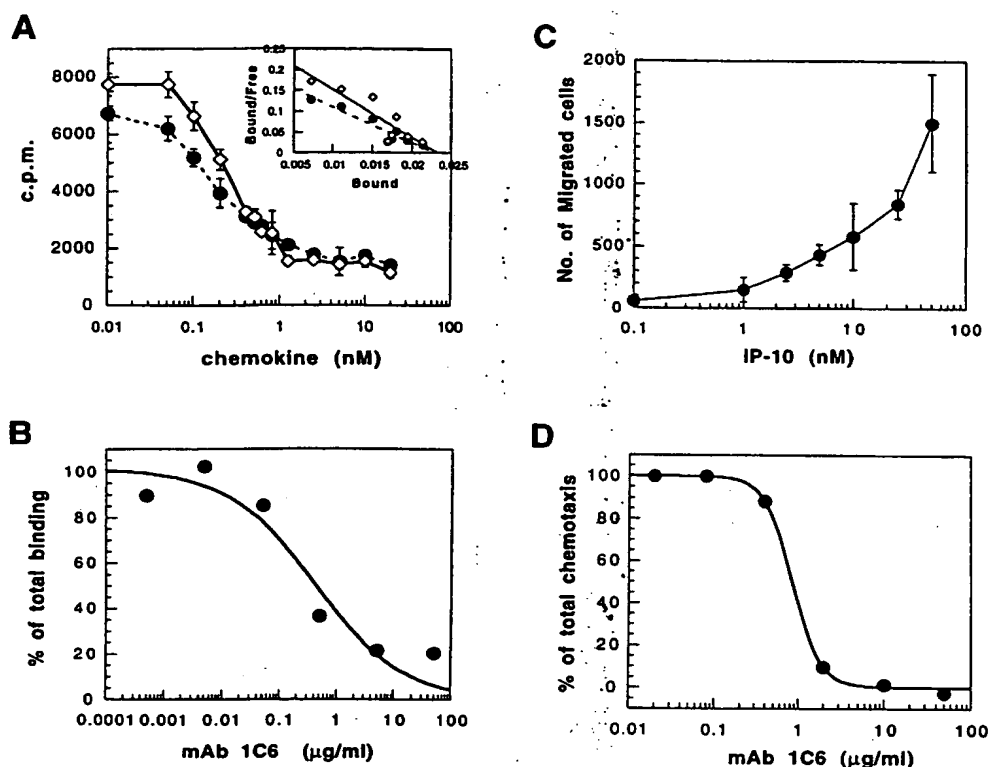


Figure 3. mAb 1C6 inhibition of IP-10 binding and chemotaxis. (A) High affinity binding of radiolabeled IP-10 to activated T cells. Human T cells were activated by anti-CD3 and IL-2 (CD3 blast cells) as described in Methods. The cells were incubated with 0.05 nM 125 I labeled IP-10 in the presence of increasing concentrations of unlabeled IP-10 (diamonds) or Mig (circles). From the competitive binding curve, Scatchard plot was calculated (inset) which gave 11,000 receptors per cell when either unlabeled IP-10 or Mig was used. The K_d s are 69 pM for IP-10 (diamonds), and 90 pM for Mig (circles). (B) mAb 1C6 inhibits 125 I-IP-10 binding to activated T cells. CD3 blasts were incubated with 0.05 nM 125 I-IP-10 in the presence of increasing concentrations of 1C6 as indicated. After 60 min at room temperature, cell pellets were washed and counted. The percentage of binding was calculated using the cpm of cells in the absence of mAb as 100%. The mAb 1C6 inhibited 50% of total binding at 160 ng/ml (IC_{50} = 160 ng/ml). (C) IP-10 mediated chemo-

taxis of activated T cells. Human CD3 blast cells were used in transendothelial chemotaxis assay towards increasing concentrations of IP-10. After 1.5 h, migrated cells were counted by flow cytometry. The number of cells in the absence of IP-10 was 57. The error bars represent SD of duplicate samples. (D) Inhibition of IP-10 mediated chemotaxis by anti-CXCR3 mAb. Human CD3 blast cell chemotaxis to 12.5 nM IP-10 was carried out in the presence of increasing concentrations of purified anti-CXCR3 mAb 1C6. The percentage of total chemotaxis was calculated using the number of cells migrated in the absence of mAb as 100%.

In this study, 5 μ g/ml of 1C6 was sufficient to achieve a total inhibition of binding, and an IC_{50} was calculated to be 160 ng/ml.

The high level expression of CXCR3 on activated T cells correlated with functional activities mediated by IP-10. In a transendothelial chemotaxis assay, activated T cells migrated to IP-10 in a dose-dependent fashion (Fig. 3 C). The number of migrated cells was similar to that induced by other CC chemokines known to induce T cell migration such as monocyte chemoattractant protein-1 (MCP-1) or MIP-1 β , ligands for CCR2 and CCR5 respectively. IP-10-mediated chemotaxis was entirely due to its interaction with CXCR3, since it was completely inhibited by 10 μ g/ml of mAb 1C6 (Fig. 3 D). The potency of this mAb to block chemokines was similar to that of other anti-chemokine receptor blocking mAbs (29).

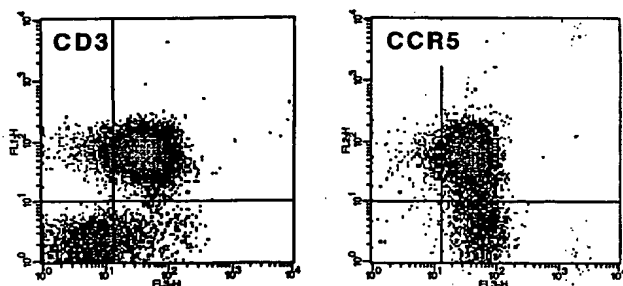
Predominance of CXCR3 $^{+}$ and CCR5 $^{+}$ lymphocytes in inflammatory sites. Rheumatoid synovial fluid is a useful source of inflammatory cells for examining features of leukocyte recruitment and function. T cells from RA synovial fluid, as well as from other inflammatory sites, have a characteristic phenotype: CD45RO $^{+}$, and high levels of adhesion molecules, such as β 1 integrins. This is similar to the phenotype of most CXCR3 $^{+}$ T cells in the blood. Lymphocytes from rheumatoid synovial fluid were assessed for CXCR3 and CCR5 expression, as well as a variety of other markers such as CD45RO. Fig. 4 A shows that synovial fluid T cells from an individual with RA were

97% CXCR3 $^{+}$, and 80% CCR5 $^{+}$, whereas blood T cells from the same individual, obtained at the same time, were only 35% CXCR3 $^{+}$, and 15% CCR5 $^{+}$ (Fig. 4 B). Similar results were obtained from three individual RA patients.

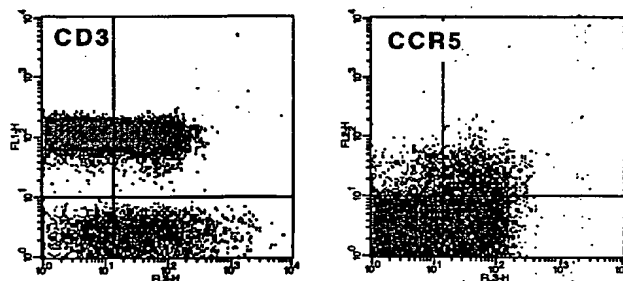
Microscopic examination of synovial biopsies from ten RA patients revealed multifocal, perivascular, variably sized accumulations of lymphocytes, lesser numbers of macrophages, and scattered neutrophils. Immunohistochemical analysis of the tissues revealed that in all biopsies, > 80% of perivascular lymphocytes were intensely immunoreactive for CXCR3 (Fig. 5 A). Lymphocytes distant from blood vessels were less intensely immunoreactive or unstained.

To determine if CXCR3 $^{+}$ lymphocytes were a prominent component of other inflammatory tissues, we performed immunohistochemical analyses of samples of chronically inflamed vaginal mucosa (n = 4) and colonic mucosa (n = 10). The vaginal samples consisted of intact squamous epithelium covering a submucosa that contained multifocal perivascular aggregates of lymphocytes, fewer macrophages and neutrophils, with lymphocytes scattered throughout the submucosa and vaginal epithelium. Immunohistochemical analysis of the tissue revealed that > 80% of perivascular lymphocytes (Fig. 5 B) and essentially 100% of the intraepithelial lymphocytes (not shown) were intensely immunoreactive for CXCR3. The colonic biopsy obtained from patients with ulcerative coli-

A synovial fluid lymphocytes



B blood lymphocytes



CXCR3 Expression



Figure 4. Expression of CXCR3 and CCR5 on synovial fluid T cells (A) and blood T cells (B) from rheumatoid arthritis patients. Synovial fluid lymphocytes and blood lymphocytes were stained for CXCR3, CCR5, and various other markers as described in Methods. Shown in the figure are CXCR3 staining versus CD3; and CXCR3 versus CCR5 gated on CD3⁺ cells. Quadrants were set based on control mAb staining. The staining shown was representative of three individuals analyzed.

tis, was characterized by focal ulceration of the colonic epithelium, and expansion of the lamina propria by large numbers of lymphocytes, fewer macrophages and neutrophils. Within the lamina propria infiltrate, > 70% of lymphocytes were immunoreactive for CXCR3, particularly below the area of epithelial ulceration. The actual proportion of cells expressing CXCR3 may be higher than this, since immunohistochemistry is not sensitive enough to detect low level receptor expression on the cell surface.

In contrast to inflamed tissues, a much lower percentage of T cells in normal lymph node expressed CXCR3 (Fig. 5 D). Approximately 20–30% of lymphocytes in the paracortex and medullary rays were immunoreactive for CXCR3, but only rare cells within cortical follicles were immunoreactive. Scattered CXCR3 immunoreactive lymphocytes were also identified within the subcapsular and medullary sinusoids. Other cell types such as smooth muscle, endothelium, and fibroblasts were uniformly nonimmunoreactive. CCR5 immunoreactive lymphocytes were fewer in number but similarly distributed. In contrast to CXCR3, CCR5 was expressed on medullary macrophages, as reported previously (20), endothelium and

vascular smooth muscle (Rottman, J.B., unpublished observations).

Discussion

Lymphocytes migrate through the body in a nonrandom fashion (2, 16). One of the best examples of this is the selective migration of activated/memory T cells to certain tissues and inflammatory lesions (30, 31). Activated and memory T cells express higher levels of some adhesion molecules that facilitate their binding to inflamed endothelium. Nevertheless, in many cases, the expression of adhesion molecules, per se, fails to explain the selectivity of a leukocyte for a particular tissue or microenvironment. The chemokines and their receptors represent another layer where selectivity can operate, possibly in combination with adhesion mechanisms. Some chemokine receptors are expressed on leukocytes in a highly restricted manner, notably CCR3, the eotaxin receptor, on eosinophils, basophils, TH2 cells (29, 32, 33), and the IL-8 receptors on neutrophils (6, 34). Just how important the chemokine system is for the selective localization of leukocyte subsets is uncertain, although inhibition of chemokines has profound effects on certain inflammatory reactions (23).

Given that chemokine receptors play a fundamental role for leukocyte migration, attention has focused on identifying relevant receptors on T cells. Until now, analyses of the precise role of various chemokine receptors on T cells has been difficult, since specific reagents have not been available. In this study, we identified, at the protein level, one of the important chemokine receptors for T cells, CXCR3. In earlier studies, Northern blot analysis indicated that CXCR3 was restricted to activated T cells (14). Staining of blood leukocytes with mAbs to CXCR3 revealed, however, that CXCR3 is much more widely expressed, for example on blood T cells, and a small proportion of B cells and NK cells. It is possible that the CXCR3 protein was produced during previous activation and remains displayed on, but no longer actively synthesized by peripheral blood lymphocytes. T cells activated *in vitro* express particularly high levels of CXCR3, which fits with our findings that IP-10 is one of the most potent chemoattractants for these cells, together with MCP-1 and the CCR5 ligands RANTES, MIP-1 α , and MIP-1 β . In fact, expression and regulation of CXCR3 were similar to that of CCR5, since both were found to be expressed by activated/memory T cells, and both showed the same pattern of downregulation and upregulation after T cell activation and IL-2 stimulation.

CXCR3 and CCR5 appear to mark subsets of lymphocytes with a capacity for migration to inflammatory sites. Identifying the nature of this lymphocyte subset is important for understanding the cellular and molecular mechanisms of inflammation, and for designing strategies for immunosuppression. CXCR3⁺ and CCR5⁺ T cells in blood are generally $\beta 1$ integrin^{hi}, CD45RO⁺, CD45RA^{low}, a phenotype consistent with previous activation. The T cells that infiltrate the inflamed synovium are also $\beta 1$ integrin^{hi}, CD45RO⁺, CD45RA^{low} (30, 35), and also CXCR3⁺ and mostly CCR5⁺ (this study). We still need to determine whether the actions of IP-10 or Mig, resulting in the recruitment of CXCR3⁺ lymphocytes, is the reason for the distinctive phenotype of migrating cells, or whether another chemokine such as a CCR5 ligand is responsible. An alternative explanation for the high expression of CXCR3 or CCR5 on inflammatory cells is upregulation by inflammatory

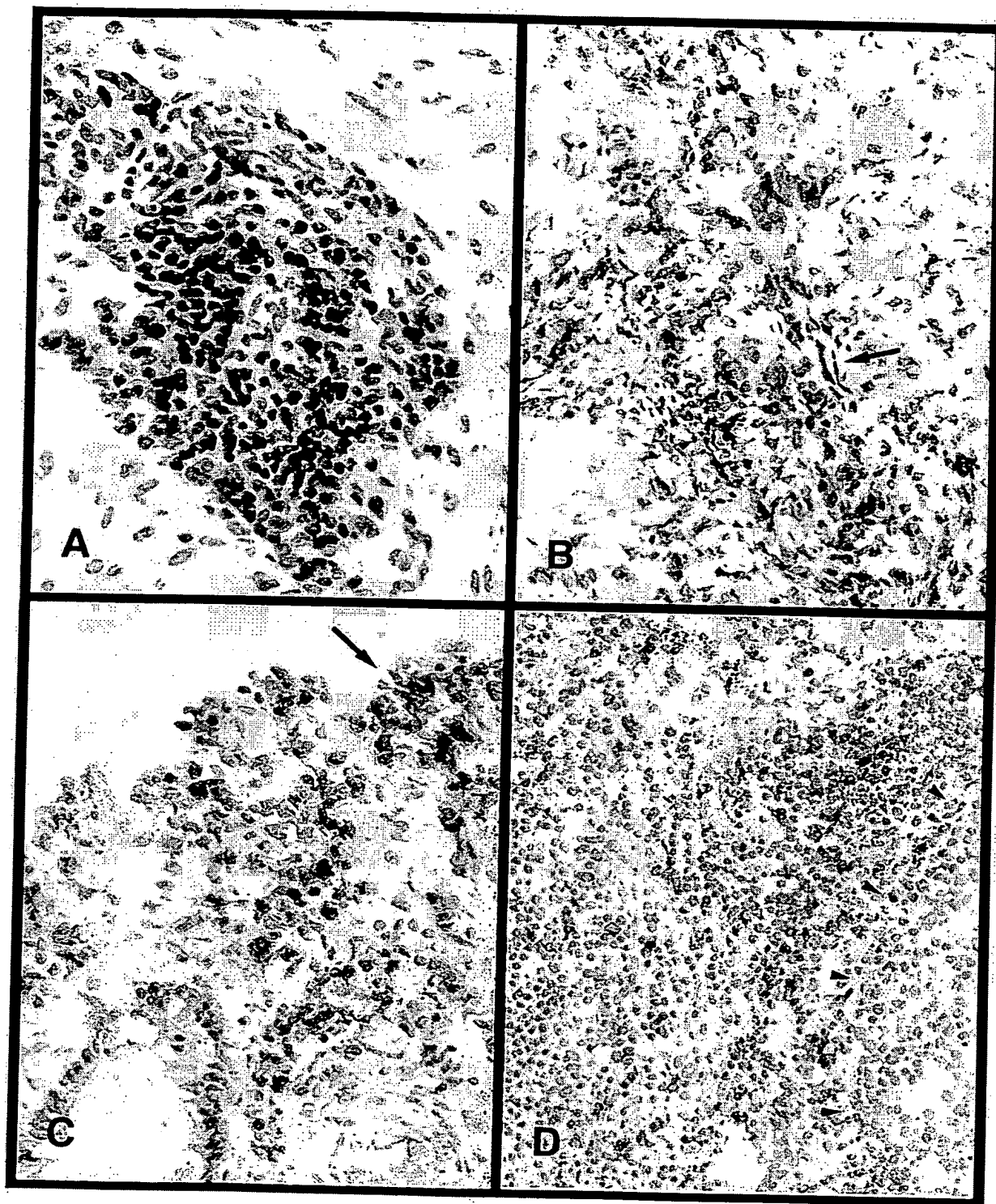


Figure 5. Enrichment of CXCR3⁺ lymphocytes in inflamed tissues. (A) Immunohistochemical detection of CXCR3 in a synovial biopsy from a patient with rheumatoid arthritis. A small blood vessel is surrounded by a thick aggregate of CXCR3 immunoreactive lymphocytes; $\times 200$. (B) Immunohistochemical detection of CXCR3 in chronic vaginitis. Numerous CXCR3 immunoreactive lymphocytes are present in the perivascular space (arrow) and adjacent stroma; $\times 100$. (C) Immunohistochemical detection of CXCR3 in ulcerative colitis. The superficial lamina propria contains numerous CXCR3⁺ lymphocytes immediately beneath an area of discontinuous colonic epithelium (arrow); $\times 200$. (D) CXCR3 Expression in a normal human lymph node. CXCR3⁺ cells are scattered throughout the paracortex. Rare CXCR3⁺ cells are present within lymphoid follicles (arrowheads).

cytokines, after extravasation. However, perivascular expression of CXCR3 (Fig. 5) and CCR5 (not shown) at the sites of inflammation and our finding that upregulation of CXCR3 and CCR5 in vitro takes many days would argue against these receptors being upregulated at the site of inflammation.

Blocking interaction of chemokines and their receptors should be useful therapeutically in autoimmune diseases or transplant rejection, in which particular receptors and their ligands may be responsible for the recruitment of cells. We have generated mAbs that effectively block CCR3 (29), CXCR1 (25), CXCR2 (25), and CCR5 (36). There is as yet no clarity on how chemokines bind to their 7-transmembrane receptors, although RANTES, MIP-1 α , and MIP-1 β have been found to bind to CCR5 through the second extracellular loop, and this can be blocked totally with a mAb specific for this loop (36). The anti-CXCR3 mAb 1C6 was able to inhibit completely the binding and chemotactic activity of IP-10 on activated T cells. mAb 1C6 is directed to the first 37 residuals of the NH₂ terminus, and so this region is of particular importance for ligand binding. Reactivity of 1C6 with shorter synthetic peptides narrowed the epitope to the first 15 amino acids (Qin, S., unpublished observations). The NH₂-terminal regions of CXCR1 and CXCR2 are also critical for IL-8 binding (25, 37), and the NH₂-terminal region of CCR2b is sufficient in itself to bind MCP-1 (38).

In conclusion, we have established that CXCR3 is expressed abundantly on human T cells, and particularly on those T cells associated with activation and inflammation, and the expression of CXCR3 closely resembled that of CCR5. We anticipate that an understanding of the role of these two receptors in inflammatory diseases, particularly those with a strong T cell involvement should help in the design of therapies to inhibit leukocyte recruitment and suppress adverse inflammatory reactions.

Acknowledgments

We thank Dr. Walter Newman and Dr. Craig Gerard for advice during the course of these experiments, Dr. Ian Clark-Lewis for the supply of certain chemokines, and Dr. Jim Campbell, Dr. Paul Ponath, Dr. Lijun Wu, and Dr. Greg LaRosa for various L1.2 chemokine receptor transfectants.

References

- Springer, T.A. 1994. Traffic signals for lymphocyte recirculation and leukocyte emigration: the multistep paradigm. *Cell* 76:301-314.
- Butcher, E.C., and L.J. Picker. 1996. Lymphocyte homing and homeostasis. *Science* 272:60-66.
- Baggiolini, M., B. Dewald, and B. Moser. 1997. Human chemokines: an update. *Annu. Rev. Immunol.* 15:675-705.
- Mackay, C.R. 1997. Chemokines: what chemokine is that? *Curr. Biol.* 7: R384-R386.
- Moser, B., M. Loetscher, L. Piali, and P. Loetscher. 1997. Lymphocyte responses to chemokines. *Int. Rev. Immunol.* In press.
- Qin, S., G. LaRosa, J.J. Campbell, H. Smith-Heath, N. Kassam, X. Shi, L. Zeng, E.C. Butcher, and C.R. Mackay. 1996. Expression of monocyte chemoattractant protein-1 and interleukin-8 receptors on subsets of T cells: correlation with transendothelial chemotactic potential. *Eur. J. Immunol.* 26:640-647.
- Carr, M.W., S.J. Roth, E. Luther, S.S. Rose, and T.A. Springer. 1994. Monocyte chemoattractant protein 1 acts as a T-lymphocyte chemoattractant. *Proc. Natl. Acad. Sci. USA* 91:3652-3656.
- Taub, D.D., P. Proost, W.J. Murphy, M. Anver, D.L. Longo, J. van Damme, and J.J. Oppenheim. 1995. Monocyte chemoattractant protein-1 (MCP-1), -2, and -3 are chemotactic for human T lymphocytes. *J. Clin. Invest.* 95:1370-1376.
- Bleul, C.C., R.C. Fuhlbrigge, J.M. Casasnovas, A. Aiuti, and T.A.

Springer. 1996. A highly efficacious lymphocyte chemoattractant, stromal cell-derived factor 1 (SDF-1). *J. Exp. Med.* 184:1101-1110.

10. Bleul, C.C., M. Farzan, H. Choe, C. Parolin, I. Clark-Lewis, J. Sodroski, and T.A. Springer. 1996. The lymphocyte chemoattractant SDF-1 is a ligand for LESTRE/fusin and blocks HIV-1 entry. *Nature* 382:829-833.

11. Oberlin, E., A. Amara, F. Bachelier, C. Bessia, J.-L. Virelizier, F. Arenzana-Seisdedos, O. Schwartz, J.-M. Heard, I. Clark-Lewis, D.F. Legler, M. Loetscher, M. Baggiolini, and B. Moser. 1996. The CXCR3 chemokine SDF-1 is the ligand for LESTRE/fusin and prevents infection by T cell line-adapted HIV-1. *Nature* 382:833-835.

12. Bleul, C.C., L. Wu, J.A. Hoxie, T.A. Springer, and C.R. Mackay. 1997. The HIV coreceptors CXCR4 and CCR5 are differentially expressed and regulated on human T lymphocytes. *Proc. Natl. Acad. Sci. USA* 94:1925-1930.

13. Taub, D.D., A.R. Lloyd, K. Conlon, J.M. Wang, J.R. Ortaldo, A. Harada, K. Matsushima, D.J. Kelvin, and J.J. Oppenheim. 1993. Recombinant human interferon-inducible protein 10 is a chemoattractant for human monocytes and T lymphocytes and promotes T cell adhesion to endothelial cells. *J. Exp. Med.* 177:1809-1814.

14. Loetscher, M.L., B. Gerber, P. Loetscher, S.A. Jones, L. Piali, I.C. Lewis, M. Baggiolini, and B. Moser. 1996. Chemokine receptor specific for IP-10 and Mig: structure, function and expression in activated T lymphocytes. *J. Exp. Med.* 184:963-969.

15. Liao, F., R.L. Rabin, J.R. Yannelli, L.G. Koniaris, P. Vanguri, and J.M. Farber. 1995. Human Mig chemokine: biochemical and functional characterization. *J. Exp. Med.* 182:1301-1314.

16. Mackay, C.R. 1993. Homing of naive, memory and effector lymphocytes. *Curr. Opin. Immunol.* 5:423-427.

17. Kaplan, G., A.D. Luster, G. Hancock, and Z.A. Cohn. 1987. The expression of a γ interferon-induced protein (IP-10) in delayed immune responses in human skin. *J. Exp. Med.* 166:1098-1108.

18. Ransohoff, R.M., T.A. Hamilton, M. Tani, M.H. Stoler, H.E. Shick, J.A. Major, M.L. Estes, D.M. Thomas, and V.K. Tuohy. 1993. Astrocyte expression of mRNA encoding cytokines IP-10 and JE/MCP-1 in experimental autoimmune encephalomyelitis. *FASEB (Fed. Am. Soc. Exp. Biol.) J.* 7:592-600.

19. Kondo, T., A.C. Novick, H. Toma, and R.L. Fairchild. 1996. Induction of chemokine gene expression during allogeneic skin graft rejection. *Transplantation (Baltimore)* 61:1750-1757.

20. Wu, L., W.A. Paxton, N. Kassam, N. Ruffing, J.B. Rottman, N. Sullivan, H. Choe, J. Sodroski, W. Newman, R.A. Koup, and R.C. Mackay. 1997. CCR5 levels and expression pattern correlate with infectability by macrophage-tropic HIV-1 in vitro. *J. Exp. Med.* 185:1681-1691.

21. Schall, T.J., K. Bacon, K.J. Toy, and D.V. Goeddel. 1990. Selective attraction of monocytes and T lymphocytes of the memory phenotype by cytokine RANTES. *Nature* 347:669-671.

22. Taub, D.D., K. Conlon, A.R. Lloyd, J.J. Oppenheim, and D.J. Kelvin. 1993. Preferential migration of activated CD4⁺ and CD8⁺ T cells in response to MIP-1 α and MIP-1 β . *Science* 260:355-358.

23. Strieter, R.M., T.J. Standiford, G.B. Huffnagle, L.M. Colletti, N.W. Lukacs, and S.L. Kunkel. 1996. "The good, the bad, and the ugly." The role of chemokines in models of human disease. *J. Immunol.* 156:3583-3586.

24. Ponath, P.D., S. Qin, D.J. Ringler, I. Clark-Lewis, J. Wang, N. Kassam, H. Smith, X. Shi, J.-A. Gonzalo, W. Newman, et al. 1996. Cloning of the human eosinophil chemoattractant, eotaxin: expression, receptor binding and functional properties provide a mechanism for the selective recruitment of eosinophils. *J. Clin. Invest.* 97:604-612.

25. Wu, L., N. Ruffing, X. Shi, W. Newman, D. Soler, C.R. Mackay, and S. Qin. 1996. Discrete steps in binding and signaling of interleukin-8 with its receptor. *J. Biol. Chem.* 271:31202-31209.

26. Wu, L., N. Gerard, R. Wyatt, H. Choe, C. Parolin, N. Ruffing, A. Borsetti, A.A. Cardoso, E. Desjardins, W. Newman, et al. 1996. CD4-induced interaction of primary HIV-1 gp120 glycoproteins with the chemokine receptor CCR-5. *Nature* 384:179-183.

27. Campbell, J.J., S. Qin, K.B. Bacon, C.R. Mackay, and E.C. Butcher. 1996. The biology of chemokine and classical chemoattractant receptors: differential requirements for adhesion-triggering versus chemotactic responses in lymphoid cells. *J. Cell Biol.* 134:255-266.

28. Coligan, J.E., A.M. Kruisbeek, D.H. Margulies, E.M. Shevach, and W. Strober. 1992. Current Protocols in Immunology. John Wiley and Sons, New York. 2.5.1-2.5.12.

29. Heath, H., S. Qin, P. Rao, L. Wu, G. LaRosa, N. Kassam, P. Ponath, and C.R. Mackay. 1997. Chemokine receptor usage by human eosinophils. The importance of CCR3 demonstrated using an antagonistic monoclonal antibody. *J. Clin. Invest.* 99:178-184.

30. Pitzalis, C., G. Kingsley, D. Haskard, and G. Panayi. 1988. The preferential accumulation of helper-inducer T lymphocytes in inflammatory lesions: evidence for regulation by selective endothelial and homotypic adhesion. *Eur. J. Immunol.* 18:1397-1404.

31. Salmi, M., D.P. Adrew, E.C. Butcher, and S. Jalkanen. 1995. Dual binding capacity of mucosal immunoblasts to mucosal and synovial endothelium in humans: dissection of the molecular mechanisms. *J. Exp. Med.* 181:137-149.

32. Uguccioni, M., C.R. Mackay, B. Ochsenberger, P. Loetscher, S. Rhis, G. LaRosa, P. Rao, P. Ponath, M. Baggiolini, and C.A. Dahinden. 1997. High ex-

pression of the chemokine receptor CCR3 in human blood basophils. Role in activation by eotaxin, MCP-4 and other chemokines. *J. Clin. Invest.* 108:1137-1143.

33. Sallusto, F., C.R. Mackay, and A. Lanzavecchia. 1997. Selective expression of the eotaxin receptor CCR3 by human T helper 2 cells. *Science*. 277: 2005-2007.

34. Chuntharapai, A., J. Lee, C.A. Hebert, and K.J. Kim. 1994. Monoclonal antibodies detect different distribution patterns of IL-8 receptor A and IL-8 receptor B on human peripheral blood leukocytes. *J. Immunol.* 153:5682-5688.

35. Oppenheim-Marks, N., and P.E. Lipsky. 1997. Migration of naive and memory T cells. *Immunol. Today*. 18:456-457.

36. Wu, L., G. LaRosa, N. Kassam, C.J. Gordon, H. Heath, N. Ruffing, H.

Chen, J. Humblas, M. Samson, M. Parmentier, et al. 1997. Interaction of chemokine receptor CCR5 with its ligands: multiple domains for HIV-1 gp120 binding and a single domain for chemokine binding. *J. Exp. Med.* 186:1373-1381.

37. Chuntharapai, A., J. Lee, J. Burnier, W.I. Wood, C. Hebert, and K.J. Kim. 1994. Neutralizing monoclonal antibodies to human IL-8 receptor A map to the NH2-terminal region of the receptor. *J. Immunol.* 152:1783-1789.

38. Monteclaro, F.S., and I. Charo. 1996. The amino-terminal extracellular domain of the MCP-1 receptor, but not the RANTES/MIP-1alpha receptor, confers chemokine selectivity. Evidence for a two-step mechanism for MCP-1 receptor activation. *J. Biol. Chem.* 271:19084-19092.

Enhanced expression of eotaxin and CCR3 mRNA and protein in atopic asthma. Association with airway hyperresponsiveness and predominant co-localization of eotaxin mRNA to bronchial epithelial and endothelial cells

Sun Ying¹, Douglas S. Robinson¹, Qiu Meng¹, James Rottman², Russ Kennedy², Douglas J. Ringler², Charles R. Mackay², Bruce L. Daugherty³, Martin S. Springer³, Stephen R. Durham⁴, Timothy J. Williams⁵ and A. Barry Kay¹

¹ Allergy and Clinical Immunology, National Heart and Lung Institute, Imperial College School of Medicine, London, GB

² Leukosite Inc., Cambridge, USA

³ Merck Research Laboratories, Rahway, USA

⁴ Upper Respiratory Medicine National Heart and Lung Institute, Imperial College School of Medicine, London, GB

⁵ Applied Pharmacology, National Heart and Lung Institute, Imperial College School of Medicine, London, GB

Eotaxin is a newly discovered C-C chemokine which preferentially attracts and activates eosinophil leukocytes by acting specifically on its receptor CCR3. The airway inflammation characteristic of asthma is believed to be, at least in part, the result of eosinophil-dependent tissue injury. This study was designed to determine whether there is increased expression of eotaxin and CCR3 in the bronchial mucosa of asthmatics and whether this is associated with disease severity. The major sources of eotaxin and CCR3 mRNA were determined by co-localization experiments. Bronchial mucosal biopsy samples were obtained from atopic asthmatics and normal non-atopic controls. Eotaxin and CCR3 mRNA were identified in tissue sections by *in situ* hybridization (ISH) using radiolabeled riboprobes and their protein product visualized by immunohistochemistry (IHC). Co-localization experiments were performed by double ISH/IHC. Eotaxin and CCR3 (mRNA and protein) were significantly elevated in atopic asthmatics compared with normal controls. In the asthmatics there was a highly significant inverse correlation between eotaxin mRNA⁺ cells and the histamine provocative concentration causing a 20% fall in FEV₁ (PC₂₀). Cytokeratin-positive epithelial cells and CD31⁺ endothelial cells were the major source of eotaxin mRNA whereas CCR3 co-localized predominantly to eosinophils. These data are consistent with the hypothesis that damage to the bronchial mucosa in asthma involves secretion of eotaxin by epithelial and endothelial cells resulting in eosinophil infiltration mediated via CCR3. Since selective (eotaxin) and non-selective C-C chemokines such as RANTES, MCP-3 and MCP-4 all stimulate eosinophils via CCR3, this receptor is potentially a prime therapeutic target in the spectrum of diseases involving eosinophil-mediated tissue damage.

Key words: Eotaxin / CCR3 / Asthma

Received Sept. 9, 1997;
accepted Oct. 15, 1997.

1 Introduction

There is substantial evidence that injurious agents released from infiltrating eosinophil leukocytes make an important contribution to the airway inflammation characteristic of asthma [1–3]. Eosinophil recruitment from

[17493]

the microcirculation of the airways is initiated by locally generated soluble chemical signals, i.e. "chemoattractants". The selective recruitment of eosinophils in allergic reactions suggests that endogenous chemoattractants specific for this leucocyte type are important *in vivo*.

Recently, a potent eosinophil chemoattractant protein has been purified and sequenced from bronchoalveolar fluid of allergen-challenged, sensitized guinea pigs [4, 5].

This protein, a C-C chemokine named "eotaxin", was shown to be highly selective for eosinophils [5]. The high potency of guinea pig eotaxin on human eosinophils [5] provided evidence for the existence of a human eotaxin homologue and a human eotaxin receptor. Primers based on the guinea pig protein sequence were used to obtain the cDNA of guinea pig eotaxin [6, 7], mouse eotaxin [7, 8] and human eotaxin [9-11]. The three known eotaxins are all highly potent and selective eosinophil chemoattractants. The gene for human eotaxin maps to chromosome 17 and the peptide is expressed constitutively in several organs and tissues. Subsequently, an eotaxin receptor designated CCR3 has been identified [11-13]. This G protein-coupled, 7-transmembrane-domain receptor is present in high numbers on human eosinophils and, unlike other members of the C-C chemokines which generally act on several receptors, eotaxin only signals via the CCR3 receptor. Other C-C chemokines, e.g. RANTES and MCP-3, also bind to the CCR3 receptor but with lower affinity [12, 13]. RANTES [14], MCP-3 [15] and the recently described MCP-4 [16, 17] all have the ability to stimulate eosinophils with varying potency, but they are nonselective and stimulate other cell types, such as monocytes and T cells, in addition (reviewed in [18]). A further C-C chemokine, eotaxin-2, has recently been cloned and expressed [19]. This protein exhibits *in vitro* activity similar to eotaxin.

There have been extensive studies on the role of eotaxin in animal models. The protein is potent in inducing eosinophil accumulation *in vivo* [4, 5] and exhibits marked synergism with IL-5 [20]. Increased expression of eotaxin mRNA and protein has been observed in allergic inflammation in the lung [6, 21] but is not restricted to allergic reactions [8]. All the eosinophil chemoattractant activity in bronchoalveolar fluid from allergen challenged/sensitized guinea pigs was shown to be neutralized by an antibody to eotaxin [22]. However, targeted disruption

of the eotaxin gene resulted in only a partial suppression of eosinophil accumulation in challenged/sensitized mice, implying that other mediators can compensate for loss of the chemokine [23].

Eotaxin has been identified in association with many cell types, including T cells, macrophages and epithelial cells [8-10]. It has also been described in lesions of patients with the inflammatory bowel diseases, ulcerative colitis and Crohn's disease [10]. The precise cell sources of asthma-associated eotaxin in the airway remain to be established.

There is considerable evidence to implicate eosinophil granulocytes in the pathogenesis of asthma. For example, in bronchial biopsy specimens from atopic asthma patients there are direct correlations between disease severity and the number of eosinophils [2,3] and IL-5 mRNA⁺ cells [24, 25]. Furthermore, in bronchoalveolar lavage fluid, the concentration of major basic protein derived from the eosinophil crystalloid granule correlates significantly with the degree of airway responsiveness [26].

For these reasons we have compared the expression of eotaxin and CCR3 (mRNA and protein) in endobronchial mucosal bronchial biopsy samples obtained from atopic asthmatics and normal, non-atopic, non-asthmatic controls and related our findings to disease severity and the infiltration of eosinophils into the bronchial submucosa. We have also identified the cell sources of eotaxin and CCR3 mRNA.

2 Results

Details of the study population are shown in Table 1. The atopic asthmatics (AA) and controls (NC) were comparable in terms of age and gender. As expected, com-

Table 1. Clinical details and the numbers of EG2⁺ eosinophils infiltrated into bronchial biopsies of patients and controls^{a)}

Patient group	Age (years)	Gender (F/M)	Total Serum IgE (IU/ml)	Blood Eosinophils (%)	EG2 ⁺ Eosinophils (0.202 mm ²)	FEV ₁ (% pred)	Histamine PC ₂₀ (mg/ml)
Atopic asthmatics (n = 20)	28.5 (22-61)	9/11	453 ^{b)} (57-3749)	3.5 ^{c)} (0.1-14.2)	9.0 ^{c)} (2.0-19.5)	85 ^{d)} (55-104)	1.82 ^{ac)} (0.16-4.0)
Normal controls (n = 10)	23.5 (20-40)	3/7	9 (4-29)	0.5 (0.1-1.7)	3.7 (0.0-5.6)	102.5 (92-110)	>16

a) All data are expressed as median (range).

b) $p < 0.0001$ versus normal controls.

c) $p < 0.0005$ versus normal controls.

d) $p < 0.005$ versus normal controls.

Table 2. Distribution of eotaxin mRNA⁺ cells and percentage of cells expressing eotaxin mRNA within the epithelium and submucosa of bronchial biopsies from asthmatics ($n = 6$)^{a)}

	Distribution of eotaxin mRNA ⁺ cells (% eotaxin mRNA ⁺ cells)	% of cell co-expressing eotaxin mRNA (% mRNA ⁺ cells)
Epithelium		
Cytokeratin ⁺ epithelial cells	68 ± 7	50 ± 17
CD68 ⁺ macrophages	12 ± 3	22 ± 5
CD3 ⁺ T cells	11 ± 5	30 ± 8
Tryptase ⁺ mast cells	4 ± 1	40 ± 16
Elastase ⁺ neutrophils	1 ± 1	14 ± 9
EG2 ⁺ eosinophils	1 ± 1	2 ± 2
CD31 ⁺ endothelial cells	0 ± 0	0 ± 0
Submucosa		
CD31 ⁺ endothelial cells	70 ± 3	36 ± 3
CD68 ⁺ macrophages	9 ± 1	9 ± 1
CD3 ⁺ T cells	8 ± 2	6 ± 2
Tryptase ⁺ mast cells	6 ± 1	12 ± 3
EG2 ⁺ eosinophils	4 ± 1	4 ± 1
Elastase ⁺ neutrophils	3 ± 1	6 ± 3
Actin ⁺ smooth muscle cells	0 ± 0	0 ± 0

a) A combination of ISH and IHC (employing mAb against several phenotype markers as indicated) was used.

pared with NC, the asthmatics had elevated total serum IgE, blood eosinophils and increased numbers of bronchial mucosal EG2⁺ eosinophils.

By *in situ* hybridization (ISH) and immunohistochemistry (IHC) eotaxin⁺ cells were identified in the epithelium and throughout the submucosa, either as isolated cells or as aggregates. On the other hand, CCR3 mRNA⁺ and immunoreactive cells were observed predominantly in the submucosa. Since large areas of the epithelium from asthmatics were disrupted (as previously reported [27, 28], quantification, i.e. cell counts, were confined to the submucosa.

The number of eotaxin and CCR3 (mRNA and protein) – positive cells per unit surface area was significantly elevated in asthmatics when compared with NC (Fig. 1). In the asthmatics there were significant inverse correlations between eotaxin mRNA⁺ cells ($p = 0.006$), eotaxin protein⁺ cells ($p = 0.017$), CCR3 mRNA⁺ cells ($p = 0.026$), CCR3 protein⁺ cells ($p = 0.018$) and the histamine provocative concentration causing a 20% fall in FEV₁ (PC₂₀) (Fig. 2). There were also significant correlations between EG2⁺ cells and eotaxin mRNA⁺ cells ($p = 0.001$),

Table 3. Distribution of CCR3⁺ mRNA cells and the percentage of cells expressing mRNA in the submucosa of bronchial biopsies from asthmatics ($n = 6$)

	Distribution of CCR3 mRNA ⁺ cells (% CCR3 mRNA ⁺ cells)	% of cell co-expressing CCR3 mRNA (% mRNA ⁺ cells)
EG2 ⁺ eosinophils	81 ± 4	89 ± 3
CD68 ⁺ macrophages	8 ± 2	6 ± 1
Tryptase ⁺ mast cells	5 ± 1	8 ± 3
Elastase ⁺ neutrophils	3 ± 1	4 ± 4
CD3 ⁺ T cells	1 ± 1	1 ± 0
CD31 ⁺ endothelial cells	1 ± 0	1 ± 0
Actin ⁺ smooth muscle cells	0 ± 0	0 ± 0

eotaxin protein ($p = 0.001$), CCR3 mRNA ($p = 0.001$) and CCR3 protein ($p = 0.001$).

The phenotypes of cells expressing eotaxin and CCR3 mRNA were determined by sequential IHC and non-radioactive ISH. In the epithelium almost 70 % of the total eotaxin mRNA⁺ cells were cytokeratin⁺ cells with 50% of these epithelial cells being mRNA⁺ (Table 2). CD68⁺ macrophages and CD3⁺ T cells accounted for 12 and 11% of the total eotaxin mRNA⁺, respectively, whereas only 6% was attributable to tryptase⁺ mast cells, elastase⁺ neutrophils, EG2⁺ eosinophils and CD31⁺ endothelial cells. In the submucosa 70 % of the eotaxin mRNA⁺ cells were CD31⁺ endothelial cells, the remainder co-localizing to CD68⁺, CD3⁺, tryptase⁺, EG2⁺ and elastase⁺ cells. As much as 36 % of the CD31⁺ cells were mRNA⁺ for eotaxin. Approximately 81 % of the CCR3 mRNA⁺ cells were eosinophils and 89 % of the eosinophils were positive (Table 3). Of the remainder 13 % of the CCR3⁺ cells were distributed amongst macrophages and mast cells. Examples of single and double ISH and IHC for eotaxin and CCR3 are shown in Fig. 3.

3 Discussion

Data from man and experimental animals support the view that asthma and airway inflammation is dependent on interactions between T cells and eosinophils, although the mechanism of selective eosinophil infiltration has thus far been unclear. It is hypothesized that after inhalation of specific allergen there is activation of Th2-type T cells which leads to the elaboration of IL-4 and IL-5 [29]. These cytokines are critical for IgE production and eosinophil maturation and activation.

There is strong evidence in the guinea pig [5, 6, 22] and mouse [7, 8, 30, 31] that eotaxin has a major role in eosinophil recruitment in allergic airways inflammation and that this is T cell dependent [31]. Other evidence suggests that IL-4 can up-regulate eotaxin mRNA in the mouse [7]. Further, a marked synergism between eotaxin and IL-5 has been observed in eosinophil recruitment [20, 30]. Our present results indicate that eotaxin may play an important role in selective eosinophil infiltration in man. There appears to be constitutive expression of eotaxin and CCR3 (Fig. 1) as shown by clear mRNA signals and positive immunostaining in normal controls, but the expression was markedly enhanced in asthma, particularly in subjects with airway hyperresponsiveness.

In other studies immunostaining of human nasal polyp tissue demonstrated that the presence of eosinophils was associated with eotaxin immunoreactivity in several cell types, *i.e.* epithelial cells, mononuclear cells, spindle cells, endothelial cells and eosinophils themselves [9]. Further, a recent study of eotaxin mRNA in bronchial biopsy samples from asthmatic patients reported increased expression in epithelial cells, T cells, macrophages and eosinophils [32].

In the present detailed investigation of bronchial biopsies from asthmatic patients we found increased mRNA and protein expression for eotaxin and its receptor CCR3. In the epithelium, co-localization studies showed eotaxin mRNA predominantly in epithelial cells with some expression in macrophages, T cells and mast cells. In the submucosa predominant expression was in endothelial cells, with limited expression in macrophages, T cells, mast cells and neutrophils. CCR3 mRNA was mainly associated with eosinophils with limited expression by macrophages and mast cells. A recent report identified CCR3 on blood basophils by PCR [33]. However, in the absence of a precise phenotypic marker the presence of basophils in bronchial biopsies from ongoing chronic asthma is controversial and remains to be established. It will be difficult to determine the mechanisms involved in up-regulating eotaxin in different cell types in the *in vivo* setting. Other cytokines may be involved in regulating eotaxin production; for example, it has been shown that TNF- α and IL-1 β stimulate eotaxin production in pulmonary epithelial cell lines *in vitro* [34]. Sallusto et al. [35] have recently described CCR3 expression by human Th2 cell lines. This observation may be of particular relevance in explaining allergic mechanisms of recruitment of Th2 type lymphocytes. In our present study of baseline, mild asthma, there were only 1 % of CD3⁺/CCR3⁺ cells (Table 3). Biopsies from severe, or chronic, asthma with a strong T cell signal will be required to identify CCR3⁺/IL-4⁺/CD3⁺ in allergic tissue reactions in man. The functional significance of CCR3 expression by cell types other than

eosinophils, and the potential consequences for therapy targeted at CCR3 are important future questions.

CCR3 was described as chemokine receptor expressed by eosinophils [12, 13], and in our study there was a significant correlation between CCR3 mRNA and protein expression and EG2⁺ eosinophils in the airway mucosa in the asthmatics. Although eotaxin and the recently reported eotaxin-2 are the only eosinophil-specific chemokines described to date, other chemokines, including RANTES [14], MCP-3 [36] and MCP-4 [16] may contribute to eosinophil recruitment in asthma. However, in our recent report [37] we showed that although RANTES and MCP-3 mRNA⁺ cell numbers were elevated in bronchial biopsy samples from asthma when compared with controls, their numbers did not correlate with clinical features such as the degree of airway hyperresponsiveness. Eotaxin, on the other hand, gave significant correlations (Fig. 2). Nevertheless it may be that different phases of allergic airways inflammation involve either mixed eosinophil/mononuclear cell infiltrates mediated by RANTES and MCP or selective eosinophil accumulation mediated by eotaxin. Further detailed studies will be required to delineate these mechanisms. The eosinophil is particularly attractive as a therapeutic target in asthma (in the absence of helminth infection) as a selective deletion of the accumulation of this cell type would negate pathogenesis associated with eosinophils, leaving host defence systems involving mononuclear cells intact. The observation that eotaxin, RANTES and MCP all stimulate eosinophils via CCR3 [38] makes this receptor a prime target for blockade by small molecule antagonists. If such compounds are developed successfully, they would also be applicable to other diseases, such as allergic eczema, idiopathic pulmonary fibrosis, sarcoidosis, Churg-Strauss syndrome and graft rejection.

The demonstration of increased eotaxin and CCR3 mRNA and protein expression in asthma compared with normal controls and their relation to bronchial hyperresponsiveness suggests that these molecules may serve as important targets for appropriate therapeutic strategies.

4 Materials and methods

4.1 Patient population

Thirty volunteers were included in this study (Table 1). They consisted of 10 non-atopic non-asthmatic controls and 20 mild to moderate symptomatic asthmatics. All were recruited from the Allergy Clinic, Royal Brompton Hospital, London, and from volunteers responding to advertisements. Asthma was defined as (1) a clear clinical history with current

symptoms, (2) evidence of more than 20 % reversibility of the forced expiratory volume in one second (FEV₁) either spontaneously or after inhaled β_2 -agonists and/or a histamine PC₂₀ provocation test of <6 mg/ml in the previous 2 weeks. A histamine PC₂₀ provocation test was performed in all atopic asthmatics within 2 weeks of the bronchoscopy day, using the method described by Hargreave et al. [39]. Atopy was defined by a positive skin prick test (wheal diameter of over 3 mm following subtraction of the negative control) to extracts of one or more aeroallergens (including house dust mite, mixed grass pollen, mixed tree pollen, mixed moulds, cat fur and dog dander). Using the CAP system (Pharmacia Diagnostics, Sweden) all atopics demonstrated a positive radioallergosorbent test (RAST) >0.70 IU/ml to one or more of these allergens. Non-atopic controls were defined by negative skin prick tests to a wide range of local aeroallergens in the presence of a positive histamine control. They also had a serum IgE concentration within the normal range of this laboratory (0–150 IU/ml) and negative RAST tests to 25 common aeroallergens. All IgE and RAST measurements were performed in the same laboratory. All subjects were non-smokers. All asthmatics were treated with inhaled β_2 -agonists and had not taken inhaled corticosteroids for the previous 2 weeks or oral corticosteroids in the previous 6 months. Exclusion criteria included age <18 years or >65 years, FEV₁ <60 % of the predicted value on the proposed bronchoscopy day, oral corticosteroid therapy, evidence of acute or chronic infection, pregnancy, breastfeeding, or any chronic medical illness other than asthma. The study was approved by the Ethics Committee of the Royal Brompton Hospital, London.

4.2 Fiberoptic bronchoscopy

Bronchoscopy was performed using an Olympus model IT30 bronchoscope with 2.8 mm channel (Olympus Corporation, Tokyo, Japan) as previously described [40]. Briefly, all subjects (asthmatics and controls) underwent bronchoscopy after premedication with 2.5 mg salbutamol by nebulizer and 0.6 mg of atropine and 5–10 mg midazolam administered intravenously. Local anesthesia of the vocal cords, trachea, and bronchial tree was induced with 2 % and 4 % lidocaine. After inspection of the airways, biopsies were taken from the right middle, lower and upper lobe bronchi using Olympus alligator forceps (model FB20C). Biopsies were fixed in freshly prepared 4 % paraformaldehyde in PBS for 2 h, washed twice for 1 h with 15 % sucrose in PBS (pH 7.4), embedded in OCT compound (Bayer, Basingstoke, GB), snap-frozen and stored at –80 °C until used.

4.3 *In situ* hybridization

Sections (6 μ m) were freshly cut from frozen bronchial biopsies onto slides coated with 0.1 % poly-L-lysine (BDH, Leicester, GB) and air-dried overnight at room temperature. All reagents were from Sigma Chemicals, unless otherwise indi-

cated. Based on sequencing, a 308-bp cDNA fragment of human eotaxin [10] (3' UTR region bp 803–1201) and a 1056-bp cDNA fragment of human CCR3 [13] (encoding region) were inserted into PCR Bluescript and pSP72 vectors, respectively. Riboprobes were prepared from cDNA for eotaxin and CCR3 as previously described [24, 41]. Briefly, riboprobes (antisense or sense) were synthesized in the presence of adenine triphosphate (ATP), guanosine triphosphate (GTP), cytosine triphosphate (CTP), and [³⁵S]uridine triphosphate (UTP), and appropriate RNA polymerases (T7, SP6 or T3), respectively.

Slides were defrosted for the experimental procedure. Permeabilization, prehybridization, and hybridization protocols were as described previously [24, 41]. Incubation in N-ethyl maleimide, iodoacetamide, and triethanolamine reduced non-specific binding of the ³⁵S-labeled probes. Negative controls employed hybridization with the sense probe and pretreatment of slides with RNase A (Promega, Southampton, GB) prior to hybridization with the antisense probe. For autoradiography, slides were dipped into K-5 emulsion (Ilford, Basildon, GB) and exposed at 4 °C for 2 weeks in absolute darkness in a desiccated environment. The slides were developed (D-19 developing solution; Eastman Kodak Co., Rochester NY), rinsed and counterstained with Harris hematoxylin. Dense deposits of silver grains on autoradiographs were present over cells expressing cytokine mRNA. In some experiments sections were counterstained with chromotrope 2R. Slides were counted in duplicate blind to the patients' clinical status using an eyepiece graticule, as previously described [24, 41]. Results were expressed as the total number of positive cells per 0.202 mm² of submucosa. The coefficient of variability of the duplicate counts obtained from all slides was less than 5 %.

4.4 Immunohistochemistry

Immunohistochemistry was performed using alkaline phosphatase anti-alkaline phosphatase (APAAP) as described previously [41, 42] with some modification. Rabbit anti-mouse Ig, APAAP, and control IgG1 were purchased from Dako (High Wycombe, GB). Anti-human eotaxin mAb (10C11 and 2G6) were prepared as described [9] and tested exhaustively to exclude cross-reactivity with other chemokines including MCP-4. Optimal concentrations of all antibodies used were determined in pilot experiments. Briefly, the sections were incubated with 20 % horse serum in PBS for 20 min, then incubated overnight at room temperature with anti-human eotaxin (10C11, 1:10) or 2G6 (1:50) or polyclonal rabbit anti-CCR3 [13] (1:1,000) in 20 % horse serum/PBS. More than 99 % of peripheral blood eosinophils (purified by immunomagnetic selection) were immunoreactive with anti-CCR3. PBMC gave negative staining. For eotaxin immunohistochemistry sections were then treated with monoclonal rabbit anti-mouse IgG (1:30, 30 min) and APAAP (1:30, 30 min), respectively. For immunostaining of CCR3,

sections were incubated with mouse anti-rabbit IgG mAb (1:30, 30 min), then treated with rabbit anti-mouse and APAAP, respectively, as above. Positive cells stained red after development with Fast Red. Omission or substitution of the primary antibody with an irrelevant antibody of the same species was used as a negative control. The sections were counted in duplicate, under blind conditions to the patients' clinical status. Results were expressed as the total number of positive cells per square millimeter of submucosa. The coefficient of variability of the duplicate counts obtained from all slides was less than 5 %. No immunoreactivity was observed in sections stained with omission of the primary rat antibody or substitution of this antibody with an irrelevant antibody of the same species.

4.5 Sequential IHC and ISH

To identify the cell source of eotaxin and CCR3 mRNA, sequential IHC/ISH was employed as previously described [42]. Briefly, cell phenotypes were first identified by IHC using the APAAP technique and phenotype-specific murine mAb. The mAb used were directed against human epithelial cells (cytokeratin, clone No: MNF 116), endothelial cells (CD31, clone No: JC/70A), macrophages (CD68, clone No: EBM 11), mast cell tryptase (clone No: AA1), neutrophil elastase (clone No: NP57), smooth muscle actin (clone No: 1A4) (Dako), T cells (CD3; Becton Dickinson, Cowley, Oxford, GB), and eosinophil cationic protein (EG2; Pharmacia, Uppsala, Sweden). For negative controls the primary Ab was replaced either with non-specific mouse Ig or Tris-buffered saline. Sections from six atopic asthmatics with high expression of eotaxin and CCR3 mRNA were chosen. After developing with Fast Red for cell phenotypes, ISH was performed using digoxigenin-labeled riboprobes [42] specific for eotaxin and CCR3 mRNA. The mRNA-positive signals (dark blue colour) were visualized by using NBT/BCIP (4-nitro blue tetrazolium/5-bromo-4-chloro-3-indolyl phosphate) (Sigma, Poole, GB) as the chromogen [42]. The numbers of positive cells expressing phenotypic markers (red colour), eotaxin and CCR3 mRNA (dark blue colour), or both (mixed colours) were counted in the epithelial area and submucosa in whole sections. The results were expressed as the percentage distribution of cells expressing eotaxin or CCR3 mRNA, or the percentage co-expressed by each cell type.

4.6 Statistical analysis

Data were analyzed using a statistical package (Minitab Release 7, Minitab Inc., State College, PA). Non-parametric statistical tests (Mann-Whitney U test) were used in the analysis, and median values and range are presented in the text and the accompanying figures and tables. Correlation coefficients were obtained by Spearman's rank-order method. *p* values less than 0.05 were considered significant.

Acknowledgement: This study was supported by the Medical Research Council (GB), the National Asthma Campaign (GB) and the Wellcome Trust (GB).

5 References

- 1 Frigas, E., Loegering, D. A., Solley, G. O., Farrow, G. M. and Gleich, G. J., Elevated levels of the eosinophil granule major basic protein in the sputum of patients with bronchial asthma. *Mayo Clin. Proc.* 1981. 56: 345–353.
- 2 Bousquet, J., Chanez, P., Lacoste, J. Y. et al., Eosinophilic inflammation in asthma. *N. Engl. J. Med.* 1990. 323: 1033–1039.
- 3 Bradley, B. L., Azzawi, M., Jacobson, M., Assoufi, B., Collins, J. V., Irani, A.-M. A., Schwartz, L. B., Durham, S. R., Jeffery, P. K. and Kay, A. B., Eosinophils, T-lymphocytes, mast cells, neutrophils and macrophages in bronchial biopsy specimens from atopic subjects with asthma: Comparison with biopsy specimens from atopic subjects without asthma and normal control subjects and relationship to bronchial hyperresponsiveness. *J. Allergy Clin. Immunol.* 1991. 88: 661–674.
- 4 Griffiths-Johnson, D. A., Collins, P. D., Rossi, A. G., Jose, P. J. and Williams, T. J., The chemokine, eotaxin, activates guinea-pig eosinophils *in vitro* and causes their accumulation into the lung *in vivo*. *Biochem. Biophys. Res. Commun.* 1993. 197: 1167–1172.
- 5 Jose, P. J., Griffiths, J. D., Collins, P. D., Walsh, D. T., Moqbel, R., Totty, N. F., Truong, O., Hsuan, J. J. and Williams, T. J., Eotaxin: a potent eosinophil chemoattractant cytokine detected in a guinea pig model of allergic airways inflammation. *J. Exp. Med.* 1994. 179: 881–887.
- 6 Jose, P. J., Adcock, I. M., Griffiths-Johnson, D. A., Berkman, N., Wells, T. N., Williams, T. J. and Power, C. A., Eotaxin: cloning of an eosinophil chemoattractant cytokine and increased mRNA expression in allergen-challenged guinea pig lungs. *Biochem. Biophys. Res. Commun.* 1994. 205: 788–794.
- 7 Rothenberg, M. E., Luster, A. D. and Leder, P., Murine eotaxin: an eosinophil chemoattractant inducible in endothelial cells and in IL-4-induced tumor suppression. *Proc. Natl. Acad. Sci. USA* 1995. 92: 8960–8964.
- 8 Gonzalo, J. A., Jia, G.-Q., Aguirre, V., Coyle, A., Jenkins, N., Katz, H., Lichtman, A., Copeland, N., Kopf, M. and Gutierrez-Ramos, J. C., Mouse eotaxin expression parallels eosinophil accumulation during lung allergic inflammatory reactions but is not restricted to a Th2-type response. *Immunity* 1996. 4: 1–14.
- 9 Ponath, P. D., Qin, S., Ringler, D. J., Clark-Lewis, I., Wang, J., Kassam, N., Smith, H., Shi, X., Gonzalo, J.-A., Newman, W., Gutierrez-Ramos, J.-C. and Mackay,

- C. R., Cloning of the human eosinophil chemoattractant, eotaxin. Expression, receptor binding, and functional properties suggest a mechanism for the selective recruitment of eosinophils. *J. Clin. Invest.* 1996. 97: 604-612.
- 10 Garcia-Zepeda, E., Rothenberg, M. E., Ownbey, R. T., Celestin, J., Leder, P. and Luster, A. D., Human eotaxin is a specific chemoattractant for eosinophil cells and provides a new mechanism to explain tissue eosinophilia. *Nature Med.* 1996. 2: 449-456.
- 11 Kitaura, M., Nakajima, T., Imai, T., Harada, S., Combadere, C., Tiffany, H. L., Murphy, P. M. and Yoshie, O., Molecular cloning of human eotaxin, an eosinophil-selective CC chemokine, and identification of a specific eosinophil eotaxin receptor, CC chemokine-receptor 3. *J. Biol. Chem.* 1006. 271: 7725-7730.
- 12 Ponath, P. D., Qin, S., Post, T. W., Wang, J., Wu, L., Gerard, N. P., Newman, W., Gerard, C. and Mackay, C. R., Molecular cloning and characterization of a human eotaxin receptor expressed selectively on eosinophils. *J. Exp. Med.* 1996. 183: 2437-2448.
- 13 Daugherty, B. L., Siciliano, S. J., De Martino, J. A., Malkowitz, L., Sirotina, A. and Springer, M. S., Cloning, expression, and characterization of the human eosinophil eotaxin receptor. *J. Exp. Med.* 1996. 183: 2349-2354.
- 14 Kameyoshi, Y., Dorschner, A., Mallet, A. I., Christophers, E. and Schroder, J. M., Cytokine RANTES released by thrombin-stimulated platelets is a potent attractant for human eosinophils. *J. Exp. Med.* 1992. 176: 587-592.
- 15 Dahinden, C. A., Geiser, T., Brunner, T., Von Tscharner, V., Caput, D., Ferrara, P., Minty, A. and Baggiolini, M., Monocyte chemotactic protein 3 is a most effective basophil- and eosinophil-activating chemokine. *J. Exp. Med.* 1994. 179: 751-756.
- 16 Uguccioni, M., Loetscher, P., Forssmann, U., Dewald, B., Li, H., Lima, S. H., Li, Y., Breider, B., Garotta, G., Thelen, M. and Baggiolini, M., Monocyte chemoattractant protein 4 (MCP-4), a novel structural and functional analog of MCP-3 and eotaxin. *J. Exp. Med.* 1996. 183: 2379-2384.
- 17 Stellato, C., Collins, P., Li, H., White, J., Ponath, P. D., Newman, W., Soler, D., Le Rosa, G., Schwiebert, L. M., Bickel, C., Liu, M., Bochner, B., Williams, T. J. and Schleimer, R., Production of the novel CC chemokine MCP-4 by airway cells and comparison of its biological activity to other CC chemokines. *J. Clin. Invest.* 1997. 99: 926-936.
- 18 Baggiolini, M. and Dahinden, C. A., CC chemokines in allergic inflammation. *Immunol. Today* 1994. 15: 127-133.
- 19 Forssmann, U., Uguccioni, M., Loetscher, P., Dahinden, C. A., Langen, H., Thelen, M. and Baggiolini, M., Eotaxin-2, a novel CC chemokine that is selective for the chemokine receptor CCR3, and acts like eotaxin on human eosinophil and basophil leukocytes. *J. Exp. Med.* 1995. 185: 2171-2176.
- 20 Collins, P. D., Marleau, S., Griffiths, J. D., Jose, P. J. and Williams, T. J., Cooperation between interleukin-5 and the chemokine eotaxin to induce eosinophil accumulation *in vivo*. *J. Exp. Med.* 1995. 182: 1169-1174.
- 21 Rothenberg, M. E., Luster, A. D., Lilly, C. M., Drazen, J. M. and Leder, P., Constitutive and allergen-induced expression of eotaxin mRNA in the guinea-pig lung. *J. Exp. Med.* 1995. 181: 1211-1216.
- 22 Humbles, A. A., Conroy, D. M., Marleau, S., Rankin, S. M., Palframan, R. T., Proudfoot, A. E. I., Wells, T. N. C., Li, D., Jeffery, P. K., Griffiths-Johnson, D. A., Williams, T. J. and Jose, P. J., Kinetics of eotaxin generation and its relationship to eosinophil accumulation in allergic airways disease: Analysis in a guinea pig model *in vivo*. *J. Exp. Med.* 1997. 186: 1-12.
- 23 Rothenberg, M. E., MacLean, J. A., Pearlman, E., Luster, A. D. and Leder, P., Targeted disruption of the chemokine eotaxin partially reduces antigen-induced tissue eosinophilia. *J. Exp. Med.* 1997. 186: 785-790.
- 24 Hamid, Q., Azzawi, M., Ying, S., Moqbel, R., Wardlaw, A. J., Corrigan, C. J., Bradley, B., Durham, S. R., Collins, J. V., Jeffery, P. K., Quint, D. J. and Kay, A. B., Expression of mRNA for interleukin-5 in mucosal bronchial biopsies from asthma. *J. Clin. Invest.* 1991. 87: 1541-1546.
- 25 Robinson, D. S., Ying, S., Bentley, A. M., Meng, Q., North, J., Durham, S. R., Kay, A. B. and Hamid, Q., Relationships among numbers of bronchoalveolar lavage cells expressing messenger ribonucleic acid for cytokines, asthma symptoms, and airway methacholine responsiveness in atopic asthma. *J. Allergy Clin. Immunol.* 1993. 92: 397-403.
- 26 Wardlaw, A. J., Dunnette, S., Gleich, G. J., Collins, J. V. and Kay, A. B., Eosinophils and mast cells in bronchoalveolar lavage in mild asthma: relationship to bronchial hyperreactivity. *Am. Rev. Respir. Dis.* 1988. 137: 62-69.
- 27 Laitinen, L. A., Heino, M., Laitinen, A., Kava, T. and Haahtela, T., Damage of the airway epithelium and bronchial reactivity in patients with asthma. *Am. Rev. Respir. Dis.* 1985. 131: 599-606.
- 28 Jeffery, P. K., Wardlaw, A. J., Nelson, F. C., Collins, J. V. and Kay, A. B., Bronchial biopsies in asthma: an ultrastructural, quantitative study and correlation with hyperreactivity. *Am. Rev. Respir. Dis.* 1989. 140: 1745-1753.

- 29 Corrigan, C. J. and Kay, A. B., T cells and eosinophils in the pathogenesis of asthma. *Immunol. Today* 1992, 13: 501-506.
- 30 Rothenberg, M., Ownbey, R., Mehlhop, P., Loisel, P., Van de Rijn, M., Bonventre, J., Oettgen, H., Leder, P. and Luster, A., Eotaxin triggers eosinophil selective chemotaxis and calcium flux via a distinct receptor and induces pulmonary eosinophilia in the presence of interleukin-5 in mice. *Mol. Med.* 1996, 2: 334-348.
- 31 MacLean, J. A., Ownbey, R. and Luster, A. D., T cell-dependent regulation of eotaxin in antigen-induced pulmonary eosinophilia. *J. Exp. Med.* 1996, 184: 1461-1469.
- 32 Mattoli, S., Stacey, M. A., Sun, G., Bellini, A. and Marini, M., Eotaxin expression and eosinophilic inflammation in asthma. *Biochem. Biophys. Res. Commun.* 1997, 236: 299-301.
- 33 Yamada, H., Hirai, K., Miyamasu, M., Ikura, M., Misaki, Y., Shoji, S., Takaishi, T., Kasahara, T., Morita, Y. and Ito, K., Eotaxin is a potent chemotaxin for human basophils. *Biochem. Biophys. Res. Commun.* 1997, 231: 365-368.
- 34 Lilly, C. M., Nakamura, H., Kesselman, H., Nagler-Anderson, C., Asano, K., Garcia-Zepeda, E. A., Rothenberg, M. E., Drazen, J. M. and Luster, A. D., Expression of eotaxin by human lung epithelial cells: induction by cytokines and inhibition by glucocorticoids. *J. Clin. Invest.* 1997, 99: 1767-1773.
- 35 Sallusto, F., Mackay, C. R. and Lanzavecchia, A., Selective expression of the eotaxin receptor CCR3 by human T helper 2 cells. *Science* 1997 (in press).
- 36 Noso, N., Proost, P., Van Damme, J. and Schroder, J. M., Human monocyte chemotactic protein-2 and 3 (MCP-2 and MCP-3) attract human eosinophils and desensitize the chemotactic responses towards RANTES. *Biochem. Biophys. Res. Commun.* 1994, 200: 1470-1476.
- 37 Humbert, M., Ying, S., Corrigan, C. J., Menz, G., Barkans, J., Pfister, R., Meng, Q., Van Damme, J., Opdenakker, G., Durham, S. R. and Kay, A. B., Bronchial mucosal expression of the CC chemokine genes RANTES and MCP-3 in symptomatic atopic and non-atopic asthmatics: relationship to EG2⁺ eosinophils and the eosinophil-active cytokines IL-5, GM-CSF and IL-3. *Am. J. Resp. Cell Mol. Biol.* 1997, 16: 1-8.
- 38 Heath, H., Qin, S., Rao, P., Wu, L., Le Rosa, G., Kasam, N., Ponath, P. D. and Mackay, C. R., Chemokine receptor usage by human eosinophil. *J. Clin. Invest.* 1997, 99: 178-184.
- 39 Hargreave, F. E., Ryan, G., Thompson, N. C., O'Byrne, P. M., Latimer, K., Juniper, E. F. and Dolovich, J., Bronchial responsiveness to histamine or methacholine in asthma: measurement and clinical significance. *J. Allergy Clin. Immunol.* 1981, 68: 347-355.
- 40 Humbert, M., Robinson, D. S., Assoufi, B., Kay, A. B. and Durham, S. R., Safety of fiberoptic bronchoscopy in asthmatics and control subjects and effect on asthma control over two weeks. *Thorax* 1996, 51: 664-669.
- 41 Ying, S., Taborda-Barata, L., Meng, Q., Humbert, M. and Kay, A. B., The kinetics of allergen-induced transcription of messenger RNA for monocyte chemotactic protein-3 and RANTES in the skin of human atopic subjects: relationship to eosinophil, T cell, and macrophage recruitment. *J. Exp. Med.* 1995, 181: 2153-2159.
- 42 Ying, S., Humbert, M., Barkans, J., Corrigan, C. J., Pfister, R., Menz, G., Larché, M., Robinson, D. S., Durham, S. R. and Kay, A. B., Expression of IL-4 and IL-5 mRNA and protein product by CD4⁺ and CD8⁺ T cells, eosinophils, and mast cells in bronchial biopsies obtained from atopic and nonatopic (intrinsic) asthmatics. *J. Immunol.* 1997, 158: 3539-3544.

Correspondence: A. Barry Kay, Allergy and Clinical Immunology, National Heart & Lung Institute, Imperial College School of Medicine, Dovehouse Street, London, SW3 6LY, GB
 Fax +44-171 376 3138; e-mail: a.b.kay@ic.ac.uk

THE ROLE OF MONOCYTE CHEMOATTRACTANT PROTEIN-1 (MCP-1) IN THE PATHOGENESIS OF COLLAGEN-INDUCED ARTHRITIS IN RATS

HIROOMI OGATA^{1,2}, MOTOHIRO TAKEYA¹, TEIZO YOSHIMURA³, KATSUMASA TAKAGI² AND KIYOSHI TAKAHASHI^{1*}

¹Second Department of Pathology, Kumamoto University School of Medicine, Kumamoto, Japan

²Department of Orthopedic Surgery, Kumamoto University School of Medicine, Kumamoto, Japan

³Immunopathology Section, Laboratory of Immunobiology, National Cancer Institute, Frederick Cancer Research and Development Center, Frederick, Maryland, U.S.A.

SUMMARY

Collagen-induced arthritis was produced in rats by intradermal immunization with type II collagen and the expression and production of monocyte chemoattractant protein-1 (MCP-1) were examined by immunohistochemistry, enzyme-linked immunosorbent assay (ELISA), and Northern blot analysis. Two to three weeks after the immunization, the hindfeet showed swelling and redness, followed by the development of severe arthritis, particularly in the ankle joints. During this period, prominent infiltration of neutrophils and macrophages was observed. Sandwich ELISA and Northern blot analysis revealed that MCP-1 concentrations in the joint lavages and MCP-1 mRNA levels in the joint tissues both peaked at 2 weeks after the immunization. By immunohistochemistry, various types of cells, particularly neutrophils, macrophages, synovial cells, and vascular endothelial cells, stained positively for MCP-1. Finally, injection of a neutralizing monoclonal antibody against rat MCP-1 significantly decreased the number of exudate macrophages in the lesions and reduced the ankle swelling by about 30 per cent compared with controls. These results suggest that MCP-1 plays a critical role in this model in the recruitment of monocytes and in the development of arthritis. © 1997 by John Wiley & Sons, Ltd.

J. Pathol. 182: 106-114, 1997.

No. of Figures: 11. No. of Tables: 1. No. of References: 34.

KEY WORDS—monocytes; macrophages; monocyte chemoattractant protein; pathogenesis; arthritis; rat model

INTRODUCTION

The infiltration and activation of monocyte/macrophages in the synovial joints are important in the pathogenesis of inflammatory joint diseases such as rheumatoid arthritis (RA). The activated macrophages play a key role in the progression and regression of the inflammatory processes by secreting various cytokines, growth factors, and proteases.^{1,2} As for the mechanisms of macrophage infiltration, various chemokines such as monocyte chemoattractant protein-1 (MCP-1),^{3,4} macrophage inflammatory protein (MIP)-1 α (LD78),² MIP-1 β (Act2),⁵ and RANTES (regulated on activation, normal T expressed and secreted)⁶ are known to induce direct movement of blood monocytes or macrophages. Among these factors, MCP-1 is one of the most potent monocyte chemoattractants and is detected in various pathological conditions.⁷ In addition to its chemotactic activity for monocytes, MCP-1 is also reported to attract other types of leukocytes such as basophils, eosinophils, or lymphocytes *in vitro*.^{8,9}

As previously reported, the MCP-1 concentration in joint fluids from RA patients was significantly higher than that from osteoarthritis.^{1,10} Increased production of MCP-1 by macrophages or synovial cells from RA patients suggests an important role for MCP-1 in

macrophage accumulation in the disease,^{1,11} but the role of MCP-1 in the development and progression of RA remains unclear.

To study the role of MCP-1 in RA, we immunized rats with native type II collagen and produced collagen-induced arthritis, which is a useful experimental model of human rheumatoid arthritis.^{12,13} The cell types infiltrating in the joint lesions were determined immunohistochemically by using a panel of mouse monoclonal antibodies (MAbs) against rat macrophages and their subpopulations, neutrophils, or lymphocytes and their subsets. We also performed immunohistochemical double staining with anti-rat MCP-1 antibody to identify MCP-1-producing cells. The concentration of MCP-1 in joint fluids and sera was measured by sandwich ELISA. Finally, anti-rat MCP-1 monoclonal antibody was intraperitoneally injected to investigate the biological role of MCP-1 in the progression of the arthritis.

MATERIALS AND METHODS

Animals

Specific pathogen-free female DR/BB Wor-UTM rats (DR/BB rats), 7-9 weeks old, were purchased from Seiwa Breeding Company for Experimental Animals (Fukuoka, Japan) and kept under conventional laboratory conditions at the Laboratory Animal Center of the Kumamoto University School of Medicine.

*Correspondence to: Kiyoshi Takahashi, MD, Second Department of Pathology, Kumamoto University School of Medicine, 2-2-1 Honjo, Kumamoto 860, Japan.

Table 1—Characteristics and reactivity of anti-rat monoclonal antibodies

Antibody	Isotype	Site of recognition	Reactive cells
ED1	IgG1	Cytoplasm	Monocytes, most macrophages, dendritic cells ¹⁴
ED2	IgG2a	Cell membrane	Resident or tissue-fixed macrophages ¹⁴
TRPM-3	IgG2a	Cell membrane	Exudate or monocyte-derived macrophages, certain macrophage subpopulations in lymphoid organs ¹⁵
OX6	IgG1	Cell membrane	Ia antigen-presenting macrophages, dendritic cells, and B cells ¹⁶
W3/25	IgG1	Cell membrane	T-helper lymphocytes, macrophages ¹⁷
OX8	IgG1	Cell membrane	T-suppressor/cytotoxic lymphocytes ¹⁸
RP-1	IgG2a	Cell membrane	Neutrophils and bone marrow cells ¹⁹
MEP-1	IgG1	Cell membrane	Mesenchymal cells and fibroblasts ²⁰
OX62	IgG1		Dendritic cells in lymphoid and non-lymphoid tissues ²¹

Induction of arthritis

Bovine type II collagen (Nitta Gelatin Inc., Osaka, Japan) was dialysed against 0.01 M acetic acid and emulsified together with an equal volume of Freund's incomplete adjuvant (Difco, Detroit, MI, U.S.A.) at 4°C. DR/BB rats were immunized by intradermally injecting 1 ml of the emulsion containing 1.5 mg/ml native type II collagen in multiple sites on the back.

Arthritis evaluation

After immunization, swelling of the hind paws was quantified by measuring the thickness of the ankle from the medial to lateral malleolus with slide calipers. Results could be reproducibly expressed to the nearest 0.1 mm. The ratio of thickness of arthritic paw to normal paw was defined as the paw thickness index and was calculated for each rat.

Immunohistochemistry

For immunohistochemistry, we utilized a panel of mouse MABs. The characteristics of each Ab are summarized in Table 1. A mouse MAB clone, B4, which specifically reacts to rat MCP-1,²² was used to detect MCP-1. ED1, ED2, OX6, W3/25, and OX62 were purchased from Serotec (Oxford, UK.). OX8 was purchased from Pharmingen (San Diego, CA, U.S.A.). RP-1 was a kind gift from Dr F. Sando, Department of Immunology and Parasitology, Yamagata University School of Medicine, Japan. TRPM-3, MEP-1, and B4 were produced in our laboratory. TRPM-3, MEP-1, ED1, ED2, OX6, W3/25, OX8, and RP-1 were used at a dilution of 1:100; B4 at 1:50, and OX62 at 1:2.

Whole ankle tissues were fixed in 2 per cent periodate-lysine-paraformaldehyde fixative for 4°C for 4 h immediately after resection. After fixation, the tissues were rinsed with phosphate-buffered saline (PBS) containing 10, 15, and 20 per cent sucrose and 20 per cent sucrose+10 per cent glycerol for 12 h; embedded in OCT compound (Miles, Elkhart, IN, U.S.A.); frozen in liquid nitrogen; and cut into 10 µm thick sections on a cryostat with a tungsten carbide-tipped knife (Bright, Huntington, U.K.). The indirect immunoperoxidase

method was employed for immunohistochemical staining. Briefly, after the inhibition of endogenous peroxidase (PO) activity by periodic acid treatment,²³ the sections were incubated with each MAB overnight at 4°C. After three washes with PBS for 5 min each, PO-conjugated sheep anti-mouse immunoglobulin (Ig) F(ab')₂ (Amersham, Poole, U.K.) diluted to 1:100 was applied for 45 min as the second step. For visualization of the PO, 3,3'-diaminobenzidine (Sigma Chemical Corp., St. Louis, MO, U.S.A.) was used as substrate in 0.05 M Tris-HCl buffer (pH 7.6) containing 0.01 per cent H₂O₂. Nuclei were counter-stained with haematoxylin. Control slides were incubated with normal mouse serum or isotype-matched non-relevant antibodies instead of the first antibodies; the results were invariably negative.

The number of positively stained cells was counted in high-power fields on each section and the average number of cells/mm² was calculated. Immunohistochemical examination of tissues at each stage was carried out on at least three specimens prepared from three different rats.

Immunohistochemical double staining

Joint tissues were stained with B4 for MCP-1 as described in the section on immunohistochemistry. After visualization of PO activity with 3,3'-diaminobenzidine as substrate to give a brown colour, the sections were rinsed in 0.1 M glycine-HCl buffer (pH 2.2) to remove Abs. The same sections were then incubated overnight with one of the anti-rat MABs: ED1, ED2, TRPM-3, OX6, W3/25, OX8, or RP-1. After washing with PBS, the sections were incubated with rabbit anti-mouse immunoglobulin (Ig) (Dako, Carpinteria, CA, U.S.A.) at room temperature for 1 h. The sections were washed with Tris-buffered saline (pH 7.6) and incubated with alkaline phosphatase anti-alkaline phosphatase (Dako) at room temperature for 1 h. The sections were subsequently incubated with a mixture of 0.2 mM naphthol AS-MX phosphate, 1 mM fast blue BB salt, and 1 mM levamisole (Sigma) in 50 mM Tris-HCl buffer (pH 8.7) at room temperature for 15 min. A positive reaction gave a blue colour. The percentages of cells that were double positive for MCP-1 and for one of the cell type-specific MABs were calculated.

Quantitation of rat MCP-1 by sandwich ELISA

Immediately after resection, tissues were rinsed with PBS and 1 ml of RPMI 1640 (Nissui, Tokyo, Japan) was injected into joints. The ankle joints were cut and the joint effusions were washed out. The medium was centrifuged and the cell-free supernatants were collected. The supernatant and serum from each animal were stored at -80°C until used. MCP-1 ELISA was carried out according to the method reported previously.²³ Briefly, a microtitre plate (Nunc, Roskilde, Denmark) was coated with one of the mouse anti-rat MCP-1 MAbs, B4 or C4²² at 4°C overnight. After repeated washing and blocking, serial dilution of recombinant rat MCP-1 and test samples were applied to the plate. The incubation was done at 37°C for 90 min with subsequent washing. Then rabbit polyclonal anti-rat MCP-1 antibody was added. After the incubation and washing, PO-conjugated donkey anti-rabbit Ig F(ab')₂ (Amersham) was added and the plate was incubated at room temperature for 60 min. After washing, the plate was incubated with *o*-phenylenediamine dihydrochloride (Sigma) and the colour was read spectrophotometrically at 405 nm; the sensitivity of the assay was 0.078 ng/ml.

RNA isolation and Northern blot analysis

Total cellular RNA was isolated by an acid guanidinium phenol-chloroform method from each ankle tissue including synovium. RNA isolation and Northern hybridization were performed according to the protocol reported previously.²³

Injection of an anti-rat MCP-1 neutralizing MAb

We have reported previously the production of MAbs against rat MCP-1.²² To clarify the neutralizing activity of the MAbs, 100 μl of 2×10^{-9} M rat recombinant MCP-1 was incubated with the same volume of serial dilutions of each MAb purified on a protein G-Sepharose column at room temperature for 10 min and then monocyte chemotactic activity was assayed with human peripheral blood mononuclear cells.²⁴

After immunization with type II collagen, anti-rat MCP-1 MAb (clone C4, 1 mg/kg body weight) was injected intraperitoneally (i.p.) every other day. As a control study, an irrelevant isotype-matched MAb, HBM-1,²⁵ was injected. The paw thickness index and the numbers of infiltrating cell subpopulations in the antibody-treated group were compared with those of the control group.

Statistical analysis

The significance of the data was evaluated by the Student's *t*-test or one factor ANOVA repeated measures test, and *P* values <0.05 were considered significant.

RESULTS

Development of collagen-induced arthritis

Redness and swelling appeared in the hindfeet around 10 days after the immunization, peaked at 2–3 weeks,

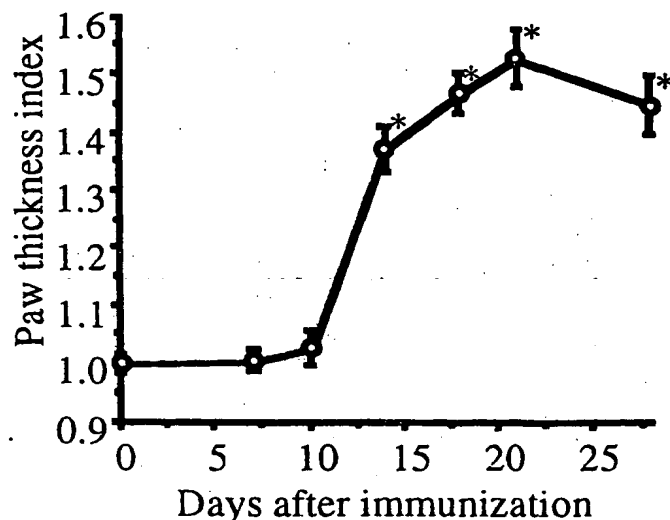


Fig. 1—The ratio of arthritic paw thickness to normal paw thickness was defined as the paw thickness index. The index peaked at 2–3 weeks after immunization and reached about 1.5. It was significant in comparison with the control rats (* $P < 0.01$).

and diminished thereafter. The paw thickness index (ratio of arthritic/normal paw thickness) peaked at about 1.5 at 3 weeks after the immunization (Fig. 1).

Histologically, there was no inflammatory reaction in the ankle joints 1 week after the immunization. After 2 weeks, proliferation of the synovial lining cells and infiltration of large numbers of mononuclear and polymorphonuclear leukocytes were observed in the synovium and joint space, accompanied with oedema in soft tissues, erosion of cartilages, and pannus formation. In the oedematous soft tissues, increased numbers of plump, spindle, or reticular fibroblasts were observed, probably due to fibroblast proliferation.

Three weeks after the immunization, proliferation of the synovial lining cells and fibroblasts were found, along with a marked infiltration of mononuclear and polymorphonuclear leukocytes. Erosion of cartilage, fibrosis, and pannus formation progressed by this time. Four weeks after the immunization, infiltration of inflammatory cells in the synovial tissues and oedema in the soft tissues decreased, whereas pannus formation, tissue destruction, fibrosis, and fibrous ankylosis increased. Soft X-ray examination revealed marked destructive changes in the joints (data not shown).

Infiltration of inflammatory cells in the inflammatory synovium

In normal joints, synovial cells were stained positively with ED1 and ED2 (Figs 2A and 2B). The immunoreactivity of ED1 and ED2 with synovial A cells has been previously reported by Verschure *et al.*,²⁶ suggesting that the ED1- and ED2-positive cells in the normal joints are synovial A cells. Resident macrophages distributed in the periarticular soft tissues were ED2-positive (Fig. 2B). Small numbers of synovial A cells were positive for TRPM-3 in the normal joints (Fig. 2C). A few cells among the synovial lining cells were positive

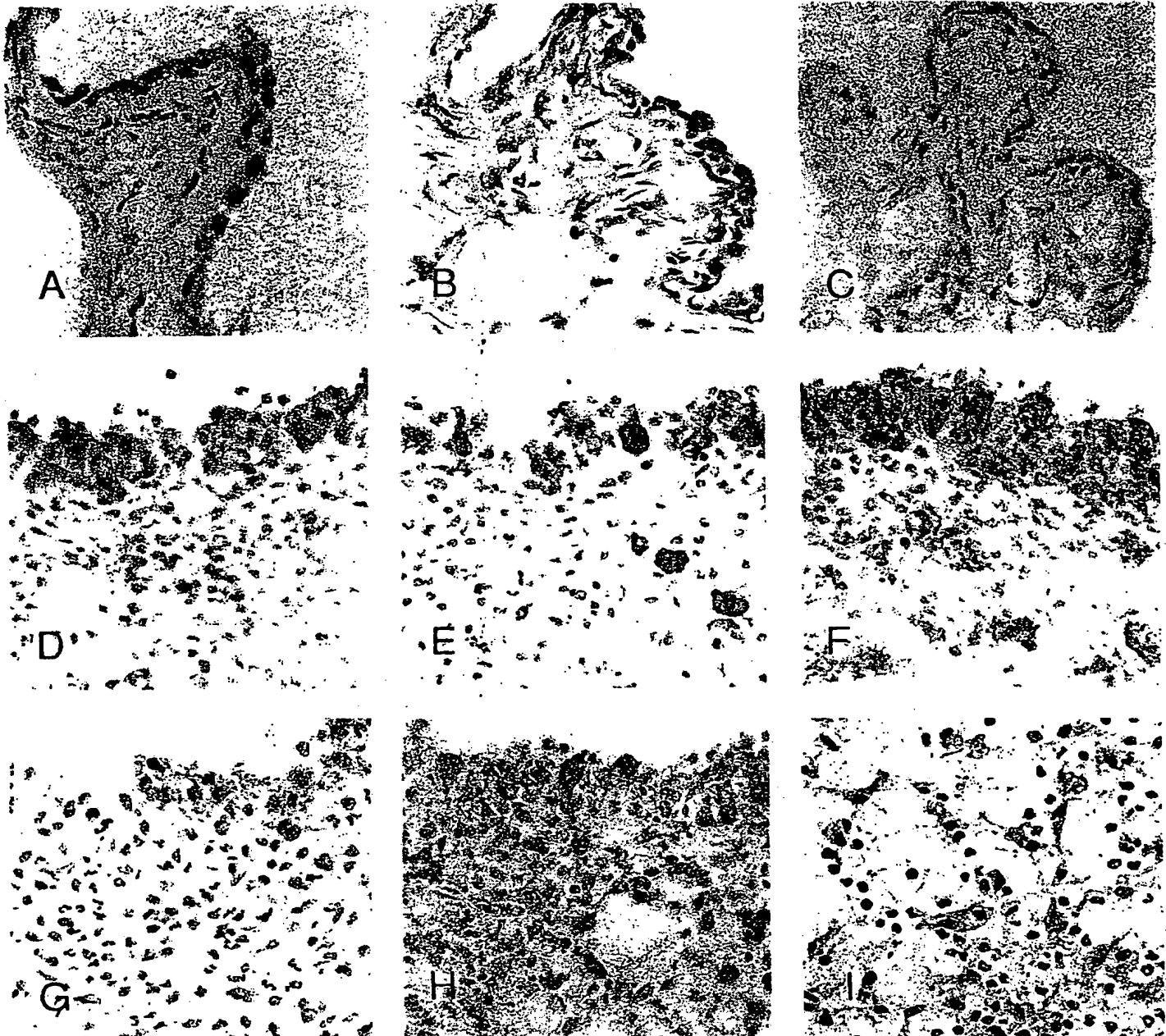


Fig. 2—Immunohistochemical staining with MAbs. In the normal joint, synovial A cells positive for ED1 (A) and ED2 (B), and a few synovial A cells weakly positive for TRPM-3 (C) can be observed. In the arthritic lesions, ED1-, ED2-, and TRPM-3-positive cells increase in number at 2 weeks after immunization (D–F). In the same stage, synovial B cells express a weak immunoreactivity for MEP-1 (G), and many macrophages and small round cells show positive reactions for OX6 (H) in the inflamed synovium. Plump, reticular, or spindle-shaped fibroblasts stain positively with MEP-1 in the inflamed periarticular soft tissue (I).

for OX6 or W3/25. These W3/25-positive cells closely resembled macrophages. OX8-, RP-1-, or MEP-1-positive cells were not detected in the normal joints.

One week after the immunization, there were no changes in the distribution pattern of ED1-, ED2- or TRPM-3-positive macrophages or OX6- or W3/25-positive cells in the joints. Two weeks after the immunization, a large number of RP-1-positive neutrophils infiltrated into the joint space, synovial sublining layers, and periarticular soft tissues. The number of

ED1-positive cells increased in both synovial lining and sublining layers, and also in the periarticular soft tissues (Fig. 2D). The number of ED2-positive cells slightly increased (Fig. 2E). A large number of TRPM-3-positive cells were detected, especially in the synovial lining layer (Fig. 2F). In the thickened or hyperplastic synovial membranes, some synovial cells (probably synovial B cells) showed MEP-1 immunoreactivity (Fig. 2G). The number of OX6-positive cells increased in the joint space, synovial lining, and sublining layers (Fig. 2H).

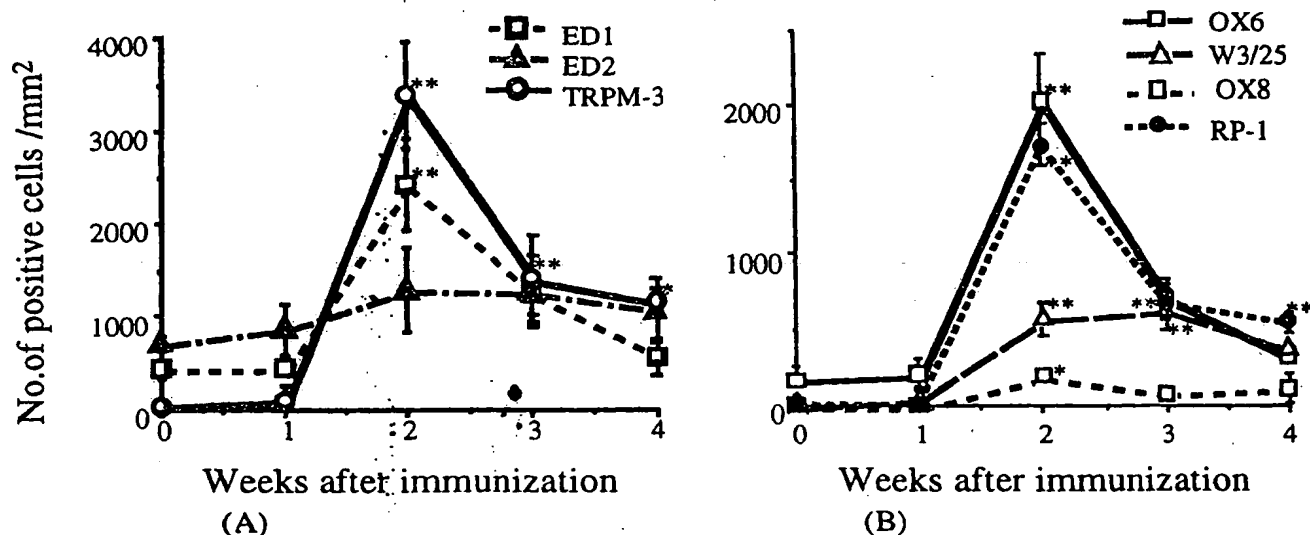


Fig. 3—(A) Number of cells positive for anti-rat macrophage MAbs ED1, ED2, and TRPM-3. Each bar indicates mean \pm standard deviation. (B) Numerical change in inflammatory cells positive for OX6, W3/25, OX8, or RP-1. ED1-, TRPM-3-, OX6-, W3/25-, OX8-, and RP-1-positive cells increase significantly at 2 weeks after immunization (* P <0.05; ** P <0.01).

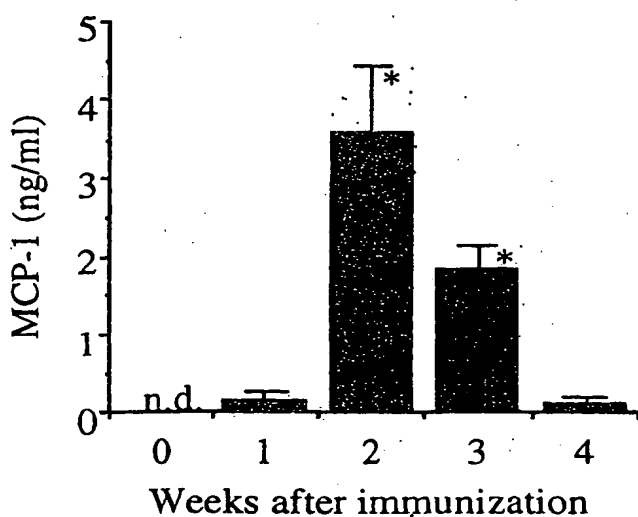


Fig. 4—Quantitation of rat MCP-1 by sandwich ELISA. The MCP-1 level in the joint lavage was increased significantly at 2–3 weeks after immunization (* P <0.01). In the serum, MCP-1 was not detectable at any time.

OX62-positive dendritic cells were sparsely distributed in the connective tissues (data not shown). The number of W3/25-positive macrophages increased in the synovium. Small round cells, of which the cell surface staining pattern with W3/25 was typical for helper T cells, were sparsely distributed in the sublining layer and periarticular soft tissues (data not shown). A few OX8-positive cells were detected in the sublining layer and soft tissues (data not shown). Staining with MEP-1 MAb indicated that plump, spindle-, or reticular-shaped cells in the synovial membranes and surrounding tissues were fibroblasts (Fig. 2I).

Three weeks after the immunization, the numbers of RP-1-positive neutrophils, ED1- or TRPM-3-positive

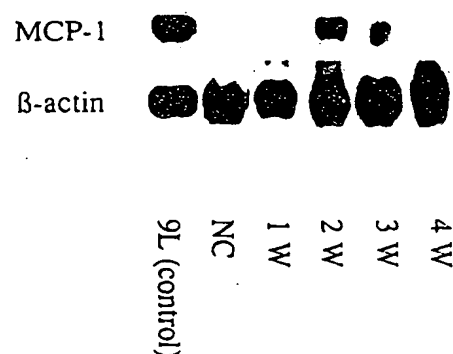


Fig. 5—Northern blot analysis shows marked expression of rat MCP-1 mRNA at 2 weeks after immunization. 9L is a rat glioma cell known to produce rat MCP-1.

macrophages, and OX6-, W3/25-, OX8-positive macrophages or lymphocytes decreased. ED2-positive cells were scattered in the synovium and in the periarticular soft connective tissues. Figure 3 shows kinetics of ED1-, ED2-, TRPM-3-, OX6-, W3/25-, OX8-, and RP-1-positive cell infiltration in the joints after the immunization.

Detection of MCP-1 in synovial lavage fluids, sera, and synovial tissues by sandwich ELISA, Northern blot analysis, and immunohistochemistry

MCP-1 concentrations in the joint lavage fluids and sera were measured by ELISA each week after immunization. As shown in Fig. 4, the MCP-1 concentrations in the lavage fluids peaked at 2 weeks after immunization and declined thereafter. In the sera, MCP-1 was not detected throughout the experimental period.

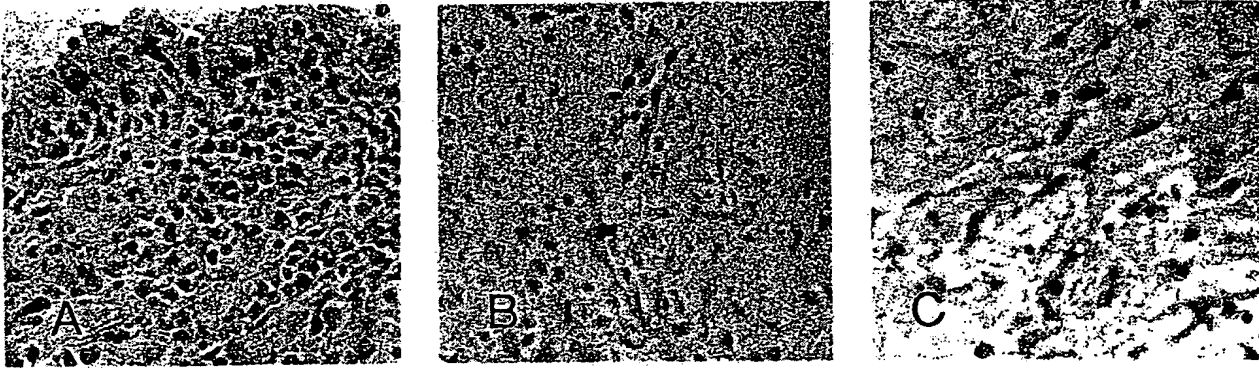


Fig. 6—Immunohistochemical staining with a MAb against rat MCP-1 (B4) in the rat ankle joint at 2 weeks after immunization. In the inflammatory synovial lesions, infiltrated neutrophils, synovial lining cells, macrophages in the sublining layer or connective tissue, and lymphocytes stain positively for B4 (A); endothelial cells of a blood capillary are positive (B); and plump, swollen, or activated fibroblasts are positive in the oedematous soft tissues (C)

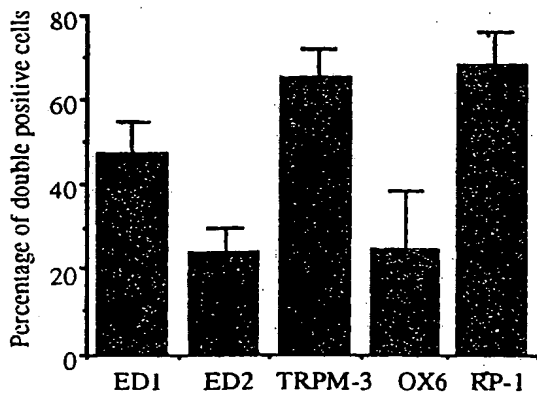


Fig. 7—Percentage of MCP-1-expressing cells in each cell subpopulation

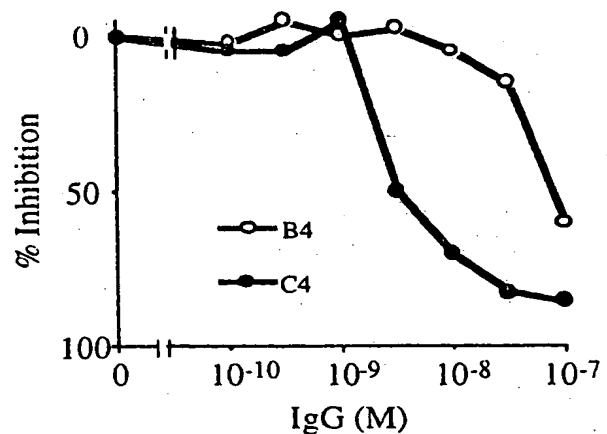


Fig. 8—Chemotactic activity assay with peripheral blood mononuclear cells. Clone C4 neutralized about 70–80 per cent of rat MCP-1 activity at 1:3 (MCP-1:C4) molar ratio *in vitro*. Clone B4 (see Methods) had a lower neutralizing activity

Total cellular RNA extracted from each joint was analysed for MCP-1 mRNA by Northern analysis. Accumulation of MCP-1 mRNA was detected at 2–3 weeks after the immunization (Fig. 5).

Immunohistochemistry with an anti-MCP-1 MAb demonstrated no MCP-1-positive cells until 1 week after the immunization. However, a large number of MCP-1-positive cells were detected at 2 weeks in the inflammatory synovial tissues (Fig. 6). Infiltrating leukocytes and synovial cells showed moderate to intense immunoreactivities for MCP-1 (Fig. 6A). Endothelial cells or perivascular adventitial cells of small blood vessels (Fig. 6B) and plump, swollen, or activated fibroblasts were also stained positively for MCP-1 (Fig. 6C). The number of MCP-1-positive cells decreased at 3–4 weeks. Some cells resembling macrophages were still positive for MCP-1 at 3–4 weeks.

To identify the cell types of the MCP-1-producing cells, the tissue sections were double stained for MCP-1 and cell surface markers. Figure 7 shows the percentages of MCP-1-positive cells in each ED1-, ED2-, TRPM-3-, OX6-, and RP-1-positive cell population. TRPM-3-positive macrophages and RP-1-positive neutrophils were strongly positive for MCP-1. None of the W3/25-

or OX8-positive cells was stained positively with the anti-rat MCP-1 MAb.

Suppressive effects of anti-rat MCP-1 MAb on collagen-induced arthritis

As shown in Fig. 8, one of the MAbs, clone C4, neutralized about 70–80 per cent of rat MCP-1 activity at 1:3 (MCP-1:C4) molar ratio *in vitro*; this MAb was therefore used for *in vivo* experiments.

In the rats treated with the control MAb, no changes were noted in the development of arthritis compared with the untreated group. In contrast, paw swelling of the hindfeet in the anti-rat MCP-1-treated rats was decreased by about 27 and 33 per cent of that of untreated rats at 2 and 3 weeks after the immunization, respectively (Fig. 9). Although some arthritic changes were still observed in the anti-MCP-1-treated rats, destruction of the joints was significantly reduced. The numbers of ED1-, ED2-, and especially TRPM-3-

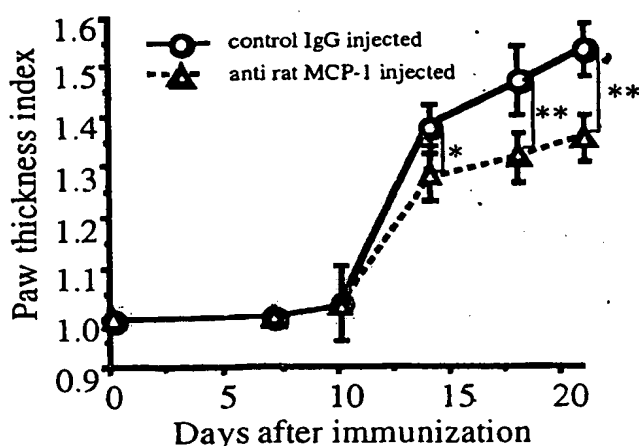


Fig. 9.—Hindfeet swelling was suppressed significantly by injection of anti-rat MCP-1 MAb. * $P < 0.05$; ** $P < 0.01$.

positive macrophages in the anti-MCP-1-treated rats were also reduced, compared with the untreated rats (Figs 10 and 11).

DISCUSSION

In the present investigation, collagen-induced arthritis was produced in rats by immunizing rats with type II collagen. Swelling and leukocyte infiltration in the ankle joints peaked at 2 weeks, followed by destruction of articular tissues, fibroblastic proliferation, and fibrous ankylosis. These histopathological changes are consistent with those described in previous studies.^{13,27} To analyse the types of leukocytes infiltrating the inflammatory lesions, we utilized a panel of MAbs for immunohistochemistry as listed in Table 1. RP-1-positive neutrophils and ED-1- or TRPM-3-positive exudate-type macrophages were the major cell

populations infiltrating into the joints. The number of infiltrating cells peaked at 2 weeks after the immunization and decreased at 3–4 weeks. In contrast, the number of ED2-positive resident macrophages was not significantly changed.

The concentration of MCP-1 in the joint lavage fluids and the expression of MCP-1 mRNA in the joint tissues peaked at 2 weeks and decreased at 3–4 weeks. These changes correlated with the increases in the number of ED-1- or TRPM-3-positive macrophages in the joints, suggesting that MCP-1 induces the infiltration of monocytes into the lesions. In contrast, the number of ED2-positive macrophages did not correlate with the elevation of MCP-1 concentration in the joint lavage fluids or with the expression of MCP-1 mRNA in the tissues. These data coincide with our previous studies on monocyte/macrophage infiltration into lung injuries induced by intratracheal instillation of bleomycin,²² or into transplanted tumours which produced a high amount of MCP-1.²³ In our recent study, we have also shown that an injection of recombinant rat MCP-1 into rat skin causes monocyte infiltration but no increase in resident macrophages (data not shown).

In addition to its monocyte chemotactic activity, MCP-1 has been reported to be a chemoattractant for CD45RO-positive lymphocytes *in vitro*.⁹ Recently, Rand *et al.* reported that an injection of anti-MCP-1 antibody inhibited lymphocyte infiltration in a rat delayed-type hypersensitivity model.²⁸ In the present study, increases in the number of W3/25-positive helper T cells and OX8-positive suppressor/cytotoxic T cells were found in the inflammatory synovial tissues, but they were not suppressed by injection of anti-rat MCP-1. In the present study, we were not able to examine the infiltration of CD45RO-positive T cells, since no CD45RO antigen has yet been identified on rat T cells. Further investigation is necessary to determine whether MCP-1 directly attracts lymphocytes *in vivo*.

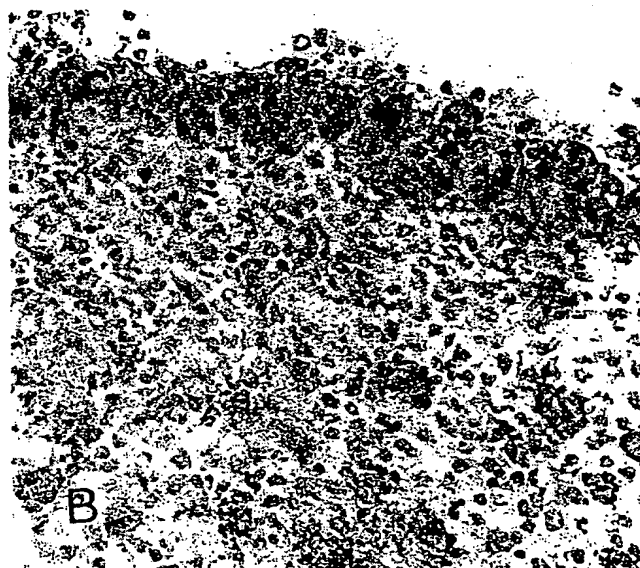


Fig. 10.—The number of TRPM-3-positive cells is decreased by injection of anti-rat MCP-1 MAb (A), compared with control rats (B).

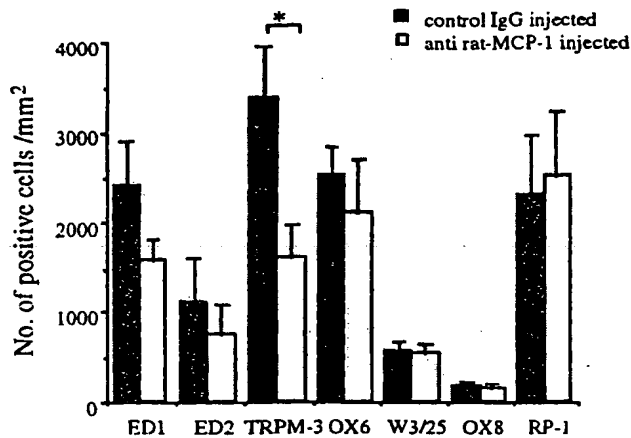


Fig. 11—The number of TRPM-3-positive cells was reduced significantly by injection of anti-rat MCP-1 MAb. * $P < 0.01$.

In the transgenic mice overexpressing MCP-1 in the basal cells of the epidermis,²⁹ a significant infiltration of CD45- and Ia-positive dendritic/Langerhans cells was demonstrated in the dermis. In the present study, the number of OX6-positive (Ia-positive) cells was increased in the inflammatory synovial tissues. However, OX62-positive dendritic cells were only sparsely distributed in the connective tissues in this arthritis model.

MCP-1 immunoreactivity was found in the synovial cells, neutrophils, macrophages, endothelial cells, adventitial cells of small blood vessels, and fibroblasts 2 weeks after the immunization. The number of MCP-1-positive cells decreased at 3–4 weeks, but macrophages continued to show MCP-1 immunoreactivity. An intense immunoreactivity for MCP-1 in macrophages and vascular endothelial cells in this collagen-induced arthritis model is in agreement with results reported for RA in humans.^{1–11} The frequency of MCP-1 expression among MCP-1-positive cells in the inflammatory joints was highest in macrophages and neutrophils. This result is consistent with that of rat lung injuries and granuloma formation induced by bleomycin,²² zymosan, or silica instillation.³⁰ Although Villiger *et al.* reported the expression of MCP-1 in cultured cartilaginous cells *in vitro*,³¹ we could not confirm MCP-1 immunoreactivity in cartilaginous cells in the inflammatory joints.

A significant reduction in the number of TRPM-3-positive macrophages in the inflammatory synovial tissues was found in the rats injected with C4. Inhibition of TRPM-3-positive macrophage infiltration by the injection of anti-MCP-1 MAb was 52 per cent of that in the control rats; this might be due to incomplete inhibition of MCP-1 activity by the MAb injected or the presence of other monocyte chemoattractants produced in the lesion such as RANTES, MIP-1 α , MIP-1 β , or other plasma-derived chemotactic factors.

Cellular and humoral immunological responses against type II collagen are involved in the pathogenesis of collagen-induced arthritis.³² In previous studies, suppression of arthritis was demonstrated by the administration of anti-T-cell receptor or anti-CD4 MAb, suggesting that T cells play an essential role in the development of arthritis.^{33,34} In the present study, the

first report of treatment for experimental arthritis with MAb against rat MCP-1, we could not inhibit the infiltration of lymphocytes in the joint tissues, but we were able to reduce the swelling of the joints by 30 per cent and to suppress significantly the infiltration of monocytes into the inflammatory joint tissues. Thus, inhibition of MCP-1 production in the joints may be useful in RA therapy, because MCP-1 appears to play an important role in recruiting monocytes that actively produce and release various cytokines, enzymes, or bioactive substances.

ACKNOWLEDGEMENT

We thank Dr Kiichi Kakimoto (Department of Immunology, School of Medicine, University of Occupational and Environmental Health, Fukuoka, Japan) for valuable advice in producing experimental arthritis.

REFERENCES

- Harigai M, Hara M, Yoshimura T, Leonard EJ, Inoue K, Kashiwazaki S. Monocyte chemoattractant protein-1 (MCP-1) in inflammatory joint diseases and its involvement in the cytokine network of rheumatoid synovium. *Clin Immunol Immunopathol* 1993; 69: 83–91.
- Koch AE, Kunkel SL, Harlow LA, *et al.* Macrophage inflammatory protein-1 alpha. A novel chemotactic cytokine for macrophages in rheumatoid arthritis. *J Clin Invest* 1994; 93: 921–928.
- Yoshimura T, Robinson EA, Tanaka S, Appella E, Kuratsu J, Leonard EJ. Purification and amino acid analysis of two human glioma-derived monocyte chemoattractants. *J Exp Med* 1989; 169: 1449–1459.
- Yoshimura T, Takeya M, Takahashi K. Molecular cloning of rat monocyte chemoattractant protein-1 (MCP-1) and its expression in rat spleen cells and tumor cell lines. *Biochem Biophys Res Commun* 1991; 174: 504–509.
- Robinson L, Keystone EC, Schall TJ, Gillett N, Fish EN. Chemokine expression in rheumatoid arthritis (RA): evidence of RANTES and macrophage inflammatory protein (MIP)-1 beta production by synovial T cells. *Clin Exp Immunol* 1995; 101: 398–407.
- Schall TJ, Bacon K, Toy KJ, Goeddel DV. Selective attraction of monocytes and T lymphocytes of the memory phenotype by cytokine RANTES. *Nature* 1990; 347: 669–671.
- Uguccioni M, D'Apuzzo M, Loetscher M, Dewald B, Baggiolini M. Actions of the chemotactic cytokines MCP-1, MCP-2, MCP-3, RANTES, MIP-1 alpha and MIP-1 beta on human monocytes. *Eur J Immunol* 1995; 25: 64–68.
- Yoshimura T, Leonard EJ. In: Cytokines, 1992: 131–152.
- Carr MW, Roth SJ, Luther E, Rose SS, Springer TA. Monocyte chemoattractant protein 1 acts as a T-lymphocyte chemoattractant. *Proc Natl Acad Sci USA* 1994; 91: 3652–3656.
- Loetscher P, Dewald B, Baggiolini M, Seitz M. Monocyte chemoattractant protein 1 and interleukin 8 production by rheumatoid synovial cells. Effects of anti-rheumatic drugs. *Cytokine* 1994; 6: 162–170.
- Koch AE, Kunkel SL, Harlow LA, *et al.* Enhanced production of monocyte chemoattractant protein-1 in rheumatoid arthritis. *J Clin Invest* 1992; 90: 772–779.
- Trentham DE, Townes AS, Kang AH. Autoimmunity to type II collagen: An experimental model of arthritis. *J Exp Med* 1977; 146: 857–868.
- Watson WC, Thompson JP, Terato K, Cremer MA, Kang AH. Human HLA-DRB1 gene hypervariable region homology in the Biobreeding BB rat: selection of the diabetic-resistant subline as a rheumatoid arthritis research tool to characterize the immunopathologic response to human type II collagen. *J Exp Med* 1990; 172: 1331–1339.
- Dijkstra CD, Dopp EA, Joling P, Kraal G. The heterogeneity of mononuclear phagocytes in lymphoid organs. Distinct macrophage subpopulations in the rat recognized by monoclonal antibodies ED1, ED2 and ED3. *Immunology* 1985; 54: 589–598.
- Takeya M, Hsiao L, Takahashi K. A new monoclonal antibody, TRPM-3, binds specifically to certain rat macrophage populations. Immunohistochemical and immunoelectron microscopic analysis. *J Leukoc Biol* 1987; 41: 187–195.
- Heuff G, van der Ende M, Boutkan H, *et al.* Macrophage populations in different stages of induced hepatic metastasis in rats: an immunohistochemical analysis. *Scand J Immunol* 1993; 38: 10–16.
- White RA, Mason DW, Williams AF, Galfrie G, Milstein C. T-lymphocyte heterogeneity in the rat: separation of functional subpopulations using a monoclonal antibody. *J Exp Med* 1978; 148: 664–673.

18. Brideau FJ, Carter PB, McMaster WR, Mason DW, Williams AF. Two subsets of rat T lymphocytes defined with monoclonal antibodies. *Eur J Immunol* 1980; 10: 609-615.
19. Gotoh S, Itoh M, Fujii Y, Arai S, Senda F. Enhancement of the expression of a rat neutrophil-specific cell surface antigen by activation with phorbol myristate acetate and concanavalin A. *J Immunol* 1986; 137: 643-650.
20. Tsuchiya T, Takahashi K, Takeya M, Hosokawa Y, Hattori T, Takagi K. Immunohistochemical, quantitative immunoelectron microscopic, and DNA cytofluorometric characterization of chemically induced rat malignant fibrous histiocytoma. *Am J Pathol* 1993; 143: 431-445.
21. Brennan M, Puklavec M. The MRC OX-62 antigen: a useful marker in the purification of rat veiled cells with the biochemical properties of an integrin. *J Exp Med* 1992; 175: 1457-1465.
22. Sakanashi Y, Takeya M, Yoshimura T, Feng L, Morioka T, Takahashi K. Kinetics of macrophage subpopulations and expression of monocyte chemoattractant protein-1 (MCP-1) in bleomycin-induced lung injury of rats studied by a novel monoclonal antibody against rat MCP-1. *J Leukoc Biol* 1994; 56: 741-750.
23. Yunashiro S, Takeya M, Nishi T, et al. Tumor-derived monocyte chemoattractant protein-1 induced intratumoral infiltration of monocyte-derived macrophage subpopulation in transplanted rat tumors. *Am J Pathol* 1994; 145: 856-867.
24. Yoshimura T, Takeya M, Takahashi K, Kuratsu J, Leonard EJ. Production and characterization of mouse monoclonal antibodies against human monocyte chemoattractant protein-1. *J Immunol* 1991; 147: 2229-2233.
25. Kohda Y, Takeya M, Arima S, Nakayama M, Sato T, Takahashi K. Production of two novel monoclonal antibodies against human renal glomeruli and their application to the immunohistochemical investigation of crescentic glomerulonephritis. *J Pathol* 1994; 172: 45-52.
26. Verschure PJ, Van Noorden CJF, Dijkstra CD. Macrophages and dendritic cells during the early stages of antigen-induced arthritis in rats: immunohistochemical analysis of cryostat section of the whole knee joint. *Scand J Immunol* 1989; 29: 371-381.
27. Caulfield JP, Hein A, Trentham RD, Trentham DE. Morphologic demonstration of two stages in the development of type II collagen-induced arthritis. *Lab Invest* 1982; 46: 321-343.
28. Rand ML, Warren JS, Mansour MK, Newman W, Ringler DJ. Inhibition of T cell recruitment and cutaneous delayed-type hypersensitivity-induced inflammation with antibodies to monocyte chemoattractant protein-1. *Am J Pathol* 1996; 148: 855-864.
29. Nakamura K, Williams IR, Kupper TS. Keratinocyte-derived monocyte chemoattractant protein-1 (MCP-1): analysis in a transgenic model demonstrates that MCP-1 can recruit dendritic and Langerhans cells to skin. *J Invest Dermatol* 1996; 105: 635-643.
30. Setoguchi K, Takeya M, Akaike T, et al. Expression of inducible nitric oxide synthase and its involvement in pulmonary granulomatous inflammation of rats. *Am J Pathol* 1996; 149: 2005-2022.
31. Villiger PM, Terkeltaub R, Lotz M. Monocyte chemoattractant protein-1 (MCP-1) expression in human articular cartilage. *J Clin Invest* 1992; 90: 488-496.
32. Trentham DE, Townes AS, Kang AH, David JR. Humoral and cellular sensitivity to collagen in type II collagen-induced arthritis in rats. *J Clin Invest* 1978; 61: 89-96.
33. Goldschmidt TJ, Holmdahl R. Anti-T cell receptor antibody treatment of rats with established autologous collagen-induced arthritis: suppression of arthritis without reduction of anti-type II collagen autoantibody levels. *Eur J Immunol* 1991; 21: 1327-1330.
34. Williams RO, Mason LJ, Feldmann M, Maini RN. Synergy between anti-CD4 and anti-tumor necrosis factor in the amelioration of established collagen-induced arthritis. *Proc Natl Acad Sci USA* 1994; 91: 2762-2766.

Effect of Regular Inhaled Albuterol on Allergen-induced Late Responses and Sputum Eosinophils in Asthmatic Subjects

G. M. GAUVREAU, M. JORDANA, R. M. WATSON, D. W. COCKCROFT, and P. M. O'BYRNE

Asthma Research Group, Departments of Medicine and Pathology, McMaster University, Hamilton; and Division of Respiratory Medicine, Department of Medicine Royal University Hospital, Saskatoon, Saskatchewan, Canada

Treatment with inhaled β_2 -agonists immediately before allergen inhalation inhibits allergen-induced early, but not late asthmatic responses (LAR). By contrast, 2 wk treatment with inhaled albuterol increases airway responses to inhaled allergen. We examined the effects of regular albuterol treatment on allergen-induced increases in inflammatory cells in blood and induced sputum. Ten mild, stable allergic asthmatics inhaled albuterol (800 μ g/day) or placebo for 7 d in a controlled, randomized, double-blind, crossover study. Allergen inhalation was performed 12 h after the final dose. Methacholine airway responsiveness and blood samples were analyzed before and 24 h after, and induced sputum was obtained before, 7 h and 24 h after allergen. Allergen significantly reduced methacholine PC₂₀, increased blood eosinophil numbers, and numbers of sputum neutrophils, EG2 positive and meta-chromatic cells ($p < 0.05$), without significant differences between treatments. Albuterol treatment significantly increased the LAR compared to placebo treatment ($p = 0.003$) and significantly enhanced the number of sputum eosinophils ($p = 0.009$) and sputum ECP ($p = 0.04$) at 7 h but not 24 h post-allergen ($p > 0.05$). We conclude that regular use of inhaled albuterol significantly increases the LAR to inhaled allergen, in association with an increase in the number of sputum eosinophils and the release of ECP, suggesting albuterol increases the late response by increasing eosinophil influx into the airways. Gauvreau GM, Jordana M, Watson RM, Cockcroft DW, O'Byrne PM. Effect of regular inhaled albuterol on allergen-induced late responses and sputum eosinophils in asthmatic subjects.

AM J RESPIR CRIT CARE MED 1997;156:1738-1745.

Airway inflammation is an important characteristic in patients with current symptomatic asthma. This has been demonstrated by increased numbers of inflammatory cells, particularly eosinophils, mast cells and lymphocytes present in bronchial biopsies (1) bronchoalveolar lavage fluid (BAL) (2) and sputum (3) from asthmatics when compared to nonasthmatics. Allergen challenge is a valuable laboratory model for the study of the pathogenesis of airway inflammation in asthma. Allergen inhalation results in acute bronchoconstriction in sensitized subjects, and in 50–60% of adult subjects, this is followed by a late bronchoconstrictor response (LAR), which is associated with the development of allergen-induced airway hyperresponsiveness (4), and increases in the number of airway inflammatory cells, particularly eosinophils and meta-chromatic cells (MCC), in bronchial biopsies (5), BAL (6), and induced sputum (7, 8). Sputum induction is a safe, nonin-

vasive method of directly obtaining repeated samples of airway secretions (3). Measurements of inflammatory cells from sputum are repeatable (9), demonstrate changes associated with airway responses after inhaled allergen (8), and has been shown to demonstrate the effects of a therapeutic intervention with inhaled corticosteroids (10).

Inhaled β_2 -adrenoceptor agonists are the most effective bronchodilator agents for the symptomatic treatment of asthma. β_2 -agonists reverse airway obstruction primarily by relaxing airway smooth muscle (11). In addition, β_2 -agonists are potent inhibitors of the release of histamine and newly synthesized mediators from activated mast cells (12) *in vitro*, and β_2 -adrenoceptors have been found on other immune cells including macrophages, eosinophils, neutrophils and lymphocytes, and may modulate adhesion of inflammatory cells through a cAMP-dependant kinase (13). Thus, these *in vitro* studies suggest that β_2 -agonists may have some anti-inflammatory properties for the treatment of asthma.

However, recent studies have demonstrated that regular treatment with β_2 -agonists increase airway responsiveness to nonallergic stimuli (14, 15), and enhance allergen-induced late bronchoconstrictor responses (16, 17). Regular treatment with albuterol is also associated with increased levels of activated eosinophils in bronchial biopsies (18). Given the association between allergen-induced airway responses and airway eosinophilia (3, 6, 7, 10), we hypothesized that regular treatment with inhaled β_2 -agonist might also enhance the allergen-induced

(Received in original form August 13, 1996 and in revised form May 7, 1997)

This study was supported by an operating grant from the Medical Research Council of Canada.

Dr. Jordana is a Career Scientist of the Ontario Ministry of Health and Dr. O'Byrne is a Medical Research Council of Canada Senior Scientist.

Correspondence and requests for reprints should be addressed to Dr. P. M. O'Byrne, Department of Medicine, Rm 3U-1 Health Sciences Center, McMaster University, 1200 Main St West, Hamilton, ON, L8N 3Z5 Canada.

Am J Respir Crit Care Med Vol 156, pp 1738–1745, 1997

TABLE 1
SUBJECT CHARACTERISTICS, ALLERGEN DOSE, AND TREATMENT RANDOMIZATION

Subject Number	Age (yr)	Gender	FEV ₁ (% predicted)	Methacholine PC ₂₀ (mg/ml)	Inhaled Allergen	Allergen Dilution	Order of Treatment	Rescue Medication
1	20	F	91.9	6.71	HDM	1:16	A/P	0/0
2	24	M	93.8	2.58	Cat	1:128	A/P	0/1
3	21	F	93.4	1.91	HDM	1:1,024	P/A	1/0
4	21	M	77.6	3.06	Ragweed	1:256	P/A	1/2
5	21	F	93.6	0.37	HDM	1:1,024	P/A	0/0
6	21	F	82.7	3.41	Ragweed	1:128	A/P	0/0
7	20	M	81.1	1.30	HDM	1:512	P/A	4/0
8	21	F	81.9	0.87	HDM	1:512	A/P	1/0
9	21	M	70.5	5.76	Grass	1:1,024	A/P	0/0
10	22	M	96.1	1.59	Grass	1:16	P/A	0/0

Definition of abbreviations: FEV₁ = forced expiratory volume in 1 second; methacholine PC₂₀ = provocative concentration of methacholine for 20% reduction in FEV₁; F = female; M = male; HDM = house dust mite; P = placebo treatment; A = albuterol treatment; rescue medication = number of occasions during A or P treatment when two puffs ipratropium bromide was inhaled to relieve bronchoconstriction.

airway eosinophilia. Therefore, the purpose of this study was to determine whether regular treatment with the inhaled β_2 -agonist, albuterol, administered for 1 wk, a duration of treatment known to enhance the allergen-induced late bronchoconstrictor responses (17), influences allergen-induced changes in inflammatory cells, particularly eosinophils, in blood and in the airways as assessed by changes in induced sputum.

METHODS

Subjects

Fourteen nonsmoking subjects (Table 1) with mild atopic asthma (eight female, six male), were selected for the study because of a previously documented allergen-induced early and late bronchoconstrictor response of at least 15% reduction in the forced expiratory volume in 1 s (FEV₁) during a screening period, and gave signed consent to participate in the study. Inhalation challenge with the allergen diluent, 0.9% saline, was completed during the screening period in order to correct the allergen-induced fall in FEV₁ for normal airflow variability during the allergen challenge day. Four of the subjects dropped out of the study due to protocol violations. Two of these subjects were unable to inhale the same three doses of allergen at all three allergen inhalation challenges, because of marked bronchoconstriction at the lowest inhaled dose of allergen during the albuterol treatment period. Two subjects were excluded from the study because their diary cards indicated they had used albuterol instead of the medication provided as a rescue medication during the study. The statistical analysis was performed on results from the remaining 10 subjects. This sample size was considered sufficient, as a previous study has shown that eight or more subjects can demonstrate a 50% change in the LAR with a power of > 90%, using the same methodology employed in this study (19). The study was approved by the Ethics Committee of McMaster University Health Sciences Center. Subjects were not exposed to sensitizing allergens and did not have asthma exacerbations or respiratory tract infections for at least four weeks prior to entering the study. All subjects had stable asthma with FEV₁ greater than 70% of predicted normal on all study days before allergen inhalation. Subjects used no regular medication other than infrequent (< twice weekly) inhaled β_2 -agonist as required to treat their symptoms. Ipratropium bromide replaced β_2 -agonists as a rescue medication during the study period. All medications were withheld for at least 8 h before each visit, and subjects were instructed to refrain from rigorous exercise, tea, or coffee in the morning before visits to the laboratory.

Study Design

The study was carried out with a double blind, placebo-controlled, randomized, two-period cross-over design (Figure 1). During each pe-

riod, subjects were treated with either inhaled albuterol 200 μ g (2 puffs) four times daily (Ventolin; Glaxo Canada, Toronto, Ontario), or an identical placebo 2 puffs four times daily for 1 wk. Each treatment period consisted of four visits to the laboratory. Baseline measurements of FEV₁, the provocative concentration of methacholine causing a 20% fall in FEV₁ (PC₂₀), blood and induced sputum differential and total cell counts were determined before treatment and on the 7th day of treatment with albuterol or placebo. Allergen challenges were carried out the following morning, 12 h after treatment was discontinued, and FEV₁ was measured for the next 7 h. Sputum samples were obtained during the late response, 7 h after allergen inhalation, 19 h after treatment was discontinued. Sputum could not be induced earlier than 7 h, because of the requirement of pretreatment with inhaled β_2 -agonists before sputum induction, which would interfere with subsequent measures of allergen-induced airway responses. Blood was not obtained 7 h after allergen because allergen-induced eosinophilia has not been shown to occur at this time after allergen inhalation (20). Methacholine PC₂₀, blood and sputum samples were obtained 24 h post-allergen, 36 h after treatment was discontinued. Each treatment period was separated by a washout period of at least 3 wk.

Laboratory Procedures

Methacholine inhalation test. Methacholine inhalation challenge was performed as described by Cockcroft (21). Subjects inhaled normal saline, then doubling concentrations of methacholine phosphate from a Wright nebulizer for 2 min. FEV₁ was measured at 30, 90, 180, and 300 s after each inhalation. Spirometry was measured with a Collins water-sealed spirometer and kymograph. The test was terminated when a fall in FEV₁ of 20% of the baseline value occurred, and the methacholine PC₂₀ was calculated.

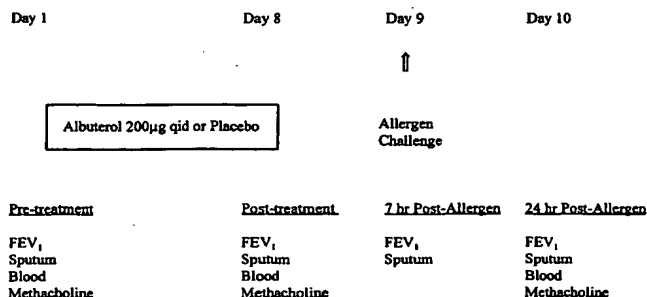


Figure 1. Study design.

Allergen Inhalation Test

Allergen challenge was performed as described by O'Byrne and coworkers (22). The allergen producing the largest skin wheal diameter was diluted in normal saline. The concentration of allergen extract for inhalation was determined from a formula described by Cockcroft and coworkers (23) using the results from the skin test and the methacholine PC₂₀. The starting concentration of allergen extract for inhalation was two doubling concentrations below that predicted to cause a 20% fall in FEV₁. The same doses of allergen were administered during each treatment period, and the FEV₁ was measured at 10, 20, 30, 40, 50, 60, 90, and 120 min post allergen inhalation, then each hour until 7 h after allergen inhalation. The early bronchoconstrictor response was taken to be the largest fall in FEV₁ within 2 h after allergen inhalation, and the late response was taken to be the largest fall in FEV₁ between 3 h and 7 h after allergen inhalation. The area under the curve was determined during the early (0–2 h) and late (3–7 h) response by plotting the response using graphics software (Fig P.; Fig P Software Corporation, Durham, NC), which calculated the area of the FEV₁-time response. All allergen challenges were performed with the same allergen dose utilized during the screening challenge.

Differential blood counts. Blood was collected into heparinized tubes by direct venipuncture, and blood smears were made for differential staining (Diff Quik; American Scientific Products, McGaw Park, IL). Differential cell counts were obtained from the mean of two slides with 300 cells counted per slide. Total leukocyte count was determined using a hemocytometer (Neubauer Chamber; Hauser Scientific, Blue Bell, PA), and cell populations were expressed as the number per ml blood by dividing by the total number of cells counted, and multiplying by the total leukocyte count.

Sputum analysis. Sputum was induced and processed using the method described by Popov and coworkers (24). Subjects inhaled 3%, 4%, then 5% saline for 7 min each. The induction was stopped when an adequate sample was obtained, or if the FEV₁ dropped 20% from baseline. Cell plugs with little or no squamous epithelial cells were selected from the sample using an inverted microscope, separated from saliva, and weighed. Samples were aspirated in two times their volume of 0.1% dithiothreitol (Sputolysin, Calbiochem Corp., San Diego, CA)

and two times their volume of Dulbecco's phosphate buffered saline (Gibco, Grand Island, NY). The cell suspension was filtered through a 52 μ m nylon gauze (BNSH Thompson, Scarborough, ON, Canada) to remove debris, then centrifuged at 1,500 rpm for 10 minutes. Supernatants were collected and stored at -70° C for fluid phase measurements of eosinophil cationic protein (ECP) by radioimmunoassay (Pharmacia, Uppsala, Sweden). The total cell count was determined using a hemocytometer (Neubauer Chamber) and expressed as the number of cells per ml sputum. Cells were resuspended in Dulbecco's phosphate buffered saline (DPBS) at $0.75\text{--}1.0 \times 10^6/\text{ml}$. Cytospins were prepared on glass slides using 50 μ l of cell suspension and a Shandon III cytocentrifuge (Shandon Southern Instruments, Sewickly, PA), at 300 rpm for 5 min. Differential cell counts were obtained from the mean of two slides with 400 cells counted per slide stained with Diff Quik. The same observer counted all study slides, and the reproducibility of the cell counts using these methods is excellent (9). For example, the interclass correlation coefficient is 0.97 for sputum eosinophils. Metachromatic cell (MCC) (mast cells and basophils) counts on slides stained with toluidine blue, were obtained from the mean of two slides with 5,000 cells observed on each slide. Cell types were enumerated by dividing by the total number of cells counted, and multiplying by the total cell count per milliliter of sputum. If possible, cytospins were also prepared on apex coated slides and fixed for 10 min in periodate-lysine-paraformaldehyde for immunocytochemical staining for ECP. Slides were stained with a mouse monoclonal antihuman antibody directed against cleaved ECP (EG2) (Kabi Pharmacia, Uppsala, Sweden) which was diluted in 1.0% BSA (Sigma Chemical Co.) and wash buffer made up of DPBS, 0.01 M HEPES buffer (Boehringer Mannheim Canada Ltd., Burlington, ON) and 0.01% saponin (Sigma Chemical Co.), and were incubated overnight at a concentration of 1 μ g/ml. Labeling of EG2 was detected by the alkaline phosphatase anti-alkaline phosphatase method (25). Mouse IgG1 (Sigma Chemical Co.) was used as a negative control. The percentage of EG2 positive cells was determined from a count of 500 cells under light microscopy, and were expressed as the number of EG2 positive cells per ml of sputum. These slides were also double stained with 10 μ g/ml FITC for 10 min,

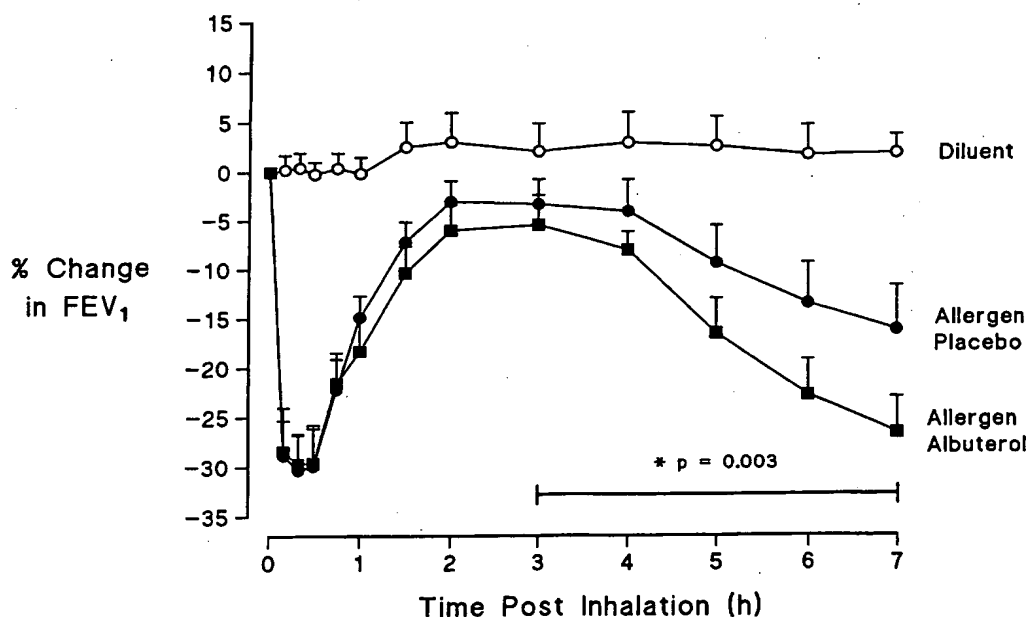


Figure 2. Allergen-induced airway responses. Percent change in FEV₁ (mean and SEM) after inhalation of diluent (open circles), allergen with albuterol treatment (closed squares), and allergen with placebo treatment (closed circles). The late (3–7 h) asthmatic response to allergen was significantly enhanced with albuterol ($p = 0.003$).

TABLE 2
ALLERGEN-INDUCED EARLY AND LATE AIRWAY RESPONSES, AND METHACHOLINE RESPONSIVENESS
AFTER 7 d REGULAR ALBUTEROL TREATMENT VERSUS PLACEBO

	Placebo	Albuterol	p Value
Early response, maximum fall in FEV ₁ , %	-34.3 ± 3.7	-32.2 ± 3.8	0.53
Early response, area under the curve	63.2 ± 10.4	79.3 ± 9.7	0.11
Late response, maximum fall in FEV ₁ , %	-18.2 ± 3.6	-28.3 ± 3.1	0.003
Late response, area under the curve	46.1 ± 15.9	72.8 ± 9.3	0.04
PC ₂₀ , log difference pre-post allergen, mg/ml	0.50	0.54	0.73

Definition of abbreviations: FEV₁ = forced expiratory volume in 1 second; PC₂₀ = provocative concentration of methacholine for 20% reduction in FEV₁.

Early and late responses are shown as the mean ± SEM and methacholine PC₂₀ is shown as the geometric mean ± GSEM.

which is a specific stain for eosinophils (26–28). The level of eosinophil activation was determined by examination of 100 fluorescent cells for appearance of immunolocalization of the EG2 antibody, and expressed as the number of EG2 positive/100 eosinophils.

Statistical Analysis

Methacholine PC₂₀ measurements are made by linear interpolation of log dose response curves resulting in logarithmic values for PC₂₀, which are then subjected to statistical analysis. Summary statistics for methacholine PC₂₀ are expressed as geometric mean and geometric standard error of the mean (GSEM). All other summary statistics are expressed as mean and SEM. Two-tailed Student's *t* test for paired observations was used to compare the early and late airway responses to allergen. The effects of 7 d treatment with placebo and albuterol treatment on airway and blood cellular and log transformed sputum cellular changes were analyzed, using a one-way repeated measured ANOVA,

for the effects of treatment. The effects of placebo and albuterol treatment on allergen-induced airway and blood cellular and log transformed sputum cellular changes from post treatment baseline, were analyzed using a two-factor repeated measures ANOVA, for the effects of time and treatment (29). As not all subjects had an adequate number of sputum slides for EG2 staining, complete sets of slides were only available from six subjects to compare the effects of 7 d albuterol treatment on baseline activated eosinophils, and from three subjects to compare the effects of albuterol in allergen-induced increases in activated eosinophils. All sputum cellular data were log transformed prior to analysis.

RESULTS

The allergen-induced late bronchoconstrictor response was significantly enhanced after albuterol treatment when com-

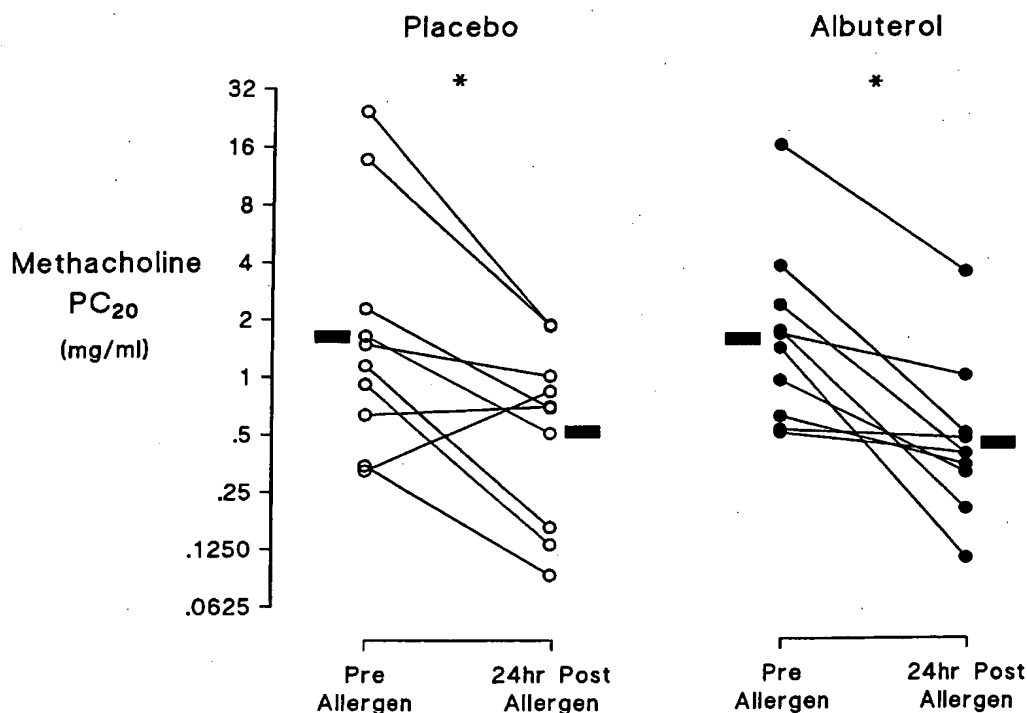


Figure 3. Allergen-induced methacholine hyperresponsiveness. Individual and geometric mean methacholine PC₂₀ (solid bars) values before treatment, after 7 d of 800 µg/day albuterol (solid circles) or placebo (open circles), and 24 h after allergen inhalation. Allergen-induced methacholine airway hyperresponsiveness was not significantly different between albuterol and placebo treatments. *Significant allergen-induced change from post-treatment baseline.

TABLE 3
THE EFFECT OF ALBUTEROL ON ALLERGEN-INDUCED CHANGES IN SPUTUM
MEASURED 7 AND 24 HOURS AFTER ALLERGEN INHALATION

	Pre-treatment		Post-treatment		7 h Post-allergen		24 h Post-allergen	
	Placebo	Albuterol	Placebo	Albuterol	Placebo	Albuterol	Placebo	Albuterol
Sputum								
Eosinophils, $\times 10^4/\text{ml}$ sputum	12 \pm 5	14 \pm 5	12 \pm 3	8 \pm 2	91 \pm 62*	220 \pm 156*†	166 \pm 78*	75 \pm 22*
Neutrophils, $\times 10^4/\text{ml}$ sputum	88 \pm 21	167 \pm 105	214 \pm 77	124 \pm 50	264 \pm 66*	373 \pm 106*	146 \pm 32*	242 \pm 105*
MCC, $\times 10^3/\text{ml}$ sputum	1.1 \pm 0.5	1.1 \pm 0.5	4.7 \pm 2.3	1.4 \pm 0.6	9.0 \pm 5.0*	6.8 \pm 2.0*	17.5 \pm 7.3	4.8 \pm 1.9*
ECP, $\mu\text{g}/\text{ml}$ supernatant	0.4 \pm 0.1	0.8 \pm 0.2	1.1 \pm 0.6	0.8 \pm 0.4	1.8 \pm 0.6*	4.3 \pm 1.8*†	8.1 \pm 3.5*	5.1 \pm 2.3*
EG2 positive, eosinophils/100	86.7 \pm 7.9	64.6 \pm 17.9	81.1 \pm 13.4	57.2 \pm 13.6	60.0 \pm 17.0	48.2 \pm 10.8	67.7 \pm 14.1	57.5 \pm 18.5
Blood								
Eosinophils, $\times 10^4/\text{ml}$	36 \pm 6	37 \pm 8	39 \pm 7	35 \pm 7			58 \pm 10*	56 \pm 6*
Neutrophils, $\times 10^4/\text{ml}$	452 \pm 47	417 \pm 48	412 \pm 35	394 \pm 36			421 \pm 46	474 \pm 51

Values shown are the mean \pm SEM.

* $p < 0.05$ significant difference between pre and post-allergen inhalation.

† $p < 0.05$ significant difference between placebo and albuterol.

pared to placebo (Figure 2). The maximal % fall in FEV₁ during the late response was $28.3 \pm 3.1\%$ after albuterol treatment and $18.2 \pm 3.6\%$ after placebo treatment ($p = 0.003$) and the area under the curve was also significantly increased ($p = 0.04$) (Table 2). The early bronchoconstrictor response was not significantly changed after albuterol treatment versus placebo (Figure 2). The maximal % fall in FEV₁ during the early response was $32.2 \pm 3.8\%$ after albuterol treatment and $34.2 \pm$

3.7% after placebo treatment (Table 2). Rescue medication with ipratropium bromide was rarely required during either of the treatment periods (Table 1).

The methacholine PC₂₀ decreased significantly 24 h after allergen inhalation after albuterol treatment from 1.55 mg/ml (GSEM 1.37) to 0.44 mg/ml (GSEM 1.32) ($p = 0.002$) and after placebo treatment from 1.62 mg/ml (GSEM 1.54) to 0.51 mg/ml (GSEM 1.38) ($p = 0.002$) (Figure 3), however, there

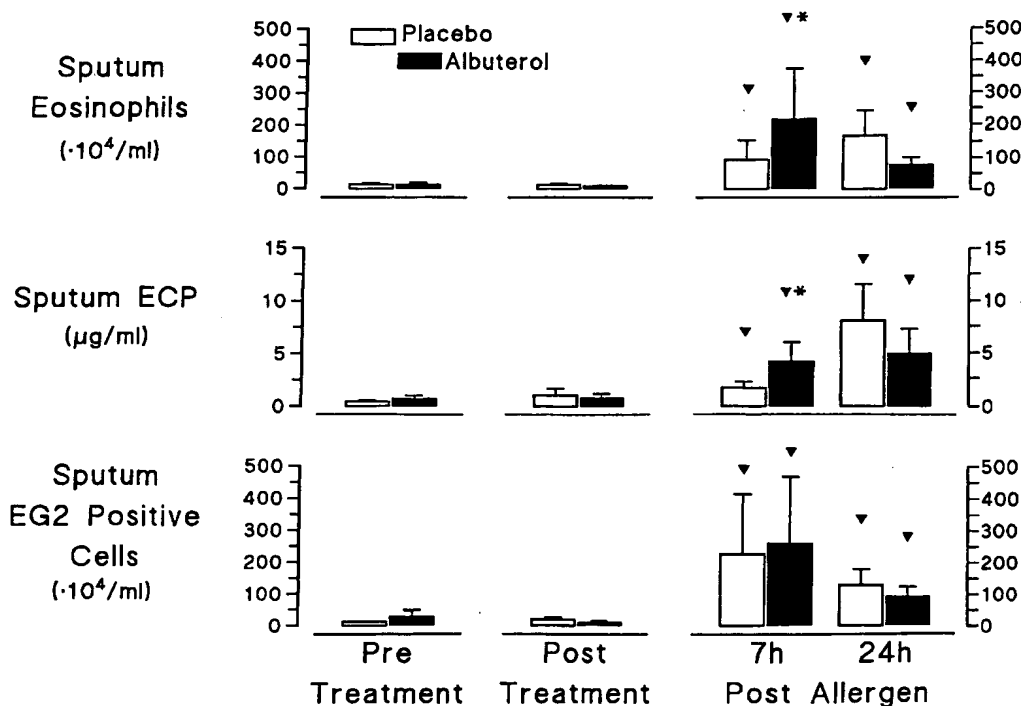


Figure 4. Allergen-induced increase of eosinophils, activated eosinophils, and eosinophil cationic protein in induced sputum. Number of sputum eosinophils (top panel), sputum fluid phase ECP (middle panel), and activated eosinophils (bottom panel) before treatment, after 7 d of 800 $\mu\text{g}/\text{day}$ albuterol (solid bars) or placebo (open bars), and at 7 and 24 h after allergen inhalation. *Significant allergen-induced change from post-treatment baseline. †Significant allergen-induced difference between albuterol and placebo treatments.

was no difference in the magnitude of the allergen-induced increase in airway responsiveness between albuterol and placebo treatments (Table 2).

Allergen inhalation increased the number of eosinophils per milliliter in sputum both at 7 h after allergen, during the late bronchoconstrictor response, and 24 h after allergen when methacholine airways responsiveness was increased ($p = 0.01$). Albuterol treatment, however, significantly enhanced the numbers of eosinophils per milliliter in sputum 7 h after allergen to $220 \pm 156 \times 10^4/\text{ml}$ when compared to $91 \pm 62 \times 10^4/\text{ml}$ after placebo treatment ($p = 0.009$) (Figure 4). This difference was no longer present in sputum 24 h after allergen, the number of eosinophils being $75 \pm 22 \times 10^4/\text{ml}$ after albuterol treatment and $166 \pm 78 \times 10^4/\text{ml}$ after placebo treatment ($p = 0.31$) (Table 3, Figure 4). The absolute change in the number of allergen-induced eosinophils at 7 h was greater after albuterol treatment in nine subjects, as compared with the change after placebo treatment, and decreased in one subject (Figure 5).

The concentration of ECP increased significantly after allergen inhalation from $1.1 \pm 0.6 \mu\text{g}/\text{ml}$ during placebo to $1.8 \pm 0.6 \mu\text{g}/\text{ml}$ at 7 h and $8.1 \pm 3.5 \mu\text{g}/\text{ml}$ at 24 h after allergen ($p = 0.00001$). During albuterol treatment, the concentration of fluid phase sputum ECP increased from $0.8 \pm 0.4 \mu\text{g}/\text{ml}$ to $4.3 \pm 1.8 \mu\text{g}/\text{ml}$ at 7 h and $5.1 \pm 2.3 \mu\text{g}/\text{ml}$ at 24 h after allergen (Table 3, Figure 4). As with the number of sputum eosinophils, the allergen-induced increase in the concentration of sputum ECP was significantly enhanced by albuterol at 7 h after allergen inhalation ($p = 0.045$). The allergen-induced changes in the number of eosinophils was correlated with the concentration of fluid phase ECP ($p = 0.00004$, $r = 0.62$). The number of EG2 positive eosinophils significantly increased after allergen inhalation during placebo, from $18 \pm 7 \times 10^4/\text{ml}$ to $223 \pm 188 \times 10^4/\text{ml}$ at 7 h and $127 \pm 50 \times 10^4/\text{ml}$ at 24 h after allergen, and during albuterol treatment, from $10 \pm 5 \times$

$10^4/\text{ml}$ to $258 \pm 207 \times 10^4/\text{ml}$ at 7 h and $91 \pm 32 \times 10^4/\text{ml}$ at 24 h after allergen ($p = 0.004$) (Table 3, Figure 4). However, we did not observe a significant effect of albuterol treatment on allergen-induced increases in EG2 positive cells ($p = 0.29$).

There was a significant correlation between the magnitude of the LAR (expressed as area under the curve) and the increase in sputum fluid phase ECP ($r = 0.67$, $p = 0.002$), and between the maximal fall in FEV_1 and the increase in sputum ECP ($r = 0.56$, $p = 0.015$). There was no significant correlation between the allergen-induced increase in the number of sputum eosinophils and the magnitude of the LAR ($r = 0.18$), or maximal fall in FEV_1 ($r = 0.18$).

Allergen inhalation also increased the numbers of sputum neutrophils ($p = 0.04$) and the numbers of MCC ($p = 0.02$) measured 7 and 24 h after allergen inhalation, however there was no significant difference between albuterol and placebo treatments either at 7 or 24 h (Table 3).

The number of blood eosinophils increased significantly 24 h after allergen inhalation after albuterol treatment from $35.1 \pm 7.5 \times 10^4/\text{ml}$ to $56.1 \pm 6.4 \times 10^4/\text{ml}$ ($p = 0.001$) and after placebo treatment from $38.9 \pm 7.4 \times 10^4/\text{ml}$ to $57.7 \pm 9.5 \times 10^4/\text{ml}$ ($p = 0.001$). This increase was the same magnitude for placebo and albuterol treatment periods (Table 3). The number of blood neutrophils measured 24 h after allergen inhalation did not change significantly after 7 d of albuterol treatment, and there was no difference in allergen-induced changes between albuterol and placebo (Table 3).

Regular use of albuterol for 7 d did not significantly alter the baseline FEV_1 , being $3.3 \pm 0.2 \text{ L}$ after albuterol treatment and $3.5 \pm 0.2 \text{ L}$ after placebo treatment, or the baseline methacholine PC_{20} , being $1.55 \text{ mg}/\text{ml}$ (GSEM 1.37) after albuterol treatment, and $1.62 \text{ mg}/\text{ml}$ (GSEM 1.54) after placebo. Also, regular albuterol treatment for 7 d did not significantly change the numbers of baseline blood eosinophils or neutrophils, nor

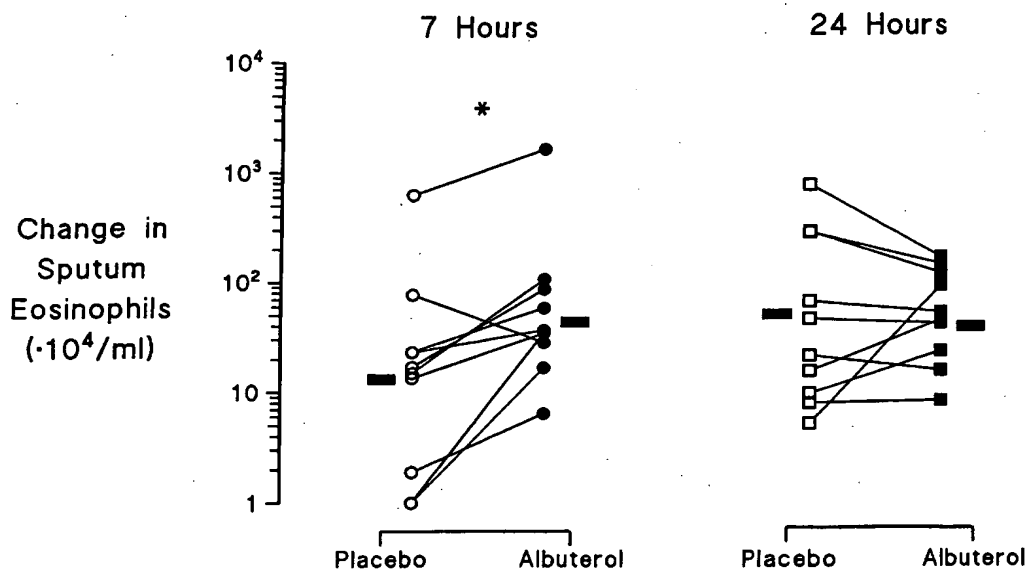


Figure 5. Allergen-induced change in sputum eosinophil numbers. The allergen-induced changes (post-allergen minus pre-allergen) in the number of sputum eosinophils (circles) after regular albuterol treatment for 7 d (closed symbols) or placebo (open symbols) and 7 h (circles) and 24 h (squares) after allergen inhalation. The geometric means are also shown (closed rectangles). As the difference from baseline was negative in two subjects on placebo treatment at 7 h after allergen inhalation, zero was used to complete the figure. *Significant allergen-induced difference between albuterol and placebo treatments.

the number of sputum inflammatory cells; eosinophils or activated eosinophils, MCC or neutrophils, nor the concentration of ECP measured in sputum (Table 3).

DISCUSSION

This study confirms previous reports which have demonstrated that regular treatment with inhaled albuterol increases allergen-induced late responses (16, 17). Use of ipratropium bromide as a rescue medication was infrequent and similar during both treatment periods, and should not bias the results. The allergen-induced late response is associated with airway inflammation, particularly increases in airway eosinophils and MCC (8). We have previously demonstrated that the number of eosinophils and the number of EG2 positive cells in sputum increase by 7 h after allergen inhalation, and remain elevated at 24 h (10). We therefore hypothesized that the increase in allergen-induced late responses may be caused by albuterol-induced increases in allergen-induced airway inflammation, as measured by changes in induced sputum.

Consistent with this hypothesis, albuterol enhanced allergen-induced sputum eosinophils and ECP at 7 h after allergen inhalation, during the late response, but there were no significant increases in the number of sputum neutrophils or MCC. This suggests the albuterol-enhanced late response may be associated with increased numbers of eosinophils rather than neutrophils or MCC, and is supported by the observation that sputum ECP levels in the present study, and sputum eosinophils in other studies of patients with asthma (30, 31) correlate with parameters of airflow obstruction.

We did not confirm the observations of Maestrelli and coworkers (31), who demonstrated a significant correlation between the magnitude of bronchoconstriction after isocyanate inhalation and the increase in sputum eosinophil counts. It is possible that this lack of correlation is because of different mechanisms involved. The lack of correlation is more likely due to large intersubject variability in the magnitude of allergen-induced eosinophilia, which has previously been described (8), and suggests the need for a larger subject sample size to further investigate the relationship between airway responses and airway eosinophilia. However, the level of ECP in sputum correlated well with airway responses, supporting the relationship between eosinophil activation and airflow obstruction.

The allergen inhalation was started 12 h after the last dose of albuterol, which is longer than its duration of pharmacological action. This suggests that the increases in allergen-induced late responses and eosinophil influx during the late response are a consequence of events in the airways which persist for 8–12 h after the pharmacological effects of albuterol are over. In addition, there was no difference in allergen-induced airway hyperresponsiveness measured at 24 h, between albuterol and placebo treatments, which was 36 h after the last dose of albuterol. This suggests that the untoward effects of albuterol on allergen-induced responses are short-lived. We did not observe a difference in blood or sputum eosinophils measured 24 h after allergen inhalation, suggesting albuterol may locally enhance allergen-induced eosinophilia in the airways, 7 h after allergen-inhalation, by altering the kinetics of eosinophil influx across the airway. The time course of the changes in allergen-induced airway eosinophils after albuterol treatment also suggests that the rate of trafficking of eosinophils through the airway may be increased. Thus, regular treatment with albuterol may lead to a faster onset of the appearance of eosinophils in the airways, as well as a faster resolution, as sputum eosinophils

were slightly but not statistically lower 24 h following allergen, without altering the trafficking of other inflammatory cells. However, there is no direct evidence, as yet, to support any of these hypotheses.

Measurement of induced sputum is a sensitive indicator of eosinophilic airway inflammation, and it can be used to distinguish between different types of airway inflammation (32). Using induced sputum, we have recently demonstrated that treatment with inhaled steroid therapy for 7 d caused a significant reduction of sputum eosinophils and EG2 positive cells (activated eosinophils) (10) associated with complete attenuation of the late response and significant reduction of allergen-induced airway hyperresponsiveness. In the present study, we also found an allergen-induced increase in both the number of eosinophils and the number of activated eosinophils. Quantification of eosinophils dual stained with FITC and EG2 demonstrated that the ratio of eosinophils localizing EG2 did not change after allergen inhalation (Table 3). This indicates that the allergen-induced increase in activated eosinophils into sputum is due to an influx of eosinophils into the airways rather than an increased level of activation of airway eosinophils. These results support our earlier observations with allergen-induced eosinophilia (10). Furthermore, albuterol may be enhancing the influx of eosinophils into the airway without affecting their level of activation.

The mechanism of the albuterol-induced increases in allergen-induced airway eosinophils was not investigated in this study. Short term treatment with albuterol has been reported to down-regulate pulmonary β_2 -receptors *in vivo* in humans (33). Down-regulation of β_2 -receptors on immune cells may render these cells more easily activated to participate in airways inflammation due to overexpression of adhesion molecules.

Finally, it is also possible that the enhanced late bronchoconstrictor response with albuterol treatment is not only associated with increased influx of eosinophils into the airways, but also may be associated with tolerance to the broncho-protective effect of the inhaled β_2 -agonist (34). Desensitization of β_2 -adrenoceptor-induced cAMP formation has been observed in cultured airway smooth muscle cells (36), and this response *in vivo* may render subjects less able to respond to endogenous catecholamines.

In this study, one week regular treatment with albuterol did not have an effect on baseline FEV₁, methacholine PC₂₀, allergen-induced early responses, or baseline numbers of inflammatory cells measured in peripheral blood or sputum. Studies with longer term regular treatment of β_2 -agonist have shown increased airway hyperresponsiveness to nonallergic stimuli (14, 15), and increased EG2 positive cells in bronchial biopsies (18). It may require a similar length of albuterol treatment to demonstrate increased indices of inflammation in peripheral blood or sputum in this group of mild asthmatics.

The clinical consequences of the effect of regular albuterol use on allergen-induced airway responses and inflammation are not known. However, it is a concern that one reason for asthmatics to increase their usage of inhaled β_2 -agonists is during allergen exposure, when asthma symptoms increase. Whether or not this repeated use of an inhaled β_2 -agonist during regular and repeated allergen inhalation, rather than the single, high dose allergen inhalation used in this study to elicit late responses, further enhances allergen-induced responses and eosinophil influx requires further study.

In conclusion, this study confirms previous observations that regular treatment with inhaled β_2 -agonist enhances the allergen-induced late bronchoconstrictor response. In addition, this study demonstrates an enhancement of allergen-induced eosinophil influx into the airways with regular albuterol treat-

ment, suggesting that albuterol enhances the late bronchoconstrictor response to inhaled allergen by increasing the rate of influx of airway eosinophils.

Acknowledgment: The authors thank T. Rerecich for technical assistance, J. Otis for help in the preparation of the manuscript, and Dr. G. Norman for statistical advice.

References

- Bradley, B. L., M. Azzawi, M. Jacobson, B. Assoufi, J. V. Collins, A. A. Irani, L. B. Schwartz, S. R. Durham, P. K. Jeffery, and A. B. Kay. 1991. Eosinophils, T-lymphocytes, mast cells, neutrophils, and macrophages in bronchial biopsy specimens from atopic subjects with asthma: comparison with biopsy specimens from atopic subjects without asthma and normal control subjects and relationship to bronchial hyperresponsiveness. *J. Allergy Clin. Immunol.* 88:661-674.
- Kirby, J. G., F. E. Hargreave, G. J. Gleich, and P. M. O'Byrne. 1987. Bronchoalveolar cell profiles of asthmatic and nonasthmatic subjects. *Am. Rev. Respir. Dis.* 136:379-383.
- Pin, I., P. G. Gibson, R. Kolendowicz, A. Girgis-Gabardo, J. A. Denburg, F. E. Hargreave, and J. Dolovich. 1992. Use of induced sputum cell counts to investigate airway inflammation in asthma. *Thorax* 47: 25-29.
- Cartier, A., N. C. Thomson, P. A. Frith, R. Roberts, and F. E. Hargreave. 1982. Allergen-induced increase in bronchial responsiveness to histamine: relationship to the late asthmatic response and change in airway caliber. *J. Allergy Clin. Immunol.* 70:170-177.
- Crimi, E., M. Chiamomondia, M. Milanese, G. A. Rossi, and V. Brusasco. 1991. Increased numbers of mast cells in bronchial mucosa after the late-phase asthmatic response to allergen. *Am. Rev. Respir. Dis.* 144:1282-1286.
- Aalbers, R., H. F. Kauffman, B. Vrugt, G. H. Keoter, and J. G. R. De Monchy. 1993. Allergen-induced recruitment of inflammatory cells in lavage 3 and 24 h after challenge in allergic asthmatic lungs. *Chest* 103: 1178-1184.
- Fahy, J. V., J. Liu, H. Wong, and H. A. Boushey. 1994. Analysis of cellular and biochemical constituents of induced sputum after allergen challenge: a method for studying allergic airway inflammation. 1994. *J. Allergy Clin. Immunol.* 93:1031-1039.
- Pin, I., A. P. Freitag, P. M. O'Byrne, A. Girgis-Gabardo, R. M. Watson, J. Dolovich, J. A. Denburg, and F. E. Hargreave. 1992. Changes in the cellular profile of induced sputum after allergen-induced asthmatic responses. *Am. Rev. Respir. Dis.* 145:1265-1269.
- Pizzichini, E., M. M. M. Pizzichini, A. Efthimiadis, S. Evans, M. M. Morris, D. Squillace, G. J. Gleich, J. Dolovich, and F. E. Hargreave. 1996. Indices of airway inflammation in induced sputum: reproducibility and validity of cell and fluid-phase measurements. *Am. J. Respir. Crit. Care Med.* 154:308-317.
- Gauvreau, G. M., J. Doctor, R. M. Watson, M. Jordana, and P. M. O'Byrne. 1996. Effects of inhaled budesonide on allergen-induced airway responses and airway inflammation. *Am. J. Respir. Crit. Care Med.* 154:1267-1271.
- Barnes, P. J. 1986. Neural control of human airways in health and disease. *Am. Rev. Respir. Dis.* 134:1289-1314.
- Church, M. K., and J. Hirol. 1987. Inhibition of IgE-dependent histamine release from human dispersed lung mast cells by anti-allergic drugs and albuterol. *Br. J. Pharmacol.* 90:421-429.
- Panettieri, R. A., Jr., A. L. Lazaar, E. Pure, and S. Albelda. 1995. Activation of cAMP-dependent pathways in human airway smooth muscle cells inhibits TNF- α -induced ICAM-1 and VCAM-1 expression and T lymphocyte adhesion. *J. Immunol.* 154:2358-2365.
- Kerrebijn, K. F., E. E. M. van Essen-Zandvliet, and J. J. Neijens. 1987. Effect of long-term treatment with inhaled corticosteroids and beta-agonists on the bronchial responsiveness in children with asthma. *J. Allergy Clin. Immunol.* 79:653-659.
- Vathenen, A. S., A. J. Knox, B. G. Higgins, J. R. Britton, and A. E. Tattersfield. 1988. Rebound increase in bronchial responsiveness after treatment with inhaled terbutaline. *Lancet* i:554-557.
- Cockcroft, D. W., C. P. McParland, S. A. Britto, V. A. Swystun, and B. C. Rutherford. 1993. Regular inhaled albuterol and airway responsiveness to allergen. *Lancet* 342:833-837.
- Cockcroft, D. W., P. M. O'Byrne, V. A. Swystun, and R. Bhagat. 1995. Regular use of inhaled albuterol and the allergen-induced late asthmatic response. *J. Allergy Clin. Immunol.* 96:44-49.
- Manolitsas, D. N., J. Wang, J. L. Devalia, C. J. Trigg, A. E. McAulay, and R. J. Davies. 1995. Regular albuterol, nedocromil sodium, and bronchial inflammation in asthma. *Am. J. Respir. Crit. Care Med.* 151: 1925-1930.
- Inman, M. D., R. Watson, D. W. Cockcroft, B. J. O. Wong, F. E. Hargreave, and P. M. O'Byrne. 1995. Reproducibility of allergen-induced early and late asthmatic responses. *J. Allergy Clin. Immunol.* 95:1191-1195.
- Dahl, R., P. Venge, and I. Olsson. 1978. Variations of blood eosinophils and eosinophil cationic protein in serum in patients with bronchial asthma. *Allergy* 33:211-215.
- Cockcroft, D. M. 1985. Measure of airway responsiveness to inhaled histamine or methacholine: method of continuous aerosol generation and tidal breathing inhalation. In F. E. Hargreave and A. J. Woolcock, editors. *Airway Responsiveness: Measurement and Interpretation*. Astra Pharmaceuticals Canada Ltd., Mississauga, ON 22-28.
- O'Byrne, P. M., J. Dolovich, and F. E. Hargreave. 1987. Late asthmatic response. *Am. Rev. Respir. Dis.* 136:740-756.
- Cockcroft, D. W., K. Y. Murdock, J. Kirby, and F. E. Hargreave. 1987. Prediction of airway responsiveness to allergen from skin sensitivity to allergen and airway responsiveness to histamine. *Am. Rev. Respir. Dis.* 135:264-267.
- Popov, T. A., R. Gottschalk, R. Kilendowicz, J. Dolovich, P. Powers, and F. E. Hargreave. 1994. The evaluation of a cell dispersion method of sputum examination. *Clin. Exp. Allergy* 24:778-783.
- Girgis-Gabardo, A., N. Kanai, J. A. Denburg, F. E. Hargreave, M. Jordana, and J. Dolovich. 1994. Immunocytochemical detection of granulocyte-macrophage colony-stimulating factor and eosinophil cationic protein in sputum cells. *J. Allergy Clin. Immunol.* 93:945-947.
- Nonaka, M., R. Nonaka, K. Wooley, E. Adelroth, K. Miura, Y. Ockhara, M. Glibetic, K. Nakano, P. O'Byrne, J. Dolovich, and M. Jordana. 1995. Distinct immunohistochemical localization of IL-4 in human inflamed airway tissues. *J. Immunol.* 155:3234-3244.
- Johnston, N. W., and J. Bienenstock. 1974. Abolition of non-specific fluorescent staining of eosinophils. *J. Immunol. Methods* 4:189-194.
- Filley, W. V., G. M. Kephart, D. E. Holley, and G. J. Gleich. 1982. Identification by immunofluorescence of eosinophil granule major basic protein in lung tissues of patients with bronchial asthma. *Lancet* 2(8288): 11-16.
- Snedecor, G. W., and W. G. Cochran. 1989. *Statistical Methods*, 8th ed. Iowa State University Press, Ames. 55-57, 374-396.
- Virchow, J. C., Jr., U. Holscher, and C. Virchow, Sr. 1992. Sputum ECP levels correlate with parameters of airflow obstruction. *Am. Rev. Respir. Dis.* 146:604-606.
- Maestrelli, P., P. G. Calcagni, M. Saetta, A. Di Stefano, J. J. Hosselet, A. Santonastaso, L. M. Fabbri and C. E. Mapp. 1994. Sputum eosinophilia after asthmatic responses induced by isocyanates in sensitized subjects. *Clin. Exper. Allergy* 24:29-34.
- Gibson, P. G., A. Girgis-Gabardo, M. M. Morris, S. Mattoli, J. M. Kay, J. Dolovich, J. Denburg, and F. E. Hargreave. 1989. Cellular characteristics of sputum from patients with asthma and chronic bronchitis. *Thorax* 44:693-699.
- Hayes, M. J., F. Qing, C. G. Rhodes, S. U. Rahman, P. W. Ind, S. Srisakandan, T. Jones, and J. M. B. Hughes. 1996. In vivo quantification of human pulmonary β -adrenoceptors: effect of β -agonist therapy. *Am. J. Respir. Crit. Care Med.* 154:1277-1283.
- O'Connor, B. J., S. L. Aikman, and P. J. Barnes. 1992. Tolerance to the nonbronchodilator effects of inhaled β_2 -agonists in asthma. *N. Engl. J. Med.* 327:1204-1208.
- Hall, I. P., K. Daykin, and S. Widdop. 1993. β_2 -adrenoceptor desensitization in cultured human airway smooth muscle. *Clin. Science* 84:151-157.

Cloning of the Human Eosinophil Chemoattractant, Eotaxin

Expression, Receptor Binding, and Functional Properties Suggest a Mechanism for the Selective Recruitment of Eosinophils

Paul D. Ponath,* Shixin Qin,* Douglas J. Ringer,* Ian Clark-Lewis,† Juan Wang,* Nasim Kassam,* Heidi Smith,* Xiaojie Shi,* Jose-Angel Gonzalo,* Walter Newman,* Jose-Carlos Gutierrez-Ramos,* and Charles R. Mackay*

*LeukoSite, Inc., Cambridge, Massachusetts 02142; †Biomedical Research Center and Biochemistry and Molecular Biology Department, University of British Columbia, Vancouver, British Columbia, Canada; and †Center for Blood Research, Harvard Medical School, Boston, Massachusetts

Abstract

The CC chemokine eotaxin, identified in guinea pigs and also recently in mice, may be a key element for the selective recruitment of eosinophils to certain inflamed tissues. Using a partial mouse eotaxin cDNA probe, the human eotaxin gene was cloned and found to be 61.8 and 63.2% identical at the amino acid level to guinea pig and mouse eotaxin. Human eotaxin protein was a strong and specific eosinophil chemoattractant in vitro and was an effective eosinophil chemoattractant when injected into the skin of a rhesus monkey. Radiolabeled eotaxin was used to identify a high affinity receptor on eosinophils ($0.52 \text{ nM } K_d$), expressed at 4.8×10^4 sites per cell. This receptor also bound RANTES and monocyte chemotactic protein-3 with lower affinity, but not macrophage inflammatory protein-1 α . Eotaxin could desensitize calcium responses of eosinophils to RANTES and monocyte chemotactic protein-3, although RANTES was able to only partially desensitize eosinophil calcium responses to eotaxin. Immunohistochemistry on human nasal polyp with antieotaxin mAbs showed that certain leukocytes as well as respiratory epithelium were intensely immunoreactive, and eosinophil infiltration occurred at sites of eotaxin upregulation. Thus eotaxin in humans is a potent and selective eosinophil chemoattractant that is expressed by a variety of cell types in certain inflammatory conditions. (*J. Clin. Invest.* 1996. 97:604–612.) Key words: chemokines • cytokines • inflammation • eosinophils • chemotaxis

Introduction

Chemoattractant cytokines (chemokines) play an important role in the recruitment of leukocytes to inflammatory lesions (1–4). Over 20 different chemokines have been identified to date, and different chemokines show characteristic biologic activity for distinct subsets of leukocytes. IL-8 is predominantly a

neutrophil chemoattractant (2, 5), while monocyte chemotactic protein (MCP)-1 serves predominantly as a monocyte and T cell chemoattractant (6, 7). Chemokines are produced by a variety of cell types, particularly in inflamed tissue, and endothelial-bound chemokines may provide a migration cue to circulating leukocytes, by signaling through seven transmembrane-spanning G-protein-coupled receptors on the leukocyte (8, 9). The notion that chemokines and their receptors play a fundamental role in the recruitment of leukocytes to inflamed tissues is supported by animal models in which anti-IL-8 mAbs inhibit neutrophil recruitment (10–12) and in IL-8 receptor knockout mice in which neutrophil recruitment to inflammatory sites is impaired (13).

Eosinophilic leukocytes also selectively accumulate in some inflammatory tissues, particularly in response to parasitic infection, and also as a result of IgE-mediated reactions such as rhinitis and allergic asthma (14–16). A number of factors have been described as being chemotactic for human eosinophils, including PAF (17), C5a (18), IL-16 (19), and the chemokines RANTES and MCP-3 (20–23), although all of these factors are chemotactic for other cell types. The striking accumulation of eosinophils in certain tissues suggest that there may be factors that are chemotactic specifically for eosinophils. A CC chemokine termed eotaxin was identified as the predominant eosinophil chemoattractant in the bronchoalveolar lavage fluid of allergen-challenged guinea pigs (24). Eotaxin was highly potent in guinea pigs, inducing substantial eosinophil accumulation at a 1–2 pmol dose in the skin. Northern blot analysis demonstrated eotaxin mRNA in the lungs of naive and sensitized guinea pigs, although allergen challenge led to considerably increased levels (25, 26).

To examine the biology of human eotaxin and its role in disease, we cloned a human homologue of guinea pig eotaxin. Human eotaxin mediated the selective migration of eosinophils, both in vitro and in vivo. Ligand binding and calcium desensitization studies indicated that eotaxin shares a novel receptor with RANTES and MCP-3 on eosinophils, distinct from the CC chemokine receptors CKR-1 (the macrophage inflammatory protein (MIP)-1 α /RANTES receptor) (27, 28) and CKR-2a,b (the MCP-1 receptors) (29). Based on the high affinity of eotaxin for its receptor and its selective activity, eotaxin appears to be an important chemokine for human eosinophil function.

Address correspondence to Charles R. Mackay, LeukoSite, Inc., 215 First Street Cambridge, MA 02142. Phone: 617-621-9350; FAX: 617-621-9349; E-mail: 71444.1022@compuserve.com

Received for publication 19 September 1995 and accepted in revised form 24 October 1995.

J. Clin. Invest.

© The American Society for Clinical Investigation, Inc.
0021-9738/96/02/0604/09 \$2.00
Volume 97, Number 3, February 1996, 604–612

1. Abbreviations used in this paper: $[Ca^{2+}]_i$, intracellular cytosolic free calcium; MCP, monocyte chemotactic protein; MIP, macrophage inflammatory protein.

Methods

Library screening, cDNA isolation, Northern hybridizations. A mouse clone, designated clone 28, containing a partial mouse eotaxin cDNA encoding murine eotaxin amino acids 17–61 was digested with EcoRI to release a 135-bp fragment (29a). This fragment was labeled by random priming using a kit from Boehringer Mannheim Biochemicals (Indianapolis, IN) following the manufacturer's recommended labeling protocol. This probe was used to screen a human genomic library purchased from Clontech (Palo Alto, CA) using standard molecular biology techniques (30). Hybridization with the mouse clone 28 probe was in $6\times$ SSC containing $2\times$ Denhardt's solution and $25\text{ }\mu\text{g/ml}$ denatured salmon sperm DNA overnight at 65°C . The membranes were rinsed twice in $2\times$ SSC, 0.05% SDS at 65°C followed by two washes (15 min each) in $0.2\times$ SSC, 0.1% SDS at 55°C . One phage clone, designated clone 25, was found to contain a nucleotide sequence with significant similarity to the mouse and guinea pig eotaxin clones and was the subject of further analysis.

Human spleen mRNA was purchased from Clontech. The following primers, derived from genomic sequence analysis were used to amplify clone 25 cDNA from human spleen mRNA, 5' primer: 5'-GGATCCAACATGAAGGTCTCCG, 3' primer: 5'-GAATTCT-TATGGCTTTGGAG-TTGGAG. 200 ng of spleen mRNA was reverse transcribed with oligo dT. $2\text{ }\mu\text{l}$ of this cDNA was amplified with 100 pmol of each primer in a final reaction mixture containing 60 mM Tris-HCl, pH 8.5, 2.0 mM MgCl_2 , 200 mM dNTPs, and 2.5 U Taq polymerase. The cycle parameters for PCR were as follows: 95°C , 1 min; 25 cycles of 94°C , 30 s; 68°C , 10 s; 72°C , 10 s; 72°C , 6 min. The PCR fragment was digested with EcoRI and BamHI and cloned into appropriate vectors for further analysis.

Multiple tissue Northern blots were purchased from Clontech and probed with the full-length human clone 25 cDNA labeled as described above for the mouse clone 28 probe. The blots were prehybridized for 2 h at 68°C in ExpressHyb™ solution (Clontech) followed by hybridization for 1 h at the same temperature. The blots were washed twice for 20 min in $2\times$ SSC, 0.05% SDS at 65°C followed by two washes for 20 min in $0.2\times$ SSC, 0.1% SDS at 65°C . Under these conditions, the full-length human clone 25 probe hybridizes with a single fragment on genomic Southern blots (data not shown).

Preparation of human eosinophils, neutrophils, and PBMC. Human neutrophils were isolated from heparinized venous blood by Percoll density gradient centrifugation ($d=1.088$) at room temperature (31). RBCs were removed by hypotonic lysis. Eosinophils were isolated from the blood of individuals with high levels of circulating blood eosinophils (5–17%) by combined density gradient centrifugation and negative selection with anti-CD16 magnetic beads (32). Briefly, the granulocyte fraction from the Percoll centrifugation was incubated with CD16 microbeads (Miltenyi Biotec Inc., Sunnyvale, CA) for 30 min. Cells were then passed through a MACS column (Miltenyi Biotec Inc.), and eosinophils were collected in the flow through. Eosinophil purity was $>99\%$ as determined by analysis of Diff-Quik-stained cytocentrifugation preparations by light microscopy. PBMCs were obtained as described (31).

Chemokines and chemotaxis. Recombinant human chemokines were obtained from Peprotech Inc. (Rocky Hill, NJ). Human eotaxin was synthesized using solid-phase methods that were optimized and adapted to a fully automated peptide synthesizer (430A; Applied Biosystems, Inc., Foster City, CA) as described elsewhere (33). Leukocyte chemotaxis was assessed using a modification of a transendothelial assay (6). The endothelial cells used for this assay were the endothelial cell line ECV 304 (34), obtained from the European Collection of Animal Cell Cultures (Porton Down, UK). Endothelial cells were cultured on 6.5-mm diameter Transwell culture inserts (Costar Corp., Cambridge, MA) with a $3.0\text{-}\mu\text{m}$ pore size. Culture media for ECV 304 cells consisted of M199 + 10% FCS, L-glutamine, and antibiotics. Assay media consisted of equal parts RPMI 1640 and M199, with 0.5% BSA. 24 h before the assay, 2×10^5 ECV 304 cells were plated onto each insert of the 24-well chemotaxis plate, and in-

cubated at 37°C . Chemotactic factors (diluted in assay medium) were added to the 24-well tissue culture plates in a final vol of $600\text{ }\mu\text{l}$. Endothelial-coated Transwells were inserted into each well and 10^6 leukocytes were added to the top chamber in a final vol of $100\text{ }\mu\text{l}$. The plate was then incubated at 37°C in 5% $\text{CO}_2/95\%$ air for 1–4 h, depending on the leukocyte type being studied. The cells that had migrated to the bottom chamber were counted using flow cytometry. $500\text{ }\mu\text{l}$ of the cell suspension from the lower chamber was placed in a tube, and relative cell counts were obtained by acquiring events for a set time period of 30 s. This counting method was found to be highly reproducible, and enabled gating on the leukocytes and the exclusion of debris or other cells. Counts obtained in this way matched closely those obtained by counting with a microscope.

Measurement of intracellular cytosolic free calcium $[\text{Ca}^{2+}]_i$. Eosinophils were labeled with the fluorochrome Fluo-3 (Molecular Probes, Eugene, OR) according to the manufacturer's recommendations. Briefly, $50\text{ }\mu\text{g}$ of Fluo-3 was dissolved in $44\text{ }\mu\text{l}$ of DMSO and diluted to $10\text{ }\mu\text{M}$ with modified Gay's buffer (MGB; 5 mM KCl, 147 mM NaCl, 0.22 mM KH_2PO_4 , 1.1 mM Na_2HPO_4 , 5.5 mM glucose, 0.3 mM $\text{MgSO}_4\cdot 7\text{H}_2\text{O}$, 1 mM MgCl_2 , and 10 mM Hepes, pH 7.4). Cells were resuspended in MGB to 10^7 cells/ml, and incubated with an equal vol of 10 mM Fluo-3 mix for 30 min at room temperature. Cells were then washed twice with MGB and resuspended at 2×10^6 cells/ml in MGB. The $[\text{Ca}^{2+}]_i$ was measured on the FACScan®, by analyzing FL1 (linear scale) versus time.

mAbs. mAbs were produced against human eotaxin by immunizing mice with $10\text{ }\mu\text{g}$ of synthesized Eotaxin, three times over a period of 4 wk. The first immunization was intraperitoneal with Freund's complete adjuvant, the second was intraperitoneal with Freund's incomplete adjuvant, and the final immunization was protein alone intravenous. 4 d after the last immunization, the spleen was taken, and cell fusion was performed using the cell line SP2/O, as described (31).

ELISA. ELISA was performed by coating $50\text{ }\mu\text{l}$ of eotaxin or recombinant MCP-1, MCP-3, or other chemokines onto 96-well Maxi-sorp plates (Nunc Inc., Naperville, IL), at a concentration of $2\text{ }\mu\text{g/ml}$ in carbonate buffer, for at least 4 h at 4°C . $300\text{ }\mu\text{l/well}$ of blocking buffer (PBS + 1% BSA) was added for at least 2 h, or until the day of the assay. Plates were washed $4\times$ with PBS/Tween 20, and $50\text{ }\mu\text{l}$ of mAb supernatant was added to each well and incubated at 37°C for 1 h. Plates were washed $4\times$ with PBS/Tween 20 and alkaline phosphatase-conjugated second antibody (Jackson ImmunoResearch Laboratories, Inc., West Grove, PA) diluted 1:500 in PBS was added to each well. After an incubation at 37°C for 30 min, plates were washed $4\times$ with PBS/Tween 20. The substrate used for the color reaction was *p*-nitrophenylphosphate dissolved in diethanolamine buffer (Bio-Rad Laboratories, Richmond, CA). Plates were read at 410 nm on an ELISA reader.

Immunohistochemistry. Immunohistochemical analysis for human eotaxin protein was performed on formalin-fixed, paraffin-embedded samples of nasal polyps using techniques previously described (35, 36). Briefly, deparaffinized sections were postfixated in 0.6% H_2O_2 in methanol for 20 min at room temperature to remove endogenous peroxidase activity, followed by blocking with PBS/10% goat serum for 30 min at room temperature. Anti-human eotaxin mAb (or irrelevant mAb) was then used as neat tissue culture supernatant overnight at 4°C , followed by biotinylated goat anti-mouse IgG (Vector Laboratories, Burlingame, CA), and avidin-biotin-peroxidase complexes (Vector Laboratories). Diaminobenzidine was used as the chromagen and Mayer's hematoxylin as the counterstain. Sections immunostained for eotaxin were compared to step sections with hematoxylin and eosin to evaluate spatial associations with eosinophil infiltration.

Ligand binding assay. ^{125}I -labeled RANTES were purchased from DuPont NEN (Boston, MA), with a sp act of $2,200\text{ Ci/mM}$. ^{125}I -labeled eotaxin was produced using the Bolton Hunter reagent (DuPont NEN), as described (31). The specific activity of radiolabeled eotaxin was calculated to be 180 Ci/mM . Chemokine binding to target cells was carried out using a modified method previously re-

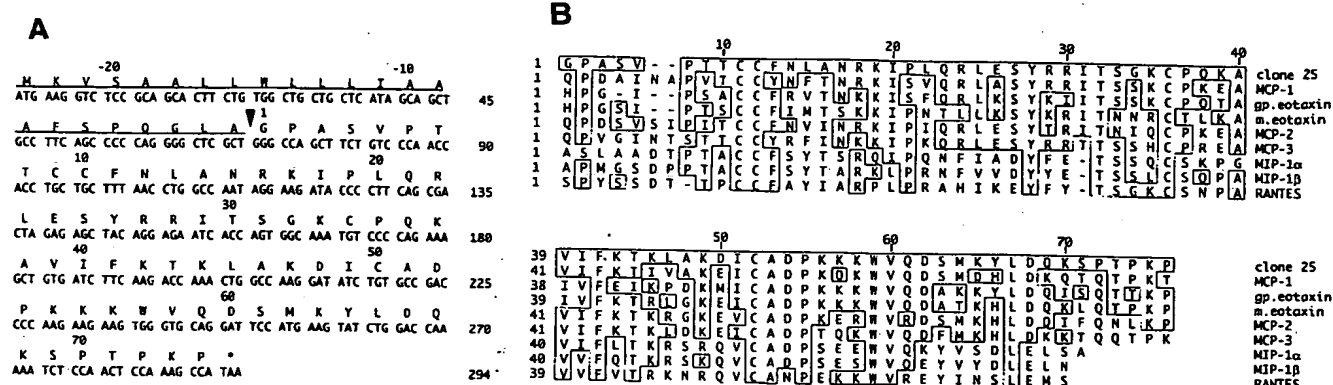


Figure 1. (A) Nucleotide sequence and deduced amino acid sequence of human clone 25 cDNA coding region. The underlined amino acids correspond to the predicted signal sequence with the arrowhead indicating the predicted signal peptidase cleavage site. (B) Amino acid sequence alignment of the predicted mature clone 25 protein with other human CC chemokines as well as guinea pig and mouse eotaxin. Amino acid numbering is relative to clone 25, and amino acids identical to clone 25 are boxed. These sequence data are available from GenBank under accession number U34780.

ported (37). Cells were washed once in PBS and resuspended in binding buffer (50 mM Hepes, 1 mM CaCl_2 , 5 mM MgCl_2 , and 0.5% BSA) at a concentration of $1 \times 10^7/\text{ml}$. Aliquots of 50 μl (5×10^5 cells) were dispensed into microfuge tubes, followed by the addition of cold competitor and radiolabeled chemokines as indicated in the text. The final reaction vol was 200 μl . Nonspecific binding was determined by incubating cells with radiolabeled chemokines in the presence of 250–500 nM of cold chemokines. After 60-min incubation at room temperature, the cells were washed three times, with 1 ml of binding buffer plus 0.5 M NaCl. Cell pellets were then counted. All experiments were carried out using duplicates and repeated at least three times. Curve fit was calculated by Kaleidagraph software (Synergy Software, Reading, PA).

In vivo assessment of eosinophil recruitment. A male adult rhesus monkey was injected intradermally at nine sites on the back with 10, 100, or 1,000 pmol of either eotaxin, RANTES, or BSA in 0.1 ml PBS. Full thickness skin biopsies (6 mm) were taken from these sites at 4 h after injection. These tissues were fixed in formalin, embedded in paraffin, and sectioned for histological analysis by staining with hematoxylin and eosin. Quantitative, computer-assisted morphometric analysis of skin sections was performed using a Quantimet 500 Image Analyzer (Leica Inc., Deerfield, IL). The relative density (number cells/ mm^2) of eosinophils was enumerated on at least five random fields per section just adjacent to and including the postcapillary venules of the superficial vascular plexus. Cells were selected based on the color wavelength generated from eosin-stained cytoplasmic granules of eosinophils, and color selection criteria were identical on all sections analyzed. The number of eosinophils/ mm^2 of dermis was then calculated.

Results

Cloning of a human eotaxin. A candidate human homologue of guinea pig eotaxin was cloned using the following approach. First, using degenerate primers deduced from the guinea pig sequence (25), a partial cDNA for a candidate mouse eotaxin was cloned (29a). Screening of a human genomic library with a mouse probe yielded 11 phage which were plaque purified and analyzed by restriction digest. One phage, designated clone 25, contained a 1.0-kb HindIII and a 5.5-kb Pst fragment which hybridized with the murine eotaxin probe. These fragments were subcloned, sequenced, and found to contain a nucleotide

sequence with significant similarity to other chemokine genes. To determine if this genomic clone encoded a functional gene, specific primers were used to amplify a cDNA. Fig. 1 A shows the nucleotide sequence and predicted amino acid sequence of the amplified product from human spleen mRNA. Clone 25 encodes a 97 amino acid protein including a putative hydrophobic leader peptide of 23 amino acids with a leader peptidase cleavage site predicted by amino acid consensus and comparison with other chemokine sequences. This protein is a member of the CC chemokine family as indicated by the cysteine pair at amino acid position 9 and 10 in Fig. 1 A.

Fig. 1 B shows an amino acid sequence alignment of the predicted mature clone 25 protein with other members of the CC chemokine family. This protein shows highest amino acid sequence identity to human MCP-1 and human MCP-2, both at 64.5% followed by mouse eotaxin, guinea pig eotaxin, and human MCP-3 with 63.2, 61.8, and 57.7%, respectively. Lower amino acid sequence identity is observed with human MIP-1 β (36.8%), human RANTES (34.2%), and human MIP-1 α (32.9%). Interestingly, further comparison shows that clone 25 shares with both guinea pig and mouse eotaxin a two amino acid deletion between positions 5 and 6 (Fig. 1 B) suggesting that clone 25 is the human homologue of the murine and guinea pig eotaxin genes. Comparison of the putative NH_2 terminus of clone 25 shows, however, that it does not share either the glutamine residue essential for optimal MCP-1 function (38) or the basic histidine residue present in both the mouse and guinea pig eotaxin sequence. A comparison between clone 25 and the guinea pig and mouse eotaxins also shows that the NH_2 terminus is poorly conserved, with only the two prolines at amino acid positions 2 and 6 completely conserved. Amino acids 51–62 are absolutely conserved, and based on the nuclear magnetic resonance structure of RANTES, this region is hypothesized to form a loop connecting a β -sheet of the chemokine core with the COOH-terminal α -helix (39).

Screening of multiple tissue Northern blots containing 2 μg of poly A + selected RNA revealed a major hybridizing message at ~ 0.8 kb with the highest level of expression in the small intestine and colon (Fig. 2). There was also a detectable level of expression in heart. No detectable level of mRNA ex-

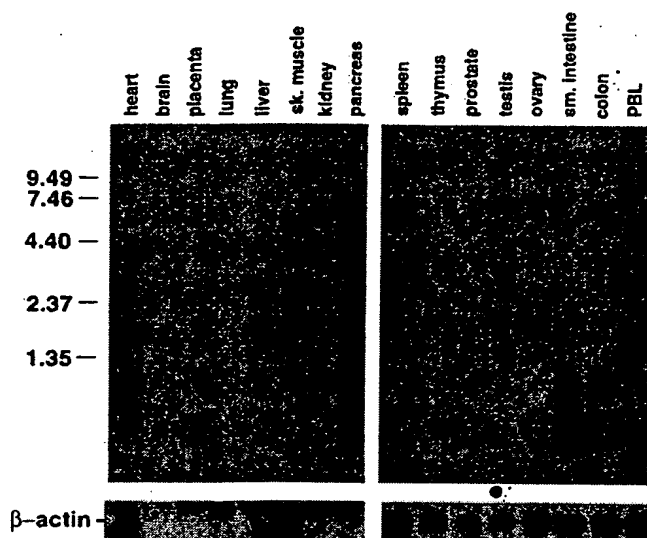


Figure 2. Northern analysis of ~2 µg of oligo-dT-selected RNA from various human tissues. Blots were purchased from Clontech and hybridized as described in Methods. After boiling in 0.5% SDS to remove specific probe, the blots were rehybridized with a β-actin control.

pression was evident in other tissues under the conditions described, however clone 25 cDNA has been amplified by PCR from spleen, thymus, and purified eosinophils (not shown).

In vitro chemotactic response of human leukocytes to a putative human eotaxin. The protein encoding clone 25 (deduced from the nucleotide sequence) was chemically synthesized and folded, following procedures used previously for other CC chemokines (38). Human eosinophils, neutrophils, monocytes, and lymphocytes were assessed for their response to different concentrations of this as well as other chemokines in a sensitive transendothelial chemotaxis assay (Fig. 3). The chemokine encoded by clone 25 was a strong chemoattractant for eosinophils, and usually showed a similar activity to RANTES and MCP-3, two well characterized eosinophil chemoattractants (20–23). We observed only modest chemotaxis of human eosinophils to MIP-1α or IL-8 in normal donors, although eosinophils from an individual with a history of asthma and very high eosinophil levels responded to these chemokines. The chemokine encoded by clone 25 was not chemotactic for human neutrophils or lymphocytes (Fig. 3) and mediated only a weak response in monocytes at very high doses (> 1,000 ng/ml). Anti-CD3-activated T cells were unresponsive at all concentrations tested (not shown). The use of endothelial cells in the chemotaxis assay enables a significant improvement in signal to noise (6, 40), sometimes reaching values of 400:1. In bare filter chemotaxis assays, the typical bell shaped curve was obtained, and the concentration of eotaxin that yielded the greatest eosinophil migration was 100 ng/ml. A checkerboard analysis with various concentrations of clone 25 protein showed that the migration of eosinophils was chemotactic rather than chemokinetic.

In vivo recruitment of rhesus monkey eosinophils to a putative human eotaxin. To test the in vivo role of the chemokine encoded by clone 25, an adult rhesus monkey was injected intradermally with 10, 100, or 1,000 pmol of either clone 25 pro-

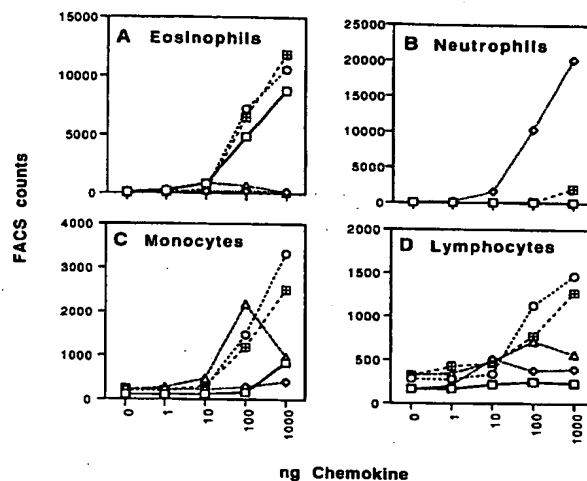


Figure 3. Chemotactic responses of human leukocytes to eotaxin and other chemokines. Human eosinophils (A), neutrophils (B), monocytes (C), and lymphocytes (D) were assessed in transendothelial chemotaxis assays to 1, 10, 100, and 1,000 ng/ml of various chemokines. Cells migrating from the top well of the Transwell to the bottom well were enumerated by counting for 30 s with a FACScan®. The endothelial cells used for coating the polycarbonate membrane of the Transwell were ECV304 cells. Values are a representative experiment of at least six performed. □, eotaxin; ◇, IL-8; ○, RANTES; △, MIP-1α; ▽, MCP-3.

tein, human RANTES, or BSA. Histologic assessment and quantitative image analysis of skin biopsies showed no recruitment of eosinophils with BSA at doses of 10 and 100 pmol, and only a rare isolated eosinophil at 1,000 pmol (Fig. 4). The greatest eosinophil recruitment was observed at the injection site for 1,000 pmol of clone 25 protein, or human RANTES, which was characterized histologically by foci consisting of 5–10 eosinophils adjacent to postcapillary venules of the superficial vascular plexus in the dermis, as well as clusters of eosinophils scattered throughout the dermal collagen bundles. The chemokine encoded by clone 25 elicited recruitment of eosinophils at 10, 100, and 1,000 pmol, whereas RANTES elicited a response only at 1,000 pmol. Although nonspecific dermal recruitment of occasional neutrophils was apparent in all specimens, including those injected with BSA, the leukocyte

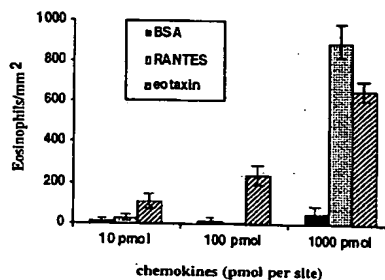


Figure 4. Recruitment of eosinophils to the skin of a rhesus monkey injected with clone 25 protein, RANTES, or BSA. An adult rhesus monkey was injected intradermally with 10, 100, or 1,000 pmol of either clone 25 protein, RANTES, or BSA. Full thickness

skin biopsies (6 mm) were taken from these sites at 4 h after injection, and histologic assessment and quantitative image analysis of skin biopsies was performed. The relative density (number cells/mm²) of eosinophils was enumerated on at least 5 random fields/section just adjacent to and including the postcapillary venules of the superficial vascular plexus.

types recruited to the clone 25-challenged site were > 90% eosinophils. In contrast, although eosinophils were recruited to the 1,000 pmol RANTES injection site, increased numbers of perivascular mononuclear cells were observed in all RANTES injection sites, similar to the infiltrate observed in a previous study with dogs (41).

Because of the high sequence similarity between clone 25 and guinea pig eotaxin, and the fact that this chemokine is selectively chemotactic for eosinophils *in vitro* and *in vivo*, this chemokine will henceforth be referred to as human eotaxin.

Human eotaxin desensitizes $[Ca^{2+}]_i$ responses of eosinophils to most CC chemokines. The transient elevation in $[Ca^{2+}]_i$ in cells upon chemokine binding can be used to monitor receptor activation, and the desensitization that occurs through a given receptor can provide some insight into receptor usage by different agonists (20, 42, 43). Fluo-3-loaded eosinophils (> 99% purity) showed a strong, rapid, and transient rise in $[Ca^{2+}]_i$ after stimulation with 50 nM of human eotaxin (Fig. 5). A similar

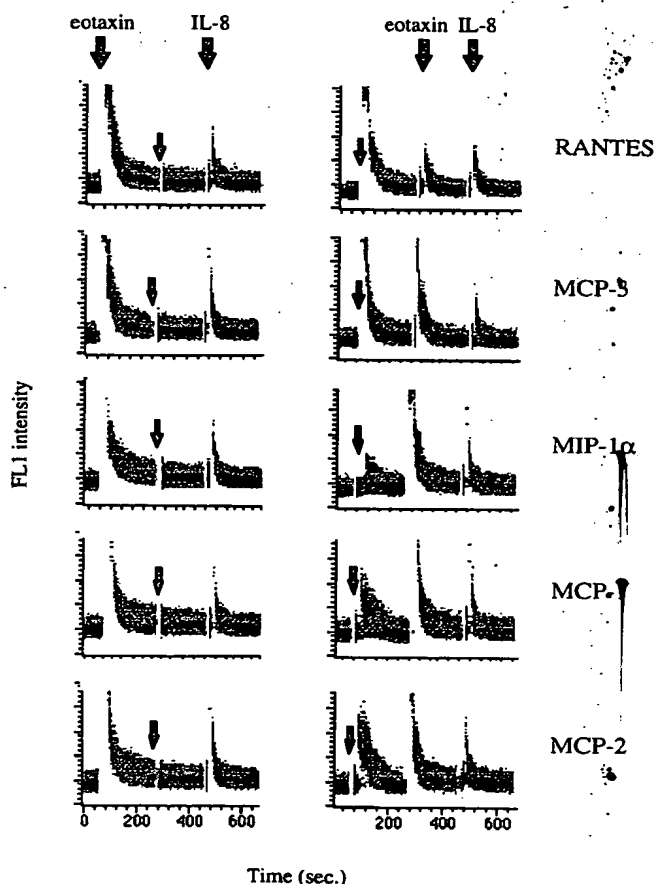


Figure 5. Changes in the cytosolic free calcium concentration in human eosinophils in response to various chemokines. In the first set of experiments (left hand plots), eotaxin was added first, followed by a test chemokine indicated on the right of the figure, followed by IL-8. In the second set of experiments (right hand plots), test chemokine were added first, followed by eotaxin, followed by IL-8. Chemokines were added at the points indicated by arrows to a final concentration of 50 nM. In this experiment, IL-8 induced a calcium flux on a proportion of eosinophils and was used for control purposes at 50 nM. FL1, linear scale.

response was observed with 50 nM human RANTES, and 50 nM MCP-3. An advantage of using the FACScan® for $[Ca^{2+}]_i$ analysis is that the proportion of cells responding to a given ligand can be assessed. All eosinophils responded to eotaxin, RANTES, and MCP-3, but only a proportion (~20–30%) responded to MIP-1α, IL-8, or MCP-1, although these values were variable from donor to donor. 50 nM of human eotaxin was able to completely desensitize eosinophils to subsequent stimulation with 50 nM RANTES, MCP-3, MCP-1, MIP-1α, and MCP-2 (Fig. 5). In addition, 50 or 100 nM RANTES could only partially desensitize eosinophils to subsequent stimulation with 50 nM of human eotaxin. However a range of concentrations of MCP-3, MCP-2, MCP-1, or MIP-1α (10–100 nM) were unable to desensitize subsequent responses to eotaxin. In all of the analyses, IL-8 was used as a control, since none of the CC chemokines could desensitize eosinophil responses to IL-8.

Human eotaxin binds with high affinity to a receptor on eosinophils. The expression of the receptor for eotaxin on eosinophils was examined using ligand binding with radiolabeled eotaxin and RANTES. Fig. 6A shows the binding of ^{125}I -labeled eotaxin to human eosinophils, in the presence of increasing concentrations of "cold" competitors. ^{125}I -labeled eotaxin bound to eosinophils, and this binding could be competed efficiently with cold eotaxin. Binding could also be competed with cold MCP-3 and RANTES, although MCP-3 and RANTES competed less efficiently than eotaxin for ^{125}I -

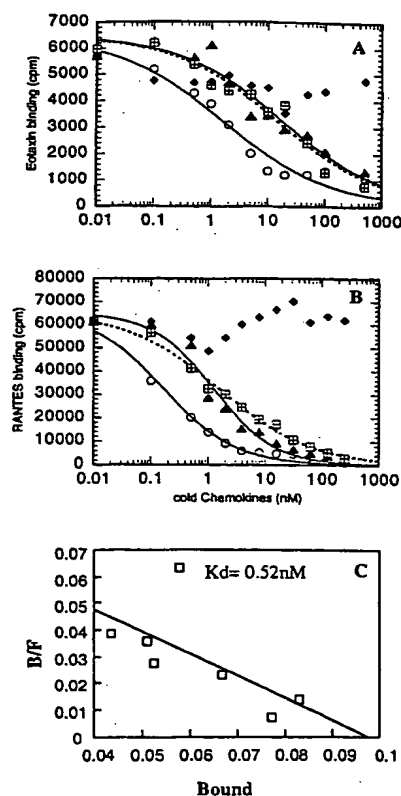


Figure 6. Competitive binding of chemokines to human eosinophils. Purified human eosinophils were resuspended in binding buffer (50 mM Hepes supplemented with 0.5% BSA, 1 mM $CaCl_2$, and 5 mM $MgCl_2$). Into each microfuge tube were added 5×10^5 eosinophils, various concentrations of unlabeled chemokines, and 1 nM radiolabeled eotaxin (A), or 0.1 nM radiolabeled RANTES (B). After 60 min at room temperature, the cell pellets were washed and counted as described in Methods. Points generated by cold MIP-1α could not be analyzed by the curve fit program as there was no competition at the concentrations used. C shows a Scatchard plot using unlabeled eotaxin to com-

pete with radiolabeled eotaxin binding to human eosinophils. It reveals a K_d of 0.52 nM and 4.8×10^4 binding sites per cell. These data are representative of at least three experiments. O, eotaxin; ▲, RANTES; ■, MCP-3; ◆, MIP-1α.

Table 1. Properties of a Panel of Antieotaxin mAbs

mAb	Isotype	Specificity*	Neutralizing activity†	Staining paraffin sections‡
6H9	IgG1	eotaxin	—	+
5E9	IgG1	eotaxin	—	+
5H2	IgG1	eotaxin	—	+
6D9	IgG1	eotaxin	—	+
9H3	IgG2b	eotaxin	+	—
3C7	IgG1	eotaxin	+	—
6E6	IgG1	eotaxin, MCP-1, MCP-3	—	ND

* Specificity was determined by ELISA using plates coated with eotaxin, MCP-1, MCP-3, RANTES, or MIP-1 α . † Neutralizing ability was assessed by mAb inhibition of ¹²⁵I-labeled eotaxin binding to human eosinophils and by inhibition of chemotaxis. ‡ mAb staining of paraffin sections was assessed using human nasal polyp.

labeled eotaxin binding. MIP-1 α was not able to compete with ¹²⁵I-labeled eotaxin binding under the conditions used, suggesting that eotaxin binding to eosinophils was through a receptor other than CKR-1 (the MIP-1 α /RANTES receptor). This was confirmed using CC CKR1-expressing transfectants and cell lines; ¹²⁵I-labeled eotaxin was unable to bind these cells, and cold eotaxin was unable to compete with ¹²⁵I-labeled RANTES binding (not shown). Competitive binding by unlabeled eotaxin produced a Scatchard plot (Fig. 6 C), which revealed a single binding site for eotaxin on eosinophils, a K_d of 0.52 nM, and 4.8×10^4 binding sites per cell. Scatchard plots using ¹²⁵I-labeled RANTES revealed similar binding sites per cell. In a similar set of experiments, eosinophils were incubated with ¹²⁵I-labeled RANTES (Fig. 6 B), and increasing concentrations of cold eotaxin, RANTES, MCP-3, or MIP-1 α . Binding of ¹²⁵I-labeled RANTES to human eosinophils could be efficiently competed with cold eotaxin, and eotaxin was a much more efficient competitor than cold MCP-3 or RANTES.

Expression of eotaxin in tissues and upregulation at a site of eosinophil recruitment. A panel of 50 mAbs was produced to human eotaxin by immunizing mice with the chemically synthesized material, and screening for specific mAbs by ELISA. The majority of the mAbs were found to be specific for eotaxin, in that they showed strong reactivity with eotaxin, and no reactivity with human MCP-1, MCP-3, RANTES, or MIP-1 α , as assessed by ELISA. Several of the mAbs recognized an epitope shared between eotaxin, MCP-3, and MCP-1. The properties of seven select mAbs are outlined in Table 1. Two of the eotaxin-specific mAbs were noted for their ability to block the binding of ¹²⁵I-labeled eotaxin to human eosinophils, and/or the chemotaxis of eosinophils to eotaxin in transendothelial chemotaxis assays. Four of the mAbs were able to recognize an epitope of human eotaxin that is preserved in paraffin-embedded tissue specimens.

Immunohistochemical analysis was performed with a representative mAb, 6H9, using human nasal mucosa and polyp tissue with pronounced submucosal eosinophil infiltration. Eotaxin staining was localized most strongly to overlying ciliated pseudostratified columnar epithelium (Fig. 7). Various leukocyte types also stained positively, including eosinophils, lymphocytes, and macrophages (Fig. 7). Care was taken to ensure the eosinophil staining was bona fide and not due to endoge-

nous peroxidase. No immunoreactivity to any cell type was recognized in the same tissue using an irrelevant IgG1 mAb. There was a strong correlation between eosinophil infiltration within the mucosa and submucosa of the polyp and eotaxin expression to resident cells and leukocytes. Specifically, in areas of eosinophil localization in polyp tissue, there was an increase in the number of antieotaxin immunoreactive macrophages, endothelial cells, fibroblasts, smooth muscle cells, lymphoid cells, epithelial cells, and eosinophils, when compared to uninvolved nasal mucosa. In addition, there was a concomitant increase in staining intensity of immunoreactive cells in the polyp tissue compared to adjacent uninvolved nasal mucosa.

Discussion

Here we identify a novel human chemokine that is selectively chemotactic for eosinophils. Based on sequence similarity and function, this chemokine can be considered a human equivalent of guinea pig and murine eotaxin. A hallmark of guinea pig eotaxin is its high degree of specificity for eosinophils, which sets it apart from the other eosinophil chemoattractants such as C5a, PAF, RANTES, and MCP-3, which are chemotactic for other leukocyte types. Human eotaxin was highly selective for eosinophils, although at very high doses it was chemotactic for a very small number of monocytes, possibly due to low affinity binding to a monocyte CC chemokine receptor. Human eotaxin was usually as effective as RANTES or MCP-3 as an eosinophil chemoattractant, although we did observe donor to donor variation in the relative response to eotaxin, RANTES, and MCP-3. The nature of an individual's eosinophils, such as activation status or exposure to IL-5, may affect the responses of eosinophils to different chemokines.

Studies with a single rhesus monkey showed that human eotaxin was also effective at recruiting eosinophils to challenged skin sites. A study in guinea pigs showed that eotaxin induced substantial eosinophil accumulation in the skin at a 1–2 pmol (24), which is a much lower dose than what we found to be optimal in our study. The recruitment of eosinophils to tissues may relate not only to the presence of chemokine within the tissue, but also other factors such as the relative numbers of eosinophils within the blood. IL-5 has been found to synergize with eotaxin in the recruitment of guinea pig eosinophils to challenged sites; the IL-5 functioned in the mobilization of eosinophils from the bone marrow to the blood, and the eotaxin acted locally for the recruitment of eosinophils (44). IL-5 is an eosinophil differentiation and activating factor (15) and has been found to affect responsiveness of eosinophils to IL-8 (45). RANTES injections into the skin of a rhesus monkey led to the recruitment of both eosinophils and mononuclear cells to the challenged sites, similar to a previous report using dogs (41) and consistent with the in vitro chemotactic profile of RANTES in humans.

The existence of an eosinophil-specific chemokine may explain the highly selective accumulation of eosinophils in some inflammatory sites. This may have important implications, since excessive recruitment of eosinophils to mucosal tissues may contribute to the pathogenesis of asthma and other human diseases (16, 46). Northern blot analysis as well as immunohistochemistry confirmed previous studies in guinea pig that eotaxin in humans is expressed constitutively in some tissues (25, 26). Our Northern blot analysis correlates well with that reported for guinea pig eotaxin with the exception of lung

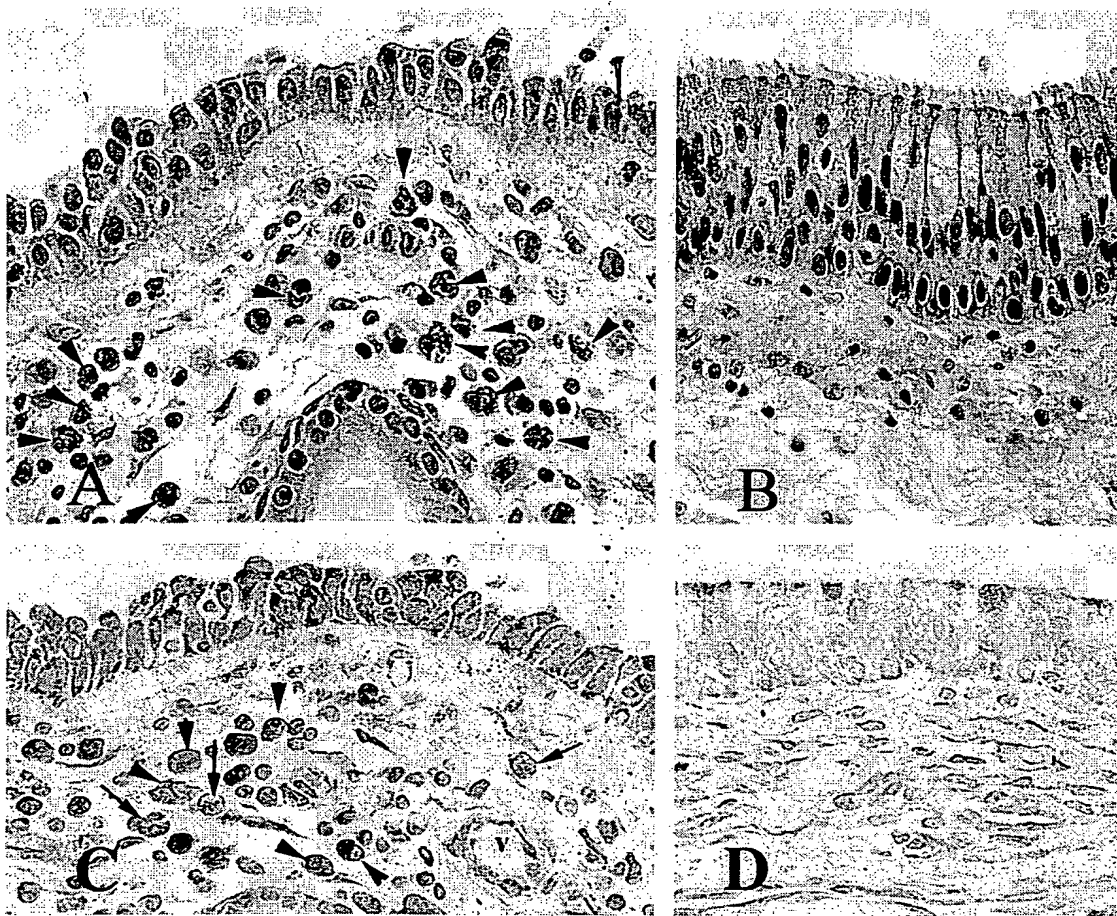


Figure 7. Photomicrographs of human nasal polyp (*A* and *C*) and adjacent nasal mucosa (*B* and *D*). The polyp (*A*) is characterized by extensive submucosal infiltration by eosinophils (arrowheads) and attenuation of the overlying respiratory epithelium. Immunoperoxidase staining of step sections of the polyp (*C*) with antieotaxin mAb 6H9 revealed intense immunoreactivity to epithelium, endothelium lining venules (*v*), eosinophils (arrows), mononuclear cells (arrowheads), and spindle cells. In contrast, the adjacent respiratory tissue is characterized by normal pseudostratified columnar epithelium and no eosinophil infiltration (*B*), and immunostaining for eotaxin shows only light constitutive immunoreactivity to epithelium and submucosal mesenchymal cells (*D*). (*A* and *B*) Hematoxylin and eosin, $\times 1,450$; (*C* and *D*) ABC-peroxidase technique with Mayer's hematoxylin, $\times 1,450$.

where it appears to be expressed more abundantly in guinea pig. A striking similarity between guinea pig and human was the presence of eotaxin message in the heart, but not in skeletal muscle. The expression in heart may relate to the pathogenesis of endomyocardial fibrosis, a condition which is common in patients with hypereosinophilic syndrome (47). A comprehensive analysis of the expression of eotaxin by immunohistochemistry was beyond the scope of this study. However, an analysis of inflamed nasal mucosal tissue revealed intense staining of respiratory epithelium, endothelial cells, leukocytes, and fibroblasts. These cell types are well characterized for their ability to produce other chemokines, such as MCP-1 and MIP-1 α (48–50). Of particular interest was the staining of eosinophils in mucosal tissue by antieotaxin mAbs. An autocrine production of eosinophilic chemotactic cytokines, yielding an amplification loop for eosinophil entry to mucosal tissue, has been proposed as a possible contributing factor in asthma and other allergies (14). We cannot exclude, however, the possibility that this staining resulted from receptor-bound material. The preliminary analysis of eotaxin expression in na-

sal polyp showed a correlation between eosinophil recruitment and upregulated expression of eotaxin, although more tissues will need to be assessed before a definitive statement can be made. Staining for other eosinophilic chemokines did not reveal such a strong correlation (D.J. Ringler, unpublished observations), although the association between chemokine expression and the presence of inflammatory cells is still poorly understood and the conditions that give rise to eosinophil recruitment to a tissue are likely to be multifactorial.

The selective migration of eosinophils to eotaxin would suggest the existence of a receptor for eotaxin expressed only on eosinophils. The ligand binding experiments and $[Ca^{2+}]_i$ analysis indicated that the dominant eosinophil eotaxin receptor also binds RANTES and MCP-3. These three ligands are the most potent chemokines for inducing eosinophil chemotaxis in vitro. Previous calcium desensitization studies (21, 22) implicated a RANTES/MCP-3 receptor on eosinophils that was distinct from CKR-1 (the MIP-1 α /RANTES receptor) identified by Neote et al. (27) and Gao et al. (28). Our $[Ca^{2+}]_i$ analysis showed that eotaxin could effectively desensitize eosin-

ophils to subsequent $[Ca^{2+}]_i$ responses to virtually all CC chemokines. This suggests that eotaxin is causing homologous desensitization of an eotaxin/MCP-3/RANTES receptor, and possibly cross-desensitization of other receptors. Cross-desensitization of chemoattractant receptors is well documented (51), and could result from a desensitization of the pathways leading to Ca^{2+} mobilization, downstream from receptor/G-protein interactions (51). Alternatively, eotaxin may bind and signal through more than one receptor, although we have found that eotaxin does not bind to CKR-1 (unpublished observation). Our binding experiments support the existence of an "eotaxin/RANTES/MCP-3" receptor, although eotaxin appears to have a much stronger binding affinity for this receptor than RANTES or MCP-3. Nevertheless the *in vitro* chemotactic response of eosinophils to RANTES and MCP-3 was usually similar to that seen with eotaxin, suggesting that binding affinity does not correlate strictly with chemotactic activity. The number of binding sites for eotaxin on eosinophils (4.8×10^4 receptors per cell) is much higher than the levels of expression of CKR-1 or CKR-2 on monocytes ($< 3,000$ per cell) (7, 41, 52) but is similar to the levels of IL-8 receptors on neutrophils ($\sim 6 \times 10^4$ sites per cell) (53). We have cloned a novel CC chemokine receptor from human eosinophils that mediates the binding and signaling of eotaxin, RANTES, and MCP-3 (Ponath, P., et al., manuscript submitted). This receptor is 72% identical to the CKR-1 and is very similar to an eosinophil-restricted CC chemokine receptor reported recently by another group (54). The selective binding of eotaxin to a receptor on eosinophils, coupled with production of eotaxin by certain inflammatory cells and epithelium, provides a mechanism for the selective recruitment of eosinophils to inflamed mucosal tissue.

The relative contribution of eotaxin versus other chemoattractants in various eosinophil-related diseases will be an important topic for further investigation. Eotaxin will be a valuable tool for exploring the molecular mechanisms for eosinophil traffic, and possibly for the discovery of eosinophil CC chemokine receptor antagonists for blocking eosinophil recruitment in diseases such as asthma.

Acknowledgments

We thank Drs. Craig Gerard, Greg LaRosa, Dulce Soler, Eugene Butcher, and Tim Springer for assistance during the course of these experiments and for suggestions in the preparation of this manuscript. We also thank Michelle Rand and Michael Mansour for technical assistance, Dr. Prabhat Sehgal of the New England Regional Primate Center for assistance with the non-human primate experiments, and Dr. Richard Sibley (Stanford University School of Medicine, Stanford, CA) for supplying human nasal polyp.

Chemical synthesis work was supported by National Institutes of Health grant RO1 GM-50969-01.

References

- Springer, T.A. 1994. Traffic signals for lymphocyte recirculation and leukocyte emigration: the multistep paradigm. *Cell* 76:301-314.
- Baggiolini, M., B. Dewald, and B. Moser. 1994. IL-8 and related chemotactic cytokines-CXC and CC chemokines. *Adv. Immunol.* 55:97-179.
- Miller, M.D., and M.S. Krangel. 1992. Biology and biochemistry of the chemokines: a family of chemotactic and inflammatory cytokines. *Crit. Rev. Immunol.* 12:17-46.
- Schall, T.J., and K.B. Bacon. 1994. Chemokines, leukocyte trafficking, and inflammation. *Curr. Opin. Immunol.* 6:865-873.
- Oppenheim, J.J., C.O. Zachariae, N. Mukaida, and K. Matsushima. 1991. Properties of the novel proinflammatory supergene "intercrine" cytokine family. *Annu. Rev. Immunol.* 9:617-648.
- Carr, M.W., S.J. Roth, E. Luther, S.S. Rose, and T.A. Springer. 1994. Monocyte chemoattractant protein 1 acts as a T-lymphocyte chemoattractant. *Proc. Natl. Acad. Sci. USA* 91:3652-3656.
- Ernst, C.A., Y.J. Zhang, P.R. Hancock, B.J. Rutledge, C.L. Corless, and B.J. Rollins. 1994. Biochemical and biologic characterization of murine monocyte chemoattractant protein-1. Identification of two functional domains. *J. Immunol.* 152:3541-3549.
- Tanaka, Y., D.H. Adams, S. Hubscher, H. Hirano, U. Siebenlist, and S. Shaw. 1993. T-cell adhesion induced by proteoglycan-immobilized cytokine MIP-1 beta. *Nature (Lond.)* 361:79-82.
- Murphy, P.M. 1994. The molecular biology of leukocyte chemoattractant receptors. *Annu. Rev. Immunol.* 12:593-633.
- Broadbent, V.C., A.M. Boylan, J.M. Hoeffel, K.J. Kim, M. Sadick, A. Chuntharapai, and C.A. Hebert. 1994. Neutralization of IL-8 inhibits neutrophil influx in a rabbit model of endotoxin-induced pleurisy. *J. Immunol.* 152:2960-2967.
- Mulligan, M.S., M.L. Jones, M.A. Bolanowski, M.P. Baganoff, C.L. Deppeler, D.M. Meyers, U.S. Ryan, and P.A. Ward. 1993. Inhibition of lung inflammatory reactions in rats by an anti-human IL-8 antibody. *J. Immunol.* 150:5585-5595.
- Sekido, N., N. Mukaida, A. Harada, I. Nakanishi, Y. Watanabe, and K. Matsushima. 1993. Prevention of lung reperfusion injury in rabbits by a monoclonal antibody against interleukin-8. *Nature (Lond.)* 365:654-657.
- Cacalano, G., J. Lee, K. Kikly, A.M. Ryan, S. Pitts-Meek, B. Hultgren, W.I. Wood, and M.W. Moore. 1994. Neutrophil and B cell expansion in mice that lack the murine IL-8 receptor homolog. *Science (Wash. DC)* 265:682-684.
- Weller, P.F. 1992. Roles of eosinophils in allergy. *Curr. Opin. Immunol.* 4:782-787.
- Gleich, G.J., C.R. Adolphson, and K.M. Leiferman. 1993. The biology of the eosinophilic leukocyte. *Annu. Rev. Med.* 44:85-101.
- Kay, A.B., and C.J. Corrigan. 1992. Asthma. Eosinophils and neutrophils. *Br. Med. Bull.* 48:51-64.
- Wardlaw, A.J., R. Moqbel, O. Cromwell, and A.B. Kay. 1986. Platelet-activating factor. A potent chemotactic and chemokinetic factor for human eosinophils. *J. Clin. Invest.* 78:1701-1706.
- Fernandez, H.N., P.M. Henson, A. Otani, and T.E. Hugli. 1978. Chemotactic response to human C3a and C5a anaphylatoxins. I. Evaluation of C3a and C5a leukotaxis *in vitro* and under simulated *in vivo* conditions. *J. Immunol.* 120:109-115.
- Rand, T.H., W.W. Cruikshank, D.M. Center, and P.F. Weller. 1991. CD4-mediated stimulation of human eosinophils: lymphocyte chemoattractant factor and other CD4-binding ligands elicit eosinophil migration. *J. Exp. Med.* 173:1521-1528.
- Rot, A., M. Krieger, T. Brunner, S.C. Bischoff, T.J. Schall, and C.A. Dahinden. 1992. RANTES and macrophage inflammatory protein 1.alpha induce the migration and activation of normal human eosinophil granulocytes. *J. Exp. Med.* 176:1489-1495.
- Dahinden, C.A., T. Geiser, T. Brunner, V. von Tschanner, D. Caput, P. Ferrara, A. Minty, and M. Baggiolini. 1994. Monocyte chemoattractant protein 3 is a most effective basophil- and eosinophil-activating chemokine. *J. Exp. Med.* 179:751-756.
- Baggiolini, M., and C.A. Dahinden. 1994. CC chemokines in allergic inflammation. *Immunol. Today* 15:127-133.
- Kameyoshi, Y., A. Dorschner, A.I. Mallet, E. Christophers, and J.M. Schroder. 1992. Cytokine RANTES released by thrombin-stimulated platelets is a potent attractant for human eosinophils. *J. Exp. Med.* 176:587-592.
- Jose, P.J., D.A. Griffiths-Johnson, P.D. Collins, D.T. Walsh, R. Moqbel, N.F. Totty, O. Truong, J.J. Hsuan, and T.J. Williams. 1994. Eotaxin: a potent eosinophil chemoattractant cytokine detected in a guinea pig model of allergic airways inflammation. *J. Exp. Med.* 179:881-887.
- Jose, P.J., I.M. Adcock, D.A. Griffiths-Johnson, N. Berkman, T.N. Wells, T.J. Williams, and C.A. Power. 1994. Eotaxin: cloning of an eosinophil chemoattractant cytokine and increased mRNA expression in allergen-challenged guinea-pig lungs. *Biochem. Biophys. Res. Commun.* 205:788-794.
- Rothenburg, M.E., A.D. Luster, C.M. Lilly, J.M. Drazen, and P. Leder. 1995. Constitutive and allergen-induced expression of eotaxin mRNA in the guinea pig lung. *J. Exp. Med.* 181:1211-1216.
- Neote, K., D. DiGregorio, J.Y. Mak, R. Horuk, and T.J. Schall. 1993. Molecular cloning, functional expression, and signaling characteristics of a C-C chemokine receptor. *Cell* 72:415-425.
- Gao, J.L., D.B. Kuhns, H.L. Tiffany, D. McDermott, X. Li, U. Francke, and P.M. Murphy. 1993. Structure and functional expression of the human macrophage inflammatory protein 1 alpha/RANTES receptor. *J. Exp. Med.* 177:1421-1427.
- Charo, I.F., S.J. Myers, A. Herman, C. Franci, A.J. Connolly, and S.R. Coughlin. 1994. Molecular cloning and functional expression of two monocyte chemoattractant protein 1 receptors reveals alternative splicing of the carboxyl-terminal tails. *Proc. Natl. Acad. Sci. USA* 91:2752-2756.
- Gonzalo, J.A., G.-Q. Jia, V. Aguirre, A. Coyle, N. Jenkins, H. Katz, A. Lichtman, N. Copeland, M. Kopf, and J.C. Gutierrez-Ramos. 1996. The expression of mouse eotaxin parallels eosinophil accumulation during lung allergic in-

flammatory reactions but is not restricted to a TH2 type response. *Immunity*. In press.

30. Sambrook, J., E.F. Fritsch, and T. Maniatis, editors. 1989. *Molecular Cloning. A Laboratory Manual*. 2nd ed. Cold Spring Harbor Laboratory Press, Cold Spring Harbor, NY.
31. Coligan, J.E., A.M. Kruisbeek, D.H. Margulies, E.M. Shevach, and W. Strober, editors. 1992. *Current Protocols in Immunology*. John Wiley and Sons, Inc., New York.
32. Hansel, T.T., J.D. Pound, D. Pilling, G.D. Kitas, M. Salmon, T.A. Gentile, S.S. Lee, and R.A. Thompson. 1989. Purification of human eosinophils by negative selection using immunomagnetic beads. *J. Immunol. Methods*. 122:97-103.
33. Clark-Lewis, I., B. Moser, A. Walz, M. Baggiolini, G.J. Scott, and R. Aebbersold. 1991. Chemical synthesis, purification, and characterization of two inflammatory proteins, neutrophil activating peptide 1 (interleukin-8) and neutrophil activating peptide. *Biochemistry*. 30:3128-3135.
34. Takahashi, K., Y. Sawasaki, J.-I. Hata, K. Mukai, and T. Goto. 1990. Spontaneous transformation and immortalization of human endothelial cells. *In Vitro Cell & Dev. Biol.* 25:265-274.
35. Ringler, D.J., W.W. Hancock, N.W. King, N.L. Letvin, M.D. Daniel, R.C. Desrosiers, and G.F. Murphy. 1987. Immunophenotypic characterization of the cutaneous exanthem of SIV-infected rhesus monkeys. Apposition of degenerative Langerhans cells and cytotoxic lymphocytes during the development of acquired immunodeficiency syndrome. *Am. J. Pathol.* 126:199-207.
36. Ringler, D.J., W.W. Hancock, N.W. King, and G.F. Murphy. 1987. Characterization of nonhuman primate epidermal and dermal dendritic cells with monoclonal antibodies. A study of Langerhans cells and indeterminate cells in the rhesus monkey. *Lab. Invest.* 56:313-320.
37. Van Riper, G., S. Siciliano, P.A. Fischer, R. Meurer, M.S. Springer, and H. Rosen. 1993. Characterization and species distribution of high affinity GTP-coupled receptors for human rantes and monocyte chemoattractant protein 1. *J. Exp. Med.* 177:851-856.
38. Gong, J.H., and L.I. Clark. 1995. Antagonists of monocyte chemoattractant protein 1 identified by modification of functionally critical NH₂-terminal residues. *J. Exp. Med.* 181:631-640.
39. Skelton, N.J., F. Aspiras, J. Ogez, and T.J. Schall. 1995. Proton NMR assignments and solution conformation of RANTES, a chemokine of the C-C type. *Biochemistry*. 34:5329-5342.
40. Smith, W.B., J.R. Gamble, I. Clark-Lewis, and M.A. Vadas. 1991. Interleukin-8 induces neutrophil transendothelial migration. *Immunology*. 72:65-72.
41. Meurer, R., G. Van Riper, W. Feeney, P. Cunningham, D. Hora, M.S. Springer, D.E. MacIntyre, and H. Rosen. 1993. Formation of eosinophilic and monocytic intradermal inflammatory sites in the dog by injection of human RANTES but not human monocyte chemoattractant protein 1, human macrophage inflammatory protein 1 alpha, or human interleukin 8. *J. Exp. Med.* 178:1913-1921.
42. Bischoff, S.C., M. Krieger, T. Brunner, A. Rot, V.V. Tschanner, M. Baggiolini, and C.A. Dahinden. 1993. RANTES and related chemokines activate human basophil granulocytes through different G protein-coupled receptors. *Eur. J. Immunol.* 23:761-767.
43. Bischoff, S.C., M. Krieger, T. Brunner, and C.A. Dahinden. 1992. Monocyte chemotactic protein 1 is a potent activator of human basophils. *J. Exp. Med.* 175:1271-1275.
44. Collins, P.D., S. Marleau, D.A. Griffiths-Johnson, P.J. Jose, and T.J. Williams. 1995. Cooperation between interleukin-5 and the chemokine eotaxin to induce eosinophil accumulation in vivo. *J. Exp. Med.* 182:1169-1174.
45. Schweizer, R.C., B.A. Welmers, J.A. Raaijmakers, P. Zanen, J.W. Lamers, and L. Koenderman. 1994. RANTES- and interleukin-8-induced responses in normal human eosinophils: effects of priming with interleukin-5. *Blood*. 83:3697-3704.
46. Gleich, G.J., C.R. Adolphson, and K.M. Leiferman, editors. 1992. *Eosinophils. Inflammation: Basic Principles and Clinical Correlates*. 2nd ed. J.I. Gallin, I.M. Goldstein and R. Snyderman, editors. Raven Press, Ltd., New York. 663-700.
47. Weller, P.F., and G.J. Bubley. 1994. The idiopathic hypereosinophilic syndrome. *Blood*. 83:2759-2779.
48. Standiford, T.J., M.W. Rolfe, S.L. Kunkel, J.P. Lynch, M.D. Burdick, A.R. Gilbert, M.B. Orringer, R.I. Whyte, and R.M. Strieter. 1993. Macrophage inflammatory protein-1 alpha expression in interstitial lung disease. *J. Immunol.* 151:2852-2863.
49. Yu, X., and D.T. Graves. 1995. Fibroblasts, mononuclear phagocytes, and endothelial cells express monocyte chemoattractant protein-1 (MCP-1) in inflamed human gingiva. *J. Periodontol.* 66:80-88.
50. Sousa, A.R., S.J. Lane, J.A. Nakhosteen, T. Yoshimura, T.H. Lee, and R.N. Poston. 1994. Increased expression of the monocyte chemoattractant protein-1 in bronchial tissue from asthmatic subjects. *Am. J. Respir. Cell Mol. Biol.* 10:142-147.
51. Tomhave, E.D., R.M. Richardson, J.R. Didsbury, L. Menard, R. Snyderman, and H. Ali. 1994. Cross-desensitization of receptors for peptide chemoattractants. Characterization of a new form of leukocyte regulation. *J. Immunol.* 153:3267-3275.
52. Yoshimura, T., and E.J. Leonard. 1990. Identification of high affinity receptors for human monocyte chemoattractant protein-1 on human monocytes. *J. Immunol.* 145:292-299.
53. Moser, B., C. Schumacher, V. von Tschanner, I. Clark-Lewis, and M. Baggiolini. 1991. Neutrophil-activating peptide 2 and gro/melanoma growth-stimulatory activity interact with neutrophil-activating peptide 1/interleukin 8 receptors on human neutrophils. *J. Biol. Chem.* 266:10666-10671.
54. Combadiere, C., S.K. Ahuja, and P.M. Murphy. 1995. Cloning and functional expression of a human eosinophil CC chemokine receptor. *J. Biol. Chem.* 270:16491-16494.

Eosinophil Recruitment to the Lung in a Murine Model of Allergic Inflammation

The Role of T Cells, Chemokines, and Adhesion Receptors

Jose-Angel Gonzalo,* Clare M. Lloyd,* Leonor Kremer,* Elizabeth Finger,* C. Martinez-A.,* M.H. Siegelman,[§] Myron Cybulsky,^{||} and Jose-Carlos Gutierrez-Ramos*

*The Center for Blood Research, Inc. and The Department of Genetics, Harvard Medical School, Boston, Massachusetts; [†]Centro Nacional de Biotecnología, CSIC, U.A.M. Madrid, Spain; [‡]Department of Pathology, Southwestern Medical Center at Dallas, University of Texas, Dallas, Texas; and [§]Division of Pathology, Brigham and Women's Hospital, Boston, Massachusetts 02115

Abstract

Eosinophil accumulation is a distinctive feature of lung allergic inflammation. Here, we have used a mouse model of OVA (ovalbumin)-induced pulmonary eosinophilia to study the cellular and molecular mechanisms for this selective recruitment of eosinophils to the airways. In this model there was an early accumulation of infiltrating monocytes/macrophages in the lung during the OVA treatment, whereas the increase in infiltrating T-lymphocytes paralleled the accumulation of eosinophils. The kinetics of accumulation of these three leukocyte subtypes correlated with the levels of mRNA expression of the chemokines monocyte chemoattractant peptide-1/JE, eotaxin, and RANTES (regulated upon activation in normal T cells expressed and secreted), suggesting their involvement in the recruitment of these leukocytes. Furthermore, blockade of eotaxin with specific antibodies in vivo reduced the accumulation of eosinophils in the lung in response to OVA by half. Mature CD4⁺ T-lymphocytes were absolutely required for OVA-induced eosinophil accumulation since lung eosinophilia was prevented in CD4⁺-deficient mice. However, these cells were neither the main producers of the major eosinophilic chemokines eotaxin, RANTES, or MIP-1 α , nor did they regulate the expression of these chemokines. Rather, the presence of CD4⁺ T cells was necessary for enhancement of VCAM-1 (vascular cell adhesion molecule-1) expression in the lung during allergic inflammation induced by the OVA treatment. In support of this, mice genetically deficient for VCAM-1 and intercellular adhesion molecule-1 failed to develop pulmonary eosinophilia. Selective eosinophilic recruitment during lung allergic inflammation results from a sequential accumulation of certain leukocyte types, particularly T cells, and relies on the presence of both eosinophilic chemoattractants and adhesion receptors. (*J. Clin. Invest.* 1996. 98:2332-2345.) **Key words:** lung eosinophilia • leukocytes • chemotactic cytokines • integrins • selectins

Introduction

Lung eosinophilia is a fundamental trait of allergic asthma and infiltration of the airways by eosinophils appears to be central in the pathogenesis of this disease (1-3). The traffic of eosinophils to the sites of allergic reactions is presumed to be regulated at three distinct levels: (a) adhesion receptors (selectins and integrins) that mediate transient or firm adhesion to inflamed vascular endothelium; (b) activating factors (cytokines, chemokines, and chemoattractants) that induce expression of selectins and their ligands, and that activate eosinophil integrins and their endothelial counter-receptors, thus attracting this leukocyte subtype to the inflammatory site; and (c) leukocytes that are present at the inflammation site and which regulate the expression and release of these activating factors (4-9). Despite the fact that most molecules or cells involved at any of these three regulation levels are not eosinophil specific, they can provide sufficient combinatorial diversity to allow selective recruitment of eosinophils to the lung in vivo (6, 10).

Eosinophils express several adhesion receptors such as β 1 and β 2 integrins, E-selectin and P-selectin ligands (11), and L-selectin (11, 12). These surface molecules enable them to interact with the vascular endothelium. Eosinophil transendothelial migration in vitro can be partially inhibited by blocking the interactions of lymphocyte function-associated antigen 1 (LFA-1)¹ and very late activation antigen 4 (VLA-4) with intercellular adhesion molecule 1 (ICAM-1), and vascular cell adhesion molecule 1 (VCAM-1) on endothelial cells, respectively (4, 5, 13, 14). Inhibition of this transmigration can be increased by blocking with an anti-E-selectin mAb (15). Recent in vivo experiments document that antigen-induced eosinophil infiltration of the mouse trachea is prevented by blocking VCAM-1-VLA-4, but not ICAM-1-LFA-1 interactions (16). In contrast, the in vivo administration of an anti-ICAM-1 mAb leads to decreased eosinophil infiltration and attenuated airway hyperreactivity in a primate model of chronic airway inflammation (17).

Chemoattractants, such as platelet activating factor and leukotriene B₄, and several human chemokines, including monocyte chemoattractant peptide 3 (MCP-3), macrophage in-

Address correspondence to Dr. Jose-Carlos Gutierrez-Ramos, The Center For Blood Research Incorporated, Harvard Medical School, 200 Longwood Avenue, Boston, MA 02115. Phone: 617-278-3240; FAX: 617-278-3030; E-mail: gutierrez@cbrv1.med.harvard.edu

Received for publication 20 June 1996 and accepted in revised form 9 September 1996.

J. Clin. Invest.

© The American Society for Clinical Investigation, Inc.

0021-9738/96/11/2332/14 \$2.00

Volume 98, Number 10, November 1996, 2332-2345

1. Abbreviations used in this paper: BAL, bronchoalveolar lavage; ICAM-1, intercellular adhesion molecule-1; LFA-1, lymphocyte function-associated antigen 1; MCP, monocyte chemoattractant peptide; MIP, macrophage inflammatory protein; OVA, ovalbumin; RANTES, regulated upon activation in normal T cells expressed and secreted; VCAM-1, vascular cell adhesion molecule-1; VLA-4, very late activation antigen 4; wt, wild-type.

flammatory protein 1 α (MIP-1 α), and regulated upon activation in normal T cells expressed and secreted (RANTES) have been reported to elicit significant migration of eosinophils (11, 18, 19). Recently, eotaxin, a chemokine that is highly efficient in inducing migration of eosinophils, has been identified and extensively studied in guinea pigs (20, 21), mice (22, 23), and humans (24).

Pathological processes that result in lung eosinophilia may involve antigen-induced T cell activation through macrophages or other antigen presenting cells, T cell cytokine release, specific sensitization of mast cells, and release of activating mediators by macrophages (8). Macrophages are able to amplify the inflammatory response and to increase eosinophil proliferation and survival by virtue of their potential to generate a variety of proinflammatory mediators and cytokines (25–28).

There is a strong correlation between the level of cytokines released by activated T cells and the degree of eosinophil-mediated tissue damage in the lung (29, 30). Eosinophils and lymphocytes tend to appear in certain types of inflammatory lesions in the absence of a marked neutrophilic infiltration (31, 32). Indeed, the accumulation of eosinophils at sites of allergic reactions has been directly correlated with the production of T cell cytokines such as IL-5, IL-3, and GM-CSF, which are known to stimulate eosinophil maturation, activation, and survival (33–36) and IL-4, which enhances the endothelial expression of VCAM-1 (37–40). VCAM-1 upregulation may augment the migration of eosinophils but not of neutrophils, which lack VLA-4 (14).

Selective activation of adhesion molecules on eosinophils and endothelial cells by leukocyte cytokines (IL-4, IL-1 β , TNF- α) (15, 39, 41) and production of eosinophilic chemokines (RANTES, eotaxin) by different cell types (23, 42) could promote eosinophil migration and their subsequent accumulation in the tissue. Cooperation between these groups of mediators has been demonstrated during *in vivo* recruitment of eosinophils (43).

The molecular cloning and functional characterization of the leukocyte integrins, their endothelial Ig gene superfamily ligands, and of selectins has made it possible to construct mutant mice to address the roles of these molecules in different pathological situations *in vivo* (44, 45). This, together with the identification and cloning of specific chemokines, facilitates the determination of the molecular and cellular basis of migration of different leukocytes and its regulation during inflammation. Here, using a mouse model of lung eosinophilia *in vivo* based on the repeated exposure of mice to aerosolized ovalbumin (OVA) (23), we analyze (a) the kinetics of accumulation in the lung of several leukocyte subtypes during the OVA treatment; (b) the correlation between the accumulation of specific leukocyte subtypes and the expression of several chemokines (RANTES, eotaxin, MCP-1/JE, MIP-1 α , and TCA-3) in eosinophilic lungs; (c) the effects of the blockade of eotaxin *in vivo* on the kinetics of accumulation of eosinophils; (d) the specific role of B-, CD4 $^{+}$ - and CD8 $^{+}$ -T-lymphocytes during lung eosinophilia by studying the response to the OVA treatment in mice lacking these leukocyte subtypes; (e) changes in the expression of these chemokines and adhesion receptors in the absence of these lymphocyte subtypes during lung eosinophilia *in vivo*; and (f) the contribution of the individual adhesion receptors ICAM-1, VCAM-1, P-selectin, and L-selectin to the eosinophil accumulation in this model by using mice that have been made genetically deficient in these molecules.

Methods

Mice and *in vivo* procedures. 8–10-wk-old male and female C57BL/6J, RAG-1, and P-selectin-deficient mice were purchased from the Jackson Laboratory (Bar Harbor, ME) and kept in the Center for Blood Research Specific Pathogen Free mouse facility. CD4- and CD8-deficient mice (46, 47) were provided by Dr. Tak W. Mak (AMGEN Institute, Toronto, Canada), and CD3 ϵ transgenic mice (48) were kindly provided by Dr. C. Terhorst (Beth Israel Hospital, Boston, MA). L-selectin-deficient mice were generated and provided by Dr. M. Siegelman. Since VCAM-1-null mutant mice are embryonic lethal (49), VCAM-1-hypomorphic mutant mice were used for these studies (50). These mutant mice were generated by a targeted deletion in domain 4 of the VCAM-1 molecule (which eliminates the main α 4 integrin binding site). The mRNA level of the truncated VCAM-1 molecule in the hypomorphic mutants used here is 95% reduced compared to wild type (wt) levels (50 and not shown). Also, the affinity of the remaining truncated VCAM-1 to α 4 integrins is presumably greatly diminished as shown previously *in vitro* (51). ICAM-1-deficient mice were previously generated by us (52). Mice designated as wt in the results section are littermates of these mutants that have a mixed genetic background 129sv \times C57BL/6J. Pulmonary eosinophilia in response to OVA (Sigma Chemical Co., St. Louis, MO) was generated in these groups of mice as described (23). The murine model of lung eosinophilia used here consists of an initial phase of sensitization and a second phase of induction of the response. Thus, mice were sensitized with intraperitoneal OVA (0.1 mg/mouse) on day 1 followed by exposure to aerosolized antigen (2% OVA for 5 min on day 8 and 1% OVA for 20 min on days 15–21) to induce the response. At different times after allergen challenge, animals were killed by barbiturate overdose and analyzed. PBS (intraperitoneal and aerosolized) was administered to mice as a negative control. The following number of mice of the indicated strains were used per time point in three individual experiments: 10, 4, and 4 C57BL/6J mice per time point for experiments shown in Figs. 1, 4 A, and 6, respectively; 4 RAG-1, CD4 and CD8-deficient mice, and 4 CD3 ϵ transgenic mice per time point for experiments shown in Fig. 4 A; 4 ICAM-1, VCAM-1, and P-selectin-mutant mice and 3 L-selectin-mutant mice per time point for experiments shown in Fig. 6. In one series of blocking experiments, mice were injected with neutralizing polyclonal Abs against murine eotaxin (20 μ g/mouse, *i.v.*) 30 min before OVA administration on days 20 and 21 and then analyzed 3 h after allergen challenge on day 21. OVA-treated control mice were injected with the same amount of control Ab (rabbit immunoglobulin fraction; Dako Corp., Santa Barbara, CA) at the same time points indicated during treatment. No endotoxin contamination was detected in all reagents used, as assessed by LAL assay (BioWhittaker, Walkersville, MD).

Bronchoalveolar lavage (BAL) was essentially performed as described (23). Briefly, at the different time points indicated after the last aerosol exposure, the airways of the mice were lavaged via a tracheal cannula with 1 ml of PBS. The resulting BAL fluid was immediately centrifuged (700 g, 5 min, 4°C) and BAL cells were then washed twice and resuspended in 1 ml of PBS.

Immunohistochemical phenotyping and quantitation of leukocytes. The number and type of leukocytes were determined in lung sections and BAL fluid. Excised lungs from OVA-treated mice were obtained at the indicated time points, fixed in 10% formalin, embedded in paraffin (Tissue-Tek, Miles Inc., Somerset, MA), and sectioned at 5 μ m on a microtome (Reichert-Jung, Vienna). To determine the number of eosinophils, a sensitive method dependent on the presence of a cyanide-resistant endogenous peroxidase was used (23).

To determine the number of lymphocytes, macrophages, and neutrophils and to analyze the expression of ICAM-1 and VCAM-1 protein, remaining portions of the excised lungs were rolled in Tissue Tek OCT compound (Cryoform, IEC, Needham Heights, MA), snap frozen in liquid nitrogen and stored at -70°C . Cryosections (4 μ m) were cut onto microscope slides, dried for 2 h, and fixed for 20 min in

acetone at 4°C. Fixed sections were stained with mAb directed against Thy 1.2 (53-2.1), Mac-1 (M1/70), GR.1 (RB6-8C5), and IgM (II/41) from PharMingen (San Diego, CA) and ICAM-1 (YN1/1.7.4) and VCAM-1 (mK2.2) kindly provided by Drs. Springer and Lobb, respectively, using an avidin/biotin staining method. All incubations were carried out under humidified conditions and slides were washed between steps (twice for 5 min each in 0.1 M phosphate buffered saline, pH 7.4). Sections were overlaid with 20% fetal calf serum in PBS for 15 min and incubated for 1 h at room temperature with the mAbs described above. Bound ab was visualized by incubation with biotinylated sheep anti-rat immunoglobulin (Dako Corp.) and then with streptavidin peroxidase complex (Dako Corp.) both diluted in 1% normal mouse serum/PBS (NMS/PBS), and incubated for 30 min. Finally slides were flooded with peroxidase substrate solution (400 mg diaminobenzidine in 10 ml of PBS, containing 0.01% hydrogen peroxide) for 10 min. Control sections were included where mAb, biotinylated anti-rat immunoglobulin or streptavidin complex were selectively omitted.

Number of leukocyte subtypes was determined in four high power fields (at a magnification of 40; total area 0.5 mm²) per section (duplicate sections per mouse and time point were examined). These high power fields were selected randomly under a low power of magnification (×4) at which leukocyte subtypes were not visible and compared with the number of leukocytes present in control mice.

To determine the number and type of leukocytes in the BAL fluid, samples were applied to glass slides by cytocentrifugation (5 × 10⁵ cells/slide), air dried for 10 min and then immersed in Wright-Giemsa stain (Fisher Diagnostics, Pittsburgh, PA), rinsed with distilled water, air dried, and mounted. Percentage of eosinophils, lymphocytes, neutrophils, and macrophages was determined by counting their number in eight high power fields (at a magnification of 40; total area 0.5 mm²) per area selected by the same criteria as above and dividing this number by the total number of cells per high power field. To obtain the absolute number of each leukocyte subtype in the lavage, these percentages were multiplied by the total number of cells recovered from the BAL fluid.

Measurement of mRNA expression by Northern blots. Total RNA from eosinophilic lungs of OVA-sensitized wt mice (1, 3, and 6 h after treatment on days 15, 18, and 21) and from lungs of OVA-treated mutant mice (3 h after challenge on days 15, 18, and 21) was isolated using the guanidinium thiocyanate/acid phenol procedure (53). RNA from lungs of PBS-treated mice at the same time points was used as a control. Northern blots (54) were performed with 20 µg of total RNA indicated above, fractionated in a 1.5% agarose/formaldehyde gel, and blotted onto a nylon membrane (Genescreen; DuPont, Wilmington, DE). Membranes were probed using ³²P-labeled mouse probes for eotaxin (23), RANTES (55), MCP-1/JE (56), MIP-1α (57), and TCA-3 (58) applied in 50% formamide hybridization solution at 42°C for 18 h. Blots were washed in 2 × SSC/1% SDS at 45°C and exposed at -70°C on Kodak XAR5 film.

Anti-eotaxin antibody generation. Polyclonal Abs against murine eotaxin were prepared according to standard methods (59). Briefly, 100 µg of purified recombinant eotaxin (23) were inoculated into rabbits together with complete Freund's adjuvant and challenged at different time points after immunization. Ab titers were determined in an ELISA using recombinant eotaxin as immobilized antigen. Rabbit serum was first depleted of antihuman IgG Abs by passage over a human IgG column and anti-eotaxin Abs were purified from the flow through on a eotaxin affinity column. Bound Ab were eluted with 0.1 mol/liter acetic acid/0.12 mol/liter NaCl (pH, 3.0), immediately neutralized with 1 mol/liter Tris (pH, 8.8), dialyzed against three changes of PBS, and stored at -70°C in 10% glycerol/PBS.

For production of mAbs against eotaxin 10-wk-old Wistar rats were immunized in the hind footpad with KLH-coupled recombinant eotaxin using a standard protocol used by us previously (60). 8 d after immunization popliteal lymph nodes were removed and fused with the murine plasmacytoma P3X63Ag8.653 (60). 12 d after fusion, supernatants from growing wells were screened by ELISA for the

presence of anti-eotaxin Abs. Positive supernatants were studied in Western blot analysis against eotaxin produced by transfected cells. Positive hybridomas were stabilized by limiting dilution using BALB/c mouse thymocytes as a feeder layer until stable Ab production was achieved.

Affinity purified rabbit polyclonal Abs and rat mAbs were shown to recognize a specific band in a Western blot against eotaxin-containing supernatant but not against the supernatant of mock-transfected cells (data not shown).

Determination of eotaxin protein expression within lung tissue.

The level of expression of eotaxin protein was determined in sections from lungs of OVA-treated mice and controls. Sections were prepared as detailed above and staining was accomplished using a modified avidin/biotin staining method. All incubations were carried out under humidified conditions and slides were washed twice between steps for 5 min each in 0.1 M PBS supplemented with 0.2% gelatin (PBSG). Sections were overlaid with 20% normal rabbit serum in PBS for 15 min and then incubated overnight at 4°C with monoclonal anti-eotaxin diluted 1:2 in PBS with 0.1% BSA and 0.1% sodium azide. Endogenous peroxidase was subsequently blocked by incubation for 20 min in methanol containing 0.3% hydrogen peroxide. Non-specific staining due to cross reaction with endogenous avidin or biotin was blocked by incubation with avidin solution followed by biotin solution, both for 20 min. Bound monoclonal Ab was visualized by incubation with biotinylated rabbit anti-rat immunoglobulin diluted in 10% normal mouse serum PBS, and then streptavidin peroxidase complex prepared according to manufacturer's instructions (both from Dako Corp.), and incubated for 1 h each. Finally, slides were flooded with peroxidase substrate solution (20 mg diaminobenzidine in 10 ml PBS, containing 0.01% hydrogen peroxide) for 10 min before counter staining with hematoxylin. Control slides were either stained with an irrelevant Ab (anti-TR5) (61) or biotinylated anti-rat immunoglobulin or streptavidin complex were selectively omitted.

Results

Characterization of leukocyte accumulation in the mouse lung in response to OVA. To characterize leukocyte types recruited to lung airways and parenchyma after antigen challenge, as well as their time of arrival to this organ, preimmunized mice (day 1) were challenged with repeated aerosolized exposure to OVA (days 8 and 15-21). At different time points (0, 1, 3, 6, and 12 h) after exposure to OVA on days 15, 18, and 21 of treatment, leukocytes present in the BAL fluid and in the lung parenchyma were enumerated (Fig. 1). Analysis of the pulmonary infiltration at these two levels (in the airways by BAL or in the parenchyma by counting leukocytes in the tissue) demonstrated a marked increase in the total number of leukocytes present in this tissue. We have previously characterized the kinetics of lung eosinophil accumulation in this model (23). Briefly, a progressive increase in the number of eosinophils is detected in lung tissue and BAL, reaching a maximum level at day 21 of treatment. Each day after OVA administration there is a transient increase in BAL and tissue eosinophils which is maximal at 3 h. Kinetics of eosinophil infiltration are shown in the bottom of Fig. 1 for comparison with the other leukocyte subtypes. Lymphocyte accumulation in BAL and lung tissue follows a similar profile to that of eosinophils, in that within 6-12 h after OVA challenge on day 15, we detected a fivefold increase in the number of T-lymphocytes in lung tissue (Fig. 1). On days 18 and 21 of OVA treatment, a progressive increase in tissue infiltrating T-lymphocytes was evident. This increase peaks at 3 h at both time points and constitutes 20- and 25-fold for T-lymphocytes on days 18 and 21, respectively, and is readily detectable within 1 h after the OVA inhalation. The

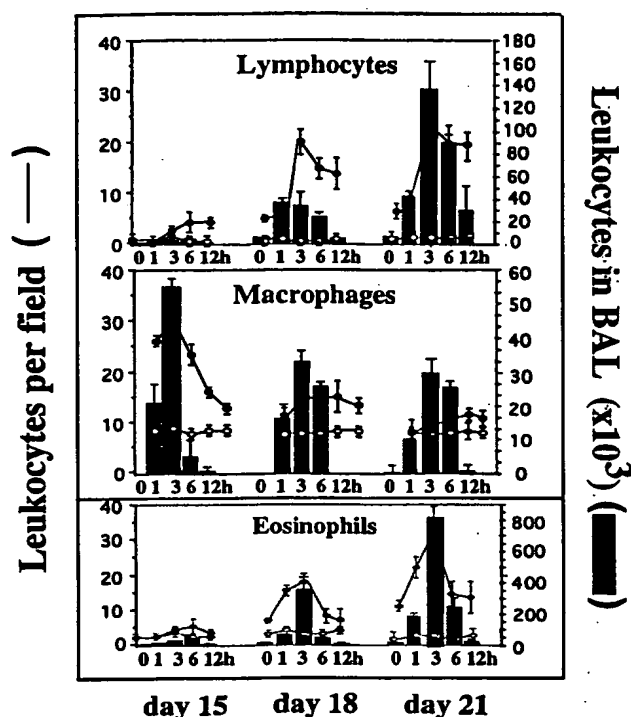


Figure 1. Pulmonary accumulation of lymphocytes and monocytes/macrophages in response to OVA treatment. Lymphocyte and macrophage infiltration in lung sections (dots) and BAL fluid (bars) are shown on days 15, 18, and 21 of OVA treatment at the different time points indicated. The treatment is described in detail in the Methods section. Solid circles and open circles represent the numbers of the indicated cell types counted in lung sections of experimental and control mice, respectively. The kinetics of eosinophil accumulation at the same time points is shown for comparison in the figure. Error bars indicate the standard deviation of the average of each cell type counted in four high power fields per lung in 3 individual experiments with 10 OVA-treated mice per time point and experiment. Total number of eosinophils, lymphocytes, and monocytes/macrophages in the BAL fluid was calculated as the product of the total cellularity of the BAL and the percentage of each cell type. Each value was corrected for background by subtracting values of control mice from OVA-treated littermates.

number of lymphocytes present in the BAL fluid also increases during the course of this treatment and becomes maximal 3 h after OVA administration on day 21 (15-fold increase; Fig. 1). It should be noted that 12 h after OVA administration, the number of total lymphocytes in BAL fluid decreases to almost basal levels while tissue infiltrates (perivascular and peribronchiolar) remain well above basal levels in the lung (as was observed for eosinophils).

The kinetics of macrophage accumulation in the lung during the response to OVA is inverse to that described above for eosinophils and lymphocytes. Macrophage accumulation peaks 3 h after OVA administration on day 15 by 3–4-fold in lung tissue and by 50-fold in BAL fluid (Fig. 1). Increased numbers of macrophages were also observed in both lung tissue and BAL fluid on days 18 and 21 although to a lesser degree than on day 15. At all time points examined the number of infiltrating macrophages decreases almost to basal levels by 12 h after last OVA administration.

No significant and persistent increase in neutrophil, B-lymphocyte, and mast cell numbers was detected during the course of this treatment when OVA and control mice were compared (data not shown).

Chemokine expression during the development of OVA-induced lung eosinophilia. Since chemokines are important inflammatory mediators involved in the recruitment and activation of leukocytes at sites of inflammation, we tried to correlate OVA-induced eosinophil, T-lymphocyte, and macrophage accumulation with the expression of chemokines specific for these cell subtypes. We assessed the expression of mRNA for murine RANTES (CD4⁺ T cell and eosinophil chemoattractant) (62), MCP-1/JE, (macrophage chemoattractant) (63), MIP-1 α (monocyte and eosinophil chemoattractant) (64, 65), TCA-3 (neutrophil and monocyte chemoattractant) (66), and eotaxin (eosinophil chemoattractant) (23) during lung eosinophilia. Northern blots of total RNA isolated from lungs of OVA-treated mice on days 15, 18, and 21 (1, 3, and 6 h after OVA inhalation) revealed a comparable pattern of RANTES and eotaxin mRNA expression (Fig. 2 A). Induction of MCP-1/JE mRNA in response to OVA challenge was maximal at 3 h after OVA-administration on day 15 of treatment. On the same day, 6 h after antigen challenge significant MCP-1/JE mRNA expression was still detectable. On days 18 and 21, Northern blot analyses revealed a transient increase in MCP-1/JE mRNA expression detected 3 h after OVA administration (Fig. 2 A). The mRNA expression of TCA-3 was virtually undetectable during the course of this treatment and there was no discernible increase at any time point after OVA challenge (Fig. 2 A). Finally, the pattern of mRNA expression for MIP-1 α was not distinguishable from that described above for RANTES or eotaxin (Fig. 2 A).

Among the chemokines examined above, eotaxin is the most selective regarding the chemoattraction of eosinophils (20, 67). In addition, its transcription profile correlates well with the accumulation of eosinophils in vivo. To determine the predominant cell type(s) producing eotaxin in this model and the relevance of eotaxin expression in the accumulation of eosinophils in vivo, we generated Abs against eotaxin. The

Table I. Properties of a Panel of Anti-eotaxin mAbs

mAb	ELISA	Western blot	Staining lung sections*	Neutralizing activity†
mEOT-1	+	++	++	ND
mEOT-2	+	++	++	ND
mEOT-3	+	+	–	ND
mEOT-4	+	–	–	ND
mEOT-5	+	++	++	ND
mEOT-6	+	++	++	ND
mEOT-7	+	++	++	ND
mEOT-8	+	+	–	ND
mEOT-9	+	+	–	ND
polyEOT	+	++	ND	+

*Immunohistochemical staining was performed as described in Methods using lungs from OVA-treated mice. †Neutralizing activity of the anti-eotaxin polyclonal antibody was assessed previously in vitro by transmigration experiments (97% blocking). (++) and (+) Strong and weak reactivity in Western blots and immunohistochemistry. (–) No staining. (ND) Not determined.

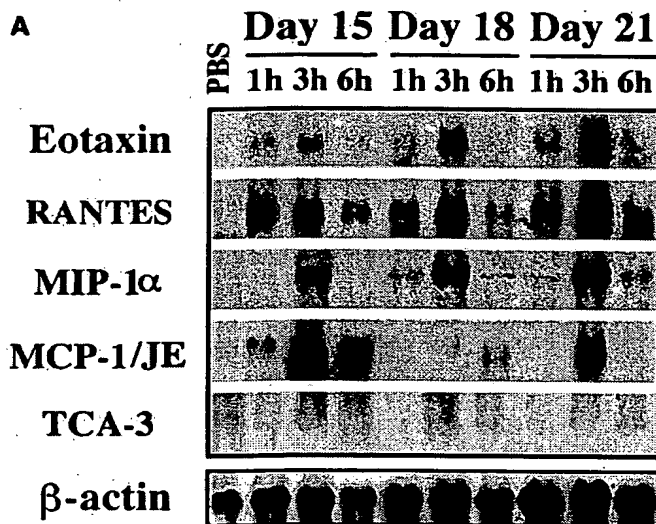
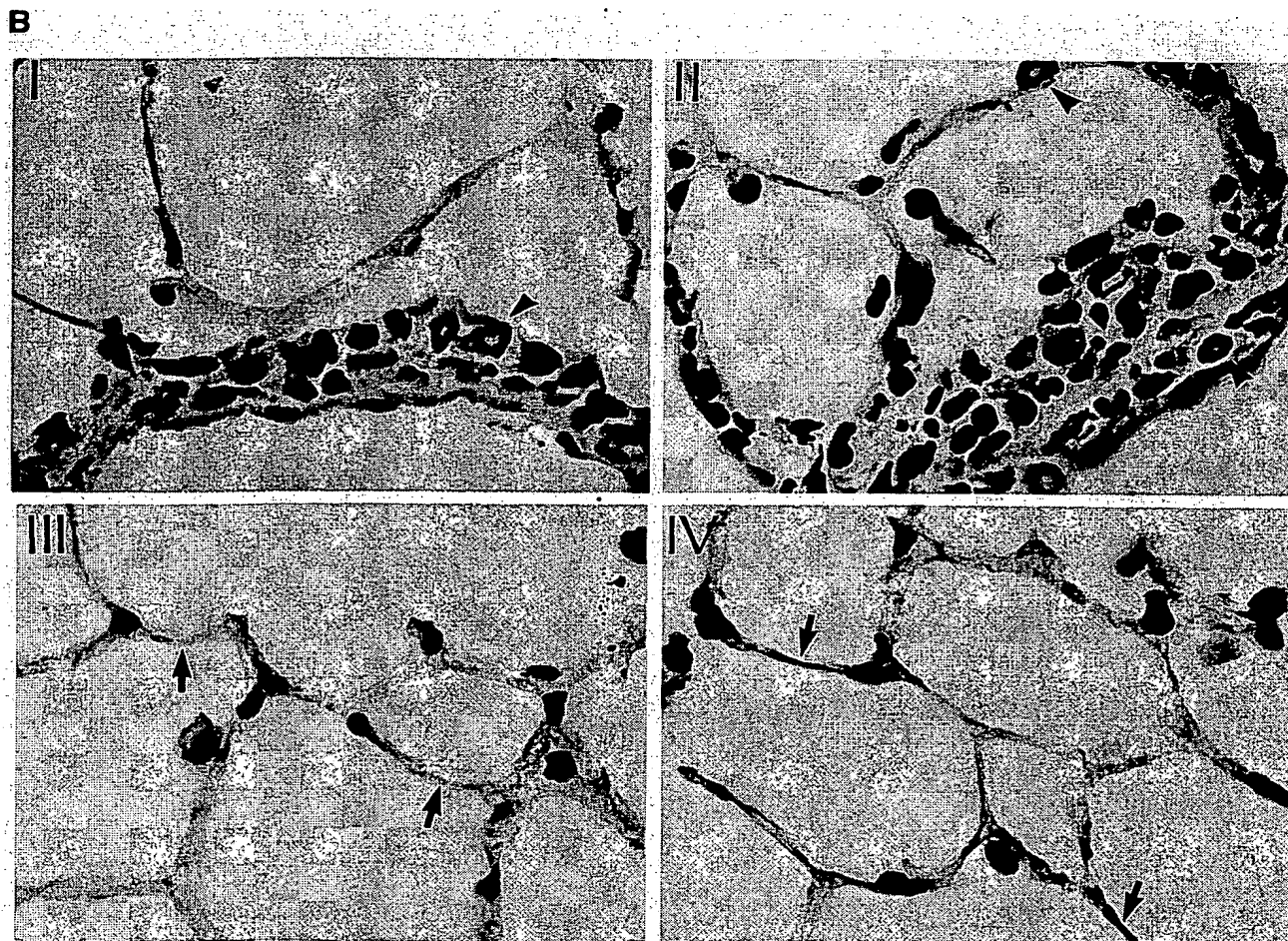


Figure 2. Chemokine expression during lung eosinophilia. (A) Expression of eotaxin, RANTES, MIP-1 α , MCP-1/JE, and TCA-3 mRNAs in the lung during OVA treatment. On days 15, 18, and 21, total RNA from lungs of OVA-treated mice was extracted 1, 3, and 6 h after antigen administration. In a control group, mice were treated with aerosolized PBS instead of OVA. Eotaxin, RANTES, MCP-1/JE, MIP-1 α , and TCA-3 mRNA induction was determined by Northern blot. Chemokine expression of one representative mouse out of four is shown. Lower panel shows a control hybridization of the blot with a β -actin probe. (B) Immunohistochemical staining of lung sections from OVA-treated mice on day 21, 3 h after OVA inhalation (I, II, and IV) and a PBS control (III). Sections were stained with anti-eotaxin mAb (mEOT-1) (see Methods) (II, III, and IV) or a negative control isotype matched mAb (I). Note that positive staining, seen as a brown precipitate, is not detected in infiltrating cells (arrowheads) but is observed in resident lung cells, in particular the alveolar endothelium (arrows). $\times 1,000$.



properties of nine selected mAbs and one polyclonal Ab are outlined in Table I. All these Abs were determined to be specific for eotaxin by ELISA. Five of the eotaxin specific mAbs showed strong reactivity in Western blots and were able to recognize an epitope of mouse eotaxin that is preserved in frozen sections of lung. The anti-eotaxin polyclonal Ab was noted for

its ability to block the *in vitro* transmigration of eosinophil to eotaxin by 97% (Table I and data not shown). Neutralizing properties of mAbs are currently being investigated. Immunohistochemical analysis of eotaxin protein expression in sections of eosinophilic lungs from OVA-treated mice was performed. Our results show that most of the eotaxin protein expressed

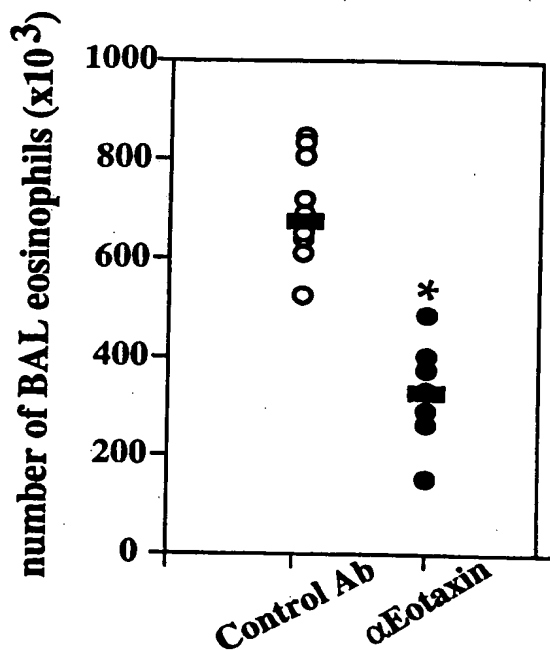


Figure 3. In vitro blockade of eotaxin with specific neutralizing Abs during OVA-induced eosinophilia. 30 min before antigen challenge on the last two days of OVA treatment, mice were injected with neutralizing Abs against eotaxin as described in the Methods section. OVA-treated control mice were injected with control Ab at the same time points indicated. BAL fluid was obtained 3 h after OVA treatment on day 21 and number of eosinophils was determined. Each circle represents a single control mouse (open circle) or a single test mouse (closed circle) analyzed. Bars represent the mean of each group. Significant difference between groups was determined using the Student's *t* test (**P* < 0.001).

can be attributed to resident lung cells (Fig. 2B). In particular, increased expression was observed in alveolar epithelial cells after OVA treatment confirming our previous data obtained by in situ hybridization (23). Few, if any, of the leukocytes that constitute perivascular infiltrates (mainly eosinophils and lymphocytes) showed positive staining at late stages of OVA-induced eosinophilia (Fig. 2B).

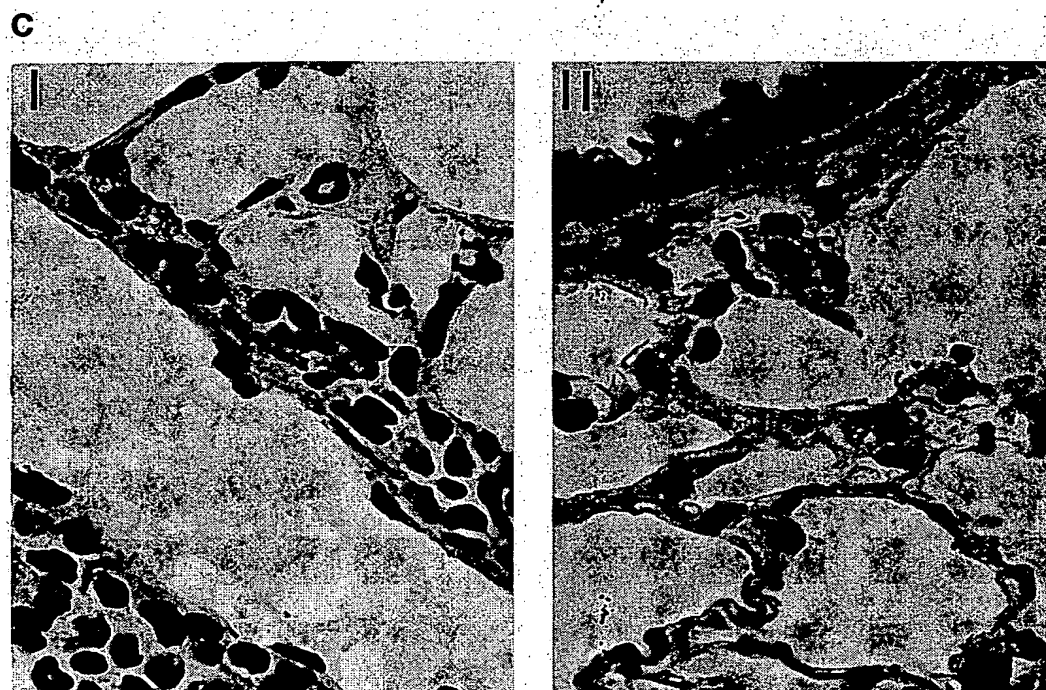
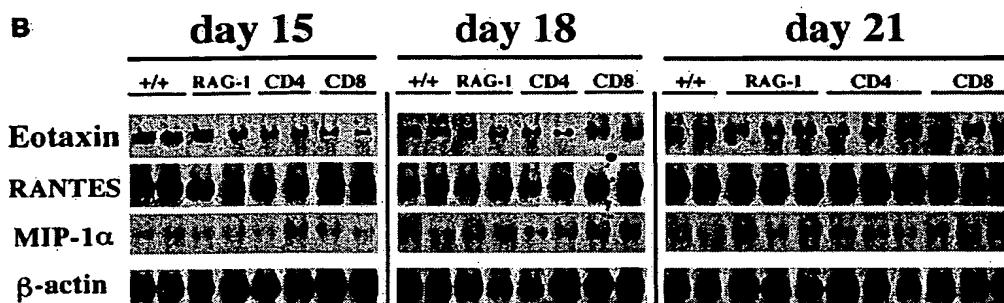
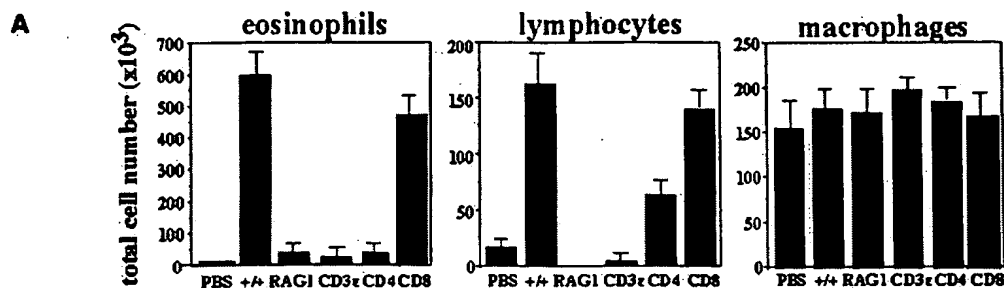
To determine the particular contribution of eotaxin to the development of OVA-induced lung eosinophilia, blocking experiments in vivo with anti-eotaxin polyclonal Abs were performed. Intravenous administration of anti-eotaxin Abs resulted in a 56% reduction of eosinophils in BAL when compared with OVA-treated control mice (Fig. 3).

Role of lymphocytes in pulmonary eosinophilia: response of mice with selective immunodeficiencies to OVA. In the light of the distinct kinetics of lymphocyte and macrophage accumulation in this model and, particularly of the parallel kinetics of eosinophil and lymphocyte accumulation, we evaluated the contribution of these cell types to the induction of eosinophilia in vivo. To dissect the specific role that different lymphocyte subtypes may play in the accumulation of eosinophils in this model, we studied the response of RAG-1-deficient mice (T and B cell-deficient) (68) and CD3 ϵ transgenic mice (T and NK cell-deficient) (48), as well as mice lacking either CD4⁺ or CD8⁺ T-lymphocytes (46, 47) to the OVA treatment. 3 h after OVA challenge on day 21, BAL fluid from these immunodeficient mice was obtained and leukocyte subtypes were enumerated.

Fig. 4A shows that there is almost a complete reduction in the number of infiltrating eosinophils recovered from the BAL fluid of OVA-treated RAG-1-deficient mice and CD3 ϵ transgenic mice when compared with OVA-treated wt littermates. We observed a small but detectable population of lymphocytes (1/20 of that found in wt mice) in the BAL fluid of CD3 ϵ transgenic mice at the same time point analyzed (Fig. 4A). To further investigate whether CD4⁺ and/or CD8⁺ T-lymphocytes are both required for the induction of eosinophilia in this model, mice lacking either CD4⁺ or CD8⁺ T-lymphocytes were also examined (Fig. 4A). We observed a comparable reduction of eosinophils in the BAL of CD4-deficient mice to that found in RAG-1-deficient mice or CD3 ϵ transgenic mice. In contrast, CD8-deficient mice subjected to the same treatment showed no significant changes in BAL eosinophilia when compared to OVA-treated wt littermates (Fig. 4A). In addition, a similar degree of lymphocyte infiltration was found in wt and CD8-deficient mice (Fig. 4A) suggesting that a significant fraction of the infiltrating lymphocytes belong to the CD4⁺ lineage (~70%, as shown by the numbers of lymphocytes in CD4-deficient mice, Fig. 4A). The number of macrophages (Fig. 4A) and neutrophils (data not shown) recovered from the BAL fluid of these mutant mice remained comparable to their corresponding wt littermates at this time point of the OVA treatment. Similarly, maximal macrophage accumulation occurred on day 15 in both groups of mice (data not shown).

To exclude the chance that cells might have migrated into the interstitium but not progressed into the airways in the absence of CD4⁺ T cells, lung sections from OVA-treated RAG-1, and CD4-deficient mice (3 h after OVA challenge on day 21) were prepared and the number of eosinophils in the parenchyma was counted. No eosinophil infiltration was detected in the lungs of these mutant mice when compared with wt or CD8-mutant mice (data not shown and Figs. 4C, and 5).

To rule out the possibility that pulmonary eosinophil accumulation in response to OVA was delayed rather than abrogated in RAG-1 and CD4-deficient mice, BAL fluid obtained 7 h after OVA administration on day 21 was analyzed. As was detected at the 3 h time point, no eosinophil infiltration was seen at this later time point in these mutants (data not shown). Wt and CD8-mutant mice showed similar numbers of infiltrating eosinophils at this time point (data not shown). To exclude the possibility that prevention of lung eosinophilia after exposure to OVA in these mutant mice was due to impaired bone marrow eosinophil differentiation resulting from an intrinsic lack of IL-5-producing CD4⁺ T cells, IL-5 was intravenously administered and 1 h later, numbers of eosinophils recovered from the blood of the different IL-5-treated mutant mice were determined. No differences were detected in the number of circulating eosinophils shortly after IL-5 injection in mutant mice that did not develop OVA-induced BAL eosinophilia (i.e., CD4 or RAG-1-mutant mice) when compared with those found in wt and CD8-deficient mice (data not shown). To exclude the possibility that functional differentiation of eosinophils was affected in CD4-deficient mice, IL-5 was administered both intravenously and intraperitoneally daily over 1 wk. 2 h after the final IL-5 injection, eosinophil accumulation into the peritoneum of these treated CD4-deficient mice was evaluated. Peritoneal eosinophilia was not impaired in these mutant mice when compared with wt littermates (data not shown).



efficient mice on day 21 of treatment, is shown. Expression of β -actin was used to determine the quality and quantity of the RNA. (C) Expression of eotaxin protein in CD4^{-/-} mice after OVA administration. Immunohistochemical staining was performed in frozen sections from OVA treated CD4^{-/-} mice (II) or OVA-treated wt littermates (I) with anti-eotaxin mAb (mEOT-1). Eotaxin is clearly expressed within alveolar macrophages and alveolar epithelial cells in CD4^{-/-} mice, although no infiltrating leukocytes were observed. $\times 1,000$

Chemokine expression during lung eosinophilia in lymphocyte deficient mice. To determine whether the absence of eosinophilia in RAG-1 and CD4-deficient mice was related to changes in the expression of eosinophilic chemokines such as

eotaxin, RANTES, and MIP-1 α , Northern analyses were performed using RNA from the lungs of these mutant mice at different time points after OVA treatment. Fig. 4B shows that in RAG-1 and CD4-deficient mice, which do not develop OVA-

Figure 4. Role of lymphocyte subsets in lung eosinophilia and its correlation with chemokine mRNA expression. (A) OVA-induced leukocyte accumulation in the BAL fluid of lymphocyte-deficient mice. BAL fluid from CD3 ϵ transgenic mice and from RAG-1, CD4-, or CD8-deficient mice was obtained 3 h after OVA administration on day 21 of OVA treatment. Numbers of (left) eosinophils, (middle) lymphocytes, and (right) macrophages were calculated as the product of the total cellularity of the BAL and the percentage of each cell type. Data represent the mean \pm SEM for three representative experiments with four mice in each group ($n = 12$). Numbers of infiltrating eosinophils, lymphocytes, and macrophages in the BAL fluid of two different control groups of mice (control group 1 "PBS": PBS-treated C57BL/6J or wt 129sv/C57BL/6J mice; control group 2 "+/+": OVA-treated wt 129sv/C57BL/6J mice) on day 21 is also shown. (B) Expression of the eosinophilic chemokines eotaxin, RANTES, and MIP-1 α mRNAs in the lung of lymphocyte-deficient mice during OVA treatment. Northern blot analysis was performed using total RNA (20 μ g) extracted from lungs of RAG-1, CD4-, and CD8-deficient mice, 3 h after OVA administration on days 15, 18, and 21. Total RNA from the lungs of OVA-treated wt mice at the same time points was used as a control. Expression of two representative wt mice out of five at each time point, two out of five immunodeficient mice on days 15 and 18, and three out of five immunode-

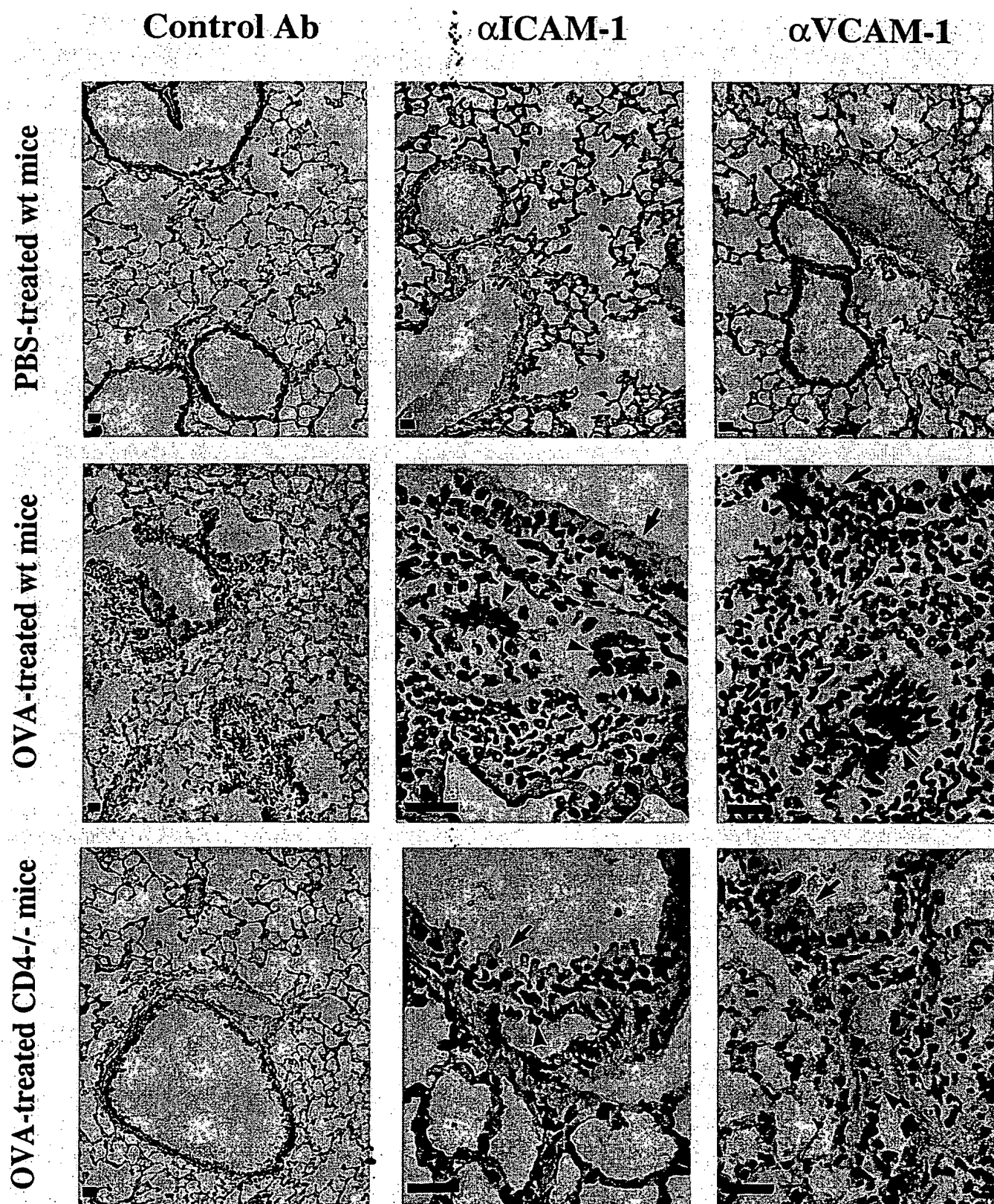


Figure 5. ICAM-1 and VCAM-1 expression in the eosinophilic lung. Frozen sections of lungs from OVA-treated wt (middle row) or CD4-deficient mice (bottom row) and of PBS-treated wt mice (top row) were stained with anti-ICAM-1 (middle column) or anti-VCAM-1 (right column) mAbs and then counterstained with hematoxylin. Pictures of lung sections from the same groups of mice stained with isotype-matched irrelevant control (left column) are included for comparison. Arrows indicate the position of airways and arrowheads of vessels. Bar, 50 μ m.

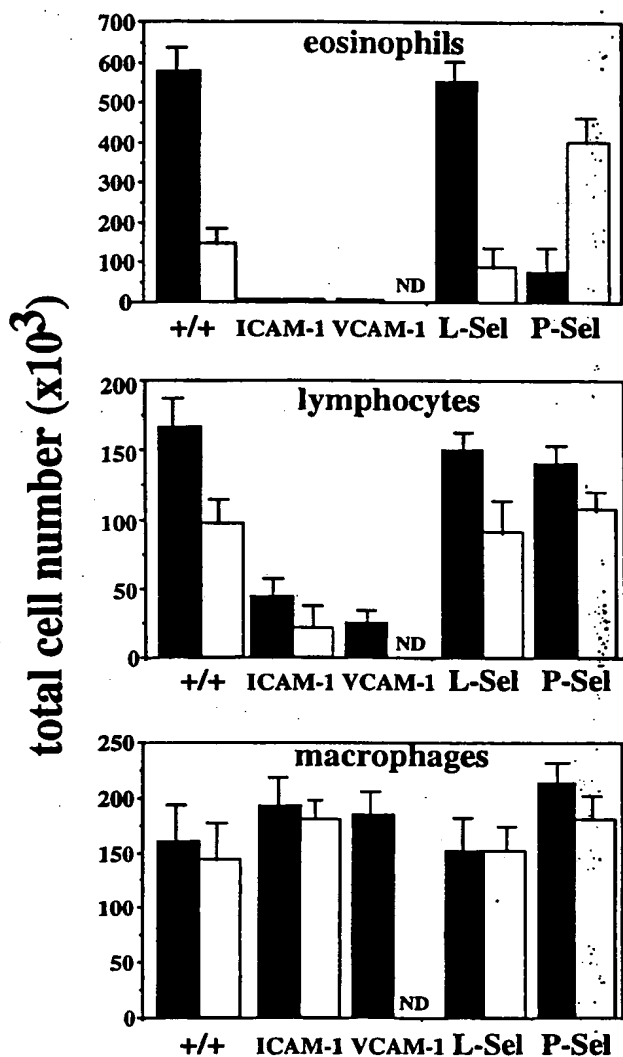


Figure 6. Enumeration of leukocytes (eosinophils, lymphocytes, and macrophages) in the BAL fluid of different adhesion receptor deficient mice in response to OVA. BAL fluid from ICAM-1, VCAM-1, L-selectin-, and P-selectin-mutant mice was obtained 3 (black bars) or 7 h (white bars) from different groups of mice after OVA administration on day 21 of treatment. OVA-treated wt 129sv/C57BL/6J mice were used as control (+/+). Numbers of eosinophils (top), lymphocytes (middle), and macrophages (bottom) were calculated as the product of the total cellularity of the BAL and the percentage of each cell type. Figure shows mean \pm SEM for three individual experiments with 4 OVA-treated mice per time point and experiment with the exception of L-selectin-deficient mice (3 mice per time point) and VCAM-1-deficient mice. (ND, not analyzed at 7 h after OVA treatment).

induced pulmonary eosinophilia, there was a significant level of expression of eotaxin, RANTES, and MIP-1 α (especially on day 21 which coincides with maximal eosinophilia in wt mice). The levels of expression of these chemokines in CD4 or RAG-1-deficient mice were comparable to those found in OVA-treated wt and CD8-deficient mice (Fig. 4B). To evaluate parity between chemokine mRNA expression and chemokine protein production in the CD4-deficient mice, eotaxin protein expression was examined in sections of lungs from OVA-

treated CD4-deficient mice. Even though there was no infiltration in the lungs from these mice there was at least as much, if not more, eotaxin expression within sections, correlating with the mRNA data (Fig. 4C). An increase in the amount of eotaxin immunodetected on macrophages was noted (Fig. 4C). Experiments are underway to confirm this finding at the molecular level.

Adhesion receptor expression during lung eosinophilia in lymphocyte-deficient mice. The mRNA expression of key eosinophilic chemokines (eotaxin and RANTES) was virtually unaffected in lymphocyte-deficient mice during the response to OVA in vivo. Therefore, we examined changes in the expression of selected adhesion receptors involved in eosinophil extravasation (11, 14) to determine whether suboptimal upregulation of adhesion receptor expression in lymphocyte-deficient mice could account for the lack of eosinophil accumulation observed in these mutant mice during the OVA treatment. To this end we assessed the protein expression of ICAM-1 and VCAM-1 genes by immunohistochemistry in frozen sections of the lungs of CD4-deficient mice and wt mice after OVA treatment on day 21 (3 h after challenge). Similar expression of ICAM-1 is observed in wt and CD4-deficient mice in vascular and alveolar endothelium (Fig. 5). In contrast, although strong expression of VCAM-1 was observed in wt mice after OVA-treatment (Fig. 5), it was only weakly expressed in vessels in OVA-treated CD4-deficient mice and untreated wt mice (Fig. 5). PBS-treated mice showed minimal expression of both ICAM-1 and VCAM-1 (Fig. 5).

Role of selected adhesion receptors in pulmonary eosinophilia: response to OVA in adhesion receptor deficient mice. The eosinophil-endothelial cell interactions required for extravasation necessitates enhanced expression of endothelial adhesion molecules and eosinophil surface integrins (11, 14). From the results presented in the previous section and from the work of others (16), we hypothesized that the expression of VCAM-1 and ICAM-1 is critically regulated by T-lymphocyte-derived cytokines and is essential for the development of lung eosinophilia. To test this hypothesis, we used ICAM-1-deficient mice and VCAM-1-hypomorphic mutant mice to evaluate the specific contribution of these adhesion receptors to OVA-induced pulmonary eosinophilia. Since eosinophils express P-selectin ligands and L-selectin, mice deficient for these molecules were also used in these experiments. On day 21, 3 h after OVA administration, which correspond with maximum eosinophilia in wt mice, no eosinophil accumulation was observed either in the BAL fluid (Fig. 6) or in lung tissue (data not shown) of ICAM-1-deficient mice and VCAM-1-hypomorphic mutant mice. At the same time point, the total number of BAL lymphocytes in these mutant mice was reduced by more than 65 and 85% in ICAM-1 and VCAM-1-mutant mice respectively, compared to OVA-treated wt littermates (Fig. 6). Analysis of eosinophil accumulation in L-selectin-deficient mice in response to OVA showed that L-selectin is not essential for induction or maintenance of pulmonary eosinophilia. No differences in the number of BAL eosinophils were found in these mutant mice compared to control animals (Fig. 6). When numbers of BAL lymphocytes were analyzed, L-selectin-mutant mice showed an identical lymphocyte accumulation to that observed in wt littermates (Fig. 6). The BAL fluid of P-selectin-deficient mice showed only 20% of the eosinophil infiltration 3 h after the last OVA inhalation when compared to wt littermates (Fig. 6). Interestingly, at the same time

point no reduction in the number of BAL lymphocytes was detected (Fig. 6). When P-selectin-deficient mice were analyzed 7 h after the last OVA challenge, we detected a 2.5-fold increase in the number of eosinophils in BAL fluid when compared with the OVA-treated wt mice at the same time point (Fig. 6). ICAM-1 and VCAM-1-mutant mice did not show any increase in eosinophil infiltration by 7 h after last OVA administration (Fig. 6). No significant differences were found in macrophage accumulation in the BAL fluid of the different mutant mice and wt littermates after challenge with OVA (Fig. 6). The lack of adhesion receptors may result in impaired eosinophil differentiation. Therefore, deficient mice were injected intravenously with IL-5. No subsequent differences in the numbers of circulating eosinophils were detected among these IL-5-injected mutant and wt mice (data not shown).

Discussion

In this report we have used a mouse model of OVA-induced pulmonary eosinophilia *in vivo* to demonstrate that (a) there is a differential accumulation of leukocyte subtypes in the lung during the response to OVA, consisting of an early accumulation of infiltrating macrophages and a late increase of T-lymphocytes and eosinophils; (b) the mRNA expression of specific chemokines (eotaxin, RANTES, and MCP-1/JE) parallels infiltration of lungs by these three leukocyte subtypes; (c) neutralization of eotaxin *in vivo* with specific Ab reduces OVA-induced lung eosinophilia by 50%; (d) mature CD4⁺ T cells are absolutely required for OVA-induced eosinophil migration and accumulation in the lung; (e) the presence of T cells is not required for the expression of the eosinophilic chemokines RANTES, MIP-1 α , and eotaxin or for their proper regulation; (f) the expression of RANTES and eotaxin is not sufficient to induce eosinophil accumulation in the absence of CD4⁺ T cells *in vivo*; (g) the presence of CD4⁺ T cells is critical for the proper enhancement of VCAM-1, but not ICAM-1 expression, in the lung during OVA treatment; and (h) the absence of ICAM-1 or VCAM-1 prevents the development of pulmonary eosinophilia whereas expression of L-selectin and P-selectin is not essential to achieve lung eosinophil accumulation *in vivo*.

The accumulation of eosinophils and T-lymphocytes in the lung is parallel, and is preceded by a transient accumulation of macrophages. This differential accumulation correlates with a distinct pattern of expression of specific chemokines. The recruitment of leukocytes from the blood to sites of inflammation is strongly regulated *in vivo* by mechanisms that allow selective leukocyte-endothelial cell recognition. These mechanisms display total specificity in relation to the stimulus inducing inflammation, cell response, and the tissue site involved. Based on a murine model of lung eosinophilia induced by the repeated exposure of mice to aerosolized OVA (23), we have analyzed cell subtypes involved in eosinophilia. We describe here that there is a macrophage accumulation at the early stages of challenge and that T-lymphocytes parallel eosinophil infiltration. Whereas eosinophils and T-lymphocytes were predominant on day 21 in both BAL and lung tissue, macrophages were the most abundant leukocyte type on day 15 in the lungs of OVA-treated mice (Fig. 1). These two events characterize pulmonary eosinophilia in this model. No significant and ordered neutrophil or B cell accumulation was detected during the course of OVA treatment (data not shown). Mast cells,

which have been described as participating in eosinophil-mediated inflammatory reactions (69), are not significantly increased during the development of this model of antigen-induced eosinophilia (data not shown).

The presence of infiltrating macrophages in the lung during the sensitization phase (day 8; data not shown) and early stage of OVA challenge (Fig. 1) is consistent with the hypothesis that these leukocytes play a prominent role in airway hyperresponsiveness (8, 27). To dissect the specific role that macrophages might play in this model of OVA-induced eosinophilia, we attempted to eliminate macrophages *in vivo* using the drug dichloromethylene-diphosphonate (Cl₂MDP) encapsulated in liposomes (70). Although a clear reduction (60%) in BAL pulmonary eosinophilia was detected in Cl₂MDP-treated mice after OVA-challenge, these experiments were unsatisfactory due to the incomplete depletion of macrophages and to possible secondary effects of the drug (data not shown). The study of the role of macrophages in lung eosinophilia using a genetically "clean" system is hampered by the lack of availability of macrophage deficient mice. Mice lacking M-CSF (op/op) or GM-CSF expression or both, still have significant numbers of alveolar macrophages (71, 72). Thus, although our preliminary results suggest a participation of macrophages in the early phases of lung eosinophilia, the final confirmation of these results awaits the development of better tools (macrophage-deficient mice) to address this issue.

Interestingly, we found that MCP-1/JE expression correlates with lung macrophage accumulation whereas the expression of RANTES and eotaxin is concomitant with lymphocyte and eosinophil infiltration (Fig. 2 A). The expression pattern of MIP-1 α mRNA reflects that seen for eotaxin and RANTES rather than the mRNA pattern observed for MCP-1/JE (Fig. 2 A). This result suggests that MIP-1 α is playing a role in the recruitment of eosinophils in our model and is in accordance with the recent description of MIP-1 α as an eosinophilic chemokine (65). Taken together these findings indicate that there is a differential expression of chemokines during OVA-induced eosinophilia *in vivo* which directly correlates with the arrival of specific leukocyte types in the lung.

Of the chemokines able to attract eosinophils, eotaxin appears to be one of the most efficient (20, 67). This has led us and others to suggest that this chemokine might play a key role in lung allergic eosinophilia. In fact, neutralization of eotaxin at day 21 in our model demonstrated that this chemokine is responsible for the recruitment of approximately half of the eosinophils that accumulate in the BAL fluid in response to allergen challenge (Fig. 3). We are presently evaluating further the specific contribution of eotaxin at different times of this allergic response in the lung, as well as its overall contribution to this process. Our results indicate that most of the infiltrating leukocytes (eosinophils, lymphocytes, and monocytes) are not producing eotaxin protein, at least at the time of maximal eosinophilia (day 21, 3 h after OVA inhalation). We have previously reported that lymphocytes and monocytes can produce eotaxin mRNA after activation *in vitro* (23). Similarly, Ponath et al. reported that human eosinophils are able to produce eotaxin mRNA (67). However, at the point of maximal eosinophilia *in vivo*, these three cell types do not overtly produce eotaxin protein. Rather, the principal cells producing eotaxin in response to OVA in this model are resident lung cells (mainly epithelial cells and alveolar macrophages with some possible contribution from endothelial cells).

The presence of CD4⁺ T cells is essential for the development of lung eosinophilia *in vivo*, but not for the expression of eosinophilic chemokines. To evaluate the relevance of lymphocytes and of specific subpopulations in OVA-induced eosinophil accumulation in the lung and the putative role that these cells might play, we have used mice lacking specific lymphocyte subtypes. Here we demonstrate that there is no OVA-induced eosinophil accumulation in the BAL fluid of RAG-1-deficient mice (lacking T- and B-lymphocytes) (68) or CD3 ϵ transgenic mice (lacking T and NK cells) (48) (Fig. 4 A). This suggests that T cells are required for the induction of lung eosinophilia and that B cells are not sufficient to induce this physiological response. Since we did not detect any significant lymphocyte infiltration in CD3 ϵ transgenic mice, the OVA-induced lymphocyte infiltrate must be composed predominantly of T cells (Fig. 4 A). This was confirmed by stained lung sections from OVA-treated mice with an anti-IgM mAb (data not shown). Furthermore, the prevention of eosinophil accumulation in BAL and lung tissue in CD4⁺ T-lymphocyte-deficient, but not in CD8⁺ T-lymphocyte-deficient mice after OVA-challenge (Figs. 4, 5, and data not shown) demonstrates that CD4⁺ T-lymphocytes are required for the induction and development of lung eosinophilia.

A number of studies have showed that airway hyperresponsiveness and pulmonary inflammation can be associated with a Th2 pattern of cytokine expression (37, 73–76). As yet, there has been no direct evidence that T-lymphocytes mediate *in vivo* antigen-induced eosinophilia. As demonstrated using SCID mice, airway hyperreactivity induction requires the presence of lymphocytes (75) but the association of airway hyperreactivity and pulmonary eosinophil infiltration is still not understood since neither IL-5 or eosinophils support airway hyperreactivity in an *in vivo* murine model of pulmonary inflammation (75). Elegant and thorough studies have demonstrated a key role for CD4⁺ T cells in the development of tracheal (77) or pulmonary (78) antigen-induced eosinophil infiltration by mAb-depletion of CD4⁺ T cells. However, a critical role for CD8⁺ T cells in the development of lung eosinophilia and airway responsiveness has also been documented in another model of airway sensitization in which priming by intraperitoneal injection of OVA was omitted (79). Expression of chemokines during CD4⁺- or CD8⁺ T cell-dependent eosinophilia in these two different mouse models is currently being investigated in our laboratory. These results illustrate that the contribution of CD4⁺ or CD8⁺ T cells to eosinophil accumulation is dependent upon the particular methods used to induce allergic inflammation. In addition, the results obtained from all these experiments are conditioned by the finding that human eosinophils also express the CD4 receptor (14) and by possible secondary effects mediated by the injection of mAbs *in vivo*. In this study we use a "clean" genetic deficiency to demonstrate that the absence of CD4⁺ T-lymphocytes (but not CD8⁺ T cells) abolishes pulmonary eosinophilia without affecting eosinophil differentiation. On the other hand, in these immunodeficient mice it is difficult to decide whether the interference with the sensitization and/or with the induction phase of the response to OVA results in the lack of eosinophil infiltration. We are evaluating the OVA-induced immune response in lymphocyte-deficient mice as well as establishing the role that B and T cells play in both the sensitization and challenge phases by depletion of these particular lymphocyte subtypes at different time points of the treatment. This will lead us to a better

characterization of both the sensitization and induction phases of the response in our murine model of lung eosinophilia. Another possible explanation for the absence of eosinophilia in CD4-deficient mice could be a decrease in the number of bone marrow or peripheral blood eosinophils because of the CD4 deficiency. CD4-deficient mice and wt littermates were found to have similar basal levels of eosinophils in peripheral blood before treatment (data not shown). After OVA treatment, it is possible that levels of peripheral blood eosinophils are lower in CD4-deficient mice. We could not test this hypothesis directly by evaluating increases in peripheral blood eosinophils in OVA-treated CD4-deficient mice because no such increase is detected after treatment of wt mice in this model. Instead, we took advantage of the fact that intravenous IL-5 induces a rapid reduction in the number of eosinophils in bone marrow due to their mobilization to the blood (43). We did not detect any differences in the number of IL-5-mobilized circulating eosinophils among these wt and mutant mice (not shown). In addition, eosinophil accumulation in the peritoneum of CD4-deficient mice after repeated peritoneal administration of IL-5 suggests that these leukocytes maintain their ability to extravasate *in vivo*, at least to the peritoneum.

We hypothesized that CD4⁺ lymphocytes might be essential for the development of lung eosinophilia because they produce or regulate the expression of eosinophilic chemokines or because they regulate the upregulation/activation of critical adhesion receptors used by eosinophils during their transmigration *in vivo*. As shown above, the infiltrating cells in the lung are not the main producers of at least one eosinophilic chemokine, eotaxin (Fig. 2 B). Therefore, we would not expect a reduction of eotaxin or RANTES expression in CD4-deficient mice. However, CD4⁺ T-lymphocytes can provide signals that regulate the expression of these chemokines by epithelial and endothelial cells. To test these possibilities, we studied the RNA expression of eotaxin and RANTES in lymphocyte-deficient mice.

The mRNA expression of chemokines able to induce eosinophil recruitment (eotaxin, RANTES, and MIP-1 α) after OVA administration, is not influenced in lymphocyte-deficient mice. In RAG-1 and CD4-deficient mice, that are resistant to OVA-induced pulmonary eosinophilia, there exist significant levels of eotaxin, RANTES, and MIP-1 α expression when compared with OVA-treated wt and CD8-deficient mice. This finding was subsequently confirmed at the protein level for eotaxin. Based on these results, we can conclude that the expression of these chemokines alone is not sufficient to drive leukocyte recruitment *in vivo* and, that CD4⁺ T cells, which are absolutely required for induction of eosinophilia, do not regulate the expression of these eosinophilic chemokines. Possible candidates capable of regulating the expression of chemokines in the lung of lymphocyte-deficient mice could be mast cells or macrophages. On the other hand, the expression of these eosinophilic chemokines in RAG-1-deficient mice or CD4-deficient mice is not due to a non-specific response to large doses of OVA or to the effect of some contaminant since we have recently reported that the novel eosinophilic chemokine MCP-5 (80) is expressed in the lung of wt mice but not of RAG-1-deficient mice after OVA treatment (80).

The expression of selected adhesion molecules is T-lymphocyte dependent. The expression of ICAM-1 and VCAM-1 is critical for the accumulation *in vivo* of eosinophils in the lung. The process of eosinophil-endothelial cell interactions

involves several adherence pathways (14). Eosinophils can bind to ICAM-1 and to VCAM-1 by means of LFA-1 and VLA-4, respectively. They also express L-selectin and ligands for P-selectin (11, 12). We examined the expression of both ICAM-1 and VCAM-1 proteins in our model of OVA-induced eosinophilia in wt and CD4-deficient mice. While OVA-treated wt and CD4-deficient mice exhibited similar staining patterns of ICAM-1 protein expression in alveoli and blood vessels (Fig. 5) a differential staining pattern was clearly observed for VCAM-1, where increased vascular endothelial staining was detected in OVA-treated wt, but not in CD4-deficient mice (Fig. 5). This implies that adhesion molecules are differentially modulated by CD4⁺ T cells since we have shown that VCAM-1, but not ICAM-1, is dramatically increased in the presence, but not absence, of these cells, and that CD4⁺ T cells are not directly involved in the regulation of ICAM-1 protein expression.

We have examined the role that the adhesion receptors ICAM-1, VCAM-1, P-selectin, and L-selectin play in OVA-induced pulmonary eosinophilia by using mice lacking these adhesion molecules. Our studies in vivo demonstrate that eosinophil migration into the lung tissue (data not shown) and BAL fluid (Fig. 6) is abolished in the absence of ICAM-1 and VCAM-1. Previous in vivo blocking experiments have shown that VCAM-1/VLA-4 interactions play a predominant role in controlling antigen-induced eosinophil and T cell recruitment into the mouse trachea but ICAM-1/LFA-1 interactions are only critical in regulating T cell recruitment in the same model of inflammation (16). Studies of eosinophil transmigration in vitro have reported a 24% reduction in IL-1 or TNF- α -induced eosinophil migration by using mAb against ICAM-1 while the combination of anti-E-selectin, anti-VCAM-1, and anti-ICAM-1 mAbs resulted in additive inhibition of transmigration (15). Our results indicate that OVA-induced eosinophil accumulation in the lung requires interactions mediated by ICAM-1 and VCAM-1 with their counter-receptors. In both strains of adhesion receptor-deficient mice, no eosinophils were detected in BAL fluid after OVA treatment (Fig. 6). Furthermore, T cell infiltration is also affected in ICAM-1 and VCAM-1-mutant mice. We found a 32 and 14% lymphocyte accumulation in the BAL fluid of OVA-treated ICAM-1-deficient mice and VCAM-1-hypomorphic mutant mice, respectively, when compared with OVA-treated wt controls (Fig. 6). Since CD4⁺ T-lymphocytes are essential for the development of pulmonary eosinophilia during OVA treatment, we can not conclude from these experiments whether ICAM-1 and/or VCAM-1 play a critical role in lung eosinophilia either by directly mediating eosinophil-endothelium interactions or by facilitating CD4⁺ T cell activation and/or infiltration, or both effects together. Adoptive transfer experiments into deficient mice are underway in our laboratory to address this question.

In contrast, the absence of L-selectin and P-selectin expression does not prevent the development of pulmonary eosinophilia in this model. The number of BAL leukocyte subtypes remained comparable in L-selectin-deficient mice and wt littermates at the different time points analyzed (3 and 7 h) after OVA administration on day 21 (Fig. 6). Three hours after OVA challenge on the same day, P-selectin-deficient mice have fewer eosinophils in the lung than wt mice. BAL fluid obtained from these treated mice showed 20% of the eosinophil accumulation observed in wt littermates without reduction in the number of infiltrating lymphocytes (Fig. 6). Since lympho-

cyte migration remains unaffected, the reduced eosinophilia at this time point might be directly attributable to the effect of the P-selectin deficiency. However, the increase in the number of eosinophils (2.5-fold over the control at this time point) in the BAL fluid of OVA-treated P-selectin-deficient mice obtained 7 h after OVA challenge, suggests that in the absence of P-selectin-mediated interactions, eosinophil accumulation in the lung is suboptimal and therefore delayed in vivo. However, P-selectin is not essential for the development of eosinophilia since in the absence of P-selectin expression, eosinophils and endothelial cells use alternative adhesion pathways that allow delayed eosinophil migration into the lung.

Numbers of macrophages (Fig. 6) and neutrophils (data not shown) present in the BAL fluid of OVA-treated mutant mice were also similar when compared with wt animals (data not shown). The only exception was a 40% reduction in neutrophils in ICAM-1-deficient mice (not shown). This reduction was also detectable in these mutant mice even before treatment and may be related to the fact that ICAM-1 is required for neutrophils to migrate into tissues (52).

The study of leukocytes and the molecules that they produce or upregulate during recruitment and accumulation of specific leukocyte subsets into sites of inflammation, may lead to the development of therapeutic approaches able to inhibit the pathogenesis of allergic inflammation. Asthma is a complex syndrome that involves recruitment of eosinophils and their accumulation in the lung. Although murine models of lung inflammation do not completely represent the complexity of this syndrome, they may delineate particular pathways operating within it. The results presented here using one particular murine model together with additional information yielded from other, different, models of lung inflammation may contribute to a better comprehension of the mechanisms implicated in the establishment of eosinophilia within the inflammatory lung.

Acknowledgments

The authors are indebted to Drs. C. Mackay, C. Gerard, and B. Rollins for critical reading of this manuscript; to Drs. M. Dorf, T. Schall, and B. Rollins for providing MIP-1 α , RANTES, and MCP-1/JE probes, respectively; to Drs. Tak W. Mak, Laura Martin (AMGEN Institute), and C. Terhorst (Beth Israel Hospital, Boston, MA) for their help in providing CD4- and CD8-deficient mice and CD3 ϵ transgenic mice, respectively; to Dr. L. Kobzic for advice on lung histology; Dr. M. Soares for her helpful discussions; and to C. Gomez Mouton and M. Catalina for their skillful work.

This work has been funded by National Institutes of Health grants HL 148675-02, CiCyT PB93-0317, HL94-10-B, HL36028 and the Aplastic Foundation of America. J-A. Gonzalo is a recipient of postdoctoral fellowship from the Spanish Ministry for Science. M. Cybulski is an established investigator of the American Heart Association. J-C. Gutierrez-Ramos is the Amy C. Potter fellow.

References

1. Spry, C.J. 1971. Mechanism of eosinophilia. *Cell Tissue Kinet.* 4:351-364.
2. De Monchy, J.G.R., H.F. Kauffman, P. Venge, G.H. Koeter, H.M. Jansen, H.J. Sluiter, and K. de Vries. 1985. Bronchoalveolar eosinophilia during allergen-induced late asthmatic reactions. *Am. Rev. Respir. Dis.* 131:373-380.
3. Gleich, G. 1990. The eosinophilic and bronchial asthma. Current understanding. *J. Allergy Clin. Immunol.* 85:422-436.
4. Lamas, A.C., C.M. Mulroney, and R.P. Schleimer. 1988. Studies on the adhesive interaction between purified human eosinophils and cultured vascular endothelial cells. *J. Immunol.* 140:1500-1505.
5. Walsh, G.M., A. Hartnell, A.J. Wardlaw, K. Kurihara, C.J. Sanderson,

- and A.B. Kay. 1990. IL-5 enhances the in vitro adhesion of human eosinophils, but not neutrophils, in a leukocyte integrin (CD11/18)-dependent manner. *Int. Arch. Allergy Appl. Immunol.* 94:174-178.
6. Butcher, E.C. 1991. Leukocyte-endothelial cell recognition: three (or more) steps to specificity and diversity. *Cell* 67:1033-1036.
7. Lasky, L.A. 1992. Selectins: interpreters of cell-specific carbohydrate information during inflammation. *Science (Wash. DC)* 258:964-969.
8. Drazen, J.M., J.P. Arm, and K.F. Austen. 1996. Sorting out the cytokines of asthma. *J. Exp. Med.* 183:1-5.
9. Springer, T.A. 1994. Traffic signals for lymphocyte recirculation and leukocyte emigration: the multistep paradigm. *Cell* 76:301-314.
10. Schweighoffer, T., and S. Shaw. 1992. Adhesion cascades: diversity through combinatorial strategies. *Curr. Opin. Cell Biol.* 4:824-831.
11. Resnick, M.B., and P.F. Weller. 1993. Mechanisms of eosinophil recruitment. *Am. J. Respir. Cell. Mol. Biol.* 8:349-355.
12. Lewinsohn, D.M., R.F. Bargatz, and E.C. Butcher. 1987. Leukocyte-endothelial cell recognition: evidence of a common molecular mechanism shared by neutrophils, lymphocytes and other leukocytes. *J. Immunol.* 138:4313-4319.
13. Walsh, G.M., J.J. Mermod, A. Hartnell, A.B. Kay, and A.J. Wardlaw. 1991. Human eosinophil, but not neutrophil, adherence to IL-1-stimulated human umbilical vascular endothelial cells is a4b1 (very late antigen-4) dependent. *J. Immunol.* 146:3419-3426.
14. Weller, P.F., T.H. Rand, S.E. Goetz, G. Chi-Rosso, and R.J. Lobb. 1991. Human eosinophil adherence to vascular endothelium mediated by binding to VCAM-1 and ELAM-1. *Proc. Natl. Acad. Sci. USA* 88:7430-7433.
15. Ebisawa, M., B.S. Bochner, S.N. Georas, and R.P. Schleimer. 1992. Eosinophil transendothelial migration induced by cytokines. I. Role of endothelial and eosinophil adhesion molecules in IL-1b-induced transendothelial migration. *J. Immunol.* 149:4021-4028.
16. Nakajima, H., H. Sano, T. Nishimura, S. Yoshida, and I. Iwamoto. 1994. Role of vacuolar cell adhesion 1/very late activation antigen 4 and intercellular adhesion molecule 1/lymphocyte function-associated antigen 1 interactions in antigen-induced eosinophil and T cell recruitment into the tissue. *J. Exp. Med.* 179:1145-1154.
17. Wegner, C., R. Gundel, P. Reily, N. Haynes, L. Letts, and R. Rothlein. 1990. Intercellular adhesion molecule-1 (ICAM-1) in the pathogenesis of asthma. *Science (Wash. DC)* 247:456-459.
18. Dahinden, C.A., T. Geiser, T. Brunner, V. von Tscharnar, D. Caput, P. Ferrara, A. Minty, and M. Baggiolini. 1994. Monocyte chemoattractant protein 3 is most effective basophil- and eosinophil-activating chemokine. *J. Exp. Med.* 179:751-756.
19. Rot, A., M. Krieger, T. Brunner, S.C. Bischoff, T.J. Schall, and C.A. Dahinden. 1992. RANTES and macrophage inflammatory protein 1 alpha induce the migration and activation of normal human eosinophil granulocytes. *J. Exp. Med.* 176:1489-1495.
20. Jose, P.J., D.A. Griffiths-Johnson, P.D. Collins, D.T. Walsh, R. Moqbel, N.F. Totty, O. Truong, J.J. Hsuan, and T.J. Williams. 1994. Eotaxin: a potent eosinophil chemoattractant cytokine detected in a guinea pig model of allergic airways inflammation. *J. Exp. Med.* 179:881-887.
21. Rothenberg, M.E., A.D. Luster, C.M. Lilly, J.M. Drazen, and P. Leder. 1995. Constitutive and allergen-induced expression of eotaxin mRNA in the guinea pig lung. *J. Exp. Med.* 181:1211-1216.
22. Rothenberg, M.E., A.D. Luster, and P. Leder. 1995. Murine eotaxin: an eosinophil chemoattractant inducible in endothelial cells and in interleukin 4-induced tumor suppression. *Proc. Natl. Acad. Sci. USA* 92:8960-8964.
23. Gonzalo, J.A., G.-Q. Jia, V. Aguirre, D. Friend, A.J. Coyle, N.A. Jenkins, G.S. Lin, H. Katz, A. Litchman, N. Copeland, et al. 1996. Mouse eotaxin expression parallels eosinophil accumulation during lung allergic inflammation but it is not restricted to a Th2-type response. *Immunity* 4:1-14.
24. Ponath, P.D., S. Qin, D.J. Ringler, I. Clark-Lewis, J. Wang, N. Kassam, H. Smith, X. Shi, J.-A. Gonzalo, W. Newman, et al. 1996. Cloning of the human eosinophil chemoattractant, eotaxin. *J. Clin. Invest.* 97:604-612.
25. Fels, A.O.S., N.A. Pawlowski, and E.B. Cramer. 1982. Human alveolar macrophages produce leukotriene B4. *Proc. Natl. Acad. Sci. USA* 79:7866-7870.
26. Chervenick, P.A., and A.F. LoBuglio. 1972. Human blood monocytes: stimulators of granulocyte and mononuclear colony formation in vitro. *Science (Wash. DC)* 178:164-169.
27. Elias, J.A., A.D. Schreiber, and K. Gostilo. 1985. Differential interleukin-1 elaboration by unfractionated and density fractionated human alveolar macrophages and blood monocytes. *J. Immunol.* 135:3198-3204.
28. Lopez, A.F., D.J. Williams, and J.R. Gamble. 1986. Recombinant human granulocyte-macrophage colony-stimulating factor stimulates in vitro mature human neutrophil and eosinophil function, surface receptor expression and survival. *J. Clin. Invest.* 78:1220-1228.
29. Bradley, B.L., M. Azzawi, M. Jacobson, B. Assoufi, J.V. Collins, A.-M.A. Irani, L.B. Schwartz, S.R. Durham, P.K. Jeffery, and A.B. Kay. 1991. Eosinophils, T-lymphocytes, mast cells, neutrophils and macrophages in bronchial biopsy specimens from atopic subjects with asthma: comparison with biopsy specimens from atopic subjects without asthma and normal control subjects and relationship to bronchial hyperresponsiveness. *J. Allergy Clin. Immunol.* 88:661.
30. Bentley, A.M., P. Maestrelli, M. Saetta, L.M. Fabbri, D.S. Robinson, B.L. Bradley, P.K. Jeffery, S.R. Durham, and A.B. Kay. 1992. Activated T-lymphocytes and eosinophils in the bronchial mucosa in isocyanate-induced asthma. *J. Allergy Clin. Immunol.* 89:821-829.
31. Frew, A.J., and A.B. Kay. 1990. Eosinophils and T-lymphocytes in late phase allergic reactions. *J. Allergy Clin. Immunol.* 85:422-429.
32. Walker, C., J.C. Virchow, P.L.B. Bruijnzel, and K. Blaser. 1991. T cell subsets and their soluble products regulate eosinophilia in allergic and non-allergic asthma. *J. Immunol.* 146:1829-1835.
33. Sanderson, C.J. 1992. Interleukin-5, eosinophils and disease. *Blood* 79:3101-3109.
34. Bousquet, J., P. Chanwz, J.Y. Lacoste, G. Barneon, N. Ghavaman, I. Enander, P. Venge, S. Ahlstedt, J. Simony-Lafontaine, P. Godard, and P.-B. Michel. 1990. Eosinophilic inflammation in asthma. *N. Engl. J. Med.* 323:1033-1039.
35. Basten, A., and P.B. Beeson. 1970. Mechanism of eosinophilia. II. Role of the lymphocytes. *J. Exp. Med.* 131:1288-1294.
36. Sanderson, C.J., D.J. Warren, and M. Strath. 1985. Identification of a lymphokine that stimulates eosinophil differentiation in vitro. *J. Exp. Med.* 162:60-69.
37. Robinson, D.S., Q. Hamid, S. Ying, A. Tsiocopoulos, J. Barkans, A.M. Bentley, C. Corrigan, S.R. Durham, and A.B. Kay. 1992. Predominant Th2-like bronchoalveolar T-lymphocyte population in atopic asthma. *N. Engl. J. Med.* 326:298-303.
38. Del Prete, G.F., E. Maggi, P. Parronchi, I. Chretien, A. Jiri, D. Macchia, M. Ricci, J. Banachereau, J. De Vries, and S. Romagnani. 1988. IL-4 is an essential factor for the IgE synthesis induced in vitro by human T cell clones and their supernatants. *J. Immunol.* 140:4193-4199.
39. Briscoe, D.M., R.S. Cotran, and J.S. Pober. 1992. Effects of tumor necrosis factor, lipopolysaccharide and IL-4 on the expression of vascular cell adhesion molecule-1 in vivo. *J. Immunol.* 149:2954-2961.
40. Schleimer, R.P., S.A. Sterbinsky, J. Kaiser, C.A. Bickel, D.A. Klunk, and K. Tomioka. 1992. IL-4 induces adherence of human eosinophils and basophils but not neutrophils to endothelium. Association with expression of VCAM-1. *J. Immunol.* 148:1086-1092.
41. Pober, J.S., M.A. Gimbrone, L.A. Lapierre, D.L. Mendrick, W. Fiers, R. Rothlein, and T.A. Springer. 1986. Overlapping patterns of activation of human endothelial cells by interleukin-1, tumor necrosis factor and immune interferon. *J. Immunol.* 137:1893-1896.
42. Schall, T.J., J. Jongstra, B.J. Dyer, J. Jorgensen, C. Clayberger, M.M. Davis, and A.L. Krensky. 1989. A human T cell-specific molecule is a member of a new gene family. *J. Immunol.* 141:1018-1025.
43. Collins, P.D., S. Marleau, D.A. Griffiths-Johnson, P.J. Jose, and T.J. Williams. 1995. Cooperation between interleukin-5 and the chemokine eotaxin to induce eosinophil accumulation in vivo. *J. Exp. Med.* 182:1169-1174.
44. Carlos, T.M., and J.M. Harlan. 1994. Leukocyte-endothelial adhesion molecules. *Blood* 84:2068-2101.
45. Ley, K. 1996. Gene-targeted mice in leukocyte adhesion research. *Microcirculation*. In press.
46. Rahemtulla, A., W.P. Fung-Leung, M.W. Schilham, T.M. Kundig, S. Sambhara, A. Narendran, A. Arabian, A. Wakeham, C. Paige, J., R.M. Zinkernagel, et al. 1991. Normal development and function of CD8⁺ cells but markedly decreased helper cell activity in mice lacking CD4. *Nature (Lond.)* 353:180-184.
47. Fung-Leung, W.-P., M.W. Schilham, A. Rahemtulla, T.M. Kundig, M. Vollenweider, J. Potter, W. van Ewijk, and T.W. Mak. 1991. CD8 is needed for development of cytotoxic T cells but not helper T cells. *Cell* 65:443-449.
48. Wang, B., C. Biron, J. She, J. Sancho, L.C.P., K. Higgins, M. Sunshine, E. Lacy, N. Lonberg, and C. Terhorst. 1994. High level expression of the cytoplasmic tail of CD3-ε in transgenic mice blocks both early T-lymphocytes and natural killer cell development. *Proc. Natl. Acad. Sci. USA* 91:9402-9406.
49. Gurtner, G.C., V. Davis, H. Li, M.J. McCoy, A. Sharpe, and M.I. Cybulsky. 1995. Targeted disruption of the murine VCAM1 gene: essential role of VCAM-1 in chorioallantoic fusion and placentation. *Genes Dev.* 9:1-14.
50. Li, H., M. Iiyama, M. DiChiara, G.C. Gurtner, D.S. Milstone, and M.I. Cybulsky. 1996. A Hypomorphic VCAM-1 Mutation Rescues the Embryonic Lethal Null Phenotype and Reveals a Requirement for VCAM-1 in Inflammation. *FASEB J.* In press.
51. Chuluyan, H.E., L. Osborn, R. Lobb, and A.C. Issekutz. 1995. Domains 1 and 4 of vascular cell adhesion molecule-1 (CD106) both support very late activation antigen-4 (CD49d/CD29)-dependent monocyte transendothelial migration. *J. Immunol.* 155:3135-3143.
52. Xu, H., J.A. Gonzalo, Y. St. Pierre, I.R. Williams, T.S. Kupper, R.S. Cotran, T.A. Springer, and J.-C. Gutierrez-Ramos. 1994. Leukocytosis and resistance to septic shock in intercellular adhesion molecule 1-deficient mice. *J. Exp. Med.* 180:95-109.
53. Chomczynski, P., and N. Sacchi. 1987. Single-step method of RNA isolation by acid guanidinium thiocyanate-phenol-chloroform extraction. *Anal. Biochem.* 162:156-159.
54. Sambrook, J., Fritsch, E.F., and Maniatis, T. 1989. Molecular Cloning: A Laboratory Manual. 2nd Ed. Cold Spring Harbor Laboratory Press, Cold

Spring Harbor, NY.

55. Heeger, P., G. Wolf, C. Meyers, M.J. Sun, S.C. O'Farrell, A.M. Krensky, and E.G. Neilson. 1992. Isolation and characterization of cDNA from renal tubular epithelium encoding murine RANTES. *Kidney Int.* 41:220-226.
56. Rollins, B.J., E.D. Morrison, and C.D. Stiles. 1988. Cloning and expression of JE, a gene inducible by platelet-derived growth factor and whose product has cytokine-like properties. *Proc. Natl. Acad. Sci. USA.* 85:3738-3742.
57. Widmer, U., V.D. Yang, K.R. Manogue, B. Sherry, and A. Cerami. 1991. Genomic structure of murine macrophage inflammatory protein-1 α and conservation of potential regulatory sequences with a human homolog, LD781². *J. Immunol.* 146:4031-4040.
58. Burd, P.R., G.J. Freeman, S.D. Wilson, M. Berman, R. DeKruyff, P.R. Billings, and M.E. Dorf. 1987. Cloning and characterization of a novel T cell activation gene. *J. Immunol.* 139:3126-3132.
59. Harlow, E., and D. Lane. 1988. *Antibodies: A Laboratory Manual*. Cold Spring Harbor Press, Cold Spring Harbor, NY.
60. Lin, G., E. Finger, and J.C. Gutierrez-Ramos. 1995. Expression of CD34 in endothelial cells, hematopoietic progenitors and nervous cells in fetal and adult mouse tissues. *Eur. J. Immunol.* 25:1508-1516.
61. Van Vliet, E., M. Melis, and W. Van Ewijk. 1984. Monoclonal Antibodies to stromal cell types of the mouse thymus. *Eur. J. Immunol.* 14:524-529.
62. Schall, T.J., K. Bacon, K.I. Toy, and D.V. Goeddel. 1990. Selective attraction of monocytes and T lymphocytes of the memory phenotype by cytokine RANTES. *Nature (Lond.)*. 347:669-671.
63. Ernst, C.A., Y.J. Zhang, P.R. Hancock, B.J. Rutledge, C.L. Corless, and B.J. Rollins. 1994. Biochemical and biologic characterization of murine monocyte chemoattractant protein-1. *J. Immunol.* 152:3541-3549.
64. Davatelis, G., P. Tekamp-Olson, S.D. Wolpe, K. Hermen, C. Luedke, C. Gallegos, D. Coit, J. Merryweather, and A. Cerami. Cloning and characterization of a cDNA for murine macrophage inflammatory protein (MIP), a novel monokine with inflammatory and chemokinetic properties. *J. Exp. Med.* 167: 1939-1946.
65. Post, T.W., C.R. Bozic, M.E. Rothenberg, A.D. Luster, N. Gerard, and C. Gerard. 1995. Molecular characterization of two murine eosinophil β chemokine receptors. *J. Immunol.* 155:5299-5305.
66. Luo, Y., J. Laning, S. Devi, J. Mak, T.J. Schall, and M.E. Dorf. 1994. Biologic activities of the murine b-Chemokine TCA3. *J. Immunol.* 153:4616-4624.
67. Ponath, P.D., S. Qin, T.W. Post, J. Wang, L. Wu, N.P. Gerard, W. Newman, C. Gerard, and C.R. Mackay. 1996. Molecular cloning and characterization of a human eotaxin receptor expressed selectively on eosinophils. *J. Exp. Med.* 183:2437-2448.
68. Mombaerts, P., J. Iacomini, R.S. Johnson, K. Herrup, S. Tonegawa, and V. Papaioannou. 1992. RAG-1-deficient mice have no mature B and T lymphocytes. *Cell* 68:869-877.
69. Gordon, J.R., and Galli, S. 1990. Mast cells as a source of both pre-formed and immunologically inducible TNF-alpha/cachectin. *Nature (Lond.)*. 346:274-277.
70. Van Rooijen, N. 1989. The liposome-mediated macrophage "suicide" technique. *J. Immunol. Methods.* 124:1-21.
71. Begg, S., J. Radley, J. Pollard, O. Chisholm, and I. Bertoncello. 1993. Delayed hematopoietic development in op/op mice. *J. Exp. Med.* 177:237-242.
72. Lieschke, G.J., E. Stanley, D. Grail, G. Hodgson, V. Sinickas, J.A.M. Gall, R.A. Sinclair, and A.R. Dunn. 1994. Mice lacking both macrophage- and granulocyte-macrophage colony-stimulating factor have macrophages and co-existent osteopetrosis and severe lung disease. *Blood.* 84:27-35.
73. Walker, C., E. Bode, L. Boer, T.T. Hansel, K. Blaser, and J.C. Virchow Jr. 1992. Allergic and non-allergic asthmatics have distinct patterns of T-cell activation and cytokine production in peripheral blood and bronchoalveolar lavage. *Am. Respir. Dis.* 146:109-115.
74. Gavett, S.H., D.J. O'Hearn, X. Li, S.-K. Huang, F.D. Finkelman, and M. Wills-Karp. 1995. Interleukin 12 inhibits antigen-induced airway hyperresponsiveness, inflammation, and Th2 cytokine expression in mice. *J. Exp. Med.* 182: 1527-1536.
75. Corry, D.B., H.G. Folkesson, M.L. Warnock, D.J. Erle, M.A. Matthay, J.P. Wiener-Kronish, and R.M. Locksley. 1996. Interleukin 4, but not interleukin 5 or eosinophils, is required in a murine model of acute airway hyperreactivity. *J. Exp. Med.* 183:109-117.
76. Foster, P.S., S.P. Hogan, A.J. Ramsay, K.I. Matthaei, and I.G. Young. 1996. Interleukin 5 deficiency abolishes eosinophilia, airways hyperreactivity, and lung damage in a mouse asthma model. *J. Exp. Med.* 183:195-201.
77. Nakajima, H., I. Iwamoto, S. Tomoe, R. Matsumura, H. Tomioka, K. Takatsu, and S. Yoshida. 1992. CD4⁺ T-lymphocytes and interleukin-5 mediate antigen-induced eosinophil infiltration into the mouse trachea. *Am. Rev. Respir. Dis.* 146:374-377.
78. Gavett, S.H., X. Chen, F. Kinkelman, and M. Wills-Karp. 1994. Depletion of murine CD4⁺ T lymphocytes prevents antigen-induced airway hyperactivity and pulmonary eosinophilia. *Am. J. Respir. Cell Mol. Biol.* 10:587-593.
79. Hamelmann, E., A. Oshiba, J. Paluh, K. Bradley, J. Loader, T.A. Potter, G.L. Larsen, and E.W. Gelfand. 1996. Requirement for CD8⁺ T cells in the development of airway hyperresponsiveness in a murine model of airway sensitization. *J. Exp. Med.* 183:1719-1729.
80. Jia, G.-Q., J.A. Gonzalo, C. M. Lloyd, L. Kremer, L. Lu, C. Martinez-A., B.K. Wershil, and J.C. Gutierrez-Ramos. 1996. Distinct expression and function of the novel mouse chemokine MCP-5 in lung allergic inflammation. *J. Exp. Med.* 184:1939-1952.

Upregulation of Interleukin 8 by Oxygen-deprived Cells in Glioblastoma Suggests a Role in Leukocyte Activation, Chemotaxis, and Angiogenesis

By Isabelle Desbaillets, Annie-Claire Diserens, Nicolas de Tribolet, Marie-France Hamou, and Erwin G. Van Meir

From the Laboratory of Tumor Biology and Genetics, Neurosurgery Department, University Hospital (CHUV), 1011 Lausanne, Switzerland

Summary

Leukocyte infiltration and necrosis are two biological phenomena associated with the development of neovascularization during the malignant progression of human astrocytoma. Here, we demonstrate expression of interleukin (IL)-8, a cytokine with chemotactic and angiogenic properties, and of IL-8-binding receptors in astrocytoma. IL-8 expression is first observed in low grade astrocytoma in perivascular tumor areas expressing inflammatory cytokines. In glioblastoma, it further localizes to oxygen-deprived cells surrounding necrosis. Hypoxic/anoxic insults on glioblastoma cells in vitro using anaerobic chamber systems or within spheroids developing central necrosis induced an increase in IL-8 messenger RNA (mRNA) and protein expression. mRNA for IL-8-binding chemokine receptors CXCR1, CXCR2, and the Duffy antigen receptor for chemokines (DARC) were found in all astrocytoma grades by reverse transcription/PCR analysis. In situ hybridization and immunohistochemistry localized DARC expression on normal brain and tumor microvascular cells and CXCR1 and CXCR2 expression to infiltrating leukocytes. These results support a model where IL-8 expression is initiated early in astrocytoma development through induction by inflammatory stimuli and later in tumor progression increases due to reduced microenvironmental oxygen pressure. Augmented IL-8 would directly and/or indirectly promote angiogenesis by binding to DARC and by inducing leukocyte infiltration and activation by binding to CXCR1 and CXCR2.

Astrocytomas are the most common and lethal human primary brain tumors and can be subdivided into low grade astrocytoma (WHO grade II), anaplastic astrocytoma (grade III), and glioblastoma (grade IV) according to cellularity, cellular pleomorphism, degree of neovascularization, and the presence of necrosis (1). Glioblastoma can occur de novo or as the recurrence of a grade II or III astrocytoma. Little is known about the molecular mediators inducing the biological changes occurring during this progression. Here we address two interesting biological features of these tumors: development of tumor-induced neovascularization and the use of this vascular network by lymphoid/myeloid cells for tumor infiltration.

As for other tumor types, the progression of astrocytoma is dependent on the development of new blood supply (2, 3). New blood vessels appear in low grade astrocytoma; these vessels are anatomically indistinguishable from those found in the surrounding normal brain. In the malignant phase of the disease, vessel density increases and the neovessels acquire an abnormal architecture, becoming extensively convoluted with the formation of vascular glom-

eruli, showing lumen occlusion, and displaying hyperplasia of the smooth muscle/pericyte and endothelial cell layers (1, 3). Maximal vessel density is reached in glioblastoma which is among the most vascularized tumors (4). Paradoxically, this increase in vessels is accompanied by the development of necrosis, the pathognomonic criterion that distinguishes glioblastoma from anaplastic astrocytoma (1, 3). The precise mechanism(s) at the origin of this tissue death are unresolved, but at least two factors are believed to contribute to its genesis. One is the outgrowth of blood supply by a rapidly growing tumor leading to tissue hypoxia/anoxia. The second is thrombotic occlusion of vessels, conducive to tissue ischemia (1).

Parallel to vessel development, astrocytomas are often infiltrated with numerous lymphoid/myeloid cells extravasating from newly formed tumor vessels. These are predominantly macrophages and CD8 T lymphocytes, but, B cells, NK cells, and CD4 T cells are also present (5, 6). It is unclear whether these infiltrates participate in an antitumor response or contribute indirectly to tumor expansion by secretion of growth factors or cytokines. Clearly, they are in-

efficient at eradicating tumor growth and do not appear to relate to a favorable prognosis (7, 8). The precise mechanism leading to infiltration in astrocytoma is unknown, but it is likely to involve both adhesion molecules (9, 10) and chemoattractants (11, 12).

IL-8 is a candidate molecule that may play a role in both of these processes. Belonging to the subfamily of chemokines blueprinted by a C-X-C amino acid cystein motif (see review in reference 13), IL-8 is secreted by many different cell types and is a chemoattractant for neutrophils, T lymphocytes, and basophils (14–19). Furthermore, recent work has demonstrated that IL-8 is a mediator of angiogenesis. IL-8 induces endothelial cell chemotactic and proliferative activity (20–22) and mediates neovascularization in rat and rabbit corneas in the absence of inflammation (23–24), as well as in the rat mesenteric window assay (25). IL-8 is secreted by a variety of tumor cells (see review in reference 13), promotes growth of bronchogenic carcinoma (26) and nonsmall cell lung cancer (22), and correlates with metastatic potential of human melanoma cells in nude mice (27).

Three IL-8-binding receptors participate in the biological responses mediated by this cytokine: C-X-C chemokine receptor 1 (CXCR1/IL-8RA), C-X-C chemokine receptor 2 (CXCR2/IL-8RB), and the Duffy antigen receptor for chemokines (DARC).¹ Although IL-8 is the only chemokine known to bind to CXCR1, CXCR2 is shared with all C-X-C chemokines carrying the amino acid motif E-L-R-C-X-C. DARC is a promiscuous receptor for many C-X-C and C-C chemokines and serves as a site of anchorage for infection by malaria parasite *Plasmodium vivax* (28, 29).

We previously demonstrated that IL-8 is synthesized in vivo during all stages of astrocytoma progression (12). Here we examine which physiological mechanisms regulate IL-8 expression during the progression of human astrocytoma, and elucidate whether this secretion mediates a biological response in these tumors. We demonstrate that two mechanisms are likely to be involved in IL-8 secretion: early induction by the presence of inflammatory signals such as IL-1 and TNF, and late induction by a change in the physiology of the tumor, namely, a decrease in oxygen levels due to ischemia/hypoxia. Expression of IL-8 receptors CXCR1 and CXCR2 on a subset of infiltrating leukocytes, and of DARC on tumor microvasculature supports a role for IL-8 in leukocyte attraction, activation, and angiogenesis.

Materials and Methods

Cell Culture, Spheroid Formation, and Anoxic Treatments. Human glioblastoma cell lines U87MG (endogenous WTp53; tumorigenic in immunocompromised mice), LN-229 (mutant p53, tumorigenic), LN-Z308 (p53-null, tumorigenic), and T98G (mutant p53, nontumorigenic) were grown as previously described (30). To

induce anoxia, cells were incubated in an Oxoid gas generating anaerobic system chamber (Unipath Ltd., Hampshire, UK) using hydrogen, CO₂, and a palladium catalyst to remove all traces of oxygen (final anoxic conditions: 93% hydrogen, 7% CO₂). Cells (1.5×10^6) were plated in tissue culture dishes 48 h before anoxic induction. When the cultures reached 80% confluence, fresh culture medium (DMEM–5% FCS) was added and dishes were incubated under normoxic or anoxic conditions for different times. To allow spheroid formation, LN-229 cells were trypsinized and 2×10^4 cells were seeded in 0.5% agar-coated wells (GIBCO BRL, Gaithersburg, MD). Culture medium was changed every 2 d and spheroids were incubated for 4–11 d until necrosis formation. Spheroids were then embedded in Tissue-Tek OCT4583 (Miles Inc., Elkhart, IN) and snap frozen in liquid nitrogen. Serial sections of 5- μ m thickness were then processed for in situ hybridization or immunohistochemistry.

Preparation of Conditioned Media for Measurement of IL-8 Production by ELISA. Culture supernatants of LN-229 were collected after 4, 12, and 24 h under normoxic or hypoxic conditions, centrifuged at 1,000 g, aliquoted, and stored at -80°C until tested. ELISA was done in duplicate using a commercially available assay system according to the manufacturer's instructions (R&D Sys. Inc., Minneapolis, MN). The minimal detection limit was 3 pg/ml of recombinant human IL-8 in the culture medium.

Tissue Specimens and Immunohistochemistry. Astrocytoma specimens and nontumoral brain tissue from pharmacoresistant epilepsy patients were snap frozen in refrigerated isopentane and stored at -80°C . Cystat tissue or spheroid sections were incubated with optimal concentrations of the following primary antibodies: anti-IL-8 hybridoma 46E5 (31), anti-CXCR1/IL-8RA hybridoma 5A12-5, anti-CXCR2/IL-8RB hybridoma 6C6-1C (18), anti-DARC polyclonal antibody 6615 and corresponding rabbit preimmune serum (32), and purified monoclonal antibody preparations against glial fibrillary acidic protein (GFAP) clone 6F2 (Dako, Copenhagen, Denmark), T cell marker CD3 clone SK7 (Becton Dickinson, Basel, Switzerland), and isotype-matched mouse immunoglobulins as negative controls (Dako). The sections were then incubated for 25 min with a biotinylated anti-mouse IgG horse antibody (Vector Labs., Burlingame, CA), followed by a 25-min incubation with peroxidase-labeled avidin. The chromogens used were 3-amino-9-ethylcarbazole (Sigma Chemical Co., St. Louis, MO) or 3,3'-diaminobenzidine (Fluka Chemie AG, Buchs, Switzerland). Counterstaining was done with hematoxylin for 30 s.

RNA Extraction and Reverse Transcriptase/PCR. Total RNA from resected human astrocytomas (5 grade II, 7 grade III, and 12 grade IV) and from four cell lines (LN-229, T98G, LN-Z308, and U87MG) were extracted with TRIzol Reagent as described by the manufacturer (GIBCO BRL). The reverse transcription (RT)/PCR was done with 1 μ g of total RNA as previously described (11). The following primer pairs were used; annealing temperatures, MgCl₂ concentrations, and amplicon sizes are indicated in brackets. For IL-8: 5' primer (5' ATG ACT TCC AAG CTG GCC GTG 3'), and 3' primer (5' CTC TTC AAA AAC TTC TCC CGA CTC TTA AGT ATT 3') [65°C, 1.5 mM, 298 bp]; for CXCR1: primer A (5' GAG GTT GTG TGT GGA AGG TG 3'), and primer B (5' AGG TTG ATG TTT TGG CAG TG 3') [64°C, 1 mM, 476 bp]; for CXCR2: primer A (5' GCT CTA GAG CTG GGC AAC AAT ACA GCA AACT 3') and primer B (5' CCA TCG ATG GGC ACT TAG GCA GGA GGT CTTA 3') [60°C, 1.5 mM, 493 bp]. RT controls included reactions without mouse Moloney leukemia virus (MMLV) reverse transcriptase and without RT product.

¹Abbreviations used in this paper: DARC, Duffy antigen receptor for chemokines; GFAP, glial fibrillary acidic protein; mRNA, messenger RNA; RT, reverse transcription; VEGF, vascular endothelial growth factor.

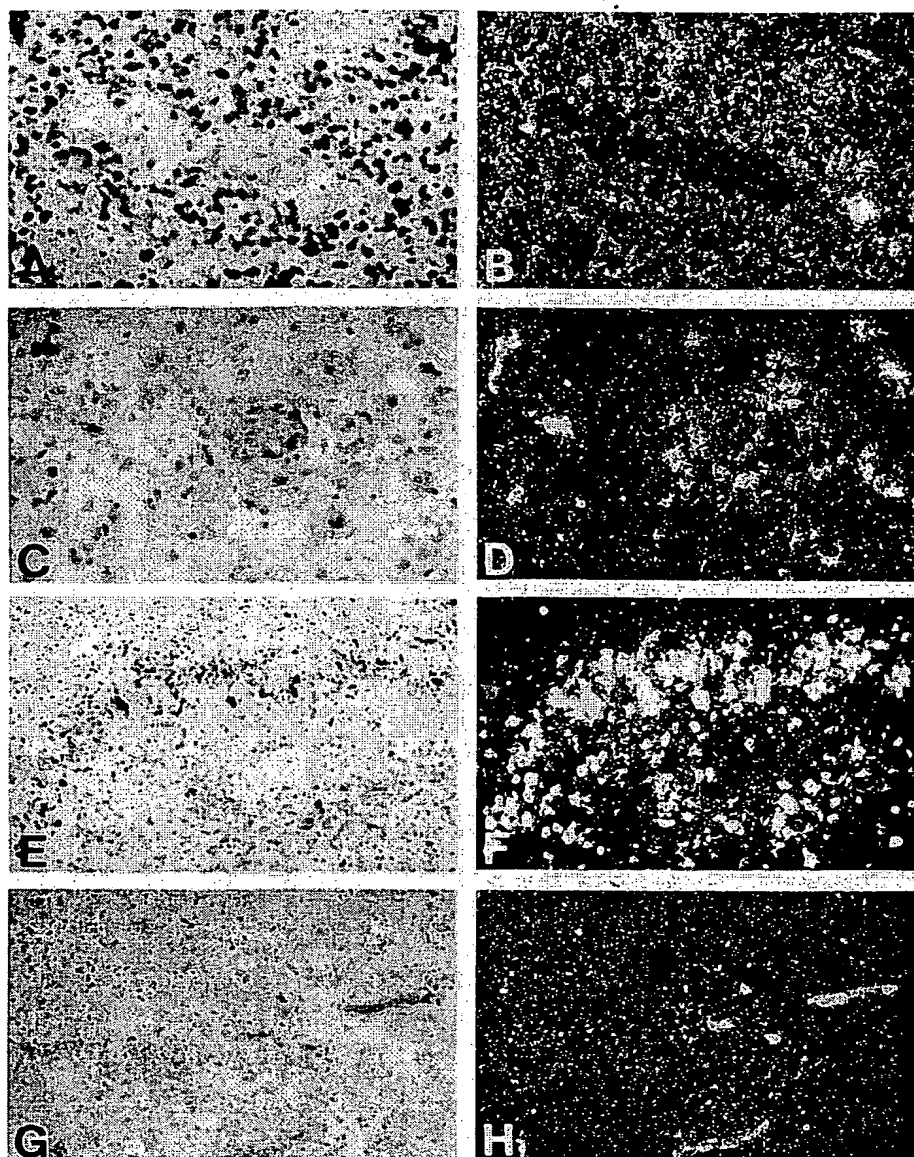


Figure 1. Detection of IL-8 mRNA in glioblastoma sections by in situ hybridization. (A–F) Antisense IL-8 cRNA probe, (G and H) sense IL-8 cRNA probe (negative control). Sections were derived from glioblastoma No. 921 for A and C (bright field) and B and D (dark field), and glioblastoma No. 882 for E and G (bright field) and F and H (dark field). (A and B were also used for immunohistochemistry with an anti-GFAP antibody (A, red filaments; B, green filaments). (E–H) Pseudopalisading cells separate a necrotic tumor area with numerous dying cells with pyknotic nuclei (top) from a viable richly vascularized tumor area (bottom). Bright areas in H are tumor vessels.

Northern Blot Analysis. 10 μ g of RNA/sample were electrophoresed through a 1% agarose formaldehyde gel and blotted onto a nitrocellulose membrane (Hybond N; Amersham, Aylesbury, UK) as previously described (11). The blots were hybridized with the following probes labeled by random primed DNA labeling kit (Boehringer Mannheim, Indianapolis, IN): a 298-bp PCR fragment of IL-8 cDNA (see above), a 500-bp EcoRI–BamHI fragment of human vascular endothelial growth factor (VEGF) cDNA (plasmid pBluescript KS-VEGF), a 1,100-bp PstI–EcoRI fragment of β actin cDNA (plasmid pAL41), and a 280-bp EcoRI fragment of the bovine 28S ribosomal DNA gene.

In Situ Hybridization. In situ hybridization was performed as previously described (11) using the following cRNA sense and antisense probes labeled with 35 S-UTP during in vitro transcription reactions with T3 or T7 RNA polymerase: a 240-bp PstI–EcoRI fragment of the IL-8 cDNA, a 477-bp EcoRI–XhoI CXCR1 cDNA fragment (33), a 1,510-bp EcoRI–XhoI CXCR2

cDNA fragment (34), and, as a positive control, a BamHI–EcoRI VEGF₁₆₅ cDNA fragment.

Results

Previous work established that IL-8 is produced in patients with all grades of astrocytoma progression. Interestingly, immunohistochemistry showed predominant IL-8 localization on tumor cells or macrophages in perivascular areas with leukocytic infiltrates and on pseudopalisading cells surrounding necrosis (12), a spatial pattern that is compatible with a role in chemotaxis and/or angiogenesis. However, localization of cytokine secretion sites on this basis may be misleading and be the result of cytokine sequestration rather than production. To unequivocally identify the

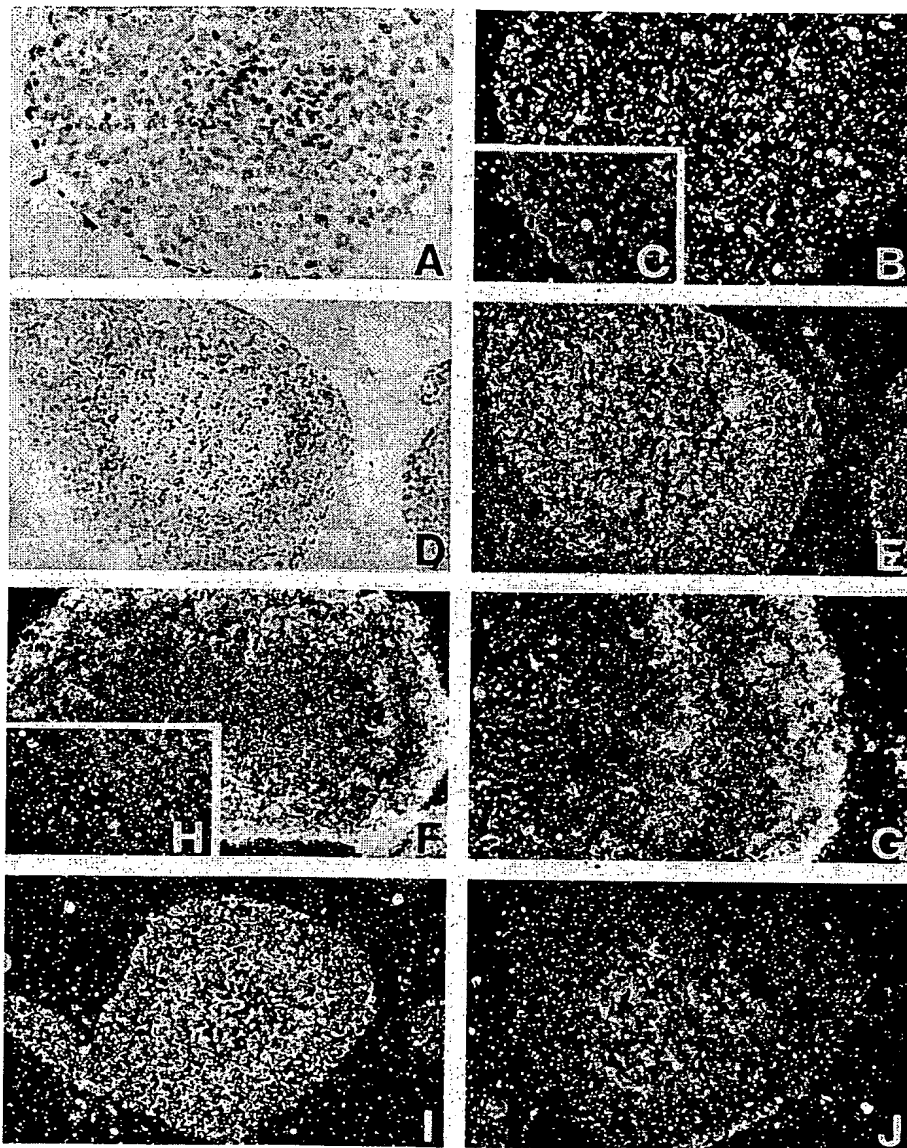


Figure 2. Detection of IL-8 and VEGF mRNAs on spheroid sections of glioblastoma cell line LN-229 by in situ hybridization. (A, B, and D-G) Antisense IL-8 cRNA probe, (C and H) sense IL-8 cRNA probe (negative control). Green area in H corresponds to necrosis. (I) Antisense VEGF cRNA probe. (J) VEGF cRNA probe (negative control). (A-C) 4-d-old spheroid, magnification of 20; (D-J) 10-d-old spheroids with central necrosis, magnification of 10. Spheroid in F and G was incubated for 24 h with TNF (100 U/ml) before sectioning.

IL-8 producer cells in these areas, we performed in situ hybridization with sense and antisense IL-8 cRNA probes on ex vivo glioblastoma samples. IL-8 messenger RNA (mRNA) was found in areas surrounding blood vessels, both in those showing a lumen (Fig. 1, A and B) and in those with glomeruloid microvascular proliferation (Fig. 1, C and D) characteristic of glioblastoma (1). This confirms the spatial pattern of expression observed previously with in situ immunoprecipitation (12). Moreover, elevated IL-8 mRNA levels were observed in cells surrounding necrosis (Fig. 1, E and F). These cells form a particular structure called pseudopalisade and are believed to undergo severe stress due to oxygen deprivation (1). Controls with sense probes on adjacent sections were negative (Fig. 1, G and H). Staining of these sections (Fig. 1 A) or adjacent sections (not shown) with an antibody against GFAP, a glial lineage marker, suggested

that the cells expressing IL-8 mRNA were either of glial origin (astrocytoma cells or reactive astrocytes) or cells infiltrating the tumor in areas with intricate patterns of GFAP expression.

The correlation of IL-8 expression and tumor cell proximity to necrosis prompted us to investigate whether there was a causal relationship. Therefore, we used an experimental model system in which necrosis forms at the center of a multicellular tumor spheroid (35, 36). These spheroids can be easily manipulated in vitro, the appearance of necrosis is dependent on spheroid size (150–300 μ M diameter), and measurement of oxygen content in the necrotic region showed that it was anoxic (35). Another advantage of this model is that it allows examination of inducing events linked to necrosis formation without the in vivo complications linked to the presence of nontumoral cells (microvessel

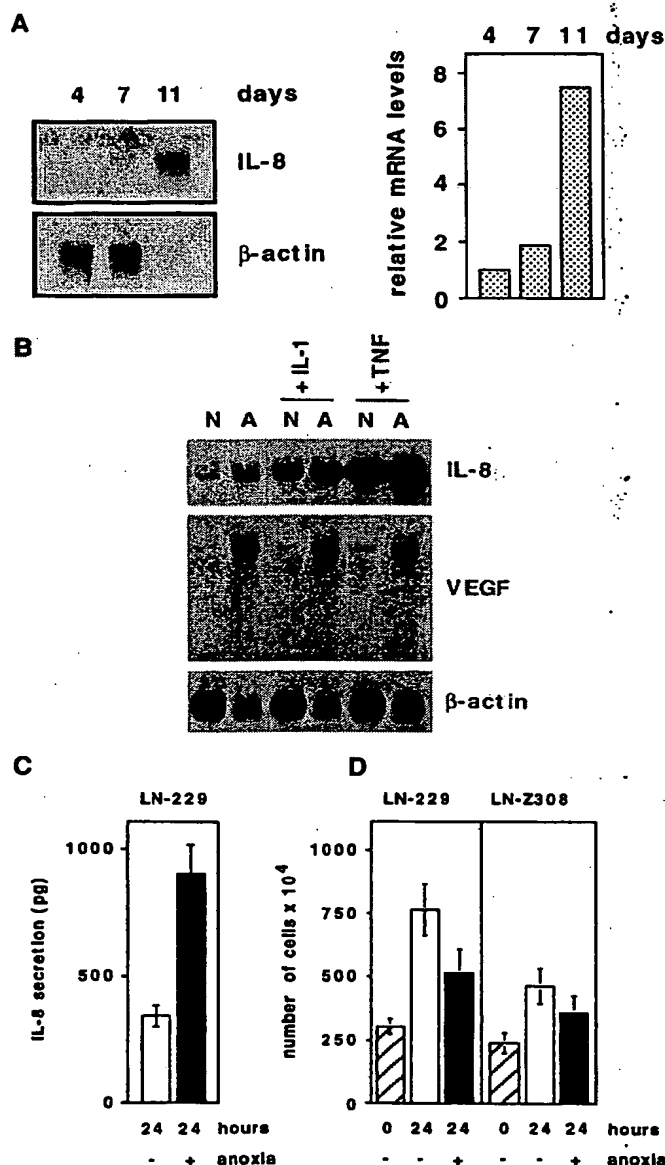


Figure 3. Measurement of IL-8 mRNA and protein levels in glioblastoma cells exposed to anoxia. (A) Time course of IL-8 mRNA levels in LN-229 glioblastoma cell spheroids by Northern blotting (left) and graphical display of relative mRNA levels (right). 10 μ g of total RNA extracted from 4-, 7-, and 11-d-old spheroids is displayed in each lane. (This normalizes for cell content in spheroids.) (B) Northern blot with RNA extracted from LN-229 glioblastoma cells, incubated for 24 h in an anoxia-generating chamber system. N, normoxia; A, anoxia; IL-1, simultaneous IL-1 β treatment at 10 U/ml for 24 h; TNF, TNF- α treatment at 100 U/ml for 24 h. (C) Measurement of IL-8 by ELISA (picogram per milligram of total cellular protein) in conditioned media of LN-229 cells after 24 h of normoxic (white column) or anoxic (black column) treatment. Standard deviations (vertical bars) of triplicates were calculated. (D) Analysis of cell number and viability of glioblastoma cell lines upon anoxic treatment. LN-229 (left) and LN-Z308 (right) glioblastoma cells were stained with trypan blue and counted before (hatched columns) and after a 24-h treatment under normoxic (white columns) or anoxic (black columns) conditions. Standard deviations of triplicates (vertical bars) were calculated. The amount of cells permeable to trypan blue was insignificant and is not presented in the graph.

cells, microglia, and infiltrating leukocytes). Spheroids were produced from glioblastoma cells and analyzed for IL-8 mRNA expression by in situ hybridization and Northern blotting before and after appearance of central necrosis. Slight constitutive IL-8 mRNA expression was found in small spheroids without necrosis (diameter of $<150 \mu$ m) under the culture conditions used (Fig. 2, A and B); this likely reflects serum stimulation of IL-8 expression as previously shown in monolayer cultures (12). In larger spheroids (>10 d old) with central necrosis, a ring-like augmentation of IL-8 mRNA levels was observed (Fig. 2, D and E). This increase in IL-8 mRNA could be the result of an inductive event in the stressed cells lining necrosis or an inhibition of IL-8 mRNA expression in the peripheral cell layer at the contact of culture medium. To discriminate between these two possibilities, we incubated the spheroids with TNF- α , an inflammatory cytokine known to induce IL-8 mRNA production. Increase of IL-8 mRNA was now observed both in the cells lining necrosis and in those at the periphery of the spheroid (Fig. 2, F and G), showing that the peripheral cells have not become refractory to an IL-8-inducing stimulus. In situ hybridization of these spheroids with a VEGF antisense probe (Fig. 2 I) showed that the mRNA increases observed for both IL-8 and VEGF were similar in both intensity and perinecrotic localization. Control sense cRNA probes for IL-8 (Fig. 2, C and H) and VEGF (Fig. 2 J) were negative.

To obtain a quantitative estimate of the increase in IL-8 mRNA production as a result of necrosis development over time, we performed Northern blotting on 10 μ g total RNA (thus normalizing for differences in cell numbers between young and old spheroids) extracted from 4-, 7-, and 11-d-old spheroids. Total IL-8 mRNA content of spheroids increased significantly from days 4 to 7 by 2-fold, and from days 4 to 11 by 7.5-fold (Fig. 3 A). These results demonstrate that establishment of a necrotic area in glioblastoma spheroids is sufficient to generate an increase in IL-8 mRNA steady state levels in glioblastoma cells, and that this induction is not dependent on nontumoral accessory cells.

Induction of IL-8 expression could be the direct result of physiological conditions of minimal oxygen supply or related to the presence of factors produced either by dying cells or liberated by cell lysis during necrosis. To discriminate between these possibilities, we placed monolayer glioblastoma cell cultures under experimental conditions of oxygen deprivation using anaerobic chambers (see Materials and Methods). These chambers generate complete anoxia within a time frame of 6–8 h due to oxygen consumption by a palladium catalyst. Using this system we were able to demonstrate an increase in IL-8 mRNA levels, as do IL-1 or TNF treatments, in glioblastoma cell lines LN-229 (Fig. 3 B), U87MG, LN-Z308, and T98G (not shown), a panel representative of the genetic and biological heterogeneity of glioblastoma (37). IL-8 mRNA peaked between 12 and 24 h after induction (not shown) and resulted in augmentation of secreted IL-8 in culture medium as measured by ELISA (Fig. 3 C). Similar results were obtained in cells in-

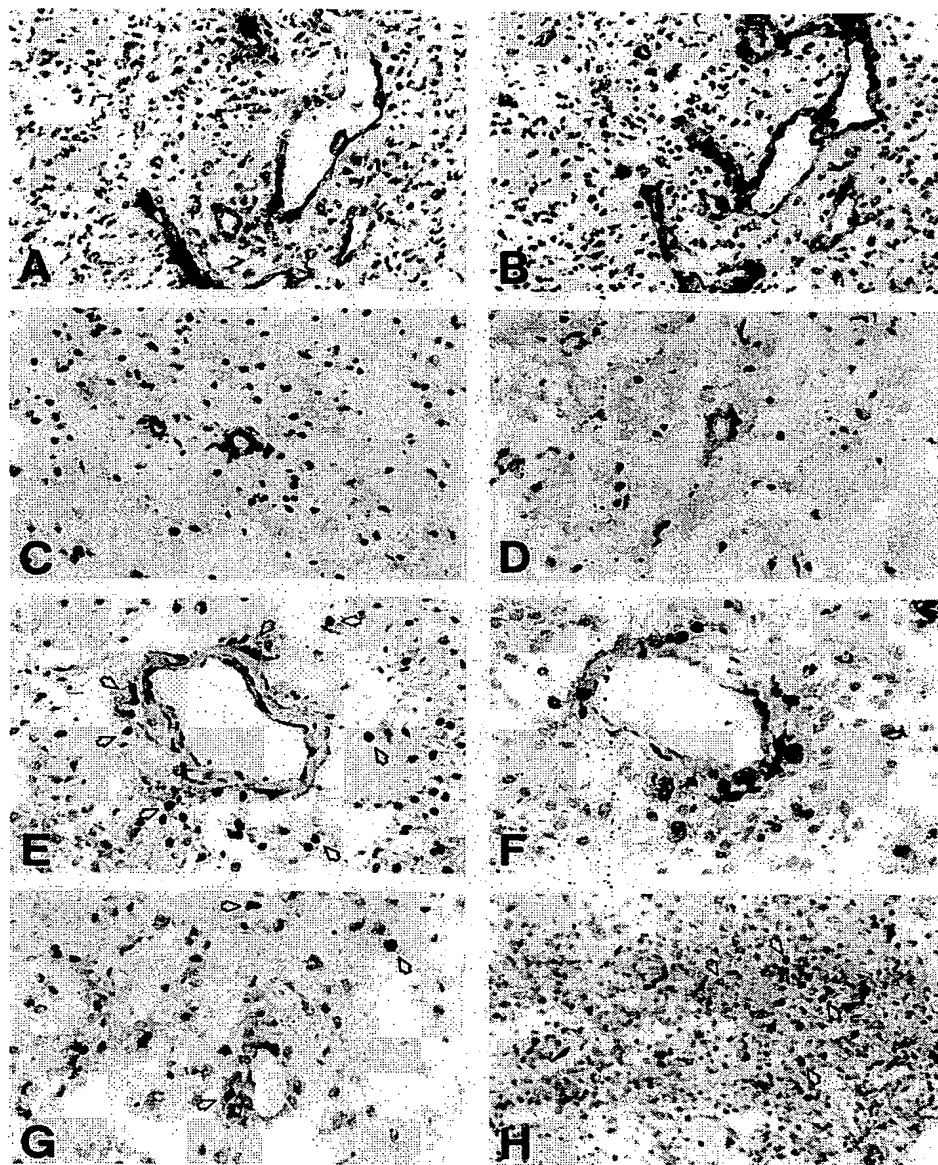


Figure 4. Detection of IL-8-binding receptors in glioblastoma by immunohistochemistry. DARC (A) and factor VIII (B) expression on microvascular cells of glioblastoma No. 1069. DARC (C) and preimmune serum (D) staining on nontumoral brain No. T265CN. CXCR1 (E) and CD3 (F) staining on glioblastoma No. 906. CXCR2 staining on sections with vessels (G) or in a perinecrotic region (H) of glioblastoma No. 842. Examples of positive cells are shown by arrows.

cubated under a gas mixture composed of 95% N₂ and 5% CO₂ (not shown). Cell counting before and after the 24-h anoxic treatment showed moderate reduction in cell numbers (by 20–30%) as compared to untreated cells (Fig. 3 D), due to a reduced proliferation rate under anoxia. Examination of morphology and membrane integrity by exclusion of trypan blue did not show loss of cell viability and there was no cell detachment from the monolayer. This demonstrates that IL-8 induction is not due to cell products released from lysing cells, but rather a biological response to anoxic stress. Furthermore, the induction was obtained irrespective of the endogenous wild-type or mutant p53 gene status of the cell lines analyzed (37), suggesting that it was not linked to hypoxia-induced p53 (38). This is particularly relevant since consensus binding sites for the p53

transcription factor (39) are present in the IL-8 gene. To directly evaluate whether WTP53 could increase IL-8 mRNA levels, we used a clone of glioblastoma cell line T98G in which WTP53 expression can be conditionally induced by dexamethasone (40). No difference in IL-8 mRNA content was found in p53-induced and noninduced cells by Northern blotting (not shown).

The biological relevance of IL-8 expression in glioblastoma depends on the presence of cells with receptors capable of binding IL-8. Therefore, we evaluated whether IL-8 might have autocrine and/or paracrine functions in vivo. First, we examined CXCR1, CXCR2, and DARC mRNA expression by RT/PCR. CXCR1 mRNA was found in 5 of 5 grade II, 1 of 7 grade III, and 8 of 12 grade IV astrocytoma. CXCR2 mRNA was found in 5 of 5 grade II, 6 of 7

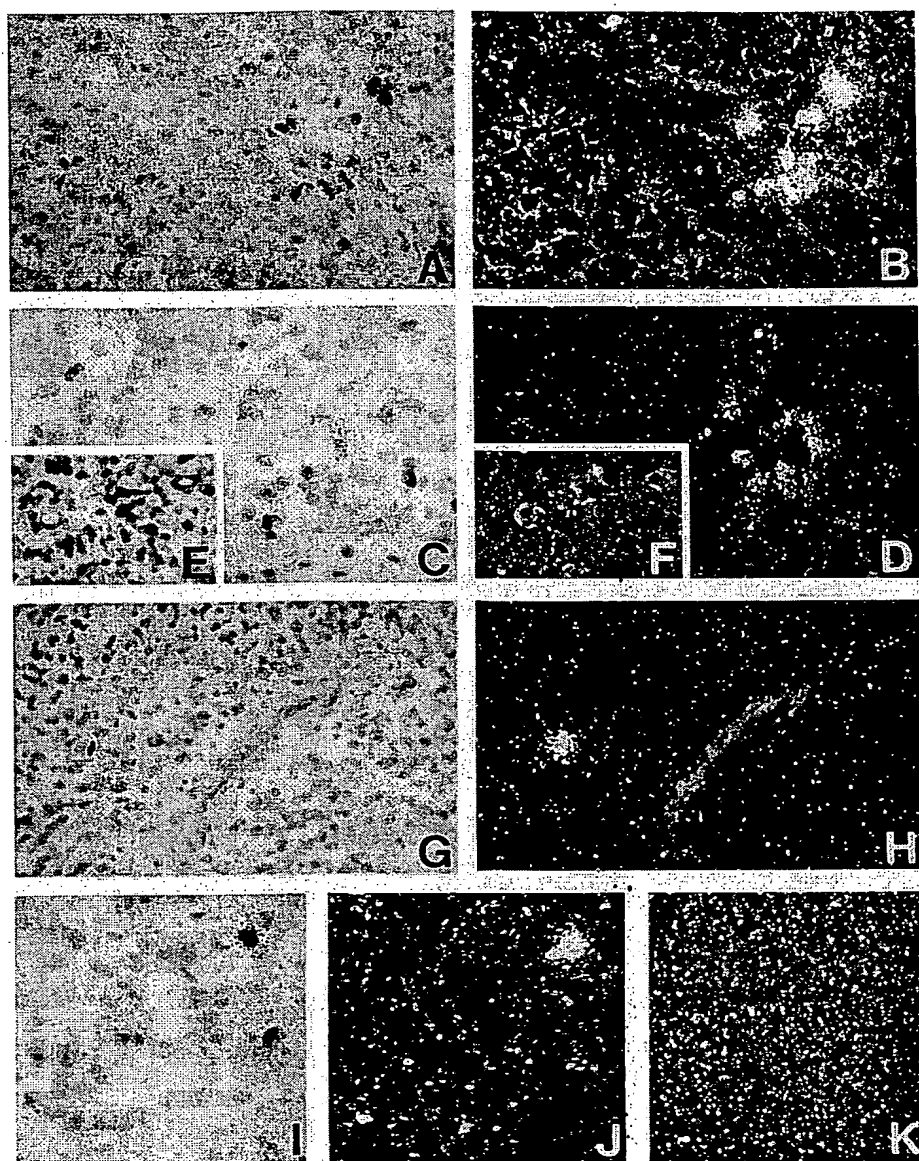


Figure 5. Detection of IL-8-binding receptors CXCR1 and CXCR2 mRNAs in glioblastoma sections by in situ hybridization. (A–D) Antisense CXCR1 cRNA probe, (E and F) negative control sense CXCR1 cRNA probe, (G–J) antisense CXCR2 cRNA probe, (K) negative control sense CXCR2 cRNA probe. Sections were derived from glioblastoma No. 921 for A and G (bright field) and B and H (dark field), glioblastoma No. 892 for C and E (bright field) and D and F (dark field), and glioblastoma No. 882 for I (bright field), J and K (dark field). Immunohistochemistry with an anti-GFAP antibody was used for sections A and B (A, red filaments, and B, green-brown filaments) and with an anti-smooth muscle actin antibody for E and F.

grade III, and 11 of 12 grade IV. DARC mRNA was found in 3 of 5 grade II, 5 of 7 grade III, and 10 of 12 grade IV (results not shown). This suggested that IL-8 may serve a biological function during the progression of human astrocytoma in vivo, either on tumor cells or on accessory cells. Next, we examined which cell types expressed IL-8-binding receptors in vivo by immunohistochemistry (representative stainings are shown in Fig. 4). Very interestingly, DARC was specifically expressed by microvascular cells in 5 of 6 grade II, 5 of 6 grade III, and 14 of 19 grade IV astrocytomas (Fig. 4 A) with a staining pattern similar to the one obtained for factor VIII, a microvascular marker (Fig. 4 B). DARC expression was also present on 5 of 5 nontumoral brains (Fig. 4 C). Control stainings with preimmune serum was negative on all samples (Fig. 4 D). In contrast,

for both CXCR1 and CXCR2, isolated positive cells were found surrounding blood vessels. For CXCR1, 2 of 9 grade II, 1 of 3 grade III, and 5 of 18 grade IV were positive (Fig. 4 E), and for CXCR2, 1 of 9 grade II, 0 of 3 grade III, and 5 of 18 grade IV (Fig. 4 G). Staining of adjacent sections for CD3, a specific marker of T lymphocytes (Fig. 4 F), and CD15, a macrophage marker (not shown), showed infiltrates in these areas, suggesting expression by a subset of T lymphocytes and/or macrophages. Unfrequently, numerous CXCR2 positive cells were found close to necrosis (Fig. 4 H).

To confirm the CXCR1- and CXCR2-expressing cells detected by immunohistochemistry, we performed in situ hybridization on three glioblastomas. Specific signals for both CXCR1 (Fig. 5, A–D) and CXCR2 (Fig. 5, G–J)

mRNAs were found on small isolated cells surrounding vessels, with a morphology compatible with lymphoid or myeloid infiltrates. Double staining with an anti-GFAP antibody failed to associate these cells with GFAP filaments (Fig. 5 A). Control with sense probes for CXCR1 (Fig. 5, E and F) and CXCR2 (Fig. 5 K) were negative. These data are consistent with expression by infiltrating leukocytes and confirm immunostaining results.

Discussion

Morphological examination of the malignant progression of astrocytoma shows that the transition to the most malignant form (glioblastoma) is defined by the appearance of necrosis (1). It is intriguing that a decrease in physiological oxygen pressure, ultimately lethal to tumor cells, coincides with maximal tumor aggressiveness. This raises the question as to whether the hypoxic/ischemic conditions increasing at this stage are a consequence or a cause of increased malignancy. The appearance of necrosis is also closely associated with the ultimate changes in the angiogenic phenotype of glioblastoma. The mRNA for VEGF, an endothelial-specific angiogenic mitogen, is upregulated by hypoxia in glioma cells *in vitro* and is overexpressed in cells lining necrotic areas *in vivo* (41, 42, 36). VEGF receptor type 2 mRNA is upregulated on endothelial cells in glioblastoma, and studies with animal models of glioma have shown that vessel development and tumor growth were partially inhibited by anti-VEGF antibodies (43), overexpression of a dominant negative VEGF receptor mutant (44), or antisense VEGF gene constructs (45, 46). These results demonstrate that hypoxic regulation of VEGF is of biological consequence for the angiogenic phenotype associated with the transition to the most malignant form of astrocytoma. The factors inducing neovascularization in the early phases of astrocytoma development are less well characterized (3). The presence of residual tumor upon anti-VEGF treatment further suggests that more than one factor ensures angiogenic supply to support astrocytoma growth.

Finally, because astrocytoma cells also secrete angiogenic inhibitors (47) and cytokines such as IL-6 (30) or leukemia inhibitory factor (LIF) (our unpublished results) with anti-angiogenic properties (48), the final angiogenic response will be determined by the balance between positive and negative regulators (2).

Here we demonstrate that IL-8, another soluble biological mediator with angiogenic and chemotactic properties, is upregulated in cells surrounding necrosis in glioblastoma and that IL-8-binding receptors are concomitantly expressed *in vivo*. IL-8 is the best studied member of the chemokines, a class of cytokines extensively analyzed for their ability to attract and activate leukocytes during inflammation (see review in reference 13). It has previously been demonstrated that upon induction by inflammatory cytokines IL-1 and TNF astrocytoma cells release a variety of cytokines *in vitro*, including biologically active IL-8 (see review in reference 49). *In vivo*, it was unclear whether cytokine expression resulted from indirect induction by tu-

mor-related inflammatory responses or was directly linked to tumor growth and progression.

We now confirm the presence of IL-8 expression in astrocytoma and show that it is likely to occur by two distinct mechanisms during the progression of astrocytoma. Initial upregulation may be mediated by stimulatory signals such as proinflammatory cytokines (e.g., IL-1 or TNF), which induce IL-8 in astrocytoma cells *in vitro* and can be present in glioma, in glioma-associated cyst fluid, and in cerebrospinal fluid derived from glioma patients (see review in reference 49). Later in disease progression, strong IL-8 upregulation is observed in cells surrounding necrotic areas in glioblastoma, suggesting further induction by hypoxia/ischemia. This hypothesis was sustained by increased IL-8 mRNA and protein expression upon *in vitro* exposure of glioblastoma cells to anoxia as monolayer cultures or in the central necrosis of three-dimensional spheroids. These experiments further showed that this increase was not dependent on nontumoral accessory cells or on stimulation by factors released by dying tumor cells. Thus, IL-8 increase in late stage astrocytoma is most likely to be due to physiological changes in oxygen pressure occurring during tumor growth, although we cannot exclude participation of accessory cells such as macrophages, microglia, or reactive astrocytes *in vivo*.

The influence of altered oxygen concentrations on IL-8 expression has previously been demonstrated in the context of ischemia reperfusion. Human umbilical vein endothelial cells were shown to upregulate IL-8 during hypoxia (50) as were monocytes during reoxygenation (51). Here, we show that similar IL-8-inducing events may occur in the pathologic process of cancer. Tumor cells and/or tumor-infiltrating macrophages or microglia upregulate IL-8 expression which may play important functions in tumor angiogenesis and tumor immune interactions through paracrine stimulation of cognate receptors. Upregulation of IL-8 in tumor endothelial cells was not observed in astrocytoma, and may reflect differences in endothelial subtypes, the abnormal structure of the tumor endothelium, as well as tissue environment (12) or rapid internalization after binding to DARC (52).

IL-8 induction is relevant to the biology of the tumor since we detected the expression of IL-8 receptor mRNA and protein. Tumor cells did not express IL-8 receptors *in vivo* demonstrating that IL-8 does not participate in an autocrine growth regulatory loop mediated by any of these three receptors. However, IL-8 receptor expression pattern suggests two functions for IL-8 in astrocytoma.

First, the constitutive expression of the DARC receptor on normal brain and tumor microvasculature supports an angiogenic function for IL-8 in astrocytoma. This is sustained by a recent report in which the angiogenic factors present in the supernatant of glioma cell lines were evaluated in an *in vitro* angiogenic assay using human microvascular endothelial cells. The authors showed with antibody neutralization assays that the angiogenic response was primarily due to IL-8 or the combination of VEGF and bFGF, depending on the cell line analyzed (53). Clearly,

further *in vivo* studies will have to establish whether IL-8 and other angiogenic chemokines are essential contributors to the angiogenic response seen in astrocytoma, whether this response is mediated by DARC, and whether they act in synergy with VEGF or represent alternative angiogenic routes. This is, to our knowledge, the first report of DARC expression on tumor vasculature. The presence of DARC on normal endothelial cells lining postcapillary venules in kidney, spleen, lung, and brain (32, 29, 54), cells potentially constitutively responsive to IL-8, may implicate DARC in early tumor angiogenesis. It is noteworthy that this vascular staining is not the result of vessel cell or extracellular matrix binding of DARC released from erythrocytes, since this staining was maintained in individuals lacking erythroid DARC gene expression, due to a mutation disrupting a binding site for the GATA1 erythroid transcription factor in the DARC gene promoter (52, 55). Furthermore, these results designate DARC as a prime candidate endothelial receptor to explain endothelial cell binding and direct angiogenic responses mediated by IL-8 (20–22, 56, 57). This should stimulate the deciphering of the downstream effector mechanisms, likely the demonstration that DARC elicits an intracellular signal upon ligand binding in microvascular cells. Lastly, due to the promiscuous nature of the DARC receptor, a variety of C-C and C-X-C chemokines expressed by astrocytoma (see review in reference 49) may bind tumor microvascular cells. The convergence of a large panel of potentially angiogenic cytokines (58) in the use of a single microvascular receptor, might designate DARC as a target of choice for therapeutic interference at what might become the "Achilles' heel" of chemokine redundancy.

Second, the expression of CXCR1 and CXCR2 on a subset of infiltrating lymphoid and/or myeloid cells is compatible with a role for IL-8 as chemotactic and activating agent for leukocytes in astrocytoma, as suggested in other systems (14, 15, 17–19). It will be of interest to further characterize this leukocyte subset and to study its function

in the tumor immune system relationship and as an indirect elicitor of angiogenesis through cytokine release (59, 60). It should also be mentioned that if IL-8 chemoattracts T lymphocytes, other astrocytoma-expressed leukocyte chemoattractants, such as MCP-1 (11, 61) are certainly involved, since CXCR1 and CXCR2 expression was found on only a fraction of leukocytic infiltrates. The reasons for the rare occurrence of neutrophils in astrocytoma/glioblastoma despite functional IL-8 inducing signals are unknown and were previously discussed (12). Additional hypotheses include inappropriate expression of homing signals, such as specific selectins (62), potential killing of Fas-expressing neutrophils (63) by Fas ligand expressed by tumor cells (64, 65), disappearance/physiological downregulation by receptor desensitization (66), excessive release of IL-8 in circulation leading to saturation (67), or inactivation of chemoattractant ability due to cleavage by aminopeptidase N (CD13) (68).

In conclusion, our results support a model where early in astrocytoma development tumor-related inflammatory responses trigger IL-8 and VEGF release. This would elicit direct and/or indirect angiogenic responses through binding of IL-8 to the DARC receptor expressed constitutively on brain microvascular cells and CXCR1 and CXCR2 receptors on leukocytes. Chemoattracted leukocytes infiltrate the tumor and their activation induces release of cell products/cytokines with angiogenic potential. VEGF release induced by inflammatory signals might exert its first action when VEGFR1 expression appears in low grade astrocytoma (3). Later in astrocytoma progression and in *de novo* glioblastoma, induction of IL-8 and VEGF production by reduced oxygen pressure and appearance of expression of VEGFR2 (3) would further contribute, besides other factors, to the florid microvascular proliferation characteristic of glioblastoma. The understanding of the molecular mechanisms at the origin of tumor neovascularization, especially at early disease stages, should permit the development of new therapeutic modalities targeted at specific angiogenic effectors.

We would like to thank Drs. M. Buckingham, J.F. Brunet, W.E. Holmes, H. Marti, P.M. Murphy, A.O. Pogo, S.X. Qin, M. Sticherling, and H. Weich for plasmids, antibodies, and nontumoral brain samples. We would also like to show our appreciation to Drs. P.-Y. Dietrich, M. Gassmann, R. Kessler, M. Pepper, A.O. Pogo, E. Reichmann, and P.R. Walker for helpful advice and reading the manuscript.

This work was supported by Swiss National Science Foundation grants no. 31-39634.93 (to N. de Tribolet), 31-39356, and 4037-044729 (to E.G. Van Meir), by the Swiss Cancer Research Foundation grant KFS172-9-1995 (to E.G. Van Meir), by the Swiss and Vaud Anti-Cancer Leagues grants FOR254 and SKL116-7-1995 (to N. de Tribolet) and the San Salvatore Foundation (to E.G. Van Meir).

Address correspondence to Erwin G. Van Meir, Laboratory of Tumor Biology and Genetics, Neurosurgery Department, University Hospital (CHUV), 1011 Lausanne, Switzerland. Phone: +41-21-314-2582; FAX: +41-21-314-2587; E-mail: evanmeir@hola.hospvd.ch

Received for publication 6 May 1997 and in revised form 23 July 1997.

References

- Kleihues, P., P.C. Burger, and B.W. Scheithauer. 1995. Histological typing of tumors of the central nervous system. Springer-Verlag, Berlin. 11-14.
- Hanahan, D., and J. Folkman. 1996. Patterns and emerging mechanisms of the angiogenic switch during tumorigenesis. *Cell*. 86:353-364.
- Plate, K.H., and W. Risau. 1995. Angiogenesis in malignant gliomas. *Glia*. 15:339-347.
- Brem, S., R. Cotran, and J. Folkman. 1972. Tumor angiogenesis: a quantitative method for histological grading. *J. Natl. Cancer Inst.* 48:347-356.
- Paine, J.T., H. Handa, T. Yamasaki, J. Yamashita, and S. Miyatake. 1986. Immunohistochemical analysis of infiltrating lymphocytes in central nervous system tumors. *Neurosurgery (Baltim.)*. 18:766-772.
- Kuppner, M.C., M.F. Hamou, and N. de Tribolet. 1988. Immunohistological and functional analyses of lymphoid infiltrates in human glioblastomas. *Cancer Res.* 48:6926-6932.
- Rossi, M.L., N.R. Jones, E. Candy, J.A. Nicoll, J.S. Compton, J.T. Hughes, M.M. Esiri, T.H. Moss, F.F. Cruz Sanchez, and H.B. Coakham. 1989. The mononuclear cell infiltrate compared with survival in high-grade astrocytomas. *Acta Neuropathol.* 78:189-193.
- Stavrou, D., A.P. Anzil, W. Weidenbach, and H. Rodt. 1977. Immunofluorescence study of lymphocytic infiltration in gliomas. Identification of T-lymphocytes. *J. Neurol. Sci.* 33:275-282.
- Kuppner, M.C., M.-F. Hamou, and N. de Tribolet. 1990. Activation and adhesion molecule expression on lymphoid infiltrates in human glioblastomas. *J. Neuroimmunol.* 29:229-238.
- Rosenman, S.J., P. Shrikant, L. Dubb, E.N. Benveniste, and R.M. Ransohoff. 1995. Cytokine-induced expression of vascular cell adhesion molecule-1 (VCAM-1) by astrocytes and astrocytoma cell lines. *J. Immunol.* 154:1888-1899.
- Desbaillets, I., M. Tada, N. de Tribolet, A.C. Diserens, M.F. Hamou, and E.G. Van Meir. 1994. Human astrocytomas and glioblastomas express monocyte chemoattractant protein-1 (MCP-1) in vivo and in vitro. *Int. J. Cancer.* 58:240-247.
- Van Meir, E.G., M. Ceska, F. Effenberger, A. Walz, E. Grouzmann, I. Desbaillets, K. Frei, A. Fontana, and N. de Tribolet. 1992. Interleukin-8 is produced in neoplastic and infectious diseases of the human central nervous system. *Cancer Res.* 52:4297-4305.
- Baggiolini, M., B. Dewald, and B. Moser. 1994. Interleukin-8 and related chemotactic cytokines-CXC and CC chemokines. *Adv. Immunol.* 55:97-179.
- Larsen, C.G., A.O. Anderson, E. Appella, J.J. Oppenheim, and K. Matsushima. 1989. The neutrophil-activating protein (NAP-1) is also chemotactic for T lymphocytes. *Science (Wash. DC)*. 243:1464-1466.
- Leonard, E.J., A. Skeel, T. Yoshimura, K. Noer, S. Kutvirt, and D. Van Epps. 1990. Leukocyte specificity and binding of human neutrophil attractant/activation protein-1. *J. Immunol.* 144:1323-1330.
- Wilkinson, P.C., and I. Newman. 1992. Identification of IL-8 as a locomotor attractant for activated human lymphocytes in mononuclear cell cultures with anti-CD3 or purified protein derivative of *Mycobacterium tuberculosis*. *J. Immunol.* 149:2689-2694.
- Babi, L.F.S., B. Moser, M.T.P. Soler, R. Moser, P. Loetscher, B. Villiger, K. Blaser, and C. Hauser. 1996. The interleukin-8 receptor B and CXC chemokines can mediate transendothelial migration of human skin homing T cells. *Eur. J. Immunol.* 26:2056-2061.
- Qin, S.X., G. Larosa, J.J. Campbell, H. Smithheath, N. Kassam, X.J. Shi, L. Zeng, E.C. Butcher, and C.R. Mackay. 1996. Expression of monocyte chemoattractant protein-1 and interleukin-8 receptors on subsets of T cells—correlation with transendothelial chemotactic potential. *Eur. J. Immunol.* 26:640-647.
- Ross, J.S., K. Mistry, K.B. Bacon, and R.D. Camp. 1991. Characterisation of the in vitro responsiveness of lymphocyte subsets to locomotor stimuli by immunocytochemical methods. *J. Immunol. Methods.* 140:219-225.
- Koch, A.E., P.J. Polverini, S.L. Kunkel, L.A. Harlow, L.A. Di Pietro, V.M. Elner, S.G. Elner, and R.M. Strieter. 1992. Interleukin-8 as a macrophage-derived mediator of angiogenesis. *Science (Wash. DC)*. 258:1798-1801.
- Szekanecz, Z., M.R. Shah, L.A. Harlow, W.H. Pearce, and A.E. Koch. 1994. Interleukin-8 and tumor necrosis factor- α are involved in human aortic endothelial cell migration. The possible role of these cytokines in human aortic aneurysmal blood vessel growth. *Pathobiology.* 62:134-139.
- Arenberg, D.A., S.L. Kunkel, P.J. Polverini, M. Glass, M.D. Burdick, and R.M. Strieter. 1996. Inhibition of interleukin-8 reduces tumorigenesis of human non-small cell lung cancer in SCID mice. *J. Clin. Invest.* 97:2792-2802.
- Strieter, R.M., S.L. Kunkel, V.M. Elner, C.L. Martonyi, A.E. Koch, P.J. Polverini, and S.G. Elner. 1992. Interleukin-8. A corneal factor that induces neovascularization. *Am. J. Pathol.* 141:1279-1284.
- Hu, D.E., Y. Hori, and T.P. Fan. 1993. Interleukin-8 stimulates angiogenesis in rats. *Inflammation.* 17:135-143.
- Norby, K. 1996. Interleukin-8 and de novo mammalian angiogenesis. *Cell Prolif.* 29:315-323.
- Smith, D.R., P.J. Polverini, S.L. Kunkel, M.B. Orringer, R.I. Whyte, M.D. Burdick, C.A. Wilke, and R.M. Strieter. 1994. Inhibition of interleukin 8 attenuates angiogenesis in bronchogenic carcinoma. *J. Exp. Med.* 179:1409-1415.
- Singh, R.K., M. Gutman, R. Radinsky, C.D. Bucana, and I.J. Fidler. 1994. Expression of interleukin 8 correlates with the metastatic potential of human melanoma cells in nude mice. *Cancer Res.* 54:3242-3247.
- Premack, B.A., and T.J. Schall. 1996. Chemokine receptors: gateways to inflammation and infection. *Nat. Med.* 2:1174-1178.
- Horuk, R., A. Martin, J. Hesselgesser, T. Hadley, Z.H. Lu, Z.X. Wang, and S.C. Peiper. 1996. The Duffy antigen receptor for chemokines: structural analysis and expression in the brain. *J. Leukocyte Biol.* 59:29-38.
- Van Meir, E.G., Y. Sawamura, A.-C. Diserens, M.-F. Hamou, and N. de Tribolet. 1990. Human glioblastoma cells release interleukin 6 in vivo and in vitro. *Cancer Res.* 50:6683-6688.
- Sticherling, M., J.M. Schroder, and E. Christophers. 1989. Production and characterization of monoclonal antibodies against the novel neutrophil activating peptide NAP/IL-8. *J. Immunol.* 143:1628-1634.
- Chaudhuri, A., S. Nielsen, M.-L. Elkjaer, V. Zbrzezna, F. Fang, and A.O. Pogo. 1997. Detection of duffy antigen in the plasma membranes and caveolae of vascular endothelial and epithelial cells of nonerythroid organs. *Blood.* 89:701-712.

33. Holmes, W.E., J. Lee, W.J. Kuang, G.C. Rice, and W.I. Wood. 1991. Structure and functional expression of a human interleukin-8 receptor. *Science (Wash. DC)*. 253:1278-1280.
34. Murphy, P.M., and H.L. Tiffany. 1991. Cloning of complementary DNA encoding a functional human interleukin-8 receptor. *Science (Wash. DC)*. 253:1280-1283.
35. Mueller-Klieser, W.F., and R.M. Sutherland. 1982. Oxygen tensions in multicell spheroids of two cell lines. *Br. J. Cancer*. 45:256-264.
36. Shweiki, D., M. Neeman, A. Itin, and E. Keshet. 1995. Induction of vascular endothelial growth factor expression by hypoxia and by glucose deficiency in multicell spheroids: implications for tumor angiogenesis. *Proc. Natl. Acad. Sci. USA*. 92:768-772.
37. Van Meir, E.G., T. Kikuchi, M. Tada, H. Li, A.C. Diserens, B.E. Wojcik, H.-J.S. Huang, T. Friedmann, N. de Tribolet, and W.K. Cavenee. 1994. Analysis of the p53 gene and its expression in human glioblastoma cells. *Cancer Res.* 54:649-652.
38. Graeber, T.G., C. Osmanian, T. Jacks, D.E. Housman, C.J. Koch, S.W. Lowe, and A.J. Giaccia. 1996. Hypoxia-mediated selection of cells with diminished apoptotic potential in solid tumours. *Nature (Lond.)*. 379:88-91.
39. Kern, S.E., K.W. Kinzler, A. Bruskin, D. Jarosz, P. Friedman, C. Prives, and B. Vogelstein. 1991. Identification of p53 as a sequence-specific DNA-binding protein. *Science (Wash. DC)*. 252:1708-1711.
40. Mercer, W.E., M.T. Shields, M. Amin, G.J. Sauve, E. Appella, J.W. Romano, and S.J. Ullrich. 1990. Negative growth regulation in a glioblastoma tumor cell line that conditionally expresses human wild-type p53. *Proc. Natl. Acad. Sci. USA*. 87:6166-6170.
41. Plate, K.H., G. Breier, H.A. Weich, and W. Risau. 1992. Vascular endothelial growth factor is a potential tumour angiogenesis factor in human gliomas in vivo. *Nature (Lond.)*. 359:845-848.
42. Shweiki, D., A. Itin, D. Soffer, and E. Keshet. 1992. Vascular endothelial growth factor induced by hypoxia may mediate hypoxia-initiated angiogenesis. *Nature (Lond.)*. 359:843-845.
43. Kim, K.J., B. Li, J. Winer, M. Armanini, N. Gillett, H.S. Phillips, and N. Ferrara. 1993. Inhibition of vascular endothelial growth factor-induced angiogenesis suppresses tumour growth in vivo. *Nature (Lond.)*. 362:841-844.
44. Millauer, B., L.K. Shawver, K.H. Plate, W. Risau, and A. Ullrich. 1994. Glioblastoma growth inhibited in vivo by a dominant-negative Flk-1 mutant. *Nature (Lond.)*. 367:576-579.
45. Cheng, S.Y., H.J.S. Huang, M. Nagane, X.D. Ji, D.G. Wang, C. Shih, W. Arap, C.M. Huang, and W.K. Cavenee. 1996. Suppression of glioblastoma angiogenicity and tumorigenicity by inhibition of endogenous expression of vascular endothelial growth factor. *Proc. Natl. Acad. Sci. USA*. 93:8502-8507.
46. Saleh, M., S.A. Stacker, and A.F. Wilks. 1996. Inhibition of growth of C6 glioma cells in vivo by expression of antisense vascular endothelial growth factor sequence. *Cancer Res.* 56:393-401.
47. Van Meir, E.G., P.J. Polverini, V.R. Chazin, H.-J.S. Huang, N. de Tribolet, and W.K. Cavenee. 1994. Release of an inhibitor of angiogenesis upon induction of wild type p53 expression in glioblastoma cells. *Nat. Genet.* 8:171-176.
48. Pepper, M.S., S.J. Mandriota, J.-D. Vassalli, L. Orci, and R. Montesano. 1996. Angiogenesis-regulating cytokines: activities and interactions. In *Current Topics in Microbiology and Immunology*. U. Günthert and W. Birchmeier, editors. Springer-Verlag, Berlin. 31-67.
49. Van Meir, E.G., 1995. Cytokines and tumors of the central nervous system. *Glia*. 15:264-288.
50. Karakurum, M., R. Shreenivas, J. Chen, D. Pinsky, S.D. Yan, M. Anderson, K. Sunouchi, J. Major, T. Hamilton, K. Kuwabara et al. 1994. Hypoxic induction of interleukin-8 gene expression in human endothelial cells. *J. Clin. Invest.* 93:1564-1570.
51. Metinko, A.P., S.L. Kunkel, T.J. Standiford, and R.M. Strieter. 1992. Anoxia-hyperoxia induces monocyte-derived interleukin-8. *J. Clin. Invest.* 90:791-798.
52. Peiper, S.C., Z.X. Wang, K. Neote, A.W. Martin, H.J. Showell, M.J. Conklyn, K. Osborne, T.J. Hadley, Z.H. Lu, J. Hesselgesser, and R. Horuk. 1995. The Duffy antigen/receptor for chemokines (DARC) is expressed in endothelial cells of Duffy negative individuals who lack the erythrocyte receptor. *J. Exp. Med.* 181:1311-1317.
53. Wakabayashi, Y., T. Shono, M. Isono, S. Hori, K. Matsushima, M. Ono, and M. Kuwano. 1995. Dual pathways of tubular morphogenesis of vascular endothelial cells by human glioma cells: vascular endothelial growth factor/basic fibroblast growth factor and interleukin-8. *Jpn. J. Cancer Res.* 86:1189-1197.
54. Hadley, T.J., Z.H. Lu, K. Wasniewska, A.W. Martin, S.C. Peiper, J. Hesselgesser, and R. Horuk. 1994. Postcapillary venule endothelial cells in kidney express a multispecific chemokine receptor that is structurally and functionally identical to the erythroid isoform, which is the Duffy blood group antigen. *J. Clin. Invest.* 94:985-991.
55. Tournamille, C., Y. Colin, J.P. Cartron, and C. Le Van Kim. 1995. Disruption of a GATA motif in the Duffy gene promoter abolishes erythroid gene expression in Duffy-negative individuals. *Nat. Genet.* 10:224-228.
56. Rot, A., E. Hub, J. Middleton, F. Pons, C. Rabeck, K. Thierer, J. Wintle, B. Wolff, M. Zsak, and P. Dukor. 1996. Some aspects of IL-8 pathophysiology. III: Chemokine interaction with endothelial cells. *J. Leukocyte Biol.* 59:39-44.
57. Schonbeck, U., E. Brandt, F. Petersen, H.-D. Flad, and H. Loppnow. 1995. IL-8 specifically binds to endothelial but not to smooth muscle cells. *J. Immunol.* 154:2375-2383.
58. Strieter, R.M., P.J. Polverini, S.L. Kunkel, D.A. Arenberg, M.D. Burdick, J. Kasper, J. Dzubba, J. Van Damme, A. Walz, D. Marriott et al. 1995. The functional role of the ELR motif in CXC chemokine-mediated angiogenesis. *J. Biol. Chem.* 270:27348-27357.
59. Brogi, E., T. Wu, A. Namiki, and J.M. Isner. 1994. Indirect angiogenic cytokines upregulate VEGF and bFGF gene expression in vascular smooth muscle cells, whereas hypoxia upregulates VEGF expression only. *Circulation*. 90:649-652.
60. Ryuto, M., M. Ono, H. Izumi, S. Yoshida, H.A. Weich, K. Kohno, and M. Kuwano. 1996. Induction of vascular endothelial growth factor by tumor necrosis factor α in human glioma cells. Possible roles of SP-1. *J. Biol. Chem.* 271:28220-28228.
61. Takeshima, H., J. Kuratsu, M. Takeya, T. Yoshimura, and Y. Ushio. 1994. Expression and localization of messenger RNA and protein for monocyte chemoattractant protein-1 in human malignant glioma. *J. Neurosurg.* 80:1056-1062.
62. Moynagh, P.N., D.C. Williams, and L.A. O'Neill. 1994. Activation of NF- κ B and induction of vascular cell adhesion molecule-1 and intracellular adhesion molecule-1 expression

- in human glial cells by IL-1. Modulation by antioxidants. *J. Immunol.* 153:2681-2690.
63. Liles, W.C., P.A. Kiener, J.A. Ledbetter, A. Aruffo, and S.J. Klebanoff. 1996. Differential expression of Fas (CD95) and Fas ligand on normal human phagocytes: implications for the regulation of apoptosis in neutrophils. *J. Exp. Med.* 184:429-440.
 64. Saas, P., P.R. Walker, M. Hahne, A.-L. Quiquerez, V. Schnuriger, G. Perrin, L. French, E.G. Van Meir, N. de Tribolet, J. Tschopp, and P.-Y. Dietrich. 1997. Fas ligand expression by astrocytoma in vivo: maintaining immune privilege in the brain? *J. Clin. Invest.* 99:1173-1178.
 65. Gratas, C., Y. Tohma, E.G. Van Meir, M. Klein, M. Tenan, N. Ishii, O. Tachibana, P. Kleihues, and H. Ohgaki. 1997. Fas ligand expression in glioblastoma cell lines and primary astrocytic brain tumors. *Brain Pathol.* 7:863-869.
 66. Sabroe, I., T.J. Williams, C.A. Hebert, and P.D. Collins. 1997. Chemoattractant cross-desensitization of the human neutrophil IL-8 receptor involves receptor internalization and differential receptor subtype regulation. *J. Immunol.* 158: 1361-1369.
 67. Simonet, W.S., T.M. Hughes, H.Q. Nguyen, L.D. Trebasky, D.M. Danilenko, and E.S. Medlock. 1994. Long-term impaired neutrophil migration in mice overexpressing human interleukin-8. *J. Clin. Invest.* 94:1310-1319.
 68. Kanayama, N., Y. Kajiwar, J. Goto, E. el Maradny, K. Maehara, K. Andou, and T. Terao. 1995. Inactivation of interleukin-8 by aminopeptidase N (CD13). *J. Leukocyte Biol.* 57: 129-134.

CHEMOKINES INDUCE MIGRATIONAL RESPONSES IN HUMAN BREAST CARCINOMA CELL LINES

Sara J. YOUNGS¹*, Selman A. ALI², Dennis D. TAUB³ and Robert C. REES²

¹Institute for Cancer Studies, University of Sheffield Medical School, Sheffield, UK

²Department of Life Sciences, Nottingham Trent University, Nottingham, UK

³Clinical Services Program, NCI-FCRDC, Frederick, MD

Chemokines have been shown to chemoattract and activate different leukocyte populations. Here we report the *in vitro* effect of macrophage inflammatory protein (MIP)-1 α , MIP-1 β , regulated on activation, normal T-cells, expressed and secreted (RANTES), monocyte chemoattractant protein-1 (MCP-1), interleukin-8 (IL-8), interferon inducible protein-10 (IP-10), neutrophil-activating peptide-2 (NAP-2), growth-related protein (GRO)- α and GRO- γ , on the migration of 3 human breast carcinoma cell lines, MCF-7, T47D and ZR-75-1, using a microchemotaxis chamber to assess migration across fibronectin-coated polycarbonate membranes. MCF-7 cells responded chemotactically to all chemokines tested in a pattern which was dose and time dependent, although responses to the different chemokines were variable. ZR-75-1 responded to MIP-1 β and GRO- α , giving maximum migration indices of 3.7 and 5.3, respectively, and exhibited a migratory response to MIP-1 α , IL-8 and MCP-1 although to a lower degree. T47D was unresponsive to the chemokines tested, but both MCF-7 and T47D cells bound radiolabelled ligands with binding constants (Kd) ranging from 0.6 to 2.2 nM and 0.6 to 2.1 nM, respectively. The specificity of the chemotactic response of MCF-7 to MIP-1 α and MIP-1 β was confirmed using chemokine-specific neutralising antibodies and heat denaturation, and was demonstrated to involve G protein and cyclic AMP signalling pathways. MIP-1 β and MIP-1 α were shown to induce changes in the organisation of the actin cytoskeleton and the level of F-actin in MCF-7 cells, as determined using flow cytometric analysis and confocal microscopy. Our results show that breast carcinoma cells can respond to chemokines, and suggests a potential role for these molecules in the process of tumour cell migration, invasion and metastasis. *Int. J. Cancer* 71:257-266, 1997.
© 1997 Wiley-Liss, Inc.

Chemokines are an ever expanding family of proinflammatory cytokines with more than 20 recognised family members, the majority showing between 20 and 80% homology in their amino acid sequences and possessing a conserved 4 cysteine residues motif (Baggiolini *et al.*, 1994). The separation into the α and β subfamilies is based on 2 criteria: the presence or the absence, respectively, of an intervening amino acid residue located between the first 2 of the 4 conserved cysteines, and the clustering of genes encoding the α and β chemokines to human chromosomes 4 and 17, respectively. Murine lymphotactin (Kerner *et al.*, 1994) and the human homologue SCM-1 (Yoshida *et al.*, 1995) contain only 2 of the 4 conserved cysteines found in the other family members and constitute a distant third subfamily (the C or γ type subfamily).

All chemokine family members have been shown to induce the directional migration of particular inflammatory cell types, including granulocytes, monocytes and lymphocytes (Baggiolini *et al.*, 1994). These proteins have also been shown to be active over a wide concentration range and are produced by a variety of cell types in response to primary proinflammatory mediators such as IL-1, tumour necrosis factor- α and endotoxins. Unlike the classical leukocyte chemoattractants (*e.g.*, C5a and leukotriene B₄) which show little specificity of responder cells, chemokines induce cell-specific recruitment to sites of production (Baggiolini *et al.*, 1994). Many of the α chemokines have been shown to induce neutrophil migration and activation predominantly, while having little or no effect on monocytes and macrophages. However, several α subfamily members have been shown to act on T-cells,

melanocytes, smooth muscle cells and keratinocytes (Baggiolini *et al.*, 1994). In contrast, β chemokines are for the most part inactive on neutrophils but chemoattract and activate monocytes, macrophages, T- and B-lymphocytes and NK cells, as well as eosinophils and basophils (Baggiolini *et al.*, 1994).

The molecular basis of tumour cell invasion and migration at primary or secondary sites *in vivo* is not fully understood, although response to external stimulants is believed to influence the process of cell motility (Helman and Thiele, 1991). Alteration in cell-cell adhesion and the secretion and activation of proteolytic enzymes (Helman and Thiele, 1991) are believed to be essential for optimal tumour cell invasion through and across the extracellular barriers, and the interaction with chemotactic factors may represent a critical step in this process (Helman and Thiele, 1991). While it is clear that several chemokines regulate leukocyte motility and recruitment into inflamed tissue, the spectrum of action of individual chemokine members on tumour cell behaviour remains to be defined. Wang *et al.* (1990) reported that IL-8 induces the haptotactic migration of A2058 human melanoma cells *in vitro* while other groups have alluded to the influence of chemokines on tumour cell proliferation (Lanig *et al.*, 1994) and tumour angiogenesis (Strieter *et al.*, 1995), as well as the production of chemokines by tumour cells (Negus *et al.*, 1995). In particular, the production of a broad range of chemokines by invasive tumour cells has been the basis of a model of passive counter current invasion (Opdenakker and van Damme, 1992a,b). In this model human cell-derived chemokines attract and activate leukocytes and these, in turn, degrade the extracellular matrix and indirectly promote tumour cell migration toward blood vessels (Opdenakker and van Damme, 1992a,b). The results of the present study demonstrate that a broad range of chemokines, but especially those belonging to the β chemokine subfamily induce the migration of breast cancer cell lines *in vitro*. These data infer a potential role for chemokines as co-factors involved in tumour cell motility/migration, possibly representing a rate-limiting step in the metastatic cascade.

MATERIAL AND METHODS

Cells

MCF-7, T47D and ZR-75-1 human breast carcinoma cell lines were used. The MCF-7 cell line was isolated from a pleural effusion of a 69-year-old female patient with metastatic mammary carcinoma (Soule *et al.*, 1973); it retains a number of properties

Abbreviations: CTX, cholera toxin; GRO, growth-related peptide; IL, interleukin; IP-10, interferon inducible protein-10; MCP-1, monocyte chemoattractant protein-1; MIP-1, macrophage inflammatory protein-1; NAP-2, neutrophil-activating peptide-2; NK, natural killer; PTx, pertussis toxin; RANTES, regulated on activation, normal T-cells, expressed and secreted.

Contract grant sponsor: Yorkshire Cancer Research Campaign.

*Correspondence to: the Institute for Cancer Studies, University of Sheffield Medical School, Beech Hill Road, Sheffield S10 2RX, U.K. Fax: 0114 2713515.

Received 20 August 1996; revised 4 November 1996

expressed by breast epithelium *in vivo*, e.g., the cytoplasmic estrogen receptor and the capacity of forming domes. The T47D cell line was derived from the pleural effusion of a 54-year-old patient with disseminated carcinoma of the breast (Keydar *et al.*, 1978), and ZR-75-1 was derived from a malignant ascitic effusion in a 63-year-old woman (Engel *et al.*, 1978). These lines are well-differentiated epithelial cell lines, and all contain 4 classes of hormone receptor (Sommers *et al.*, 1994). All cell lines were cultured in Dulbecco's modified Eagle's medium (Life Technologies, Paisley, UK), supplemented with 10% FCS (Life Technologies) at 37°C in a 5% CO₂ and 95% air humidified atmosphere.

The chemokines used in the study were human recombinant forms obtained from Preprotech (Rocky Hills, MD) and R&D Systems (Minneapolis, MN).

Cell migration assay

Tumour cells were assessed for migratory ability using a 48-well microchemotaxis chamber (Neuroprobe, Cabin John, MD). The chemoattractant (serum or chemokine) was added to the lower wells, overlaid with a fibronectin (Sigma, Poole, UK) coated 8 µm pore polyvinylpyrrolidone-coated polycarbonate membrane (Neuroprobe). Membranes were coated with fibronectin for 2 hr at 37°C using a concentration of 6.5 µg/ml; 50 µl of a cell suspension containing 3×10^5 cells/ml were added to each of the upper wells and the chamber incubated for 5 hr at 37°C in a humidified atmosphere of 5% CO₂. The non-migrated cells were removed from the upper surface of the membrane by gently wiping the surface and the cells attached to the lower surface of the membrane, fixed with methanol (BDH, Lutterworth, UK), stained with Harris' haematoxylin (Life Technologies) and then counted using light microscopy.

To determine the specificity of the response to the chemokines, neutralising anti-MIP-1α and -MIP-1β antibodies (50 µg/ml) (R&D Systems) were used; antibodies were mixed with the chemokines just prior to use in the assay. Heat denaturation studies were also performed by incubating MIP-1α and MIP-1β in a boiling water bath for 30 min before addition to the lower wells of the chemotaxis chamber (data not shown).

To distinguish chemotaxis from chemokinesis, a checkerboard assay (in which varying concentrations of chemokine are added to the upper well only, the lower well only or both the upper and lower wells) was used. If cell movement was present only in the presence of a concentration gradient, this migration was considered to be chemotaxis.

Pertussis and cholera toxin treatment

Prior to assessment of tumour cell migration, cells were treated with various concentrations of PTx or CTx (0.1–1,000 ng/ml) (Sigma) for 90 min at 37°C. Cells were then washed twice with serum-free media, re-suspended at 3×10^5 cells/ml and then placed in the upper wells of the chemotactic chamber. The effect of PTx on MIP-1α-, MIP-1β- and RANTES- induced migration, as well as CTx on MIP-1α- and MIP-1β- induced migration, was assessed.

Chemokine binding assays

Binding conditions for MIP-1α, MIP-1β, RANTES, MCP-1 and IL-8 were carried out as previously described (Wang *et al.*, 1993). Chemokine binding was carried out as follows: 2×10^6 cells, cultured overnight in serum-free medium to synchronize the tumour cell populations, were incubated in duplicate with increasing concentrations of ¹²⁵I-labeled chemokines in a modified binding medium (RPMI 1640 containing 1 mg/ml of BSA, 25 mM HEPES and 0.05% sodium azide, pH 7.4) in a total volume of 200 µl. The residual non-specific binding was determined by parallel incubation of ¹²⁵I-labeled chemokine in the presence of 100-fold excess of unlabeled ("cold") chemokine. After incubation at 4°C for 90 min, the cells were pelleted through a 10% sucrose/PBS cushion. The tips of the tubes containing cells were cut, and radioactivity was determined on a gamma counter. The residual non-specific bound radioactivity associated with cells in the

presence of unlabeled chemokine was subtracted from the total bound radioactivity to yield specific binding. The data were analyzed using the Biosoft (Edinburgh, UK) RADLIG program. The displacement curves for ¹²⁵I-chemokines to MCF-7 and T47D cells were generated by incubating these tumour cells with a constant concentration of radiolabeled chemokine for 2 hr at 4°C in the presence of increasing concentrations of unlabeled ligands. The cells were then pelleted through a sucrose cushion and the radioactivity associated with cell pellets determined (data not shown).

Actin polymerisation assays

Assessment by confocal microscopy. Cells were seeded on fibronectin-coated glass coverslips in 6-well tissue culture plates for 30 min and then incubated with MIP-1β (1 ng/ml) or with 0.01% BSA (Sigma) for 5, 15, 30 and 45 min at 37°C in a humidified atmosphere of 5% CO₂. Cells were then washed with PBS and fixed with 3% paraformaldehyde (BDH) for 20 min at room temperature (RT). The coverslips were then placed in acetone (BDH) for 5 min at -20°C and then washed with PBS 3×. Cells were then incubated in TRITC-labelled phalloidin (200 ng/ml) (Sigma) for 45 min at RT. Cells were washed with PBS and distilled water 3× and the coverslips mounted using glycerol/PBS (1:1). Cells were visualised using a confocal microscope.

Assessment by flow cytometry. Cells were prepared for flow cytometric analysis to quantitate the changes in staining with FITC-labelled phalloidin (a specific F-actin label) (Sigma), following treatment of cells with the chemokines MIP-1α and MIP-1β (1 ng/ml). Cells were seeded in 6-well plates for 24 hr and then placed in serum-free Dulbecco's modified Eagle's medium for 48 hr to synchronise the cell population prior to harvesting. Cells were then counted (using the Trypan blue exclusion) and re-suspended at 1×10^6 cells/ml. Cells were treated with chemokine (1 ng/ml), after which 250 µl of the sample were removed mixed with 250 µl of lysis fixative solution (6% paraformaldehyde containing 200 µg/ml lysophosphatidylcholine [Sigma] and 1.5 µg/ml FITC-labelled phalloidin) and incubated for 20 min at RT. Samples were then analysed by flow cytometric analysis using a Becton Dickinson (Oxford, UK) FACS Vantage.

Data analysis

Significant values were calculated using Students *t* test. Results are expressed as either mean number of cells migrating per 3 wells in 5 microscopic fields or as migration index (MI).

$$MI = \frac{\text{number of cells migrating to test}}{\text{number of cells migrating to negative control}}$$

RESULTS

The chemotactic response of MCF-7, T47D and ZR-75-1 breast carcinoma cells to α and β chemokines

The chemotactic response of MCF-7 cells to α and β chemokines was assessed using a microchemotaxis chamber after incubation for 5 hr at 37°C. Time course experiments determined that a 5 hr incubation was optimal for MCF-7 migration; previous studies have reported that tumour cells require a longer incubation period than leukocyte populations (Yabkowitz *et al.*, 1993). Although significant migration of MCF-7 cells was observed with the α and β chemokines tested (Fig. 1a,b), the β chemokines elicited a greater chemotactic response than many of the α chemokines. MIP-1α (in 5 of 6 experiments), MIP-1β (in 5 of 6 experiments) and RANTES (in 6 of 6 experiments) induced significant ($p < 0.05$) migration of MCF-7 cells, with mean migration indices of 7.4 ± 2.5 , 5.8 ± 2.8 and 8.3 ± 2.8 for MIP-1α, MIP-1β and RANTES, respectively ($n = 4$) (Fig. 1a). MCP-1 induced significant migration of MCF-7 cells in 3 of 4 experiments, with a mean MI of 4.5, with maximal migration observed with a concentration of 100 ng/ml. In contrast, MIP-1α and MIP-1β induced optimal migration at 1 ng/ml and RANTES at 10 ng/ml (Fig. 1a).

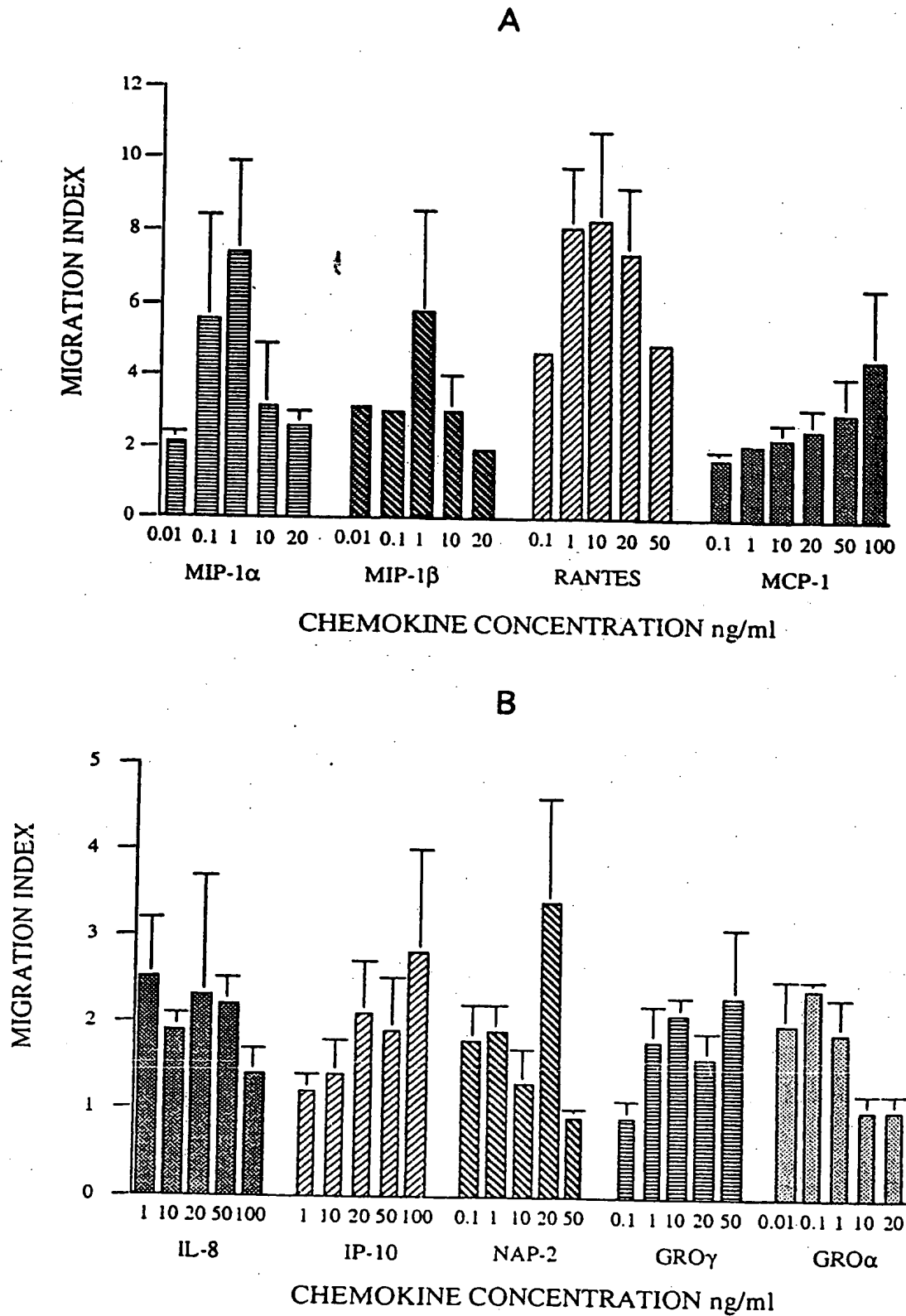


FIGURE 1. - (a and b) Migration responses of MCF-7 cells to α and β chemokines. Migration assays to assess the ability of the α and β chemokines to induce MCF-7 cells to migrate were performed using a modified Boyden chamber assay (see Material and Methods). Chemokine was added to the lower chamber and $50 \mu\text{l}$ of 3×10^5 cells/ml were added to the upper wells of a 48-well microchemotaxis chamber and migration across a fibronectin-coated polycarbonate membrane ($8 \mu\text{m}$ pore size) assessed after 5 hr. The numbers of migrated cells in 5 high power microscopic fields were counted in triplicate wells. Data are expressed as the mean migration index (see Material and Methods) from four experiments.

The α chemokines IL-8, IP-10, NAP-2, GRO- α and GRO- γ also induced significant migration of MCF-7 cells ($p < 0.05$) in more than 50% of the chemotaxis experiments (Fig. 1b). However, the response was less frequently observed and generally gave a lower MI with MCF-7 cells compared with the β chemokines (Fig. 1). The optimal concentration of chemokine required for migration varied with the individual chemokine (range of 1–100 ng/ml) as seen with the β chemokines. IL-8 elicited a mean migration index of 2.5 ± 0.7 at a concentration of 50 ng/ml ($n = 4$), while NAP-2, GRO- α , GRO- γ and IP-10 achieved mean MIs of 3.4, 2.4, 2.3 and 2.8, respectively with varying concentrations depending on the chemokine ($n = 4$) (Fig. 1). Figure 2 shows MCF-7 cell migration to MIP-1 α , compared with the background migration observed using 0.1% BSA which is used in the storage of the chemokines and in diluent solutions and here as a negative control. BSA at concentrations ranging from 0.001 to 0.5% induced similar low levels of migration.

The responses of MCF-7 cells to the α and β chemokines were compared with those of 2 other breast carcinoma cell lines, ZR-75-1 and T47D. ZR-75-1 exhibited a migratory response toward MIP-1 α , MIP-1 β , IL-8, MCP-1 and GRO- α . The mean MIs achieved were 3.1 (range, 2.6–3.7) for MIP-1 β and 3.6 (range, 2.2–5.1) for GRO- α . The response to MIP-1 α , IL-8 and MCP-1 were of a lower order, giving an MI of between 2 and 3 (Table I). In contrast, the breast cancer line cells T47D did not migrate in response to any of the chemokines tested (Table I). Breast carcinoma cells of similar origin may therefore show distinct migratory patterns to specific chemokines.

Chemotaxis vs. chemokinesis of MCF-7 cells to MIP-1 α and MIP-1 β

To discriminate between random motility (chemokinesis) and concentration-dependent cell migration (chemotaxis) to the chemokines (MIP-1 α and MIP-1 β), checkerboard analysis was performed, by adding chemokine to either the upper or lower chamber or to both chambers of the chemotaxis plate ($n = 3$), using a

TABLE I - SUMMARY OF MCF-7, T47D AND ZR-75-1 BREAST CARCINOMA CELL MIGRATION TO α AND β CHEMOKINES¹

Chemokine	Chemotactic response of cell lines ²		
	MCF-7	T47D	Zr-75-1
MIP-1 α	++	—	+
MIP-1 β	++	—	++
RANTES	++	—	—
MCP-1	++	—	+
IL-8	+	—	+
NAP-2	+	—	—
GRO- α	+	—	++
GRO- γ	+	—	—
IP-10	+	—	—

¹The chemotactic response of MCF-7 cells was compared with that of 2 other breast carcinoma cell lines, T47D and ZR-75-1. ²The following was used to indicate the *in vitro* response of the cells to chemokines: —: no response; +: 2- to 3-fold increase in migration above background; ++: >3-fold increase in migration (above background).

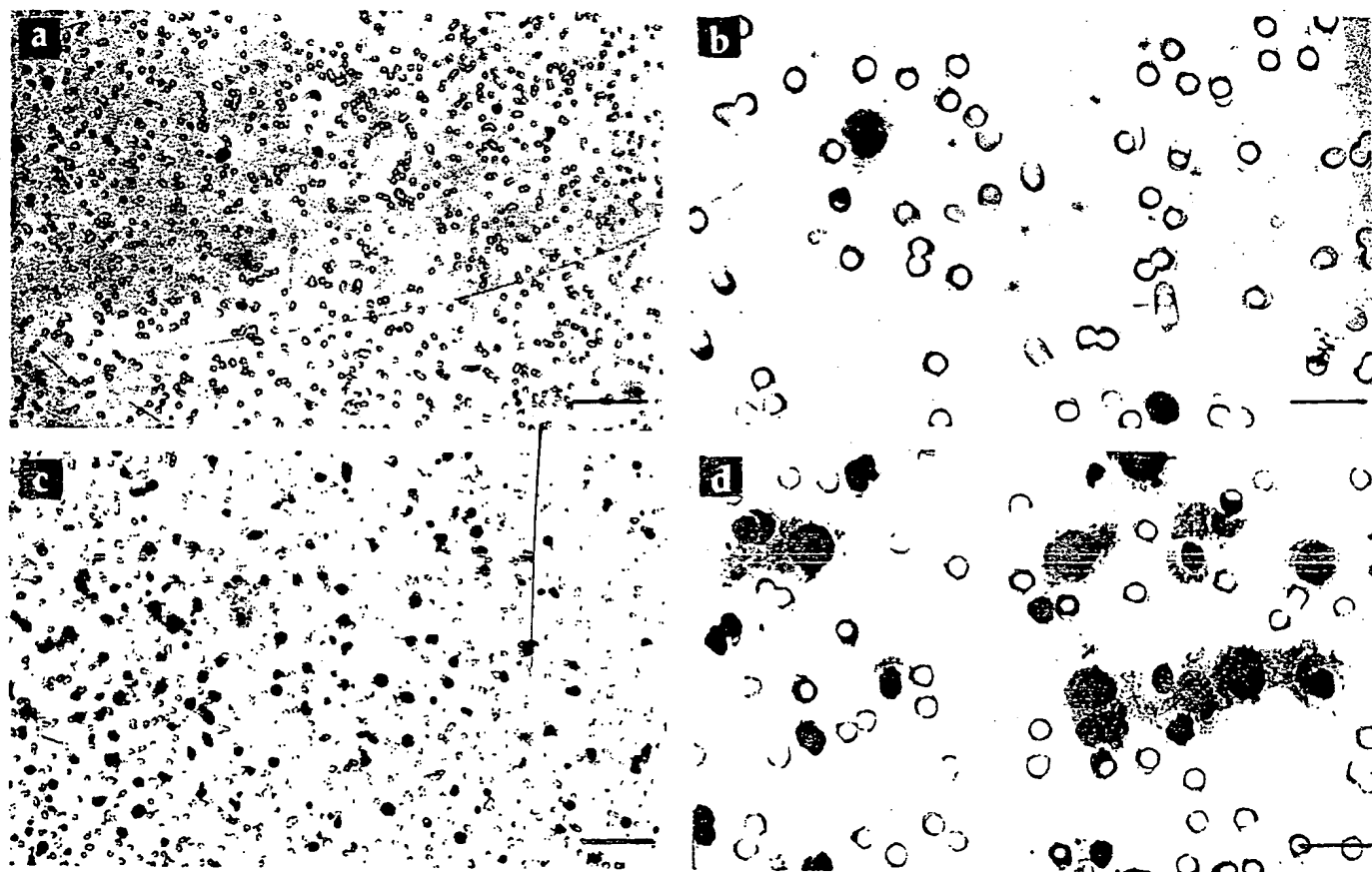


FIGURE 2. - Migration of MCF-7 cells to 0.1% BSA and MIP-1 α . MCF-7 cell migration to 0.1% BSA (a and b) and to MIP-1 α 1 ng/ml (c and d) are shown to illustrate the level of migration induced by MIP-1 α using a 48-well microchemotaxis chamber (see Material and Methods). Similar migration was observed using MIP-1 β , 1 ng/ml and RANTES, 10 ng/ml. Scale bars: a and c: 10 μ m; b and d: 2.5 μ m.

concentration range of 0.01–1 ng/ml. The results shown in Table II (top) demonstrate that MIP-1 α induces MCF-7 migration in a dose- and gradient-dependent manner. The presence of MIP-1 α in both the upper and lower chamber abrogated MCF-7 cell migration, confirming that the majority of the migration of MCF-7 cells to MIP-1 α was chemotaxis and concentration gradient dependent. MIP-1 β -induced MCF-7 cell migration was inhibited when the concentration in the upper well was higher than in the lower well, but not when both wells contained a similar MIP-1 β concentration (Table II (bottom)). These experiments show that chemokine migratory responses rely in part on the presence of a concentration gradient, although this may not always be the case.

Specificity of chemokine-induced MCF-7 cell migration

The specificity of MIP-1 α - and MIP-1 β -induced MCF-7 cell migration was investigated using neutralising concentrations of affinity-purified anti-MIP-1 α and -MIP-1 β antibody to inhibit the response. MIP-1 α and MIP-1 β (0.1–10 ng/ml) and polyclonal antibody to MIP-1 α and MIP-1 β (50 μ g/ml) were mixed prior to addition to the wells of the lower chamber. The results (Figure 3) demonstrate that MCF-7 cell migration was significantly inhibited toward all concentrations of MIP-1 β in the presence of anti-MIP-1 β antibody. Similar results were observed with MIP-1 α (data not shown). The presence of a control antibody did not inhibit the chemotactic response to either MIP-1 α or MIP-1 β . These results provide additional evidence that MIP-1 α - and MIP-1 β -induced migration of MCF-7 cells is not random and is chemokine specific. Similarly, inactivation of MIP-1 α and MIP-1 β by boiling for 30 min abrogated their ability to induce MCF-7 cell chemotaxis (data not shown).

PTx and CTx inhibit chemokine-induced MCF-7 cell migration

Previous studies have demonstrated that both PTx and CTx can inhibit chemokine-induced leukocyte migration *in vitro* (Sozzani *et al.*, 1995). Prior to assay for chemotaxis, MCF-7 cells were incubated with either CTx or PTx (concentration range, 0.1–1,000 ng/ml) in serum-free medium for 90 min at 37°C. The cells were washed twice and assayed for chemotaxis toward MIP-1 β and MIP-1 α (1 ng/ml) and RANTES (10 ng/ml). Both PTx and CTx inhibited the MIP-1 α - and MIP-1 β -induced chemotaxis of MCF-7 cells (Fig. 4a,b; $n = 3$). The IC₅₀ (concentration causing a 50% reduction in number of migrating cells) for both toxins was 7 ng/ml for MIP-1 β -induced migration, and 0.3 and 0.1 ng/ml for MIP-1 α -induced migration with PTx and CTx, respectively. PTx was also shown to inhibit RANTES-induced migration of MCF-7 cells with an IC₅₀ of 0.08 ng/ml. Medium-treated control cells responded to MIP-1 α , MIP-1 β and RANTES in all experiments, and background migration to 0.1% BSA was 18 ± 3 cells per 5 high power

fields. PTx and CTx (0.5–1 μ g/ml) were not toxic to MCF-7 cells assessed after a 90 min incubation, using the Trypan blue exclusion test. These results suggest that the response of MCF-7 cells to β chemokines is active utilising receptors which signal both G protein and adenylate cyclase-dependent pathways.

Both MCF-7 and T47D cells express α and β chemokine binding sites on their cell surface

Ligand binding studies were used to demonstrate chemokine binding to tumour cell surface receptors, and Scatchard analysis was performed on the results to assess receptor affinity and numbers. The results (Table III) for MCF-7 demonstrate the presence of significant numbers of high-affinity (K_d between 0.6 and 2.2 nM) specific binding sites for MIP-1 α , MIP-1 β , RANTES, MCP-1 and IL-8. In agreement with the chemotaxis results, MCF-7 cells appear to express higher levels of MIP-1 β -specific binding sites (number per cell = 1,843–2,232), and in addition similar numbers of IL-8 binding sites (1,894–2,250, $K_d = 1.8$ –2.2 nM), although the chemotactic response to IL-8 is weaker than that to MIP-1 β . Through displacement analysis, this IL-8 receptor appears to be the promiscuous receptor type B as [¹²⁵I]-IL-8 binding can be completely displaced by GRO- α and NAP-2 (data not shown), both of which induced similar levels of migration as that seen with IL-8.

Similarly, T47D cells also express high levels of high-affinity α and β chemokine-specific binding sites on their cell surface (Table III). However, while this cell line expresses similar levels of chemokine binding sites to that of MCF-7 cells, T47D cells do not migrate in response to the α and β chemokines *in vitro*. In addition, both cell lines express similar levels of integrin molecules on their surface, in particular VLA-5, CD18, CD28 and to a lesser extent VLA-4 (data not shown). These results suggest that the expression of chemokine-specific binding sites on the cell surface of a tumour cell does not necessarily predict their ability to migrate.

Effect of MIP-1 α and MIP-1 β on the actin cytoskeleton organisation in MCF-7 cells

The effect of MIP-1 α and MIP-1 β (1 ng/ml) on the F-actin content of MCF-7 cells was investigated using flow cytometry which allowed us to quantitate FITC-labelled phalloidin staining following treatment with each chemokine. The fluorescence intensity of the cytoskeletal staining with FITC-labelled phalloidin may be taken as a measure of the relative content of F-actin. In 4 of 6 experiments, a significant increase in the level of cytoskeletal staining was observed after treatment for 1 min with MIP-1 β (Fig. 5). Figure 5 shows the results of 3 assays in which the level of F-actin expression following MIP-1 β treatment was increased and sustained during the 30 min observation period. However, the time course of this response was variable, and a 4th experiment showed a gradual decline to background expression 20 min following treatment of the cells with MIP-1 β (data not shown). MIP-1 α also increased the F-actin staining in 4 of 5 experiments, but the level of the response was less than that produced by MIP-1 β (data not shown). Studies using confocal microscopy indicate that there is also a redistribution of the F-actin within the cell, after treatment with MIP-1 β for 45 min (Fig. 6a,b). Intense F-actin staining was visible following treatment near the periphery of the cells and in most cases was polarised toward one side of the cell (Fig. 6a,b).

DISCUSSION

Chemokines are a rapidly expanding superfamily of inflammatory cytokines, and their relevance in promoting leukocyte migration to sites of inflammation is becoming increasingly apparent (Baggiolini *et al.*, 1994). Our findings suggest that this family of proteins may also play a prominent role in tumour cell migration which could result in enhanced invasive and metastatic propensity.

TABLE II DIRECTIONAL MIGRATION (CHEMOTAXIS) AND INCREASED MOTILITY (CHEMOKINESIS) OF MCF-7 CELLS TO MIP-1 α AND MIP-1 β

Concentration, upper well (ng/ml)	Concentration in lower well (ng/ml)			
	0	0.01	0.1	1
MIP-1α				
0	12.0 \pm 2.0	21.7 \pm 7.0	10.7 \pm 1.2	50.7 \pm 13.3*
0.01	16.7 \pm 3.2	12.3 \pm 2.1	10.5 \pm 7.8	41.0 \pm 1.7**
0.1	13.3 \pm 2.1	5.7 \pm 1.2	5.3 \pm 2.5	28.0 \pm 21.7
1	8.3 \pm 3.5	17.0 \pm 2.0	11.7 \pm 3.2	20.0 \pm 2.8
MIP-1β				
0	9.5 \pm 0.7	48.0 \pm 7.8**	38.7 \pm 13.6*	49.5 \pm 13.4**
0.01	9.3 \pm 3.4	24.0 \pm 8.5*	17.7 \pm 2.1*	35.0 \pm 5.7**
0.1	10.5 \pm 2.1	10.7 \pm 3.2	43.7 \pm 16.4*	92.3 \pm 28.7**
1	6.0 \pm 3.6	11.0 \pm 2.0	12.5 \pm 4.9	56.3 \pm 8.1**

*Data are expressed as mean number of migrated cells per 5 fields (\pm SD) after 5 hr incubation ($n = 2$).

*Significant ($p < 0.05$) migration of MCF7 cells across the membrane compared with control migration in the absence of chemokine.

**Significant ($p < 0.01$) migration of MCF7 cells across the membrane compared with control migration in the absence of chemokine.

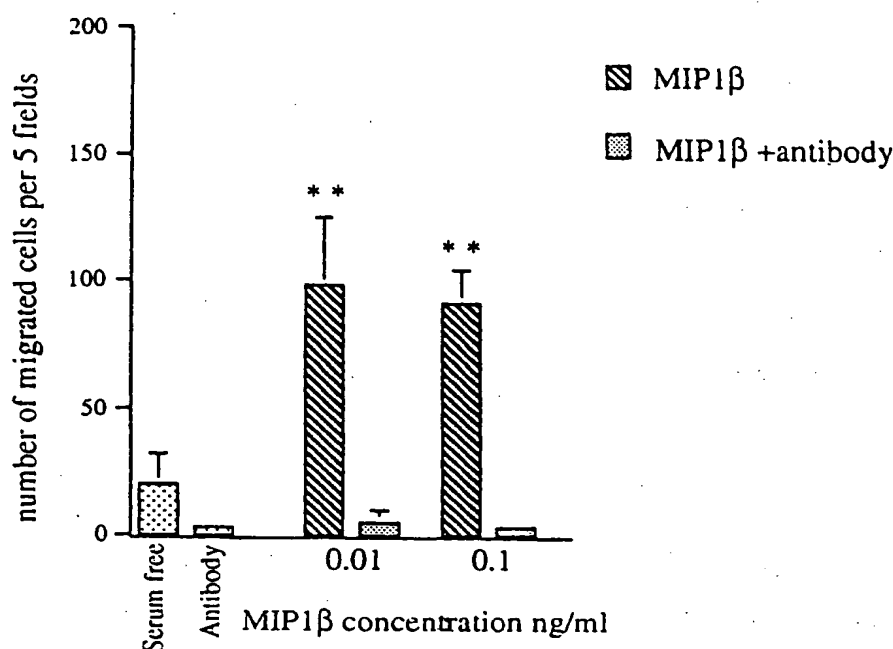


FIGURE 3. – Neutralisation of MIP-1β-induced migration with anti-MIP-1β antibodies. MCF-7 cell migration induced by MIP-1β was assessed in the presence and absence of antibody to MIP-1β. Chemokine (0.01–0.1 ng/ml) and antibody (50 μg/ml) were mixed just prior to addition to the lower wells of the chemotaxis chamber. Data are expressed as the mean number of cells per 5 high power fields for triplicate wells in four experiments (\pm SD). Similar results were obtained with the MIP-1α antibody.

A 48-well chemotaxis chamber was used to study the migratory responses of 3 human breast carcinoma cell lines (across a fibronectin-coated polycarbonate membrane) to α and β chemokines. Fibronectin-coated membranes were used to facilitate the presentation of the chemokines to the tumour cells, since haptotaxis data with MCF-7 cells demonstrates that matrix-bound chemokines are more effective than soluble chemokines (data not shown) and aid in integrin-mediated adhesion and de-adhesion. As chemokines are known to alter the avidity of integrin molecules for their ligands (here fibronectin), adding fibronectin to the assay permits uropod formation and the development of a leading edge.

The MCF-7 cell line was established from a well-differentiated epithelial breast carcinoma and retains many of the properties of normal breast epithelial cells (Soule *et al.*, 1973). This line exhibited a significant chemotactic response to both the α and β chemokines in our current study. MIP-1α, MIP-1β and RANTES were the most potent inducers of MCF-7 cell migration, while MCP-1 and many of the α chemokines elicited a significant but lower chemotactic response. Previous studies using IL-8 and GRO-α were shown to induce the haptotactic migration of human melanoma cells *in vitro* (Wang *et al.*, 1990), but in the present study, a lower order of migration was observed to the α chemokines compared with the responses elicited by the β chemokines. The migratory response of MCF-7 cells to MIP-1α and MIP-1β appeared to be due to chemotaxis, although in some instances with MIP-1β some migration was found to be due to random motility. Migration induced by MIP-1α and MIP-1β was also shown to be chemokine specific using antibody neutralisation analysis and through protein denaturation studies.

By using bacterial toxins we have shown that intoxication with PTx and CTx inhibited the migration of MCF-7 cells in response to MIP-1α, MIP-1β and RANTES. These toxins are known to ADP-ribosylate the α subunits of various G proteins, resulting in modification of these proteins, and it has previously been shown that both these toxins inhibit the chemokine-mediated migratory response of many cell types (Sozzani *et al.*, 1995). These results lead us to conclude that chemokine receptor-mediated cell signal-

ling of MCF-7 cells in response to the β chemokines involves G-proteins and adenylate cyclase-dependent pathways, similar to other cell types (Sozzani *et al.*, 1995).

The chemotactic responses of MCF-7 cells to the α and β chemokines was compared with that of 2 other breast carcinoma cell lines, T47D and ZR-75-1. All 3 of these breast cancer cell lines are similar in that they were all derived from well-differentiated epithelial tumours (determined due to their high expression of catenins and lower expression of vimentin; Sommers *et al.*, 1994) and contain 4 classes of steroid hormone receptor [MCF-7 and ZR-75-1 have been shown to be hormonally responsive (Engel *et al.*, 1978; Soule *et al.*, 1973)]. Their chemotactic responses to the α and β chemokines were varied. T47D cells failed to respond to any of the chemokines tested (with less than 20 cells present per 5 high power fields with any of the chemotactic factors used). ZR-75-1 cells exhibited potent migratory responses to MIP-1β and GRO-α, giving mean MIs of 3.1 and 3.6, respectively. ZR-75-1 cells also exhibited a response to MIP-1α, IL-8 and MCP-1 although showing a lower extent of migration (MI, 2–3), but did not respond to RANTES, IP-10, NAP-2 or GRO-γ. These data demonstrate that cell lines of similar origin can demonstrate distinct migratory patterns to the individual chemokines.

Appreciable numbers of binding sites for the β chemokines and IL-8 were detected on the cell surface of MCF-7 and T47D cells in

FIGURE 4. – (a and b). Chemokine-induced MCF-7 migration is PTx and CTx sensitive. Prior to assessment of migration, MCF-7 cells were treated with various concentrations of either PTx (a) or CTx (b) for 90 min at 37°C. The cells were then washed 3× with PBS and placed in the upper wells of the chemotaxis chamber; migration to MIP-1α, MIP-1β and RANTES was assessed after 5 hr. Background migration was 15 ± 3.5 with both treatments. Data are expressed as the mean number of migrated cells in 5 high power microscopic fields (\pm SD) from a representative experiment. Total number of experiments performed = 3. *, Significant ($p < 0.05$) reduction in MCF-7 cell migration following toxin treatment.

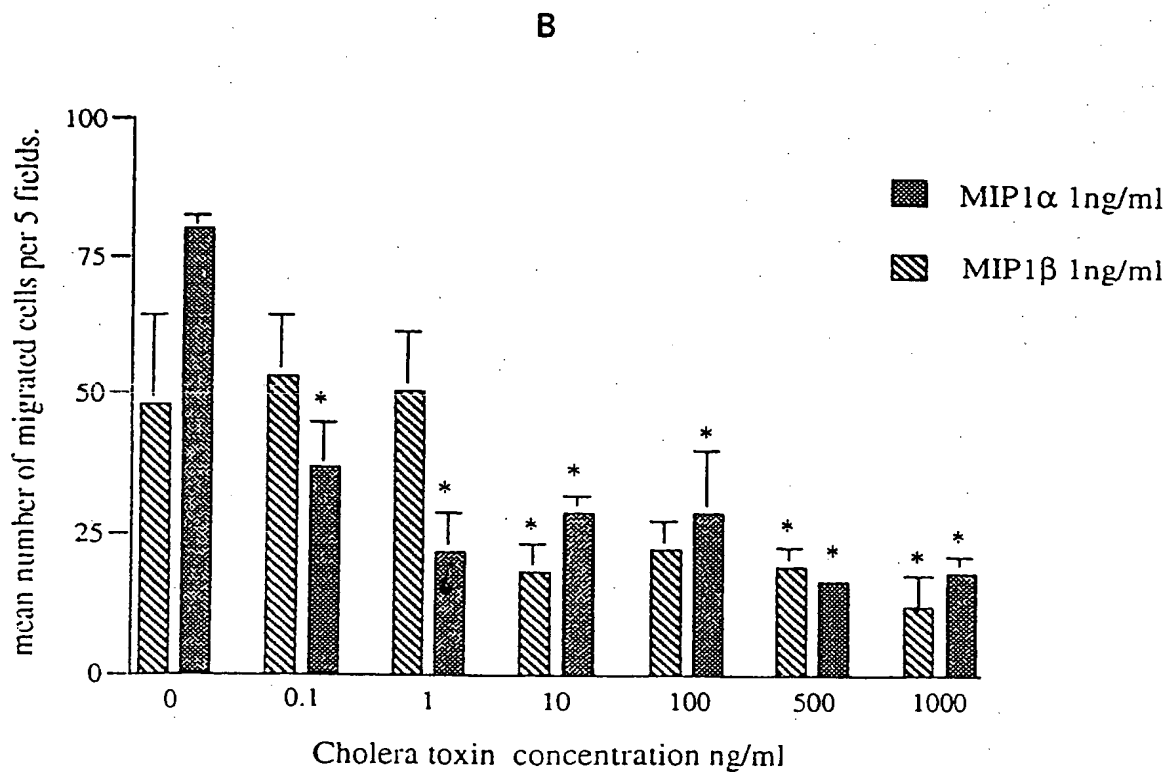
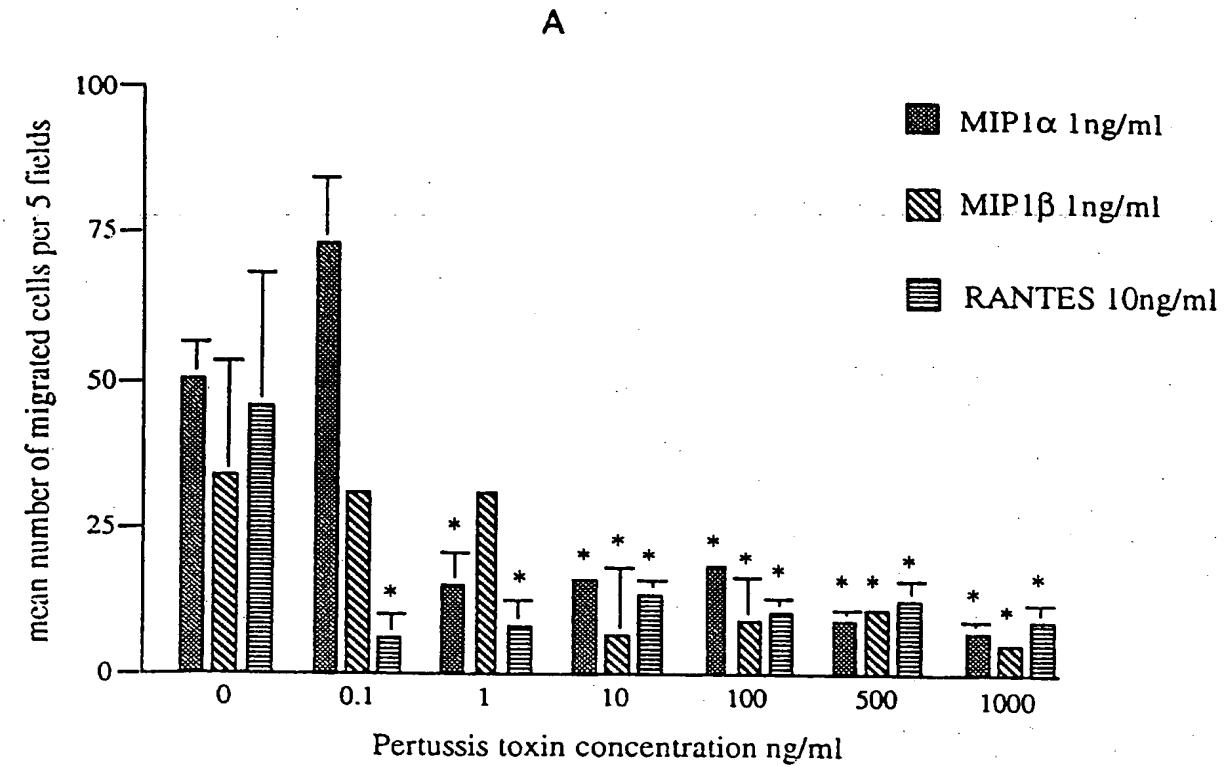


FIGURE 4

TABLE III - SCATCHARD ANALYSIS FOR CHEMOKINE RECEPTOR EXPRESSION BY MCF-7 AND T47D TUMOUR CELLS¹

Tumour cells	Chemokine ²	Binding sites/cell ¹	K _d (nM) ¹	No.
MCF-7	MIP-1 α	645-912	0.8-1.5	3
	MIP-1 β	1,843-2,232	0.6-1.2	3
	RANTES	927-1,215	0.8-1.4	2
	MCP-1	824-1,050	1.2-1.8	2
	IL-8	1,894-2,350	1.8-2.2	3
T47D	MIP-1 α	544-712	0.6-1.2	3
	MIP-1 β	824-1,025	1.1-1.9	3
	RANTES	1,124-1,312	1.7-2.1	3
	MCP-1	1,032-1,436	0.8-1.1	3
	IL-8	2,434-3,235	0.9-2.0	2

¹MCF-7 and T47D cells were grown overnight in serum-free medium prior to performing binding assays to determine receptor density and affinity. ²Various concentrations of chemokines labeled with [¹²⁵I] were incubated at RT in sodium azide for 90 min. Matching replicates contained a 100 \times excess of unlabeled ligands. After incubation, the tumour cells were layered on a 10% sucrose/PBS cushion. The tubes were then centrifuged at RT for 30 sec. Both supernatant (free) and pellets (bound) were collected and counted in a gamma counter. ³The number of binding sites per cell and the K_d values were analysed by non-linear regression calculated using the Biosoft RADLIG program.

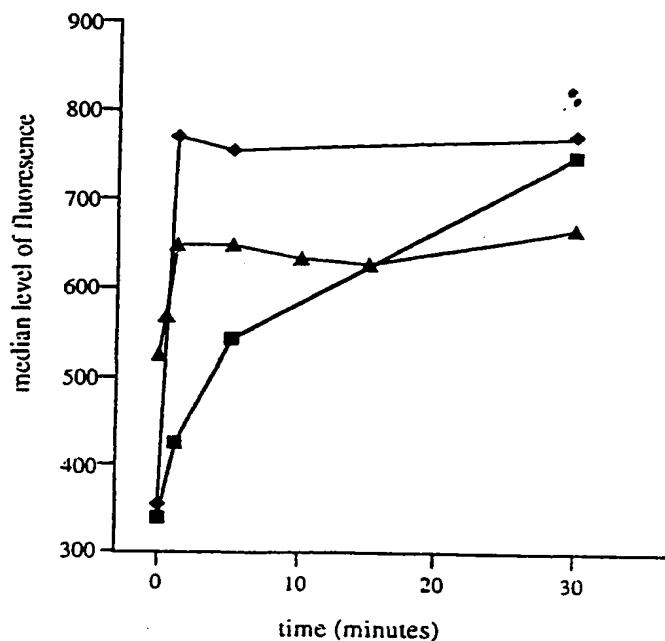


FIGURE 5. - Time course of effect of MIP-1 β on the F-actin content of MCF-7 cells. To determine the MIP-1 β -induced changes in the F-actin content of MCF-7 cells, the cells were stimulated with MIP-1 β (1 ng/ml), after which 250 μ l of the cell suspension was removed and mixed with 250 μ l of lysis fixative solution (see Material and Methods) for 20 min. Staining of samples was assessed by flow cytometric analysis. Data are expressed as the median level of fluorescence as detected by the flow cytometer in three experiments (n = 6); similar results were shown for MIP-1 α -treated MCF-7 cells.

vitro. Human MIP-1 α , MIP-1 β , RANTES, MCP-1 and IL-8 receptors have also been detected on a number of leukocytic cell populations (Sozzani *et al.*, 1995). In the present report we have observed that MCF-7 cells express high levels of MIP-1 α , MIP-1 β , RANTES and MCP-1 binding sites on their cell surface with affinities similar to those described for monocytes (Sozzani *et al.*, 1995). Scatchard analyses (data not shown) using these tumour

cells have demonstrated the presence of only a single class of high-affinity binding sites for each of these chemokines. Approximately 10-15% of the β chemokine binding to MCF-7 cells is blocked by the addition of soluble heparin, and this does not explain most of the binding observed. Surprisingly, the T47D cell line, which does not migrate in response to the chemokines *in vitro*, expresses significant levels of α and β chemokine-binding sites on the cell surface. This failure to migrate in response to the chemokines was found not to be due to differences in expression of integrin molecules since MCF-7 and T47D cells express similar levels of VLA-5, CD18, CD28 and VLA-4 (data not shown). We have observed a similar discrepancy with human NK cells (Taube *et al.*, 1995) which express IL-8 receptors but do not migrate in response to IL-8. These results suggest that chemokine receptor expression by a particular cell population does not necessarily result in migration in response to the chemokine, since the functional status of the receptors will determine if a cell will respond to a given stimulus. The lack of response seen with T47D may be due to the presence of non-functional receptors on the cell surface, which bind the protein but do not trigger any signalling responses. Studies to determine signalling responses in these cells stimulated by the chemokines should clarify this point.

Tumour cell motility is an important step in the intricate process leading to the formation of metastases, and tumour cells demonstrating an increased metastatic potential are more motile than non-metastatic tumour cells or most normal cells (Lester and McCarthy, 1992). Morphological studies of rat sarcoma cells have shown that the structure of the actin network relates to the malignant potential of cell lines and determines their level of motility (Pokorna *et al.*, 1994). In T lymphoma cells (BW5147 cell line), the motility and F-actin content of non-invasive variants have been compared with invasive variants, in which a high level of actin polymerisation is a prerequisite for pseudopod formation and necessary for infiltration of these cells into tissue (Vershueren *et al.*, 1994). Our data show that there is a significant increase in the level of FITC-labelled phalloidin staining of MCF-7 cells after treatment with MIP-1 α and MIP-1 β (1 ng/ml), which is a measure of their relative content of F-actin. An overall increase in F-actin staining was observed in response to the chemokine treatment, representing a recruitment of F-actin to the cell cytoskeleton from a cytoplasmic pool of G-actin rather than a redistribution of cytoskeletal F-actin. Results using confocal microscopy indicate that a redistribution of the cytoskeletal F-actin occurs within 45 min, with movement of F-actin toward the periphery of the cell in a polarised manner. These results indicate that there is a rapid polymerization of F-actin following stimulation with MIP-1 α and MIP-1 β , and a redistribution of the cytoskeletal actin within cells.

Studies have been undertaken to evaluate the potential of chemokines in promoting tumour rejection. Murine tumours engineered to express high levels of MCP-1 show a reduced tumour growth *in vivo* compared with control non-transfected cells (Rollins and Sunday, 1991), although Hirose *et al.* (1995) failed to confirm this finding, and MCP-1 transfection into cells may even lead to an enhanced tumour take. Additionally, MIP-1 α and IL-8 when expressed by tumour cells may suppress tumour growth, while MIP-2 appears to be ineffective (Hirose *et al.*, 1995). Other results also suggest that IL-8 expressed within human tumours may enhance leukocyte recruitment into the tissue and promote angiogenesis (Strieter *et al.*, 1995). The consequences of chemokine production within the tumour environment is unclear and should depend on which chemokines are produced, their concentration and localisation in the tissue, and appropriately expressed receptors. One suggested role of chemokine production within the tumour mass is to activate and attract leukocyte subpopulations into the tumour mass (Opdenakker and van Damme, 1992b). Once there they could contribute to the protease load in the tissue and help the process of cell invasion. To invade out of primary mass, tumour cells must be capable of directional migration; one solution to this

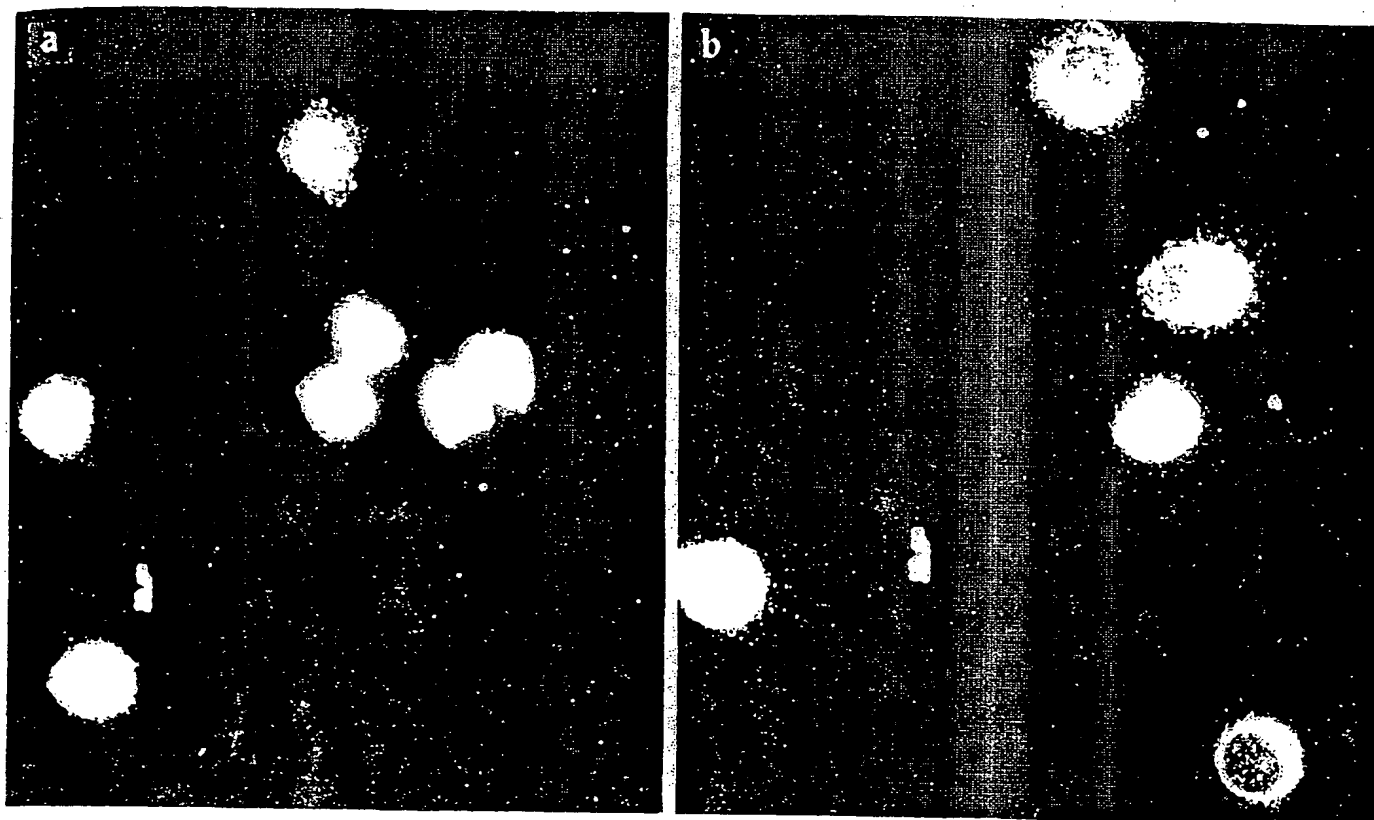


FIGURE 6. – MIP-1 β induces changes in the localisation of F-actin with MCF-7 cells. MCF-7 cells were seeded on glass coverslips, stimulated with MIP-1 β , fixed and then stained with TRITC-labeled phalloidin (a specific F-actin label) for 30 mins. The cells were then washed 2 \times and the coverslips mounted on glass slides using glycerol/PBS (1:1). Cells were visualised using a confocal microscope. Control cells demonstrating nuclear localisation (a) and cells treated with MIP-1 β for 45 min showing redistribution of F-actin to the cytoplasm and polarisation toward a leading edge (b) are shown. These changes were observed in all three tests performed. Scale bar = 10 μ m.

problem is the proposed passive counter current model of invasion and metastasis. This suggests that infiltrating leukocytes create channels in the tissue toward blood or lymph vessels as they migrate; tumour cells can passively move along such channels (Opdenakker and van Damme, 1992a).

Our results indicate that β chemokines can induce migration and cytoskeletal changes in human breast carcinoma cell lines *in vitro* and suggest a potential role for these molecules in the processes of tumour cell migration, invasion and possibly metastasis. A compre-

hensive evaluation of their biological significance *in vivo* and their association with tumour aggression is in progress.

ACKNOWLEDGEMENTS

We thank Dr. J. Lawry for his help with the flow cytometry analysis and the Yorkshire Cancer Research Campaign for supporting this work.

REFERENCES

- BAGGIOLINI, M., DEWALD, D. and MOSER, B., Interleukin 8 and related chemotactic cytokines CXC and CC chemokines. *Adv. Immunol.*, **53**, 97–179 (1994).
- ENGEL, L.W., YOUNG, N.A., TRALKA, T.S., LIPPMAN, M.E., O'BRIEN, S.J. and JOYCE, M.J., Establishment and characterisation of three new continuous cell lines derived from human breast carcinomas. *Cancer Res.*, **38**, 3352–3364 (1978).
- HELMAN, L.J. and THIELE, C.J., New insights into the causes of cancer. *Pediatr. Clin. North Amer.*, **38**, 201–221 (1991).
- HIROSE, K., HAKOZAKI, M., NYUNOYA, Y., KOBAYASHI, Y., MATSUSHITA, K., TAKENOUCHI, T., MIKATA, A., MUKAIDA, N. and MATSUSHIMA, K., Chemokine gene transfection into tumour cells reduced tumourigenicity in nude mice in association with neutrophilic infiltration. *Brit. J. Cancer*, **72**, 708–714 (1995).
- KELNER, G.S., KENNEDY, J., BACON, K.B., KLEYENSTEUBER, S., LARGAESPADA, D.A., JENKINS, N.E., COPELAND, N.G., BAZAN, J.F., MOORE, K.W., SCHALL, T.J. and ZLOTNIK, A., Lymphotactin: a cytokine that represents a new class of chemokine. *Science*, **266**, 1395–1399 (1994).
- KEYDAR, I., CHEN, L., KARBY, S., WILSON, F.R., DELAREA, J., RADU, M., CHAITIK, S. and BRENNER, H.J., Establishment and characterization of a cell line of human breast carcinoma origin. *Cancer Res.*, **38**, 659–670 (1978).
- LANING, J., KAWASAKI, H., TANAKA, E., LUO, Y. and DORF, M.E., Inhibition of *in vivo* tumor growth by the beta chemokine TCA3. *J. Immunol.*, **154**, 4625–4635 (1994).
- LESTER, B.R. and MCCARTHY, J.B., Tumor cell adhesion to the extracellular matrix and signal transduction mechanisms implicated in tumor cell motility, invasion and metastasis. *Cancer Metastasis Rev.*, **11**, 31–44 (1992).
- NEGUS, R.P.M., ALLAVENA, P., SOZZANI, S., MANTOVANI, A. and BALKWILL, F.R., The detection and localisation of monocyte chemoattractant protein 1 (MCP-1) in human ovarian cancer. *J. clin. Invest.*, **95**, 2391–2396 (1995).

- OPDENAKKER, G. and VAN DAMME, J., Chemotactic factors, passive invasion and metastasis of cancer cells. *Immunol. Today*, **13**, 463-464 (1992a).
- OPDENAKKER, G. and VAN DAMME, J., Cytokines and proteases in invasive processes: molecular similarities between inflammation and cancer. *Cytokine*, **4**, 251-258 (1992b).
- POKORNA, E., JORDAN, P.W., O'NEILL, C.H., ZICHA, D., GILBERT, C.S. and VESELY, P., Actin cytoskeleton and motility in rat sarcoma cell populations with different metastatic potential. *Cell Motility Cytoskeleton*, **28**, 25-33 (1994).
- ROLLINS, B.J. and SUNDAY, M.E., Suppression of tumor formation *in vivo* by expression of the JE gene in malignant cells. *Mol. Cell Biol.*, **11**, 3125-3131 (1991).
- SOMMERS, C.L., BYERS, S.W., THOMPSON, E.W., TORRI, J.A. and GELMANN, E.P., Differentiation state and invasiveness of human breast cell lines. *Breast Cancer Res. Treat.*, **31**, 325-335 (1994).
- SOULE, H.D., VAZQUEZ, J., LONG, A., ALBERT, S. and BRENNAN, M., A human cell line from a pleural effusion derived from a breast carcinoma. *J. nat. Cancer Inst.*, **51**, 1409-1416 (1973).
- SOZZANI, S., LOCATI, D., ZHOU, D., RIEPPI, M., LUINI, W., LAMORSE, G., BIANCHI, G., POLENTARUTTI, N., ALLAVENE, P. and MANTOVANI, A., Receptor, signal transduction and spectrum of action of monocyte chemotactic protein 1 and related chemokines. *J. Leukocyte Biol.*, **57**, 788-794 (1995).
- STRIETER, R.M., PULVERINI, P.J., ARENBERG, D.A. and KUNKEL, S.L., The role of CXC chemokines as regulators of angiogenesis. *Shock*, **4**, 155-159 (1995).
- TAUB, D.D., SAYERS, T.J., CARTER, C.R.D. and ORTALDO, O.R., Alpha and beta chemokines induce NK cell migration and enhanced NK mediated cytotoxicity. *J. Immunol.*, **155**, 3877-3888 (1995).
- VERSCHUEREN, H., VAN DER TAELEN, I., DEWIT, J., DE BRAEKELEER, J. and BAETSELIER, P., Metastatic competence of BW5147 T lymphoma cell line is correlated with *in vitro* metastasis. *J. Leukocyte Biol.*, **55**, 552-556 (1994).
- WANG, J.M., SHERRY, B., FIVASH, M.J., KELVIN, D.J. and OPPENHEIM, J.J., Human recombinant macrophage inflammatory protein-1 α and -1 β and monocyte chemotactic and activating factor utilize common and unique receptors on human monocytes. *J. Immunol.*, **150**, 3022-3029 (1993).
- WANG, M.J., TARABOLETTI, G., MATSUSHIMA, K., VAN DAMME, J. and MANTOVANI, A., Induction of haptotactic migration of melanoma cells by neutrophil activating protein/Interleukin 8. *Biochem. biophys. Res. Commun.*, **169**, 165-170 (1990).
- YABKOWITZ, R., MANSFIELD, P.J., DIXIT, V.M. and SUCHARD, S.J., Motility of human carcinoma cells in response to thrombospondin: relationship to metastatic potential and thrombospondin structure domains. *Cancer Res.*, **53**, 378-387 (1993).
- YOSHIDA, T., IMAI, T., KAKIZAKI, M., HISHIMURA, M. and YOSHIE, O., Molecular cloning of a novel C or γ type chemokine SCM-1. *FEBS Lett.*, **360**, 155-159 (1995).

Association of Macrophage Infiltration with Angiogenesis and Prognosis in Invasive Breast Carcinoma¹

Russell D. Leek, Claire E. Lewis, Ruth Whitehouse, Michael Greenall, Jane Clarke, and Adrian L. Harris²

Imperial Cancer Research Fund Molecular Oncology Laboratory, University of Oxford Institute of Molecular Medicine [R. D. L., R. W., A. L. H.], Nuffield Department of Pathology and Bacteriology [R. D. L., C. E. L.], and Department of Surgery [M. G., J. C.], University of Oxford, John Radcliffe Hospital, Headington, Oxford OX3 9DU, England

Abstract

Angiogenesis is a key process in tumor growth and metastasis and is a major independent prognostic factor in breast cancer. A range of cytokines stimulate the tumor neovasculature, and tumor-associated macrophages have been shown recently to produce several important angiogenic factors.

We have quantified macrophage infiltration using Chalkley count morphometry in a series of invasive breast carcinomas to investigate the relationship between tumor-associated macrophage infiltration and tumor angiogenesis, and prognosis. There was a significant positive correlation between high vascular grade and increased macrophage index ($P = 0.03$), and a strong relationship was observed between increased macrophage counts and reduced relapse-free survival ($P = 0.006$) and reduced overall survival ($P = 0.004$) as an independent prognostic variable. These data indicate a role for macrophages in angiogenesis and prognosis in breast cancer and that this cell type may represent an important target for immunoinhibitory therapy in breast cancer.

Introduction

Angiogenesis is important in tumor growth and metastasis. Recent studies have shown microvessel density in tumors to be a major prognostic factor in various forms of cancer, including invasive carcinoma of the breast. Moreover, high microvessel density gives independent prognostic information for both relapse-free and overall survival (1).

Angiogenesis is a multistep process involving the formation of new capillaries from an existing vascular network with remodeling of the extracellular matrix, endothelial cell migration and proliferation, capillary differentiation, and anastomosis. The neovasculature within tumors is highly proliferative compared to normal vessels, and several factors are known to stimulate angiogenesis, including VEGF,³ bFGF, EGF/transferring growth factor α , TNF- α , platelet-derived endothelial cell growth factor/thymidine phosphorylase, hepatocyte growth factor/scatter factor, and insulin-like growth factor I (2).

In invasive breast carcinomas, the neoplastic cell population is often outnumbered by such stromal cells as TAMs, which can comprise more than 50% of the total tumor mass (3). It is thought that monocytes in the peripheral circulation are recruited to the tumor site by the release of the chemotactic cytokines, monocyte chemotactic protein-1 (4), CSF-1 (5), granulocyte macrophage-CSF (6), and VEGF (7) by such tumors. Once recruited, monocytes differentiate to be-

come TAMs and are modified in the tumor microenvironment to secrete several growth factors, such as EGF (8), TNF- α (9), VEGF, and bFGF (10).

There are drugs that inhibit macrophage function, such as Lino-mide, which is antiangiogenic *in vivo* but not *in vitro* (11). This effect is mediated by its ability to inhibit both the entry of macrophages into tumors and their secretion of TNF α (12). Furthermore, a recent study has reported that prolonged immunosuppression reduced the incidence of breast cancer in a large cohort of patients, suggesting that breast cancer is in some way promoted by immune mechanisms (13).

Collectively, these findings have led to increased interest in the role of TAMs in the regulation of tumor development and angiogenesis and prompted us to evaluate the relationship between TAM infiltration and tumor angiogenesis in a series of invasive breast carcinomas. We also correlated macrophage infiltration with overall and relapse-free survival for the same set of patients. To study the relationship between angiogenesis and macrophage infiltration, a variation of the Chalkley point-counting method for assessment of vascular density (14) was employed in a similar fashion to assess the macrophage density (M ϕ I) for each tumor.

Materials and Methods

Immunohistochemistry. A consecutive series of 101 breast carcinomas was assessed for vascular grade and M ϕ I. The endothelial cell marker CD31 and the commonly used macrophage marker CD68 were stained immunohistochemically using the mouse monoclonal antibodies JC70a (DAKO) and KP1 (DAKO) on 5- μ m sections of routinely processed paraffin-embedded biopsies to identify blood vessels and macrophages, respectively. The alkaline phosphatase antialkaline phosphatase method was used to amplify the primary antibody signal, and the stain was developed using a new fuchsin substrate kit (DAKO), yielding an insoluble red reaction product. A hematoxylin nuclear counterstain was also applied.

To evaluate the spatial distribution of macrophage hot spots and their relationships to areas of angiogenesis, a subset of 46 cases was double stained for CD68 and Von Willebrand factor (formerly factor VIII-related antigen, an endothelial cell marker). Double staining of Von Willebrand factor and CD68 was achieved using a peroxidase-labeled EPOS rabbit polyclonal antibody (identifying blood vessels; DAKO) with the mouse monoclonal antibody KP1 (identifying macrophages). The peroxidase-labeled anti-Von Willebrand factor antibody was applied first; this is a single step method, and 3,3'-diaminobenzidine (DAKO) was used as the chromogen, yielding an insoluble brown reaction product. This was followed by the monoclonal antibody KP1 utilizing the standard alkaline phosphatase antialkaline phosphatase method and new fuchsin substrate as the chromogen. This produced single sections with blood vessels stained brown and macrophages stained red, and a hematoxylin nuclear counterstain was also applied.

ER and EGFR. Estrogen receptor analysis was performed using the method described by the European Organization for Research and Treatment of Cancer Breast Cancer Co-operative group (15). Tumors with cytoplasmic estrogen receptor levels of more than 5 fmol/mg of protein were considered positive. The EGFR level was determined using a ligand binding method described previously (16). Tumors with an EGFR level of greater than 20 fmol/mg of protein were considered positive.

Received 8/7/96; accepted 8/28/96.

The costs of publication of this article were defrayed in part by the payment of page charges. This article must therefore be hereby marked advertisement in accordance with 18 U.S.C. Section 1734 solely to indicate this fact.

¹ This project was funded by the Imperial Cancer Research Fund, P. O. Box 123, Lincoln's Inn Fields, London WC2A 3PX, England.

² To whom requests for reprints should be addressed.

³ The abbreviations used are: VEGF, vascular endothelial cell growth factor; bFGF, basic fibroblast growth factor; TNF α , tumor necrosis factor α ; CI, confidence interval; TAM, tumor-associated macrophage; M ϕ I, macrophage index; CSF, colony-stimulating factor; ER, estrogen receptor; EGF, epidermal growth factor; EGFR, EGF receptor; CVC, Chalkley vessel count.

Vascular and Macrophage Index. Microvessel density was assessed in the three most vascular areas or "hot spots" following a brief scan of the entire section at low power. For each area, an eyepiece-mounted 25-point Chalkley array graticule was used to assess the vascular grade using a $\times 25$ objective lens with a $\times 10$ eyepiece as described by Fox *et al.* (14). The mean of the three Chalkley counts was used for the subsequent statistical analysis. To assess the M ϕ I, the same Chalkley point-counting method was employed to assess the three areas of densest macrophage infiltration. Similar to the method employed for vascular enumeration, the Chalkley point array was rotated so that the maximum number of points coincided with stained macrophages, and a count was taken. The vascular and macrophage hot spots are chosen rather than random fields, because these areas are thought to be the most biologically important regions.

The double-stained sections were assessed for vascular index and M ϕ I simultaneously by first scanning the section at low power to find the three most highly vascularized areas. Each area was then assessed for vascularity using the Chalkley point array and then immediately assessed for M ϕ I using the same method. The section was then scanned again to determine the three densest areas of macrophage infiltration; each area was then assessed for M ϕ I and then assessed immediately for vascularity.

Statistical Analysis. Spearman rank and pairwise correlation were used to investigate relationships between continuous patient and tumor variables, and a χ^2 test for categorical variables. Survival curves were plotted using the method of Kaplan and Meier, and the log rank test and Cox univariate duration model were used to evaluate differences between life tables. A Cox multivariate proportional hazard model was used to investigate the overall effect of patient and tumor variables on survival. The analysis was performed using Stata release 3.1 (Stata Corp., College Station, Texas).

Results

Correlation of M ϕ I with Angiogenesis. Data from the series of breast tumors examined was divided by tertiles into three categories corresponding to low, medium, and high vascular grade. We have reported previously that the upper third group by vascular grade has a worsened prognosis when compared to the middle and lower groups (14). When comparing the mean M ϕ I for the three vascular groups, it was found that the mean M ϕ I for the high-vascular grade group was significantly higher than that found for the combined lower and middle-vascular grade groups ($P = 0.03$; Fig. 1a). This demonstrates a positive correlation between high vascular grade and increased M ϕ I.

Spatial Relationships between Areas of Angiogenesis and Macrophage Activity. The three most dense areas of macrophage content were enumerated simultaneously for macrophage and vascular density; this was followed by the three most dense areas of vascular activity being evaluated in the same manner. The overall results are presented in Fig. 1b, where it is shown that there is an inverse relationship between macrophage density and vascular density. That is, the highly angiogenic areas were poorly populated with macrophages when compared to the more macrophage-dense fields, which were similarly poorly vascularized. Macrophage density in low-angiogenesis areas was higher than in high angiogenesis areas ($P < 0.0001$). Angiogenesis was higher in low macrophage areas than high-macrophage areas ($p < 0.0001$). This inverse relationship was maintained when highly vascularized and poorly vascularized tumors were examined separately.

Correlation of M ϕ I with Relapse-free and Overall Survival. In this series of cases, a total of 91 patients were evaluable for survival. Taking M ϕ I as a continuous variable in a univariate Cox proportional hazard model, increasing M ϕ I was a significant indicator of worsened prognosis for both relapse-free and overall survival [(for relapse-free survival, $P = 0.01$, hazard ratio = 1.03 (CI, 1.00–1.06), for overall survival, $P = 0.05$, hazard ratio = 1.03 (CI 1.00–1.07)]. Two cut points for M ϕ I were chosen corresponding to the median (12) and the upper third (18). At the median cut point, 41 cases were in the low

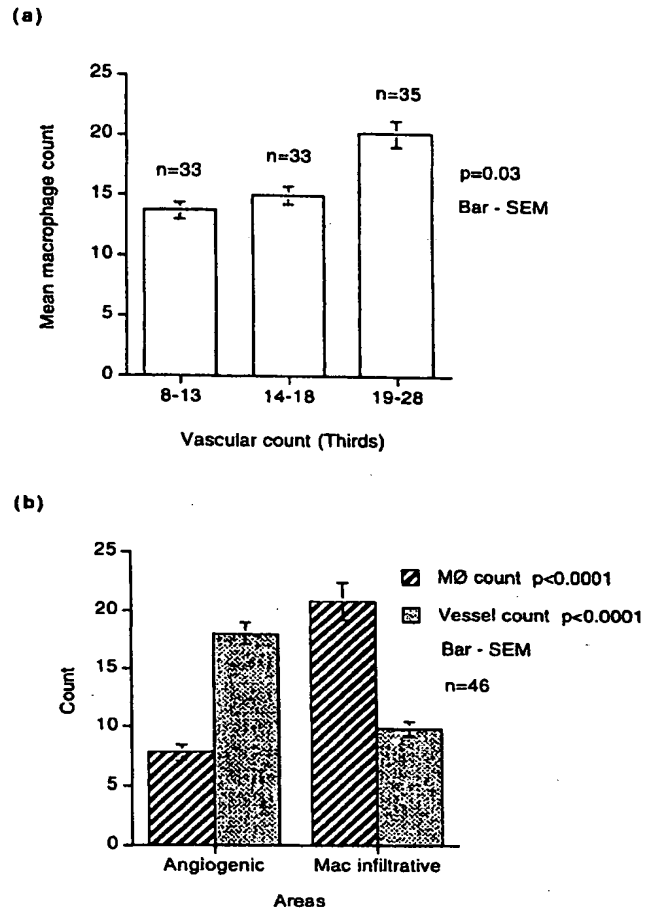


Fig. 1. Macrophage infiltration and angiogenesis. a, comparison of macrophage infiltration with degree of vascularization (split into thirds). b, distribution of macrophages in relation to areas of angiogenesis.

(<12) category, with 50 cases falling into the high (≥ 12) category, whereas, using the upper tertile cut point, 60 cases fell into the low (<18) category, with 31 cases being in the high (≥ 18) category.

Comparing M ϕ I to relapse-free survival, at the median cut point a higher relapse rate occurred in the high-M ϕ I category (hazard ratio = 3.2, $P = 0.007$; Fig. 2a). Likewise, using the upper third cut point, there was an increased relapse rate in the high-M ϕ I group (hazard ratio = 2.73, $P = 0.008$).

When examining the effect of M ϕ I on overall survival, a similar effect was observed with higher death rates at above the median (hazard ratio = 11.19, $P = 0.0036$; Fig. 2b) and in the upper third M ϕ I class (hazard ratio = 3.4, $P = 0.0233$).

Examining node-negative tumors separately, using the median cut point for M ϕ I, it was found that M ϕ I was a significant predictor of poorer outcome for relapse-free survival in this group ($P = 0.013$).

When angiogenesis was examined for its effects on survival, it was found that cases that were highly angiogenic had a worse overall and relapse-free survival rate than cases in the low-angiogenesis group (for overall survival, $P = 0.02$; for relapse-free survival, $P = 0.009$).

Multivariate Survival Analysis. Because it was shown that the cases with high M ϕ I above the median have a worse prognosis, multivariate analysis was carried out with other factors.

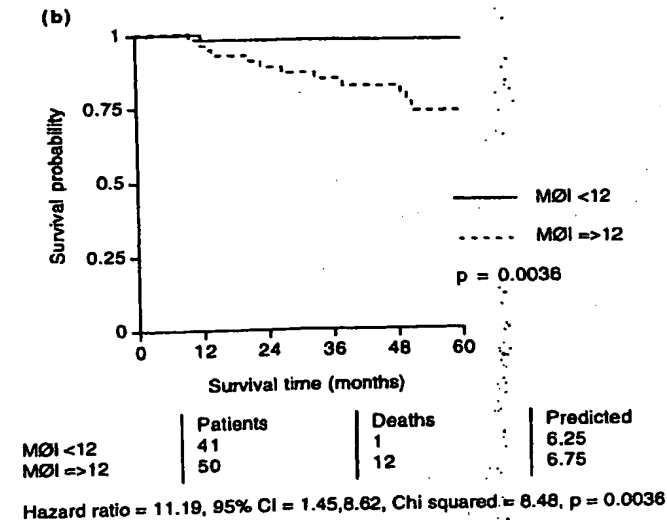
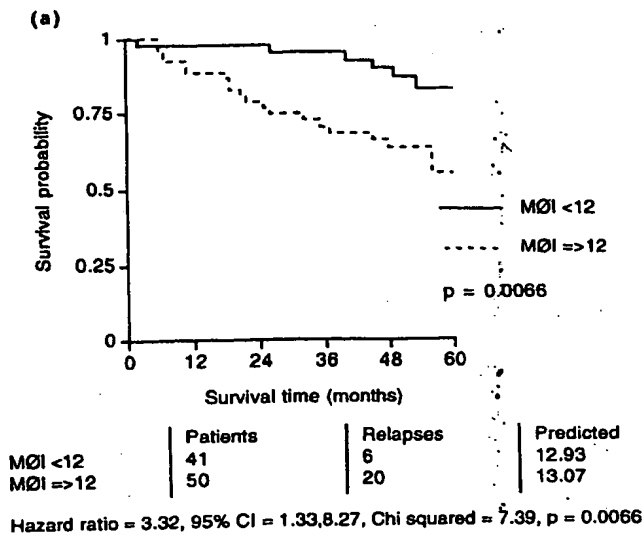


Fig. 2. Macrophage infiltration and survival. a, relapse-free survival at median MφI cut point. b, overall survival at median MφI cut point.

MφI was significant as an independent prognostic indicator for both relapse-free and overall survival ($P = 0.038$ and $P = 0.037$, respectively), with high MφI indicating worse prognosis (Table 1). When macrophages are taken into account, angiogenesis was not significant, although it was the most significant of the other factors. A separate multivariate analysis excluding MφI showed CVC to be independently prognostic for relapse-free survival ($P = 0.018$), but in this group, CVC failed marginally to achieve significance for overall survival ($P = 0.081$), although it was the most significant of all the other factors, with the exception of node status.

Interaction of MφI with Angiogenesis and Effects on Survival. Because both vascular grade and MφI were found to prognostically significant, and there was a positive correlation between the two factors, we assessed the interactions between MφI and angiogenesis and their effects on relapse-free and overall survival. The median MφI cut point was used in these analyses.

Dividing the series of cases into high and low vascular grade, it was

found that for relapse-free survival, MφI was able to split the low-vascular grade group into two, with high-MφI cases having a worsened prognosis when compared to the low-MφI cases ($P = 0.023$; Fig. 3). A similar finding was observed when examining overall survival, with MφI again splitting the low-vascular grade group ($P = 0.0017$). However, in the high-vascular grade group, MφI was unable to split the series into two more prognostically significant subgroups in either relapse-free ($P = 0.71$) or overall survival ($P = 0.72$).

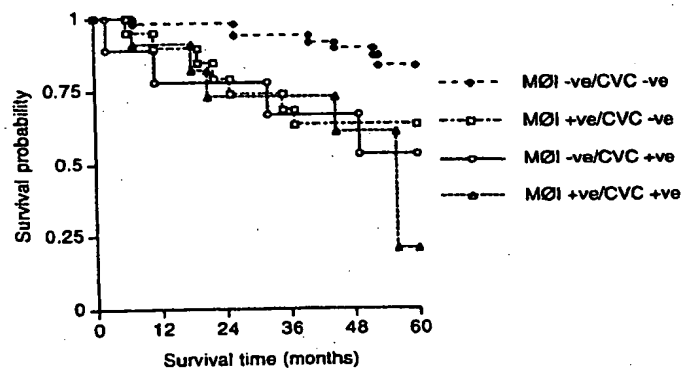
Dividing the series by high and low MφI, it was found that vascular grade was able to further stratify the low-MφI group into two prognostically different subgroups for both relapse-free ($P = 0.022$; Fig. 3) and overall survival ($P = 0.0005$), with the high vascular grade category having the worse prognosis. This was not observed when vascular grade was used to stratify the high-MφI group of cases ($P = 0.43$ for relapse-free survival; $P = 0.84$ for overall survival).

Comparison of MφI with Other Prognostic Variables. MφI was compared to other patient and tumor variables, including age, tumor size, nodal status, grade, ER, and EGFR. Split by median, using χ^2 tests at cut point 12 for MφI, no significant associations were evident.

Discussion

We have shown that there is a significant and positive correlation between angiogenesis and macrophages in breast tumors, with highly vascular tumors having higher numbers of macrophages. This observation could be due either to the presence of more vessels, allowing the infiltration of more macrophages, or the proangiogenic activity of macrophages inducing the proliferation, migration, and differentiation of endothelial cells.

Although the former explanation cannot be excluded, the latter appears to be more likely in light of recent evidence showing that macrophages play an important role in promoting angiogenesis by secreting proangiogenic cytokines and/or enzymes that degrade the extracellular matrix (10). Also in favor of the latter is the observation that the areas of greatest macrophage density or macrophage hot spots



CVC split by MφI

CVC + / MφI + } $p = 0.71$
CVC + / MφI - }

CVC - / MφI + } $p = 0.023$
CVC - / MφI - }

MφI split by CVC

MφI + / CVC + } $p = 0.43$
MφI + / CVC - }

MφI - / CVC + } $p = 0.022$
MφI - / CVC - }

Fig. 3. Effects of interaction between macrophage infiltration and angiogenesis on survival. -ve, negative; +ve, positive.

MACROPHAGE INFILTRATION IN BREAST CARCINOMA

Table 1 Multivariate Cox proportional hazard analysis

Prognostic indicator	Cut point	Overall survival			Relapse-free survival		
		Hazard	95% CI	P value	Hazard	95% CI	P value
MφI	12	9.43	1.15-77.3	0.037	2.79	1.06-7.33	0.038
CVC	7	3.57	0.87-14.5	0.076	2.19	0.89-5.41	0.089
Age	50	1.60	0.29-8.93	0.593	1.18	0.42-3.33	0.758
ER	10	0.72	0.19-2.68	0.623	0.68	0.27-1.70	0.405
EGFR	20	0.66	0.17-2.64	0.558	0.68	0.26-1.80	0.443
Nodes	0	6.09	1.58-23.5	0.009	1.91	0.78-4.64	0.155
Size	2	1.09	0.28-4.30	0.900	2.48	0.82-7.48	0.108

are situated away from the vascular hot spots, implying active migration rather than accumulation in areas around blood vessels. This type of distribution has also been noted by Hildenbrand *et al.*, who also observed a positive relationship between high macrophage grade and increased expression of urokinase-plasminogen activator in breast cancer (17).

The factors that induce macrophage hot spots are not clear but may include necrosis and hypoxia. Angiogenesis occurs in vascular hot spots (14), which are biologically important because they provide a route through which tumor cells can metastasize. Tumor cells in the nonvascular regions experience hypoxic stress and/or undergo cell death. Macrophages may then migrate into these areas, chemotactically following a gradient of substances released by stressed cells such as lactate, low oxygen, and/or VEGF released by the hypoxic tumor cells themselves. Once in these hypoxic areas, they may become angiogenically active, and it has been shown previously that experimental hypoxia can induce the release of bFGF by monocytic cells *in vitro* (18). Upon induction or completion of angiogenesis in that area, macrophages may then move away or undergo apoptosis.

Focal macrophage infiltration also appears to be an important prognostic factor in invasive carcinoma of the breast, being predictive of a worsened outcome and of reduced relapse-free and overall survival when MφI is high. Indeed, from these data it would seem that MφI is a more powerful predictor of survival than nodal status, again suggesting that macrophages may have a direct role in disease progression. Other studies have found associations between higher levels of macrophage infiltration and markers of poor prognosis such as Ki-67 (17), and Pupa *et al.* (19) have described a positive correlation between macrophage infiltration and *c-erbB2* as well as high grade in invasive breast carcinoma. However, in a large series of 1207 cases, they found that the presence of a general lymphoplasmacytic infiltrate in these poor prognosis groups did improve outcome. Also, it was seen in a subset of 72 cases of *c-erbB2*-positive cases that the lymphoplasmacytic infiltrate had a high proportion of macrophages, although the group for which the macrophage proportions were known was not analyzed for survival, and the macrophages were not quantified.

A minority of low-angiogenic tumors in this study were seen to have high macrophage counts and *vice versa*. This shows that macrophages are not necessarily a major angiogenic influence in all highly vascular tumors, and it will be of interest to assess angiogenic factors expressed in these two types of tumors. Also, tumors with high MφIs and low angiogenesis may not yet have developed increased vascularization, because this type of study represents only a single point in the evolution of a tumor. Tumors that have both low vascular grade and low MφI may represent an early stage in the induction of angiogenesis and may have been destined to progress to highly vascularized tumors with a greater macrophage density at a later stage.

Both angiogenesis and MφI were seen to be prognostic factors, and these appear to be related. When the survival data for vascular grade and MφI are combined, it is observed that high vascular grade can

predict a worsened outcome in the low MφI subclass of cases (but is unable to split the high-MφI subclass into two prognostically different groups). Also, MφI can split the low-vascular grade group into two prognostically different groups. This suggests that if either factor is high, the pathway toward metastasis and poorer outcome is favored; if either is low, then the other factor generates a poor prognosis pathway. If both factors are high, prognosis is not significantly worsened than when either is high, possibly because they act via a similar final pathway.

Taken together, our data indicate that TAMs may play a central role in tumor angiogenesis and tumor progression, and that assessment of MφI could be used clinically to predict outcome in breast cancer patients. It is also apparent that the TAM population of breast carcinomas could be an effective target for future antiangiogenic therapies. Recent findings suggest that this could be achieved using interleukin 10 and Linomide. In mice, transplantable tumors transfected with interleukin 10 show lower levels of macrophage infiltration than their nontransfected counterparts (20), whereas treatment of tumor-bearing rats with Linomide markedly reduced the tumor infiltration and TNFα secretion of macrophages as well as the degree of tumor neovascularization (12). On the basis of the data presented here, breast cancer is a key tumor type for assessing these new therapies.

References

- Weidner, N., Semple, J. P., Welch, W. R., and Folkman, J. Tumor angiogenesis and metastasis: correlation in invasive breast carcinoma. *N. Engl. J. Med.*, 324: 1-8, 1991.
- Leek, R. D., Harris, A. L., and Lewis, C. E. Cytokine networks in solid human tumors: regulation of angiogenesis. *J. Leukoc. Biol.*, 56: 423-435, 1994.
- O'Sullivan, C., and Lewis, C. E. Tumour-associated leucocytes: friends or foes in breast carcinoma. *J. Pathol.*, 172: 229-235, 1994.
- Graves, D. T., and Valente, A. J. Monocyte chemotactic proteins from human tumor cells. *Biochem. Pharmacol.*, 41: 333-337, 1991.
- Scholl, S. M., Pallud, C., Beuvon, F., Hacene, K., Stanley, E. R., Rohrschneider, L., Tang, R., Pouillart, P., and Lidereau, R. Anti-colony-stimulating factor-1 antibody staining in primary breast adenocarcinomas correlates with marked inflammatory cell infiltrates and prognosis. *J. Natl. Cancer Inst.*, 86: 120-126, 1994.
- Fu, Y. X., Cai, J. P., Chin, Y. H., Watson, G. A., and Lopez, D. M. Regulation of leukocyte binding to endothelial tissues by tumor-derived GM-CSF. *Int. J. Cancer*, 50: 585-588, 1992.
- Clauss, M., Gerlach, M., Gerlach, H., Brett, J., Wang, F., Familletti, P. C., Pan, Y. C., Olander, J. V., Connolly, D. T., and Stern, D. Vascular permeability factor: a tumor-derived polypeptide that induces endothelial cell and monocyte procoagulant activity, and promotes monocyte migration. *J. Exp. Med.*, 172: 1535-1545, 1990.
- O'Sullivan, C., Lewis, C. E., Harris, A. L., McGee, J. O'D. Secretion of epidermal growth factor by macrophages associated with breast carcinoma. *Lancet*, 342: 148-149, 1993.
- Pusztai, L., Clover, L. M., Cooper, K., Starkey, P. M., Lewis, C. E., and McGee, J. O'D. Expression of tumour necrosis factor α and its receptors in carcinoma of the breast. *Br. J. Cancer*, 70: 289-292, 1994.
- Lewis, C. E., Leek, R., Harris, A. L., and McGee, J. O'D. Cytokine regulation of angiogenesis in breast cancer: the role of tumor-associated macrophages. *J. Leukoc. Biol.*, 57: 747-751, 1995.
- Ichikawa, T., Lamb, J. C., Christensson, P. J., Hartley-Asp, B., and Isaacs, J. T. The antitumor effects of the quinoline-3-carboxamide linomide on dunning R-3327 rat prostatic cancers. *Cancer Res.*, 52: 3022-3028, 1992.
- Vukanovic, J., and Isaacs, J. T. Linomide inhibits angiogenesis, growth, metastasis, and macrophage infiltration within rat prostatic cancers. *Cancer Res.*, 55: 1499-1504, 1995.
- Stewart, T., Tsai, S. C., Grayson, H., Henderson, R., and Opelz, G. Incidence of *de-novo* breast cancer in women chronically immunosuppressed after organ transplantation. *Lancet*, 346: 796-798, 1995.

MACROPHAGE INFILTRATION IN BREAST CARCINOMA

14. Fox, S. B., Leek, R. D., Weekes, M. P., Whitehouse, R. M., Gatter, K. C., and Harris, A. L. Quantitation and prognostic value of breast cancer angiogenesis: comparison of microvessel density, Chalkley count, and computer image analysis. *J. Pathol.*, 177: 275-283, 1995.
15. European Organization for Research and Treatment of Cancer Breast Cancer Co-Operative Group. Revision of the standards for the assessment of hormone receptors in human breast cancer: report of the second E. O. R. T. C. Workshop, held on 16-17 March, 1979, in the Netherlands Cancer Institute. *Eur. J. Cancer*, 16: 1513-1515, 1980.
16. Nicholson, S., Sainsbury, J. R., Needham, G. K., Chambers, P., Farndon, J. R., and Harris, A. L. quantitative assays of epidermal growth factor receptor in human breast cancer: cut-off points of clinical relevance. *Int. J. Cancer*, 42: 36-41, 1988.
17. Hildenbrand, R., Dilger, I., Horlin, A., and Stutte H. J. Urokinase and macrophages in tumour angiogenesis. *Br. J. Cancer*, 72: 818-823, 1995.
18. Kuwabara, K., Ogawa, S., Matsumoto, M., Koga, S., Clauss, M., Pinsky, D. J., Leavy, J., Witte, L., Joseph, S. J., Furie, M. B., Torcia, G., Cozzolino, F., Karnad, T., and Stern, D. M. Hypoxia-mediated induction of acidic/basic fibroblast growth factor and platelet-derived growth factor in mononuclear phagocytes stimulates growth of hypoxic endothelial cells. *Proc. Natl. Acad. Sci. USA*, 92: 4606-4610, 1995.
19. Pupa, S. M., Bufalino, R., Invernizzi, A. M., Andreola, S., Rilke, F., Lomardi, L., Colnaghi, M. I., and Menard, S. Macrophage infiltrate and prognosis in c-erbB-2-overexpressing breast carcinomas. *J. Clin. Oncol.*, 14: 85-94, 1996.
20. Richter, G., Kruger, K. S., Hein, G., Huls, C., Schmitt, E., Diamantstein, T., and Blankenstein, T. Interleukin 10 transfected into Chinese hamster ovary cells prevents tumor growth and macrophage infiltration. *Cancer Res.*, 53: 4134-4137, 1993.

Brief Reviews

Cytokines and Cell Adhesion Molecules in Cerebral Ischemia

Experimental Bases and Therapeutic Perspectives

Leonardo Pantoni, Cristina Sarti, Domenico Inzitari

Abstract—The possibility of reopening an occluded cerebral artery by means of thrombolysis has renewed interest in a number of the several mechanisms that are active during acute cerebral ischemia. Over recent years, it has become apparent that leukocytes play a central role not only during the healing stage of brain infarction but also during the early phases of cerebral ischemia, when it is postulated that these cells produce harmful effects, particularly in the presence of reperfusion. This review is based on the critical analysis of more than 150 publications dealing with the role of leukocytes and some inflammatory mediators (cytokines, chemokines, and adhesion molecules) in cerebral ischemia. Animal studies indicate that leukocyte involvement is promoted by a variety of inflammatory molecules produced immediately after the onset of cerebral ischemia. Considerable experimental evidence suggests that these mediators play a key role in the progression from ischemia to irreversible injury (ie, cellular death and necrosis). However, the precise role of each molecule alone remains to be further elucidated as well as in relation to the complex network existing among different mediators. Progress in our understanding of the inflammatory mechanisms operating in cerebral ischemia has enabled the testing of new compounds with promising results in animals; in contrast, one recent controlled trial of an anti-leukocyte molecule in acute stroke patients showed negative results. This discrepancy may derive in part from our incomplete understanding of the complexity of the inflammatory mechanisms involved in cerebral ischemia. Our analysis suggests that until sufficient knowledge of the underlying disease mechanisms is acquired, more care should be taken when testing new and potentially efficacious drugs in stroke patients.

The scenario of acute ischemic stroke therapy is rapidly evolving, and thrombolysis has recently been approved for use in stroke patients by USA authorities. However, therapeutic recanalization of an occluded cerebral artery still appears to be a potentially risky option that can be applied only in the case of selected patients.^{1,2} The main limitation of cerebral thrombolysis is the narrow, 3-hour therapeutic "window" during which the thrombolytic agent has to be administered to be effective³; beyond this time limit, its effectiveness is neutralized by the high risk of cerebral hemorrhage.⁴

The rationale for the use of a number of other pharmacological treatments for acute stroke currently under study in both animals and humans is based on recent advances in the pathophysiology of brain ischemia, one of the most rapidly expanding and promising areas of which is the role of inflammation in stroke. This role involves (1) the molecules that form part of the inflammatory response and participate in the pathophysiological cascade after an ischemic insult and (2) the inflammatory or infectious processes that may predispose or precipitate atherothrombotic stroke.⁵⁻⁸ In this review, we reexamine some aspects of inflammation in acute stroke by focusing on the role of leukocytes and leukocyte-related

molecules, with the aim of providing the background necessary to understand the rationale of newly emerging therapeutic approaches. Our review is limited to experimental and human data concerning some of the inflammatory mechanisms active during the acute phase of cerebral ischemia.

Histological Inflammatory Aspects in Acute Cerebral Ischemia

An inflammatory reaction is a common response of the brain parenchyma to various forms of insult. It is histologically characterized by the infiltration of leukocytes, which in the case of cerebral ischemia are mainly polymorphonuclear leukocytes and monocytes/macrophages.⁹ Human data are scarce: an increased number of leukocytes has been documented in the cerebrospinal fluid of acute stroke patients 2 to 3 days after stroke¹⁰; a high number of radiolabeled polymorphonuclear leukocytes have been shown in slightly perfused brain areas as early as 6 to 12 hours after the ictus¹¹; and one autopsy study described intense leukocyte infiltration of the brain parenchyma 2 to 3 days after the stroke.¹²

However, the inflammatory response of ischemic brain parenchyma has been more thoroughly explored in animal

Received September 26, 1997; revision accepted December 3, 1997.

From the Department of Neurological and Psychiatric Sciences, University of Florence, Florence, Italy.

Correspondence to Leonardo Pantoni, MD, Department of Neurological and Psychiatric Sciences, University of Florence, Viale Morgagni 85, 50134 Firenze, Italy.

E-mail neuroinz@cesit1.unifi.it

(*Arterioscler Thromb Vasc Biol.* 1998;18:503-513.)

© 1998 American Heart Association, Inc.

Selected Abbreviations and Acronyms

CINC	= cytokine-induced neutrophil chemoattractant
ICAM	= intercellular adhesion molecule
IFN	= interferon
IL	= interleukin
MCA	= middle cerebral artery
MCP	= monocyte chemoattractant protein
MIP	= macrophage inflammatory protein
TGF	= transforming growth factor
TNF	= tumor necrosis factor

models. An increased number of polymorphonuclear leukocytes in the microvessels or ischemic brain parenchyma have been found in various species.¹³⁻²¹ Until recently, it was assumed that this inflammatory reaction was delayed, secondary to tissue necrosis, and was intended to remove tissue debris from the infarcted area. In rats with permanent occlusion of one MCA, leukocytes (particularly polymorphonuclear cells) can be recognized in the microvessels as early as 30 minutes after occlusion.²² In the same model, necrosis is detected only 72 to 96 hours after MCA occlusion.^{23,24} This study and others suggest that at least the early arrival of leukocytes in the brain parenchyma is independent of the presence of necrosis, and this idea leads to the hypothesis that these cells play a role in the progression from ischemia to brain infarction.

There are a number of mechanisms by which leukocytes may produce deleterious effects on ischemic parenchyma. It has been proposed that leukocytes obstruct the microvessels and contribute toward the so-called "no-reflow" phenomenon¹⁶; ie, the lack of complete recovery of cerebral blood flow in the ischemic area after reperfusion.²⁵ This plugging of microvessels under ischemic conditions may be the result of an interaction with endothelial cells, mediated by adhesion molecules and/or the loss of cell deformability due to actin polymerization and pseudopod projections.^{26,27} As reviewed by Härtl et al,²⁸ other detrimental effects of leukocytes during ischemia may be due to: (1) the release of vasoconstrictive mediators, such as superoxidase anions, thromboxane A₂, endothelin-1, and prostaglandin H₂²⁹; (2) an alteration in cerebral artery vasoreactivity; and (3) the release of cytotoxic enzymes, free oxygen radicals, NO, and products of the phospholipid cascade. The release of proteolytic enzymes such as elastase might damage endothelial cell membranes and the basal lamina, alter the blood-brain barrier, and contribute to the formation of postischemic edema. In addition, loss of the integrity of the endothelial cell-basal lamina lining might facilitate the escape of red blood cells and the hemorrhagic transformation of a brain infarct.^{30,31}

The view that leukocytes may cause additional damage to potentially still-viable tissue during acute cerebral ischemia is indirectly supported by data showing a smaller infarct volume in neutropenic animals than in normal controls.³²⁻³⁵ Furthermore, a significant correlation has been found in humans between the degree of leukocyte accumulation and infarct volume as assessed by CT.¹¹ The arrival of leukocytes in the ischemic area is a multistep process.³⁶ They first marginate in the venules, then adhere to endothelial cells, and finally

migrate into the brain parenchyma. During each of these three steps, their functions are regulated by the inflammation-related molecules that are produced soon after the onset of cerebral ischemia.

Cytokines and Cerebral Ischemia

The signals mediating the entry of leukocytes into the ischemic area have not yet been completely elucidated, but a number of clues suggest that cytokines play a key role in this process. Cytokines are low-molecular-weight glycoproteins that act as intercellular messengers and are produced by macrophages, monocytes, lymphocytes, endothelial cells, fibroblasts, platelets, and many other cell types. To produce cytokines, all of these cells need to be activated.³⁷ Cytokines act at very low concentrations on specific target-cell receptors, whose expression is modulated by the cytokines themselves. Binding of cytokines to receptors activates intracellular second-messenger systems (yet to be identified) and subsequently, protein kinases and phosphatases. These proteins cause gene regulation through the activity of transcription factors.³⁷ Cytokines are considered to be among the principal mediators of immunologic and inflammatory responses. In vitro, cytokines can be produced by astrocytes, neurons, and endothelial and microglia cells,³⁸⁻⁴⁰ and there are observations suggesting that this also holds true in humans affected by brain ischemia.⁴¹

Cytokines may have various functions during cerebral ischemia: on the one hand, they can attract leukocytes and stimulate the synthesis of adhesion molecules in leukocytes, endothelial cells, and other cells, thus promoting the inflammatory response of damaged cerebral tissue; on the other, they can facilitate thrombogenesis by increasing the levels of plasminogen-activating inhibitor-1, tissue factor, and platelet-activating factor^{42,43} and by inhibiting tissue plasminogen activator and protein S.⁴⁴ Examination of this last aspect is beyond the scope of the present review.

IL-1

IL-1 exists in two separate forms (α and β), which have only one-third sequence homology. IL-1 is overexpressed during brain ischemia, as documented by the induction of IL-1 β mRNA synthesis in rats with permanent MCA occlusion,^{45,46} transient global forebrain ischemia,⁴⁷⁻⁵⁰ or a ligated carotid artery associated with hypoxia.⁵¹ Attempts to detect IL-1 in the peripheral blood of stroke patients have so far been unsuccessful, conceivably because of its low plasma levels.⁵²

Evidence that IL-1 may play a deleterious role in cerebral ischemia derives from the observation that rats with a transient MCA occlusion have a larger brain infarction when recombinant human IL-1 β is injected into the lateral ventricle immediately after reperfusion.⁵³ Similar results have been obtained in rats with a permanent MCA occlusion.⁵⁴ The intraventricular injection of recombinant human IL-1 β also enhances the formation of brain edema and increases both the number of neutrophils in ischemic areas and neutrophil-endothelial cell adhesion.⁵³ The complex functions of IL-1 are mediated by specific cell-surface receptors and regulated by the IL-1 receptor antagonist.⁵⁵ Two main receptors for IL-1 have been identified; type I is present in many cell types and

binds IL-1 α and IL-1 β with similar affinity.⁵⁶ Type II is found on the surface of B cells, neutrophils, and macrophages and shows higher affinity for IL-1 β .⁵⁶ Types I and II are regulated differently in brain ischemia and may thus play separate roles. In spontaneously hypertensive rats, the mRNA for the type I IL-1 receptor is relatively highly expressed in the normal cortex, with a marked increase 5 days after cerebral ischemia.⁵⁵ Type II mRNA has low basal expression and a peak 12 hours after the onset of ischemia.⁵⁵ The possible mechanisms of intracellular signal transduction for IL-1 on peripheral immune cells include effects on cAMP, protein kinase C, and protein phosphorylation⁵⁶; these effects remain to be proved in brain ischemia. The IL-1-receptor interaction is quickly followed by the induction of immediate-early genes such as *c-jun* and *c-fos*.⁵⁷

Studies showing a reduction in infarct size after the administration of IL-1 antagonists or inhibitors provide further evidence of the importance of IL-1 in cerebral ischemia.^{53,58-64} The possible harmful mechanisms induced or activated by IL-1 include fever, increased heart rate and arterial blood pressure, enhancement of *N*-methyl-D-aspartate-mediated injury, proliferation of microglia, release of arachidonic acid, and stimulation of NO synthesis.⁶⁵ At present, the most widely recognized functions of IL-1 appear to be the induction of endothelial cell adhesion molecule expression and the promotion of neutrophil tissue infiltration.

TNF- α

TNF- α gene upregulation has been demonstrated in transient⁶⁶ and prolonged^{51,67} cerebral ischemia by the increased synthesis of TNF- α mRNA in the parenchyma. TNF- α plasma levels have also been found to be higher in acute stroke patients than in healthy control subjects.⁶⁸

The effects of TNF- α are mediated by specific receptors, the most well known of which are two proteins called p75 and p55 (according to their molecular weight).⁶⁹ The binding of TNF- α to its receptor is followed by the activation of a variety of proteins, such as protein kinase C, tyrosine kinase, mitogen-activated protein kinase, phospholipase A₂, and phosphatidylcholine-specific phospholipase C.⁷⁰ Among these, the mitogen-activated protein kinases are the most extensively studied, and they are divided into three main families: (1) the extracellular signal-regulated kinases, which are activated by growth factors; (2) the c-Jun NH₂-terminal kinases; and (3) the p38 kinases. The last two groups are activated by proinflammatory cytokines.^{71,72} The second step in the TNF- α signal transduction pathway, as for other cytokines, is intranuclear, with the activation of several transcription factors. One of these, nuclear factor- κ B, translocates from the cytoplasm to the nucleus, where it activates the promoter of the genes for adhesion molecules and other cytokines.⁷³

Like IL-1, TNF- α induces the expression of adhesion molecules by glial and endothelial cells,⁷⁴ thus favoring neutrophil adherence and accumulation in microvessels.⁶⁷ TNF- α is also involved in blood-brain barrier alterations, a proadhesive-procoagulant transformation of endothelial cell surfaces, and glial cell activation.⁷⁴ However, its role in cerebral ischemia remains to be established. Barone et al⁷⁵

showed that administration of TNF- α exacerbated the ischemic injury provoked by MCA occlusion in spontaneously hypertensive rats, although TNF- α toxicity was not related to direct neuronal damage, and also demonstrated that anti-TNF- α antibodies have a neuroprotective effect.⁷⁵ Similarly, the inhibition of TNF- α in mice with permanent MCA occlusion leads to a smaller infarct volume.⁷⁶ However, not all studies agree about the deleterious role of TNF- α in brain ischemia. When TNF- α is administered to mice 48 hours before MCA occlusion, it induces a protective effect.⁷⁷ Furthermore, the fact that mice lacking TNF- α receptors show a larger infarct area after MCA occlusion than do normal controls⁷⁸ suggests that TNF- α may be beneficial in the poststroke recovery phase. Finally, the specificity of TNF- α expression after cerebral ischemia has been challenged by preliminary human data showing that TNF- α is also expressed in the contralateral, nonischemic hemisphere.⁷⁹

IL-6

IL-6 plays a central role in host defense as well as in acute and chronic inflammatory activities^{80,81} and is expressed in response to various forms of brain injury.⁸¹⁻⁸⁵ In the rat, IL-6 mRNA is overexpressed 3 hours after permanent MCA occlusion and reaches a peak at 12 hours; its expression remains high for at least 24 hours.⁸⁶

Higher IL-6 levels have been detected in the peripheral blood of patients with acute cerebral ischemia than in control subjects.^{52,87-89} Increased plasma and cerebrospinal fluid IL-6 levels are correlated with a larger infarct size on CT and magnetic resonance imaging scans^{87,88} and with a poorer clinical outcome,⁵² although it is not clear whether this simply reflects an overproduction of IL-6 by larger lesions or a directly damaging effect of IL-6 itself. In addition, it has not yet been completely elucidated whether IL-6 exerts anti-inflammatory or proinflammatory effects or both. Its anti-inflammatory effect depends on the inhibition of IL-1 and TNF- α production via a negative-feedback mechanism and stimulation of the production of their circulating antagonists: soluble TNF- α receptor and IL-1 receptor antagonist.^{80,90} Part of the anti-inflammatory function of IL-6 can be attributed to its ability to induce the release of corticotropin and cortisol^{91,92} and to promote the expression of acute-phase proteins^{93,94} that have antiproteinase and oxygen-scavenger functions.⁸¹ On the other hand, it has also been shown that IL-6 induces phospholipase A₂ gene expression and as a consequence, stimulates the production of leukotrienes, prostaglandins, and platelet activating factor,⁹⁵ all of which are involved in ischemic brain damage.⁹⁶

TGF- β

TGF- β is a cytokine that is known to regulate and stimulate cell proliferation and differentiation and to play a central role in tissue repair mechanisms.⁹⁷ In rats exposed to 10 minutes of global cerebral ischemia, increased expression of TGF- β mRNA is seen after 6 hours throughout the brain; this expression increases further at day 2 and subsides thereafter.⁹⁸

One recent human autopsy study has found TGF- β mRNA overexpression in ischemic tissue in comparison with samples taken from the contralateral, nonischemic side.⁹⁹ The

highest expression of TGF- β mRNA was detected in the tissue surrounding the infarction (the penumbra zone).⁹⁹ A so-far-unexplained finding is that serum TGF- β levels are lower in acute stroke patients than in control subjects, perhaps owing to an accumulation of this cytokine in the ischemic tissue.⁸⁹

Preliminary results indicate that TGF- β may play a protective role in brain ischemia.¹⁰⁰⁻¹⁰⁴ Some of the proposed reasons for this beneficial effect include (1) reduced neutrophil adherence to endothelial cells¹⁰⁵; (2) suppression of the release of potentially harmful oxygen- and nitrogen-derived products by macrophages^{106,107}; (3) the promotion of angiogenesis in the penumbra area⁹⁹; and (4) a reduction in the expression and efficacy of other cytokines, such as TNF- α ,^{108,109} possibly by blocking p38 kinase and the consequent inhibition of the TNF- α transduction mechanism.¹¹⁰

IFN- γ

IFN- γ is a protein produced by activated CD4⁺ and CD8⁺ T cells and, to a lesser degree, by natural killer cells.¹¹¹ IFN- γ is not produced by central nervous system cells, and its release at this level is possible only when a breakdown of the blood-brain barrier allows infiltration of lymphocytes into the brain parenchyma. Although the role of IFN- γ (and of all the IFNs) in brain ischemia has not been specifically addressed, blood-brain barrier damage and leukocyte penetration are among the first consequences of ischemic cerebral insults. Among many different functions, IFN- γ induces the expression of a variety of cytokines by stimulating p38 kinase¹¹⁰ and of class II major histocompatibility complex. Major histocompatibility complex is essential for macrophages to recognize antigen, and thus, IFN- γ could play a crucial role in the development of brain necrosis after an ischemic insult. Another possible role of IFN- γ in cerebral ischemia is the production of NO, with a consequent cytotoxic effect on brain cells; in vitro, IFN- γ stimulates the production of interferon regulatory factor-1, which induces NO synthase mRNA expression.¹¹²

Cell Adhesion Molecules in Cerebral Ischemia

Cell-Cell Adhesion

The adhesion of leukocytes to the endothelial surface and their subsequent migration from the microvessels into the brain parenchyma is mediated by a variety of molecules located on the surface of both leukocytes and endothelial cells. Adhesion molecules are conventionally divided into four main families, each of which has a different function: integrins, the immunoglobulin superfamily, cadherins, and selectins.¹¹³ Under normal conditions, there is little or no cell-surface expression of adhesion molecules¹¹⁴; their expression is induced by various inflammatory processes, such as cerebral ischemia, with the upregulation mediated by cytokines. Among the most studied adhesion molecules are ICAM-1 (immunoglobulin superfamily), which is located on the endothelial surface, and its leukocyte counterpart, integrin CD11/CD18; many others are currently under investigation. A number of animal studies have documented the upregulation of endothelial-leukocyte adhesion molecule 1 (also called E-selectin) in the microvessels,¹¹⁵⁻¹¹⁷ ICAM-1,¹¹⁸⁻¹²²

and P-selectin¹¹⁸ after focal cerebral ischemia in rodents and in nonhuman primates.

The possible relevance of adhesion molecules to the pathogenesis of ischemic brain damage has recently been corroborated by two studies demonstrating that, in comparison with normal controls, mice belonging to an ICAM-1-deficient strain show a marked reduction in cerebral infarction size after transient MCA occlusion.^{35,123} As reviewed by Feuerstein et al,⁷⁴ cytokines can also induce the in vitro expression of adhesion molecules in astrocytes, oligodendrocytes, and microglia. It is postulated that the presence of adhesion molecules on the surface of glial cells may facilitate the postischemic migration of leukocytes through the brain parenchyma.⁷⁴

One observation with potential clinical relevance is that the expression of adhesion molecules caused by administration of IL-1, TNF- α , and IFN- γ is higher in endothelial cell cultures from spontaneously hypertensive rats than in those derived from normotensive rats.¹²⁴ This finding suggests that ischemic injuries of comparable severity may lead to more severe consequences in hypertensive individuals.

Upregulation of adhesion molecules has been documented in human stroke patients. In a preliminary study, leukocytes from patients suffering an ischemic stroke or transient ischemic attack showed increased CD11a expression within 72 hours of the onset of symptoms in comparison with control subjects matched for age and risk factors.¹²⁵ Sobel et al¹²⁶ detected increased ICAM-1 expression on the surface of vessels from cerebral cortical infarcts in four patients. Soluble isoforms of adhesion molecules, which are believed to be shed from the surfaces of activated cells, can be quantified in serum: in comparison with normal control subjects, patients with acute stroke showed an initial increase in serum endothelial-leukocyte adhesion molecule-1 levels (up to 24 hours after stroke) and persistently increased levels of vascular cell adhesion molecule-1 (up to 5 days).¹²⁷ This temporal pattern is in line with the current view that selectins, such as endothelial-leukocyte adhesion molecule-1, mediate the initial low-affinity interaction between leukocytes and endothelial cells and promote the margination and rolling of leukocytes in the blood stream; subsequently, it is vascular cell adhesion molecule-1 (immunoglobulin superfamily) that causes the tight leukocyte-endothelial attachment and transendothelial migration.

When evaluating the levels of adhesion molecules in patients with cerebrovascular diseases, consideration should be given to the possible confounding effect of risk factors for atherosclerosis, a condition involving chronic inflammatory endothelial activation.¹²⁸ In acute ischemic stroke patients, serum ICAM-1 levels have been found to be lower than¹²⁹ or the same as¹²⁷ those of asymptomatic control subjects matched for age, sex, and a number of vascular risk factors. It can also be hypothesized that because of the long period (up to 72 hours) for enrolling patients, in one of these two studies,¹²⁹ the theoretical initial peak serum level of adhesion molecules could no longer be detected after they had bound to leukocytes and endothelial cells.

Cell-Matrix Adhesion

Another group of adhesion molecules is involved in cell-matrix interaction. Integrins, the most widely studied adhesion molecules of this group, are heterodimeric membrane glycoproteins formed by the combination of an α - and a β -subunit with an intracellular and an extracellular domain.¹¹³ At the basal membrane level, integrins connect endothelial cells to extracellular components, such as laminin and collagen. In the brain, endothelial cells, astrocytes, and the basal membrane contribute to form the blood-brain barrier, and their interconnection is mediated by integrins. Damage to these molecules may therefore lead to severe damage of the blood-brain barrier. Wagner et al¹³⁰ have demonstrated that integrin $\alpha_6\beta_4$, that under physiological conditions mediates the interaction between astrocytes and extracellular matrix, is rapidly damaged during focal cerebral ischemia/reperfusion. Other integrins play an important role in inflammatory neoangiogenesis, wound repair, and ontogenesis and may therefore be important for tissue repair after an ischemic insult. Among these, integrin $\alpha_v\beta_3$, a receptor for molecules sharing the common arginine-glycine-aspartic acid (RGD) sequence (eg, vitronectin, fibrinogen, fibronectin, and laminin), is expressed in basal ganglia microvessels in a nonhuman primate model of ischemia/reperfusion as early as 2 hours after MCA occlusion.¹³¹ The binding of ligand to integrins modifies the conformation of their intracellular domain so as to interfere with the cytoskeleton alignment, modify cellular structure, and confer on the cell the ability to migrate. Through these mechanisms, $\alpha_v\beta_3$ might play a role during the first stages of vascular reorganization after cerebral ischemia.

Chemokines in Cerebral Ischemia

As IL-1 β and TNF- α play a major role in promoting adhesion between endothelial cells and leukocytes, they are poor attractants for polymorphonuclear leukocytes and monocytes; other chemoattractant cytokines (the so-called chemokines) are believed to be specifically involved in guiding leukocytes through the parenchyma and toward the ischemic area.

Chemokines are low-molecular-weight molecules characterized by the presence, as a common structural pattern, of four cysteine residues and are divided into two main families (C-X-C and C-C chemokines) according to the presence or absence of an amino acid between the residues of the two most amino-proximal cysteines.³⁶ This structural distinction is reflected in vitro by a peculiar effect on different cell types: C-X-C chemokines tend to attract neutrophils, whereas C-C chemokines preferentially act on monocytes/macrophages. Each chemokine family binds to specific receptors formed by seven transmembrane domains that activate G proteins and subsequently an intracellular kinase cascade.¹³² Chemokine production and secretion are stimulated by a number of compounds, such as bacterial lipopolysaccharide, IL-1 α and -1 β , and TNF- α .³⁶

Few chemokines have so far been studied in some detail in experimental cerebral ischemia. Significant expression of CINC mRNA has been detected in the ischemic areas of spontaneously hypertensive rats 6 hours after permanent MCA occlusion¹³³; this expression peaks at 12 hours and

rapidly decreases at 24 hours. CINC has been shown to be homologous to three "gro" human proteins and "KC" in the mouse, and all of them are molecules acting predominantly as neutrophil chemoattractants.¹³⁴ In a model of rat transient focal ischemia, the first detectable level of CINC in the brain was observed 3 hours after reperfusion and preceded leukocyte infiltration.¹³⁵ In the sera of the same animals, a high concentration of CINC was found 60 minutes after MCA occlusion, with the peak concentration being reached 3 hours after reperfusion; a reduction in levels was observed between 6 and 48 hours.¹³⁵

The temporal expression of MCP-1 in brain ischemia follows that of CINC. High levels of MCP-1 mRNA have been found in the brains of rats with transient and permanent MCA occlusion at 6 hours, with the highest expression occurring between 12 hours and 2 days^{136,137}; increased MCP-1 expression was still detectable 5 days after permanent MCA occlusion.¹³⁶ The observations that in vitro IL-1 β and TNF- α induce MCP-1 gene expression¹³⁸ and that in vivo MCP-1 mRNA temporal expression follows that of IL-1 β and TNF- α mRNA^{45,67} suggest that IL-1 β and TNF- α induce MCP-1 expression in cerebral ischemia. According to Gourmal et al,¹³⁹ 6 hours to 2 days after MCA occlusion, MCP-1 mRNA is present in rat astrocytes surrounding the ischemic tissue. After 4 days, MCP-1 mRNA is found in macrophages and microglial cells in the infarcted tissue.

The mRNA of another member of the C-C chemokine family, MIP-1 α , has been found to be overexpressed in cerebral ischemic areas.¹³⁷ This chemokine attracts monocytes and macrophages and modulates their activity in tissue undergoing an inflammatory process. Kim et al¹³⁷ found that the temporal expression of MIP-1 α parallels that of MCP-1 and that the distribution of MIP-1 α -positive cells was similar to that of activated astrocytes. MIP-1 α infused into the subarachnoid space of rabbits treated with Gram-negative bacteria initially attracts neutrophils and subsequently monocytes.¹⁴⁰ If this sequence also holds true in cerebral ischemia, this molecule could be in part responsible for the switch from a leukocyte- to a macrophage-based inflammatory response. The temporal profile of CINC, MCP-1, and MIP-1 α expression is in line with that of leukocyte accumulation in the ischemic brain parenchyma of nonhuman primates. In these models, polymorphonuclear cells are detected 24 to 72 hours after the onset of ischemia, followed at 7 to 16 days by monocyte and macrophage infiltration.^{9,13}

In vitro, smooth muscle cells stimulated by IFN and IL-1 β or TNF- α produce IFN-inducible protein-10, which is a chemoattractant for macrophages and activated T lymphocytes.¹⁴¹ Inducible protein-10 mRNA expression has been demonstrated in the rat after endothelial damage by balloon angioplasty.¹⁴¹ Because endothelial damage occurs during brain ischemia, it seems possible that this molecule could also play a role in this latter pathological condition.

The number of discovered chemokines is continuously growing, and so far, more than 20 members of this cytokine family have been identified. It is likely that in the future, the activity of other chemokines may be found to be increased after cerebral ischemia and their function elucidated.

Experimental Anti-Leukocyte Interventions

On the basis of the progress made in our understanding of inflammatory-like mechanisms in cerebral ischemia, an increasing number of molecules are currently being investigated in animals for their possible effectiveness in human acute stroke.

One group of studies has focused on therapeutic strategies related to the role of proinflammatory cytokines. The intraventricular and systemic administration of IL-1 receptor antagonist into rats reduces the volume of infarction caused by MCA occlusion^{54,59,62,64} or the ligation of one carotid artery associated with hypoxia.⁶¹ This reduction in infarct size is accompanied by a decreased number of leukocytes in the ischemic hemisphere and improved neurological function.⁶² Similar results have been achieved by means of the topical application of anti-IL-1 β neutralizing antibody,⁵³ zinc protoporphyrin,^{53,60,63} and fragments of lipocortin-1,⁵⁸ all of which act as IL-1 inhibitors. TGF- β administration has led to less severe histological damage in a rabbit model of embolic stroke¹⁰⁰ as well as in rats subjected to permanent MCA occlusion,¹⁰¹ transient global ischemia,¹⁰⁴ and hypoxia-ischemia cerebral insult.¹⁰³

A second group of studies has concentrated on molecules that are capable of blocking the adhesion between endothelial cells and leukocytes. The administration of anti-CD11b/CD18 monoclonal antibodies at various times after reperfusion reduces infarct volume in rats with MCA occlusion^{142,143} in a dose-dependent manner,¹⁴⁴ although single administration of the same drug 1 hour after permanent MCA occlusion led to less striking effects.¹⁴⁵ Treatment with antibodies against ICAM-1 or integrin CD11b/CD18 is also capable of reducing the number of apoptotic cells in the ischemic brain area.¹⁴⁶

The use of anti-ICAM-1 antibodies reduces infarct volume and the number of tissue polymorphonuclear leukocytes in rats with transient MCA occlusion,^{147,148} but the treatment is ineffective when administered to animals with permanent occlusion.¹⁴⁹ The same dichotomy between transient and permanent ischemia has been shown in one model of spinal cord ischemia.¹⁵⁰ These observations suggest that drugs blocking leukocyte-endothelial adhesion are effective only in the presence of reperfusion.

Because monoclonal antibodies are immunogenic and might have collateral effects in stroke patients, new nonimmunogenic molecules are now being tested in animal models with encouraging results.^{151,152} These are peptides or glycoproteins, which are produced by bacteria and which structurally or functionally mimic cell adhesion molecules and inhibit leukocyte function.

Conclusions

Leukocytes and Inflammatory Mediators in Cerebral Ischemia

The studies reviewed in this article emphasize the possible role of cytokines and cell adhesion molecules in the development of cerebral damage caused by an ischemic insult. Early overexpression of these inflammatory mediators promotes the recruitment of leukocytes in the ischemic area and represents a key mechanism for the evolution of tissue

damage. Leukocytes are in fact believed to have a deleterious effect in brain ischemia. In the microvessels, they first adhere to endothelial cells, interfering with local cerebral blood flow and enhancing the ischemic insult. Subsequently, leukocytes proceed through the endothelial lining and accumulate in the ischemic area, where they release a number of toxic molecules that contribute to the development of an infarction.

Relevance of Animal Models

Most of the evidence comes from animal studies; only preliminary observations relating to humans are available. It is plausible that our knowledge of the role of inflammation in human stroke will considerably expand in the future, in terms of both new molecules and a more precise definition of their action, but it is likely that animal models will continue to represent a fundamental source of information. The possibility that leukocyte alterations in experimental models may be determined by the surgical procedures used to induce the ischemic insult or by anesthesia has been refuted in a nonhuman primate model.¹⁵³ Moreover, the use of sham-operated animals (ie, animals in which all of the phases of the surgical procedure except artery occlusion are reproduced) makes it possible to control for the influence of surgery and anesthesia. Some of the substantial advantages of experimental models are the following: (1) The possibility of knowing the exact time of onset of ischemia means that the temporal pattern of the expression of the molecules under study can be investigated; (2) Access to brain tissue for pathological observation is simple; (3) New drugs can be tested. Nevertheless, it should be borne in mind that most of the conclusions are based on rodent experiments because data from nonhuman primate models (which are probably of greater relevance to human disease) are still scarce.

Therapeutic Perspectives

Acute stroke therapy is probably destined to change over the next few years. One of the crucial turning points will be definition of the time interval during which the administration of drugs is likely to be efficacious (therapeutic window), which is not easy because of individual patient variability. Most of the trials carried out so far suggest a very narrow (3 hours) therapeutic window, which in the case of thrombolytic agents, is due more to the increased occurrence of hemorrhagic transformation than a lack of efficacy beyond this limit. Animal and human studies have shown that the evolution of a brain infarct progresses over a longer period of time,^{23,24,154,155} and so the reopening of an artery could also be advantageous at a later time.

New drugs counteracting cytokine-mediated damage or opposing leukocyte-endothelial cell adhesion are already being investigated in animals with encouraging results. One perspective for the use of drugs capable of interfering with inflammation-related mechanisms is the possibility of widening the therapeutic window; in a rabbit model of embolic stroke, administration of anti-ICAM-1 antibodies has been shown to extend the time during which the thrombolytic agent was effective in dissolving blood clots.¹⁵⁶ The timing of arrival of many stroke patients to the emergency department¹⁵⁷ seems compatible with potential drug interventions

designed to interfere with inflammatory mediators and the natural evolution of the ischemic lesion. The inflammatory response of the cerebral parenchyma, with the above-discussed harmful implications, develops over days after the onset of ischemia in the animal,²⁰ and this is probably also true in humans.¹² Therefore, these therapeutic strategies could theoretically be undertaken far beyond the strict time limit of thrombolysis with some beneficial effects.

Possible future pharmacological treatments could be based on the inhibition of proinflammatory mediators (perhaps IL-1 and TNF- α) or enhancement of the effect of others (IL-6 and TGF- β). Some cytokines and chemokines, such as IFN- γ and MIP-1, seem to play a role in the passage from the first phase of the inflammatory response, characterized by the presence of polymorphonuclear cells, to the second, with monocyte and macrophage invasion and the development of frank necrosis. Blocking these molecules could prevent part of the brain parenchyma from becoming necrotic. Interfering with adhesion between leukocytes and endothelial cells represents a second therapeutic option. On the other hand, attempts could be made to potentiate the role of integrins that promote cell remodeling and neovascularization. Other targets for a possible pharmacological approach are the specific transduction pathway signals (eg, intracytoplasmic kinases) that are critical for cytokine production and their effects.

Caveats and Limitations

An understanding of the role of leukocytes and the mediators of inflammation in cerebral ischemia may have a very great impact on therapy, but a few notes of caution should be outlined. Although it currently seems that some cytokines, such as IL-1, have a detrimental effect and that others, such as TGF- β and IL-6, might be protective in some way, the precise effect of each mediator is still not completely known. Moreover, some data exist challenging the view that leukocytes are active in favoring the progression from cerebral ischemia to necrosis.¹⁵⁸⁻¹⁶⁰

The expectations aroused by animal studies have been somewhat dampened by the results of the first human trial using an anti-ICAM-1 murine monoclonal antibody (Enlimomab, Boehringer Ingelheim). In this double-blind, placebo-controlled trial, 625 patients with acute ischemic stroke were randomized within the first 6 hours of symptom onset to receive either anti-ICAM-1 antibodies (160 mg IV the first day, followed by 40 mg/d for 2 to 5 days after onset) or placebo.¹⁶¹ The 90-day outcome as measured by the modified Rankin Scale showed an improvement in 33% of the patients on placebo versus 27% of those receiving active treatment. Side effects (mainly fever, infections, and pneumonia) were recorded in 44% of the Enlimomab and 30% of the placebo patients; serious adverse effects (stroke progression, brain edema, and hemorrhagic transformation of the infarction) were observed in 22% of the Enlimomab versus 16% of the placebo patients; both of these differences were statistically significant. Moreover, the occurrence of cases of aseptic meningitis in the Enlimomab group underlines the limitations due to the immunogenic effect of this drug.

Is There Still a Role for Anti-Leukocytes Interventions in Human Stroke?

However, before setting aside anti-ICAM-1 antibodies as another ineffective drug in acute ischemic stroke, the preliminary results of the Enlimomab study should be critically considered. First of all, anti-leukocyte interventions appear to be particularly effective against reperfusion injury. Anti-ICAM-1 antibodies have been tested and proved efficacious in models of transient^{146-148,150} but not permanent¹⁴⁹ focal ischemia, presumably the condition of most of the patients enrolled in the Enlimomab trial. As shown by Bowes et al,¹⁵⁶ the use of anti-ICAM-1 might be beneficial only in combination with thrombolysis. Second, the time and route of drug administration could be crucial: in none of the reviewed animal studies was the first dose of anti-ICAM-1 antibodies delayed beyond 1 hour after reperfusion, and systemic administration could lead to a reduction in host defenses and a predisposition to infections. Finally, given the increased frequency of fever and aseptic meningitis among the treated patients, the immunogenic role of anti-ICAM-1 antibodies needs to be weighed very carefully.

In the light of the above considerations, among others, a multitherapeutic approach for ischemic stroke can be foreseen.¹⁶² The testing of new anti-leukocyte drugs in humans probably requires further elucidation of the pathophysiological role that these cells play during cerebral ischemia. At present, it would be dangerous to simply dismiss those drugs that may prove to be efficacious in different target populations.

Acknowledgment

The authors thank Thomas DeGraba, MD (National Institute of Neurological Disorders and Stroke, Stroke Branch, National Institutes of Health, Bethesda, Md) for his helpful revision of the manuscript.

References

1. Riggs JE. Tissue-type plasminogen activator should not be used in acute ischemic stroke. *Arch Neurol.* 1996;53:1306-1308.
2. Furlan AJ, Kanot G. When is thrombolysis justified in patients with acute ischemic stroke? A bioethical perspective. *Stroke.* 1997;28:214-218.
3. The National Institute of Neurological Disorders and Stroke rt-PA Stroke Study Group. Tissue plasminogen activator for acute ischemic stroke. *N Engl J Med.* 1995;333:1581-1587.
4. Wardlaw JM, Warlow CP, Counsell C. Systematic review of evidence on thrombolytic therapy for acute ischaemic stroke. *Lancet.* 1997;350:607-614.
5. Syrjänen J, Valtonen VV, Iivanainen M, Kaste M, Huttunen JK. Preceding infection as an important risk factor for ischaemic brain infarction in young and middle aged patients. *BMJ.* 1988;296:1156-1160.
6. Grau AJ, Bugge F, Heindl S, Steichen-Wiehn C, Banerjee T, Mainwald M, Rohlf M, Suhr H, Fiehn W, Becher H, Hacke W. Recent infection as a risk factor for cerebrovascular ischemia. *Stroke.* 1995;26:373-379.
7. Macko RF, Ameriso SF, Barndt R, Clough W, Weiner JM, Fisher M. Precipitants of brain infarction: roles of preceding infection/inflammation and recent psychological stress. *Stroke.* 1996;27:1999-2004.
8. Bova IV, Bornstein NM, Korczyn AD. Acute infection as a risk factor for ischemic stroke. *Stroke.* 1996;27:2204-2206.
9. Kochanek PM, Hallenbeck JM. Polymorphonuclear leukocytes and monocytes/macrophages in the pathogenesis of cerebral ischemia and stroke. *Stroke.* 1992;23:1367-1379.
10. Sörnäs R, Ostlund H, Müller R. Cerebrospinal fluid cytology after stroke. *Arch Neurol.* 1972;26:489-501.

11. Akopov SE, Simonian NA, Grigorian GS. Dynamics of polymorphonuclear leukocyte accumulation in acute cerebral infarction and their correlation with brain tissue damage. *Stroke*. 1996;27:1739-1743.
12. Chuaqui R, Tapia J. Histologic assessment of the age of recent brain infarcts in man. *J Neuropathol Exp Neurol*. 1993;52:481-489.
13. Garcia JH, Kamijyo Y. Cerebral infarction: evolution of histopathological changes after occlusion of a middle cerebral artery in primates. *J Neuropathol Exp Neurol*. 1974;33:408-421.
14. Hallenbeck JM, Dutka AL, Tanishima T, Kochanek PM, Kumaroo KK, Thompson CB, Obrenovitch TP, Contreras TJ. Polymorphonuclear leukocyte accumulation in brain regions with low blood flow during the early posts ischemic period. *Stroke*. 1986;17:246-253.
15. Barone FC, Hillegas LM, Price WJ, White RF, Lee EV, Feuerstein GZ, Sarau HM, Clark RK, Griswold DE. Polymorphonuclear leukocyte infiltration into cerebral focal ischemic tissue: myeloperoxidase activity assay and histologic verification. *J Neurosci Res*. 1991;29:336-345.
16. del Zoppo GJ, Schmidt-Schönbein GW, Mori E, Copeland BR, Chang CM. Polymorphonuclear leukocytes occlude capillaries following middle cerebral artery occlusion and reperfusion in baboons. *Stroke*. 1991;22:1276-1283.
17. Barone FC, Schmidt DB, Hillegas LM, Price WJ, White RF, Feuerstein GZ, Clark RK, Lee EV, Griswold DE, Sarau HM. Reperfusion increases neutrophils and leukotriene B₄ receptor binding in rat focal ischemia. *Stroke*. 1992;23:1337-1348.
18. Dereski MO, Chopp M, Knight RA, Chen H, Garcia JH. Focal cerebral ischemia in the rat: temporal profile of neutrophil responses. *Neurosci Res Commun*. 1992;11:179-186.
19. Clark RK, Lee EV, Fish CJ, White RF, Price WJ, Jonak ZL, Feuerstein GZ, Barone C. Development of tissue damage, inflammation and resolution following stroke: an immunohistochemical and quantitative planimetric study. *Brain Res Bull*. 1993;31:565-572.
20. Clark RK, Lee EV, White RF, Jonak ZL, Feuerstein GZ, Barone FC. Reperfusion following focal stroke hastens inflammation and resolution of ischemic injury. *Brain Res Bull*. 1994;35:387-392.
21. Zhang R-L, Chopp M, Chen H, Garcia JH. Temporal profile of ischemic tissue damage, neutrophil response, and vascular plugging following permanent and transient (2H) middle cerebral artery occlusion in the rat. *J Neurol Sci*. 1994;125:3-10.
22. Garcia JH, Liu K-F, Yoshida Y, Lian J, Chen S, del Zoppo GJ. Influx of leukocytes and platelets in an evolving brain infarct (Wistar rat). *Am J Pathol*. 1994;144:188-199.
23. Garcia JH, Yoshida Y, Chen H, Li Y, Zhang ZG, Lian J, Chen S, Chopp M. Progression from ischemic injury to infarct: following middle cerebral artery occlusion in the rat. *Am J Pathol*. 1993;142:623-635.
24. Garcia JH, Liu K-F, Ho K-L. Neuronal necrosis after middle cerebral artery occlusion in Wistar rats progresses at different time intervals in the caudoputamen and the cortex. *Stroke*. 1995;26:636-643.
25. Ames A, Wright LW, Kowade M, Thurston JM, Majors G. Cerebral ischemia, II: the no-reflow phenomenon. *Am J Pathol*. 1968;52:437-453.
26. Schmid-Schönbein GW, Usami S, Skalak R, Chien S. The interaction of leukocytes and erythrocytes in capillary and postcapillary. *Microvasc Res*. 1980;19:45-70.
27. Sutton DW, Schmid-Schönbein GW. Elevation of organ resistance due to leukocyte perfusion. *Am J Physiol*. 1992;262:H1648-H1650.
28. Härtl R, Schürer L, Schmid-Schönbein GW, del Zoppo G. Experimental antileukocyte interventions in cerebral ischemia. *J Cereb Blood Flow Metab*. 1996;16:1108-1119.
29. Hamann GF, del Zoppo GJ. Leukocyte involvement in vasomotor reactivity of the cerebral vasculature. *Stroke*. 1994;25:2117-2119.
30. Hamann GF, Okada Y, Fritridge R, del Zoppo GJ. Microvascular basal lamina antigens disappear during cerebral ischemia and reperfusion. *Stroke*. 1995;26:2120-2126.
31. Hamann GF, Okada Y, del Zoppo GJ. Hemorrhagic transformation and microvascular integrity during focal cerebral ischemia/reperfusion. *J Cereb Blood Flow Metab*. 1996;16:1373-1378.
32. Bednar MM, Raymond S, McAuliffe T, Lodge PA, Gross CG. The role of neutrophils and platelets in a rabbit model of thromboembolic stroke. *Stroke*. 1991;22:44-50.
33. Chen H, Chopp M, Bodzin G. Neutropenia reduces the volume of cerebral infarct after transient middle cerebral occlusion in the rat. *Neurosci Res Commun*. 1992;11:93-99.
34. Matsuo Y, Onodera H, Shiga Y, Nakamura M, Ninomiya M, Kihara T, Kogure K. Correlation between myeloperoxidase-quantified neutrophil accumulation and ischemic brain injury in the rat: effects of neutrophil depletion. *Stroke*. 1994;25:1469-1475.
35. Connolly ES Jr, Winfree CJ, Springer TA, Naka Y, Liao H, Yan SD, Stern DM, Solomon RA, Gutierrez-Ramos J-C, Pinsky DJ. Cerebral protection in homozygous null ICAM-1 mice after middle cerebral artery occlusion: role of neutrophil adhesion in the pathogenesis of stroke. *J Clin Invest*. 1996;97:209-216.
36. Furie MB, Randolph GJ. Chemokines and tissue injury. *Am J Pathol*. 1995;146:1287-1301.
37. Howard MC, Miyajima A, Coffmann R. T-cell-derived cytokines and their receptors. In: We P, ed. *Fundamental Immunology*. 3rd ed. New York, NY: Raven Press Ltd; 1993:763-800.
38. Fontana A, Kristensen F, Dubi R, Gerns D, Weber E. Production of prostaglandin E and interleukin-1 like factor by cultured astrocytes and C6 glioma cells. *J Immunol*. 1982;129:2413-2418.
39. Giuliani D, Baker TJ, Shih LN, Lachman LB. Interleukin-1 of central nervous system is produced by ameboid microglia. *J Exp Med*. 1986;164:594-604.
40. Lechan RM, Clark TBD, Cannon JG, Shaw AR, Dinarello CA, Reichlin S. Immunoreactive IL-1 β localization in the rat forebrain. *Brain Res*. 1990;514:135-140.
41. Tomimoto H, Akiguchi I, Wakita H, Kinoshita A, Ikemoto A, Nakamura S, Kimura J. Glial expression of cytokines in the brains of cerebrovascular disease patients. *Acta Neuropathol (Berl)*. 1996;92:281-287.
42. Bevilacqua MP, Pober JS, Majeau GR, Cotran RS, Gimbrone MA Jr. Interleukin 1 (IL-1) induces biosynthesis and cell surface expression of procoagulant activity in human vascular endothelial cells. *J Exp Med*. 1984;160:618-623.
43. Conway EM, Bach R, Rosenberg RD, Konigsberg WH. Tumor necrosis factor enhances expression of tissue factor mRNA in endothelial cells. *Thromb Res*. 1989;53:231-241.
44. Nawroth PP, Handley DA, Esmon CT, Stern DM. Interleukin-1 induces endothelial cell procoagulant while suppressing cell-surface anticoagulant activity. *Proc Natl Acad Sci U S A*. 1986;83:3460-3464.
45. Liu T, McDonnell PC, Young PR, White RF, Siren AL, Hallenbeck JM, Barone FC, Feuerstein GZ. Interleukin-1 β mRNA expression in ischemic rat cortex. *Stroke*. 1993;24:1746-1751.
46. Butini M, Sauter A, Boddeke HWGM. Induction of interleukin-1 β mRNA after focal cerebral ischemia in the rat. *Mol Brain Res*. 1994;23:126-134.
47. Minami M, Kuraishi Y, Yabuuchi K, Yamazaki A, Satoh M. Induction of interleukin-1 β mRNA in rat brain after transient forebrain ischemia. *J Neurochem*. 1992;58:390-392.
48. Wiessner C, Gehrmann J, Lindholm D, Topper R, Kreutzberg GW, Hossmann KA. Expression of transforming growth factor-beta 1 and interleukin-1 beta mRNA in rat brain following transient forebrain ischemia. *Acta Neuropathol (Berl)*. 1993;86:439-446.
49. Yabuuchi K, Minami M, Katsumata S, Yamazaki A, Satoh M. An in situ hybridization study on interleukin-1 β mRNA induced by transient forebrain ischemia in the rat brain. *Mol Brain Res*. 1994;26:135-142.
50. Yoshimoto T, Houkin K, Tada M, Abe H. Induction of cytokines, chemokines, and adhesion molecule mRNA in a rat forebrain reperfusion model. *Acta Neuropathol (Berl)*. 1997;93:154-158.
51. Szaflarski J, Burtrum D, Silverstein FS. Cerebral hypoxia-ischemia stimulates cytokine gene expression in perinatal rats. *Stroke*. 1995;26:1093-1100.
52. Fassbender K, Rossol S, Kammer T, Daffertshofer M, Wirth S, Dollman M, Hennerici M. Proinflammatory cytokines in serum of patients with acute cerebral ischemia: kinetics of secretion and relation to the extent of brain damage and outcome disease. *J Neurol Sci*. 1994;122:135-139.
53. Yamasaki Y, Matsuura N, Shozuhara H, Onodera H, Itoyama Y, Kogure K. Interleukin-1 as a pathogenetic mediator of ischemic brain damage in rats. *Stroke*. 1995;26:676-681.
54. Loddick SA, Rothwell NJ. Neuroprotective effects of human recombinant interleukin-1 receptor antagonist in focal cerebral ischaemia in the rat. *J Cereb Blood Flow Metab*. 1996;16:932-940.
55. Wang X, Barone FC, Aiyar NV, Feuerstein GZ. Interleukin-1 receptor antagonist gene expression after focal stroke in rats. *Stroke*. 1997;28:155-162.
56. Dinarello CA. Interleukin-1 and interleukin-1 antagonism. *Blood*. 1991;77:1627-1652.
57. Muegge K, Williams TM, Kant J, Karin M, Chiu R, Schmidt A, Siebenlist U, Young HA, Durum SK. Interleukin-1 costimulatory activity on the interleukin-2 promoter via AP-1. *Science*. 1989;246:249-251.

58. Relton JK, Strijbos PJLM, O'Shaughnessy CT, Carey F, Forder RA, Tilders FJH, Rothwell NJ. Lipocortin-1 is an endogenous inhibitor of ischemic damage in the rat brain. *J Exp Med*. 1991;174:305-310.
59. Relton JK, Rothwell NJ. Interleukin-1 receptor antagonist inhibits ischaemic and excitotoxic neuronal damage in the rat. *Brain Res Bull*. 1992;29:243-246.
60. Yamasaki Y, Suzuki T, Yamaya H, Matsuura N, Onodera H, Kogure K. Possible involvement of interleukin-1 in ischemic brain edema formation. *Neurosci Lett*. 1992;142:45-47.
61. Martin D, Chinookoswong N, Miller G. The interleukin-1 receptor antagonist (rhIL-1ra) protects against cerebral infarction in a rat model of hypoxia-ischemia. *Exp Neurol*. 1994;130:362-367.
62. Garcia JH, Liu K-F, Relton JK. Interleukin-1 receptor antagonist decreases the number of necrotic neurons in rats with middle cerebral artery occlusion. *Am J Pathol*. 1995;147:1477-1486.
63. Kadoya C, Domino EF, Yang GY, Stern JD, Betz AL. Preischemic but not postischemic zinc protoporphyrin treatment reduces infarct size and edema accumulation after temporary focal cerebral ischemia in rats. *Stroke*. 1995;26:1035-1038.
64. Relton JK, Martin D, Thompson RC, Russell DA. Peripheral administration of interleukin-1 receptor antagonist inhibits brain damage after focal cerebral ischemia in the rat. *Exp Neurol*. 1996;138:206-213.
65. Rothwell NJ, Relton JK. Involvement of interleukin-1 and lipocortin-1 in ischemic brain damage. *Cerebrovasc Brain Metab Rev*. 1993;5:178-198.
66. Wang X, Yue TL, Barone FC, White RF, Gagnon RC, Feuerstein GZ. Concomitant cortical expression of TNF- α and IL-1 β mRNA follows early response gene expression in transient focal ischemia. *Mol Chem Neuropathol*. 1994;23:103-114.
67. Liu T, Clark RK, McDonnell PC, Young PR, White RF, Barone FC, Feuerstein GZ. Tumor necrosis factor- α expression in ischemic neurons. *Stroke*. 1994;25:1481-1488.
68. Elneihoum AM, Falke P, Axelsson L, Lundberg E, Lindgärde F, Ohlsson K. Leukocyte activation detected by increased plasma levels of inflammatory mediators in patients with ischemic cerebrovascular diseases. *Stroke*. 1996;27:1734-1738.
69. Smith CA, Farrah T, Goodwin RG. The TNF receptor superfamily of cellular and viral proteins: activation, costimulation, and death. *Cell*. 1994;76:959-962.
70. Kolesnick R, Golde DW. The sphingomyelin pathway in tumor necrosis factor and interleukin-1 signaling. *Cell*. 1994;77:321-328.
71. Davis RJ. MAPKs: new JNK expands the group. *Trends Biochem Sci*. 1994;19:470-473.
72. Blumberg PM, Johnson GL. Diversity in function and regulation of MAP kinase pathways. *Trends Biochem Sci*. 1994;19:236-240.
73. Heller RA, Konkre M. Tumor necrosis factor receptor-mediated signaling pathways. *J Cell Biol*. 1994;126:5-9.
74. Feuerstein GZ, Liu T, Barone FC. Cytokines, inflammation, and brain injury: role of tumor necrosis factor- α . *Cerebrovasc Brain Metab Rev*. 1994;6:341-360.
75. Barone FC, Arvin B, White RF, Miller A, Webb CL, Willette RN, Lysko PG, Feuerstein GZ. Tumor necrosis factor- α : a mediator of focal ischemic brain injury. *Stroke*. 1997;28:1233-1244.
76. Nawashiro H, Martin D, Hallenbeck JM. Inhibition of tumor necrosis factor and amelioration of brain infarction in mice. *J Cereb Blood Flow Metab*. 1997;17:229-232.
77. Nawashiro H, Tasaki K, Ruetzler CA, Hallenbeck JM. TNF- α pretreatment induces protective effects against focal cerebral ischemia in mice. *J Cereb Blood Flow Metab*. 1997;17:483-490.
78. Bruce AJ, Boling W, Kindy MS, Peshon J, Kraemer PJ, Carpenter MK, Holtberg FW, Mattson MP. Altered neuronal and microglial responses to excitotoxic and ischemic brain injury in mice lacking TNF receptors. *Nat Med*. 1996;2:788-794.
79. Vidman TR, Carpen O, Paetau A, Karjalainen-Lindsberg M-L, Lindsberg PJ. Production of tumor necrosis factor- α (TNF- α) in infarcted human brain. *Stroke*. 1997;28:255. Abstract.
80. Hirano T. The biology of interleukin-6. *Chem Immunol*. 1992;51:153-180.
81. Akira S, Taga T, Kishimoto T. Interleukin-6 in biology and medicine. *Adv Immunol*. 1993;54:1-78.
82. McClain C, Cohen D, Phillips R, Ott L, Young B. Increased plasma and ventricular fluid interleukin-6 levels in patients with head injury. *J Lab Clin Med*. 1991;118:225-231.
83. Woodroffe MN, Sarna GS, Wadhwa M, Hayes JM, Loughlin AJ, Tinker A, Cuzner ML. Detection of interleukin-1 and interleukin-6 in adult rat brain, following mechanical injury, by in vivo microdialysis: evidence of a role for microglia in cytokine production. *J Neuroimmunol*. 1991;33:227-236.
84. Yan HQ, Banos MA, Herregodts P, Hooghe R, Hooghe-Peters EL. Expression of interleukin (IL)-1 β , IL-6 and their respective receptors in the normal rat brain after injury. *Eur J Immunol*. 1992;22:2963-2971.
85. Mathiesen T, Andersson B, Loftén A, von Holst H. Increased interleukin-6 levels in cerebrospinal fluid following subarachnoid hemorrhage. *J Neurosurg*. 1993;78:562-567.
86. Wang X, Yue TL, Young PR, Barone FC, Feuerstein GZ. Expression of interleukin-6, c-fos, and zif268 mRNA in rat ischemic cortex. *J Cereb Blood Flow Metab*. 1995;15:166-171.
87. Beamer NB, Coull BM, Clark WM, Hazel JS, Silberger JR. Interleukin-6 and interleukin-1 receptor antagonist in acute stroke. *Ann Neurol*. 1995;37:800-805.
88. Tarkowski E, Rosengren L, Blomstrand C, Wikkelö C, Jensen C, Ekholm S, Tarkowski A. Early intrathecal production of interleukin-6 predicts the size of brain lesion in stroke. *Stroke*. 1995;26:1393-1398.
89. Kim JS, Yoon SS, Kim YH, Ryu JS. Serial measurement of interleukin-6, transforming growth factor- β , and S-100 protein in patients with acute stroke. *Stroke*. 1996;27:1553-1557.
90. Tilg H, Trehu E, Atkins MB, Dinarello CA, Mier JW. Interleukin-6 (IL-6) as an anti-inflammatory cytokine: induction of circulating IL-1 receptor antagonist and soluble tumor necrosis factor receptor p55. *Blood*. 1994;83:113-118.
91. Salas MA, Evans SW, Levell MJ, Whicher JT. Interleukin-6 and ACTH act synergistically to stimulate the release of corticosterone from adrenal gland cells. *Clin Exp Immunol*. 1990;79:470-473.
92. Jones TH. Interleukin-6 an endocrine cytokine. *Clin Endocrinol (Oxf)*. 1994;40:703-713.
93. Geiger T, Andus T, Klapproth J, Hirano T, Kishimoto T, Heinrich PC. Induction of rat acute-phase proteins by interleukin-6 in vivo. *Eur J Immunol*. 1988;18:717-721.
94. Heinrich PC, Castell JV, Andus T. Interleukin-6 and the acute phase response. *Biochem J*. 1990;265:621-636.
95. Crowl RM, Stoller TJ, Conroy RR, Stoner CR. Induction of phospholipase A2 gene expression in human hepatoma cells by mediators of the acute phase response. *J Biol Chem*. 1991;266:2647-2651.
96. Raichle ME. The pathophysiology of brain ischemia. *Ann Neurol*. 1983;13:2-10.
97. Wahl SM. Transforming growth factor beta (TGF- β) in inflammation: a cause and a cure. *J Clin Immunol*. 1992;12:61-74.
98. Lehrmann E, Kiefer R, Finsen B, Diemer NH, Zimmer J, Hartung HP. Cytokines in cerebral ischemia: expression of transforming growth factor beta-1 (TGF- β 1) mRNA in the postischemic adult rat hippocampus. *Exp Neurol*. 1995;131:114-123.
99. Krupinski J, Kumar P, Kumar S, Path FRC, Kaluza J. Increased expression of TGF- β 1 in brain tissue after ischemic stroke in humans. *Stroke*. 1996;27:852-857.
100. Gross CE, Bednar MM, Howard DB, Sporn MB. Transforming growth factor- β 1 reduces infarct size after experimental cerebral ischemia in a rabbit model. *Stroke*. 1993;24:558-562.
101. Prehn JH, Backhaus C, Kriegstein J. Transforming growth factor-beta 1 prevents glutamate neurotoxicity in rat neocortical cultures and protects mouse neocortex from ischemic injury in vivo. *J Cereb Blood Flow Metab*. 1993;13:521-525.
102. Gross CE, Howard DB, Dooley RH, Raymond SJ, Fuller S, Bednar MM. TGF- β 1 post-treatment in a rabbit model of cerebral ischemia. *Neuro Res*. 1994;16:465-470.
103. McNeill H, Williams C, Guan J, Dragunow M, Lawlor P, Sirimanee E, Nikolic K, Gluckman P. Neuronal rescue with transforming growth factor-beta 1 after hypoxic-ischaemic brain injury. *Neuroreport*. 1994;14:901-904.
104. Henrich-Noack P, Prehn JHM, Kriegstein J. TGF- β 1 protects hippocampal neurons against degeneration caused by transient global ischemia: dose-response relationship and potential neuroprotective mechanisms. *Stroke*. 1996;27:1609-1615.
105. Gamble JR, Vadas MA. Endothelial adhesiveness for blood neutrophils is inhibited by transforming growth factor- β . *Science*. 1988;242:97-99.
106. Tsunawaki S, Sporn M, Ding A, Nathan C. Deactivation of macrophages by transforming growth factor- β . *Nature*. 1988;334:260-262.
107. Ding A, Nathan CF, Graycar J, Derynck R, Stuehr DJ, Srinivasan S. Macrophage deactivating factor and transforming growth factors- β 1, - β 2, - β 3 inhibit induction of macrophage nitrogen oxide synthesis by IFN- γ . *J Immunol*. 1990;145:940-944.

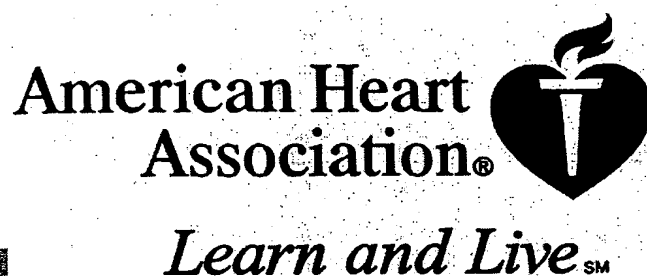
108. Lieberman AP, Pitha PM, Shin HS, Shin ML. Production of tumor necrosis factor and other cytokines by astrocytes stimulated with lipopolysaccharide or a neurotropic virus. *Proc Natl Acad Sci U S A*. 1989; 86:6348-6352.
109. Lefer AM, Tsao P, Aoki N, Palladino MA Jr. Mediation of cardioprotection by transforming growth factor- β . *Science*. 1990;249:61-64.
110. Rose DM, Winston BW, Chan ED, Riches DWH, Henson PM. Interferon- γ and transforming growth factor- β modulate the activation of mitogen-activated protein kinases and tumor necrosis factor- α production induced by Fc γ -receptor stimulation in murine macrophages. *Biochem Biophys Res Commun*. 1997;238:256-260.
111. Ijzermans JNM, Marquet RL. Interferon-gamma: a review. *Immunobiology*. 1989;179:456-473.
112. Kamijo R, Harada H, Matsuyama T, Bosland M, Gerecitano J, Shapiro D, Le J, Koh SI, Kimura T, Green SJ, Mak TW, Taniguchi T, Vilcek J. Requirement for transcription factor IRF-1 in NO synthase induction in macrophages. *Science*. 1994;263:1612-1615.
113. Frenette PS, Wagner DD. Adhesion molecules, part I. *N Engl J Med*. 1996;334:1526-1529.
114. Osborn L. Leukocyte adhesion to endothelium in inflammation. *Cell*. 1990;62:3-6.
115. Wang X, Yue TL, Barone FC, Feuerstein GZ. Demonstration of increased endothelial-leukocyte adhesion molecule-1 mRNA expression in rat ischemic cortex. *Stroke*. 1995;26:1665-1669.
116. Haring H-P, Berg EL, Tsurushita N, Tagaya M, del Zoppo GJ. E-selectin appears in nonischemic tissue during experimental focal cerebral ischemia. *Stroke*. 1996;27:1386-1392.
117. Zhang RL, Chopp M, Zhang ZG, Phillips ML, Rosenbloom CL, Cruz R, Manning A. E-selectin on focal cerebral ischemia and reperfusion in the rat. *J Cereb Blood Flow Metab*. 1996;16:1126-1136.
118. Okada Y, Copeland BR, Mori E, Tung MM, Thomas WS, del Zoppo GJ. P-selectin and intercellular adhesion molecule-1 expression after focal brain ischemia and reperfusion. *Stroke*. 1994;25:202-211.
119. Wang X, Siren A-L, Liu Y, Yue T-L, Barone FC, Feuerstein GZ. Upregulation of intercellular adhesion molecule 1 (ICAM-1) on brain microvascular endothelial cells in rat ischemic cortex. *Mol Brain Res*. 1994;26:61-68.
120. Zhang R-L, Chopp M, Zaloga C, Zhang ZG, Jiang N, Gautam SC, Tang WX, Tsang W, Anderson DC, Manning AM. The temporal profiles of ICAM-1 protein and mRNA expression after transient MCA occlusion in the rat. *Brain Res*. 1995;682:182-188.
121. Jander S, Kraemer M, Schroeter M, Witte OW, Stöhl G. Lymphocytic infiltration and expression of intercellular adhesion molecule-1 in photochemically induced ischemia of the rat cortex. *J Cereb Blood Flow Metab*. 1995;15:42-51.
122. Kato H, Kogure K, Liu X-H, Araki T, Itoyama Y. Progressive expression of immunomolecules on activated microglia and invading leukocytes following focal cerebral ischemia in the rat. *Brain Res*. 1996;734:203-212.
123. Soriano SG, Lipton SA, Wang YF, Xiao M, Springer TA, Gutierrez-Ramos JC, Hickey PR. Intercellular adhesion molecule-1 deficient mice are less susceptible to cerebral ischemia-reperfusion injury. *Ann Neurol*. 1996;39:618-624.
124. McCarron RM, Wang L, Siren AL, Spatz M, Hallenbeck JM. Adhesion molecules on normotensive and hypertensive rat brain endothelial cells. *Proc Soc Exp Biol Med*. 1994;205:257-262.
125. Kim JS, Chopp M, Chen H, Levine SR, Carey JL, Welch KMA. Adhesive glycoproteins CD11a and CD18 are upregulated in the leukocytes from patients with ischemic stroke and transient ischemic attacks. *J Neurol Sci*. 1995;128:45-50.
126. Sobel RA, Mitchell ME, Fronden G. Intercellular adhesion molecule-1 (ICAM-1) in cellular immune reactions in the human central nervous system. *Am J Pathol*. 1990;136:1309-1316.
127. Fassbender K, Mössner R, Motsch L, Kischka U, Grau A, Hennerici M. Circulating selectin- and immunoglobulin-type adhesion molecules in acute ischemic stroke. *Stroke*. 1995;26:1361-1364.
128. Davies MJ, Gordon JL, Gearing AJ, Pigott R, Woolf N, Katz D, Kyriakopoulos A. The expression of adhesion molecules ICAM-1, VCAM-1, PECAM, and E-selectin in human atherosclerosis. *J Pathol*. 1993;171:223-229.
129. Clark WM, Coull BM, Briley DP, Mainolfi E, Rothlein R. Circulating intercellular adhesion molecule-1 levels and neutrophil adhesion in stroke. *J Neuroimmunol*. 1993;44:123-126.
130. Wagner S, Tagaya M, Koziol JA, Quaranta V, del Zoppo GJ. Rapid disruption of an astrocyte interaction with the extracellular matrix mediated by integrin $\alpha_5\beta_1$ during focal cerebral ischemia/reperfusion. *Stroke*. 1997;28:858-865.
131. Okada Y, Copeland BR, Hamann GF, Koziol JA, Cheresch DA, del Zoppo GJ. Integrin $\alpha_5\beta_1$ is expressed in selected microvessels after focal cerebral ischemia. *Am J Pathol*. 1996;149:37-44.
132. Baggiolini M, Dewald B, Moser B. Human chemokines: an update. *Annu Rev Immunol*. 1997;15:675-705.
133. Liu T, Young PR, McDonnell PC, White RF, Barone FC, Feuerstein GZ. Cytokine-induced neutrophil chemoattractant mRNA expressed in cerebral ischemia. *Neurosci Lett*. 1993;164:125-128.
134. Watanabe K, Konishi K, Fujioka M, Kinoshita S, Nakagawa H. The neutrophil chemoattractant produced by the rat kidney epithelioid cell line NRK-52E is a protein related to CINC/KC/gro protein. *J Biol Chem*. 1989;264:19559-19563.
135. Yamasaki Y, Matsuo Y, Matsuura N, Onodera H, Itoyama Y, Kogure K. Transient increase of cytokine-induced neutrophil chemoattractant, a member of the interleukin-8 family, in ischemic brain areas after focal ischemia in rats. *Stroke*. 1995;26:318-323.
136. Wang X, Yue TL, Barone FC, Feuerstein GZ. Monocyte chemoattractant protein-1 messenger RNA expression in rat ischemic cortex. *Stroke*. 1995;26:661-666.
137. Kim JS, Gautam SC, Chopp M, Zaloga C, Jones ML, Ward PA, Welch KMA. Expression of monocyte chemoattractant protein-1 and macrophage inflammatory protein-1 after focal cerebral ischemia in the rat. *J Neuroimmunol*. 1995;56:127-134.
138. Sica A, Wang JM, Colotta F, Dejana E, Mantovani A, Oppenheim JJ, Larsen CG, Zachariae COC, Matsushima K. Monocyte chemotactic and activating factor gene expression induced in endothelial cells by IL-1 and tumor necrosis factor. *J Immunol*. 1990;144:3034-3038.
139. Gourmal NG, Buttini M, Limonta S, Sauter A, Boddeke HWGM. Differential and time-dependent expression of monocyte chemoattractant protein-1 mRNA by astrocytes and macrophages in rat brain: effects of ischemia and peripheral lipopolysaccharide administration. *J Neuroimmunol*. 1997;74:35-44.
140. Saukkonen K, Sande S, Cioffe C, Wolpe S, Sherry B, Cerami A, Tuomanen E. The role of cytokines in the generation of inflammation and tissue damage in experimental gram-positive meningitis. *J Exp Med*. 1989;171:439-448.
141. Wang X, Yue T-L, Ohlstein EH, Sung C-P, Feuerstein GZ. Interferon-inducible protein-10 involves vascular smooth muscle cell migration, proliferation, and inflammatory response. *J Biol Chem*. 1996;271:24286-24293.
142. Chopp M, Zhang RL, Chen H, Li Y, Jiang N, Rusche JR. Postischemic administration of an anti-Mac-1 antibody reduces ischemic cell damage after transient middle cerebral artery occlusion in rats. *Stroke*. 1994;25:869-876.
143. Zhang ZG, Chopp M, Tang WX, Jiang N, Zhang RL. Postischemic treatment (2-4 h) with anti-CD11b and anti-CD18 monoclonal antibodies are neuroprotective after (2h) focal cerebral ischemia in the rat. *Brain Res*. 1995;698:79-85.
144. Chen H, Chopp M, Zang RL, Bodzin G, Chen Q, Rusche JR, Todd RF. Anti-CD11b monoclonal antibody reduces ischemic cell damage after transient focal cerebral ischemia in rat. *Ann Neurol*. 1994;35:458-463.
145. Garcia JH, Liu K-F, Bree MP. Effects of CD11b/18 monoclonal antibody on rats with permanent middle cerebral artery occlusion. *Am J Pathol*. 1996;148:241-248.
146. Chopp M, Li Y, Jiang N, Zhang RL, Prostak J. Antibodies against adhesion molecules reduce apoptosis after transient middle cerebral artery occlusion in rat brain. *J Cereb Blood Flow Metab*. 1996;16:578-584.
147. Zhang RL, Chopp M, Zaloga C, Jiang N, Jones ML, Miyasaka M, Ward PA. Anti-ICAM-1 antibody reduces ischemic cell damage after transient middle cerebral artery occlusion in the rat. *Neurology*. 1994;44:1747-1751.
148. Matsuo Y, Onodera H, Shiga Y, Shozuhara H, Ninomiya M, Kihara T, Tamatani T, Miyasaka M, Kogure K. Role of cell adhesion molecules in brain injury after transient middle cerebral artery occlusion in the rat. *Brain Res*. 1994;656:344-352.
149. Zhang RL, Chopp M, Jiang N, Tang WX, Prostak J, Manning AM, Anderson DC. Anti-intercellular adhesion molecule-1 antibody reduces ischemic cell damage after transient but not permanent middle cerebral artery occlusion in the Wistar rat. *Stroke*. 1995;26:1438-1443.
150. Clark WM, Madden KP, Rothlein R, Zivin JA. Reduction of central nervous system ischemic injury by monoclonal antibody to intercellular adhesion molecule. *J Neurosurg*. 1991;75:623-627.

151. Jiang N, Moyle M, Soule H, Rote WE, Chopp M. Neutrophil inhibitory factor is neuroprotective after focal ischemia in rats. *Ann Neurol*. 1995;38:935-942.
152. Zhang RL, Chopp M, Tang WX, Zhang ZG, Putney SD, Starzyk RM. Synthetic peptide derived from the *Bordetella pertussis* bacterium reduces infarct volume after transient middle cerebral artery occlusion in the rat. *Neurology*. 1996;46:1437-1441.
153. Ember JA, del Zoppo GJ, Mori E, Thomas WS, Copeland BR, Hugli TE. Polymorphonuclear leukocyte behavior in a nonhuman primate focal ischemia model. *J Cereb Blood Flow Metab*. 1994;14:1046-1054.
154. Baron JC, von Kummer R, del Zoppo GJ. Treatment of acute ischemic stroke: challenging the concept of a rigid and universal time window. *Stroke*. 1995;26:2219-2221.
155. Marchal G, Beaudouin V, Rioux P, de la Sayette V, Le Doze F, Viader F, Derlon JM, Baron JC. Prolonged persistence of substantial volumes of potentially viable tissue after stroke: a correlative PET-CT study with voxel-based data analysis. *Stroke*. 1996;27:599-606.
156. Bowes MP, Rothlein R, Fagan SC, Zivin JA. Monoclonal antibodies preventing leukocyte activation reduce experimental neurologic injury and enhance efficacy of thrombolytic therapy. *Neurology*. 1995;45:815-819.
157. Azzimondi G, Bassein L, Fiorani L, Nonino F, Montaguti U, Celin D, Re G, D'Alessandro R. Variables associated with hospital arrival time after stroke: effect of delay on the clinical efficiency of early treatment. *Stroke*. 1997;28:537-542.
158. Aspey BS, Jessimer C, Pereira S, Harrison MJG. Do leukocytes have a role in the cerebral no-reflow phenomenon? *J Neurol Neurosurg Psychiatry*. 1989;52:526-528.
159. Takeshima R, Kirsch JR, Koehler RC, Gomoll AW, Traystman RJ. Monoclonal leukocyte antibody does not decrease the injury of transient focal cerebral ischemia in cats. *Stroke*. 1992;23:247-252.
160. Hayward NJ, Elliott PJ, Swayer SD, Bronson RT, Bartus RT. Lack of evidence for neutrophil participation during infarct formation following focal cerebral ischemia in the rat. *Exp Neurol*. 1996;139:188-202.
161. The Enlimomab Acute Stroke Trial Investigators, Sherman DG. The Enlimomab Acute Stroke Trial: final results. *Neurology*. 1997;48:A270. Abstract.
162. Hallenbeck JM, Frerichs KU. Stroke therapy: it may be time for an integrated approach. *Arch Neurol*. 1993;50:768-770.

KEY WORDS: cerebral ischemia ■ cytokines ■ cell adhesion molecules ■ leukocytes ■ therapy

Arteriosclerosis, Thrombosis, and Vascular Biology

JOURNAL OF THE AMERICAN HEART ASSOCIATION



Cytokines and Cell Adhesion Molecules in Cerebral Ischemia : Experimental Bases and Therapeutic Perspectives

Leonardo Pantoni, Cristina Sarti and Domenico Inzitari

Arterioscler. Thromb. Vasc. Biol. 1998;18;503-513

Arteriosclerosis, Thrombosis, and Vascular Biology is published by the American Heart Association,
7272 Greenville Avenue, Dallas, TX 72514

Copyright © 2005 American Heart Association. All rights reserved. Print ISSN: 1079-5642. Online
ISSN: 1524-4636

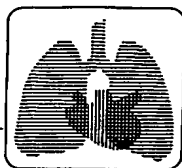
The online version of this article, along with updated information and services, is
located on the World Wide Web at:

<http://atvb.ahajournals.org/cgi/content/full/18/4/503>

Subscriptions: Information about subscribing to Arteriosclerosis, Thrombosis, and Vascular
Biology is online at
<http://atvb.ahajournals.org/subscriptions/>

Permissions: Permissions & Rights Desk, Lippincott Williams & Wilkins, 351 West Camden
Street, Baltimore, MD 21202-2436. Phone 410-5280-4050. Fax: 410-528-8550. Email:
journalpermissions@lww.com

Reprints: Information about reprints can be found online at
<http://www.lww.com/static/html/reprints.html>



laboratory and animal investigations

Effect of Exposure of Guinea Pigs to Cigarette Smoke on Elastolytic Activity of Pulmonary Macrophages*

Raul H. Sansores, MD; Raja T. Abboud, MD; Carina Becerril, MSc; Martha Montañó, MSc; Carlos Ramos, MSc; Beatriz Vanda, MSc; and Moises L. Selman, MD, FCCP

Study objective: To determine the effect of exposure to cigarette smoke on the elastolytic activity of guinea pigs' alveolar macrophages (AMs), and to compare elastolytic activity of AMs obtained by BAL with that of lung macrophages (LMs) obtained from minced lung tissue.

Methods: AMs were obtained by BAL from seven adult guinea pigs exposed to cigarette smoke for 5 d/wk during 6 weeks, as well as from age-matched control guinea pigs. From each animal, one lung was used to obtain LMs by mincing and teasing the lung, followed by enzymatic digestion and isolation of mononuclear cells by Hypaque-Ficoll separation. The other lung was inflated and fixed to quantitate emphysema by the destructive index (DI). Elastolytic activity (microgram of elastin degraded by 10^6 macrophages) was determined at 24, 48, and 72 h, by culturing AMs and LMs (1×10^6 cells in 1 mL of medium) in ^3H -elastin-coated wells.

Results: In animals exposed to cigarette smoke, the total number of BAL cells ($8.6 \pm 2.1 \times 10^6$) and DI (21.8 ± 8.1) were significantly higher than in nonexposed animals ($6.4 \pm 1.8 \times 10^6$, $p < 0.05$ for cells, and 12.1 ± 4.1 , $p < 0.01$ for DI). Elastolytic activity of AMs from smoke-exposed guinea pigs was significantly higher at 24, 48, and 72 h than elastolytic activity of AMs from control animals (19.0 ± 9.4 vs 10.0 ± 5.3 , $p < 0.05$ at 72 h). Likewise, elastolytic activity of LMs was significantly higher in exposed than nonexposed guinea pigs (11.8 ± 7.7 vs 7.4 ± 5.0 at 72 h, $p < 0.05$). Elastolytic activity of LMs was not significantly different from elastolytic activity of AMs, both in exposed guinea pigs (11.8 ± 7.7 vs 19.0 ± 9.4 at 72 h) and nonexposed animals (7.4 ± 5.0 vs 10.0 ± 5.3 at 72 h). **Conclusions:** These results indicate that elastolytic activity of both AMs and LMs of guinea pigs increases significantly after exposure to cigarette smoke and that AMs and LMs have similar elastolytic activities.

(CHEST 1997; 112:214-19)

Key words: cigarette smoke exposure; elastase; elastolytic activity; emphysema; lung macrophages

Abbreviations: AM=alveolar macrophage; COHb=carboxyhemoglobin; DI=destructive index; EA=elastolytic activity; LM=lung macrophage; NS=not significant; PMSF=phenylmethyl-sulfonyl-fluoride

The current hypothesis of the pathogenesis of emphysema postulates that an imbalance between proteases and antiproteases leads to the destructive changes in the lung parenchyma.¹ Neuro-

phils have been considered to be the main cells involved in this elastolytic injury.² However, there is more recent evidence suggesting that alveolar macrophages (AMs) may play a prominent role in the degradation of lung elastin.³⁻⁵ Studies of the elastolytic properties of lung macrophages (LMs) as well as their possible role in mechanisms leading to emphysema have been based on AMs retrieved from BAL.³⁻⁷ However, because these AMs are not directly in contact with the interstitial matrix, the macrophages resident in the lung interstitium may be the more relevant cell in relation to potential elastolytic damage of lung parenchyma.

In this context, our study had two aims; first to evaluate the effect of cigarette smoke exposure on

*From the Instituto Nacional de Enfermedades Respiratorias (Drs. Sansores and Selman, Mr. Ramos, and Mss. Becerril, Montañó, and Vanda), México, DF, México, and the Respiratory Division, Vancouver Hospital and Health Sciences Centre (Dr. Abboud), University of British Columbia, Vancouver, BC, Canada.

Supported in part by CONACYT grant F-643-M9406. Manuscript received October 14, 1996; revision accepted December 12, 1996.

Reprint requests: RH Sansores, Instituto Nacional de Enfermedades Respiratorias, Talpan 4502, Col. Sección 16, CP 14080, México DF, México

AM elastolytic activity (EA) in guinea pigs, and second to compare the EA of AMs with that of macrophages extracted from lung tissue (predominantly interstitial macrophages) both in guinea pigs exposed and not exposed to cigarette smoke.

MATERIALS AND METHODS

Preparation of Elastin-Coated Culture Plates

³H-elastin was prepared by reductive alkylation of bovine ligamentum nuchae elastin (Elastin Products Company, Owensville, Mo) using sodium borohydride [³H] hydride⁸ as previously reported.⁹ Culture plates were prepared by spreading evenly 250 µg of the ³H-elastin suspension (specific activity=1,584 cpm/µg) on the inside bottom of 16-mm wells of 24-well tissue culture plates (Costar; Cambridge, Mass). The elastin was dried at 45°C and the ³H-elastin-coated plates were then stored at 4°C until used.

Experimental Exposure to Cigarette Smoke

Approval from the Institutional Animal Research Committee was obtained. Seven adult guinea pigs weighing 600 to 650 g were exposed to the smoke of 20 commercial nonfilter cigarettes per day, for 5 d/wk, during 6 weeks. The smoke exposure was accomplished by enclosing the animals (three or four at a time) in a plastic chamber 100 cm long, 60 cm wide, and 80 cm high, which had two holes on one lower edge that held two cigarettes used for smoke exposure. The animals were exposed to the smoke by lighting the cigarettes and inhaling the smoke through the chamber using a suction vacuum attached to the opposite upper corner of the chamber; in this manner, the smoke was dispersed throughout the chamber. The cigarettes were lit and "smoked" over a period of 10 min and followed by a period of 10 to 20 min without cigarette smoking. The cycle was repeated until a total of 20 cigarettes were "smoked" over a period of about 5 h. To confirm that this system led to significant smoke inhalation, we obtained blood measurement of carboxyhemoglobin (COHb) by co-oximetry in another group of animals exposed to cigarette smoke under identical conditions. As control group for the effects of cigarette smoke exposure, we studied seven guinea pigs placed in a similar chamber for a similar period of time for 5 d/wk during 6 weeks under the same conditions but without using any cigarette, so that only room air was being aspirated into the chamber.

Bronchoalveolar Lavage

After 6 weeks of experimental or sham exposure, guinea pigs were anesthetized by intraperitoneal injection of pentobarbital (28 mg/kg). A tracheostomy was performed under sterile conditions and a 0.21-cm catheter was introduced into the trachea. Guinea pig lungs were washed very gently by instilling five aliquots of 10 mL of saline solution each. The fluid recovered from the lavage was kept on ice until analysis. Cells in the BAL were separated from the lavage fluid by centrifugation at 4°C. The sedimented cells were washed twice in Hanks' balanced salt solution and then resuspended in serum-free RPMI 1640 medium containing 25 mmol/L Hepes buffer, 2 mmol/L glutamine, 100 U/mL penicillin, and 10 mg/mL streptomycin (GIBCO; Grand Island, NY). The number of macrophages per milliliter was determined by counting the cells in a hemocytometer and cell viability was analyzed by trypan blue exclusion. Slide prepa-

rations were prepared to determine the BAL cell differential count. Cell counting was performed on a total of 300 cells by a pathologist unaware of the origin of the fluid. The cell suspension was adjusted to a count of 1×10^6 macrophages per milliliter for assay of elastolytic activity.

Preparation of LMs

To further remove AMs from the lung, two additional BALs with 10 mL of saline solution each were performed. After the lavage, the animals were killed with an intraperitoneal overdose of sodium pentobarbital. The left lung was used for the histologic study and the right lung for obtaining LMs. The right lung was minced into pieces of 2 to 4 mm with scissors and excess blood was removed by rinsing the lung pieces with saline solution. The tissue was then incubated with RPMI-1640 medium and trypsin (166 µg/mL EDTA (66 µg/mL) for 30 min at 37°C. To remove particulate matter, the medium was filtered through gauze and then centrifuged for 10 min at 1,500 g at 4°C. The cell pellet was resuspended in medium and the LMs were separated by using a Hypaque-Ficoll gradient.¹⁰

The LMs were washed twice in medium and then centrifuged. The LMs in the pellet were considered to be predominantly interstitial macrophages; they were resuspended in RPMI-1640 medium, counted, and adjusted to a concentration of 1×10^6 LM per milliliter. Cell viability was determined by trypan blue exclusion.

Measurements of AM and LM EA

EA in AMs and LMs was measured by the method originally described by Chapman and Stone³ and later used by other investigators.^{4,9} Prior to use, the ³H-elastin-coated wells of culture plates were washed three times with phosphate-buffered saline solution and then loaded in duplicate (or in triplicate depending on the total amount of available cells) with either 1 (or 0.5) mL of either AMs or LMs in RPMI-1640 at 1×10^6 cells per milliliter. For every assay, blanks (RPMI-1640 without cells) in duplicate were routinely included and used to correct for non-specific release of radioactive elastin. The cell cultures were then incubated at 37°C, 100% humidity, and 95% air-5% CO₂ for 2 h for allowing macrophages to adhere to the ³H-elastin-coated wells, and then nonadherent cells were removed. The wells with ³H-elastin and the adherent macrophages were then filled with 1 (or 0.5) mL of RPMI-1640 supplemented with 1% (vol/vol) nonessential amino acids and 10% fetal (vol/vol) bovine serum, and the culture plates were returned to the incubator for culture periods up to 72 h. Every 24 h, the medium was removed and stored at 4°C until analysis, and replaced by fresh medium. At the end of the 72-h incubation period, the samples of each 24-h incubation were spun in a microcentrifuge (13,000 × g at 4°C for 5 min) and 100 µL of the supernatants was assayed for solubilized ³H-elastin by scintillation counting in 10 mL of Aquasol-2 (New England Nuclear; Dupont, UK). Results of the EA in micrograms of elastin degraded per 100 µL of medium were calculated as follows:

$$\frac{(\text{cpm macrophage sample} - \text{cpm blank})}{\text{specific activity of } ^3\text{H-elastin}}$$

Results were then expressed as microgram of elastin degraded by 10^6 cells by dividing the total amount of elastin degraded in each well by the number of macrophages in that well.

Experiments to Control for Possible Differences Due to Method

Effect of Hypaque-Ficoll: Since LMs were isolated by using the Hypaque-Ficoll gradient method, and AMs were not, we deter-

mined if AMs had similar EA whether or not they were obtained by using Hypaque-Ficoll. Therefore, a separate experiment was made with three additional guinea pigs to compare EA of AMs prepared from BAL without and with the use of Hypaque-Ficoll.

Trypsin Treatment: To determine the influence of the enzymatic digestion with trypsin used during recovery of LMs on EA, AMs from three guinea pigs exposed to cigarette smoke and obtained as described previously were assayed for EA without and after incubation with trypsin for 30 min. The EA from AMs subjected to enzymatic treatment was then compared with EA of the AMs without trypsin exposure.

Effect of Neutrophil-Derived Elastase: To determine the possible contribution of EA derived from neutrophils on the determined macrophage EA, AMs from three guinea pigs exposed to cigarette smoke and obtained as described previously were assayed for EA without and with the addition of 100 mmol/L of phenylmethyl-sulfonyl fluoride (PMSF), a potent inhibitor of neutrophil elastase.

Histologic Assessment

After fixation with 10% buffered formalin at a constant pressure of 25 cm H₂O, the left lung was processed for morphologic evaluation. Five-micrometer sections were stained with hematoxylin-eosin and examined on light microscopy by a pathologist who did not know whether the animal had been exposed to cigarette smoke. To assess the degree of parenchymal destruction, lung samples were further evaluated by using the destructive index (DI) described by Sackett et al.¹¹ Light microscopy at 10X magnification was used to grade the stained sections of the lung. For each tissue, 20 nonoverlapping fields randomly chosen from one slide were examined with an ocular with cross hair and 36 points. Any field containing structures, like vessels or airways, whose maximal diameter was larger than 0.60 mm was not used for the analysis. Alveoli or alveolar ducts lying under these points were classified as normal or destroyed. They were considered to be normal when they were surrounded by intact or continuous walls or when these walls were disrupted only in one place. Alveolar spaces were considered to be destroyed when the wall of an alveolus was disrupted in two or more places or there were three or more disruptions of contiguous alveoli. DI was calculated according to the following formula: $DI = 100 \times D / (D + N)$, where D indicates "destroyed" and N indicates "normal."

Statistical Analysis¹²

The unpaired Student's *t* test was used for comparing results in nonexposed and smoke-exposed animals, while the paired *t* test was used when comparing the two types of macrophages from the same animal. The *p* values <0.05 were considered to indicate a statistically significant difference.

Table 1—BAL Cell Profile (Mean ± SD)

	Total Cells, ×10 ⁶	Macrophages, %	Neutrophils, %	Lymphocytes, %
Smoke exposed	8.6 ± 2.1	65.85 ± 15	11 ± 7.4	22.2 ± 8.4
Control animals	6.4 ± 1.8	63.85 ± 15	7 ± 3.1	27.8 ± 5.9
<i>p</i> Value	<0.05	NS	NS	NS

RESULTS

After 6 weeks of tobacco smoke or air exposure, there were no significant differences in body weight between the two groups of guinea pigs. A significant increase in the mean level of COHb was observed in the cigarette smoke-exposed animals (19.3 ± 5.4% vs 6.5 ± 3.2% in the control group; *p* < 0.05). Table 1 shows the cell profile from BAL. The total amount of cells was significantly higher in smoke-exposed guinea pigs compared with control animals (8.6 ± 2.1 vs 6.4 ± 1.8, *p* < 0.05). Macrophages were the most prevalent cell population in both groups of animals, but no significant differences were found in any type of inflammatory cells. The cell viability was always higher than 90%.

Histologic Assessment

Morphologic changes are illustrated in Figure 1. The lungs of all cigarette smoke-exposed guinea pigs showed inflammatory changes as foci of interstitial

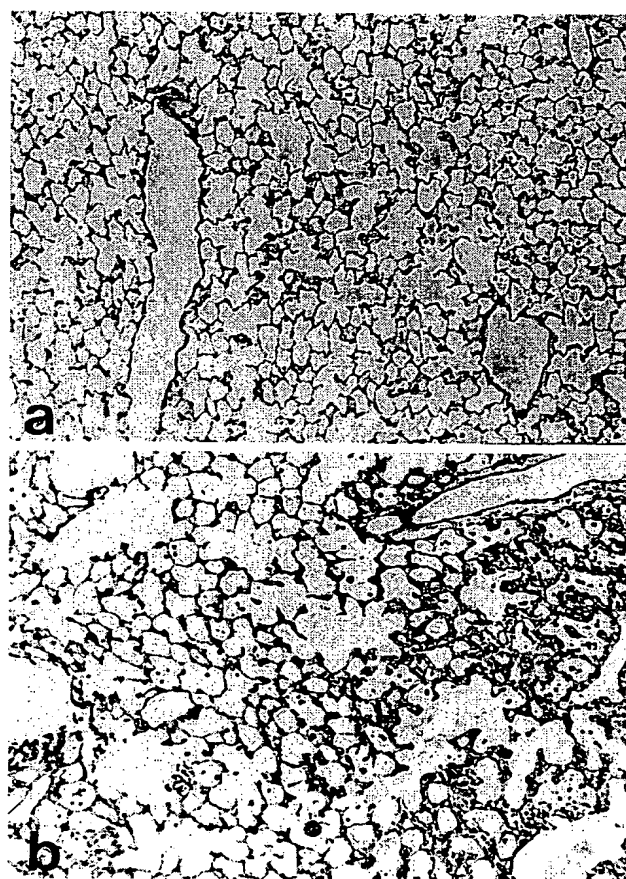


FIGURE 1. Top (a): normal lung. Bottom (b): smoke-exposed lung exhibiting peribronchiolar, interstitial, and intra-alveolar inflammation, with areas of rupture of the alveolar septa can be seen (hematoxylin-eosin, original magnification ×4).

and intra-alveolar infiltration by lymphocytes and macrophages and in some cases by polymorphonuclear cells. In most animals, lesions compatible with bronchiolitis were found. Areas of disruption of alveolar septa were noticed mainly under the pleura, and this observation was corroborated by the DI that was significantly higher in guinea pigs exposed to cigarette smoke (21.76 ± 8.11) than in the control animals (12.17 ± 4.11 ; $p=0.016$).

Elastolytic Activity

Results of EA of AMs and LMs derived from control and smoke-exposed animals are shown in Table 2. In general, mean values of EA obtained from AMs tended to be higher than those obtained from LMs in both tobacco smoke-exposed animals and control animals. However, no significant differences between the two cell preparations were found by the paired *t* test. EA of both types of macrophages increased with duration of culture. EA of AMs was significantly higher in smoke-exposed guinea pigs compared with the control animals at all time intervals of culture. Similar results were observed with LMs, although no significant difference was observed at 72-h culture.

Effect of Hypaque-Ficoll Separation, Trypsin Treatment, and PMSF on EA

We first determined if the total number of cells recovered was affected by the use of Hypaque-Ficoll. The mean number of cells obtained from the BAL of three guinea pigs exposed to cigarette smoke was $10.93 \pm 5.8 \times 10^6$. Half of the BAL was processed to obtain mononuclear cells by using the Hypaque-Ficoll method and a total of $5.06 \pm 4.69/10^6$ cells were recovered. This number was not significantly different from the $5.41 \pm 5.3/10^6$ cells in the remaining half of the BAL not subjected to Hypaque-Ficoll. In addition, EA (microgram of degraded elastin $\times 10^6$ cells) of AMs purified by the Hypaque-Ficoll separation was not different from AMs not treated with Hypaque-Ficoll (24 ± 7 vs 22 ± 8 at 72 h (p =not significant [NS])).

Since enzymatic digestion with trypsin was used to obtain LMs, we additionally evaluated EA from AMs after incubation with this enzyme. Our results show that EA from AMs treated with trypsin exhibited a consistently lower EA by a factor of $17 \pm 3\%$ ($n=6$ assays from three guinea pigs). When EA of LMs from all the experiments (shown in Table 2) was adjusted by using this factor to correct for the trypsin effect, EA of LMs still remained slightly lower by 15 to 20% than the corresponding AM values. PMSF treatment did not significantly affect EA; the EA of AMs with PMSF at 72 h was 22 ± 4 , while that of AMs without PMSF was 23 ± 6 ($p=NS$).

DISCUSSION

The evaluation of the EA of AMs or LMs raises two issues: first, whether the observed EA is really due to the macrophages and not to neutrophils, and second, if the so-called LMs are indeed coming from the interstitium of the lung. It was assumed in this article that the cells responsible for the EA were macrophages based on stained cytopsin preparations of the obtained cells. Contaminating neutrophils were removed after a 2-h period of incubation to allow adherence of macrophages prior to determination of EA. This adherence step indicates that the EA determined was due to macrophages and not to nonadherent cells such as neutrophils. Furthermore, in a separate experiment (with three guinea pigs), EA of AMs obtained with the Hypaque-Ficoll method to remove contaminating neutrophils was the same as that obtained without Hypaque-Ficoll, supporting the notion that in our assay, there was no EA due to neutrophils. Moreover, the routine use of fetal bovine serum rich in serine proteinases inhibitors such as α_1 -antitrypsin in all cultures would inhibit any elastase derived from neutrophils but not macrophages.³ The addition of PMSF, a potent inhibitor of neutrophil elastase, did not affect cultured AM EA, indicating that there was no EA derived from neutrophils.

The best method to determine the origin of the macrophages from lung tissue is by cell markers

Table 2—EA of AMs and LMs of Control and Cigarette Smoke-Exposed Guinea Pigs

Time, h	μg of Degraded Elastin $\times 10^6$ Cells					
	Nonexposed		<i>p</i>	Exposed		<i>p</i>
	AM	LM		AM	LM	
24	4.72 ± 2.10	2.97 ± 2.37	NS	$8.94 \pm 2.65^*$	$6.41 \pm 1.95^†$	NS
48	7.67 ± 3.71	5.13 ± 3.49	NS	$15.21 \pm 6.07^*$	$10.12 \pm 4.54^†$	NS
72	9.99 ± 5.26	7.36 ± 4.99	NS	$19.01 \pm 9.42^*$	$11.82 \pm 7.68^†$	NS

*AM exposed vs nonexposed AM, $p < 0.05$.

†Exposed LM vs nonexposed LM, $p < 0.05$.

‡Exposed LM vs nonexposed LM, $p = NS$.

specific for alveolar but not for interstitial macrophages, but we were unable to use these techniques. We attempted to decrease contamination of LMs by AMs by washing out the lung with an excess of saline solution after the BAL, and by rinsing and eliminating the remaining blood from the tissue while processing the tissue cells. These maneuvers would not completely eliminate the resident macrophages in the alveoli and the blood. The studies by Dethloff and Lehnert¹³ indicate that such preparations considered to be of interstitial macrophages would have significant contamination of AMs. However, Weissler and coworkers¹⁴ observed that macrophages obtained from minced lung tissue (as we did) are functionally different from those obtained by BAL, in terms that they induce significantly more T-cell proliferation in a mixed leukocyte reaction, suggesting macrophages different from AMs. Despite this possible contamination of LMs by AMs, our results clearly suggest that EA of LMs increases significantly after exposure to cigarette smoke.

Significant exposure to cigarette smoke was clearly demonstrated by the levels of COHb (19%) in smoke-exposed guinea pigs. However, the nonexposed animals also had high levels of COHb (about 6%) in comparison to human levels. The reason for this finding is not clear; a possible explanation is that the levels were tested in a co-oximeter standardized for determining human blood COHb and not guinea pig COHb.

Significant inflammatory and parenchymal changes compatible with early emphysema were observed in guinea pigs exposed to cigarette smoke, indicating that even the degree of exposure to tobacco smoke that we used (5 h/d, 5 d/wk for 6 weeks) was deleterious. This is not surprising since Wright and Churg¹⁵ have previously observed changes of emphysema in guinea pigs exposed to the smoke of 10 cigarettes during 5 d/wk for 1 to 12 months. Furthermore, we have previously demonstrated that foci of moderate peribronchiolar, interstitial, and intra-alveolar inflammation are observed in the same model at 4 weeks exposure.¹⁶

Our findings of increased EA in both AMs and LMs from guinea pigs exposed to cigarette smoke suggest that increased EA by LMs may contribute to the observed destructive changes in the lung parenchyma. Supporting this point of view are the findings of increased EA in smokers as reported by Chapman and Stone³ and reviewed by Shapiro and associates.¹⁷ Actually, it is important to point out that macrophages are the most abundant inflammatory cells found in BAL of cigarette smokers, as well as in respiratory bronchioles where emphysematous changes are first manifested.^{18,19} Moreover, Finkelstein et al²⁰ have recently demon-

strated that the extent of lung destruction in human emphysema is directly related to the number of AMs and T lymphocytes, but not with the number of neutrophils.

Despite the numerous studies on pathogenetic mechanisms in emphysema using BAL, to our knowledge, our study is the first one to attempt to compare EA of both AMs and LMs. The importance of attempting to evaluate interstitial macrophages' enzymatic activity through the use of minced lung tissue is that the interstitial macrophages, in contrast to AMs, are in closer contact with the elastic fibers that may be more susceptible to elastolysis by interstitial than AMs. Nevertheless, our results showed that the EA of these two types of macrophages is similar both in smoke-exposed and in nonexposed guinea pigs.

There was a nonsignificant trend for the LMs to show a lower EA than the AMs. This tendency was not modified after correcting for the putative enzymatic effect of trypsin, to which the tissue cells were submitted during their isolation.

In general, our results support the notion that AMs and LMs are similar in a variety of activities, as has been demonstrated in other different studies. For example, Adamson and coworkers²¹ compared rat alveolar and interstitial macrophage activity to stimulate fibroblasts after exposure to silica and asbestos. They found that the two macrophage populations responded equally to particles with respect to secretion of fibroblast growth factors.

However, the time course of EA of guinea pig AMs and LMs is comparable to that previously reported by Senior et al,⁴ Chapman and Stone,³ and Ofulue et al⁹ regarding EA of human AMs; the slight differences in the amount of degraded elastin and in the time course of elastin degradation may be due to the species difference.

In summary, our study indicates that cigarette smoke exposure in guinea pigs not only induces changes compatible with emphysema, as has been reported previously, but also results in a significant increase of EA by macrophages that may contribute in part to the destructive changes observed in emphysema. The enzyme(s) responsible for this activity deserve further study, but the recently described metalloelastase, and the 92-kd gelatinase B, both secreted by macrophages, are strong candidates.²² Actually, an increase in 92-kd type IV collagenase expression by macrophages has been found previously in this experimental model.²³ Our study also suggests that the EA of macrophages from minced lung tissue is similar to that observed in macrophages obtained from BAL.

REFERENCES

- 1 Evans MD, Pryor WA. Cigarette smoking, emphysema and damage to alpha-1-proteinase inhibitor. *Am J Physiol (Lung Cell Mol Physiol 10)* 1994; 266:L593-611
- 2 Snider GL, Ciccolella DE, Morris SM, et al. Putative role of neutrophil elastase in the pathogenesis of emphysema. *Ann NY Acad Sci* 1991; 624:45-59
- 3 Chapman HG, Stone OL. Comparison of human neutrophil and alveolar macrophages elastolytic activity *in vitro*: relative resistance of macrophage elastolytic activity to serum and alveolar proteinase inhibitors. *J Clin Invest* 1984; 74:1693-1700
- 4 Senior RM, Connelly NL, Cury JD, et al. Elastin degradation by human alveolar macrophages: a prominent role of metalloproteinase activity. *Am Rev Respir Dis* 1989; 139:1251-56
- 5 Snider GL. Emphysema: the first two centuries and beyond: a historical overview, with suggestions for future research. *Am Rev Respir Dis* 1992; 146:1334-44
- 6 Sibille Y, Reynolds YH. Macrophages and polymorphonuclear neutrophils in lung defense and injury. *Am Rev Respir Dis* 1990; 141:471-501
- 7 Rodriguez RT, White RR, Senior RM, et al. Elastase release from human alveolar macrophages: comparison between smokers and non-smokers. *Science* 1977; 198:313-14
- 8 Gordon S, Werb Z, Cohn ZA. Methods for detection of macrophage secretory enzymes. In: Bloom EB, David JR, eds. *In vitro* methods in cell-mediated and tumor immunity. New York: Academic Press, 1976; 349-51
- 9 Ofulue AF, Sansores RH, Abboud RT. Effect of assay conditions on measurement of elastolytic activity of alveolar macrophages in culture and characterization with proteinase inhibitors. *Clin Biochem* 1994; 27:13-20
- 10 Boyum A. Isolation of mononuclear cells and granulocytes from human blood. *Scand J Clin Lab Invest* 1968; 21(suppl 97):77-89
- 11 Saetta M, Shiner R, Kim W, et al. Destructive index: a measurement of lung parenchymal destruction in smokers. *Am Rev Respir Dis* 1985; 131:764-69
- 12 Bailar JC, Mosteller F. Medical uses of statistics. 2nd ed. Boston: NEJM Books, 1992
- 13 Dethloff LA, Lehnert BE. Compartmental origin of pulmonary macrophages harvested from mechanically disrupted lung tissue. *Exp Lung Res* 1987; 13:361-83
- 14 Weissler JC, Lyons CR, Lipscomb MF, et al. Human pulmonary macrophages: functional comparison of cells obtained from whole lung and bronchoalveolar lavage. *Am Rev Respir Dis* 1986; 133:473-77
- 15 Wright J, Churg A. Cigarette smoke causes physiologic and morphologic changes of emphysema in the guinea pig. *Am Rev Respir Dis* 1990; 142:1422-28
- 16 Selman M, Montañó M, Ramos C, et al. Tobacco smoke-induced lung emphysema in guinea pigs is associated with increased interstitial collagenase. *Am J Physiol (Lung Cell Molec Physiol 15)* 1996; 271:L734-43
- 17 Shapiro SD, Campbell EJ, Welgus HG, et al. Elastin degradation by mononuclear phagocytes. *Ann NY Acad Sci* 1991; 624:69-80
- 18 Merchant RK, Schwartz DA, Helmers RA, et al. Bronchoalveolar lavage cellularity: the distribution in normal volunteers. *Am Rev Respir Dis* 1992; 146:448-53
- 19 Niewoehner DE, Kleinerman J, Rice DB. Pathologic changes in the peripheral airways of young cigarette smokers. *N Engl J Med* 1974; 291:755-58
- 20 Finkelstein R, Fraser RS, Ghezzi H, et al. Alveolar inflammation and its relation to emphysema in smokers. *Am J Respir Crit Care Med* 1995; 152:1666-72
- 21 Adamson IYR, Letourneau HL, Bowden DH. Comparison of alveolar and interstitial macrophages in fibroblast stimulation after silica and long or short asbestos. *Lab Invest* 1991; 64:339-44
- 22 Shapiro SD. Elastolytic metalloproteinases produced by human mononuclear phagocytes: potential roles in destructive lung disease. *Am J Respir Crit Care Med* 1994; 150(suppl): S160-64
- 23 Segura L, Ramirez R, Ramos C, et al. Upregulation of 92 kDa type IV collagenase (MMP-9) in an experimental model of pulmonary emphysema [abstract]. *FASEB J* 1995; 9(3):A431

Effect of exposure of guinea pigs to cigarette smoke on elastolytic activity of pulmonary macrophages

RH Sansores, RT Abboud, C Becerril, M Montano, C Ramos, B Vanda and ML Selman

Chest 1997;112;214-219

This information is current as of January 12, 2006

Updated Information & Services	Updated information and services, including high-resolution figures, can be found at: http://www.chestjournal.org
Citations	This article has been cited by 6 HighWire-hosted articles: http://www.chestjournal.org#otherarticles
Permissions & Licensing	Information about reproducing this article in parts (figures, tables) or in its entirety can be found online at: http://www.chestjournal.org/misc/reprints.shtml
Reprints	Information about ordering reprints can be found online: http://www.chestjournal.org/misc/reprints.shtml
Email alerting service	Receive free email alerts when new articles cite this article sign up in the box at the top right corner of the online article.
Images in PowerPoint format	Figures that appear in CHEST articles can be downloaded for teaching purposes in PowerPoint slide format. See any online article figure for directions.

A M E R I C A N C O L L E G E O F
 C H E S T
P H Y S I C I A N S

CHEST[®]

THE CARDIOPULMONARY
AND CRITICAL CARE JOURNAL

FOR PULMONOLOGISTS, CARDIOLOGISTS, CARDIOTHORACIC SURGEONS,
CRITICAL CARE PHYSICIANS, AND RELATED SPECIALISTS

**Effect of exposure of guinea pigs to cigarette smoke on elastolytic activity of
pulmonary macrophages**


RH Sansores, RT Abboud, C Becerril, M Montano, C Ramos, B Vanda and ML
Selman

Chest 1997;112;214-219

This information is current as of January 12, 2006

The online version of this article, along with updated information and services, is
located on the World Wide Web at:
<http://www.chestjournal.org>

CHEST is the official journal of the American College of Chest Physicians. It has been published monthly since 1935. Copyright 2005 by the American College of Chest Physicians, 3300 Dundee Road, Northbrook IL 60062. All rights reserved. No part of this article or PDF may be reproduced or distributed without the prior written permission of the copyright holder. ISSN: 0012-3692.

A M E R I C A N C O L L E G E O F
 C H E S T
P H Y S I C I A N S

Macrophages Promote Prosclerotic Responses in Cultured Rat Mesangial Cells: A Mechanism for the Initiation of Glomerulosclerosis

IZABELLA Z. A. PAWLUCZYK and KEVIN P. G. HARRIS

Department of Nephrology, Leicester General Hospital, Leicester, United Kingdom.

Abstract. Glomerulosclerosis is the final outcome of a number of different causes of glomerular injury, during which the structures of the glomerulus are obliterated by extracellular matrix. Accumulating evidence suggests that infiltrating macrophages play a pivotal role in the progression to glomerulosclerosis. The present study defines the role played by macrophages at both cellular and molecular levels in the initiation of the sclerotic process in cultured rat mesangial cells. Macrophage-conditioned medium (MPCM) generated from thioglycollate-elicited, lipopolysaccharide-stimulated macrophages upregulated mesangial cell fibronectin production in a dose- and time-dependent manner, independently of cell proliferation. Immunoprecipitation of metabolically labeled ^{35}S -fibronectin confirmed that the matrix protein was synthesized *de novo*. The genes for fibronectin and the matrix proteins laminin and collagen IV were also found to be upregulated 2.86 ± 0.24 -, 4.94 ± 0.17 -, and 3.03 ± 0.31 -fold over controls, respectively ($P < 0.001$). Macrophage modulation of matrix turnover was suggested by an upregulation of both transin and

tissue inhibitor of metalloproteinase-1 gene transcription. Transforming growth factor (TGF) β_1 , platelet-derived growth factor, tumor necrosis factor (TNF) α , or interleukin (IL)-1 β could not be detected in the MPCM *per se*; however, TGF β_1 and platelet-derived growth factor AB were found to be secreted into mesangial cell culture supernatants. Secretion was augmented 1.69 ± 0.16 - and 2.28 ± 0.28 -fold, respectively (both $P < 0.001$), in response to MPCM. Northern blot analysis demonstrated that protein secretion had been preceded by upregulation of the genes for these cytokines (2.2 ± 0.4 -fold [$P < 0.001$] and 5.7 ± 1.2 -fold [$P < 0.004$], respectively). Incubation of MPCM with either neutralizing antibody or the growth factor receptor antagonist suramin demonstrated that TGF β_1 played a significant, although minor, role in MPCM-stimulated fibronectin production. In conclusion, this study provides compelling evidence for a direct role of macrophages in the progression to glomerulosclerosis. (J Am Soc Nephrol 8: 1525-1536, 1997)

The histological characteristics of numerous experimental and human glomerular diseases that ultimately progress to glomerulosclerosis are expansion of the glomerular mesangium and deposition of extracellular matrix (1). The etiology of progressive renal scarring is complex and multifactorial, but considerable evidence, largely from animal studies, now suggests that macrophages could play an important pathogenetic role in this process.

For example, the administration of puromycin aminonucleoside (PAN) to rats causes the nephrotic syndrome, which is associated with a glomerular macrophage infiltrate at day 11, coinciding with peak proteinuria (2). Although the nephrotic syndrome resolves, the rats subsequently develop progressive glomerulosclerosis. Maneuvers that abolish the glomerular macrophage infiltrate during the acute nephrotic phase in this model, such as a diet free of essential fatty acids (3) or whole-body X-irradiation (4), are able to prevent the subse-

quent progression to glomerulosclerosis. A glomerular infiltrate is also an early response to renal ablation, a lesion also known to progress to glomerulosclerosis (5,6). After uninephrectomy, for example, an infiltrate occurs within 1 to 2 wk of surgery, before the observation of histological changes by light microscopy, the detection of microalbuminuria, or the development of renal scarring (5). Glomerular macrophage depletion by X-irradiation has been shown to ameliorate the progression of the glomerular injury in the remnant kidney model (6), further supporting an effector role for these cells in mediating glomerulosclerosis.

Factors elaborated by these infiltrating cells could alter the phenotypic expression of the resident glomerular cells with respect to their proliferative and matrix-producing capacities. Much research has recently been carried out regarding the role of various cytokines and growth factors in the modulation of glomerular cell proliferation and matrix synthesis. In PAN nephrosis, the macrophage infiltrate has been shown to occur in temporal association with increased glomerular transforming growth factor (TGF) β and fibronectin gene expression (7). Furthermore, immunohistochemical labeling studies have demonstrated that the TGF β protein staining corresponds locally with ED-1-positive macrophages (7). More recently, in the same model, it has been reported that TGF β mRNA is ex-

Received November 26, 1996. Accepted March 26, 1997.

Correspondence to Dr. Kevin P. G. Harris, Department of Nephrology, Leicester General Hospital, Leicester LE5 4PW, England.

1046-6673/08010-1525\$03.00/0

Journal of the American Society of Nephrology

Copyright © 1997 by the American Society of Nephrology

pressed by glomerular macrophages, thus identifying these cells as a potential cellular source of the profibrogenic cytokine (8). Okuda *et al.* have also reported that the level of TGF β mRNA and the number of cells producing TGF β protein was higher in glomeruli isolated from Thy-1 nephritic rats than in glomeruli from normal rats (9). Subsequently, in the same model, it was shown that administration of a neutralizing antibody to TGF β resulted in a significant suppression of extracellular matrix production with a concomitant reduction in the degree of histological damage (10). Further support for a pathogenic role for TGF β in renal scarring has been provided by the observation that *in vivo* transfection of the TGF β gene increases the production of extracellular matrix deposition in the kidney (11).

These observations provide a strong, although correlative, case for TGF β mediating the adverse effects of macrophages in the scarring process. However, it seems unlikely that one cytokine acting alone would be solely responsible for mediating mesangial matrix accumulation, given the potential cytokine interactions involving autocrine loops and paracrine pathways that could be involved in this process. Instead, the process of scarring likely requires a number of factors acting in concert.

The present study, therefore, was undertaken to determine the precise role played by macrophages at both cellular and molecular levels in the initiation of the sclerotic process in mesangial cells—functionally the most important cells within the glomerulus.

Materials and Methods

Unless stated otherwise, chemicals and reagents were obtained from Sigma Chemical Co. (Poole, United Kingdom).

Culture of Rat Mesangial Cells

Glomerular cells were cultured from the glomerular explants of adult Wistar rat kidneys, using standard techniques (12). The cells were cultured in RPMI 1640 supplemented with 20% heat-inactivated fetal calf serum (FCS), 100 μ g/ml penicillin (Life Technologies), 100 μ g/ml streptomycin (Life Technologies), 5 μ g/ml bovine insulin, and 2 mM glutamine (Life Technologies). Cultured cells were characterized by their typical stellate fusiform morphology, their positive staining for the Thy-1 antigen, and their resistance to the toxic effects of D-valine.

Mesangial cells of passages 2 through 10 were cultured in 24-well plates (ICN Flow, Oxfordshire, United Kingdom) or 25-cm² flasks (Corning, High Wycombe, United Kingdom), allowed to grow to confluence, and then made quiescent in medium containing 0.5% FCS for 72 h before use.

Isolation of Macrophages and Preparation of Macrophage-Conditioned Media

Macrophages were obtained from adult Wistar rats by injecting 10 ml of 3% thioglycollate broth into the peritoneal cavity. After 5 d, the peritoneal cavity was lavaged with 20 ml of cold Hanks' balanced salt solution (HBSS). The majority (~90%) of the exudate cells obtained in this way were macrophages, as judged by positive immunohistochemical staining for the rat monocyte/macrophage marker ED-1. Macrophage-conditioned medium (MPCM) was prepared using a

modified method of Kohan and Schreiner (13). The exudate cells were purified by temporarily plating them at a cell density of 5×10^5 cell/ml in 25-cm² tissue culture flasks. After 2 h of incubation at 37°C in a humidified 5% CO₂/95% air atmosphere, nonadherent cells were removed by washing with HBSS buffered with 20 mM Hepes. The macrophages were then stimulated with lipopolysaccharide (LPS) (from *Escherichia coli* 026 B6) at a final concentration of 1 μ g/ml for 16 h, and then washed three times and cultured for an additional 48 h in serum-free RPMI. The MPCM was harvested and centrifuged for 10 min at 2000 rpm, and then frozen at -20°C until needed.

Culture of Mesangial Cells in the Presence of Macrophages or MPCM

Confluent quiescent mesangial cells were exposed to thioglycollate-elicited peritoneal macrophages at final (macrophage) cell densities of 0, 3.13×10^4 , 6.25×10^4 , 12.5×10^4 , and 25×10^4 cells/ml per well. In parallel, macrophages at the same cell densities were cultured directly on the 24-well plates as controls.

In additional experiments, confluent quiescent mesangial cells were exposed to a 50% solution of MPCM. The final concentration of FCS remained at 0.5%. The cultures were maintained in this medium for up to 7 d. The tissue culture supernatants were harvested and centrifuged for 30 s at $11,600 \times g$ to remove cell debris and were then stored at -20°C for subsequent analysis of soluble fibronectin or the cytokines TGF β , platelet-derived growth factor (PDGF), tumor necrosis factor (TNF) α , or interleukin (IL)-1 β .

Preparation of Cell Lysates

After removal of tissue culture supernatants, cell monolayers were washed with PBS, scraped into 1% Nonidet P40 in wash buffer (PBS containing 0.3 M NaCl and 1% Tween 20), and then incubated at room temperature for approximately 30 min. The cell scrapings were then transferred to 2-ml tubes, sonicated for 5 s, and centrifuged for 30 s at $11,600 \times g$. Sonication and centrifugation were repeated, and the lysate supernatants were assayed for fibronectin and total cell protein.

Effect of Suramin on MPCM

To assess the contribution of TGF β and PDGF to MPCM-mediated fibronectin production, the antihelminthic, polyanionic drug suramin was used. Suramin has been shown to antagonize the binding of growth factors such as TGF β and PDGF to their receptors (14,15). Confluent, quiescent mesangial cells were exposed to MPCM, in combination with 150 μ g/ml suramin, for 24 h. Supernatants and cell lysates were assayed for fibronectin.

TGF β and PDGF Cell-Binding Assays

Confluent, quiescent mesangial cells in 24-well plates were fixed with 200 μ l/well 0.25% glutaraldehyde for 10 min at room temperature. The plate was washed twice with 2 ml of HBSS/well. The fixed mesangial cells were then treated with 200 μ l/well of either 10 ng/ml TGF β (or PDGF) \pm 150 μ g/ml suramin or medium \pm 150 μ g/ml suramin for 1 h at room temperature. After incubation, the plate was washed three times with enzyme-linked immunosorbent assay (ELISA) wash buffer and blocked with 2% bovine serum albumin (BSA) (in wash buffer) for 30 min. A total of 200 μ l of rabbit anti-TGF β (or goat anti-human PDGF) was added to each well and incubated for 1 h at room temperature. After three washes, 200 μ l/well of goat anti-rabbit Ig-horseradish peroxidase (HRP)-conjugated antibody (Dako, High Wycombe, United Kingdom) at 1:1000 dilution (or rabbit anti-goat Ig-HRP [Dako] at 1:5000 dilution) was

added to each well and incubated for an additional hour at room temperature. After three more washes, 200 μ l/well 1,2-phenylenediamine dihydrochloride substrate solution was added (see section, Fibronectin ELISA, below). The reaction was stopped with 200 μ l of 1 M H_2SO_4 . Duplicate 200- μ l aliquots from each of the 24 wells were transferred to the wells of a 96-well plate, and the optical density was determined.

Effect of Neutralizing Anticytokine Antibodies on MPCM

Mesangial cells were exposed to: (1) MPCM, in combination with either 10 μ g/ml rabbit pan-specific anti-TGF β , goat anti-human PDGF, goat anti-murine TNF α , or goat anti-murine IL-1 β ; (2) MPCM, in combination with a "cocktail" of neutralizing antibodies (10 μ g/ml each of α TGF β , α PDGF, α TNF α , and α IL-1 β); and (3) cytokines (natural human TGF β , natural human PDGF, recombinant murine TNF α , and recombinant murine IL-1 β ; 2.5 ng/ml of each), in combination with the "cocktail" of neutralizing anticytokine antibodies. Incubations were carried out for 7 d, after which cell lysates, supernatants, or both, were assayed for fibronectin. All cytokines and anticytokine antibodies were purchased from R&D Systems, Inc. (Minneapolis, MN).

Fibronectin ELISA

Culture supernatants or cell lysates were assayed for fibronectin, using an inhibition ELISA. A total of 60 μ l of rat plasma fibronectin standard (19 to 5000 ng/ml) (Calbiochem, Nottingham, United Kingdom), supernatant sample, or cell lysate was incubated with an equal volume of rabbit anti-rat fibronectin diluted 1:2000 in wash buffer at 4°C overnight. Fifty microliters of this reaction mixture was then transferred to each well of a 96-well microtiter plate (Nunc Immuno-plate, Roskilde, Denmark) that had been precoated at 4°C overnight with rat plasma fibronectin (1 μ g/ml in 0.05 M carbonate buffer, pH 9.6) and blocked with 2% BSA in wash buffer for 1 h at room temperature. The plate was incubated with the reaction mixture at room temperature for 2 h. After washing each well four times, 50 μ l of goat anti-rabbit IgG conjugated to HRP (Dako) was added to the well and incubated at room temperature for 1 h. After four more washes, 50 μ l of 0.67 mg/ml 1,2 phenylenediamine dihydrochloride was added in 0.03 M citrate buffer, pH 5.0, containing 0.012% H_2SO_4 , and absorbance was read at 492 nm on a Titertek Multiskan Plus microtiter plate reader (Flow Laboratories, Oxfordshire, United Kingdom).

Cytokine ELISA

Cytokine measurements were carried out on culture supernatants, using commercially available ELISA assays for the following cytokines: human TGF β (Predicta, Genzyme Diagnostics, R&D Systems), human PDGF-AB (Biotrak, Amersham), rat TNF α (Factor-Test-X, Genzyme Diagnostics), and IL-1 β (Intertest-1 β -X, Genzyme Diagnostics). Assays were carried out according to the manufacturer's instructions.

DNA Assay

Cell monolayers were washed four times with ice-cold 0.9% wt/vol NaCl and then scraped into 10% ice-cold perchloric acid (PCA). The wells were washed with further aliquots of 10% PCA, after which the washings were pooled, vortexed, and spun at 3000 \times g for 10 min at 4°C. After discarding the supernatants, 500 μ l of fresh 10% PCA was added, and the solution was hydrolyzed by heating at 70°C in a water bath for 20 min. After hydrolysis, the tubes were chilled on ice to

precipitate as much protein as possible. The tubes were then centrifuged for 10 min at 3000 \times g at 4°C to spin down the protein precipitate, which was subsequently analyzed for protein concentration. The supernatants containing the DNA were transferred to plastic test tubes. A total of 250 μ l of diphenylamine reagent (1 g of diphenylamine/25 ml of glacial acetic acid) followed by 50 μ l of acetaldehyde solution (1.6 mg/ml in water) was added to the 250- μ l cell hydrolysate or calf thymus DNA standard (0 to 200 μ g/ml). The mixture was vortexed and incubated at 25 to 30°C for 16 to 20 h. The absorbance of the reaction solution was read at 595 and 710 nm, and the difference between the absorbances at the two wavelengths was calculated. (Light scattering at 710 nm was measured to eliminate any effects arising from the slight turbidity of the samples.) A standard curve of change in absorbance versus DNA concentration was constructed, from which the DNA concentration was determined.

Protein Determination

For cell monolayers that had been precipitated with PCA for DNA determinations, the cell protein content was measured by the method of Lowry *et al.* (16), using BSA standards. The protein content of cell lysates dissolved in Nonidet P40 was determined using a commercial BioRad DC protein assay, using BSA standards.

[3H]Thymidine Incorporation Assays

Mesangial cell proliferation was measured by [3H]thymidine incorporation. Confluent, quiescent mesangial cells were exposed to MPCM or medium alone for 3 d. Then, 1 μ Ci/well [3H]thymidine (Amersham) was added directly to each well. The cells were incubated for an additional 24 h, after which the culture media were discarded and the wells rinsed once with PBS. One milliliter of 0.1 mM cold thymidine in RPMI + 0.5% FCS was then added to each well and incubated at 37° for 20 min. The wells were washed once with ice-cold PBS, twice with 10% trichloroacetic acid, and then once with PBS again. A total of 250 μ l of 0.5 M NaOH was added to each well, and the plate was incubated at 60 to 70°C for 30 min to dissolve the cell monolayer. Two hundred microliters of cell lysate from each well was added to 4 ml of Ecoscint A scintillation fluid (National Diagnostics, Mansville, NJ), followed by 20 μ l of concentrated HCl. 3H activity was counted on an LKB 1219 liquid scintillation counter (LKB Instruments, Bromma, Sweden).

Identification of Newly Synthesized Fibronectin

Biosynthetic Labeling with ^{35}S -Methionine. Confluent, quiescent mesangial cells were exposed to MPCM or medium alone diluted 1:1 in methionine-free RPMI (Sigma) for 3 d. Eighteen hours before termination of the experiment, each well was pulsed with 50 μ Ci of ^{35}S -methionine (Amersham). The culture media were retained, and the cell monolayers were washed twice in PBS. Cell lysates were prepared as described above.

Immunoprecipitation. To immunoprecipitate the newly synthesized fibronectin, 20 μ l of goat anti-rat fibronectin (Calbiochem) was added to 500 μ l of culture medium or 200 μ l of cell lysate. Normal goat serum was used as control. The samples were incubated overnight at 4°C. Fifty microliters of insoluble protein A cell suspension (10% wet vol/vol of nonviable *S. aureus* [Cowan strain] cells in 0.04 M sodium phosphate buffer, pH 7.2, 0.15 M NaCl, and 0.05% sodium azide) was then added to precipitate out the antigen:antibody complexes and then incubated for 4 h at 4°C. The samples were centrifuged for 10 min at 3000 \times g, and the pellets were washed three times with ice-cold immunoprecipitation buffer (PBS containing 0.5 M NaCl, 0.1% sodium dodecyl sulfate [SDS], and 1% Triton X-100, pH

7.4), vortexing the pellet thoroughly between each wash. Finally, the pellets were washed with ice-cold PBS and dissolved in 70 μ l of SDS-polyacrylamide gel electrophoresis (PAGE) sample buffer containing 3% SDS and 10% 2-mercaptoethanol and heated for 7 min in a boiling water bath. The dissolved pellets were centrifuged in a microfuge for 30 s.

The radiolabeled proteins were resolved by SDS-PAGE on 5% polyacrylamide gels. Newly synthesized proteins were detected by autoradiography of dried gels. Bands were quantified by scanning densitometry on an LKB Ultrascan densitometer (LKB Instruments).

Northern Blotting

Confluent, quiescent mesangial cells were exposed to MPCM or medium alone for 24 h. Total RNA was extracted using TRIzol reagent (Life Technologies), according to the manufacturer's instructions. Aliquots (30 μ g) of RNA were electrophoresed on a 1% agarose gel containing 1.9% formaldehyde in MOPS (3-(*N*-morpholino)propanesulfonic acid). The resolved RNA was transferred onto Hybond-N nylon membranes (Amersham) by capillary action using 20 \times SSC (1 \times SSC = 15 mM trisodium citrate, 150 mM sodium chloride). The membranes were prehybridized for 4 h at 37 or 42°C (depending on probe) with 200 μ g/ml denatured salmon sperm DNA in 50% formamide, 1% SDS, 5 \times Denhardt's, and 5 \times saline-sodium phosphate ethylenediaminetetra-acetic acid (SSPE) [1 \times SSPE = 11.5 mM sodium phosphate, 150 mM sodium chloride, 1 mM EDTA]. The membranes were then hybridized overnight with a [32 P]dCTP cDNA probe that had been Klenow DNA polymerase-labeled, using a random primer labeling system (Prime-a-Gene, Promega) in fresh buffer (same composition as prehybridization buffer). After hybridization, the membranes were washed twice with 1% SDS, 2 \times SSPE at room temperature, twice with 0.2% SDS, 0.2% SSPE at 65°C, then exposed to X-Omat LS film (Kodak) with intensifier screens at -70°C. Membranes were subsequently stripped in boiling 5% SDS, 0.5 \times SSPE before reprobing. Densitometric analysis of the transcripts was carried out on a BioRad GS 700 imaging scanner. RNA loading was normalized using a cDNA probe for cyclophilin. Cyclophilin expression was not affected by treatment with MPCM (data not shown).

Probes

All of the cDNA probes were generous gifts. cDNA for rat fibronectin was from Dr. R. O. Hynes (Massachusetts Institute of Technology) (17); murine α 1 (IV) collagen and laminin B1 chain cDNA were from Dr. Kurkinen (Department of Medicine and Dentistry of New Jersey-Rutgers Medical School, Piscataway, NJ) (18,19); murine TGF β 1 was from Dr. R. Akhurst (Department of Medical Genetics, Glasgow University, Glasgow, Scotland) (20); murine PDGF B chain was from Dr. C. D. Stiles (Dana Farber Cancer Institute, Harvard Medical School, Boston, MA) (21); murine tissue inhibitor of metalloproteinase (TIMP)-1 cDNA was from Dr. D. T. Denhardt (Department of Biochemistry, Rutgers University, Piscataway, NJ); rat transin was from Professor R. Breathnach (Laboratoire de Recherche, Nantes, France) (22); and human cyclophilin was from SmithKline Beecham Pharmaceuticals.

Statistical Analyses

Data were expressed as means \pm SEM. For comparison of means between two groups, an unpaired *t* test was used. To compare values between multiple groups, ANOVA with a Bonferroni correction was applied. Statistical significance was defined as *P* < 0.05.

Results

Effect of Macrophage/Mesangial Cell Coculture on Fibronectin Production

Macrophages cultured in the presence of 0.5% FCS for 3 d generated small amounts of secreted fibronectin dose dependently (Figure 1). Mesangial cells also constitutively secreted fibronectin. However, direct coculture of macrophages with mesangial cells resulted in a synergistic increase in fibronectin production proportional to the number of added macrophages (Figure 1).

Effect of MPCM on Mesangial Cell Fibronectin Production

To verify that the macrophage effect on mesangial cell fibronectin production was due to secreted factors and could occur independently of cell:cell contact, mesangial cells were exposed to MPCM.

Although macrophages cultured for 3 d in 0.5% FCS secreted fibronectin, the matrix protein could not be detected in MPCM *per se*. Cultured mesangial cells constitutively secreted low levels of fibronectin into the culture medium (Table 1). Addition of MPCM significantly enhanced this production

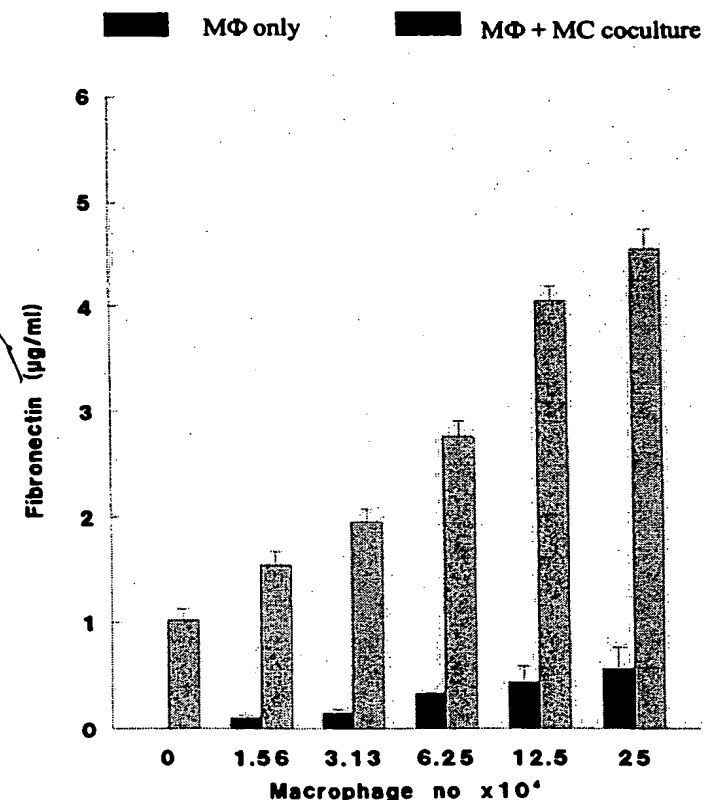


Figure 1. Effect of macrophage/mesangial cell coculture on fibronectin production. Increasing numbers of macrophages were cultured alone or in combination with confluent, quiescent mesangial cells for 3 d in medium containing 0.5% fetal calf serum (FCS). Tissue culture supernatants were assayed for fibronectin. Results are means \pm SEM of eight wells.

Table 1. Time course of fibronectin secretion in response to MPCM^a

Day	Fibronectin ($\mu\text{g/ml}$)	
	Medium	MPCM
0	0	0
3	1.21 ± 0.13	4.48 ± 0.46
5	1.83 ± 0.18	5.92 ± 0.46
7	2.34 ± 0.37	9.40 ± 1.15

^a Mesangial cells were incubated with MPCM for 3, 5, and 7 d. Supernatants were assayed for fibronectin. Values are means \pm SEM ($n = 3$) each carried out in quadruplicate. MPCM, macrophage-conditioned medium.

with time (Table 1). The effect of MPCM demonstrated a clear dose dependency (Figure 2A), which was maintained when fibronectin production was expressed as a function of total cell DNA (Figure 2B) or protein (Figure 2C), indicating that the effect was not secondary to an increase in cell number.

MPCM also caused an increase in cell-associated fibronectin. Of the total amount of fibronectin produced by mesangial cells, approximately 80% was secreted into the supernatant, whereas 20% was cell-associated ($427.5 \pm 59 \text{ ng}/\mu\text{g}$ cell protein in supernatant *versus* $80.1 \pm 16.1 \text{ ng}/\mu\text{g}$ cell protein in cell lysate). Values are means \pm SEM ($n = 4$).

The increase in fibronectin was not a result of residual or contaminating endotoxin in the MPCM activating the mesangial cells, because addition of LPS to a final concentration of $1 \mu\text{g/ml}$ directly to mesangial cells did not result in an increase in constitutive fibronectin levels in either the secreted or cell-associated forms (data not shown).

Effect of MPCM on Mesangial Cell Proliferation

[³H]Thymidine incorporation assays were used to assess mesangial cell proliferation in response to MPCM. MPCM suppressed mesangial cell proliferation dose dependently: the greater the concentration of MPCM, the lower the incorporation of [³H]thymidine (Figure 3).

Effect of MPCM on De Novo Fibronectin Synthesis

To assess whether the observed increase in fibronectin levels was due to an increase in protein synthesis, biosynthetic labeling of fibronectin was carried out. Autoradiographs of the immunoprecipitated, biosynthetically labeled fibronectin showed that exposure of mesangial cells to MPCM resulted in an increased fibronectin synthesis over that of medium alone (Figure 4, A and B). Densitometric analysis of the 220-kD fibronectin band from three independent experiments showed 5.9- and 4.4-fold increases over control in the secreted and cell-associated forms of MPCM-induced fibronectin, respectively (0.31 ± 0.06 *versus* 0.053 ± 0.007 , $P < 0.001$, and 0.31 ± 0.07 *versus* 0.073 ± 0.016 , $P < 0.005$ arbitrary densitometric units).

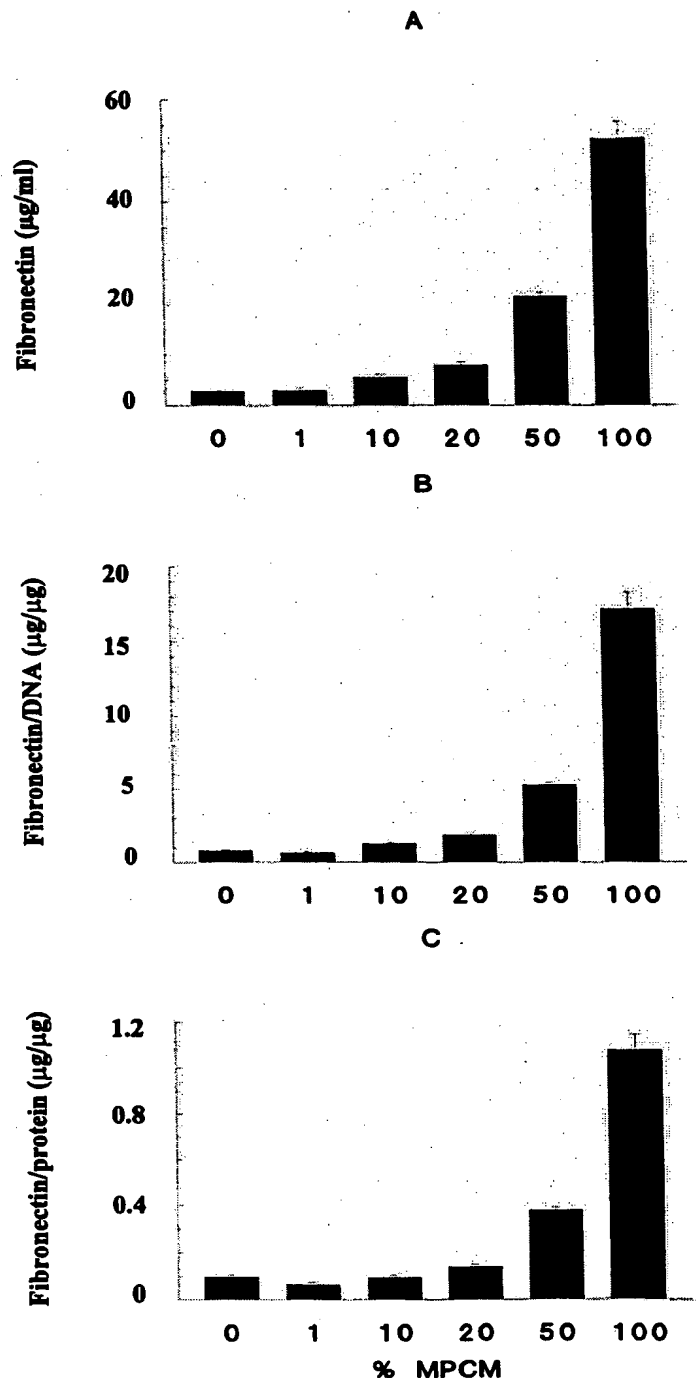


Figure 2. Effect of macrophage-conditioned medium (MPCM) on mesangial cell fibronectin production. Confluent, quiescent mesangial cells were incubated with 0, 1, 10, 20, 50, and 100% MPCM for 7 d. Culture supernatants were assayed for fibronectin. Cell lysates were assayed for total cell DNA and total cell protein. Results are expressed as micrograms of fibronectin secretion per milliliter (A), per microgram of cell DNA (B), and per microgram of cell protein (C). A representative experiment from three experiments carried out in quadruplicate is shown.

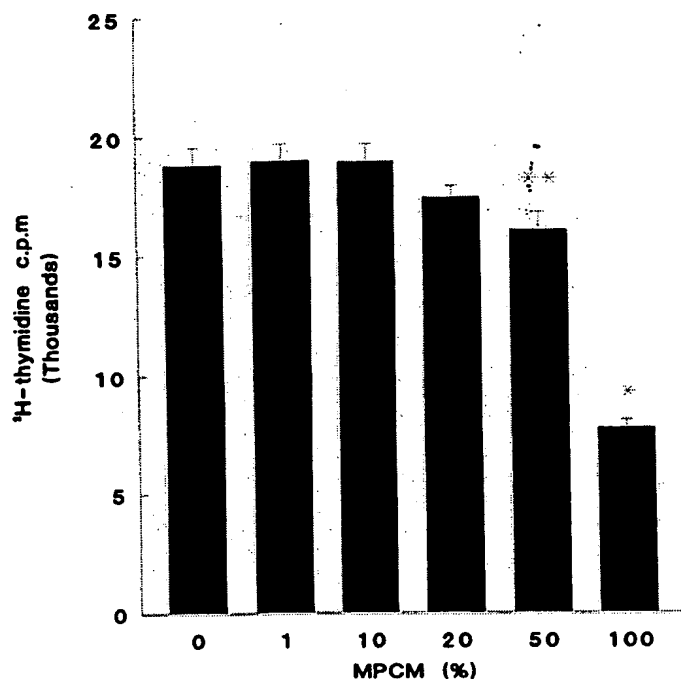


Figure 3. Effect of dose of MPCM on mesangial cell proliferation. A total of $1 \mu\text{Ci/ml}$ [^3H]thymidine was added to mesangial cells exposed to 0, 1, 10, 20, 50, and 100% MPCM. Results are means \pm SEM of eight wells. * $P < 0.001$; ** $P < 0.003$ versus medium alone (0% MPCM).

Effect of MPCM on Mesangial Cell Extracellular Matrix Gene Transcription

Figure 5 illustrates that there was an increase in mesangial cell fibronectin mRNA in quiescent rat mesangial cells exposed to MPCM for 24 h. Analysis of the 8-kb fibronectin band by scanning densitometry showed that fibronectin mRNA was increased 2.9 ± 0.24 -fold ($P < 0.001$, $n = 5$) over control cells exposed to medium alone (normalizing for RNA loading with cyclophilin). A second, larger transcript (>9.49 kb) was also seen, but was not included for analysis in this study. As well as message for fibronectin, the genes for the matrix proteins collagen IV ($\alpha 1$ (IV) collagen) and laminin (B1 chain) were also upregulated 3.1 ± 0.3 -fold ($P < 0.001$, $n = 4$) and 4.9 ± 0.2 -fold ($P < 0.001$, $n = 4$), respectively (Figure 5).

Effect of MPCM on Mesangial Cell Transin and TIMP-1 Gene Transcription

Stromelysin or rat transin is a matrix metalloproteinase (MMP) that is able to degrade various matrix components, including fibronectin (23). Northern blot analysis demonstrated that MPCM induced *de novo* transin expression in mesangial cells, whereas TIMP-1 mRNA was upregulated 15.2 ± 2.5 -fold ($P < 0.001$, $n = 6$) over control levels (Figure 6).

Detection of Growth Factors in MPCM and Tissue Culture Supernatants

TGF β , PDGF, TNF α , and IL-1 β are cytokines whose presence in the glomerulus has been associated with the progres-

sion to glomerulosclerosis. None of the cytokines could be detected in MPCM using the commercially available ELISA. After concentration of MPCM 20 \times using Amicon Centriprep 3 concentrators (Amicon), TGF β , PDGF, and IL-1 β remained undetectable, although TNF α was detected at a concentration of 90 pg/ml. However, TGF β and PDGF-AB were detected in mesangial cell culture supernatants (2.56 ± 0.69 and 1.18 ± 0.22 ng/ml, respectively), suggesting that these cytokines were autocrinally secreted by mesangial cells. Furthermore, this autocrinal secretion was upregulated 1.69 ± 0.16 - and 2.29 ± 0.28 -fold, respectively ($P < 0.001$, $n = 8$), in response to MPCM. The secreted TGF β was in the latent, or inactive, form, since it could not be detected in the assay unless the samples had been activated by acidification.

Northern blot analysis demonstrated that the observed increase in secreted cytokines in response to MPCM had been preceded by an upregulation of message for these cytokines (Figure 7). TGF β mRNA transcription was upregulated 2.2 ± 0.4 -fold ($P < 0.001$, $n = 4$) and PDGF B chain mRNA 5.7 ± 1.2 -fold ($P = 0.004$, $n = 5$) over control levels (Figure 7). Neither TNF α nor IL-1 β could be reliably detected in tissue culture supernatants from mesangial cells exposed to MPCM.

Effect of Suramin on MPCM-Mediated Mesangial Cell Fibronectin Production

To ascertain the contribution of autocrinally secreted TGF β and PDGF to the observed increase in fibronectin levels, the growth factor receptor antagonist suramin was used. Binding of exogenously added TGF β and PDGF to fixed mesangial cells could readily be detected under control conditions, as evidenced by an increase in A_{492} (Table 2). Addition of suramin significantly decreased detectable, bound TGF β and PDGF. Indeed, addition of suramin produced A_{492} readings that were similar to those observed in medium without exogenously added cytokines (i.e., background), confirming that suramin could effectively abolish TGF β and PDGF binding to mesangial cells by interfering with cytokine receptor binding.

Exposure of mesangial cells to MPCM, in combination with 150 $\mu\text{g/ml}$ suramin, resulted in a reduction of secreted fibronectin to $83.8 \pm 4.4\%$ ($P = 0.02$, $n = 3$) and a reduction of cell-associated fibronectin to $59.5 \pm 3.0\%$ ($P = 0.005$, $n = 3$) of control levels. Suramin had no statistically significant effect on basal fibronectin production by mesangial cells.

Effect of Neutralizing Antibodies on MPCM-Mediated Fibronectin Production

In an alternative approach to assessing the contribution of known cytokines to the observed effects of MPCM, mesangial cells were exposed to a panel of neutralizing antibodies. Anti-TGF β significantly reduced MPCM-mediated supernatant fibronectin production to $72.9 \pm 3.7\%$ of untreated MPCM ($P < 0.001$, $n = 5$) and cell-associated fibronectin production to $66.3 \pm 6.8\%$ ($P = 0.003$) (Table 3). Antibodies to PDGF, TNF α , and IL-1 β had no significant effect, suggesting that these cytokines, at least individually, played no role in MPCM-mediated fibronectin production. (Antibody concentrations of up to 50 $\mu\text{g/ml}$ did not produce any greater reduction in

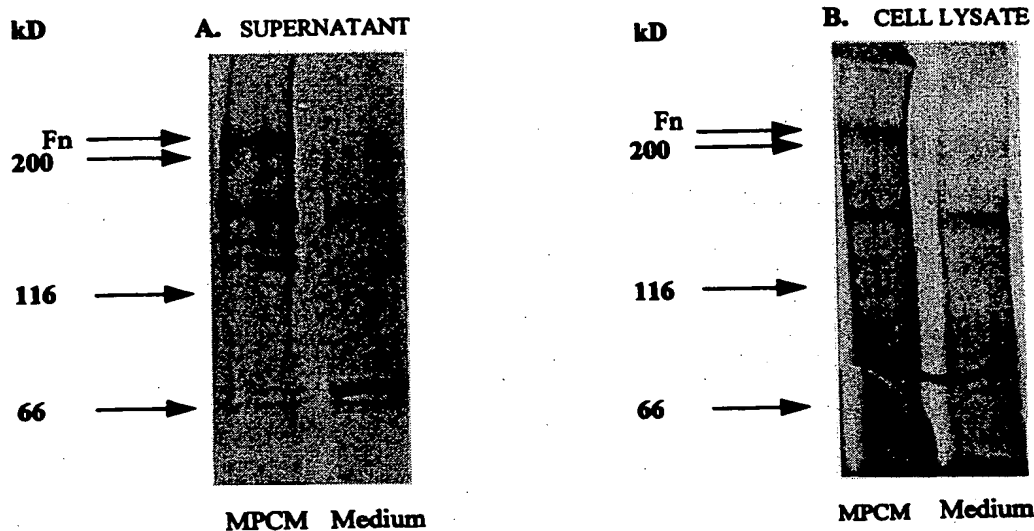


Figure 4. Effect of MPCM on *de novo* fibronectin synthesis. Autoradiograph of immunoprecipitated supernatant (A) and cell-associated ^{35}S -fibronectin (B). A representative autoradiograph from three experiments is shown.

fibronectin production by mesangial cells [data not shown].) A "cocktail" of neutralizing antibodies to the cytokines TGF β , PDGF, TNF α , and IL-1 β was effectively able to abolish fibronectin secretion stimulated by exogenously added cytokines (6.7 ± 5.7 , $P < 0.001$) (Figure 8A). However, the same cocktail was only able to reduce MPCM-stimulated fibronectin secretion to $77.9 \pm 7.4\%$ of untreated MPCM ($P = 0.04$, $n = 3$) (Figure 8B), a degree of reduction that was no greater than that observed with anti-TGF β alone.

Discussion

The present study demonstrates that macrophage-derived factors can initiate renal scarring directly, by production of matrix proteins, and also indirectly, via the production of profibrogenic cytokines and modulation of matrix turnover.

In the current study, MPCM caused cultured mesangial cells to secrete fibronectin in a time- and dose-dependent manner. The fibronectin was derived from mesangial cells since the matrix protein was not detected in the MPCM *per se*, although fibronectin was secreted by macrophages cultured for 3 d in medium containing 0.5% FCS. This is in agreement with observations by other investigators who demonstrated that human and mouse macrophages also secrete fibronectin (24,25). The function of macrophage fibronectin may be to aid binding of macrophages to mesangial cells, because Dubois *et al.* (26) have shown that, *in vitro*, rat peritoneal macrophages preferentially bind to rat mesangial cells via interactions with fibronectin expressed on the macrophage cell surface. However, our data indicate that macrophages can induce mesangial cell fibronectin production independently of macrophage:mesangial cell contact. This increase in fibronectin secretion could not be accounted for by endotoxin contamination of MPCM, because addition of LPS directly to mesangial cells had no effect on basal fibronectin production.

Northern blot analysis, taken together with the biosynthetic

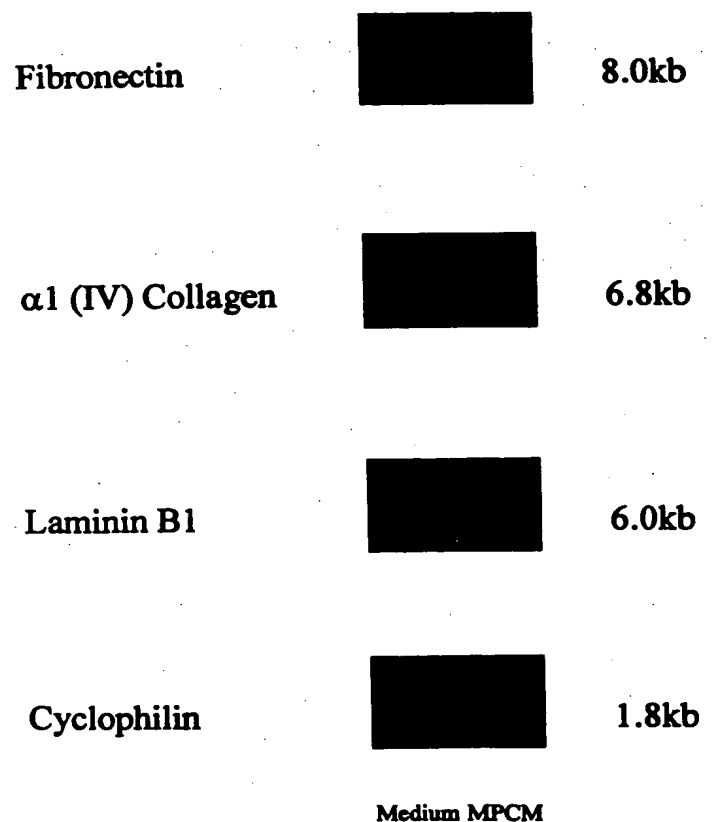


Figure 5. Effect of MPCM on mesangial cell extracellular matrix gene transcription. Northern blot analysis was carried out on RNA extracted from mesangial cells incubated with MPCM or medium alone for 24 h. RNA was probed for fibronectin, $\alpha 1$ (IV) collagen IV, and laminin B1 chain. Representative blots from four to five experiments are presented.

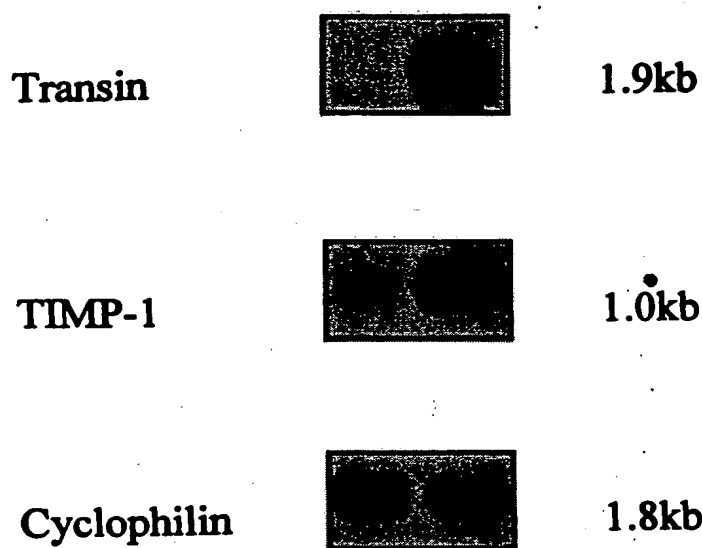


Figure 6. Effect of MPCM on mesangial cell transin and tissue inhibitor of metalloproteinase-1 (TIMP-1) gene transcription. Northern blot analysis of mesangial cell RNA after treatment with MPCM or medium alone. Representative blots from five and six experiments, respectively, are shown.

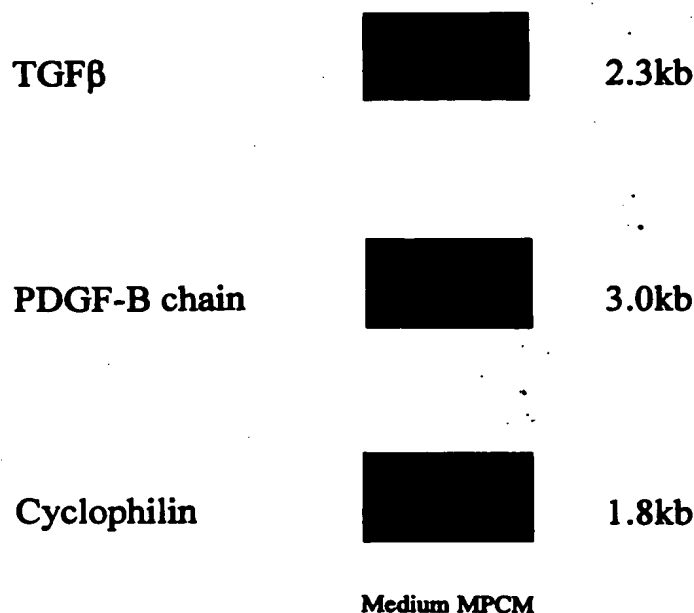


Figure 7. Effect of MPCM on TGFβ and PDGF B chain gene transcription. Northern blot analysis of mesangial cell RNA after treatment with MPCM or medium alone. One representative blot from five experiments is shown.

labeling studies, suggests that the MPCM-mediated upregulation of mesangial cell fibronectin production occurs, at least in part, as a result of increased mRNA transcription and protein

Table 2. Effect of suramin on the binding of TGFβ and PDGF to mesangial cells^a

Group	A ₄₉₂	
	Control	+ Suramin
Medium	0.327 ± 0.007	0.326 ± 0.003
TGFβ	0.456 ± 0.008	0.370 ± 0.008 ^b
PDGF	0.438 ± 0.007	0.346 ± 0.007 ^b

^a Glutaraldehyde-fixed mesangial cells were incubated with 10 ng/ml of either TGFβ or PDGF in the presence or absence of 150 μg/ml suramin. Bound cytokine was detected using anti-TGFβ or anti-PDGF antibodies followed by the appropriate horseradish peroxidase-labeled second antibody and colorimetric analysis (expressed as A₄₉₂). Each value represents means ± SEM of six wells (one of three representative experiments). A, absorbance; TGF, transforming growth factor; PDGF, platelet-derived growth factor.

^b *P* < 0.001 versus corresponding suramin-untreated cells.

Table 3. Effect of neutralizing antibodies on MPCM-mediated fibronectin production

Group	Fibronectin (% of MPCM)	
	Supernatant	Cell Lysate
MPCM	100	100
αTGFβ	72.9 ± 3.7 ^b	66.3 ± 6.8 ^c
αIL-1β	107.0 ± 4.8	110.5 ± 7.5
αPDGF	102.5 ± 5.3	95.0 ± 7.1
αTNFα	100.1 ± 0.6	99.0 ± 7.2

^a Mesangial cells were exposed to MPCM in combination with antibodies (α) to TGFβ, IL-1β, PDGF, or TNFα. Supernatants and cell lysates were assayed for fibronectin. Values are means ± SEM (*n* = 3 to 5), each carried out in quadruplicate. IL, interleukin; TNF, tumor necrosis factor.

^b *P* < 0.001.

^c *P* = 0.003 versus untreated MPCM.

synthesis. However, MPCM was also found to induce the expression of mRNA for the MMP transin and to upregulate mRNA for TIMP-1. Although upregulation of message does not always suggest translation of protein, a number of reports have suggested that TIMP-1 mRNA expression and protein secretion are tightly coupled (27). These observations suggest that macrophage-derived products may also modulate matrix turnover, and they raise the possibility that fibronectin accumulation could also result from a net decrease in degradation rate, depending on the balance between MMP and TIMP-1 production. However, the fivefold accumulation in fibronectin protein as assessed by both the ELISA and immunoprecipitation studies confirms that the net effect of macrophage-derived products is the accumulation of matrix proteins.

The observed increase in fibronectin levels was not secondary to a stimulation of cell proliferation. When fibronectin secretion was expressed per unit cell DNA or cell protein, the

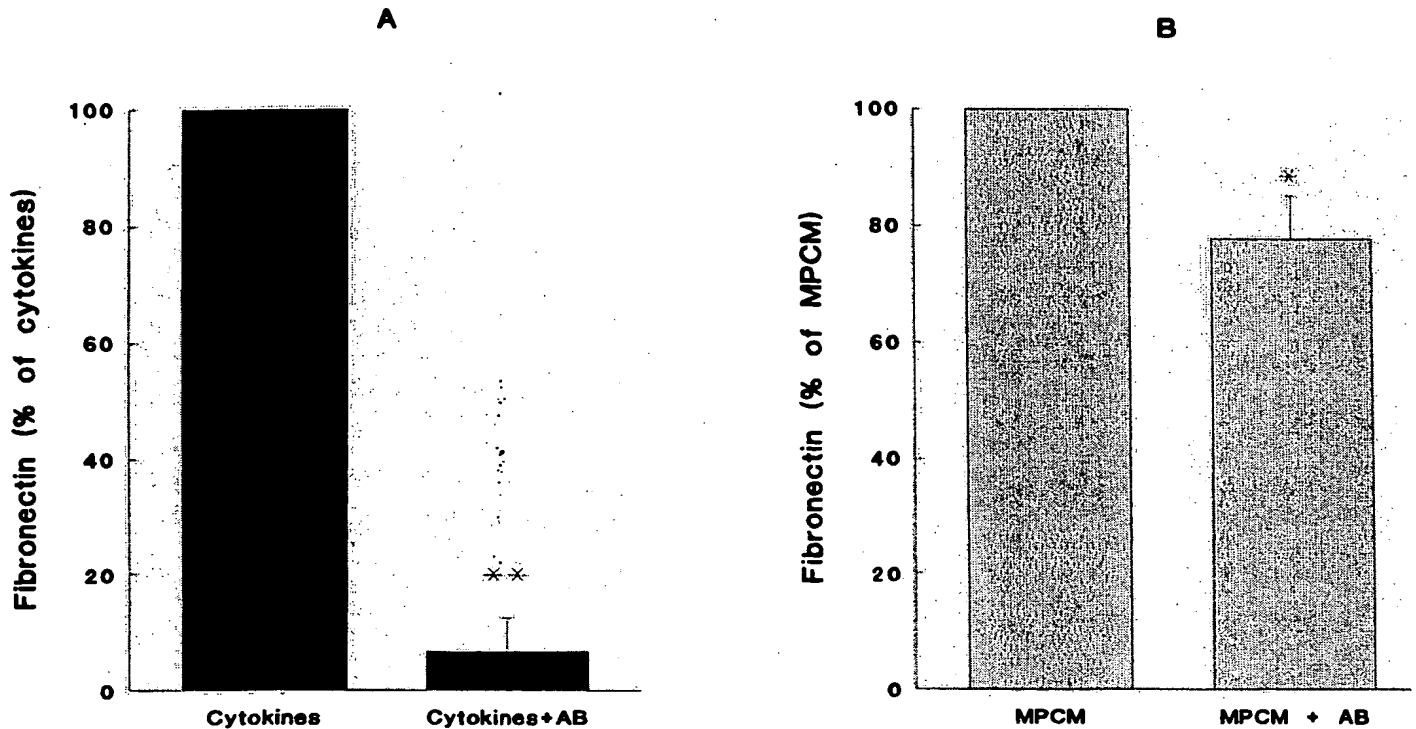


Figure 8. Effect of a cocktail of neutralizing antibodies on MPCM and cytokine-mediated fibronectin production. Mesangial cells were exposed to cytokines (Panel A) or MPCM \pm a cocktail of neutralizing anticytokine antibodies (AB) (Panel B). Supernatants were assayed for fibronectin. Values are means \pm SEM ($n = 3$), each carried out in quadruplicate. * $P = 0.04$; ** $P < 0.001$ versus MPCM.

effects of MPCM were still observed. [^3H]Thymidine incorporation assays showed that MPCM actually suppressed mesangial cell proliferation, or at least [^3H]thymidine uptake. The suppressive effect of MPCM is in agreement with the findings of Ooi *et al.* (28), who demonstrated suppression of mesangial cell proliferation by murine MPCM derived from endotoxin-treated mice. These observations contrast with those of other researchers who have found that MPCM can stimulate mesangial cell proliferation (29–32). The differences between these studies may be a function of the concentration of mitogenic factors in MPCM, because Mattana and Singhal (33) found that macrophage supernatants had both stimulatory and suppressive effects on mesangial cell proliferation, depending on the concentration of the supernatant used. Alternatively, the disparity may be due to the particular experimental conditions used.

At present, it is not clear whether the factor(s) suppressing proliferation and inducing fibronectin production are identical. Many *in vivo* studies have reported that cell proliferation precedes matrix accumulation, which has led to the formulation of the hypothesis that mesangial cell proliferation and accumulation of extracellular matrix are inextricably linked (34). Eng *et al.* (35), however, were able to demonstrate that the two processes could be partially dissociated. They demonstrated that administration of interferon- γ to anti-Thy-1 nephritic rats significantly reduced cell proliferation while increased levels of matrix deposition were maintained. These *in vivo* experiments thus concur with the findings reported in the study presented here, *i.e.*, that proliferation and matrix synthe-

sis can be dissociated. This is further supported by the findings of Groggel and Hughes, who demonstrated that heparan sulfate could stimulate rat mesangial cell matrix production while decreasing cell number (36), and those of Zhu *et al.* (37), who demonstrated that light chains isolated from patients with biopsy-proven light-chain deposition disease were able to increase mesangial cell fibronectin, laminin, and collagen IV in the absence of cell proliferation.

Laminin and collagen are matrix proteins more commonly associated with the basement membrane, although they are present in the mesangium in small amounts. Under pathophysiological conditions, increased amounts of these matrix proteins are found in the mesangium. This study demonstrates that MPCM produces an increase in mesangial cell production of these three matrix proteins, consistent with the notion that macrophage-derived products play a role in the development of glomerulosclerosis. The combined expression of fibronectin, laminin, and collagen IV in mesangial cells has been reported previously in a number of other experimental systems, including: (1) exposure to high glucose conditions (38); (2) after stimulation with thromboxane (39); and (3) after treatment with morphine-stimulated macrophages (30). Differential expression of the three matrix proteins has also been described (40). The extracellular matrix in sclerosed mesangial areas generally contains these matrix proteins, although the exact composition varies among diseases. Whether the production of the three matrix proteins occurs in a coordinated manner in response to one factor via the activation of a common tran-

scriptional element or whether each matrix protein is independently regulated by several different factors is yet to be elucidated. TGF β , for example, has been shown to directly stimulate the activity of α 2(I) collagen promoter (41) and the fibronectin promoter (42) in human cell lines, and it has been speculated that matrix genes, often coexpressed after stimulation with TGF β , might be activated by a common transcriptional factor such as nuclear factor κ B (43).

TGF β has been shown to be expressed in many conditions, leading to glomerulosclerosis. Ding *et al.*, in experiments on PAN-nephrotic rats, have tentatively identified glomerular macrophages as a potential source of TGF β (8). In the current study, TGF β was not detected in MPCM *per se*, although mesangial cells were shown to constitutively secrete TGF β (and PDGF-AB) into their culture media, and this autocrine secretion was further upregulated in response to MPCM. The secreted TGF β was found to be in the latent or inactive form, in accord with the findings of other investigators (44).

The experiments with the neutralizing antibodies suggest that, with the exception of TGF β , the other cytokines, individually, play no role in MPCM-mediated fibronectin production. The antibodies used in this study were neutralizing for either mouse or human cytokines and were able to completely block the activity of exogenously added human or mouse cytokines at the concentration used; whether they would also neutralize endogenous rat cytokines is difficult to ascertain with the current, limited availability of rat cytokines. However, it is noteworthy that higher concentrations of antibody (50 μ g/ml) demonstrated no additional effect. Moreover, suramin, whose action to inhibit growth factor binding would be species-independent, demonstrated a comparable (and no greater) reduction in fibronectin accumulation to those seen with the anti-TGF β neutralizing antibody. Taken together, the data suggest that TGF β plays a small but significant role in MPCM-mediated fibronectin production. However, the majority of the fibronectin-stimulating activity in MPCM cannot be attributed to this growth factor. The identity of the factor(s) responsible for the majority of the stimulatory activity remains to be elucidated. Although TGF β has been implicated in the pathogenesis of glomerulosclerosis (45), it is of note that Border and associates have reported that in rat mesangial cells expression of fibronectin, laminin, and collagen IV is not substantially affected by TGF β , as demonstrated by immunoprecipitation of metabolically labeled culture supernatants (46).

Whether the macrophage model used in this study, *i.e.*, thioglycollate-elicited, LPS-stimulated peritoneal macrophages, represents or reflects the effects of infiltrating macrophages found in conditions of renal disease is unclear. To date, the precise activation state of infiltrating macrophages has not been fully described and no doubt varies according to a number of criteria, including cell origin, maturity, and environmental and immunological factors (47,48). However, certain comparisons can be made between the present *in vitro* system and the pathophysiological *in vivo* conditions. Infiltrating macrophages are, in a broad sense, elicited into the glomerulus by the actions of chemokines, etc. Macrophage adherence to plastic surface has been shown to mimic the spreading of these cells to

vascular surfaces (49). *In vitro*, the process of adhesion itself has been shown to upregulate the gene transcription of certain cytokines, which are generally not translated until they have received a second signal from agents such as LPS (50). In addition, it has been shown previously that peritoneal macrophages behave in a qualitatively similar way to glomerular macrophages. For example, peritoneal and glomerular macrophages from diet-induced hypercholesterolemic and PAN-nephrotic rats both exhibit an upregulation of TGF β gene expression (10). The current studies clearly demonstrate that macrophage-derived products can induce potent profibrogenic characteristics in mesangial cells. The use of MPCM more closely mimics the likely events occurring *in vivo* than those studies that used heterologous, purified recombinant proteins (traditionally associated with macrophages) added in "industrial," or at least nonphysiological, concentrations to achieve similar effects.

In conclusion, this study provides direct evidence of a role for macrophages in the development of glomerulosclerosis; macrophage secretory products comprise all of the elements required for the initiation of the sclerotic process, as evidenced by the upregulation of the expression of proteins, genes, or both, for matrix proteins and profibrogenic growth factors and the ability to modulate matrix turnover by augmenting the mRNA expression of both the MMP transin and the inhibitor of matrix degradation TIMP-1.

Although TGF β plays an important role in the fibrogenic process, other factors, some of which are yet to be identified, are also involved.

Acknowledgments

The authors acknowledge Dr. Tim Johnson of the Sheffield Kidney Institute for transforming the original gift cDNA-containing plasmids into bacteria and Jez Brown for assistance with animal handling. Some of the data presented in this article were presented at the 1996 American Society of Nephrology Meeting held November 3 to 6 in New Orleans, LA. A large portion of this work was funded by a grant from the National Kidney Research Fund, Huntingdon United Kingdom.

References

1. Klahr S, Schreiner GF, Ichikawa I: Progression in renal disease. *N Engl J Med* 318: 1657-1666, 1988
2. Schreiner GF, Cotran RS, Unanue ER: Modulation of Ia and leukocyte common antigen expression in rat glomeruli during the course of glomerulonephritis and aminonucleoside nephrosis. *Lab Invest* 51: 524-533, 1984
3. Diamond JR, Pesek I, Ruggieri S, Karnovsky MJ: Essential fatty acid deficiency during acute puromycin nephrosis ameliorates late renal injury. *Am J Physiol* 257: F798-F807, 1989
4. Diamond JR, Pesek-Diamond I: Sublethal X-irradiation during acute puromycin nephrosis prevents late renal injury: Role of macrophages. *Am J Physiol* 260: F779-F786, 1991
5. Harris KPG, Baker F, Walls J: Early increase in glomerular leukocyte number after a reduction in renal mass: Implication for the pathogenesis of glomerulosclerosis. *Clin Sci* 85: 27-31, 1993
6. Van Goor H, Van der Horst ML, Fidler V, Grond J: Glomerular macrophage modulation affects mesangial expansion in the rat after renal ablation. *Lab Invest* 66: 564-571, 1992

7. Ding G, Pesek-Diamond I, Diamond JR: Cholesterol, macrophages and gene expression of TGF β_1 and fibronectin during nephrosis. *Am J Physiol* 264: F577-F584, 1993
8. Ding G, Van Goor H, Frye J, Diamond JR: Transforming growth factor β expression in macrophages during hypercholesterolaemic states. *Am J Physiol* 267: F937-F943, 1994
9. Okuda S, Languino LR, Ruoslahti E, Border WA: Elevated expression of transforming growth factor β and proteoglycan production in experimental glomerulonephritis: Possible role in expansion of the mesangial extracellular matrix. *J Clin Invest* 86: 453-462, 1990
10. Border WA, Okuda S, Languino LR, Sporn MB, Ruoslahti E: Suppression of experimental glomerulosclerosis by anti-serum against transforming growth factor β . *Nature (Lond)* 346: 371-374, 1990
11. Isaka Y, Fujiwara Y, Veda N, Kaneda Y, Kamada T, Imai E: Glomerulosclerosis induced by in vivo transfection of transforming growth factor β or platelet-derived growth factor gene in the rat kidney. *J Clin Invest* 92: 2597-2601, 1993
12. Foidart JB, Dechenne CA, Mahieu P, Creutz CE, De Mey J: Tissue culture of normal glomeruli: Isolation and morphological characterisation of two homogeneous cell lines. *Invest Cell Pathol* 2: 15-26, 1979
13. Kohan DE, Schreiner GF: Interleukin-1 modulation of renal epithelial glucose and amino acid transport. *Am J Physiol* 254: F879-F886, 1988
14. Coffey RJ, Leof EB, Shipley GD, Moses HL: Suramin inhibition of growth factor receptor binding and mitogenicity in AKR-2B cells. *J Cell Physiol* 132: 143-148, 1987
15. Betholtz C, Johnsson A, Heldin CH, Westermark B: Efficient reversion of simian sarcoma virus-transformation and inhibition of growth factor-induced mitogenesis by suramin. *Proc Natl Acad Sci USA* 83: 6440-6444, 1986
16. Lowry OH, Rosenbrough NJ, Farr AL, Randall RJ: Protein measurements with the Folin reagent. *J Biol Chem* 193: 265-275, 1951
17. Schwarzbauer JE, Tamkun WJ, Lemischka IR, Hynes RO: Three different fibronectin mRNAs arise by alternate splicing within the coding region. *Cell* 35: 421-431, 1983
18. Kurkinen M, Condon MR, Blumberg B, Barlow DP, Quinones S, Saus J, Pihlajaniemi T: Extensive homology between the carboxy-terminal peptides of mouse $\alpha 1(\text{IV})$ and $\alpha 2(\text{IV})$ collagen. *J Biol Chem* 262: 8496-8499, 1987
19. Barlow DP, Green NM, Kurkinen M, Hogan BLM: Sequencing of laminin B chain cDNAs reveals C-terminal regions of coiled-coil alpha helix. *EMBO J* 3: 2355-2362, 1984
20. Millan F, Denhez F, Kondaiah P, Ackurst R: The embryonic gene expression patterns of TGF β_1 , 2 and 3 suggest differential developmental function in vivo. *Development* 111: 131-144, 1991
21. Mercola M, Wang C, Kelly J, Brownlee C, Jackson-Grusby L, Stiles C, Bowen-Pope DF: Selective expression of PDGF A and its receptor during early mouse embryogenesis. *Dev Biol* 138: 114-122, 1990
22. Nicholson R, Murphy G, Breathnach R: Human and rat malignant tumour associated mRNAs encode a stromelysin-like metalloproteinase. *Biochemistry* 28: 5195-5203, 1989
23. Matrisian LM: Metalloproteinases and their inhibitors in matrix remodeling. *Trends Genet* 6: 121-125, 1990
24. Alitalo K, Hovi T, Vaheri A: Fibronectin is produced by human macrophages. *J Exp Med* 151: 602-613, 1980
25. Werb Z, Chin JR: Biosynthetic radiolabeling of cellular and secreted proteins of mononuclear phagocytes. In: *Methods for Studying Mononuclear Phagocytes*, edited by Adams DO, Edelson PJ, Koren H, New York, Academic, 1981, pp 861-872
26. Dubois CH, Goffinet G, Foidart JB, Dechenne CA, Foidart JM, Mahieu PR: Evidence for a particular binding capacity of rat peritoneal macrophages to rat glomerular mesangial cells in vitro. *Eur J Clin Invest* 12: 239-246, 1982
27. Jones CL, Buch S, Post M, McCulloch L, Liu E, Eddy AA: Pathogenesis of interstitial fibrosis in chronic purine aminonucleoside nephrosis. *Kidney Int* 40: 1020-1031, 1991
28. Ooi YM, Weiss MA, Hsu A, Ooi BS: Mechanisms of suppression of mouse mesangial cell proliferation by macrophage supernatants. *J Immunol* 130: 1790-1795, 1983
29. Lovett DH, Ryan JL, Sterzel RB: Stimulation of rat mesangial cell proliferation by macrophage interleukin-1. *J Immunol* 130: 1790-1795, 1983
30. Mattana J, Singhal PC: Macrophage Fc receptor activity modulates mesangial cell proliferation and matrix synthesis. *Am J Physiol* 266: F568-F575, 1994
31. Singhal PC, Mattana J, Garg P, Arya M, Shan Z, Gibbons N, Franki N: Morphine-induced macrophage activity modulates mesangial cell proliferation and matrix synthesis. *Kidney Int* 49: 94-102, 1996
32. Weissgarten J, Berman S, Averbukh Z, Cohn M, Golik A, Cohen N, Modai D: Renal mononuclear cells secrete a factor triggering mesangial cell proliferation. *Nephrol Dial Transplant* 8: 118-121, 1993
33. Mattana J, Singhal PC: Macrophage supernatants have both stimulatory and suppressive effects on mesangial cell proliferation. *J Cell Physiol* 154: 289-293, 1993
34. Striker LJ, Doi T, Elliot S, Striker GE: The contribution of glomerular mesangial cells to progressive glomerulosclerosis. *Semin Nephrol* 9: 318-328, 1989
35. Eng E, Floege J, Young BA, Couser WG, Johnson RJ: Does extracellular matrix expansion in glomerular disease require mesangial cell proliferation? *Kidney Int* 45(Suppl 45): 44-47, 1994
36. Groggel GC, Hughes ML: Heparan sulphate stimulates extracellular matrix protein synthesis by mesangial cells in culture. *Nephron* 71: 197-202, 1995
37. Zhu L, Herrera GA, Murphy-Ullrich JE, Huang Z-Q, Sanders PW: Pathogenesis of glomerulosclerosis in light chain deposition disease: Role for transforming growth factor β . *Am J Pathol* 147: 375-385, 1995
38. Ayo SH, Radnik RA, Garoni J, Glass FW II, Kreisberg JJ: High glucose causes an increase in extracellular matrix proteins in cultured mesangial cells. *Am J Pathol* 136: 1339-1348, 1990
39. Bruggeman LA, Pelicoro JA, Horigan EA, Klotman PE: Thromboxane and prostacyclin differentially regulate murine extracellular matrix gene expression. *Kidney Int* 43: 1219-1225, 1993
40. Wagner C, Braunger M, Beer M, Rother K, Hansch GM: Induction of matrix protein synthesis in human glomerular mesangial cell by the terminal complement complex. *Exp Nephrol* 2: 51-56, 1994
41. Rossi P, Karsenty G, Roberts AB, Roche NS, Sporn MB, de Crombrughe B: A nuclear factor 1 binding site mediates the transcriptional activation of a type 1 collagen promoter by transforming growth factor β . *Cell* 52: 405-414, 1988
42. Dean DC, Newby RF, Bourgeois S: Regulation of fibronectin biosynthesis by dexamethasone, transforming growth factor β and cAMP in human cell lines. *J Cell Biol* 106: 2159-2170, 1988
43. Roberts AB, Flanders KC, Kondaiah P, Thompson NL, Ob-

- berghen-Schilling E, Wakefield LM, Rossi P, de Crombrughe DH, Heine U, Sporn MB: Transforming growth factor β : Biochemistry and roles in embryogenesis, tissue repair and remodelling and carcinogenesis. *Recent Prog Horm Res* 44: 157-197, 1988
44. Kaname S, Vehida S, Ogata E, Kurokawa K: Autocrine secretion of transforming growth factor β in cultured rat mesangial cells. *Kidney Int* 42: 1319-1327, 1992
45. Border WA, Ruoslahti E: Transforming growth factor β : The dark side of tissue repair. *J Clin Invest* 90: 1-7, 1992
46. Border WA, Okuda S, Languino LR, Ruoslahti E: Transforming growth factor β regulates production of proteoglycans by mesangial cells. *Kidney Int* 37: 689-695, 1990
47. Hibbs JB Jr, Taintor RR, Chapman HA Jr, Weinberg JB: Macrophage tumour killing: Influence of local environment. *Science* 197: 279-282, 1977
48. Chapman HA Jr, Hibbs JB Jr: Modulation of macrophage tumoricidal capability by components of normal serum: A central role for lipid. *Science* 197: 282-285, 1977
49. Doherty DE, Haslett C, Tonnesen MG, Henson PM: Human monocyte adherence: A primary effect of chemotactic factor on the monocyte to stimulate adherence to human endothelium. *J Immunol* 138: 1762-1771, 1987
50. Haskill S, Johnson C, Eierman D, Becker S, Warren K: Adherence induces selective mRNA expression of monocyte mediators and proto-oncogenes. *J Immunol* 140: 1690-1694, 1988

Renal Expression of Monocyte Chemoattractant Protein-1 in Lupus Autoimmune Mice

CARLA ZOJA,* XUE-HUI LIU,* ROBERTA DONADELLI,* MAURO ABBATE,*
DAVIDE TESTA,* DANIELA CORNA,* GIULIA TARABOLETTI,*
ANNUNCIATA VECCHI,[†] QIANG GANG DONG,[†] BARRETT J. ROLLINS,[‡]
TULLIO BERTANI,*[§] and GIUSEPPE REMUZZI*[§]

Mario Negri Institute for Pharmacological Research, *Bergamo, Italy, [†]Milano, Italy; [§]Division of Nephrology and Dialysis, Azienda Ospedaliera, Ospedali Riuniti di Bergamo, Bergamo, Italy, [‡]Department of Medicine, Dana-Farber Cancer Institute, Boston, Massachusetts.

Abstract. Mononuclear cell infiltration in glomeruli and renal interstitium is a prominent feature of some types of glomerulonephritis, including lupus nephritis. The mechanism(s) underlying monocyte influx into the kidney is not fully understood. Recently, monocyte chemoattractant protein-1 (MCP-1) has been identified as a chemotactic factor involved in the recruitment of monocytes/macrophages in the glomeruli of rats with mesangioproliferative as well as anti-glomerular basement membrane glomerulonephritis. In the study presented here, renal MCP-1 mRNA expression in New Zealand Black x New Zealand White (NZB/W) F1 mice, a model of genetically determined immune complex disease that mimics systemic lupus in humans, was investigated. Northern blot analysis revealed a single 0.7 kb MCP-1 transcript of very low intensity in kidneys from 2-month-old NZB/W mice that had not yet developed proteinuria nor renal damage. Message levels,

which increased markedly with the progression of nephritis and in association with mononuclear cell infiltration, were 10- and 15- fold higher in 8-10-month-old mice than in 2-month-old mice. By *in situ* hybridization, increased expression of MCP-1 mRNA was demonstrated in glomeruli and, even more striking, in tubular epithelial cells. Western blot analysis demonstrated increased expression of MCP-1 protein in kidneys of 10-month-old NZB/W mice, consistent with MCP-1 mRNA data. When NZB/W mice were treated with cyclophosphamide up to 12 months of age, expression of MCP-1 in the renal tissue remained low, the influx of inflammatory cells did not appear, and glomerular and tubular structures remained well preserved. These data suggest that elevated MCP-1 might act as a signal for inflammatory cells to infiltrate the kidney in lupus nephritis. (J Am Soc Nephrol 8: 720-729, 1997)

The New Zealand Black x New Zealand White (NZB/W) F1 hybrid mice spontaneously develop an autoimmune disease that closely resembles systemic lupus erythematosus (SLE) in humans (1,2). The disease manifests with circulating antibodies to nucleic acid and endogenous antigens, renal immune deposits, and proteinuria. The resulting progressive glomerulonephritis is the primary cause of death in these animals. Mononuclear inflammatory cells infiltrate glomeruli and renal interstitium of mice with experimental lupus and humans with lupus nephritis (3,4). The precise mechanism(s) governing inflammatory cell recruitment into the kidney is unknown, despite sparse data implying a role of recently discovered chemoattractants and/or adhesion molecules (5,6). Among novel chemoattractants, a family of proinflammatory cytokines—chemokines (7)—including the monocyte chemoattractant protein-1 (MCP-1), a potent chemoattractant for mono-

cytes (8,9) and for T lymphocytes (10,11), can theoretically play a pivotal role (12). MCP-1 expression and production can be regulated by cytokines and other inflammatory mediators in several cell types, including endothelial cells (13-15), mesangial cells (16,17), tubular epithelial cells (18), and monocytes/macrophages (19). Of relevance is the observation that in cultured mouse mesangial cells, binding of IgG aggregates and IgG complexes to specific Fc receptors increased MCP-1 mRNA and promoted the synthesis of the corresponding protein product (20,21). The above data can be taken to indicate that MCP-1 may act in glomerular immune complex disease as a critical molecule to the full expression of local inflammatory reaction. Actually, some data indicate that MCP-1 is overexpressed in glomeruli taken from rats with anti-thymocyte antibody-induced glomerulonephritis (22), as well as from rats with anti-glomerular basement membrane (GBM) glomerulonephritis (23,24). Moreover, immunohistochemical studies have shown increased staining for MCP-1 in renal tissue from patients with renal diseases associated with inflammatory cell accumulation in glomeruli or interstitium (23,25). Our group has recently shown that patients with active lupus nephritis had high levels of urinary MCP-1 as compared with lupus patients studied in the inactive phase of the disease or with healthy controls (26), which would suggest that in lupus nephritis,

Received January 11, 1996. Accepted December 30, 1996.

Correspondence to Dr. Carla Zoja, Mario Negri Institute for Pharmacological Research, Via Gavazzeni 11 24125 Bergamo, Italy.

1046-6673/98/05-0720\$03.00/0

Journal of the American Society of Nephrology

Copyright © 1997 by the American Society of Nephrology

excessive renal MCP-1 could contribute to mononuclear cell migration into the kidney.

In the study presented here, we sought to investigate in lupus-prone NZB/W mice (1) renal MCP-1 mRNA expression at different time courses during the development of renal lesions; (2) the sites of MCP-1 mRNA in the kidney; (3) the effect of immunosuppressant therapy on renal MCP-1 expression.

Materials and Methods

Experimental Design

NZB/W F1 female mice (Charles River Italia., Calco, Italy), 2 months of age at the start of the experiment, were used in these studies. Animal care and treatment were conducted in conformity with the institutional guidelines in compliance with national and international laws and policies (EEC Council Directive 86/609, OJL 358, Dec 1987; NIH Guide for the Care and Use of Laboratory Animals, NIH Publication No. 85-23, 1985). All animals were housed in a constant-temperature room with a 12-h dark, 12-h light cycle and fed a standard diet. Animals were divided into four groups, which were euthanized at 2, 6, 8, and 10 months of age, respectively. At the beginning of the study, groups 1, 2, and 3 were of $N = 9$ mice each, and group 4 was of $N = 12$ mice. At 2 months of age, before the onset of renal disease (1,2) all mice were housed in metabolic cages and 24-h urines were collected for determination of basal urinary protein excretion levels. Baseline values of urinary protein excretion ranged from 0.50 to 2.90 mg/day. Thus levels exceeding 3 mg/day were considered abnormal. Urinary protein excretion was then measured every month. Serum BUN levels were measured at the end of the experimental period. At the time that the animals were euthanized, renal tissue specimens were removed for (1) histologic analysis by light (all mice) and electron microscopy ($N = 5$ mice for each group, randomly selected); (2) RNA extraction and Northern blot analysis (all mice); (3) *in situ* hybridization ($N = 3$ mice for each group, randomly selected); and (4) Western blot analysis ($N = 3$ mice of groups 1 and 4, randomly selected).

Two additional groups of NZB/W F1 mice ($N = 15$ for each group) were treated with cyclophosphamide at the dose of 25 mg/kg ip once a week or vehicle—phosphate buffer solution (PBS)—starting at 3 months of age until 12 months. In all mice, urinary protein excretion was evaluated every month. At the time that the animals were euthanized, renal tissue specimens were removed for renal morphology (all mice), Northern blot analysis (all remaining mice of vehicle group and $N = 6$ mice, randomly selected, for cyclophosphamide group), and *in situ* hybridization. For comparison, five CD-1 (ICR) BR untreated mice were followed until 12 months of age.

Renal Morphology

Light Microscopy. Fragments of renal cortex were fixed in Dubosq-Brazil, dehydrated in alcohol, and embedded in paraffin. Sections (3 μ m each) were stained with hematoxylin and eosin, Masson's trichrome, and periodic acid-Schiff's reagent. Each biopsy included at least 100 glomeruli. Glomerular endocapillary hypercellularity was quantitated by a scoring system from 0 to 3+ (0, no hypercellularity; 1+, mild; 2+, moderate; and 3+, severe). Extracapillary proliferation was graded from 0 to 3+ (0, no hypercellularity; 1+, <25% of glomeruli involved; 2+, 25%–50% of glomeruli involved; and 3+, >50% of glomeruli involved). Glomerular deposits were graded from 0 to 3+ (0, no deposits; 1+, <25% of glomeruli involved; 2+, 25%–50% of glomeruli involved; and 3+, >50% of

glomeruli involved). Glomerular sclerosis was graded from 0 to 3+ (0, no sclerosis; 1+, sclerosis affecting <25% of glomeruli; 2+, sclerosis affecting 25%–50% of glomeruli; and 3+, sclerosis affecting >50% of glomeruli). Tubular (atrophy, casts, and dilatation) and interstitial changes (fibrosis and inflammation) were graded from 0 to 3+ (0, no changes; 1+, changes affecting <25% of the sample; 2+, changes affecting 25%–50% of the sample; and 3+, changes affecting >50% of the sample). At least 100 glomeruli were scored per mouse, and 10–18 fields per mouse were examined at low magnification (10 \times) for histologic scoring of the interstitium. All renal biopsies have been analyzed by the same pathologist, blind to the nature of the experimental groups.

Electron Microscopy. Small fragments of kidney were fixed in 2.5% glutaraldehyde in 0.1 M cacodylate buffer (pH 7.4) for 4 h at 4°C. Samples were washed in cacodylate buffer and subsequently postfixed in 1% osmium tetroxide for 1 h. After a brief wash in cacodylate buffer, they were dehydrated through ascending grades of alcohol and embedded in Epon resin. Sections were cut on an LKB V ultramicrotome (Bromma, Sweden). Semithin sections were stained with toluidine blue in borax and examined by light microscopy. Ultrathin sections were stained with uranyl acetate and lead citrate, and then they were examined with a Zeiss EM 109.

RNA Isolation and Northern Blot Analysis

Total RNA was isolated from mouse kidneys by the guanidium isothiocyanate/cesium chloride procedure, as previously described (27). For mRNA preparation, total RNA of kidneys of each group of NZB/W mice was pulled together. Poly (A)+ RNA was selected by oligo (dT)-cellulose column chromatography (mRNA separator, Clontech, Palo Alto, CA). Then, 7 μ g of mRNA were fractionated on 1.2% agarose gel and blotted onto synthetic membranes (Gene Screen Plus, New England Nuclear, Boston, MA). Plasmid containing murine JE/MCP-1 probe was kindly provided by Dr. Charles D. Stiles (Harvard Medical School and Dana-Farber Cancer Institute, Boston, MA). MCP-1 mRNA was detected by using the 577 basepair (bp) of MCP-1 cDNA (28). The cDNA fragment of MCP-1 was labeled with α^{32} PdCTP by random-primed method (29). Membranes were hybridized for 20 h at 60°C with 1.5×10^6 cpm-labeled probe, and the filters were washed as previously described (30) and exposed to x-ray film for autoradiography. Membranes were subsequently probed with a glyceraldehyde-3-phosphate dehydrogenase (GAPDH) cDNA (31), taken as the internal standard of equal loading of the samples on the membrane. MCP-1 mRNA optical density was normalized to that of the constitutively released GAPDH gene expression. Data of MCP-1 mRNA levels ($N = 3$ experiments) were analyzed by one-way analysis of variance using the Tukey test for multiple comparisons. Statistical significance was defined as $P < 0.05$.

Preparation of Digoxigenin-Labeled Murine JE/MCP-1 Riboprobes

The murine JE/MCP-1 antisense and sense RNA probes were synthesized and labeled by *in vitro* transcription using digoxigenin-labeled uridine triphosphate. A 577-bp murine JE/MCP-1 cDNA was cloned into the EcoRI site of the pGEM-1 vector between SP6 and T7 promoters (gift from Dr. Charles D. Stiles). The plasmid was linearized with the appropriate restriction enzymes, SacI (antisense murine JE/MCP-1, T7 polymerase) and SmaI (sense murine JE/MCP-1, SP6 polymerase), and purified by phenol/chloroform extraction and ethanol precipitation. Linearized plasmid was resuspended in diethyl pyrocarbonate (DEPC)-treated water. Transcription of 1 μ g linearized plasmid was performed using a DIG RNA labeling Kit (Boehringer-

Mannheim Biochemica, Mannheim, Germany). The reaction products were ethanol precipitated and stored at 70°C until use. Labeling efficiency of the riboprobe was estimated by comparison with 10-fold serial dilutions of a digoxigenin-labeled control riboprobe (Boehringer Mannheim Biochemica) and direct detection of the labeled riboprobe with anti-digoxigenin antibodies. Riboprobe concentrations were adjusted to be equivalent on the basis of the labeling efficiency before use in the *in situ* hybridization studies.

In Situ Hybridization

Ten percent neutral buffered formalin-fixed and paraffin-embedded renal tissues were cut at 4 μ m and floated onto 2% 3-aminopropyltriethoxysilane (APES) (Sigma Chemical, St. Louis, MO) coated slides. Sections were heat-fixed for 30 min at 65°C and deparaffinized. After a 30-min incubation in 5 mmol/L levamisole, the sections were washed in PBS and in DEPC-treated water for 5 min, respectively, and then immersed in 0.2 mol/L HCl for 20 min. Then, the sections were deproteinized by digestion with 40 μ g/mL proteinase K (Sigma) for 10 min at 37°C, washed in 0.2% glycine for 5 min twice and in PBS for 10 min, and postfixed with 1.5% paraformaldehyde-1.5% glutaraldehyde for 1 min. After rinsing twice for 5 min in PBS, sections were dehydrated through a graded ethanol series and air dried. The sections were hybridized with the RNA probes at the final concentrations of 0.1–0.5 ng/ μ l in 2 \times SSC, 10% dextran sulfate, 1 \times Denhardt's solution, 20 mM Vanadyl Ribonucleoside Complex (GIBCO BRL, Life Technologies, Gaithersburg, MD), 0.1 M sodium phosphate under sealed coverslips and incubated overnight in a moist chamber at 42°C. They were washed in 0.2 \times SSC and then blocked with a buffer blocking solution (50 mg/mL skimmed dried milk, 150 mM NaCl in 100 mM Tris HCl, pH 7.8) at room temperature for 15 min, and the sections were incubated with anti-digoxigenin antibody conjugated with alkaline phosphatase (Boehringer-Mannheim Biochemica) at the dilution of 1:750 for 30 min at 37°C. Colorimetric detection with nitro blue tetrazolium and 5-bromo-4-chloro-3-indolyl phosphate (Boehringer-Mannheim Biochemica) was then performed, and the sections were mounted in 60% glycerol and examined by light microscopy. The negative controls included: (1) hybridization with the sense probe, (2) RNase (100 μ g/ml in 10 mM Tris HCl, pH 8.0, 1 mM ethylenediaminetetraacetate) pretreatment before hybridization, and (3) omission of either the antisense RNA probe or the anti-digoxigenin antibody.

Western Blot Analysis

For Western blot analysis, kidneys from NZB/W 2- and 10-month-old mice were homogenized in lysis buffer containing 0.1 M Tris pH 6.8, 4% sodium dodecyl sulfate (SDS), 10% β -mercaptoethanol, and 1 mM Pefabloc (Boehringer-Mannheim Biochemica). The samples were incubated for 20 min at room temperature with 0.5 mg/ml DNase I (Boehringer-Mannheim Biochemica) and 10 mM MgCl₂, and then centrifuged at 15,000 rpm for 2 h. After determination of protein concentration in the supernatant by the Coomassie method (Bio-Rad Protein Assay, Bio-Rad, Hercules, CA), samples (50 μ g/lane) were electrophoresed on 15% SDS-polyacrylamide gels in reducing conditions. Proteins were then transferred to a nitrocellulose filter for 2 h at 100 V. To block nonspecific binding sites, the membrane was incubated in PBS + 5% low-fat dry milk for 1 h at room temperature, and then for 20 h at room temperature with purified monoclonal antibodies: hamster anti-mouse MCP-1 2H5 (0.5 μ g/ml) (32) or rat anti-mouse MCP-1 ECE.2 (0.8 μ g/ml), prepared as described below. After incubation with peroxidase conjugated rabbit anti-hamster IgG (Jackson Immuno Research Laboratories Inc., West Grove, PA) for

2H5 and peroxidase conjugated sheep anti-rat IgG (Amersham Life Science, Amersham, UK) for ECE.2 for 1 h at room temperature, the reactivity was detected with ECL detection reagent (Amersham Life Science). Molecular weights of the immunoreactive bands were estimated by running aside a mixture of molecular standards (GIBCO, Grand Island, NY). Recombinant mouse MCP-1 was used as reference (32). To confirm the specificity of the reaction, in one experiment one of two identical membranes was incubated with ECE.2 and the other one with ECE.2 in the presence of the MCP-1 peptide it recognizes.

Monoclonal Antibody Generation

Male Lewis rats (Charles River Italia, Calco, Italy) were immunized with a synthetic peptide—prepared as previously described (33)—spanning residues 102–130 of mouse MCP-1 (32) conjugated with keyhole limpet hemocyanin (Sigma Chemical, St. Louis, MO). Hybridomas were generated as previously reported (34) and screened for MCP-1 reactivity with enzyme-linked immunosorbent assay. Monoclonal antibody ECE.2 (IgG1 class) was specific for mouse, but not human, recombinant MCP-1 and was purified from serum-free supernatants by ammonium sulfate precipitation and size-exclusion chromatography (35).

Analytical

Urinary protein concentration was determined by the Coomassie blue G dye-binding assay with bovine serum albumin as standard (36). Renal function was assessed as BUN on serum samples using an enzymatic UV Rate by Sincron CX-5 (Beckman, Fullerton, CA). BUN levels exceeding 30 mg/dl were considered abnormal (normal range in our laboratory: 14–29 mg/dl). BUN data were expressed as mean \pm SE.

Results

Life Survival in NZB/W Mice

Up to 6 months of age, all NZB/W mice were alive. At 8 and 10 months of age, the percentage of survival was 67% and 42%, respectively.

Time Course of Proteinuria and Renal Function in NZB/W Mice

Cumulative frequency of proteinuria >3 mg/day in NZB/W mice at different stages of the disease is shown in Table 1. At 2 months of age, none of the animals was proteinuric. Thereafter, cumulative percentage of proteinuric mice progressively increased over time, reaching 92% at 10 months of age.

Renal function—as evaluated by serum BUN measurements—was normal up to 6 months of age (2 months, 24.4 \pm 2.1; 6 months, 21.9 \pm 1.3 mg/dl), but deteriorated at 8 and 10 months. This was reflected in elevations of BUN values (8 months, 139.5 \pm 45.6; 10 months, 133.7 \pm 39.8 mg/dl).

Renal Morphologic Changes in NZB/W Mice at Different Stages of the Disease

Data of renal morphologic analysis by light microscopy in NZB/W mice at different months of age are shown in Table 1. At 2 months, mice did not exhibit changes in the glomeruli, interstitium, tubules, and vessels. At 6 months, light microscopy analysis revealed only mild glomerular changes characterized by mild endocapillary hypercellularity not associated

Table 1. Cumulative frequency of proteinuria (>3 mg/day) and renal histology in NZB/W mice at different stages of the disease

Months of Age	Cumulative % Proteinuric Mice*	Endocapillary Hypercellularity	Extracapillary Proliferation	Glomerular Hyaline Deposits	Glomerular Sclerosis	Interstitial Fibrosis or Inflammation	Tubular Damage
2	0	0	0	0	0	0	0
6	22	0.37 (0-1)	0	0	0	0	0.11 (0-1)
8	55	1.88 (1-2)	0.44 (0-1)	1.33 (0-3)	0.44 (0-1)	1.44 (0-3)	1.22 (0-3)
10	92	1.72 (1-2)	1.00 (0-3)	2.09 (1-3)	0.91 (0-3)	1.81 (1-3)	1.72 (0-3)

* Each point reflects the current level of proteinuria in surviving mice, as well as the last measurement in deceased mice. Values of renal histological parameters are mean scores; ranges are in parenthesis.

with obvious damage in the tubules, interstitium, and vessels. At 8 and 10 months, glomerular changes were pronounced, with endocapillary hypercellularity associated with a focal extracapillary proliferation. Immune type of deposits was detected in the mesangium and on subendothelial aspect of GBM. Interstitial inflammation, fibrosis, and tubular damage were severe. Global or segmental sclerotic changes were confined to <25% of glomeruli.

By electron microscopy analysis of kidneys from NZB/W mice at 2 months of age, the only glomerular lesion consisted of focal electron-dense deposits within the GBM or on the subepithelial aspect of GBM in some animals. At 6 months, glomerular changes included inflammatory cells in the capil-

lary lumina, as well as diffuse electron-dense deposits in the mesangium and on the subepithelial aspect of GBM. At 8 and 10 months, lesions worsened, with more inflammatory cells accumulating in the glomerular capillaries, and numerous mesangial, subendothelial, intramembranous, and subepithelial electron-dense deposits. These findings agree with previously published observations in this model (37,38).

Renal MCP-1 Gene Expression in NZB/W Mice

The time course of renal MCP-1 gene induction—monitored by Northern blot analysis—during the evolution of the disease in NZB/W lupus mice is given in Figure 1. A single 0.7 kb MCP-1 mRNA transcript of very low intensity was detected in kidneys from 2-month-old NZB/W mice. Message levels increased markedly with time. Thus, as revealed by densitometric analysis of the autoradiographic signals, renal MCP-1 mRNA levels in 6-, 8-, and 10-month-old mice were 2- ($P < 0.05$), 10-, and 15- ($P < 0.01$) fold higher, respectively, than those of 2-month-old mice (Figure 2).

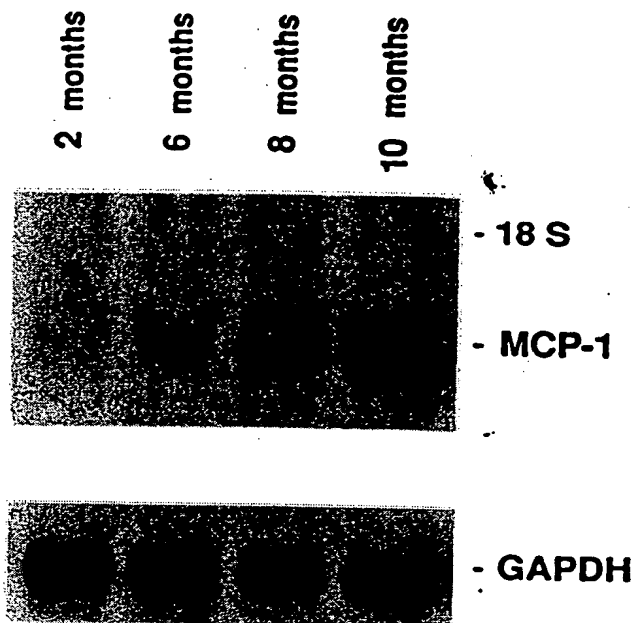


Figure 1. Time-dependent renal expression of MCP-1 mRNA in NZB/W lupus mice from a representative Northern blot ($N = 3$ experiments). mRNA ($7 \mu\text{g}$) obtained from pooled kidneys of NZB/W mice at 2 ($N = 9$), 6 ($N = 9$), 8 ($N = 6$), and 10 ($N = 5$) months of age was blotted onto synthetic membranes which were hybridized sequentially with α - ^{32}P -labeled murine JE/MCP-1 (top) and glyceraldehyde-3-phosphate dehydrogenase (GAPDH) (bottom) cDNA probes.

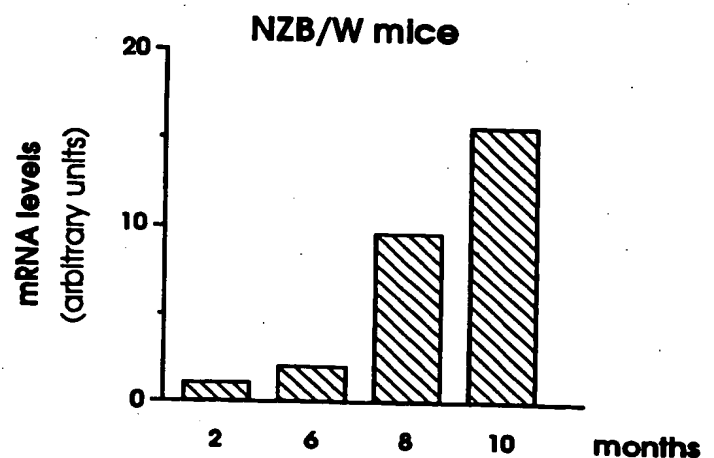


Figure 2. Corresponding densitometry of the autoradiograph reported in Figure 1 shows MCP-1 mRNA expression in kidneys from NZB/W mice at different stages of the disease. The optical density of the autoradiographic signals was quantitated and calculated as the ratio of MCP-1 to GAPDH mRNA. The mRNA levels of 6, 8, and 10 months were calculated by assuming the optical density of 2 months as unit.

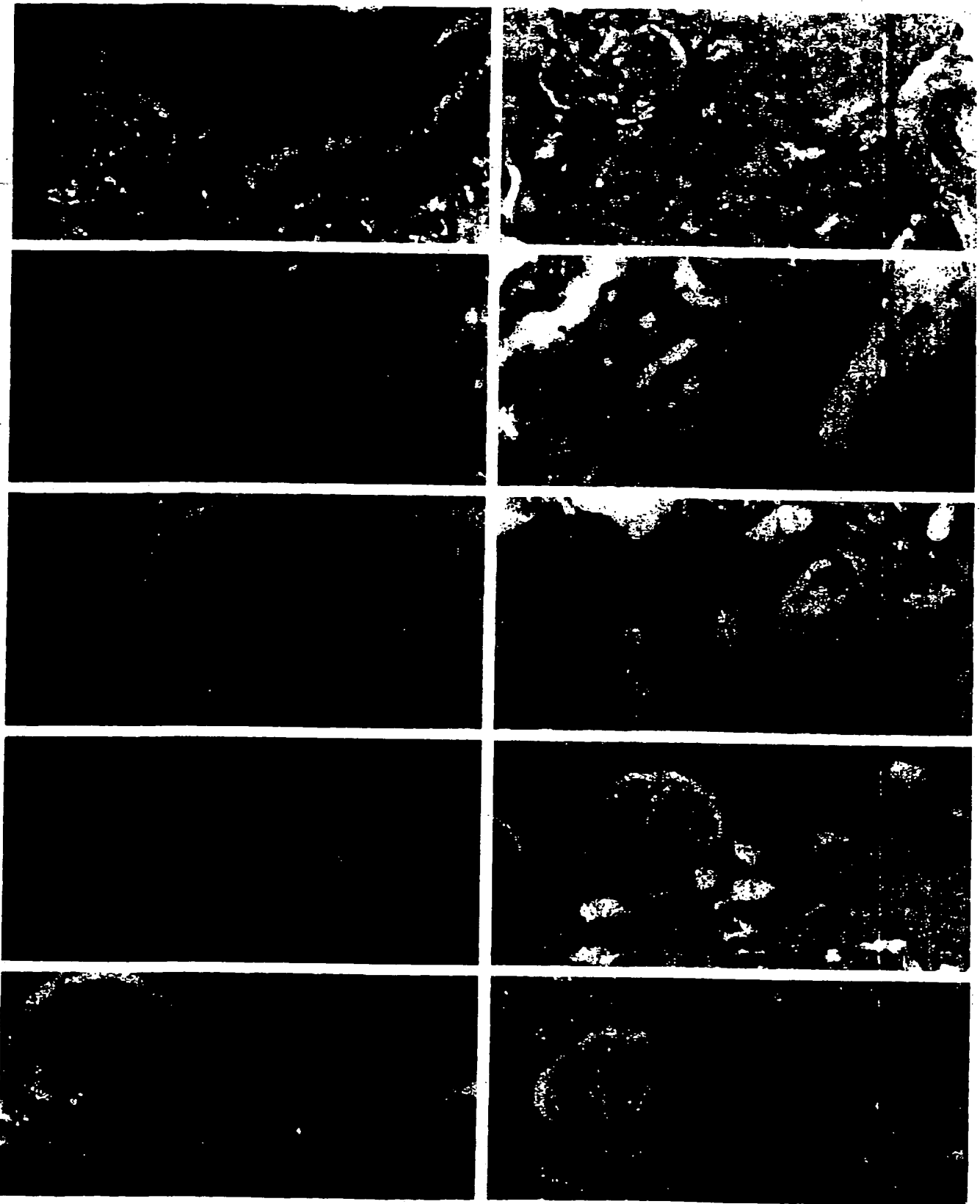


Figure 3. Photomicrographs showing MCP-1 mRNA in kidneys from NZB/W mice and a control CD mouse by *in situ* hybridization (digoxigenin d-UTP-labeled murine MCP-1 probe, alkaline phosphatase reporter system). Hybridization signal can be seen in some glomerular and tubular epithelial cells in a kidney from a 2-month-old NZB/W mouse (a). The signal is more intense both in glomeruli and tubules in

In Situ Hybridization

In situ hybridization was performed with antisense JE/ MCP-1 RNA probe to localize MCP-1 mRNA expression at the cellular level on kidneys of NZB/W lupus mice in different stages of the disease. Hybridization signal of mainly perinuclear or cytoplasmic pattern was clearly detectable in the renal cortex. In 2-month-old mice, the signal was observed in glomerular cells. When these cells were situated peripherally in glomerular tuft, they could be confidently identified as visceral and parietal epithelial cells. Some endothelial and mesangial cells were also labeled. MCP-1 mRNA was also present in some tubular epithelial cells (Figure 3a). The intensity of the labeling increased progressively in NZB/W mice at 6, 8, and 10 months of age, in agreement with the results of the Northern blot analysis (Figure 3b-f). The most intense signals were found in tubules. At 6 months, increased MCP-1 mRNA staining in glomeruli was associated with endocapillary proliferative lesions. The staining was present both in resident glomerular cells and in infiltrating cells. The tubular MCP-1 mRNA staining at this time was not yet clearly associated with the presence of inflammatory cells in interstitium (Figure 3b). Conversely, there were interstitial infiltrates in kidneys of 8- and 10-month-old mice, and the inflammatory cells stained positive for MCP-1 mRNA. Most of the staining, however, was found in the tubules, which were also adjacent to sites of accumulation of inflammatory cells (Figure 3c-f). Signal in areas of glomerular sclerosis was weak or absent. No hybridization was detected in negative control sections pretreated with RNase before incubation with antisense MCP-1 RNA probe, or in sections incubated with the corresponding sense MCP-1 probe (Figure 3 g).

Renal MCP-1 Protein Expression in NZB/W Mice

As shown in Figure 4, Western blot analysis of proteins extracted from kidneys of 10-month-old NZB/W mice, performed with two monoclonal antibodies against mouse MCP-1 revealed three bands with an apparent molecular mass of approximately 30, 18, and 14 kd corresponding to heavily and partially glycosylated forms of MCP-1 (32,39). By contrast, in the kidney extract of 2-month-old NZB/W mice, only a faint band of 14 kd was detected, and no higher molecular weight bands were observed, thus confirming our results at the mRNA level. The specificity of the reaction was confirmed by the fact that no band was observed when Western blotting was performed on 10-month-old NZB/W kidney extract with ECE.2 in the presence of the peptide it recognizes (data not shown).

Effect of Cyclophosphamide on Renal MCP-1 Expression in NZB/W Mice

Two groups of NZB/W mice up to 12 months of age were treated with cyclophosphamide or vehicle. An additional group of 12-month-old CD1(ICR)BR normal mice was used as control. At the end of the observation period, all cyclophosphamide-treated mice were alive, and none of them had proteinuria of >3 mg/day. Only mild glomerular changes were observed by light microscopy analysis (mean scores, endocapillary hypercellularity: 0.6; extracapillary hypercellularity: 0; hyaline deposits: 0.3; tubulo-interstitial damage: 0; glomerular sclerosis: 0). By contrast, in the vehicle-treated group, only 20% of mice survived, and the cumulative percentage of proteinuric mice was 93%. Glomerular and tubulo-interstitial changes were severe (mean scores, endocapillary and extracapillary proliferation: 1.3; hyaline deposits: 2; glomerular sclerosis: 1.7; tubulo-interstitial damage: 1.7). Northern blot analysis showed that cyclophosphamide treatment prevented the increase in renal MCP-1 mRNA that occurred in untreated NZB/W lupus mice of the same age (Figures 5 and 6, $P < 0.01$). Renal MCP-1 transcript levels of 12-month-old control mice that did not exhibit any glomerular or tubulo-interstitial damage (mean score for all the parameters considered: 0) remained lower than levels of untreated 12-month-old lupus mice ($P < 0.01$), thus excluding that upregulation of MCP-1 in NZB/W lupus mice was a consequence of aging. In accordance with Northern blot experiments, *in situ* hybridization showed that in kidneys of cyclophosphamide-treated mice (Figure 3j), the intensity of MCP-1 mRNA staining was dramatically decreased compared with that of untreated mice of the same age (Figure 3i) and similar to that observed in 2-month-old NZB/W mice (Figure 3a) that had not yet developed the disease. In kidneys of 12-month-old normal mice, the signal for MCP-1 was comparable to that observed in 2-month-old NZB/W mice (Figure 3h).

Discussion

The first finding of the study presented here is that MCP-1 mRNA is upregulated in the kidneys of mice with lupus nephritis. Specifically, using Northern blot analysis, we have demonstrated that renal MCP-1 message levels increased progressively with the development of the disease in NZB/W lupus mice, being 10- and 15- fold higher at 8 and 10 months than at 2 months of age, when mice showed no sign of renal disease. Overexpression of MCP-1 in renal tissue paralleled mononuclear cell accumulation, as indicated by the morphologic analysis performed at different time points during the development of the renal disease.

kidneys from 6-month-old (b) and 8-month-old (c) NZB/W mice. At 8 months, inflammatory cells positive for MCP-1 mRNA are observed in an area showing abundant MCP-1 mRNA in tubules (d). Kidney at 10 months (e, f). Most tubules and a crescent are strongly stained (e). MCP-1 mRNA staining is also present in the cells of a perivascular infiltrate (f). Negative control using MCP-1 sense probe (g). CD1 (ICR) BR normal 12-month-old mouse (h). A glomerulus and some tubular epithelial cells reveal very small amount of staining. A strong MCP-1 hybridization signal is present both in tubules and inflammatory cells in the interstitium in a kidney of a 12-month-old NZB/W mouse (i). Renal MCP-1 mRNA expression is dramatically decreased in a 12-month-old mouse treated with cyclophosphamide (j). (Magnification, $\times 200$.) Reproduction of this figure in color was made possible by a grant from Angelini Ricerche S. P. A., S. Polombre, Rome, Italy.

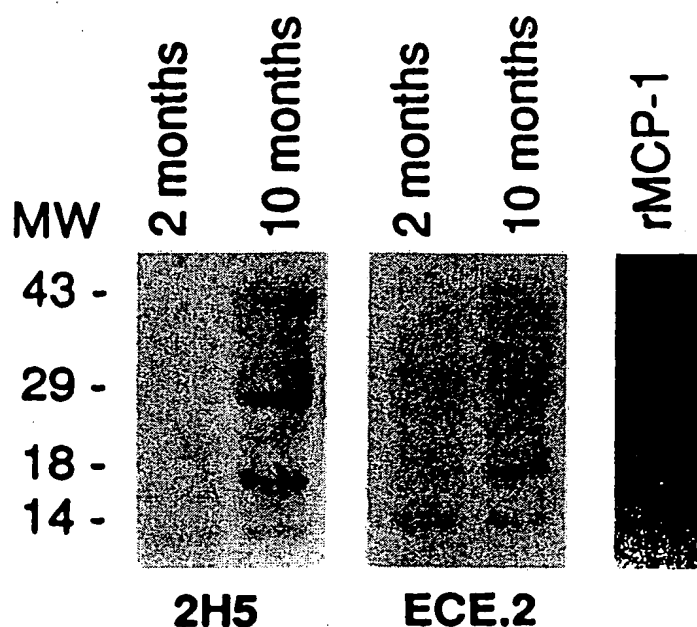


Figure 4. Western blot analysis of renal expression of MCP-1 protein in NZB/W lupus mice (representative of $N = 2$ experiments). Proteins extracted from kidneys of 2- and 10-month-old NZB/W mice ($N = 3$ mice for each group) were applied to 15% sodium dodecyl sulfate (SDS)-polyacrylamide gel in reducing conditions and then transferred to nitrocellulose membrane. The membranes were subsequently probed for antigenic MCP-1 with hamster anti-mouse MCP-1 moAb 2H5 (32) or rat anti-mouse MCP-1 moAb ECE.2 (see Methods) as the primary antibody, followed by peroxidase conjugated secondary antibodies. The blots were developed using an ECL system. Relative positions of molecular weight markers (kd) are indicated. Mouse recombinant MCP-1 was used as reference.

Infiltrates of mononuclear cells within the glomeruli in lupus, as in many other glomerulonephritis conditions, precede the development of glomerular structural lesions and are very likely to contribute to tubulo-interstitial damage (40,41). Old studies established the fundamental role of mononuclear cells in initiating and monitoring renal injury in immune complex disease. Thus, the evidence is available to show that macrophage depletion abrogated proteinuria and effectively prevented subsequent injury in experimental glomerulonephritis (42). More recently, the myriad of macrophage proinflammatory functions are being elucidated, and the various molecules responsible for the different effects are now at least partially identified (43,44). Among these are cytokines synthesized and released by macrophages infiltrating the glomerulus, either in human or experimental immune-mediated glomerulonephritis (43,44), platelet-activating factor, and reactive oxygen species (45). Other data tend to suggest that infiltrating macrophages are involved in renal disease progression to the extent that they participate in glomerular crescent formation and appear directly responsible for glomerular fibrin deposition by virtue of their surface-related property of expressing procoagulant activity (46,47). Despite so many studies on the role of monocytes/macrophages in glomerulonephritis, data on signaling

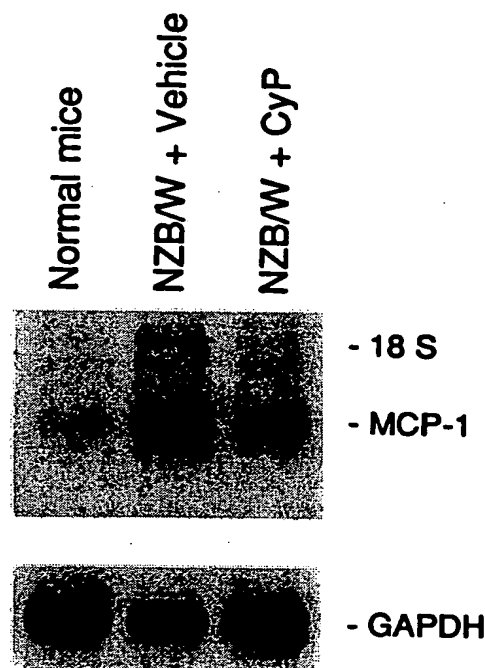


Figure 5. Renal MCP-1 mRNA expression in 12-month-old NZB/W lupus mice given vehicle or cyclophosphamide (CyP) and in 12-month-old CD1 (ICR) BR normal mice (representative Northern blot of $N = 3$ experiments). mRNA (7 μ g) obtained from kidneys of 12-month-old NZB/W mice given vehicle ($N = 3$) or cyclophosphamide ($N = 6$) and from 12-month-old CD1 (ICR) BR normal mice ($N = 5$) was blotted onto synthetic membranes, which were hybridized sequentially with α - 32 P-labeled murine JE/MCP-1 (top) and glyceraldehyde-3-phosphate dehydrogenase (GAPDH) (bottom) cDNA probes.

events to drive them into the glomerulus are very few. Advances in basic mechanisms governing macrophage chemotaxis and on the different proteins involved have provided an opportunity to unravel the issue. In this context, we have concentrated on MCP-1, a member of the β chemokine (C-C chemokine) subfamily (7,48), which corresponds to the product of the early response gene, JE, of the mouse (19). MCP-1 is a chemotactic factor (8–11) that, in addition, induces the respiratory burst in human monocytes (49); activates monocytes to synthesize cytokines, including interleukin-1 and interleukin-6 (50); and upregulates adhesion molecule expression on monocytes (50), which results in increased adhesion of monocytes to endothelial cells (51). All of these properties make MCP-1 a potent pro-inflammatory molecule. Experimental data are available showing that MCP-1 can be regarded as a good candidate in the sequence of signaling events leading to kidney infiltration by inflammatory cells. In rat anti-Thy 1.1 glomerulonephritis, expression of glomerular MCP-1 increased markedly in the early phase of mesangial immune complex formation 30 min after disease induction, when infiltration of monocytes/macrophages started to occur (22). MCP-1 message levels were reduced during the subsequent phase of mesangiolysis (at 24 h) and increased again during proliferative glomerulonephritis (at 5 and 21 days). Decomplementation of rats

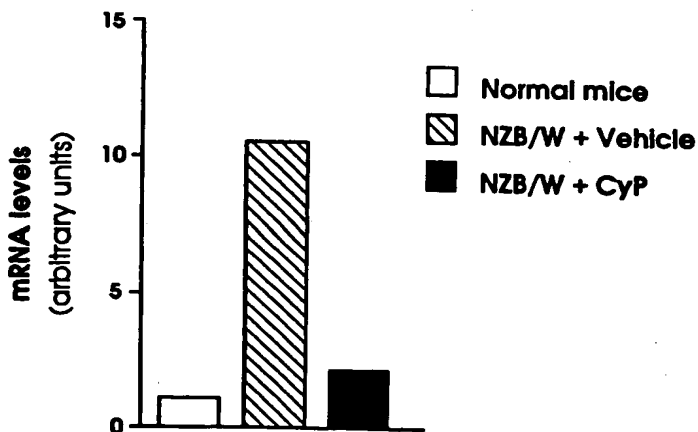


Figure 6. Corresponding densitometry of the autoradiograph reported in Figure 5 shows MCP-1 mRNA expression in kidneys from 12-month-old CD1 (ICR) BR normal mice and 12-month-old NZB/W mice given vehicle or cyclophosphamide (CyP). The optical density of the autoradiographic signals was quantitated and calculated as the ratio of MCP-1 to GAPDH mRNA. The mRNA levels of NZB/W mice were calculated by assuming the optical density of control mice as unit.

prevented MCP-1 induction and glomerular influx of monocytes/macrophages. Other studies showed that in rats with anti-GBM glomerulonephritis, glomerular MCP-1 mRNA increased in association with the monocyte influx and correlated with expression of immunoreactive MCP-1 in the nephritic glomeruli (23).

To study the distribution of MCP-1 mRNA in the kidney, we performed *in situ* hybridization experiments on renal tissue from NZB/W lupus mice of different ages. MCP-1 mRNA was detected in the glomerular epithelial, endothelial, and mesangial cells, as well as in tubules and interstitium. The intensity of the signal increased progressively with the evolution of the disease, in accordance with the Northern blot analysis results. Western blot experiments revealed an increased expression of MCP-1 protein in the renal tissue of 10-month-old as compared with 2-month-old NZB/W mice, which was consistent with MCP-1 mRNA data. Our *in vivo* findings agree with *in vitro* studies showing the capability of both glomerular and tubular epithelial cells in culture to express and produce MCP-1 in response to cytokines and other inflammatory mediators (16–18), a phenomenon that, at least in glomerular mesangial and endothelial cells, is mediated by the activation of NF- κ B and AP-1 transcription factors (52,53). In mice with lupus nephritis, gene expression of interleukin-1 and tumor necrosis factor α is increased in the renal cortex (54), which might imply that cytokines act as regulatory molecules for the observed MCP-1 overexpression. Mesangial cells are also induced by IgG and immune complexes to release MCP-1 upon engagement of Fc receptors (20,21). In the study presented here, increased MCP-1 mRNA was detected in glomeruli at 6 months, a time of early accumulation of mononuclear cells in capillary lumina. Additionally, consistent with previous studies (37,38), we detected diffuse electron-dense deposits by electron microscopy

in the mesangium at this time. These findings together may suggest that immune complexes, particularly those deposited in the mesangium, act to trigger MCP-1-mediated pathways of glomerular mononuclear cell accumulation in NZB/W mice, similar to other experimental diseases like anti-Thy 1.1 (22) and anti-GBM glomerulonephritis (23,24) in rats.

Our finding of a remarkable increase of MCP-1 mRNA in tubular cells of NZB/W lupus mice of 8 and 10 months of age might explain, at least in part, the accumulation of mononuclear cells observed in renal interstitium. Recent experiments by Harris *et al.* (55) have shown an upregulation of MCP-1 mRNA expression in proximal tubular cells in culture exposed to albumin and transferrin-iron at concentrations similar to those found in proteinuric urine. It is tempting to speculate that in lupus nephritis, tubular overexpression of MCP-1 might be the consequence of the excessive tubular reabsorption of proteins ultimately leading to interstitial inflammation.

Patients with lupus nephritis studied in the active phase of the disease had higher levels of urinary MCP-1 than in the inactive phase (26). Administration of high-dose steroids to patients with active disease significantly reduced urinary MCP-1. In harmony with the above human findings are additional data from the study presented here, indicating that cyclophosphamide given to NZB/W mice up to 12 months of age effectively limited proteinuria and renal damage and prevented upregulation of renal MCP-1 gene as assessed by Northern blot and *in situ* hybridization experiments.

When interpreting data on the effect of steroids and cyclophosphamide on renal MCP-1 upregulation in lupus nephritis, the possibility that these drugs inhibit B cell activation and antibody synthesis should not be overlooked. This will prevent immune complex formation, regardless of the contributing role of MCP-1.

In summary, our results show a progressive, time-dependent upregulation of renal MCP-1 gene during the course of nephritis in NZB/W lupus mice that closely parallels the time course of mononuclear cell infiltration in the kidney. These data can be taken to suggest that MCP-1 acts as a major signaling molecule for mononuclear cell recruitment at the glomerular and tubulo-interstitial level, at least in murine models of SLE. In the past few years, attempts to block cytokine activity have been made by neutralizing antibodies, receptor antagonists, or soluble receptors (56). Molecules that effectively antagonize the biological activity of MCP-1—if available in the near future—may possibly find an important role in the therapy of lupus nephritis.

Acknowledgments

We thank Daniela Cavallotti for technical assistance. We are greatly indebted to Dr. Charles D. Stiles (Department of Microbiology and Molecular Genetics, Harvard Medical School, and Dana-Farber Cancer Institute, Boston, MA) for providing JE/MCP-1 probe. We also thank Dr. Alberto Mantovani (Mario Negri Institute, Milano, Italy) for discussion and guidance in preparation of anti-MCP-1 antibody, Dr. Luca De Gioia (Mario Negri Institute, Milano, Italy) for preparing MCP-1 synthetic peptide, and Dr. Paolo Ruggiero (Centro Ricerche Dompé, Biotechnologie, L'Aquila, Italy) for helpful advice.

References

- Howie JB, Helyer BJ: The immunology and pathology of NZB mice. *Adv Immunol* 9: 215-266, 1968
- Theofilopoulos AN, Dixon FJ: Etiopathogenesis of murine SLE. *Immunol Rev* 55: 179-216, 1981
- Alexopoulos E, Seron D, Hartley RB, Cameron S: Lupus nephritis: Correlation of interstitial cells with glomerular function. *Kidney Int* 37: 100-109, 1990
- D'Agati VD, Appel GB, Estes D, Knowles II, Pirani CL: Monoclonal antibody identification of infiltrating mononuclear leukocytes in lupus nephritis. *Kidney Int* 30: 573-581, 1986
- Bruijn JA, Dinklo NJCM: Distinct patterns of expression of inter-cellular adhesion molecule-1, vascular cell adhesion molecule-1, and endothelial-leukocyte adhesion molecule-1 in renal disease. *Lab Invest* 69: 329-335, 1993
- Brady HR: Leukocyte adhesion molecules: Potential targets for therapeutic intervention in kidney diseases [commentary]. *Curr Opin Nephrol Hypertens* 2: 171-182, 1993
- Oppenheim JJ, Zachariae CO, Mukalda N, Matsushima K: Properties of the novel proinflammatory supergene "intercrine" cytokine family. *Annu Rev Immunol* 9: 617-648, 1991
- Yoshimura T, Robinson EA, Tanaka S, Appella E, Leonard EJ: Purification and amino acid analysis of two human monocyte chemoattractants produced by pyrohemagglutinin-stimulated human blood mononuclear leukocytes. *J Immunol* 142: 1956-1962, 1989
- Leonard EJ, Yoshimura T: Human monocyte chemoattractant protein-1 (MCP-1). *Immunol Today* 11: 97-101, 1990
- Carr MW, Roth SJ, Luther E, Rose SS, Springer TA: Monocyte chemoattractant protein-1 acts as a T-lymphocyte chemoattractant. *Proc Natl Acad Sci U S A* 91: 3652-3656, 1994
- Taub DD, Proost P, Murphy WJ, Anver M, Longo DL, van Damme J, Oppenheim JJ: Monocyte chemotactic protein-1 (MCP-1), -2, and -3 are chemotactic for human T lymphocytes. *J Clin Invest* 95: 1370-1376, 1995
- Luckow B, Schlondorff D: The monocyte chemoattractant protein 1. In: *Molecular Nephrology: Kidney Function in Health and Disease*, edited by Schlondorff D, Bonventre JV, New York, Marcel Dekker, Inc., 1995, pp 653-671
- Sica A, Wang JM, Colotta F, Dejana E, Mantovani A, Oppenheim JJ, Larsen C, Zachariae CO, Matsushima K: Monocyte chemotactic and activating factor gene expression induced in endothelial cells by IL-1 and TNF. *J Immunol* 144: 3034-3038, 1990
- Rollins BJ, Yoshimura T, Leonard EJ, Pober JS: Cytokine-activated human endothelial cells synthesize and secrete a monocyte chemoattractant, MCP-1/JE. *Am J Pathol* 136: 1229-1233, 1990
- Kakizaki Y, Waga S, Sugimoto K, Tanaka H, Nukii K, Takeya M, Yoshimura T, Yokoyama M: Production of monocyte chemoattractant protein-1 by bovine glomerular endothelial cells. *Kidney Int* 48: 1866-1874, 1995
- Zoja C, Wang JM, Bettoni S, Sironi M, Renzi D, Chiaffarino F, Abboud HE, van Damme J, Mantovani A, Remuzzi G, Rambaldi A: Interleukin 1 β and tumor necrosis factor induce gene expression and production of leukocyte chemotactic factors, colony-stimulating factors and interleukin 6 in human mesangial cells. *Am J Pathol* 138: 991-1003, 1991
- Rovin BH, Yoshimura T, Tan L: Cytokine-induced production of monocyte chemoattractant protein-1 by cultured human mesangial cells. *J Immunol* 148: 2148-2153, 1992
- Prodjosudjadi W, Gerritsma JSJ, Klar-Mohamad N, Gerritsen AF, Bruijn JA, Daha MR, van Es LA: Production and cytokine-mediated regulation of monocyte chemoattractant protein-1 by human proximal tubular epithelial cells. *Kidney Int* 48: 1477-1486, 1995
- Yoshimura T, Yuhki N, Moore SK, Appella E, Lerman MI, Leonard EJ: Human monocyte chemoattractant protein-1 (MCP-1): Full-length cDNA cloning, expression in mitogen-stimulated blood mononuclear leukocytes, and sequence similarity to mouse competence gene JE. *FEBS Lett* 244: 487-493, 1989
- Hora K, Satriano JA, Santiago A, Mori T, Stanley ER, Shan Z, Schlondorff D: Receptors for IgG complexes activate synthesis of monocyte chemoattractant peptide 1 and colony stimulating factor 1. *Proc Natl Acad Sci U S A* 89: 1745-1749, 1992
- Satriano JA, Hora K, Shan Z, Stanley ER, Mori T, Schlondorff D: Regulation of monocyte chemoattractant protein-1 and macrophage colony-stimulating factor-1 by IFN- γ , tumor necrosis factor- α , IgG aggregates, and cAMP in mouse mesangial cells. *J Immunol* 150: 1971-1978, 1993
- Stahl RAK, Thaiss F, Disser M, Helmchen U, Hora K, Schlondorff D: Increased expression of monocyte chemoattractant protein-1 in anti-thymocyte antibody-induced glomerulonephritis. *Kidney Int* 44: 1036-1047, 1993
- Rovin BH, Rumancik M, Tan L, Dickerson J: Glomerular expression of monocyte chemoattractant protein-1 in experimental and human glomerulonephritis. *Lab Invest* 71: 536-542, 1994
- Tang WW, Yin S, Wittwer AJ, Qi M: Chemokine gene expression in anti-glomerular basement membrane antibody glomerulonephritis. *Am J Physiol* 269: F323-F330, 1995
- Prodjosudjadi W, Gerritsma JSJ, van Es LA, Daha MR, Bruijn JA: Monocyte chemoattractant protein-1 in normal and diseased human kidneys: An immunohistochemical analysis. *Clin Nephrol* 44: 148-155, 1995
- Noris M, Bernasconi S, Casiraghi F, Sozzani S, Gotti E, Remuzzi G, Mantovani A: Monocyte chemoattractant protein-1 is excreted in excessive amounts in the urine of patients with lupus nephritis. *Lab Invest* 73: 804-809, 1995
- Rambaldi A, Young DC, Griffin ID: Expression of the M-CSF (CSF-1) gene by human monocytes. *Blood* 69: 1409-1413, 1987
- Rollins BJ, Morrison ED, Stiles CD: Cloning and expression of JE a gene inducible by platelet-derived growth factor and whose product has cytokine-like properties. *Proc Natl Acad Sci U S A* 85: 3738-3742, 1988
- Feinberg AP, Volgestein B: A technique for radiolabeling DNA restriction endonuclease fragments to high specific activity. *Anal Biochem* 132: 6-13, 1983
- Noris M, Morigi M, Donadelli R, Aiello A, Foppolo M, Todeschini M, Orisio S, Remuzzi G, Remuzzi A: Nitric oxide synthesis by cultured endothelial cells is modulated by flow conditions. *Circ Res* 76: 536-543, 1995
- Forth P, Marty L, Piechaczyk KM, el Sabrouy S, Dani C, Jeanteur P, Blanchard JM: Various rat adult tissues express only one major mRNA species from the glyceraldehyde 3-phosphate-dehydrogenase multigenic family. *Nucleic Acids Res* 13: 1431-1432, 1985
- Luo Y, Laning J, Hayashi M, Hancock PR, Rollins B, Dorf ME: Serologic analysis of the mouse beta chemokine JE/monocyte chemoattractant protein-1. *J Immunol* 153: 3708-3715, 1994
- Selvaggini C, De Gioia L, Cantù L, Ghibaudi E, Diomedè L, Passerini F, Forloni G, Bugiani O, Tagliavini F, Salmona M: Molecular characteristics of a protease-resistant, amyloidogenic neurotoxic peptide homologous to residues 106-126 of the prion protein. *Biochem Biophys Res Commun* 194: 1380-1386, 1993

34. Vecchi A, Garlanda C, Lampugnani LMG, Resnati M, Matteucci C, Stoppacciaro A, Schnurch H, Risau W, Ruco L, Mantovani A, Dejana E: Monoclonal antibodies specific for endothelial cells of mouse blood vessels: Their application in the identification of adult and embryonic endothelium. *Eur J Cell Biol* 63: 247-254, 1994
35. Coligan JE, Kruisbeek AM, Margulies DH, Shevach EM, Strober W, editors: *Current Protocols in Immunology*, Vol. 1, Unit 2, New York, John Wiley and Sons, 1994
36. Read SM, Northcote DH: Minimization of variation in the response to different proteins of the Coomassie blue G dye-binding assay for protein. *Anal Biochem* 116: 53-64, 1981
37. Balow JE: Lupus nephritis. *Ann Intern Med* 106: 79-94, 1987
38. McGiven AR, Lynraven GS: Glomerular lesions in NZB/NZW mice: Electron microscopic study of development. *Arch Pathol* 85: 250-261, 1968
39. Fuentes ME, Durham SK, Swerdel MR, Lewin AC, Barton DS, Megill JR, Bravo R, Lira SA: Controlled recruitment of monocytes and macrophages to specific organs through transgenic expression of monocyte chemoattractant protein-1. *J Immunol* 155: 5769-5776, 1995
40. Schreiner GF: The role of the macrophage in glomerular injury. *Semin Nephrol* 3: 268-275, 1991
41. Remuzzi G, Zoja C, Bertani T: Glomerulonephritis. *Curr Opin Nephrol Hypertens* 2: 465-474, 1993
42. Holdsworth SR, Neall TJ, Wilson CB: Abrogation of macrophage-dependent injury in experimental glomerular nephritis in the rabbit: Use of an anti-macrophage serum. *J Clin Invest* 68: 686-698, 1981
43. Main IW, Nikolic-Paterson DJ, Atkins RC: T cells and macrophages and their role in renal injury. *Semin Nephrol* 12: 395-407, 1992
44. Cattell V: Macrophages in acute glomerular inflammation. *Kidney Int* 45: 945-952, 1994
45. Nathan CF: Secretory products of macrophages. *J Clin Invest* 80: 319-326, 1987
46. Holdsworth SR, Tipping PG: Macrophage-induced glomerular fibrin deposition in experimental glomerulonephritis in the rabbit. *J Clin Invest* 76: 1367-1374, 1985
47. Glassock RJ: The pathogenesis of crescentic glomerulonephritis in man. In: *Glomerular Injury 300 Years After Morgagni*, edited by Bertani T, Remuzzi G, Milan, Wichtig Editore, 1983, pp 195-204
48. Furie MB, Randolph GJ: Chemokines and tissue injury. *Am J Pathol* 146: 1287-1301, 1995
49. Rollins BJ, Walz A, Baggiolini M: Recombinant human MCP-1/JE induces chemotaxis, calcium flux and the respiratory burst in human monocytes. *Blood* 78: 1112-1116, 1991
50. Jiang Y, Beller DI, Frendl G, Graves DT: Monocyte chemoattractant protein-1 regulates adhesion molecule expression and cytokine production in human monocytes. *J Immunol* 148: 2423-2428, 1992
51. Shyy Y-J, Wickham LL, Hagan JP, Hsieh H-J, Hu Y-L, Telian SH, Valente AJ, Sung K, Chien S: Human monocyte colony-stimulating factor stimulates the gene expression of monocyte chemotactic protein-1 and increases the adhesion of monocytes to endothelial monolayers. *J Clin Invest* 92: 1745-1751, 1993
52. Rovin BH, Dickerson JA, Tan LC, Hebert CA: Activation of nuclear factor-kB correlates with MCP-1 expression by human mesangial cells. *Kidney Int* 48: 1263-1271, 1995
53. Kakizaki Y, Sugimoto K, Waga S, Tanaka H, Yokoyama M: Transcription factors NF-kB and AP-1 regulate gene expression of monocyte chemoattractant protein-1 (MCP-1) by bovine glomerular endothelial cells (GEN) [Abstract]. *J Am Soc Nephrol* 6: 833, 1995
54. Boswell JM, Yui MA, Burt DW, Kelley VE: Increased tumor necrosis factor and IL-1 β gene expression in the kidneys of mice with lupus nephritis. *J Immunol* 141: 3050-3054, 1988
55. Harris DCH, Chen J: Monocyte chemoattractant protein-1 (MCP-1) mRNA expression in response to protein in rat proximal tubule cells in culture [Abstract]. *J Am Soc Nephrol* 6: 1015, 1995
56. Abbate M, Remuzzi G: Glomerulonephritis: From new knowledge on the mechanisms of tissue damage to novel therapies. *Curr Opin Nephrol Hypertens* 4: 374-382, 1995

Early Influx of Glomerular Macrophages Precedes Glomerulosclerosis in the Obese Zucker Rat Model¹

Stéphanie Lavaud, Odile Michel, Caroline Sassy-Prigent, Didier Heudes, Raymond Bazin, Jean Bariéty, and Jacques Chevallier,² with the technical assistance of Marie-France Bélair and Chantal Mandet

S. Lavaud, O. Michel, C. Sassy-Prigent, D. Heudes, J. Bariéty, J. Chevallier, M.-F. Bélair, C. Mandet, Unité de Recherche "Immunopathologie Humaine," INSERM U430, Hôpital Broussais, Paris, France

R. Bazin, Unité de Recherche "Physiopathologie de la Nutrition," INSERM U177, Les Cordeliers, Paris, France
(J. Am. Soc. Nephrol. 1996; 7:2604-2615)

ABSTRACT

Because hyperlipidemia and macrophage influx appear to play a key role in the genesis of renal glomerulosclerosis, this study examined the temporal relationship between hyperlipidemia (triglycerides and cholesterol), mononuclear cell influx, changes in glomerular structure, and expansion of the extracellular matrices in obese Zucker rats, which rapidly develop hyperlipidemia and spontaneous glomerulosclerosis. Lean and obese Zucker rats were fed a standard diet, and were euthanized at 14 days, 1, 3, 6, 9, and 12 months. Plasma lipid, insulin, and creatinine levels were measured, and the presence of inflammatory cells in the glomerulus was assessed by immunohistochemistry on kidney sections. Plasma lipids and insulin and macrophage density were significantly greater in obese than in lean rats as early as 1 month. Computer-assisted image analysis was used to evaluate the glomerular domain surface areas. The morphometric measurements showed that glomeruli of obese rats rapidly became hypertrophied after 3 months, as a result of a very large increase in the mesangial domain. The expression of genes for extracellular matrix components and inhibitors of extracellular matrix proteinases (TIMP-1 and TIMP-2) was monitored in microdissected glomeruli. Reverse transcription-polymerase chain reaction showed increases in mRNA for Type IV collagen and fibronectin and for the two metalloproteinase inhibitors, each of which might participate in this matrix expansion. Thus, the development of hyperlipidemia plus macrophage influx at a very early age may initiate a

sequence of events leading to glomerulosclerosis later on.

Key Words: *Inflammation, hyperlipidemia, extracellular matrix, morphometry, RT-PCR*

Diffuse glomerulosclerosis and focal and segmental glomerular hyalinosis (FSGH) (1) (often called focal and segmental glomerulosclerosis (2)) occur in diverse circumstances including aging; hypertension; metabolic disorders such as diabetes, obesity or hyperlipidemia; partial nephrectomy; and intoxication by puromycin aminonucleoside (reviewed in References 1 and 2). Among the different factors implicated in the pathogenesis of these lesions, the accumulation of circulating monocytes/macrophages within the glomerular tuft has been described in almost all circumstances of FSGH (3), suggesting that several mechanisms involved in glomerulosclerosis are analogous to those observed in atherosclerosis (4). In this respect, disturbances of lipoprotein metabolism may accelerate the onset of glomerulosclerosis (5).

The obese Zucker rat is a model of spontaneous glomerulosclerosis (6-8). Obesity, an autosomal recessive trait accompanied by hyperlipidemia, develops at an early age (8, reviewed in Reference 9). Obese rats also suffer from mild glucose intolerance and peripheral insulin resistance similar to that found in humans with Type II diabetes (10). These metabolic abnormalities precede the development of proteinuria and glomerular injury in obese rats (8,11). Lean littermates have normal serum lipids (11,12) and normal renal structure and function (6). The glomerular hemodynamic function of obese rats and their lean littermates is not significantly different and is probably not involved in the pathogenesis of glomerulosclerosis in this strain (13).

Several studies have been published on the putative mechanisms involved in the pathogenesis of diffuse glomerulosclerosis and FSGH in Zucker rats, but little attention has been paid to the early events occurring in the glomeruli of weaning animals when metabolic disorders begin to worsen. The importance of a monocyte/macrophage influx during and after the weaning period is not known, although hypertriglyceridemia, hypercholesterolemia, and hyperinsulinemia develop markedly. We have, therefore, attempted to examine the contribution of inflammation to the initiation and development of diffuse glomerulosclerosis and FSGH lesions in obese rats, by analyzing the temporal relationship between hyperlipidemia and hyperinsulinemia, the mononuclear cell influx, changes in glomer-

¹ Received March 28, 1996. Accepted August 12, 1996.

² Correspondence to Dr. J. Chevallier, Immunopathologie Rénale et Vasculaire, INSERM U 430, Hôpital Broussais, 96 Rue Didot, 75674 Paris Cedex 14, France.

1046-6673/97/12-2604\$03.00/0

Journal of the American Society of Nephrology
Copyright © 1996 by the American Society of Nephrology

ular structure, and the expansion of the glomerular tuft. Little is known about the composition of the expanded matrices observed in the sclerosed glomeruli of Zucker rats, or about the change in the balance between the synthesis and degradation of extracellular matrix components (ECM) that occurs with age. Accordingly, to consider only the matrix expansion within the glomerulus, we used microdissected glomeruli from lean and obese rat kidneys to follow the kinetics of messenger RNA expression of some major ECM components (Types I, III, and IV collagens, and fibronectin) and of the specific proteinase inhibitors TIMP-1 and TIMP-2.

METHODS

Animals

Male lean (Fa/fa) and obese (fa/fa) Zucker rats were identified and selected at 4 wk of age by visual examination of inguinal fat deposit. They were raised under standard husbandry conditions, fed regular laboratory chow *ad libitum* (A04; Villemoisson, Epinay sur Orge, France) and had free access to water until euthanization at 5 wk (1 month), 3, 6, 9, and 12 months of age. A second group of 14-day-old suckling Zucker pups (Fa/fa and fa/fa) were euthanized, and the obese genotype was determined by plotting inguinal fat pad weight against body weight (14).

Animal care complied with the Principles of Laboratory Animal Care formulated by the National Society for Medical Research and the Guide for the Care and Use of Laboratory Animals (National Institutes of Health Publication 86-23, revised 1989; authorization 00577, 1989, Paris, France).

Blood Pressure, Serum Creatinine, Insulin, Lipids, and Urine Proteins

Conscious systemic blood pressure (BP) was measured by a tail-cuff system (Ugo Basile Apex, Varese, Italy). Blood was collected from animals at the time of euthanization into tubes containing heparin as anticoagulant for serum lipid and creatinine assays. These samples were centrifuged and aliquots of plasma were frozen and stored at -20°C . Twenty-four-hour urine samples were collected from fasting animals housed individually in metabolic cages with free access to water. Triglycerides and total cholesterol were determined by the enzymatic and colorimetric GPO-PAP and CHOD-PAP methods respectively (Boehringer, Mannheim, Germany). Serum and urine creatinine concentrations were measured on a Synchron CX7 Beckman analyser (Beckman, Fullerton, CA). Proteinuria was determined enzymatically using the Coomassie Protein Assay Reagent with BSA as standard (Pierce, Rockford, IL). Serum insulin levels were measured by RIA (CIS, Gif sur Yvette, France) with a rat insulin standard (Novo, Copenhagen, Denmark).

Kidney Structure

Lean and obese rats aged 1, 3, 6, 9, and 12 months, were anesthetized with pentobarbital (ip, 0.1 mL/100 g body wt) and the kidneys were removed and weighed. For light microscopy, transverse sections at the hilus were directly frozen in liquid nitrogen, others were fixed in alcoholic Bouin's solution, embedded in paraffin, sectioned (4- μm thick), and stained with Masson's trichrome or silver methenamine, according to routine histological staining. For electron microscopy, small samples of the kidney cortex were fixed in 2%

glutaraldehyde/0.2 M cacodylate buffer, dehydrated in acetone, and embedded in Glucidether 100 (Merck, Darmstadt, Germany).

Masson's trichrome stained sections of at least 100 glomeruli were evaluated for the presence of FSGH lesions. The percentage of glomeruli having FSGH lesions was determined for each tissue specimen, and a severity index was calculated for each glomerulus by using the equation:

$$\frac{(S1 \times 1/4) + (S2 \times 1/2) + (S3 \times 3/4) + (S4 \times 1)}{\text{total number of glomeruli}}$$

where S is the number of glomeruli with FSGH involving 1/4, 1/2, 3/4, and 4/4 of the glomerulus.

Morphometric Measurements

The thickness of the glomerular basement membrane (GBM) was evaluated from electron micrographs enlarged to a magnification of 42,000. Only capillaries in which the plasma membrane of the foot processes was clearly visible along the basement membrane were considered to guarantee that the section was perpendicular to the GBM. The width of the lamina densa was measured with a ruler oriented at a right angle to the GBM, in areas not directly contiguous to the mesangial matrix. At least three glomeruli were examined from each rat, with a minimum of five capillary sections surveyed in each glomerulus. The exact magnification of the image was calculated using diffraction grating replica standard (Polaron Equipment, Watford, U.K.).

Morphometric determination of the different glomerular domains and parameters was done using an automated image-analyzing system on transverse kidney sections processed with silver methenamine staining, which reveals the extracellular matrices. The image-analyzing system was composed of a light microscope (Nacht; Microvision, Evry, France), a black-and-white video camera (Cohu, San Diego, CA), an image-analysis processor (NS-15000, Nacht), and a microcomputer to store the data and pilot the processor using a personal program written in C language. The image-analysis processor, based on the principles of mathematical morphology, digitizes microscopic images into 512×512 pixel images within 256 gray levels. The digitized images were submitted to predefined transformation allowing automatic measurements of selected glomerular morphometric parameters (15). The glomeruli were measured with a $\times 25$ objective, yielding a final calibration of $0.4219 \mu\text{m}/\text{pixel}$. Any variability in the staining intensity of the sections could be corrected by calibrating the image according to the defined gray levels. The glomerular parameters measured were: (1) total glomerular surface area delimited by the internal edge of the Bowman's capsule; (2) urinary space surface area; (3) cumulative surface area of the capillary lumen sections; (4) glomerular tuft surface area, defined by the total glomerular measurement minus the urinary space; (5) mesangial surface area, defined by the glomerular tuft measurement minus areas of the capillary lumens and the glomerular capillary free walls (see Figure 1). Although the individual capillary lumen section surface area was not obtained by the program used in the automated image analysis, the mean capillary section surface area was estimated by dividing the cumulative surface area of the capillary lumen by the number of capillary sections. The total number of glomeruli necessary to yield convergent data was established at 30 glomeruli per rat (15). The observer, unaware of the code of the sections, measured 30 glomeruli randomly over the depth of the cortex on each kidney section. Glomeruli show-

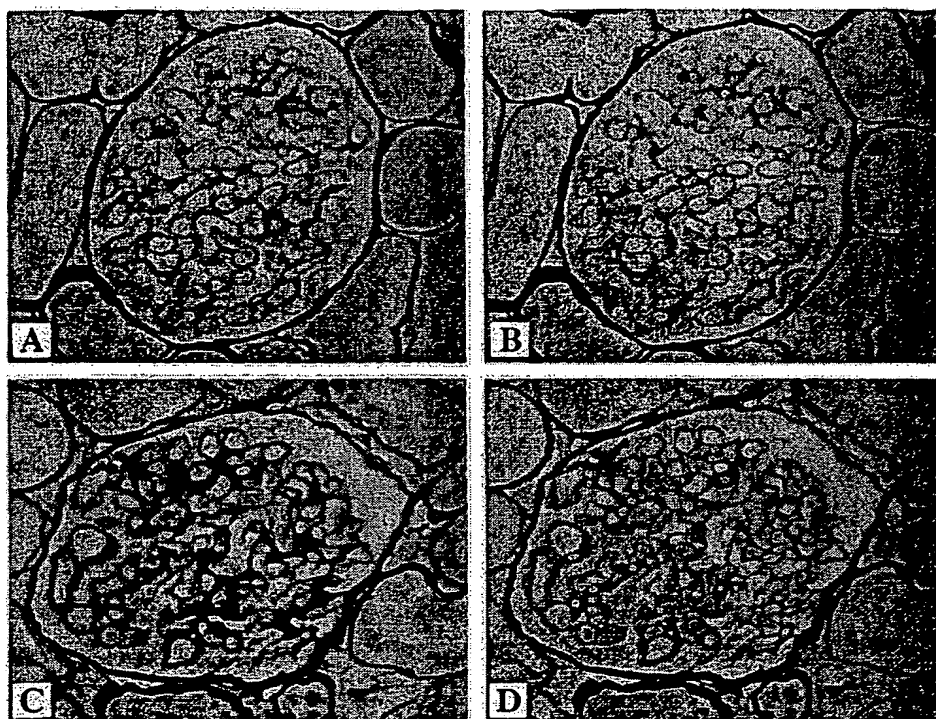


Figure 1. Digitized images of the glomerulus of a 12-month-old lean rat (A, B) and an obese rat (C, D). A and C, images of the glomerulus within 256 gray levels. B and D, mesangial domain selected from the preceding image. This mesangial domain was more expanded in obese than in lean rat glomeruli. (Original magnification, $\times 350$).

ing clear glomerular tuft retraction or extensive FSGH were not measured because, in these cases, differences between matrices, remnant capillary lumen sections, and urinary spaces were indistinguishable.

Immunohistochemical Studies

The differentiation and activation of intraglomerular mononuclear cells was assessed by incubating frozen sections from rats aged 14 days, 1, 3, 6, or 9 months for 60 min at room temperature (RT) with a panel of mouse monoclonal antibodies diluted in Tris-buffered saline pH 7.4, containing 0.1% BSA (Sigma Chemical, St Louis, MO): (1) ED₁, diluted 1:1000 (Serotec, Oxford, UK), specific for a monocyte/macrophage cytoplasmic antigen (16); (2) ED₂, diluted 1:1000 (Serotec, Oxford, UK), considered to be a marker of tissue-resident macrophages (16); (3) OX₆, diluted 1:50 (Sera-Lab; Crawley Down, Sussex, UK), which detects the MHC Class II Ia antigen; and (4) W3/25 diluted 1:50 (Serotec, Oxford, UK), which reacts with a CD4 epitope and binds to T lymphocyte helper cells and to a monocyte/macrophage subpopulation (17, 18). FSGH lesions were particularly well developed in the glomeruli of the 12-month-old obese rats, making the estimation of mononuclear cell densities difficult and imprecise. This age group was therefore not included in the immunohistochemical study. The sections were washed in Tris-buffered saline and incubated with rabbit anti-mouse immunoglobulin antibody (Dako Corporation, Carpinteria, CA) and alkaline-anti-phosphatase alkaline complexes (diluted 1:75) (Dako). The enzyme was revealed with freshly prepared Fast Red Substrate System (Dako) containing 0.33 mg/mL le-

vamisole (Sigma) to reduce the staining background. Sections were counterstained with hematoxylin. The number of positive cells in each glomerulus was counted, with a minimum of 50 glomeruli surveyed per kidney section.

The presence of matrix protein was assessed by incubating frozen sections from rats aged 1, 3, 6, or 9 months for 60 min at RT with antibodies (Institut Pasteur Lyon, France) diluted in Tris/0.1% BSA buffer (pH 7.2), such as: (1) an IgG fraction of polyclonal rabbit anti-mouse Type IV collagen (1:20); (2) anti-rat Type III collagen rabbit immune serum (1:5); and (3) anti-rat Type I collagen rabbit immune serum (1:5). The sections were then incubated with a fluorescein-conjugated anti-rabbit swine antibody (Dako).

Preparation of Isolated Microdissected Glomeruli

The expression of genes for ECM components and inhibitors of ECM proteinases was monitored in glomeruli microdissected from a second series of lean and obese rats (1, 3, 6, 9, and 14 months old), after modifications of the technique described by Peten *et al.* (19). Rats were anesthetized with pentobarbital and the left kidney was perfused at 4°C, first with solution I (135 mM NaCl, 1 mM Na₂HPO₄, 1.2 mM Na₂SO₄, 1.2 mM MgSO₄, 5 mM KCl, 2 mM CaCl₂, 5.5 mM glucose, and 5 mM *N*-hydroxyethylpiperazine-*N'*-2-ethanesulfonic acid, pH 7.4) and then with 3 mL of the solution I containing 1 mg/mL Type I collagenase (300 U/mg) (Sigma) and 1 mg/mL BSA (Sigma). Small, superficial fragments of the kidney cortex were rapidly excised and transferred to a microdissecting dish, placed on ice, containing solution I

supplemented with 1.2 U/ μ L RNasin, a RNase inhibitor (Promega, Madison, WI) and 1 mM dithiothreitol (Sigma). Glomeruli were separated from tubules and from afferent and efferent arterioles and removed from their Bowman's capsules under a binocular microscope. A total of 20 glomeruli were taken from each rat, and placed in acid guanidium thiocyanate solution for RNA extraction by the phenol/chloroform method.

Reverse Transcription and Polymerase Chain Reaction Analysis

The mRNA were extracted from glomeruli from three rats in each group and pooled to ensure sufficient material for the subsequent polymerase chain reaction (PCR) analysis. They were reverse transcribed into cDNA with oligo(dT) and MMLV reverse transcriptase (Gibco-BRL, Gaithersburg, MD). The reverse transcription products were amplified with primers for mouse fibronectin (upper primer: 5'-TTA TGA CGA TGG GAA GAC CTA-3'; lower primer: 5'-GTG GGG CTG GAA AGA TTA CTC-3'; product length, 295 base pairs (bp)), for mouse $\alpha 1$ (IV) collagen (upper primer: 5'-TCG GCT ATT CCT TCG TGA TG-3'; lower primer: 5'-TCT CGC TTC TCT CTA TGG TG-3'; product length, 185 bp), for mouse $\alpha 1$ (III) collagen (upper primer: 5'-TGC CCA CAG CCT TCT ACA CCT-3'; lower primer: 5'-CAG CCA TTC CTC CCA CTC CAG-3'; product length, 244 bp), for mouse $\alpha 2$ (I) collagen (upper primer: 5'-TGT TCG TGG TTC TCA GGG TAG-3'; lower primer: 5'-TTG TCG TAG CAG GGT TCT TTC-3'; product length, 254 bp), for mouse TIMP-1 (upper primer: 5'-CCC CAG AAA TCA ACG AGA CCA-3'; lower primer: 5'-ACA CCC CAC AGC CAG CAC TAT-3'; product length, 303 bp), for mouse TIMP-2 (upper primer: 5'-GCA GGA GGA GAT GTA GCA AGG-3'; lower primer: 5'-CGG GGA GGA GAT GTA GCA AGG-3'; product length, 162 bp) and for GAPDH (upper primer: 5'-GTG AAG GTC GGA GTC AAC G-3'; lower primer: 5'-GGT GAA GAC GCC AGT GGA CTC-3'; product length, 299 bp). All PCR were carried out in 25 μ L of a mixture containing 10 mM dNTP, 1 \times PCR buffer (10 mM Tris-HCl, pH 8.3, 50 mM KCl, 40% dimethyl sulfoxide, 0.001% gelatin, $MgCl_2$ [1 mM for Type IV collagen, TIMP-1, TIMP-2, and GAPDH primers; 1.5 mM for fibronectin primers and Type I collagen primers; 0.75 mM for Type III collagen primers] and 2.5 U amplitaq polymerase [Perkin-Elmer Cetus, Norwalk, CT]). Each sample was incubated in a DNA thermal cycler (Perkin-Elmer Cetus) at 55 to 58°C for 25 to 30 cycles, depending on the primer. The PCR fragments were analyzed by electrophoresis on 2% agarose gels and visualized by ethidium bromide staining. Polaroid photographs of ethidium bromide-stained gels were digitized into 512 \times 512 pixel gray-scale images. The amount of nucleic acid was determined by densitometric analysis of the dots. The intensities of the cDNA bands for each protein were normalized to the GAPDH band intensities. All experiments were performed in duplicate.

Statistical Analysis

Results are expressed as means \pm SE. Statistical analysis was carried out using two-way analysis of variance with age and genotype as factors. Statistical significance was achieved if $P < 0.05$. In cases of interaction between the factors, one-factor analysis of variance was used at one level of the other factor. Data were analyzed using Statview 4.0 software (Abacus Concept Inc., Berkeley, CA).

RESULTS

Both lean and obese Zucker rats increased in weight with age, almost two times faster between 1 and 3 months than in the following period (Table 1). The obese rats were significantly heavier than age-matched lean littermates at and after 3 months of age, with body weights 40 to 50% greater. The cumulative weights of the two kidneys also increased with age in both groups of animals, more rapidly in the obese than in lean rats, the difference being significant at 9 and 12 months. However, the growth of the kidney with respect to the body weight remained roughly similar in the two groups of animals (Table 1). Mean systolic tail-cuff blood pressure increased slightly and similarly in both lean and obese groups between 3 and 12 months (Table 1).

Serum levels of cholesterol and triglycerides were higher in obese than in lean Zucker rats as early as 1 month (Table 1). Cholesterol levels increased twofold in obese rats between 1 and 12 months and triglyceride levels increased sevenfold. Plasma insulin levels, higher in the obese than in the lean group on and after 1 month, plateaued at 3 to 6 months and declined thereafter. No differences existed between the two groups by 12 months (Table 1). Serum creatinine concentration increased with age in the same manner in both groups of animals up to 9 months, but rose dramatically thereafter in obese rats (Table 1).

The creatinine clearance rate decreased with age in the obese group, dropping from 2.0 ± 0.8 mL/min at 3 months to 0.5 ± 0.1 mL/min at 12 months, but remained close to 1.3 mL/min in lean rats of any age (1.2 ± 0.3 mL/min at 3 months and 1.4 ± 0.1 mL/min at 12 months). Proteinuria developed markedly in obese rats between 3 and 9 months of age and stabilized thereafter. At 9 and 12 months, proteinuria was nearly 20 times greater in the obese rats than in the lean littermates (302.8 ± 50.7 and 16.5 ± 11.8 mg/24 h, respectively, at 12 months).

There was no sign of FSGH in lean-rat kidneys until 12 months. At 12 months, a faint FSGH, with a low severity index of 2, was detectable and affected 2% of the glomeruli. On the contrary, the incidence of FSGH in obese rats was 2% (severity index: 2) at 6 months and rapidly increased in quantity and severity to affect 26% of the glomeruli at 9 months with a severity index of 15, with no further development of the lesion thereafter. Histopathological examination of the kidney revealed a moderate tubulopathy in the obese group at 6 months, which worsened with age, affecting all of the obese animals after 9 months with the presence of tubular casts and cystic formations. Cystic formations were generally close to the most damaged glomeruli of the examined kidney section, and were often associated with areas of interstitial fibrosis.

The automated morphometric analysis revealed that glomeruli and glomerular tufts increased in size, in both obese and lean rat kidneys. They were larger in the obese group than in the lean group at all ages but

TABLE 1. Evolution of weights, blood pressure, and blood chemistries with age in obese rats and lean littermates^a

Parameter	Age (months)				
	1	3	6	9	12
Body weight (g)					
Lean	123.5 ± 5	345 ± 2	398 ± 10	440 ± 1	471 ± 10 ^b
Obese	128 ± 7	411 ± 14 ^c	594 ± 11 ^c	656 ± 12 ^c	654 ± 34 ^{b,c}
Two-Kidney Weight (g)					
Lean	1.18 ± 0.05	2.38 ± 0.06	2.79 ± 0.08	2.89 ± 0.10	3.23 ± 0.05 ^b
Obese	1.19 ± 0.08	2.57 ± 0.16	3.11 ± 0.13	4.29 ± 0.26 ^c	5.12 ± 0.56 ^{b,c}
Kidney Weight/100 g Body Weight					
Lean	0.95 ± 0.02	0.69 ± 0.01	0.70 ± 0.01	0.66 ± 0.01	0.64 ± 0.01 ^b
Obese	0.93 ± 0.03	0.62 ± 0.03	0.52 ± 0.01 ^c	0.66 ± 0.04	0.81 ± 0.12 ^b
Systolic Blood Pressure (mm Hg)					
Lean		108 ± 8	124 ± 2	129 ± 2	131 ± 2 ^b
Obese		103 ± 6	127 ± 3	129 ± 3	134 ± 2 ^b
Cholesterol (mg/dL)					
Lean	87 ± 3	126 ± 9	103 ± 7	112 ± 4	101 ± 6
Obese	139 ± 5 ^c	175 ± 10 ^c	242 ± 7 ^c	299 ± 31 ^c	288 ± 24 ^{b,c}
Triglycerides (mg/dL)					
Lean	29 ± 6	33 ± 10	10 ± 4	48 ± 13	71 ± 12 ^b
Obese	55 ± 5 ^c	191 ± 19 ^c	273 ± 97 ^c	382 ± 43 ^c	415 ± 33 ^{b,c}
Insulin (μU/mL)					
Lean	36 ± 7	27 ± 2	31 ± 3	49 ± 4	44.9 ± 6.4 ^b
Obese	77 ± 7 ^c	239 ± 56 ^c	230 ± 21 ^c	123 ± 12.5 ^c	71 ± 12 ^b
Creatinine (μM/L)					
Lean	37 ± 1	46 ± 2	51 ± 3	58 ± 3	60 ± 5 ^b
Obese	31 ± 1 ^c	36 ± 6	57 ± 3	73 ± 26	176 ± 52 ^{b,c}

^a N = six rats per group except in 12-month obese group where N = five rats.^b Age effect: $P < 0.001$.^c Lean versus obese: $P < 0.05$.

12 months (Figure 2A). The whole glomerular surface area began to decline in the obese group between 9 and 12 months. The urinary space surface area remained constant between 3 and 9 months, and tended to decline thereafter (Figure 2A). The cumulative surface area of the capillary lumen sections and the number of cut sections of the capillary lumen are shown in Figure 2B. These two parameters indicated significant differences with age in the two groups of rats. However, the curves had to be divided into two parts. The first part, from 1 to 3 months, corresponded to the growing period of the kidney (Table 1, Figure 2A) whereas the second period covered 3 to 12 months. When only the second period was considered, on and after 3 months of age, neither the cumulative surface area nor the number of capillary lumen sections changed significantly in the obese or lean group of animals (age effect between 3–12 months, $P = 0.16$ for both groups). With age, the mesangial domain increased in size in the two groups of animals, with a sharp expansion in obese rat kidneys between 6 and 12 months (Figures 1, 2C). At 12 months, the mesangial domain was three times larger in obese than in lean animals. Whereas in the 12-month-old obese rat kidneys, the glomerulus, urinary, and the capillary lumen surface areas tended to decline (Figure 2, A and

B), the mesangial domain continued to expand in old obese rats (Figure 2C). The Bowman's capsule basement membrane became thicker with age in both groups of animals (lean, $1.9 \pm 0.3 \mu\text{m}$ versus 2.4 ± 0.1 ; obese, 1.8 ± 0.3 versus 2.9 ± 0.1 at 3 months and 12 months, respectively).

Electron microscopy showed that the GBM regularly thickened between 3 months and 12 months by a factor of 1.8 in lean rats ($0.119 \mu\text{m} \pm 0.003$ versus $0.217 \mu\text{m} \pm 0.018$, $N =$ three rats) and by a factor of 2.4 in obese rats ($0.123 \mu\text{m} \pm 0.003$ versus $0.287 \mu\text{m} \pm 0.018$, $N =$ three rats) (Figure 3). The difference between lean and obese rats became statistically significant at 12 months ($P < 0.05$).

Macrophage-ED₁⁺ cell density increased 3.5-fold in obese rat glomeruli between 15 days and 1 month and remained high for the following periods (Figure 4A). In lean rats, the density of such ED₁-positive cells increased moderately (twofold) in early life and remained stable after 1 month, at a much lower level (almost twofold less) than in obese rats. Ia⁺ cell density (Ox6-detected cell) (Figure 4B) increased in lean and obese rat glomeruli between 14 days and 1 month. Thereafter, this density remained roughly constant in the lean group (if the 14-day data are excluded, the statistical analysis did not show any age effect: $P = 0.1$). On the

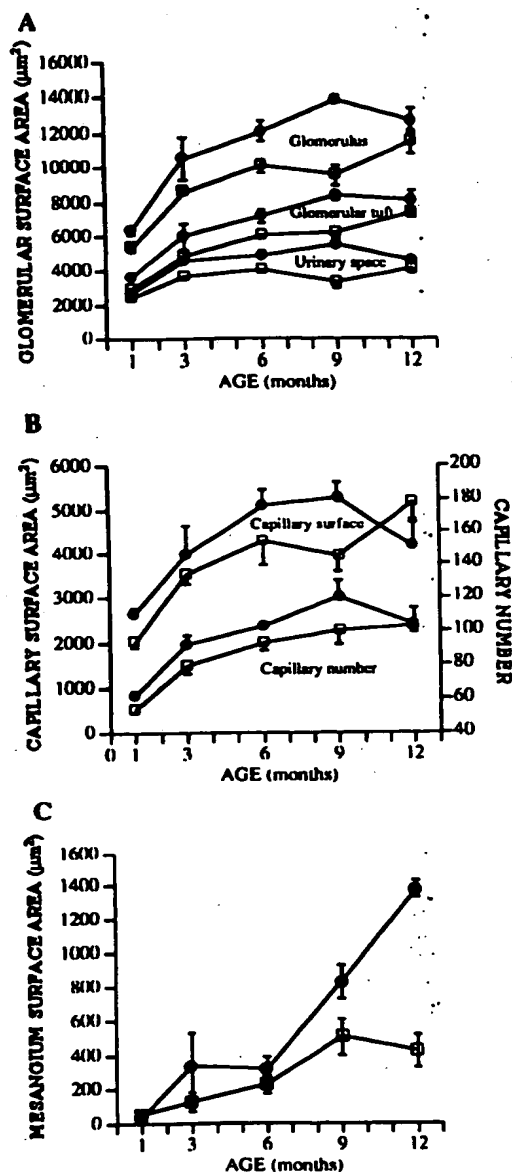


Figure 2. Morphometric measurements of the glomerular domains in lean and obese Zucker rat kidneys. Filled circles, obese rats; squares, lean rats. A: The whole glomerulus and the glomerular tuft increased in size with age in both obese and lean rats (age effect: $P < 0.001$ for both parameters), but was greater in obese than in lean rats (lean versus obese $P < 0.001$). The glomerular size tended to decline after 9 months. The urinary space surface area increased significantly in both groups between 1 and 12 months (age effect: $P < 0.001$; lean versus obese $P < 0.001$), but this age effect was concentrated in the 1-to-3-months growing period, with no change thereafter except a tendency to a decline at 12 months. B: The cumulative surface area of the capillary lumen sections and the number of section profiles per glomerulus significantly increased with age in both groups between 1 and 12 months (age effect: $P < 0.001$) but

contrary, la^+ cell density continuously increased with age in the obese rat glomeruli. At 9 months, there were significantly more la^+ cells in obese than in lean rat glomeruli. The number of $CD4^+$ cells per glomerulus (recognized by W3/25: T cells and monocyte/macrophage subpopulation) was always low compared with the number of other cell types (Figure 4C). Again, at 9 months, obese rats had statistically more cells per glomerulus than did lean animals. There was no ED_2 antibody labeling in any case.

The change in mRNA synthesis for extracellular matrix proteins is shown in Figure 5. $\alpha_1(IV)$ collagen (Figure 5B) and fibronectin (Figure 5C), which are among the major components of the mesangial matrix, were actively synthesized in younger animals. Thereafter, the mRNA synthesis in the two groups of rats varied. In lean rats, $\alpha_1(IV)$ collagen and fibronectin mRNA decreased with age, whereas in obese rats, after a decrease at 3 months, they regularly increased until 14 months. Messenger RNA for $\alpha_2(I)$ collagen (Figure 5D) was barely detected after 1 month of age and did not change, no matter what the experimental group and the age of the animals were, except for a sharp increase in 9-month-old obese rats. No mRNA for Type III collagen was detected in any rats of either group, at any age. These observations were paralleled by the immunodetection of the proteins in the glomeruli in kidney sections (Figure 6). Levels of mRNA for TIMP-1 and TIMP-2 slowly decreased in lean rats to reach minima in 9- and 14-month-old animals but they remained constant in obese rats, with a peak at 9 months (Figure 5, E and F). They then increased 5.2-fold (TIMP-1) and 4.5-fold (TIMP-2) in obese rats as compared with lean rats.

DISCUSSION

With age, FSGH developed dramatically in obese Zucker rats between 6 and 9 months, affecting 25% of the glomeruli. In comparison, only 2% of the glomeruli show FSGH at 36 months in a model of true kidney aging, the Wistar (WAG)/Rij rat raised in specific pathogen-free conditions (15). Automated image analysis showed that all glomerular domains markedly increased in size during the first 3 months of life in obese and lean animals. This corresponds to the developing phase of young animals and kidneys. Thereafter, the glomeruli rapidly became hypertrophied in obese rat kidneys, as in aging (15), because of enlargement of the glomerular tuft after the age of 3

remained constant if we ignore the growing period (1-3 months). There were more capillary sections in obese rat kidneys than in lean rat kidneys ($P < 0.05$; $N =$ three rats/group). C: The mesangial domain enlarged in both groups of rats between 1 and 12 months (age effect: $P < 0.01$), with a marked increase at 6 to 9 months in obese rat glomeruli. The mesangial surface area in 12-month-old obese animals was three times greater than in lean rats ($P < 0.001$; $N =$ three rats/group).

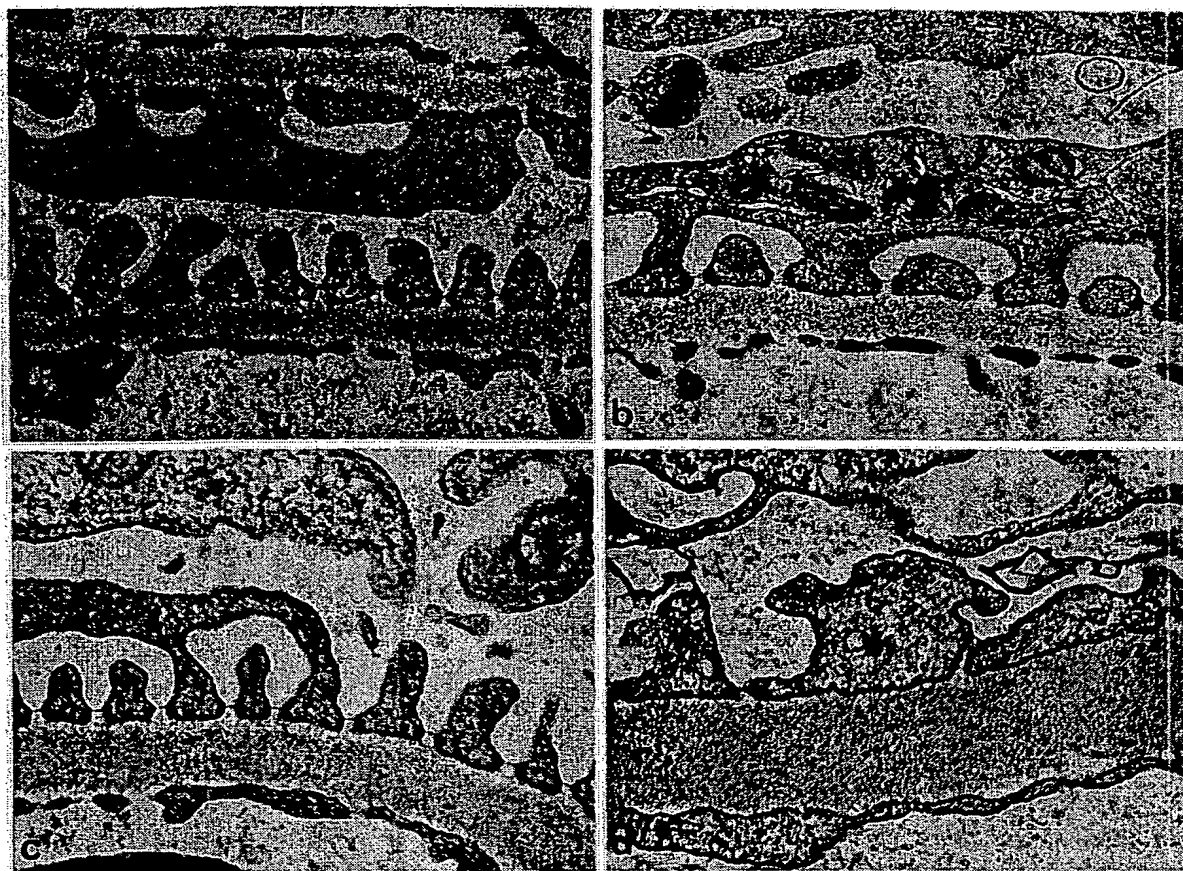


Figure 3. Electron micrographs of glomerular basement membrane in lean (A, C) and obese (B, D) rat kidneys. Glomerular basement membrane significantly increased in size between 3 (A, B) and 12 months (C, D) in both groups of animals, but this thickening was more pronounced in obese rats than in lean rats ($N = 3$ rats/group). (Original magnification, $\times 40,000$).

months. This was caused by a specific, large increase in argyrophilic extracellular matrices (GBM and mesangial matrix) with no statistical significant change in the number of capillary lumen sections or their surface area, or in the urinary space, between 3 and 12 months, except for a tendency to decline in the oldest animals. Contrary to human diabetic nephropathy, in which mesangial expansion could lead to glomerular functional deterioration in insulin-dependent diabetes mellitus by restricting the glomerular vasculature (20), the expansion of the glomerular tuft did not modify the capillaries in these obese Zucker rats, at least until 9 months, as was observed in true aging (15). Thereafter, although the mesangial domain was still expanding, a tendency toward a decline in glomerulus, urinary space, and capillary surface areas was observed at 12 months, a result that was significantly confirmed at 15 months in another series of animals (Michel *et al.*, manuscript in preparation). This decline is not an artifact of measurements, as glomeruli showing manifest glomerular tuft retraction or extensive FSGH were not taken into account because glomeru-

lar structures were almost indistinguishable in these cases. It is probably a result of an impairment in the GFR (as shown by the decrease in creatinine clearance and a rise in creatinemia), indirectly provoked by a general alteration of the tubulointerstitial area, a phenomenon observed in progressive renal diseases (reviewed in Reference 21). This hypertrophy of the glomerular tuft might be associated with the genetic character of the Zucker rats or a consequence of hyperlipidemia and the associated events (cytokine and eicosanoid production) (22) rather than being directly induced by a glomerular hyperfunction, as micropuncture experiments indicate that glomerular hemodynamic alterations play little role in the initiation of glomerular injury in this strain of rats (13,23).

Because the interaction between serum lipids, macrophages, and mesangial cell activation must play a key role in the pathogenesis of glomerulosclerosis, we investigated the correlation between hyperlipidemia and trapping of monocytes/macrophages in the mesangial matrix in young Zucker pups. The number of ED₁⁺ macrophages markedly increased in obese pups

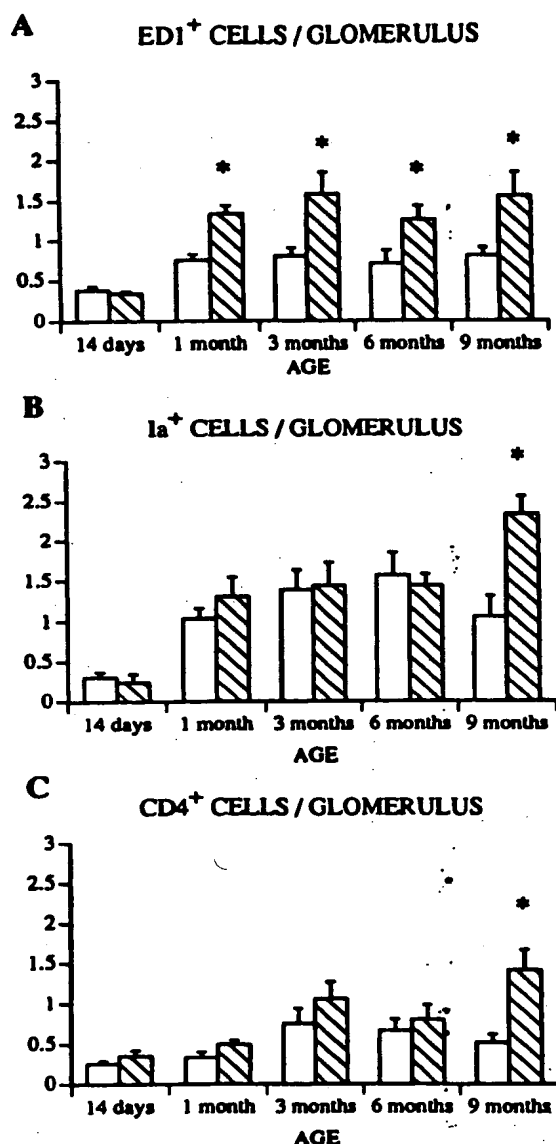


Figure 4. Immunohistochemical detection of ED₁⁺ (monocytes/macrophages), OX₆⁺ (MHC Class II Ia⁺ cells) and W3/25⁺ (T helper CD₄⁺ cells) cells (hatched bars, obese rats; open bars, lean rats). Macrophages (A) invaded the glomeruli of very young obese rats (14 days to 1 month) and their number per glomerulus remained significantly higher in obese than in lean rats (lean versus obese group: $P < 0.001$). In contrast, Ia⁺ cells (B) and CD₄⁺ cells (C) differed significantly in the two experimental groups only at 9 months ($P < 0.05$; $N =$ six rats per group).

in the very first weeks after weaning (Figure 4). This macrophage density remained low in lean rats from 1 to 12 months, and was similar to the value found during true kidney aging in the Wistar (WAG)/Rij model (Lavaud, unpublished observations). These

cells were not glomerular-resident macrophages, as they were not labeled by the ED₂ antibody (24), but our study does not discriminate between the local proliferation of recently recruited monocytes and a continuous influx of circulating cells with age. Although obese rats always had significantly more ED₁⁺ cells than lean rats, this number (close to two cells per glomerulus) remained lower than the densities generally seen in other experimental models of glomerulosclerosis, such as nephrotoxic serum nephritis (25), partial nephrectomy (26), or aminonucleoside nephrosis (27), but are in agreement with those seen by Magil and Fröhlich (28) in obese Zucker rats and Mai *et al.* (29) in hypertension-induced renal injury. It is interesting to note that the use of an antibody which reveals all of the MHC Class II Ia⁺ antigens instead of specific ED₁⁺ monocytes/macrophages did not seem adequate to detect the early inflammatory cells involved in the genesis of glomerulosclerosis in this strain of rat: in younger obese rats, the density of Ia⁺ cells (which was low and similar to the ED₁⁺ cell density) did not differ from that seen in lean littermates (Figure 4B) or in the Wistar/Rij model (Lavaud, unpublished observations). This indicates that other cells (for example, a subset of mesangial cells [30]) probably intervene in the Ia⁺ labeling. The number of Ia⁺ cells was significantly increased in 9-month-old obese rats, as were CD₄⁺ T helper lymphocytes and/or a subpopulation of monocytes/macrophages recognized by W3/25 antibody. This shows that inflammation involving major inflammatory cell types was taking place in the glomeruli in parallel with the development of tubular lesions and interstitial fibrosis seen in aged obese rat kidney.

Lipoproteins and oxidized lipoproteins play a major role in the recruitment and/or activation of macrophages (4). In obese Zucker rats, hyperlipidemia was associated with significant increases in serum very-low-density lipoprotein triglycerides and very-low-density lipoprotein cholesterol, which occurred very early and massively accumulated thereafter (9,11). This study shows that hyperlipidemia (triglyceridemia and cholesterolemia) and glomerular macrophage density are already dramatically greater in 1-month-old obese rats than in their lean littermates. This close relationship between hyperlipidemia and macrophages is in agreement with the observation that lipid-supplemented diets, which induced hyperlipidemia and glomerulosclerosis in some animal models, increase the number of macrophage cells in the early stages of glomerular injury (22). Conversely, diets reducing hyperlipidemia should decrease the number of glomerular macrophages. Kasiske *et al.* (31) succeeded in reducing glomerular injury by feeding rats polyunsaturated diets, but found no decrease in the number of Ia⁺ cells trapped into the mesangium of 9-month-old obese Zucker rats. This could be because of the fact that they did not use the specific ED₁ antibody but a broader-range antibody to detect macrophages.

A mRNA for GAPDH

le ob le ob le ob le ob le ob
1 m 3 m 6 m 9 m 14 m

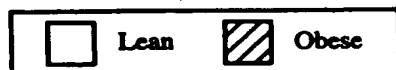
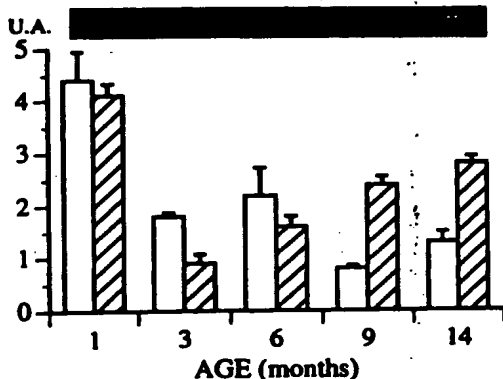
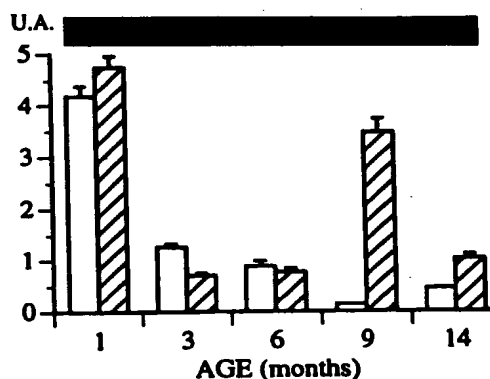
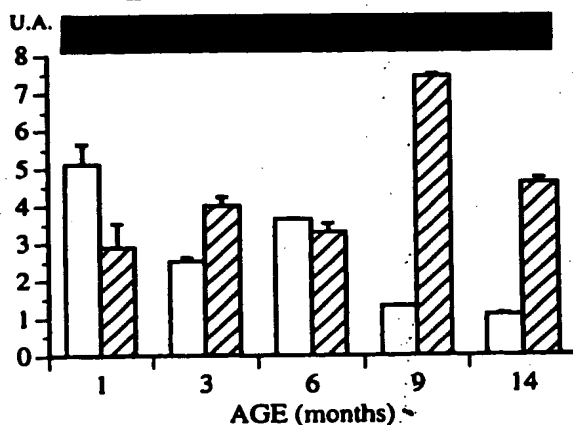
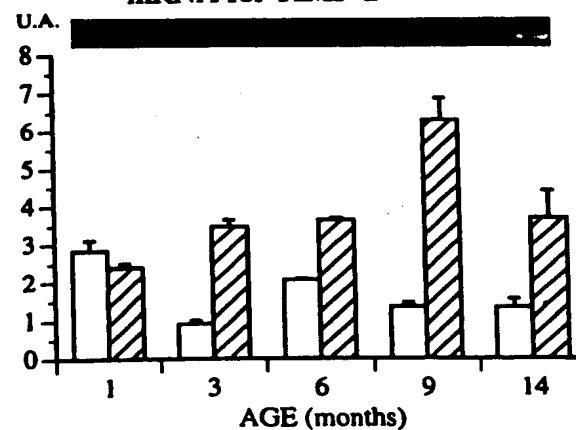
**B** mRNA for α_1 coll IV**C** mRNA for Fibronectin**D** mRNA for α_2 coll I**E** mRNA for TIMP-1**F** mRNA for TIMP-2

Figure 5. Synthesis of messenger RNA for α_1 (IV), α_2 (I) collagens, fibronectin, TIMP-1, and TIMP-2 in isolated, microdissected glomeruli from lean and obese rat kidneys. After an early phase of maturation of the glomeruli, as evidenced by the 1-month values, α_1 (IV) collagen (B) and fibronectin (C) mRNA decreased in lean rats, but increased between 3 and 14 months in obese animals. However, α_2 (I) collagen mRNA were barely detected after 1 month of age and did not change in either the experimental group regardless of the age of the animals, except for a sharp increase in 9-month-old obese rats. TIMP-1 (E) and TIMP-2 (F) mRNA decreased in lean rats to reach low values in 9- and 14-month-old animals, but were still synthesized in obese rats with a peak at 9 months. Glomerular mRNA isolated from three rats were pooled in each age group. Experiments were run in duplicates. The intensities of the cDNA bands for each protein were normalized to the GAPDH band intensities (A).

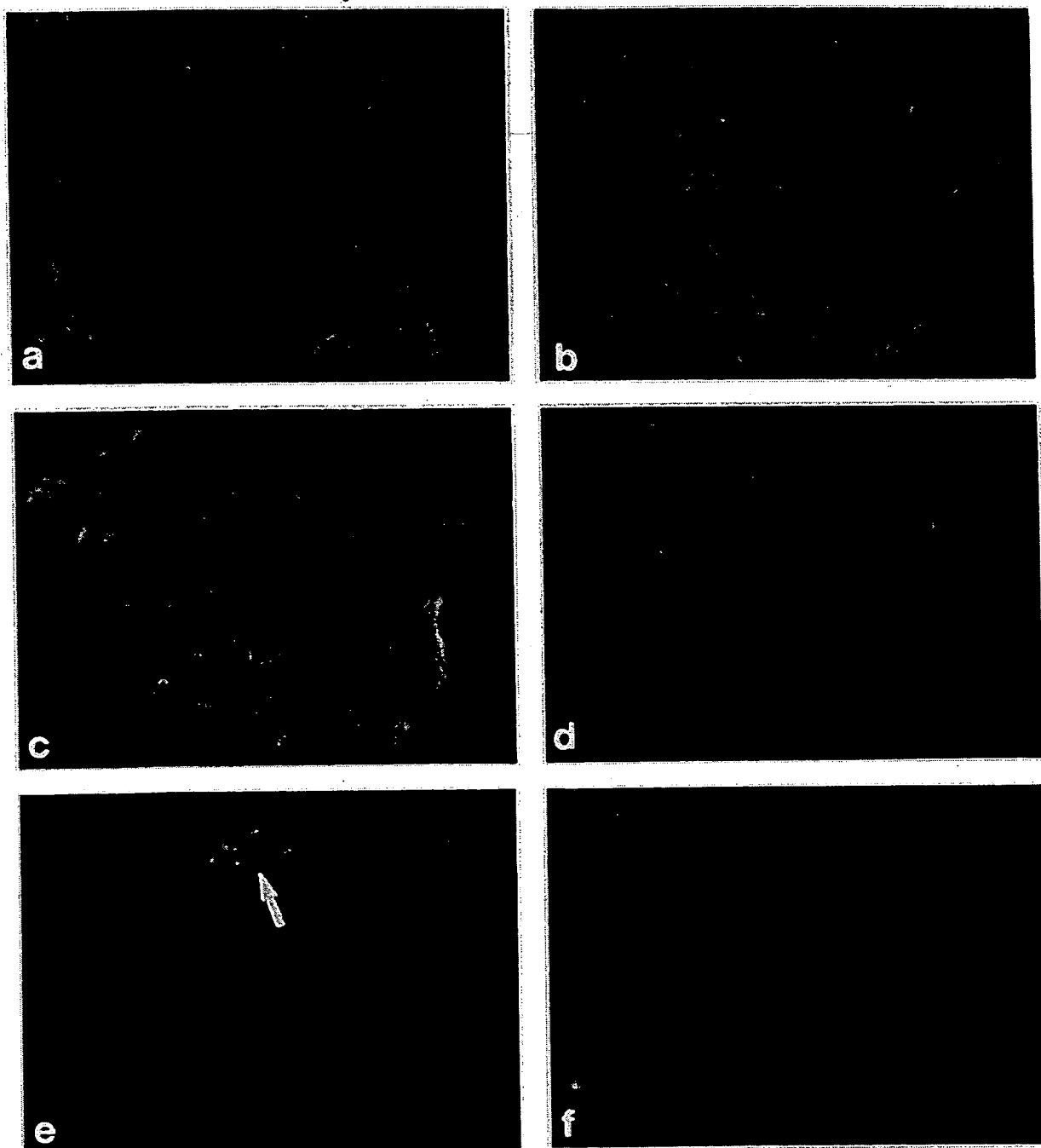


Figure 6. Immunofluorescence detection of Types I, III, and IV collagens in obese (A, C, E, F) and lean (B, D) rat kidneys. With age, Type IV collagen accumulated in obese and lean rat glomeruli, but more in obese than in lean animals (A, B: 3-month-old rats; C, D: 9-month-old rats). Type I collagen was barely seen in 9-month-old obese-rat glomeruli, associated with foci of FSGH lesions (E, arrow). Type III collagen was not detected in any group (F: 9-month-old obese-rat glomerulus). (Original magnification: A through D, $\times 500$; E, $\times 300$; F, $\times 600$).

Activated macrophages can stimulate both mesangial cell proliferation and their synthesis activity via several cytokines and growth factors, as shown by

studies on animal and human mesangial cells in culture (32). Lipoproteins also directly stimulate mesangial cells (33). Although this study provides no

precise information on mesangial cell hyperplasia, it shows that extracellular matrices (GBM and mesangial matrix) largely expand with age in the glomeruli of obese rats. This expansion is associated with a net increase in Type IV collagen and fibronectin (mRNA and proteins) and occurs late after a significant increase in plasma lipids, in parallel with the development of proteinuria and the beginning of kidney-function impairment. This influence of hyperlipidemia and macrophages on the upregulation of fibronectin mRNA was also found in experimental nephrotic syndrome induced by puromycin aminonucleoside (34). The synthesis of fibronectin and $\alpha 1(\text{IV})$ collagen mRNA continued to increase until the rats were 12 months old, whereas the macrophage density did not vary after 3 months. This could indicate that there is an autocrine production of cytokines by mesangial cells in the cascade of events initiated by the lipoproteins and the activation of monocytes/macrophages. This increase in fibronectin and $\alpha 1(\text{IV})$ collagen mRNA could also be the result of hyperinsulinemia, which reached a peak at 3 to 6 months, as insulin seems to be a potent factor in mesangial matrix accumulation *in vitro* (35). We also detected a band corresponding to $\alpha 2(\text{I})$ collagen mRNA and the protein itself in 9-month-old obese rats when FSGH lesions were well established. This is in agreement with the results of Floege *et al.* (36), who found Type I collagen in the remnant kidney model. Type III collagen mRNA and protein remained undetectable, whereas it has been found in a diabetic model (37). As the expansion of ECM components is the result of the balance between synthesis and degradation of the components, we looked for a possible reduction in protein degradation by checking the mRNA for TIMP-1 and TIMP-2, enzymes that specifically inhibit 72-kd metalloproteinase (TIMP-1) and 92-kd gelatinase (TIMP-2). These metalloproteinases are involved in the degradation of the major matrix components, Types IV and V collagens, fibronectin, proteoglycans, elastin, and laminin (38). The synthesis of both TIMP-1 and TIMP-2 mRNA increased in obese animals in parallel. Our results are in agreement with those of Guijarro *et al.* (22), who found increased glomerular TIMP-2 mRNA in a rat model of dietary-induced hypercholesterolemia. This synthesis of TIMP-1 and TIMP-2 mRNA in microdissected glomeruli is probably a result of the glomerular constitutive cells, primarily mesangial cells (39). However, the inhibition of the ECM degradation could also be partly mediated by infiltrating macrophages, as they produce collagenase inhibitors (40).

In summary, we have shown that the glomerular macrophage density is markedly greater in 1-month-old obese Zucker rats than in their lean littermates. This increase parallels the worsening of hyperlipidemia in the obese animals in the very first few days after weaning. Hyperlipidemia associated with hyperinsulinemia develops in preobese pups from 10 days onward (9). Low- and very-low-density lipoproteins are known to activate mesangial cells and to stimulate

the production of chemokines (reviewed in Reference 5). Mesangial cells and endothelial cells also alter low-density lipoproteins to form minimally modified and oxidized low-density lipoproteins, which are cytotoxic for endothelial cells, aggravating the recruitment of macrophages by newly synthesized adhesion molecules and via the production of chemokines (reviewed in Reference 41). The invasion of glomeruli by monocytes/macrophages, which occurs on and after weaning, is probably the result of the increases in lipoproteins at very early ages in these obese Zucker pups. Thus, this study underscores the importance of the Zucker fa/fa rats as an appropriate model for examining the relationship between obesity, early changes in plasma lipids, plasma insulin, glucose intolerance, and the cellular and molecular events involved in the genesis of glomerulosclerosis.

ACKNOWLEDGMENTS

We acknowledge the skillful technical assistance of Mr. Michel Paing in photography. We also thank Dr Srinivas Kaveri (INSERM U430) for helpful discussions during the preparation of the manuscript. Part of this work was supported by Biologie du Vieillessement Grant BV1 94007 from the Délégation à la Recherche Clinique, Assistance Publique, Hôpitaux de Paris. Stéphanie Lavaud and Marie-France Bélaïr are supported by the Claude Bernard Association.

REFERENCES

1. Bariéty J, Chevalier J, Michel O, Nochy D, Callard P. La biopsie rénale dans la hyalinose segmentaire et focale des glomérules. In: D. Droz and B. Lantz, Eds. *La Biopsie Rénale*. Paris: Les Editions INSERM; 1996:109-134.
2. D'Agati V: The many masks of focal segmental glomerulosclerosis. *Kidney Int* 1994;46:1223-1241.
3. Van Goor H, Ding GH, Kees-Folts D, Grond J, Schreiner GF, Diamond JR: Macrophages and renal disease. *Lab Invest* 1994;71:456-464.
4. Wheeler DC, Chana RS: Interactions between lipoproteins, glomerular cells and matrix. *Miner Electrolyte Metab* 1993;19:149-164.
5. Keane WF, Madias NE, Harrington JT, *et al.*: Lipids and the kidney. *Kidney Int* 1994;46:910-920.
6. Kasiske BL, Cleary MP, O'Donnell MP, Keane WF: Effects of genetic obesity on renal structure and function in the Zucker rat. *J Lab Clin Med* 1985;106:598-604.
7. Shimamura T: Relationship of dietary intake to the development of glomerulosclerosis in obese Zucker rats. *Exp Mol Pathol* 1982;36:423-434.
8. Zucker LM: Hereditary obesity in the rat associated with hyperlipemia. *Ann NY Acad Sci* 1965;131:447-458.
9. Krief S, Bazin R: Genetic obesity: Is the defect in the sympathetic nervous system? A review through developmental studies in the preobese Zucker rat. *Proc Soc Exp Biol Med* 1981;168:528-538.
10. Ionescu E, Sauter JF, Jeanrenaud B: Abnormal oral glucose tolerance in genetically obese (fa/fa) rats. *Am J Physiol* 1985;248:E500-E506.
11. Kamanna VS, Kirschenbaum MA: Association between very low density lipoprotein and glomerular injury in obese Zucker rats. *Am J Nephrol* 1993;13:53-58.
12. Schirardin H, Bach A, Schaeffer A, Bauer M, Weryha A: Biological parameters of the blood in the genetically obese Zucker rat. *Arch Int Physiol Biochim* 1979;87:275-289.
13. O'Donnell MP, Kasiske BL, Cleary MP, Keane WF: Effects of genetic obesity on renal structure and function in the Zucker rat. II. Micropuncture studies. *J Lab Clin Med* 1985;106:605-610.
14. Lavau M, Bazin R: Inguinal fat pad weight plotted versus body weight as a method of genotype identification, in 16-day-old Zucker rats. *J Lipid Res* 1982;23:941-943.

15. Heudes D, Michel O, Chevalier J, et al: Effect of chronic ANG-I converting enzyme inhibition on aging processes. I. Kidney structure and function. *Am J Physiol* 1994; 266:R1038-R1051.
16. Dijkstra CD, Döpp EA, Joling P, Kraal G: The heterogeneity of mononuclear phagocytes in lymphoid organs: Distinct macrophage subpopulations in the rat recognized by monoclonal antibodies ED1, ED2 and ED3. *Immunology* 1985;54:589-599.
17. Barclay AN: The localization of populations of lymphocytes defined by monoclonal antibodies in rat lymphoid tissues. *Immunology* 1981;42:593-600.
18. Eddy AA, Crary GS, Michael AF: Identification of lymphohemopoietic cells in the kidneys of normal rats. *Am J Pathol* 1986;124:335-342.
19. Peten EP, Garcia-Perez A, Terada Y, et al: Age-related changes in α -1 and α -2-chain type IV collagen mRNAs in adult mouse glomeruli: Competitive PCR. *Am J Physiol* 1992;263:F951-F957.
20. Mauer SM, Steffes MW, Ellis EN, Sutherland DER, Brown DM, Goetz FC: Structural-functional relationships in diabetic nephropathy. *J Clin Invest* 1984;74: 1143-1155.
21. Burton CJ, Walls J: Proximal tubular cell proteinuria and tubulo-interstitial scarring. *Nephron* 1994;68:287-293.
22. Gujjarro C, Kaslake BL, Kim Y, O'Donnell M, Lee HS, Keane WF: Early glomerular changes in rats with dietary-induced hypercholesterolemia. *Am J Kidney Dis* 1995;26:152-161.
23. Schmitz PG, O'Donnell MP, Kaslake BL, Katz SA, Keane WF: Renal injury in obese Zucker rats: Glomerular hemodynamic alterations and effects of enalapril. *Am J Physiol* 1992;263:F496-F502.
24. Lan HY, Nikolic-Paterson DJ, Mu W, Atkins RC: Local macrophage proliferation in the progression of glomerular and tubulointerstitial injury in rat anti-GBM glomerulonephritis. *Kidney Int* 1995;48:753-760.
25. Baba N, Shimokama T, Watanabe T: Effects of hypercholesterolemia on initial and chronic phases of rat nephrotoxic serum nephritis: Development of focal segmental glomerulosclerosis, analogous to atherosclerosis. *Virchows Arch B Cell Pathol* 1993;64:97-105.
26. Van Goor H, Van der Horst MLC, Fidler V, Grond J: Glomerular macrophage modulation affects mesangial expansion in the rat after renal ablation. *Lab Invest* 1992;66:564-571.
27. Diamond JR, Ding G, Frye J, Pesek-Diamond I: Glomerular macrophages and the mesangial proliferative response in the experimental nephrotic syndrome. *Am J Pathol* 1992;141:887-894.
28. Magli AB, Frohlich JJ: Monocytes and macrophages in focal glomerulosclerosis in Zucker rats. *Nephron* 1991; 59:131-138.
29. Mai M, Gelger H, Hilgers KF, et al: Early interstitial changes in hypertension-induced renal injury. *Hypertension* 1993;22:754-765.
30. Schreiner GF: The mesangial phagocyte and its regulation of contractile cell biology. *J Am Soc Nephrol* 1992; 2:S74-S82.
31. Kasiske BL, O'Donnell MP, Lee H, Kim Y, Keane WF: Impact of dietary fatty acid supplementation on renal injury in obese Zucker rats. *Kidney Int* 1991;39:1125-1134.
32. Cattell V: Macrophages in acute glomerular inflammation. *Kidney Int* 1994;45:945-952.
33. Pai RM, Kirschenbaum MA, Kamanna VS: Low-density lipoprotein stimulates the expression of macrophage colony-stimulating factor in glomerular mesangial cells. *Kidney Int* 1995;48:1254-1262.
34. Ding GH, Pesek-Diamond I, Diamond JR: Cholesterol, macrophages, and gene expression of TGF- β 1 and fibronectin during nephrosis. *Am J Physiol* 1993;264: F577-F584.
35. Abrass CK, Spicer D, Raugi GJ: Induction of nodular sclerosis by insulin in rat mesangial cells in vitro: Studies of collagen. *Kidney Int* 1995;47:25-37.
36. Floege J, Alpers CE, Burns MW, et al: Glomerular cells, extracellular matrix accumulation, and the development of glomerulosclerosis in the remnant kidney model. *Lab Invest* 1992;66:485-497.
37. Abrass CK, Peterson CV, Raugi GJ: Phenotypic expression of collagen types in mesangial matrix of diabetic and non diabetic rats. *Diabetes* 1988;37:1695-1702.
38. Ries C, Petrides PE: Cytokine regulation of matrix metalloproteinase activity and its regulatory dysfunction in disease. *Biol Chem Hoppe-Seyler* 1995;376:345-355.
39. Martin J, Davies M, Thomas G, Lovett DH: Human mesangial cells secrete a GBM-degrading neutral proteinase and a specific inhibitor. *Kidney Int* 1989;36:790-801.
40. Nathan CF: Secretory product of macrophages. *J Clin Invest* 1987;79:319-326.
41. Demuth K, Myara I, Moatti N: Biologie de la cellule endothéliale et athérogenèse. *Ann Biol Clin* 1995;53: 171-189.

Adhesion Molecules Expression in Noncrescentic Acute Post-Streptococcal Glomerulonephritis¹

Maria Pia Rastaldi,² Franco Ferrario, Lin Yang, Stefania Tunesi, Antonio Indaco, Hequn Zou, and Giuseppe D'Amico

M.P. Rastaldi, F. Ferrario, L. Yang, S. Tunesi, A. Indaco, H. Zou, G. D'Amico, Renal Immunopathology Center, Division of Nephrology, San Carlo Borromeo Hospital, Milan, Italy

(J. Am. Soc. Nephrol. 1996; 7:2419-2427)

ABSTRACT

Clinicopathological features of 11 cases of non-crescentic acute post-streptococcal glomerulonephritis (APSGN) were reviewed. Intraglomerular and interstitial leukocytes and their possible correlation with the adhesion molecules intercellular adhesion molecule-1 (ICAM-1), vascular cell adhesion molecule-1 (VCAM-1), and endothelial leukocyte adhesion molecule-1 (ELAM-1/E-selectin) were investigated by an immunohistochemical method. Intraglomerular leukocytes were primarily granulocytes (11.4 ± 10 cells/glomerular cross-section) and monocytes-macrophages (13.4 ± 19.4 cells/glomerular cross-section). The granulocytes outnumbered monocytes-macrophages in 7 of 11 specimens. The number of intraglomerular leukocytes correlated with proteinuria at the time of renal biopsy. Intraglomerular ICAM-1 staining was strongly positive in all biopsies, especially when intraglomerular monocytes-macrophages prevailed. Expression of intraglomerular VCAM-1 and E-selectin in diseased kidneys did not differ from that in normal kidneys. Interstitial leukocytes were primarily monocytes-macrophages (158.9 ± 96.8 cells/mm²) and T lymphocytes (102.2 ± 63.9 cells/mm²). The number of interstitial leukocytes, especially monocytes-macrophages, correlated with serum creatinine level at the time of biopsy. Interstitial ICAM-1 staining was strongly positive on tubules, peritubular capillaries, and small vessels. The tubular positivity for ICAM-1 correlated with the number of interstitial monocytes-macrophages. Interstitial VCAM-1 and E-selectin were expressed as in normal kidney tissues. The data from this study demonstrate that APSGN is characterized by the presence of both intraglomerular and interstitial leukocyte infiltration, corre-

lating respectively with proteinuria and serum creatinine at the time of renal biopsy. Among the adhesion molecules studied, ICAM-1 seems the most involved in leukocyte recruitment, especially in that of monocytes-macrophages.

Key Words: Leukocyte infiltration, ICAM-1, VCAM-1, E-selectin, acute post-streptococcal glomerulonephritis

Acute post-streptococcal glomerulonephritis (APSGN) is histologically characterized by the presence of enlarged glomeruli containing an increased number of cells. The hypercellularity results from the proliferation of resident cells and from leukocyte infiltration (1,2). Polymorphonuclear leukocytes are the most easily identified cells and may be present in large numbers, but monocytes-macrophages have also been detected in both human and experimental models of the disease (1-3). In human studies using histochemical methods and electron microscopy, a high number of intraglomerular monocytes was found, especially in the early acute stage of the disease (4,5). In experimental serum sickness models, Sano (6) and Striker *et al.* (7) showed that much of the glomerular hypercellularity resulted from monocytes. In recent immunohistochemical studies, a few intraglomerular T lymphocytes were also found (8,9). Besides the acute glomerular involvement, an interstitial leukocyte infiltration, ranging from mild to severe, was also frequently described (1,2).

In recent years, it has become evident from many experimental and *in vivo* studies that adhesion molecules play a key role in inflammatory and immune responses (10-13). Intercellular adhesion molecule-1 (ICAM-1) and vascular cell adhesion molecule-1 (VCAM-1) are constitutionally expressed on many different cell types, where they can be upregulated by cytokines and other mediators of inflammation (14,15). It is well known that the major ligand of ICAM-1, the β_2 -integrin LFA-1, is present on all leukocytes, whereas the ligand of VCAM-1, the β_1 -integrin VLA-4, is absent on neutrophils and present on lymphocytes and monocytes (16-20). The binding between VCAM-1 and VLA-4 is considered a preferential way of monocyte adhesion (21-23). Recent experimental studies (24-26) have shown that E-selectin (ELAM-1) expression is restricted to cytokine-stimulated endothelium, is prominent in acute inflammatory lesions, and correlates with the large influx of neutrophils.

We reviewed the clinicopathological features in 11 patients with APSGN to study (using an immunohistochemical method) intraglomerular and interstitial

¹ Received February 9, 1996. Accepted May 9, 1996.

² Correspondence to Dr. M.P. Rastaldi, Division of Nephrology, San Carlo Borromeo Hospital, Via Pio II, 3, 20153 Milano, Italy.

1046-6673/97/11-2419\$03.00/0

Journal of the American Society of Nephrology
Copyright © 1996 by the American Society of Nephrology

infiltrating cells and their possible correlation with the expression of the adhesion molecules ICAM-1, VCAM-1, and E-selectin.

METHODS

Patients

Eleven patients (6 men and 5 women) with a mean age of 30.9 yr (range, 10 to 67), showing clinical and histological evidence of nonrescendent APSGN, were studied.

At the time of admission to our hospital, all patients showed increased antistreptolysin O (normal value < 200 IU/mL) titers (ranging from 250 to 800 IU/mL) and decreased C3 serum levels. In seven patients, a decreased serum C4 level was also present.

The interval time between streptococcal infection (a pharyngo-tonsillitis infection in all patients) and the onset of nephropathy ranged from 7 to 22 days (mean value (m.v.), 14.18 ± 5.34 days). The renal onset was an acute nephritic syndrome in seven patients, a nephrotic syndrome in one patient, and macroscopic hematuria in three patients. The mean prebiopsy follow-up period was 28.2 days (range, 7 to 75 days).

Serum creatinine concentration at the time of renal biopsy (RB) ranged from 61.8 to 866.3 $\mu\text{mol/L}$ (m.v., 274.0 ± 290.5 $\mu\text{mol/L}$) and proteinuria from 0.1 to 11.7 g per day (m.v., 3.16 ± 3.49).

Kidney Tissue

Kidney tissue was obtained from all patients and, for comparison, from five cadaveric kidneys that could not be grafted because of vascular abnormalities. Tissue samples for light microscopy were fixed in Bouin's fluid, embedded in paraffin, and stained according to standard techniques. For immunofluorescence and immunoperoxidase staining, the unfixed renal tissue was embedded in OCT compound (Miles Scientific, Naperville, IL), snap-frozen in a mixture of isopentane and dry ice, and stored at -80°C . Subsequently, 5- μ sections were placed on slides and stored at -20°C until they were immunostained.

Immunoperoxidase Labeling

We used an avidin-biotin technique, in which a biotinylated secondary antibody reacts with several peroxidase-conjugated streptavidin molecules. In brief, after incubation with 0.5% avidin (Sigma Chimica, Gallarate, Milan, Italy) and 0.01% biotin (Sigma) to suppress endogenous avidin-binding activity, tissue sections were incubated with the primary antibody. We used the following monoclonal antibodies: CD45 (monoclonal mouse anti-human leukocyte common antigen; Immunotech, Marseille Cedex, France), CD3 (monoclonal rabbit anti-human T-lymphocyte; Dako, Glostrup, Denmark), CD68 (monoclonal mouse anti-human monocyte-macrophage; Dako), CD15 (monoclonal mouse anti-human granulocyte; Dako), CD19 (monoclonal mouse anti-human B-lymphocyte; Dako), CD54 (monoclonal mouse anti-human ICAM-1; Serotec, Kidlington, Oxford, England), CD106 (monoclonal mouse anti-human VCAM-1; Serotec), CD62E (monoclonal mouse anti-human E-selectin; Serotec).

After being washed, the sections were sequentially fixed in a methanol- H_2O_2 solution (to block endogenous peroxidase) and incubated with the secondary biotinylated antibody (Dako) and with the peroxidase-labeled streptavidin (Dako). Peroxidase activity was detected with 3,5-diaminobenzidine (DAB, Dako), then sections were counterstained with Harry's

hematoxylin (BDH, Poole, England), dehydrated, and mounted in Entellan (Merck, Darmstadt, Germany).

Specificity of labeling was demonstrated by the lack of staining after substitution of phosphate-buffered saline for the primary antibody.

Quantitative Evaluation

All peroxidase-stained sections had five or more glomeruli and were evaluated by two independent observers who were blinded to any histological or clinical information. Minor differences were subsequently resolved by conference.

Immunohistological reaction intensity and/or quantity was evaluated separately for glomeruli, tubuli, vessels, and interstitium. Intraglomerular infiltrating cells were expressed as number of cells per glomerular cross section (gcs).

The interstitial labeled cells were counted using an eyepiece graticule (Leitz, Periplan 6F 12.5 \times MF mounted in a Leitz-Dialux 20 microscope; Leitz-Wetzlar, Germany) in ten consecutive fields, avoiding glomeruli and large vessels; the results were expressed as number of positive cells per square millimeter.

Results were evaluated using the mean and the standard deviation of the mean.

Intraglomerular, tubular, and vessel staining of adhesion molecules were scored semiquantitatively on a four-point scale: no staining, 0; focal staining, 1; diffuse staining, 2; massive staining, 3. Tubular staining was scored in ten consecutive fields per biopsy. Means and standard deviations of the scores were calculated.

Statistical significances ($P < 0.05$) were analyzed using *t* test and regression test.

RESULTS

Histological Features

By light microscopy, we found the presence of endocapillary proliferation and intraglomerular leukocyte infiltration of variable degrees, ranging from mild to intense. Extracapillary proliferation was absent in all cases. Subepithelial deposits (humps) were seen by light microscopy in ten biopsies. In eight cases, interstitial infiltration was also evident, ranging from mild to severe.

Immunofluorescence was typically positive for C3, with a granular "starry sky" pattern.

Electron microscopy was performed in five cases, confirming the intraglomerular leukocyte infiltration and the presence of subepithelial deposits (humps).

Immunohistochemical Features

Intraglomerular infiltration and adhesion molecule expression. The results are shown in Table 1.

Intraglomerular infiltration ranged from 7.9 to 70 cells/gcs (m.v., 23.8 ± 21 CD45+ cells/gcs). These cells were primarily monocytes-macrophages (m.v., 13.4 ± 19.4 CD68+ cells/gsc) and granulocytes (m.v., 11.4 ± 10 CD15+ cells/gsc) with less evidence of T lymphocytes (m.v., 1.9 ± 1.4 CD3+ cells/gcs) (Figure 1). No B lymphocytes were found. In seven cases, the granulocytes were prevalent, whereas in four cases (Table 1: PT 8 through 11), monocytes-macrophages outnumbered granulocytes. The number of intraglo-

TABLE 1. Intraglomerular infiltration and adhesion molecule expression^a

PT	CD45	CD3	CD68	CD15	CD19	CD54	CD106	CD62E
1	1.9	0.8	0.9	1.3	0	1	0	0
2	3.4	0.9	1.3	2.3	0	1	0	0
3	5.7	1.3	2.1	2.7	0	1	0	0
4	20	0.8	3.1	19.1	0	1	0	0
5	37.6	5.5	13.1	18.3	0	1	0	0
6	31.3	1.3	16.3	26.8	0	1	0	0
7	36.3	2.7	2.6	29.6	0	1	0	0
8	10.3	2.6	6.3	1	0	2	0	0
9	7.6	2	7.5	3	0	2	0	0
10	37.8	1	27.6	14.1	0	3	0	0
11	70	2.4	66.4	7.4	0	3	0	0
m.v. \pm SD	23.8 \pm 21	1.9 \pm 1.4	13.4 \pm 19.4	11.4 \pm 10.7				

^a PT, patient; m.v., mean value; SD, standard deviation.

merular leukocytes correlated with the degree of urinary proteins at RB (Figure 2).

Although a positive trend between the number of intraglomerular leukocytes and the prebiopsy follow-up was present, we did not find a statistical significance between these parameters even when the interval between onset of streptococcal infection and biopsy was considered.

Glomerular ICAM-1 staining, which in normal kidneys was present only on the endothelium, appeared stronger and more diffuse in all diseased kidneys. The four cases with a prevalent monocyte-macrophage infiltration demonstrated the most diffuse and intense ICAM-1 positivity (Figure 3). Furthermore, ICAM-1 did not correlate with glomerular nephritis duration. Glomerular VCAM-1 only lined the Bowman's capsule, as it also appeared in the normal kidneys, and was occasionally positive on scattered cells. Glomerular E-selectin was always negative, as in normal tissues.

Interstitial infiltration and adhesion molecule expression. The presence of a diffuse interstitial infiltration (Table 2, Figure 4), ranging from mild to intense (m.v., 245.6 ± 137.9 CD45+ cells/mm²), was found with immunohistochemical evaluation in all biopsies, characterized by monocytes-macrophages (m.v., 158.9 ± 96.8 CD68+ cells/mm²) and T lymphocytes (m.v., 102.2 ± 63.9 CD3+ cells/mm²). The number of interstitial granulocytes was low (m.v., 15.7 ± 14.6 CD15+ cells/mm²).

Although only two patients showed high serum creatinine levels, we found a significant correlation between the number of interstitial leukocytes, primarily monocytes-macrophages, and serum creatinine level at RB (Figure 5). Some infiltrating cells were also positive for ICAM-1 (m.v., 82.7 ± 59.1), VCAM-1 (m.v., 33.6 ± 25.4), and E-selectin (m.v., 4.6 ± 9.5) (Table 2).

Tubules and vessels. In normal kidneys, interstitial E-selectin was negative and tubular epithelial cells had no ICAM-1, although some tubules were positive for VCAM-1. Some capillaries expressed both ICAM-1 and VCAM-1, the latter also being positive on some small vessels.

In APSGN biopsies, ICAM-1 showed an intense positivity involving all the interstitial components: tubules, peritubular capillaries, and small vessels (Figure 6).

Interstitial VCAM-1 did not significantly differ from normal kidneys and E-selectin was positive only rarely on interstitial capillaries.

We found a significant correlation between ICAM-1 tubular expression and the CD68 interstitial infiltration (Figure 7).

DISCUSSION

The primary histological feature in APSGN is the presence of a diffuse and global glomerular hypercellularity, resulting from proliferation of resident cells and leukocyte infiltration (1,2). In agreement with previous human immunohistochemical studies (8,9), our data showed that intraglomerular leukocytes were primarily granulocytes and monocytes-macrophages. In particular, monocytes-macrophages outnumbered granulocytes in four cases. There were few T lymphocytes, and no B lymphocytes were found.

In experimental serum sickness models, Sano (6) and Striker *et al.* (7) found that much of the glomerular hypercellularity resulted from monocytes, and Hunsicker *et al.* (27) found that the peak proteinuria coincided with the time of intraglomerular monocyte accumulation. In our cases, also confirming previous results obtained by our group, the number of intraglomerular leukocytes correlated with urinary proteins at RB (4) and not with serum creatinine levels (28), suggesting that the acute glomerular involvement is responsible more for protein losses than for the impairment of renal function.

The mechanism of acute and transient intraglomerular leukocyte accumulation in APSGN is still not well known. In recent years, it has become more and more clear that adhesion molecules are essential for leukocyte entry to the tissue (10-13). Most authors (12,26,29-31) agree that leukocyte adhesion to the endothelium may be schematically divided into two

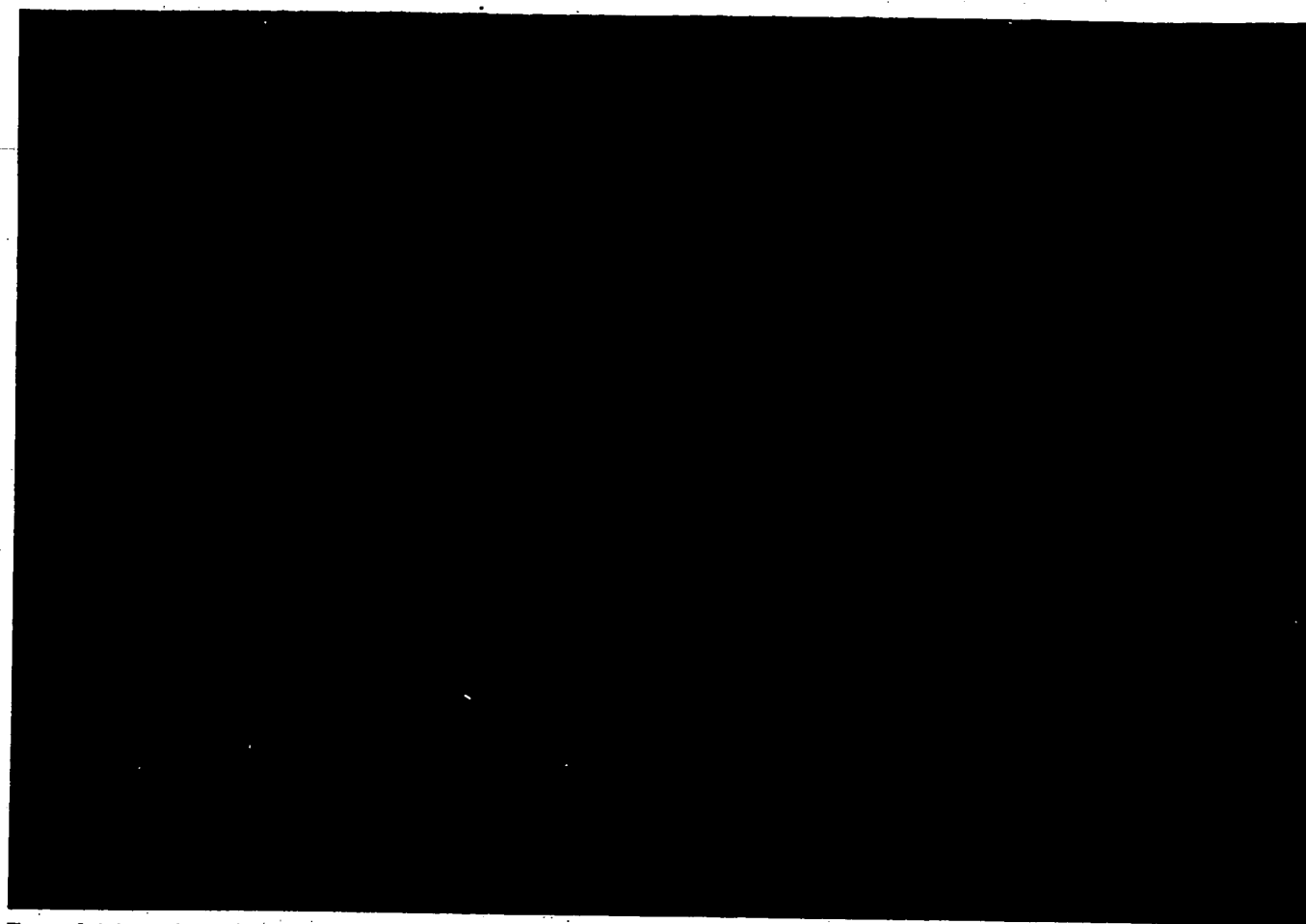


Figure 1. Intense intraglomerular leukocyte infiltration (a) primarily resulting from granulocytes (b) and macrophages (c). There are few intraglomerular T lymphocytes (d). (Immunoperoxidase stain; original magnification: a-c, $\times 10$; d, $\times 20$).

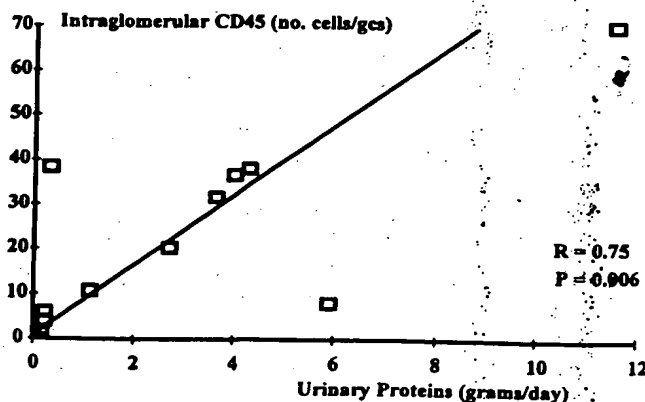


Figure 2. Correlation between intraglomerular leukocytes and urinary proteins at the time of renal biopsy. gcs, glomerular cross-section.

steps: first, the interaction between selectins (as E-selectin) and their carbohydrate ligands induces leukocytes to roll onto endothelium. The second step is characterized by the interaction between leukocyte integrins and endothelial immunoglobulin (Ig)-like molecules (as ICAM-1 and VCAM-1), and produces the immobilization that precedes diapedesis. ICAM-1 and VCAM-1 are constitutively expressed on many different cell types, where they can be upregulated by cytokines and other mediators of inflammation (14,15). It is well known that the major ligand of ICAM-1, the β_2 -integrin LFA-1, is present on all leukocytes, whereas the ligand of VCAM-1, the β_1 -integrin VLA-4, is absent on neutrophils and present on lymphocytes and monocytes (16-20).

In normal glomeruli, we found, as have many other authors (32-34), a constitutive expression of ICAM-1 on endothelial cells, whereas VCAM-1 was present on Bowman's capsule and E-selectin was negative. All of our cases with noncrescentic APSGN showed an in-

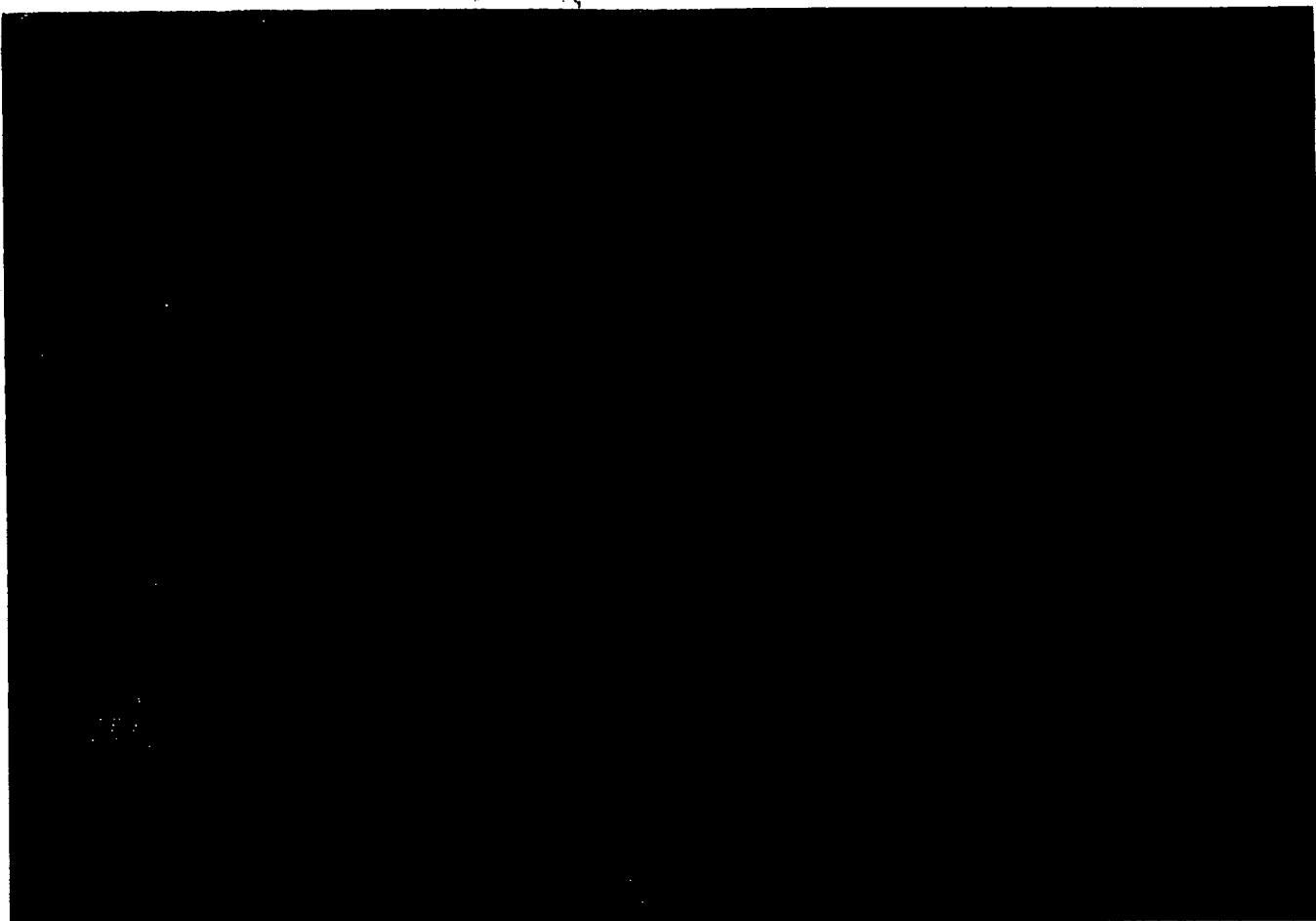


Figure 3. Intraglomerular adhesion molecule expression. (a, b) Evident endothelial and mesangial ICAM-1 positivity characterized by variable intensity. (c, d) VCAM-1 and ELAM-1 expression are not different from normal tissue. (Immunoperoxidase stain; original magnification, $\times 20$).

TABLE 2. Interstitial Infiltration

Monoclonal Antibodies	Normal Tissue (no. of cells/mm ² (m.v. \pm SD))	APSGN Biopsies (no. of cells/mm ² (m.v. \pm SD))	P Value
CD45	72.1 \pm 53.8	245.6 \pm 137.9	0.001
CD3	26.5 \pm 23.3	102.2 \pm 63.9	0.001
CD68	44.1 \pm 32.9	158.9 \pm 96.8	0.001
CD15	0.9 \pm 1.52	15.7 \pm 14.6	0.003
CD54	2.2 \pm 1.5	82.7 \pm 59.1	0.0005
CD106	2.8 \pm 1.4	33.6 \pm 25.4	0.001
CD62E	0	4.6 \pm 9.5	0.08

creased intraglomerular ICAM-1 expression, with a particular intensity in the four cases in which monocytes-macrophages outnumbered granulocytes. An increased expression of intraglomerular ICAM-1 that significantly correlated with the number of glomerular monocytes-macrophages was recently found in APSGN by Parra *et al.* (35), suggesting that in APSGN, ICAM-1

is primarily involved in the glomerular monocyte-macrophage infiltration.

VCAM-1, through the interaction with its ligand VLA-4, is thought to be a preferential way of monocyte recruitment (21–23). Nevertheless, in our specimens, VCAM-1 was almost negative in the glomerular tufts, as it also appears in the normal kidney.

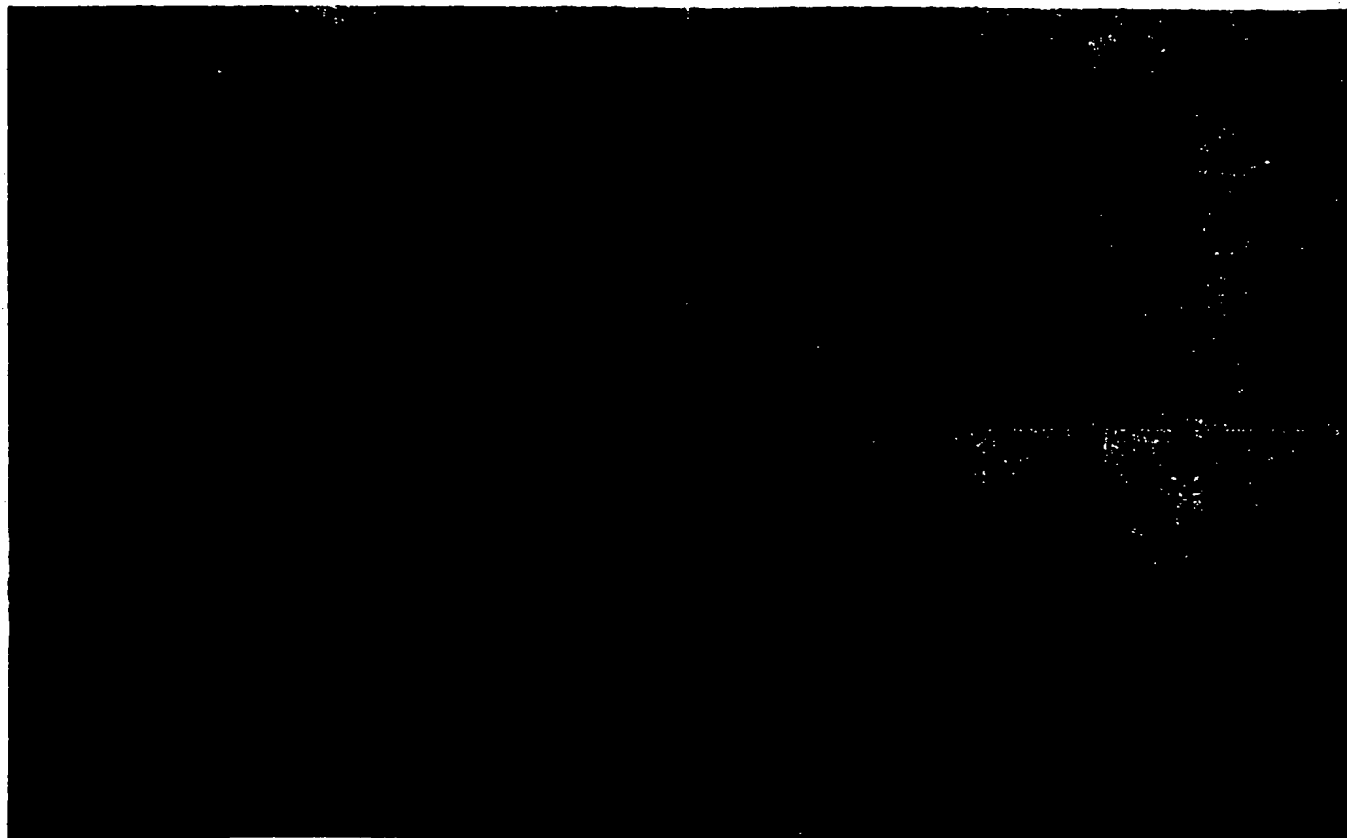


Figure 4. Intense and diffuse interstitial leukocyte infiltration (a) resulting from macrophages (b) and T lymphocytes (c). A low number of interstitial granulocytes was present (d). (Immunoperoxidase stain; original magnification: a-c, $\times 10$; d, $\times 20$).

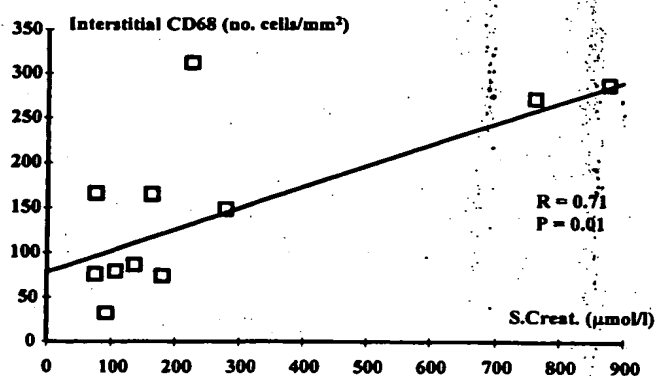


Figure 5. Correlation between interstitial macrophages and serum creatinine (S.Creat.) level at renal biopsy.

In a previous study on renal vasculitis (36) and in 18 cases of IgAGN showing necrotizing-extracapillary lesions (data not published), our group has found an intense positivity of VCAM-1, strictly corresponding to the areas of necrotizing-extracapillary damage with evident monocyte-macrophage accumulation. With a double-staining procedure, we identified the parietal

epithelial cells positive for VCAM-1 in the crescents, whereas in the necrotic areas it was quite impossible to determine exactly what type of cell was positive. Furthermore, in our experience, VCAM-1 was negative in the tuft of 21 cases of cryoglobulinemic glomerular nephritis, characterized by a massive monocyte infiltration but the absence of extracapillary proliferation. Therefore, all of our data seem to confirm the hypothesis that intraglomerular VCAM-1 might be particularly involved in the monocyte recruitment in necrotizing-extracapillary damage. Obviously, when using only immunohistochemistry, we can hypothesize but not demonstrate that VCAM-1 glomerular positivity is linked to a different mechanism of monocyte recruitment.

Recent experimental studies have shown that E-selectin is absent on normal endothelium before cytokine stimulation (24,25). Its expression, although also involved in chronic inflammation (37,38), is prominent in acute inflammatory lesions and correlates with the large influx of neutrophils (25, 26). On the other hand, it has been found that the cytoplasmic domain of E-selectin contains tyrosin residues that have been suggested to mediate the internalization of

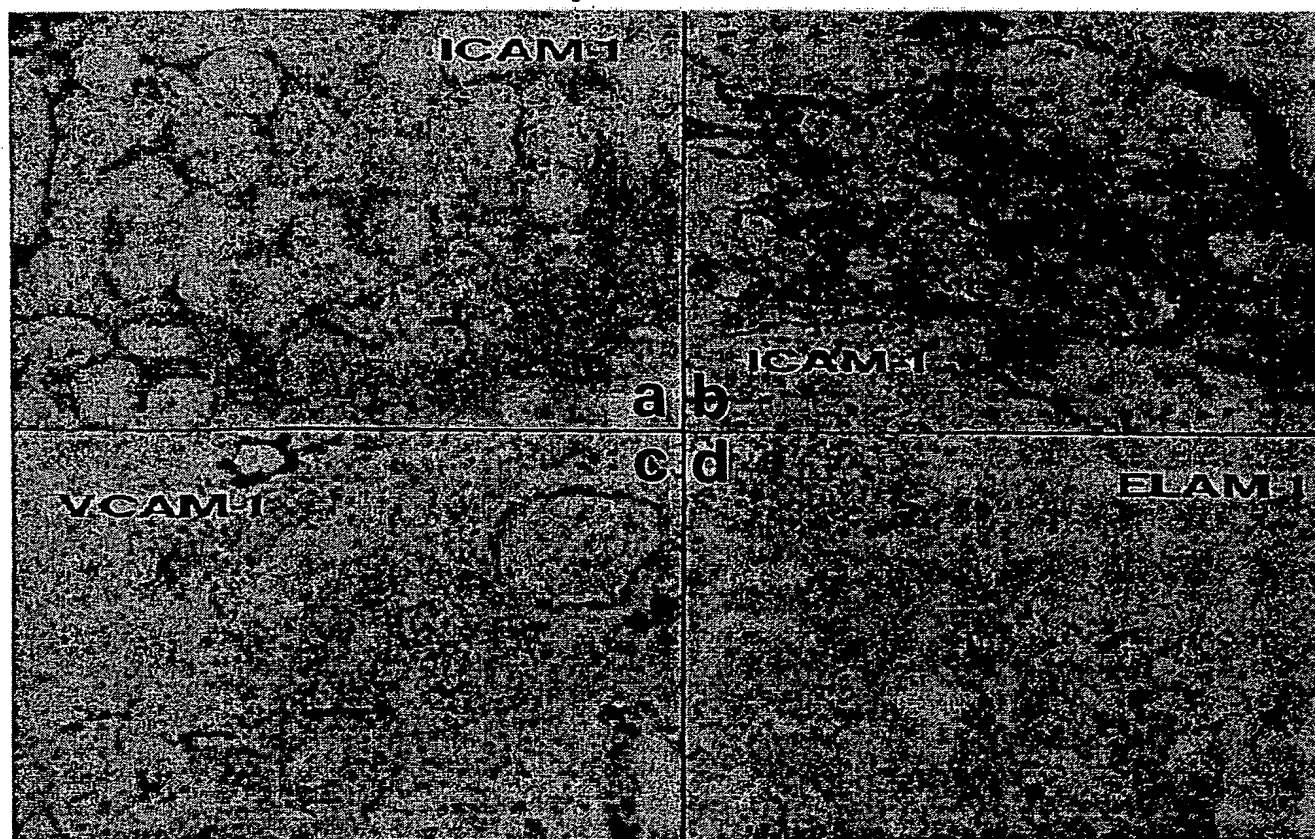


Figure 6. Intense and diffuse ICAM-1 positivity (a, b) involving all of the interstitial components. Interstitial VCAM-1 (c) does not significantly differ from normal kidneys. ELAM-1 (d) is positive only rarely on interstitial small vessels. (Immunoperoxidase stain; original magnification: a, c, d, $\times 10$; b, $\times 20$).

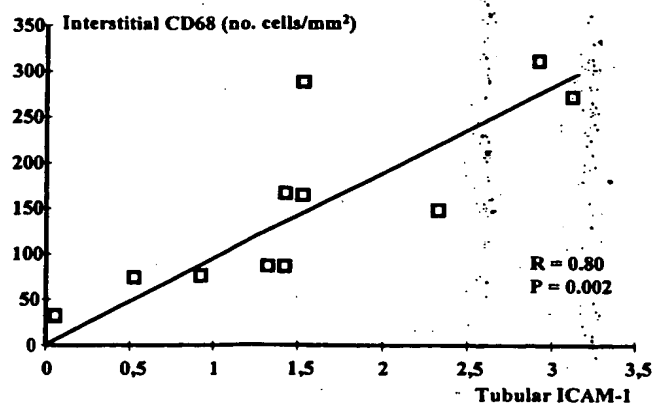


Figure 7. Correlation between interstitial macrophages and tubular ICAM-1 expression.

other transmembrane domains (39). This may account for the short half-life of E-selectin at the cell surface (12,40), and may also explain the complete intraglomerular negativity that we found in APSGN.

Many authors have described in APSGN the presence of diffuse interstitial infiltration ranging from mild to severe, and sometimes associated with focal accumulation of mononuclear leukocytes and polymorphonucleates (1,2). By light microscopy, we found interstitial infiltrations of varying degrees in eight patients. With immunohistochemistry, all cases showed a diffuse interstitial infiltration primarily composed by monocytes-macrophages and T lymphocytes. A few granulocytes were also present. The number of interstitial infiltrating cells significantly differed from those found in normal kidneys.

The greater sensitivity of immunohistochemistry to detect infiltrating leukocytes was also underlined by Alexopoulos *et al.* in membranous glomerulonephritis (41), and, in our opinion, confirms the benefits of routine use of monoclonal antibodies on renal biopsies to more precisely determine quantity and quality of interstitial leukocyte infiltration.

In 1977, Bohle *et al.* (42), using morphometric analysis, discovered for the first time a correlation between serum creatinine levels and the increase in interstitial volume in acute endocapillary glomerulo-

nephritis, and explained the correlation on the basis of a reduction of RBF brought about by compression of the postglomerular vasculature.

In our patients, we could not find any correlation between the presence of interstitial edema and the degree of renal failure. Moreover, it is well known that in both primary and secondary glomerular nephritis, the intensity of interstitial infiltration better correlates with the impairment of GFR than do glomerular lesions (43-45).

In our cases, taking into account that a very high serum creatinine level was present in only two patients, a significant correlation between interstitial infiltration, and in particular of monocytes-macrophages, and serum creatinine level at RB was found. Therefore, also considering the absence of correlation between intraglomerular infiltration and serum creatinine level, our data might suggest that the interstitial inflammation may also be responsible for the functional damage in acute processes.

In our specimens, we also found some cells expressing adhesion molecules, primarily ICAM-1 and VCAM-1. The presence of adhesion molecules on leukocyte surface was suggested by Brady *et al.* (46) to be important in cell-cell and cell-matrix interactions to promote transcellular biosynthesis of lipoxigenase products, therefore enhancing the inflammatory process.

In the interstitium of our patients, we found ICAM-1 to be strongly expressed, and to involve tubules, peritubular capillaries, and small vessels. Moreover, the tubular ICAM-1 expression significantly correlated with the interstitial monocyte-macrophage number, further suggesting that ICAM-1 in nonrescued APSGN is especially involved in acute monocyte recruitment. In effect, interstitial VCAM-1 and E-selectin did not show substantial differences from normal kidneys.

In conclusion, our data demonstrate that APSGN is characterized by the presence of both intraglomerular and interstitial leukocyte infiltration that respectively correlate with proteinuria and serum creatinine at RB. Among the adhesion molecules studied, ICAM-1 seems to be the most involved in recruitment of both intraglomerular and interstitial leukocytes, especially of monocytes.

REFERENCES

1. Silva FG. Acute postinfectious glomerulonephritis and glomerulonephritis complicating persistent bacterial infection. In: Heptinstall RH, ed. *Pathology of the Kidney*, 4th ed. Boston: Little, Brown; 1992:297-388.
2. Rodriguez-Iturbe B. Poststreptococcal glomerulonephritis. In: Massry SG, Glasscock RJ, eds. *Textbook of Nephrology*, 3rd ed. Baltimore: Williams & Wilkins; 1995: 698-703.
3. Holdsworth SR, Neale TJ, Wilson CB: The participation of macrophages and monocytes in experimental immune complexes glomerulonephritis. *Clin Immunol Immunopathol* 1980;15:510-524.
4. Ferrario F, Castiglione A, Colasanti G, Barbiano di Belgioioso G, Bertoli S, D'Amico G: The detection of monocytes in human glomerulonephritis. *Kidney Int* 1985;28:513-519.
5. Monga G, Mazzucco G, Barbiano di Belgioioso G, Busnach G: Monocyte infiltration and glomerular hypercellularity in human acute and persistent glomerulonephritis. Light and electron microscopic, immunofluorescence and histochemical investigation on twenty-eight cases. *Lab Invest* 1981;44:381-387.
6. Sano M: Participation of monocytes in glomerulonephritis in acute serum sickness of rabbit. *Acta Pathol Jpn* 1976;26:423-427.
7. Striker GE, Mannick M, Tung MY: Role of marrow-derived monocytes and mesangial cells in removal of immune complexes from renal glomeruli. *J Exp Med* 1979;149:127-132.
8. Parra G, Platt JL, Falk RJ, Rodriguez-Iturbe B, Michael AF: Cell populations and membrane attack complex in glomeruli of patients with post-streptococcal glomerulonephritis. Identification using monoclonal antibodies by indirect immunofluorescence. *Clin Immunol Immunopathol* 1984;33:324-332.
9. Cameron JS, Nolasco F, Hartley B: Glomerular T-cells and macrophages in crescentic and non-crescentic proliferative glomerulonephritis [Abstract]. *Kidney Int* 1986; 29:267A.
10. Springer TA: Adhesion receptors of the immune system. *Nature (Lond)* 1990;46:425-434.
11. Lasky LA: Selectins: Interpreters of cell-specific carbohydrate information during inflammation. *Science* 1992; 258:964-969.
12. Carlos TM, Harlan JM: Leukocyte-endothelial adhesion molecules. *Blood* 1994;84:2068-2101.
13. Dal Canton A: Adhesion molecules in renal disease. *Kidney Int* 1995;48:1687-1696.
14. Rothlein R, Czajkowski M, O'Neill MM, Marlin SD, Mainolfi E, Merluzzi VJ: Induction of intercellular adhesion molecule-1 on primary and continuous cell lines by pro-inflammatory cytokines. *J Immunol* 1988;141: 1665-1669.
15. Carlos T, Kovach N, Schwartz B, et al.: Human monocytes bind to two cytokine-induced adhesive ligands on cultured human endothelial cells: Endothelial leukocyte adhesion molecule-1 and vascular cell adhesion molecule-1. *Blood* 1991;77:2266-2271.
16. Rothlein R, Dustin ML, Marlin SD, Springer TA: A human intercellular adhesion molecule (ICAM-1) distinct from LFA-1. *J Immunol* 1986;137:1270-1274.
17. Marlin SD, Springer TA: Purified intercellular adhesion molecule-1 (ICAM-1) is a ligand for lymphocyte function-associated antigen 1 (LFA-1). *Cell* 1987;51:813-819.
18. Osborn L, Hession C, Tizard R, et al.: Direct expression cloning of vascular cell adhesion molecule-1 (VCAM-1), a cytokine-induced endothelial protein that binds to lymphocytes. *Cell* 1989;59:1203-1211.
19. Rice GE, Munro JM, Bevilacqua MP: Inducible cell adhesion molecule 110 (ICAM-110) is an endothelial receptor for lymphocytes. *J Exp Med* 1990;171:1369-1374.
20. Wuthrich RP: Intercellular adhesion molecules and vascular cell adhesion molecule-1 and the kidney. *J Am Soc Nephrol* 1992;3:1201-1211.
21. Butcher EC: Leukocyte-endothelial cell recognition: Three (or more) steps to specificity and diversity. *Cell* 1991;67:1033-1036.
22. Cattell V: Macrophages in acute glomerular inflammation. *Kidney Int* 1994;45:945-952.
23. Bruijn JA, De Heer E: Adhesion molecules in renal diseases. *Lab Invest* 1995;72:387-394.
24. Bevilacqua MP, Pober JS, Mendrick DL, Cotran RS, Gimbrone MA: Identification of an inducible endothelial-leukocyte adhesion molecule, E-LAM 1. *Proc Natl Acad Sci USA* 1987;84:9238-9242.
25. Munro JM, Pober JS, Cotran RS: Recruitment of neutrophils in the local endotoxin response: Association with de novo endothelial expression of endothelial leukocyte adhesion molecule-1. *Lab Invest* 1991;64:295-298.
26. Kishimoto TK, Rothlein R: Integrins, ICAMs, and selectins: Role and regulation of adhesion molecules in neu-

- trophil recruitment to inflammatory sites. *Adv Pharmacol* 1994;25:117-119.
27. Hunsicker LG, Shearer TP, Plattner SB, Weisenburger D: The role of monocytes in serum sickness nephritis. *J Exp Med* 1979;150:413-425.
 28. Ferrario F, Kourilsky O, Morel-Maroger L: Acute endocapillary glomerulonephritis in adults: A histologic and clinical comparison between patients with and without initial acute renal failure. *Clin Nephrol* 1983;19:17-23.
 29. Pober JS, Cotran RS: The role of endothelial cells in inflammation. *Transplantation* 1990;50:537-544.
 30. Briscoe DM, Cotran RS: Role of leukocyte-endothelial cell adhesion molecules in renal inflammation: In vitro and in vivo studies. *Kidney Int* 1993;44(S42):S27-S34.
 31. Brady HR, Denton MD, Jimenez W, Takata S, Palliser D, Brenner BM: Chemoattractants provoke monocyte adhesion to human mesangial cells and mesangial cell injury. *Kidney Int* 1992;42:480-487.
 32. Bruijn JA, Dinklo NJCM: Distinct patterns of expression of intercellular adhesion molecule-1, vascular cell adhesion molecule-1 and endothelial-leukocyte adhesion molecule-1 in renal disease. *Lab Invest* 1993;69:329-335.
 33. Hill PA, Main IW, Atkins RC: ICAM-1 and VCAM-1 in human renal allograft rejection. *Kidney Int* 1995;47:1383-1391.
 34. Brady HR: Leukocyte adhesion molecules and kidney diseases. *Kidney Int* 1994;45:1285-1300.
 35. Parra G, Romero M, Henriquez-La Roche C, Pineda R, Rodriguez-Iturbe B: Expression of adhesion molecules in post-streptococcal glomerulonephritis. *Nephrol Dial Transplant* 1994;9:1412-1417.
 36. Rastaldi MP, Ferrario F, Tunesi S, Yang L, D'Amico G: Intraglomerular and interstitial leukocyte infiltration, adhesion molecules and IL-1 α expression in 15 cases of ANCA-associated renal vasculitis. *Am J Kidney Dis* 1996;1:48-57.
 37. Koch AE, Burrows JC, Haines GK, Carlos TM, Harlan JM, Leibovich SJ: Immunolocalization of endothelial and leukocyte adhesion molecules in human rheumatoid and osteoarthritic synovial tissues. *Lab Invest* 1991;64:313-320.
 38. Picker LJ, Kishimoto TK, Smith CW, Warnock RA, Butcher EC: ELAM-1 is an adhesion molecule for skin-homing T cells. *Nature (Lond)* 1991;349:796-799.
 39. Pearce BMF: Receptors compete for adaptors found in plasma coated pits. *EMBO J* 1988;7:3331-3337.
 40. Von Asmuth EJU, Smeets EF, Ginsel LA, Onderwater JJM, Leeuwenberg JFM, Buurman WA: Evidence for endocytosis of E-selectin in human endothelial cells. *Eur J Immunol* 1992;22:2519-2525.
 41. Alexopoulos E, Seron D, Hartley RB, Nolasco F, Cameron JS: Immune mechanisms in idiopathic membranous nephropathy: The role of the interstitial infiltrates. *Am J Kidney Dis* 1989;13:404-412.
 42. Bohle A, Bader R, Grund KE, Mackensen S, Neunhofer J: Serum creatinine concentration and renal interstitial volume: Analysis of correlations in endocapillary (acute) glomerulonephritis and in moderately severe mesangioliproliferative glomerulonephritis. *Virchows Arch (Pathol Anat)* 1977;375:87-92.
 43. Hooke DH, Gee DC, Atkins RC: Leukocyte analysis using monoclonal antibodies in human glomerulonephritis. *Kidney Int* 1987;31:964-972.
 44. Nath KA: Tubulointerstitial changes as a major determinant in the progression of renal damage. *Am J Kidney Dis* 1992;20:1-17.
 45. D'Amico G, Ferrario F, Rastaldi MP: Tubulointerstitial damage in glomerular diseases: Its role in the progression of renal damage. *Am J Kidney Dis* 1995;26:124-132.
 46. Brady HR, Papayanni A, Serhan C: Leukocyte adhesion promotes biosynthesis of lipoxigenase products by transcellular routes. *Kidney Int* 1994;45(S45):S90-S97.

Intervention of crescentic glomerulonephritis by antibodies to monocyte chemotactic and activating factor (MCAF/MCP-1)

TAKASHI WADA,* HITOSHI YOKOYAMA,* KENGO FURUICHI,* KEN-ICHI KOBAYASHI,* KENJI HARADA,[†] MASANOBU NARUTO,[†] SHAO-BO SU,[‡] MARIKO AKIYAMA,[‡] NAOFUMI MUKAIDA,[‡] AND KOUJI MATSUSHIMA^{‡1}

First Department of Internal Medicine, School of Medicine, Kanazawa University, Kanazawa; [†]Basic Research Laboratories, Toray Industries, Inc., Kamakura; and [‡]Department of Pharmacology, Cancer Research Institute, Kanazawa University, Kanazawa, Japan

ABSTRACT We investigated the pathophysiological role of a potent macrophage (M ϕ) chemotactic cytokine (chemokine), monocyte chemotactic and activating factor/monocyte chemoattractant protein-1 (MCAF/MCP-1), in an animal model of crescentic glomerulonephritis. Administration of a small dose of nephrotoxic sera induced severe proliferative and necrotizing glomerulonephritis, with crescentic formation in the early phase and glomerulosclerosis in the later phase, in Wistar-Kyoto rats. MCAF/MCP-1 protein was detected immunohistochemically in glomeruli, vascular endothelial cells, and tubular epithelial cells in the early phase of injured kidney tissues but not in normal ones. Anti-MCAF/MCP-1 antibodies decreased the number of M ϕ in glomeruli, and prevented crescentic formation and the fusion of epithelial cell foot process in nephritic rats, thereby decreasing the excreted amounts of protein to normal levels on days 3 and 6. Furthermore, anti-MCAF/MCP-1 antibodies remarkably reduced glomerulosclerosis and improved renal dysfunction as well as proteinuria in the later phase (56 days). These results indicate that MCAF/MCP-1 essentially participates in the impairment of renal functions associated with crescentic glomerulonephritis by recruiting and activating M ϕ .—Wada, T., Yokoyama, H., Furuichi, K., Kobayashi, K.-i., Harada, K., Naruto, M., Su, S.-B., Akiyama, M., Mukaida, N., Matsushima, K. Intervention of crescentic glomerulonephritis by antibodies to monocyte chemotactic and activating factor (MCAF/MCP-1). *FASEB J.* 10, 1418–1425 (1996)

Key Words: chemokine · glomerular base membrane · macrophage · proteinuria

In Wistar-Kyoto (WKY)² rats, a very small dose of nephrotoxic sera (NTS) induces severe proliferative and necrotizing glomerulonephritis with crescentic formation (1, 2). This type of glomerulonephritis is caused by the antibodies reactive with Goodpasture's antigen, and is characterized by linear deposition of IgG in the glomerular

basement membrane (GBM), widespread crescentic formation, and glomerulosclerosis, resembling human crescentic glomerulonephritis. In human glomerulonephritis, crescentic formation is usually associated with poor prognosis. In this model, the infiltration of T lymphocytes and monocytes/macrophages (M ϕ) with a few neutrophils is the earliest and most prominent pathological change. Moreover, M ϕ as well as CD8-positive T lymphocytes have been postulated to be involved in both the development of glomerular lesions and crescentic formation (1). However, the precise roles of M ϕ in the development of glomerular lesions and crescentic formation have not been determined.

A chemokine, monocyte chemotactic and activating factor (MCAF) (also known as monocyte chemoattractant protein-1, MCP-1 or JE), is secreted either constitutively or after induction with mitogens, cytokines, or growth factors by a variety of cell types including lymphocytes, fibroblasts, endothelial cells, smooth muscle cells, and several tumor cell lines in vitro (3–5). Recent studies indicate that MCAF/MCP-1 is also produced by mesangial cells in response to low density lipoprotein (LDL), IL-1, or TNF- α in vitro (6–8). Moreover, increased expression of MCAF/MCP-1 transcript or protein has been observed on renal tissues from human lupus nephritis and experimental glomerulonephritis models (9–12). However, no direct evidence has been provided on the role of MCAF/MCP-1 in the infiltration and activation of M ϕ or crescentic formation in glomerulonephritis. Hence, we evaluated the role of MCAF/MCP-1 in crescentic glomerulonephritis in WKY rats by administering specific

¹To whom correspondence should be addressed, at: Department of Pharmacology, Cancer Research Institute, Kanazawa University, 13-1 Takara-machi, Kanazawa, 920 Japan.

²Abbreviations: Ccr, creatinine clearance; FGF, fibroblast growth factor; GBM, glomerular base membrane; M ϕ , macrophage; MIP, macrophage inflammatory protein; MCP, monocyte chemoattractant protein; MCAF, monocyte chemotactic and activating factor; NTS, nephrotoxic sera; PAS, periodic acid-Schiff; PCNA, proliferating cell nuclear antigen; PDGF, platelet-derived growth factor; ROI, reactive oxygen intermediate; WKY, Wistar-Kyoto.

polyclonal neutralizing anti-MCAF/MCP-1 antibodies that were prepared against recombinant rat MCAF/MCP-1.

MATERIALS AND METHODS

Animals

Inbred male WKY rats (Charles River Japan Inc., Atsugi, Kanagawa, Japan), aged 12 wk, were quarantined for at least 1 wk at the Animal Research Center of Kanazawa University to confirm the absence of disease before use. Animals were fed standard rat chow and given free access to water under 24 h light control. All the procedures used in the animal experiments complied with the standards set out in the *Guideline for the Care and Use of Laboratory Animals in Takara-machi Campus of Kanazawa University*.

Expression of rat recombinant MCAF/MCP-1 and preparation of polyclonal antibodies against rat MCAF/MCP-1

An expression vector pSCFV-1 (a generous gift from Chugai Pharmaceutical Co. Ltd., Tokyo, Japan) that contained a tryptophane promoter and a leader sequence of the bacterial *pel B* gene (13) was chosen to express rat MCAF/MCP-1 as a secreted form in *Escherichia coli*. Rat MCAF/MCP-1 cDNA (14) was obtained by reverse transcriptase-polymerase chain reaction (RT-PCR) using total RNA from lipopolysaccharide-stimulated rat spleen cells and was cloned into pSCFV-1 and transduced into *E. coli* HB101. The transformant was cultured in a modified M9 medium with 3-indole acrylic acid at 37°C for 24 h. The culture fluids were centrifuged at 4600 × g for 10 min and the pellet was washed with 10 mM Tris-HCl (pH 7.5), 25% sucrose twice. The cell pellet was further washed with 10 mM Tris-HCl (pH 7.5), 25% sucrose, 1 mM EDTA. All the supernatants during these procedures were pooled; the pH was adjusted to 5.0 with acetic acid, applied to a heparin agarose column (Pharmacia-Biotech, Uppsala, Sweden), and eluted by 1 M NaCl-0.02 M Na phosphate buffer (pH 7.5). The eluate was then applied to a Superose 12 gel filtration column equipped with an FPLC system (Pharmacia-Biotech) and dialyzed against 0.02 M Na-phosphate buffer (pH 7.5). The dialyzed sample was further applied to a heparin column (TSK Heparin-5PW, Tosoh, Tokyo, Japan) equipped with a Pharmacia-LKB Pump 2248 system and eluted by a linear gradient of NaCl in the range of 0–1 M in 0.02 M Na-phosphate buffer (pH 7.5). The fractions containing rat MCAF/MCP-1 were monitored by sodium dodecyl sulfate-polyacrylamide gel electrophoresis (SDS-PAGE) analysis. The final product showed a single band on SDS-PAGE stained with Coomassie brilliant blue, and its amino acid sequence of amino terminus was identical to the one reported for mature rat MCAF/MCP-1 (14).

Antibodies and reagents

Goat and rabbit polyclonal antibodies were prepared by repeated immunization of animals with purified, recombinant rat MCAF/MCP-1. IgG fraction was purified from immunized or normal animal sera by using a protein A agarose column (Pharmacia-Biotech). On Western blotting analysis, the goat antibodies detected a single band in the same fraction as recombinant rat MCAF/MCP-1 when concanavalin A-stimulated spleen culture supernatant was fractionated by using a heparin-high performance liquid chromatography (data not shown). The goat antibodies did not show any cross-reactivities against recombinant rat RANTES (Pepro-Tech, Rocky Hill, N.J.) on Western blotting analysis (data not shown). Rat GBM was prepared by the method of Krakower and Green-son (15). Three Japanese white rabbits were immunized subcutaneously with sonicated GBM emulsified in complete Freund's adjuvant (Iatron, Tokyo, Japan). Boosters were given several times using GBM with incomplete Freund's adjuvant (Iatron). Blood was drawn 7 days after the last booster and sera were prepared by centrifugation after coagulation. Before use, the NTS were heat-decomplemented and absorbed twice with an equal volume of packed rat red blood cells and

rabbit liver powder overnight at 4°C. An indirect immunofluorescence analysis using the NTS gave rise to a sharp linear fluorescence only along the GBM and the tubular basement membranes in frozen sections of normal Wistar rats, indicating the specificity of the serum.

Monocyte chemotaxis assay

Monocyte chemotaxis assay using rat peripheral blood mononuclear cells was performed in essentially the same way described previously (5). In some experiments, recombinant rat MCAF/MCP-1 (10 ng/ml) was preincubated with the indicated concentrations of anti-rat MCAF/MCP-1 antibodies at 4°C for 30 min before the chemotaxis assay.

Experimental design

On day 0, male WKY rats aged 12 wk were injected intravenously with 0.1 ml of NTS. Either anti-MCAF/MCP-1 polyclonal antibodies or normal goat IgG at a dose of 2.5 mg in 0.5 ml of physiological saline was administered intravenously at the same time. Groups of six rats were killed on days 3, 6, 14, and 56. Urine samples were collected using a metabolic cage at five time intervals: from day -1 to the time of injection of NTS on day 0, and from day 2, 5, 13, or 55 to the time of death.

Histopathological studies

One portion of the renal tissue was fixed in 10% buffered formalin, followed by embedding in paraffin and staining with periodic acid-Schiff (PAS) reagents. The sections were evaluated under light microscopy by two independent observers without any prior knowledge of the experimental design. To avoid variation in the shape of the glomeruli, we chose glomeruli of the same diameter from a vascular pole. The total number of cells was determined on at least 10 glomeruli of each rat and expressed as the number per glomerulus. The number of crescentic formation in at least 30 glomeruli of each rat was measured and expressed as a percentage of positive glomeruli of the total. We defined the lobes of each glomerulus according to the location of mesangial areas so that each glomerulus contained more than four lobes in a particular glomerulus. Glomerular sclerosis was expressed as an index in all glomeruli of each rat, graded on an arbitrary scale (0, none; 1, one lobe; 2, two lobes; 3, three lobes; 4, more than four lobes). Another portion of renal tissue was frozen rapidly and immunostained directly with fluorescein isothiocyanate (FITC)-conjugated, anti-proliferating cell nuclear cell antigen (PCNA; Leinco Technologies Inc., St. Louis, Mo.; No. 033L245) or indirectly with either a mouse monoclonal antibody against rat tissue monocytes and macrophages, ED1 (IgG₁, BMA Biomedicals Ltd., Switzerland) or a mouse monoclonal antibody against the rat CD8 molecules (IgG₁, Cedarlane, Hornby, Ontario, Canada; No. 0412). Positive cells were counted on at least 30 randomly chosen glomeruli. Renal tissues obtained from four normal WKY rats were used as negative controls. FITC-conjugated anti-rabbit IgG (Organon Teknika Corporation; No. 38236), FITC-conjugated anti-rat C3 (Organon Teknika Corporation; No. 38810), and FITC-conjugated anti-rat IgG (Organon Teknika Corporation; No. 38731) were used for direct immunofluorescence. The amount and extent of fluorescence were evaluated for at least 50 glomeruli and graded on an arbitrary scale from 0 to 3 (negative, scattered, weakly diffuse, and strongly diffuse) by two independent observers with no prior knowledge of the experimental design. Several portions of each specimen were prefixed with 2.5% glutaraldehyde and postfixed with 4% osmic acid, progressively dehydrated in an alcohol series, embedded in Epok 812, and cut into ultrathin sections. These were double-stained with uranyl acetate and lead citrate and were examined by electron microscopy (Hitachi H-600, Tokyo, Japan).

Immunohistochemical detection of MCAF/MCP-1

The presence of MCAF/MCP-1 protein was examined immunohistochemically on frozen tissue specimens by using an indirect avidin-biotinylated alkaline phosphatase complex method (12) with rabbit anti-rat MCAF/MCP-1 antibodies. In some experiments, the antibodies were preabsorbed with an excess amount of recombinant rat MCAF/MCP-1 before the analyses. Two observers without any prior knowledge about

experimental designs independently examined the immunohistochemical findings.

Determination of urinary protein, blood urea nitrogen, and creatinine concentrations

Urinary protein concentrations were determined by the pyrogallol red method using human serum albumin as a standard (16). Urinary protein excretion was expressed as the total amount excreted in 24 h. Blood urea nitrogen, serum, and urinary creatinine levels were measured using an automated analyzer (Hitachi, Tokyo, Japan) according to the manufacturer's instructions.

Statistical analysis

The mean and standard error were calculated on all parameters determined in this study. Statistical analyses were performed using paired and unpaired Student's *t* test and ANOVA test. *P* < 0.05 was accepted as statistically significant.

RESULTS

Neutralizing activities of anti-rat MCAF/MCP-1 antibodies

We first examined the effects of anti-rat MCAF/MCP-1 antibodies on rat MCAF/MCP-1-induced monocyte chemotaxis. Recombinant rat MCAF/MCP-1 induced rat monocyte chemotaxis, with a maximal effect at 10 ng/ml (Fig. 1) as reported on human MCAF/MCP-1-induced human monocyte chemotaxis (4, 5), indicating that the expressed protein has full biological activities. Goat anti-

rat MCAF/MCP-1 antibodies, but not normal goat IgG, inhibited rat-MCAF/MCP-1-induced monocyte chemotaxis by nearly 50% at a MCAF/MCP-1 to antibody molar ratio of about 1: 100 (Fig. 1), suggesting that the antibody can neutralize the biological activities of rat MCAF/MCP-1 effectively.

Histopathological studies

Immunofluorescence analysis revealed no deposition of rabbit IgG in glomeruli from four normal WKY rats (data not shown). Rabbit IgG was intensely detected in a linear pattern along the glomerular capillaries from NTS-injected rats treated with the control IgG or anti-MCAF/MCP-1 antibodies. Rat IgG and C3 were also detected, but the intensity was similarly faint. Semiquantitative evaluation of deposition revealed no significant difference in the deposition of rabbit IgG, rat IgG, and rat C3 between glomeruli from rats treated with anti-MCAF/MCP-1 antibodies and those given a control IgG (data not shown).

Three days after NTS injection, endocapillary proliferation, pathologically characterized by the presence of endothelial cell proliferation and inflammatory cell infiltration, was observed in glomeruli in the rats treated with a control IgG (Fig. 2c). At the same time point, the animals treated with the anti-MCAF/MCP-1 antibodies exhibited only a mild increase in mononuclear cells in glomeruli, without endocapillary proliferation (Fig. 2b). On day 6, severe glomerular lesions developed in rats treated with a control IgG. In the injured renal tissues, endocapillary proliferation, severe necrotizing lesions, and crescentic formation were observed (Fig. 2e, f). The increase in the number of total glomerular cells was also observed at 3 days after NTS injection and reached a maximum at day 6 (Table 1). Moreover, a considerable number of PCNA- and ED1-positive cells infiltrated into glomeruli, starting at day 3 and reaching a peak at day 6 (Table 1) as previously reported (1). The infiltration of CD8-positive T lymphocytes, which are characteristic of this model, reached a maximal level on day 3 and decreased thereafter. The increases in number of total cells, PCNA-, and ED-1-positive cells, but not CD8-positive T cells, were significantly reduced by the administration of anti-MCAF/MCP-1 antibodies on days 3 and 6 (Table 1). The formation of crescentic lesions as well as necrotizing lesions, observed on day 6 in animals treated with a control IgG was reduced by the administration of anti-MCAF/MCP-1 antibodies (Fig. 2d and Table 1).

Electron microscopical analyses demonstrated little fusion of epithelial foot processes in the free wall of the glomerular capillaries from four normal rats (data not shown). Epithelial cell foot processes fused severely in all tufts, especially near infiltrated leukocytes, as examined on day 6 in diseased glomeruli from each of six rats treated with the control IgG (Fig. 3A). However, in six NTS-injected rats treated with anti-MCAF/MCP-1 antibodies, fusion of epithelial foot processes barely oc-

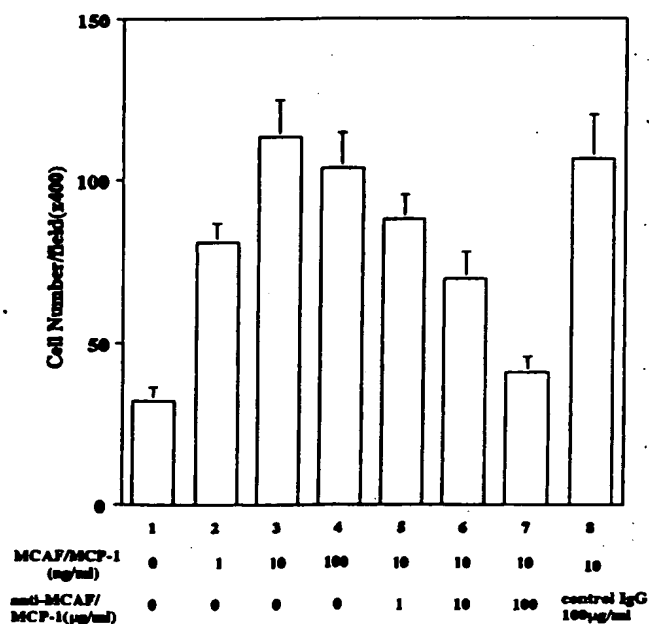


Figure 1. Monocyte chemotaxis assay. Monocyte chemotaxis assay was performed using rat peripheral blood mononuclear cells on medium (lane 1) or rat MCAF/MCP-1 (lane 2, 1 ng/ml; lanes 3, and 5 to 8, 10 ng/ml; lane 4, 100 ng/ml) pre-incubated with goat anti-rat MCAF/MCP-1 antibodies (lane 5, 1 µg/ml; lane 6, 10 µg/ml; lane 7, 100 µg/ml) or a control IgG (lane 8, 100 µg/ml). After incubation, the number of migrated cells were determined as described in Materials and Methods.

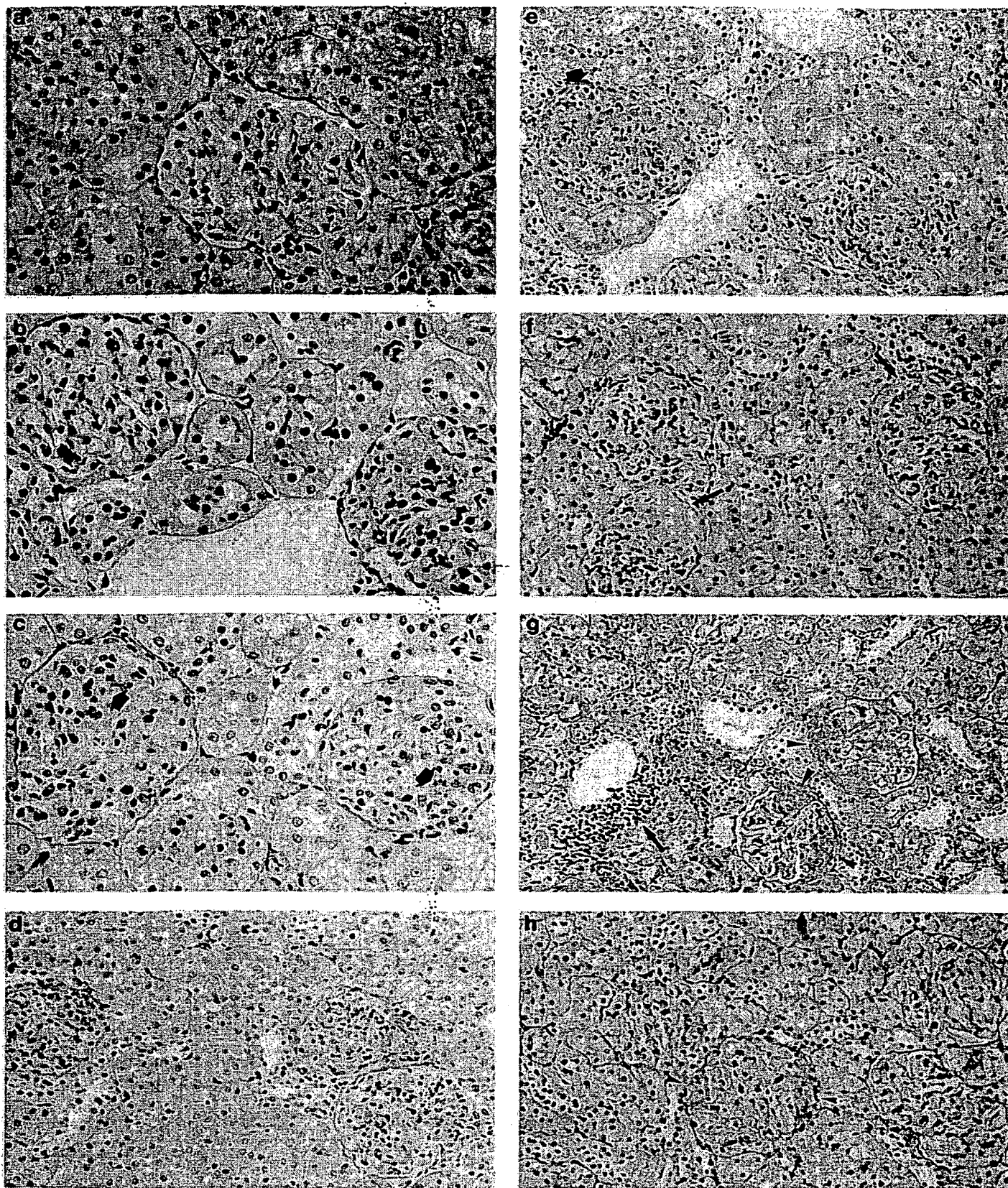


Figure 2. Light micrographical analysis on renal tissues. Histopathological examination was performed using PAS-stained renal tissues obtained from a control rat (a), nephritic rat treated with the anti-MCAF/MCP-1 antibodies (b, d, h) or the control IgG (c, e-g) on days 3 (b, c), 6 (d-f), and 56 (g, h). Arrows in panels c, e-g indicate endocapillary proliferation, crescentic formation, a necrotizing lesion and an interstitial lesion, respectively. Arrowheads in panels g and h represent glomerular sclerotic changes. Original magnification is as follows: a-c) $\times 310$; d-h) $\times 160$.

TABLE 1. Inhibition of pathological changes in the early phase by anti-MCAF antibodies^a

	Normal rat	Day 3		Day 6	
		Control IgG	anti-MCAF	Control IgG	anti-MCAF
Crescentic formation, %	0	15.2 ± 1.0	7.0 ± 1.0 ^b	38.9 ± 5.5	26.1 ± 1.3 ^c
Total cell number cells/glomerulus	55.3 ± 1.1	88.9 ± 3.1	59.6 ± 2.0 ^b	136.4 ± 6.2	103.4 ± 6.0 ^c
PCNA-positive cells cells/glomerulus	1.8 ± 0.5	4.1 ± 0.2	2.9 ± 0.2 ^b	6.9 ± 0.2	4.7 ± 0.3 ^b
ED1-positive cells cells/glomerulus	0.8 ± 0.1	10.1 ± 0.2	7.2 ± 0.1 ^b	11.7 ± 0.4	9.0 ± 0.2 ^b
CD8-positive cells cells/glomerulus	0.2 ± 0.02	2.7 ± 0.2	2.4 ± 0.1	1.3 ± 0.1	1.3 ± 0.1

^aValues are given as mean ± SEM. Statistical analyses are based on unpaired *t* test and ANOVA test. ^b*P* < 0.01, compared to control IgG-treated rats. ^c*P* < 0.05.

curred, even though leukocytes infiltrated in glomerular capillaries (Fig. 3B). Collectively, these results indicated that the antibodies improved pathological changes observed during the early phase.

On day 56, control IgG-treated animals exhibited marked degree of glomerulosclerosis as well as interstitial lesions (Table 2 and Fig. 2g). A single injection of anti-MCAF/MCP-1 antibodies at the start of inflammatory reaction significantly reduced glomerulosclerosis in this later phase (Table 2 and Fig. 2h), suggesting the crucial role of MCAF/MCP-1 in the pathogenesis of this type of crescentic glomerulosclerosis.

Immunohistochemical detection of MCAF/MCP-1 protein in renal tissues

Renal tissues from all nephritic rats on day 3 were examined immunohistochemically for the presence of antigenic MCAF/MCP-1. MCAF/MCP-1-positive cells were observed in the diseased glomeruli, vascular endothelial cells, and tubular epithelial cells (Fig. 4A). The staining was specific for MCAF/MCP-1, as the polyclonal antibodies preabsorbed with recombinant rat MCAF/MCP-1 failed to stain (Fig. 4B). Moreover, in the glomeruli from normal rats, MCAF/MCP-1 was not detected immunohistochemically (data not shown). These results suggested the local production of MCAF/MCP-1 in the process of NTS-induced crescentic glomerulonephritis.

Effects of anti-MCAF/MCP-1 antibodies on the urinary excretion of protein and renal dysfunction

We finally evaluated the effects of anti-MCAF/MCP-1 antibodies on proteinuria as well as renal dysfunction.

Twenty-eight normal untreated rats excreted minute amounts of protein in the urine. In contrast, all six of the nephritic rats treated with the control IgG excreted markedly elevated amounts of protein in the urine on days 3 and 6. The administration of anti-MCAF/MCP-1 antibodies dramatically decreased the excreted amount of proteinuria and reversed to normal levels on days 3 and 6 (Fig. 5). Moreover, proteinuria on day 56 but not on day 14 was improved markedly by a single injection of anti-MCAF/MCP-1 antibodies (Table 2). On day 56, control IgG-treated animals developed renal dysfunction as evidenced by increased blood urea nitrogen levels and reduced creatinine clearance (Ccr), as reported previously (1). A single administration of anti-MCAF/MCP-1 antibodies decreased blood urea nitrogen levels and prevented the reduction of Ccr significantly, inferring that the treatment could prevent also chronic renal dysfunction.

DISCUSSION

WKY rats developed crescentic glomerulonephritis, leading to glomerulosclerosis with progressive renal dysfunction by the administration of a small dose of NTS. In this study, we observed that the administration of anti-MCAF/MCP-1 antibodies completely prevented proteinuria and lessened histological changes, with significant inhibition of Mφ infiltration in the early phase. Moreover, the treatment prevented glomerulosclerosis as well as renal dysfunction in the later phase. Although the antibodies used in this study was highly specific to rat MCAF/MCP-1, we cannot completely exclude the remote possibility that the antibodies showed some cross-reactivities against closely related chemokines MCP-2 and

TABLE 2. Improvement of laboratory data and glomerulosclerosis in the later phase by anti-MCAF/MCP-1 antibodies

	Day 14		Day 56	
	Control IgG	anti-MCAF	Control IgG	anti-MCAF
Urinary protein, mg/24 h	98.7 ± 12.7	78.7 ± 26.8	173.7 ± 22.4 ^a	63.5 ± 33.2 ^b
24 h Ccr, ml/min	1.47 ± 0.07	1.40 ± 0.16	0.99 ± 0.10 ^a	1.23 ± 0.08 ^c
Blood urea nitrogen, mg/dl	21.4 ± 3.1	20.3 ± 3.7	33.2 ± 2.0 ^b	24.5 ± 2.6 ^b
Glomerular sclerosis, index/glomerulus	0.47 ± 0.09	0.37 ± 0.09	0.95 ± 0.19 ^a	0.47 ± 0.06 ^b

Values are given as mean ± SEM. Statistical analyses are based on unpaired *t* test or Wilcoxon signed rank test. ^a*P* < 0.05, compared to day 14. ^b*P* < 0.05. ^c*P* = 0.06 compared to control IgG-treated rats.

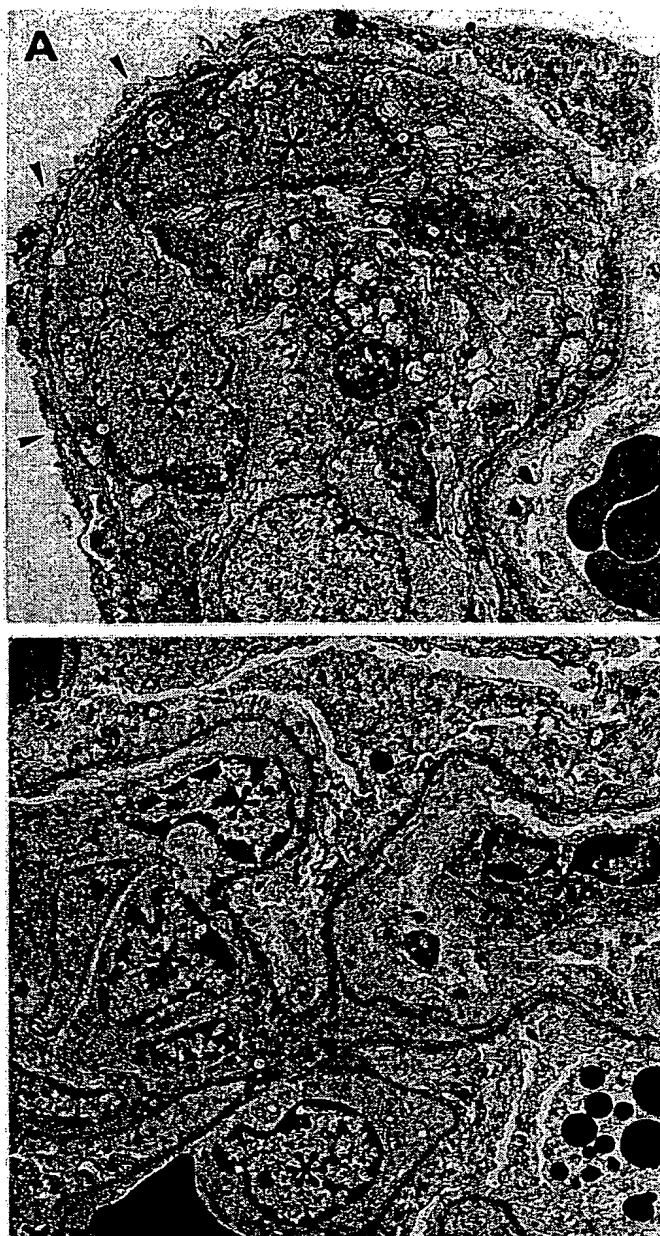


Figure 3. Representative electron micrographs of glomeruli. Electron micrographical analyses were performed on glomeruli from rats treated with the control IgG (A) or the anti-MCAF/MCP-1 antibodies (B). Arrowheads and asterisks indicate the fusion of epithelial foot processes and infiltrated leukocytes. Original magnification $\times 1500$.

MCP-3. Nevertheless, these results suggested that MCAF/MCP-1 or its closely related chemokines may govern the entire course of this type of crescentic glomerulonephritis.

Infiltration of various types of leukocytes has been documented on human glomerulonephritis as well as animal models (17–19). Although several independent groups observed that antibodies against either IL-1 or TNF- α prevented leukocyte infiltration as well as proteinuria (20), neither cytokine possessed direct chemotactic

activities against leukocytes (21), raising the possibility that an additional chemotactic factor (or factors) plays a role in inducing leukocyte infiltration. Renal tissue cells, such as mesangial cells and endothelial cells, and infiltrated leukocytes could both produce a potent M ϕ chemotactic and activating cytokine MCAF/MCP-1 in vitro (6–8). Moreover, increased expression of MCAF/MCP-1 has been documented on glomerular lesions of another experimental glomerulonephritis model (9–11). Herein, our immunohistochemical analyses also demonstrated the presence of MCAF/MCP-1 in the injured kidney tissues. These results would imply that MCAF/MCP-1 was locally produced in glomeruli during the processes of renal injuries.

Semiquantitative evaluation of deposition revealed no significant difference in the deposition of rabbit IgG, rat IgG, and rat C3 between glomeruli from rats treated with anti-MCAF/MCP-1 antibodies and those given a control IgG. Thus, MCAF/MCP-1 might be involved in the processes after anti-GBM antibody has been deposited and complement system has been activated (19).

The administration of anti-MCAF/MCP-1 antibodies did not completely prevent ED1-positive M ϕ infiltration. Since this polyclonal antibody preparation potentially inhibits the biological activity of rat MCAF/MCP-1 (50% inhibition at about 100-fold excess molar ratio of polyclonal antibodies to MCAF/MCP-1) and completely prevented the appearance of proteinuria, it is very unlikely that the dose of anti-MCAF/MCP-1 antibodies was not enough to neutralize MCAF/MCP-1. Similarly in the case of IgA immune complex-induced lung injury model, pulmonary injury but not the increase in the M ϕ number was completely blocked by the intravenous administration of anti-MCAF/MCP-1 antibodies (22). Thus, these results suggest the simultaneous generation of additional chemotactic cytokines, chemokines for M ϕ such as MCP-2, MCP-3, RANTES, and macrophage inflammatory protein (MIP)-1 α , β (21). This possibility was supported by the facts that inflammatory stimuli including LPS, IL-1, and TNF- α stimulated various types of cells to produce MIP-1 α and β (21) as well as MCAF/MCP-1.

The administration of anti-MCAF/MCP-1 antibodies also reduced the number of PCNA-positive cells in glomeruli on days 3 and 6. PCNA is a nuclear protein markedly up-regulated from late G₁ through the M phase of the cell cycle (23); PCNA-positive cells are reported to belong to mesangial cells or α -smooth-muscle-cell associated protein-positive cells (24), in addition to ED1-positive M ϕ (25). Hence, anti-MCAF/MCP-1 antibodies might also affect the proliferation and/or migration of nonleukocytic cells in glomeruli. Activated M ϕ could release platelet-derived growth factor (PDGF) and basic fibroblast growth factor (bFGF), which vigorously stimulate mesangial cell proliferation (26). Thus, anti-MCAF/MCP-1 treatment might inhibit the release of mesangial cell proliferation factors such as bFGF or PDGF by M ϕ . This could prevent mesangial cell proliferation and eventually the development of glomerulosclerosis.



Figure 4. Immunohistochemical examination for expression of MCAF/MCP-1 protein in renal tissue. Immunohistochemical analyses were performed on renal tissues obtained from rats treated with the control IgG on day 3 as described in Materials and Methods using rabbit anti-rat MCAF/MCP-1 polyclonal antibodies with (B) or without (A) preabsorption with excess amount of rat recombinant MCAF/MCP-1. Asterisks, arrowheads, and an arrow indicate glomeruli, vascular endothelial cells, and tubular epithelial cells, respectively. Original magnification $\times 160$.

Several independent groups claim the significance of the interaction of CD8-positive T lymphocytes as well as monocytes/M ϕ with mesangium in the pathogenesis of glomerulonephritis, particularly crescentic glomerulonephritis (1, 27). MCAF/MCP-1 has been reported to exhibit a potent chemotactic activity against T lymphocytes in vitro (28). However, there was no significant difference of the CD8-positive T lymphocyte numbers in glomeruli between the control IgG-treated rats and anti-MCAF/MCP-1 antibodies-treated rats. Thus, our results indicate that MCAF/MCP-1 is not a main factor in determining the infiltration of CD8-positive T lymphocytes, at least in this model; rather, that MCAF/MCP-1 could induce the glomerular injury and crescentic formation via the infiltration and activation of M ϕ , but not CD8-positive T lymphocytes.

In contrast to incomplete inhibition of M ϕ infiltration, anti-MCAF/MCP-1 antibodies improved renal dysfunction in the later phase as well as proteinuria. Electron microscopical analyses demonstrated that anti-MCAF/MCP-1

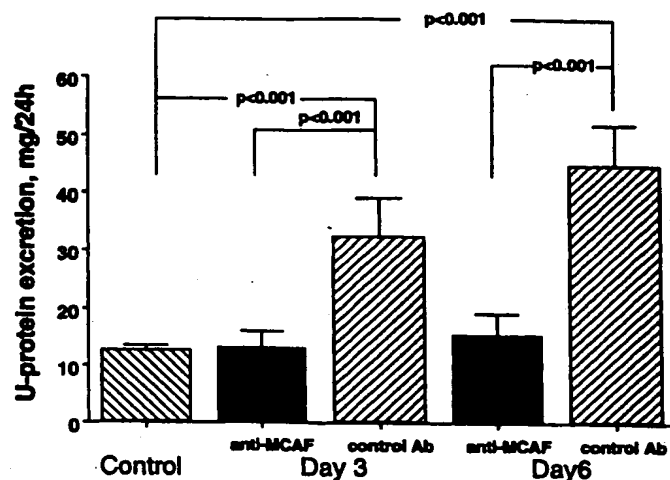


Figure 5. Effects of anti-MCAF/MCP-1 antibodies on urinary protein excretion. Results from normal rats, rats treated with control antibody, and rats treated with anti-MCAF/MCP-1 antibodies are shown. The administration of anti-MCAF/MCP-1 antibodies markedly decreased proteinuria both on days 3 and 6 ($P < 0.001$, respectively).

treatment prevented the fusion of epithelial foot processes even in glomerular capillaries where M ϕ infiltrated, inferring that anti-MCAF/MCP-1 treatment prevented glomerular injury almost completely. The involvement of lysosomal enzymes, nitrous oxide (NO), and reactive oxygen intermediates (ROI) from leukocytes has been reported to play an essential role in inducing tissue injury in glomerulonephritis (29). MCAF/MCP-1 has been documented to induce release of lysosomal enzymes and generation of superoxide anions (21) from M ϕ in addition to chemotaxis of leukocytes. Hence, we presumed the role of MCAF/MCP-1 in the establishment of renal injury in this model as follows. Locally produced MCAF/MCP-1 at the early phase induced the infiltration and activation of M ϕ /monocytes, which caused renal pathology by releasing effector molecules such as PDGF, bFGF, lysosomal enzymes, NO, and ROI. A single injection of anti-MCAF/MCP-1 antibodies blocked the initial and essential event, the infiltration and activation of M ϕ /monocytes, and prevented the subsequent renal dysfunction.

This study has, for the first time, provided evidence on the essential roles of MCAF/MCP-1 in the chronic as well as the acute phase of crescentic glomerulonephritis in any species. Thus, the administration of an antagonist to MCAF/MCP-1, such as a humanized anti-human MCAF/MCP-1 monoclonal antibody and specific receptor antagonists, would be a key to future treatment of M ϕ -dominant human glomerulonephritis, particularly chronic ones. [7]

We are grateful to Dr. Naohisa Tomoeugi (Kanazawa Medical College, Japan) for his kind advice.

REFERENCES

- Kawasaki, K., Yaoita, E., Yamamoto, T., and Kihara, I. (1992) Depletion of CD8 positive cells in nephrotoxic serum nephritis of WKY rats. *Kidney Int.* 41, 1517-1526

2. Nishikawa, K., Guo, Y. J., Miyasaka, M., Tamatani, T., Collins, B., Sy, M. S., McCluskey, R. T., and Andres, G. (1993) Antibodies to intercellular adhesion molecule 1/lymphocyte function-associated antigen 1 prevent crescentic formation in rat autoimmune glomerulonephritis. *J. Exp. Med.* 177, 667-677
3. Rollins, B. J., Stier, P., Ernst, T. E., and Wong, C. G. (1989) The human homologue of the JE gene encodes a monocyte secretory protein. *Mol. Cell. Biol.* 9, 4687-4695
4. Yoshimura, T., Robinson, E. A., Tanaka, S., Appela, E., and Leonard, E. J. (1989) Purification and amino acid analysis of two human monocyte chemoattractants produced by phytohemagglutinin-stimulated human blood mononuclear cells. *J. Immunol.* 142, 1956-1962
5. Matsushima, K., Larssen, C. G., DuBois, C. C., and Oppenheim, J. J. (1989) Purification and characterization of a novel monocyte chemotactic and activating factor produced by a human myelomonocytic cell line. *J. Exp. Med.* 169, 1485-1490
6. Brown, Z., Strieter, R. M., Neild, G. H., Thompson, R. C., Kunkel, S. L., and Westwick, J. (1992) IL-1 receptor antagonist inhibits monocyte chemotactic peptide 1 generation by human mesangial cells. *Kidney Int.* 42, 95-101
7. Rovin, B. H., and Tan, L. C. (1993) LDL stimulates mesangial fibronectin production and chemoattractant expression. *Kidney Int.* 43, 218-225
8. Schmodder, R. L., Strieter, R. M., and Kunkel, S. L. (1993) Interferon- γ regulation of human cortical epithelial cell-derived monocyte chemotactic peptide-1. *Kidney Int.* 44, 43-49
9. Stahl, R. A. K., Thaisz, F., Disser, M., Helmchen, U., Hora, K., and Schloendorff, D. (1993) Increased expression of monocyte chemoattractant protein-1 in anti-thymocyte antibody-induced glomerulonephritis. *Kidney Int.* 44, 1036-1047
10. Rovin, B. H., Rumancik, M., Tan, L., and Dickerson, J. (1994) Glomerular expression of monocyte chemoattractant protein-1 in experimental and human glomerulonephritis. *Lab. Invest.* 71, 536-542
11. Tang, W. W., Feng, L., Mathison, J. C., and Wilson, C. B. (1994) Cytokine expression, up-regulation of intercellular adhesion molecule-1, and leukocyte infiltration in experimental tubulointerstitial nephritis. *Lab. Invest.* 70, 631-638
12. Wada, T., Yokoyama, H., Su, S.-B., Mukaida, N., Iwano, M., Dohi, K., Takahashi, Y., Sasaki, T., Furuichi, K., Segawa, C., Hisada, Y., Ohta, S., Takasawa, K., Kobayashi, K.-I., and Matsushima, K. (1996) Monitoring urinary levels of monocyte chemotactic and activating factor reflects disease activity of lupus nephritis. *Kidney Int.* 49, 761-767
13. Better, M., Chang, C. P., Robinson, R. R., and Horwitz, A. H. (1988) *Escherichia coli* secretion of an active chimeric antibody fragment. *Science* 240, 1041-1043
14. Yoshimura, T., Takeya, M., and Takahashi, K. (1991) Molecular cloning of rat monocyte chemoattractant protein-1 (MCP-1) and its expression in rat spleen cells and tumor cells. *Biochem. Biophys. Res. Commun.* 174, 504-509
15. Krakower, C. A., and Greenspan, S. A. (1951) Localization of nephrotoxic antigen within the isolated renal glomerulus. *Arch. Pathol.* 51, 629-639
16. Wada, T., Tomosugi, N., Naito, T., Yokoyama, H., Kobayashi, K., Mukaida, N., and Matsushima, K. (1994) Prevention of proteinuria by the administration of anti-interleukin 8 antibody in experimental acute immune complex-induced glomerulonephritis. *J. Exp. Med.* 180, 1135-1144
17. Wada, T., Yokoyama, H., Tomosugi, N., Hisada, Y., Ohta, S., Naito, T., Kobayashi, K., Mukaida, N., and Matsushima, K. (1994) Detection of urinary interleukin-8 in glomerular diseases. *Kidney Int.* 46, 455-460
18. Camussi, G., Tetta, C., Bussolino, F., Turello, E., Brentjens, J., Montrucchio, G., and Andres, G. (1990) Effect of leukocyte stimulation on rabbit immune complex glomerulonephritis. *Kidney Int.* 38, 1047-1055
19. Mulligan, M. S., Johnson, K. J., Todd, R. F., III, Issekutz, T. B., Miyasaka, M., Tamatani, T., Smith, C. W., Anderson, D. C., and Ward, P. A. (1993) Requirement for leukocyte adhesion molecules in nephrotoxic nephritis. *J. Clin. Invest.* 91, 577-587
20. Egidio, J., Gomez-Chiarri, M., Ortiz, A., Bustos, C., Alonso, J., Gomez-Guerrero, C., Gomez-Garre, D., Lopez-Armada, M. J., Plaza, J., and Gonzalez, E. (1993) Role of tumor necrosis factor- α in the pathogenesis of glomerular diseases. *Kidney Int.* 43 (Suppl. 39), S59-S61
21. Baggiolini, M., Dewald, B., and Moser, B. (1994) Interleukin-8 and related chemotactic cytokines—CXC and CC chemokines. *Adv. Immunol.* 55, 97-179
22. Jones, M. L., Mulligan, M. S., Flory, C. M., Ward, P. A., and Warren, J. S. (1992) Potential role of monocyte chemoattractant protein 1/JE in monocyte/macrophage-dependent IgA immune complex alveolitis in the rat. *J. Immunol.* 149, 2147-2154
23. Kurki, P., Vandelaan, M., Dolbeare, F., Gary, J., and Tan, E. M. (1986) Expression of proliferating cell nuclear antigen (PCNA)/cyclin during the cell cycle. *Exp. Cell Res.* 166, 209-219
24. Johnson, R. J., Iida, H., Alpers, C. E., Majecky, M. W., Schwartz, S. M., Protal, P., Gordon, K., and Gown, A. M. (1991) Expression of smooth muscle cell phenotype by rat mesangial cells in immune complex nephritis. *J. Clin. Invest.* 87, 847-858
25. Lan, H. Y., Nikolic-Paterson, D. J., Mu, W., and Atkins, R. C. (1995) Local macrophage proliferation in the progression of glomerular and tubulointerstitial injury in rat anti-GBM glomerulonephritis. *Kidney Int.* 48, 753-760
26. Nathan, C. F. (1987) Secretory products of macrophages. *J. Clin. Invest.* 79, 319-326
27. Nolasco, F., Cameron, J.S., Hartley, B., Coelho, A., Hildreth, G., and Reuben, R. (1987) Intraglomerular T cells and monocytes in nephritis: Study with monoclonal antibodies. *Kidney Int.* 31, 1160-1166
28. Carr, M. W., Roth, S. J., Luther, E., Rose, S. S., and Springer, T. A. (1994) Monocyte chemoattractant protein1 acts as a T-lymphocyte chemoattractant. *Proc. Natl. Acad. Sci. USA* 91, 3652-3656
29. Johnson, R. J., Couser, W. G., Chi, E. Y., Adler, S., and Klebanoff, S. J. (1987) New mechanism for glomerular injury: Myeloperoxidase-hydrogen peroxidase-halide system. *J. Clin. Invest.* 79, 1379-1387

Received for publication December 26, 1995.

Accepted for publication June 18, 1996.

Perivascular T Cells Express the Pro-Inflammatory Chemokine RANTES mRNA in Multiple Sclerosis Lesions

J. HVAS*†, C. McLEAN‡, J. JUSTESEN§, G. KANNOURAKIS¶, L. STEINMAN*, J. R. OKSENBERG†† & C. C. A. BERNARD†

*Department of Medical Microbiology and Immunology, University of Aarhus, Århus, Denmark; †The Neuroimmunology Laboratory, La Trobe University, Bundoora, Victoria, Australia; ‡Department of Pathology, the University of Melbourne, Parkville, Victoria, Australia; §Department of Molecular and Structural Biology, University of Aarhus, Århus, Denmark; ¶L.A.R.C.H. Cancer Research Unit, Royal Children's Hospital, Parkville, Victoria, Australia; Department of Neurology and Neurological Science, Stanford University Medical Centre, Stanford, CA, USA; and ††Department of Neurology, University of California, San Francisco, CA, USA

(Received 18 November 1996; Accepted in revised form 20 March 1997)

Hvas J, McLean C, Justesen J, Kannourakis G, Steinman L, Oksenberg JR, Bernard CCA. Perivascular T Cells Express the Pro-Inflammatory Chemokine RANTES in Multiple Sclerosis Lesions. *Scand J Immunol* 1997;46:195–203

Multiple sclerosis (MS) is an inflammatory demyelinating disease of the central nervous system (CNS), characterized by accumulation of mononuclear cells. The pathogenesis of MS is complex and probably involves soluble immune mediators, particularly cytokines, and activated memory T cells, that are thought to migrate into the CNS. During lesion formation in MS, cytokines regulate cell functions, such as cell recruitment and migration. Because the chemokine RANTES play a role in both activating and recruiting leucocytes, particularly memory T cells into inflammatory sites, the authors have assessed RANTES mRNA levels at the site of lesions. Expression levels were analysed in brain samples and compared with neurological, infectious and other controls. RANTES was expressed by activated perivascular memory T cells, predominantly located at the edge of active plaques. While RANTES mRNA was detected in all 17 MS brains analysed, it was only found in six of the 14 control patients and generally at a lower expression level. In view of the regulatory and chemotactic properties of RANTES, these results imply that RANTES in MS lesions may play an important role in the activation and/or selective accumulation of memory T cells and, thereby, in the pathogenic events associated with MS.

Dr J. Hvas, Department of Medical Microbiology and Immunology, The Bartholin Building, University of Aarhus, Århus 8000C, Denmark

INTRODUCTION

Multiple sclerosis (MS) is an inflammatory disease of the central nervous system (CNS) characterized by localized myelin destruction [1–3]. While MS is thought to be the result of an autoimmune attack toward myelin proteins, the aetiology and pathogenesis of this disease remain largely unknown [1–3]. It is known that at the site of demyelination, the perivascular infiltrating cells consist predominantly of macrophages and CD4⁺ activated T cells secreting various cytokines [2–6]. Such activated T cells are thought to migrate from the peripheral lymphoid system to the CNS via the blood–brain barrier (BBB) [7, 8]. Some pro-inflammatory cytokines, such as tumour necrosis factor- α (TNF- α) and interferon- γ (IFN- γ), have been implicated

as important mediators of inflammation and demyelination in this disease [9, 10].

Chemokines are major regulatory proteins of leucocyte activation and recruitment in inflammation and immunity [11–13]. They are subdivided into two groups, C-X-C and C-C, depending on whether or not there is an intervening amino acid between the first two cysteines [12]. The chemokines of the C-X-C class, act mainly on neutrophils, whereas the C-C chemokines stimulate mononuclear cells with various degrees of specificity. RANTES (regulated upon activation, normal T-cell expressed and secreted) is a member of the C-C class, that may have important biological activities in inflammatory lesions, such as those seen in MS. Indeed, RANTES has been shown to be a chemotactic factor for monocytes, unstimulated as well as activated CD4⁺

T cells of the memory phenotype (CD45RO) that are of particular interest since they are known to accumulate at the sites of MS lesions [2, 14, 15]. Furthermore, RANTES expression has been observed in cultured T-cell lines that are antigen-specific and growth factor-dependent [16]. The cellular distribution of factors controlling the regulation of the RANTES gene has not yet been extensively characterized, but it is known that the production of RANTES is induced in endothelial cells by TNF- α , IFN- γ and inhibited by the T-helper 2-type cytokines interleukin-4 (IL-4) and IL-13 [17].

RANTES plays an important role in inflammatory recruitment leading to cell activation and directional migration of specific leucocyte subsets as well as contributing to the activation of integrin-mediated adhesion which allows the trans-endothelial migration of inflammatory cells [18]. It is noteworthy that *in situ* hybridization studies have revealed that RANTES mRNA is present in synovial lining cells of patients with rheumatoid arthritis [12, 19], in delayed-type hypersensitivity reaction [20] and that RANTES is involved in cell-mediated transplant rejection [21]. A recent study of RANTES expression in the murine animal model of MS, experimental autoimmune encephalomyelitis (EAE) showed induction of this chemokine in the spinal cord 1 to 2 days before the clinical signs were apparent [22]. In the present study we have analysed the expression of RANTES at the site of lesion in 26 brain samples from 17 MS patients. RANTES was detected in all samples analysed and co-localized to perivascular T cells, which makes RANTES a possible candidate in the pathogenesis of MS by selectively attracting CD45RO T cells and perhaps facilitating their entry into the CNS.

MATERIALS AND METHODS

Source of post-mortem tissue and blood samples. Post-mortem material (8–24 h old), stored at -80°C , was obtained from the Neuroimmunology Laboratory Tissue Bank, La Trobe University, Victoria, the Monash Medical Centre, Victoria, Australia and from the Rocky Mountain Multiple Sclerosis Centre, Englewood, CO, USA. Our tissue study included 17 patients with MS, all with clinically definite MS according to the criteria of Weiner & Ellison [23] with a mean age of 61 years (range 38–81). Control tissue samples were obtained from two groups of individuals. The first one referred to as neurology and infectious controls (NI) included one patient with Alzheimer's disease, one patient with epilepsy and one patient who died from septicæmia. The second group, referred to as other patient (OP) controls comprised 11 individuals who died of miscellaneous causes including three drug overdoses, three motor car accidents and one each, cardiac failure, abdominal haemorrhage, pulmonary thrombosis, atherosclerosis and non-defined with a mean age of 59 years (range 26–91). Two types of samples were tested, one, referred to as CNS tissue, included rapidly frozen or paraffin-embedded autopsy material from different brain regions; MS plaque lesions, parietal lobe, frontal lobe, temporal lobe, occipital lobe, cerebellum, meninges, brainstem, spinal cord as well as cerebrospinal fluid (CSF). The other samples, referred to as lymphoid tissue, were obtained from spleen and lymph node.

RNA isolation and cDNA synthesis. Total RNA was extracted from 0.1–1 g of tissue samples or from CSF (5–10 ml) according to the method of Chomczynski & Sacchi [24]. Total RNA (0.25 μg) was

reverse transcribed (RT) into first strand cDNA as previously reported [25]. To verify the quality of the RNA and/or efficiency of cDNA synthesis, a preliminary polymerase chain reaction (PCR) assay was performed on an aliquot of the cDNA sample using oligonucleotide primers specific for the ubiquitously expressed gene β -actin (Table 1). Occasionally, the RT efficiency was estimated by measuring $\alpha^{32}\text{P}$ -dCTP incorporation and found to be approximately 80%. To ensure both accuracy and reproducibility of the RT and PCR assay, large volumes of 'master' solutions, were initially prepared, aliquots taken and stored at -80°C until required. The template and enzyme were added prior to the experimentation.

PCR amplification. Five microlitres of cDNA was combined in a 50 μl reaction volume, with 2.5 U of Amplitaq (Perkin Elmer, Glen Waverley, Victoria, Australia), 5 μl of $10\times$ PCR buffer I (Perkin Elmer), and 0.5 μM of RANTES and β -actin-specific oligonucleotide primers (Table 1). Pairs of primers were chosen so that the amplified fragment spanned an intron, allowing any possible contamination of RNA with genomic DNA to be distinguished. The specificity of the primers for the PCR amplification was tested according to the procedure routinely in use in our laboratory, Southern hybridization and sequencing [25].

Pre-PCR mis-priming and primers creating dimers were inhibited by using the hot start method [26]. The standard PCR profile used was: denaturation at 94°C for 30 s, annealing at 64°C for 30 s and extension at 72°C for 45 s, for 22 cycles on a Perkin Elmer-Cetus 480 DNA Thermal Cycler using thin-walled tubes. For each RANTES experiment, a positive control using β -actin or TNF- α primers was included and a negative control, which contained all test reagents, except the cDNA, was set up in parallel. For comparison of mRNA levels among different RNA samples, RT and PCR were performed simultaneously using reagents from a single master mix. Each sample was tested on at least three separate occasions by PCR and Southern blotting.

Southern blot and computer imaging analysis. Ten microlitres of amplified PCR product was separated by gel electrophoresis, transferred onto Hybond N^{+} membranes (Amersham, Castle Hill, NSW, Australia). Membranes were prehybridized for 1–4 h in $5\times$ SSC, $1\times$ Denhardt's solution, 100 $\mu\text{g}/\text{ml}$ salmon sperm DNA, 0.1% SDS, and hybridized for 4–12 h at 60°C with 1 pmol/ml of a radioactive ^{32}P -labelled oligonucleotide probe specific for RANTES and/or β -actin (Table 1). Each membrane was autoradiographed on Kodak XAR-5 film for 1–5 days and/or a Phosphor Imager screen (Molecular Dynamics, Sunnyvale, CA, USA) for $\frac{1}{2}$ –1 day. An additional 2-week exposure generally failed to detect additional RANTES gene products. Filters probed in parallel with a horseradish peroxidase-labelled RANTES or β -actin probe (data not shown), gave a similar pattern of hybridization. Typically, several exposures were made for the same blot to ensure that band intensities were within an appropriate range for densitometric analysis. The quantification of RANTES was determined by computer imaging analysis of the RANTES intensity relative to the β -actin band intensity (Fig. 1). Southern blot results on membranes and/or on auto-radiograms (Fig. 2) were scanned using a Molecular Dynamics phosphor-imager or densitometer (Molecular Dynamics, Sunnyvale, CA, USA) according to the manufacturer's instructions.

Semi-quantitative RT-PCR. Semi-quantitative analyses of RANTES mRNA levels were performed according to our standardized protocol where all tests are performed within the exponential range of the PCR reaction and are reproducible. In short, the technique has been shown suitable to compare the relative levels of RANTES gene expression in human tissue samples and can detect a minimum of a fourfold difference in mRNA levels between two RNA samples derived from equal amounts of total RNA (data not shown). Since PCR products will only reflect the

Table 1. RANTES, β -actin and TNF- α primers used for PCR in this study^a

Sequences	
Primers	
RANTES L ^b	5'-CCA TAT TCC TCG GAC ACC ACA CCC TGC T-3'
RANTES R	5'-CAT CTC CAA AGA GTT GAT GTA CTC CCG A-3'
β -actin L ^c	5'-GGT GAT GAC CTG GCC GTC AGG CAG CTC GTA-3'
β -actin R	5'-AAC CCC AAG GCC AAC CGC GAG AAG ATG ACC-3'
TNF- α L ^d	5'-CAG AGG GAA GAG TT CCC AG-3'
TNF- α R	5'-CCT TGG TCT GGT AGG AGA CG-3'
Probes	
RANTES	5'-CTA CAC CAG TGG CAA GTG CTC CAA CCC AGC-3'
β -actin	5'-GCC CTG GAC TTC GAG CAA GAG ATG GCC ACG-3'
TNF- α	5'-TTA TCT CTC AGC TCC-3'

^a PCR amplification with the RANTES, TNF- α or β -actin primers, gave fragments of, respectively, 198, 330 and 417 base pair.

^b The RANTES primers and probes were designed from the RANTES cDNA sequence, Genbank acc. no. M21121 [16]. RANTES L is localized on the cDNA sequence at position 99–123 (exon 1 and 2 boundary), RANTES R at 279–303 (exon 3) and RANTES probe at 179–197 (exon 2).

^c The TNF- α primers and probes were from the human TNF- α cDNA sequence Genbank acc. no. X01394. TNF- α L match position 327–346 in the signal peptide and TNF- α R match position 632–651 in exon 4 and TNF probe match position 503–517 in exon 3 [41].

^d The β -actin primers and probes were designed from the β -actin cDNA Genbank sequence M10277 [42]. Primer positions on the spliced cDNA are β -actin L 307–324 (exon 2), β -actin R 724–741 (exon 3) and the β -actin probe 685–702 (exon 3).

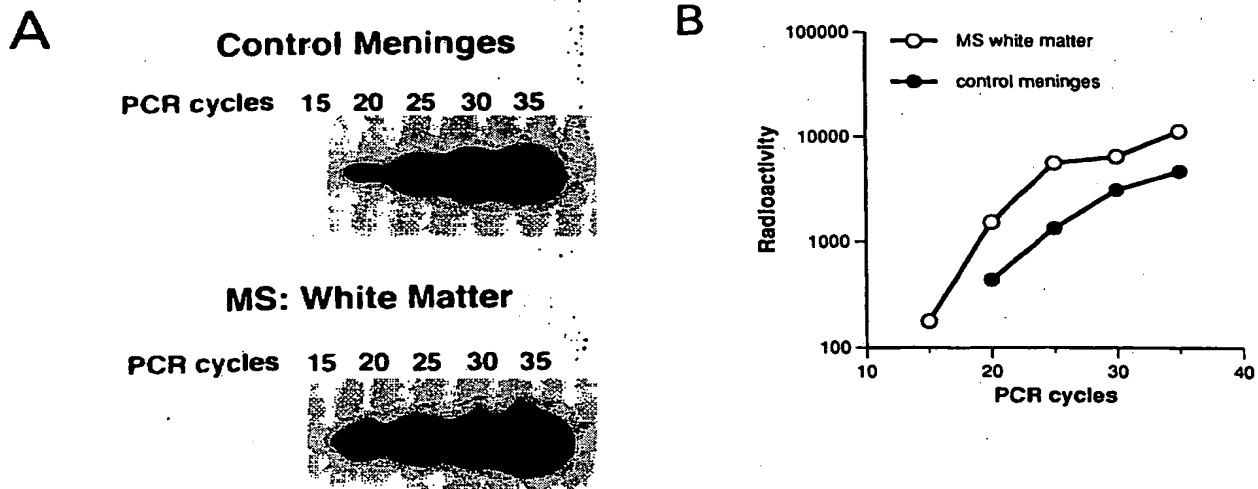


Fig. 1. Relation between number of PCR cycles and rate of RANTES amplification. (A) Phosphorimager photographs of filter with 25 ng total RNA from MS white matter or control meninges that were reverse transcribed and amplified between 15 and 35 cycles of PCR using RANTES primer. (B) Schematic representation of scanning data from A, above, showing that at 22 cycles of PCR, both analysed samples are within the exponential phase (units in counts).

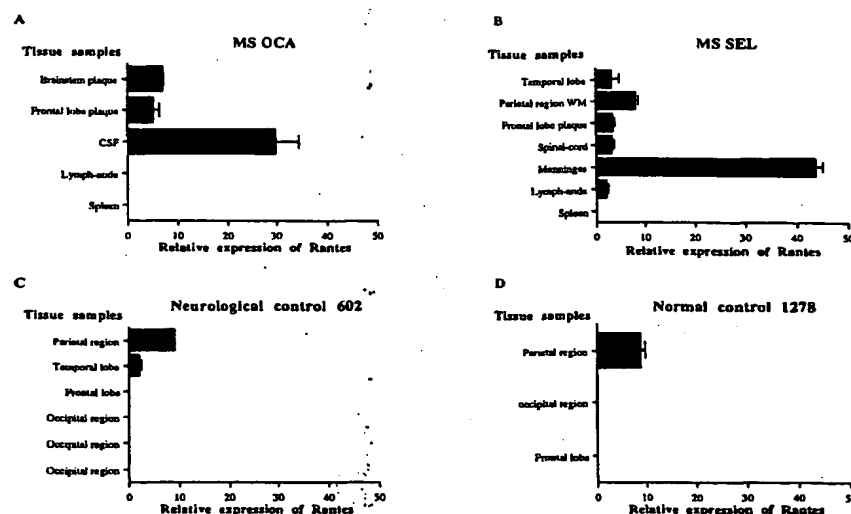


Fig. 2. Comparison of RANTES mRNA expression in different samples from MS patients and controls. The relative amount of RANTES PCR product obtained from the different samples was distinguished by size, processed by Southern blot analysis and quantified by scanning densitometry of autoradiograms. Each bar represents the mean of at least three experiments \pm SEM. (A) Five CNS and two lymphoid samples from one MS patient; (B) three CNS and two lymphoid samples from a MS patient; (C) six different brain samples from a neurological control with epilepsy; (D) three samples from a normal control, who died from a heroin overdose.

relative level of mRNA when other experimental variables, such as efficiency of RT, amplification, etc., are equalized, each experiment was designed and performed in such a way that the different samples to be compared were RT and amplified at the same time using aliquots of reagent from the same master mix. In order to quantify the RANTES mRNA expression, the amount of radioactivity on the filters or the density of bands on the autoradiogram was plotted against the template concentration and/or the number of PCR cycles to select reaction conditions within the exponential phase that are linear (Fig. 1). The relative value of RANTES expression was calculated from the phosphorimager scanning value of RANTES divided by the value of β -actin from the same experiment and lane on the scanned filter and multiplied by 100 to give relative percentages. The means were calculated by adding up values from several experiments and dividing the sum by the number of experiments.

In situ hybridization. *In situ* hybridization on formalin-fixed, paraffin-embedded tissues of cerebrum, cerebellum and brainstem was performed as described by Coghlan *et al.* [27], using oligonucleotide probes labelled with [35 S]dATP. Multiple sections from the different area of two MS and two control brains were analysed. Briefly, 25 pmol of oligonucleotide probe was end-labelled with 25 μ Ci [35 S]dATP (Du pont, North Ryde, NSW, Australia) using 25 units of terminal transferase (Boehringer Mannheim, Castle Hill, NSW, Australia) in 20 μ l of the manufacturer's reaction buffer, 6.25 mM CoCl_2 , then incubated at 37°C for 1 h. Then, 3.3 μ Ci of labelled probe in 100 μ l hybridization buffer was added to each tissue section analysed, and incubated overnight at 37°C with coverslips. Control-sense, non-sense, and positive anti-sense oligonucleotides were used. The sequence of the RANTES and TNF- α anti-sense probes is shown as TNF- α R and RANTES R primers in Table 1. Sections were stained with haematoxylin and eosin. Routinely, duplicate sections were made and one set was developed after 1 week and the second after 2–6 weeks.

Immunohistochemistry. Formalin-fixed, paraffin-embedded tissues of cerebrum, cerebellum and brainstem were cut at 4 μ m thickness and immunostained with DAKO antibodies to UCHL1 (clone CD45RO), CD68, L26 (clone CD20) (Dako Corporation, Carpinteria, CA, USA) and glial fibrillar acidic protein (GFAP) (Dako Corporation) according to the manufacturer's guidelines. Parallel sections were also stained with haematoxylin, eosin and Luxol fast blue.

RESULTS

RANTES expression in MS brains

Preliminary ELISA analysis of sera from MS patients, showed more than double the amount of RANTES compared to healthy, normal donor sera. (mean 120 ng/ml, range 50–210 ng/ml, $n = 16$) (data not shown). To determine whether the chemokine RANTES mRNA was specifically expressed in MS patients at the site of lesions, we performed PCR analysis on brain samples obtained from 17 MS patients, from 11 OP controls and three NI patients (Table 2). RANTES mRNA was detected in all the 26 samples obtained from the MS patients. In contrast such transcripts could only be detected in four out of the 18 samples (22%) of the OP control and in five out of the 12 (42%) brain samples from the NI controls group (an epilepsy, an Alzheimer's disease and a septicemia patient) (Table 2). Of these five positive samples from the NI group, two were from the patient that died from septicemia and two were from the patient with epilepsy. All four samples known to contain T cells [25, 28].

Having demonstrated that RANTES mRNA could not only be detected in MS brain, but also in some control brain samples, we

Table 2. Relative expression of RANTES mRNA

Brain tissues	Mean ^a (%) \pm SEM
MS	
WM ^b	66.3 \pm 0.1
WM	53.4 \pm 1.0
Meninges	43.5 \pm 1.5
WM	20.0 \pm 3.4
WM	18.3 \pm 0.0
Occipital	16.3 \pm 1.3
WM	10.6 \pm 0.3
WM Cerebellum	10.6 \pm 0.6
WM	9.5 \pm 0.5
WM Parietal	8.2 \pm 0.4
WM Brainstem plaque	7.1 \pm 0.1
WM	7.1 \pm 0.8
WM plaque	6.0 \pm 1.0
Parietal	5.4 \pm 0.3
Frontal plaque	5.3 \pm 1.1
Spinal cord	5.0 \pm 0.9
Frontal plaque	3.5 \pm 0.3
Occipital	3.5 \pm 0.9
Spinal cord	3.3 \pm 0.5
Frontal lobe	3.1 \pm 0.0
Temporal lobe	
WM	2.8 \pm 0.2
Spinal cord	2.1 \pm 0.0
Temporal lobe plaque	1.3 \pm 0.2
Grey matter	1.3 \pm 0.6
Plaque (old)	0.6 \pm 0.0
Neurological and infectious controls	
EPI	
Parietal	9.1 \pm 0.1
Occipital	0.0 \pm 0.0
Occipital	0.0 \pm 0.0
Occipital	0.0 \pm 0.0
Temporal	2.1 \pm 0.3
Frontal	0.0 \pm 0.0
ALZ	
Frontal	0.0 \pm 0.0
Brainstem	0.0 \pm 0.0
Cerebellum	6.5 \pm 1.4
Occipital	0.0 \pm 0.0
SEP	
WM	7.4 \pm 1.1
Meninges	2.5 \pm 0.5
Other patient controls	
Parietal	8.9 \pm 1.0
Temporal	4.6 \pm 0.5
Temporal	4.5 \pm 0.1
Parietal	4.1 \pm 0.7
Frontal	0.0 \pm 0.0
Parietal	0.0 \pm 0.0
Frontal	0.0 \pm 0.0
Temporal	0.0 \pm 0.0
Occipital	0.0 \pm 0.0
Parietal	0.0 \pm 0.0

Table 2. Continued

Brain tissues	Mean ^a (%) \pm SEM
Parietal	0.0 \pm 0.0
WM	0.0 \pm 0.0
Occipital	0.0 \pm 0.0
Frontal	0.0 \pm 0.0
WM	0.0 \pm 0.0
WM frontal	0.0 \pm 0.0
Occipital	0.0 \pm 0.0
Occipital	0.0 \pm 0.0

^a Mean of RANTES mRNA relative to β -actin, of at least three experiments.

^b WM, white matter.

next examined if the level of RANTES mRNA expression, was higher in MS than in control subjects. As a prelude for these studies we first assessed the validity of our PCR method to quantitatively measure the level of RANTES mRNA in a variety of samples. For this we asked whether: first, the quantification is affected by the number of PCR cycles; second, if the quantification is linear with respect to the amount of mRNA present; and finally, if the method is reproducible. As shown in Fig. 1, 22 cycles of PCR with 25 ng total RNA were found to be optimal to fulfil this set of criteria for RANTES and β -actin (data not shown). Using such experimental conditions, a higher expression of RANTES mRNA in this MS white matter was found as compared to that in a control meninges as exemplified in Fig. 1. Levels of RANTES mRNA expression fluctuated within, as well as between, MS and control patients (Table 2). Among the 26 MS brain samples examined, the expression of RANTES mRNA relative to β -actin expression range from 0.6% to 66.3%, with a mean of 13.8% (Table 3). This is in contrast to the results obtained with the two control groups where the maximum relative levels were 9.1% (mean 2.4%) and 8.9% (mean 1.1%) for the NI and other patient controls, respectively (Table 3).

Relative expression of RANTES mRNA in different MS brain regions

In order to determine whether the large variation in levels of RANTES mRNA observed between patients could be due to the type of brain tissue examined, we assessed the level of RANTES mRNA in different regions of the brains as well as different plaques sampled from the same patients (Fig. 2). When possible, the expression of RANTES in different brain regions was also compared to that of the corresponding CSF and/or lymphoid tissues (Fig. 2). As illustrated in Fig. 2A and B, no clear association could be found between the level of RANTES expression and the type of brain tissue sampled. For example, in the MS patient OCA (Fig. 2A) the highest expression of RANTES was found in the CSF, while the two plaques only

Table 3. Relative expression of RANTES mRNA in brain and lymphoid tissues^a

Tissue	MS ^b		NI controls ^c		OP controls ^d	
	CNS	Lymphoid	CNS	Lymphoid	CNS	Lymphoid
Maximum	63.3%	2.6%	9.1%	20.8%	9.9%	0%
Minimum	0.6%	0%	0%	0%	0%	0%
Mean \pm SEM	13.8% \pm 15.8	0.5% \pm 0.9	2.4% \pm 3.3	10.1% \pm 11	1.1% \pm 2.5	0%

^aRANTES mRNA expression in % relative to the expression of β -actin.^bThe data are based on 26 CNS and 12 lymphoid samples from 17 MS patients.^cNI (neurological and infectious) controls included: Alzheimer's disease (1), epilepsy (1) and septicaemia (1), where the CNS and lymphoid data were based on 30 and six samples, respectively.^dThe data from OP (Other patient) controls were based on 51 CNS and six lymphoid samples from 11 patients (Table 2).

showed moderate levels of this chemokine, with no detectable transcripts in lymph nodes and spleen (Fig. 2A).

While differences were observed when multiple areas of the same MS brain were analysed, no correlation with the expression levels of RANTES mRNA could be made on the basis of sex, duration of disease, or the region of brain analysed. In the OP and NI control groups, the expression level of RANTES was generally low and only localized in limited areas of the brain (Fig. 2C & D).

Localization of RANTES in MS brain

Having demonstrated that RANTES can be consistently detected in different regions of the MS brains, we next tried to determine, using immunohistochemistry and *in situ* hybridization, if RANTES expression was associated with a specific cell type within the inflammatory lesion (Fig. 3). For this, we analysed multiple brain samples from two MS patients and two controls. Both controls brains did not show RANTES expression in any of the analysed areas and one of the MS patients, a long-term chronic case of MS, showed a very low RANTES expression in one plaque (data not shown). In contrast a MS patient, who died from chronic progressive MS 2 years after diagnosis and where the routine immunohistochemistry indicated the presence of multiple plaques throughout the cerebrum, cerebellum and brainstem, showed RANTES expression in several plaques (Fig. 3A & B). The age of the plaques varied, as indicated by the macrophage and astrocyte activity. Several of the plaques showed active demyelination, as confirmed by the loss of Luxol fast blue staining, and the presence of plump macrophages immunostaining with CD68 containing myelin debris and reactive astrocytes immunostaining with GFAP (data not shown). Prominent perivascular T cells of the CD45RO subtype were present in these active plaques, as determined by staining with UCHL1 (Fig. 3E). Only occasional perivascular B cells immunostained with L26 were seen (data not shown). Within some chronic plaques, an active edge was apparent, which by *in situ* hybridization showed macrophage expression of TNF- α as found in all non-chronic

plaques (data not shown). Chronic plaques showed well demarcated areas of demyelination with few, if any, residual macrophages or astrocytes and replacement gliosis. Perivascular CD45RO T cells were still present but not as prominent as in the more active areas (Fig. 3F). *In situ* hybridization with [³⁵S]dATP labelled RANTES oligoprobes (Table 1) revealed that RANTES mRNA localization was within perivascular T cells (Fig. 3A & B). This appeared more prominent at the active edge of the plaque than within chronic areas (Fig. 3A & B).

DISCUSSION

In this study we describe, for the first time, the presence of RANTES mRNA in MS brains.

RANTES is a potent chemoattractant, especially to activated T-helper cells of the memory type which are believed to play a crucial role in both MS and in EAE, the animal model of MS [2, 29, 30]. Other chemokines are found to be up-regulated in wound healing [31], atherosclerosis [32] and rheumatoid arthritis [33], while RANTES is more likely to be involved in chronic inflammation or allergic late-phase reaction [34, 35].

RANTES was detected in all the 26 brain samples analysed by PCR from 17 MS patients. Quantitative RT-PCR was used in the present study to examine levels of mRNA coding for RANTES in various tissue samples. The expression levels of RANTES mRNA in MS brain were significantly higher than in controls, in some white matter samples (Table 3). On the basis of the results presented in Table 2, it would appear that the expression of RANTES in MS brain samples can be arbitrarily grouped into three levels; High expression (30–40%), more frequently found in some white matter samples; medium expression (\approx 10%), observed in most plaque and white matter samples; and low expression (\approx 5%), seen in other brain or spinal cord samples. All samples used in the PCR analyses had been characterized macroscopically and thus small plaques may have, occasionally, gone undetected. This might explain the relative high expression in some white matter samples with no visible plaques. Indeed, our *in-situ* study showed that the RANTES mRNA is mainly

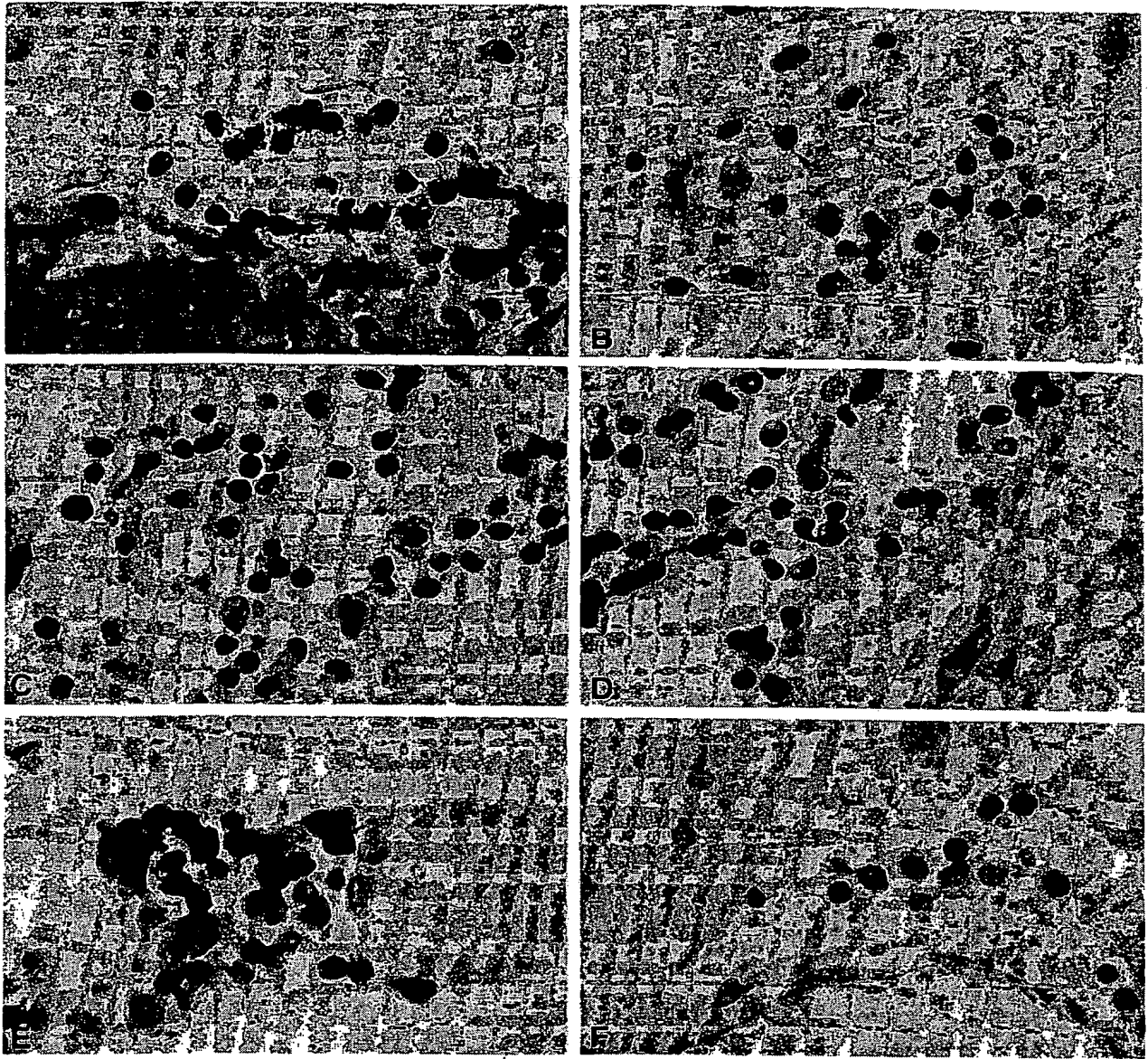


Fig. 3. Prominent RANTES mRNA expression in perivascular lymphocytes in the active lesions of a MS brain. (A–D) *In situ* hybridization with [³⁵S]dATP-labeled RANTES mRNA oligo probes in MS brain. (A) Active edge of a MS plaque; (B) old plaque area, gliotic, inactive, periventricular area of a MS plaque; (C,D) negative controls using sense RANTES probes on active and inactive MS plaques, respectively; (E,F) immunostaining with CD45RO, clone UCHL1, of active new areas of plaque and older areas with gliosis, respectively (areas are the same as above). Counterstaining with haematoxylin and in (A)–(D) also eosin; magnification $\times 1000$.

expressed at the edge of active plaques (Fig. 3). Studying the expression of RANTES mRNA by *in situ* hybridization not only confirmed our PCR findings, but also demonstrated the relative low frequency of RANTES-transcribing cells in the brain, all of which have the phenotype of T cells. Preliminary *in situ* hybridization data of RANTES mRNA in MS brain by Woodroffe *et al.* gave a similar expression pattern [36]. In addition, our

preliminary data showed that another C-C chemokine macrophage inflammatory protein (MIP)-1 α was also predominantly expressed at the active plaque edge but strictly by endothelial cells (data not shown).

Since this *in situ* hybridization technique is not as sensitive as PCR it was not possible to detect any RANTES expression in the two control brains analysed. The reason for the expression of

RANTES mRNA in the control brains is not clear, but could perhaps be the result of a general inflammation or infection as indicated by relatively high levels of RANTES expression in the lymphoid tissues of such patients. However, low levels of RANTES have been detected in normal human peripheral blood lymphocytes and are known to be involved in activation and trafficking of lymphocytes [15, 37].

An important question raised by our findings is whether or not RANTES is directly involved in the demyelinating process, or merely recruits non-myelin-specific T cells, trafficking into the CNS, as a consequence of BBB breakdown. During an acute attack of MS, the predominant pattern of cytokine secretion resembles that of T-helper 1 cells (i.e. IFN- γ and TNF- α) [38]. IFN- γ stimulates RANTES gene expression in macrophages [19], whereas TNF- α stimulates RANTES gene expression in fibroblasts, mesangial cells, and renal epithelial cells [17, 19, 39]. Our co-localization of RANTES mRNA with TNF- α and MIP-1 α in mainly active plaques in serial sections, together with the general expression of RANTES mRNA in MS brains, would suggest that RANTES participates in the attraction of appropriate autoreactive T-cell subsets into the lesion. In this context, it is particularly relevant to note that a recent analysis of human T-cell migration in a chimeric severe combined immunodeficiency disease (SCID) mouse model reconstituted with human T cells revealed RANTES induced T-cell infiltration into sites of RANTES injection [15, 40]. In addition, evidence that RANTES plays an important role in CNS inflammation has recently been demonstrated in mice with EAE [22]. In this study, aimed at defining the profile of chemokines and their respective role in the inflammatory process occurring during EAE, it was shown that RANTES mRNA was elevated just before the onset of clinical signs of paralysis and reaches a maximum level at the peak of the clinical symptoms. This suggests that RANTES is able to recruit the specific leucocytes needed for disease expression.

In view of the extraordinary ability of RANTES to attract specific T-cell subsets, this molecule may have an important role in conditions where T cells predominate, such as in autoimmune diseases, certain neoplasms, and chronic inflammatory conditions. Indeed, if the actions of the RANTES cytokines *in vivo* mirror those exhibited *in vitro*, they may mediate essential processes in lymphocyte trafficking through their ability to target distinct subsets of immune effector cells. As we learn more about the expression of RANTES and other chemokines in early and late stages of this disease, it should become possible to design appropriate forms of intervention, including therapy by implantation of chemokine genes. Furthermore, investigation of these molecules and their properties could provide key insights into basic immune function and lead to advances in the clinical manipulation of autoimmune disorders, cancer, atherosclerosis, acquired immune deficiency syndrome and chronic inflammation.

ACKNOWLEDGMENTS

The authors wish to express their appreciation to Mrs Roslyn Clark and cand. scient. Mette Munch for expert assistance and

advice, and Dr Ronald S. Murray, Rocky Mountain MS Centre, Englewood, CO for providing some MS samples. Jonna Hvas was a recipient of a Fellowship from the Danish Medical Research Council.

REFERENCES

- Bernard CCA, Carnegie PR, Mackay IR. Immunoregulatory mechanisms in experimental autoimmune encephalomyelitis and multiple sclerosis. In: Adams CWM, Tourtellotte WW, Hallpike JF. eds. *Multiple Sclerosis*. London: Chapman & Hall, 1983;479–511.
- Raine CS. Multiple sclerosis: a pivotal role for the T cell in lesion development. *Neuropathol Appl Neurobiol* 1991;17:265–74.
- Bernard CCA, Kerlero de Rosbo N. Multiple sclerosis: an autoimmune disease of multifactorial etiology. *Curr Opin Immunol* 1992;4:760–5.
- Prineas JW. The neuropathology of multiple sclerosis. *Handbook Clin Neurol* 1985;3:213–56.
- McFarlin DE, McFarland HF. Multiple sclerosis. *N Engl J Med* 1982;307:1183–8.
- Traugott U, Reinherz EL, Raine CS. Multiple sclerosis distribution of T cells, T cell subsets and Ia positive macrophages in lesions of different ages. *J Neuroimmunol* 1983;4:201–21.
- Sobel RA, Hafler DA, Castro EE, Morimoto C, Weiner HL. The 2H4 (CD45R) antigen is selectively decreased in multiple sclerosis lesions. *J Immunol* 1988;140:2210–14.
- Hafler DA, Duby AD, Lee SJ *et al.* Oligoclonal T lymphocytes in the cerebrospinal fluid of patients with multiple sclerosis. *J Exp Med* 1988;167:1313–22.
- Olsson T, Zhi WW, Hojberg B *et al.* Autoreactive T lymphocytes secretion of interferon- γ . *J Clin Invest* 1990;86:981–5.
- Selmaj K, Cross AH, Farooq M, Brosnan CF, Raine CS. Non-specific oligodendrocyte cytotoxicity mediated by soluble products of activated T cell lines. *J Neuroimmunol* 1991;35:261–4.
- Lloyd AR, Oppenheim JJ, Kelvin DJ, Taub DD. Chemokines regulate T cell adherence to recombinant adhesion molecules and extracellular matrix proteins. *J Immunol* 1996;156:932–8.
- Schall TJ. Biology of the RANTES/Sis cytokine family. *Cytokine* 1991;3:165–83.
- Kunkel SL, Strieter RM, Lindley IJD, Westwick J. Chemokines: new ligands, receptors and activities. *Immunol Today* 1995;16:559–61.
- Schall TJ, Bacon K, Toy KJ, Goeddel DV. Selective attraction of monocytes and T lymphocytes of the memory phenotype by cytokine RANTES. *Nature* 1990;347:669–71.
- Murphy WJ, Tian Z, Asai O. Chemokines and T lymphocyte activation. II. Facilitation of human T cell trafficking in severe combined immunodeficiency mice. *J Immunol* 1996;156:2104–11.
- Schall TJ, Jongstra J, Dyer BJ *et al.* A human T cell-specific molecule is a member of a new gene family. *J Immunol* 1988;141:1018–25.
- Marfaing-Koka A, Devergne O, Gorgone G *et al.* Regulation of the production of the RANTES chemokine by endothelial cells. *J Immunol* 1995;154:1870–8.
- Roth SJ, Carr MW, Springer TA. C-C chemokines, but not the C-X-C chemokines interleukin-8 and interferon- γ inducible protein 10, stimulate transendothelial chemotaxis of T lymphocytes. *Eur J Immunol* 1995;25:3482–8.
- Rathanaswami P, Hachicha M, Sadick M *et al.* Expression of the

- cytokine RANTES in human rheumatoid synovial fibroblasts. *J Biol Chem* 1993;268:5834-9.
- 20 Devergne O, Marfaing-Koka A, Schall TJ *et al*. Production of the RANTES chemokine in delayed-type hypersensitivity reaction: involvement of macrophages and endothelial cells. *J Exp Med* 1994;179:1689-94.
- 21 Kondo T, Norvick AC, Toma H, Fairchild RL. Induction of chemokines gene expression during allogeneic skin graft rejection. *Transplantation* 1996;61:1750-7.
- 22 Godiska R, Chantry D, Dietsch GN, Gray PW. Chemokine expression in murine experimental allergic encephalomyelitis. *J Neuroimmunol* 1995;58:167-76.
- 23 Weiner HL, Ellison GW. A working protocol to be used as a guideline for trials in multiple sclerosis. *Arch Neurol* 1983; 40:704-70.
- 24 Chomczynski P, Sacchi N. Single-step methods of RNA isolation by acid guanidinium thiocyanate-phenol-chloroform extraction. *Anal Biochem* 1987;162:156-9.
- 25 Hvas J, Oksenberg JR, Fernando R, Steinman L, Bernard CCA. $\gamma\delta$ T cell receptor repertoire in brain lesions of patients with multiple sclerosis. *J Neuroimmunol* 1993;46:225-34.
- 26 Chou Q, Russell M, Birch DE *et al*. Prevention of pre-PCR mispriming and primer dimerization improves low-copy-number amplifications. *Nucleic Acids Res* 1992;20:1717-23.
- 27 Coghlan JP, Aldred P, Harolambitis J *et al*. Hybridisation, histochemistry. *Anal Biochem* 1985;149:1-28.
- 28 Oksenberg JR, Stuart S, Begovich AB *et al*. Limited heterogeneity of rearranged T cell receptor $V\alpha$ transcripts in brain of multiple sclerosis patients. *Nature* 1990;345:344-6.
- 29 Eoli MM, Ferrarini M, Dufour A *et al*. Presence of T-cell subset abnormalities in newly diagnosed cases of multiple sclerosis and relationship with short-term clinical activity. *J Neurol* 1993;240:79-84.
- 30 Baggiolini M, Dahinden CA. CC chemokines in allergic inflammation. *Immunol Today* 1994;15:127-33.
- 31 Fahey TJ, Sherry B, Tracey KJ *et al*. Cytokine production in a model of wound healing: the appearance of MIP-1, MIP-2, cachectin/TNF and IL-1. *Cytokine* 1992;2:92-9.
- 32 Yla-Herttuala S, Lipton B, Rosenfeld M *et al*. Expression of MCP-1 in macrophage-rich areas of human and rabbit atherosclerotic lesions. *Proc Natl Acad Sci USA* 1991;88:5252-7.
- 33 Villiger PM, Terkeltaub R, Lotz M. Monocyte chemoattractant Protein-1 (MCP-1) expression in human articular cartilage. *J Clin Invest* 1992;90:488-96.
- 34 Charlesworth EN, Hood AF, Soter NA *et al*. Cutaneous late-phase response to allergen. *J Clin Invest* 1989;83:1519-26.
- 35 Frew AJ, Kay AB. UCHL1⁺ (CD45RO⁺) 'memory' T-cells predominate in the CD4⁺ cellular infiltrate associated with allergen-induced late-phase skin reactions in atopic subjects. *Clin Exp Immunol* 1991;84:270-4.
- 36 Woodroffe MN, Loughlin AJ, Newcombe J, Cuzner ML. Detection of cytokine expression in the central nervous system in multiple sclerosis. *Multiple Sclerosis* 1996;2:5-6.
- 37 Conlon K, Lloyd A, Chattopadhyay U *et al*. CD8⁺ and CD45RA⁺ human peripheral blood lymphocytes are potent sources of macrophage inflammatory protein 1 α , interleukin-8 and RANTES. *Eur J Immunol* 1995;25:751-6.
- 38 Correale J, Gilmore W, McMillan M *et al*. Patterns of cytokine secretion by autoreactive proteolipid protein-specific T cell clones during the course of multiple sclerosis. *J Immunol* 1995;154:2959-65.
- 39 Heeger P, Wolf G, Meyers C *et al*. Isolation and characterisation of cDNA from renal tubular epithelium encoding RANTES. *Kidney Int* 1992;41:220-4.
- 40 Taub DD, Conlon K, Lloyd AR *et al*. Preferential migration of activated CD4⁺ and CD8⁺ T cells in response to MIP-1 α and MIP-1 β . *Science* 1993;260:355-8.
- 41 Pennica D, Nedwin GE, Hayflick JS *et al*. Human tumor necrosis factor: precursor structure, expression and homology to lymphotoxin. *Nature* 1984;312:724-9.
- 42 Nakajima-Iijima S, Hamada H, Reddy P, Kakunaga T. Molecular structure of the human cytoplasmic b-Actin gene: interspecies homology of sequences in the introns. *Proc Natl Acad Sci USA* 1985;82:6133-7.

Macrophages in T cell line-mediated, demyelinating, and chronic relapsing experimental autoimmune encephalomyelitis in Lewis rats

I. HUITINGA, S. R. RUULS, S. JUNG*, N. VAN ROOIJEN, H.-P. HARTUNG* & C. D. DIJKSTRA

Department of Cell Biology and Immunology, Faculty of Medicine, Vrije Universiteit, Amsterdam, The Netherlands and

**Department of Neurology, Julius-Maximilians Universität, Würzburg, Germany*

(Accepted for publication 28 December 1994)

SUMMARY

About 50% of the mononuclear cells in the perivascular lesions in the central nervous system (CNS) of rats suffering from experimental allergic encephalomyelitis (EAE) are blood-borne macrophages. In this study we investigated the role of these macrophages in different variants of EAE, using a liposome-mediated macrophage depletion technique. Intravenously injected liposomes containing dichloromethylene diphosphonate (Cl_2MDP) are ingested by macrophages and cause temporary and selective elimination of these cells. Macrophage depletion during EAE induced by a T cell line specific for myelin basic protein (MBP; T cell-EAE) suppresses development of neurological signs of EAE. T cell-EAE with pronounced demyelination as induced by an additionally injected MoAb directed against myelin oligodendrocyte glycoprotein (MOG) was also significantly ameliorated after macrophage depletion. During chronic relapsing EAE (CR-EAE) the occurrence of relapses was prevented or suppressed, provided that the liposomes were injected before the initiation of a putative relapse. A chronic progressive course of CR-EAE was not modified by Cl_2MDP containing liposome treatment. Histologic examination of the CNS of liposome-treated animals confirmed decreased infiltration of macrophages into the parenchyma in the rats with T cell and AD-EAE, whereas T cells were still present.

Keywords experimental allergic encephalomyelitis macrophage dichloromethylene diphosphonate liposomes demyelination

INTRODUCTION

Experimental allergic encephalomyelitis (EAE) is an experimental autoimmune inflammatory condition of the central nervous system (CNS) that serves as a disease model for multiple sclerosis (MS) [1]. Adoptive transfer studies established the importance of T lymphocytes in the generation of clinical EAE [2,3]. However, during the effector phase of the disease, encephalitogenic T cells recruit blood-borne macrophages into the lesion sites [4]. Also active plaques of MS are characterized by impressive numbers of macrophages that are mainly located in areas of ongoing demyelination (mean ratio T cells: macrophages = 23:527) [5].

Proinflammatory effector molecules secreted by macrophages can open the blood-brain barrier, attract and activate other immune competent cells, and damage myelin [6]. In addition, macrophages are considered to be important in CR3- and Fc receptor-mediated phagocytosis of myelin [7,8].

Correspondence: Inge Huitinga, Dept. of Cell Biology and Immunology, Faculty of Medicine, Vrije Universiteit, Van der Boechorststraat 7, 1081 BT Amsterdam, The Netherlands.

Therefore, modulation of the activities of macrophages that invade the CNS during EAE and MS could offer an interesting approach to reducing tissue damage and demyelination.

In a previous study we have shown that depletion of macrophages using dichloromethylene diphosphonate (Cl_2MDP) encapsulated in liposomes suppresses actively induced acute EAE (A-EAE) almost completely [9]. Cl_2MDP -containing liposomes are ingested by macrophages, and high concentrations of intracellularly released Cl_2MDP kill the cell [10]. Free circulating Cl_2MDP is not toxic and has a half-life in the order of minutes [11]. Cl_2MDP -containing liposomes cause transient and selective elimination of macrophages in the spleen and the liver and of monocytes in the circulation [10,12,13]. Therefore, the previously reported suppression of A-EAE after macrophage depletion might also be due to interference with peripherally located macrophages which presumably have an initiating role in antigen processing and presentation to T cells, rather than to interference with macrophages as effector cells in the CNS. To bypass this problem we now depleted macrophages during EAE induced by myelin basic protein (MBP)-specific T cells (T cell-EAE) [14].

Although limited demyelination occurs during A-EAE and T cell-EAE [15], clinical signs during this acute and monophasic form of EAE are mainly attributed to oedema [16,17]. To study the role of macrophages in demyelination in EAE, we eliminated macrophages during a hyperacute demyelinating form of T cell-EAE as induced by injection of MBP-specific T cells followed by a MoAb directed against myelin oligodendrocyte glycoprotein (MOG) (AD-EAE) [18,19].

Furthermore, to mimic the situation of MS more closely, the role of macrophages in the generation of clinical relapses during low dose cyclosporin A (CsA)-induced chronic relapsing remitting EAE (CR-EAE) was studied [20]. The clinical course of CR-EAE closely resembles that of MS. The pathological findings in the brain and spinal cord of rats with CR-EAE, for example, the composition of the perivascular mononuclear cell infiltrates and the extensive demyelination [21], are also similar to those found in MS [20].

MATERIALS AND METHODS

Animals

Male Lewis rats were obtained from the Zentralinstitut für Versuchstierzucht (Hannover, Germany), and kept under standard laboratory conditions, with water and food available *ad libitum*. The animals weighed approximately 200 g at the time of EAE induction. Experiments were carried out with the approval of the responsible Bavarian government authorities.

Induction of EAE

T cell-EAE. An MBP-specific T cell line was derived from the popliteal lymph nodes of a Lewis rat immunized with guinea pig MBP in Freund's complete adjuvant (FCA) into the hind foot pad 10 days before, and established as described for a P₂-specific T cell line [14]. Before transfer T line cells were activated as follows: 3×10^5 /ml T cells were incubated with 1.5×10^7 /ml freshly isolated irradiated (30 Gy) syngeneic thymocytes as antigen-presenting cells in the presence of guinea pig MBP (20 µg/ml). After 72 h activated T cell blasts were isolated by centrifugation on Ficoll (Nyegaard & Co, Oslo, Norway) gradients. Blasts from the interface were washed twice. EAE was transferred to naive Lewis rats by injection of 4×10^6 MBP-specific T blast cells in 1 ml 0.9% NaCl into the tail vein.

AD-EAE. T cell-EAE was induced as described above. Anti-MOG MoAb was synthesized by the hybridoma cell line 8-18C5, and was produced and purified as described [18,19]. The MoAb was injected intraperitoneally on day 3 after the injection of encephalitogenic T cells in a volume of 1 ml PBS at a dose of 25 mg/kg body weight.

CR-EAE. Rats were actively immunized by a single subcutaneous injection of 80 µl guinea pig spinal cord (GPSC) emulsion in one hind foot pad. This emulsion consisted of the following ratio of components: 1 g GPSC homogenized in 1 ml saline, to which 10 mg *Mycobacterium tuberculosis* H37 RA (Difco Labs, Detroit, MI) in 1 ml FCA (Difco) were added. A chronic relapsing remitting course of the disease was induced by subcutaneous low dose injections of CsA (Sandoz, Uden, The Netherlands; 2 mg/kg bodyweight) on alternate days from day 0 until day 22 after immunization [20].

Clinical assessment

Rats were weighed and examined daily for the development of neurological signs. Clinical signs of T cell-EAE and AD-EAE were scored on a scale from 0 to 5: 0, no clinical signs; 1, loss of tip-of-tail reflex, or complete loss of tail tonus and unsteady gait; 2, paresis of the hind legs; 3, complete paralysis of the hind legs; 4, paralysis of the complete lower part of the body; 5, death due to EAE. Clinical signs of CR-EAE were scored on a scale ranging from 0 to 11: 0, no clinical signs; 1, partial loss of tail tonus; 2, complete loss of tail tonus; 3, weakness of hind limbs; 4, partial paralysis of hind limbs; 5, spastic paresis of hind limbs; 6, complete paralysis of hind limbs; 7, paralysis up to the diaphragm; 8, paralysis of the fore limbs; 9, head held sideways; 10, rotation movements; 11, death due to EAE.

Preparation of liposomes

Multilamellar mannosylated liposomes constructed of phosphatidylcholine, cholesterol and mannose were prepared as described before [9]. Briefly 70.9 mg phosphatidylcholine and 10.8 mg cholesterol (Sigma Chemical Co., St Louis, MO) were dissolved in 10 ml chloroform, and added to 3.6 mg *p*-aminophenyl- α -D-mannopyranoside (Sigma) dissolved in 2 ml methanol. This was put into a 500-ml round-bottomed flask, and dried *in vacuo* on a rotary evaporator to form a film. Subsequently the dried film was dissolved in 10 ml of chloroform and dried again. The total amount of lipids in the film was 140 µmol. The molar ratio of phosphatidylcholine: cholesterol:mannoside = 7:2:1 was chosen according to Umezawa & Eto [22]. To prepare PBS liposomes, 10 ml of PBS (0.15 M NaCl in 10 mM phosphate buffer pH 7.4) were added to the dried film, and the bottom flask was rotated until the lipid film was dispersed into liposomes; to incorporate Cl₂MDP into the liposomes, 2.5 g Cl₂MDP (maximum soluble amount; a gift of Boehringer, Mannheim, Germany) were added to the 10 ml PBS. The preparations were held for 2 h at room temperature and sonicated for 3 min at 20°C in a sonicator (50 Hz) and kept at room temperature for another 2 h or overnight at 4°C. The liposomes were centrifuged at 100 000 g for 30 min and finally resuspended carefully in 4 ml PBS.

Treatment

Experiment A. T cell-EAE was induced in 14 Lewis rats. Rats were injected intravenously with 2 ml of either Cl₂MDP liposomes ($n = 7$, treatment group) or PBS liposomes ($n = 7$, control group) 1 and 3 days after injection of the MBP-specific T cells (post-transfer (p.t.)), i.e. just before the expected manifestation of clinical signs. Six animals per group were killed for histological evaluation 7 days after the injection of the MBP-specific T cells.

Experiment B. AD-EAE was induced in 14 Lewis rats. The MoAb directed against MOG was injected intraperitoneally 3 days p.t. Rats in the treatment ($n = 7$) and control ($n = 7$) group were injected with liposomes as described above at days 1 and 3 p.t. Animals were killed at day 7 p.t. for histological investigation. In case of very severe EAE animals were killed for ethical reasons; if so a matching rat in the parallel group was killed too, to make possible histological comparison between groups on the same day p.t.

Experiment C. CR-EAE was induced in 15 Lewis rats. Rats were treated either with Cl₂MDP liposomes ($n = 7$, treatment group) or PBS liposomes ($n = 8$, control group) at days 21 and

23 after immunization (a.i.). Timing of liposome injection was based on earlier data on the mean day of onset of the first relapse (day 23 a.i.) [20]. At both days 29 and 39 after immunization, three animals of either group were killed for histological evaluation.

Statistical analysis

The significance of differences in clinical signs of EAE between two groups was analysed using a χ^2 test. Differences in day of onset of clinical signs of EAE, as well as differences in weight loss between two groups, were analysed using the Wilcoxon rank sum test.

Immunocytochemistry

Animals were killed by an i.v. injection of 0.5 ml Nembutal (Algin B.V., Maassluis, The Netherlands). Brain, spinal cord, and spleen were dissected, frozen in liquid nitrogen and stored at -20°C or -70°C . Serial cryostat sections of $10\ \mu\text{m}$ were cut, picked up on glass slides and dried in a container with silica gel. Immunocytochemistry was applied after acetone fixation to examine cellular infiltrates in the CNS and efficacy of macrophage elimination by Cl_2MDP liposomes in the spleen. The following murine MoAbs were used: anti-pan-T cell (OX-19), anti-MHC class II (OX-6), both from Serotec (Oxford, UK), and anti-rat macrophages (ED1 and ED2). ED1 recognizes a lysosomal membrane-related antigen in all rat macrophages, and ED2 recognizes an adhesion-related antigen on resident rat macrophages [23]. ED1 and OX19 were biotinylated using biotin-N-hydroxysuccinimide ester (biotin-NHS; Zymed, San Francisco, CA) in a molar ratio of biotin-NHS: MoAb = 80:1. As detection system, peroxidase-conjugated rabbit anti-mouse IgG or peroxidase-conjugated avidin (both from Dako, Tilburg, The Netherlands) was used. Antibodies and conjugates were diluted in 0.01 M PBS with 0.2% bovine serum albumin (BSA; Organon Technika, Oss, The Netherlands) and used in dilutions between 1:100 and 1:500. All incubations were carried out horizontally at room temperature. After incubation with the first antibody for 45 min, the slides were rinsed in PBS, incubated in conjugate with 1% normal rat serum for 30 min, and washed again in PBS. Peroxidase activity was demonstrated after incubation with 0.5 mg/ml 3,3'-diaminobenzidine-tetra-hydrochloride (DAB; Sigma) in 0.05 M Tris buffer pH 7.6, containing 0.03% H_2O_2 for 10 min. Sections were lightly counterstained with haematoxylin.

RESULTS

Experiment A: macrophage depletion during T cell-EAE

Mean onset of clinical disease was 3.1 ± 0.4 days post-EAE induction in the case of control liposome-treated animals, and 4.0 ± 0.0 days post-EAE induction in the case of Cl_2MDP liposome treatment ($P < 0.01$; Fig. 1). PBS liposome-treated animals all developed paresis or paralysis of the hind limbs (score 2 and 3). In contrast, affected hind limbs were not observed in the Cl_2MDP -treated animals. Tail tonus, however, was diminished for 1 or 2 days in the treated animals. Based on the incidence of hind limb paresis, the Cl_2MDP liposome-treated animals were significantly less severely affected than the PBS liposome-treated animals ($P < 0.003$).

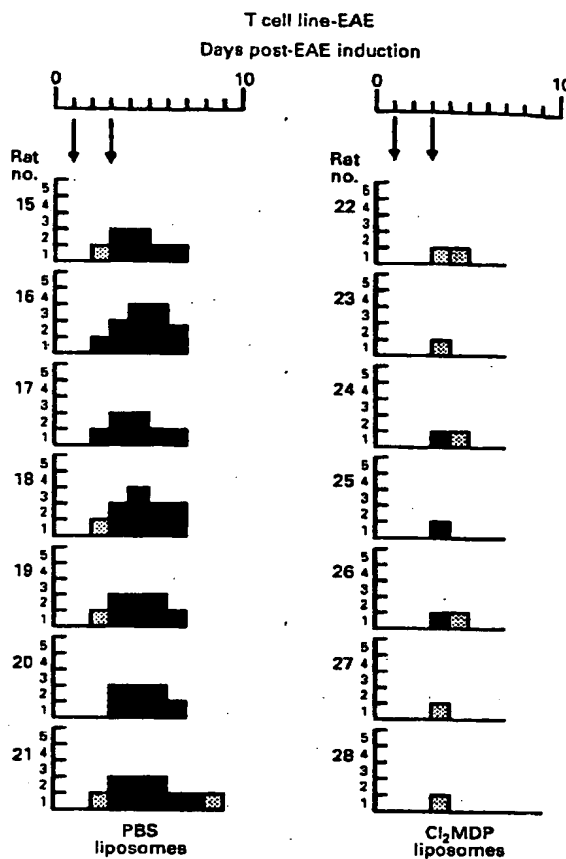


Fig. 1. Experiment A: effect of two i.v. injections (arrows) of dichloromethylene diphosphonate (Cl_2MDP) or PBS containing liposomes on clinical expression of T cell experimental allergic encephalomyelitis (EAE). Liposomes were injected 1 and 3 days post-transfer (p.t.). Clinical signs were scored as indicated in Materials and Methods. Shaded areas in grade 1 indicate loss of the tip-of-tail reflex, whereas a black box in grade 1 indicates complete loss of the tail tonus. Based on the incidence of score 2, the treated animals were less severely affected ($P < 0.003$). End of line on the time-axis of each rat indicates that the animal died due to EAE (score 5) or that the animal was killed for histology.

Weight loss during clinical EAE was significantly less in the Cl_2MDP liposome-treated rats ($P < 0.05$) compared with control animals (data not shown).

Experiment B: macrophage depletion during AD-EAE

The effect of liposome treatment on AD-EAE is shown in Fig. 2. Clinical disease in control animals developed severely after the injection of the anti-MOG MoAb beginning on day 3.7 ± 0.5 p.t. At 5 days p.t., 4/7 of the control rats had completely lost the mobility of hind limbs (score 4). Two of these rats died due to EAE (score 5), whereas the other two rats were killed at day 5 p.t. because of severity of disease. In comparison, rats which

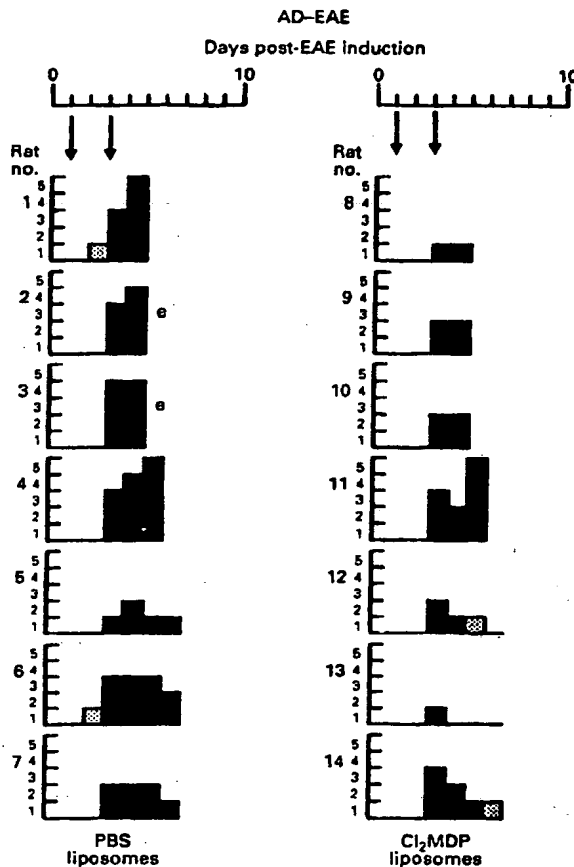


Fig. 2. Experiment B: effect of two i.v. injections (arrows) of dichloromethylene diphosphonate (Cl_2MDP) or PBS containing liposomes on clinical expression of AD-EAE. Liposomes were injected on days 1 and 3, and the myelin oligodendrocyte glycoprotein (MOG) MoAb was injected 3 days post-transfer (p.t.). Based on the incidence of score 4, the differences between treated rats and controls were statistically significant ($P < 0.02$). e, Killed for ethical reasons. Other details are as described in the legend of Fig. 1.

had been treated with Cl_2MDP liposomes were much less affected. Clinical disease in these animals started 4.0 ± 0.0 days p.t. Although one animal died due to EAE, no paralysis up to the diaphragm was seen (score 4) in any of the treated rats. Statistical analysis based on incidence of score 4 showed significant difference between treated and control group ($P < 0.02$). Weight loss was impressive in the controls, but treatment reduced weight loss considerably ($P < 0.01$) from day 4 onwards (Fig. 3).

Experiment C: macrophage depletion during CR-EAE

The effect of liposome treatment on CR-EAE is shown in Fig. 4. Animals of the control group developed either chronic relapsing remitting EAE (6/8 rats) or chronic progressive EAE (2/8

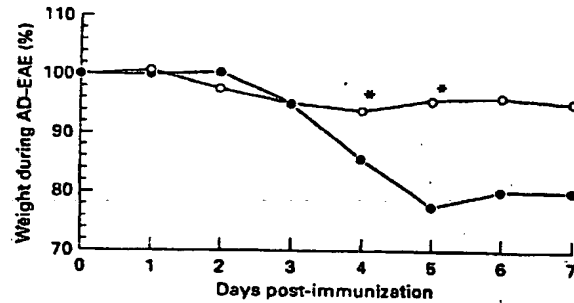


Fig. 3. Weight loss during AD-EAE treated with dichloromethylene diphosphonate (Cl_2MDP) liposomes. Weight is given in percentage of that on the day of EAE induction ($1.1 \pm \text{s.d.} < 4.9$, $n = 7$ until day 5 and $n = 3$ at days 6 and 7 post-transfer (p.t.)). *Difference between rats treated with Cl_2MDP -containing liposomes and controls is significant ($P < 0.01$). O, Cl_2MDP liposomes; ●, PBS liposomes.

rats). In the treatment group the Cl_2MDP liposomes either prevented or suppressed the clinical severity of the first relapse very efficiently (5/7 rats). Based on the number of animals with a score of at least 4 during a second attack, the difference was significant ($P < 0.006$). Interestingly, clinical signs were not suppressed by Cl_2MDP -containing liposomes in the two rats showing a chronic progressive course (2/7).

Histological investigations

Histological examination of the spleens of all Cl_2MDP liposome treatment groups showed effective elimination of macrophages (not shown).

The CNS of control rats with T cell-EAE (experiment A) revealed multiple lesions containing both macrophages and low numbers of T cells. The effect of macrophage depletion was evident in the decline of ED2⁺ macrophages in the meninges of Cl_2MDP liposome-treated animals (not shown). The CNS of these rats occasionally also showed lesions with striking dense accumulations of Ia-positive mononuclear cells in the blood vessels and within the Virchow-Robin space (Fig. 5a). This phenomenon was characteristic of Cl_2MDP liposome-treated animals; the multiple rows of tightly accumulated cells consisted of ED1⁺ macrophages as well as OX-19⁺ T cells (not shown). In control rats, such accumulations were smaller and rarer (Fig. 5b). Margination of leucocytes within vessels of Cl_2MDP liposome-treated rats was confined to inflamed blood vessels in the CNS. Within the Cl_2MDP liposome-treated animals small numbers of macrophages were still present within the parenchyma of the CNS. Surprisingly, T cells were present in lesion areas of treated rats in higher numbers (Fig. 5c) compared with controls (Fig. 5d).

Within the CNS of AD-EAE animals (experiment B), multiple inflammatory foci containing high numbers of macrophages (Fig. 6b) and to a lesser extent T cells were observed in control animals. Cl_2MDP liposome treatment was clearly reflected in a considerable reduction of the number of infiltrating macrophages (Fig. 6a), but T cells were still present in high numbers in these treated animals (not shown).

In the CNS of rats with CR-EAE (experiment C), lesions were abundant containing high numbers of ED1⁺ macrophages

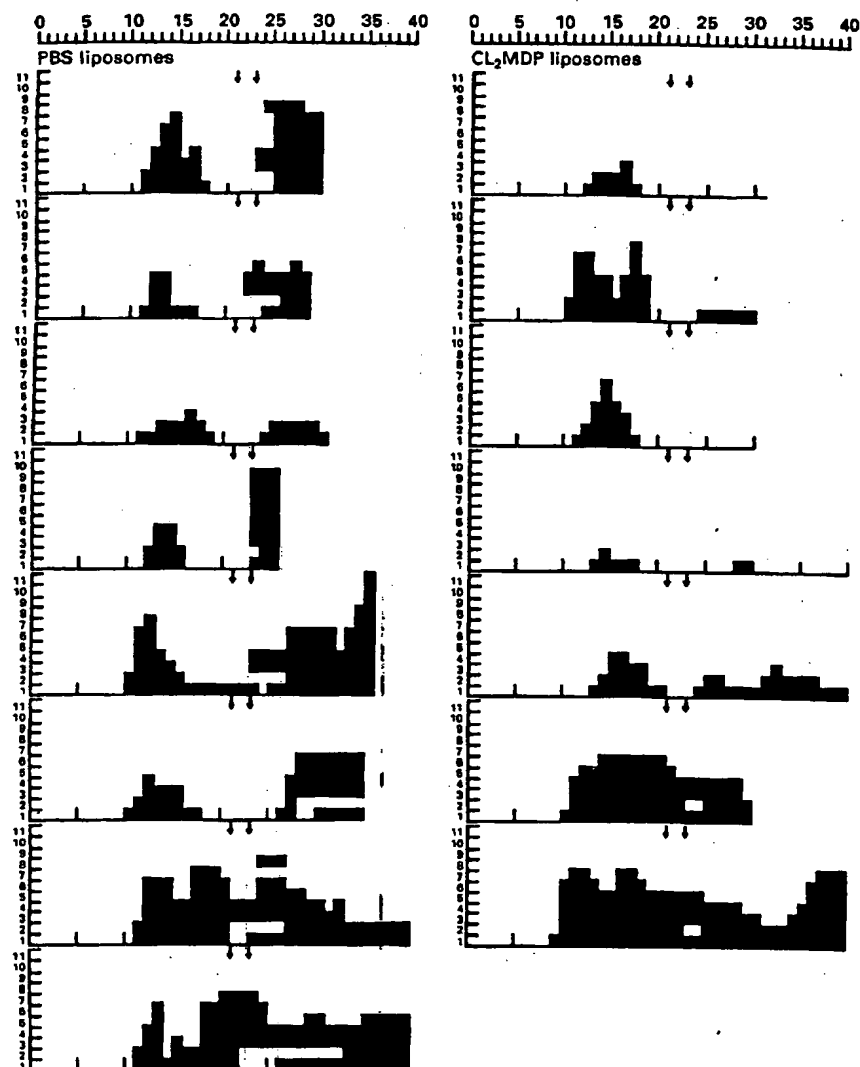


Fig. 4. Experiment C: effect of two i.v. injections (arrows) of dichloromethylene diphosphonate (Cl_2MDP) containing liposomes on clinical expression of chronic relapsing experimental autoimmune encephalomyelitis (CR-EAE). Clinical signs were scored as indicated in Materials and Methods. Based on the incidence of score 4 the severity of the relapse was significantly reduced in the Cl_2MDP liposome-treated rats ($P < 0.006$). Note that the treatment was only effective when started before a relapse during relapsing remitting CR-EAE, and not when liposomes were injected during a chronic progressive course of the disease (lowest two panels).

and OX-19⁺ T cells. No differences between treated and control rats were observed (not shown).

DISCUSSION

The results show that macrophage depletion during the EAE induced by MBP-specific T cells suppresses clinical signs almost completely. Apparently macrophages are necessary effector

cells for full-blown clinical signs of T cell-EAE. In previous studies it was found that during actively induced EAE (A-EAE) macrophage depletion, either by the use of Cl_2MDP liposomes [9] or by the use of silica [24], also suppresses expression of clinical disease markedly. However, in A-EAE it is not possible to discriminate between different functions of macrophages during different stages of EAE. Those results [9,24] can well be explained by reduced infiltration of macrophages into the

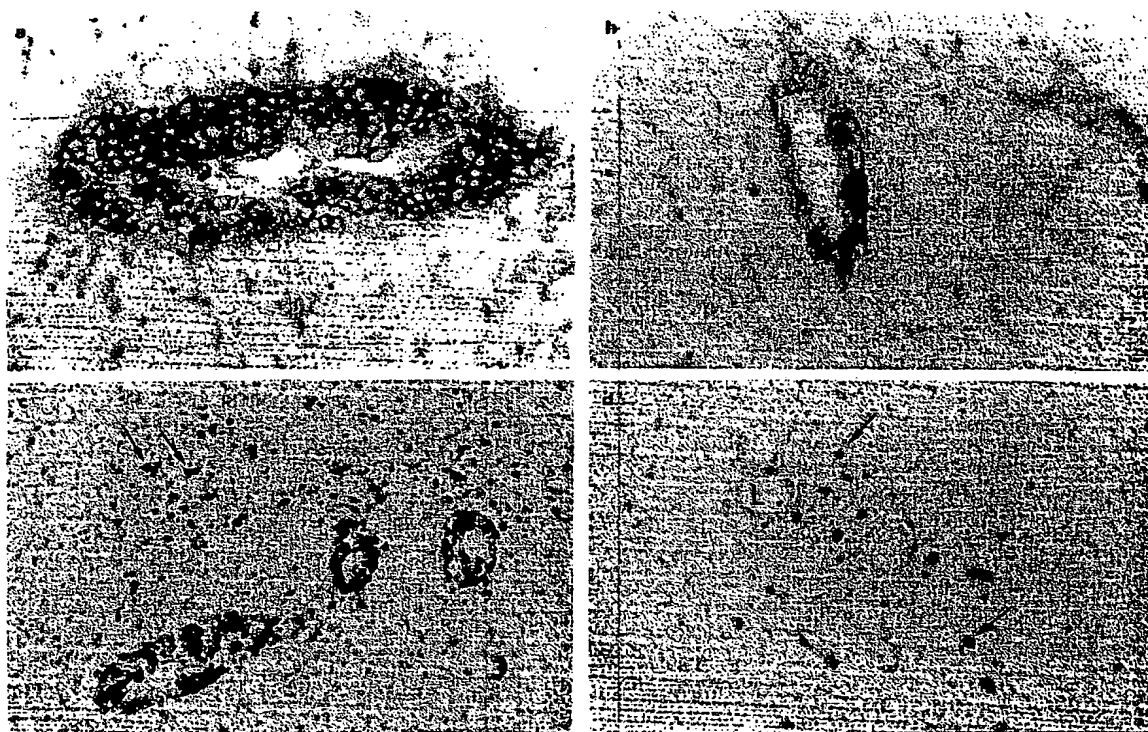


Fig. 5. Representative micrographs of immunohistochemical stainings (Ia and OX-19) of the central nervous system (CNS) of dichloromethylene diphosphonate (Cl_2MDP) liposome-treated rats (a,c) or control treated rats (b,d) with T line-EAE. Cryostat sections from the medulla oblongata were obtained 7 days post-transfer (p.t.). (a) (Cl_2MDP liposome-treated) and (b) (control-treated): Ia-positive cells accumulating along a cerebral vessel wall ($\times 1200$). (c) (Cl_2MDP liposome-treated) and (d) (control-treated): OX-19 $^+$ T cells accumulating within a vessel (c) (L, lumen) and infiltrating (arrows) into the parenchyma (c and d) ($\times 600$).

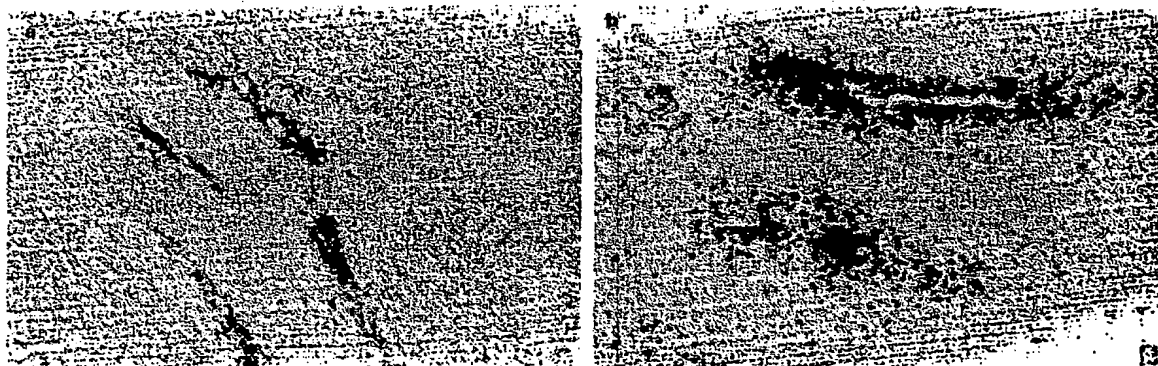


Fig. 6. Representative micrographs of immunohistochemical (ED1) stainings of the central nervous system (CNS) of a dichloromethylene diphosphonate (Cl_2MDP) liposome treated rat (a) and a control-treated rat (b) with AD-EAE. Cryostat sections from the cerebellum obtained 5 days post-transfer (p.t.) showing ED1 $^+$ macrophages within cerebral blood vessels ($\times 300$) of Cl_2MDP liposome-treated (a) and control-treated (b) rats. Note the decreased infiltration of macrophages into the parenchyma in the treated rats (a) compared with the controls (b).

012

CNS, thereby reducing local tissue damage. However, macrophage depletion may also have interfered with antigen processing and presentation at the site of immunization during the induction phase of the A-EAE, ultimately leading to impaired T cell responses and interruption of the autoimmune response. During T cell line-induced EAE, however, this induction phase is omitted. Therefore, the results of the present study unequivocally prove that macrophages which infiltrate the CNS during EAE are crucial in the development of clinical signs of EAE.

Histological evaluation after treatment with Cl_2MDP liposomes confirmed macrophage depletion in peripheral organs like the spleen and the liver, as well as the lesions in the CNS. A specific feature of CNS tissue of animals treated with Cl_2MDP containing liposomes was the occasional dense accumulations of Ia-positive cells within the Virchow-Robin space and in the blood vessels. These Ia-positive cells consisted of activated T cells as well as macrophages. Within the parenchyma, however, only macrophage numbers had decreased, whereas T cells were still present in high numbers. The blood-borne macrophages may have been damaged by ingested liposomes and become unable to migrate into the parenchyma. The reduction of macrophage infiltration was most evident in the rats with AD-EAE, that had been killed already 2 days after the last liposome injection. It is very likely that histological evidence of macrophage depletion in the CNS is most pronounced shortly after the last liposome injection. After monocyte depletion, the bone marrow releases new monocytes rapidly into the circulation [13], which may infiltrate the CNS. This may explain why the decline in number of macrophages is less evident in rats with T cell-EAE, which had been killed later after the final liposome injection. In addition, macrophage infiltration was scarcely affected by liposome treatment of animals with CR-EAE, perhaps because of the long time interval between liposome injections and histological analysis, as well as of the persistence of some inflammation after a first, untreated, clinical episode.

Activated resident microglial cells are, besides infiltrating T cells and macrophages, other putative candidates as effector cells. Mannosylated liposomes as used in this study have been described to pass the blood-brain barrier (BBB) [22]. However, we (unpublished results) and others [25] have not been able to confirm these observations. It should be noted, however, that the BBB is compromised during EAE, and Cl_2MDP -containing liposomes can be observed within perivascular lesions in the CNS of EAE rats (unpublished observations). Recent electron microscopical investigation of the CNS of Cl_2MDP liposome-treated (BN x Lewis into Lewis) bone marrow chimerae [26] with T cell-EAE, however, does not show elimination of microglia cells (Bauer *et al.*, submitted for publication). This latter study confirms massive reduction of infiltration of blood-borne macrophages into the CNS of up to 90% after Cl_2MDP liposome treatment. Also, diminished activation of microglial cells was inferred from reduced expression of ED1 and MHC class II, together with the morphology of these cells [27]. Thus, depletion of infiltrating blood-borne macrophages has indirect effects on the state of activation of microglia.

Other putative effector cells in the CNS of rats with EAE are the ED2⁺ perivascular macrophages. These are macrophages of haematogenous origin [26,28]; they are likely to be capable of ingesting high quantities of liposomes, and are therefore susceptible to the Cl_2MDP liposomes. Since they

present antigen [26], their elimination could also interfere with a crucial step in lesion formation.

Liposome-treated rats with both T cell-EAE and AD-EAE were followed for only a short period after treatment, and we therefore do not know how long the protective effects of the treatment would have lasted. However, long-term follow up of A-EAE [9] revealed that liposome-mediated macrophage depletion is long-lasting. In addition, rats with relapsing remitting CR-EAE which were observed for 17 days after the final Cl_2MDP -containing liposome injection did not show any rebound reaction to the treatment.

During AD-EAE, the anti-MOG MoAb 8-18C5 binds to myelin and causes severe demyelination [19]. Complement depletion by soluble recombinant CRI clearly demonstrates that the anti-MOG-mediated demyelination depends at least in part on C3b opsonization and terminal membrane attack complex [29], although earlier findings on the role of complement using cobra venom factor do not confirm this observation [30]. Since F(ab)_2 fragments of 8-18C5 have no effect on the clinical course of A-EAE [31], it is likely that an additional mechanism by which anti-MOG initiates demyelination *in vivo* depends on antibody-dependent cell-mediated cytotoxicity (ADCC) mediated by Fc receptors present on macrophages [29]. The results of this study demonstrate that macrophages are involved in the pathogenesis of AD-EAE, and suggest that demyelination as caused by 8-18C5 depends indeed, at least in part, on ADCC effected by macrophages.

During CR-EAE, Cl_2MDP -containing liposomes administered just before the expected beginning of a relapse suppressed clinical signs of this relapse efficiently. Interestingly, however, if rats were developing a chronic progressive course of the disease, Cl_2MDP liposome treatment had no effect at all on neurological signs. This suggests that: (i) suppression of macrophage influx into the CNS by liposomes is likely to be due to elimination of monocytes within the circulation [13] rather than the elimination of macrophages which have already infiltrated the CNS; and (ii) for each new clinical episode macrophages are newly recruited from the circulation into the CNS. It is unclear which systemic immunological event causes and precedes the clinical relapse. Relapses might also have been prevented by Cl_2MDP liposomes due to elimination of spleen macrophages as putative amplifier cells of relapse initiation. Furthermore, during the chronic progressive course of EAE there may have been enough macrophages residing in the CNS—unaffected by the Cl_2MDP liposomes—to ensure perpetuation of local inflammation.

These findings are relevant for therapeutic approaches focused on the functioning of macrophages during MS. Active lesions of MS contain numerous macrophages [5]. The fact that during CR-EAE macrophage depletion was only successful when the treatment was given just before the beginning of a relapse demonstrates the importance of finding parameters that predict a relapse. Therapeutic approaches focused on modulation of macrophages infiltrating active lesions in MS are promising, but are likely to depend on the right timing of the treatment.

ACKNOWLEDGMENTS

The authors thank Dr Hermann Schluesener for providing the MOG antibody and Dr Beate Schmidt for her help with histologic preparations.

This work has been financed by the foundations 'Vrienden MS research', 'The European Charcot Foundation for Multiple Sclerosis Research' and the Bundesministerium für Forschung und Technologie (01KD9001/8).

REFERENCES

- Raine CS. Experimental allergic encephalomyelitis and experimental allergic neuritis. In: Koetsier J, ed. *Handbook of clinical neurology*, Vol. 47, Part 3: Demyelinating diseases. Amsterdam: Elsevier Science Publ. B.V., 1985:429-66.
- Holda JH, Swanborg RH. Autoimmune effector cells I. Transfer of experimental allergic encephalomyelitis with lymphoid-cells cultured with antigen. *Eur J Immunol* 1980; 10:657-9.
- Pettinelli CB, McFarlin DE. Adoptive transfer of experimental allergic encephalomyelitis in SJL/J mice after *in vitro* activation of lymph node cells by myelin basic protein: requirement of Lyt 1, 2 T lymphocytes. *J Immunol* 1981; 127:1420-3.
- Polman CH, Dijkstra CD, Sminia T *et al.* Immunohistochemical analysis of macrophages in the central nervous system of Lewis rats with acute experimental allergic encephalomyelitis. *J Neuroimmunol* 1986; 11:215-22.
- Brück W, Schmied M, Suchanek G *et al.* Oligodendrocytes in the early course of multiple sclerosis. *Ann Neurol* 1994; 35:65-73.
- Hartung H-P, Heininger K. Non-specific mechanisms of inflammation and tissue damage in MS. *Res Immunol* 1989; 140:226-33.
- Brück W, Friede RL. Anti-macrophage CR3 antibody blocks myelin phagocytosis by macrophages *in vitro*. *Acta Neuropathol* 1990; 80:415-8.
- Huitinga I, Damoiseaux JGMC, Döpp EA *et al.* Treatment with anti-CR3 antibodies ED7 and ED8 suppresses experimental allergic encephalomyelitis in Lewis rats. *Eur J Immunol* 1993; 23:709-15.
- Huitinga I, Van Rooijen N, DeGroot CJA *et al.* Suppression of experimental allergic encephalomyelitis after elimination of macrophages. *J Exp Med* 1990; 172:1025-31.
- Van Rooijen N. The liposome-mediated macrophage 'suicide' technique. *J Immunol Methods* 1989; 124:1-7.
- Fleisch H. Biphosphonates: a new class of drugs in disease of bone and calcium metabolism. In: Baker PF, ed. *Handbook of experimental pharmacology*, Vol. 83. Berlin: Springer-Verlag, 1988:441-66.
- Van Rooijen N, Kors N, Van den Ende M *et al.* Depletion and repopulation of macrophages in spleen and liver of rat after intravenous treatment with liposome-encapsulated dichloromethylene diphosphonate. *Cell Tissue Res* 1990; 260:215-22.
- Huitinga I, Damoiseaux JGMC, Van Rooijen N *et al.* Liposome-mediated affection of monocytes. *Immunobiology* 1992; 185:11-19.
- Jung S, Toyka KV, Hartung H-P. Impact of 15-deoxyspergualin on effector cells in experimental autoimmune diseases of the nervous system in the Lewis rat. *Clin Exp Immunol* 1994; 98:494-502.
- Pender MP. Demyelination and neurological signs in experimental allergic encephalomyelitis. *J Neuroimmunol* 1987; 15:11-24.
- Simmons RD, Bernard CCA, Singer G *et al.* Experimental autoimmune encephalomyelitis—an anatomical-based explanation of clinical progression in rodents. *J Neuroimmunol* 1982; 3:307-18.
- Kerlero de Roboso N, Bernard CCA, Simmons RD *et al.* Concomitant detection of changes in myelin basic protein and permeability of blood-spinal cord barrier in acute experimental allergic encephalomyelitis by electroimmunoblotting. *J Neuroimmunol* 1985; 9:349-54.
- Linington C, Webb M, Woodhams PL. A novel myelin associated glycoprotein defined by a mouse monoclonal antibody. *J Neuroimmunol* 1988; 6:387-96.
- Schlesener HJ, Sobel RA, Linington C *et al.* A monoclonal antibody against a myelin oligodendrocyte glycoprotein induces relapses and demyelination in central nervous system autoimmune disease. *J Immunol* 1987; 139:4016-21.
- Polman CH, Matthei I, DeGroot CJA *et al.* Low-dose cyclosporin A induces relapsing remitting experimental allergic encephalomyelitis in the Lewis rat. *J Neuroimmunol* 1988; 17:209-16.
- Pender MP, Stanley GP, Yoong G *et al.* The neuropathology of chronic relapsing experimental allergic encephalomyelitis induced in the Lewis rat by inoculation with whole spinal cord and treatment with cyclosporin A. *Acta Neuropathol* 1990; 80:172-83.
- Umezawa F, Eto Y. Liposome targeting to mouse brain: mannose as a recognition marker. *Biochem Biophys Res Commun* 1988; 153:1038-43.
- Dijkstra CD, Döpp EA, Van den Berg TK *et al.* Monoclonal antibodies against rat macrophages. *J Immunol Methods* 1994; 174:21-23.
- Brosnan CF, Bornstein MB, Bloom BR. The effect of macrophage depletion on the clinical and pathologic expression of experimental allergic encephalomyelitis. *J Immunol* 1981; 126:614-20.
- Micklus MJ, Greig NH, Tung J *et al.* Organ distribution of liposomal formulations following intracarotid infusion in rats. *Biochim Biophys Acta* 1992; 1124:7-12.
- Hickey WF, Kimura H. Perivascular microglia cells of the CNS are bone marrow-derived and present antigen. *Science* 1988; 239:290-1.
- Graeber MB, Streit WJ, Kiefer R *et al.* New expression of myelomonocytic antigens by microglia and perivascular cells following lethal motor neuron injury. *J Neuroimmunol* 1990; 27:121-32.
- Graeber MB, Streit WJ, Kreutzberg GJ. Identity of ED2 positive perivascular cells in rat brain. *J Neurosci Res* 1989; 22:103-6.
- Piddlesden SJ, Storch MK, Hibbs M *et al.* Soluble recombinant complement receptor 1 inhibits inflammation and demyelination in antibody-mediated demyelinating experimental allergic encephalomyelitis. *J Immunol* 1994; 152:5477-84.
- Piddlesden S, Lassmann H, Laffan I *et al.* Antibody-mediated demyelination in experimental allergic encephalomyelitis is independent of complement membrane attack complex formation. *Clin Exp Immunol* 1991; 83:245-50.
- Linington C, Morgan BP, Scolding NJ *et al.* The role of complement in the pathogenesis of experimental allergic encephalomyelitis. *Brain* 1989; 112:895-911.

CD40–CD40 ligand interactions in experimental allergic encephalomyelitis and multiple sclerosis

(autoimmunity/T-helper cell/gp39/therapy)

KOEN GERRITSE*, JON D. LAMAN*, RANDOLPH J. NOELLE†, ALEJANDRO ARUFFO‡, JEFFREY A. LEDBETTER‡, WIM J. A. BOERSMA*, AND ERIC CLAASSEN*§¶

*Division of Immunological and Infectious Diseases, TNO Prevention and Health, POB 2215, 2301 CE, Leiden, The Netherlands; †Department of Immunology, Erasmus University, 3015 GE Rotterdam, The Netherlands; ‡Department of Microbiology, Dartmouth Medical School, Lebanon, NH 03756; and §Bristol-Myers Squibb Pharmaceutical Research Institute, Seattle, WA 98121

Communicated by J. J. van Rood, University of Leiden, Leiden, The Netherlands, September 27, 1995 (received for review December 15, 1994)

ABSTRACT We investigated the role of CD40–CD40 ligand (CD40L) interactions in multiple sclerosis (MS) and experimental allergic encephalomyelitis (EAE). Activated helper T cells expressing CD40L (gp39) surface protein were found in MS patient brain sections, but not in brain tissue sections of normal controls or patients with other neurological diseases. CD40L-positive cells were co-localized with CD40-bearing cells in active lesions (perivascular infiltrates). Most of these CD40 bearing cells proved to be of the monocytic lineage (macrophages or microglial cells), and relatively few were B cells. To functionally evaluate CD40–CD40L interactions, EAE was elicited in mice by means of proteolipid-peptide immunization. Treatment with anti-CD40L monoclonal antibody completely prevented the development of disease. Furthermore, administration of anti-CD40L monoclonal antibody, even after disease onset, shortly before maximum disability score was reached led to dramatic disease reduction. The presence of helper T cells expressing CD40L in brain tissue of MS patients and EAE animals, together with the functional evidence provided by successful experimental prevention and therapy in an animal model, indicates that blockade of CD40–CD40L-mediated cellular interactions may be a method for interference in active MS.

Interactions between CD40, constitutively expressed on B cells, and CD40 ligand [CD40L; gp39; TBAM (T-B cell activation molecules); TRAP (tumor necrosis factor-related activation protein)], transiently expressed on activated CD4⁺ T cells, are essential for B-cell responses against thymus-dependent antigens. CD40L provides a number of signals to the B cell, some of which require additional cytokine stimuli, such as upregulation of cell surface markers, homotypic adhesion, proliferation, and isotype switching (reviewed in ref. 1). *In vivo* treatment of mice with anti-CD40L monoclonal antibody (mAb) prevents thymus-dependent antibody responses (2, 3), and generation of B-cell memory (4).

Although less well described, CD40–CD40L interactions are now thought to play a role in activation of cells of the monocytic lineage as well. Treatment of human monocytes with granulocyte/macrophage colony-stimulating factor, interleukin 3 (IL-3) or interferon γ resulted in the induction of CD40 mRNA and enhancement of cell surface CD40 protein expression. CD40 was found to mediate monocyte adhesion to cells transformed to express CD40L. The CD40L-transfected cells provided a costimulatory signal for monocytes to produce tumor necrosis factor α and IL-6 in the presence of granulocyte/macrophage colony-stimulating factor or IL-3 (5).

Adoptive transfer studies have established the crucial role of CD4⁺ T-cells in experimental allergic encephalomyelitis

(EAE), but both B cells and monocytes are considered to be involved in the pathogenesis of multiple sclerosis (MS) as well. Active lesions in the central nervous system (CNS) of MS patients are characterized by mononuclear cell infiltrates. The infiltrating cells comprise T cells, B cells, and macrophages (6). About 50% of the mononuclear cells in the perivascular lesions in the CNS of EAE animals, an animal model considered to represent the effector phase of MS, are blood-borne monocytes/macrophages (7) and microglial cells (8). In Lewis rats, in which EAE was induced either by adoptive spleen cell transfer or by active immunization with CNS white-matter homogenate, the elimination of macrophages significantly suppressed the development of EAE neurological signs (7). This suggests an important functional role for macrophages in EAE.

Recently, we have detected autoantigen specific B cells in human cerebellum and cerebrum *in situ* (9). Anti-myelin basic protein (MBP)-specific B cells were found in CNS tissue sections of only MS patients, not in patients with other neurological diseases nor in CNS tissue sections of normal controls. It is not clear whether these autoantigen-specific B cells were activated by CD40L⁺ helper T (Th) cells locally in the demyelinated areas of the CNS or in peripheral lymphoid tissues.

In this study, we investigated whether interactions between CD40L on activated CD4⁺ T cells and CD40 on B cells and/or cells of the monocytic lineage are involved in development and progression of EAE and MS. Using immunohistochemistry, we evaluated expression of CD40 and CD40L in CNS tissue sections of MS autopsy material. Furthermore, functional experiments blocking CD40–CD40L interactions in a mouse EAE model were performed. Collectively, our data support the hypothesis that the CD40–CD40L system is indeed involved in EAE and MS, providing a target for therapeutic intervention.

MATERIALS AND METHODS

Histochemistry. Human autopsy CNS tissues from patients with MS ($n = 12$), normal controls, and controls with other neurological disease were obtained from the Multiple Sclerosis/Control Brain Bank (supported by the Netherlands Foundation for the Support of MS Research; Amsterdam). All histochemical analyses of both human and mouse tissues were performed on cryosections (8 μ m) from snap-frozen material. In a pilot study, selected CNS tissues of MS patients ($n = 4$) were used in which anti-MBP-specific B cells (putatively

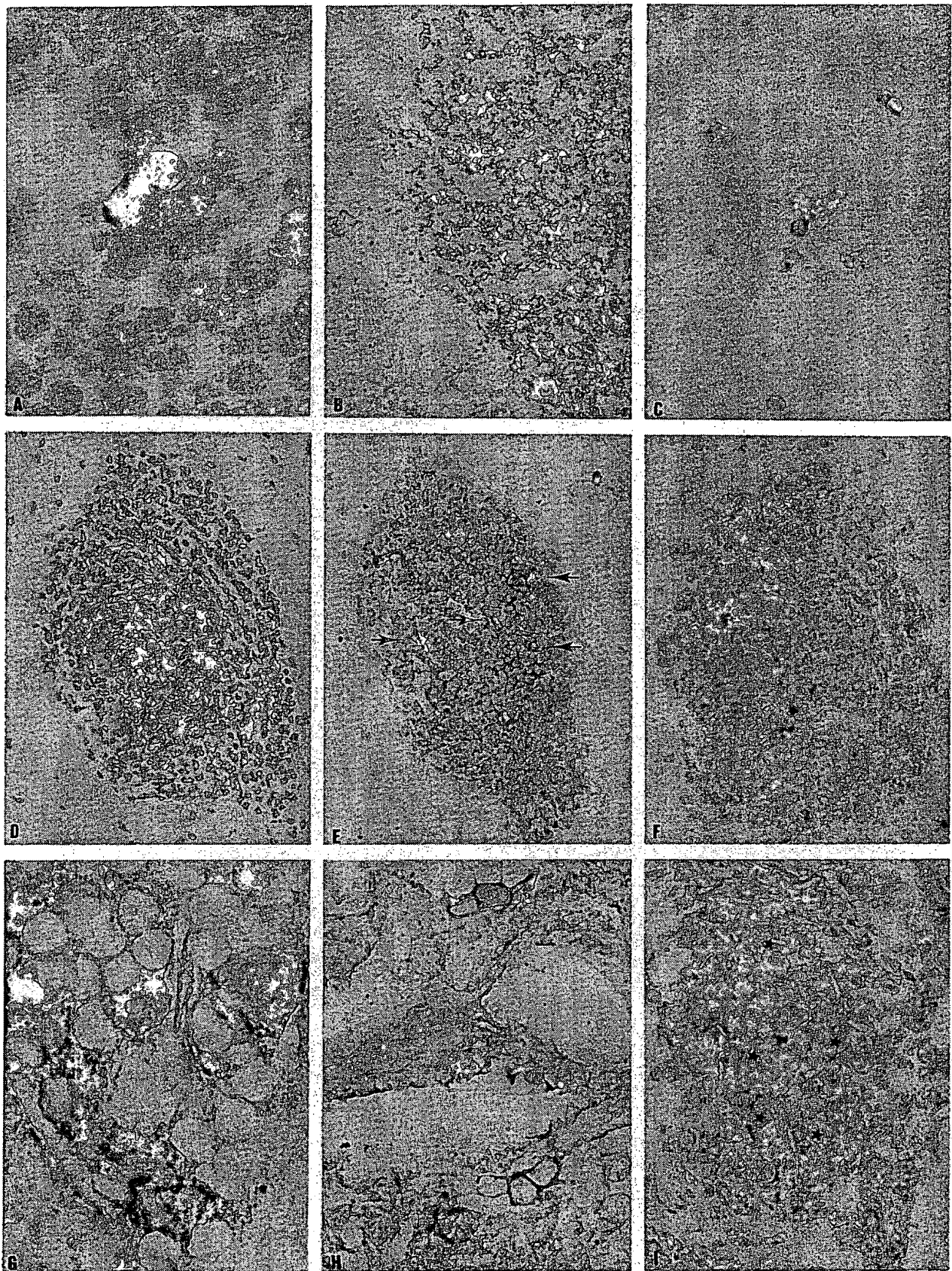


FIG. 1. (Legend appears at the bottom of the opposite page.)

bearing CD40) were detected on a previous occasion (9). CD40L⁺ cells were detected immunohistochemically in human tissue by using a CD40-Ig fusion protein, as described (3), and in the mouse with the mAb MR1 (3, 10) directly labeled with alkaline phosphatase. Alkaline phosphatase was revealed by using naphthol-AS-MX-phosphate and fast blue BB base resulting in a blue precipitate, as described (11). CD40 was revealed with a mouse anti-human CD40 antibody (5D12; a kind gift from M. de Boer, PanGenetics BV, Heemstede, The Netherlands; ref. 12), followed by rabbit-anti-mouse IgG conjugated with horseradish peroxidase (RAMPO, Dako, Denmark), and immunocytochemistry with 3-amino-9-ethylcarbazole (AEC, Sigma), resulting in a red precipitate, as described (11). CD40 was revealed in a blue color after incubation with mAb 5D12, followed by horse-anti-mouse-IgG coupled with biotin (Vector Laboratories), and subsequent application of streptavidin-alkaline phosphatase (GIBCO/BRL). Cells of the monocytic lineage (11–13) were detected by acid-phosphatase staining demonstrating endogenous enzyme activity in lysosomes by using naphthol AS-BI phosphate (Sigma), as described (11). CD11b (complement receptor 3; ref. 13) was revealed in red after incubation with Leu-15 (Becton Dickinson) followed by RAMPO and AEC. B cells were demonstrated in red as described (9) with mouse anti-human IgG/IgM directly labeled with horseradish peroxidase and revealed with AEC.

EAE Induction and Anti-CD40L mAb Administration. EAE was induced according to a standard protocol in three groups ($n = 18$) of female SJL/J mice (12–15 weeks old) by two subcutaneous injections of 75 μ g, 150 μ g, or 300 μ g of proteolipid protein (PLP) peptide in the abdominal flanks. The PLP peptide contained amino acids 139–151 of rat PLP (14). Peptide synthesis was performed by using 9-fluorenylmethoxycarbonyl (Fmoc) amino acids with the 9500 Milligen synthesizer according to standard protocols. The standard EAE-induction procedure using this peptide results in the development of acute EAE, clinically and pathologically identical to EAE induced by using whole CNS myelin or MBP (15). The emulsion contained 25 μ g of *Mycobacterium tuberculosis* organisms (H37RA; Difco) in 50 μ l of Freund's complete adjuvant and 37.5 μ g, 75 μ g, or 150 μ g of peptide in 50 μ l of phosphate-buffered saline (PBS; 0.01 M phosphate buffer, pH 7.2/0.9% NaCl). On days 0 and 2, each mouse was injected intravenously with 200 μ l of *Bordetella pertussis* suspension (10^{10} organisms per animal). Mice were injected intraperitoneally with 125 μ g of hamster anti-CD40L mAb (2, 10) in 200 μ l of PBS on days 0, 2, and 4; 4, 6, and 8; or 7, 9, and 11. Mice of the control groups received 125 μ g of normal hamster antibodies (Serva) in 200 μ l of PBS. The severity of EAE clinical signs was evaluated each day and graded according to discrete criteria (15): Disability scale (DAS) units; grade 0 = no clinical signs, grade 1 = tail weakness, grade 2 = mild paraparesis and ataxia of the hind legs, grade 3 = severe paraparesis or ataxia of the hind legs, grade 4 = moribund, grade 5 = death due to EAE. Blood samples were obtained on

days 4, 9, 14, 21, 31, and 40 by tail-vein puncture. Sera were screened in a standard direct ELISA (16) for the presence of anti-PLP peptide antibodies by using the PLP peptide at a concentration of 10 μ g/ml in PBS for coating of microtiter plates.

RESULTS

Detection of CD40L⁺ Th Cells. As shown in Fig. 1A, CD40L⁺ cells were detected in CNS tissue sections from MS patients ($n = 12$). Cells were shown to be of the Th phenotype by double staining for CD4 (data not shown). In control CNS tissue sections from normal individuals ($n = 5$) or from Alzheimer patients ($n = 5$), no cells stained with CD40-Ig fusion protein were observed (Fig. 1B). Similarly, CD40L-bearing cells could be demonstrated in cryosections of EAE mice with either CD40-Ig fusion protein (overlap of CD40-Ig and MR1 immunocytochemical staining of mouse tissue was shown before; ref. 3) or the anti-CD40L antibody MR1 (Fig. 1C; day 12 after induction of disease). CD40L-bearing cells were found in white matter lesions and not outside these lesions nor in control animals.

Detection of CD40-Bearing Cells. In Fig. 1D–I serial sections of a representative perivascular infiltrate in a cryosection of MS brain are shown. From Fig. 1D, it is clear that a majority of the infiltrating cells bear CD40. From our previous study on anti-MBP antibody production in MS brain (9), we would have expected these cells to be CD40-bearing B cells; however, only a few cells (10–20%) were B cells, on the basis of double staining for IgM/IgG and CD40 (Fig. 1E). Staining for either acid phosphatase (Fig. 1F and G) or CD11b (Fig. 1H) showed that most CD40-bearing cells belonged to the monocytic lineage. Only a very few of these cells were detected in control cerebrum tissue sections. Cells expressing CD40 and cells expressing CD40L were found in close juxtaposition after double staining (Fig. 1I), suggesting ongoing cellular interactions.

Prevention of EAE by Anti-CD40L mAb. Administration of PLP peptide resulted in EAE of dose-dependent severity. After EAE induction with 75 μ g or 300 μ g of PLP peptide (data of 150 μ g not shown), control mice or those receiving irrelevant hamster antibodies showed a significant reduction in body weight (25–30%) from day 11 until day 17 (Figs. 2 Top and 3 Top; shaded bars), the first clinical signs of EAE becoming apparent on day 11. Severe disease (most animals moribund or dead) was induced with all peptide doses. The highest average DAS score of the control groups in animals in which EAE was induced with 300 μ g of PLP peptide was 3.6, observed on days 16–23 (Fig. 3 Middle), and a score of 2.3 was observed on days 15–22 (Fig. 2 Middle) in animals in which EAE was induced with 75 μ g of PLP peptide. Strikingly, no body-weight reduction was observed in animals which were treated on days 0, 2, and 4 with 125 μ g of anti-CD40L mAb, irrespective of the peptide dose used for disease induction

FIG. 1 (on opposite page). *In vivo* evidence for involvement of CD40–CD40L interactions in EAE and MS. (A) Red, CD40L. CD40L-positive cells in a perivascular infiltrate in human MS brain. ($\times 325$.) (B) No specifically stained cells. No CD40L-positive cells were found in human brain tissues from “normal” controls or from patients with other neurological disease. Shown here is a representative section of Alzheimer brain. ($\times 40$.) (C) Blue, CD40L. CD40L-positive cells in a perivascular infiltrate of mouse brain during EAE. ($\times 200$.) Note: D–I are serial sections from the same plaque in human MS brain. (D) Red, CD40. Numerous CD40-positive cells are present. ($\times 65$.) (E) Red, IgG/IgM; blue, CD40; violet, double staining, both IgG/IgM and CD40. Only a few cells positive for CD40 also contain IgG or IgM (arrows). This indicates that only a minority of CD40-expressing cells in the infiltrates belongs to the B-cell subset (10–20%). ($\times 65$.) (F) Red, acid phosphatase. Numerous cells having acid phosphatase activity in lysosomal compartments are present. This indicates that these cells have phagocytic properties and are therefore monocytes/macrophages or microglia (monocytic lineage). ($\times 65$.) (G) Red, acid phosphatase; blue, CD40. The large majority of cells bearing CD40 on their membrane also have acid phosphatase activity in the cytoplasm. This indicates that CD40-positive cells in infiltrates are presumably monocytes and/or microglia. ($\times 650$.) (H) Red, CD11b (CR3); blue, CD40; violet, double staining, both CD11b and CD40. The large majority of CD40-positive cells also express complement receptor 3. Taken together with the acid phosphatase activity, this indicates that CD40-positive cells in infiltrates are monocytes or microglia. ($\times 325$.) (I) Red, CD40; blue, CD40L. Cells expressing CD40 and cells expressing CD40L are juxtaposed (stars). ($\times 130$.) This suggests that CD40–CD40L interactions are ongoing in perivascular infiltrates in human MS brain. For technical details of immunohistochemical staining, see *Materials and Methods*.

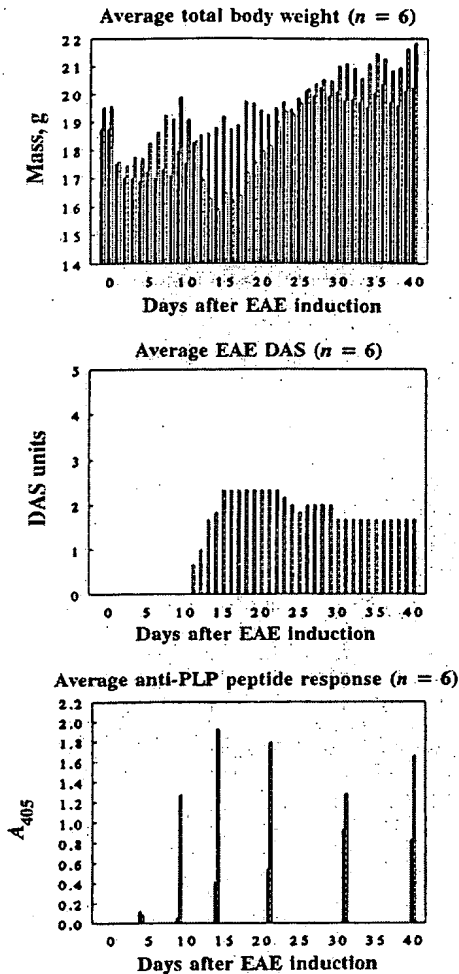


FIG. 2. Prevention of EAE induced with low-dose peptide by using anti-CD40L mAb. EAE was induced with 75 μ g of PLP peptide in female SJL/J mice ($n = 6$) according to a standard procedure. Animals were treated with anti-CD40L mAb on days 0, 2, and 4 (black bars). Control mice received normal hamster antibodies on the same days (hatched bars). The effect of anti-CD40L mAb treatment was monitored by determination of the body weight (*Top*), by evaluation of clinical signs (*Middle*; note: no black bars/no disease), and by determination of serum anti-PLP peptide antibody responses by standard direct ELISA (*Bottom*).

(Figs. 2 *Top* and 3 *Top*; black bars). Even more dramatic, MR1-treated animals showed only minimal or no clinical signs at both doses of PLP peptide used for EAE induction (Figs. 2 *Middle* and 3 *Middle*; note: no or only very low black bars). Clinical signs in the anti-CD40L-treated mice were only found when EAE was induced with the highest dose (300 μ g) of PLP peptide and disappeared on day 31, whereas clinical signs of the control group remained severe (Fig. 3 *Middle*). In control animals, anti-PLP peptide serum antibody responses were observed from day 9 until day 40, with maximal responses on day 14 (titer = 1433) and 21 (titer = 2710) after EAE induction with 75 μ g or 300 μ g of PLP peptide, respectively. In contrast, anti-PLP peptide antibody responses in animals treated with CD40L mAb on days 0, 2, and 4 were severely delayed and decreased, with highest levels on day 31 (titer = 571) and 40 (titer = 1034) after EAE induction with 75 μ g and 300 μ g of PLP peptide, respectively (Figs. 2 *Bottom* and 3 *Bottom*).

Effect of Anti-CD40L Treatment During Disease. Treatment with anti-CD40L mAb around day 6 and day 9 after EAE

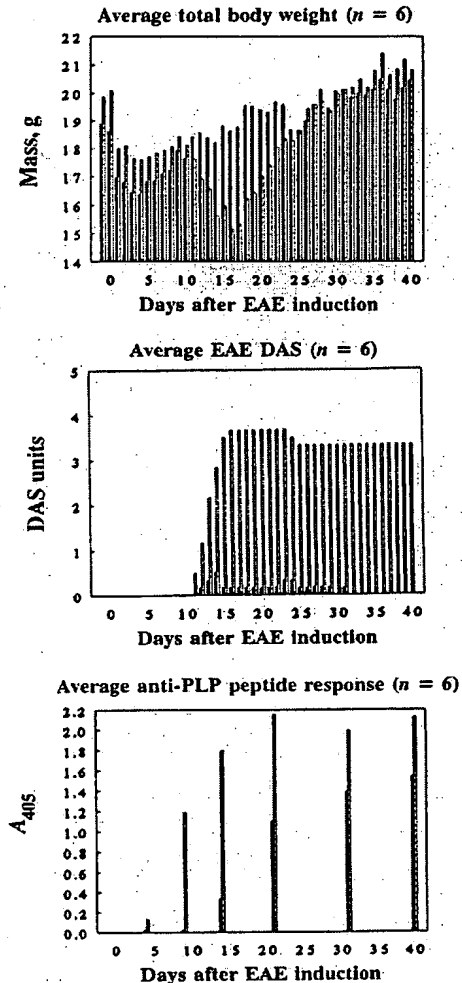


FIG. 3. Prevention of EAE induced with high-dose peptide by using anti-CD40L mAb. EAE was induced with 300 μ g of PLP peptide in female SJL/J mice ($n = 6$) according to a standard procedure. Animals were treated with anti-CD40L mAb on days 0, 2, and 4 (black bars). Control mice received normal hamster antibodies on the same days (hatched bars). The effect of anti-CD40L mAb treatment was monitored by determination of the body weight (*Top*) by evaluation of clinical signs (*Middle*; note: only very low black bars/minimal disease), and by determination of serum anti-PLP peptide antibody responses by standard direct ELISA (*Bottom*).

induction with 150 μ g of PLP peptide still resulted in blockade of disease by 80% and 67%, respectively, as compared with the complete inhibition (100%) in animals treated with anti-CD40L mAb around day 2 (Fig. 4). Of the animals treated with anti-CD40L, none died due to EAE. In control animals, the first EAE clinical signs (and death) were found on day 11.

DISCUSSION

This study provides evidence that CD40-CD40L interactions are involved in development of EAE in mice and MS in man. Functionally, treatment of mice with antibodies against CD40L both prevented development of disease (prophylaxis) and dramatically suppressed clinical signs when treatment was started after onset of disease (therapy). Histologically, cells expressing CD40 and CD40L were found in the perivascular infiltrates in the CNS of both EAE mice and MS patients but not in control tissues. Double-staining procedures revealed

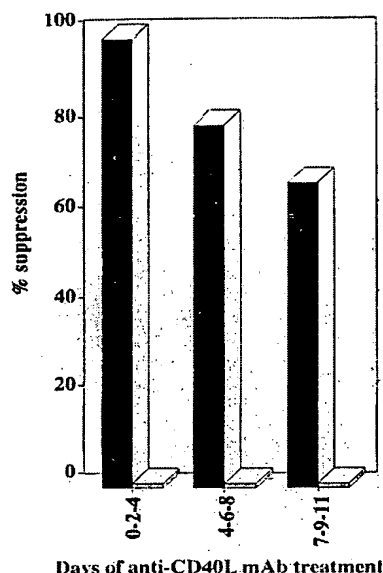


FIG. 4. Effect of delayed anti-CD40L treatment on EAE. EAE was induced with 150 μ g of PLP peptide in female SJL/J mice ($n = 6$) according to a standard procedure. Animals were treated with anti-CD40L mAb on days 0, 2, and 4; 4, 6, and 8; or 7, 9, and 11 (black bars). Control mice received normal hamster antibodies on the same days (hatched bars). The effect of anti-CD40L mAb treatment was monitored by evaluation of clinical signs. The cumulative DAS scores from day 12 until day 28 of mice treated with anti-CD40L mAb on days 0, 2, and 4 was set at 100% EAE suppression. Cumulative DAS scores from day 12 until day 28 of the other groups were related to this percentage.

that the majority of CD40-expressing cells in human MS brain were cells of the monocytic lineage, while a minority belonged to the B-cell subset. Finally, juxtaposition of CD40- and CD40L-expressing cells *in situ* was demonstrated, indicative of ongoing cellular interactions.

The interaction between CD40L on activated CD4⁺ T cells and CD40 on B cells has been shown to be indispensable for antibody responses against thymus-dependent antigens (1-4). However, recent data indicate that the CD40-CD40L axis is involved not only in humoral immunity but in development of some autoimmune diseases as well, such as collagen-induced arthritis (17) and lupus nephritis (18).

Here, we show that cells expressing CD40L could be found in perivascular infiltrates of CNS tissue of both EAE mice and MS patients but not in control tissues. Frequencies of CD40L-expressing cells in these infiltrates were modest. This is in accordance with frequencies of CD40L⁺ cells induced in the spleen by immunization of mice with thymus-dependent antigen (TNP-KLH)(3), where ~ 1 CD40L⁺ cell was found per 12 KLH-specific B cells. Cells expressing CD40 were abundantly present in perivascular infiltrates of MS brain. By using acid phosphatase and CD11b (CR3) as markers for monocytes/macrophages and microglia (8, 13), it was shown that CD40 expression was predominantly restricted to cells of the monocytic lineage, while B cells formed a minority of the CD40⁺ population.

To functionally assess the role of CD40 and its ligand, we blocked this cognate interaction *in vivo* by administration of anti-CD40L antibody in a mouse EAE model. Treatment with anti-CD40L mAb during disease induction (days 0-4) completely prevented development of disease, indicating that CD40-CD40L interactions play an important role in the induction phase of EAE. Importantly, delaying treatment with anti-CD40L mAb by initiating it shortly before maximal clinical disease score was reached, resulted in near-total suppres-

sion of disease (Fig. 4). These results indicate that CD40-CD40L interactions are not only important in the induction phase but also during the clinical phase of EAE, implying that the development of this inflammatory disease of the CNS is dependent on continuous or repeated CD40-CD40L interactions, as was shown for humoral responses against thymus-dependent antigens (1-3).

What effector mechanisms are induced by CD40-CD40L interactions in the CNS during EAE and MS? The immunocytochemical data discussed above clearly showed that the majority of CD40-bearing cells were macrophages or microglia. In addition, a small subpopulation of CD40⁺ cells belonged to the B-cell lineage. Consequently, CD40L-induced functions of both macrophages/microglia and B cells should be considered. With respect to B cells, antibodies specific for or crossreactive with myelin components may be involved in the process of demyelination in EAE (see, for example, refs. 19 and 20). However, several findings argue against a central role for B cells in development of EAE and MS. It has been convincingly demonstrated that EAE can be adoptively transferred by T cells but not by B cells (21). Furthermore, we have found only limited numbers of MBP-specific plasma cells in CNS tissue of MS patients and EAE rhesus monkeys (9). The current study demonstrates that the number of immunoglobulin-containing CD40⁺ B cells in lymphoid infiltrates of MS brain is also limited in relation to the total number of infiltrating cells and the number of CD40⁺ cells of the monocytic lineage. Finally, the anti-PLP peptide antibodies found at later time points after anti-CD40L treatment indicate that, despite intact B-cell function, no clinical signs develop. Apparently, either B-cell responses are not crucial to disease induction or B cells/antibodies become unable to induce disease after a critical susceptible period.

This leaves macrophages/microglia (CD11b⁺, acid phosphatase-containing cells; see Fig. 1 D-H) in perivascular infiltrates as the CD40-bearing population crucial to disease development. Consistent with this possibility, Huitinga *et al.* (7) have elegantly demonstrated that macrophages are required for development of EAE in rats. What macrophage effector mechanisms contributing to inflammation and/or demyelination in the CNS may be activated through CD40 triggering? Alderson *et al.* (5) have shown that CD40 triggering of human monocytes induced tumoricidal activity, and in the presence of appropriate cytokines, tumor necrosis factor α , IL-6, and IL-8 was produced. In addition, CD40 triggering induces IL-1 and IL-12 (22, 23) and can enhance nitric oxide production (24). Interestingly, antibodies against IL-12 prevent development of EAE in mice (25). It remains to be determined which of these compounds are actually produced *in vivo* in response to CD40-CD40L interactions and what their relative contributions to disease development are.

How does treatment with anti-CD40L antibody prevent disease development and suppress established disease? As we discussed before (4), anti-CD40L mAb does not induce unresponsiveness by a direct cytotoxic effect on T cells, and it does not affect the frequencies of IL-2, IL-4, and interferon γ -producing cells *in situ* (3). Collectively, these observations and the current study suggest that amelioration of EAE by anti-CD40L treatment may result from direct blocking of interaction of CD40L on activated T cells with CD40 on monocytes/macrophages and microglial cells.

Alternatively, anti-CD40L antibody may induce Th-cell unresponsiveness in EAE by interference with the CD40-related expression of additional costimulatory molecules on antigen-presenting cells, resulting in impaired antigen presentation. Other studies support this hypothesis in view of the fact that the blocking of interactions between B7 family members and their ligands *in vivo* induce a state of allo-specific T-cell unresponsiveness (26). Therefore, receptors like CD40, the triggering of which was shown to regulate the expression of

B7.1 and B7.2 (27), might play an important role in controlling tolerance and immunity.

Although further details of the mechanism(s) of action are clearly needed, the co-localization of CD40-bearing macrophages/microglia and CD40L-bearing cells in affected CNS tissue of patients suggests that CD40-CD40L interactions may play an important role in the immunopathology of MS. By analogy with the results obtained in EAE, blockade of CD40-CD40L interactions should be considered as a method to interfere in active episodes of MS as well. Preventing CD40-CD40L interactions is potentially useful in limiting duration, intensity, and neurological damage of disease exacerbations. A significant advantage of CD40L as a target for intervention, in comparison with the constitutively expressed CD40, is its transient expression restricted to activated CD4⁺ T cells. This feature allows targeting of only those T cells actively participating in the response without affecting the population of T cells at large.

MS-autopsy brain tissues were obtained from the Netherlands Brain Bank in Amsterdam (coordinator Dr. R. Ravid). We thank Dr. Mark de Boer (PanGenetics BV) for supplying the 5D12 mAb directed to human CD40. We thank Marjan van Meurs and Louis Ribbens for excellent histochemical support. This study was financially supported by the Netherlands Foundation for the Support of MS Research, projects MS89-50 (K.G.) and MS94-171 (J.D.L.), and partially supported by a pilot grant from the National Multiple Sclerosis Society and National Institutes of Health Grant AI26296 (R.J.N.).

1. Durie, F. H., Foy, T. M., Masters, S. R., Laman, J. D. & Noelle, R. J. (1994) *Immunol. Today* 15, 406-411.
2. Foy, T. M., Shepherd, D. M., Durie, F. H., Aruffo, A., Ledbetter, J. A. & Noelle, R. J. (1993) *J. Exp. Med.* 178, 1567-1575.
3. Van den Eertwegh, A. J. M., Noelle, R. J., Roy, M., Shepherd, D. M., Aruffo, A., Ledbetter, J. A., Boersma, W. J. A. & Claassen, E. (1993) *J. Exp. Med.* 178, 1555-1565.
4. Foy, T. M., Laman, J. D., Ledbetter, J. A., Aruffo, A., Claassen, E. & Noelle, R. J. (1994) *J. Exp. Med.* 180, 157-163.
5. Alderson, M. R., Armitage, R. J., Tough, T. W., Strockbine, L., Fanslow, W. C. & Spriggs, M. K. (1993) *J. Exp. Med.* 178, 669-674.
6. Traugott, U., Scheinberg, L. C. & Raine, C. S. (1982) *Ann. Neurol.* 11, 182-186.
7. Huitinga, I., Ruuls, S. R., Jung, S., Van Rooijen, N., Hartung, H.-P. & Dijkstra, C. D. (1995) *Clin. Exp. Immunol.* 100, 344-351.
8. Bauer, J., Sminia, T., Wouterlood, F. G. & Dijkstra, C. D. (1994) *J. Neurosci. Res.* 38, 365-375.
9. Gerritse, K., Deen, C., Fasbender, M., Ravid, R., Boersma, W. J. A. & Claassen, E. (1994) *J. Neuroimmunol.* 49, 153-159.
10. Noelle, R. J., Roy, M., Shepherd, D. M., Stamenkovic, I., Ledbetter, J. A. & Aruffo, A. (1992) *Proc. Natl. Acad. Sci. USA* 89, 6550-6554.
11. Van Rooijen, N., Claassen, E., Kraal, G. & Dijkstra, C. D. (1989) *Prog. Histochem. Cytochem.* 19, 1-71.
12. De Boer, M., Kasran, A., Kwekkeboom, J., Walter, H., Vandenbergh, P. & Ceuppens, J. L. (1993) *Eur. J. Immunol.* 23, 3120-3125.
13. Ulvestad, E., Williams, K., Bjerkvig, R., Tiekotter, K., Antel, J. & Matre, R. (1994) *J. Leukocyte Biol.* 56, 732-740.
14. Dautigny, A., Alliel, P. M., d'Auriol, L., Pham-Dinh, D., Nussbaum, J. L., Galibert, F. & Jolles, P. (1985) *FEBS Lett.* 188, 33-36.
15. Sobel, R. A., Tuohy, V. K., Lu, Z., Laursen, R. A. & Lees, M. B. (1990) *J. Neuropathol. Exp. Neurol.* 49, 468-479.
16. Zegers, N. D., Claassen, E., Neelen, C., Mulder, E., van Laar, J. H., Voorhorst, M. M., Berrevoets, C. A., Brinkmann, A. O., van der Kwast, T. H., Ruizeveld de Winter, J. A., Trapman, J. & Boersma, W. J. A. (1991) *Biochim. Biophys. Acta* 1073, 23-32.
17. Durie, F. H., Fava, R. A., Foy, T. M., Aruffo, A., Ledbetter, J. A. & Noelle, R. J. (1993) *Science* 261, 1328-1330.
18. Mohan, C., Shi, Y., Laman, J. D. & Datta, S. K. (1995) *J. Immunol.* 154, 1470-1480.
19. Lassmann, H., Brunner, C., Bradl, M. & Linington, C. (1988) *Acta Neuropathol.* 75, 566-576.
20. Warren, K. G. & Catz, I. (1994) *J. Neurol. Sci.* 121, 66-73.
21. Ben-Nun, A. & Cohen, I. R. (1982) *J. Immunol.* 128, 1450-1457.
22. Wagner, D. H., Stout, R. D. & Suttles, J. (1994) *Eur. J. Immunol.* 24, 3148-3154.
23. Shu, U., Kiniwa, M., Wu, C. W., Maliszewski, C., Vezzio, N., Hakimi, J., Gately, M. & Delespesse, G. (1995) *Eur. J. Immunol.* 25, 1125-1128.
24. Tian, L., Noelle, R. J. & Lawrence, D. A. (1995) *Eur. J. Immunol.* 25, 306-309.
25. Leonard, J. P., Waldburger, K. E. & Goldman, S. J. (1995) *J. Exp. Med.* 181, 381-386.
26. Tan, P., Anasetti, C., Hansen, J. A., Melrose, J., Brunvand, M., Bradshaw, J., Ledbetter, J. A. & Linsley, P. S. (1993) *J. Exp. Med.* 177, 165-173.
27. Roy, M., Aruffo, A., Ledbetter, J., Linsley, P., Kehry, M. & Noelle, R. J. (1995) *Eur. J. Immunol.* 25, 596-603.

Macrophage/Microglial-mediated Primary Demyelination and Motor Disease Induced by the Central Nervous System Production of Interleukin-3 in Transgenic Mice

Chi-Shiun Chiang,* Henry C. Powell,† Lisa H. Gold,* Ana Samimi,* and Iain L. Campbell*

*Department of Neuropharmacology, The Scripps Research Institute, La Jolla, California 92037; †Veterans Administration Research Service and Department of Pathology, University of California San Diego, La Jolla, California 92093-0612

Abstract

Activated macrophage/microglia may mediate tissue injury in a variety of CNS disorders. To examine this, transgenic mice were developed in which the expression of a macrophage/microglia activation cytokine, interleukin-3 (IL-3), was targeted to astrocytes using a murine glial fibrillary acidic protein fusion gene. Transgenic mice with low levels of IL-3 expression developed from 5 mo of age, a progressive motor disorder characterized at onset by impaired rota-rod performance. In symptomatic transgenic mice, multi-focal, plaque-like white matter lesions were present in cerebellum and brain stem. Lesions showed extensive primary demyelination and remyelination in association with the accumulation of large numbers of proliferating and activated foamy macrophage/microglial cells. Many of these cells also contained intracisternal crystalline pole-like inclusions similar to those seen in human patients with multiple sclerosis. Mast cells were also identified while lymphocytes were rarely, if at all present. Thus, chronic CNS production of low levels of IL-3 promotes the recruitment, proliferation and activation of macrophage/microglial cells in white matter regions with consequent primary demyelination and motor disease. This transgenic model exhibits many of the features of human inflammatory demyelinating diseases including multiple sclerosis and HIV leukoencephalopathy. (*J. Clin. Invest.* 1996; 97:1512–1524.) Key words: neurologic disease • multiple sclerosis • inflammation • cytokine • glial fibrillary acidic protein

Introduction

Microglia are central nervous system (CNS)¹ resident, macrophage-derived cells that comprise 10–20% of the normal

adult brain glial cells and exist largely in a resting state (1–3). These cells become functionally activated when the brain is injured or in the course of neurodegenerative disease. Pronounced activation of the macrophage/microglia in the CNS has been associated with many disorders such as multiple sclerosis (MS) (4), Parkinson's dementia (5), Alzheimer dementia (6), human immunodeficiency virus (HIV)-associated dementia (7) and radiation-induced CNS injury (8). Activation of microglia may play a role in host defense, e.g., immune activation or tissue repair, and this process could also be harmful, contributing to CNS tissue injury (3, 9–11). In support of the latter view, these cells are known to produce a number of soluble factors, including cytokines, prostaglandins, and free radicals (for reviews see references 7, 10, and 12), that are toxic to neurons in vitro. In spite of this largely circumstantial evidence, definitive information concerning the potential neuropathogenic actions of activated microglia is lacking, as are suitable animal models for studying the role of these cells in CNS disease.

Interleukin 3 (IL-3) was originally described as a T cell-derived cytokine (for review see reference 13) that acted as a hematopoietic growth factor supporting the proliferation of multipotential progenitors at the early stages of their differentiation. Subsequently, IL-3 was shown to possess potent macrophage-activating properties associated with T cell-dependent immune responses (14), (15). As a growth factor in the development of hematopoietic progenitor cells as well as mature neutrophils, eosinophils and macrophages in the bone marrow and peripheral circulation, IL-3 has been used in clinical trials in the treatment of pancytopenic disorders (16–18). Consistent with its immune regulatory properties, tumors engineered to produce murine IL-3 become heavily infiltrated by macrophages and granulocytes (19, 20). In the CNS, microglia have been reported to produce and respond to IL-3 (21). Expression of the β subunit (signal transducing) of the IL-3 receptor shows restricted distribution in the rat brain, being expressed by only macrophage/microglial cells (22). IL-3 also acts on microglia in vitro, inducing proliferation and multinucleated giant cell formation (23). Moreover, a recent report found IL-3 was detectable in post mortem brain tissue from patients with Alzheimer's disease (24). Therefore, IL-3 may play a role in the marked activation of microglia and subsequent development of neurodegeneration seen in this disease.

The development of animal models for the spontaneous and chronic activation of the CNS microglia would greatly advance attempts at better understanding the biology and pathobiology of these cells. To this end, in the present study we utilized a previously well defined transgenic approach (25, 26) using a glial fibrillary acidic protein (GFAP) expression cassette to direct the constitutive expression of the macrophage/microglial activating cytokine, IL-3, to astrocytes in the intact CNS of mice. The results indicate that so-called GFAP-IL3 transgenic mice with low levels of cerebral IL-3 expression de-

Address correspondence to Dr. Iain L. Campbell, Department of Neuropharmacology, CVN 9, The Scripps Research Institute, 10666 North Torrey Pines Road, La Jolla, CA 92037. Phone: 619-784-7092; FAX: 619-784-7377; E-Mail: icamp@scripps.edu. Chi-Shiun Chiang's present address is Department of Nuclear Science, Tsing-Hua University, Hsin-Shu, 300043, Taiwan.

Received for publication 14 September 1995 and accepted in revised form 20 December 1995.

1. Abbreviations used in this paper: CNPase, 2', 3' Cyclic Nucleotide Phosphohydrolase; CNS, central nervous system; EAE, experimental allergic encephalomyelitis; GFAP, glial fibrillary acidic protein; MBP, myelin basic protein.

J. Clin. Invest.

© The American Society for Clinical Investigation, Inc.

0021-9738/96/03/1512/13 \$2.00

Volume 97, Number 6, March 1996, 1512–1524

velop in later life a progressive motor disorder as a result of a vigorous T cell-independent macrophage/microglia-mediated demyelination process. The molecular and cellular CNS manifestations of this disorder resemble many of those observed in human inflammatory demyelinating disorders. Therefore, the GFAP-IL3 transgenic mouse represents a novel experimental model to study the role of macrophage/microglia in the pathogenesis of CNS demyelinating disease.

Methods

Generation of GFAP-IL3 transgenic mice. The overall strategy used for the generation of the GFAP-IL3 transgenic mice followed that described previously for the generation of GFAP-IL6 transgenic mice (26). The CNS and astrocyte specific expression obtained for fusion gene constructs under the control of this promoter is well documented (26, 27). Briefly, a full length cDNA encoding murine IL-3 (kindly provided by Dr. John Schrader, University of British Columbia, Vancouver, Canada) was modified by removal of the 3' untranslated region. After the addition of Not-I linkers the modified IL-3 cDNA fragment was subcloned into the Not I-digested vector pCMV (Clontech, Palo Alto, CA). A clone containing the cDNA in the correct orientation was selected and the IL-3 cDNA together with the upstream SV-40 splice donor/acceptor site and the downstream SV-40 polyadenylation signal was excised using Xho I/Sal I. This fragment was then inserted into the unique SalI restriction enzyme site of the modified murine GFAP gene used previously for IL-6 (26).

After screening for correct orientation, the GFAP-IL3 fusion gene construct was excised and purified from plasmid DNA before microinjection into fertilized eggs of (C57BL/6J \times SJL) F1 hybrid mice. Transgenic offspring were identified by slot-blot analysis of tail DNA using a 32 P-labeled SV-40 late-region cDNA fragment as a probe.

Motor function test. Motor function was assessed using a rota-rod apparatus. Rota-rod balancing requires a variety of proprioceptive, vestibular, and fine tuned motor abilities. This task has been used successfully for detecting acute drug-induced changes in motor coordination as well as neurotoxicity produced by drugs and developmental behavioral abnormalities (28, 29).

The rota-rod apparatus consisted of a rotating horizontal cylinder (30 mm) and a motor driven control unit (Omnitech, Columbus, OH). The cylinder was divided into 4 separate rotating compartments, fully enclosed to ensure that the mice did not jump out of their area. The mice were placed on the rod which was rotating at a fixed speed of 5 or 15 revolutions per minute (rpm). Automatic timers recorded the duration of time (in tenths of seconds) the mice remained on the rod, and two infrared beams at the base of each compartment determined when the mice had fallen off the rod. Each mouse was tested for three 180 s trials, with 1 min inter-trial interval at 5 rpm. After all the mice were tested at 5 rpm they were then tested at 15 rpm (about 75 min later) for three 180 s trials, with 1-min inter-trial interval. All testing occurred in low light, during the dark portion of the light/dark cycle.

Rotating rod performance was analyzed by two-way analysis of variance (group and trial) with repeated measures on the trial factor followed by Newman-Keuls post hoc test.

RNA isolation. Organs were removed and immediately snap-frozen in liquid nitrogen. Poly (A)⁺ enriched RNA was isolated by a rapid procedure (30). Briefly, frozen organs were placed in lysis buffer (10 ml; 0.2 M NaCl, 0.2 M Tris/HCl pH 7.5, 1.5 mM MgCl₂, 2% SDS, 200 μ g/ml proteinase K) and immediately homogenized. After incubation for 60 min at 45°C, the NaCl concentration of the lysate was adjusted to 0.5 M and mixed with 40 mg of oligo-dT cellulose (In Vitrogen, San Diego, CA) that had been pre-equilibrated in binding buffer (0.5 M NaCl, 0.01 M Tris/HCl pH 7.5). The mixture was then incubated at 25°C for 60 min with gentle rocking. After washing with

binding buffer, poly (A)⁺ RNA was eluted from the oligo-dT cellulose with elution buffer (0.5 ml; 0.01 M Tris/HCl pH 7.5) and precipitated in ethanol, dried and resuspended in 25 μ l elution buffer. The concentration of RNA was determined by UV spectroscopy at 260 nm.

RNAse protection assays. RPA for the detection of cytokine RNAs was performed as described previously (31–33).

Northern blot analysis. Poly (A)⁺ RNA (5 μ g) was denatured, electrophoresed in 1% agarose/2.2 M formaldehyde gels, transferred to nylon membranes, pre-hybridized in hybridization buffer (HB) (6 \times SSPE, pH 7.6, 50% formamide, 5 \times Denhardt's solution, and 0.2% SDS) containing 10 μ g/ml Salmon Sperm DNA at 45°C for 1 h, and then hybridized overnight at 45°C with 32 P-labeled cDNA probes. After autoradiographic exposure, the membrane was stripped twice in boiling water and hybridized with a different probe. Probes used were: a 932-bp cDNA fragment corresponding to the murine Ia α chain (34), a 600-bp cDNA fragment corresponding to the murine H-2D^b (35) and a 0.26-kb fragment of β -actin gene fragment (36) generated by PCR was provided by M. Nerenberg (The Scripps Research Institute, La Jolla, CA).

In situ hybridization. Animals were anesthetized and then slowly perfused intracardially with ice-cold PBS (30 ml) followed by ice-cold 4% paraformaldehyde in PBS (30 ml). After perfusion, the brain was removed and placed in ice-cold 4% paraformaldehyde/1 \times PBS (phosphate-buffered saline, pH 7.3). After overnight fixation, brains were processed, embedded in paraffin and 8- μ m sagittal sections prepared. All subsequent procedures for in situ hybridization were as described (37). 35 S-labeled cRNA to IL-3 was used as probe. The IL-3 probe was generated from a pBluescript SK⁺/– vector that contains an EcoRI/BglII fragment of the murine IL-3 cDNA used to make the GFAP fusion gene described above.

Immunocytochemical analysis. For the detection of Mac-1, CD4, CD8, B220, or Ia, mice were sacrificed by cervical dislocation and the brain was immediately removed, embedded in O.T.C medium, and snap frozen. Sagittal sections (10 μ m) were cut on a cryomicrotome, air-dried and stored at –70°C. Immediately before staining, sections were fixed in cold (–20°C) methanol:acetone (1:1) solution for 1 min and then incubated for 20 min in PBS containing 2% FCS (to reduce nonspecific reactivity). Sections were incubated first with rat monoclonal antibody to: Mac-1 (ATCC/TIB126, Rockville, MD), CD4 (L3T4; Pharmingen), CD8 α (Ly-2; Pharmingen, San Diego, CA), B220 (CD45R, Pharmingen, San Diego, CA), or Ia (Clone MS/114, Boehringer-Mannheim Indianapolis, IN), respectively, for 1 h at room temperature. For GFAP immunostaining, brain was fixed in 70% alcohol overnight at 4°C, embedded in paraffin, and sagittal sections (4 μ m) cut. The antibody used was a polyclonal rabbit anti-bovine GFAP (DAKO, Santa Barbara, CA). For all sections, bound antibody was detected with a biotinylated anti-rat or rabbit antibody followed by avidin labeled horseradish peroxidase (Sigma Chemical Co., St. Louis, MO) or alkaline phosphatase (Sigma Chemical Co.). Staining employed 3',3' diaminobenzidine (Sigma Chemical Co.) as substrate. Before mounting, sections were counter stained in Mayers hematoxylin (Sigma Chemical Co.).

Light and electron microscopy. Unless stated otherwise morphological examination of the brain was performed on G3C2 mice and age- and sex-matched normal littermates. Before killing, animals were anesthetized with an intraperitoneal injection (2 ml/kg) of a solution consisting of pentobarbital (12.5 mg/ml) and diazepam (1.25 mg/ml) in 0.9% NaCl. Brains of some animals including the high expressor and G3K1 founder transgenic animals were removed for routine histology and light microscopic examination using buffered paraformaldehyde as a fixative. Animals used for electron microscopy were anesthetized and perfused intracardially with a solution of 5% phosphate buffered glutaraldehyde. The brain was then removed and after overnight fixation at 4°C, tissues were postfixed in a 1% aqueous osmium tetroxide solution for 2 h, dehydrated using a graded series of ethanols and propylene oxide and infiltrated with resin. Overnight infiltration was followed by embedding in fresh araldite resin. Thick sections (1 μ m) were cut with glass knives and stained with paraphe-

nylenediamine (PPD) or methylene blue azure II in preparation for light microscopic examination. Ultrathin sections from selected blocks were cut with a diamond knife and stained with uranyl acetate and lead citrate before electron microscopic examination.

Western blotting. For western blot analysis, mice were killed by cervical dislocation and the cerebellum and cortices were isolated and snap frozen. The tissue was weighed and homogenized by sonication in 10 volumes of 1% SDS. Samples were centrifuged at 14,000 rpm for 30 min, and the supernatant was collected. The protein concentration was determined by Bradford analysis using commercially available reagents (BioRad, Hercules, CA). Sample corresponding to 20 μ g protein was fractionated by 15% SDS PAGE and transferred to a nylon membrane using a Mini-Protein II system (BioRad) performed according to the manufacturer's instructions. Equal loading and transfer of proteins was confirmed with amido black (Sigma Chemical Co.) staining of the membrane. The membrane was then incubated for 1 h with 5% blocking solution (nonfat milk powder, BioRad) in Tris buffered saline with 0.1% Tween, pH 7.5 (T-TBS) (BioRad). After three washes with T-TBS, the membrane was incubated for 1 h with a solution containing rabbit anti-bovine GFAP antibody (1:5000) (DAKO, Santa Barbara, CA) or rabbit anti-murine CNPase (1:2000) (obtained from Dr. Monica Carson, The Scripps Research Institute). After washing with three changes of T-TBS, the membrane was incubated for 1 h with a horseradish peroxidase labeled goat anti-rabbit IgG antibody (Invitrogen), and the bound complex detected using an ECL kit (Amersham) performed according to the manufacturer's instructions. After autoradiograph exposure, the membrane was stripped in 0.5% β -mercaptoethanol in T-TBS at 60°C for 30 min, washed in T-TBS for 15 min, and then incubated for 1 h with 5% blocking solution. The membrane then was re-probed for rabbit anti-bovine MBP (1:2000) (Chemicon, Temecula, CA) or rabbit anti-rat SNAP25 (1:2000) (obtained from Dr. Michael C. Wilson, The Scripps Research Institute). The relative change in the intensity of the individual protein bands was determined by densitometry (Personal Densitometer, Molecular Dynamics, Sunnyvale, CA).

Cell proliferation in vivo. Mice were injected intraperitoneally with [3 H]thymidine (2 μ Ci/g of body weight) ([3 H]methyl-thymidine; Amersham) in 0.5 ml of saline and were killed 4 h after injection by cervical dislocation. Brains were processed and immunostained for the Mac-1, Ia and GFAP proteins as described above. After staining, the sections were dehydrated through a series of graded alcohol solutions and air-dried. Slides were then coated with film emulsion (Type NTB3; Eastman Kodak Co., Rochester, NY) and placed in a light tight box at 4°C for 4 wk. The emulsion was developed in DEKTOL (Eastman Kodak Co.) fixed, and counterstained with Mayer's Hematoxylin solution (Sigma Chemical Co.). For visualization and photomicroscopy, slides were examined using dark-field or epifluorescence microscopy.

Astrocyte cultures and the determination of IL-3 production. Astrocyte cultures were prepared from individual neonatal (< 48 h old) offspring as described previously (38). Brain cells from the cerebrum or the cerebellum were seeded into three wells of a six-well plate (Costar Corp.) to which was added DME containing antibiotics and 10% fetal calf serum. The medium was changed twice weekly. At confluence fresh medium was added to the cultures and supernatant was collected 24 h later for IL-3 assay. IL-3 was measured by an ELISA method using a commercially available kit (Endogen, Boston, MA) that detects murine IL-3. The remaining cells were lysed in 1 ml of 1% SDS in 50 mM Tris-HCl, pH 7.4. Protein concentration of lysate was determined by BioRad protein assay reagents (BioRad) performed according to the manufacturer's instructions.

Assay of 2', 3' cyclic nucleotide phosphodiesterase (CNPase) activity. CNPase activity was measured by the method of Prohaska et al. (39) as described previously (38). Brain tissue was homogenized in 9 volumes of 0.32 M sucrose. Aliquots (0.2 ml) of homogenate were mixed with 0.5% (wt/vol) sodium deoxycholate in 0.2 M Tris-HCl pH 7.5 (0.3 ml) and incubated for 10 min at 4°C. The homogenates were

diluted in three volumes of distilled water and the protein concentration measured as described above. Homogenates (20 μ g protein) were incubated with 180 μ l of 10.5 mM 2'-3'-cAMP in 50 mM Tris-maleate pH 6.2 for 10 min at 30°C. The reaction was terminated by placing tubes in boiling water for 30 s. The solutions were returned to 30°C and 0.1 ml of 0.3M Tris, pH 9 containing 21 mM MgCl₂ and 0.72 units of alkaline phosphatase (Sigma Chemical Co.) was added and the mixture incubated at 30°C for 20 min. A mixture of isobutanol and toluene (1:1) (1.2 ml) was then added together with 1.2 ml of 1.5% (wt/vol) (NH₄)₆MO₇O₂₄·4H₂O in 0.5 M H₂SO₄. After 20 min of

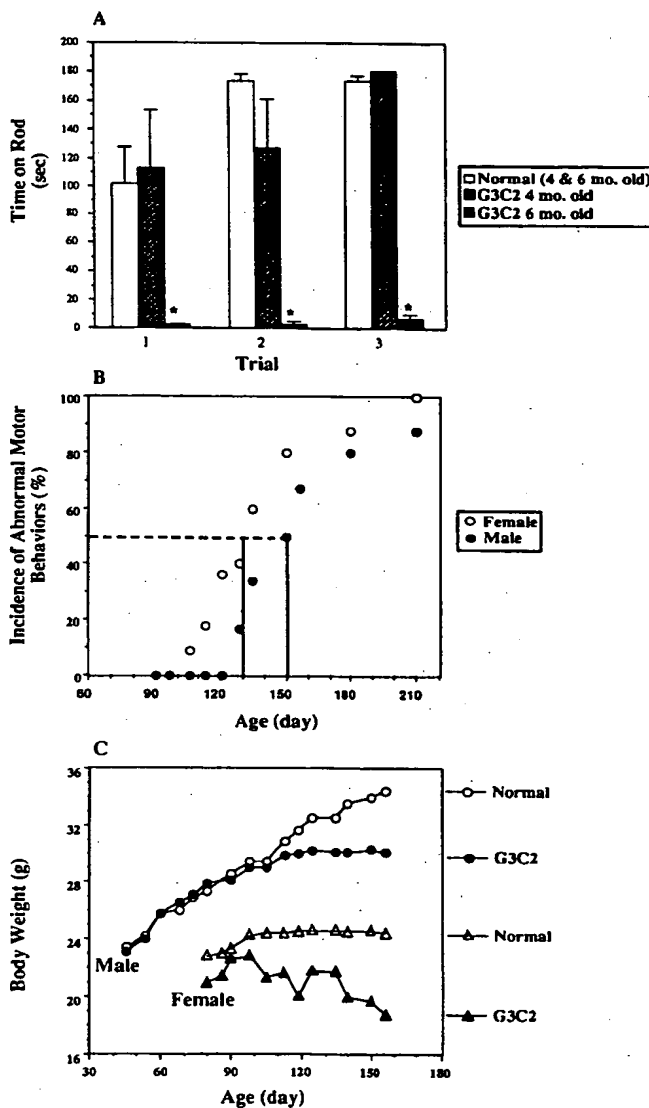


Figure 1. Altered physical characteristics of G3C2 transgenic mice. (A) Impaired performance on a rotating rod (5 rpm) in 6 month old G3C2 mice ($n = 3$) compared with that of 4-mo-old G3C2 mice ($n = 5$) and normal littermates ($n = 10$). Values represent mean \pm SEM time spent on rotating rod for 3 trials with a maximum possible duration of 180 s/trial. (B) Incidence of motor disease at different ages of G3C2 mice. (C) Body weight at different ages of G3C2 compared with normal littermates. The data of (B) and (C) was obtained from 10 mice for each group. These mice were followed until the age of 7 mo. The incidence of abnormal motor behavior, e.g. head tilting and abnormal gait, and body weight were scored once a week.

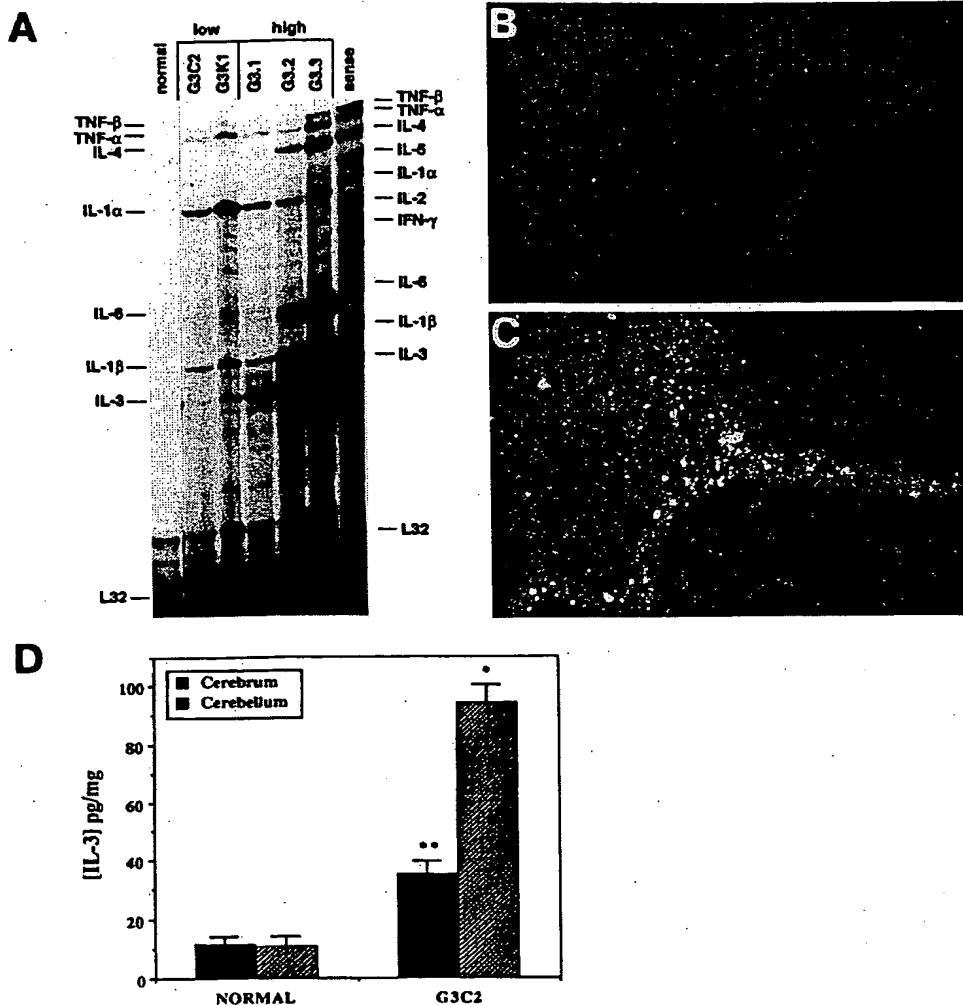


Figure 2. Analysis of cerebral transgene-encoded IL-3 expression. (A) RNase protection analysis of cytokine mRNA levels in the brain of low expressor and high expressor GFAP-IL3 mice. (B-C) Distribution of IL-3 RNA expression in the brain was assessed by in situ hybridization with an 35 S-labeled anti-sense IL-3 RNA probe. Sections shown represent cerebellum from a normal littermate (B) and the G3K1 founder mouse (C). Expression of IL-3 RNA was detectable in the transgenic specimen only and was particularly prominent in white matter tracts. (D) IL-3 production from cultured astrocytes. Compared with normal littermates, significant production of IL-3 was found from astrocytes derived from G3C2 mice. The production of IL-3 was markedly higher from astrocytes isolated from the cerebellum versus cerebrum ($P < 0.01$) of the G3C2 animals. Values represent mean \pm SEM ($n = 3$). * $P < 0.01$; ** $P < 0.05$; compared with normal.

shaking, the solutions were centrifuged at 2,200 rpm for 4 min and the absorbance of the yellow upper layer was read in a spectrophotometer at 410 nm. Activity was expressed in Units (one unit defined as one μ mole phosphate release per mg of protein per minute).

Results

Cerebral expression of IL-3 results in dose-related neurological disease. From birth, several founder generation mice displayed severe neurological disturbance with ataxia, runting, tremor, and disproportionate enlargement of the head. These animals died before reaching reproductive maturity. Pathological changes in the brain of these transgenic mice included marked cellular infiltration (with mainly macrophages, lymphocytes and to a less degree granulocytes), meningoencephalitis, hydrocephalus, gliosis, and neurodegeneration (data not shown). Two founder transgenic mice (G3K1 and G3C2) appeared healthy and normal until 4 and 5 mo of age, respectively. At this time, these animals developed abnormal motor features with head tilting, ataxia, and weakness in muscle strength. Founder G3K1 failed to breed and was killed for further analysis at 5 mo old. In contrast, founder G3C2 was mated successfully to derive a stable transgenic line. Transgenic off-

spring from the G3C2 line developed a motor disorder identical to that of the parental founder. In these animals, from onset at 5–7 mo of age, the symptoms progressed rapidly over the next 2–3 mo resulting in quadriplegia and premature death. Compared with normal age-matched littermates, symptomatic G3C2 mice were significantly impaired in a quantitative test of motor function. Performance on rotating rod (5 rpm) for female G3C2 mice at 4 and 6 mo of age and normals is shown in Fig. 1 A. Because there was no difference in rotorod performance between groups of normal mice at the two ages, the data for these groups has been pooled ($F[1,8] = 1.15$, $P > 0.05$). Although the 4-mo old transgenics performed as well as normal mice, there was a significant deficit in rotorod performance in the 6-mo-old G3C2 mice observed for all three trials ($F[2,15] = 22$, $P < 0.05$; followed by Newman-Keuls test). There was no significant group by trial interaction. Performance on the rod rotating at 15 rpm was also significantly impaired in the 6-mo-old G3C2 mice compared with 4-mo-old G3C2 mice and normals (4 and 6 mo old combined; $F[2,15] = 12.5$, $P < 0.05$, followed by Newman-Keuls test; data not shown). Studies of the incidence of motor disease (Fig. 1 B) showed that female mice tended to develop symptoms earlier than males (130 d for female vs. 150 d for male). Moreover, pregnancy in the G3C2 transgenic mice accelerated the onset

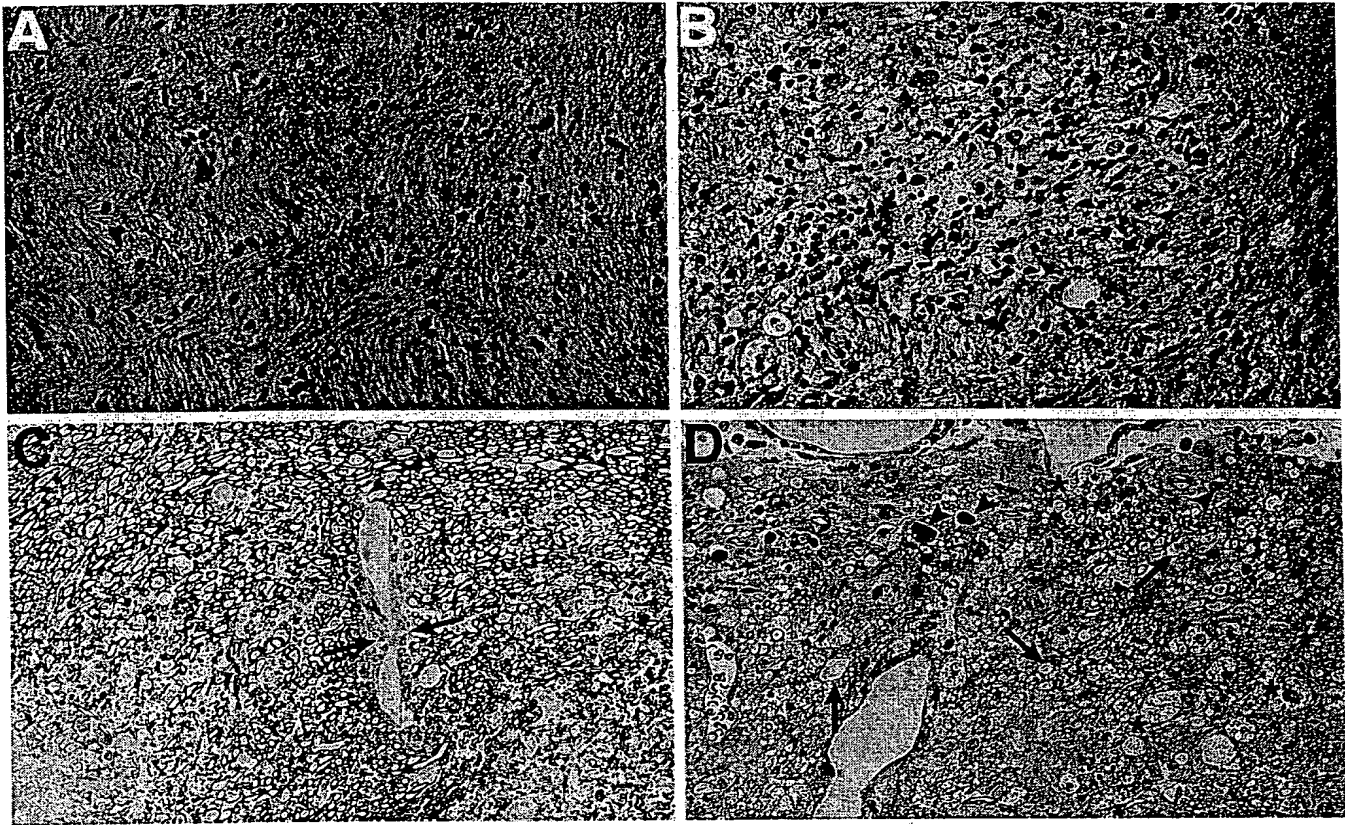


Figure 3. Focal white matter lesions and demyelination in the brain of G3C2 mice. Brains were obtained from age- and sex-matched normal littermates (A) and presymptomatic (C) or symptomatic G3C2 mice (B and D). Sections from paraffin embedded control mouse cerebellar tissue (A), stained with Luxol Fast Blue showing dense blue staining of the white matter characteristic of normal myelination. $\times 448$. In contrast, in a similarly stained specimen from the transgenic mouse (B), a hypercellular area is visible, forming a discrete plaque-like lesion in the white matter. Note the loss of blue staining associated with this lesion indicative of demyelination. $\times 448$. Plastic sections from the brainstem of presymptomatic 4-mo-old (C) and symptomatic 5.5-mo-old (D) G3C2 mice stained with methylene-blue. $\times 448$. This specimen from the presymptomatic animal shows normal myelination of white matter. However, the vessel at the center of the illustration shows perivenular cellular infiltrates (arrow). In contrast, in the symptomatic animal there is extensive loss of myelin. Demyelinated axons (arrows), myelin debris (arrowheads), and foamy macrophages (asterisks) are prominent.

of observable motor disease (not shown). Analysis of body weight revealed that G3C2 mice, in contrast to their normal littermates, failed to gain weight at the onset of motor signs (Fig. 1, B and C). Consistent with the incidence data, female G3C2 mice also showed earlier and more pronounced changes in body weight than their male transgenic littermates (Fig. 1 C).

The onset and severity of the neurological disorder in the different founders was related to the levels of transgene encoded IL-3 mRNA expression (Fig. 2 A). Thus, founders with severe, early onset neurological disease had high levels of cerebral IL-3 mRNA expression. Coincidentally, in addition to IL-3, the expression of a number of other cytokine mRNAs including those for IL-1 α , IL-1 β , IL-4, and TNF- α was also found to be significantly elevated in these mice (Fig. 2 A). In all the high IL-3 expressor transgenic mice this finding paralleled the neurohistological observation of diffuse encephalitis (not shown). Founder G3K1 expressed comparatively lower levels of IL-3 mRNA in the brain, while transgenic mice of the G3C2 line showed lowest levels of cerebral IL-3 mRNA expression. Increased cerebral expression of IL-1 α , IL-1 β and TNF- α but not IL-4 mRNA was also observed in these low expressor transgenic mice. A survey of spleen, kidney, liver, tes-

tis and skin from G3C2 transgenic animals failed to detect expression of IL-3 RNA in these peripheral organs (not shown). Localization of IL-3 RNA by in situ hybridization showed predominant expression in the white matter tracts of the cerebellum and brain stem in the G3K1 mouse (Fig. 2 C). In G3C2 mice, the level of IL-3 mRNA was too low to be detected by this method. However, production of IL-3 protein from astrocyte cultures derived from cerebrum (35.5 ± 4.3 pg/mg) and cerebellum (94.5 ± 5.7 pg/mg) (Fig. 2 D) confirmed transgene encoded IL-3 expression was also higher for astrocytes in the cerebellum in the G3C2 animals.

Low levels of cerebral IL-3 production result in primary demyelination of the white matter. To examine the pathologic correlates of the neurological disorder seen in the low expressor mice, brains from G3C2 offspring of different ages were examined by light and electron microscopy. Routine histological examination failed to reveal significant alterations in asymptomatic mice. With the onset of neurological signs, focal inflammatory lesions in white matter in the cerebellum and brain stem were prominent (Fig. 3, A and B). Increased numbers of mononuclear cells were observed in perivenular regions in the cerebellum. Myelin stains revealed demyelination

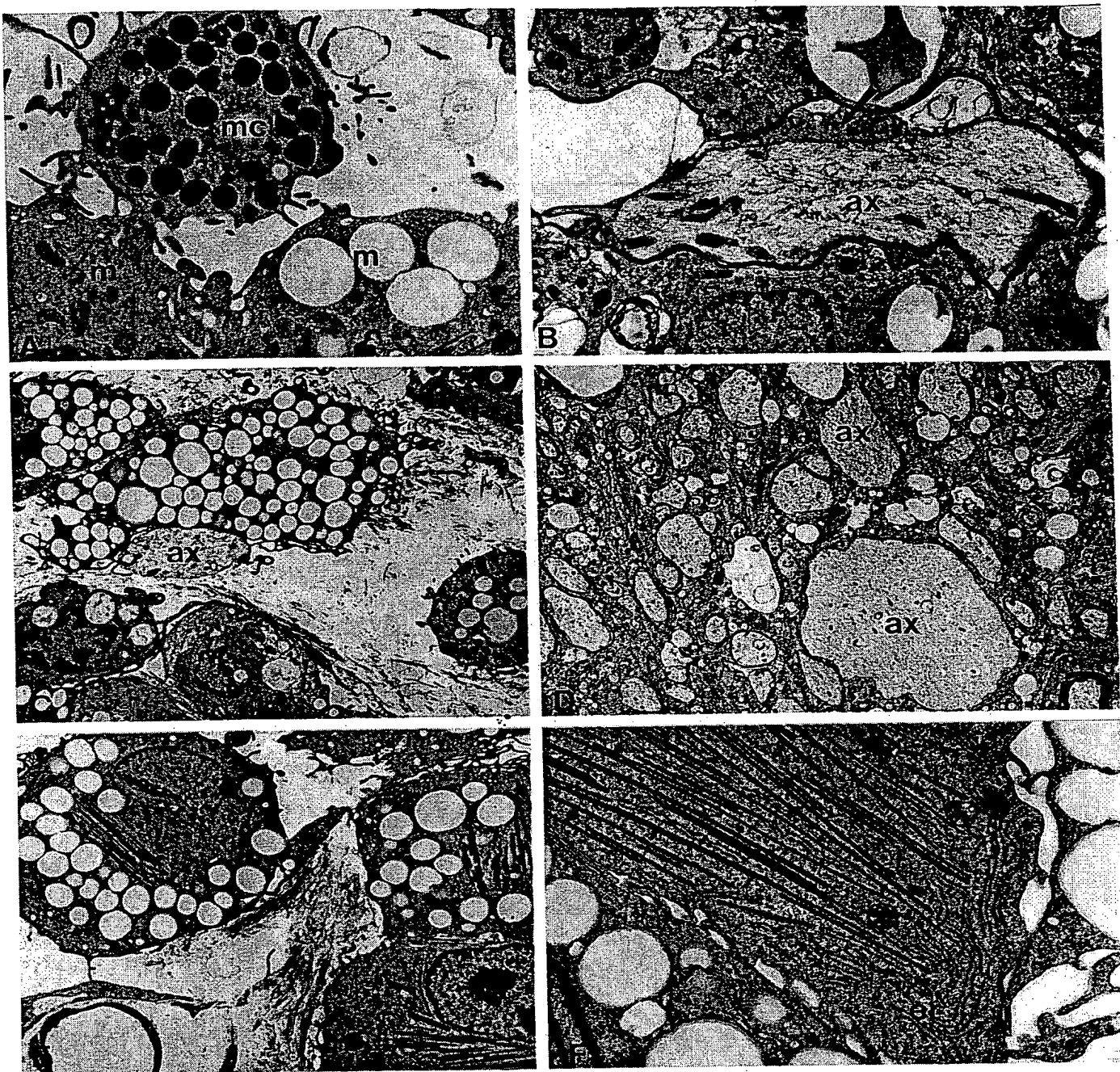


Figure 4. Ultrastructural features of demyelinating lesions in the brain stem. (A) Macrophages (M) and a mast cell (MC) represent the cell types that constitute the inflammatory infiltrate. The macrophages shown in this figure contain lipid droplets ($\times 5533$). (B) A thinly myelinated fiber undergoing demyelination with separation of myelin lamellae from the axonal surface and penetration by a process of an infiltrating cell (arrow) not connected to the myelin. The infiltrating process lies between two areas of myelinolysis ($\times 6972$). (C) A completely demyelinated axon is surrounded by a foamy macrophage. Collagen fibrils are seen in the interstitial space ($\times 3112$). (D) Axons (ax) in this field are either completely demyelinated, partially myelinated, or thinly myelinated consistent with remyelination ($\times 2490$). (E) Thin, needle-like inclusions are clustered at the center of this macrophage which also contains foamy vacuolar inclusions ($\times 3423$). (F) Polygonal "pole-shaped" crystalline inclusions appear in a cell in which there is ample endoplasmic reticulum (er). The inclusions are themselves enveloped by membranes of rough endoplasmic reticulum ($\times 8715$).

in association with white matter lesions (Fig. 3, A and B). Cerebellar cortices in transgenic animals with late stage disease exhibited disorganization of granular layer structure and the loss of Purkinje cells was also evident. One micron thick plastic

sections from the cerebellum and brainstem of 4-mo-old mice showed occasional perivenular cellular infiltrates (Fig. 3 C), as well as rare foci of active, macrophage mediated demyelination. In contrast, in symptomatic 5-mo-old transgenic mice,

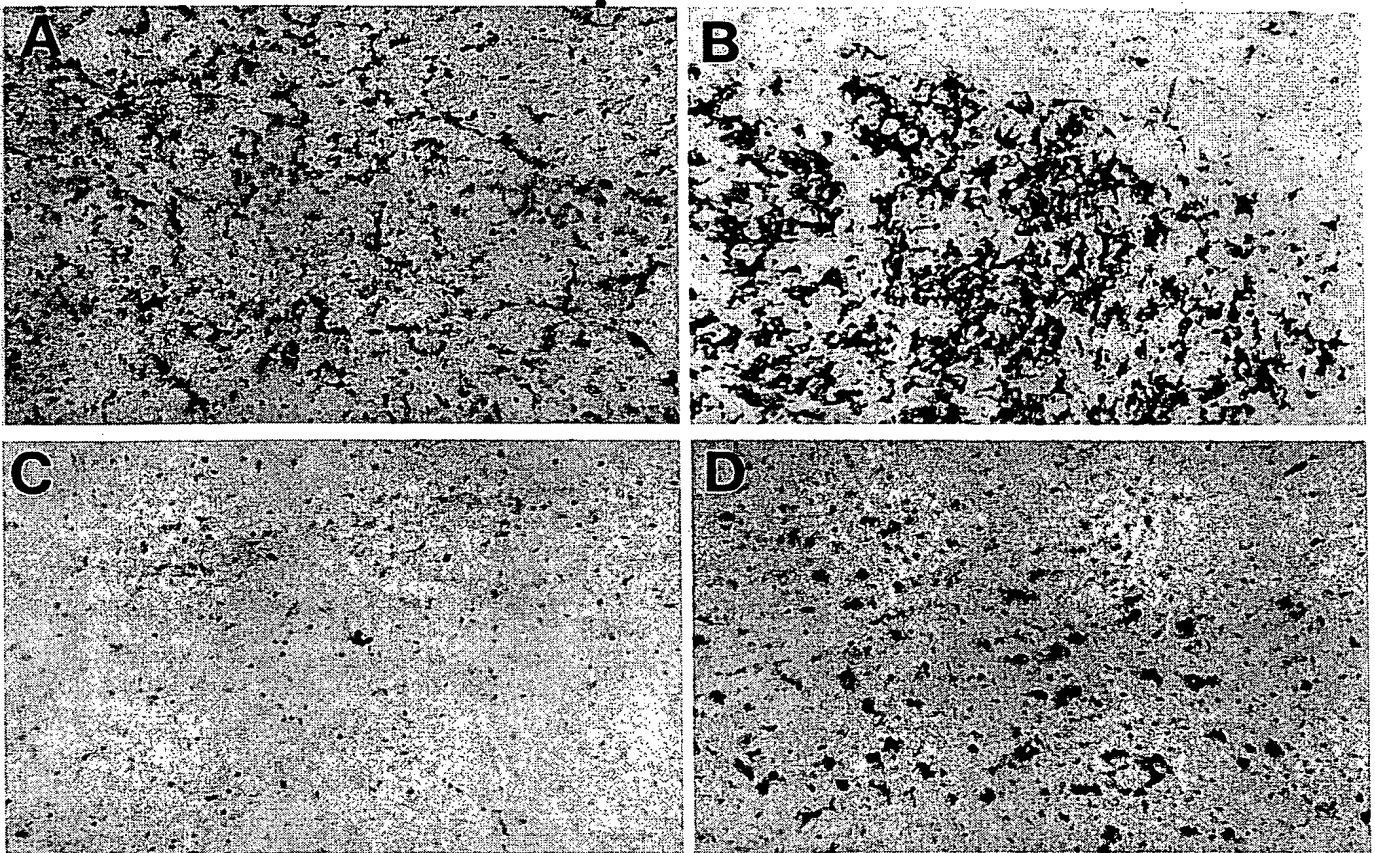


Figure 5. Prominent macrophage/microglial accumulation and activation in white matter lesions in GFAP-IL3 mice. Cryostat sections of brain from a normal (A) or a symptomatic G3C2 (B) mouse immunostained for Mac-1 showing a pronounced accumulation of strongly stained cells in a white matter lesion in the transgenic specimen. Adjacent sections immunostained for Ia revealed a significant increase in Ia⁺ cells associated with white matter lesions in the G3C2 (D) specimen compared with normal (C).

gross loss of myelin was manifest in white matter lesions with large numbers of demyelinated but normal appearing axons visible (Fig. 3 D). Large foamy macrophages were conspicuous throughout the demyelinated regions and clumps of myelin debris were also noted (Fig. 3 D). Foamy macrophages were also present on the surface of the brain stem (Fig. 4 A).

By electron microscopy, demyelination was seen in cerebellar and brain stem white matter associated with infiltration by macrophages (Fig. 4, B and C), which appeared in the parenchyma and on the axon surface (Fig. 4 B). Completely demyelinated axons were often surrounded by foamy macrophages in which the cytoplasm was filled with lipid rich vacuoles (Fig. 4 C). Contiguous axons were either partially myelinated or had inappropriately thinly myelinated sheaths consistent with remyelination (Fig. 4 D). The vast majority of demyelinated axons appeared normal indicating that myelin was the primary target for injury. The inflammatory infiltrate showed some distinctive abnormalities. Many of the lipid rich macrophages also contained crystalline "pole-like" inclusions in their endoplasmic reticulum (Fig. 4 E). Other macrophages contained exclusively crystalline inclusions which filled their cytoplasm with needle shaped profiles that were surrounded by cisternae of endoplasmic reticulum (Fig. 4 F). In the most severely affected areas of the cerebellar white matter, intense

infiltration by macrophages was accompanied by necrosis and cavitary degeneration of the white matter.

Consistent with the neuropathological findings, Western blot analysis of brain lysates from late-stage symptomatic G3C2 transgenic mice revealed a decrease in myelin basic protein (MBP) ($71.8 \pm 7.3\%$ of normal mice) and SNAP25 protein ($70.9 \pm 7.8\%$ of normal mice) contents in cerebellum but not in cerebrum. However, the oligodendrocyte specific enzyme, 2',3'-cyclic nucleotide phosphohydrolase (CNPase) was not changed in either content as assessed by Western blot or in total specific activity (cerebrum: 4.27 U for normal mice vs. 4.73 U for G3C2 mice; cerebellum: 5.26 U for normal mice vs. 5.28 U for G3C2 mice). Compared with normal controls, expression of the astrocyte protein GFAP was found to be markedly elevated ($263 \pm 31\%$) in cerebellum but not in cerebrum of symptomatic transgenic mice.

Macrophage/microglial activation and proliferation are co-incident with demyelination in white matter. To assess the activation status of the macrophage/microglial cells in the brain of G3C2 mice, brain sections were immunostained with antibodies to the complement C3 receptor (Mac-1) or the MHC class II molecule (Ia). In normal mice, weakly stained Mac-1 positive cells were distributed throughout the brain, and were particularly visible in white matter regions (Fig. 5 A). This prop-

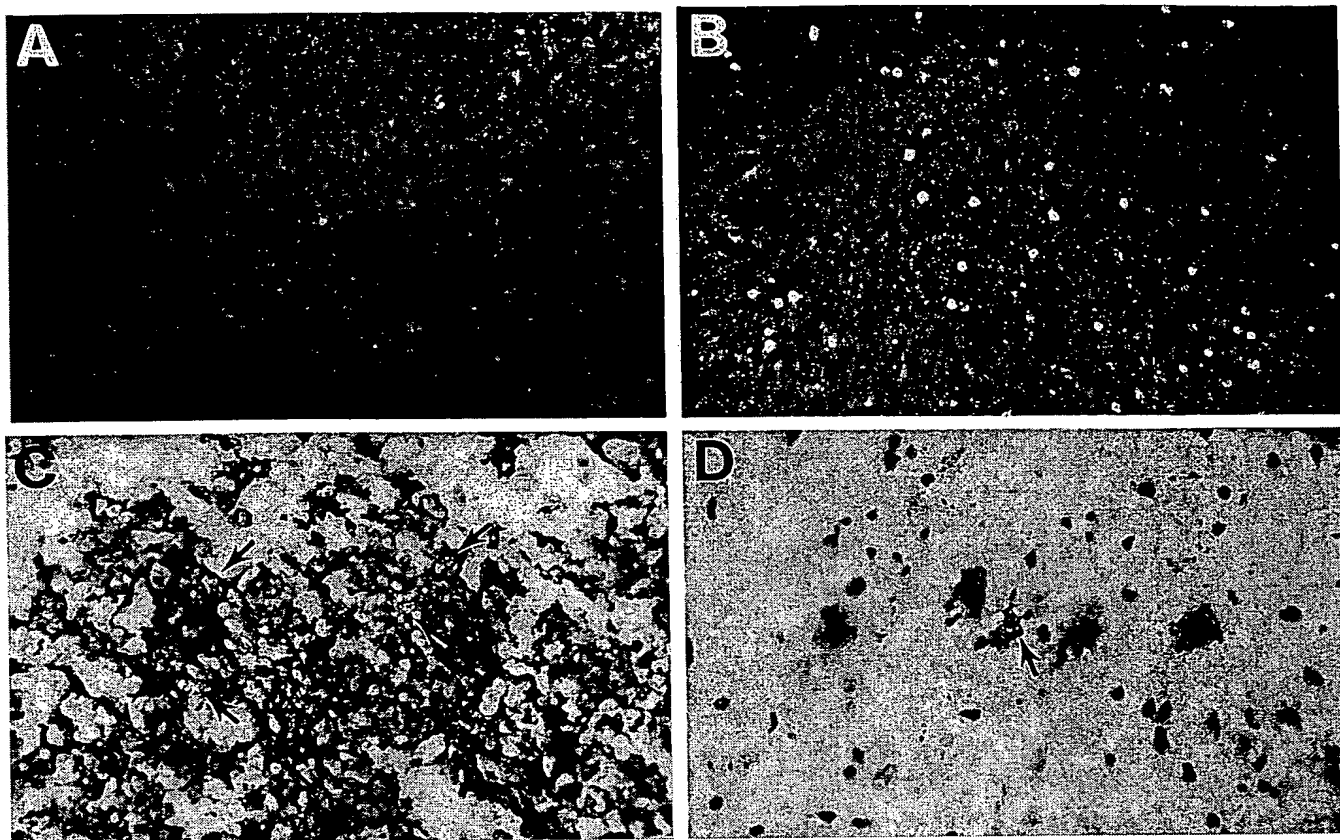


Figure 6. Marked cellular proliferation of macrophage/microglial cells in white matter lesions in GFAP-IL3 mice. Dark-field photomicrograph of autoradiographs of brain sections from normal (A) or G3C2 (B) mice after systemic injection of [^3H]thymidine. In contrast to the absence of labeling in the normal mouse, numerous labeled cells can be seen in white matter tracts and to a lesser extent in the granular layer of the cerebellum from the transgenic animal. Combined [^3H]thymidine autoradiography and immunostaining for Mac-1 (C) or Ia (D) of brain sections from a symptomatic G3C2 mouse. [^3H]thymidine labeled Mac-1 $^+$ cells were numerous in white matter lesions (arrow) while co-labeled Ia $^+$ cells (arrow) were also occasionally seen.

erty together with their highly ramified appearance identified these cells as resident resting microglia. Less numerous, but more strongly stained Mac-1 positive cells were associated with blood vessels. In contrast, in symptomatic transgenic mice, large numbers of intensely stained Mac-1 positive cells were present in white matter lesions (Fig. 5 B). The majority of these latter cells were very large with expansive cytoplasm, compatible with hyperplastic microglia and/or the foamy macrophages noted above. A smaller number of Mac-1 positive cells in these lesions, also present at perivenular sites as well as on the brain surfaces, had a compact ameboid appearance characteristic of macrophages. In normal mice, Ia positive cells were much rarer, being restricted to perivascular sites, and were presumed to represent perivascular microglia (Fig. 5 C). In contrast, in transgenic mice, increased numbers of Ia positive cells also observed in the white matter lesions although their numbers were less than the Mac-1 population (Fig. 5 D). In addition, increased numbers of Ia positive cells were also identified at perivenular sites and on brain surfaces (not shown). Consistent with the electron microscopic findings, immunostaining of adjacent sections for the lymphocytic markers CD4 (Th-cell), CD8 (Tc-cell) and B220 (B-cell) confirmed the absence of these cells in brain from normal and transgenic mice (not shown).

To investigate for possible macrophage/microglial cell proliferation, mice were injected with [^3H]thymidine and brain sections immunolabeled for Mac-1 and Ia. Adjacent sections were also immunolabeled for the astrocyte marker GFAP. In normal mice, small numbers of labeled cells were consistently identified in the subependymal plate (not shown) and rarely, if at all, in other brain areas (Fig. 6 A). These labeled cells did not stain for Mac-1, Ia or GFAP and their identity remained unknown. However, in symptomatic G3C2 mice, besides the subependymal plate, numerous labeled cells were observed particularly in focal areas of white matter of the cerebellum (Fig. 6 B), brain stem and basal ganglia. The majority of [^3H]thymidine labeled cells in these areas were Mac-1 positive (Fig. 6 C). Rare Ia positive (Fig. 6 D) and GFAP-positive (not shown) [^3H]thymidine-labeled cells were also found.

Increased MHC class II gene expression and proliferation of perivascular microglia precedes development of white matter pathology. Experiments were performed to investigate the spatiotemporal expression of the MHC class II gene in the brain of G3C2 mice. Compared with normal littermates, cerebral MHC class II mRNA levels increased progressively from as early as 2 mo of age in the transgenic mice (Fig. 7 A). In contrast, there was no significant change in the levels of MHC class I mRNA between normal control and transgenic mice up

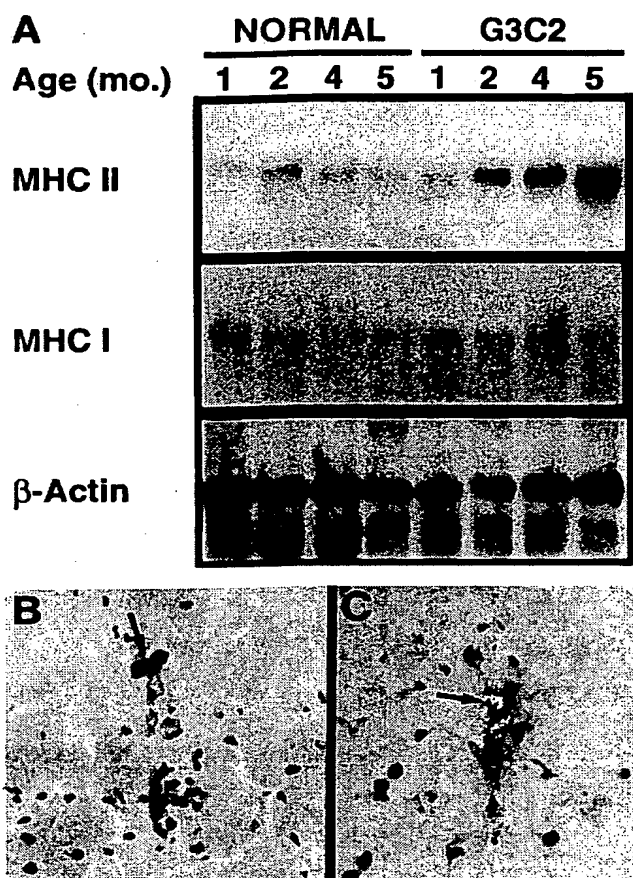


Figure 7. Early onset increased MHC-class II gene expression in the brain of G3C2 mice (A) Northern blot hybridization analysis revealed increased MHC class II mRNA was detectable in the brain from transgenic mice as early as 2 mo age. In contrast, there was no significant difference in the level of MHC class I mRNA between normal or G3C2 mice at any age studied. (B) Cryostat section of brain from a 3-mo-old G3C2 mouse immunostained for Ia showing increased levels of staining of perivascular microglia and accumulation of small numbers of Ia+ cells with an ameboid morphology (arrow). (C) Combined [³H]thymidine autoradiography and immunostaining for Ia of brain sections from a 2-mo-old G3C2 mouse showing dual labeling of perivascular cells (arrows).

to 5 mo of age. Compared with normal controls, in 2- and 3-mo-old G3C2 mice, immunostaining of brain sections revealed a generalized increase of Ia protein expression by perivascular microglial cells, particularly in subcortical, cerebellar and brain stem regions. In addition, these cells frequently appeared to be hypertrophied. An associated increase in the numbers of perivascular Ia positive cells with an ameboid morphology was also noted (Fig. 7 B). In parallel experiments utilizing [³H]thymidine incorporation studies combined with immunostaining, proliferating Ia positive perivascular cells were identified in the brain of 2- and 3-mo-old transgenic but not normal animals (Fig. 7 C).

Discussion

We have produced transgenic mice in which chronic expression of a macrophage/microglial activating factor, IL-3 (15,

21), was targeted to astrocytes using a GFAP-IL3 fusion gene construct. We demonstrated such mice developed distinct neurological disorders depending on the dose of transgene-encoded IL-3 expression. Thus, CNS expression of IL-3 at high levels resulted in a lethal early-onset acute neuroinflammatory disease, while CNS expression of this cytokine at low levels was associated with the development of a late-onset chronic progressive motor disorder. Significantly, in the latter case, the stable transgenic line G3C2 was established. The findings in this transgenic line indicated that the persistent CNS production of low levels of IL-3 promoted the recruitment, proliferation, and activation of macrophage/microglial cells in white matter regions with consequent demyelination. In affected regions of the cerebellum and brain stem, the presence of large numbers of normal appearing, but completely demyelinated axons as seen by electron microscopy, indicated unambiguously a process of active primary demyelination. While a small number of degenerating axons were also observed, this is characteristic of a demyelinating disease in which there is a vigorous inflammatory component (40). That this phenotype could have arisen from an insertional mutation or from some non-specific interference with astrocyte function, created by the transgene is improbable. First, in addition to the stable G3C2 line, a similar phenotype was exhibited by an independent GFAP-IL3 founder mouse (G3K1) that was shown to also express low levels of IL-3 in the brain. Second, in the case of both the G3C2 and the G3K1 transgenic mice, there was concordance between the CNS location for transgene encoded IL-3 expression and the principal sites of pathology. Third, the prominent involvement of macrophage/microglial cells in the evolution of the brain lesions seen in the GFAP-IL3 mice is consistent with the known ability of IL-3 to activate cells belonging to this lineage (14, 21). Finally, the pathologic and clinical profiles seen in the GFAP-IL3 mice are unique to these animals and have not been observed in other transgenic models where this GFAP construct was used to express the cytokines IL-6 (26, 32) and IFN- α (41) or the HIV coat protein gp120 (42).

Motor abnormalities in the low expressor GFAP-IL3 mice appeared with a sudden onset, typically presenting as gait disturbance starting around 5–6 mo of age, then becoming progressively more severe over the ensuing 2–3 mo, leading to complete incapacitation and premature death. Motor incoordination was estimated from rotating rod performance. This procedure permits quantification of a neurological deficit indicated by the inability of the mice to remain on a rotating rod (43). The rotating rod task has been used to characterize developmental alterations and X-irradiation induced structural disorganization of the cerebellum and other areas involved in motor control, in laboratory rodents (29, 44). Since rotating rod performance has been related to cerebellar function, and IL-3 transgenic mice exhibited pathological changes in this area, cerebellar involvement in the motor deficit observed in these mice seems probable. The abrupt transition to motor disorder was further underscored by the observations that, before the appearance of an abnormal gait, physical parameters such as body weight and motor function tests indicated these animals were indistinguishable from their non-transgenic littermates. Interestingly, the onset of motor symptoms was found to occur earlier in female versus male transgenic animals. This observation, together with the recent finding that pregnancy in GFAP-IL3 mice was associated with an earlier onset of motor

disease (unpublished observation) suggest that sex-associated factors may modulate the onset of the IL-3-induced disease process. At present the identity and mode of action of such putative factors is not known, but this issue clearly warrants further study. Significantly, the sex-associated phenomenon seen in the GFAP-IL3 mice has correlates in the human demyelinating disease, MS, where the onset is known to be earlier in females (45) and post-partum exacerbations occur more often (46).

Pathologic and molecular analysis of the brain from symptomatic low expressor GFAP-IL3 transgenic mice provided clear evidence for multiple plaque-like, white matter lesions with demyelination in the cerebellum and brain stem. Since the cerebellum and brain stem are major centers controlling motor function and coordination (47, 48), our findings indicated that a probable cause for the motor disease seen in the GFAP-IL3 mice was initially the development of extensive demyelination in the hind-brain regions. Although not specifically addressed by our studies here, it is also conceivable that white matter disease may have affected the spinal cord in the transgenic mice which would also contribute to loss of motor control. Preliminary ultrastructural examination of the spinal cord, has revealed the presence of demyelinating plaques in these transgenic mice (H.C. Powell and I.L. Campbell, unpublished observation). The subsequent parenchymal degeneration observed in the white matter likely compounded further the severity of the disorder leading eventually to complete incapacitation and death. Consistent with the absence of a detectable clinical phenotype, in presymptomatic transgenic animals, as late as 4 mo of age, routine histological examination and Western blotting for myelin and the synaptosomal protein SNAP-25, failed to reveal alterations in the brain. However, in this group of animals, the earliest ultrastructural morphologic abnormalities were noted with perivascular mononuclear cell accumulation and scant demyelination.

White matter lesions that developed in the GFAP-IL3 mice contained numerous intact axons devoid of myelin representative of primary demyelination. Dystrophic axons were also seen, however their small number as compared with the large number of healthy appearing demyelinated axons implied that demyelination was predominant and preceded any neuronal injury. Another common feature seen in these lesions was the presence of many axons circumscribed by a thin, even layer of myelin. This morphological profile, which is characteristic of remyelination (49, 50), suggested the oligodendrocytes were not only viable but also functionally active. Although we did not count oligodendrocyte numbers directly, our finding that the predominantly cell body located oligodendrocyte-specific enzyme CNPase (51) showed unaltered activity in the brain of symptomatic GFAP-IL3 mice provided further evidence for preservation of these cells. Although CNPase is also located in the myelin sheath, maintenance of this enzyme's activity has been noted in other experimental models (e.g., the shiverer mouse) (52, 53) where significant hypomyelination is known to occur and in which oligodendrocyte numbers are maintained. These changes in the GFAP-IL3 mice are similar to those seen in MS where extensive primary demyelination accompanied by some axonal abnormalities and remyelination is a feature of active plaque lesions (54). In the GFAP-IL3 mice, remyelination apparently persisted due to the maintenance of active oligodendrocyte activity. However, this finding contrasts with MS, where remyelination is a transient phenomenon associ-

ated with new white matter plaques and is thought to eventually cease because of injury to and loss of the oligodendrocytes (55-57).

A key issue raised by our studies concerns the cause of demyelination in the GFAP-IL3 mice. As discussed above, this could not be accounted for by direct injury to and/or loss of the oligodendrocytes. On the contrary, a number of observations indicated a key role of macrophage/microglial cells in mediating demyelination. First, there was a significant accumulation of these cells within the demyelinating white matter lesions. Remarkably, these lesions were almost entirely made up of cells belonging to the monocytoid lineage, while T- and B-lymphocytes were absent. On the basis of ultrastructural morphology, mast cells were the only other immunoinflammatory cells to be discerned. Second, a high proportion of the macrophage/microglial cells were in an activated state as reflected by their increased expression of the complement C3 receptor. Third, by electron microscopy, macrophage/microglial cells could be visualized surrounding myelinated axons and in some cases seen to be actively engaged in myelin stripping. Fourth, white matter lesions contained significant numbers of swollen foamy macrophages engorged with neutral lipids, presumably as a result of engulfing myelin. Therefore, these data strongly suggest that activated macrophage/microglial cells in the GFAP-IL3 mice were the primary mediators of demyelination.

Accumulation of macrophage/microglial cells within the white matter represented a cardinal and striking feature of the GFAP-IL3 mice and as discussed above was a critical event in the development of demyelination. Macrophages (14, 15) and microglia (21) are known to respond to IL-3. Therefore, their accumulation in the transgenic mice is compatible with a response of these cells to the transgene encoded cytokine. This point was further illustrated by the coincidence of macrophage/microglial accumulation with sites of transgene encoded IL-3 expression. The formation and evolution of these lesions likely resulted from multiple ongoing processes. Electron microscopic and immunostaining analysis revealed numerous macrophages on the brain surfaces as well as at perivascular sites suggesting active recruitment of these cells from the periphery was one contributing factor. Additionally, the pronounced proliferation of the Mac-1⁺ population observed in the white matter lesions indicated that local proliferation of the macrophage/microglial cells was also likely to be responsible for the accumulation of these cells. In addition to confirming its well described hematopoietic growth promoting properties (reviewed in reference 13) our findings suggest IL-3 is an effective and, at low concentrations, somewhat specific chemotactic and growth factor for macrophages. Why, in spite of continuous IL-3 production from birth, the recruitment and accumulation of the macrophage/microglial cells in the CNS of the low expressor transgenic mice was so protracted is unknown. It likely reflects, in part, a concentration related phenomenon since GFAP-IL3 mice with high levels of transgene expression exhibited florid and widespread mononuclear cell infiltration of the brain at an early age. In addition, compared with the periphery, the brain parenchyma is known to be extremely resistant to the proinflammatory actions (including recruitment of immunoinflammatory cells) of acutely injected LPS (58) and various cytokines and chemokines (59). This suggests as yet unidentified brain-specific factors may be involved in suppressing the potentially harmful actions of proinflammatory

cytokines. Modulation of these factors and possibly other priming events by IL-3 in the transgenic mice may also be required to further facilitate the recruitment and infiltration of the brain by peripheral macrophages. One such priming event could involve activation of perivascular microglia. Hypertrophy, proliferation and enhanced expression of MHC class II molecules by these cells was one of the earliest changes we could detect in the brain in GFAP-IL3 animals. Induction of MHC class II expression is part of a spectrum of changes that is associated with the activation of macrophages by IL-3 (15). How, in the GFAP-IL3 mice, these early responses by the perivascular microglia might influence circulating macrophages is presently not known. It is conceivable however, that through their intimate association with the cerebrovascular endothelium, the perivascular cells might provide signals for the recruitment and promote the initial adherence of macrophages to the endothelial cell and their subsequent extravasation. Future studies aimed at delineating the functional state of the endothelium as well as the expression of key adhesion molecules will help to resolve some of these issues.

Similar to our present findings in the GFAP-IL3 mice, activated macrophage/microglial cells are implicated as key effectors in a variety of human and experimental immune-associated demyelinating neuropathies including MS (4, 56, 60, 61), Guillain-Barre syndrome (62), HIV leukoencephalopathy (63, 64) and EAE (65), respectively. Why myelin in particular becomes the primary target for these cells, and the mechanisms underlying the demyelination process itself, remain open questions. Experiments *in vitro* show that macrophages (66) and microglia (67) in addition to becoming activated, vigorously phagocytose added myelin. A critical role of the complement C3 receptor in myelin phagocytosis has been demonstrated (68). Ultrastructural evidence in the GFAP-IL3 mice revealed myelin disruption by macrophage/microglial cells indicative of direct physical involvement of these cells in the demyelination process. Moreover, the prominent hyperexpression of complement C3 receptor by macrophage/microglial cells observed in the white matter lesions of the GFAP-IL3 mice suggest there may be a role for this molecule in the coupling and subsequent amputation of the myelin lamellae.

Demyelination in the GFAP-IL3 mice might also result indirectly from the release of soluble factors. Activated macrophages and microglia are known to produce a spectrum of soluble factors including cytokines, serine proteases, prostaglandins and reactive oxygen species that under certain conditions may mediate tissue injury (12). Disease progression in the GFAP-IL3 mice was found to be associated with increased expression of IL-1 α and to a lesser extent IL-1 β and TNF- α mRNAs. While the presence of these cytokine RNAs does not necessarily infer their activity at the protein level, it is notable in the case of TNF- α that this cytokine may damage myelin and be toxic to oligodendrocytes *in vitro* (69, 70). Recent evidence suggests the toxic actions of TNF- α to oligodendrocytes *in vitro* are mediated in part via the induction of nitric oxide (NO) (71). However, in recent studies we were unable to detect iNOS mRNA in brain from symptomatic G3C2 mice (I.L. Campbell, unpublished observation). Therefore, NO is not likely to be involved in the pathogenesis of macrophage/microglial mediated demyelination in this animal model.

In many respects, the molecular and cellular pathologic manifestations exhibited by the GFAP-IL3 mice show remarkable overlap with those in the active plaque lesions of MS.

Thus, the animal model closely resembles the histopathology of acute fulminant MS where there is frequently heavy macrophage infiltration with minimal perivascular T cell infiltration (72). Furthermore, in MS, reactive macrophage/microglial cells with increased MHC class II and complement C3 receptor expression are the predominant cells found at the leading edge of demyelinating lesions (4, 56, 60, 73). Consistent with their effector role in demyelination, fine structural studies illustrate macrophages in MS lesions separating and engulfing myelin lamellae, as well as the presence of numerous foamy macrophages engorged with neutral lipid material (54, 74, 75). The presence of intracisternal "pole like" bodies within macrophages present in active MS plaques appears to represent a unique morphological feature of this disorder (54). Interestingly, almost identical intracisternal inclusions were observed in macrophages in white matter lesions in the GFAP-IL3 mice. While the identity and function of these unusual structures are unknown, the transgenic mice now provide an opportunity to establish their nature. Mast cells are known to respond to IL-3 (13) and were present in white matter lesions in the transgenic mice. These cells which are infrequently if at all seen in the normal human brain, have been reported in demyelinating MS plaques (76). Finally, as discussed above, remyelination which was prominent in the transgenic mice is also seen in active MS plaque lesions. These similarities between the human and transgenic murine demyelinating disorders suggest there may be underlying common pathogenetic mechanisms, perhaps involving IL-3 or a related cytokine. An implication from our findings is that one role of the putative autoreactive T cells that are thought to contribute to the development of MS (57, 77), may be to provide a chronic source of macrophage recruiting and activating cytokines such as IL-3. Although IL-3 and other functionally related cytokines such as GM-CSF and CSF-1 are known to be produced by activated T cells (13), to date we are not aware of any studies that have examined for the presence of these cytokines in the active plaques of MS. However, in the related experimental disorder of EAE in mice, expression of CSF-1 is increased markedly in spinal cord before maximal clinical expression of disease (78). Furthermore, a positive correlation was recently reported between myelin basic protein-specific T cell production of IL-3 and the encephalitogenic potential of these cells when adoptively transferred to susceptible mice (79).

In conclusion, transgenic mice with low levels of cerebral IL-3 expression develop in later life a progressive motor disorder as a result of a vigorous T cell-independent macrophage/microglia-mediated demyelination process. Many of the clinicopathologic manifestations of this disorder show a striking resemblance to those observed in human inflammatory demyelinating diseases, particularly acute fulminant multiple sclerosis, suggesting the GFAP-IL3 transgenic mouse is a potentially valuable new model to study the role of macrophage/microglia in the pathogenesis of CNS demyelinating disease.

Acknowledgments

We thank Dr. Nai-Chen Yu for assistance with the preparation of astrocyte cell cultures, Ms. Laurie Turbeville and Anna Stalder for technical assistance and Jenny Price for her assistance in the development of the transgenic mice. We thank Drs. Monte V. Hobbs, Michael C. Wilson, and Monica Carson at the Scripps Research Insti-

tute for providing the cytokine RPA probe, SNAP-25 antibodies and CNPase antibody, respectively.

This paper is manuscript number 9302-NP from the Scripps Research Institute. This study was supported by U.S. Public Health Service Grants MH-47680 and MH-50426 to I.L. Campbell.

References

1. Lawson, L.J., V.H. Perry, P. Dri, and S. Gordon. 1990. Heterogeneity in the distribution and morphology of microglia in the normal adult mouse brain. *Neurosci.* 39:151-170.
2. Ling, E.-A., and W.-C. Wong. 1993. The origin and nature of ramified and amoeboid microglia: a historical review and current concepts. *GLIA.* 7:9-18.
3. Nakajima, K., and S. Kohsaka. 1993. Functional roles of microglia in the brain. *Neurosci. Res.* 17:187-203.
4. Boyle, E.A., and P.L. McGeer. 1990. Cellular immune response in multiple sclerosis plaques. *Am. J. Pathobiol.* 137:575-584.
5. McGeer, P.L., S. Itagaki, B.E. Boyes, and E.G. McGeer. 1988. Reactive microglia are positive for HLA-DR in the substantia nigra of Parkinson's and Alzheimer's disease brains. *Neurosci.* 38:1285-1291.
6. McGeer, P.L., T. Kawamata, D.G. Walker, H. Akiyama, I. Tooyama, and E.G. McGeer. 1993. Microglia in degenerative neurological disease. *GLIA.* 7:84-92.
7. Dickson, D.W., L.A. Mattiace, K. Kure, K. Hutchins, W.D. Lyman, and C.F. Brosnan. 1991. Biology of Disease: Microglia in human disease, with an emphasis on acquired immune deficiency syndrome. *Lab. Invest.* 64:135-156.
8. Chiang, C.S., W.H. McBride, and H.R. Withers. 1993. Radiation-induced astrocytic and microglial responses in mouse brain. *Radiother. Oncol.* 29:60-68.
9. Giuliani, D., K. Vaca, and M. Corpuz. 1993. Brain glia release factors with opposing actions upon neuronal survival. *J. Neurosci.* 13:29-37.
10. Davis, E.J., T.D. Foster, and W.E. Thomas. 1994. Cellular forms and functions of brain microglia. *Br. Res. Bull.* 34:73-78.
11. Colton, C.A., and D.L. Gilbert. 1993. Microglia, an *in vivo* source of reactive oxygen species in the brain. *Adv. Neurol.* 59:321-326.
12. Banati, R.B., J. Gehrmann, P. Schubert, and G.W. Kreutzberg. 1993. Cytotoxicity of microglia. *GLIA.* 7:111-118.
13. Schrader, J.W. 1986. The pan specific hemopoietin of activated T-lymphocytes (interleukin-3). *Ann. Rev. Immunol.* 4:205-230.
14. Frendl, G. 1992. Interleukin 3: from colony-stimulating factor to pluripotent immunoregulatory cytokine. *J. Immunol.* 14:421-430.
15. Frendl, G., and D.I. Beller. 1990. Regulation of macrophage activation by IL-3. *J. Immunol.* 144:3392-3399.
16. Oster, W., J. Frisch, U. Nicolay, and G. Schulz. 1988. Interleukin-3: biological effects and clinical impact. *Cancer.* 67:2712-2717.
17. Kurzrock, R., M. Talpaz, Z. Estrov, M.G. Rosenblum, and J.U. Gutterman. 1991. Phase 1 study of human recombinant interleukin-3 in patients with bone marrow failure. *J. Clin. Oncol.* 9:1241-1250.
18. Aglietta, M., F. Sanavio, A. Stacchini, S. Morelli, L. Fubini, A. Severino, P. Pasquino, C. Volta, S. Bretti, S. Tafuto et al. 1993. Interleukin-3 in vivo: kinetics of response of target cells. *Blood.* 82:2054-2061.
19. McBride, W.H., G.D. Dougherty, G.D. Wallis, O. Econo J.S., and C.-S. Chiang. 1994. Interleukin-3 in gene therapy of cancer. *Folia Biologica.* 40:62-73.
20. Pulaski, B.A., A.J. McAdam, E.K. Hutter, S. Biggar, E.M. Lord, and J.G. Frelinger. 1993. Interleukin-3 enhances the development of tumor reactive cytotoxic cells by a CD4-dependent mechanism. *Cancer Res.* 53:2112-2117.
21. Gebicke-Haerter, P.J., K. Appel, G.D. Taylor, A. Schobert, I.N. Rich, H. Northoff, and M. Berger. 1994. Rat microglial interleukin-3. *J. Neuroimmunol.* 50:203-214.
22. Appel, K., M. Buttini, A. Sauter, and P.J. Gebicke-Haerter. 1995. Cloning of rat interleukin-3 β -subunit from cultured microglia and its RNA expression *in vivo*. *J. Neurosci.* 15:5800-5809.
23. Lee, T.T., F.C. Martin, and J.E. Merrill. 1993. Lymphokine induction of rat microglia multinucleated giant cell formation. *GLIA.* 8:51-61.
24. Araujo, D.M., and P.A. Lapchak. 1994. Induction of immune system mediators in the hippocampal formation in Alzheimer's and Parkinson's diseases: selective effects on specific interleukins and interleukin receptors. *Neurosci.* 61:745-754.
25. Campbell, I.L. 1994. Cytokines in the pathogenesis of CNS disease. Studies in transgenic mice. *Int. J. Dev. Neurosci. Suppl.* 12:66.
26. Campbell, I.L., C.R. Abraham, E. Masliah, P. Kemper, J.D. Inglis, M.B.A. Oldstone, and L. Mucke. 1993. Neurologic disease induced in transgenic mice by the cerebral overexpression of interleukin 6. *Proc. Natl. Acad. Sci. USA.* 90:10061-10065.
27. Mucke, L., M.B.A. Oldstone, J.C. Morris, and M.I. Nerenberg. 1991. Rapid activation of astrocyte-specific expression of GFAP-lacZ transgene by focal injury. *New Biol.* 3:465-474.
28. Jones, B.J., and D.J. Roberts. 1968. The quantitative measurement of motor incoordination in naive mice using an accelerating rotarod. *J. Pharm. Pharmacol.* 20:302-304.
29. Laffan, E.W., C.A. Lisciotto, D.A. Gapp, and D.A. Weldon. 1989. Development of rotarod performance in normal and congenitally hypothyroid mutant mice. *Behav. Neural. Biol.* 52:411-416.
30. Badley, J.E., G.A. Bishop, T. St. John, and J.A. Frelinger. 1988. A simple, rapid method for the purification of poly A⁺ RNA. *Biotechniques.* 6:114-116.
31. Hobbs, M.V., W.O. Weigle, D.J. Noonan, B.E. Torbett, R.J. McEvilly, R.J. Koch, G.J. Cardenas, and D.N. Ernst. 1992. Patterns of cytokine gene expression by CD4⁺ T cells from young and old mice. *J. Immunol.* 150:3602-3068.
32. Chiang, C.-S., A. Stalder, A. Samimi, and I.L. Campbell. 1994. Reactive gliosis as a consequence of interleukin-6 expression in the brain. Studies in transgenic mice. *Dev. Neurosci.* 16:212-221.
33. Campbell, I.L., M.V. Hobbs, P. Kemper, and M.B.A. Oldstone. 1994. Cerebral expression of multiple cytokine genes in mice with lymphocytic choriomeningitis. *J. Immunol.* 152:716-723.
34. Benoist, C.O., D.J. Mathis, M.R. Kanter, V.E. Williams, and H.O. McDevitt. 1983. Regions of allelic hypervariability in the murine A alpha immune response gene. *Cell.* 34:169-177.
35. Reyes, A.A., M. Schold, and R.B. Wallace. 1982. The complete amino acid sequence of the murine transplantation antigen H-2Db as deduced by molecular cloning. *Immunogenetics.* 16:1-9.
36. Tokunaga, K., H. Taniguchi, K. Yoda, M. Shimizu, and S. Sakiyama. 1986. Nucleotide sequence of a full-length cDNA for mouse cytoskeletal beta-actin mRNA. *Nucleic Acids Res.* 14:2829.
37. Wilson, M.C., and G.A. Higgins. 1989. *In Situ* hybridization. *Neuro-methods.* 16:239-284.
38. Chiang, C.-S., and W.H. McBride. 1991. Radiation-enhanced TNF production by murine brain cells. *Brain Res.* 566:265-269.
39. Prohaska, J.R., D.A. Clark, and W.W. Wells. 1973. Improved rapidity and precision in the determination of brain 2',3'-cyclic nucleotide-3'-phosphohydrolase. *Anal. Biochem.* 56:272-282.
40. Powell, H.C., R.R. Myers, A.P. Mizisin, T. Olee, and S.W. Brostoff. 1991. Response of the axon and barrier endothelium to experimental allergic neuritis induced by autoreactive T cell lines. *Acta Neuropathol.* 82:364-377.
41. Campbell, I.L., L. Mucke, and K. Sandberg. 1993. Cerebral overexpression of interleukin-6 or interferon- α induces distinct neuropathology in transgenic mice. *Soc. Neurosci. Abstr.* Vol.19 (Part 1):225.
42. Toggs, S.M., E. Masliah, E.M. Rockenstein, G.F. Rall, C.R. Abraham, and L. Mucke. 1994. Central nervous system damage produced by expression of the HIV-1 coat protein gp120 in transgenic mice. *Nature (Lond.)* 367:188-193.
43. Dunham, N.W., and T.S. Miya. 1957. A note on a simple apparatus for detecting neurological deficit in rats and mice. *J. Am. Pharmaceut. Assn.* 46:208-209.
44. Pellegrino, L.J., and J. Altman. 1979. Effects of differential interference with postnatal cerebellar neurogenesis on motor performance, activity level and maze learning of rats: a developmental study. *J. Comp. Physiol. Psychol.* 93:1-33.
45. Leibowitz, U., and M. Alter. 1973. Multiple sclerosis. In *Clinical Studies of Multiple Sclerosis in Israel*. U. Leibowitz and M. Alter, editors. North-Holland Publishing Company, New York. 25-35.
46. Nelson, L.M., G.M. Franklin, and M.C. Jones. 1984. Risk of multiple sclerosis exacerbation during pregnancy and breast-feeding. *J. Am. Med. Assoc.* 259:3441-3443.
47. Thack, W.T., H.P. Goodkin, and J.G. Keating. 1992. The cerebellum and the adaptive coordination of movement. *Ann. Rev. Neurosci.* 62:403-442.
48. Lang, A.E. 1991. Movement disorder symptomatology. In *Neurology in Clinical Practice: principles, Diagnosis and Management*. W.G. Bradley, R.B. Daroff, G.M. Fenichel, and C.D. Marsden, editors. Butterworth-Heinemann Reed, New York. 320-321.
49. Prineas, J.W., R.O. Barnard, E.E. Kwon, L.R. Sharer, and E.-S. Cho. 1993. Multiple sclerosis: remyelination of nascent lesions. *Ann. Neurol.* 33:137-151.
50. Raine, C.S., and E. Wu. 1993. Multiple sclerosis: Remyelination in acute lesions. *J. Neuropathol. Exper. Neurol.* 52:199-204.
51. Shapira, R., W.C. Mobley, S.B. Thiele, M.R. Wilhelmi, A. Wallace, and R.F. Kibler. 1978. Localization of 2',3'-cyclic nucleotide-3'-phosphohydrolase of rabbit brain by sedimentation in a continuous sucrose gradient. *J. Neurochem.* 30:123-131.
52. Bird, T.D., D.F. Farrell, and S.M. Sumi. 1978. Brain lipid composition of the shiverer mouse: (genetic defect in myelin development). *J. Neurochem.* 31:387-391.
53. Mikoshiba, K., K. Nagaike, and Y. Tsukada. 1980. Subcellular distribution and developmental change of 2',3'-cyclic nucleotide 3'-phosphohydrolase in the central nervous system of the myelin-deficient shiverer mutant mice. *J. Neurochem.* 1980:465-470.
54. Rodriguez, M., and B. Scheithauer. 1994. Ultrastructure of multiple sclerosis. *Ultrastruct. Pathol.* 18:3-13.
55. Prineas, J.W., R.O. Barnard, T. Revesz, E.E. Kwon, L. Sharer, and E.-S. Cho. 1993. Multiple sclerosis. Pathology of recurrent lesions. *Brain.* 116:681-693.

56. Adams, C.W.M., R.N. Poston, and S.J. Buk. 1989. Pathology, histochemistry and immunocytochemistry of lesions in acute multiple sclerosis. *J. Neurol. Sci.* 92:291-306.
57. ffrench-Constant, C. 1994. Pathogenesis of multiple sclerosis. *Lancet.* 343:271-275.
58. Andersson, P.-B., V.H. Perry, and S. Gordon. 1992. The acute inflammatory response to lipopolysaccharide in CNS parenchyma differs from that in other body tissues. *Neurosci.* 48:169-186.
59. Andersson, P.-B., V.H. Perry, and S. Gordon. 1992. Intracerebral injection of proinflammatory cytokines or leukocyte chemotaxins induces minimal myelomonocytic cell recruitment to the parenchyma of the central nervous system. *J. Exp. Med.* 176:255-259.
60. Hauser, S.L., A.K. Bhan, F. Gilles, M. Kemp, C. Kerr, and H.L. Weiner. 1986. Immunohistochemical analysis of the cellular infiltrate in multiple sclerosis lesions. *Ann. Neurol.* 19:578-587.
61. Li, H., J. Newcombe, N.P. Groome, and M.L. Cuzner. 1993. Characterization and distribution of phagocytic macrophages in multiple sclerosis plaques. *Neuropathol. Appl. Neurobiol.* 19:214-223.
62. Griffin, J.W., G. Stoll, C.Y. Li, W. Tyro, and D.R. Cornblath. 1990. Macrophage responses in inflammatory demyelinating neuropathies. *Ann. Neurol.* 27:S64-S68.
63. Gray, F., and M.C. Lesca. 1993. HIV-related demyelinating disease. *Eur. J. Med.* 2:89-96.
64. Smith, T.W., U. DeGirolami, D. Hein, F. Bolgert, and J.-J. Hauw. 1990. Human immunodeficiency virus (HIV) leukoencephalopathy and the microcirculation. *J. Neuropathol. Exp. Neurol.* 49:357-370.
65. Brosnan, C.F., M.B. Bornstein, and B.R. Bloom. 1981. The effects of macrophage depletion on the clinical and pathologic expression of experimental allergic encephalomyelitis. *J. Immunol.* 126:614-620.
66. Friede, R.L., and W. Bruck. 1993. Macrophage functional properties during myelin degradation. *Adv. Neurol.* 59:327-336.
67. Williams, K., E. Ulvestad, A. Waage, J.P. Antel, and J. McLaurin. 1994. Activation of adult human derived microglia by myelin phagocytosis in vitro. *J. Neurosci. Res.* 38:433-443.
68. Bruck, W., and R.L. Friede. 1990. Anti-macrophage CR3 antibody blocks myelin phagocytosis by macrophages in vitro. *Acta Neuropathol.* 80:415-418.
69. Selmaj, K., C.S. Raine, M. Farooq, W.T. Norton, and C.F. Brosnan. 1991. Cytokine cytotoxicity against oligodendrocytes. *J. Immunol.* 147:1522-1529.
70. Louis, J.-C., E. Magal, S. Takayama, and S. Varon. 1993. CNTF protection of oligodendrocytes against natural and tumor necrosis factor-induced death. *Science (Wash. DC).* 259:689-692.
71. Merrill, J.E., L.J. Ignarro, M.P. Sherman, J. Melinek, and T.E. Lane. 1993. Microglial cell cytotoxicity of oligodendrocytes is mediated through nitric oxide. *J. Immunol.* 151:2132-2141.
72. Nesbit, G.M., G.S. Forbes, B.W. Scheithauer, and H. Okazaki. 1991. Multiple sclerosis: Histopathologic and MR and/or CT correlation in 37 cases at biopsy and three cases at autopsy. *Radiology.* 180:467-474.
73. Newcombe, J., H. Li, and M.L. Cuzner. 1994. Low density lipoprotein uptake by macrophages in multiple sclerosis plaques: implications for pathogenesis. *Neuropathol. Appl. Neurobiol.* 20:152-162.
74. Princeas, J.W., and R.G. Wright. 1978. Macrophages, lymphocytes and plasma cells in the perivascular compartments in chronic multiple sclerosis. *Lab. Invest.* 48:581-589.
75. Lampert, P.W. 1978. Autoimmune and virus-induced demyelinating diseases. *Am. J. Pathol.* 91:176-198.
76. Toms, R., H.L. Weiner, and D. Johnson. 1990. Identification of IgE-positive cells and mast cells in frozen sections of multiple sclerosis brains. *J. Neuroimmunol.* 30:169-177.
77. Martin, R., H.F. McFarland, and D.E. McFarlin. 1992. Immunological aspects of demyelinating diseases. *Ann. Rev. Immunol.* 10:153-187.
78. Hukower, K., C.F. Brosnan, D.A. Aquino, W. Cammer, S. Kulshretha, M.P. Guida, D.A. Rapoport, and J.W. Berman. 1993. Expression of CSF-1, c-fms, and MCP-1 in the central nervous system of rats with experimental allergic encephalomyelitis. *J. Immunol.* 150:2525-2533.
79. Zhao, M.-L., J.-Q. Xia, and R.B. Fritz. 1993. Interleukin 3 and encephalitogenic activity of SJL/J myelin basic protein-specific T cell lines. *J. Neuroimmunol.* 43:69-78.

Neutral Endopeptidase 24.11 in Neutrophils Modulates Protective Effects of Natriuretic Peptides Against Neutrophils-Induced Endothelial Cytotoxicity

Toshiyuki Matsumura, Kiyotaka Kugiyama, Seigo Sugiyama, Masamichi Ohgushi, Kyoze Yamanaka,* Makoto Suzuki,* and Hirofumi Yasue

Division of Cardiology, Kumamoto University School of Medicine, Honjo 1-1-1, Kumamoto City, Japan 860; and *Pharmacology Laboratory, New Product Development Center Pfizer Pharmaceuticals Inc., 5-2, Taketoyo-cho, Chita-gun Aichi, Japan 470-23

Abstract

This study was performed to determine effects of atrial and brain natriuretic peptides (ANP, BNP) on neutrophils-induced endothelial injury which is known to play a role in the pathophysiology of ischemia/reperfusion myocardial injury and to examine whether the effects of ANP and BNP on neutrophils are modulated by neutral endopeptidase 24.11 (NEP) in neutrophils themselves. The incubation of human neutrophils with ANP and BNP inhibited the neutrophils-induced detachment of cultured human endothelial cells (HEC). The inhibitory effect of ANP and BNP was associated with the suppressions of the neutrophils adhesiveness to HEC, CD18 expression on the neutrophils, and elastase release from the neutrophils. Coincubation with UK73967 or phosphoramidon, inhibitors of NEP, potentiated all of the effects of ANP and BNP on the neutrophil functions, and the NEP inhibitors protected degradation of ANP and BNP by the neutrophils. NEP enzymatic activity in the particulate fractions and immunoreactive NEP expression were found to increase in the neutrophils from patients with early phase of acute myocardial infarction (AMI) by 5.2- and by 4.2-fold of the neutrophils from patients with late phase of AMI, respectively. In an in vivo canine model of myocardial ischemia/reperfusion, the intravenous administration of UK73967 suppressed the neutrophil adherence to endothelium and the neutrophil accumulation in the ischemic/reperfused myocardium. The results indicate that ANP and BNP, which are known to increase in AMI, modulate the neutrophil functions and exert protective effects against the neutrophils-induced endothelial cytotoxicity. But the effects are suppressed due to their degradation by the neutrophil own NEP. Thus, neutrophil NEP, which also increases in AMI, may play a role in the pathophysiology of neutrophils-mediated ischemia/reperfusion endothelial and myocardial injury. (*J. Clin. Invest.* 1996; 97: 2192-2203). Key words: atrial natriuretic peptide • brain natriuretic peptide • CD10 • acute myocardial infarction • endothelial cells

Address correspondence to Kiyotaka Kugiyama, M.D., Division of Cardiology, Kumamoto University School of Medicine, Honjo 1-1-1, Kumamoto City, Japan 860. Phone: 96-373-5175; FAX: 96-362-3256; E-mail: miles@gpo.kumamoto-u.ac.jp

Received 20 July 1995 and accepted in revised form 22 February 1996.

J. Clin. Invest.

© The American Society for Clinical Investigation, Inc.

0021-9738/96/05/2192/12 \$2.00

Volume 97, Number 10, May 1996, 2192-2203

Introduction

Atrial natriuretic peptide (ANP)¹ and brain natriuretic peptide (BNP) are the hormones with a wide range of potent biological effects, including natriuresis, diuresis, vasodilations, and inhibitions of the renin-angiotensin-aldosterone system and the sympathetic nervous system (1-6). ANP is mainly synthesized and secreted from atria in adult mammals, while BNP is secreted mainly from the ventricles (7). We have reported that their plasma levels markedly increase in patients with acute myocardial infarction (AMI) (8, 9) as well as in those with congestive heart failure (7, 10). However, the role of ANP and BNP in the pathophysiology of AMI remains to be determined. Neutral endopeptidase 24.11 (NEP), a membrane ectoenzyme, hydrolyses and inactivates a variety of peptides including ANP and BNP at the amino side of hydrophobic amino acids (11-17). NEP is widely distributed in the body and is abundant especially in the kidney (11), lung (12), brain (13), and neutrophils (14-17). The gene of NEP has been cloned and its sequence is shown to be identical to that of a pre- β lymphocyte surface antigen (CD10), the common acute lymphoblastic leukemia antigen (CALLA) (18, 19). Earlier studies indicated that NEP in neutrophils regulates their own responsiveness to multiple inflammatory peptides including formyl-met-leu-phe (FMLP) and substance P (14-16). However, the functional significance of neutrophil NEP in myocardial ischemic events also remains unknown at the present time.

Myocardial ischemia/reperfusion cause coronary vascular injury as well as myocardial injury (20-24). Although the mechanism by which coronary vascular damage from myocardial ischemia/reperfusion occurs remains unclear, endothelial injury caused by the activated neutrophils has been shown to play an important role in this process (25-28). Thus, this study was aimed to determine the effects of ANP and BNP on neutrophils-induced endothelial injury and to examine whether the effects of ANP and BNP on neutrophils are modulated by NEP in neutrophils themselves.

Methods

Preparations of neutrophils. Peripheral blood neutrophils were purified from citrate-anticoagulated, dextran-sedimented venous blood samples from healthy volunteers over Ficoll-Hypaque gradients followed by hypotonic lysis of erythrocytes. The preparations were composed of > 96% neutrophils by Türk stain (0.01% of methylrosaniline chloride and 1.0% acetic acid), neutrophil alkaline phosphatase and

1. Abbreviations used in this paper: ANP, atrial natriuretic peptide; BNP, brain natriuretic peptide; NEP, neutral endopeptidase 24.11; OZ, opsonized zymosan; HUVECs, human umbilical vein endothelial cells; HAECs, human aortic endothelial cells; MPO, myeloperoxidase.

neutrophil esterase stain, and of > 98% viable cells by the trypan blue dye exclusion test. The isolated neutrophils were suspended in serum-free Medium 199. Neutrophils (10^6 , 5×10^6 , 10^7 cells/ml) were incubated for the indicated time with or without ANP or BNP in the presence or absence of UK73967 (Candoxatrilat, 50 μ mol/liter, Pfizer Central Research), phosphoramidon (50 μ mol/liter), or HS-142-1 (a nonpeptide antagonist for the particulate guanylyl cyclase receptor, 100 μ g/ml, Kyowa-Hakko). UK73967 and phosphoramidon have been shown to be a specific inhibitor of NEP (UK73967, NEP: K_i = 14 nmol/liter; Angiotensin converting enzyme: K_i > 10,000 nmol/liter. Phosphoramidon, NEP: K_i = 39 nmol/liter, Aminopeptidase: K_i > 10,000 nmol/liter) (29–31). Subsequently, Opsonized Zymosan (OZ, 0.5 mg/ml) or C5a (20 nmol/liter) was added into the incubation mixture with neutrophils, followed by the further incubation for the indicated time at 37°C in the same manner as we reported previously (32). The preconditioned neutrophils were examined for the assays of elastase release, respiratory burst function, cytosolic free calcium, adhesiveness to the cultured endothelial cells and toxicity to the endothelial cells (endothelial detachment) and were also used for the examinations of NEP enzymatic activity and surface expression of CD18. Neutrophils were also isolated from the peripheral blood in patients with AMI who admitted to our hospital within 12 h after onset of MI. Blood sampling was performed at the admission to hospital (counted as day 0) and at 7:00 A.M. over 4 wk, on days 1, 2, 3, 7, 14, 21, and 28 after onset of MI. The particulate fraction prepared from neutrophils in patients with AMI was used for examination of their NEP enzymatic activity. When neutrophil surface expression of NEP/CD10 was examined by fluorescence-activated cell sorter (FACS[®]), whole blood was directly subjected to the analysis with FACSscan[®] (Beckton Dickinson & Co., Mountain View, CA).

Respiratory burst function. Production of active oxygen metabolites during neutrophil activation was measured by the method of luminol-dependent chemiluminescence using the Luminescence Reader BLR-301 (ALOKA, Japan). The isolated neutrophils from the healthy volunteers (5×10^6 cells/ml) suspended in 1 ml of serum free Medium 199 without phenol red were treated with or without ANP or BNP in the presence or absence of UK73967 for 15 min at 37°C. After the incubation, luminol (0.1 mmol/liter) was added to the cuvette, followed by the addition of OZ (50 μ g/ml) to initiate neutrophil activation, and light emission was recorded.

Neutrophil elastase release. The isolated neutrophils from the healthy volunteers (10^7 cells/ml) suspended in 1 ml of serum-free Medium 199 without phenol red were treated with or without ANP or BNP in the presence or absence of UK73967, phosphoramidon or HS-142-1 for 60 min at 37°C. Thereafter, the cells were activated with OZ and then pelleted by centrifugation (27,000 g for 20 min). The hydrolytic activity of neutrophil elastase in the harvested supernatants was determined using synthetic substrate Suc-Ala-Pro-Ala-pNA as reported previously (33).

Adherence assay. Primary cultures of human umbilical vein endothelial cells (HUVECs) and the cultures of human aortic endothelial cells (HAECs) were confluent grown in 24-well plates, as we showed previously (34), and were used for this study. The isolated neutrophils from the healthy volunteers were labeled with ⁵¹Cr using the method as reported previously (35, 36). The ⁵¹Cr-labeled neutrophils suspended in serum-free Medium 199 (5×10^6 cells/ml) were treated with or without ANP or BNP in the presence or absence of UK73967 for 60 min at 37°C and then activated with OZ. The monolayers of cultured endothelial cells were rinsed three times with serum-free Medium 199 and then incubated with the preconditioned neutrophils for 20 min at 37°C in 5% CO₂ and 98% humidity. After the incubation, the incubation medium was removed and the monolayer of the endothelial cells were washed three times with PBS to remove non-adherent neutrophils, and then remained adherent cells were lysed by an overnight incubation with 2 N NaOH (1 ml/well) at 4°C. The cell lysate was collected and ⁵¹Cr activity in the lysate was counted by a Gamma Counter. The adhered neutrophils to the endothelial monolayers were expressed as a percent of the count in the to-

tal neutrophils added to a well. The endothelial cells were not detached by the 20-min incubation with the neutrophils after any preconditions.

Endothelial detachment. The confluent cultures of HUVECs and HAECs grown in 12-well plates were used for the experiment (27, 28, 37, 38). The isolated neutrophils from the healthy volunteers (10^7 cells/ml) were treated with or without ANP, BNP, or 8-bromo-guanosine 3',5'-cyclic monophosphate (8-bromo-cGMP) in the presence or absence of UK73967, phosphoramidon or HS-142-1 for 60 min at 37°C and then activated with OZ. The monolayers of cultured endothelial cells were rinsed three times with serum-free Medium 199 and then incubated with the preconditioned neutrophils at 37°C for 60 min in 5% CO₂ and 98% humidity. After the incubation, the detached endothelial cells and the nonadherent neutrophils were removed by three times washing with PBS. The remained nondetached endothelial cells in each well were harvested by trypsinization. The harvested nondetached endothelial cells were stained with Türk stain, and the number of nondetached endothelial cells were directly counted. The endothelial detachment was expressed as a percentage of the number of the nondetached endothelial cells isolated after the incubation with the neutrophils-free incubation mixture, which was performed in the parallel with the every condition of the incubations. There were few detached endothelial cells after the incubation with the neutrophils-free medium and variation in the counted number of the nondetached endothelial cells after the incubation with the neutrophils-free medium was < 1% among the wells. Thus, counted number of the nondetached endothelial cells after the incubation with the neutrophils-free medium can be assumed to be the cell number originally present in each well. The percent cell detachment was therefore calculated: [(the number of nondetached endothelial cells after the incubation with the neutrophils-free medium) – (the number of nondetached endothelial cells after the incubation with the preconditioned neutrophils)] \times 100 / (the number of nondetached endothelial cells after the incubation with the neutrophils-free medium). To confirm that the cell detachment was due to cell injury and death in this system, the detached cells after the incubation with activated neutrophils were centrifuged, washed, and replated as described in the text. Fewer than 5% of the cells were capable of replating. The lack of viability of the detached cells was also confirmed by trypan blue staining of detached cells.

NEP enzymatic activity. The neutrophils treated with the indicated agents in 1 ml of cold 25 mmol/liter 2-(N-morpholino)ethanesulfonic acid (Mes) buffer (pH 6.5) were homogenized with the glass to glass homogenizer and then sonicated (sonifier 250; Branson Corp., Danbury, CT) at 4°C. The suspension was centrifuged at 800 g for 15 min at 4°C to remove unbroken cells and nuclear materials. The supernatant was then centrifuged at 100,000 g for 60 min at 4°C for separation with cytosolic and particulate fractions. The membrane pellet (particulate fractions) was resuspended in 25 mmol/liter Mes buffer (pH 6.5) containing 0.5% Triton X-100 at 4°C for 90 min with continuous mixing. NEP enzymatic activity in the soluble particulate fraction and the cytosolic fraction of the isolated neutrophils was measured by a two-step spectrofluorometric assay using Glutaryl-Ala-Ala-Phe-4-methoxy-2-naphthylamide (4Meo-2NA) as a substrate as reported previously (12, 14, 16, 19, 39). The reaction was performed in the presence or absence of UK73967, and only the activity inhibited by UK73967 was attributed to the NEP activity.

Immunofluorescence staining and fluorescence-activated cell sorter (FACS) analysis. Cell surface NEP expression in neutrophils was detected by direct immunofluorescence evaluated by the flow cytometry. Aliquots of whole blood were pretreated for 5, 15, 30, and 60 min at 37°C with OZ or C5a, and then fixed in 1% paraformaldehyde. A part of whole blood was pretreated with ANP or BNP and then activated with OZ or C5a. After the pretreatments, 100 μ l of the blood was incubated for 30 min at 4°C in the dark with saturating concentrations (5 μ l) of the conjugated murine anti-human CD10/NEP (MoAb, J5-FITC; Coulter Immunology, Hialeah, FL) or the nonspecific IgG2a. After the incubation, the blood was washed in PBS con-

taining 1% fetal calf serum (FCS) and 0.1% NaN_3 . Thereafter, erythrocytes in the blood were lysed by adding 2 ml of ice-cold erythrocyte-lysing solution (NH_4Cl 2.08 grams; Na_2EDTA 0.0108 grams; NaHCO_3 0.21 grams in 250 ml H_2O). The remained leukocytes were then rinsed again with PBS containing 1% FCS and 0.1% NaN_3 and analyzed using FACScan. Antigen expression was expressed as the mean channel of fluorescence intensity of 10,000 cells.

Cell surface CD18 of the isolated neutrophils was also detected by direct immunofluorescence evaluated by the flow cytometry. The isolated neutrophils from the healthy volunteers were resuspended at a final concentration of 10^6 cells/ml in serum-free Medium 199 without phenol red. Aliquots of cells were then pretreated with or without ANP or BNP in the presence or absence of UK73967 at 37°C for 10 min and subsequently incubated with OZ for 10 min and then fixed in 1% paraformaldehyde. After the incubation, the cells were washed with PBS containing 1% FCS and 0.1% NaN_3 and then incubated in the dark at 4°C for 30 min with the conjugated murine anti-human CD18 (MoAb, FITC-Conjugated MHM23, DAKO A/S, Denmark) or the nonspecific IgG1 at a final concentration of 10 μl of MoAb per 100 μl of cell suspension. After the cells were washed with PBS containing 1% FCS and 0.1% NaN_3 , CD18 expression on neutrophils was analyzed by FACScan.

Measurement of cGMP levels. The isolated neutrophils from the healthy volunteers (10^7 cells/ml) were incubated with ANP (1 nmol/liter) or BNP (1 nmol/liter) at 37°C for 10 min in the presence or absence of UK73967. The incubations were done in the presence of 3-isobutyl-1-methylxanthine (IBMX; 1 mmol/liter). The reaction was terminated by the addition of trichloroacetic acid (TCA, final concentration 6%). The cell mixture was then sonicated. After centrifugation of the mixture, the supernatant was harvested and extracted with diethyl ether. After the extraction of TCA, cGMP produced in neutrophils was measured using a standard radioimmunoassay kit (^{125}I -cGMP; Amersham).

Gel filtration analysis of ^{125}I -ANP hydrolysis by neutrophils. ^{125}I -labeled α -human ANP (40 μl , 2000 Ci/mmol) was incubated for 15 min at 37°C with or without the activated neutrophils or the particulate fractions prepared from the activated neutrophils in serum-free Medium 199 in the presence or absence of UK73967 (50 $\mu\text{mol/liter}$). After the termination of the incubation by the addition of EDTA (10 mmol/liter), the incubation mixture was centrifuged, and the resulting supernatant (400 μl) was subjected to the Sephadex G-25 gel filtration chromatography (Superfine, 1.2×80 cm, Pharmacia) at a flow rate of 5 ml/h with 1 ml/tube of the fraction size. The chromatography was calibrated with ^{125}I -labeled standards of ^{125}I -ANP, ^{125}I -Phe-Arg-Tyr, free ^{125}I in the identical manner. Phe-Arg-Tyr was iodinated as reported previously (40).

Measurements of cytosolic free calcium in neutrophils. The concentration of cytosolic free calcium ($[\text{Ca}^{2+}]_i$) in neutrophils was measured using the calcium indicator fura 2, as described previously (41-43). In short, the isolated neutrophils (10^6 cells/ml) from the healthy volunteers were incubated with 2 $\mu\text{mol/liter}$ fura 2/AM in phosphate buffer containing 0.1% bovine serum albumin at 37°C for 45 min. After this, the neutrophils were washed twice with the incubation medium and resuspended at a final concentration of 10^6 cells/ml in phenol red-free Medium 199. Thereafter, the loaded neutrophils were treated with or without ANP, BNP and 8-bromo-cGMP in the presence or absence of HS-142-1 for 15 min at 37°C . Then, cell suspension (100 μl) was directly plated onto the tissue culture dish. Immediately after plating, a single cell was centered in the measuring field of the microscope photometer while it was still in suspension. Continuous monitoring of $[\text{Ca}^{2+}]_i$ was made in a single cell as it began to attach to the dishes. 5 min after plating of the neutrophils, C5a was added to the medium under the continuous monitoring of $[\text{Ca}^{2+}]_i$. $[\text{Ca}^{2+}]_i$ monitoring in a single fura 2 loaded neutrophils was continuously performed by the dual excitation microfluorimetry equipment (ARGUS 50/CA System, HAMAMATSU, Japan) coupled to an image acquisition system (Nikon inverted microscope, Nikon, Japan). This system was also equipped with a thermostated chamber allowing the cells to be main-

tained at 37°C during the entire experiment. The ratio of the fluorescence ($R = F_{340}/F_{380}$) was calibrated to express $[\text{Ca}^{2+}]_i$ using the formula, proposed previously (43, 44).

In vivo animal experiments. Healthy adult beagle dogs (10.0-13.0 kg) of either sex were anesthetized with sodium pentobarbital (30 mg/kg), intubated, and ventilated with room air by an animal respirator. The hearts were exposed through a left thoracotomy in the fifth intercostal space. The left anterior descending coronary artery (LAD) was then exposed and carefully dissected free immediately distal to the first major diagonal branch. Regional myocardial ischemia was produced by occluding LAD for 90 min and was followed by 2 h of reperfusion. UK73967 (1 mg/kg) and its vehicle were intravenously administered in 7 dogs and 7 dogs, respectively, as a bolus twice at 30 min after the LAD occlusion and at the beginning of the reperfusion. Blood samples were obtained from femoral vein. Arterial blood pressure, heart rate, and electrocardiogram were recorded continuously. Plasma ANP concentration was measured by radioimmunoassay using a commercial kit (Shionoria ANP kit, Osaka, Japan).

After the 2 h of reperfusion, heparin (10,000 units) was given intravenously and then the heart was stopped with an overdose of pentobarbital and removed from the chest. The left and right coronary arteries were cannulated and perfused with cold saline at a pressure of 75 mmHg for 30 min. Thereafter, five pieces of myocardial tissue samples (300-500 mg) were punched out from both central myocardial regions perfused by LAD and the left circumflex coronary artery (LCx), respectively. A part of each sample was fixed in 10% buffered formalin for histologic analysis with light microscopy. The remaining part of each sample from the region perfused by LAD was sectioned into small cubes and incubated in 0.1% nitroblue tetrazolium (NBT) in phosphate buffer at pH 7.4 and 37°C for 15 min to identify the injured tissue (45, 46). The tissue samples, from LAD region, that showed the negative NBT staining (the injured tissue) and the tissue samples from LCx region (the control tissue) were analyzed for myocardial myeloperoxidase activity (MPO) assay. The NBT staining did not affect MPO assay (46). Subsequently, each heart was perfused with 3% glutaraldehyde at a pressure of 75 mmHg for 30 min, then LAD 1 cm distal to the occlusion site and LCx were removed and used for the analysis with scanning electron microscopy.

Assay of myocardial myeloperoxidase (MPO). The enzyme MPO is found in the granules of neutrophils and has been used as an indicator of neutrophil emigration into tissue (45, 47). The injured myocardial tissue determined by NBT staining and the control tissue were homogenized and sonicated in 0.5% hexadecyltrimethylammonium bromide (HTAB) in 50 mmol/liter potassium phosphate buffer, pH 6.0. The mixture was centrifuged at 12,500 g for 30 min at 4°C . The supernatants were then collected and reacted with 0.167 mg/ml of *o*-dianisidine dihydrochloride and 0.0005% H_2O_2 in 50 mmol/liter phosphate buffer at pH 6.0. The change in absorbance was measured spectrophotometrically at 460 nm. One unit of myeloperoxidase is defined as the quantity of enzyme hydrolyzing 1 mmol peroxide/min at 25°C .

Scanning electron microscopy of coronary arteries and light microscopy of myocardial tissues. The coronary arteries removed from the heart were then placed in 3% glutaraldehyde in 0.1 mol/liter phosphate buffer for 24 h, and then the arteries were cut into longitudinal-sections with razor blades to expose the luminal surface. The sections were immersed in 1% tannic acid (Katayama Chemical Inc., Osaka, Japan) in phosphate buffer overnight at 4°C to increase tissue reactivity with osmium tetroxide (so-called "conductive-staining"). The sections were then rinsed with water for 2 h and fixed with 1% OsO_4 in distilled water for 2 h at 4°C . The specimens were dehydrated in ethanol series, infiltrated in 100% *t*-butanol, frozen, freeze-dried by evaporation under vacuum, mounted on aluminum stubs, and coated with a 20 to 30 nm layer of platinum alloy in an ion coater (Eiko Engineering Inc., Ibaragi, Japan). The specimens were observed at an accelerating voltage of 15 kV with a JSM 6400FK scanning electron microscope (JEOL Inc., Tokyo, Japan).

Myocardial tissues from regions perfused by LAD and LCx were fixed in 10% phosphate buffered formalin, embedded in paraffin, sectioned, and stained with hematoxylin and eosin.

Antibodies and reagents. α -Human ANP, BNP-32 (Human), and Suc-Ala-Pro-Ala-pNA were obtained from Peptide Institute, Inc., Minoh, Japan. UK73967 was supplied by Pfizer Central Research, Sandwich, UK. HS-142-1 was supplied by Kyowa-Hakko, Tokyo, Japan. A mouse anti-human CD10 MoAb (J5-FITC, IgG2a) was obtained from Coulter Immunology, Hialeah, FL. A mouse anti-human CD18 MoAb (FITC-Conjugated MHM23, IgG1) was from DAKO A/S, Denmark. cGMP radioimmunoassay kit, ^{51}Cr , ^{125}I , and ^{125}I -labeled α -human ANP were from Amersham, Buckinghamshire, UK. Phe-Arg-Tyr was from BACHEM, Bubendorf, Switzerland. All reagents for cell culture were from GIBCO (Grand Island, NY). Other chemicals were from Sigma Chemical Co. (St. Louis, MO).

Statistical analysis. All values were expressed as mean \pm SEM. Statistical analysis of the data was performed by Student's *t* test for paired or unpaired observations. When more than two groups were compared, ANOVA was used. Values were considered to be statistically different at $P < 0.05$.

Results

The inhibitory effects of ANP or BNP on the neutrophil functions and their potentiations by NEP inhibitor. The pretreatment of neutrophils with ANP or BNP inhibited endothelial detachment by the activated neutrophils in a dose-dependent manner (Fig. 1). The adhesiveness of the activated neutrophils to the

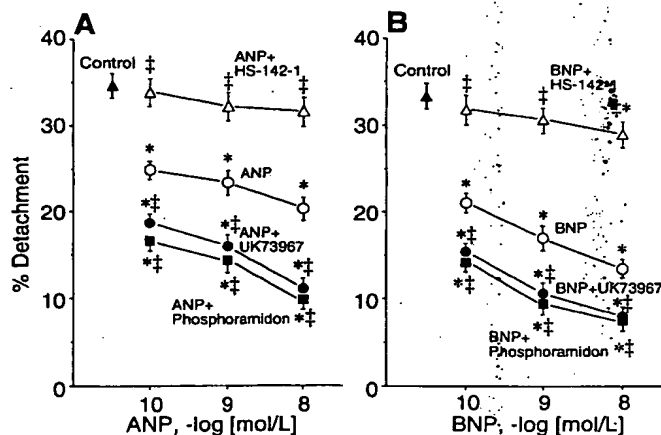


Figure 1. Effects of ANP and BNP in the combination with or without UK73967, phosphoramidon or HS-142-1 on the neutrophils-induced endothelial cell detachment. The isolated neutrophils from the healthy volunteers (10^7 cells/ml) were pretreated with ANP (A) or BNP (B) in the presence or absence of UK73967 (a specific inhibitor of NEP, 50 $\mu\text{mol/liter}$), phosphoramidon (50 $\mu\text{mol/liter}$), HS-142-1 (an antagonist for the particulate guanylyl cyclase receptor, 100 $\mu\text{g/ml}$), and the pretreated neutrophils were subsequently activated with OZ, and the preconditioned neutrophils were incubated with the monolayer of the cultured HUVECs, as described in the text. (Δ) Control, activated neutrophils with no pretreatment; (\circ) activated neutrophils after pretreatment with ANP or BNP; (\triangle) activated neutrophils after pretreatment with ANP or BNP in the presence of HS-142-1; (\bullet) activated neutrophils after pretreatment with ANP or BNP in the presence of UK73967; (\blacksquare) activated neutrophils after pretreatment with ANP or BNP in the presence of phosphoramidon. Values are shown as mean \pm SEM ($n = 6-10$). * $P < 0.01$ vs. control (Δ); $^{\dagger}P < 0.01$ vs. activated neutrophils after pretreatment with ANP or BNP (\circ).

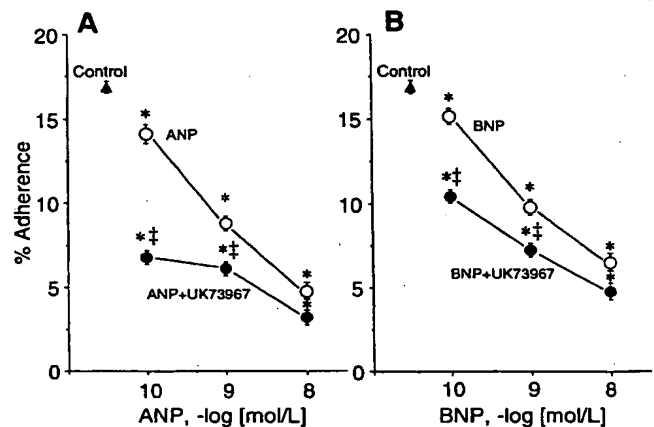


Figure 2. Effects of ANP and BNP in the combination with or without UK 73967 on the neutrophils adherence to endothelial cells. ^{51}Cr -labeled neutrophils (5×10^6 cells/ml) from the healthy volunteers were activated with OZ after pretreatment with ANP (A) or BNP (B) in the presence or absence of UK73967 (a specific inhibitor of NEP, 50 $\mu\text{mol/liter}$), and the preconditioned neutrophils were incubated with the monolayer of the cultured HUVECs, as described in the text. (Δ) Control, activated neutrophils with no pretreatment; (\circ) activated neutrophils after pretreatment with ANP or BNP; (\bullet) activated neutrophils after pretreatment with ANP or BNP in the presence of UK73967 (a specific inhibitor of NEP, 50 $\mu\text{mol/liter}$). Values are shown as mean \pm SEM ($n = 6-10$). * $P < 0.01$ vs. control (Δ); $^{\dagger}P < 0.01$ vs. activated neutrophils after pretreatment with ANP or BNP (\circ).

cultured endothelial cells (Fig. 2) and elastase release from the activated neutrophils (Fig. 3) were also inhibited by the pretreatment of neutrophils with ANP or BNP in a dose-dependent manner. Co-incubation of the neutrophils with UK73967

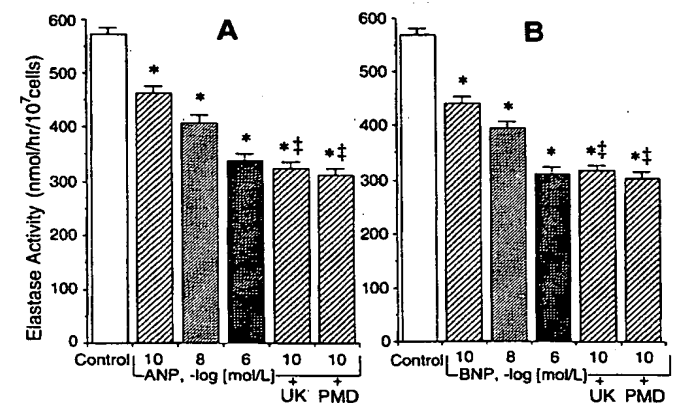


Figure 3. Effects of ANP and BNP in the combination with or without UK 73967 or phosphoramidon on elastase release from the isolated neutrophils. The isolated neutrophils from the healthy volunteers (10^7 cells/ml) suspended in 1 ml of serum-free Medium 199 without phenol red were activated with OZ after pretreatment with or without ANP (A) or BNP (B) in the presence or absence of UK73967 (a specific inhibitor of NEP, 50 $\mu\text{mol/liter}$), or phosphoramidon (PMD, 50 $\mu\text{mol/liter}$) for 60 min at 37°C , as described in the text. Values are shown as mean \pm SEM ($n = 6-10$). * $P < 0.01$ vs. control (activated neutrophils with no pretreatment); $^{\dagger}P < 0.01$ vs. activated neutrophils after pretreatment with ANP (0.1 nmol/liter) alone or BNP (0.1 nmol/liter) alone, respectively.

Table I. Effects of ANP or BNP on Reactive Oxygen Production of Neutrophils Activated with OZ

Treatments	Integrated count (cpm $\times 10^3$) ^a	Peak count (cpm $\times 10^3$) ^b
No pretreatment	1.1 \pm 0.1	0.1 \pm 0.1
OZ alone	117.8 \pm 6.9 [‡]	11.0 \pm 0.6 [‡]
ANP+OZ	114.5 \pm 5.2 [‡]	10.5 \pm 0.4 [‡]
ANP+UK73967+OZ	113.9 \pm 8.5 [‡]	10.1 \pm 0.8 [‡]
BNP+OZ	116.7 \pm 3.0 [‡]	10.4 \pm 0.4 [‡]
BNP+UK73967+OZ	114.0 \pm 6.1 [‡]	10.3 \pm 0.5 [‡]

Details of the method were described in the text. ^aIntegrated count means the sum of chemiluminescence counts integrated for 15 min after the activation. ^bPeak count means the maximal counts within 15 min after the activation. Concentrations of ANP, BNP, and UK73967 were 1 nmol/liter, 1 nmol/liter, and 50 μ mol/liter, respectively. Values are shown as mean \pm SEM ($n = 6-10$). [‡] $P < 0.01$ vs. no pretreatment.

or phosphoramidon potentiated the inhibitory effects of ANP or BNP on the neutrophils-induced endothelial detachment, the adhesiveness of the neutrophils to the endothelial cells and on the elastase release from the neutrophils (Figs. 1-3). The inhibitory effects of ANP or BNP on the adhesion of neutrophils to endothelium and neutrophils-mediated endothelial detachment and their potentiation by NEP inhibitor were comparable between the experiments using HUVECs and those using HAECs (data not shown). The pretreatment of neutrophils with UK73967 or phosphoramidon alone had no effect on elastase release from the activated neutrophils (elastase activity [nmol/h/10⁷ cells]: control; 573 \pm 10, UK73967 alone; 570 \pm 11, phosphoramidon alone; 569 \pm 10, $n = 6-10$, $P = NS$) and also had no effect on the neutrophils adhesion to the endothelial cells and endothelial detachment by the neutrophils (data not shown). The pretreatment with ANP or BNP had no effect on the total and peak chemiluminescence counts of the neutrophils activated with OZ as shown in Table I.

The studies with flow cytometry showed that the pretreatment of neutrophils with ANP or BNP inhibited CD18 expression on the activated neutrophils (Table II). Co-incubation with UK73967 potentiated the inhibitory effect of ANP or BNP on CD18 expression on the activated neutrophils. The

Table II. Cell Surface CD18 Expression on Isolated Neutrophils

Treatments	Mean channel of fluorescence intensity
No pretreatment	37.0 \pm 0.4
OZ alone	67.3 \pm 1.2
ANP+OZ	58.0 \pm 1.6*
ANP+UK73967+OZ	38.0 \pm 0.3**
BNP+OZ	44.7 \pm 0.8*
BNP+UK73967+OZ	39.0 \pm 1.0**
UK73967+OZ	67.1 \pm 1.0

Cell surface CD18 immunoreactive expression was analyzed using FACScan. Details of the method were described in the text. Concentrations of ANP, BNP, and UK73967 were 1 nmol/liter, 1 nmol/liter, and 50 μ mol/liter, respectively. Values are shown as mean \pm SEM ($n = 6-10$). * $P < 0.01$ vs. OZ alone; ** $P < 0.01$ vs. ANP+OZ or BNP+OZ.

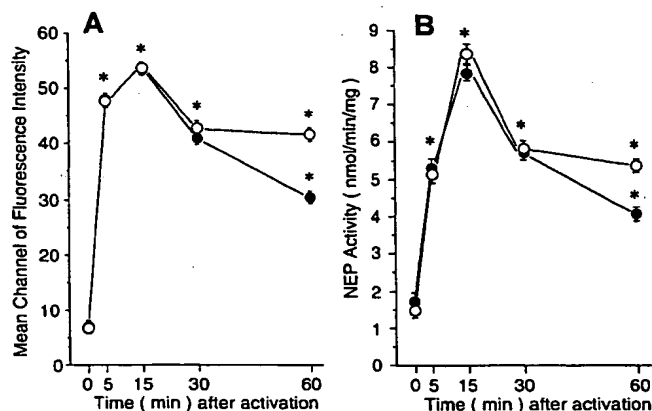


Figure 4. Time courses of NEP/CD10 immunoreactive expression and NEP enzymatic activity on the surface membrane of the human neutrophils stimulated with OZ or C5a. (A) NEP immunoreactive expression. (B) NEP enzymatic activity. (O) Neutrophils activated by OZ; (●) neutrophils activated by C5a. Values are shown as mean \pm SEM ($n = 6$ in each experiment), * $P < 0.01$ vs. time 0 (before activation).

pretreatment of neutrophils with UK73967 alone had no effect on CD18 expression on the activated neutrophils.

NEP enzymatic activity and immunoreactive expression on the surface membrane of neutrophils. NEP enzymatic activity in the particulate fraction and NEP/CD10 immunoreactive expression on the surface membrane of neutrophils were up-regulated within 5 min after the exposure to OZ or C5a (Fig. 4). The NEP enzymatic activity and NEP/CD10 immunoreactive expression on the surface membrane of neutrophils from the peripheral blood in patients with AMI were also up-regulated in the early phase of AMI (Figs. 5 and 6), but the NEP expressions were gradually decreased and returned to the same levels of control subjects within 7 d after the MI onset. In contrast with the NEP activity in the cell surface membrane, the activ-

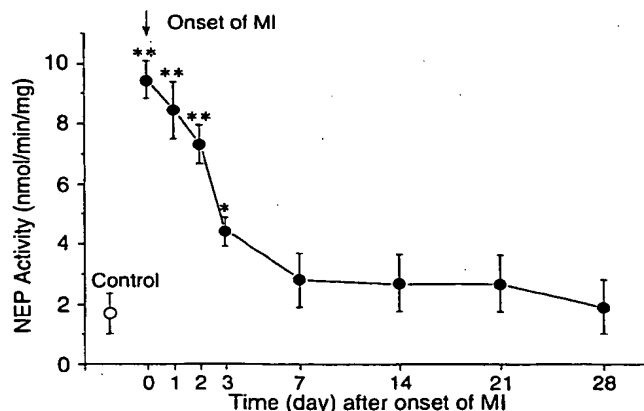


Figure 5. Time course of human neutrophil membrane NEP enzymatic activity in patients with acute myocardial infarction (AMI). Neutrophil NEP enzymatic activity in the particulate fraction of neutrophils from patients with AMI (●, $n = 8$) and of neutrophils from control subjects (○, $n = 6$). Details of the method were described in the text. Values are shown as mean \pm SEM, * $P < 0.05$, ** $P < 0.01$ vs. control subjects (○).

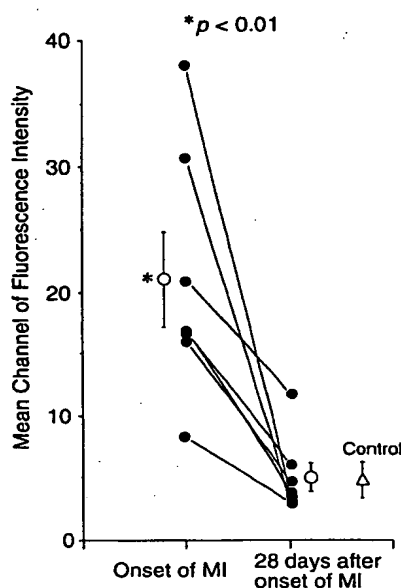


Figure 6. FACS analysis of human neutrophil NEP/CD10 immunoreactive expression in patients with acute myocardial infarction (AMI). Details of the method were described in the text. * $P < 0.01$ vs. 28th day after MI onset and control subjects (Δ).

ity in the cytosolic fraction decreased in neutrophils activated with OZ and in those from patients with early phase of AMI as shown in Table III. Total NEP activity in the particulate plus cytosolic fractions of neutrophils activated with OZ and of neutrophils from patients with early phase of AMI was not significantly different from that of nonactivated neutrophils and neutrophils in patients with late phase of AMI, respectively (Table III). Pretreatment of neutrophils with cycloheximide or actinomycin D did not affect the up-regulations of NEP enzymatic activity or immunoreactive expression on the surface membrane of the activated neutrophils (Table IV). Pretreatment with ANP or BNP did not affect the up-regulation of NEP/CD10 immunoreactive expression on the surface membrane of the activated neutrophils (mean channel of fluorescence intensity: OZ alone; 54.0 ± 3.8 , ANP [1 nmol/liter] + OZ;

Table III. Neutrophil NEP Activities in the Particulate and Cytosolic Fractions

Samples	Particulate % of total activity	Cytosol % of total activity	Total activity nmol/min/mg
No treated neutrophils	21.9 ± 2.4	78.1 ± 2.5	8.6 ± 0.4
Activated neutrophils	$97.0 \pm 1.3^*$	$3.0 \pm 0.8^*$	8.8 ± 0.1
Neutrophils in late phase of AMI	18.6 ± 1.8	81.4 ± 2.4	9.4 ± 0.3
Neutrophils in early phase of AMI	$97.2 \pm 1.4^\dagger$	$2.8 \pm 0.1^\dagger$	9.6 ± 0.2

No treated neutrophils, neutrophils isolated from healthy volunteers were treated without OZ but in the identical manner with neutrophils activation with OZ; Activated neutrophils, neutrophils isolated from healthy volunteers were incubated with OZ; Neutrophils in late phase of AMI, neutrophils isolated from the peripheral circulation in patients with AMI on 28th day after onset; Neutrophils in early phase of AMI, neutrophils isolated from the peripheral circulation in patients with AMI on the day of the onset. Values are shown as mean \pm SEM ($n = 6-10$). * $P < 0.01$ vs. no treated neutrophils; $^\dagger P < 0.01$ vs. neutrophils in late phase of AMI.

Table IV. Effects of Cycloheximide or Actinomycin D on the NEP Enzymatic Activity and Immunoreactive Expression on the Surface Membrane of the Activated Neutrophils

Treatment	Mean channel of fluorescence intensity	NEP activity nmol/min/mg
No treatment	7.9 ± 0.6	3.3 ± 0.2
OZ alone	$54.0 \pm 3.8^*$	$8.5 \pm 0.3^*$
Cycloheximide+OZ	$53.9 \pm 1.8^*$	$8.6 \pm 0.4^*$
Actinomycin D+OZ	$53.3 \pm 2.2^*$	$8.7 \pm 0.2^*$

Details were described in the text. No treatment, neutrophils from healthy volunteers were treated without OZ but in the identical manner with neutrophils activation with OZ; OZ alone, neutrophils from healthy volunteers were activated with OZ; Cycloheximide+OZ, neutrophils from healthy volunteers were preincubated with cycloheximide (40 μ mol/liter) and subsequently activated by OZ; Actinomycin D+OZ, neutrophils from healthy volunteers were preincubated with actinomycin D (150 nmol/liter) and subsequently activated by OZ. Values are shown as mean \pm SEM ($n = 6$ in each experiment). * $P < 0.01$ vs. no treatment.

54.1 ± 2.1 , BNP [1 nmol/liter] + OZ; 53.8 ± 1.8 , $n = 6$ in each experiment, $P = \text{NS}$). There were no significant differences in the NEP enzymatic activity and NEP/CD10 immunoreactive expression in the surface membrane of the neutrophils in early phase of AMI between the patients treated with and without the infusion of tissue plasminogen activator (data not shown).

Roles of cGMP on the effects of ANP and BNP. The incubation of neutrophils with ANP (1 nmol/liter) or BNP (1 nmol/liter) induced cGMP generation in neutrophils, which peaked at 5–10 min and lasted for 30 min after the start of the incubation with ANP or BNP, and co-incubation with UK73967 potentiated the effect of ANP or BNP on cGMP generation (Fig. 7). The incubation of neutrophils with ANP or BNP in the combination with HS-142-1, an antagonist for the particulate guanylyl cyclase receptor, attenuated the inhibitory effects of ANP or BNP on the endothelial detachment by the activated neutrophils (Fig. 1) and on the elastase release from the activated neutrophils (elastase activity [nmol/h/ 10^6 cells]: control; 573 ± 10 , ANP [1 nmol/liter] alone; 430 ± 12 ,[§] ANP [1 nmol/liter] + HS-142-1; 520 ± 15 ,^{§§} BNP [1 nmol/liter] alone; 423 ± 10 ,[§] BNP [1 nmol/liter] + HS-142-1; 484 ± 12 ,^{§§} $n = 6-10$, * $P < 0.01$ vs. ANP [1 nmol/liter] alone, $^\dagger P < 0.01$ vs. BNP [1 nmol/liter] alone, $^\ddagger P < 0.01$ vs. control). The pretreatment of neutrophils with 8-bromo-cGMP inhibited the endothelial detachment by the activated neutrophils (Fig. 8) and elastase release from the activated neutrophils (elastase activity [nmol/h/ 10^6 cells]: control; 573 ± 10 , 8-bromo-cGMP [0.1 mmol/liter]; 410 ± 19 ,^{*} 8-bromo-cGMP [1 mmol/liter]; 331 ± 17 ,^{*} $n = 6-10$, * $P < 0.01$ vs. control), mimicking the results obtained from the experiment using ANP or BNP.

The effect of UK73967 on ^{125}I -ANP degradation by neutrophils. After a 15-min incubation of ^{125}I -ANP with the particulate fraction from the activated neutrophils, 2 main hydrolysis products were detected by gel filtration chromatography analysis; one corresponds to ^{125}I -Phe-Arg-Tyr and the other corresponds to the undetermined degradation product of ^{125}I -ANP presumably cleaved between residues Cys-105 and Phe-106, accompanied by a minor peak corresponding to free ^{125}I (Fig. 9). When ^{125}I -ANP was incubated with the activated neutro-

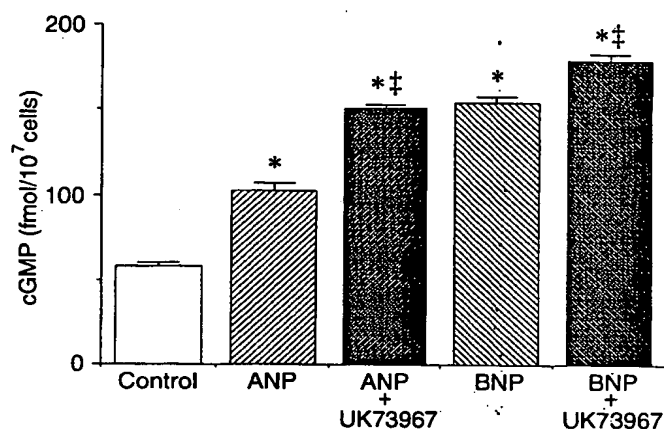


Figure 7. Effects of ANP and BNP in the combination with or without UK73967 on cyclic GMP levels in human neutrophils. Details of the method were described in the text. Concentrations of ANP, BNP, and UK73967 were 1 nmol/liter, 1 nmol/liter, and 50 μ mol/liter, respectively. Values are shown as mean \pm SEM ($n = 5$ in each experiment). * $P < 0.01$ vs. control (nontreated neutrophils); ‡ $P < 0.01$ vs. neutrophils treated with ANP (1 nmol/liter) alone or BNP (1 nmol/liter) alone, respectively.

phils, three peaks were also observed and co-incubation with UK73967 protected ¹²⁵I-ANP against the degradation by the activated neutrophils as shown in Fig. 9.

The effects of ANP and BNP on $[Ca^{2+}]_i$ during adhesion and at C5a-stimulation in single neutrophils. It has been reported that neutrophils attach and spread with significant change in $[Ca^{2+}]_i$ when suspended neutrophils are placed on the tissue culture dish (41–43). Spontaneous intracellular calcium oscillations were observed during the adhesion to the tissue culture dish in most of neutrophils. And $[Ca^{2+}]_i$ was transiently increased in response to C5a in most of neutrophils. However the oscillatory activity during the adhesion and the transients of $[Ca^{2+}]_i$ in response to C5a were not observed in all neutrophils examined. These observations were in agreement with previous reports (41–43). Table V shows that the percentages of number of the oscillatory neutrophils during adhesion and

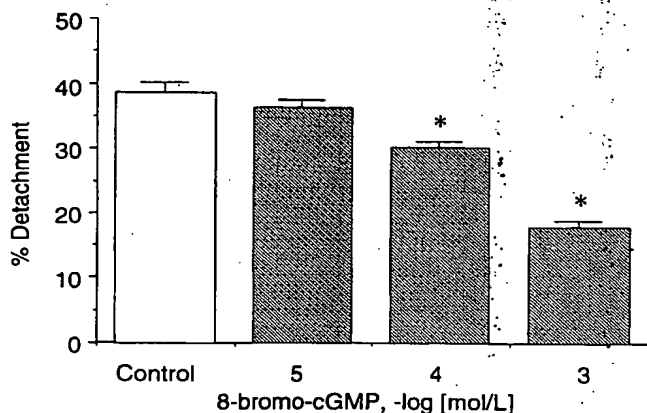


Figure 8. Effect of 8-bromo-cGMP on the endothelial detachment by the activated human neutrophils. Details of the method were described in the text. Values are shown as mean \pm SEM ($n = 6-10$). * $P < 0.01$ vs. control (the activated neutrophils without pretreatment with 8-bromo-cGMP).

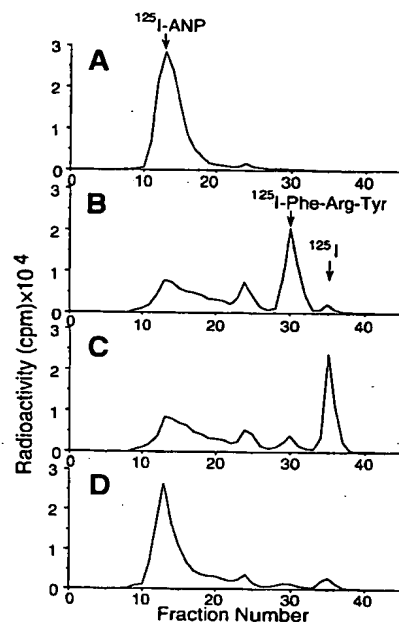


Figure 9. Effect of UK73967 (a specific inhibitor of NEP) on ¹²⁵I-ANP degradation by the activated human neutrophils. (A) Radiochromatograms of ¹²⁵I-ANP after the incubation with the neutrophils-free medium for 15 min at 37°C. (B) ¹²⁵I-ANP after the incubation with the particulate fraction from the activated neutrophils for 15 min at 37°C. (C) ¹²⁵I-ANP after the incubation with the activated neutrophils for 15 min at 37°C. (D) ¹²⁵I-ANP after the incubation with the activated neutrophils for 15 min at 37°C in the presence of UK73967 (a specific inhibitor of NEP, 50 μ mol/liter). When ¹²⁵I-ANP was incubated with the particulate fraction of the activated neutrophils or the activated neutrophils, three peaks were observed, and co-incubation with UK73967 protected ¹²⁵I-ANP against the degradation by the activated neutrophils.

the responding neutrophils to the C5a-stimulation were changed by the pretreatments and the changes in response to each of the pretreatments were in parallels with those of the peak $[Ca^{2+}]_i$ response to the pretreatments. The pretreatment with ANP or BNP reduced both the oscillatory activity of $[Ca^{2+}]_i$ during the adhesion and the transients in $[Ca^{2+}]_i$ in response to C5a stimulation with regards to the amplitude of the peaks, as shown in Table V. Co-incubation of the neutrophils with HS-142-1 attenuated the inhibitory effects of ANP or BNP on the peaks in $[Ca^{2+}]_i$ (Table V). The pretreatment of neutrophils with 8-bromo-cGMP inhibited the oscillatory activity during the adhesion and the transients in $[Ca^{2+}]_i$ at the C5a-stimulation, mimicking the results obtained from experiments using ANP or BNP (Table V).

In vivo animal experiments. Plasma level of ANP in dogs was increased at 30 min after the LAD occlusion (9.3 ± 2.1 pg/ml at baseline vs. 147 ± 35 pg/ml at 30 min after the LAD occlusion, $P < 0.05$). Plasma level of ANP at 30 min after the first injection of UK73967 or vehicle was significantly higher in dogs with UK73967 treatment than in those without UK73967 treatment (695 ± 135 pg/ml with UK73967 vs. 167 ± 40 pg/ml without UK73967, $P < 0.05$). NEP immunoreactivity and enzymatic activity were found to exist in the isolated neutrophils from the dogs by the same methods as used in the human neutrophils, described in the Methods section, and the immunoreactivity and the enzymatic activity in the dog neutrophils were also up-regulated with C5a-stimulation by 2.6- and 2.2-fold of those at baseline, respectively (cell surface immunoreactive NEP/CD10 expression by flow cytometry at baseline, 5.4 ± 0.3 mean channel fluorescence intensity. NEP activity at baseline, 0.1 ± 0.03 nmol/min/mg protein). Furthermore, the enzymatic activity in the dog neutrophils from the peripheral circulation was also increased after the myocardial ischemia/reperfusion

Table V. Effects of ANP and BNP on Peak of $[Ca^{2+}]_i$ during Adhesion and at C5a-Stimulation in Single Neutrophils

Pretreatments	Peak $[Ca^{2+}]_i$ (nmol/L)	
	During adhesion No. oscillatory cells/ No. cells studied, %	At C5a-Stimulation No. responding cells/ No. cells studied, %
No pretreatment	232±11 (15/20, 75%)	311±12 (14/19, 74%)
ANP	157±10* (10/24, 42%)	176±10* (9/22, 41%)
BNP	152±15* (10/23, 43%)	170±12* (10/23, 44%)
ANP+HS-142-1	207±12 [‡] (16/22, 73%)	288±15 [‡] (17/24, 70%)
BNP+HS-142-1	199±15 [‡] (15/22, 68%)	281±13 [‡] (13/21, 61%)
8-bromo-cGMP[0.1 mmol/L]	190±11* (9/18, 50%)	232±10* (11/19, 58%)
8-bromo-cGMP[1 mmol/L]	167±12* (8/19, 42%)	213±12* (9/19, 47%)

Values within parentheses are number of the oscillatory cells during adhesion and the responding cells at C5a-stimulation and all neutrophils studied. Peaks in $[Ca^{2+}]_i$ during adhesion and at C5a-stimulation were statistically analyzed and shown in this Table in the cells that showed the oscillatory activity and the transients of $[Ca^{2+}]_i$ in the respective conditions. Concentrations of ANP, BNP, and HS-142-1 were 1 nmol/liter, 1 nmol/liter, and 100 µg/ml, respectively. Values of peak $[Ca^{2+}]_i$ (nmol/liter) were taken from ten different preparations of neutrophils and are shown as mean±SEM. * $P < 0.01$ vs. no pretreatment; [‡] $P < 0.01$ vs. ANP; [‡] $P < 0.01$ vs. BNP.

by 2.1-fold of that at baseline. MPO activity, an indicator of neutrophils accumulation, in the ischemic/reperfused myocardial region was significantly lower in dogs with UK73967 treatment than in those without UK73967 treatment, as shown in Fig. 10. The study with light microscopy showed that there were numerous neutrophils infiltrates within vascular lumens and in the interstitium from dogs without UK73967 treatment, whereas there were only rare neutrophils present in capillaries and in the interstitium from dogs with UK73967 treatment, as shown in Fig. 11. The study with scanning electron microscopy showed that there were numerous neutrophils adhered to the coronary arterial endothelium from dogs without UK73967 treatment, whereas there were only occasional neutrophils ad-

hered to the endothelium from dogs with UK 73967 treatment, as shown in Fig. 12.

Discussion

The present study showed that ANP and BNP at the concentrations of 0.1–10 nmol/liter inhibited the detachment of the cultured endothelial cells by the neutrophils and the adhesiveness of the neutrophils to the endothelial cells. The present study also showed that the inhibitory effects of ANP and BNP were associated with the suppressions of CD18 expression on the neutrophils and of elastase release from the neutrophils. CD18 expression and elastase release of neutrophils are well-known to have important roles in the adhesion of neutrophils to the endothelium and subsequent endothelial injury (27, 28, 48, 49). Furthermore, we have previously shown that CD18 expression on the neutrophils and elastase release from the neutrophils play an essential role in the adhesion of the neutrophils to the endothelium and neutrophils-induced endothelial cytotoxicity (32). Therefore, the suppressions of CD18 expression and of elastase release by ANP and BNP may at least partly contribute to the inhibitory effects of ANP and BNP on neutrophils adhesion and cytotoxicity to the endothelial cells. Although the exact mechanisms responsible for the suppression on the neutrophil functions by ANP and BNP still remain to be elucidated, cGMP produced in neutrophils by ANP and BNP via particulate guanylyl cyclase may play a role in the mechanism of the suppressive effects of ANP and BNP. Because the present study also demonstrated that HS-142-1, an antagonist for the particulate guanylyl cyclase receptor (50, 51), attenuated the suppressive effects of ANP and BNP, and the present study showed that 8-bromo-cGMP also inhibited the neutrophils-induced endothelial detachment and elastase release from the neutrophils, mimicking the effects observed with ANP and BNP. Thus, it could be assumed that cGMP elevated by ANP and BNP may affect the intracellular processes for the functional alterations in neutrophils during activation with OZ or C5a. Furthermore, the present study showed that ANP and BNP suppressed both of the oscillatory activity of $[Ca^{2+}]_i$ during the adhesion and the transients in $[Ca^{2+}]_i$ in re-

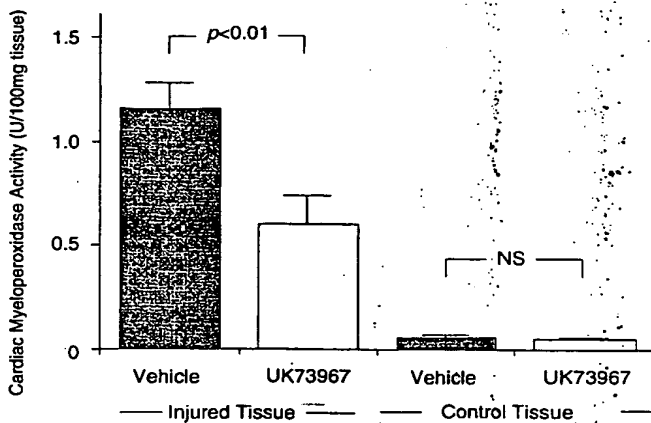


Figure 10. Effect of UK73967 treatment on cardiac MPO activity in an in vivo canine model of myocardial ischemia/reperfusion. Regional myocardial ischemia was produced by occluding LAD for 90 min and was followed by 2 h of reperfusion. UK73967 (1 mg/kg) ($n = 7$ dogs) or its vehicle ($n = 7$ dogs) was intravenously administered as a bolus twice during the myocardial ischemia/reperfusion experiments. The myocardial tissues were taken from the regions injured by the ischemia/reperfusion (Injured Tissue) and the normal perfused region (Control Tissue) and were subjected to the assay of MPO activity. Values are shown as mean±SEM.

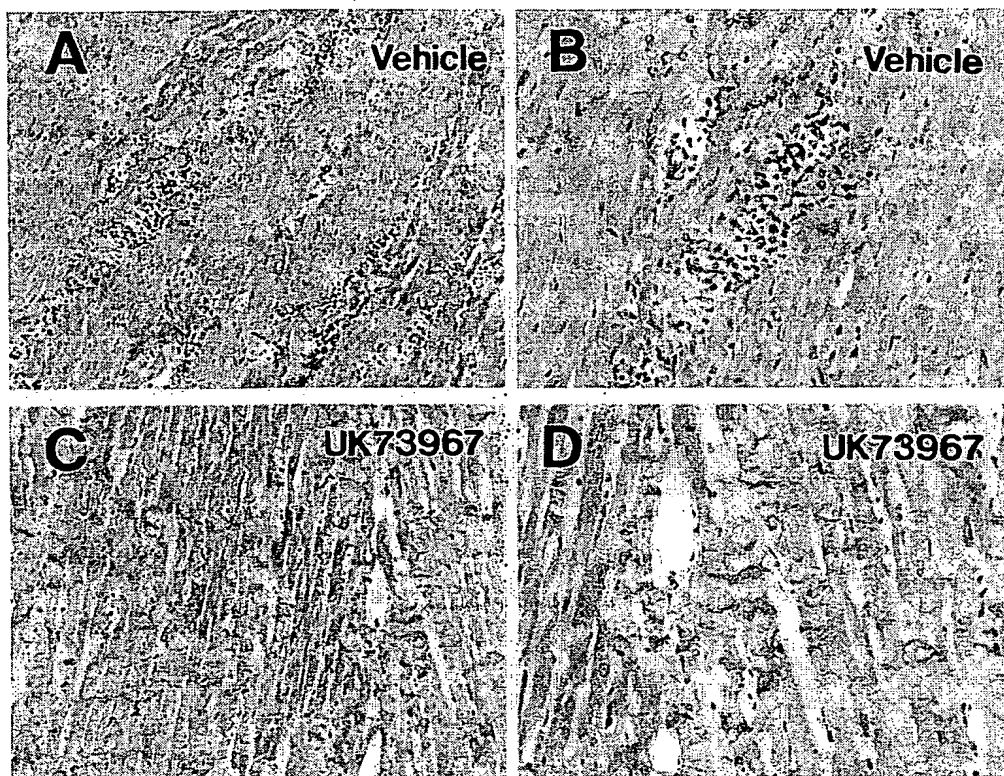


Figure 11. Light micrographs of the ischemic/reperfused myocardial tissues in an in vivo canine model. (A and B) Light micrographs of ischemic/reperfused myocardium from the dog without UK73967 treatment. Intense accumulation of neutrophils in the microvessels and the transmigration of neutrophils were apparent in the myocardium injured by ischemia/reperfusion (A, $\times 200$, B, $\times 400$). (C and D) Light micrographs of ischemic/reperfused myocardium from the dog with UK73967 treatment. Neutrophil accumulation in the microvessels and the extravascular neutrophils were much less as compared with A and B (C, $\times 200$; D, $\times 400$). Findings showing in A–D are representative of those observed in the ischemic/reperfused myocardium of the dogs treated with or without UK73967.

sponse to C5a-stimulation in neutrophils. These suppressions also appear to be mediated by cGMP since HS-142-1 attenuated the suppressive effects of ANP and BNP on $[Ca^{2+}]_i$, and 8-bromo-cGMP exhibited mimicking effects on $[Ca^{2+}]_i$ in neutrophils as observed with ANP and BNP. A rise in $[Ca^{2+}]_i$ has been implicated to have a regulatory role in various functions including adherence and elastase release in the neutrophils at

rest and at the agonists-stimulation (41–43). Thus, cGMP-mediated inhibition of intracellular calcium mobilization may be at least partially involved in the mechanisms by which ANP and BNP suppressed the neutrophil functions. Previous studies showed that cGMP inhibits the receptor-mediated intracellular signaling pathway leading to increase in $[Ca^{2+}]_i$ at the levels of protein kinase C (PKC) or G protein in various types of

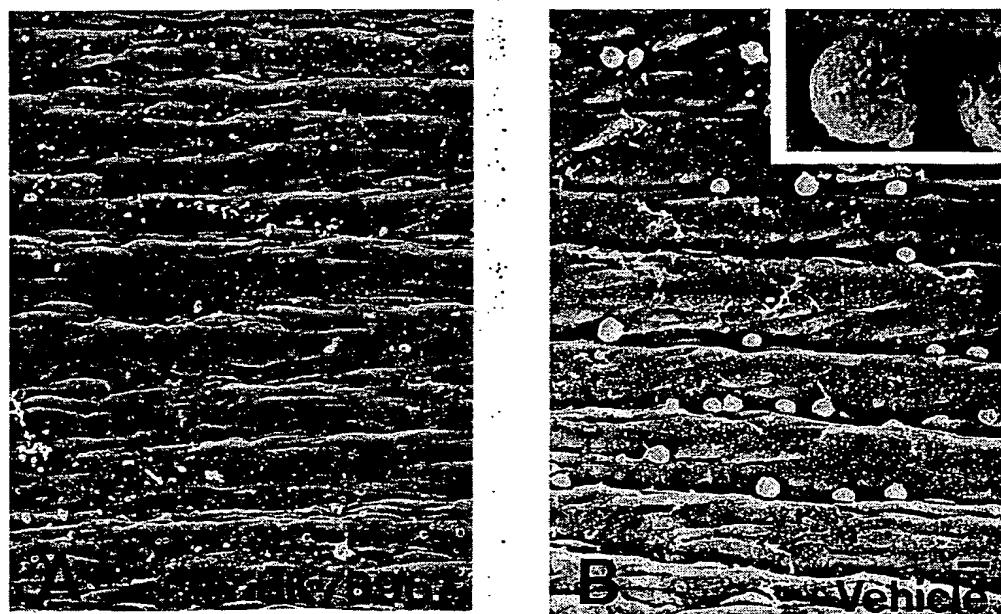


Figure 12. Scanning electron micrographs of the luminal surface of the ischemic/reperfused coronary arteries in an in vivo canine model. (A) Scanning electron micrograph of the ischemic/reperfused coronary arteries from the dog with UK73967 treatment. There were only occasional neutrophils adhered to the endothelium (Bar, 10 μ m). (B) Scanning electron micrograph of the ischemic/reperfused coronary arteries from the dog without UK73967 treatment (Bar, 10 μ m). There were numerous neutrophils adhered to the coronary arterial endothelium. (B, inset) Higher magnification illustrates neutrophils adhered to the endothelium (Bar, 60 μ m). Findings shown in A and B are representative of those observed in the ischemic/reperfused coronary arteries of the dogs treated with or without UK73967.

cells (52, 53), however, the exact role of cGMP in the signaling pathway in neutrophils is controversial (54–56). Thus, it remains undetermined at the present time which levels of the signaling pathways leading to increase in $[Ca^{2+}]_i$ in neutrophils may be affected by ANP and BNP. The effects of ANP and BNP on the neutrophil functions seems to be selective, because ANP and BNP had no effect on the respiratory burst action. It has been shown that there may be two distinct signal transduction pathways for the activation of the respiratory burst: one is Ca^{2+} -dependent and leads to PKC activation; the other is Ca^{2+} -independent and does not involve phospholipase C or PKC (57). It is thus possible that the Ca^{2+} -independent pathway may remain functional for the activation of the respiratory burst in the neutrophils treated with ANP and BNP.

We have previously shown that plasma levels of ANP and BNP increase to the concentrations of 0.01–0.03 nmol/liter and 0.03–0.1 nmol/liter, respectively, in the peripheral blood and to the concentrations of 0.3–0.6 nmol/liter and 0.8–2.0 nmol/liter, respectively, in the coronary sinus blood in patients with AMI (8). We have also reported that intravenous infusion of ANP or BNP improves left ventricular function in patients with congestive heart failure by the mechanisms of vasodilatation and natriuretic action (58, 59). Furthermore, we have previously demonstrated that intracoronary infusion of BNP dilates coronary arteries in vivo humans (60). Thus, ANP and BNP appear to exert the beneficial effects on cardiac hemodynamics. Myocardial ischemia/reperfusion in AMI causes not only myocardial injury but also coronary vascular injury, which results in further myocardial damage. It has been shown that neutrophils play a role in those setting, and that the adhesion of neutrophils to coronary endothelium and the subsequent endothelial injury by neutrophils are important steps in the coronary vascular injury occurring in the condition of myocardial ischemia and reperfusion in AMI. Therefore, considering our previous reports and the present results showing that ANP and BNP at the concentrations elevated in the coronary or peripheral circulations in patients with AMI inhibit neutrophils-induced endothelial injury, ANP and BNP elevated in the coronary circulation and in the circulatory peripheral plasma in patients with AMI could exert protective actions on the neutrophils-induced coronary vascular injury and could lead to salvage ischemic myocardium.

NEP has been shown to exist on the surface membrane of neutrophils and hydrolyze ANP and BNP. The present study demonstrated that NEP expression was up-regulated on the surface membrane of neutrophils activated with OZ or C5a and on that of the circulating neutrophils in the patients with early phase of AMI. Furthermore, the present study also demonstrated that the activated neutrophils induced ANP degradation which was attenuated with UK73967, a specific NEP inhibitor. The present study also showed that the inhibitory effects of ANP and BNP on the functions of the activated neutrophils were potentiated with NEP inhibitors. Therefore, the present results indicate that ANP and BNP exert protective effects against the neutrophils-induced endothelial injury, but the effects are suppressed by neutrophil NEP which also increases after their activation with OZ or C5a or in AMI. In this context, NEP inhibitors might have a rationale for therapeutic agent preventing neutrophils-induced endothelial injury in AMI. In fact, the present in vivo dog experiment showed that UK73967 treatment suppressed both the adhesion to endothelium and the accumulation of neutrophils in the ischemic/re-

perfused coronary vasculature and myocardial tissue. These inhibitory effects of UK73967 in vivo treatment on neutrophil-related activities (adherence to coronary vascular endothelium, accumulation in the vasculature and myocardial tissue) were at least partially mediated by the inhibition of neutrophil NEP since the present in vivo dog experiment also showed that NEP was expressed in dog neutrophils and up-regulated in the circulated peripheral dog neutrophils after the myocardial ischemia/reperfusion and in the isolated dog neutrophils after C5a activation. The present and other studies with in vivo human and animals show that levels of ANP in the peripheral circulation were increased after systemic administration of NEP inhibitor (61, 62). Thus, NEP inhibitor might inhibit neutrophils-mediated endothelial and myocardial injury and improve cardiac hemodynamics through the effect of ANP and BNP increased locally on the surface of neutrophils and systematically in the peripheral circulation by inhibition of NEP in neutrophils and in other organs.

The present results are in agreement with the previous reports by Shipp et al. and other workers showing that the responses of neutrophils to inflammatory peptides including FMLP and substance P were influenced by NEP in neutrophils themselves (14–16). A report showed that ANP weakly enhanced respiration burst activity and granule release in neutrophil response to FMLP (63). The stimulative effects of ANP on neutrophils, in that report, were independent of cGMP and were not affected by NEP in neutrophils themselves, which are in contrast with the results in the present study and in other papers (14–16). The reason for the discrepancy is unclear, but the difference in the incubating conditions and in the stimulations tested may be one of the possible reasons. They suspended neutrophils in Hanks' balanced salt solution (HBSS) while we and other workers used the culture medium such as RPMI and Medium 199 which are more physiological than HBSS. When they incubated neutrophils in culture medium of RPMI for chemotaxis assay instead of HBSS which was used for the other assays of the respiration burst activity and the granule release in the report, they showed that ANP did inhibit chemotactic activity of neutrophils in response to FMLP.

As suggested in the present study, neutrophils in patients with AMI might reduce the responses to a variety of NEP degradable peptides such as endothelin and bradykinin so on (64, 65). However, the exact mechanisms for the up-regulation of NEP in the surface membrane of neutrophils in patients with AMI remains undetermined in the present study. There are a number of reports showing that neutrophils present in the injured myocardium as well as in the circulation in AMI are on the state of activation (66). In the present in-vitro experiment, we used OZ for the neutrophils activation since OZ is a potent activator of the alternative pathway of complements, and the activation of the complement system has been shown to play a role in the neutrophils-induced myocardial injury in AMI (67, 68). In fact, the complement C5a was reported to be produced during myocardial ischemia and reperfusion via activation of neutrophils (67). And further, the present study showed that up-regulation of NEP expression was induced by OZ in neutrophils in the comparable magnitude observed with that by C5a and in early phase of AMI. Thus, complements-induced up-regulation of NEP may be one of the possible mechanisms for the increase expression of neutrophil NEP in AMI. The present study showed that up-regulation of NEP expression on the surface membrane of neutrophils after activation with OZ

seems to be independent on the de-novo protein synthesis and mRNA transcription because cycloheximide and actinomycin D were ineffective on the NEP up-regulation on the activated neutrophils. The increase in particulate NEP activity was associated with the decrease in the cytosol NEP activity without changes of total NEP activity in the neutrophils activated with OZ. The similar response of the intracellular NEP activities was observed with neutrophils from patients with early phase of AMI, comparing with neutrophils from patients with late phase of AMI and from control subjects. These present findings indicate that the up-regulation of NEP expression on the surface membrane of neutrophils after activation with OZ and of those from patients with AMI may be caused by the translocation of NEP to the plasma membrane from the intracellular compartments, supporting the results reported by Werfel et al. (69) who used C5a for the neutrophils activation.

In conclusion, ANP and BNP, which increase in AMI, modulate the neutrophil functions and exert protective effects against the neutrophils-induced endothelial cytotoxicity at the physiological concentrations. But the effects are suppressed due to their degradation by the neutrophil own NEP. Thus, neutrophil NEP, which also increases in AMI, may play a role in the pathophysiology of ischemia/reperfusion myocardial injury.

Acknowledgments

We thank Dr. Akira Hirata (Div. of Ophthalmology, Kumamoto University), and Dr. Yasuhiro Ogata (Japanese Red Cross Kumamoto Hospital).

This work was supported in part by the Grant-in-aid for Scientific Research on C07670793 from the Ministry of Education, Science and Culture in Japan.

References

1. de Bold, A.J. 1985. Atrial natriuretic factor: a hormone produced by the heart. *Science (Wash. DC)* 230:767-770.
2. Laragh, J.H. 1985. Atrial natriuretic hormone: the renin aldosterone axis and blood pressure-electrolyte homeostasis. *N. Engl. J. Med.* 313:1330-1340.
3. Needleman, P., and J.E. Greenwald. 1986. Atrial natriuretic factor: a cardiac hormone intimately involved in fluid, electrolyte, and blood pressure homeostasis. *N. Engl. J. Med.* 314:828-834.
4. Ballermann, B.J., and B.M. Brenner. 1986. Role of atrial peptides in body fluid homeostasis. *Circ. Res.* 58:619-630.
5. Genest, J., and M. Cantin. 1987. Atrial natriuretic factor. *Circulation* 75(suppl I): I-118-124.
6. Floras, J.S. 1990. Sympathoinhibitory effects of atrial natriuretic factor in normal humans. *Circulation* 81:1860-1873.
7. Yasue, H., M. Yoshimura, H. Sumida, K. Koichi, K. Kugiyama, M. Jougasaki, H. Ogawa, K. Okumura, M. Mukoyama, and K. Nakao. 1994. Localization and mechanism of secretion of B-type natriuretic peptide in comparison with those of A-type natriuretic peptide in normal subjects and patients with heart failure. *Circulation* 90:195-203.
8. Morita, E., H. Yasue, M. Yoshimura, H. Ogawa, M. Jougasaki, T. Matsumura, M. Mukoyama, and K. Nakao. 1993. Increased plasma levels of brain natriuretic peptide in patients with acute myocardial infarction. *Circulation* 88: 82-91.
9. Omland, T., T. Aarsland, A. Aakvaag, R. T. Lie, and K. Dickstein. 1993. Prognostic value of plasma atrial natriuretic factor, norepinephrine and epinephrine in acute myocardial infarction. *Am. J. Cardiol.* 72:255-259.
10. Yasue, H., K. Obata, K. Okumura, M. Kurose, H. Ogawa, K. Matsumura, M. Jougasaki, Y. Saito, K. Nakao, and H. Imura. 1989. Increased secretion of atrial natriuretic polypeptide from the left ventricle in patients with dilated cardiomyopathy. *J. Clin. Invest.* 83:46-51.
11. Erdös, E.G., and R.A. Skidgel. 1989. Neutral endopeptidase 24.11 (enkephalinase) and related regulators of peptide hormones. *FASEB J.* 3:145-151.
12. Johnson, A.R., J. Ashton, W.W. Schultz, and E.G. Erdös. 1985. Neutral metalloendopeptidase in human lung tissue and cultured cells. *Am. Rev. Respir. Dis.* 132:564-568.
13. Malfroy, B., J.P. Swerts, A. Guyon, B.P. Roques, and J.C. Schwartz. 1978. High-affinity enkephalin-degrading peptidase in brain is increased after morphine. *Nature (Lond.)* 276:523-526.
14. Connelly, J.C., R.A. Skidgel, W.W. Schulz, A.R. Johnson, and E.G. Erdös. 1985. Neutral endopeptidase 24.11 in human neutrophils: cleavage of chemotactic peptide. *Proc. Natl. Acad. Sci. USA* 82:8737-8741.
15. Shipp, M.A., G. B. Stefano, L. D'Adamio, S.N. Switzer, F.D. Howard, J. Sinisterra, B. Scharer, and E.L. Reinherz. 1990. Downregulation of enkephalin-mediated inflammatory responses by CD10/neutral endopeptidase 24.11. *Nature (Lond.)* 347:394-396.
16. Shipp, M.A., G.B. Stefano, S.N. Switzer, J.D. Griffin, and E.L. Reinherz. 1991. CD10 (CALLA)/Neutral endopeptidase 24.11 modulates inflammatory peptide-induced changes in neutrophil morphology, migration, and adhesion proteins and is itself regulated by neutrophil activation. *Blood* 78:1834-1841.
17. Iwamoto, I., A. Kimura, K. Ochiai, H. Tomioka, and S. Yoshida. 1991. Distribution of neutral endopeptidase activity in human blood leukocytes. *J. Leukocyte Biol.* 49:116-125.
18. Letarte, M., S. Vera, R. Tran, J.B.L. Addis, R.J. Onizuka, E.J. Quackenbush, C.V. Jongeneel, and R.R. McInnes. 1988. Common acute lymphocytic leukemia antigen is identical to neutral endopeptidase. *J. Exp. Med.* 168:1247-1253.
19. Shipp, M.A., N.E. Richardson, P.H. Sayre, N.R. Brown, E.L. Masteller, L.K. Clayton, J. Ritz, and E.L. Reinherz. 1988. Molecular cloning of the common acute lymphoblastic leukemia antigen (CALLA) identifies a type II integral membrane protein. *Proc. Natl. Acad. Sci. USA* 85:4819-4823.
20. Willerson, J.T., J.T. Watson, I. Hutton, G.H. Templeton, and D.E. Fixel. 1975. Reduced myocardial reflow and increased coronary vascular resistance following prolonged myocardial ischemia in the dog. *Circ. Res.* 36:771-781.
21. Ku, D.D. 1982. Coronary vascular reactivity after acute myocardial ischemia. *Science (Wash. DC)* 218:576-578.
22. VanBenthuyzen, K.M., I.F. McMurtry, and L.D. Horwitz. 1987. Reperfusion after acute coronary occlusion in dogs impairs endothelium-dependent relaxation to acetylcholine and augments contractile reactivity in vitro. *J. Clin. Invest.* 79:265-274.
23. Tsao, P.S., N. Aoki, D.J. Lefer, G. Johnson, and A.M. Lefer. 1990. Time course of endothelial dysfunction and myocardial ischemia and reperfusion in the cat. *Circulation* 82:1402-1412.
24. Lefer, A.M., P.S. Tsao, D.J. Lefer, and X. Ma. 1991. Role of endothelial dysfunction in the pathogenesis of reperfusion injury after myocardial ischemia. *FASEB J.* 5:2029-2034.
25. Mehta, J., J. Dinerman, P. Mehta, T.G.P. Saldeen, D. Lawson, W.H. Donnelly, and R. Wallin. 1989. Neutrophil function in ischemic heart disease. *Circulation* 79:549-556.
26. Servi, S.D., A. Mazzone, G. Ricevuti, A. Fioravanti, E. Bramucci, L. Angoli, G. Stefano, and G. Specchia. 1990. Granulocyte activation after coronary angioplasty in humans. *Circulation* 82:140-146.
27. Inauen, W., D.N. Granger, C.J. Meininger, M.E. Schelling, H.J. Granger, and P.R. Kvietys. 1990. Anoxia-reoxygenation-induced, neutrophil-mediated endothelial cell injury: role of elastase. *Am. J. Physiol.* 259:H925-H931.
28. Harlan, J.M., P.D. Killen, L.A. Harker, and G.E. Striker. 1981. Neutrophil-mediated endothelial injury in vitro. Mechanisms of cell detachment. *J. Clin. Invest.* 68:1394-1403.
29. Roques, B.P., F. Noble, V. Dauge, M.C. Fournie-Zalunski, and A. Beaumont. 1993. Neutral endopeptidase 24.11: structure, inhibition, and experimental and clinical pharmacology. *Pharmacol. Rev.* 45:87-146.
30. Hudgin, R.L., S.E. Charleson, M. Zimmermann, R. Mumford, and P.L. Wood. 1981. Enkephalinase: selective peptide inhibitors. *Life Sci.* 29:2593-2601.
31. Danilewicz, J.C., P.L. Barclay, I.T. Barnish, D. Brown, S.F. Campbell, K. James, G.M.R. Samuels, N.K. Terrett, and M.J. Wythes. 1989. UK-69,578, a novel inhibitor of EC 3.4.24.11 which increases endogenous ANF levels and is natriuretic and diuretic. *Biochem. Biophys. Res. Commun.* 164:58-65.
32. Sugiyama, S., K. Kugiyama, M. Ohgushi, K. Fujimoto, and H. Yasue. 1994. Lysophosphatidylcholine in oxidized low-density lipoprotein increases endothelial susceptibility to polymorphonuclear leukocyte-induced endothelial dysfunction in porcine coronary arteries. Role of protein kinase C. *Circ. Res.* 74:565-575.
33. Kawabata, K., M. Suzuki, M. Sugitani, K. Imaki, M. Toda, and T. Miyamoto. 1991. ONO-5046, a novel inhibitor of human neutrophil elastase. *Biochem. Biophys. Res. Commun.* 177:814-820.
34. Kugiyama, K., T. Sakamoto, I. Misumi, S. Sugiyama, M. Ohgushi, H. Ogawa, M. Horiguchi, and H. Yasue. 1994. Transferable lipids in oxidized low-density lipoprotein stimulate plasminogen activator inhibitor-1 and inhibit tissue-type plasminogen activator release from endothelial cells. *Circ. Res.* 73: 335-343.
35. Sugama, Y., C. Tiruppathi, K. Janakidevi, T.T. Andersen, J.W. Fenton II, and A.B. Malik. 1992. Thrombin-induced expression of endothelial P-selectin and intercellular adhesion molecule-1: a mechanism for stabilizing neutrophil adhesion. *J. Cell Biol.* 119:935-944.
36. Zimmerman, B.J., D.C. Anderson, and D.N. Granger. 1992. Neuropeptides promote neutrophil adherence to endothelial cell monolayers. *Am. J.*

Physiol. 263:G678-G682.

37. Hughes, H., B. Mathews, M.L. Lenz, and J.R. Guyton. 1994. Cytotoxicity of oxidized LDL to porcine aortic smooth muscle cells is associated with the oxysterols 7-ketocholesterol and 7-hydroxycholesterol. *Arterioscler. Thromb.* 14:1177-1185.
38. Moldow, C.F., and H.S. Jacob. 1984. Endothelial culture, neutrophil or enzymic generation of free radicals: in vitro methods for the study of endothelial injury. *Methods Enzymol.* 105:378-385.
39. Vijayaraghavan, J., A.G. Scicli, O.A. Carretero, C. Slaughter, C. Moomaw, and L.B. Hersh. 1990. The hydrolysis of endothelins by neutral endopeptidase 24.11 (enkephalinase). *J. Biol. Chem.* 265:14150-14155.
40. Gros, C., A. Souque, J.C. Schwartz, J. Duchier, A. Cournot, P. Baumer, and J.M. Lecomte. 1989. Protection of atrial natriuretic factor against degradation: diuretic and natriuretic responses after in vivo inhibition of enkephalinase (EC 3.4.24.11) by acetorphan. *Proc. Natl. Acad. Sci. USA.* 86:7580-7584.
41. Richter, J., I. Olsson, and T. Andersson. 1990. Correlation between spontaneous oscillations of cytosolic free Ca^{2+} and tumor necrosis factor-induced degranulation in adherent human neutrophils. *J. Biol. Chem.* 265:14358-14363.
42. Laudanna, C., G. Constantin, P. Baron, E. Scarpini, G. Scarlato, G. Cabrini, C. Dechecchi, F. Rossi, M.A. Cassatella, and G. Berton. 1993. Sulfatides trigger increase of cytosolic free calcium and enhanced expression of tumor necrosis factor- α and interleukin-8 mRNA in human neutrophils. *J. Biol. Chem.* 269:4021-4026.
43. Jaconi, M.E.E., R.W. Rivest, W. Schlegel, C.B. Wölheim, D. Pittet, and P.D. Lew. 1988. Spontaneous and chemoattractant-induced oscillations of cytosolic free calcium in single adherent human neutrophils. *J. Biol. Chem.* 263:10557-10560.
44. Grynkiewicz, G., M. Poenie, and R. Y.Tsien. 1985. A new generation of Ca^{2+} indicators with greatly improved fluorescence properties. *J. Biol. Chem.* 260:3440-3450.
45. Buerke, M., A.S. Weyrich, Z. Zheng, F.C.A. Gaele, M.J. Forrest, and A.M. Lefer. 1994. Sialyl lewis^x-containing oligosaccharide attenuates myocardial reperfusion injury in cats. *J. Clin. Invest.* 93:1140-1148.
46. Ma, X.-L., D.J. Lefer, A.M. Lefer, Baron, and R. Rothlein. 1992. Coronary endothelial and cardiac protective effects of a monoclonal antibody to intercellular adhesion molecule-1 in myocardial ischemia and reperfusion. *Circulation.* 86:937-946.
47. Bradley, P.P., D.A. Priebe, R.D. Christensen, and G. Rothstein. 1982. Measurement of cutaneous inflammation: estimation of neutrophil content with an enzyme marker. *J. Invest. Dermatol.* 78:206-209.
48. Lum, H., L. Gibbs, L. Lai, and A.B. Malik. 1994. CD18 integrin-dependent endothelial injury: effects of opsonized zymosan and phorbol ester activation. *J. Leukocyte Biol.* 55:58-63.
49. Woodman, R.C., P.H. Reinhardt, S. Kanwar, F.L. Johnston, and P. Kubes. 1993. Effects of human neutrophil elastase (HNE) on neutrophil function in vitro and in inflamed microvessels. *Blood.* 82:2188-2195.
50. Morishita, Y., T. Sano, K. Ando, Y. Saitoh, H. Kase, K. Yamada, and Y. Matsuda. 1991. Microbial polysaccharide, HS-142-I, competitively and selectively inhibits and binding to its guanylyl cyclase-containing receptor. *Biochem. Biophys. Res. Commun.* 176:949-957.
51. Park, K.H., and R. Levi. 1994. Hypoxic coronary vasodilatation and cGMP overproduction and blocked by a nitric oxide synthase inhibitor, but not by a guanylyl cyclase ANF receptor antagonist. *Eur. J. Pharmacol.* 256:99-102.
52. Appel, R.G., G.R. Dubyak, and M.J. Dunn. 1987. Effect of atrial natriuretic factor on cytosolic free calcium in rat glomerular mesangial cells. *FEBS Lett.* 224:396-400.
53. Rogers, J., R.G. Hughes, and E.K. Matthews. 1988. Cyclic GMP inhibits protein kinase C-mediated secretion in rat pancreatic acini. *J. Biol. Chem.* 263:3713-3719.
54. Schröder, H., P. Ney, I. Woditsch, and K. Schrör. 1990. Cyclic GMP mediates SIN-1-induced inhibition of human polymorphonuclear leukocytes. *Eur. J. Pharmacol.* 182:211-218.
55. Moilanen, E., P. Vuorinen, H. Kankaanranta, T. Metsä-Ketelä, and H. Vapaatalo. 1993. Inhibition by nitric oxide-donors of human polymorphonuclear leukocyte functions. *Br. J. Pharmacol.* 109:852-858.
56. Niu, X., C.W. Smith, and P. Kubes. 1994. Intracellular oxidative stress induced by nitric oxide synthesis inhibition increases endothelial cell adhesion to neutrophils. *Circ. Res.* 74:1133-1140.
57. Dewald, B.M., M. Thelen, and M. Baggiolini. 1988. Two transduction sequences are necessary for neutrophil activation by receptor agonist. *J. Biol. Chem.* 263:16179-16184.
58. Saito, Y., K. Nakao, K. Nishimura, A. Sugawara, K. Okumura, K. Obata, R. Sonoda, T. Ban, H. Yasue, and H. Imura. 1987. Clinical application of atrial natriuretic polypeptide in patients with congestive heart failure: beneficial effects on left ventricular function. *Circulation.* 76:115-124.
59. Yoshimura, M., H. Yasue, E. Morita, N. Sakano, M. Jougasaki, M. Kurose, M. Mukoyama, Y. Saito, K. Nakao, and H. Imura. 1991. Hemodynamic, renal, and hormonal responses to brain natriuretic peptide infusion in patients with congestive heart failure. *Circulation.* 84:1581-1588.
60. Okumura, K., H. Yasue, H. Fujii, K. Kugiyama, K. Matsuyama, M. Yoshimura, M. Jougasaki, K. Kikuta, H. Kato, H. Tanaka, H. Sumida, and K. Nakao. 1995. Effects of brain (B-type) natriuretic peptide on coronary artery diameter and coronary hemodynamic variables in humans: comparison with effects on systemic hemodynamic variables. *J. Am. Coll. Cardiol.* 25:342-348.
61. Münzel, T., S. Kurz, J. Holtz, R. Busse, H. Steinhilber, J. Hanjörg, and D. Helmut. 1992. Neurohormonal inhibition and hemodynamic unloading during prolonged inhibition of ANF degradation in patients with severe chronic heart failure. *Circulation.* 86:1089-1098.
62. Seymour, A.A., M.M. Asaad, V.M. Lanoce, S.A. Fennell, H.S. Cheung, and W.L. Rogers. 1993. Inhibition of neutral endopeptidase 3.4.24.11 in conscious dogs with pacing induced heart failure. *Cardiovasc. Res.* 27:1015-1023.
63. Wiedermann, C.J., M. Niedermühlbichler, and H. Braunsteiner. 1992. Priming of polymorphonuclear neutrophils by atrial natriuretic peptide in vitro. *J. Clin. Invest.* 89:1580-1586.
64. López Farré, A., A. Riesco, G. Espinosa, E. Digiuni, M.R. Cernadas, V. Alvarez, M. montón, F. Rivas, M.J. Gallego, J. Egido, S. Casado, and C. Caramelo. 1993. Effect of endothelin-1 on neutrophil adhesion to endothelial cells and perfused heart. *Circulation.* 88:1166-1171.
65. Skidgel, R.A., H.L. Jackman, and E.G. Erdős. 1991. Metabolism of substance P and bradykinin by human neutrophils. *Biochem. Pharmacol.* 41:1335-1344.
66. Engler, R.L., M.D. Dahlgren, M.A. Peterson, A. Dobbs, and W. Schmid-Schönbein. 1986. Accumulation of polymorphonuclear leukocytes during 3-h experimental myocardial ischemia. *Am. J. Physiol.* 251:H93-100.
67. Dreyer, W.J., L.H. Michael, T. Nguyen, C.W. Smith, D.C. Anderson, M.L. Entman, and R.D. Rossen. 1992. Kinetics of C5a release in cardiac lymph of dogs experiencing coronary artery ischemia-reperfusion injury. *Circ. Res.* 71:1518-1524.
68. Yasuda, M., K. Takeuchi, M. Hiruma, H. Iida, A. Tahara, H. Itagane, I. Toda, K. Akioka, M. Teragaki, H. Oku, Y. Kanayama, T. Takeda, W.P. Kolb, and J.D. Tamerius. 1990. The complement system in ischemic heart disease. *Circulation.* 81:156-163.
69. Werfel, T., G. Sonntag, M.H. Weber, and O. Götze. 1991. Rapid increases in the membrane expression of neutral endopeptidase (CD10), aminopeptidase N (CD13), tyrosine phosphatase (CD45), and Fc γ -RIII (CD16) upon stimulation of human peripheral leukocytes with human C5a. *J. Immunol.* 147:3909-3914.

CD4⁺ T-Lymphocytes Mediate Ischemia/Reperfusion-induced Inflammatory Responses in Mouse Liver

Ralf M. Zwacka,* Yulong Zhang,* Jeff Halldorson,** Howard Schlossberg,* Lorita Dudus,* and John F. Engelhardt*[†]

*Institute for Human Gene Therapy at the University of Pennsylvania Medical Center, Department of Molecular and Cellular Engineering, Philadelphia, Pennsylvania 19104; [†]Department of Surgery, University of Minnesota, Minneapolis, Minnesota 55455; and ^{**}Wistar Institute, Philadelphia, Pennsylvania

Abstract

The success of orthotopic liver transplantation is dependent on multiple factors including MHC tissue compatibility and ischemic/reperfusion injury. Ischemic/reperfusion (I/R) injury in the liver occurs in a biphasic pattern consisting of both acute phase (oxygen free radical mediated) and subacute phase (neutrophil-mediated) damage. Although numerous studies have given insights into the process of neutrophil recruitment after I/R injury to the liver, the exact mechanism that initiates this subacute response remains undefined. Using a T cell-deficient mouse model, we present data that suggests that T-lymphocytes are key mediators of subacute neutrophil inflammatory responses in the liver after ischemia and reperfusion. To this end, using a partial lobar liver ischemia model, we compared the extent of reperfusion injury between immune competent BALB/c and athymic nu/nu mice. Studies evaluating the extent of liver damage as measured by serum transaminases (GPT) demonstrate similar acute (3–6 h) post-I/R responses in these two mouse models. In contrast, the subacute phase (16–20 h) of liver injury, as measured by both serum GPT levels and percent hepatocellular necrosis, was dramatically reduced in T cell-deficient mice as compared with those with an intact immune system. This reduction in liver injury seen in nu/nu mice was associated with a 10-fold reduction in hepatic neutrophil infiltration. Adoptive transfer of T cell-enriched splenocytes from immune competent mice was capable of reconstituting the neutrophil-mediated subacute inflammatory response within T cell-deficient nu/nu mice. Furthermore, in vivo antibody depletion of CD4⁺ T-lymphocytes in immune competent mice resulted in a reduction of subacute phase injury and inflammation as measured by serum GPT levels and neutrophil infiltration. In contrast, depletion of CD8⁺ T-lymphocytes had no effect on these indexes of subacute inflammation. Kinetic analysis of T cell infiltration in the livers of BALB/c mice demonstrated a fivefold increase in the number of hepatic CD4⁺ T-lymphocytes within the first hour of reperfusion with no signifi-

cant change in the number of CD8⁺ T-lymphocytes. In summary, these results implicate CD4⁺ T-lymphocytes as key regulators in initiating I/R-induced inflammatory responses in the liver. Such findings have implications for therapy directed at the early events in this inflammatory cascade that may prove useful in liver transplantation. (*J. Clin. Invest.* 1997. 100:279–289.) Key words: ischemia • reperfusion • liver • T-lymphocytes • CD4

Introduction

Ischemia/reperfusion (I/R)¹-mediated injury has been studied in a number of clinically relevant diseases such as myocardial infarction, cerebrovascular diseases, and peripheral vascular diseases. With the advent of whole organ transplantation, research in the area of I/R injury has been extended to include the commonly transplanted organs kidney, liver, pancreas, and lung. In the liver, I/R injury has been demonstrated to occur in a biphasic pattern: an initial acute phase characterized by hepatocellular damage at 3–6 h and a subacute phase characterized by massive neutrophil infiltration at 18–24 h (1–6). The essential role of neutrophils in the inflammatory phase is supported by studies that demonstrate beneficial effects of neutrophil depletion using CD11b/CD18 monoclonal antibodies (2, 7, 8). These studies also support the notion that neutrophil recruitment and/or endothelial damage may also play an important role in perpetuating hepatic injury after I/R. Although numerous studies have given insight into the process of leukocyte recruitment after I/R injury in the liver, the exact mechanisms that initiate this response remain undefined.

The recruitment of neutrophils after reperfusion likely results from a complex series of ischemia-induced cellular changes in the liver and vasculature that serve to alter the adherent characteristics of neutrophils. Many ischemia-induced changes have been hypothesized to play a role in neutrophil recruitment and the perpetuation of I/R injury including: (a) the release of chemoattractants (such as oxygen free radicals) from ischemically damaged endothelium or hepatocytes (9, 10), (b) Kupffer cell and/or hepatocyte-derived production of inflammatory mediators such as TNF (11, 12), IL-1 (13, 14), and platelet-activating factor (15), (c) cellular changes in microvascular expression of surface antigens such as intercellular adhesion molecule (ICAM) and MHC class II (16), (d) vascular-associated damage creating a “no-reflow” phenomena that may trap neutrophils and further produce a second wave of ischemia (17), and/or (e) the release of superoxides by activated neutrophils that serve to perpetuate chemoattraction of in-

Address correspondence to John F. Engelhardt, Institute for Human Gene Therapy, Department of Molecular and Cellular Engineering, University of Pennsylvania Medical Center, BRBI, Room 306, Philadelphia, Pennsylvania. Phone: 215-898-6638; FAX: 215-573-8590.

Received for publication 1 May 1996 and accepted in revised form 17 April 1997.

J. Clin. Invest.

© The American Society for Clinical Investigation, Inc.
0021-9738/97/07/0279/11 \$2.00

Volume 100, Number 2, July 1997, 279–289

1. Abbreviations used in this paper: I/R, ischemia/reperfusion; ICAM, intercellular adhesion molecule; Tc, T-cytotoxic; Th, T-helper.

flammatory cell types (9, 10). Numerous studies suggest that oxygen free radical formation after reoxygenation of the liver may initiate the cascade of hepatocellular injury, necrosis, and subsequent inflammatory infiltration (17–20). For example, studies aimed at reducing reactive oxygen species after I/R injury, with xanthine oxidase inhibitor allopurinol and exogenous free radical scavengers such as SOD and catalase, have demonstrated beneficial effect (21–25). However, the source and mechanism of these free radicals remains controversial and may involve Kupffer cells, hepatocytes, extracellular xanthine oxidase in the acute phase, and neutrophils at the inflammatory stage (26–29).

The ambiguity in the field as to the mechanisms of I/R-induced liver injury results from a lack of understanding of the pathophysiologically relevant primary inciting events that lead to the subacute inflammatory responses and the ultimate decline of liver function. T-lymphocytes have been demonstrated to be key cellular mediators of granulocytic inflammatory responses through several secreted cytokines including TNF α , IFN γ , IL-4, and GM-CSF (30). These cytokines regulate proliferation, accumulation, and attraction of granulocytes to the site of injury. T cells are divided into three categories including T-helper (Th), T-cytotoxic (Tc), and T-suppressor (Ts) cells. Th cells are in turn subdivided into two categories based on their functional pattern of secreted cytokines; Th1 cells secrete IL-2 and IFN γ , but relatively little IL-4 or IL-5, whereas Th2 cells secrete IL-4 and IL-5, but little IL-2 and IFN γ (30). To better define the mechanisms of leukocyte recruitment in the liver after I/R, we sought to investigate the involvement of T-lymphocytes in this recruitment process. We reasoned that by comparing I/R responses in the liver between nu/nu and syngeneic immune competent mice, we would be able to study those responses that are specifically due to T cell functions. To this end, we compared pathophysiologic endpoints of hepatocellular and immune responses after lobar-induced I/R injury in the liver between nu/nu and BALB/c mice. These studies implicate T cell lineages in the progression of acute I/R injury to subacute inflammatory stages of leukocyte recruitment.

Methods

Mouse model of lobar I/R injury. Two mouse models including BALB/c and nu/nu mice (Harlan Sprague-Dawley Inc., Indianapolis, IN) were evaluated for I/R injury responses in the liver. Male (25 g) mice were anesthetized with ketamine/xylazine and a laparotomy was performed to expose the liver. After surgical exposure of the liver, mice were injected with heparin (100 μ g/kg) to prevent clotting of blood at long time points of ischemia. The medial largest lobe of the liver was clamped at its base using a microaneurysm clamp followed by placement of the liver and clamp back into the peritoneal cavity for 3, 60, or 90 min. Sham surgeries were performed on anesthetized and heparinized animals for which the liver was not clamped. 3-min ischemic time points were performed to control for any nonspecific hepatocellular damage induced by clamping, which was unassociated with long periods of ischemia. All animals remained anesthetized for a total of 90 min to control for any effects of anesthesia. After surgically implemented ischemia, the abdominal wall was sutured with two layers and the animals were returned to their cages. A total of four serial 12–25 μ l retro-orbital bleeds were performed on each animal at various time points including 0, 3, 6, 12, 16, 20, and 36 h postreperfusion, and serum was collected immediately by centrifugation and stored on ice. Although the number of bleeds for any one animal was limited to four, all animals were bled at 0 h to obtain an accurate baseline. After

completion of the experiment, serum GPT levels were measured using a microkinetic assay (200 μ l total volume; Sigma Chemical Co., St. Louis, MO). Typically assays were performed with 6 μ l of serum for preischemic and 2 μ l for postischemic time points. Assays were based on a variation of Sigma Chemical Co. kits to accommodate the small volumes of serum in which the change in OD_{340nm} was assessed in a 96-well microtiter plate reader (Molecular Dynamics, Sunnyvale, CA). Serum standards were used to assess the linearity of the assay and to convert values to international units per liter GPT. In total, 6–10 animals were evaluated at each time point of ischemia, and enzyme assays were performed in duplicate. Livers were harvested after the 20- or 36-h bleeds and divided into ischemic and nonischemic lobes. All tissues were divided into regionally identical quadrants that were either frozen directly in ornithine carbamyl transferase or fixed in formalin. The extent of liver damage as indicated by hepatocellular necrosis was confirmed by blinded morphometric assessment in paraffin sections (4 μ m) using a Leica DMR image analysis system to determine the percent necrotic area in liver sections. In these studies, the area of necrosis was traced by computer-assisted morphometry and the percentage of necrosis calculated from the total micrometer² area of the tissue section. In total, four sections were analyzed for each ischemic lobe tissue sample ($n = 4$ independent animals for each experimental point). Nonischemic lobes, which demonstrated no significant necrosis, except for infrequent focal areas at the surface of the liver due to surgical manipulation, were not included in this analysis. All statistical comparisons were performed using the Student's t test with significance inferred by $P < 0.05$.

Purification of T cell-enriched populations from splenocytes. Mononuclear cell suspensions were generated from spleens of immune competent BALB/c mice. Freshly isolated spleens were placed in complete RPMI (Hepes) media containing 10% FCS and cells removed by blunt dissection and scraping through a metal mesh. Cell aggregates were further separated by filtration through a 200- μ m mesh nylon screen. Splenic cells were collected by centrifugation and the red blood cells were removed by hypertonic lysis in NH₄Cl for 5 min (31). Mononuclear cells were harvested by centrifugation and washed three times in 10% FCS containing media. T cell enrichment was performed using nylon wool column chromatography as previously described (31). Briefly, sterile nylon wool (Fisher Scientific Co., Santa Clara, CA) packed columns were equilibrated in complete RPMI media and mononuclear cell fractions incubated on the column for 1 h at 37°C in 5% CO₂. Nonadherent cells (predominately T cells) were then eluted in 15 ml complete media and collected by centrifugation. The percentages of CD4⁺ and CD8⁺ T cells were assessed in nylon wool T cell-enriched fractions by flow cytometry. In these studies, 5×10^5 cells from the nylon wool column were washed once with 5% FCS/PBS and resuspended in the same buffer containing 1 μ g of PE anti-mouse CD4 and FITC anti-mouse CD8 antibodies (PharMingen, San Diego, CA) for 2 h at 4°C. Stained cells were washed three times in 5% FBS/PBS, analyzed by flow cytometry.

Adoptive transfer of T cells into nu/nu mice. T cell-enriched splenocyte fractions composed of > 80% T cells as indicated by CD4 and CD8 FACS[®] analysis (Becton Dickinson & Co., Mountain View, CA) were injected into nu/nu mice by subcapsular splenic injection 5 d before I/R experiments. Two experimental protocols were performed in which a total of either 2×10^5 or 2×10^6 cells resuspended in PBS were injected in each animal. Because the lower dose of T cells gave no experimental response, the data presented in this report represents only that from the higher dose ($n = 6$). All animals were subjected to 60 min of lobar ischemia followed by reperfusion. Blood was drawn at 0, 6, and 20 h post-I/R and analyzed for serum GPT levels. The extent of subacute I/R injury was assessed by comparing the extent of decline in serum GPT responses at 6 h to that at 20 h post-I/R.

Immunocytochemical localization of neutrophils and T cells. T cell localization studies were performed by immunofluorescent staining for CD4 and CD8 antigens in frozen (6- μ m) sections of the liver and spleen. In these studies, sections were fixed in 95% ethanol for 30 min, blocked in 20% mouse serum/PBS for 30 min, and then incubated in

1/200 dilution of rat FITC anti-mouse CD4 or rat FITC anti-mouse CD8 in the presence of 1.5% mouse serum/PBS for 18 h at 4°C. Sections were washed three times in 1.5% goat serum/PBS and coverslipped in Citifluor. These analyses were performed to assess the kinetics of T cell infiltration to the liver post-I/R and to confirm the success of T cell adoptive transfers. Kinetic T cell infiltration studies assessed ischemic lobes of livers from mice that underwent 90 min of ischemia and 1, 3, 6, 12, and 20 h of reperfusion (three independent animals were analyzed for each experimental group). Additionally, sham-operated animals were included in these analyses to assess baseline numbers of resident T-lymphocytes in the liver.

Immunofluorescent staining for neutrophils was performed on frozen sections fixed in 4% paraformaldehyde for 10 min, followed by postfixation in methanol for 10 min at -20°C. Sections were permeabilized with 0.1% Triton X-100 before blocking and incubation with a 1/500 dilution of rat anti-mouse neutrophil FITC antibody (CALTAG Labs, South San Francisco, CA). Morphometric analysis of immunoreactive neutrophils in liver sections were performed by quantifying the total numbers of immunoreactive cells in 30 random (400×) fields (five independent animals were analyzed for each experimental group). Localization of neutrophils in CD4 and CD8 T cell-depleted animals assessed 10 random fields (400×) of the ischemic liver lobes from five and three independent animals, respectively.

In vivo T cell depletion. Rat monoclonal antibodies against mouse CD4 and CD8 were generated by intraperitoneal injection of 10⁷ cells of the rat hybridoma lines GK 1.5 or 2.43, obtained from American Type Culture Collection (Rockville, MD) (32, 33), into female SCID mice. Ascites fluid was harvested and purified over an anti-rat IgG agarose (Sigma Chemical Co.) column. Positive fractions were identified by Bradford analysis and purity verified by SDS-PAGE. The positive fractions were then pooled, desalted, and concentrated into PBS using a Centricon-30 filtration system. Antibody concentrations were adjusted to 1 mg/ml. The mAb were then tested by flow cytometry analysis for antigen specificity by comparison with commercially available directly labeled anti-CD4 and -CD8 antibodies. In vivo depletion experiments were performed in 6-7-wk-old BALB/c mice by injection of 0.2 mg of affinity-purified anti-CD4 mAb (GK1.5) or anti-CD8 mAb (2.43) on two consecutive days. On day 4 after the second injection, the animals underwent 90 min of ischemia as described above and blood samples were taken at 0, 6, 12, and 20 h post-reperfusion for analysis of serum GPT. The animals were then killed and spleens from each mouse were tested for successful T cell depletion by flow cytometry analysis. In these studies, total splenocytes were isolated and purified as described above and 10⁶ cells stained with 1 µg of anti-CD8 FITC- and anti-CD4 PE-labeled antibodies in 50 µl PBS/10% FCS for 30 min on ice.

Results

Reduced subacute I/R injury response in livers from nu/nu mice. Results from both 60- and 90-min lobar liver I/R injury in both BALB/c and nu/nu mice demonstrate similar acute (3-6 h) increases (50-100-fold) in the level of serum GPT (Fig. 1, A and B) over preischemic time points. Conversely, 3-min ischemic animals showed minimal (threefold) transient increases in GPT at 3- and 6-h time points, which were likely due to nonspecific hepatocellular clamping damage. Sham-operated animals produced no detectable changes in serum transaminases, demonstrating that neither anesthesia nor serial blood draws affected these liver function enzymes. In contrast with the similar level of acute I/R-mediated liver injury seen in BALB/c and nu/nu mice, subacute (20-h) levels of serum GPT were dramatically different between these two strains. Serum GPT values of BALB/c animals that underwent 90 min ischemia demonstrated a biphasic pattern of liver injury that peaked at 6 and 20 h, representing early acute and subacute

damage, respectively. In comparison, nu/nu mice after 90 min of ischemia demonstrated a complete lack of subacute-mediated liver injury, suggesting that the inflammatory response after I/R injury in T cell-deficient mice was impaired (compare Fig. 1 A to B). Although the bimodal serum GPT phases of liver injury were not observed after 60 min of I/R, similar differences in the decline of serum GPT levels were seen during the later phases of I/R between nu/nu and BALB/c mice. At 36 h, the GPT activities for all animals returned to baseline. Morphometric analysis of the percentage of hepatocellular necrosis confirmed differences in the level of hepatic injury at 20 h post-reperfusion in BALB/c and nu/nu mice (Fig. 1, C-F). BALB/c animals subject to 60 and 90 min of ischemia demonstrated a twofold higher level of hepatocellular necrosis as compared with nu/nu mice ($P < 0.009$ and $P < 0.001$ for 60 and 90 min ischemia, respectively). In contrast, control animals subject to 3 min of ischemia demonstrated negligible levels of necrosis in both strains of mice. Differences in the extent of the bimodal serum GPT response between BALB/c animals, which had undergone 60- and 90-min of I/R injury, is likely due to differences in the extent of injury produced by these two times of ischemia and is reflected in the percent hepatocellular necrosis ($27 \pm 4.8\%$ for 60 min of ischemia vs. $62 \pm 9.0\%$ for 90 min) (Fig. 1 F). In summary, initial results comparing the time course and extent of I/R injury in the liver between nu/nu and BALB/c mice demonstrate similar patterns of acute I/R injury, but dramatic differences in the extent of subacute responses. Such findings suggest that the absence of T cells in nu/nu mice may be responsible for reduced subacute injury responses after I/R. To address this hypothesis, we attempted to reconstitute this subacute I/R response in nu/nu mice by adoptive transfer of T-lymphocytes harvested from BALB/c mice.

Adoptive transfer of T cells reconstitutes the subacute inflammatory response in nu/nu mice. Enriched populations of T cells were purified from BALB/c splenocytes using nylon wool chromatography. The extent of T cell enrichment was confirmed by flow cytometry after immunocytochemical staining with CD4 and CD8 antibodies (Fig. 2 A). These results demonstrated an 80% T cell content within glass wool-purified splenocytes. Within these T cell populations, ~25 and 55% were positive for CD8 and CD4, respectively. Adoptive transfer into nu/nu mice was performed by injection of 2×10^6 enriched T cells directly into the subcapsular region of the spleen. The successful engraftment of T cells was evaluated by immunocytochemical staining of spleens (Fig. 2) for both CD4 and CD8 antigens (epitopes that are normally absent in nu/nu mice). In these studies, nu/nu animals demonstrated no detectable CD4 and CD8 T cells within the spleen (Fig. 2, E and F) as compared with control BALB/c mice (Fig. 2, C and D). In contrast, nu/nu mice injected with enriched T-lymphocyte populations (Fig. 2, G and H) demonstrated high levels of CD4 and CD8 immunoreactive cells in the spleen. These results confirm the successful reconstitution of T-lymphocytes over the time course of these experiments.

The profile of serum GPT levels was quantified in animals after 60 min I/R in an attempt to evaluate whether adoptively transferred T cells were capable of reconstituting the subacute injury response. Results from these studies demonstrated a fourfold increase in 20-h GPT levels ($P < 0.001$) within T cell adoptively transferred nu/nu mice ($2,029 \pm 317$ U/liter) as compared with uninjected nu/nu animals (499 ± 83 U/liter). In nu/nu mice that received T cells, the extent of the subacute injury

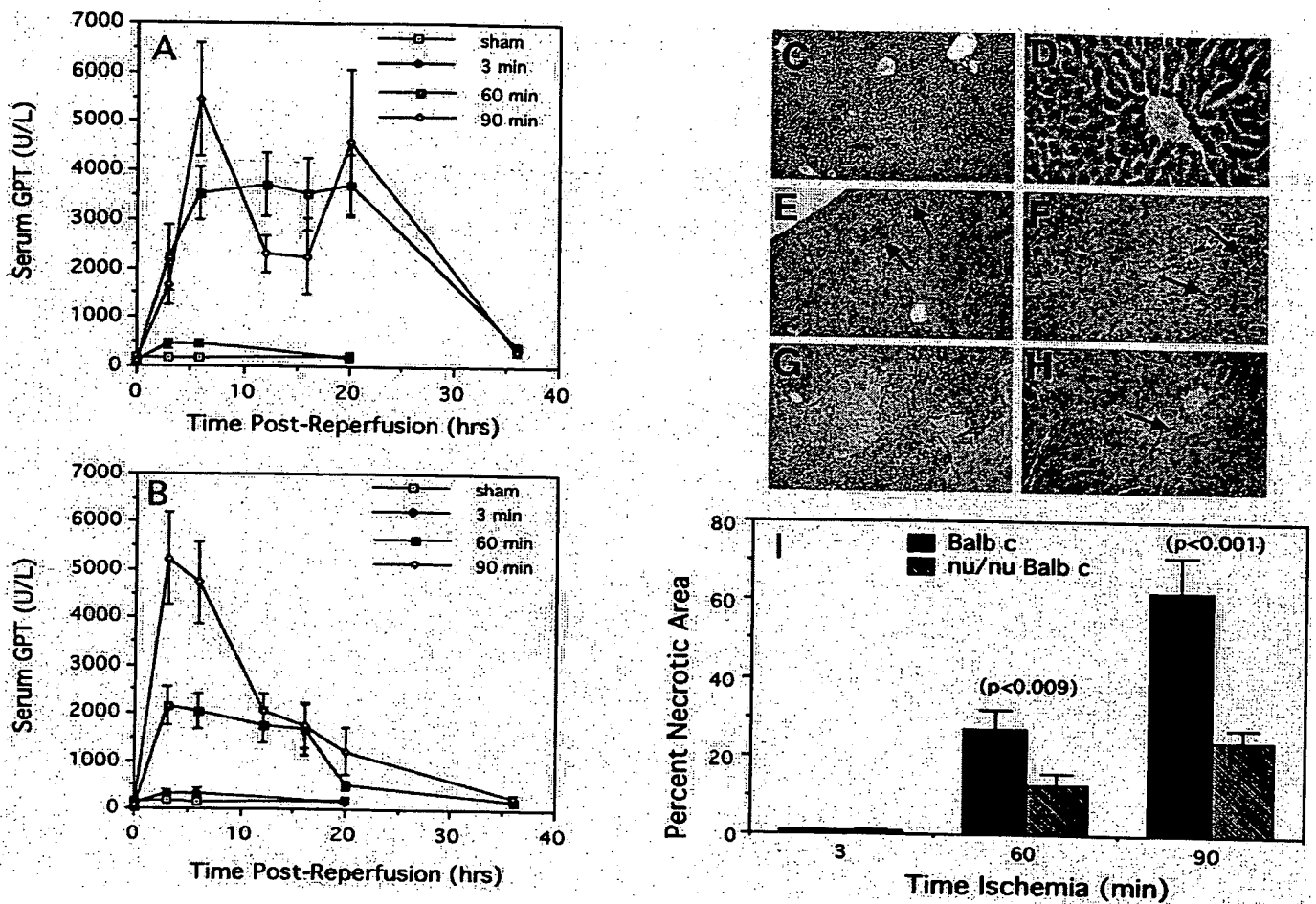


Figure 1. Differences in I/R-induced liver damage in BALB/c and nu/nu mice. BALB/c (A) and nu/nu (B) mice were subject to lobar ischemia for 3, 60, and 90 min, followed by reperfusion for a total of 20–36 h. Sham animals for which surgery was performed without ischemia were included as additional controls. Blood samples from animals were analyzed for serum GPT levels at 0, 3, 6, 12, 16, 20, and 36 h postreperfusion. For any one animal, only four serial blood draws were performed in an effort to assure minimal changes in blood volume. In 60- and 90-min ischemia experiments, the total number of independent animals for each time point were as follows: 0 ($n = 15$), 3 ($n = 6$), 6 ($n = 10$), 12 ($n = 9$), 16 ($n = 9$), 20 ($n = 10$), and 36 ($n = 6$) h. For all sham and 3-min ischemia experiments, the total number of animals for each time point presented was $n = 6$. A (BALB/c) and B (nu/nu) represent the mean \pm SEM of serum GPT values of pooled data for each group. Ischemic and nonischemic lobes were harvested for morphologic analysis of the percent hepatocellular necrosis in paraffin sections. Photomicrographs from sections of 3-min (C and D) and 60-min (E and F) BALB/c ischemic lobes are compared with ischemic lobes from nu/nu mice after 60 min of ischemia (G and H). All livers were harvested at 20 h postreperfusion for evaluation of percent hepatocellular necrosis. Panels on the left and right were taken with 4 \times and 40 \times objectives, respectively. Dashed lines outline the boundaries of necrosis while arrows point to inflammatory infiltrate. The mean percent area \pm SEM of hepatocellular necrosis is shown in I for ischemic lobes ($n = 4$ independent animals for each experimental point). Percent hepatocellular necrosis was significantly higher in BALB/c animals subject to both 60 (Student's t test, $P < 0.009$) and 90 (Student's t test, $P < 0.001$) min of ischemia as compared with nu/nu animals. No significant differences were seen in the percent necrosis between BALB/c and nu/nu livers subject to 3 min of ischemia. Nonischemic lobes did not demonstrate necrosis at any of the time points of ischemia (data not shown).

was increased to a level $\sim 50\%$ that seen in BALB/c mice ($3,704 \pm 625$ U/liter). Fig. 2B represents the cumulative data from these experiments, which compared the peak acute (6 h) GPT levels with peak subacute (20 h) serum GPT levels. Studies evaluating T cell recruitment to the liver after I/R injury in adoptive transfer experiments provided additional evidence supporting the importance of T cells in subacute phase liver damage. Nu/nu mice adoptively transferred with purified splenic T cell populations demonstrated T cell infiltration into the liver after I/R. In all cases, T cell infiltration was confined to the ischemic lobes of the liver and absent in control nonis-

chemic lobes (data not shown). These findings demonstrate that the elevated levels of CD4 $^{+}$ T cells in the livers of adoptively transferred nu/nu mice were not due to a nonspecific global increase in resident T cell in the liver, but rather a specific response to I/R injury. As seen with BALB/c mice, no significant infiltration of CD8 $^{+}$ T cells were seen in nu/nu mice adoptively transferred with purified splenic T cell populations (data not shown).

In summary, these findings demonstrate that adoptively transferred T cells were capable of reconstituting the subacute I/R injury response in nu/nu mice and suggested that T cells

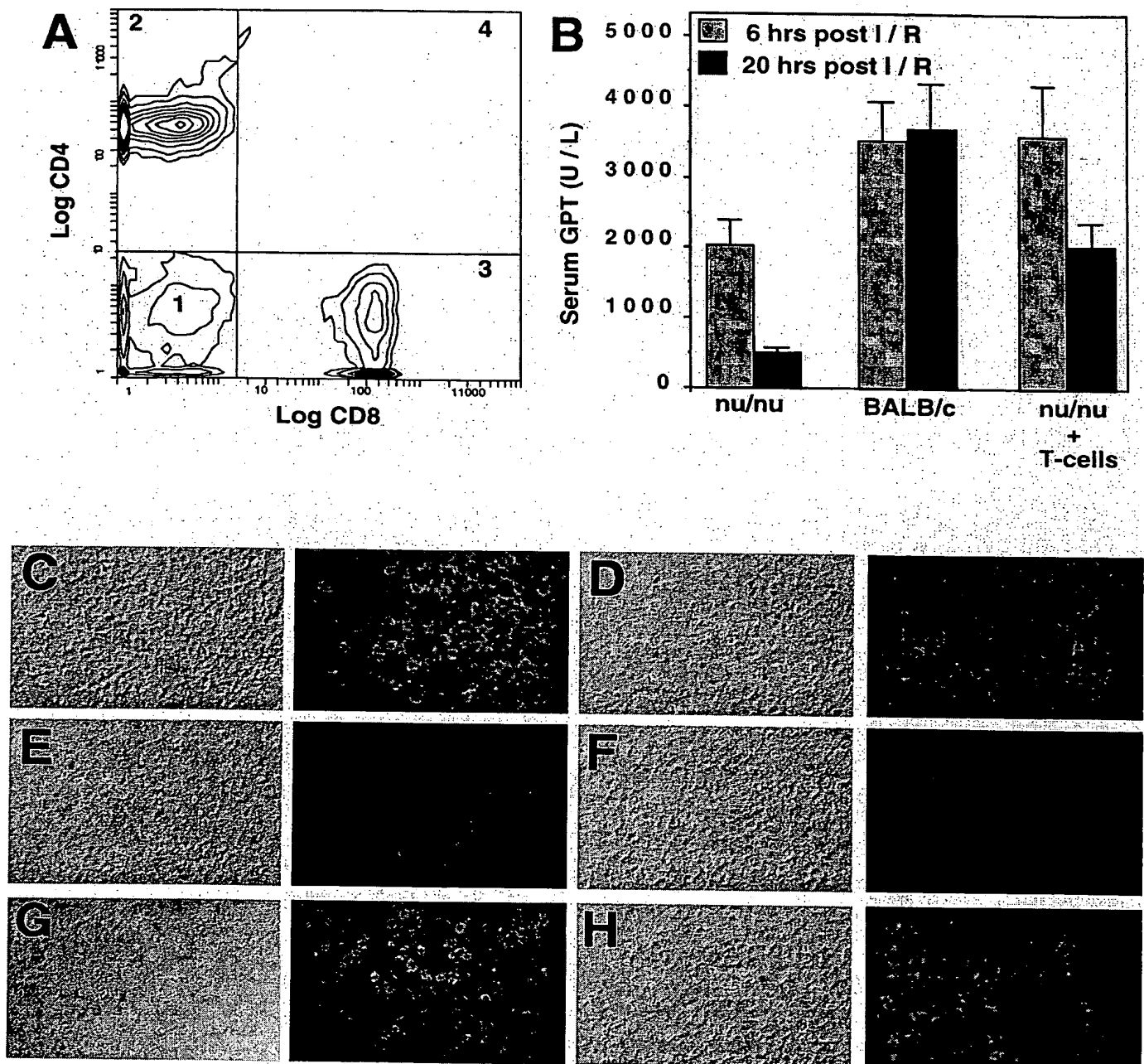


Figure 2. Adoptive transfer of T-lymphocytes into nu/nu mice. Enriched populations of T-lymphocytes were isolated from spleens of BALB/c mice by nylon wool chromatography and analyzed by flow cytometry after immunocytochemical staining with anti-mouse CD4 and CD8 antibodies (A). Results from FACS[®] analysis demonstrate an enrichment to > 80% T cells. Within these T cell fractions, ~ 25% (quadrant 3) and 55% (quadrant 2) of the splenocytes were positive for CD8 and CD4, respectively. 2×10^6 T-lymphocytes were injected into the splenic subcapsular space of recipient nu/nu mice ($n = 6$ for each experimental group). 5 d posttransfer, mice were subject to 60 min of partial lobar ischemia followed by 20 h of reperfusion. B compares serum GPT levels observed during the peak acute (6 h) and subacute (20 h) phases of post-I/R injury between nu/nu, Balb/c, and nu/nu T cell-transplanted mice. Spleens were harvested at 20 h postreperfusion to determine the efficiency of adoptive transfer by immunocytochemical analysis with CD4 and CD8 antibodies. Immunocytochemical staining of spleen-frozen sections (6 μ m) with anti-mouse CD8 FITC (C, E, and G)– and anti-mouse CD4 FITC (D, F, and H)–labeled antibodies was performed on BALB/c mice (C and D), nu/nu mice, which were uninjected (E and F), or nu/nu mice injected with T cell populations into the spleen (G and H). BALB/c and nu/nu mice serve as positive and negative controls for CD4 and CD8 staining, respectively. All panels represent photomicrographs taken with a 20 \times objective. Nomarski and fluorescent photomicrographs are shown on the left and right of each panel, respectively.

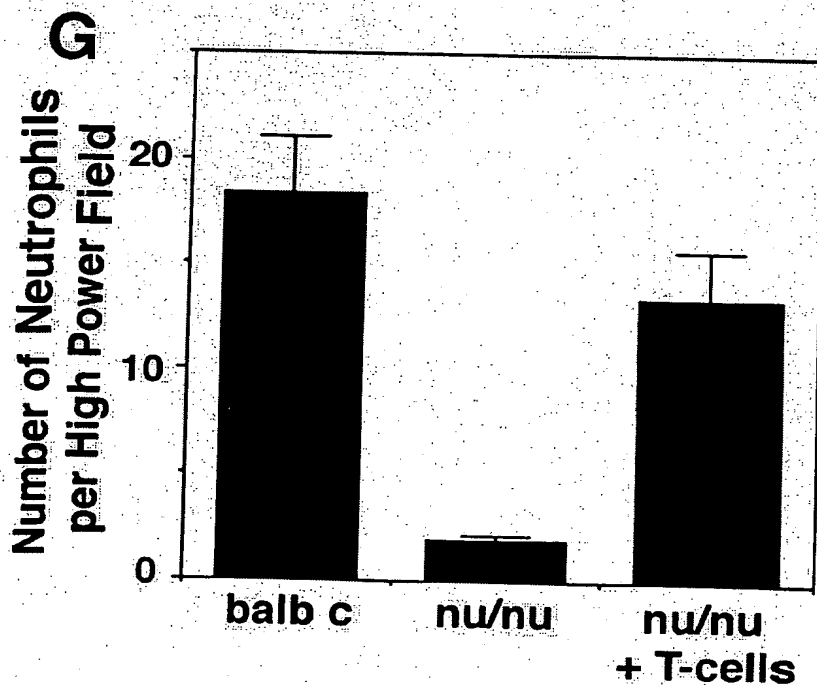
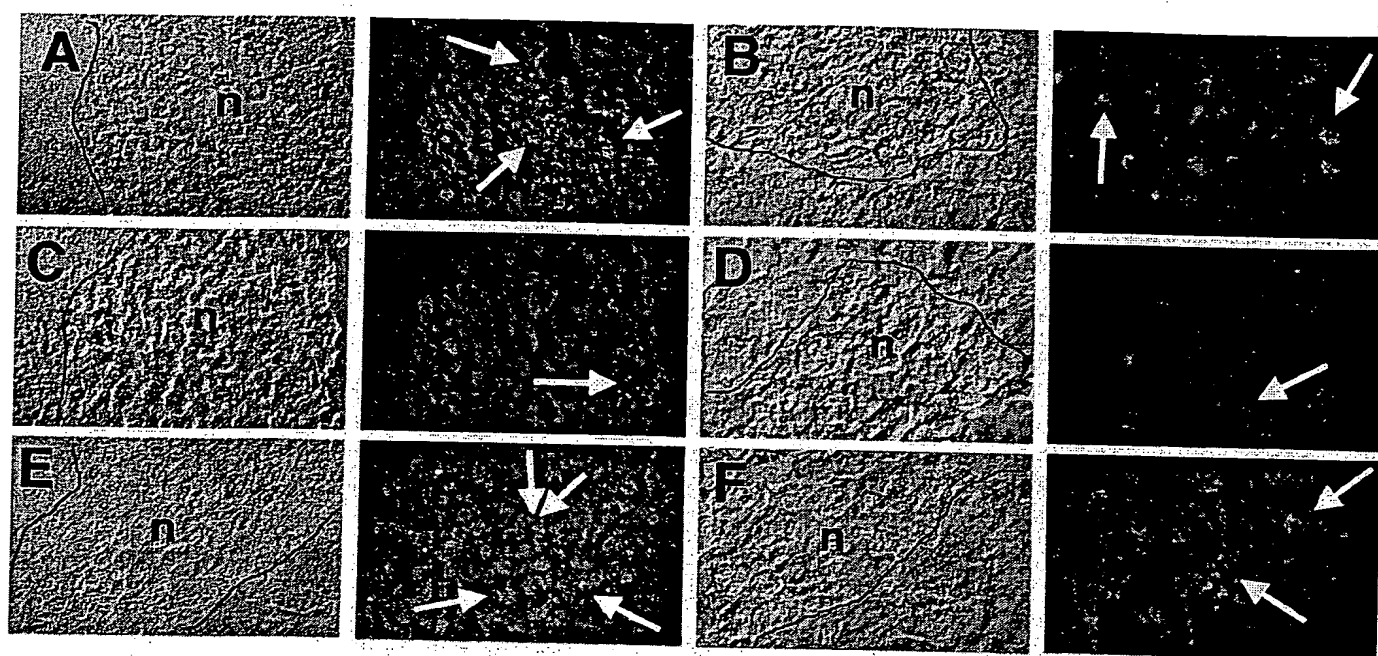


Figure 3. Immunocytochemical localization of neutrophils within T cell-defined animal models of I/R in the liver. Frozen sections (6 μ m) of ischemic livers were immunocytochemically stained for neutrophils using an anti-mouse neutrophil FITC-labeled antibody. Three experimental groups were compared for the extent of neutrophil infiltration within 60-min ischemic lobes at 20 h of reperfusion (peak neutrophil response). Immunoreactive cells were quantified from 30 fields within necrotic regions of ischemic lobes ($n = 5$ independent animals for each group). Nonischemic lobes were also analyzed but did not demonstrate detectable neutrophil infiltration (data not shown). Representative immunofluorescent photomicrographs are shown for ischemic lobes from BALB/c (A and B), nu/nu (C and D), and T cell-transplanted nu/nu mice (E and F). Nomarski and fluorescent photomicrographs are shown on the left and right of each panel, respectively. A, C, and E represent photomicrographs taken with a 10 \times objective, while B, D, and F were taken at higher magnification with a 40 \times objective. Lines within the Nomarski photomicrographs mark the boundaries of necrotic regions that demonstrate a red/orange autofluorescence using this Texas red/FITC filter cube. Arrows mark immunoreactive neutrophils with green FITC fluorescence. A summary of the quantitative analysis is depicted in G that gives the mean \pm SEM number of immunoreactive neutrophils per high power field (40 \times). The number of neutrophils in the ischemic liver lobes were significantly reduced in nu/nu mice as compared with BALB/c or nu/nu T cell transplanted mice (Student's t test, $P < 0.001$).

may be critical mediators in this phase of injury, which has been traditionally characterized as a neutrophil-mediated inflammatory response. To this end, we sought to correlate the requirement of T cells necessary for subacute phase I/R injury with the extent of neutrophil infiltration.

T cells mediate neutrophil recruitment after ischemia/reperfusion in the liver. Subacute injury after I/R has been traditionally characterized by massive neutrophil-mediated inflammatory responses. Numerous hypotheses have proposed mechanisms by which ischemic injury in the liver may mediate neutrophil recruitment, including hepatocellular cytokine production and local changes in the adherence characteristic of endothelium in the liver. Initial comparisons of I/R histopathology between nu/nu and BALB/c mice shown in Fig. 1, E-H have suggested that neutrophil recruitment may be impaired in T cell-deficient mice. These findings, together with the requirement for T cells to elicit I/R subacute liver injury, have

suggested that T-lymphocytes may be key mediators of this response. To this end, we sought to correlate differences in the level of subacute injury with the extent of the subacute neutrophil inflammatory response in nu/nu and BALB/c mice. Furthermore, by comparing nu/nu with BALB/c and T cell-reconstituted nu/nu mice, we sought to mechanistically confirm T cell involvement with the activation of neutrophil infiltration.

Immunocytochemical localization using a pan antineutrophil antibody was performed on five to six animals from each experimental category that had undergone 60 min of ischemia followed by 20 h of reperfusion. This time point was chosen for analysis since subacute liver injury peaks during this time frame. Morphometric studies quantifying the extent of neutrophil infiltration in the liver demonstrated a mean number of 18.4 ± 2.6 immunoreactive neutrophils per high power field in necrotic regions of BALB/c ischemic lobes (Fig. 3, A and B). Only infrequent immunoreactive cells were seen in nonne-

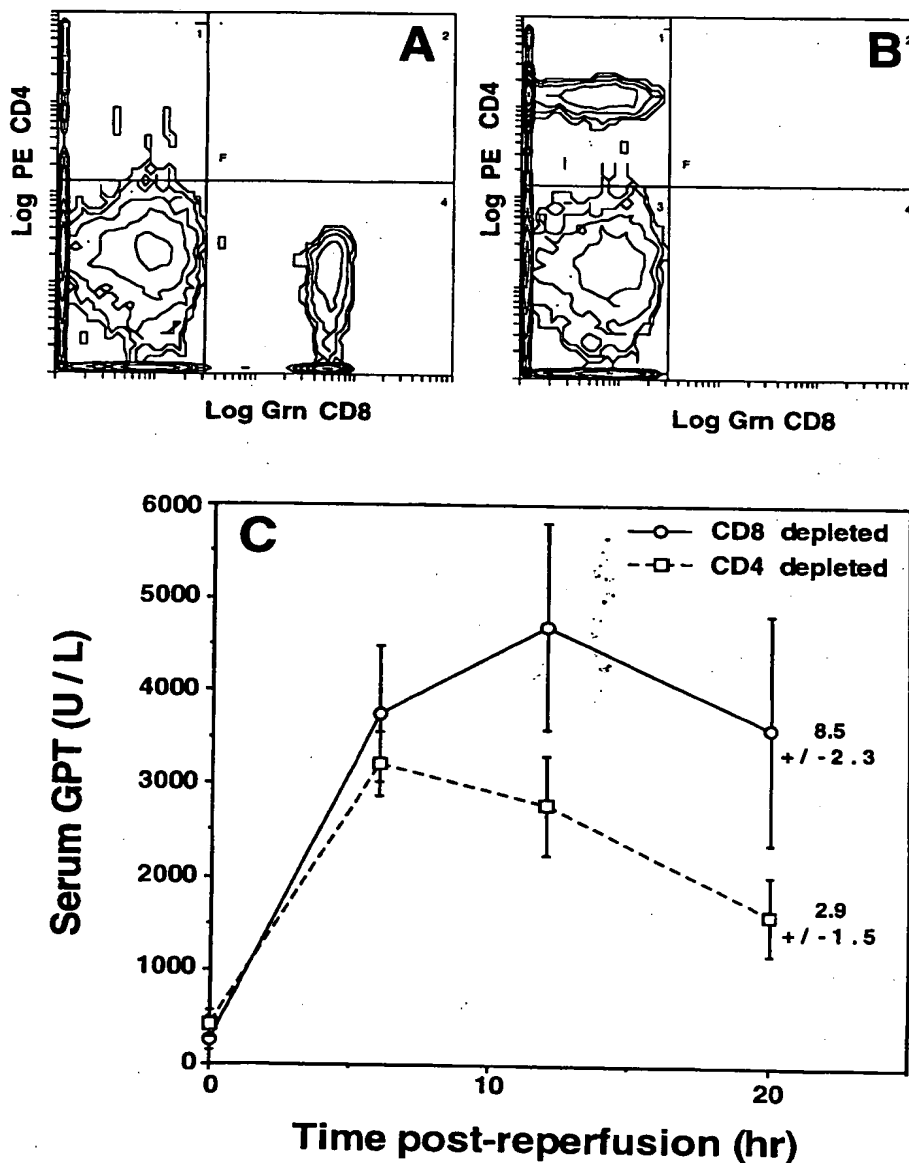


Figure 4. Modulation of I/R injury responses after in vivo depletion of CD4⁺ and CD8⁺ T-lymphocytes in BALB/c mice. 6–7-wk-old BALB/c mice were depleted of CD4⁺ ($n = 7$) or CD8⁺ ($n = 4$) T-lymphocytes by injection of affinity-purified anti-CD4 or anti-CD8 mAb on two consecutive days. 4 d after the second injection, animals underwent 90 min of partial lobar ischemia and blood samples were taken at 0, 6, 12, and 20 h postreperfusion for analysis of serum GPT. Animals were killed at 20 h post-I/R and the spleens from each mouse were tested for successful T cell depletion by FACS[®] analysis against anti-CD8 FITC- and anti-CD4 PE-labeled antibodies. The antibodies used for FACS[®] analysis recognized different epitopes from those used for in vivo depletion. FACS[®] analysis of splenocytes from CD4- (A) and CD8- (B) depleted animals are shown. The mean \pm SEM serum GPT profile for both CD4- (dashed line) and CD8- (solid line) depleted mice are given in C. GPT levels were significantly lower in CD4- as compared with CD8-depleted animals at both 12 and 20 h of reperfusion (Student's *t* test, $P < 0.05$). The mean \pm SEM number of neutrophils per 40 \times field within ischemic lobes at 20 h postreperfusion are given for both CD4- and CD8-depleted animals (shown to the right of 20-h GPT experimental values). These data demonstrate a statistically significant decrease in the number of neutrophils within ischemic lobes of CD4- as compared with CD8-depleted animals (Student's *t* test, $P < 0.05$). Quantification of neutrophil numbers was performed by immunofluorescent detection as described in the Methods.

cretic regions of ischemic lobes, while neutrophils were absent from control nonischemic lobes (data not shown). In contrast with BALB/c animals, nu/nu mice demonstrated a 10-fold reduction (1.9 ± 0.3 cells/field, $P < 0.001$) in the number of neutrophils within necrotic regions of ischemic lobes (Fig. 3, C and D). Such findings suggest that the absence of T cells in nu/nu mice may be responsible for the reduced subacute neutrophil inflammatory response seen at 20 h postreperfusion. To conclusively address this hypothesis, nu/nu mice that were adoptively transferred with an enriched population of splenic T cells were analyzed for neutrophil infiltration after I/R. T cell-transplanted mice subjected to 60 min of lobar ischemia followed by 20 h of reperfusion demonstrated a statistically significant ($P < 0.001$) sevenfold increase in the number of immunoreactive neutrophils within ischemic lobes (13.4 ± 2.3 cells/field) (Fig. 3, E and F). Control nonischemic lobes from these animals demonstrated an absence of neutrophils as similarly seen in nu/nu and BALB/c mice (data not shown), suggesting that adoptive transfer of T cells did not globally elevate circulating neutrophils in the liver, but rather specifically increased the neutrophil inflammatory response to I/R. Morphometric analysis of I/R-induced increases in the frequency of neutrophils seen in necrotic regions of the liver are summarized in Fig. 3 G. When the ratio of 20-h/6-h serum GPT levels (an index of subacute mediated injury) were grouped for all animals, including nu/nu, Balb/c, and nu/nu + T cells, and compared with the extent of neutrophil infiltration, a significant direct correlation ($r = 0.9$, $P < 0.001$ by the Spearman correlation) was observed in the frequency of neutrophil infiltration and the extent of subacute serum GPT levels. Such find-

ings substantiate the hypothesis that T-lymphocytes play a key role in the recruitment of neutrophils in subacute I/R injury.

Depletion of CD4⁺ but not CD8⁺ T cells decreases the subacute inflammatory response in BALB/c mice. To determine whether specific subsets of T cells were responsible for activating subacute inflammatory responses in the liver seen at 18–24 h after reperfusion, we selectively in vivo-depleted CD4⁺ and CD8⁺ T cells from BALB/c mice before I/R experiments. To this end, animals were injected intraperitoneally with depleting monoclonal antibodies derived from rat hybridomas directed against the CD4 or CD8 receptors. The extent of depletion was confirmed in all animals after I/R experiments by FACS[®] analysis of splenocytes with CD4 and CD8 antibodies that recognized alternative epitopes to antibodies used for depletion studies. All mice demonstrated > 95% depletion of immunoreactive CD4 or CD8 cells after depletion experiments (Fig. 4, A and B). CD4- and CD8-depleted animals were subjected to 90 min of partial lobar ischemia, and the extent of liver injury was monitored by measuring serum GPT values at 0, 6, 12, and 20 h. While there were no significant differences in baseline (0 h) and 6 h reperfusion GPT values among the different groups of animals, the GPT activities at 12 and 20 h were significantly lower ($P < 0.05$) in CD4-depleted mice as compared with the CD8-depleted group (Fig. 4 C). CD4-depleted animals demonstrated a similar pattern of GPT injury as seen in nu/nu (T cell-deficient) mice, while CD8-depleted animals more closely reproduced the pattern of injury seen in BALB/c (T cell-sufficient) mice. Furthermore, CD4-depleted BALB/c had significantly reduced ($P < 0.05$) numbers of neutrophils (2.9 ± 1.5 cells/field) as compared with CD8-depleted

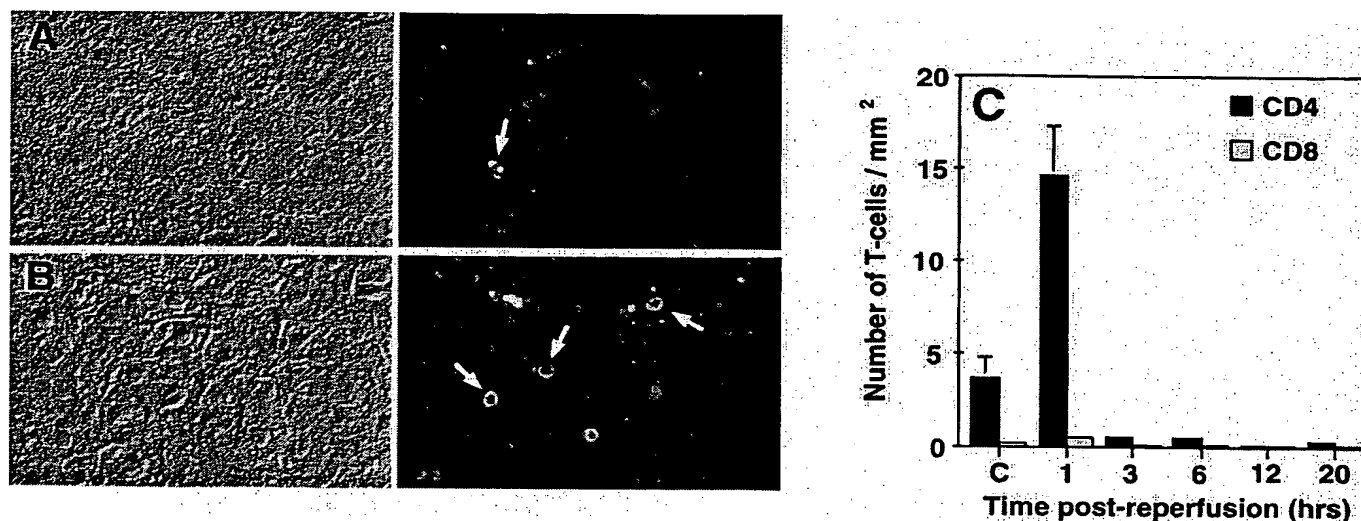


Figure 5. T-lymphocyte infiltration in the liver after I/R-induced injury. The kinetics of T-lymphocyte infiltration in the liver after 90 min of ischemia and 1, 3, 6, 12, and 20 h of reperfusion was examined by immunofluorescent staining using anti-mouse CD4 and CD8 FITC antibodies. The numbers of resident T cells were analyzed in nonischemic sham-operated control BALB/c mouse liver section from three independent mice. Total numbers of immunoreactive cells were quantitated in three nonserial sections of the ischemic lobes from three independent animals for each reperfusion time point. A is a representative image of a liver section taken from a control animal, while B represents an animal that underwent 90 min of ischemia and 1 h of reperfusion. Nomarski and fluorescent photomicrographs are shown on the left and right of each panel, respectively. All photomicrographs were taken with a 40 \times objective and arrows indicate immunoreactive CD4⁺ T-lymphocytes. C summarizes morphometric analysis quantifying the number of CD4⁺ and CD8⁺ T cells/mm² seen in control and 90-min ischemic livers that underwent 1, 3, 6, 12, and 20 h of reperfusion. Sham-operated control mice that were not subject to I/R injury are marked C. The number of immunoreactive CD4⁺ T cells within ischemic lobes increases fivefold after 1 h of reperfusion as compared with sham-operated animals (Student's *t* test, $P < 0.05$). No significant differences were seen in the extent of CD8⁺ T cell infiltration at any time points.

animals (8.5 ± 2.3 cells/field) within ischemic lobes at 20 h of reperfusion (Fig. 4 C). These results substantiate findings with adoptive transfer of T cells in nu/nu animals and provide more definitive evidence that CD4⁺ but not CD8⁺ T cell subsets are important mediators of inflammatory responses associated with subacute liver injury. To mechanistically determine when T cells may act to mediate the post-I/R subacute inflammatory response, we performed kinetic studies aimed at elucidating the time course of T-lymphocyte recruitment to the ischemic lobes of the liver after reperfusion.

Kinetics of T cell infiltration into the ischemic liver. To evaluate the temporal relationship of T cell recruitment within the inflammatory cascade after I/R in the liver, we followed the time course of T cell infiltration in postischemic and reperfused livers from BALB/c mice. To this end, we compared the number of CD4⁺ and CD8⁺ T cells in sham operated animals with mice that underwent 90 min of ischemia and 1, 3, 6, 12, and 20 h of reperfusion. Results depicted in Fig. 5, A and B demonstrate maximal fivefold increase in the infiltration of CD4⁺ T cells to ischemic lobes at 1 h postreperfusion, which decreased more than 10-fold by 3 h of reperfusion. No significant change in the extent of CD4⁺ T cell infiltration was observed at later time points of 6, 12, and 20 h postreperfusion. However, T cells were usually not found in necrotic areas of the liver, and may in part account for the decrease in total T cells/mm² at the later time points. In summary, transient CD4⁺ T cell infiltration to ischemic lobes occurred very early within the process of reperfusion and suggests that this cell type may mediate early events that activate the subacute inflammatory cascade. In contrast, no changes in the number of CD8⁺ T cells recruited to the liver were seen throughout the time course of reperfusion after 90 min of ischemia and remained at endogenous levels seen in control mouse livers (Fig. 5 A). These findings suggest that CD4⁺ T cells are likely early cellular mediators of I/R inflammatory responses.

Discussion

The mechanisms of ischemic damage in the liver associated with reoxygenation is of great clinical relevance in understanding and preventing early graft failure in orthotopic liver transplants. In addition to acute free radical-induced injury, subacute inflammatory responses play a major role in post-I/R organ injury, which leads to a decline of liver function and potentially increased organ immunogenicity leading to graft rejection. In the present study, the analysis of genetically defined T cell-deficient mice has provided a unique animal model for studying the immunology of subacute inflammatory responses after I/R in the liver. Our findings, which demonstrate a substantially reduced subacute inflammatory-mediated I/R injury response in nu/nu mice, as compared with T cell-competent BALB/c mice, suggest that T-lymphocytes are required for complete activation of post-I/R inflammatory responses. Three pathophysiologic indexes including serum GPT levels, percent hepatocellular necrosis, and neutrophil infiltration were all reduced in nu/nu mice as compared with immune competent BALB/c mice. Furthermore, the involvement of T cells in mediating subacute I/R inflammatory injury was supported by adoptive transfer experiments of T cells into nu/nu mice, which were capable of increasing both the subacute serum GPT levels (20 h) and neutrophil influx to damaged tissue.

Studies aimed at elucidating whether Tc and/or Th T cell subsets were involved in mediating this subacute inflammatory response used in vivo depletion of CD8⁺ or CD4⁺ T-lymphocytes in immune-competent BALB/c mice. Results from these experiments demonstrated that CD4⁺ but not CD8⁺ T-lymphocyte depletion was capable of reducing both the extent of injury and neutrophil infiltration during the subacute phase of I/R liver damage. These findings suggest that CD4⁺ T cells are a predominant mediator of the I/R-induced inflammatory responses. Additionally, the fact that CD4⁺ T cell influx to the liver after ischemia occurred within the first hour of reperfusion suggests that this cell type may mediate very proximal events that are responsible for activation of the subacute inflammatory cascade. In contrast, CD8⁺ T cell influx to the liver after I/R remained unchanged and suggests that this cell type does not play an important role in mediating postreperfusion inflammatory events in the liver after ischemia. In summary, these results suggest that in the absence of CD4⁺ T cells, the liver has an improved capacity to recover from oxidant-mediated damage. Furthermore, one might predict that therapeutic intervention directed at Th-lymphocyte activation pathways after I/R injury could yield substantial therapeutic benefits in transplantation through abrogation of subacute neutrophil inflammatory responses.

The mechanism(s) by which neutrophils are recruited after I/R liver injury is presently only partially understood. Previous studies have evaluated the increased adherent characteristics of neutrophils to endothelium in the liver after I/R. To this end, studies in ICAM-1-deficient transgenic mice have demonstrated the importance of this adhesion molecule in the recruitment of neutrophils in a model of LPS-induced liver damage (34). These studies demonstrated a protection against leukocytosis in the livers of ICAM-1-deficient mice treated with LPS. Furthermore, the mechanism underlying this protection was proposed to be distal to the inciting events that promote TNF α and IL-1 cytokine production, since these cytokines remained elevated in both wild-type and ICAM-1-deficient mice after LPS injury. Similarities between this toxic shock model of liver damage and that encountered in I/R-induced liver injury include the production of TNF α and IL-1 (11–13). Such hepatic cytokines have been suggested to be produced by Kupffer cells within the early phases of ischemic liver injury before reperfusion and have been implicated in amplification of subsequent neutrophil inflammatory responses (11, 12). These cytokines may have a direct role in activation of neutrophils or in contrast may activate other hematopoietic cell types (e.g., T cells) involved in regulating the injury responses to I/R in the liver. Findings from the present study have provided new insights into the potential involvement of T cell lineages in the recruitment and amplification of neutrophils to the damaged liver after I/R. Specifically, we propose that CD4⁺ T-lymphocytes may be important mediators of these responses.

CD4⁺ T cells can be subdivided into at least two subpopulations, Th1 and Th2. Th1 cells, which secrete IFN γ , TNF β , and GM-CSF (known to have stimulatory effects on Kupffer cells and neutrophils), may represent the best candidates for mediating this process of inflammation (30). Of these various T cell-secreted cytokines, IFN γ and TNF β are known to be potent activators of Kupffer cells and may likely promote local secretion of TNF α and IL-1, which in turn act to facilitate changes in endothelial adherence characteristics of neutrophils through either direct activation of neutrophils themselves or

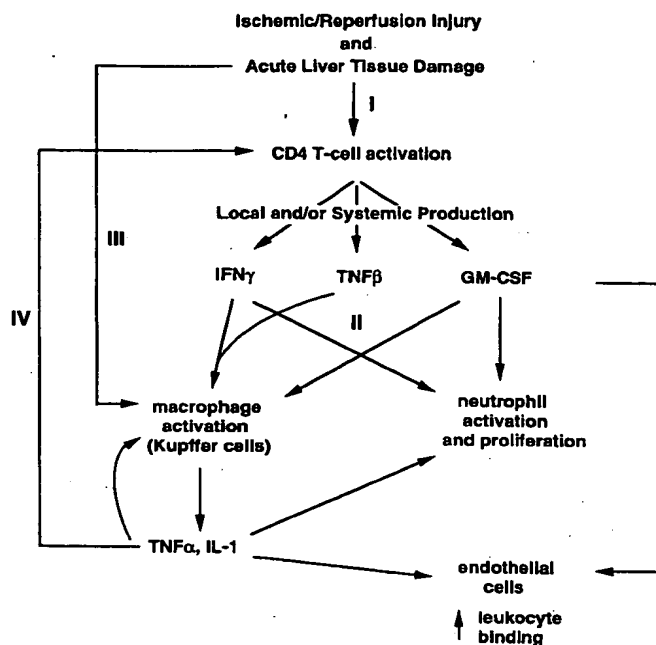


Figure 6. Potential mechanism(s) of T-lymphocytes activated inflammatory response after I/R injury in the liver. This schematic proposes potential mechanism(s) by which CD4⁺ T-lymphocytes mediate the activation of neutrophil inflammatory responses after ischemia and reperfusion in the liver. One potential hypothesis suggests that the stimulus of ischemia/reperfusion injury triggers activation directly in resident CD4⁺ T cells (pathway I). Once activated, CD4⁺ T cells may secrete a number of cytokines including IFN γ , TNF β , and GM-CSF, which either directly or indirectly (through Kupffer cell-secreted cytokines) activate neutrophils to infiltrate the liver (pathway II). Alternatively, the I/R stimulus may directly activate resident Kupffer cells within the liver (pathway III), which in turn activate circulating CD4⁺ T cells through secreted cytokines (pathway IV). Despite the present speculation as to the exact cytokine pathways by which CD4⁺ T cells interact within the amplification of neutrophil inflammatory responses after I/R injury, the significantly reduced subacute phase I/R injury in the absence of T cells demonstrates that some component of T cell activation is critical for this response.

indirectly through changes in surface adhesion molecules on endothelial cells. Furthermore, Th1-secreted IFN γ and GM-CSF may also act directly on neutrophils and enhance their partitioning to damaged liver tissue.

The primary question at present is whether T cell involvement lies proximal or distal with respect to the activation of Kupffer cell cytokine secretion, which has been demonstrated to play a major role in neutrophil recruitment. If T cell involvement lies proximal to the activation of Kupffer cells, this would imply that circulating T cells within the liver are directly activated by ischemia and reperfusion (i.e., changes in the cellular or extracellular redox state) and are potentially involved in initiating Kupffer cellular responses. Alternatively, T cells may be critical in amplifying primary Kupffer cell cytokine responses within the initial phases of injury. This hypothesis is attractive given the fact that secretion of TNF α by Kupffer cells has been suggested to occur before reperfusion. However, since CD4⁺ T cells are also resident in the liver before

reperfusion, it is impossible to rule out primary inciting activation of Kupffer cells by CD4⁺ T cells during the ischemic period. In addition, T cell-mediated effects could be amplified by other ectopic sites such as the spleen. In support of this hypothesis, a recent paper by Okuaki et al. (35) has demonstrated reduced neutrophil infiltration and attenuation of I/R injury in animals subjected to splenectomy as compared with controls. In the context of this present study, these data suggest that T cells at distant sites to the liver (e.g., the spleen) may also be involved in the inflammatory process. This action could occur by recruitment of T cells to the liver or alternatively through soluble mediators such as cytokines. Regardless of the exact mechanisms of action, since activation of CD4⁺ T cell recruitment to the liver occurs very early within the first hour of reperfusion, one would anticipate that T cells play a critical early role in amplifying the post-I/R inflammatory cascade. Fig. 6 summarizes potential mechanisms by which CD4⁺ T-lymphocytes may mediate a subacute inflammatory response in the liver after I/R injury.

Activation of naive T cells has traditionally been demonstrated to require recognition of foreign antigens bound to a self-MHC molecule together with costimulatory signals by an antigen presenting cell. However, in I/R injury, the lack of available foreign antigen's for presentation by antigen presenting cells suggests that activation of T-lymphocytes after I/R injury may occur via an antigen-independent pathway. Alternatively, self-antigens may be modified by generated reactive oxygen species so they appear foreign to T-lymphocytes. An antigen-independent activation mechanism of T-lymphocytes has recently been described by Bacon et al. (36) that involves the chemokine Rantes. Additionally, protein modifications due to oxidation with associated inflammatory responses have been postulated for cases of liver cirrhosis (37).

Despite the present lack of a defined cytokine-mediated pathway, these studies conclusively implicate T-lymphocytes as key mediators in the pathoproduction of I/R inflammatory responses in the liver. Elucidation of the cytokine pathways for T-lymphocyte activation of neutrophil recruitment in the liver after I/R may ultimately yield clinically relevant modalities for the amelioration of acute rejection in orthotopic liver transplants. Furthermore, since the major T cell subsets involved in graft rejection may be different than those involved in subacute phase post-I/R inflammatory responses (i.e., Tc [CD8⁺] versus Th [CD4⁺] cells, respectively), the rational design of effective therapies to prevent graft rejection necessitates the need for a concrete understanding of the cellular and cytokine pathways involved in these two pathophysiologically unique T cell-mediated responses. Neutrophil-mediated damage secondary to I/R injury is a pathophysiologic process seen in a number of additional organs including the heart, brain, lung, and kidney. Studies aimed at determining the T cell dependency of these post-I/R neutrophil responses, as seen in the liver, could lead to potential novel anti-T cell-directed therapies for other types of ischemically induced injuries as seen in myocardial infarction and stroke.

Acknowledgments

We thank the Wistar Institute Flow Cytometry Core and Hybridoma Core for their technical assistance.

This work was supported by National Institutes of Health grant RO1 DK51315 (J.F. Engelhardt).

References

- Hernandez, L.A., M.B. Grisham, B. Twohig, K.E. Arfors, J.M. Harlan, and D.N. Granger. 1987. Role of neutrophils in ischemia-reperfusion-induced microvascular injury. *Am. J. Physiol.* 253:699-703.
- Jaeschke, H., A. Farhood, and C.W. Smith. 1990. Neutrophils contribute to ischemia/reperfusion injury in rat liver *in vivo*. *FASEB J.* 4:3355-3359.
- Komatsu, H., A. Koo, E. Ghadishah, H. Zeng, J.F. Kuhlenskamp, M. Inoue, P.H. Guth, and N. Kopolwitz. 1992. Neutrophil accumulation in ischemic reperfused rat liver: evidence for a role for superoxide free radicals. *Am. J. Physiol.* 262:669-676.
- Langdale, L.A., L.C. Flaherty, H.D. Liggitt, J.M. Harlan, C.L. Rice, and R.K. Winn. 1993. Neutrophils contribute to hepatic ischemia-reperfusion injury by a CD18-independent mechanism. *J. Leukocyte Biol.* 53:511-517.
- Suzuki, S., L.H. Toledo-Pereyra, and F.J. Rodriguez. 1994. Role of neutrophils during the first 24 hours after liver ischemia and reperfusion injury. *Transplant. Proc.* 26:3695-3700.
- Vollmar, B., M.D. Menger, J. Glasz, R. Leiderer, and K. Messmer. 1994. Impact of leukocyte-endothelial cell interaction in hepatic ischemia-reperfusion injury. *Am. J. Physiol.* 267:786-793.
- Jaeschke, H., A.P. Bautista, Z. Spolarics, and J.J. Spitzer. 1991. Superoxide generation by Kupffer cells and priming of neutrophils during reperfusion after hepatic ischemia. *Free Radical Res. Commun.* 15:277-284.
- Jaeschke, H., A. Farhood, A.P. Bautista, Z. Spolarics, J.J. Spitzer, and S.C. Wayne. 1993. Functional inactivation of neutrophils with a Mac-1 (CD11b/CD18) monoclonal antibody protects against ischemia-reperfusion injury in rat liver. *Hepatology.* 17:915-923.
- Fantone, J.C., and P.A. Ward. 1982. Role of oxygen-derived free radicals and metabolites in leukocyte-dependent inflammatory reactions. *Am. J. Physiol.* 107:397-418.
- Flaherty, J.T., and M.L. Weisfeldt. 1988. Reperfusion injury. *Free Radical Biol. Med.* 5:409-419.
- Colletti, L.M., D.G. Remick, G.D. Burtch, S.L. Kunkel, R.M. Strieter, and D.A. Campbell. 1990. Role of tumor necrosis factor- α in the pathophysiology alterations after hepatic ischemia/reperfusion injury in the rat. *J. Clin. Invest.* 85:1936-1943.
- Colletti, L.M., S.L. Kunkel, A. Walz, M.D. Burdick, R.G. Kunkel, C.A. Wilke, and R.M. Strieter. 1995. Chemokine expression during hepatic ischemia/reperfusion-induced lung injury in the rat. *J. Clin. Invest.* 95:134-141.
- Ghezzi, P., C.A. Dinarello, M. Bianchi, M.E. Rosandich, J.E. Repine, and C.W. White. 1991. Hypoxia increases production of interleukin-1 and tumor necrosis factor by human mononuclear cells. *Cytokine.* 3:189-194.
- Suzuki, S., and L.H. Toledo-Pereyra. 1994. Interleukin 1 and tumor necrosis factor production as the initial stimulants of liver ischemia and reperfusion injury. *J. Surg. Res.* 57:253-258.
- Zhou, W., M.O. McCollum, B.A. Levine, and M.S. Olson. 1992. Inflammation and platelet-activating factor production during hepatic ischemia/reperfusion. *Hepatology.* 16:1236-1240.
- Scoazec, J.Y., F. Durand, C. Degott, D. Delautier, J. Bernuau, J. Belghiti, J.P. Benhamou, and G. Feldmann. 1994. Expression of cytokine-dependent adhesion molecules in postreperfusion biopsy specimens of liver allografts. *Gastroenterology.* 107:1094-1102.
- Koo, A., H. Komatsu, G. Tao, M. Inoue, P.H. Guth, and N. Kaplowitz. 1991. Contribution of no-reflow phenomenon to hepatic injury after ischemia-reperfusion: evidence for a role for superoxide anion. *Hepatology.* 15:507-514.
- Arthur, M.J.P., I.S. Bently, A.R. Tanner, P. Kowalski Saunders, G.H. Millward-Sadler, and R. Wright. 1985. Oxygen-derived free radicals promote hepatic injury in the rat. *Gastroenterology.* 89:1114-1122.
- Atalla, S.L., L.H. Toledo-Pereyra, G.H. MacKenzie, and J.P. Cederna. 1985. Influence of oxygen-derived free radical scavengers on ischemia livers. *Transplantation (Baltimore).* 40:584-590.
- Mathews, W.R., D.M. Guido, M.A. Fisher, and H. Jaeschke. 1994. Lipid peroxidation as molecular mechanism of liver cell injury during reperfusion after ischemia. *Free Radical Biol. Med.* 16:763-770.
- Adkinson, D., M.E. Hollwarth, J.N. Benoit, D.A. Parks, J.M. McCord, and N. Granger. 1986. Role of free radicals in ischemia-reperfusion injury to the liver. *Acta Physiol. Scand.* 548:101-107.
- Fujita, T., H. Furitsu, M. Nishikawa, Y. Takakura, H. Sezaki, and M. Hashida. 1992. Therapeutic effects of superoxide dismutase derivatives modified with mono- or polysaccharides on hepatic injury induced by ischemia/reperfusion. *Biochem. Biophys. Res. Commun.* 189:191-196.
- Hasuoka, H., K. Sakagami, and K. Orita. 1991. A new slow delivery type of superoxide dismutase prevents warm ischemia damage in swine orthotopic liver transplantation. *Transplant. Proc.* 23:693-696.
- Kawamoto, S., M. Inoue, S. Tashiro, Y. Morino, and Y. Miyauchi. 1990. Inhibition of ischemia and reflow-induced liver injury by an SOD derivative that circulates bound to albumin. *Arch. Biochem. Biophys.* 277:160-165.
- McEnroe, C.S., F.J. Pearce, J.J. Ricotta, and W.R. Drucker. 1986. Failure of oxygen-free radical scavengers to improve postischemic liver function. *J. Trauma.* 26:892-896.
- Jaeschke, H., C.V. Smith, and J.R. Mitchell. 1988. Hypoxic damage generates reactive oxygen species in isolated perfused rat livers. *Biochem. Biophys. Res. Commun.* 150:568-574.
- Jaeschke, H., and A. Farhood. 1991. Neutrophil and Kupffer cell-induced oxidant stress and ischemia-reperfusion injury in rat liver. *Am. J. Physiol.* 260:355-362.
- Kobayashi, S., and M.G. Clemens. 1992. Kupffer cell exacerbation of hepatocyte hypoxia/reoxygenation injury. *Circ. Shock.* 37:245-252.
- Mochida, S., M. Arai, A. Ohno, N. Masaki, I. Ogata, and K. Fujiwara. 1994. Oxidative stress in hepatocytes and stimulatory state of Kupffer cells after reperfusion differ between warm and cold ischemia in rats. *Liver.* 14:234-240.
- Salgame, P.R., J.S. Abrams, C. Clayberger, H. Goldstein, J. Convit, R.L. Modlin, and B.R. Bloom. 1991. Differing lymphokine profiles of functional subsets of human CD4 and CD8 T-cell clones. *Science (Wash. DC).* 254:279-282.
- Coligan, J.E., A.M. Kruisbeek, D.H. Margulies, and E.M. Shevach. 1994. Current Protocols in Immunology. W. Strober, editor. John Wiley & Sons Inc., New York. 3.1.1-3.5.16, 5.3.1-5.3.11.
- Dialynas, D.P., Z.S. Quan, K.A. Wall, A. Pierres, J. Quintans, M.R. Loken, M. Pierres, and F.W. Fitch. 1983. Characterisation of the murine T cell surface molecule designated L3T4, identified by the monoclonal antibody GK1.5: Similarities to the human Leu 3/T4 molecule. *J. Immunol.* 131:2445-2451.
- Sarmiento, M., A.L. Glasebrook, and F.W. Fitch. 1980. IgG or IgM monoclonal antibodies bearing Lyt2 antigen block T cell-mediated cytotoxicity in the absence of complement. *J. Immunol.* 125:2665-2670.
- Xu, B.-H., J.A. Gonzalo, Y. St. Pierre, I.R. Williams, T.S. Kupper, R.S. Cotran, T.A. Springer, and J. Gutierrez-Ramos. 1994. Leukocytosis and resistance to septic shock in intercellular adhesion molecule 1-deficient mice. *J. Exp. Med.* 180:95-109.
- Okuaki, Y., H. Miyazaki, M. Zeniya, T. Ishikawa, Y. Ohkawa, S. Tsuno, M. Sakaguchi, M. Hara, H. Takahashi, and G. Toda. 1996. Splenectomy-reduced hepatic injury induced by ischemia/reperfusion in the rat. *Liver.* 16:188-196.
- Bacon, K.B., B.A. Premack, P. Gardner, and T.J. Schall. 1995. Activation of dual T cell signaling pathways by the chemokine RANTES. *Science (Wash. DC).* 269:1727-1730.
- Niemelä, O., S. Parkkila, S. Ylä-Herttuala, C. Halsted, J.L. Witztum, A. Lanca, and Y. Israel. 1994. Covalent protein adducts in the liver as a result of ethanol metabolism and lipid peroxidation. *Lab. Invest.* 70:537-546.

The Role of Macrophages, Perivascular Cells, and Microglial Cells in the Pathogenesis of Experimental Autoimmune Encephalomyelitis

JAN BAUER,¹ INGE HUITINGA,¹ WEIGUO ZHAO,² HANS LASSMANN,³ WILLIAM F. HICKEY,² AND CHRISTINE D. DIJKSTRA¹

¹Department of Cell Biology and Immunology, Faculty of Medicine, Vrije Universiteit, 1081 BT, Amsterdam, The Netherlands; ²Department of Pathology, Dartmouth Medical School, Lebanon, New Hampshire 03756-0001; and ³Neurological Institute, University of Vienna, A-1090, Austria

KEY WORDS Macrophage subpopulations, Brain inflammation, Dichloromethylene diphosphonate, Liposomes

ABSTRACT Clinical signs of experimental autoimmune encephalomyelitis (EAE) in rats can be suppressed by treatment with liposomes containing dichloromethylene diphosphonate (Cl₂MDP liposomes). Here we investigated whether besides the blood-borne macrophages also ED2⁺ perivascular cells and microglia are affected by this treatment. For this purpose we examined the central nervous system of bone marrow chimeras in which EAE was induced with encephalitogenic T cells. Quantification of cell numbers of various cell types in inflammatory lesions in the spinal cord showed that after treatment with Cl₂MDP liposomes more than 95% of the bone marrow derived (I1-69⁺) macrophages were eliminated. In addition the number of ED2⁺ perivascular cells were seen to be decreased by 68% as compared to ED2⁺ cells in control liposome treated animals. However the number of these perivascular cells in Cl₂MDP liposome treated animals did not differ from the number of perivascular cells in naive animals, indicating that only newly recruited, inflammation associated, ED2⁺ macrophages were eliminated. Moreover, detection of degenerating nuclei by in situ nick translation (ISNT) in combination with staining for ED1 or ED2 showed that in the perivascular space no degenerating cells were present. Cl₂MDP liposome treatment furthermore decreased the numbers of T cells infiltrating the parenchyma by more than 50%. Instead T cells were found in large numbers in the perivascular space. Microglia did not seem to be eliminated by Cl₂MDP liposome treatment as shown by the absence of ED1⁺/ISNT⁺ cells in the CNS parenchyma. However the number of ED1⁺(I1-69⁻) microglial cells decreased by more than 80%, indicating that the activation of this cell type was impaired. It is concluded that bone marrow derived macrophages play an important role in the pathogenesis of EAE via interactions with lymphocytes and the activation of resident microglia.

© 1995 Wiley-Liss, Inc.

INTRODUCTION

Experimental autoimmune encephalomyelitis (EAE) is a T cell-dependent disease which is characterized by inflammatory lesions in the central nervous system (CNS). These parenchymal lesions consist of T lymphocytes, which preferentially use the V β 8.2 T cell recep-

tor (Lannes-Vieira et al., 1994; Tsuchida et al., 1993), and blood-borne macrophages (Paterson, 1960). Besides,

Received April 6, 1995; accepted June 27, 1995.

Address reprint requests to Christine D. Dijkstra, Department of Cell Biology and Immunology, Faculty of Medicine, Vrije Universiteit, Van Der Boechorststraat 7, 1081 BT, Amsterdam, The Netherlands.

© 1995 Wiley-Liss, Inc.

the hematogenous infiltrating macrophages and lymphocytes also cells in the CNS seem to play a role in EAE. Especially the parenchymal microglial cell is believed to participate in the immune response by upregulation of cell surface molecules such as the complement receptor 3 (Graeber et al., 1988; Matsumoto et al., 1992), CD4, and MHC class II molecules (Gehrmann et al., 1993; Matsumoto et al., 1986; Vass et al., 1986). Furthermore, microglial cells are able to produce cytokines like interleukin-1 (Bauer et al., 1993; Van Dam et al., 1992) and have phagocytic properties (Bauer et al., 1994; Graeber et al., 1989; Lassmann et al., 1993). Another cell type of interest is the perivascular cell. This cell, which is situated in the perivascular space of blood-vessels, is bone-marrow derived and can be stained with the ED2 monoclonal antibody (Graeber et al., 1989; Hickey and Kimura, 1988). The strategic location, the ability to phagocytose, the ability to present antigens in an MHC class II restricted manner (Hickey and Kimura, 1988) and to produce IL-1 (Bauer et al., 1993) demonstrates the potency of this cell to act as an immunoregulatory cell during EAE. Early studies by Brosnan et al. (1981) revealed that macrophage depletion by treatment with silica dust could suppress clinical signs of EAE. In our laboratories we developed liposomes containing the drug dichloromethylene diphosphonate (Cl_2MDP) to eliminate macrophages (Van Rooijen, 1989). In a previous study (Huitinga et al., 1990), we demonstrated that treatment with Cl_2MDP liposomes eliminated macrophages in animals with EAE. However, with the techniques applied in that study it was neither possible to assess the effects of Cl_2MDP liposome treatment on microglia and perivascular cells, nor could the effect that the Cl_2MDP liposomes exerted on macrophages which had already infiltrated in the CNS be evaluated.

Therefore, in the present study we investigated whether treatment of animals with Cl_2MDP liposomes, in addition to circulating macrophages also affects effector cells within the CNS. A problem in the study of infiltrating macrophages and microglial cells is that during EAE these cells in the CNS virtually are indistinguishable because of the similarity of immunocytological phenotype. In order to overcome this problem we used bone-marrow chimeras (Hickey and Kimura, 1988; Matsumoto and Fujiwara, 1987) which allows unequivocal identification of bone marrow derived cells by their MHC class I profile. Furthermore, degenerating cells in the CNS were identified by cytochemical visualization of nuclear DNA fragmentation using *in situ* nick translation.

MATERIALS AND METHODS

Animals

Lewis (Lew) rats (150–175 g weight) were obtained from Charles River Laboratories (Wilmington, MA). Brown Norway (BN) rats and (Lew \times BN) F_1 (150–175 g) were obtained from Harlan Sprague Dawley (India-

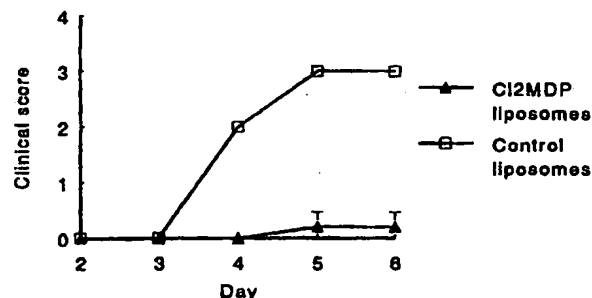


Fig. 1. Clinical course of MBP-T cell induced EAE in animals treated with control liposomes or with liposomes containing Cl_2MDP . Based on the presence of clinical signs the Cl_2MDP liposome treated animals differed significantly from the animals treated with control liposomes ($P < 0.05$).

napolis, IN). Animals were maintained in the facilities of Dartmouth Medical School under the care of a veterinarian in accordance with institutional and Federal guidelines for the treatment of rodents.

Chimeras

Chimeric rats were made as described before (Hickey and Kimura, 1988; Hickey et al., 1992). Briefly, Lewis rats (MHC type RT1^b) were crossed with BN rats (MHC type RT1ⁿ) in order to get (BN \times Lewis) F_1 hybrids (RT1^{n/b}). Bone marrow cells (1×10^6) from these hybrids were injected in irradiated (1,000 rads) BN rats. The animals were allowed to mature for 2 months prior to use in order to assure repopulation of the immune system by F_1 bone marrow derivatives.

Preparation of liposomes

Mannosylated liposomes were prepared according to Huitinga et al. (1990). Liposomes were obtained by dissolving 70.9 mg phosphatidylcholine and 10.8 mg cholesterol in 8 ml chloroform. This was added to 3.6 p-aminophenyl- α -D-mannopyranoside which was dissolved in 2 ml methanol. This mixture then was dried *in vacuo* in a round-bottomed flask connected to a rotary evaporator. After dissolving (with 100% chloroform) and a second *in vacuo* drying step, the resulting film was dispersed into liposomes after the addition of 10 ml of PBS (control liposomes) or 10 ml of PBS to which 1.89 g dichloromethylene diphosphate (a kind gift from Boehringer Mannheim, Mannheim, Germany) was added (experimental liposomes).

EAE induction and experimental design

Adoptive T cell EAE was induced by intravenous (i.v.) injection of 5×10^6 Lewis myelin basic protein (MBP) specific T cells in eleven chimeric rats (day 0) as de-

TABLE 1. Differences in localisation of cells in various compartments of the spinal cord between control liposome and Cl_2 MDP liposome treated animals^a

Staining	Meninges		Perivascular		Parenchymal	
	CON	Cl_2 MDP	CON	Cl_2 MDP	CON	Cl_2 MDP
I1-69 ⁺ /ED1 ⁻	+	++	+++	++++	+++	++
I1-69 ⁺ /ED1 ⁺	+	+/-	+++	+/-	+++	+/- ^b
I1-69 ⁻ /ED1 ⁺	-	-	-	-	+	+/- ^b
OX-6	+	+	+++	++	+++	++ ^b

^aGross examination of immunoreactivity for markers in the different compartments (meninges, perivascular space, and parenchyma) of the spinal cord was performed on single (OX-6) and double stained sections. The presence of immunoreactive cells is noted from - (no immunoreactive cells) to +++ (high numbers of immunoreactive cells). CON, control liposome treated groups; Cl_2 MDP, Cl_2 MDP liposome treated animals. Note the shift in distribution from T cells from the parenchyma to the meninges and perivascular space, the decrease in ED1 positive macrophages in all compartments and the decrease of ED1 positive microglial cells in the parenchyma.

^bWhile OX-6 immunoreactivity is found on microglial cells throughout the parenchyma, immunoreactivity for ED1 is only found on activated microglia/macrophages in lesions.

TABLE 2. Number of T cells, macrophages and microglial cells in spinal cord^a

Treatment	I1-69 ⁺ /ED1 ⁻ (lymphocytes)	I1-69 ⁺ /ED1 ⁻ (macrophages)	I1-69 ⁻ /ED1 ⁺ (microglia)
Control liposomes			
C	262.5	253.1	67.1
D	293.1	311.2	88.8
E	360.5	271.5	60.0
F	321.3	356.3	51.1
Average of group	309.35 ± 20.9	298.03 ± 22.9	66.75 ± 8.0
Cl_2 MDP			
G	87.0	8.8	10.2
H	327.3	20.3	12.5
I	64.8	6.0	14.6
J	152.7	3.5	4.3
K	161.3	5.4	11.3
Average of group	158.63 ± 46.1	8.79 ± 3.0*	10.56 ± 1.7*

^aQuantitative evaluation of cell numbers in spinal cord of animals treated with control liposomes (C-F) or Cl_2 MDP liposomes (G-K). Values represent the number of immunostained cells/mm² as measured in double staining for I1-69 and ED1. The average values of the group is given with the standard deviation.

*Different from control at $P < 0.05$ (Wilcoxon test).

scribed before (Hickey and Kimura, 1988; Hickey et al., 1991). On day 1 and day 3, nine of these 11 animals were injected i.v. with Cl_2 MDP ($n = 5$, experimental group) or PBS ($n = 4$, control group) liposomes. The remaining two chimeric rats were given no injections (except infusion of T cells) to serve as controls for the induction of EAE. The rats were observed daily for clinical signs of EAE which were graded in four categories (grade 0.5: partial loss of tail tonus, grade 1: floppy tail, grade 2: paraparesis, grade 3: paraparesis and a moribund condition). Absence of any signs resulted in clinical score 0. On day 6 after T cell transfer, material from these chimeric animals and from naive Lewis rats ($n = 4$) was sampled and used for immunocytochemistry.

Tissue sampling and immunocytochemistry

Under deep anesthesia with thiopental, on day 6, animals were perfused with 0.1 M phosphate buffer (PB, pH 7.4) followed by 4% paraformaldehyde in the same buffer. The brain, spinal cord, and spleen were removed and fixed in the same fixative for an additional 3 h. After this, part of the material was embedded in paraffin and part of the material was rinsed in PB and subsequently incubated in PB containing 10% (overnight, o/n), 15% (o/n), and 20% (8 h) sucrose before being frozen in liquid nitrogen. This material was stored

at -20°C until further use for immunocytochemistry at the light microscopical level.

Cryostat sections were picked up on gelatin coated glass slides and air dried for at least 45 min. After this, sections were used immediately for immunocytochemistry or stored at -20°C . Immunocytochemistry was done with the following antibodies: I1-69 (for recognition of bone marrow derived cells, Lewis MHC Class I, type RT1¹), ED1 (macrophages and activated microglial cells), ED2 (perivascular cells), R73 (T cells, T cell Receptor $\alpha\beta$), and OX-6 (MHC class II). ED1 and ED2 were made in our own laboratories (Dijkstra et al., 1985) (Serotec, Oxford, UK). I1-60 and R73 were generous gifts from Dr. H. Kimura and Dr. T. Hünig respectively. OX-6 was obtained from Serotec. Besides these antibodies also the marker Griffonia simplicifolia isolectin B4 (GSA I-B₄, Sigma, peroxidase conjugated) was used for recognition of resting and activated microglia. Incubations with these primary antibodies and with the lectin marker were done for 48 h at 4°C in Tris buffered saline (TBS, pH 7.8) to which 2.5% bovine serum albumin (BSA, Organon Technika, Oss, The Netherlands) and 0.5% Triton X-100 was added (TBST). The second antibody used was biotinylated rabbit anti mouse (Dakopatts, Denmark), diluted 1:100 in TBST (6 h, room temperature (RT)), as the tertiary step incubations with peroxidase conjugated avidin-biotin complex (ABC, Vectastain, Vector, diluted in TBST) was done for 2 h at

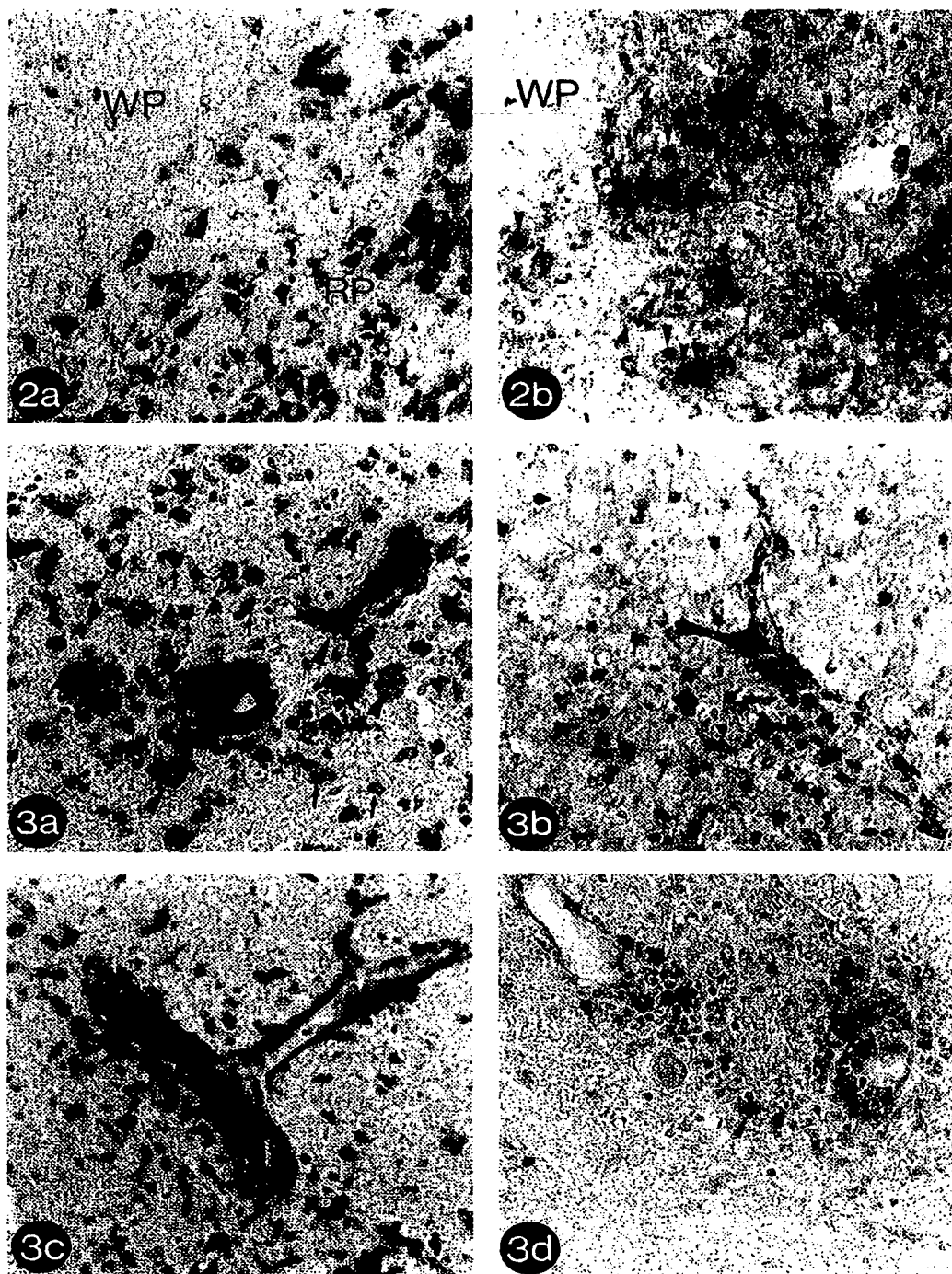


Fig. 2. Immunocytochemistry for ED1 in combination with ISNT on spleen sections. a: In control liposome treated animals macrophages stained by ED1 can be seen in the red pulp (RP) of the spleen. No ISNT signal is found in this section. WP, white pulp ($\times 600$). b: In Cl_2MDP liposome treated animals, ED1-immunoreactivity is not confined to

cells but appears as a smear in the red pulp indicating the destruction of macrophages. Unlike in Figure 2a, the ISNT signal shows many degenerated nuclei (arrows) of macrophages in the red pulp (RP). WP, white pulp ($\times 600$).

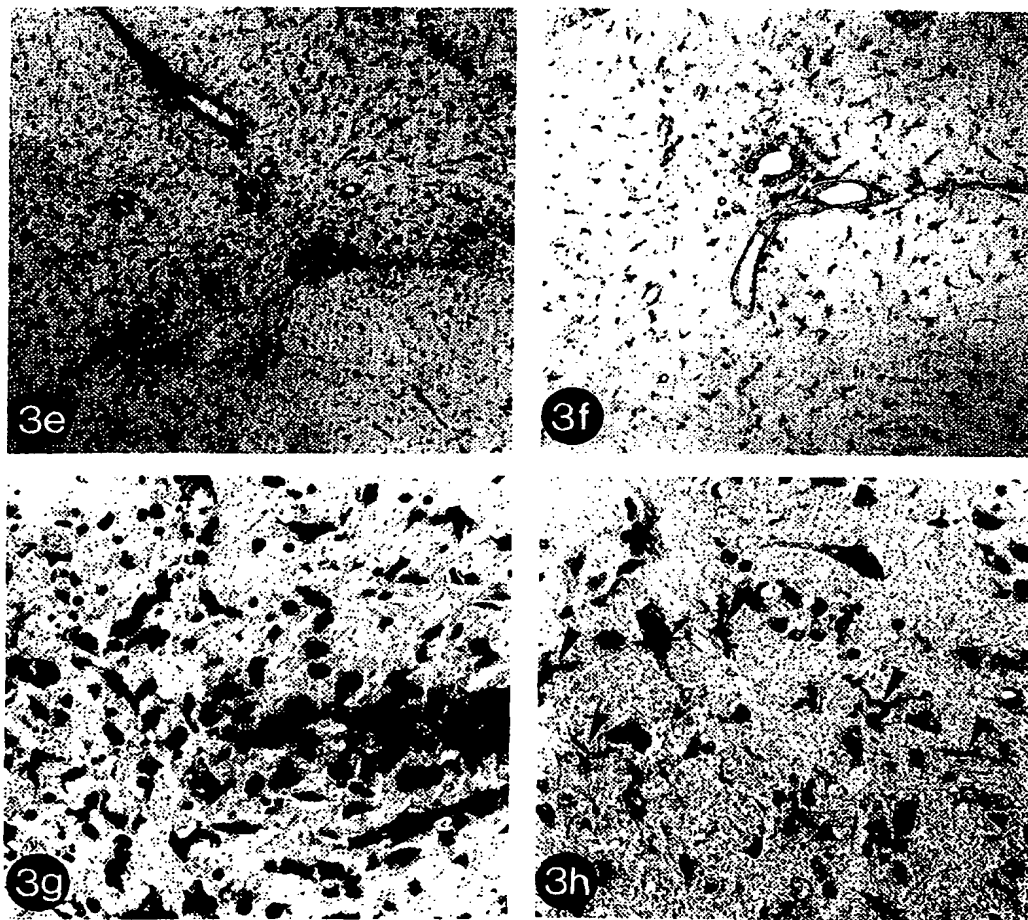


Fig. 3. a: Immunocytochemistry for I1-69 in a lesion in the spinal cord of a control liposome treated animal. Large round blood borne macrophages (arrowheads) and lymphocytes (arrows) have infiltrated the parenchyma (hematoxylin counterstain, $\times 600$). b: Staining for I1-69 in the spinal cord of an animal treated with CL₂MDP liposomes shows that in this lesion only small lymphocytes are present (hematoxylin counterstain, $\times 600$). c: Staining for ED1 in a control liposome treated animal shows intense ED1-immunoreactivity in macrophages/activated microglia, spinal cord (hematoxylin counterstain, $\times 600$). d: ED1-immunoreactivity in an animal treated with CL₂MDP liposomes shows that in this lesion in the spinal cord only some macrophages/activated microglial cells (arrowheads) are present (hematoxylin counterstain, $\times 600$). e: Histochemistry for GSA I-B₄ in the spinal cord of an animal treated with control liposomes. Throughout the spinal cord

microglial cells have lost their "resting" morphology and appear as cells with short thick processes (hematoxylin counterstain, $\times 60$). f: Histochemistry for GSA I-B₄ shows that in the spinal cord of an animal treated with CL₂MDP liposomes microglial cells have a somewhat activated morphology but stay regularly distributed in the spinal cord parenchyma ($\times 60$). g: Immunocytochemistry for OX-6 shows a lesion in the spinal cord of a control liposome treated animal. MHC class II⁺ macrophages and lymphocytes are intermingled with activated microglial cells (hematoxylin counterstain, $\times 600$). h: In the spinal cord of an animal treated with CL₂MDP liposomes, MHC class II⁺ microglial cells with somewhat thickened processes (arrowheads) are found in a regular pattern in the spinal cord parenchyma (hematoxylin counterstain, $\times 600$).

RT. Peroxidase was visualized with 3,3'-diaminobenzidine-tetra-hydrochloride. All the rinsing procedures were done with TBS. The sections were counterstained with haematoxylin.

Double staining on cyrostat sections was performed for I1-69 and ED1 according to Van den Dobbelsteen et al. (1991) with slight modifications. In brief, incubation with the first antibody (I1-69) was done for 24 h at 4°C in TBST. This incubation was followed by incubation

with an alkaline-phosphatase conjugated goat anti mouse antibody for 6 h at RT (Jackson, diluted 1:75). Alkaline phosphatase was visualized with Fast blue B base (Sigma). Incubation with the second antibody (ED1) was also done for 24 h (4°C) followed by the avidin-biotin detection method as described above. As the chromogen, amino ethyl carbazole (AEC) was used. This double staining resulted in lymphocytes being single stained (I1-69, blue), bone marrow derived macro-

perivascular cells in spinal cord

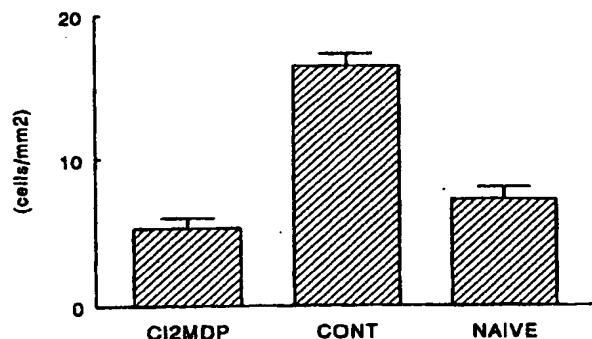


Fig. 4. The number of ED2⁺ perivascular cells was measured in spinal cord of animals treated with Cl₂MDP liposomes (Cl₂MDP), animals which received control (CONT) liposomes and in naive Lewis rats (naive). Only the Cl₂MDP liposome treated group differed significantly from the other groups ($P < 0.001$, Student's *t* test).

phages double stained (I1-69, blue; ED1, red) and activated microglial cells single stained for ED1 (red). The recognition of double staining cells was facilitated by the fact that ED1 predominantly recognizes a cytoplasmic antigen, whereas I1-69 recognizes a membranous antigen. The numbers of lymphocytes, bone marrow derived macrophages, ED2⁺ perivascular cells and microglial cells in the spinal cord were quantitatively measured according to Lassmann et al. (1993). For each animal 2–3 cross sections of the spinal cord (in total at least 10 mm²) were investigated.

In Situ Nick Translation (ISNT)

In order to detect degenerating cells, in situ nick translation was performed as described by Gold et al. (1993); 3 μ m paraffin sections containing spinal cord and spleen were deparaffinized, treated with chloroform and air dried. Next, sections were incubated in 50 μ l of the reaction mixture (consisting of 5 μ l 10 \times nick translation buffer, 1 μ l digoxigenin labeled nucleotides, and 44 μ l polymerase I) for 1 h at 37°C. As a secondary step the sections were incubated with an alkaline phosphatase labeled anti-digoxigenin F(ab')₂ antibody at a dilution of 1:250. Alkaline phosphatase was visualized with NBT/BCIP. All materials for the ISNT were obtained from Boehringer Mannheim. Subsequently, the sections were stained with monoclonal antibodies ED1 and ED2. These antibodies were visualized by a biotin-avidin-peroxidase technique (Vass et al., 1986).

Statistical evaluation

Differences in clinical signs between control and liposome treated animals were evaluated with the χ^2 test.

Differences in cell numbers of immunostained cells between control and Cl₂MDP liposome treated animals were evaluated with the Student's *t*-test or the Wilcoxon rank sum test.

RESULTS

Clinical findings

Onset of clinical disease in animals treated with control liposomes started on day 4 after transfer of T cells (mean clinical score 2.0, indicating paraparesis). The clinical score increased to a mean of 3 (moribund) on day 5 and 6. The development of clinical disease in these radiation bone marrow chimeras treated with control liposomes did not differ from the two chimeric rats with T cell EAE which did not receive liposomes. In comparison to animals treated with control liposomes, in Cl₂MDP liposome treated animals the clinical signs were markedly decreased; three animals did not develop clinical manifestations at all whereas in two animals only a mild loss of tail tonus (clinical score 0.5) was noted on day 5 and 6. Average clinical score on day 6 in these animals as a group was 0.2 (Fig. 1).

Histological findings

Spleen

Immunocytochemical staining for I1-69 in the control liposome group confirmed the successful repopulation with I1-69⁺ lymphocytes and macrophages after bone-marrow transfer (Fig. 2a). In the Cl₂MDP liposome treated group the elimination of macrophages could be seen by the absence of ED1⁺ cells in the splenic red pulp. In addition the ISNT in combination with staining for ED1 showed a strong staining in these Cl₂MDP liposome treated spleens indicating that many macrophages were degenerated (Fig. 2b).

Central nervous system

No marked differences in lesion size and number were found between uninjected control bone marrow chimeras with T cell EAE and control liposome treated bone

Fig. 5. ED2-immunoreactivity in naive Lewis rats and liposome treated rats. a: Low magnification photograph from the spinal cord of a naive Lewis rat showing several ED2⁺ perivascular cells (hematoxylin counterstain, $\times 198$). Perivascular cells indicated by arrows are shown in higher magnification in b and c ($\times 180$). d: Low magnification from a control liposome treated rat. Here, ED2⁺ cells have a macrophage appearance (hematoxylin counterstain, $\times 198$). Cell indicated by arrow is depicted in a higher magnification ($\times 810$) in e. f: Besides the cells with rounded morphology, in these animals also the perivascular cells with elongated morphology can be found ($\times 810$). Low magnification from the spinal cord of a Cl₂MDP liposome treated rat. Like in naive rats, in these animals only perivascular cells with elongated cytoplasm are found alongside blood vessel walls (hematoxylin counterstain, $\times 198$). h: Higher magnification ($\times 810$) from the cell indicated by an arrow in g. i: Second example of an ED2⁺ perivascular cell in the spinal cord of a Cl₂MDP liposome treated rat ($\times 810$).

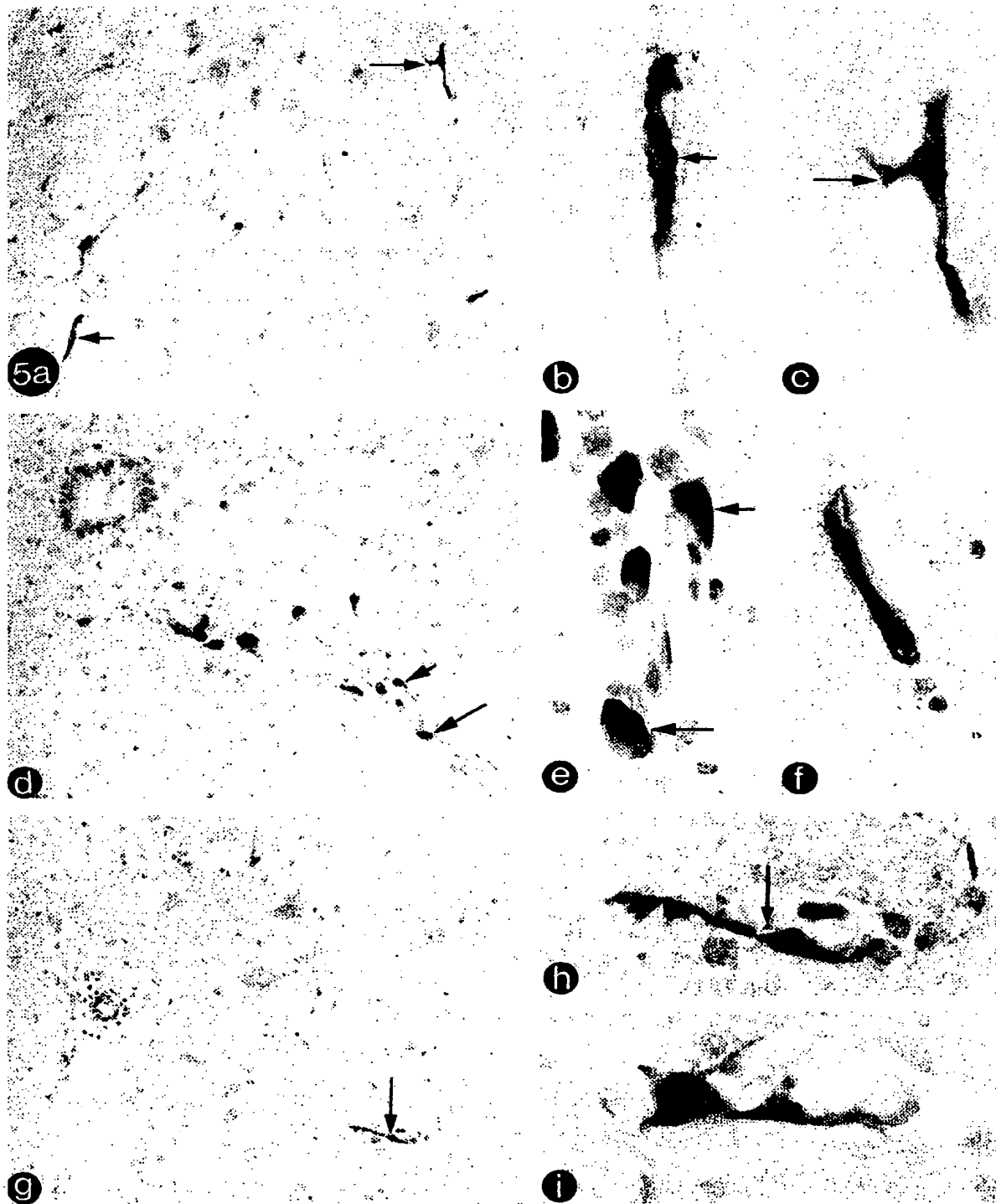


Fig. 5.

marrow chimeras with T cell EAE. Therefore, at the histological level, only differences between control and Cl_2MDP liposome groups could be detected (Table 1)

T cells

In control liposome treated rats, T cells (R73^+ , $\text{I1-69}^+/\text{ED1}^-$) in the spinal cord were found in the meninges, the perivascular space and infiltrated into the parenchyma. With double staining for I1-69 and ED1 an average of 309.35 cells/ mm^2 (see Table 2) in the parenchyma was found. Whereas in the control liposome treated animals most lymphocytes had infiltrated in the parenchyma, in Cl_2MDP liposome treated animals large numbers of lymphocytes were seen to be trapped in the perivascular space of bloodvessels and in the meninges. The average number of lymphocytes in the parenchyma in the Cl_2MDP liposome treated animals had decreased to a level of 49% compared to controls (Table 2). This decrease however was not found to be significant.

Macrophages

$\text{I1-69}^+/\text{ED1}^+$ blood-borne macrophages were found in the meninges, the perivascular space of bloodvessels and deeply infiltrated in the CNS parenchyma of control liposome treated animals (Table 1). In general these cells had an oval or rounded morphology with, in some cases, short processes (Fig. 3a,c). In the Cl_2MDP liposome treated animals the numbers of these $\text{I1-69}^+/\text{ED1}^+$ cells were markedly decreased in meninges, perivascular space, and CNS parenchyma (Table 1). Quantitation of the macrophages infiltrating into the parenchyma showed a 97% reduction of these cells (Table 2) as compared to the control group (Fig. 3b,d).

Microglial cells

In control liposome treated rats, activated microglial cells in and near EAE lesions could be recognised as $\text{I1-69}^+/\text{ED1}^+$. Many of these microglial cells did not have the rounded morphology of $\text{I1-69}^+/\text{ED1}^+$ blood-borne macrophages but had thick processes in which a string of ED1^+ granules were found. Quantitation of these cells showed that these microglial cells represented 9.9% of the cells in the double stainings (Table 1). The GSA I-B₄ marker which, besides endothelial cells, stains both resting and activated microglia, showed intense staining of cells in lesions (Fig. 3e). Furthermore, with this lectin marker it was noted that almost all of the microglial cells in the spinal cord showed the activated morphology. The staining for MHC Class II (OX-6) showed a pattern similar to the staining for GSA I-B₄ in that, besides round macrophages, the activated microglial cells with thick processes located in lesions and deeper in the parenchyma were also stained (Fig. 3g).

Quantitation of the $\text{I1-69}^+/\text{ED1}^+$ microglial cells revealed a dramatically decreased number in the Cl_2MDP liposome treated animals as compared to control liposome treated animals (Table 1). These ED1^+ microglial cells were located near lesions and were not present in the surrounding parenchyma. The ISNT technique in combination with staining for ED1 showed that there were no necrotic macrophages and/or microglial cells present in the CNS parenchyma. Staining with the GSA I-B₄ marker showed that, whereas in the control liposome treated animals almost all microglial cells morphologically looked like activated microglia, in the Cl_2MDP liposome treated animals microglial cells with thick short processes were only found in the vicinity of lesions. Unlike in control liposome treated animals, where activated microglial cells were intermingled with bone-marrow derived macrophages, most of the microglial cells (although activated in the sense that they had somewhat thicker processes) were distributed in a regular pattern over the spinal cord parenchyma (Fig. 3f). Staining with OX-6 essentially showed the same as the GSA I-B₄ staining: clearly activated microglia were present in lesions and regularly distributed microglial cells deeper in the parenchyma were found to be OX-6⁺ (Fig. 3h).

Perivascular cells

Perivascular cells and meningeal macrophages were detected with the ED2 monoclonal antibody. In the control liposome treated group a mean of 16.6 perivascular cells/ mm^2 was counted. Many of the ED2^+ cells in perivascular position had a rounded morphology (Fig. 5d-f) while ED2^+ perivascular cells in Cl_2MDP liposome treated animals had an elongated cytoplasm like in naive Lewis rat (Fig. 5a-c,g-i). The number of these perivascular cells was much higher than the number of ED2^+ cells in the Cl_2MDP liposome treated group (average of 5.2 cells/ mm^2 , Fig. 4). Comparison of the numbers of ED2^+ cells in the Cl_2MDP liposome treated animals with the numbers of ED2^+ cells in naive Lewis rats (Fig. 5a-c) showed that the number of these cells were similar and thus, resident perivascular cells seemed not to be affected (Fig. 4). In support of this determination, ISNT in combination with ED2 staining showed that no dying ED2^+ cells in the perivascular space were present.

DISCUSSION

The present study was performed in order to elucidate whether treatment with liposomes affects phagocytes within the central nervous system. Our results show that only macrophages in the periphery are depleted whereas in the CNS itself no destruction of phagocytes occurs.

Macrophages have been found to play an important role as effector cells in demyelination in EAE. These

cells can produce numerous factors known to be potentially harmful to myelin. For instance, macrophages are known to produce reactive oxygen species (ROS), nitric oxide, and TNF- α which easily can damage myelin (Konat and Wiggins, 1985; Selmaj and Raine, 1988) and the myelin producing oligodendrocytes (Griot et al., 1990; Kim and Kim, 1991; Merrill et al., 1993). Besides the production of factors as noted above, macrophages play an important role in demyelination in that they are the cells which phagocytose putatively damaged myelin sheaths (Lampert, 1965; Lassmann and Wisniewski, 1979; Pender, 1987; Raine et al., 1974). The result that macrophages after Cl_2MDP liposome treatment infiltrate the CNS only in very low numbers and that in the CNS itself, in contrast to the spleen, no degenerating macrophages are detected, indicates that depletion of these cells takes place outside the CNS. The absence of blood-borne macrophages concomitant with the marked suppression of clinical signs, confirms and strengthens the thought that this cell type plays a major role as an effector cell in EAE.

The perivascular cell with its strategic localization in the Virchow, Robin space (Hickey and Kimura, 1988) may play a crucial role in the development of EAE. By their release of IL-1 (Bauer et al., 1993) they may induce adhesion molecules like intercellular adhesion molecule-1 (ICAM-1) on endothelial cells and in this way modulate binding of leukocytes to endothelial cells (Fabry et al., 1993; Pober and Cotran, 1990), which is a first step in migration of leukocytes into the CNS. Furthermore, by their MHC class II expression they can present antigens to T cells at the BBB (Vass and Lassmann, 1990). This study shows that, although the number of ED2⁺ cells in perivascular position is much lower in the Cl_2MDP liposome treated animals as compared to control liposome treated animals, it apparently is not the resident perivascular cell itself which is eliminated. This is suggested by the finding that, although in the spleen with the ISNT technique many necrotic macrophages were found, in the perivascular space of bloodvessels no necrotic ED2⁺ cells could be detected. In addition, the number of ED2⁺ perivascular cells in Cl_2MDP liposome treated animals did not differ from perivascular cell numbers in naive Lewis rats. Taken together, these results indicate that in EAE the increase of ED2⁺ perivascular cells is correlated with infiltration of hematogenous macrophages.

This study was conducted in order to find out if besides blood-borne macrophages also microglial cells are depleted by Cl_2MDP treatment. Since with the ISNT technique in the central nervous system no degenerating ED1⁺ cells (uptake of Cl_2MDP liposomes requires phagocytosis and therefore ED1 upregulation) were detected, it is clear that after treatment with these liposomes no local destruction of microglial cells takes place. In the CNS, microglial cells have strong immunocompetent functions; phagocytosis, cytokine release, expression of immunologically functional molecules like complement receptor 3 (CR3), CD4, and MHC class II antigens are all microglial properties (Graeber et al.,

1988; Matsumoto et al., 1986; Vass et al., 1986). Depletion of blood-borne macrophages resulted in suppression of clinical signs. Thus, although activated microglial cells may have the same capabilities as infiltrating macrophages, in the absence of blood-borne macrophages, microglial cells do not take over the effector functions of these macrophages. The concomitant loss of blood-borne macrophages and the impaired activation of microglial cells suggests that macrophages may be responsible for the activation of microglial cells. Possibly macrophages may activate microglia by the release of TNF- α . This cytokine which also plays a role in demyelination is known for its stimulatory activity on macrophages (Brosnan et al., 1988) and therefore may also activate microglia. In Cl_2MDP liposome treated animals ED1 expression by microglia was decreased and their resting morphology had remained. MHC class II expression was present not only on microglial cells near lesions but also on microglial cells with long processes deeper in the unaffected parenchyma. The unaffected presence of MHC class II antigens on microglia in Cl_2MDP treated animals suggests that while macrophages may mediate activation of microglia, they are probably not involved in the upregulation of MHC class II molecules on microglia. MHC class II expression on microglial cells can be induced by IFN- γ (Vass and Lassmann, 1988). Since it is predominantly the CD4⁺ T cell which produces IFN- γ , it is likely that this cell type is responsible for the upregulation of MHC class II antigens on microglia.

In conclusion, this study shows that suppression of EAE by the use of Cl_2MDP liposomes is a result of elimination of peripheral blood-borne macrophages and not of resident perivascular cells or microglial cells. After macrophage depletion the activation of microglial cells was seen to be decreased, this implies that macrophages play a role in the activation of microglia. These results further strengthen the idea that blood-borne macrophages play a central role as effector cells in CNS inflammation.

ACKNOWLEDGMENTS

The authors thank Karis Sontrop and Keith Wegmann for help with the experiments and Dirk de Jong and Elisabeth Gurnhofer for reproducing the figures. This work was supported by grants from the Dutch foundation for the support of MS research (Vrienden MS research, projectcodes 89-38MS and 90-67MS) and by NIH award NS-27321.

REFERENCES

- Bauer, J., Berkenbosch, F., Van Dam, A.-M., and Dijkstra, C.D. (1993) Demonstration of interleukin-1 β in Lewis rat brain during experimental allergic encephalomyelitis by immunocytochemistry at the light and ultrastructural level. *J. Neuroimmunol.* 48:13-22.
- Bauer, J., Sminia, T., Wouterlood, F.G., and Dijkstra, C.D. (1994) Phagocytic activity of macrophages and microglial cells during the

- course of acute and chronic relapsing experimental autoimmune encephalomyelitis. *J. Neurosci. Res.*, 38:365-375.
- Brosnan, C.F., Bornstein, M.B., and Bloom, B.R. (1981) The effects of macrophage depletion on clinical and pathologic expression of experimental allergic encephalomyelitis. *J. Immunol.*, 126:614-620.
- Brosnan, C.F., Selmaj, K., and Raine, C.S. (1988) Hypothesis: A role for tumor necrosis factor in immune-mediated demyelination and its relevance to multiple sclerosis. *J. Neuroimmunol.*, 18:87-94.
- Dijkstra, C.D., Dopp, E.A., Joling, P., and Kraal, G. (1985) The heterogeneity of mononuclear phagocytes in lymphoid organs: Distinct macrophage subsets in the rat recognised by monoclonal antibodies ED1, ED2, and ED3. *Immunology*, 54:589-599.
- Fabry, Z., Waldschmidt, M.M., Hendrickson, D., Keiner, J., Loveman, L., Takei, F., and Hart, M.N. (1992) Adhesion molecules on murine brain microvascular endothelial cells: Expression and regulation of ICAM-1 and Lp 55. *J. Neuroimmunol.*, 36:1-11.
- Gehrmann, J., Gold, R., Linington, C., Lannes-Vieira, J., Wekerle, H., and Kreutzberg, G.W. (1993) Microglial involvement in experimental autoimmune encephalomyelitis of the central nervous system. *Glia*, 7:50-59.
- Gold, R., Schmied, M., Rothe, G., Zischler, H., Breitschopf, H., Wekerle, H., and Lassmann, H. (1993) Detection of DNA fragmentation in apoptosis: application of in situ nick translation to cell culture systems and tissue sections. *J. Histochem. Cytochem.*, 41:1023-1030.
- Graeber, M.B., Streit, W.J., and Kreutzberg, G.W. (1988) Axotomy of rat facial nerve leads to increased CR3 complement receptor expression by activated microglial cells. *J. Neurosci. Res.*, 21:18-24.
- Graeber, M.B., Streit, W.J., and Kreutzberg, G.W. (1989) Identity of ED2-positive perivascular cells in rat brain. *J. Neurosci. Res.*, 22:103-106.
- Griot, C., Vandevelde, M., Richard, A., Peterhans, E., and Stocker, R. (1990) Selective degeneration of oligodendrocytes mediated by oxygen radical species. *Free Rad. Res. Comm.*, 11:181-193.
- Hickey, W.F. and Kimura, H. (1988) Perivascular microglia are bone marrow derived and present antigen in vivo. *Science*, 239:290-292.
- Hickey, W.F., Hau, B.L., and Kimura, H. (1991) T-cell entry into the rat central nervous system. *J. Neurosci. Res.*, 28:254-260.
- Hickey, W.F., Vass, K., and Lassmann, H.J. (1992) Bone marrow derived elements in the central nervous system: An immunohistochemical and ultrastructural survey of rat chimeras. *J. Neuropathol. Exp. Neurol.*, 51:246-256.
- Huitinga, I., Van Rooijen, N., De Groot, C.J.A., Uitdehaag, B.M.J., and Dijkstra, C.D. (1990) Suppression of experimental allergic encephalomyelitis after elimination of macrophages. *J. Exp. Med.*, 172:1025-1033.
- Kim, Y.S. and Kim, S.U. (1991) Oligodendroglial cell death induced by oxygen radicals and its protection by catalase. *J. Neurosci.*, 29:100-106.
- Konat, G.W. and Wiggins R.C. (1985) Effect of reactive oxygen species on myelin membrane proteins. *J. Neurochem.*, 45:1113-1118.
- Lampert, P.W. (1965) Demyelination and remyelination in experimental allergic encephalomyelitis. *J. Neuropathol. Exp. Neurol.*, 24:371-385.
- Lannes-Vieira, J., Gehrmann, J., Kreutzberg, G.W., and Wekerle, H. (1994) The inflammatory lesion of T cell line transferred experimental autoimmune encephalomyelitis of the Lewis rat: Distinct nature of parenchymal and perivascular infiltrates. *Acta Neuropathol.*, 87:435-442.
- Lassmann, H. and Wisniewski, H.M. (1979) Chronic relapsing experimental allergic encephalomyelitis: Clinicopathological comparison with multiple sclerosis. *Arch. Neurol.*, 36:490-498.
- Lassmann, H., Schmied, M., Vass, K., and Hickey, W.F. (1993) Bone marrow derived elements and resident microglia in brain inflammation. *Glia*, 7:19-24.
- Matsumoto, Y., Hara, N., Tanaka, R., and Fujiwara, M. (1986) Immunohistochemical analysis of the rat central nervous system during experimental allergic encephalomyelitis, with special reference to Ia-positive cells with dendritic morphology. *J. Immunol.*, 136:3668-3676.
- Matsumoto, Y. and Fujiwara, M.J. (1987) Absence of donor type major histocompatibility complex class I antigen bearing microglia in the rat central nervous. *J. Neuroimmunol.*, 17:71-82.
- Matsumoto, Y., Ohmori, K., and Fujiwara, M. (1992) Microglial and astroglial reactions to inflammatory lesions of experimental autoimmune encephalomyelitis in the rat central nervous system. *J. Neuroimmunol.*, 37:23-33.
- Merrill, J.E., Ignarro, L.J., Sherman, M.P., Melinek, J., and Lane, T.E. (1993) Microglial cell cytotoxicity is mediated through nitric oxide. *J. Immunol.*, 151:2132-2141.
- Paterson, P. (1960) Transfer of allergic encephalomyelitis in rats by means of lymph node cells. *J. Exp. Med.*, 111:119-135.
- Pender, M.P. (1987) Demyelination and neurological signs in experimental allergic encephalomyelitis. *J. Neuroimmunol.*, 15:11-24.
- Pober, J.S., Cotran, R.S. (1990) Cytokines and endothelial cell biology. *Physiol. Rev.*, 70:427-451.
- Raine, C.S., Snyder, D.H., Valsamis, M.P., and Stone, S.H. (1974) Chronic experimental allergic encephalomyelitis in inbred guinea pigs: An ultrastructural study. *Lab. Invest.*, 31:369-380.
- Selmaj, K.W. and Raine, C.S. (1988) Tumor necrosis factor mediated myelin and oligodendrocyte damage in vitro. *Annal. Neurol.*, 23:339-346.
- Tsuchida, M., Matsumoto, Y., Hirahara, H., Hanawa, H., Tomiyama, K., and Abo, T. (1993) Preferential distribution of V β 8.2-positive T cells in the central nervous system of rats with myelin basic protein-induced autoimmune encephalomyelitis. *Eur. J. Immunol.*, 23:2399-2406.
- Van Dam, A.-M., Brouns, M., Louisse, S. and Berkenbosch, F. (1992) Appearance of interleukin-1 in macrophages and in ramified microglia in the brain of endotoxin-treated rats: A pathway for the induction of non-specific symptoms of sickness? *Brain Res.*, 588:291-296.
- Van den Dobbelsteen, G.P.J.M., Van Rooijen, N., Sminia, T., and Van Rees, E.P. (1991) The immune response to *Streptococcus pneumoniae* types 3 and 4 capsular polysaccharide: Detection by double immunocytochemical staining of antibody-containing cells in situ and ELISA. *J. Immunol. Methods*, 145:93-103.
- Van Rooijen, N. (1989) The liposome-mediated macrophage 'suicide' technique. *J. Immunol. Methods*, 124:1-6.
- Vass, K., Lassmann, H., Wekerle, H., and Wisniewski, H.M. (1986) The distribution of Ia antigen in the lesions of rat acute experimental allergic encephalomyelitis. *Acta Neuropathol.*, 70:149-160.
- Vass, K. and Lassmann, H. (1990) Intrathecal application of interferon gamma: Progressive appearance of MHC antigens within the rat nervous system. *Am. J. Pathol.*, 137:789-800.

Chemokine-induced Eosinophil Recruitment

Evidence of a Role for Endogenous Eotaxin In An In Vivo Allergy Model in Mouse Skin

Mauro M. Teixeira,* Timothy N.C. Wells,[‡] Nicholas W. Lukacs,[§] Amanda E.I. Proudfoot,[‡] Steven L. Kunkel,[§] Timothy J. Williams,* and Paul G. Hellewell*

*Applied Pharmacology, Imperial College School of Medicine at the National Heart and Lung Institute, London, SW3 6LY, United Kingdom; [‡]Geneva Biomedical Research Institute, Geneva, Switzerland; and [§]Department of Pathology, University of Michigan Medical School, Ann Arbor, Michigan 48109

Abstract

Selective eosinophil recruitment into tissues is a characteristic feature of allergic diseases. Chemokines are effective leukocyte chemoattractants and may play an important role in mediating eosinophil recruitment in various allergic conditions in man. Here, we describe a novel mouse model of eosinophil recruitment in which we have compared the in vivo chemoattractant activity of different C-C chemokines. Furthermore, we describe the use of antibodies to chemokines and receptor blockade to address the endogenous mechanisms involved in eosinophil recruitment in a late-phase allergic reaction in mouse skin. Intradermal injection of mEotaxin and mMIP-1 α , but not mMCP-1, mRANTES, mMCP-5, or mMIP-1 β , induced significant ¹¹¹In-eosinophil recruitment in mouse skin. Significant ¹¹¹In-eosinophil recruitment was also observed in an active cutaneous anaphylactic reaction. Pretreatment of skin sites with antieotaxin antiserum, but not an antiMIP-1 α antibody, suppressed ¹¹¹In-eosinophil recruitment in this delayed-onset allergic reaction. Similarly, desensitization of the eosinophil eotaxin receptor CCR3 with mEotaxin, or blockade of the receptor with metRANTES, significantly inhibited ¹¹¹In-eosinophil recruitment in the allergic reaction. These results demonstrate an important role for endogenous eotaxin in mediating the ¹¹¹In-eosinophil recruitment in allergic inflammation, and suggest that blockade of the CCR3 receptor is a valid strategy to inhibit eosinophil migration in vivo. (*J. Clin. Invest.* 1997. 100:1657–1666.) Key words: chemokines • chemokine receptors • eosinophils • allergy • late-phase response

Introduction

Tissue eosinophilia in the absence of a concomitant increase in the number of neutrophils is a characteristic feature of allergic and parasitic diseases (1, 2). This preferential accumulation of

eosinophils in tissue suggests that there are specific pathways used by eosinophils for their accumulation in vivo. Understanding these mechanisms would aid in developing pharmacological therapies that would block eosinophil recruitment, but not that of other leukocytes (3). Such therapies may be of benefit in allergic diseases where eosinophil recruitment inhibition is desirable, and may have considerable advantage over existing treatments (e.g., steroids) that inhibit leukocyte recruitment indiscriminately (3) and have other deleterious actions.

Recently, it has become clear that a family of chemoattractants, the chemokines, may play an important role in activation and subsequent recruitment of leukocytes in vivo (4–6). Chemokines are proteins usually ranging from 8 to 10 kD, having amino acid sequence identity of between 20 and 90% (7). These proteins generally have four conserved cysteine residues, and, depending on the presence of one amino acid between the first two cysteines, are classified as C-C (no amino acid) or C-X-C (one intervening amino acid) chemokines (8). A member (lymphotactin) of a third subfamily possessing just two cysteine residues (8), C chemokines, has also been identified, and more recently, a novel chemokine family C-X₃-C has been described (9). The main function of chemokines appears to be activation and recruitment of particular leukocyte subsets, although a number of different roles have been ascribed to these proteins (8, 10).

Chemokine action on leukocytes is mediated by a family of G protein-coupled, seven-transmembrane receptors. There are five known receptors that mediate the actions of C-C chemokines, and these receptors are differentially expressed on different leukocyte subsets (7, 10, 11). Human eosinophils have been shown to express high levels of the CCR3 receptor (40,000–400,000 receptors per cell) and this receptor appears to mediate most of the actions of C-C chemokines on eosinophils (12, 13). Eosinophils also express the CCR1 receptor, but only at 1–5% of the levels of CCR3 (13). In agreement with their ability to bind and activate these two receptors, regulated upon activation in normal T cells expressed and secreted (RANTES),¹ macrophage inflammatory protein (MIP)-1 α , monocyte chemoattractant protein (MCP)-3, MCP-4, and eotaxin have been shown to activate eosinophils in vitro (14–17). In contrast to the wealth of data demonstrating the effects of chemokines on eosinophil function in vitro, however, there has been relatively little attention paid to testing comparatively the efficacy and potency of chemokines as eosinophil

Address correspondence to Mauro M. Teixeira, Ph.D., Applied Pharmacology, Imperial College School of Medicine at the National Heart and Lung Institute, Dovehouse Street, London SW3 6LY, United Kingdom. Phone: 44-171-352-8121 ext. 3108; FAX: 44-171-351-8270; E-mail: mauro.teixeira@ic.ac.uk

Received for publication 19 March 1997 and accepted in revised form 23 July 1997.

J. Clin. Invest.

© The American Society for Clinical Investigation, Inc.

0021-9738/97/10/1657/10 \$2.00

Volume 100, Number 7, October 1997, 1657–1666

<http://www.jci.org>

1. Abbreviations used in this paper: ACA, active cutaneous anaphylactic reaction; LTB₄, leukotriene B₄; MCP, monocyte chemoattractant protein; MIP, macrophage inflammatory protein; OVA, ovalbumin; PAF, platelet activating factor; RANTES, regulated upon activation in normal T cells expressed and secreted.

chemoattractants *in vivo*. In addition, only a few studies have demonstrated a role for endogenous chemokines in mediating eosinophil recruitment in response to antigen challenge *in vivo* (18–21). This fact is particularly important since there is clinical evidence to suggest an important role for chemokines in mediating eosinophil recruitment in various allergic conditions in man (for review see references 4 and 6). In this study, we describe a novel mouse model of eosinophil recruitment in which we have compared the *in vivo* chemoattractant activity of different C-C chemokines. Furthermore, we describe the use of antibodies to chemokines and receptor blockade in addressing the endogenous mechanisms involved in eosinophil recruitment in a late-phase allergic reaction in mouse skin.

Methods

Animals. Female CBA/Ca mice (18–20 g) were purchased from Harlan (Bicester, United Kingdom). CBA/Ca mice overexpressing the murine IL-5 gene (Tg1 mice [22]) were obtained from GlaxoWellcome (Stevenage, United Kingdom) and were bred in-house.

Reagents. The following compounds were purchased from Sigma Chemical Company (Poole, United Kingdom): ovalbumin (OVA), BSA, and 2-mercaptopyridine-*N*-oxine. Dulbecco's PBS (calcium- and magnesium-free, pH 7.4), and HBSS were from Life Technologies Ltd. (Paisley, United Kingdom). Percoll and dextran (T500) were from Pharmacia (Milton Keynes, United Kingdom). C16 platelet-activating factor (PAF) was from Bachem U.K. (Saffron Walden, United Kingdom), and leukotriene B₄ (LTB₄) was from Cascade (Reading, United Kingdom). Human recombinant C5a (C5a) was a gift from Dr. J. van Oostrum, Ciba Geigy (Summit, NJ). ¹²⁵I-HSA and ¹¹¹InCl₃ were obtained from Amersham International (Little Chalfont, United Kingdom). mEotaxin, hEotaxin, hMIP-1α, hRANTES, hMCP-3, hMCP-4, mMCP-5, and affinity-purified rabbit IgG were purchased from PeproTech Inc. (London, United Kingdom). mMIP-1α, mMCP-1, mKC, mMIP-2, mMIP-1β, anti-CD2, anti-B220, and affinity-purified anti-MIP-1α polyclonal antibody were purchased from R & D Systems (Abingdon, United Kingdom). mRANTES was a kind gift of Dr. I. Clark-Lewis, University of British Columbia, Vancouver, Canada. metRANTES was synthesized by GlaxoWellcome.

Anti-eotaxin antiserum. Rabbit anti-mEotaxin antibodies were prepared by multiple-site immunization of New Zealand White rabbits with recombinant mEotaxin in complete Freund's adjuvant. Rabbits were boosted with mEotaxin in incomplete Freund's adjuvant at 2-wk intervals for 1 mo after the original immunization, and were boosted when titers began to fall. Polyclonal antibodies were titered by direct ELISA, and were specifically verified by their failure to cross-react with mIL-3, mIL-1α/β, mTNF-α, mMIP-1α, IL-6, mJE, mMIP-1β, mC10, hMCP-1, hIL-8, hRANTES, hMIP-1α, hTNF-α, hEotaxin, and hMIP-1β. The ability of these antibodies to neutralize eosinophil chemotaxis was verified using *in vitro* chemotactic assays at a dilution of 1:1,000. This dilution was able to inhibit the eosinophil chemotactic response to 30 ng/ml of eotaxin by ~80% (data not shown).

Purification and radiolabeling of mouse eosinophils. Eosinophils were purified from the blood of CBA/Ca mice overexpressing the IL-5 gene. In our transgenic mouse colony, eosinophils accounted for ~60% of circulating blood leukocytes (data not shown). Blood was obtained by cardiac puncture (three to four donor mice per experiment), and red blood cells were sedimented using Dextran (T500, one part blood to four parts Dextran 1.25%). The leukocyte-rich supernatant was removed, centrifuged (300 g, 7 min), and layered onto a discontinuous four-layer Percoll gradient (densities: 1.070, 1.075, 1.080, and 1.085 g/ml). The gradients were centrifuged at 1,500 g for 25 min at 20°C, and eosinophils and lymphocytes were collected from the 1.080/1.085 interface. Lymphocytes were removed by using negative immunoselection with rat anti-mouse CD2 and B220 mAbs on a MACS BS col-

umn according to guidelines set by the manufacturers (Miltenyi Biotec Inc., Camberley, United Kingdom). In brief, the eosinophil and lymphocyte pellet was resuspended in PBS/BSA (10⁷ cells in 500 μl), and was incubated with 10 μg/ml of anti-CD2 and 7.5 μg/ml of anti-B220 for 20 min on ice. The cells were washed and resuspended in PBS/BSA (80 μl of PBS/BSA per 10⁷ cells). 20 μl of goat anti-rat IgG microbeads (Miltenyi Biotec Inc.) per 10⁷ cells were added, and the cells were incubated for a further 20 min at 6–8°C. The cell suspension was run through an immunomagnetic selection column, and the eosinophils were collected with the column effluent. The eosinophils purified this way were >95% pure and >98% viable. Flow cytometric analysis of purified eosinophils showed these cells to express similar amounts of CD11/CD18, very late activation antigen 4 (VLA-4), and L-selectin as granulocytes (~97% eosinophils) in whole blood of IL-5 transgenic mice (data not shown).

For the *in vivo* experiments, eosinophils were radiolabeled as previously described for guinea pig cells (23, 24). In brief, purified mouse eosinophils were incubated with ¹¹¹In (~100 μCi in 10 μl) chelated to 2-mercaptopyridine-*N*-oxine (40 μg in 0.1 ml of 50 mM PBS, pH 7.4) for 15 min at room temperature. Cells were then washed twice in PBS/BSA, and were finally resuspended at a final concentration of 10⁷ ¹¹¹In-eosinophils/ml. Eosinophils taken through the labeling procedure without addition of ¹¹¹InCl₃ exhibited no detectable changes in cell adhesion molecule expression (data not shown).

For the *in vitro* experiments measuring intracellular calcium, eosinophils were loaded with Fura-2 as previously described for guinea pig cells (25). Purified eosinophils (5 × 10⁶ cells/ml in PBS with 0.25% BSA) were loaded with fura-2-acetoxymethyl ester (1.0 μM, 30 min at 37°C). After two washes, eosinophils were resuspended at 10⁶ cells/ml in PBS buffer containing 10 mM Hepes, 0.25% BSA, and 1 mM calcium, and were stored on ice.

Immunization procedure. Animals were immunized with ovalbumin (OVA) adsorbed to aluminium hydroxide gel as previously described (26). In brief, mice were injected subcutaneously on days 1 and 8 with 0.2 ml of a solution containing 100 μg of OVA and 70 μg of aluminium hydroxide (Reheiss, Dublin, Ireland). 7–8 d after the last immunization, the animals were anaesthetized and shaved, and antigen (OVA 0.1 and 1.0 μg per site) was injected intradermally. The allergic reaction in mouse skin will be referred to as an active cutaneous anaphylactic (ACA) reaction.

Evaluation of eosinophil recruitment in mouse skin. 10 min after intravenous injection of ¹¹¹In-eosinophils (10⁶ ¹¹¹In-eosinophils/mouse), each animal received up to six intradermal injections (50 μl vol) of recombinant chemokines (1–30 pmol/site), PAF (1.5–500 pmol/site), LTB₄ (1.5–500 pmol/site), or hC5a (1.5–50 pmol/site). Recruitment of ¹¹¹In-eosinophils was allowed to occur over a period of 4 h, after which the animals were killed, and the number of ¹¹¹In-eosinophils per skin site was quantified after counting on a gamma counter (Canberra Packard, Berks, United Kingdom). In some experiments, ¹²⁵I-human serum albumin (¹²⁵I-HSA, ~5 μCi) was added to the ¹¹¹In-eosinophils before the cell suspension was injected intravenously. In these experiments, skin sites were counted in the gamma counter, and the counts for each isotope were cross-channel corrected for spillover. Extravasation of ¹²⁵I-HSA was expressed as μl of plasma, and was calculated by dividing the number of counts in each skin site by the number of counts in 1 μl of plasma.

For the experiments assessing ¹¹¹In-eosinophil recruitment in ACA reactions, animals were injected intradermally with antigen 4 h before the intravenous injection of radiolabeled cells, and ¹¹¹In-eosinophil recruitment was measured over a period of 4 h. Thus, ¹¹¹In-eosinophil recruitment in the ACA reaction was measured from 4 to 8 h after intradermal injection of antigen. At the end of the 4-h measurement period, blood was obtained by cardiac puncture, and the number of circulating ¹¹¹In-eosinophils was calculated.

Time course experiments were carried out to evaluate the optimal measurement periods for ¹¹¹In-eosinophil recruitment induced by eotaxin and LTB₄. Animals were given an intradermal injection of the chemoattractant 4 h, 3 h, 2 h, 1 h, and just before intravenous injection.

tion of radiolabeled cells. ^{111}In -eosinophil recruitment was assessed over a period of 1 h. Thus, the following measurement periods were considered in the time course: 0–1 h, 1–2 h, 2–3 h, 3–4 h, and 4–5 h.

Treatment with anti-MIP-1 α polyclonal antibody, antieotaxin antiserum, and metRANTES. To test the efficacy of anti-MIP-1 α antibody and antieotaxin antiserum, these agents were mixed with chemokines before intradermal injection of the mixture in mouse skin. To block the activity of endogenously generated chemokines, both the anti-MIP-1 α polyclonal antibody and antieotaxin antiserum were given intradermally into sites of 4-h-old ACA reactions just before intravenous injection of radiolabeled eosinophils. Anti-MIP-1 α was used at a dose of 50 μg per site when used with MIP-1 α , and at 100 μg per site when used in sites of ACA reactions. Affinity-purified rabbit IgG was used as control. Antieotaxin antiserum was used as a 5 and 20% dilution in PBS when used with eotaxin, and as a 20% dilution when used in sites of ACA reactions. Nonimmune rabbit serum was used as control. MetRANTES (5 $\mu\text{g}/\text{mouse}$) or saline (100 μl) were given subcutaneously at a remote site 30 min before injection of ^{111}In -eosinophils. metRANTES had no significant effect on the levels of circulating ^{111}In -eosinophils measured at 2 or 4 h after their intravenous injection (data not shown). This dose of metRANTES was chosen based on its ability to induce maximal inhibition of the recruitment of eosinophils in the lungs of allergen challenged mice (T.N.C. Wells, unpublished observations). In some experiments, ^{111}In -eosinophils were pretreated with 10^{-8} M mEotaxin at 37°C before their intravenous administration.

Measurement of changes in intracellular calcium. 10 min before their use, Fura-2-loaded eosinophils were warmed to 37°C , and 300- μl aliquots were dispensed into quartz cuvettes. Changes in fluorescence after activation with mEotaxin (10^{-10} – 10^{-8} M), mMIP-1 α (10^{-10} – 10^{-8} M), or LTB $_4$ (10^{-7} M) were monitored at 37°C using a fluorimeter (LS50; Perkin-Elmer Corp., Beaconsfield, Bucks, United Kingdom) at excitation wavelengths 340 and 380 nm, and emission wavelength 510 nm. MetRANTES was used at a concentration of 10^{-6} M. For cross-desensitization experiments, the trace was allowed to return to baseline levels before addition of a further stimulus. $[\text{Ca}^{2+}]_i$ levels were calculated using the ratio of the two fluorescence readings and a K_d for Ca^{2+} binding at 37°C of 224 nM (27).

Statistical analysis. All results are presented as the mean \pm SEM. Normalized data were analyzed by one-way ANOVA, and differences between groups was assessed using the Student-Newman-Keuls post-test. A P value < 0.05 was considered significant. Percent inhibition of ^{111}In -eosinophil recruitment in skin was calculated by subtracting background values obtained in response to intradermal PBS injection.

Results

Effects of lipid mediators and hC5a on ^{111}In -eosinophil recruitment in mouse skin. Initial experiments were designed to assess the effects of chemoattractant agents previously shown to induce the direct recruitment of eosinophils *in vivo* (24, 28). The intradermal injection of PAF, LTB $_4$, and hC5a induced a dose-dependent ^{111}In -eosinophil recruitment when measured over a 4-h period (Fig. 1). PAF-induced ^{111}In -eosinophil recruitment was maximal at 50 pmol/site, and there was significant cell recruitment at 5 pmol/site. LTB $_4$ was more effective than PAF, but significant ^{111}In -eosinophil recruitment was only observed at doses ≥ 15 pmol/site (Fig. 1). C5a induced significant ^{111}In -eosinophil recruitment at 50 pmol/site, but it was less effective than were the other two mediators tested at similar doses (Fig. 1). PAF, LTB $_4$, and hC5a induced significant oedema formation in mouse skin (for example: PBS, 2.4 ± 0.5 μl of plasma; PAF, 50 pmol/site, 7.4 ± 1.2 μl ; LTB $_4$, 150 pmol/site, 4.5 ± 0.2 μl ; C5a, 50 pmol/site, 4.9 ± 1.5 μl ; $n = 5$).

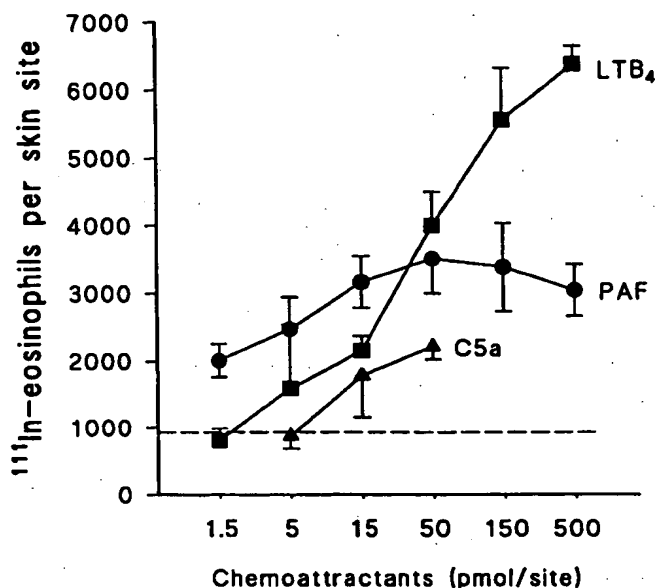


Figure 1. Recruitment of ^{111}In -eosinophils to the skin of mice injected with LTB $_4$, PAF, and hC5a. Eosinophils were purified from the blood of IL-5-transgenic mice, labelled with ^{111}In and 10^6 ^{111}In -eosinophils injected intravenously into nontransgenic CBA/Ca mice. 10 min later, the animals received intradermal injections of LTB $_4$ (1.5–500 pmol/site), PAF (1.5–500 pmol/site), or hC5a (5–50 pmol/site). After 4 h, the animals were killed, and ^{111}In -eosinophils accumulating at skin sites were quantified in a gamma counter. The dashed line represents background recruitment of ^{111}In -eosinophils in sites injected with PBS. Results are expressed as the mean \pm SEM for 5–6 animals.

Time-course experiments showed that maximal recruitment of ^{111}In -eosinophils in response to LTB $_4$ occurred over the first 2 h with little ^{111}In -eosinophil over the next h (Fig. 2). PAF- and hC5a-induced ^{111}In -eosinophil was also maximal over the first 2 h (data not shown).

Comparative effects of C-C chemokines on ^{111}In -eosinophil recruitment in mouse skin. The following recombinant murine C-C chemokines were tested for their ability to induce ^{111}In -eosinophil recruitment in mouse skin: eotaxin, MIP-1 α , MIP-1 β , RANTES, MCP-5, and MCP-1/JE. Intradermal injection of mEotaxin and mMIP-1 α , but not mMIP-1 β , mRANTES, mMCP-1, or mMCP-5, resulted in significant ^{111}In -eosinophil recruitment over the 4-h measurement period (Fig. 3). mEotaxin-induced ^{111}In -eosinophil recruitment was significant at 1.0 pmol/site, and was not maximal at the highest dose tested (Fig. 3). mMIP-1 α -induced ^{111}In -eosinophil recruitment was significant at 3.0 pmol/site, and peaked around 30 pmol/site (Fig. 3). Comparable doses of mEotaxin were significantly more effective than was mMIP-1 α when compared in the same animal (Fig. 4a). None of the chemokines at the doses tested above induced any significant oedema formation as assessed by extravasation of ^{125}I -HSA (for example: PBS, 2.4 ± 0.3 μl of plasma; mEotaxin, 30 pmol/site, 2.5 ± 0.7 μl ; mMIP-1 α , 30 pmol/site, 2.8 ± 0.4 μl , $n = 4$ –5). In contrast to LTB $_4$, mEotaxin-induced ^{111}In -eosinophil recruitment was more protracted, and significant cell recruitment was observed even when measured from 4–5 h after intradermal injection (Fig. 2).

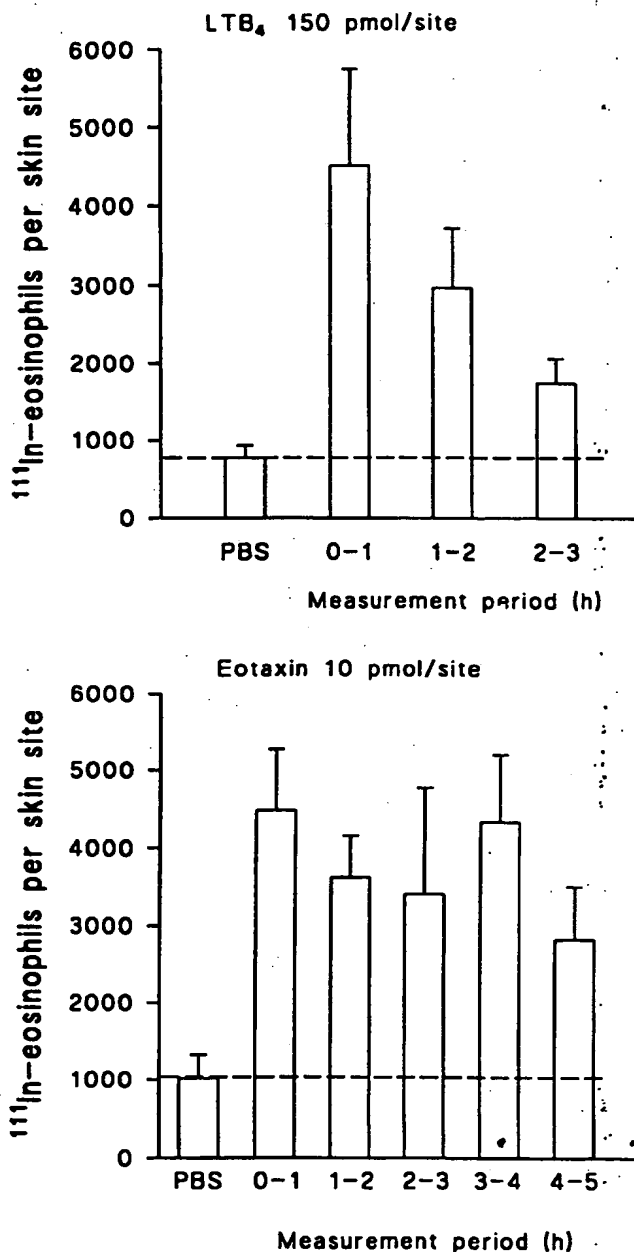


Figure 2. Time course of ¹¹¹In-eosinophil recruitment after intradermal administration of LTB₄ and mEotaxin in mouse skin. Eosinophils were purified from the blood of IL-5-transgenic mice, labelled with ¹¹¹In and 10⁶ ¹¹¹In-eosinophils injected intravenously into nontransgenic CBA/Ca mice. Animals were given an intradermal injection of LTB₄ (150 pmol/site) or mEotaxin (10 pmol/site) 4 h, 3 h, 2 h, 1 h, and just before intravenous injection of radiolabelled cells, and ¹¹¹In-eosinophil recruitment was assessed over a period of 1 h. The animals were then killed, and ¹¹¹In-eosinophils accumulating at skin sites quantified in a gamma counter. The dashed line represents background recruitment of ¹¹¹In-eosinophils in sites injected with PBS. Results are expressed as the mean ± SEM for four animals.

The following human recombinant chemokines were tested for their ability to induce ¹¹¹In-eosinophil recruitment in mouse skin: eotaxin, MIP-1α, MCP-3, MCP-4, and RANTES. Similar to the results described above, hEotaxin and hMIP-1α (Fig. 4 b),

but not hMCP-3, hMCP-4, or hRANTES, induced significant ¹¹¹In-eosinophil recruitment (data not shown). Fig. 4 b depicts the effects of similar doses of hEotaxin and hMIP-1α when injected intradermally into mouse skin. Similar to its murine counterparts, hEotaxin was more effective than was hMIP-1α, and significant ¹¹¹In-eosinophil recruitment was observed at doses as low as 1.0 pmol/site of hEotaxin (Fig. 4 b).

The murine recombinant C-X-C chemokines KC and MIP-2 induced no significant recruitment of ¹¹¹In-eosinophils when injected intradermally in doses of up to 30 pmol/site (data not

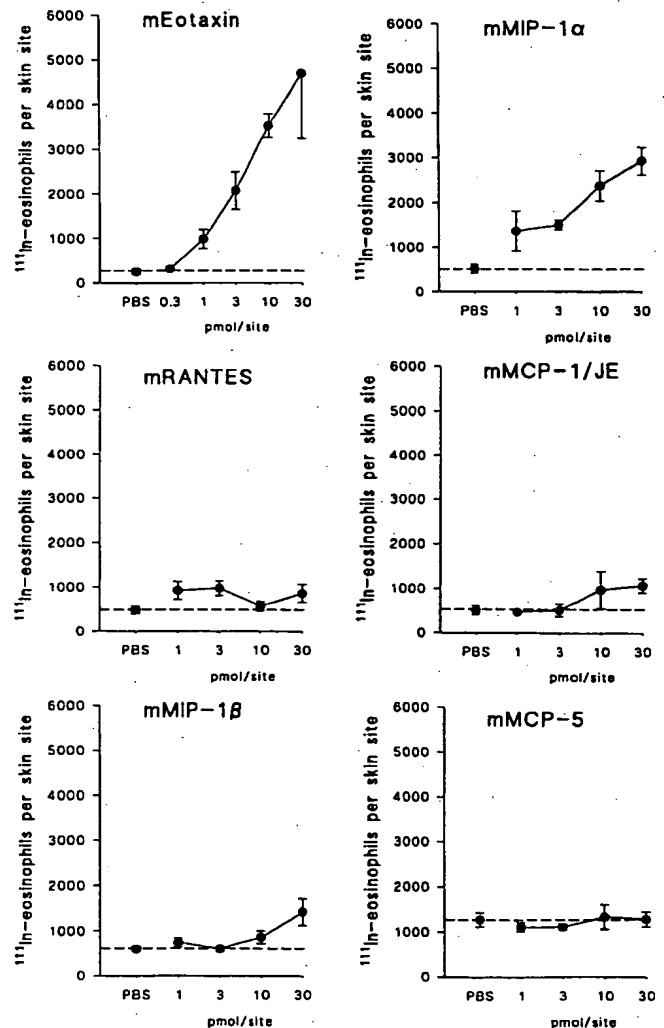


Figure 3. Comparison of eosinophil-recruiting activities of murine C-C chemokines in mouse skin. Eosinophils were purified from the blood of IL-5-transgenic mice, labelled with ¹¹¹In and 10⁶ ¹¹¹In-eosinophils injected intravenously into nontransgenic CBA/Ca mice. 10 min later, the animals received intradermal injections of mEotaxin (0.3–30 pmol/site), mMIP-1α (1–30 pmol/site), mMIP-1β (1–30 pmol/site), mMCP-1/JE (1–30 pmol/site), mRANTES (1–30 pmol/site), and mMCP-5 (1–30 pmol/site). After 4 h, the animals were killed, and ¹¹¹In-eosinophils accumulating at skin sites were quantified in a gamma counter. The dashed lines represent background recruitment of ¹¹¹In-eosinophils in sites injected with PBS. Results are expressed as the mean ± SEM for 4–6 animals.

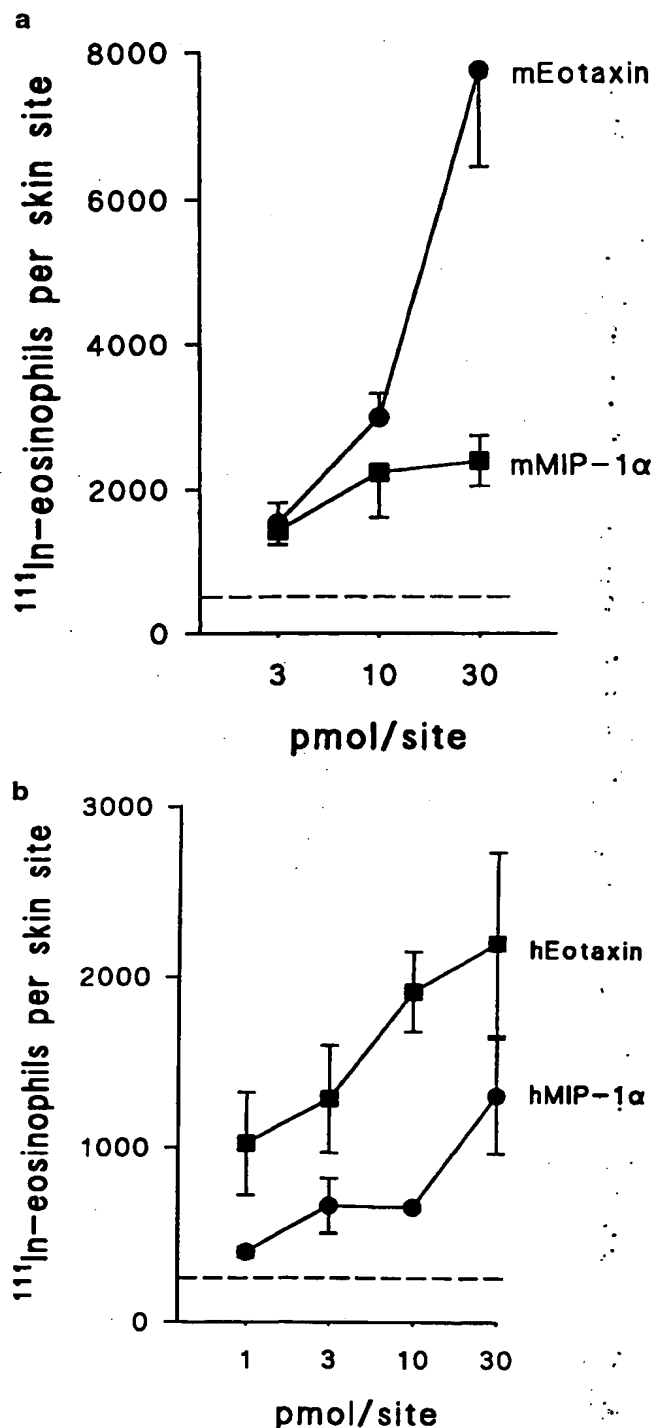


Figure 4. Eosinophil recruitment in mouse skin induced by injection of murine or human eotaxin and MIP-1 α . Eosinophils were purified from the blood of IL-5-transgenic mice, labelled with ^{111}In and 10^6 ^{111}In -eosinophils injected intravenously into nontransgenic CBA/Ca mice. 10 min later, (a) mEotaxin (3–30 pmol/site) and mMIP-1 α (3–30 pmol/site) or (b) hEotaxin (1–30 pmol/site) and hMIP-1 α (1–30 pmol/site) were injected intradermally in the same animals. After 4 h, the animals were killed, and ^{111}In -eosinophils accumulating at skin sites were quantified in a gamma counter. The dashed line represents background recruitment of ^{111}In -eosinophils in sites injected with PBS. Results are expressed as the mean \pm SEM for 4–6 animals.

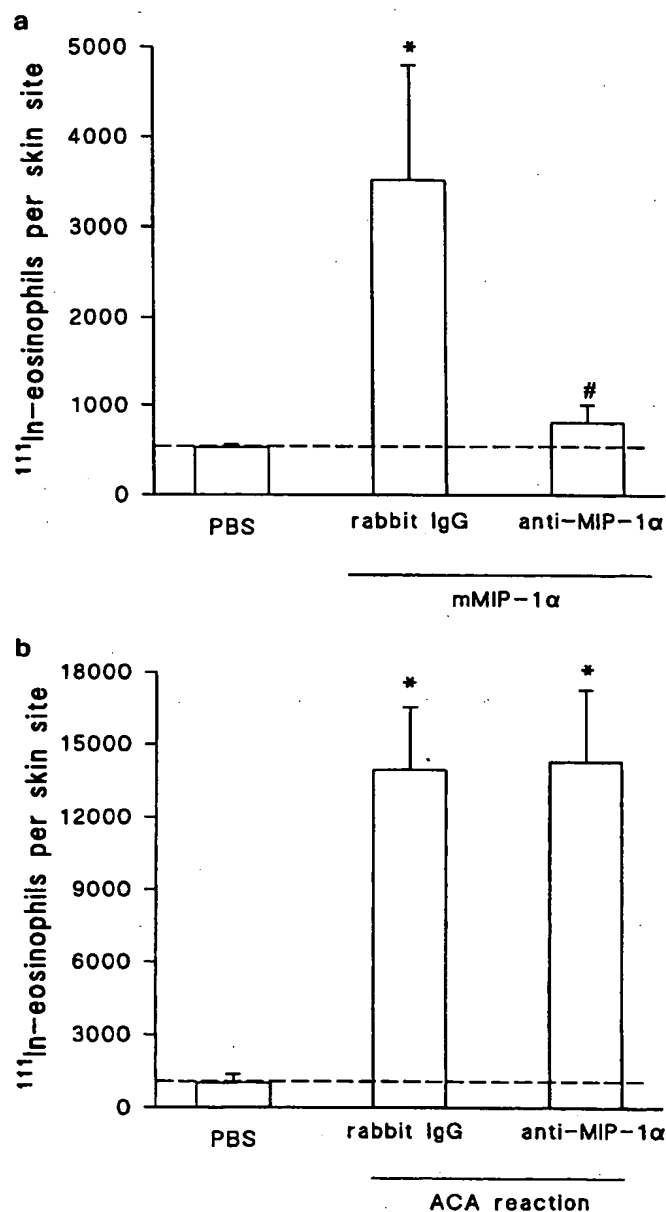


Figure 5. Effects of anti-MIP-1 α polyclonal antibody on ^{111}In -eosinophil recruitment induced by (a) mMIP-1 α and (b) in a delayed-onset allergic reaction in mouse skin. Eosinophils were purified from the blood of IL-5-transgenic mice, labelled with ^{111}In and 10^6 ^{111}In -eosinophils injected intravenously into nontransgenic CBA/Ca mice. OVA (1 $\mu\text{g}/\text{site}$) was administered intradermally 4 h before, and mMIP-1 α (10 pmol/site) 10 min after, intravenous injection of ^{111}In -eosinophils. Rabbit anti-mMIP-1 α polyclonal antibody or purified rabbit IgG were coinjected with mMIP-1 α (50 $\mu\text{g}/\text{site}$), or injected intradermally into sites of 4–8 h ACA reactions (100 $\mu\text{g}/\text{site}$) just before the intravenous injection of cells. All experiments were performed in sensitized animals. After 4 h, the animals were killed, and ^{111}In -eosinophils accumulating at skin sites were quantified in a gamma counter. The dashed line represents background recruitment of ^{111}In -eosinophils in sites injected with PBS. Results are expressed as the mean \pm SEM for five animals. * $P < 0.05$ when compared with PBS, and # $P < 0.05$ when compared with sites treated with rabbit IgG.

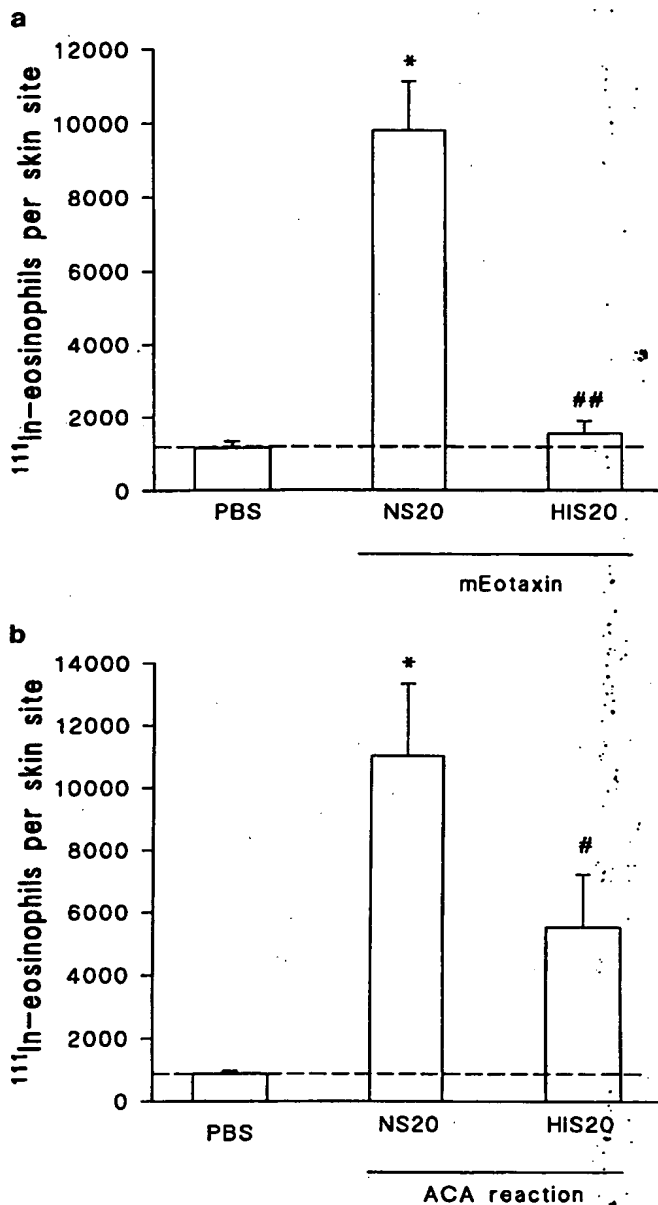


Figure 6. Suppression of ¹¹¹In-eosinophil recruitment induced by (a) mEotaxin and (b) in a delayed-onset allergic reaction in mouse skin by an antieotaxin antiserum. Eosinophils were purified from the blood of IL-5-transgenic mice, labelled with ¹¹¹In and 10⁶ ¹¹¹In-eosinophils injected intravenously into nontransgenic CBA/Ca mice. OVA (1 µg/site) was administered intradermally 4 h before, and mEotaxin (10 pmol/site) 10 min after intravenous injection of ¹¹¹In-eosinophils. Rabbit antieotaxin antiserum (HIS, 20% dilution in PBS) or rabbit nonimmune serum (NS, 20% dilution in PBS) was coinjected with mEotaxin, or injected intradermally into sites of 4–8 h ACA reactions just before intravenous injection of cells. After 4 h, the animals were killed, and ¹¹¹In-eosinophils accumulating at skin sites were quantified in a gamma counter. The dashed line represents background recruitment of ¹¹¹In-eosinophils in sites injected with PBS. Results are expressed as the mean ± SEM for five animals. **P* < 0.05 when compared with PBS. # and ## denote *P* < 0.05 and *P* < 0.01, respectively, when compared with sites treated with rabbit serum (NS).

shown). In contrast, histological analysis of skin sites injected with both C-X-C chemokines revealed a marked neutrophil infiltrate without any infiltrating eosinophils (data not shown).

Effects of anti-MIP-1α polyclonal antibody and antieotaxin antiserum on ¹¹¹In-eosinophil recruitment in a delayed-onset allergic reactions in mouse skin. To examine the role of MIP-1α and eotaxin in allergic inflammation in mouse skin, we evaluated the effects of antibodies that bind and neutralize these chemokines. Ovalbumin-sensitized mice were challenged with OVA and ¹¹¹In-eosinophil recruitment assessed from 4–8 h after antigen challenge, a period at which maximal ¹¹¹In-eosinophil recruitment occurs (M.M. Teixeira and P.G. Hellewell, unpublished observations). At a dose of 50 µg/site, the rabbit anti-mMIP-1α polyclonal antibody reduced ¹¹¹In-eosinophil recruitment induced by mMIP-1α to basal levels (Fig. 5 a). In contrast, the anti-mMIP-1α antibody used at 100 µg/site failed to modify ¹¹¹In-eosinophil recruitment in the 4–8 h ACA reaction (Fig. 5 b).

We then examined the effects of a rabbit anti-mEotaxin antiserum on ¹¹¹In-eosinophil recruitment induced by mEotaxin and in the 4–8 h ACA reaction. Dilutions of 5 and 20% of the antiserum in PBS blocked ¹¹¹In-eosinophil recruitment induced by mEotaxin by 45% and 94%, respectively (Fig. 6 a).

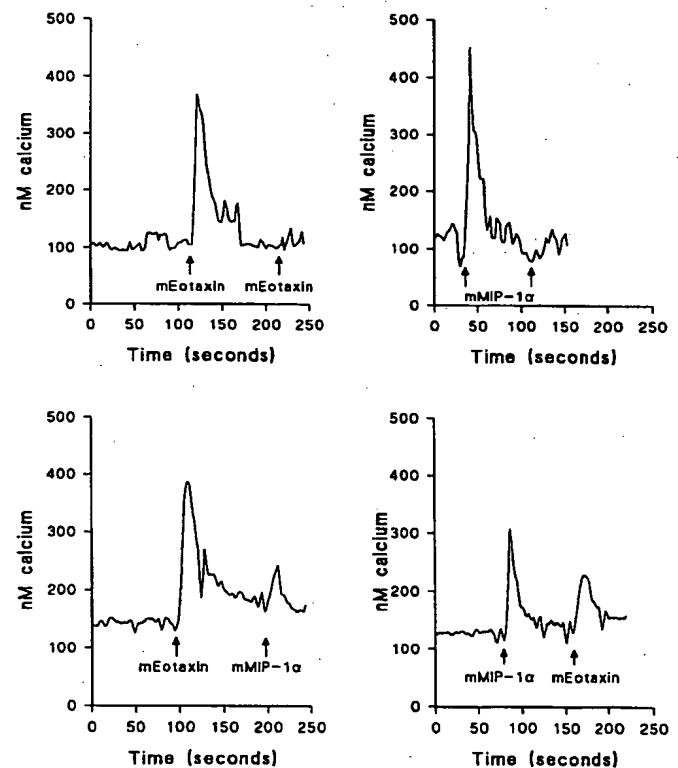


Figure 7. Changes in the intracellular calcium levels in murine eosinophils in response to mEotaxin and mMIP-1α. Eosinophils were purified from the blood of IL-5-transgenic mice and labelled with Fura-2. Changes in fluorescence after activation with eotaxin (10⁻⁸ M) and MIP-1α (10⁻⁸ M) were monitored at 37°C using a fluorimeter. The arrows indicate the time of addition of the stimulus. Results are representative of at least four experiments using cells from different donors.

The 20% antiserum dilution was then chosen to be tested against the ACA reaction. As shown in Fig. 6 *b*, intradermal injection of antieotaxin antiserum into sites of ACA reaction just before intravenous injection of ^{111}In -eosinophils, inhibited the recruitment of these cells by 55%. Together, these results suggest an important role for eotaxin, but not for MIP-1 α , in mediating eosinophil migration into sites of delayed-onset allergic inflammation in mouse skin.

Effects of mEotaxin and mMIP-1 α on intracellular calcium levels in eosinophils. Activation of eosinophils with mEotaxin induced a significant elevation in the intracellular calcium levels in eosinophils (Fig. 7). mEotaxin-induced calcium elevation was detected at concentrations $> 10^{-10}$ M eotaxin, and was maximal at 10^{-8} M (data not shown). Similarly, mMIP-1 α -induced intracellular calcium elevation in eosinophils (Fig. 7) was detected at concentrations greater than 2×10^{-9} M, and was maximal at 2×10^{-8} M (data not shown). As shown in Fig. 7, mEotaxin completely desensitized responses to further stimulation with mEotaxin, and significantly inhibited by 73% ($n = 5$) responses to a further stimulation with mMIP-1 α . Similarly, mMIP-1 α desensitized responses to itself, and partially inhibited by 52% ($n = 4$) the intracellular calcium elevation induced by a second stimulation with mEotaxin (Fig. 7). Neither mEotaxin or mMIP-1 α modified responses to a subsequent stimulation with LTB $_4$ (data not shown; see also Fig. 8 *a*).

Effects of desensitization and blockade of the eotaxin receptor on ^{111}In -eosinophil recruitment in a delayed-onset allergic reaction in mouse skin. As shown in Fig. 7, mEotaxin desensitized eosinophils to a further stimulation by mEotaxin or mMIP-1 α . To establish whether desensitized eosinophils would be impaired in their capacity to recruit *in vivo*, aliquots of the same batch of ^{111}In -eosinophils were pretreated with buffer or 10^{-8} M mEotaxin for 10 min at 37°C, and were injected intravenously into recipient animals. Compared with buffer pretreatment, pretreatment with mEotaxin significantly attenuated ^{111}In -eosinophil recruitment into skin sites induced by mEotaxin, mMIP-1 α , and in the 4–8 h ACA reaction by 51, 60, and 65%, respectively (Table I). In contrast, ^{111}In -eosinophil recruitment induced by LTB $_4$ was not altered (Table I). Pretreat-

ment of eosinophils with mEotaxin did not reduce significantly the number of ^{111}In -eosinophils circulating at 4 h (control, $7.2 \pm 0.9\%$ of total ^{111}In -eosinophils injected; mEotaxin-treated, $5.4 \pm 1.6\%$, $n = 4$).

Extension of hRANTES by retaining the initiating methionine produces a potent antagonist at the CCR1 receptor (29). To assess whether metRANTES would also inhibit the murine eotaxin receptor, we evaluated the effects of metRANTES on elevation of intracellular calcium induced by mEotaxin. As seen in Fig. 8 *a*, metRANTES significantly reduced mEotaxin- but not LTB $_4$ - induced intracellular calcium elevation in eosinophils. Thus, in addition to blocking the action of chemokines on the human CCR1 receptor (29), metRANTES also blocks the action of chemokines on the murine CCR3 receptor. Next we examined the effects of systemic treatment with metRANTES on the ^{111}In -eosinophil recruitment induced by mEotaxin and in the 4–8 h ACA reaction; metRANTES (5 $\mu\text{g}/\text{mouse}$) was administered subcutaneously 30 min before the intravenous injection of ^{111}In -eosinophils. As seen in Fig. 8 *b*, metRANTES blocked ^{111}In -eosinophil recruitment induced by eotaxin and in the ACA reaction by 45 and 68%, respectively, but had no effect on the response to LTB $_4$.

Discussion

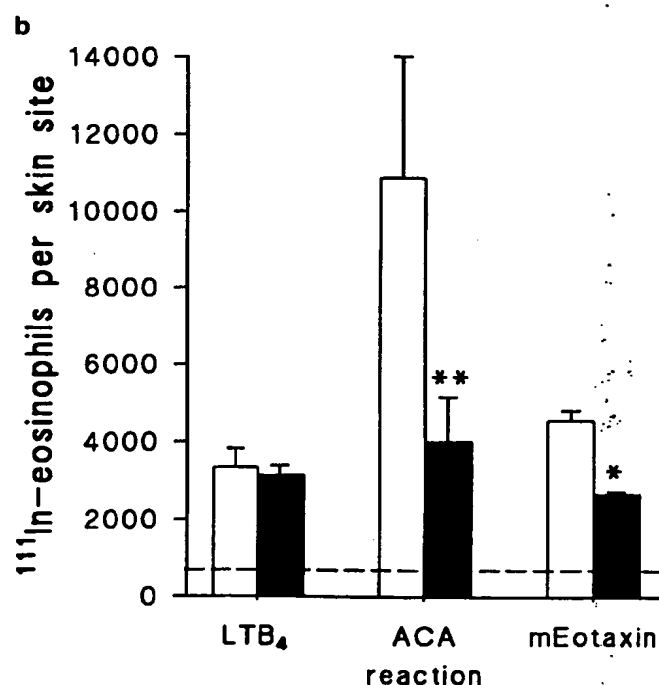
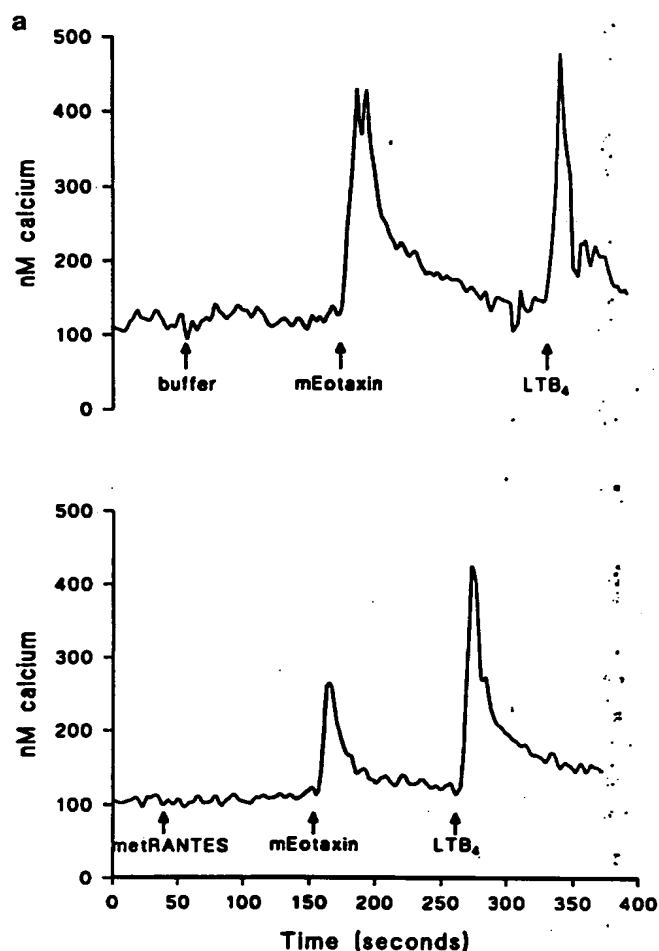
There is considerable evidence in support of an important role for eosinophils in the pathophysiology of allergic diseases such as asthma and atopic dermatitis (2, 30, 31). A detailed understanding of the molecular mechanisms that govern the eosinophil recruitment into tissues during inflammation is essential if eosinophil-specific pharmacological therapies are to be developed for treatment of allergic diseases (3). In this study, using eosinophils purified from the blood of IL-5 transgenic mice, we have evaluated and compared the *in vivo* capacity of C-C chemokines to induce eosinophil recruitment, and have assessed the role of endogenous eotaxin and of the eotaxin receptor in mediating eosinophil migration into sites of delayed-onset allergic inflammation in mouse skin.

Initial studies were carried out to investigate the chemoattractant effects of mediators previously shown to induce eosinophil recruitment when injected intradermally in the skin of guinea pigs, namely PAF, LTB $_4$, and C5a (24, 28). These inflammatory mediators induced significant cell recruitment and oedema formation when injected intradermally. Although LTB $_4$ appeared to be more effective than the other mediators, PAF induced significant migration of cells at doses as low as 5 pmol/site. Next, we examined the effects of a range of chemokines previously shown to stimulate various eosinophils functions *in vitro* (14–17, 32). Of the chemokines tested, only eotaxin and MIP-1 α induced significant recruitment of ^{111}In -eosinophils, but eotaxin was consistently more effective than was MIP-1 α . In agreement with studies evaluating the *in vitro* activation of murine eosinophils (33, 34), both human and murine recombinant proteins induced significant recruitment of ^{111}In -eosinophils. Although RANTES appears to activate human eosinophils via the eotaxin receptor CCR3 (6, 14), neither mRANTES nor hRANTES induced significant recruitment of ^{111}In -eosinophils in mouse skin. This result is consistent with the lack of effect of hRANTES on the levels of intracellular calcium in murine and guinea pig eosinophils (16, 35, 36), but contrasts with the capacity of hRANTES to induce eosinophil recruitment in dog (37) and Rhesus monkey

Table I. Desensitization of the Eotaxin Receptor Suppresses ^{111}In -eosinophil Recruitment in a Delayed-onset Allergic Reaction in Mouse Skin

Stimulus	^{111}In -eosinophils per skin site*	
	Control	mEotaxin-pretreated
PBS	772 \pm 56	662 \pm 103
LTB $_4$ 150 pmol	3166 \pm 210	3170 \pm 294
mEotaxin 10 pmol	2881 \pm 434	1705 \pm 617*
mMIP-1 α 10 pmol	2160 \pm 350	1212 \pm 117*
ACA reaction (1 μg of OVA)	15441 \pm 6219	5823 \pm 1010*

^{111}In -eosinophils were pretreated with buffer (control) or 10^{-8} M mEotaxin for 10 min at 37°C and injected intravenously into recipient animals. OVA was administered intradermally into sensitized animals 4 h before, and direct-acting chemoattractants just after, the intravenous injection of ^{111}In -eosinophils. Their recruitment was measured after a further 4 h. Results are mean \pm SEM for four animals in each group. * $P < 0.05$.



(38) skin. Moreover, the chemokines mMIP-1 β , mMCP-1/JE, hMCP-3, and hMCP-4 failed to trigger calcium flux in eosinophils (36), and failed to induce significant ¹¹¹In-eosinophil recruitment in our in vivo model. Finally, mMCP-5 failed to induce significant recruitment of ¹¹¹In-eosinophils when injected intradermally in mouse skin. This result is consistent with the lack of ability of this chemokine to activate murine eosinophils in vitro (39).

The lipid mediators and C5a induced significant oedema formation at the doses tested, but none of the chemokines had this effect. These results are in contrast to the swelling-inducing activity of hMIP-1 α and hMCP-1 when injected into the footpad of mice (40). In the latter study, immediate swelling was accompanied by mast cell degranulation and cell recruitment, although a more direct measure of increased vascular permeability was not assessed (40). Thus, it is unclear whether chemokine-induced swelling was due to oedema formation, or just to local cell infiltration. As we failed to observe any oedema formation in response to the intradermal injection of chemokines and mast cell degranulation, our results suggest that mast cell degranulation is unlikely to explain the observed recruitment of ¹¹¹In-eosinophils. Thus, our results suggest that the chemokines eotaxin and MIP-1 α are potent and effective direct inducers of ¹¹¹In-eosinophil recruitment in mouse skin.

Like human eosinophils (12), eosinophils purified from IL-5 transgenic mice have been shown to possess two receptors that mediate the action of chemokines CCR1 and CCR3 (41). To investigate whether eotaxin and MIP-1 α could activate eosinophils purified from the blood of IL-5 transgenic mice via a distinct or the same receptor, we assessed the ability of these chemokines to induce cross-desensitization of the calcium response. Both eotaxin and MIP-1 α desensitized the intracellular calcium elevation when cells were activated by the same chemokine subsequently, and markedly desensitized responses to each other at the concentrations used. As eotaxin appears not to bind to the CCR1 receptor, it is possible that both eotaxin and MIP-1 α induce intracellular calcium elevation in eosinophils by activating the CCR3 receptor. This possibility is

Figure 8. Modulation by metRANTES of (a) mEotaxin-induced intracellular calcium elevation in eosinophils, and (b) ¹¹¹In-eosinophil recruitment induced by mEotaxin, LTB₄, and in a delayed-onset allergic reaction in mouse skin. (a) Eosinophils were purified from the blood of IL-5-transgenic mice and labeled with Fura-2. Eosinophils were pretreated with buffer or MetRANTES (10⁻⁶ M) for 2 min, and were then activated with eotaxin (10⁻⁸ M). Changes in fluorescence were monitored at 37°C using a fluorimeter. The arrows indicate the time of stimulus addition. Results are representative of two experiments using cells from different donors. (b) Eosinophils were purified from the blood of IL-5-transgenic mice, labelled with ¹¹¹In and 10⁶ ¹¹¹In-eosinophils injected intravenously into nontransgenic CBA/Ca mice. OVA (1 μ g/site) was administered intradermally 4 h before, and mEotaxin (10 pmol/site) and LTB₄ (150 pmol/site) 10 min after intravenous injection of ¹¹¹In-eosinophils. MetRANTES (5 μ g/mouse, closed bars) or saline (open bars) was given subcutaneously 30 min before intravenous injection of ¹¹¹In-eosinophils. After 4 h, the animals were killed, and ¹¹¹In-eosinophils accumulating at skin sites were quantified in a gamma-counter. The dashed lines represent background recruitment of ¹¹¹In-eosinophils in sites injected with PBS. Results are expressed as the mean \pm SEM for 4–8 animals. * and ** denote $P < 0.05$ and $P < 0.01$, respectively, when compared with saline-treated animals.

in agreement with the ability of murine and human MIP-1 α to bind the mCCR3 receptor (41), but not the hCCR3 receptor (12, 13). An alternative explanation for the data, however, is that there is cross-desensitization between the CCR1 and CCR3 receptors. In this respect, it has recently been reported that MIP-1 α and eotaxin signaled via two distinct pathways (CCR1 and CCR3, respectively) in murine eosinophils purified from spleen of IL-5 transgenic mice (36, 42). These results suggest that eotaxin appears to activate the mCCR3 receptor, and MIP-1 α the mCCR1 receptor. Moreover, our results suggest that there is receptor cross-desensitization that might occur through distinct receptors as reported for chemoattractant receptors on human neutrophils (43). Further studies using receptor-specific tools are needed to clarify and evaluate the intracellular mechanisms underlying CCR1 and CCR3 receptor cross-desensitization in mouse eosinophils.

Because exogenous MIP-1 α and eotaxin induced effective recruitment of ¹¹¹In-eosinophils, we evaluated whether blockade of the action of the endogenous chemokines would modulate the recruitment of ¹¹¹In-eosinophils in sites of allergic inflammation in mouse skin. Intradermal administration of an anti-MIP-1 α polyclonal antibody completely inhibited recruitment of ¹¹¹In-eosinophils induced by MIP-1 α , but failed to modulate the recruitment of these cells in the 4–8-h ACA reaction. These results contrast with previous studies demonstrating an important role for MIP-1 α in mediating eosinophil recruitment in the lung of *Schistosoma mansoni* egg antigen-sensitized and -challenged animals (20). In the latter studies, however, the anti-MIP-1 α antibody was given before antigen challenge, and could thus modulate migration of mononuclear cells into the lung, or reduce their activation before eosinophil recruitment. In agreement with this hypothesis, MIP-1 α has been shown to play an important role in directing the chemoattraction of mononuclear inflammatory cells in the T-cell-mediated autoimmune disease, experimental autoimmune encephalomyelitis (44). Alternatively, there could be a differential role for MIP-1 α in mediating eosinophil recruitment in the lung (20) and skin (this study) of mice. In this respect, we have observed no effect of a polyclonal anti-MIP-1 α on eosinophil recruitment induced by intradermal injection of *Schistosoma* egg antigen in sensitized mice (M.M. Teixeira and P.G. Hellewell, unpublished observations).

In contrast to the lack of effect of the anti-MIP-1 α antibody, an antiserum raised against mEotaxin suppressed ¹¹¹In-eosinophil recruitment into sites of 4–8 h ACA reaction by 55%; the first study to demonstrate a role for endogenous eotaxin in mediating eosinophil recruitment into cutaneous sites of allergic inflammation. Moreover, the results are in agreement with previous studies assessing the role of endogenous eotaxin in mediating recruitment of eosinophils into the lung of allergen-sensitized mice (18, 21). Thus, blockade of eotaxin with a polyclonal antibody (18) or by target disruption of the eotaxin gene (21) showed inhibition of 56 and 70% of the number of eosinophils in the bronchoalveolar lavage fluid of mice. Similarly, there was a 50% inhibition of eosinophil recruitment into the eyes of eotaxin-deficient mice challenged with antigens of the parasite *Onchocerca volvulus* (21). Together, these studies provide strong evidence to suggest an important role for eotaxin in inducing eosinophil recruitment into sites of allergic inflammation in different tissues.

We have previously shown that blocking the eotaxin receptor with the human chemokine RANTES blocked eosinophil

recruitment in response to eotaxin in guinea pig skin (35). To evaluate whether intervention at the level of the eotaxin (CCR3) receptor would also modulate eosinophil recruitment into sites of allergic inflammation in mouse skin, two strategies were used; blockade of the receptor with metRANTES, and desensitization of the receptor with mEotaxin. Extension of hRANTES by the retention of the initiating methionine produces a protein that is a potent antagonist at the human CCR1 receptor (29). The demonstration that metRANTES also blocks the effects of mEotaxin on murine eosinophils both in vitro and in vivo demonstrates that metRANTES also acts on the mEotaxin receptor CCR3. These results are consistent with the capacity of hRANTES to act as antagonist of eotaxin-induced elevation in intracellular calcium in murine (data not shown) and guinea pig eosinophils (35). When administered systemically, metRANTES inhibited eosinophil recruitment into sites of allergic inflammation in mouse skin by 68%. Similarly, pretreatment of eosinophils with eotaxin at a concentration that desensitized eosinophils to further stimulation by eotaxin and MIP-1 α , inhibited eosinophil recruitment in sites of allergic inflammation by 65%. Interestingly, eosinophil recruitment induced by exogenous eotaxin was less inhibited by these two strategies than were responses in sites of ACA reactions. In contrast to the ACA reaction where mediators are likely to be released continuously over a protracted period, exogenous administration of eotaxin achieves a high local concentration (2×10^{-7} M) that declines. The latter may be more difficult to inhibit, and indeed the ability of eotaxin to desensitize itself has been reported to be dose-dependent, and not observed with high concentrations of the chemokine (36). Future studies with better CCR3 receptor antagonists should clarify the reasons underlying the lesser inhibition of exogenous eotaxin-induced eosinophil recruitment.

Recently, Heath et al. (45) reported that an antibody that recognizes the human CCR3 receptor effectively blocked the action of different eosinophil-active chemokines on human eosinophils in vitro. Taken together with our in vivo observations, these results suggest that blockade of the CCR3 receptor is a valid strategy to inhibit eosinophil migration in vivo, and that development of drugs that block the human CCR3 is a feasible strategy for treatment of allergic diseases in man.

Acknowledgments

This work was funded by the National Asthma Campaign and The Wellcome Trust. M.M. Teixeira is a recipient of postdoctoral fellowship from Novartis, Switzerland. N.W. Lukacs and S.L. Kunkel were supported by National Institutes of Health grants AI36302 and HL35276, respectively.

References

1. Weller, P.F. 1991. The immunobiology of eosinophils. *N. Engl. J. Med.* 324:1110–1118.
2. Butterfield, J.H., and K.M. Leiferman. 1993. Eosinophil-associated diseases. In *Immunopharmacology of Eosinophils*. H. Smith and R.M. Cook, editors. Academic Press Limited, London. 152–192.
3. Teixeira, M.M., T.J. Williams, and P.G. Hellewell. 1995. Mechanisms and pharmacological manipulation of eosinophil accumulation in vivo. *Trends Pharmacol. Sci.* 16:418–423.
4. Lukacs, N.W., R.M. Strieter, S.W. Chensue, and S.L. Kunkel. 1996. Activation and regulation of chemokines in allergic airway inflammation. *J. Leukocyte Biol.* 59:13–17.
5. Schall, T.J., and K.B. Bacon. 1994. Chemokines, leukocyte trafficking, and inflammation. *Curr. Opin. Immunol.* 6:865–873.

6. Kita, H., and G.J. Gleich. 1996. Chemokines active on eosinophils: potential roles in allergic inflammation. *J. Exp. Med.* 183:2421-2426.
7. Power, C.A., and T.N.C. Wells. 1996. Cloning and characterization of human chemokine receptors. *Trends Pharmacol. Sci.* 17:209-213.
8. Bacon, K.B., and T.J. Schall. 1996. Chemokines as mediators of allergic inflammation. *Int. Arch. Allergy Immunol.* 109:97-109.
9. Bazan, J.F., K.B. Bacon, G. Hardiman, W. Wang, D.R. Greaves, A. Zlotnik, and T.J. Schall. 1997. A new class of membrane-bound chemokine with a CX₃C motif. *Nature (Lond.)* 385:640-644.
10. Murphy, P.M. 1996. Chemokine receptors: structure, function and role in microbial pathogenesis. *Cytokine Growth Factor Rev.* 7:47-64.
11. Mackay, C.R. 1996. Chemokine receptors and T cell chemotaxis. *J. Exp. Med.* 184:799-802.
12. Ponath, P.D., S. Qin, T.W. Post, J. Wang, L. Wu, N.P. Gerard, W. Newman, C. Gerard, and C.R. Mackay. 1996. Molecular cloning and characterization of a human eotaxin receptor expressed selectively on eosinophils. *J. Exp. Med.* 183:2437-2448.
13. Daugherty, B.L., S.J. Siciliano, J. DeMartino, L. Malkowitz, A. Sironi, and M.S. Springer. 1996. Cloning, expression and characterization of the human eosinophil eotaxin receptor. *J. Exp. Med.* 183:2349-2354.
14. Kameyoshi, Y., A. Dorschner, A.I. Mallet, E. Christophers, and J. Schröder. 1992. Cytokine RANTES released by thrombin-stimulated platelets is a potent attractant for human eosinophils. *J. Exp. Med.* 176:587-592.
15. Rot, A., M. Krieger, T. Brunner, S.C. Bischoff, T.J. Schall, and C.A. Dahinden. 1992. RANTES and macrophage inflammatory protein 1 α induce the migration and activation of normal human eosinophil granulocytes. *J. Exp. Med.* 176:1489-1495.
16. Jose, P.J., D.A. Griffiths-Johnson, P.D. Collins, D.T. Walsh, R. Moqbel, N.F. Totty, O. Truong, J.J. Hsuan, and T.J. Williams. 1994. Eotaxin: a potent eosinophil chemoattractant cytokine detected in a guinea-pig model of allergic airways inflammation. *J. Exp. Med.* 179:881-887.
17. Ugucioni, M., P. Loetscher, U. Forssmann, B. Dewald, H. Li, S.H. Lima, Y. Li, B. Kreider, G. Garotta, M. Thelen, and M. Baggiolini. 1996. Monocyte chemoattractant protein 4 (MCP-4), a novel structural and functional analogue of MCP-3 and eotaxin. *J. Exp. Med.* 183:2379-2384.
18. Gonzalo, J., C.M. Lloyd, L. Kremer, E. Finger, C. Martinez-A., M.H. Siegelman, M.I. Cybulsky, and J. Gutierrez-Ramos. 1996. Eosinophil recruitment to the lung in a murine model of allergic inflammation. The role of T cells, chemokines and adhesion receptors. *J. Clin. Invest.* 98:2332-2345.
19. Lukacs, N.W., S.L. Kunkel, R.M. Strieter, K. Warming, and S.W. Chensue. 1993. The role of macrophage inflammatory protein 1 α in Schistosoma mansoni egg-induced granulomatous inflammation. *J. Exp. Med.* 177:1551-1559.
20. Lukacs, N.W., R.M. Strieter, C.L. Shaklee, S.W. Chensue, and S.L. Kunkel. 1995. Macrophage inflammatory protein-1 α influences eosinophil recruitment in antigen-specific airway inflammation. *Eur. J. Immunol.* 25:245-251.
21. Rothenberg, M.E., J.A. MacLean, E. Pearlman, A.D. Luster, and P. Leder. 1997. Targeted disruption of the chemokine eotaxin partially reduces antigen-induced tissue eosinophilia. *J. Exp. Med.* 184:1-6.
22. Dent, L.A., M. Strath, A.L. Mellor, and C.J. Sanderson. 1990. Eosinophilia in transgenic mice expressing interleukin 5. *J. Exp. Med.* 172:1425-1431.
23. Teixeira, M.M., A.G. Rossi, T.J. Williams, and P.G. Hellewell. 1994. Effects of phosphodiesterase isoenzyme inhibitors on cutaneous inflammation in the guinea-pig. *Br. J. Pharmacol.* 112:332-340.
24. Faccioli, L.H., S. Nourshargh, R. Moqbel, F.M. Williams, R. Sehmi, A.B. Kay, and T.J. Williams. 1991. The accumulation of ¹¹¹In-eosinophils induced by inflammatory mediators in vivo. *Immunology* 73:222-227.
25. Teixeira, M.M., M.A. Gienbycz, M.A. Lindsay, and P.G. Hellewell. 1997. Pertussis toxin reveals distinct early signalling events in platelet-activating factor-, leukotriene B₄- and C5a-induced eosinophil homotypic aggregation in vitro and recruitment in vivo. *Blood* 89:4566-4573.
26. Das, A.M., R.J. Flower, P.G. Hellewell, M.M. Teixeira, and M. Perretti. 1997. A novel murine model of allergic inflammation to study the effect of dexamethasone on eosinophil recruitment. *Br. J. Pharmacol.* 121:97-104.
27. Grynkiewicz, G., M. Poenie, and R.Y. Tsien. 1985. A new generation of Ca²⁺ indicators with greatly improved fluorescence properties. *J. Biol. Chem.* 260:3440-3450.
28. Teixeira, M.M., and P.G. Hellewell. 1994. Effect of a 5-lipoxygenase inhibitor, ZM 230487, on cutaneous allergic inflammation in the guinea-pig. *Br. J. Pharmacol.* 111:1205-1211.
29. Proudfoot, A.E.I., C.A. Power, A.J. Hoogerwerf, M. Montjovent, F. Borlat, R.E. Offord, and T.N.C. Wells. 1996. Extension of recombinant human RANTES by the retention of the initiating methionine produces a potent antagonist. *J. Biol. Chem.* 271:2599-2603.
30. Djukanovic, R., W.R. Roche, J.W. Wilson, C.R.W. Beasley, O.P. Twen-tyman, P.H. Howarth, and S.T. Holgate. 1990. Mucosal inflammation in asthma. *Am. Rev. Respir. Dis.* 142:434-457.
31. Leiferman, K.M. 1989. Eosinophils in atopic dermatitis. *Allergy (Copenhagen)* 44:20-26.
32. Jia, G., J. Gonzalo, C. Lloyd, L. Kremer, L. Lu, C. Martinez-A., B.K. Wershil, and J. Gutierrez-Ramos. 1996. Distinct expression and function of the novel mouse chemokine monocyte chemoattractant protein-5 in lung allergic inflammation. *J. Exp. Med.* 184:1939-1951.
33. Gonzalo, J., G. Jia, V. Aguirre, D. Friend, A.J. Coyle, N.A. Jenkins, G. Lin, H. Katz, A. Lichtman, N. Copeland, et al. 1996. Mouse eotaxin expression parallels eosinophil accumulation during lung allergic inflammation but it is not restricted to a Th2-type response. *Immunity* 4:1-14.
34. Gao, J., and P.M. Murphy. 1995. Cloning and differential tissue-specific expression of three mouse β chemokine receptor-like genes, including the gene for a functional macrophage inflammatory protein-1 α receptor. *J. Biol. Chem.* 270:17494-17501.
35. Marleau, S., D.A. Griffiths-Johnson, P.D. Collins, Y.S. Bakhle, T.J. Williams, and P.J. Jose. 1996. Human RANTES acts as a receptor antagonist for guinea pig eotaxin in vitro and in vivo. *J. Immunol.* 157:4141-4146.
36. Rothenberg, M.E., R. Ownby, P.D. Mehlhop, P.M. Loiselle, M. Van de Rijn, J.V. Bonventre, H.C. Oettgen, P. Leder, and A.D. Luster. 1996. Eotaxin triggers eosinophil-selective chemotaxis and calcium flux via distinct receptor and induces pulmonary eosinophilia in the presence of interleukin 5 in mice. *Mol. Med.* 2:334-348.
37. Meurer, R., G. van Riper, W. Feeney, P. Cunningham, D. Hora, M.S. Springer, D.E. MacIntyre, and H. Rosen. 1993. Formation of eosinophilic and monocytic intradermal inflammatory sites in the dog by injection of human RANTES but not human monocyte chemoattractant protein 1, human macrophage inflammatory protein 1 α , or human interleukin 8. *J. Exp. Med.* 178:1913-1921.
38. Ponath, P.D., S. Qin, D.J. Ringler, I. Clark-Lewis, J. Wang, N. Kassam, H. Smith, X. Shi, J. Gonzalo, W. Newman, et al. 1996. Cloning of the human eosinophil chemoattractant, eotaxin. Expression, receptor binding and functional properties suggest a mechanism for the selective recruitment of eosinophils. *J. Clin. Invest.* 97:604-612.
39. Sarafi, M.N., E.A. Garcia-Zepeda, J.A. MacLean, I.F. Charo, and A.D. Luster. 1997. Murine monocyte chemoattractant protein (MCP)-5: a novel CC chemokine that is a structural and functional homologue of human MCP-1. *J. Exp. Med.* 185:99-109.
40. Alam, R., D. Kumar, D. Anderson-Walters, and P.A. Forsythe. 1994. Macrophage inflammatory protein-1 α and monocyte chemoattractant peptide-1 elicit immediate and late cutaneous reactions and activate murine mast cells in vivo. *J. Immunol.* 152:1298-1303.
41. Post, T.W., C.R. Bozic, M.E. Rothenberg, A.D. Luster, N. Gerard, and C. Gerard. 1995. Molecular characterization of two murine eosinophil β chemokine receptors. *J. Immunol.* 155:5299-5306.
42. Gao, J., A.I. Sen, M. Kitauro, O. Yoshie, M.E. Rothenberg, P.M. Murphy, and A.D. Luster. 1996. Identification of a mouse eosinophil receptor for the CC chemokine eotaxin. *Biochem. Biophys. Res. Commun.* 223:679-684.
43. Sabroe, I., T.J. Williams, C.A. Hebert, and P.D. Collins. 1997. Chemoattractant cross-desensitization of the human neutrophil IL-8 receptor involves receptor internalization and differential receptor subtype regulation. *J. Immunol.* 158:1361-1369.
44. Karpus, W.J., N.W. Lukacs, B.L. McRae, R.M. Strieter, S.L. Kunkel, and S.D. Miller. 1995. An important role for the chemokine macrophage inflammatory protein 1- α in the pathogenesis of the T cell-mediated disease, experimental autoimmune encephalomyelitis. *J. Immunol.* 155:5003-5010.
45. Heath, H., S. Qin, L. Wu, G. LaRosa, N. Kassam, P.D. Ponath, and C.R. Mackay. 1997. Chemokine receptor usage by human eosinophils. The importance of CCR3 demonstrated using an antagonistic monoclonal antibody. *J. Clin. Invest.* 99:178-184.

COLITIS

Selective depletion of neutrophils by a monoclonal antibody, RP-3, suppresses dextran sulphate sodium-induced colitis in rats

MASAAKI NATSUI,* KATSUTOSHI KAWASAKI,[†] HIDEAKI TAKIZAWA,*
SHUN-ICHI HAYASHI,* YASUNOBU MATSUDA,* KAZUHITO SUGIMURA,*
KEIICHI SEKI,* RINTARO NARISAWA,* FUJIRO SENDO[‡] AND HITOSHI ASAKURA*

**Third Department of Internal Medicine, Niigata University School of Medicine, [†]Department of Pathology, Institute of Nephrology, Niigata University School of Medicine, Niigata and [‡]Department of Parasitology, Yamagata University School of Medicine, Yamagata, Japan*

Abstract Administration of dextran sulphate sodium to animals induces acute colitis characterized by infiltration of large numbers of neutrophils into the colonic mucosa, which histologically resembles human active ulcerative colitis. It has been reported that neutrophils and the reactive oxygen metabolites produced by them are involved in the progress of ulcerative colitis. This study was intended to clarify their roles by using this animal model. First, possible sources and species of reactive oxygen metabolites were determined using luminol-dependent chemiluminescence with addition of enzyme inhibitors and reactive oxygen metabolite scavengers. Next, to examine whether neutrophils and hypochlorous acid derived from them contribute to tissue injury, we administered RP-3, a monoclonal antibody capable of selectively depleting neutrophils, and taurine, a hypochlorous acid scavenger, to rats treated with dextran sulphate sodium. Addition of azide, taurine, catalase, superoxide dismutase and dimethyl sulphoxide into colonic mucosal scrapings significantly inhibited chemiluminescence production, but allopurinol and indomethacin had no effects. These results suggest that excessive hypochlorous acid, hydrogen peroxide, superoxide anion and hydroxyl radical are generated by the inflamed colonic mucosa. Intraperitoneal injections of RP-3 significantly suppressed bleeding, tissue myeloperoxidase activity, chemiluminescence production and erosion formation. On the other hand, administration of taurine tended to inhibit bleeding and erosion formation to some extent, although it could not significantly suppress them. These data suggest that neutrophils play an important role in the development of this colitis and that hypochlorous acid might be one of the causes of tissue injury induced by neutrophils.

Key words: colitis, dextran sulphate sodium, monoclonal antibody, neutrophil depletion.

INTRODUCTION

Although many factors have been implicated in the pathogenesis of ulcerative colitis (UC),^{1,2} its precise mechanism remains unclear. It has been proposed that neutrophils play an important role in its development, as marked infiltration of neutrophils has been identified in the colonic mucosa of patients with active UC.³ They are generally understood to contribute to the inflammatory response by secreting a variety of proteases, producing reactive oxygen metabolites (ROM), and synthesizing and releasing leukotrienes.⁴

Oral administration of dextran sulphate sodium (DSS) induces colitis in animals, which histologically mimics human UC.⁵⁻⁷ It has been reported that the actions of DSS on colonic epithelial cells, macrophages, and intestinal microflora are likely to be involved in the

pathogenesis of this colitis.^{5,6,8-10} On the other hand, we and other investigators have described the accumulation of numerous neutrophils and the excessive production of ROM in the DSS-treated colonic mucosa.^{3,7,11} Therefore, we hypothesized that neutrophils participated in the development of DSS-induced colitis. The present study was designed to investigate the role of neutrophils and the involvement of ROM derived from them in this model.

METHODS

Animals

Male Wistar rats (Charles River Japan, Kanagawa, Japan) weighing 180-200 g were housed separately in

Correspondence: Dr Masaaki Natsui, Third Department of Internal Medicine, Niigata University School of Medicine, Asahimachi-dori 1-757, Niigata 951, Japan.

Accepted for publication 23 July 1997.

524

cages under standard laboratory conditions and allowed free access to pelleted chow and tap water.

Induction of colitis

Colitis was induced by giving 9% (w/v) DSS (5000 mol weight; Wako Jyunyaku Co., Tokyo, Japan) dissolved in distilled water (DW) as drinking water for 3 days. Normal control animals were given DW for the same period. They were killed under pentobarbital anaesthesia after 3 days of the treatment.

Ex vivo luminol-dependent chemiluminescence assay

After death, the colon (except for the caecum) was removed and divided into four equal segments. Because DSS-induced inflammation was obviously dominant in the distal colon,⁵ the most distal segment was used in this assay. The mucosa scraped from this segment was placed in 980 μ L of Hanks' balanced salt solution (HBSS; Gibco BRL, Grand Island, NY, USA) and suspended by vortex for a few seconds. The suspension was equally divided and mixed with 500 μ L of HBSS with or without an enzyme inhibitor/a ROM scavenger in scintillation test tubes. The following reagents were used as inhibitors or scavengers: azide (final concentration, 1 mmol/L; Sigma Chemical Co., St. Louis, MO, USA); catalase (from bovine liver, 3000 U/mL; Sigma); taurine (20 mmol/L; Sigma); superoxide dismutase (SOD, from bovine erythrocytes, 300 U/mL; Sigma); dimethyl sulphoxide (DMSO, 5%; Sigma); allopurinol (400 mg/mL; Sigma); and indomethacin (100 mmol/L; Sigma).^{12,13} They were all dissolved in HBSS on the experimental day. The sample was placed in a chemiluminometer (Lumat LB9501; Berthold, Germany) and mixed with 10 μ L of luminol (Sigma) solution (30 mmol/L luminol and 60 mmol/L triethylamine in distilled water). The light emission was measured for 1 min immediately after addition of luminol. Chemiluminescence values were expressed as c.p.m. per mg of dry tissue after subtraction of background photon counts.

In vivo RP-3 and taurine administration assays

Monoclonal antibody (RP-3)

RP-3 is a monoclonal antibody established by hybridization of mouse myeloma cells and spleen cells of BALB/c mice sensitized with peritoneal neutrophils of Wistar-King-Aptakemann/Hok rats, and can selectively deplete rat neutrophils.¹⁴ About 2 weeks after pristane-treated BALB/c mice (Charles River Japan) were given an intraperitoneal injection of 1×10^7 hybridoma cells cultured *in vitro*, ascitic fluid rich with RP-3 was obtained. The fluid was centrifuged at 1700 g for 5 min and the supernatant was purified by precipitation with ammonium sulphate, dialysed against phosphate-buffered saline (PBS), and stored at -70°C until use. A preliminary study confirmed that an intra-

peritoneal injection of RP-3, at a dose of 60 mg/kg bodyweight, depleted circulating neutrophils to less than $100/\text{mm}^3$ within 6–24 h (data not shown).

Experimental design

To examine the role of neutrophils, animals were randomized into three groups: rats treated with DSS plus RP-3 (RP-3-treated group, $n=22$), DSS plus PBS (RP-3-control group, $n=24$), and DW plus PBS (normal group, $n=10$). They received four intraperitoneal injections of 1 mL of RP-3 (at a dose of 60 mg/kg) or PBS. The initial injection was made 6 h before oral administration of 9% DSS or DW, and the following injections were performed every 24 h.

To estimate the involvement of hypochlorous acid (HOCl) produced by neutrophils, animals were divided into two groups: rats treated with DSS plus taurine, an HOCl scavenger (taurine-treated group, $n=19$), and DSS plus PBS (taurine-control group, $n=19$).^{15,16} Seven intraperitoneal injections of 1 mL of 10% taurine or PBS were given to them. The initial injection was made using the same protocol as used for RP-3, and the others were performed every 12 h. The consumption of DSS solution per rat was measured every day. They were killed after 3 days of the treatment, and the most distal colonic segment was prepared in the same way as in the *ex vivo* luminol-dependent chemiluminescence (LDCL) assay for the determination of myeloperoxidase (MPO) activity, LDCL, and histological changes.

Assessment of clinical symptoms

Bodyweight, stool consistency, and the presence of macroscopic anal bleeding were observed every day. Faecal occult blood was also examined every day using haemoccult test Wako (Wako Jyunyaku Co.), and its degree was evaluated according to the five-grade system in arbitrary units. These data were scored according to a modification of the criteria of Cooper *et al.* (Table 1).⁷

Determination of circulating neutrophil counts

Blood samples were collected from the tail vein at 12 h after injections of RP-3 and taurine. Neutrophil, eosinophil, monocyte, and lymphocyte counts were calculated on the basis of leucocyte counts using Burkert's chamber and a triplicate of 100 cells in May-Giemsa stained blood smears.

Determination of tissue myeloperoxidase activity

Tissue MPO activity was determined by the method of Krawisz *et al.*¹⁷ Briefly, the mucosa scraped from the most distal colonic segment was homogenized in hexadecyltrimethylammonium bromide (HTAB; Sigma) buffer (0.5% HTAB in 50 mmol/L phosphate buffer, pH 6.0) on ice for 60 s. The suspension was sonicated for 10 s,

Table 1 Criteria for scoring of clinical symptoms

Score	Weight loss (%)	Stool consistency*	Faecal occult blood
0	None	Normal	-
1	1-5		+
2	5-10	Loose stool	2+
3	10-15		3+
4	> 15	Diarrhoea	4+

*Normal stool, well formed pellets; Loose stool, pasty stool which does not adhere to anus; Diarrhoea, liquid stool which adheres to anus.

freeze-thawed three times, and centrifuged at 10 000 *g* for 10 min, after which the supernatant was assayed for MPO activity. The supernatant (0.1 mL) was combined with 2.9 mL of 50 mmol/L phosphate buffer, pH 6.0, containing 0.167 mg/mL *O*-dianisidine hydrochloride (Sigma) and 0.0005% hydrogen peroxide (H_2O_2). The change in absorbance at 460 nm was measured with a spectrophotometer (U-3200; Hitachi Ltd, Tokyo, Japan). One unit of MPO activity was defined as that degrading 1 mmol of H_2O_2 per min at 25°C.

Determination of luminol-dependent chemiluminescence

The mucosal scraping from the most distal colonic segment was suspended in 990 mL of HBSS, mixed with 10 μ L of luminol solution, and placed in the chemiluminometer.

Quantitative assessment of erosion formation and infiltrating neutrophil and eosinophil counts in erosions

The most distal colonic segment was fixed in 10% buffered formalin. It was further divided into eight equal cross subsegments and embedded in paraffin. Two serial cross-sections for each subsegment were prepared. One was stained with haematoxylin and eosin (HE), and another was stained for chloroacetate esterase with naphthol AS-D chloroacetate and slightly counterstained with haematoxylin.^{18,19} The erosion and muscularis mucosa lengths in the eight subsegments were measured with an image analyser (Image Command 5098; Olympus, Tokyo, Japan). The ratio of the total erosion length to the total muscularis mucosa length was defined as 'erosion index'. Erosion areas and the numbers of neutrophils and eosinophils assembling there were also measured with the image analyser. Since neutrophils and mast cells are stained by naphthol AS-D chloroacetate procedure, neutrophils were identified by observing both the staining and the nuclear morphology. Their counts per unit area were calculated by dividing their total counts by the total erosion area.

Statistical analysis

In the *ex vivo* LDCL assay, the differences in the effects on LDCL between the various reagents and HBSS were assessed using the paired *t*-test. In both *in vivo* RP-3 and taurine administration assays, the presence of macroscopic anal bleeding between the treated group and the control group was compared using the χ^2 -test, and faecal occult blood was compared using the Mann-Whitney *U*-test. The differences in tissue MPO activity and LDCL were determined using Scheffé's test after one-way ANOVA. The differences in circulating and infiltrating inflammatory cell counts were examined using Student's *t*-test. Parametric data were expressed as mean \pm SD, while non-parametric data were expressed as median and range. The differences were considered significant if *P* value was < 0.05.

RESULTS

Effects of inhibitors and scavengers on luminol-dependent chemiluminescence

The data of the *ex vivo* LDCL assay are summarized in Fig. 1. The DSS-treated colonic mucosa produced marked elevations (6-9-fold) in LDCL compared with the normal mucosa. The addition of azide, catalase, taurine, SOD, and DMSO to the tissue suspension significantly (*P* < 0.05) suppressed LDCL production by the DSS-treated mucosa. In contrast, allopurinol and indomethacin had no significant effects on LDCL production. More than 92% of cells were found to be viable before the determination of LDCL by trypan blue exclusion.

Effects of RP-3 and taurine on DSS-induced colitis

Consumption of DSS solution

The severity of DSS-induced colitis is dependent on the consumption of DSS solution. There were no significant differences in the consumption of DSS solution between the RP-3-treated group (75 ± 12 mL/3 days, *n* = 22) and its control group (79 ± 14 mL/3 days, *n* = 24), and between the taurine-treated group (79 ± 10 mL/3 days, *n* = 19) and its control group (78 ± 9 mL/3 days, *n* = 19).

Clinical symptoms

The intraperitoneal injections of RP-3 significantly (*P* < 0.05) inhibited both macroscopic anal bleeding and faecal occult blood on day 3 compared with the control rats (Table 2), but did not affect either bodyweight nor stool consistency (data not shown). Taurine tended to suppress both macroscopic bleeding and occult blood on day 3, although significant differences were not demonstrated (Table 3).

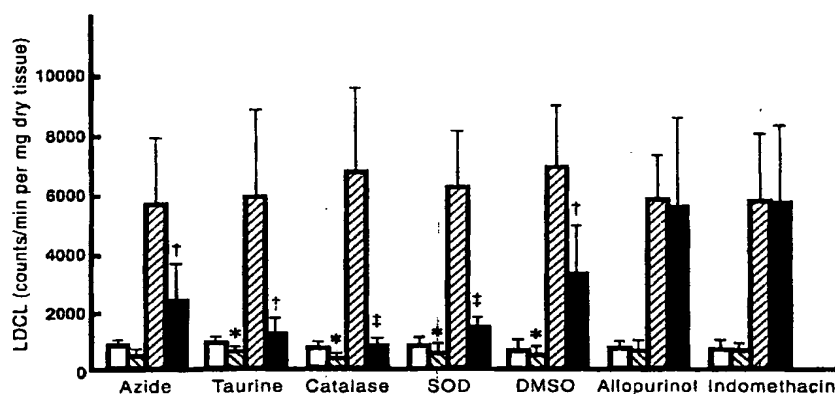


Figure 1 Effects of enzyme inhibitors and reactive oxygen metabolites (ROM) scavengers on LDCL. Each bar represents the mean value in five rats. □, Normal mucosa with Hanks' balanced salt solution (HBSS); ▨, normal mucosa with each reagent; ▤, dextran sodium sulphate (DSS)-treated mucosa with HBSS; ■, DSS-treated mucosa with each reagent; SOD, superoxide dismutase; DMSO, dimethyl sulphoxide. *Significantly different ($P < 0.05$) from normal mucosa with HBSS. † and ‡, Significantly different ($P < 0.05$ and $P < 0.01$, respectively) from DSS-treated mucosa with HBSS.

Circulating neutrophil counts

To examine the effectiveness of the treatment with RP-3, the numbers of various circulating cells were counted. RP-3 decreased circulating neutrophil counts to less than 5% of the control level (Fig. 2), but did not at all affect the numbers of eosinophils, monocytes, and lymphocytes from days 0 to 3 (data not shown). Taurine had no significant effects on the numbers of these cells including neutrophils (data not shown).

Tissue myeloperoxidase activity

Tissue MPO activity has been frequently used as an index of the accumulation of neutrophils within tissue. Although the administration of RP-3 significantly ($P < 0.05$) depressed tissue MPO activity compared with the control rats and succeeded in lowering it to the normal level (Table 2), taurine had no significant effect on MPO activity (Table 3).

Luminol-dependent chemiluminescence

The administration of RP-3 and taurine resulted in a significant ($P < 0.01$ and $P < 0.05$, respectively) reduction in LDCL compared with the control rats, but failed to lower it to the normal level (Tables 2, 3).

Erosion index and infiltrating neutrophil and eosinophil counts in erosions

Figure 3 shows typical histological features in the RP-3-treated group and its control group. The administration of 9% DSS for 3 days induced extensive erosions (a)

with prominent infiltration of neutrophils with chloroacetate activity (b). In contrast, the treatment with RP-3 produced smaller erosions (c) with fewer neutrophils (d). The administration of RP-3 statistically significantly reduced the erosion index ($P < 0.05$) and neutrophil counts in erosions ($P < 0.001$) compared with the control rats (Table 2). Taurine showed a tendency to decrease the erosion index, but no significant difference was found (Table 3). While many eosinophils were found in erosions, RP-3 and taurine had no significant effects on its counts (Tables 2,3).

DISCUSSION

Reactive oxygen metabolites have been reported to be increased in both colonic mucosa and peripheral blood of patients with inflammatory bowel disease (IBD), and the antioxidants, such as SOD and glutathione, have been shown to be decreased in their colonic mucosa.^{12,20-23} Sulphasalazine and 5-aminosalicylic acid, which are frequently used in the treatment for IBD, have been demonstrated to be potent ROM scavengers.^{24,25} Therefore, ROM are now regarded as one of the main causes of tissue injury in IBD. Potential sources of ROM in the gastrointestinal tract include oxidases such as xanthine oxidase within epithelial cells and NADPH oxidase of resident macrophages.²⁶ Neutrophils and monocytes which arrive at the inflammatory foci produce additional ROM via NADPH oxidase, MPO, and enzymes involved in arachidonate metabolism.^{12,27}

Luminol-dependent chemiluminescence is a sensitive and simple method capable of detecting ROM. However, it is non-specific, because luminol is oxidized by any oxidant to produce chemiluminescence. Therefore, we attempted to identify the sources and

Table 2 Effects of RP-3 treatment on various parameters

	Normal	RP-3 control	RP-3 treated
Faecal occult blood on day 3 (U)	NA	3 (1-4) (n = 24)	2 (0-4) [‡] (n = 22)
Tissue MPO activity ($\times 10^{-3}$ U/mg wet tissue)	1.52 \pm 0.48 (n = 5)	3.01 \pm 0.72* (n = 5)	1.64 \pm 0.75 [‡] (n = 5)
LDCL (counts/min per mg dry tissue)	869.9 \pm 216.4 (n = 5)	5118.3 \pm 1837.4 [‡] (n = 11)	3123.3 \pm 1213* [‡] (n = 9)
Erosion index (%)	NA	4.08 \pm 2.20 (n = 8)	1.57 \pm 1.02 [‡] (n = 8)
Neutrophil counts in erosion (per mm ²)	NA	534 \pm 161 (n = 8)	119 \pm 37 [‡] (n = 8)
Eosinophil counts in erosion (per mm ²)	NA	258 \pm 72 (n = 8)	221 \pm 60 (n = 8)

NA, Not applicable; * and [‡], significantly different ($P < 0.05$ and $P < 0.001$, respectively) from normal group; [‡], [§] and [†], significantly different ($P < 0.05$, $P < 0.01$ and $P < 0.001$, respectively) from control group.

MPO, Myeloperoxidase; LDCL, luminol-dependent chemiluminescence.

Table 3 Effects of taurine treatment on various parameters

	Taurine control	Taurine treated
Faecal occult blood on day 3 (U)	3 (1-4) (n = 19)	2 (1-4) (n = 19)
Tissue MPO activity ($\times 10^{-3}$ U/mg wet tissue)	3.33 \pm 0.56 (n = 6)	3.03 \pm 0.53 (n = 6)
LDCL (counts/min per mg per dry tissue)	6029.8 \pm 3445.0 (n = 6)	2348.9 \pm 1626.2 [†] (n = 6)
Erosion index (%)	4.30 \pm 2.95 (n = 7)	2.74 \pm 2.64 (n = 7)
Neutrophil counts in erosion (per mm ²)	532 \pm 102 (n = 7)	495 \pm 97 (n = 7)
Eosinophil counts in erosion (per mm ²)	247 \pm 65 (n = 7)	241 \pm 70 (n = 7)

*Significantly different ($P < 0.05$) from control group. MPO, Myeloperoxidase; LDCL, luminol-dependent chemiluminescence.

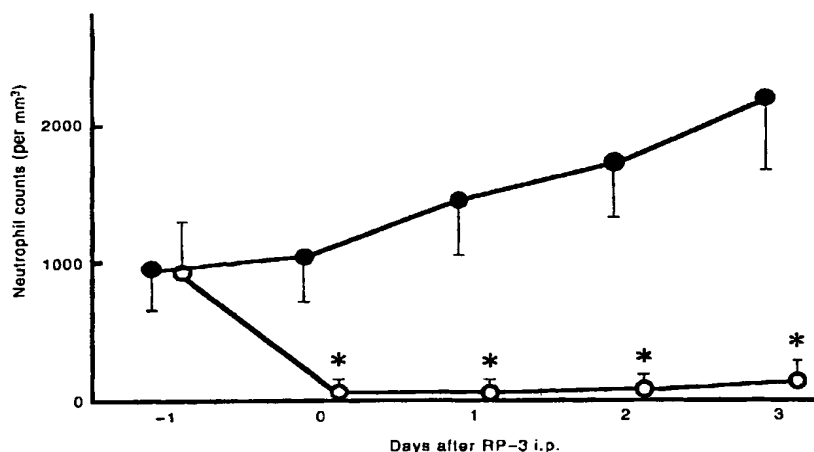


Figure 2 Effect of RP-3 treatment on circulating neutrophil counts. ●, RP-3 control (n = 24); ○, RP-3 treated (n = 22). *Significantly different ($P < 0.001$) from control group.

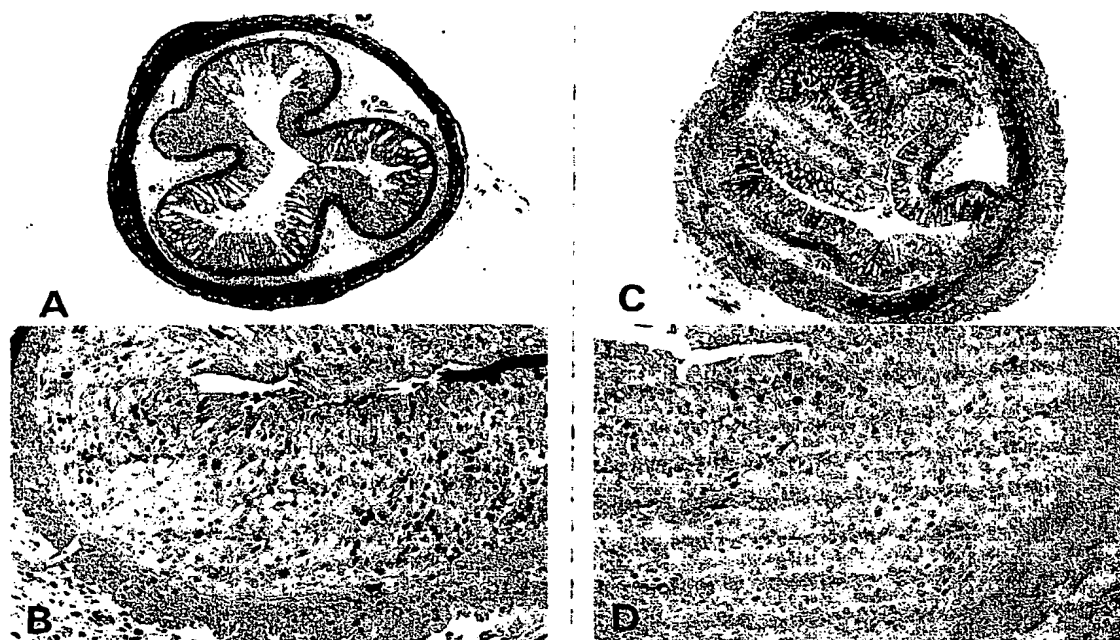


Figure 3 Representative histological appearance of colonic segments. (a) A colonic wall from RP-3-control group (HE $\times 20$). (b) A magnified view of Fig. 3a (naphthol AS-D, chloroacetate esterase, $\times 160$). Many neutrophils are strongly positive. (c) A colonic wall from RP-3-treated group (HE $\times 20$). (d) A magnified view of Fig. 3c, (naphthol AS-D chloroacetate esterase, $\times 160$).

species of ROM by addition of enzyme inhibitors and ROM scavengers to the mucosal scrapings. A significant decrease in LDCL by addition of azide is probably largely caused by its inhibition of MPO indispensable for HOCl production (Fig. 1). However, other pathways cannot be excluded as azide also inhibits other haem proteins such as catalase and cytochrome P450, and quenches singlet oxygen and hydroxyl radical ($\cdot\text{OH}$).^{12,13} The inhibition of LDCL production by taurine implies excessive HOCl production in this system (Fig. 1). However, it has been known that H_2O_2 and HOCl can efficiently co-oxidize luminol to enhance chemiluminescence.²⁸ It appears likely that taurine inhibits LDCL production by not only scavenging HOCl but also blocking co-oxidation of luminol by H_2O_2 and HOCl. Neutrophils almost exclusively contain MPO and so they are considered to be the main site of HOCl production.²⁶ As monocytes contain less MPO and lose it when they mature into tissue macrophages, monocytes but not macrophages can generate HOCl.^{29,30} Hypochlorous acid is a powerful oxidant which may attack membrane-associated targets. Moreover, it also inactivates antiproteases which inhibit elastase, and activates both collagenase and gelatinase released from neutrophils. In this way, neutrophils can create an environment where these proteolytic enzymes can break down tissue.³¹ As

H_2O_2 is relatively stable as a ROM and unable to efficiently oxidize luminol, it is likely that catalase decreases LDCL by scavenging H_2O_2 available as a precursor of HOCl and $\cdot\text{OH}$.^{4,26} The addition of SOD, a superoxide anion ($\text{O}_2^{\cdot-}$) scavenger, suppressed LDCL production (Fig. 1), suggesting that $\text{O}_2^{\cdot-}$ is one of the ROM responsible for luminol oxidation. Because the spontaneous dismutation of $\text{O}_2^{\cdot-}$ proceeds rapidly, the cytotoxicity associated with $\text{O}_2^{\cdot-}$ is generally ascribed to its role as a precursor of more powerful ROM.^{4,26} A significant decrease in LDCL by preincubation with DMSO, an $\cdot\text{OH}$ scavenger, suggests that $\cdot\text{OH}$ is also one of the ROM detected in the inflamed mucosa (Fig. 1). It is possible that $\cdot\text{OH}$ is produced by iron-catalysed oxidation of H_2O_2 (Fenton's reaction), since the inflamed mucosa contains erythrocytes/haemoglobin/haem.³² Because H_2O_2 is consumed by MPO prior to the Fenton's reaction, neutrophils with a large amount of MPO limit $\cdot\text{OH}$ formation, but macrophages without MPO may enhance it.³³ Dimethyl sulphoxide and catalase seem to prevent iron-catalysed oxidation of luminol by scavenging $\cdot\text{OH}$ and H_2O_2 . The $\cdot\text{OH}$ is a strong oxidant, but there has been little convincing evidence that it plays a major pathogenic role in human IBD or animal experimental colitis.¹² Neither allopurinol nor indomethacin affected LDCL (Fig. 1), indicating that a xanthine/xanthine oxidase

system and cyclo-oxygenase metabolites of arachidonate are probably not involved in ROM production.

As we demonstrated that many neutrophils assembled in erosions¹¹ and that HOCl was increased in the colonic mucosal scrapings, we assumed that neutrophils might be involved in the development of this colitis by producing HOCl. To determine whether neutrophils contribute to tissue injury, we rendered rats neutropenic by administering RP-3. Neutropenia led to a reduction not only of tissue MPO activity, but also of macroscopic anal bleeding, faecal occult blood, the erosion index, and LDCL (Table 2). These data indicated that infiltrating neutrophils are important in the progression of this model. Next, to examine whether HOCl influences tissue damage, we injected taurine to rats. Although taurine did not scavenge all HOCl, it significantly diminished LDCL and tended to improve macroscopic bleeding, occult blood, and the erosion index to some extent. These results illustrate that HOCl might be involved in tissue injury in this model.

Previous studies have attempted to prevent neutrophils from infiltrating into the colonic mucosa by administration of antineutrophil serum, anti-CD18 antibody, or leuadin which inhibits the expression of β_2 -integrins.^{34,39} Despite a significant decrease in tissue MPO activity, not all of these studies demonstrated improvement in gross and histological changes. It is difficult to account for the discrepancies between our data and theirs, but the direct mucosal toxicity of acetic acid or trinitrobenzene sulphonic acid/ethanol which they used to induce colitis might have been stronger than that of DSS as those agents produced colitis sooner and more severely than DSS.

Despite a satisfactory decrease in tissue MPO activity, RP-3 could not reduce LDCL to the normal level and not completely inhibit erosion formation (Table 3). Thus, in estimating the pathogenesis of DSS-induced colitis, we should consider not only neutrophils, but also other factors. Dextran sulphate sodium may directly damage colonic epithelial cells, since it has been shown to inhibit proliferation of rat small intestinal epithelial cells and mouse colon epithelial carcinoma cells *in vitro*.^{8,9} Okayasu *et al.*⁵ histologically demonstrated the phagocytosis of DSS by many macrophages, and Dieleman *et al.*⁹ demonstrated the increased production of macrophage-derived cytokines, such as tumour necrosis factor and interleukin-1 β , in DSS-induced colitis. These findings support the hypothesis that DSS phagocytosed by macrophages activates these cells and initiates tissue injury. In this study it was found that many eosinophils gathered into erosions (Tables 2,3) and it has been reported that they can yield more ROM than neutrophils in certain conditions.⁴⁰ Thus, eosinophils as well as monocytes and macrophages^{29,33} may have produced the remnant LDCL which RP-3 failed to suppress, and participated in the formation of this colitis. In addition, various changes in the intestinal microflora population caused by DSS may influence this model.¹⁰

In this context, it should be concluded that: (i) various ROM are excessively produced in the rat colonic mucosa damaged by DSS; (ii) neutrophils play a pivotal role in the progress of DSS-induced colitis;

and (iii) because the *in vivo* administration of taurine as a HOCl scavenger had a tendency to prevent this colitis, HOCl might be one of the candidates involved in tissue injury caused by neutrophils.

REFERENCES

- 1 Krisner JB, Shorter RG. Recent developments in non-specific inflammatory bowel disease. *N. Engl. J. Med.* 1982; 306: 775-84.
- 2 Cello JP, Schneiderman DJ. Ulcerative colitis. In: Sleisenger M, eds. *Gastrointestinal Disease*. Philadelphia: WB Saunders, 1989; 1435-77.
- 3 Morson BC. Pathology of ulcerative colitis. In: Krisner JB, Shorter RG, eds. *Inflammatory Bowel Disease*. Philadelphia: Lea Febinger, 1980; 281-95.
- 4 Winterbourn CC. Neutrophil oxidants: production and reactions. In: Das DK, Essman WB, eds. *Oxygen Radicals: Systemic Events and Disease Processes*. Basel: Karger, 1990; 31-70.
- 5 Okayasu I, Hatakeyama S, Yamada M, Ohkusa T, Inagaki Y, Nakaya R. A novel method in the induction of reliable experimental acute and chronic ulcerative colitis in mice. *Gastroenterology* 1990; 98: 694-702.
- 6 Ohkusa T. Production of experimental ulcerative colitis in hamsters by dextran sulfate sodium and change in intestinal microflora. *Jpn. J. Gastroenterol.* 1985; 82: 1327-36.
- 7 Cooper HS, Murthy SNS, Shah RS, Sedergran DJ. Clinicopathologic study of dextran sulfate sodium experimental murine colitis. *Lab. Invest.* 1993; 69: 238-49.
- 8 Yan Chen. Effect of dextran sulfate sodium on the proliferative activity of intestinal crypt epithelial cells. *Gastroenterology* 1994; 106: A663.
- 9 Dieleman LA, Ridwan BU, Tennyson GS, Beagley KW, Bucy RP, Elson CO. Dextran sulfate sodium-induced colitis occurs in severe combined immunodeficient mice. *Gastroenterology* 1994; 107: 1643-52.
- 10 Ohkusa T, Yamada M, Takenaga T *et al.* Protective effect of metronidazole in experimental ulcerative colitis induced by dextran sulfate sodium. *Jpn. J. Gastroenterol.* 1987; 84: 2337-46.
- 11 Takizawa H, Shintani N, Natsui M *et al.* Activated immunocompetent cells in rat colitis mucosa induced by dextran sulfate sodium and not complete but partial suppression of colitis by FK506. *Digestion* 1995; 56: 259-64.
- 12 Simmonds NJ, Allen RE, Stevens TRJ, Van Someren RNM, Blake DR, Rampton DS. Chemiluminescence assay of mucosal reactive oxygen metabolites in inflammatory bowel disease. *Gastroenterology* 1992; 103: 186-96.
- 13 Keshavarzian A, Sedghi S, Kanofsky J *et al.* Excessive production of reactive oxygen metabolites by inflamed colon: analysis by chemiluminescence probe. *Gastroenterology* 1992; 103: 177-85.
- 14 Sekiya S, Gotoh S, Yamashita T, Watanabe T, Saitoh T, Sendo F. Selective depletion of rat neutrophils by *in vivo* administration of a monoclonal antibody. *J. Leukoc. Biol.* 1989; 46: 96-102.
- 15 Nakashima T, Taniko T, Kuriyama K. Therapeutic effect of taurine administration on carbon tetrachloride-induced hepatic injury. *Jpn. J. Pharmacol.* 1982; 32: 583-9.

- 16 Venkatesan N, Chandrakasan G. In vivo administration of taurine and niacin modulate cyclophosphamide-induced lung injury. *Eur. J. Pharmacol.* 1994; 292: 75-80.
- 17 Krawisz JE, Sharon P, Stenson WF. Quantitative assay for acute intestinal inflammation based on myeloperoxidase activity. *Gastroenterology* 1984; 87: 1344-50.
- 18 Yam LT, Li CY, Crosby WH. Cytochemical identification of monocytes and granulocytes. *Am. J. Clin. Pathol.* 1971; 55: 283-90.
- 19 Jaeschke H, Farhood A, Fisher MA, Smith CW. Sequestration of neutrophils in the hepatic vasculature during endotoxemia is independent of β_2 integrins and intercellular adhesion molecule-1. *Shock* 1996; 6: 351-6.
- 20 Suematsu M, Suzuki M, Kitahara T et al. Increased respiratory burst of leukocytes in inflammatory bowel disease - the analysis of free radical generation by using chemiluminescence probe. *J. Clin. Lab. Immunol.* 1987; 24: 125-8.
- 21 Mulder TPJ, Verspaget HW, Janssens AR, Pena AS, Griffioen G, Weterman IT. Decreased levels of antioxidant proteins in the intestinal mucosa of patients with inflammatory bowel disease (IBD). *Gut* 1990; 31: A465 (abstract).
- 22 Lauterburg BH, Bilzer M, Rowedder E, Inauen W. Decreased glutathione in inflamed mucosa in man. Possible role of hypochlorous acid and prevention by 5-aminosalicylic acid. In: MacDermott RP, eds. *Inflammatory Bowel Disease: current status and future approach*. New York: Elsevier Science Publishers BV, 1988; 273-6.
- 23 Buffinton GD, Doe WF. Depleted mucosal antioxidant defences in inflammatory bowel disease. *Free Radic. Biol. Med.* 1995; 19: 911-18.
- 24 Miyachi Y, Yoshioka A, Imamura S, Niwa Y. Effect of sulfasalazine and its metabolites on the generation of reactive oxygen species. *Gut* 1987; 28: 190-5.
- 25 Williams JG, Hallett MB. Effect of sulphasalazine and its metabolite, 5-aminosalicylic acid, on toxic oxygen metabolite production by neutrophils. *Gut* 1989; 30: 1581-9.
- 26 Grisham MB, Granger DN. Neutrophil-mediated mucosal injury. Role of reactive oxygen metabolites. *Dig. Dis. Sci.* 1988; 33: S6-15.
- 27 Blake DR, Allen RE, Lunec J. Free radicals in biological systems-a review oriented to inflammatory processes. *Br. Med. Bull.* 1987; 43: 371-85.
- 28 Brestel EP. Co-oxidation of luminol by hypochlorite and hydrogen peroxide implications for neutrophil chemiluminescence. *Biochem. Biophys. Res. Commun.* 1985; 126: 482-8.
- 29 Johansson A, Dahlgren C. Characterization of the luminol-amplified light-generating reaction induced in human monocytes. *J. Leukoc. Biol.* 1989; 45: 444-51.
- 30 Wang JF, Komarov P, de Groot H. Luminol chemiluminescence in rat macrophages and granulocytes: the role of NO, O₂^-/H₂O₂, and HOCl. *Arch. Biochem. Biophys.* 1993; 304: 189-96.
- 31 Weiss SJ. Tissue destruction by neutrophils. *N. Engl. J. Med.* 1989; 320: 365-76.
- 32 Tatsu Y, Yoshikawa S. Homogeneous chemiluminescent immunoassay based on complement-mediated hemolysis of red blood cells. *Ann. Chem.* 1990; 62: 2103-6.
- 33 Britigan BE, Coffman TJ, Adelberg DR, Cohen MS. Mononuclear phagocytes have the potential for sustained hydroxyl radical production. *J. Exp. Med.* 1988; 168: 2367-72.
- 34 Sekizuka E, Grisham MB, Li M, Deitch EA, Granger DN. Inflammation-induced intestinal hyperemia in the rat: role of neutrophils. *Gastroenterology* 1988; 95: 1528-34.
- 35 Wallace JL, Keenan CM. Leukotriene B₄ potentiates colonic ulceration in the rat. *Dig. Dis. Sci.* 1990; 35: 622-9.
- 36 Yamada T, Zimmerman BJ, Specian RD, Grisham MB. Role of neutrophils in acetic acid-induced colitis in rats. *Inflammation* 1991; 15: 399-411.
- 37 Buell MG, Berin MC. Neutrophil-independence of the initiation of colonic injury. *Dig. Dis. Sci.* 1994; 39: 2575-88.
- 38 Wallace JL, Higa A, McKnight GW, MacIntyre DE. Prevention of experimental colitis by a monoclonal antibody which inhibits leukocyte adherence. *Inflammation* 1992; 16: 343-54.
- 39 Noronha-Blob L, Lowe VC, Muhlhauser RO, Burch RM. NPC 15669, an inhibitor of neutrophil recruitment, is efficacious in acetic acid-induced colitis in rats. *Gastroenterology* 1993; 104: 1021-9.
- 40 Petreccia DC, Nauseef WM, Clark RA. Respiratory burst of normal human eosinophils. *J. Leukoc. Biol.* 1987; 41: 283-8.

Depletion of T Lymphocytes with Immunotoxin Retards the Progress of Experimental Allergic Encephalomyelitis in Rhesus Monkeys

Huaizhong Hu,* Scott Stavrou,* Belinda Cairns Baker,† Carlo Tornatore,† Joshua Scharff,* Paul Okunieff,‡ and David M. Neville, Jr.*¹

*Section on Biophysical Chemistry, Laboratory of Molecular Biology, National Institute of Mental Health, National Institutes of Health, Building 36, Room 1B08, 36 Convent Drive, Bethesda, Maryland 28092-4034; †Molecular Therapeutics Section, Laboratory of Molecular-Medicine, National Institute of Neurological Disorders and Stroke, National Institutes of Health, Bethesda, Maryland; and ‡Radiation Oncology Branch, National Cancer Institute, National Institutes of Health, Bethesda, Maryland

Received November 25, 1996; accepted February 6, 1997

FN18-CRM9 is an anti-rhesus anti-CD3 immunotoxin that can transiently deplete T cells to 1% of initial values in both the blood and lymph node compartments and can induce long-term tolerance to mismatched renal allografts. We have investigated the ability of this immunotoxin to interdict the course of an experimental rhesus T-cell-driven autoimmune disease, experimental allergic encephalomyelitis (EAE) induced by myelin basic protein. Monkeys showing CSF pleocytosis were then treated with FN18-CRM9 alone or in combination with cranial irradiation (325 or 650 cGy). EAE in nontreated control monkeys progressed rapidly. Paralysis occurred 4-6 days after CSF pleocytosis. Paralysis was either delayed or never occurred in treated monkeys, and histopathology revealed few inflammatory plaques that were notable for their low or absent T cell content. While T cells repopulate in the periphery posttreatment, they do not return to the CNS in large numbers, suggesting that the newly repopulated T cells have lost their previously acquired CNS homing capability. Anti-CD3 immunotoxin may be useful in treating clinical T-cell-driven autoimmune diseases such as rheumatoid arthritis and multiple sclerosis.

INTRODUCTION

Experimental allergic encephalomyelitis (EAE) is an inflammatory T-cell-mediated autoimmune disease of the central nervous system that can be induced in a number of species by immunization with CNS components such as myelin basic protein (MBP) and adjuvant (1-6). In humans, MBP-reactive T cells are thought to initiate acute disseminated encephalomyelitis that

follows infection or vaccination (4). EAE has also served for the testing of therapies for multiple sclerosis with variable predictive results (7). EAE is a far from perfect model for multiple sclerosis. In part this is due to the variability of the model in different genetic backgrounds, observed in both inbred rodents and outbred nonhuman primates. In the latter case the disease ranges between monophasic and self-limiting, relapsing-remitting and monophasic hyperacute. However, more than any other disease model, EAE has contributed to current concepts of T-cell-mediated organ-specific immunity and has permitted a dissection of immune effector and suppressor mechanisms (7).

T lymphocytes play a central role in the induction phase of EAE. This has been demonstrated by adoptive transferring of MBP-reactive T cells to induce EAE in naive syngeneic rodents and in unimmunized *Callithrix jacchus* marmoset (1, 2, 4). Moreover, it has been shown recently that T cell receptor transgenic mice specific for MBP develop spontaneous EAE at a very high incidence (8). However, it is less clear what part T cells play in the ongoing disease, and what part is played by other activated cells that have the capacity to secrete chemokines such as monocytes, macrophages, and astrocytes (9-11) and the capacity to present CNS antigens.

We have recently constructed an immunotoxin (IT) composed of an anti-rhesus monkey CD3 monoclonal antibody (mAb), FN18, and a binding site mutant of diphtheria toxin (DT), CRM9 (12). This immunotoxin, FN18-CRM9, is an analogue of UCHT1-CRM9, an anti-human CD3 immunotoxin which is capable of regressing established xenografted human T cell (Jurkat) tumors in nude mice via protein synthesis inhibition (13). A truncated toxin engineered fusion protein version of UCHT1-CRM9 has also been constructed that displays resistance to blockade by human anti-DT antibodies arising from immunizations with DT toxoid (14). When FN18-CRM9 was given iv to a group of rhesus

¹ To whom correspondence should be addressed.

monkeys, blood and lymph node T cells were depleted within 48 h in a dose-dependent manner to levels as low as 1% of initial values. Other blood cells were not affected. This resulted in a marked population inversion of T and B cells in the blood and lymph node compartments. T cell repopulation then occurred and was rapid in juvenile animals (2–4 weeks) and slower in older animals (12). Monkeys treated in this manner become tolerized to mismatched renal allografts (15). This novel immunotoxin enabled us to investigate EAE progression in the absence of the peripheral T cell population that experienced immunization with the encephalitogenic MBP. In some monkeys in this study we combined IT with cranial irradiation for the purpose of inducing CNS T cell cyto-reduction. This was done because of concern that T cells within the CNS blood-brain barrier sanctuary might not be accessible to blood compartment IT and might not be depleted. We report in this communication that IT-induced transient T cell depletion with or without cranial irradiation markedly attenuates EAE progression and greatly reduces CNS cellular infiltrates, eliminating detectable perivascular infiltrates in some monkeys.

MATERIALS AND METHODS

Animals. Thirteen rhesus monkeys (*Macaca mulatta*) 4–6 years of age obtained from the Texas Primate Center (Alice, Texas) comprised this study. All were negative for antibodies directed at diphtheria toxin.

Immunotoxin construction. FN18 is a murine IgG1 monoclonal antibody directed at rhesus CD3 and activates T cells in the presence of mixed mononuclear cells (16). CRM9 is a binding site mutant of DT, and has only 1/300 the systemic toxicity of wild-type DT (17). The immunotoxin, FN18–CRM9, was synthesized as previously described by thiolating both FN18 and CRM9 moieties and then crosslinking with bismaleimido-hexane. The 1:1 complex used in this study was purified by size exclusion (12).

EAE induction and treatment. Rhesus monkeys were used in accordance with NIH guidelines in a protocol approved by the NIMH ACUC. Monkey brain MBP (lot 95 from African green monkeys) purified by the batch method was kindly provided by G. E. Deibler (18). We modified a protocol kindly supplied by L. M. Rose and E. C. Alvord Jr. in which the ratio of monkey MBP to heat-killed mycobacteria is set at 2:1. Aqueous MBP at 20 mg/ml was emulsified with an equal volume of complete Freund's adjuvant (DIFCO) containing 10 mg/ml heat-killed *Mycobacterium tuberculosis* (H37 RA, DIFCO Laboratories, Detroit, MI). Each rhesus monkey was immunized with intradermal injection of 0.2 ml emulsion distributed between two sites above the ankle on both hind legs. In 12 monkeys cerebrospinal fluid (CSF), 1.5-ml samples, was collected by punc-

ture into the subarachnoid space at the cisternal magna. This was done once a day for 5 consecutive days starting from 11 days after the immunization. The 13th monkey was used to provide lymph node T and B cell data pre- and post-IT.

Four monkeys were used as nontreated controls, 4 were treated with FN18–CRM9 alone, and 4 were treated with FN18–CRM9 in conjunction with cranial irradiation. The first 8 monkeys were immunized as pairs and were randomly assigned prior to immunization to either the nontreatment group or the FN18–CRM9 treatment group. FN18–CRM9 was administered to monkeys in 2 split doses by intravenous bolus infusion at a total amount of 0.2 mg/kg. The first dose of the immunotoxin was given to monkeys on the same day when an increase in CSF WBC > 30 cells/ μ l was detected. This day was considered as Day 0. The second dose of FN18–CRM9 was infused on Day 2. Radiation was given in one fraction of 650 cGy (monkeys 1144, 1109), one fraction of 325 cGy (1181), or two daily fractions of 325 cGy (1106) using opposed lateral shaped X-ray fields generated by a linear accelerator. The radiation was delivered to anesthetized air-breathing animals on Day 1 following CSF pleocytosis (1109, 1181, 1144) or Day 3 (1106) and covered the entire cranial vault down to C2 with shielding of the orbit, oral cavity, pharynx, and most of the parotid. The dose rate was \approx 100 cGy/min. Monkeys with EAE were monitored at least twice each day. The disease activity was scored as 0–5 using an EAE scoring system described previously by Massacesi and co-workers (3) and detailed in the legend to Fig. 1. EAE monkeys were euthanized under the following conditions: 1, obvious neurologic signs such as ataxia and tremors lasting 2 days or an inability of self feeding; 2, one or more limbs paralyzed; 3, 60 days after the immunization. Monkeys were euthanized by intravenous injection of 3 ml euthanasia-5 solution (Veterinary Laboratories Inc., Lenexa, KS). Brains and brain stems were surgically removed immediately following euthanasia and saline perfusion through the left ventricle and stored at -80°C for histologic examination.

Flow cytometry. Both blood and CSF samples were analyzed with flow cytometry utilizing a lysis method (12). The following mAb reagents that have been demonstrated to be reactive to rhesus monkey lymphocytes were used (19): fluorescein isothiocyanate (FITC)- or phycoerythrin (PE)-conjugated mAbs reactive with the lymphocyte surface antigens CD3 (FN18–FITC, this lab), CD20 (B1-PE, Coulter Corp., Hialeah, FL), CD4 (OKT4–FITC, Ortho Diagnostic Systems Inc., Raritan, NJ), CD8 (DK25–PE, DAKO Corporation, Carpinteria, CA), CD2 (T11–PE, Coulter), CD16 (3G8–FITC, AMAC, Inc., Westbrook, ME), CD25 (IL-2R1–PE, Coulter), CD45RA (2H4–PE, Coulter).

to very low levels compared with that before IT treatment ($P < 0.01$). These low levels of T cells remained for about 10–14 days. Note also the marked inversion of the lymph node T/B cell ratio.

Previous studies showed that EAE in rhesus monkeys had an acute onset and caused death within days (5, 6). This is confirmed by our data. As shown in Fig. 1A, EAE in all 4 nontreated control monkeys reached grade 3 disease within 3 days after the onset and required euthanasia. Of the 8 experimental monkeys, 4 were treated with intravenous infusion of FN18-CRM9, and the remaining 4 had cranial irradiation in addition to FN18-CRM9. Survival status of these monkeys is depicted in Fig. 1B. The 4 monkeys treated with FN18-CRM9 survived from 11 to 45 days before euthanasia, significantly longer than the control monkeys ($P < 0.01$). One of them, 1225, survived disease free, and was euthanized subject to the 2 months time schedule in the protocol. In the 4 monkeys treated with FN18-CRM9 plus cranial irradiation, one died several hours after the irradiation, possibly due to irradiation-induced acute CNS syndrome. Therefore, this monkey is not included in the analysis. The other 3 monkeys experienced vomiting, dyspnea, and tremors within 30 min postirradiation. Two of them also developed a facial cellulitis that lasted for 7–20 days. However, these 3 monkeys survived the early side effects of cranial irradiation and the cellulitis, and lived on for 10 to 44 days before euthanasia. Among over 50 rhesus monkeys treated to their whole body with a total dose of 1300 cGy in two daily fractions for bone marrow transplantation studies at this center, there have been no acute deaths, no evidence of seizure activity, no parotitis, or evidence of facial cellulitis.

EAE progress to stage 2 or 3 disease in the treated monkeys was either retarded (1224, 1203, 1216, and 1106), or halted to a condition showing only minor symptoms such as loss of appetite, decreased activity, and weight loss (1144 and 1181) or no symptoms (1225).

T cell repopulation. Blood and lymph node T cells remained at a very low levels for about 7 days after

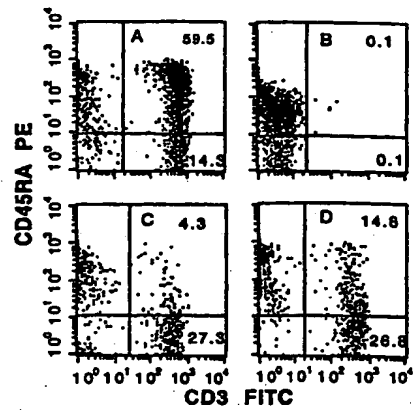


FIG. 4. CD3⁺CD45RA⁺ cells repopulate earlier than CD3⁺CD45RA⁻ cells in blood of FN18-CRM9-treated monkeys. Blood samples were taken 1 day before immunotoxin treatment (A) and after treatment on Days 1 (B), 17 (C), and 41 (D) and analyzed with flow cytometry (data from monkey 1181).

treatment, and then started to repopulate (Figs. 2 and 3). In the 3 long-term survivors (Fig. 1B), only one (1225) repopulated blood T cells to a level close to that before treatment, and the other 2 failed to achieve a complete repopulation. CD4⁺ and CD8⁺ T cells repopulated simultaneously in most of the monkeys (data not shown). Comparing the T cell data in the blood between the monkeys treated with FN18-CRM9 only and those treated with FN18-CRM9 plus cranial irradiation, no obvious difference was observed (Fig. 2). T cell repopulation in the blood was consistently initiated by CD3⁺CD45RA⁻ cells, and only until about 25 days after the treatment did the CD3⁺CD45RA⁺ cells appear in a significant proportion (Fig. 4).

CSF T cell numbers also dropped quickly after IT treatment as did granulocytes. In 4 monkeys where data are available CSF T cells decreased to 1–3% of initial values after immunotoxin treatment. Most of this change occurred in the first 48 hr. Unlike T cells in the blood, CSF T cells remained at low levels in the follow-up period (Fig. 5B). In contrast, T cells in nontreated monkeys increased severalfold within days (Fig. 5A).

The inflammatory response at the immunization sites of the treated monkeys fluctuated in accordance with the blood T cell status. The injection sites became red and swollen 1 day after the immunization, and the involved area was about 0.8 × 0.8 cm. This remained until Day 9 when the inflammatory area enlarged to approximately 2.0 × 1.5 cm, and became ulcerated in the middle. This severe local reaction started to resolve 1 day after the first dose of FN18-CRM9 and ulcers sealed within 3 days. However, the inflammation re-

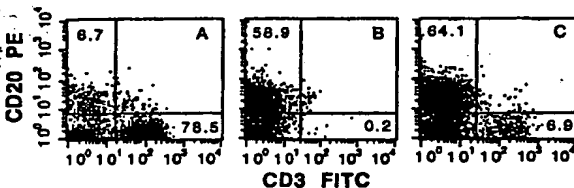


FIG. 3. Lymph node lymphocyte population phenotypes before (A) and 4 and 11 days after FN18-CRM9 (B and C, respectively) by FACS in a single EAE monkey (964). The immunotoxin induces a marked inversion of the normal T/B cell ratio (lower right/upper left quadrants).

), normal
riparasis;
and 1224
on.

ver oc-
such a
edomi-
mpho-
ally be-
y com-
small
Both
former
cells
ch was
blood

gress.
hesus
unized
alysis
e and
eased

25
24
18
15
33
34
36
31

keys
RM9

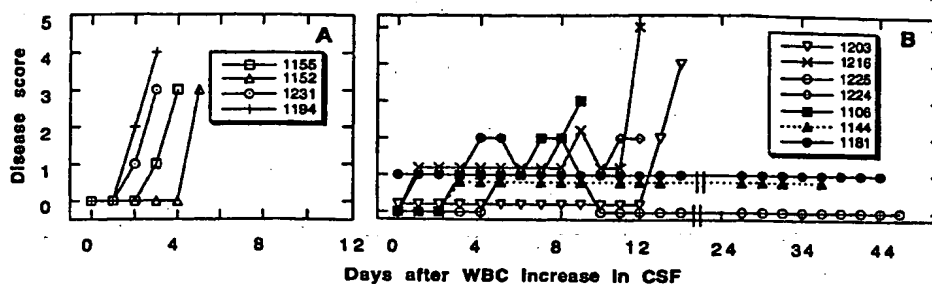


FIG. 1. EAE disease process in nontreated (A) and treated monkeys (B). EAE was scored following a scoring system (3): 0, normal neurologic exam; 1, lethargy, anorexia, weight loss; 2, ataxia, tremor; 3, blindness, paraplegia, hemiplegia; 4, quadriplegia, quadriparesis; and 5, moribund. Day 0 means the time when WBC increase in CSF was detected for the first time. Monkeys 1203, 1216, 1225, and 1224 were treated with FN18-CRM9, and 1106, 1144, and 1181 (filled symbols) were treated with FN18-CRM9 and cranial irradiation.

Immunohistochemistry. Immunohistochemical staining was carried out on frozen brain sections using a previously described protocol (20) employing a secondary anti-mouse horseradish peroxidase antibody and diaminobenzidine (Sigma) chromagen. Primary mAbs used were all of mouse origin: anti-human vimentin (1:50 dilution, DAKO), anti-human MHC class I (W6/32) hybridoma supernatant, anti-human HLA-DR (1:50 dilution, Becton-Dickinson), anti-human CD11b (1:50 dilution, Serotec), anti-human CD68 (1:100 dilution, DAKO), anti-rhesus CD3 (FN18 3 mg/ml 1:100 dilution) (16), anti-human Thy 1 (1:50 dilution, Chemicon), anti-human CD4 (1:25 dilution, Ortho Diagnostic Systems Inc.), anti-human CD8 (1:50 dilution, DAKO). Both primary and secondary antibodies were applied in rhesus sera diluted 1:5 in bovine serum albumin.

RESULTS

Increased WBC in CSF predict the clinical onset of EAE. All monkeys (with the exception of 964) were monitored by CSF examination via the cisterna magna for 5 days starting 11 days postimmunization. This procedure was well tolerated and in itself did not induce pleocytosis (>30 cells/ μ l). Four of these monkeys were used as nontreatment controls, and the rest were treated at the time of the first detectable WBC increase in CSF. Among the 4 control monkeys clinical EAE occurred 2–6 days after the observed WBC increase in CSF, approximately 15–20 days after the immunization (Fig. 1A). The early symptoms of EAE included apathy, loss of appetite, and weak hind limbs, with rapid deterioration to paralysis.

The first CSF samples displaying increased WBC in all 12 monkeys contained 31–700 cells/ μ l (normal range 0–7 cells/ μ l), including monocytes, eosinophils, lymphocytes, and neutrophils. In half of the samples eosinophils occupied a high percentage, 22–78%. In

contrast, this high percentage of eosinophils never occurred in the blood ($<5\%$). In samples without such a high percentage of eosinophils, monocytes predominated proportionally, ranging from 42 to 81%. Lymphocytes were about 10–25%, and neutrophils usually below 10%. The lymphocyte population was mainly composed of T cells (60–90%) in the FACS analysis. A small proportion of B cells ($<5\%$) was also observed. Both CD4⁺ and CD8⁺ cells were present, with the former having a slightly higher percentage. CD3⁺CD25⁺ cells ranged from 5 to 24% in these CSF samples, which was 4 times higher than their counterparts in the blood (data not shown).

T cell depletion slows down the disease progress. FN18-CRM9 transiently depletes T cells in rhesus monkeys (12). This also occurs in MBP immunized monkeys as shown in Figs. 2 and 3 by FACS analysis on blood and macerated lymph node taken before and after IT treatment. CD3⁺ cells in the blood decreased

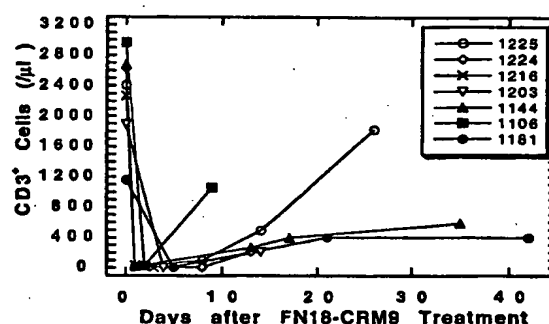


FIG. 2. T cell depletion and repopulation in blood of monkeys treated with FN18-CRM9 by FACS. The first day of FN18-CRM9 treatment is recorded as Day 0.

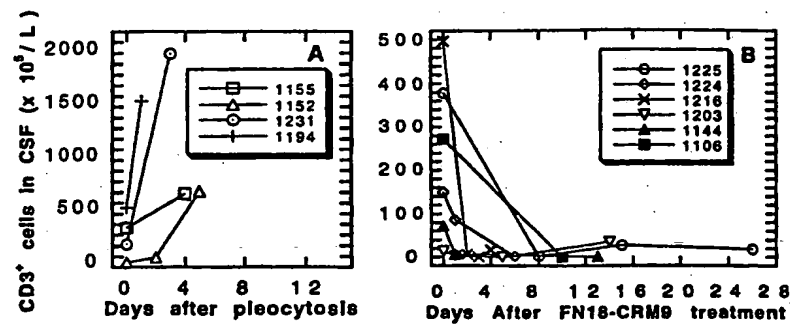


FIG. 5. T cells in CSF increased in nontreated EAE animals (A) and were depleted in EAE monkeys treated with FN18-CRM9 (B). Day 0 is either the date of detecting the first CSF sample with increased WBC (A) or the first FN18-CRM9 treatment (B).

turned at the same area, and ulceration reoccurred in monkeys with repopulated T cells (1225, 1144, 1181).

Immunohistochemistry. As seen in Table 1 and in Figs. 6A–6E, the nontreatment EAE cohort had numerous large perivascular inflammatory plaques throughout the white matter of the hemispheres easily identified in sections stained with specific markers or with hematoxylin alone. These plaques were remarkable for marked up-regulation of vimentin in the parenchyma adjoining the plaques, consistent with acutely reactive astrocytes. The parenchyma was also notable for up-regulation of both MHC class I and II (MHC class I > MHC class II). Although double staining was not done, the MHC class I expression is probably on microglial cells and astrocytes given the diffuse nature of the staining. The MHC class II expression is more restricted and probably represents expression by microglial cells. The inflammatory infiltrate was notable for marked macrophage infiltration as seen by the extraordinary CD68 (Fig. 6A) and CD11b expression. CD4⁺ and CD8⁺ cells also constituted a sig-

nificant population of cells in the infiltrates, further confirmed by the staining for CD3 (Fig. 6B). MHC class I and class II expression in these inflammatory plaques was also quite remarkable (Figs. 6C and 6D), again class I expression being greater than class II expression.

In contrast to the untreated EAE cohort, the cohort treated with FN18-CRM9 or FN18-CRM9 plus irradiation had no identifiable inflammatory plaques in the hemispheres in 4/5 treated monkeys subjected to histochemistry (Figs. 6F–6J and 6K–6O). However, small and large vessels often exhibited enhanced CD68 staining (Fig. 6K), and occasional plaques were seen in the brain stem (Figs. 6P and 6Q). Rare to no CD3⁺, CD4⁺, or CD8⁺ cells could be identified in these infiltrates (Fig. 6Q). The plaques in the fifth monkey consisted predominately of CD11b- and CD68-expressing macrophages (Figs. 6R and S). Again, few CD3⁺, CD4⁺, or CD8⁺ cells could be identified in these infiltrates (Fig. 6S). The brain parenchyma of immunotoxin-treated animals euthanized before 15 days of active disease dem-

TABLE 1
Summary of Histopathology

Monkey	Therapy	Disease duration days	Terminal disease score	Plaques brain	Plaques brain stem	CD68	CD3	CD4	CD8	MHC I	MHC II	Vimentin
1231	—	4	3	62 ± 11	nd	4+	3+	3+	3+	4+	4+	4+
1194	—	6	4	42 ± 6	nd	4+	3+	2+	3+	4+	4+	4+
1203	IT	14	4	<1	nd	r	—	—	—	bv	—	—
1106	IT + R	9	3	<1	3 ± 0	3+	—	—	—	4+	2+	2+
1225	IT	45	0	<1	nd	r	—	—	—	bv	—	4+
1181	IT + R	44	1	<1	<1	r	r	—	—	bv	—	4+
1144	IT + R	35	1	68 ± 10	16 ± 5	4+	1+	—	—	4+	3+	4+

Note. IT, immunotoxin; IT + R, immunotoxin + cranial irradiation; bv, blood vessels only; nd, not done. Percentage of cells in plaque staining for antigen: —, 0%; r, rare isolated cell; 1+, 1–10%; 2+, 10–33%; 3+, 34–66%; 4+, 67–100%. Plaque quantitation: 3 noncontiguous sections covering at least 10 cm² were scanned under low power, plaques were counted, averaged and are reported per 10 cm² of tissue.

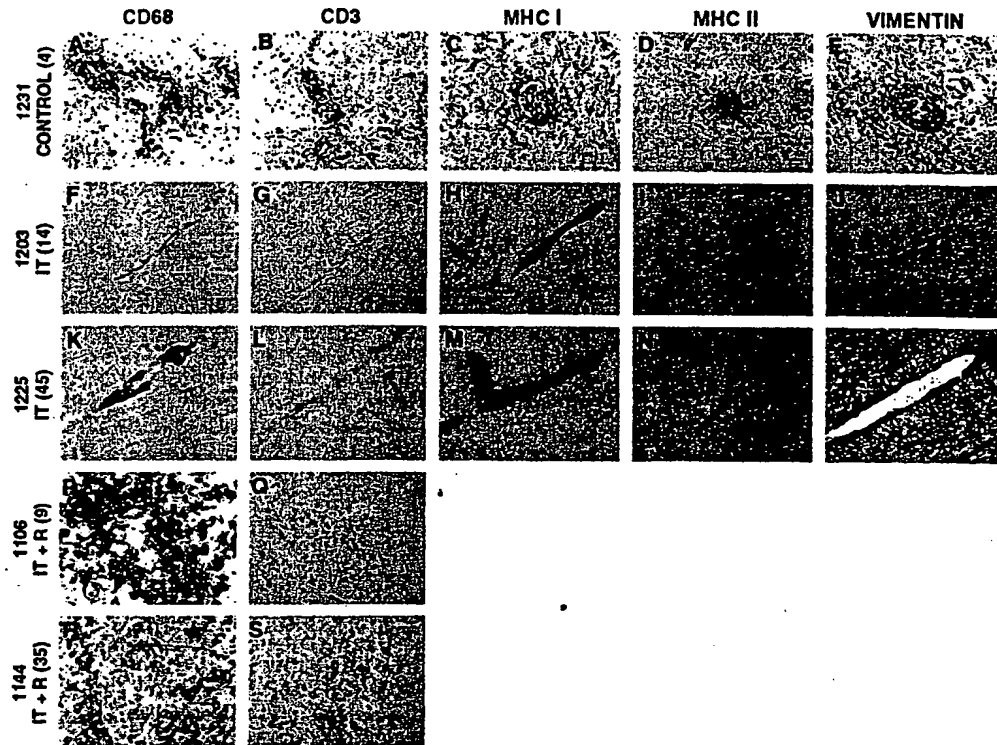


FIG. 6. Immunohistochemistry. Rows display contiguous sections of brain or brain stem that were stained for cell surface epitopes by secondary immunoperoxidase methodology and counterstained with hematoxylin. Positive epitope staining is brown. Epitope staining is delineated by the column heading and is constant by column. Rows are signed by the monkey number, the treatment (as in Table 1) and the disease duration in parentheses. When identifiable the field covers the same histological structure, otherwise the field is from the same general area of the section. A-E shows a typical perivascular plaque in a nontreated EAE monkey brain. Perivascular plaques were not observed in most treated monkey brains (F-J and K-O) but were seen in the brain stem (P-Q and R-S). However, these plaques while containing macrophages (P and R) were largely devoid of CD3⁺ T cells (Q and S) in contrast to untreated EAE monkeys (B). Printed magnification is 100 \times . See Results for detailed comments.

onstrated little gliosis as seen by vimentin staining (Fig. 6J) in contrast to animals surviving 35-45 days where gliosis was marked (Fig. 6O).

DISCUSSION

Nonhuman primate models of EAE have the advantage of sharing considerable similarity with the human immune system. We chose to evaluate anti-CD3 immunotoxin as a treatment for a T-cell-driven autoimmune diseases in rhesus monkeys because of the availability of the anti-rhesus anti-CD3 antibody FN18. We induced a highly consistent monophasic form of the disease having a narrow window between immunization and disease onset by using a 2:1 ratio of monkey MBP

to heat-killed mycobacteria. This relatively small window allowed us to predict EAE onset by performing serial CSF WBC and FACS analyses. CSF pleocytosis occurred 1-5 days before the appearance of clinical signs in 10 of 11 monkeys, and allowed us to initiate early treatment. This method of early prediction of subsequent EAE is much simpler than MRI. It is based on the observation that in rodent EAE the meninges and subarachnoid space are infiltrated with inflammatory cells before brain and spinal tissue (21) and in some models before the onset of neurological signs (10). We reasoned that if this were the case in rhesus EAE, CSF pleocytosis should likely precede clinical EAE. The consistency of this model permits therapeutic evaluations with a relatively small group of monkeys and is in our

IRM9 (B).

her con-
class I
plaques
in class
on.
cohort
irradi-
in the
o histo-
small
stain-
in the
CD4⁺,
litrates
sisted
macro-
4⁺, or
s (Fig.
ed an-
dem-

mentin

4+
4+
—
2+
4+
4+
4+

plaque
tiguous
issue.

opinion preferable to EAE treatment evaluations where treatment is initiated prior to any signs of disease onset (9, 11).

Treatment with immunotoxin lowered CSF pleocytosis to near normal levels within 3 days. Treatment also dramatically prolonged the survival time of EAE monkeys. In nontreated monkeys EAE progressed rapidly, and these monkeys required euthanasia within 3 days after EAE onset having reached a disease score of 3 or greater. Thus there was a striking negative correlation between the average CSF T cell count and the survival time ($R = 0.93$) in nontreated monkeys but not in treated monkeys ($R = 0.24$), indicating that treatment attenuated a major correlate of the disease process. Histopathology on these nontreated monkeys showed numerous brain perivascular plaques containing T cells and macrophages. In the treated monkeys EAE manifested either as a delayed acute process (survival time was prolonged to 2 weeks), or as a mild form, reflected by loss of appetite, weakness, and weight loss (survival time was 35 days or the last day of the protocol, Days 44–45). Histopathology was performed on two monkeys euthanized during a delayed acute process. The hemispheres of these brains were nearly normal. However, the brain stem of the animal treated with immunotoxin plus radiation displayed a single plaque devoid of identifiable T cells and mild gliosis. The occasional brain stem plaque could have been responsible for the clinical deterioration seen in the delayed acute-phase animals. However, the observed plaque was not centered on an intact vessel and may represent an old, rather than a new lesion. Two of the three animals euthanized between Days 35 and 45 during the mild form of the disease and subjected to histopathology failed to show plaques. However, all of these animals exhibited marked gliosis. The third treated monkey exhibiting a clinical mild form of the disease showed about the same number of perivascular plaques seen in nontreated animals but T cells were infrequent. Again, marked gliosis was present. It is not clear whether this gliosis represents a late response to the early acute disease or whether it represents an ongoing chronic process. No differences were apparent between the radiation and nonradiation treatment groups.

Therapies previously shown to prolong survival time in nonhuman primate EAE include treatment with corticosteroids or antibiotics plus high dose MBP (22), monoclonal anti-CD4 (5, 23), and a monoclonal antibody cross-reactive with RhLA II (6). Although there was some reduction noted in the histopathology in these treated animals, major changes compared to nontreatment groups were not noted (5, 6, 23, 24). In particular, perivascular cellular infiltrates, the hallmark of new lesions, contained T cells after treatment. In contrast, immunotoxin treatment produced a reduction in the number and size of new perivascular brain le-

sions. The striking feature was that these lesions when present were largely devoid of T cells.

In 4 monkeys where data are available CSF T cells decreased to 1–3% of initial values after immunotoxin treatment. Most of this change occurred in the first 48 hr. The decline of T cells might be due to a leak of IT into the CSF through partial disruption of the blood-brain barrier, but this is unlikely since we could not detect therapeutic levels of IT in the CSF as we could in blood by ELISA (data not shown). More likely these T cells have a short CNS half-life either due to cell death or recirculation to the venous system along with the bulk CSF. Their decline indicates that they are not being replaced. The reduction of brain T cell and macrophage infiltrates seen in treated animals compared to untreated animals also probably occurs through lack of replacement since in self-limiting rodent EAE these infiltrates regress within 10 days (25). The residual macrophage infiltrates that are seen in the treatment groups may represent continued macrophage infiltration driven by residual vascular damage or a very small number of residual T cells. These could have survived immunotoxin therapy due to the sanctuary provided by the blood-brain barrier. This was the reason for providing an IT plus cranial irradiation group in this study. Since activated T cells are radiation sensitive with a D_0 estimated to be 52 cGy (13), 325 cGy could achieve a 1.8 log reduction of this cell type. However, in this limited study we could not detect a significant difference between IT alone and IT plus radiation. A trend toward longer survival in the group receiving radiation may or may not be real. It is possible that early radiation may inactivate CNS T cells more quickly than IT which probably works by preventing reseeding. Early radiation-induced inactivation of CNS T cells might limit CNS damage in this acute disease process.

Animals in this study were hypersensitive to acute radiation-induced phenomenon. Whole brain radiation at the doses delivered is associated with only rare nausea or transient asymptomatic parotid swelling in human subjects, a negligible rate of seizure, and no deaths (26). Likewise, whole body radiation to other rhesus monkeys in our laboratory, using a dose two to four times the dose used in this study has resulted in no acute deaths, seizures, or parotitis. The frequency of facial swelling, seizure activity, and probably CNS syndrome seen in the current study suggests that EAE (or immunotoxin) predisposed irradiated cells in the brain and probably to the salivary gland to depolarize (27), apoptose (28), or release cytotoxic factors (29) that caused edema and/or necrosis.

Most of the treated monkeys surviving at 12–21 days had begun to repopulate their blood T cells by this time to a range of 250–500 cells/ μ l. By 3 weeks the inflammatory lesions at the immunization sites which had regressed 48 hr after IT treatment showed a recrudescence.

cence of inflammation and began to ulcerate again. One monkey, 1225, was tested for PPD sensitivity at Day 41 and was strongly positive. These findings indicate that the repopulated T cells could exhibit delayed-type hypersensitivity reactions. Mycobacterial antigens were continually present since the draining immunization sites continued to shed heat-killed acid fast bacteria from the adjuvant. However, T cells did not apparently repenetrate the blood-brain barrier in large numbers as evidenced by repeated CSF FACS analysis and histopathology at the time of euthanasia.

The difference in behavior of repopulated T cells toward tissue depots containing mycobacterial antigens versus CNS MBP may reflect the very low level or absence of peripheral MBP at the time of T cell repopulation. In rat EAE bromodeoxyuridine labeling has shown that most of the MBP-specific T cell proliferation occurs in the periphery as opposed to the CNS (30). The severity of the initial disease is also very sensitive to the MBP dose (5). This suggests that in active EAE the number of peripheral MBP-reactive T cells is a major variable that determines the magnitude of the CNS cellular infiltrates and the severity of the disease, a fact demonstrated in passive EAE (31). It seems reasonable to speculate that the postimmunotoxin-repopulated T cell population contains a greatly reduced number of MBP-reactive effector cells compared to the population at the time of treatment. We think that this is the most likely mechanism to explain the beneficial effect of immunotoxin at late times following T cell repopulation. This could reflect a decrease in the number of T cells carrying TCR specific for MBP. However, there are other possible mechanisms that might be operative during the T cell depletion and subsequent repopulation phases. Part of the effect could be due to alterations in the functions of the repopulated T cells capable of binding MBP. For example, the naive phenotype CD3⁺ CD45RA⁺ is very underrepresented in the early repopulation period. Alternatively, repopulation during the disease process might induce a switch (immune deviation) in phenotype from T_H1 to T_H2 that would give the appearance of tolerance to MBP (32). Anti-CD3 immunotoxin has been shown to induce tolerance to rhesus renal allografts mismatched at both MHC class I and class II loci. Tolerance was shown by the acceptance of donor skin grafts and the rejection of third party grafts. This appears to take several months to develop indicating an active immune process (15). However, the mechanism of this process has not yet been delineated. One possible mechanism is that during the depletion phase the ratio of non-professional antigen-presenting cells (B cells) greatly exceeds the number of T cells. It has been suggested that this population inversion which is akin to the neonatal state favors tolerance over immunization (33). Whether a similar tolerizing processes to autoimmune-inducing antigens could be operative in the immunotoxin toxin

treatment of autoimmune diseases remains to be elucidated.

ACKNOWLEDGMENTS

We thank M. Jonker for making FN18 available, J. Shiloach for production of CRM9, and the NIMH veterinary staff for their expertise and help.

REFERENCES

- Pettinelli, D. B., and McFarlin, C. E., *J. Immunol.* 127, 1420, 1981.
- Zamvil, S., Nelson, P., Trotter, J., Mitchell, D., Knobler, R., Fritz, R., and Steinman, L., *Nature* 317, 355, 1985.
- Massaccesi, L., Joshi, N., Lee-Parritz, D., Rombos, A., Letvin, N. L., and Hauser, S. L., *J. Clin. Invest.* 90, 399, 1992.
- Genain, C., Lee-Parritz, D., Nguyen, M.-H., Massaccesi, L., Joshi, N., Ferrante, R., Hoffman, K., Moseley, M., Letvin, N. L., and Hauser, S. L., *J. Clin. Invest.* 94, 1339, 1994.
- Rose, L. M., Alvord, E. C., Jr., Hruby, S., Jackevicius, S., Petersen, R., Warner, N., and Clark, E. A., *Clin. Immunol. Immunopathol.* 45, 405, 1987.
- van Lambelgen, R., and Jonker, M., *Clin. Exp. Immunol.* 67, 305, 1987.
- Massaccesi, L., Genain, C. P., Lee-Parritz, D., Letvin, N. L., Canfield, D., and Hauser, S. L., *Ann. Neurol.* 37, 519, 1995.
- Lafaille, J. L., Nagashima, K., Katsuki, M., and Tonegawa, S., *Cell* 78, 399, 1994.
- Huitinga, I., van Rooijen, N., de Groot, C. J. A., Uitdehaag, B. M. J., and Dijkstra, C. D., *J. Exp. Med.* 172, 1025, 1990.
- Polman, C. H., Dijkstra, C. D., Sminia, T., and Koetsier, J. C., *J. Neuroimmunol.* 11, 215, 1986.
- Karpus, W. J., Lukacs, N. W., McRae, B. L., Strieter, R. M., Kunkel, S. L., and Miller, S. D., *J. Immunol.* 155, 5003, 1995.
- Neville, D. M., Jr., Scharff, J., Hu, H. Z., Rigaut, K., Shiloach, J., Slingerland, W., and Jonker, M., *J. Immunother.* 19, 85, 1996.
- Neville, D. J., Jr., Scharff, J., and Srinivasachar, K., *Proc. Natl. Acad. Sci. USA* 89, 2585, 1992.
- Thompson, J., Hu, H., Scharff, J. E., and Neville, D. M., Jr., *J. Biol. Chem.* 270, 28037, 1995.
- Knechtle, S. J., Vargo, D., Fechner, J., Zhai, Y., Wang, J., Hanaway, M. J., Scharff, J., Hu, H., Knapp, L., Watkins, D., and Neville, D. M., Jr., *Transplantation* 63, 1, 1997.
- Nooij, F. J. M., Jonker, M., and Balner, H., *Eur. J. Immunol.* 16, 975, 1986.
- Neville, D. J., Jr., Srinivasachar, K., Stone, R., and Scharff, J., *J. Biol. Chem.* 264, 14653, 1989.
- Deibler, G. E., Martenson, R. E., and Kies, M. W., *Prep. Biochem.* 2, 139, 1972.
- Reimann, K. A., Waite, B. C. D., Lee-Parritz, D. E., Lin, W., Uchanska-Ziegler, B., O'Connell, M. J., and Letvin, N., *Cytometry* 17, 102, 1994.
- Tornatore, C., Baker-Cairns, B., Yadid, G., Hamilton, R., Meyers, K., Atwood, W., Cummins, A., Tanner, V., and Major, E., *Cell Transplant.* 5, 145, 1996.
- Shin, T., Kojima, T., Tanuma, N., Ishihara, Y., and Matsumoto, Y., *J. Neuroimmunol.* 56, 171, 1995.
- Shaw, C.-M., Alvord, E. C., Jr., and Hruby, S., *Ann. Neurol.* 24, 738, 1988.

23. Jonker, M., Van Lambalgen, R., Mitchell, D. J., Durham, S. K., and Steinman, L., *J. Autoimmun.* 1, 399, 1988.
24. Rose, L. M., Richards, T. L., Petersen, R., Peterson, J., Hraby, S., and Alvord, E. C., Jr., *Clin. Immunol. Immunopathol.* 59, 1, 1991.
25. Allen, S. J., Baker, D., O'Neill, J. K., Davison, A. N., and Turk, J. L., *Cell. Immunol.* 146, 335, 1993.
26. Diener-West, M., Dobbins, T. W., Phillips, T. L., and Nelson, D. F., *Int. J. Radiat. Oncol. Biol. Phys.* 16, 669, 1989.
27. Todd, D. G., and Mikkelsen, R. B., *Cancer Res.* 54, 5224, 1994.
28. Fuks, Z., Persaud, R. S., Alfieri, A., McLoughlin, M., Ehleiter, D., Schwartz, J. L., Seddon, A. P., Cordon-Cardo, C., and Haimovitz-Friedman, A., *Cancer Res.* 54, 2582, 1994.
29. Hallahan, D. E., Haimovitz-Friedman, A., Kufe, D. W., Fuks, Z., and Weichselbaum, R. R., in "Important Advances in Oncology" eds. (DeVita, V. T., Hellman, S., and Rosenberg, S. A., Eds.), p. 71. Lippincott Philadelphia, 1993.
30. Ohmori, K., Hong, Y., Fujiwara, M., and Matsumoto, Y., *Lab. Invest.* 68, 54, 1992.
31. Zeine, R., and Owens, T., *J. Neuroimmunol.* 40, 57, 1992.
32. Forsthuber, T., Yip, H. C., and Lehmann, P. V., *Science* 271, 1728, 1996.
33. Ridge, J. P., Fuchs, E. J., and Matzinger, P., *Science* 271, 1723, 1996.

Heparin-binding Transforming Growth Factor α -*Pseudomonas* Exotoxin A

A HEPARAN SULFATE-MODULATED RECOMBINANT TOXIN CYTOTOXIC TO CANCER CELLS AND PROLIFERATING SMOOTH MUSCLE CELLS*

(Received for publication, October 5, 1992)

Enrique A. Mesri†, Robert J. Kreitman‡, Ya-Min Fu§, Stephen E. Epstein§, and Ira Pastan†¶

From the †Laboratory of Molecular Biology, Division of Cancer Diagnosis Biology and Centers, National Cancer Institute and the §Cardiology Branch, National Heart Lung and Blood Institute, National Institutes of Health, Bethesda, Maryland 20892

TGF α -PE40, a recombinant toxin in which transforming growth factor α (TGF α) is fused to a mutant form of *Pseudomonas* exotoxin, is selectively cytotoxic to cells bearing epidermal growth factor (EGF) receptors. Heparin binding EGF-like growth factor is a potent mitogen for smooth muscle cells capable of binding to both the EGF receptor and to immobilized heparin (Higashiyama, S., Abraham, J., Miller, J., Fiddes, J., and Klagsbrun, M. (1991) *Science* 251, 936-938). To study the effect of the heparin-binding domain in a chimeric toxin targeted to the EGF receptor, we fused the DNA sequence corresponding to the putative NH₂-terminal heparin-binding (HB) domain of HB-EGF to chimeric toxins composed of TGF α and two different recombinant forms of *Pseudomonas* exotoxin (PE). One of these is a truncated form of PE devoid of the binding domain (TGF α -PE38); another is a mutant form of full-length toxin containing inactivating mutations in the binding domain and an altered carboxyl terminus (TGF α -PE^{4E}KDEL). The resulting chimeric toxins HB-TGF α -PE38 and HB-TGF α -PE^{4E}KDEL were expressed in *Escherichia coli* as inclusion bodies, refolded, and purified by heparin affinity chromatography. Both of the toxins were eluted from heparin at 0.8 M NaCl, in contrast to their respective TGF α toxins which were eluted at 0.15 M. Binding studies on A431 cells showed that the HB-TGF α toxins bound to the EGF receptor with an affinity similar to that of the TGF α toxins. However, cell killing studies on a panel of malignant cell lines showed that cytotoxicity was strongly affected by the presence of the HB domain. Cell lines expressing high numbers of EGF receptors such as A431 and KB were less sensitive to toxins containing the HB domain. Cells with low number of EGF receptors had similar responses to both types of toxins (MCF-7 and LNCaP) or were more sensitive to the toxin with the added HB domain (HEP-G2). HB-TGF α -PE^{4E}KDEL was over 10-fold more cytotoxic against proliferating vascular smooth muscle cells (VSMC) than to quiescent VSMC. Moreover, HB-TGF α -PE^{4E}KDEL was 6-fold more potent than TGF α -PE^{4E}KDEL to proliferating VSMC. Competition studies with EGF and/or heparin showed that heparin blocks the cytotoxicity of HB-TGF toxins and the in-

hibitory action of heparin is stronger in cells expressing lower number of EGF receptors. In addition, experiments with heparitinase-treated cells showed that in cells with low numbers of EGF receptors the binding of the HB domain to cell surface heparan sulfate proteoglycans appears to facilitate the internalization of the toxin. We conclude that addition of a HB domain to TGF α -PE38 or TGF α -PE^{4E}KDEL confers the ability to bind to and to be modulated by heparin-like molecules and increases their cytotoxicity to cells expressing low numbers of EGF receptor and proliferating smooth muscle cells.

The use of targeted toxins is a promising approach for the therapy of cancer and autoimmune diseases, as well as other disorders (Pastan *et al.*, 1986, 1992; Pastan and FitzGerald, 1989; Vitetta *et al.*, 1987). Initially, toxins were chemically coupled to antibodies and growth factors in order to kill target cells with differential surface properties (Vitetta *et al.*, 1987; Pastan *et al.*, 1992). Advances in the recombinant DNA field have made it possible to construct chimeric toxins from genes encoding growth factors or single chain antibodies fused to toxin genes (Pastan *et al.*, 1992).

One of the toxins that has proven versatile in producing chimeric toxins is *Pseudomonas* exotoxin A (PE)¹ (Pastan *et al.*, 1986, 1992; Pastan and FitzGerald, 1989). PE is a 66-kDa molecule that kills animal cells by inhibition of protein synthesis (Iglewski and Kabat, 1975). In order to kill a cell, the toxin must first be internalized by receptor-mediated endocytosis, and then must translocate to the cytosol where it catalyzes the ADP-ribosylation of elongation factor-2 (FitzGerald *et al.*, 1980). Crystallographic studies have identified three major domains in PE (Allured *et al.*, 1986). Domain Ia enables PE to bind to the PE receptor (Hwang *et al.*, 1986; Jinno *et al.*, 1988), and domain II is involved in the processing and translocation of the toxin to the cytosol (Hwang *et al.*, 1986; Ogata *et al.* 1990). Domain III contains the ADP-ribosylating activity (Hwang *et al.*, 1986). In addition, amino acids at the COOH-terminal residues of PE, REDLK, are required to route the toxin to an intracellular compartment from which it can translocate to the cytosol

* The costs of publication of this article were defrayed in part by the payment of page charges. This article must therefore be hereby marked "advertisement" in accordance with 18 U.S.C. Section 1734 solely to indicate this fact.

¶ To whom all correspondence should be addressed: Lab. of Molecular Biology, National Cancer Institute, National Institutes of Health, 9000 Rockville Pike, Bldg. 37, Rm. 4E16, Bethesda, MD 20892. Tel.: 301-497-4797; Fax: 301-402-1344.

¹ The abbreviations used are: PE, *Pseudomonas* exotoxin; SMCs, smooth muscle cells; VSMCs, vascular smooth muscle cells; HB, heparin binding; TP38, TGF α -PE38; HB-TP38, HB-TGF α -PE38; TP4EK, TGF α -PE^{4E}KDEL; HB-TP4EK, HB-TGF α -PE^{4E}KDEL; HSPG, heparan sulfate proteoglycan; EGFR, EGF receptor; BES, N,N-bis(2-hydroxyethyl)-2-aminoethanesulfonic acid; TGF α , transforming growth factor α ; FBS, fetal bovine serum; kb, kilobase(s).

(Chaudhary *et al.*, 1990a). If the COOH terminus, REDLK, is changed to the known endoplasmic reticulum retention sequence, KDEL, toxin activity is increased (Chaudhary *et al.*, 1990a; Seetharam *et al.*, 1991). The function of domain Ib, a 4-kDa segment between domains II and III is unknown, and much of it has been deleted without loss of activity (Siegall *et al.*, 1989).

To kill specific target cells, domain I of PE can be replaced by various ligands, such as growth factors (TGF α , interleukin 6, acidic FGF, insulin-like growth factor 1) (Chaudhary *et al.*, 1987; Siegall *et al.*, 1988, 1989a, 1989b; Prior *et al.*, 1991), single chain antibodies (Chaudhary *et al.*, 1989; Brinkmann *et al.*, 1991), and other molecules capable of specifically targeting the toxin (Chaudhary *et al.*, 1988). The residual toxin portion can contain domain II, part of domain Ib, and domain III (PE38). In addition, growth factors like aFGF and TGF α have been fused to mutants of full-length PE (PE^{EB}) (Chaudhary *et al.*, 1990b; Kreitman *et al.*, 1991a; Siegall *et al.*, 1991) that have mutations in domain Ia making the toxin incapable of binding to the PE receptor. The resulting chimeric toxins bind to and selectively kill cells expressing appropriate surface molecules. One of these chimeric toxins, TGF α -PE40, selectively kills cells expressing high numbers of EGF receptors (EGFR). These include many cancer cell lines, as well as proliferating smooth muscle cells (Siegall *et al.*, 1989b; Epstein *et al.*, 1991). This chimeric toxin has also been shown to have anti-tumor activity in mice carrying subcutaneous tumors (Pai *et al.*, 1991; Heimbrosk *et al.*, 1990) and is currently being tested as a possible therapy for human bladder cancer. However, the amount of TGF α -PE40 and related toxins that can be administered systemically is limited by liver toxicity, which is due to the relatively high number of EGF receptors on liver cells. In addition, these chimeric toxins have a short half-life in the blood stream. To prolong the half-life of chimeric toxins, protease sites have been removed (Brinkmann *et al.*, 1992), and protein domains such as the C_{H2} domain of IgG have been added (Batra *et al.*, 1992). Recent studies have also demonstrated that the bFGF has an increased half-life when administered with heparin (Whalen *et al.*, 1989).

Very recently, two heparin-binding growth factors which bind to the EGFR have been described; these include the heparin-binding EGF-like growth factor (HB-EGF) (Higashiyama *et al.*, 1991) and amphiregulin (Shoyab *et al.*, 1989). HB-EGF is a growth factor which is highly mitogenic to smooth muscle cells (SMCs). Proliferation of vascular SMCs is implicated in several vascular disorders such as atherosclerosis and restenosis following angioplasty (Ross, 1986; Austin *et al.*, 1987; Woolf, 1990). Since proliferating VSMCs produce HB-EGF (Yoshisumi *et al.*, 1992) and display high numbers of EGFRs (Epstein *et al.*, 1991), an HB-EGF autocrine loop has been postulated as a cause of SMC hyperplasia (Klagsbrun *et al.*, 1992). Cytotoxic agents capable of targeting proliferating VSMC might be useful to treat these disorders. Chimeric toxins targeted by TGF α and aFGF have been assayed on proliferating VSMC and are currently being tested both *in vitro* and *in vivo* as possible therapies for restenosis following angioplasty (Epstein *et al.*, 1991; Lindner *et al.*, 1991; Casscells *et al.*, 1992; Biro *et al.*, 1992).

The mature HB-EGF polypeptide, in addition to containing an EGF like domain, has an N terminus rich in lysine and arginine residues. It is believed that this basic amino acid sequence confers HB activity to the molecule without affecting its affinity for the EGFR and facilitates its mitogenic activity (Higashiyama *et al.*, 1991, 1992). We designed two new chimeric toxins having both a HB and an EGFR binding

function by fusing the HB domain from HB-EGF to TGF α -PE38 or TGF α -PE^{EB}KDEL. In this manner we generated chimeric toxins bearing a binding domain composed of a chimeric ligand HB-TGF α , which presumably will be functionally equivalent to HB-EGF. These two new chimeric toxins allowed us to address several questions. Does the HB domain improve the ability of TGF α to target proliferating VSMCs? Does the HB domain increase the activity of the new recombinant toxin toward certain cancer cell lines? Finally, by comparing the activities of HB-TGF toxins and their respective TGF toxins we could determine the importance of the HB domain in the interaction of the toxins with target cells and gain insight into the biological role of the HB domain of HB-EGF.

MATERIALS AND METHODS

Human Cancer Cell Lines—Most cell lines were from the American Type Culture Collection (Rockville, MD) and were cultured and maintained as suggested by the supplier. HUT-102 cells were a gift from Dr. T. Waldmann (National Cancer Institute, National Institutes of Health). TE-671, D-54MG, and NCI 417D were generously provided by Dr. D. Bigner (Department of Pathology, Duke University Medical Center, Durham, NC).

Smooth Muscle Cells—Cultured VSMC were isolated from Sprague-Dawley rats (200–250 g) by the explant method as previously described (Epstein *et al.*, 1991). VSMC were maintained in medium-199 (M199) (Biofluids, Rockville, MD), 2 mM L-glutamine, 100 units/ml penicillin, and 100 μ g/ml streptomycin, supplemented with 10% fetal bovine serum (FBS) for rapidly proliferating cells or 0.5% FBS for quiescent cells. Identification of VSMC was confirmed by their typical morphological character and immunocytochemical staining by anti-muscle actin. VSMC were used between passages 11 and 13.

Plasmid Construction—The plasmid pCS10 encodes TGF α -PE38, which is identical to TGF α -PE40 except that it is missing amino acids 365–380 of PE. Like TGF α -PE40, it contains an *NdeI* site at the 5' end of the coding region and an *NcoI* site near codon 18 of TGF α (Fig. 1B). pCS10 was cut with *NdeI*, and an 87-mer oligonucleotide duplex flanked by *NdeI* sites was ligated to the vector. The 5' end of the inserted sequence contained a *NdeI*-*NheI* fragment of sequence T-ATG-GTC-AGG-CTA-TCT-TCG-AAA-CCT-CAG-GCG encoding for the 9 amino-terminal residues of HB-EGF. This new plasmid pRK4391 was converted to a high copy number plasmid pRK4391 f + T. The 1.0-kb *XbaI*-*XhoI* fragment of pRK4391 was ligated to the 3.4-kb *XbaI*-*XhoI* fragment of p7018 (Batra *et al.*, 1990), resulting in pRK4391 f + T. This plasmid was digested with *NcoI* and *NheI*, and then a three fragment ligation was performed using two oligonucleotide duplexes. The resulting plasmid pRK4392 encodes HB-TGF α -PE38. The 5'-terminal portion of its coding sequence was determined by DNA sequencing and is shown in Fig. 1B. To make pEMHB4E encoding HB-TGF α -PE^{EB}, the 257-bp *XbaI*-*SphI* fragment of pRK4392 was ligated to the 4.9-kb *XbaI*-*SphI* fragment of pVC34E/4E, which encodes for TGF α -PE^{EB} (Kreitman *et al.*, 1991b). Plasmids pEMHB4EK or pEMT4EK, encoding for TGF α -PE^{EB}KDEL or HB-TGF α -PE^{EB}KDEL, respectively, were made by ligating the 0.36-kb *BamHI*-*EcoRI* fragment of pCSF4K to the 4.8-kb *EcoRI*-*BamHI* fragment of pVC34/4E or pEMHB4E, respectively. Plasmids pRK4392 and pEMHB4EK showing the relevant restriction sites together with the structure of the four chimeric toxins are shown in Fig. 1B.

Expression and Purification of the Chimeric Toxins—Expression, refolding, and purification of the HB-TGF α chimeric toxins were accomplished by a modification of previously published methods (Kreitman *et al.*, 1991a, 1991b; Buchner *et al.*, 1992). *Escherichia coli* BL21 (ADE3) (Studier and Moffat, 1986), transformed with the specific plasmid, was grown to an OD₆₀₀ of 1. Expression was induced by the addition of isopropyl-1-thio- β -D-galactopyranoside (United States Biochemicals, Cleveland, OH). Cells were harvested after 90 min of induction, and spheroplasts were prepared by osmotic shock. Inclusion bodies, obtained from the spheroplasts by sonication, were denatured with guanidine-HCl 7 M containing 0.3 M dithioerthreitol. Renaturation and refolding was achieved by 100-fold dilution into Tris, pH 8.0, containing 0.4 M arginine, 2 mM EDTA, and 4.9 g/liter GSSG. After stirring at 4 °C for 20 h, the renaturing solution was dialyzed against 20 mM Tris buffer, pH 7.4, containing 100 mM urea and 50 mM NaCl. The dialyzed protein was centrifuged 30 min at

18,000 revolutions/minute on a Sorvall SS-34 rotor, filtered through a 0.22- μ m filter, and loaded on an Econo-pak heparin column (Bio-Rad). The Econo-pak column was eluted with a 0–1 M NaCl gradient (20 ml) in 20 mM Tris, pH 7.4. The fractions eluting from 0.4 to 0.9 M NaCl were pooled, diluted to a final NaCl concentration of 150 mM, and loaded onto a TSK-heparin column (Toso-Haas, Philadelphia, PA), washed with 0.15 M NaCl, and eluted with a 20-ml 0.15–1 M NaCl gradient. Each fraction was characterized by cytotoxic activity toward A431 cells, SDS-polyacrylamide gel electrophoresis (Laemmli 1970), and analytical size exclusion chromatography (TSK-3000 gel, Toso-Haas, Philadelphia, PA). For the expression and purification of TGF α chimeric toxins, we used the protocol previously described (Kreitman *et al.*, 1991a, 1991b) without any modification. aFGF-PE⁴²KDEL was obtained as described (Siegal *et al.*, 1991).

Cytotoxicity Assays—Cytotoxicity assays were performed as described (Kreitman *et al.*, 1991a, 1991b). Adherent cells were plated 24 h prior to toxin addition in 96-well plates at a density of 1×10^5 cells/ml. After incubating with toxins at 37 °C for 16–18 h, 1 μ Ci of [³H]leucine was added to each well, and the cells were incubated for 4 additional h. After freeze/thawing, the cells were harvested onto Filtermat papers and counted in a Betaplate scintillation counter (Wallac-Pharmacia, Gaithersburg, MD). The counts/minute data reported from cytotoxicity assays were the medians of triplicate experiments, each of which generally deviated from their means by less than 10%. ID₅₀ values and cytotoxicity profiles reported are representative of several confirmatory assays. Cytotoxicity assays in VSMC were performed as described before (Epstein *et al.*, 1991). Briefly, VSMC were plated 48 h prior to toxin addition in 24-well plates at a density of 1×10^5 cells/ml. After incubating with toxins for 48 h, 5 μ Ci of [³H]leucine was added to each well. The following steps were same as above.

Effect of Heparin, EGF, and Heparitinase on Cytotoxicity—For preincubation assays, toxins at a concentration of 4 μ g/ml were incubated for 15 min with heparin (10 units/ml) (Upjohn, Kalamazoo, MI) at 22 °C. The heparin-treated toxins were diluted and assayed as described above. For assays in presence of heparin, heparin was added to the cells with the toxin. For competition experiments, 2 h before adding the toxin, plates were cooled on ice, and EGF (GIBCO-BRL, Gaithersburg, MD) was added to the plates up to 4 μ g/ml. Plates were incubated at 4 °C for 90 min with gentle rocking. Toxins with or without heparin were then added, and the assay was continued as described above. For heparitinase digestion, heparitinase (Linhardt *et al.*, 1990) (heparitinase III, heparan sulfate lyase, EC 4.2.2.8, ICN Biochemicals, Costa Mesa, CA) was added to the cells up to 1 milliunit/ml 3 h prior to toxin addition. The assay was then continued as described above.

Binding Displacement Assays—Displacement assays were performed as described (Kreitman *et al.*, 1991a, 1991b). A431 cells were plated at 8×10^3 cells/ml/well in 24-well plates. Twenty-four h later the medium was discarded, and the adherent cells were washed two times with ice-cold binding buffer (Dulbecco's modified Eagle's medium containing 1 mg/ml bovine serum albumin and 50 mM BES, pH 6.8). Plates were then placed on ice, and 200 μ l of binding buffer containing 0.5 ng of [¹²⁵I]-EGF (0.1 μ Ci/ng, Du Pont-New England Nuclear) and 100, 10, 1, or 0.1 nM of toxins or controls was added. After incubation at 4 °C with gentle rocking, the binding solution was aspirated and the cells washed three times with cold binding buffer. The cells were then lysed by the addition of 0.5 ml of lysis buffer (10 mM Tris-HCl, pH 7.4, 0.5% SDS, EDTA 1 mM) and bound [¹²⁵I]-EGF was quantitated with a gamma detector. Results represent the median value of triplicates. Binding profiles are representative of at least three experiments with similar data.

RESULTS

Construction of the Heparin-binding TGF α Chimeric Toxins—To determine the effect of adding a heparin-binding domain to a chimeric toxin composed of TGF α and mutant forms of PE, we took advantage of the recent discovery of HB-EGF which binds both to heparin and to the EGFR (Higashishima *et al.*, 1991) (Fig. 1A). We combined the proposed HB region of HB-EGF with two forms of TGF α -PE. As shown in Fig. 1B, we made recombinant fusion proteins in which the putative HB domain of HB-EGF was placed at the amino terminus of TGF α -PE38 (TP38). The binding region of the resulting chimeric toxin, HB-TGF α -PE38 (HB-

TP38), is functionally equivalent to HB-EGF because it contains both a heparin-binding domain and a EGFR-binding domain, and also shares a high degree of sequence homology (Fig. 1A). To obtain a chimeric toxin with high cytotoxic activity, the HB domain was also fused to TGF α -PE⁴²KDEL (TP4EK) to obtain HB-TGF α -PE⁴²KDEL (HB-TP4EK).

Expression and Purification of HB-TGF α Toxins and Heparin Affinity Chromatography—After expression of each plasmid in *E. coli*, the chimeric protein accumulated in inclusion bodies. To obtain the recombinant protein in a soluble, active form, the inclusion bodies were dissolved in a denaturing buffer and the protein renatured and refolded as described previously (Kreitman *et al.*, 1991a; Buchner *et al.*, 1992). The soluble protein was purified by heparin affinity chromatography on a TSK-heparin column (Fig. 2A). The latter was used both as a purification step and also to measure the affinity of the chimeric toxin to heparin. For this measurement TP38 and TP4EK were employed as negative controls and aFGF-PE⁴²KDEL as a positive control (Siegal *et al.*, 1991). As shown in Fig. 2A, HB-TP38 and HB-TP4EK elute from the TSK-heparin column as two peaks, one at 0.6 M and the other at 0.8 M NaCl. Protein eluting within these peaks showed a similar degree of purity (90%) as deduced by SDS-polyacrylamide gel electrophoresis (Fig. 2B). However, the protein eluting at 0.8 M NaCl was 10-fold more cytotoxic to A431 cells than the protein eluting at 0.6 M (data not shown). Typical yields for the toxin eluting at 0.8 M NaCl were 600–1000 μ g/liter of a culture induced at OD₆₀₀ 1.0. Since TP38 and TP4EK eluted from heparin at 0.15 M NaCl we can conclude that the HB domain of the HB-EGF conferred to this chimeric toxin the ability to bind to heparin.

Cytotoxicity to A431 Cells and Binding to the EGFR of the HB-TGF α -PEs—Since HB-EGF and EGF bind to the EGFR of A431 cells with similar affinities (Higashiyama *et al.*, 1991, 1992), we anticipated the cytotoxic activities of HB-TP38 and HB-TP4EK toward A431 cells might be similar to those of TP38 and TP4EK. To measure cytotoxic activity, different concentrations of each toxin were incubated with cells overnight, and protein synthesis was monitored by measuring [³H] leucine incorporation (Fig. 3). As shown in Table I, HB-TP38 and HB-TP4EK were both very cytotoxic to A431 cells, with ID₅₀ values 1.0 and 0.12 ng/ml, respectively. However, TP38 and TP4EK were 20- and 4-fold more cytotoxic, with ID₅₀ values of 0.05 and 0.03 ng/ml, respectively. Excess EGF (4 μ g/ml) completely blocked the cytotoxicity of the HB-TGF α -PEs for A431 cells (see below), and the toxins displayed very low cytotoxicity to cells without EGFRs (HUT-102, data not shown) indicating the specificity of these toxins for the EGFR.

To test whether the decrease in cytotoxicity of HB-TGF α chimeric toxins toward A431 cells was due to a decrease in the affinity of the HB toxins for the EGFR, we measured the ability of the chimeric toxins to displace EGF from A431 cells. As shown in Fig. 4A, the concentrations of HB-TP38 and HB-TP4EK necessary for 50% displacement of the [¹²⁵I]-EGF (IC₅₀) were slightly lower (10 and 6 nM, respectively) than the IC₅₀s for TP38 and TP4EK (20 and 11 nM, respectively). Therefore, the HB-TGF α toxins bind to the receptor with the same or slightly higher affinity than their respective TGF α -PE toxins. This results indicate that the 4–20-fold decrease in cytotoxic activities of the HB-TGF α chimeric toxins (Fig. 3 and Table I) is not due to a decrease in their affinity for the EGFR. Thus, interactions with cellular components other than the EGFR are probably important in determining the cytotoxicity of the HB-TGF α toxins.

Cytotoxicity of HB-TGF α -PEs to Various Human Cancer Cell Lines—If the interactions between cell components and

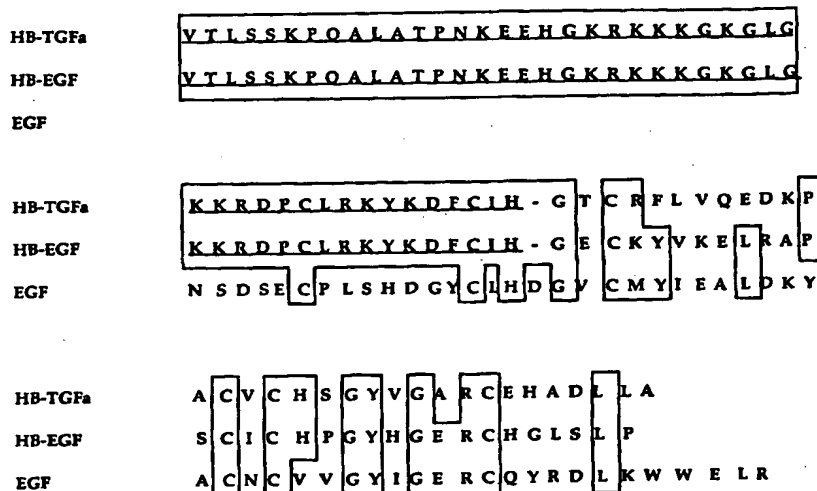
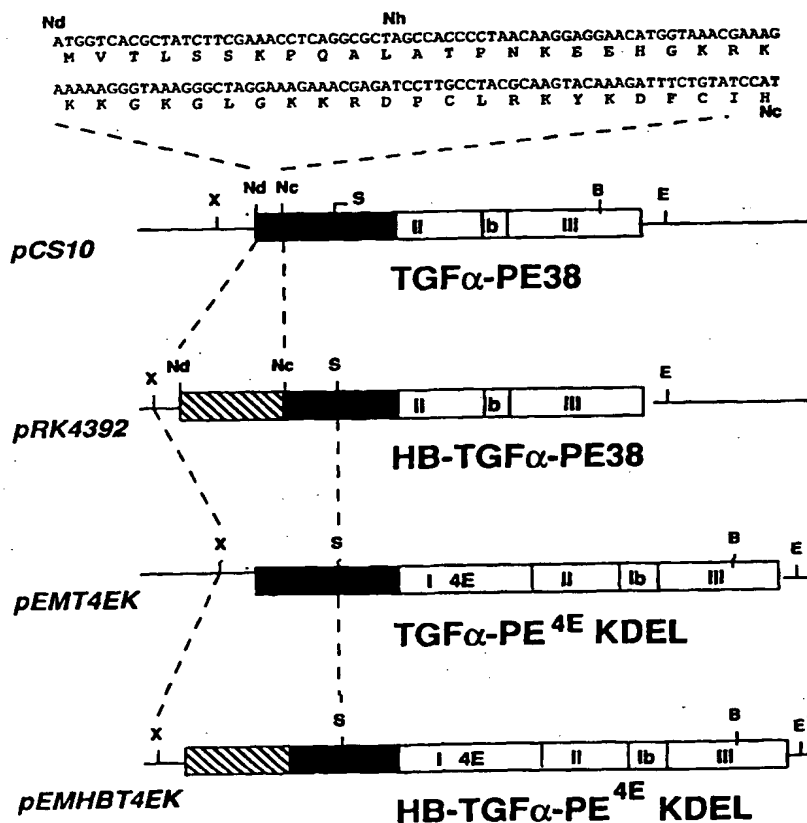
A

FIG. 1. A, amino acid sequence comparison between HB-EGF (Higashiyama *et al.*, 1991), EGF (Gregory, 1975), and HB-TGF α . Boxed residues indicate identity with the corresponding residue of HB-EGF. Underlined are the residues encompassing the HB domain. B, DNA and amino acid sequence of the HB domain of HB-EGF and the structure of plasmids encoding for the TGF α and HB-TGF α toxins. Abbreviation of restriction enzymes: E, *Eco*RI; B, *Bam*HI; Nc, *Nco*I; Nd, *Nde*I; Nh, *Nhe*I; S, *Sph*I; X, *Xba*I. ■, TGF α sequences; □, PE sequences; ▨, HB (Met amino acids 1-45 of mature HB-EGF) (Higashiyama *et al.*, 1991).

B

met- (aa 1-45) HB-EGF = HB



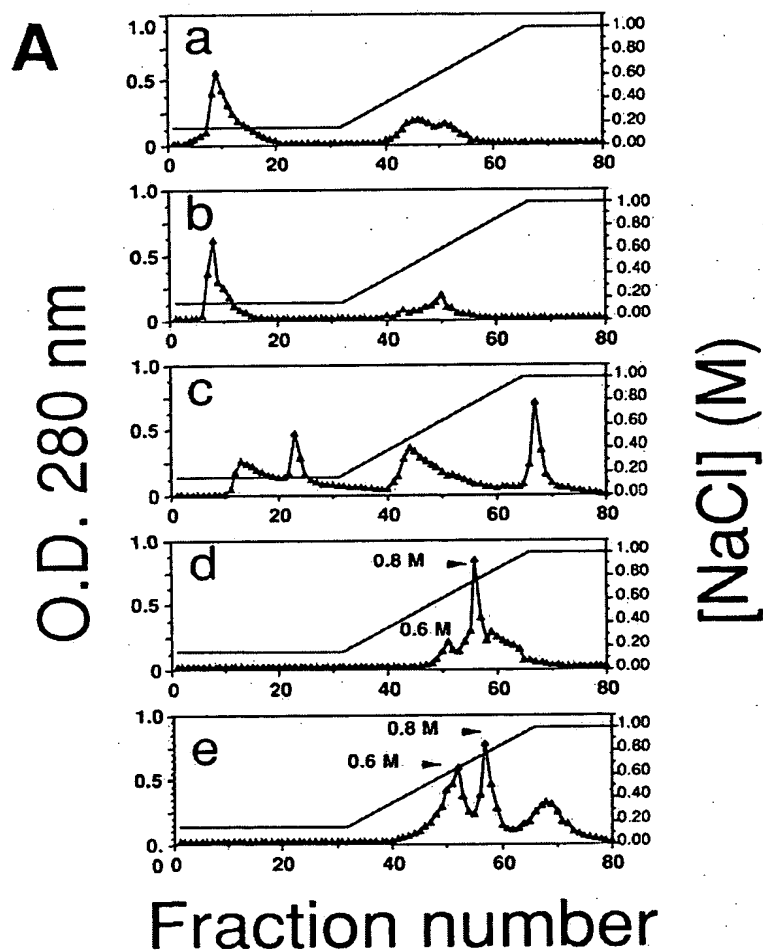
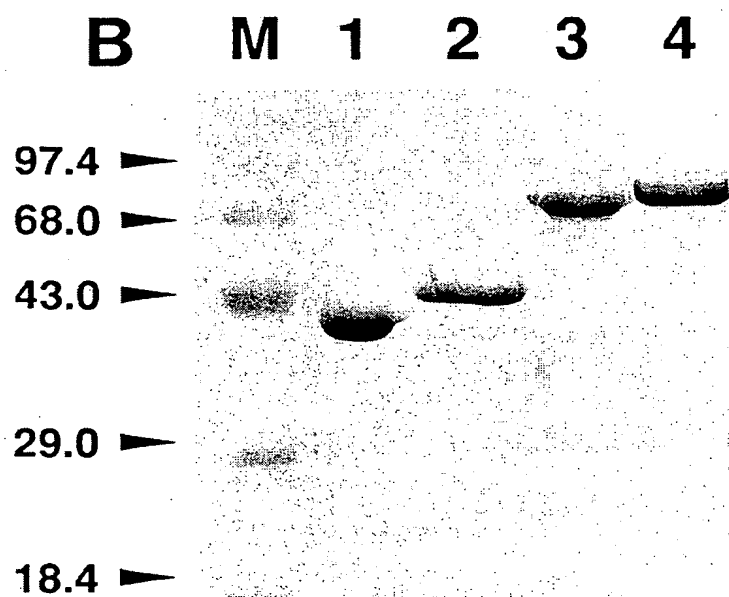


FIG. 2. *A*, heparin affinity chromatography profiles on TSK-heparin columns of TP38 (*a*), TP4EK (*b*), aFGF-PE^{KDEL} (*c*), HB-TP38 (*d*), and HB-TP4EK (*e*). —, NaCl molarity; Δ , OD 280 nm. *B*, purified fractions eluted from TSK chromatography (TGF α -PE toxins) or TSK-heparin chromatography (HB-TGF α -PE toxins) analyzed by SDS-polyacrylamide gel electrophoresis on a 12% polyacrylamide gel and stained with Coomassie Blue. Lane 1, molecular mass standards; lane 2, TP38; lane 3, HB-TP38; lane 4, TP4EK; lane 5, HB-TP4EK.



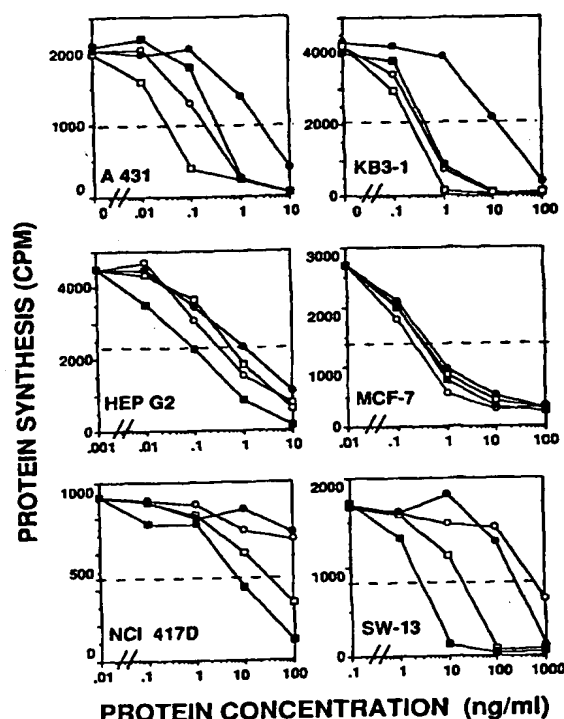


FIG. 3. Cytotoxicity assay of TGF α and HB-TGF α toxins on human cancer cell lines. O, TP38; \square , TP4EK; \bullet , HB-TP38; \blacksquare , HB-TP4EK; ---, 50% [3 H]leucine incorporation.

TABLE I

Cytotoxicity of TGF α and HB-TGF α toxins toward different human cancer cell lines

Cell lines (cancer type)	ID ₅₀			
	TP38	HB-TP38	TP4EK	HB-TP4EK
	ng/ml			
A431 (epidermoid)	0.05	1	0.03	0.12
KB3-1 (epidermoid)	0.4	20	0.35	0.7
COLO 205 (colon)	0.25	7	0.25	0.35
HT-29 (colon)	1.5	8	ND	0.5
CRL 1739 (gastric)	0.5	7	0.35	0.5
HEP G2 (hepatoma)	1.5	2	0.5	0.1
LNCAP (prostate)	0.15	0.4	0.15	0.3
MCF-7 (breast)	0.4	0.5	0.5	0.5
MDA-MB-468 (breast)	0.15	3	ND*	0.3
NCI 417D (lung)	1000	1000	30	7
MG63 (osteosarcoma)	0.7	50	ND	0.3
TE-671 (rhabdomyosarcoma)	1	8	1	1
U-251 (glioblastoma)	0.05	0.5	0.05	0.05
D-54MG (glioma)	0.5	5	0.3	0.3
SW-13 (adrenal)	650	250	20	2.5

* ND, not determined.

the HB domain are the cause of differences in the cytotoxic activities between HB-TGF α -PE and TGF α -PE toxins, we expected to find different cytotoxic responses among different cell lines. Therefore, the cytotoxic activities of HB-TP38 and HB-TP4EK and their respective TGF α -PE forms were measured on a panel of 15 cancer cell lines. As shown in Fig. 3 and Table I, the ID₅₀ values of the chimeric toxins and the relative toxicity of HB-TGF α toxins compared to those without the HB domain varied widely among the different cell lines. In the cell lines A431, Colo205, CRL 1739, KB, MG63, U-251, and D-54MG, TP38 was at least 10-fold more cytotoxic than HB-TP38. In none of the cell lines, except A431, was the

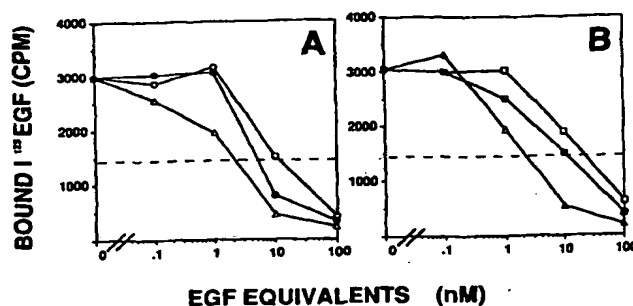


FIG. 4. Displacement of binding of 125 I-EGF to A431 cells by TGF α and HB-TGF α chimeric toxins. Panel A, Δ , EGF; O, TP38; \bullet , HB-TP38. Panel B, Δ , EGF; \square , TP4EK; \blacksquare , HB-TP4EK.

TABLE II

Effect of heparin on the cytotoxicity of heparin binding toxins on various human cancer cell lines

Cytotoxicity experiments were carried out in presence of 2.5 μ /ml of heparin. -, indicates no effect on the cytotoxicity. +, indicates an inhibitory effect on the cytotoxicity, with less than a 5-fold increase in the ID₅₀. ++, indicates an inhibitory effect of 5-10-fold increase in the ID₅₀. +++, indicates an inhibitory effect of more than 10-fold increase in the ID₅₀. A, indicates an increase in the cytotoxicity, with at least a 3-fold decrease in the ID₅₀.

	TP4EK	HB-TP4EK
A431	-	-
CRL 1739	-	+
KB3-1	-	+
LNCAP	-	+
SW-13	-	++
U-251	A	++
NCI 417D	-	++
COLO 205	-	+++
D-54MG	-	+++
HEP G2	-	+++
TE-671	-	+++
MCF-7	-	+++

cytotoxic effect of TP4EK more than 2-fold greater than that of HB-TP4EK (Table I). On cell lines HEPG2, H-421, and SW-13, HB-TP4EK was 4-8-fold more cytotoxic than TP4EK. In all the cell lines except MCF-7 and LNCaP, HB-TP4EK was much more cytotoxic (8-145-fold) than HB-TP38. These data show that the HB-chimeric toxin containing the full-length mutant PE toxin ending in KDEL (PE^{KDEL}) had more cytotoxic activity than the truncated form (PE38). Moreover, the addition of the HB domain to TP4EK maintained much of the cytotoxicity of the TGF α -PE toxin to most of the cell lines tested and improved its cytotoxicity toward several cell lines.

Effect of Heparin on the Cytotoxicity of HB-TGF α -PEs—To study the influence of interactions involving the HB domain on cytotoxicity, we used soluble heparin. When the heparin-binding toxins were preincubated with heparin prior to testing their cytotoxicity, the only cell line which consistently showed a modification of cytotoxicity was the glioblastoma cell line U-251. In this cell line, the sensitivity to HB-TP4EK increased 3.5-fold after the preincubation of the toxin with heparin (data not shown). When cells and toxins were exposed to 10 μ g/ml (2.5 units/ml) of heparin, most of the cell lines but not A431 showed a specific dose-dependent inhibition in the cytotoxicity of HB-TP4EK (Table II and Fig. 5). Fig. 5 shows that even concentrations of heparin up to 100 units/ml did not affect the sensitivity of A431 cells to HB-TP4EK. The cytotoxic activity of TP4EK was also not significantly modified by heparin either by preincubation or

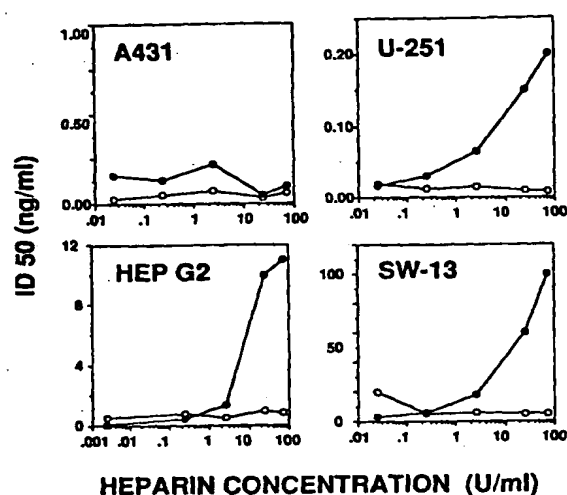


FIG. 5. Effect of heparin on the cytotoxicity of ID₅₀ (○) TP4EK and HB-TP4EK (●) on different cell lines. Cytotoxicity assays were performed in the presence of the indicated concentration of heparin, as described in text.

by addition of heparin to the cytotoxicity assay. Therefore, the addition of the HB domain confers the ability of the toxins to be modulated by heparin, suggesting a role for interactions of the HB domain with cellular components on the cytotoxicity of HB-TGF α toxins.

Competition Studies with EGF and Heparin—The enhanced cytotoxicity of the HB-TGF α toxins toward some cell lines, and the inhibition by heparin suggests that the HB domain, in addition to the EGFR-binding domain, plays a role in the binding and internalization of the HB-TGF α toxins. To determine the importance to toxin internalization of both the EGFR and the putative receptor for the HB domain, we performed competition assays using an excess of EGF with or without excess heparin. Fig. 6A shows that the cytotoxicity of TP4EK and HB-TP4EK toward A431 and KB cells is completely blocked by EGF. Similar results were found with CRL 1739 cells (data not shown). Conversely, the cytotoxicity to LNCAP and SW-13 cells was not competed by EGF (data not shown). Finally, in HEPG2 and MCF-7 cells (and U-251, data not shown) the extent of EGF competition achieved for HB-TP4EK was much lower than that for TP4EK (Fig. 6A). In all cases the lack of competition was overcome by the addition of heparin (Fig. 6A), further suggesting that interactions with the HB domain in some cell lines affects toxin binding and/or internalization.

Like other growth factors carrying heparin-binding domains such as bFGF, the HB-TGF α toxins may bind to heparan sulfate chains present on cell surface heparan sulfate proteoglycans (HSPGs) (Klagsbrun and Baird, 1991; Rapraeger *et al.*, 1991). To test whether the binding to HSPG was involved in the internalization of HB-TGF α toxins, we performed cytotoxicity experiments after treatment of the cells with heparitinase, an enzyme that specifically degrades heparan sulfate chains (Linhardt *et al.*, 1990; Rapraeger *et al.*, 1991). As shown in Fig. 6B, treatment with heparitinase decreased the toxicity of HB-TP4EK on HEP G2 cells and MCF-7 cells, but did not alter the cytotoxicity of both the TGF α and HB-TGF α toxins to A431 cells. This result, together with the data from the competition experiment, indicates that in HEPG2 and MCF-7 cells binding of the HB domain to HSPG is involved in the internalization of HB-TGF α toxins. Moreover, in HEPG2 cells in which the HB-

TP4EK is more cytotoxic than TP4EK, treatment with heparitinase decreased the cytotoxicity of the HB toxin to a value similar to TP4EK, indicating that the enhancement of the cytotoxicity by the HB domain is due to binding to cell surface heparan sulfates.

HB-TGF α -PE as a Cytotoxic Agent to Rapidly Proliferating Smooth Muscle Cells—Because proliferation of SMCs is associated with vascular disease processes such as restenosis after angioplasty and atherosclerosis (Ross, 1986; Austin *et al.*, 1987; Woolf, 1990) and because HB-EGF is a much more potent growth factor for VSMC than EGF (Higashiyama *et al.*, 1991), we wished to determine the cytotoxic activity of the HB-TGF α toxins to proliferating VSMC. Accordingly, we compared the cytotoxic activity of HB-TGF α and TGF α toxins to rapidly proliferating SMC (growing in 10% FBS) or to quiescent SMC (growing in 0.5% FBS). Table III shows that TP38, HB-TP4EK, and TP4EK were more cytotoxic to proliferating smooth muscle cells than to quiescent VSMC. HB-TP4EK is over 10-fold more cytotoxic to proliferating VSMC than to quiescent VSMC. This differential effect was previously shown using TGF α and aFGF chimeric toxins (Epstein *et al.*, 1991; Biro *et al.*, 1991) and ascribed to a proliferation induced up-regulation of EGFR and FGF receptors. Most importantly, we found in this study that HB-TP4EK is 6-fold more potent toward proliferating vascular SMCs than TP4EK (ID₅₀ 0.25 ng/ml versus 1.5 ng/ml). We also tested the effect of heparin in this system, and we found that heparin also selectively inhibited the cytotoxicity of the HB-TGF α toxins against vascular SMCs (Table III). TP38 and TP4EK, however, showed an increased cytotoxicity in the presence of heparin. These results indicate that both HB-TP4EK or the combination of TGF α toxins and heparin may constitute highly cytotoxic agents to target proliferating VSMC.

DISCUSSION

The objective of the present work was to test the effect of the putative heparin-binding domain from HB-EGF on the activity of toxins targeted to the EGFR. We found that the addition of the HB domain to TP38 and TP4EK conferred an ability to bind to heparin and changed cytotoxic activity toward a panel of cancer cell lines and SMCs. Inclusion of the HB domain did not substantially alter the affinity of the chimeric toxins for the EGFR. However, the specific heparin inhibition of the activity of the HB-TGF α toxins and the results of competition experiments with EGF and experiments with heparitinase indicated that binding of the heparin-binding domain to cell surface heparan sulfate proteoglycans is involved in the uptake of the toxin.

Expression, Refolding, and Purification of the HB-TGF α -PEs—The production of a recombinant toxin having the bifunctional ligand HB-TGF α posed several problems. Since these proteins are produced in *E. coli* as inclusion bodies, the protein must be denatured and then renatured to acquire its active conformation. Although our HB-TGF α ligand was very similar to HB-EGF (Fig. 1A), we did not know if we attached HB-TGF α to PE that the resulting molecule would fold correctly. Our results showed that after renaturation under controlled conditions, HB-TGF α toxins bound to immobilized heparin and eluted at 0.8 M NaCl. TP38 and TP4EK renatured under the same conditions eluted from heparin at 0.15 M NaCl. These results indicate that the HB domain from HB-EGF is a polypeptide sequence capable of conferring high affinity heparin binding to another molecule. Therefore, we conclude that the heparin-binding domain of HB-EGF is contained within its amino-terminal 42 residues.

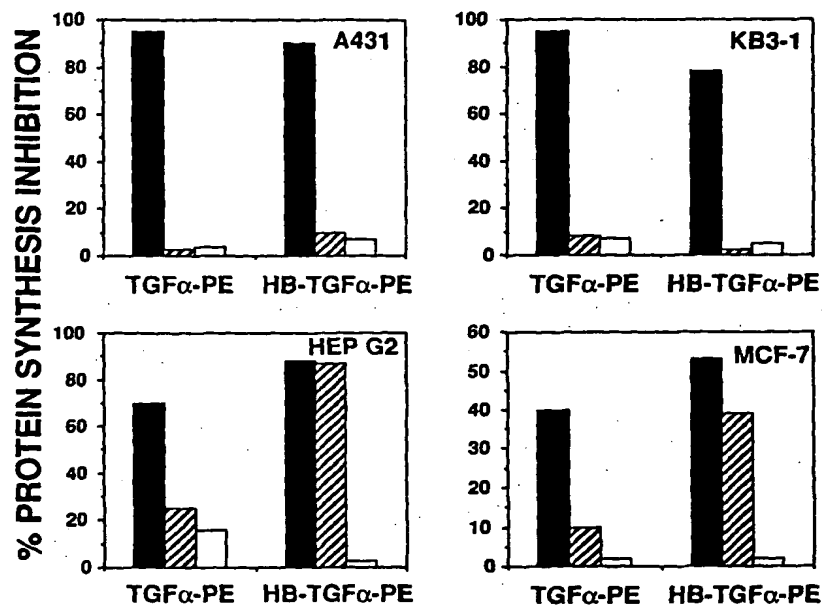
A

FIG. 6. A, competition of the cytotoxicity of TP4EK and HB-TP4EK by heparin and EGF. The cytotoxic assay was performed in the presence of 4 μ g/ml of EGF (▨), 4 μ g/ml of EGF plus 2.5 units/ml of heparin (□), or with no additions (■). Bars represent % inhibition of [3 H]-leucine incorporation at the following toxin concentration: A431 cells, 10 ng/ml; KB cells, 10 ng/ml; HEP G2 cells, 10 ng/ml; MCF-7 cells, 100 ng/ml. B, effect of treatment with heparitinase on the cytotoxicity of TGF α and HB-TGF α toxins. ▨, without heparitinase. ■, cells were incubated with 1 milliunit/ml of heparitinase at 37 °C for 3 h before toxin addition.

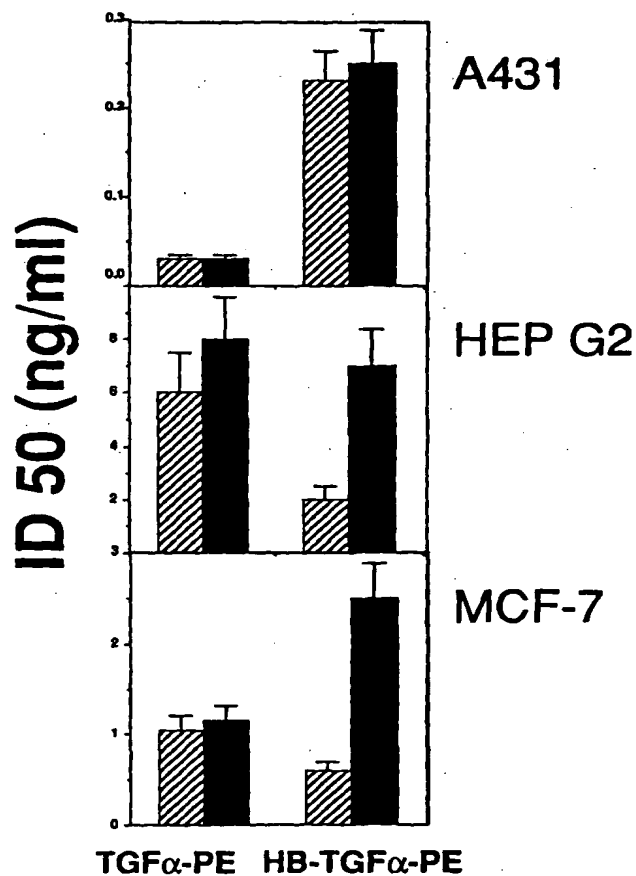
B

TABLE III
Cytotoxicity of heparin-binding TGF α toxins to smooth muscle cells:
effect of heparin on quiescent and rapidly proliferating cells

Toxin	ID ₅₀ (ng/ml)			
	Quiescent (0.5% fetal bovine serum)		Proliferating (10% fetal bovine serum)	
	-HEP ^a	+HEP ^a	-HEP	+HEP
TP38	15	ND ^c	2.5	0.12
HB-TP38	>1000	ND	100	>1000
TP4EK	4	1.5	1.5	0.6
HB-TP4EK	3	70	0.25	15

^a Control experiments.

^b Cytotoxicity experiments were carried out in presence of 2.5 units/ml of heparin.

^c ND, not done.

TABLE IV
Relative cytotoxicity of HB-TGF toxins, and competition by heparin and EGF, for cells with different levels of EGF receptor surface expression

	Rec $\times 10^5$	ID ₅₀ HB-TGF α -PE/ ID ₅₀ TGF α -PE		Competition	
		-PE38	-PE ⁴² KDEL	Heparin	EGF
A431	3000	20	4	-	++
KB3-1	200	50	2	+	+
LNCAP	20	2.5	2	+	-
HEP-G2	9	1.6	0.2	+++	-
MCF7	0.8	1.2	1	+++	-

The next question was whether the new molecule was cytotoxic to target cells. We used cytotoxicity as an indication that the toxin was binding to the EGFR and was also efficiently processed within cells in order to display its ADP-ribosylation activity in the cytosol of target cells. The protein eluting at 0.8 M NaCl probably contains a better folded HB domain than in fractions eluting at 0.6 M NaCl. Furthermore, HB-TGF α toxins that eluted at 0.8 M were more cytotoxic and bound to the EGFR with 10-fold higher affinity than those eluting at 0.6 M (data not shown). The cytotoxic activity of TGF α and HB-TGF α chimeric toxins toward a panel of target cell lines showed that cell lines could be less sensitive, show little or no change, or become more sensitive upon addition of the HB domain. These results, together with the binding and competition studies, indicate that the HB domain interacts with cellular components to modify the activity of the TGF α toxin. In Table IV, the results of the relative cytotoxicity of TGF α and HB-TGF α toxins toward cell lines with known numbers of EGFR are summarized. Cell lines are ordered according to their EGFR number. It is apparent that for cells displaying high numbers of EGFRs, TP38 and TP4EK are more cytotoxic than HB-TP38 and HB-TP4EK, respectively. The cytotoxicity of HB-TGF α toxins toward these cells is less sensitive to heparin inhibition but very sensitive to excess EGF. On the other hand, for cell lines displaying low numbers of EGFR, HB-TGF α toxins are of equal or greater cytotoxicity than their respective TGF α toxins. In these cell lines the cytotoxicity of HB-TGF α toxins is less sensitive to inhibition by EGF but more sensitive to inhibition by heparin, and also affected by heparitinase treatment (see Fig. 6B). Thus, in cells with low numbers of EGFRs, the heparin-binding domain is involved in the increase in cytotoxic activity. Furthermore, our results indicate that the HB domain binds to cell surface HSPGs, which facilitates internalization of the toxin. This indicates that HB-TGF α toxins may function as chimeric toxins with two ligands. We have previously found that cell lines expressing high numbers

of EGFRs were more sensitive to TGF α toxin if it did not contain interleukin 6 as an additional ligand (Kreitman *et al.*, 1991b). However, as in the present study, cells with a low number of EGFRs were more sensitive to TGF α toxins if they contained an additional ligand (Kreitman *et al.*, 1991b).

The reason for the decrease in the cytotoxicity caused by the HB domain in cell lines with high numbers of EGFRs is unclear. In A431 cells the HB domain neither modifies binding to the EGFR nor affects the cytotoxicity when bound to heparin. Moreover, the cytotoxicity to A431 cells is not modified by treatment with heparitinase indicating that the binding to HPSG is not involved in the cytotoxic activity in this cell line. In most of the cell lines we observed that the relative differences in cytotoxicity between HB-TGF α and TGF α toxins decreased when we replaced both the toxin portion by PE⁴² and the COOH terminus of the toxin by KDEL (see Table I). This improvement may be due to better processing and/or intracellular targeting of the toxin (Ogata *et al.*, 1986; Chaudhary *et al.*, 1990; Seetharam *et al.*, 1991; Siegall *et al.*, 1991). It is possible that these functions are impaired in most of the cell lines when the HB domain is present, but are less impaired for toxins bearing PE⁴²KDEL.

We postulate at least two mechanisms by which the binding of the HB domain to HSPG can increase cytotoxicity. In cells expressing high levels of HSPG, the increase in the local concentration of toxin on the surface of the cell may facilitate the binding of the toxin to the EGF receptor (Ruoslahti and Yamaguchi, 1991). HSPG may also internalize HB-TGF α toxins; endocytosis of heparin sulfate proteoglycans has been demonstrated (Yanagishita and Hascall, 1992). Other heparin-binding growth factors such as basic FGF and acidic FGF have been shown to bind cell surface HSPG (Klagsbrun and Baird, 1991; Rapraeger *et al.*, 1991). However, unlike HB-TGF α and HB-EGF they need to bind either to heparin or heparan sulfate to acquire a conformation capable of binding to their high affinity receptor (Klagsbrun and Baird, 1991). Since TGF α displays full binding activity to the EGFR, our results indicate that heparin like molecules exert a modulatory effect on the binding of the HB-TGF α ligand to the EGFR through the HB domain. We suspect the addition of a HB domain may confer the ability to be modulated by heparin to other ligands.

HB-TGF α as a Targeting Ligand to Vascular Smooth Muscle Cells—We expected HB-TGF α toxins to be more cytotoxic toward proliferating VSMC because HB-EGF is more mitogenic and binds more avidly to smooth muscle cells than does EGF (Higashishima *et al.*, 1991). The 60-fold competition of the cytotoxicity of HB-TP4EK by heparin suggests that the HB domain of the molecule binds to surface HSPG and this facilitates internalization. One important question is why the cytotoxicity of TGF α toxins improves with heparin. A possible explanation is that the antiproliferative activity of heparin in SMC may enhance the cytotoxicity of TGF α chimeric toxins (Karnovsky *et al.*, 1989; Edelman *et al.*, 1990). The transient proliferation of medial smooth muscle cells and their subsequent migration to the intima and continued proliferation is one of the causes of restenosis after angioplasty (Austin *et al.*, 1987). Agents such as like HB-TP4EK, a molecule capable of specifically targeting rapidly proliferating VSMC, while preserving normally growing VSMC (see Table III), merits investigation in the treatment of this common disorder (Epstein *et al.*, 1991).

CONCLUSIONS

By adding a HB domain from HB-EGF in a recombinant toxin composed of TGF α fused to mutant forms of PE, we

generated two new cytotoxic agents, HB-TP38 and HB-TP4EK. The HB domain enables the toxin to bind with high affinity to heparin. This characteristic allows the toxin to interact with and to be modulated by heparan sulfate proteoglycans of the cell and by exogenous heparin. Our experiments show several ways in which this interaction can be exploited: HB-TGF toxins often have enhanced cytotoxicity to malignant cell lines that express low levels of EGFR and might be useful in targeting proliferating VSMC. Addition of exogenous heparin might decrease the hepatic toxicity of HB-TGF α toxins, while preserving cytotoxic activity to malignant cells expressing high numbers of EGFRs. Finally, such toxins are useful in studying the biology of heparan sulfate proteoglycans and may give important insights into the biology and physiology of heparin-binding growth factors which bind to the EGFR.

Acknowledgments—We greatly appreciate the assistance of E. Lovelace and A. Harris in culturing the cell lines. We thank E. Gott and A. Jackson for editorial assistance. E. A. M. would like to dedicate this paper to his mother Frida Schlaen (1937–1982).

REFERENCES

- Allured, V. S., Collier, R. J., Carroll, S. F., and McKay, D. B. (1986) *Proc. Natl. Acad. Sci. U. S. A.* **83**, 1320–1324.
- Austin, G. E., Ratliff, N. B., Hollman, J., Tabeil, S., and Philips, D. (1987) *J. Am. Coll. Cardiol.* **6**, 369–375.
- Batra, J. K., Kasturi, S., Gallo, M. G., Voorman, R. L., Maio, S. M., Chaudhary, V. K., and Pastan, I. (1992) *Mol. Immunol.*, in press.
- Biro, S. S., Siegall, C. B., Fu, Y.-M., Speir, E., Pastan, I., and Epstein, S. E. (1992) *Circ. Res.* **71**, 640–645.
- Brinkmann, U., Pai, L. H., FitzGerald, D. J., and Pastan, I. (1991) *Proc. Natl. Acad. Sci. U. S. A.* **88**, 8616–8620.
- Brinkmann, U., Pai, L. H., FitzGerald, D. J., and Pastan, I. (1992) *Proc. Natl. Acad. Sci. U. S. A.* **89**, 3065–3069.
- Buchner, J., Pastan, I., and Brinkmann, U. (1992) *Anal. Biochem.* **205**, 263–270.
- Caascells, W., Lappi, D. A., Olwin, B. B., Wai, C., Siegman, M., Speir, E. H., Sasse, J., and Baird, A. (1992) *Proc. Natl. Acad. Sci. U. S. A.* **89**, 7159–7163.
- Chaudhary, V. K., FitzGerald, D. J., Adhya, S., and Pastan, I. (1987) *Proc. Natl. Acad. Sci. U. S. A.* **84**, 4538–4542.
- Chaudhary, V. K., Mizukami, T., Fuerst, T. R., FitzGerald, D. J., Moss, B., Pastan, I., and Berger, E. A. (1988) *Nature* **335**, 369–372.
- Chaudhary, V. K., Queen, C., Junghans, R. P., Waldmann, T. A., FitzGerald, D. J., and Pastan, I. (1989) *Nature* **339**, 394–397.
- Chaudhary, V. K., Jinno, Y., FitzGerald, D., and Pastan, I. (1990a) *Proc. Natl. Acad. Sci. U. S. A.* **87**, 308–312.
- Chaudhary, V. K., Jinno, Y., Gallo, M. G., FitzGerald, D. P., and Pastan, I. (1990b) *J. Biol. Chem.* **265**, 16306–16310.
- Edelman, E. R., Adams, D. H., and Karnovsky, M. J. (1990) *Proc. Natl. Acad. Sci. U. S. A.* **87**, 3773–3777.
- Epstein, S. E., Siegall, C. B., Biro, S., Fu, Y., FitzGerald, D., and Pastan, I. (1991) *Circulation* **84**, 778–787.
- FitzGerald, D. J. P., Morris, R. E., and Saelinger, C. B. (1980) *Cell* **21**, 867–873.
- Gregory, H. (1975) *Nature* **257**, 235–237.
- Heimbrook, D. C., Sturdivant, S. M., Ahern, J. D., Balishin, N. L., Patrick, D. R., Edwards, G. M., Defeo, J. D., FitzGerald, D. J., Pastan, I., and Oliff, A. (1990) *Proc. Natl. Acad. Sci. U. S. A.* **87**, 4697–4701.
- Higashiyama, S., Abraham, J., Miller, J., Fiddes, J., and Klagsbrun, M. (1991) *Science* **251**, 936–938.
- Higashiyama, S., Lau, K., Besner, G. E., Abraham, J. A., and Klagsbrun, M. (1992) *J. Biol. Chem.* **267**, 6205–6212.
- Hwang, J., FitzGerald, D. J., Adhya, S., and Pastan, I. (1987) *Cell* **48**, 129–136.
- Iglewski, B. H., and Kabat, D. (1975) *Proc. Natl. Acad. Sci. U. S. A.* **72**, 2284–2288.
- Jinno, Y., Chaudhary, V. K., Kondo, T., Adhya, S., FitzGerald, D. J., and Pastan, I. (1988) *J. Biol. Chem.* **263**, 13203–13207.
- Karnovsky, M. J., Wright, T. C. J., Castellot, J. J., Choay, J., Lormeau, J.-C., and Petitou, M. (1989) *Ann. N. Y. Acad. Sci.* **556**, 268–281.
- Klagsbrun, M., and Baird, A. (1991) *Cell* **67**, 229–231.
- Klagsbrun, M., Marikowski, M., Abraham, J., Thompson, S., Damm, D., and Higashiyama, S. (1992) *J. Cell Biochem.* **16A**, 6.
- Kreitman, R. J., Chaudhary, V. K., Siegall, C., FitzGerald, D. J., and Pastan, I. (1991a) *Bioconjugate Chem.* **3**, 1992.
- Kreitman, R. J., Siegall, C. B., Chaudhary, V. K., FitzGerald, D. J., and Pastan, I. (1991b) *Bioconjugate Chem.* **3**, 63–68.
- Laemmli, U. K. (1970) *Nature* **227**, 680–685.
- Lindner, V., Lappi, D. A., Baird, A., Majack, R. A., and Reidy, M. A. (1991) *Circ. Res.* **68**, 106–113.
- Linhardt, R. J., Turnbull, J. E., Wang, H. M., Loganathan, D., and Gallagher, J. T. (1990) *Biochemistry* **29**, 2611–2617.
- Ogata, M., Chaudhary, V. K., Pastan, I., and FitzGerald, D. J. (1990) *J. Biol. Chem.* **265**, 20678–85.
- Pai, L. H., Gallo, M., FitzGerald, D. J., and Pastan, I. (1991) *Cancer Res.* **51**, 2808–2812.
- Pastan, I., and FitzGerald, D. (1989) *J. Biol. Chem.* **264**, 15157–15160.
- Pastan, I., Willingham, M. C., and FitzGerald, D. J. P. (1986) *Cell* **47**, 641–648.
- Pastan, I., Chaudhary, V., and FitzGerald, D. J. (1992) *Annu. Rev. Biochem.* **61**, 331–354.
- Prior, T. I., Helman, L. J., FitzGerald, D. J., and Pastan, I. (1991) *Cancer Res.* **51**, 174–180.
- Rapraeger, A. C., Krufka, A., and Olwin, B. B. (1991) *Science* **252**, 1705–1708.
- Ross, R. (1986) *N. Engl. J. Med.* **314**, 488–500.
- Ruoslahti, E., and Yamaguchi, Y. (1991) *Cell* **64**, 867–869.
- Seetharam, S., Chaudhary, V. K., FitzGerald, D., and Pastan, I. (1991) *J. Biol. Chem.* **266**, 17376–17381.
- Shoyab, M., Plowman, G., McDonald, V., Bradley, J. G., and Todaro, G. J. (1989) *Science* **243**, 1074–1076.
- Siegall, C. B., Chaudhary, V. K., FitzGerald, D. J., and Pastan, I. (1988) *Proc. Natl. Acad. Sci. U. S. A.* **85**, 9738–9742.
- Siegall, C. B., Chaudhary, V. K., FitzGerald, D. J., and Pastan, I. (1989a) *J. Biol. Chem.* **264**, 14256–14261.
- Siegall, C. B., Xu, Y.-H., Chaudhary, V. K., Adhya, S., FitzGerald, D., and Pastan, I. (1989b) *FASEB J.* **3**, 2647–2652.
- Siegall, C. B., Epstein, S. E., Speir, E., Hla, T., Forough, R., Maciag, T., FitzGerald, D. J., and Pastan, I. (1991) *FASEB J.* **5**, 2843–2844.
- Studier, F. W., and Moffatt, B. A. (1986) *J. Mol. Biol.* **189**, 113–130.
- Vitetta, E. S., Fulton, R. J., May, R. D., Till, M., and Uhr, J. W. (1987) *Science* **238**, 1098–1104.
- Whalen, G. F., Shing, S., and Folkman, J. (1989) *Growth Factors* **1**, 157–164.
- Woolf, N. (1990) *Br. Med. Bull.* **46**, 960–985.
- Yanagishita, M., and Hascall, V. C. (1992) *J. Biol. Chem.* **267**, 9451–9454.
- Yoshisumi, M., Kourembanas, S., Temizer, D. H., Cambria, R. P., Quertermous, T., and Lee, M.-E. (1992) *J. Biol. Chem.* **267**, 9467–9469.

Recombinant Toxins Containing Human Granulocyte-Macrophage Colony-Stimulating Factor and Either Pseudomonas Exotoxin or Diphtheria Toxin Kill Gastrointestinal Cancer and Leukemia Cells

By Robert J. Kreitman and Ira Pastan

The granulocyte-macrophage colony-stimulating factor receptor (GM-CSFR) is a potential target for toxin-directed therapy, because it is overexpressed on many leukemias and solid tumors and apparently not on stem cells. To investigate the potential therapeutic use of GM-CSF toxins, we fused human GM-CSF to truncated forms of either Pseudomonas exotoxin (PE) or diphtheria toxin (DT) and tested the cytotoxicity of the resulting GM-CSF-PE38KDEL and DT388-GM-CSF on human gastrointestinal (GI) carcinomas and leukemias. Toward gastric and colon cancer cell lines, GM-CSF-PE38KDEL was much more cytotoxic than DT388-GM-CSF, with IC_{50} s (concentration resulting in 50% inhibition of protein synthesis) of 0.5 to 10 ng/mL compared with 4 to 400 ng/mL, respectively. In contrast, toward leukemia lines and fresh bone marrow cells DT388-GM-CSF was more cytotoxic than GM-CSF-PE38KDEL. The cytotoxicity of both GM-CSF-PE38KDEL and DT388-GM-CSF toward the human cells was specific, because it could be competed by an ex-

cess of GM-CSF. Binding studies indicated that human GM-CSF receptors were present on all of the human GI and leukemic cell lines tested, at levels of 540 to 3,700 sites per cell ($k_d = 0.2$ to 2 nmol/L), and the number of sites per cell did not correlate with the cell type. A similar pattern of cytotoxicity was found with recombinant immunotoxins binding to the transferrin receptor, in that anti-TFR(Fv)-PE38KDEL was much more cytotoxic than DT388-anti-TFR(Fv) toward GI cells, but both were similar in their cytotoxic activity toward leukemia cells. The fact that PE is more effective than DT in killing GI but not leukemic tumor cells targeted by GM-CSF indicates a fundamental difference in the way PE or DT gains access to the cytosol in these cells. GM-CSF-PE38KDEL and DT388-GM-CSF deserve further evaluation as possible treatments for selected tumors.

This is a US government work. There are no restrictions on its use.

GRANULOCYTE-MACROPHAGE colony-stimulating factor (GM-CSF) is a cytokine responsible for the growth, differentiation, and functional enhancement of granulocytes and macrophages.¹⁻³ Human GM-CSF is 127 amino acids long and binds to hematopoietic cells via high-affinity ($k_d = 10$ to 50 pmol/L) receptors composed of α and β subunits.⁴⁻⁸ GM-CSF is used to attenuate the myelosuppressive effects of chemotherapy in the treatment of not only hematologic malignancies but also solid tumors,⁹ and it has been shown that GM-CSF usually does not stimulate the growth of solid tumors.¹⁰ However, like leukemias,¹¹ solid tumors, including renal, lung, breast, and gastrointestinal carcinomas, also express GM-CSF receptors (GM-CSFRs), at least the low affinity α component ($k_d = 0.7$ to 2 nmol/L).¹²⁻¹⁶

Recent studies have shown that GM-CSFR is absent on the most immature hematopoietic progenitors but increases in expression during maturation.¹⁷ This finding suggests that the GM-CSFR may be a useful target for recombinant toxins or immunotoxins, which contain a cell binding protein linked to a protein toxin. Murine GM-CSF has recently been fused to truncated diphtheria toxin and the resulting DT₃₉₀mGM-CSF was cytotoxic to murine GM-CSFR-bearing cells.¹⁸ A

chemical conjugate of human GM-CSF with saporin was shown to kill mouse cells transfected with the human receptor.¹⁹ To determine the utility of GM-CSFR as a means to target human hematologic and solid tumors, we fused human GM-CSF to truncated forms of Pseudomonas exotoxin (PE) or diphtheria toxin (DT).

PE is a 66-kD protein that, like DT, kills cells by binding to a receptor, internalizing via a coated pit, translocating its active fragment into the cytosol, and enzymatically ADP-ribosylating elongation factor-2.^{20,21} The x-ray crystallographic structure of PE indicates three major domains, and mutational analysis has elucidated which domains are responsible for the several steps necessary to kill cells.^{22,23} Domain Ia, which is composed of amino acids 1 through 252, functions to bind the toxin to the PE receptor. Domain III (amino acids 400 through 613) contains the enzymatic activity that ADP-ribosylates EF2. Domain II (amino acids 253 through 364) undergoes proteolytic processing and is responsible for translocating to the cytosol the 37-kD carboxyl terminus of PE that contains the ADP ribosylating activity. DT also undergoes proteolytic processing,²⁴ but its amino terminus contains the ADP-ribosylating activity and is translocated to the cytosol. Accordingly, in chimeric DT-containing toxins, the ligand replaces the toxin's binding domain at the carboxyl terminus. Conversely, in PE-containing chimeric toxins, the ligand replaces the toxin's binding domain at the amino terminus. The truncated form of PE used in the present study ends in KDEL, which has been shown to improve the cytotoxicity of PE-containing toxins and to increase binding of the toxin fragment to the KDEL receptor, which probably transports it to the endoplasmic reticulum, where it can translocate to the cytosol.²⁵⁻²⁷

MATERIALS AND METHODS

Plasmid construction. The polymerase chain reaction (PCR) was performed using a PCR kit from Perkin Elmer Cetus (Norwalk, CT). Denaturation temperature was 94°C for 1 minute, annealing was at 55°C for 2 minutes, and polymerization was at 72°C for 3 minutes,

From the Laboratory of Molecular Biology, Division of Cancer Biology, National Cancer Institute, National Institutes of Health, Bethesda, MD.

Submitted July 1, 1996; accepted February 13, 1997.

Address reprint requests to Ira Pastan, MD, Laboratory of Molecular Biology, Division of Cancer Biology, National Cancer Institute, National Institutes of Health, 37/4E16, 37 Convent Dr MSC 4255, Bethesda, MD 20892.

The publication costs of this article were defrayed in part by page charge payment. This article must therefore be hereby marked "advertisement" in accordance with 18 U.S.C. section 1734 solely to indicate this fact.

This is a US government work. There are no restrictions on its use. 0006-4971/97/9001-0043\$0.00/0

with 10 seconds of extension per cycle. Plasmids were sequenced using an Applied Biosystems Taq Dyedexy cycle-sequencing kit and an automated sequencer (Applied Biosystems, Foster City, CA). The cDNA encoding human GM-CSF and containing *Nde* I and *Hind*III restriction sites at the ends was obtained from a human spleen cDNA library (Clontech, Palo Alto, CA) using primers BK-134 (5'-gcc-tgc-agg-cat-atg-gca-ccc-gcc-cgc-tgc-ccc-agg-ccc-3') and BK144 (3'-ctg-acg-acc-ctc-ggt-cag-gtc-ctc-att-cga-act-taa-gcc-5'). The 0.41-kb *Nde* I-*Hind*III fragment was then ligated into the 3.0-kb *Nde* I-*Hind*III fragment of pRKL4.²⁸ The resulting plasmid, pRKGM2, contained the reported GM-CSF-encoding sequence,⁶ except for mutations of codons 83 (cac→cgc), 86 (cag→cgg), and 97 (gca→gcg). The mutations at codons 83 and 86 were repaired using revertant primers that separately amplified codons 1 through 87 and 79 through 127. Primers for the first amplification were BK-145 (5'-gga-gat-ata-cat-atg-gca-cca-gca-cga-tcg-cca-agg-cca-agg-cag-ccc-tgg-3') and BK-147 (3'-ggg-aac-tgg-tac-tac-cga-tcg-gtg-atg-ttc-gtc-gtg-5'), and for the second amplification were BK-146 (5'-atg-gct-agg-cac-tac-aag-cag-cac-tgc-cct-cca-acc-3') and BK-148 (3'-ctg-acg-acc-ctc-ggt-cat-gtc-ctt-cga-aga-act-taa-5'). The two overlapping fragments were used as a template for amplification with BK-145 and BK-148. The 0.39-kb *Nde* I-*Hind*III fragment of the final amplification product was then ligated to the 4.5-kb fragment of pRKB3F,²⁹ resulting in pRKGM9K, which had the correct sequence encoding GM-CSF-PE38KDEL. The 0.39-kb *Nde* I-*Hind*III fragment from pRKGM9K was then ligated to the 4.2-kb *Nde* I-*Hind*III fragment of pVCDT1-IL2,³⁰ resulting in pRKDTGM, which encodes DT388-GM-CSF. To make HB9K, encoding anti-TFR(Fv)-PE38KDEL, the 0.35-kb *Nde* I-*Bam*HI and 0.35-kb *Bam*HI-*Hind*III fragments of plasmid pJBDT1-anti-TFR(Fv)³¹ were ligated to the 4.1-kb *Nde* I-*Hind*III fragment of pRK749K.³²

Protein expression and purification. The method for expressing pRKGM9K, pRKDTGM, pRKHB9K, and pJBDT1-anti-TFR(Fv) and purifying the respective recombinant toxins GM-CSF-PE38KDEL, DT388-GM-CSF, anti-TFR(Fv)-PE38KDEL, and DT388-anti-TFR(Fv) differed slightly from the protocol previously reported.³³ *Escherichia coli* BL21/ADE3 cells³⁴ were transformed with each plasmid and grown overnight on LB-ampicillin plates. The transformed cells were cultured in superbroth containing 5 g/L glucose, 1.4 mmol/L MgSO₄, and 100 µg/mL ampicillin. At an OD₆₀₀ of 2 to 3.5, protein synthesis was induced for 90 to 120 minutes with 1 mmol/L isopropyl-B-D-thiogalactopyranoside. The harvested cell paste was resuspended using a Tissuemizer tip (Thomas, Swedesboro, NJ) in TES buffer (50 mmol/L Tris, pH 8, 100 mmol/L NaCl, and 20 mmol/L EDTA) containing 180 µg/mL lysozyme. After incubating at 22°C for 1 hour, the cells were resuspended again and centrifuged at 27,000g for 50 minutes. The pellet was washed by resuspension and centrifugation three or four times with TES buffer containing 2.5% Triton-X-100 and then four times with TES. The inclusion bodies were resuspended in 5 to 10 mL of denaturation buffer (7 mol/L guanidine-HCl, 0.1 mol/L Tris, pH 8.0, and 5 mmol/L EDTA) by sonication or tissuemizing and diluted to a protein concentration of 10 mg/mL. The protein was reduced with dithioerythritol (65 mmol/L) for 4 to 24 hours at 22°C and rapidly diluted in a thin stream into refolding buffer (0.1 mol/L Tris, pH 8.0, 0.5 mol/L arginine-HCl, 2 mmol/L EDTA, and 0.9 mmol/L oxidized glutathione). After incubating at 10°C for 36 to 72 hours, the refolding buffer was either diluted 10-fold with water or dialyzed against 0.02 mol/L Tris, pH 7.4, 1 mmol/L EDTA, and 0.1 mol/L urea. The filtered protein was then purified by Qsepharose and MonoQ (Pharmacia, Piscataway, NJ) anion exchange and finally by sizing chromatography. The yield of purified active monomeric protein was 7.5% to 10% of total denatured recombinant protein.

Cytotoxicity assay. N87 gastric carcinoma cells were obtained from Dr R. King (Georgetown University, Washington, DC),³⁵ HUT-

102 adult T-cell leukemia (ATL) cells were obtained from Dr T. Waldmann (National Institutes of Health), and the other cell lines were available from ATCC (Rockville, MD). A total of 1.5×10^4 cells/well were plated in 96-well plates; 24 hours later, toxin or control molecules were added and incubated for 48 hours in final volumes of 200 µL. The cells were pulsed for 4 to 6 hours with [³H]-leucine 1 µCi/well, harvested, and counted. Bone marrow mononuclear cells were obtained from a patient with lymphocytic leukemia and from a normal donor for allogeneic bone marrow transplantation by Ficoll centrifugation, as described.³⁶ The marrow mononuclear cells (0.4 to 1×10^6 /well) were incubated for 60 hours with toxin or control molecules in 100-µL aliquots of media consisting of 88% leucine-free RPMI, 2% RPMI, and 10% fetal bovine serum. The cells were then pulsed for 6 to 8 hours with [³H]-leucine at 2 µCi/well, harvested, and counted. The IC₅₀ was the concentration of toxin required for 50% protein synthesis inhibition.

Binding assay. Clinical grade GM-CSF was purchased from Immunex (Seattle, WA) and desalted on a PD-10 column (Pharmacia, Piscataway, NJ), equilibrated, and eluted with phosphate-buffered saline (PBS). Na [¹²⁵I] (1 mCi; Amersham, Arlington Heights, IL) was added to a 100 µL volume of PBS containing GM-CSF (50 µg), sodium phosphate, pH 7.5 (150 mmol/L), and chloramine T (3.3 µg). After incubating for 2 minutes at 22°C, sodium metabisulfite (83 µg) was added and the [¹²⁵I]-GM-CSF purified on a PD-10 (Pharmacia) column equilibrated and eluted with 0.2% human serum albumin in PBS. HB21 (also termed anti-TFR-IgG), the monoclonal antibody to the transferrin receptor,³⁷ was labeled the same way except using 75 µg of anti-TFR-IgG and 10 µg of chloramine T. To determine the number of GM-CSF sites per cell, cells were incubated in 96-well U-bottom plates in binding buffer (RPMI containing 0.1% bovine serum albumin and 0.2% NaN₃) containing increasing concentrations of [¹²⁵I]-GM-CSF with or without a 100-fold excess of unlabeled GM-CSF. After 30 minutes at 37°C, the cells were centrifuged and washed once with binding buffer and then counted. This method was easier and more reproducible than centrifuging the cells through n-butyl phthalate and counting the cell pellets. To determine the binding affinity of unlabeled toxins relative to that of GM-CSF, U937 cells (4.8×10^4 /well) were plated in U-bottom 96-well plates in binding buffer and incubated with 1.2 nmol/L [¹²⁵I]-GM-CSF with and without different concentrations of re-

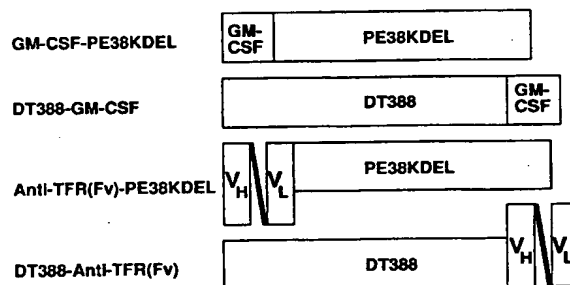


Fig 1. Schematic diagram of the recombinant toxins used. GM-CSF-PE38KDEL, encoded by pRKGM9K, contains the 127 amino acids of human GM-CSF followed by amino acids 253 through 364 and 381 through 608 of PE and then the sequence KDEL. DT388-GM-CSF, encoded by pRKDTGM, contains the first 388 amino acids of DT followed by human GM-CSF. Anti-TFR(Fv)-PE38KDEL and DT388-anti-TFR(Fv), encoded by pRKHB9K and pJBDT1-anti-TFR(Fv), respectively, contain the same toxin domains as the respective GM-CSF toxins, but the ligand is the single-chain Fv of an antitransferrin receptor antibody.

Table 1. Cytotoxicity of Recombinant Toxins Containing Human GM-CSF

Cell Line	Cell Type	IC ₅₀ (ng/mL) ± SD	
		GM-CSF-PE38KDEL	DT388-GM-CSF
LS174T	Colon	2.2 ± 0.7	70 ± 18
SW403	Colon	0.9 ± 0.5	15 ± 0.6
N87	Gastric	0.45 ± 0.2	3.7 ± 0.1
HTB-103	Gastric	9.5 ± 7.5	400 ± 300
HL60	Promyelocytic	> 100	0.4 ± 0.2
TF-1	Erythroleukemia	22 ± 8	0.02 ± 0.01
U937	Monocytic	9.5 ± 5.5	0.04 ± 0.02

Cells were plated in 96-well plates at 1.5×10^4 /well and incubated at 37°C for 24 hours. The cells were then incubated with recombinant toxins for 24 to 48 hours and [³H]-leucine for 4 to 6 hours.

combinant toxins. The relative binding affinity of the immunotoxins containing anti-TFR(Fv) was determined similarly using HUT-102 cells (8×10^5 /well) and 0.1 nmol/L [¹²⁵I]-anti-TFR-IgG.

RESULTS

The fact that GM-CSFR is overexpressed on solid tumors and leukemia cells but is undetectable on the earliest hematopoietic progenitor cells¹¹⁻¹⁷ makes the GM-CSFR a potential target molecule. To determine whether GM-CSF can direct bacterial toxins to kill GM-CSF-expressing tumor cells, we fused GM-CSF to truncated forms of PE or DT and tested the resulting fusion toxins for cytotoxicity and binding.

Preparation of recombinant GM-CSF toxins. Figure 1 shows schematic diagrams of GM-CSF-PE38KDEL and DT388-GM-CSF. As confirmed by the DNA sequence analysis, the first molecule contains the 127 amino acid human GM-CSF ligand at the amino terminus of the truncated toxin,

which consists of amino acids 253 through 364 and 381 through 608 of PE, followed by the KDEL carboxyl terminus. DT388-GM-CSF contains the first 388 amino acids of DT followed by human GM-CSF. GM-CSF was placed at the amino terminus of truncated PE and at the carboxyl terminus of truncated DT to replace the binding domains that are normally present in those positions and because a free carboxyl terminus of PE and a free amino terminus of DT is necessary for cytotoxicity.^{30,38} To properly fold the recombinant toxins, each of which contains 6 cysteine residues, the insoluble inclusion body protein was denatured, reduced, and refolded in a redox buffer as described in Materials and Methods. Each protein could be purified to near homogeneity by sodium dodecyl sulfate-polyacrylamide gel electrophoresis (gel not shown) in a yield of 10% of the total recombinant protein renatured. The purified recombinant toxins were then tested for cytotoxicity and binding.

Cytotoxicity of GM-CSF toxins. To determine the sensitivity of leukemia and GI carcinomas to GM-CSF toxins, the cells were incubated with recombinant toxins and [³H]-leucine incorporation was measured. The IC₅₀s, the concentrations of toxin necessary for 50% inhibition of protein synthesis, are listed in Table 1. For GM-CSF-PE38KDEL, the IC₅₀s on GI carcinomas ranged from 0.45 ng/mL on N87 to 9.5 ng/mL on HTB-103 cells. Leukemia cells were less sensitive to GM-CSF-PE38KDEL, with IC₅₀s ranging from 9.5 ng/mL on U937 monocytic leukemia cells to greater than 100 ng/mL on HL60 promyelocytic leukemia cells. In contrast, DT388-GM-CSF was much more cytotoxic to leukemia cells than to GI carcinomas, with IC₅₀s ranging from 0.02 ng/mL to 0.4 ng/mL on the leukemia lines compared with 3.7 ng/mL to 400 ng/mL on the GI carcinoma lines. Thus, GM-CSF-PE38KDEL was much more cytotoxic than DT388-GM-CSF on the GI carcinoma lines, whereas the reverse was true on the leukemia lines.

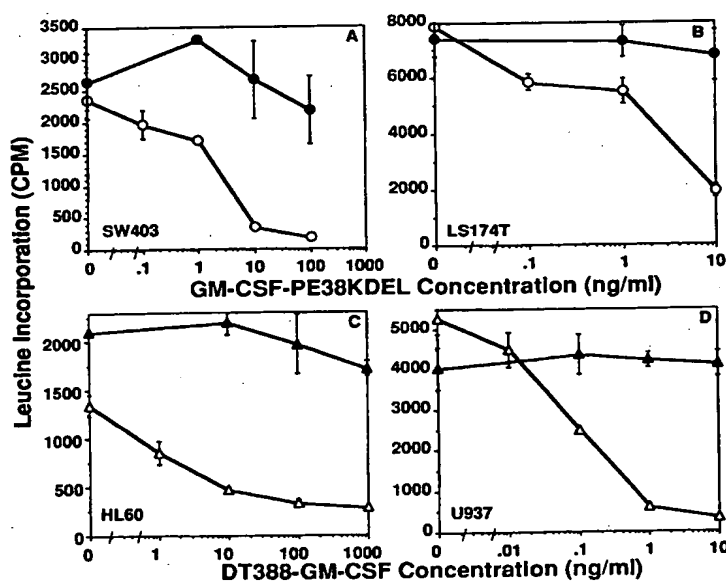
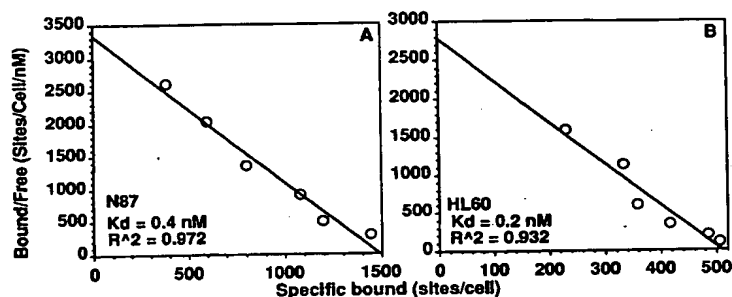


Fig 2. Cytotoxicity and specificity of GM-CSF toxins on target cells. The colon lines SW403 (A) and LS174T (B) were incubated with GM-CSF-PE38KDEL and DT388-GM-CSF was incubated with the leukemia lines HL60 (C) and U937 (D) in the presence (●, ▲) or absence (○, △) of 5 μg/mL of GM-CSF. The cells were pulsed with [³H]-leucine and harvested, and the leucine incorporation was determined.

Fig 3. Scatchard plots of [125 I]-GM-CSF binding to target cells. In (A), N87 cells ($1.3 \times 10^6/200 \mu\text{L}$ /well) were incubated with 0.15, 0.3, 0.6, 1.2, 2.4, and 4.8 nmol/L [125 I]-GM-CSF (5.7 $\mu\text{Ci}/\mu\text{g}$) in RPMI containing 0.1% bovine serum albumin and 0.2% NaN₃ for 30 minutes, washed, and counted. HL60 cells (B) were assayed similarly at 2.2×10^6 /well.



Cytotoxic specificity of the recombinant toxins containing GM-CSF. To determine whether the cytotoxicity of the recombinant GM-CSF toxins was specific in requiring internalization through the GM-CSF receptor, cytotoxicity experiments were performed where the binding of the chimeric toxins was competed by an excess of GM-CSF (2.5 to 5 $\mu\text{g}/\text{mL}$). Figure 2 shows representative cytotoxicity curves for GM-CSF-PE38KDEL and DT388-GM-CSF in the presence and absence of an excess of GM-CSF. It was found that an excess of GM-CSF prevented the cytotoxic activity of both recombinant toxins, indicating that their cytotoxic activity required binding to the GM-CSF receptor. Such specificity was also shown by GM-CSF-PE38KDEL for N87, HTB-103, TF-1, and U937 cells and by DT388-GM-CSF for TF-1, LS174T, and SW403 cells (data not shown). To determine whether the cytotoxicity of the GM-CSF toxins was only due to their binding to the GM-CSFR and did not require the action of the toxin domains, the cells were incubated with and without 5 $\mu\text{g}/\text{mL}$ of GM-CSF. In Fig 2, the points on the y-axis of each curve, where the toxin concentration equals 0, show the leucine incorporation in cells with and without 5 $\mu\text{g}/\text{mL}$ of GM-CSF. In none of the seven cell lines did GM-CSF alone result in greater than 50% inhibition of protein synthesis. Thus, the cytotoxicity of GM-CSF-PE38KDEL and DT388-GM-CSF required both binding to the GM-CSFR and also internalization and action of the toxin domains. Interestingly, the leukemic cell lines HL60 (Fig 2C) and TF-1 (data not shown) showed significant (but <twofold) stimulation with 5 $\mu\text{g}/\text{mL}$ of GM-CSF in the absence of toxin, but the solid tumors showed no significant stimulatory response to GM-CSF.

Quantitation of GM-CSFR on the target cells. The number of GM-CSFR sites per cell were quantitated by radiolabeled binding assay using [125 I]-GM-CSF on the cell lines to determine whether cytotoxic activity correlated with receptor expression. Representative Scatchard plots are shown in Fig 3. The binding assay was designed to determine the number of low-affinity sites, which outnumber the small number of high-affinity sites.^{4,8} As shown in Table 2, the number of GM-CSFR sites per cell varied somewhat from assay to assay, but the average values varied from 500 sites per cell for HTB-103 gastric cells to 3,700 sites per cell for TF-1 cells. The k_d s for the seven cell lines ranged from 0.2 to 1.9 nmol/L, consistent with low-affinity binding sites. Together with the cytotoxicity data from Table 1, it can be seen that

cytotoxicity did correlate with the number of GM-CSFR sites per cell when examining one type of cell at a time. For example, for either toxin toward the GI carcinoma lines, SW403 and N87 were more sensitive than LS174T and HTB-103 was least sensitive, matching the order of their GM-CSFR expression. Also, of the three leukemia lines, HL60 had the least numbers of sites per cell and was less sensitive to either toxin than were TF-1 or U937 cells. However, GM-CSF-PE38KDEL was more cytotoxic toward the GI lines than the leukemia lines, and DT388-GM-CSF was more cytotoxic toward the leukemia lines than the GI lines. Thus, for both recombinant toxins the difference in their cytotoxic activity toward leukemia and solid tumor cells was likely due to fundamental differences between these cell types unrelated to the numbers of receptors expressed.

Sensitivity of fresh bone marrow cells to GM-CSF toxins. To determine if the data on cell lines from patients with leukemia and GI cancer would apply to fresh human hematopoietic cells, bone marrow mononuclear cells from two donors were partially purified by Ficoll centrifugation and incubated with the recombinant toxins. The first sample was taken from normal marrow and the second from a patient whose marrow contained normal hematopoietic progenitor cells and was 50% involved with a B-cell small-cell lymphoma. As shown in Table 3, the marrow mononuclear cells were much more sensitive to DT388-GM-CSF compared with GM-CSF-PE38KDEL. In the normal marrow sample, the IC_{50} for DT388-GM-CSF was 2.1 ng/mL, compared with greater than 1,000 ng/mL for GM-CSF-

Table 2. Expression of GM-CSFR on Human Cells

Cell Line	Sites/Cell	k_d (nmol/L)
LS174T	900 \pm 700	1.7 \pm 1
SW403	3,050 \pm 900	1.6 \pm 0.5
N87	2,400 \pm 1,200	0.9 \pm 0.7
HTB-103	500 \pm 200	0.4 \pm 0.4
HL60	540 \pm 50	0.2 \pm 0.01
TF-1	3,700 \pm 1,500	0.5 \pm 0.05
U937	3,500 \pm 350	1.9 \pm 0.2

Cells were incubated at 37°C for 30 minutes with [125 I]-GM-CSF with or without a 100-fold excess of GM-CSF in RPMI media containing 1 mg/mL bovine serum albumin and 0.2% NaN₃. Unbound GM-CSF was removed from the cells either by centrifuging through n-butyl phthalate or by centrifuging and washing the cells with binding buffer.

Table 3. Sensitivity of Fresh Hematopoietic Cells to Recombinant GM-CSF Toxins

Sample	IC ₅₀ (ng/mL)	
	GM-CSF-PE38KDEL	DT388-GM-CSF
Normal bone marrow	>1,000	2.1
Marrow in lymphoma patient	>100	0.9
Normal peripheral lymphocytes	>1,000	>1,000
Peripheral blood B leukemia	>1,000	>1,000

Samples consisted of mononuclear cells obtained by Ficoll centrifugation and were incubated with recombinant toxins for 60 hours followed by [³H]-leucine for 4 to 6 hours.

PE38KDEL. The results were similar in the marrow contaminated with malignant B cells, with an IC₅₀ of 0.9 ng/mL for DT388-GM-CSF and greater than 100 ng/mL for GM-CSF-PE38KDEL. Although these marrow samples contained differentiated cells, the cytotoxicity of DT388-GM-CSF appeared directed toward the hematopoietic progenitor cells, because fresh normal or malignant lymphocytes isolated from the peripheral blood were resistant (Table 3). To determine whether the cytotoxic activity of GM-CSF toxin towards the marrow cells was specific in requiring binding to the GM-CSFR, we simultaneously tested recombinant toxin containing PE38KDEL or DT388 but not GM-CSF. As shown in Fig 4A, PE38KDEL alone³⁹ or DT388-IL2³⁰ showed no cytotoxic activity toward the normal marrow cells, and PE38KDEL was significantly less cytotoxic than GM-CSF-PE38KDEL. Thus, the cytotoxic activity of the recombinant toxins containing GM-CSF was not due to non-specific internalization into the fresh marrow cells. As shown by the Y-axis of Fig 4B, in the absence of toxin, 20 ng/mL of GM-CSF resulted in a 25% increase in protein synthesis, indicating that the cytotoxic activity of the GM-CSF toxin was not only due to their binding to the GM-CSFR on the cells but also required action of the bacterial toxins after internalization. Finally, Fig 4B shows that the cytotoxic activity of DT388-GM-CSF could be competed by 20 ng/mL of GM-CSF, confirming that its cytotoxic activity required binding to the GM-CSFR on the fresh human hematopoietic progenitor cells.

Sensitivity of GI and leukemia cells to toxins carrying another ligand. To determine whether the difference in sensitivity of GI and leukemia cells to recombinant toxins

Table 4. Sensitivity of Colon and Leukemia Lines to Recombinant Immunotoxins Binding to the Human Transferrin Receptor

Cell Line	Cell Type	IC ₅₀ (ng/mL) ± SD	
		Anti-TFR(Fv)-PE38KDEL	DT388-Anti-TFR(Fv)
LS174T	Colon	0.008 ± 0.003	0.4 ± 0.05
SW403	Colon	0.02 ± 0.007	0.7 ± 0.3
N87	Gastric	0.003 ± 0.0004	0.2 ± 0.07
HTB-103	Gastric	0.002 ± 0.0006	0.2 ± 0.06
HL60	Promyelocytic	0.4 ± 0.15	0.2 ± 0.015
TF-1	Erythroleukemia	0.018 ± 0.006	0.13 ± 0.1
U937	Monocytic	0.1 ± 0.09	0.13 ± 0.08

was due to differences in the way the cells handle the GM-CSFR or due to differences between these cells that are unrelated to the GM-CSFR, they were incubated with recombinant toxins containing a different ligand. The ligand chosen was anti-TFR(Fv), which binds to the human transferrin receptor.³¹ As shown in Fig 1, anti-TFR(Fv)-PE38KDEL contains the exact same toxin domains as GM-CSF-PE38KDEL, and DT388-anti-TFR(Fv) contains the exact same toxin domains as DT388-GM-CSF. Table 4 lists the IC₅₀s of these two recombinant immunotoxins toward the GI and leukemia cell lines. It can be seen that anti-TFR(Fv)-PE38KDEL was usually much more cytotoxic to the GI cell lines than the leukemia cell lines, with differences being as great as 200-fold. In contrast, DT388-anti-TFR(Fv) was usually more cytotoxic to the leukemia cells than to the GI carcinoma cells, with the differences being less than 10-fold. Thus, regardless of the targeting ligand, GI carcinomas were more sensitive than leukemias to PE38KDEL, and leukemias were more sensitive than GI carcinomas to DT388.

Assessment of the relative affinities of the recombinant toxins. To compare the cytotoxic activities of GM-CSF-PE38KDEL or anti-TFR(Fv)-PE38KDEL with those of DT388-GM-CSF and DT388-anti-TFR(Fv), respectively, one must take into consideration quantitative differences in the binding of the ligands, depending on whether the ligand is located at the amino or carboxyl terminus of the toxin. To determine the relative binding affinity of the recombinant toxins, they were tested for their ability to displace radiolabeled ligand. In Fig 5A, the amount of [¹²⁵I]-GM-CSF bound to U937 cells is shown as a function of increasing

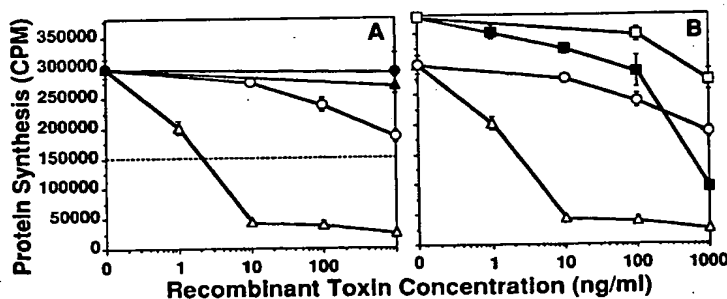
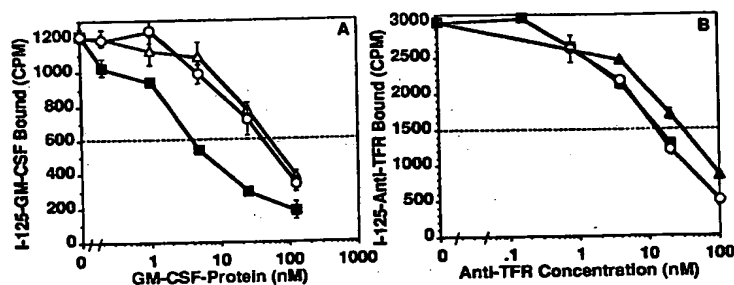


Fig 4. Cytotoxicity of recombinant toxins towards normal bone marrow cells. Normal marrow mononuclear cells ($10^6/0.1$ mL well) were incubated with DT388-GM-CSF (Δ) or GM-CSF-PE38KDEL (\circ) for 60 hours and pulsed with [³H]-leucine. In (A), the cells were incubated in parallel with the negative control molecules PE38KDEL (\bullet) or DT388-IL2 (Δ). In (B), the cells were also incubated with DT388-GM-CSF (\blacksquare) or GM-CSF-PE38KDEL (\square) in the presence of 20 ng/mL of GM-CSF.

Fig 5. Displacement analysis of recombinant toxins. In (A), U937 cells (4.5×10^5 /well) were incubated with [125 I]-GM-CSF and the indicated concentrations of GM-CSF (■), GM-CSF-PE38KDEL (○), or DT388-GM-CSF (Δ). In (B), HUT-102 cells (8×10^5 /well) were incubated with [125 I]-anti-TFR-IgG and the indicated concentrations of anti-TFR-IgG (■), anti-TFR(Fv)-PE38KDEL (○), or DT388-anti-TFR(Fv) (Δ). The cells were harvested and counted as in Fig 3.



concentrations of either GM-CSF, GM-CSF-PE38KDEL, or DT388-GM-CSF. The EC_{50} , the concentration necessary for 50% competition of [125 I]-GM-CSF binding, was 3.9 nmol/L for GM-CSF, 41 nmol/L for GM-CSF-PE38KDEL, and 50 nmol/L for DT388-GM-CSF. In Fig 5B, the amount of [125 I]-anti-TFR-IgG binding to HUT-102 cells is shown as a function of increasing concentrations of either anti-TFR-IgG, anti-TFR(Fv)-PE38KDEL, or DT388-anti-TFR(Fv). The EC_{50} was 13 nmol/L for anti-TFR-IgG, 12 nmol/L for anti-TFR(Fv)-PE38KDEL, and 29 nmol/L for DT388-anti-TFR(Fv). Table 5 was then constructed to display the IC_{50} s for the recombinant toxins corrected for binding affinity. Lower values of IC_{50}/EC_{50} would indicate more efficient killing of cells due to processes occurring after binding. Table 5 indicates that the IC_{50}/EC_{50} ratios of GM-CSF-PE38KDEL are much less than those of DT388-GM-CSF toward GI carcinomas, whereas the reverse was true for leukemias. Similarly, the IC_{50}/EC_{50} ratios of anti-TFR(Fv)-PE38KDEL are much less than those of DT388-anti-TFR(Fv) toward GI carcinomas, but not toward leukemias. Thus, regardless of the targeting ligand, PE38KDEL was more cytotoxic toward solid tumors and DT388 was more cytotoxic toward leukemias due to processes in those cells that occur after receptor binding.

DISCUSSION

To determine the sensitivity of solid tumors and leukemias to recombinant toxins containing GM-CSF, we tested the sensitivity of such cell lines to GM-CSF-PE38KDEL and

DT388-GM-CSF. We found that, although both recombinant toxins were specifically cytotoxic to both types of cells, solid tumor cells were more sensitive to GM-CSF-PE38KDEL and leukemia cells were more sensitive to DT388-GM-CSF. This was not a phenomenon peculiar to cell lines, because fresh human marrow progenitor cells behaved similar to the leukemia lines. Based on a similar pattern of cytotoxicity using the same toxins targeted to the transferrin receptor, it appears that these differences are due to inherent differences between solid tumors and leukemias in the way by which they handle the toxins intracellularly.

It is believed that cytotoxicity by PE requires proteolytic processing by Furin between amino acids 279 and 280 and that the carboxy terminal fragment is transported by the KDEL receptor from at least the transreticular Golgi toward the endoplasmic reticulum, from which it translocates to the cytosol.^{25,38,40,41} DT is also cleaved by Furin between arginine 193 and serine 194, and arginine 193 at the carboxyl terminus of the DT fragment A is necessary for translocation.^{24,40} However, this fragment is thought to translocate from the endosome to the cytosol via membrane insertion and passage through ion-conductive channels.⁴²⁻⁴⁴ Because both PE and DT are processed by the same enzyme, both toxins ultimately ADP-ribosylate EF2 in the cytosol, and in both PE38KDEL and DT388 ADP-ribosylation activity is not altered by the ligand to which the toxin is fused (data not shown). Thus, the difference in activity between GM-CSF-PE38KDEL and DT388-GM-CSF would not be due to differences in ADP-ribosylation activity. We therefore speculate from our data that leukemic cells differ from GI carcinoma cells in the intracellular transport or translocation of protein molecules. For example, in leukemic cells, a protein molecule may have a higher chance of entering the cytosol if it can translocate directly from the endosome than if it must be transported intracellularly. Conversely, in solid tumors, proteins may not easily translocate from endosomes and may require transport to an organelle such as the endoplasmic reticulum that has preexisting pores. It is also possible that leukemic and solid tumor cells differ in the function and location of lysosomes, which may degrade toxin molecules before they reach the cytosol. So far, our data with cell lines are consistent with that on fresh cells from patients with GM-CSFR⁺ leukemia (Rozemuller et al, manuscript submitted). Because one molecule of DT⁴⁵ or PE (Willingham and Pastan, unpublished data) in the cytosol appears sufficient to kill a cell, it is very

Table 5. Cytotoxicity of Recombinant Toxins Corrected for Binding Affinity

Cell Line	IC_{50} (pmol/L)/ EC_{50} (nmol/L)			
	GM-CSF-PE38KDEL	DT388-GM-CSF	Anti-TFR(Fv)-PE38KDEL	DT388-Anti-TFR(Fv)
LS174T	1	25	0.003	0.2
SW403	0.4	5	0.007	0.35
N87	0.2	1.3	0.001	0.1
HTB-103	4	140	0.0007	0.1
HL60	>45	0.14	0.14	0.1
TF-1	10	0.007	0.006	0.07
U937	4	0.014	0.035	0.07

The IC_{50} s shown in Tables 1 and 4 were converted to picomoles per liter and divided by the EC_{50} as shown in Fig 5.

important to identify and attempt to overcome these potential impediments to translocation.

We have shown that human GM-CSF can be used to target truncated forms of either PE or DT to inhibit protein synthesis in receptor-bearing solid or hematopoietic tumor cells. Further development of these agents for the treatment of human tumors should include monkey toxicology studies, because murine GM-CSFR does not bind human GM-CSF.⁴⁶ Such studies could determine whether cytotoxicity toward GM-CSFR⁺ normal cells spares stem cells and, if so, whether hematopoietic toxicity is low enough to allow the delivery of high doses. If so, such agents could prove useful clinically in the purging of bone marrow or stem cell autografts before transplantation or in the direct systemic treatment of human leukemia and solid tumors.

ACKNOWLEDGMENT

The authors acknowledge the technical assistance of R. Beers, I. Margulies, and V. Fogg, which contributed to aspects of this work.

REFERENCES

- Miyajima A, Mui AL, Ogorochi T, Sakamaki K: Receptors for granulocyte-macrophage colony-stimulating factor, interleukin-3, and interleukin-5. *Blood* 82:1960, 1993
- Metcalf D: The granulocyte-macrophage colony-stimulating factors. *Science* 299:16, 1985
- Burgess AW, Camakaris J, Metcalf D: Purification and properties of colony-stimulating factor from mouse lung-conditioned medium. *J Biol Chem* 252:1998, 1977
- Park LS, Friend D, Gillis S, Urdal DL: Characterization of the cell surface receptor for granulocyte-macrophage colony-stimulating factor. *J Biol Chem* 261:4177, 1986
- DiPersio J, Billing P, Kaufman S, Eghtesady P, Williams RE, Gasson JC: Characterization of the human granulocyte-macrophage colony-stimulating factor receptor. *J Biol Chem* 263:1834, 1988
- Wong GG, Witek JS, Temple PA, Wilkens KM, Leary AC, Luxenberg DP, Jones SS, Brown EL, Kay RM, Orr EC, Shoemaker C, Golde DW, Kaufman RJ, Hewick RM, Wang EA, Clark SC: Human GM-CSF: Molecular cloning of the complementary DNA and purification of the natural and recombinant proteins. *Science* 228:810, 1985
- Cantrell MA, Anderson D, Cerretti DP, Price V, McKereghan K, Tushinski RJ, Mochizuki DY, Larsen A, Grabstein K, Gillis S, Cosman D: Cloning, sequence, and expression of a human granulocyte/macrophage colony-stimulating factor. *Proc Natl Acad Sci USA* 82:6250, 1985
- Hayashida K, Kitamura T, Gorman DM, Arai K, Yokota T, Miyajima A: Molecular cloning of a second subunit of the receptor for human granulocyte-macrophage colony-stimulating factor (GM-CSF): Reconstitution of a high-affinity GM-CSF receptor. *Proc Natl Acad Sci USA* 87:9655, 1990
- Fleischman RA: Southwestern Internal Medicine Conference: Clinical use of hematopoietic growth factors. *Am J Med Sci* 305:248, 1993
- Foulke RS, Marshall MH, Trotta PP, Hoff DDV: In vitro assessment of the effects of granulocyte-macrophage colony-stimulating factor on primary human tumors and derived lines. *Cancer Res* 50:6264, 1990
- Park LS, Waldron PE, Friend D, Sassenfeld HM, Price V, Anderson D, Cosman D, Andrews RG, Bernstein ID, Urdal DL: Interleukin-3, GM-CSF, and G-CSF receptor expression on cell lines and primary leukemia cells: Receptor heterogeneity and relationship to growth factor responsiveness. *Blood* 74:56, 1989
- Chiba S, Shibuya K, Piao Y, Tojo A, Sasaki N, Matsuki S, Miyagawa K, Miyazono K, Takaku F: Identification and cellular distribution of distinct proteins forming human GM-CSF receptor. *Cell Regul* 1:327, 1990
- Berdel WE, Danhauser-Riedl S, Steinhauser G, Winton EF: Various hematopoietic growth factors (interleukin-3, GM-CSF, G-CSF) stimulate clonal growth of non-hematopoietic tumor cells. *Blood* 73:80, 1989
- Baldwin GC, Gasson JC, Kaufman SE, Quan SG, Williams RE, Avalos BR, Gazdar AF, Golde DW, DiPersio JF: Nonhematopoietic tumor cells express functional GM-CSF receptors. *Blood* 73:1033, 1989
- Dippold WG, Klingel R, Kerlin M, Schwaebel W, Buschenfelde KMZ: Stimulation of pancreas and gastric carcinoma cell growth by interleukin 3 and granulocyte-macrophage colony stimulating factor. *Gastroenterology* 100:1338, 1991
- Hirsch T, Eggstein S, Frank S, Farthmann EH, Specht BV: Expression of GM-CSF and a functional GM-CSF receptor in the human colon carcinoma line SW403. *Biochem Biophys Res Commun* 217:138, 1995
- Wognum AW, Westerman Y, Visser TP, Wagemaker G: Distribution of receptors for granulocyte-macrophage colony-stimulating factor on immature CD34⁺ bone marrow cells, differentiating monomyeloid progenitors, and mature blood cell subsets. *Blood* 84:764, 1994
- Chan C, Blazar BR, Eide CR, Kreitman RJ, Vallera DA: A murine cytokine fusion toxin specifically targeting the murine granulocyte-macrophage colony-stimulating factor (GM-CSF) receptor on normal committed bone marrow progenitor cells and GM-CSF-dependent tumor cells. *Blood* 86:2732, 1995
- Lappi DA, Martineau D, Sarmientos P, Garofano L, Aranda AP, Miyajima A, Kitamura T, Baird A: Characterization of a saporin mitotoxin specifically cytotoxic to cells bearing the granulocyte-macrophage colony-stimulating factor receptor. *Growth Factors* 9:31, 1993
- Pastan I, FitzGerald D: Recombinant toxins for cancer treatment. *Science* 254:1173, 1991
- Murphy JR, vanderSpek JC: Targeting diphtheria toxin to growth factor receptors. *Semin Cancer Biol* 6:259, 1995
- Hwang J, FitzGerald DJ, Adhya S, Pastan I: Functional domains of *Pseudomonas* exotoxin identified by deletion analysis of the gene expressed in *E. coli*. *Cell* 48:129, 1987
- Allured VS, Collier RJ, Carroll SF, McKay DB: Structure of exotoxin A of *Pseudomonas aeruginosa* at 3.0 Angstrom resolution. *Proc Natl Acad Sci USA* 83:1320, 1986
- Williams DP, Wen Z, Watson RS, Boyd J, Strom TB, Murphy JR: Cellular processing of the interleukin-2 fusion toxin DAB₄₈₆-IL-2 and efficient delivery of diphtheria fragment A to the cytosol of target cells requires Arg¹⁹⁴. *J Biol Chem* 265:20673, 1990
- Kreitman RJ, Pastan I: Importance of the glutamate residue of KDEL in increasing the cytotoxicity of *Pseudomonas* exotoxin derivatives and for increased binding to the KDEL receptor. *Biochem J* 307:29, 1995
- Kreitman RJ, Batra JK, Seetharam S, Chaudhary VK, FitzGerald DJ, Pastan I: Single-chain immunotoxin fusions between anti-Tac and *Pseudomonas* exotoxin: Relative importance of the two toxin disulfide bonds. *Bioconjug Chem* 4:112, 1993
- Seetharam S, Chaudhary VK, FitzGerald D, Pastan I: Increased cytotoxic activity of *Pseudomonas* exotoxin and two chimeric toxins ending in KDEL. *J Biol Chem* 266:17376, 1991
- Kreitman RJ, Puri RK, Leland P, Lee B, Pastan I: Site-specific conjugation to interleukin 4 containing mutated cysteine residues produces interleukin 4-toxin conjugates with improved binding and activity. *Biochemistry* 33:11637, 1994
- Kreitman RJ, Puri RK, Pastan I: A circularly permuted recom-

binant interleukin 4 toxin with increased activity. *Proc Natl Acad Sci USA* 91:6889, 1994

30. Chaudhary VK, FitzGerald DJ, Pastan I: A proper amino terminus of diphtheria toxin is important for cytotoxicity. *Biochem Biophys Res Commun* 180:545, 1991

31. Batra JK, FitzGerald DJ, Chaudhary VK, Pastan I: Single-chain immunotoxins directed at the human transferrin receptor containing *Pseudomonas* exotoxin A or diphtheria toxin: Anti-TFR(Fv)-PE40 and DT388-Anti-TFR(Fv). *Mol Cell Biol* 11:2200, 1991

32. Kreitman RJ, Bailon P, Chaudhary VK, FitzGerald DJ, Pastan I: Recombinant immunotoxins containing anti-Tac(Fv) and derivatives of *Pseudomonas* exotoxin produce complete regression in mice of an interleukin-2 receptor-expressing human carcinoma. *Blood* 83:426, 1994

33. Kreitman RJ, Pastan I: Purification and characterization of IL6-PE⁴⁰, a recombinant fusion of interleukin 6 with *Pseudomonas* exotoxin. *Bioconjug Chem* 4:581, 1993

34. Studier FW, Moffatt BA: Use of bacteriophage T7 polymerase to direct selective expression of cloned genes. *J Mol Biol* 189:113, 1986

35. Batra JK, Kasprzyk PG, Bird RE, Pastan I, King CR: Recombinant anti-erbB2 immunotoxins containing *Pseudomonas* exotoxin. *Proc Natl Acad Sci USA* 89:5867, 1992

36. Kreitman RJ, Siegall CB, FitzGerald DJ, Epstein J, Barlogie B, Pastan I: Interleukin-6 fused to a mutant form of *Pseudomonas* exotoxin kills malignant cells from patients with multiple myeloma. *Blood* 79:1775, 1992

37. Batra JK, Jinno Y, Chaudhary VK, Kondo T, Willingham MC, FitzGerald DJ, Pastan I: Antitumor activity in mice of an immunotoxin made with anti-transferrin receptor and a recombinant form of *Pseudomonas* exotoxin. *Proc Natl Acad Sci USA* 86:8545, 1989

38. Chaudhary VK, Jinno Y, FitzGerald D, Pastan I: *Pseudomonas* exotoxin contains a specific sequence at the carboxyl terminus

that is required for cytotoxicity. *Proc Natl Acad Sci USA* 87:308, 1990

39. Kreitman RJ, Hansen HJ, Jones AL, FitzGerald DJ, Goldenberg DM, Pastan I: *Pseudomonas* exotoxin-based immunotoxins containing the antibody LL2 or LL2-Fab' induce regression of subcutaneous human B-cell lymphoma in mice. *Cancer Res* 53:819, 1993

40. Chiron MF, Fryling CM, FitzGerald DJ: Cleavage of *Pseudomonas* exotoxin and diphtheria toxin by a furin-like enzyme prepared from beef liver. *J Biol Chem* 269:18167, 1994

41. Ogata M, Fryling CM, Pastan I, FitzGerald DJ: Cell-mediated cleavage of *Pseudomonas* exotoxin between Arg²⁷⁹ and Gly²⁸⁰ generates the enzymatically active fragment which translocates to the cytosol. *J Biol Chem* 267:25396, 1992

42. Zhan H, Choe S, Huynh PD, Finkelstein A, Eisenberg D, Collier RJ: Dynamic transitions of the transmembrane domain of diphtheria toxin: Disulfide trapping and fluorescence proximity studies. *Biochemistry* 33:11254, 1994

43. Cabiliaux V, Mindell J, Collier RJ: Membrane translocation and channel-forming activities of diphtheria toxin are blocked by replacing isoleucine 364 with lysine. *Infect Immunity* 61:2200, 1993

44. vanderSpek J, Cassidy D, Genbauffe F, Huynh PD, Murphy JR: An intact transmembrane helix 9 is essential for the efficient delivery of the diphtheria toxin catalytic domain to the cytosol of target cells. *J Biol Chem* 269:21455, 1994

45. Yamaizumi M, Mekada E, Uchida T, Okada Y: One molecule of diphtheria toxin fragment A introduced into a cell can kill the cell. *Cell* 15:245, 1978

46. Kaushansky K, Shoemaker SG, Alfaro S, Brown C: Hematopoietic activity of granulocyte/macrophage colony-stimulating factor is dependent upon two distinct regions of the molecule: Functional analysis based upon the activities of interspecies hybrid growth factors. *Proc Natl Acad Sci USA* 86:1213, 1989

Recombinant RFB4 Immunotoxins Exhibit Potent Cytotoxic Activity for CD22-Bearing Cells and Tumors

By Elizabeth Mansfield, Peter Amlot, Ira Pastan, and David J. FitzGerald

Many B-cell malignancies express the CD22 antigen on their cell surface. To kill cells expressing this antigen, the RFB4 monoclonal antibody (MoAb) has been linked chemically with either deglycosylated ricin A chain or truncated versions of *Pseudomonas* exotoxin. These immunotoxins exhibited selective cytotoxic activity for CD22⁺ cells and antitumor activity in nude mouse models bearing human B-cell lymphomas. To construct a recombinant immunotoxin targeted to CD22, we first cloned the variable portions of the heavy and light chains of RFB4. The cloned Fv fragments were joined by a newly created disulfide bond to form a disulfide stabilized (ds) construct. The RFB4 construct was combined by gene fusion with PE38, a truncated version of PE. The recombinant immunotoxin was then expressed in

Escherichia coli, purified by column chromatography and tested for cytotoxicity activity. RFB4(dsFv)PE38 retained its binding activity for CD22, was very stable at 37°C and exhibited selective cytotoxic activity for CD22⁺-cultured cell lines. Because of its favorable binding characteristics and potency for CD22-positive cell lines, RFB4(dsFv)PE38 was tested for antitumor activity in a nude mouse model of human lymphoma. CA46 cells were injected subcutaneously and then treated with the RFB4(dsFv)PE38 immunotoxin. Antitumor activity was dose responsive and was not evident when an irrelevant immunotoxin was administered on the same schedule.

This is a US government work. There are no restrictions on its use.

LEUKEMIAS AND LYMPHOMAS are attractive targets for treatment with immunotoxins. The response of patients with B-cell malignancies has been extensively investigated in phase I/II clinical trials of immunotoxin activity.¹⁻⁴ To date, some antitumor responses have been noted but immunotoxin-mediated toxicity to normal tissue often prevented dose escalations to therapeutic levels. Several B-cell-specific antigens such as CD19, CD22, and CD40 have been targeted by immunotoxins made with plant toxins such as ricin A-chain and bacterial toxins, such as *Pseudomonas* exotoxin A (PE).⁵⁻⁷

CD22, a lineage-restricted B-cell antigen that belongs to the Ig superfamily, is expressed on the surface of many types of malignant B cells, including chronic B-lymphocytic cells (B-CLL), B lymphoma cells such as Burkitt's lymphomas, and hairy cell leukemias, as well as on normal mature B lymphocytes. CD22 is not present on the cell surface in the early stages of B-cell development and is not expressed on stem cells.⁸ Additionally, no shed antigen can be detected in normal human serum or serum from patients with CLL.⁹

RFB4 IgG is an anti-CD22 monoclonal antibody that has been chemically conjugated to both ricin and *Pseudomonas* exotoxin A (PE) and has shown excellent activity against B cells both in vitro and in vivo.^{6,10,11} RFB4 is highly specific for cells of the B lineage and has no detectable cross-reactivity with any other normal cell type.⁹ RFB4 IgG has previously been covalently coupled to both ricin A-chain and a truncated form of PE called PE35.^{6,11} These conjugate

molecules were effective against experimental lymphoma xenograft models, and in the clinical setting, the ricin-based immunotoxin also has shown some efficacy against human disease.^{1,2}

While chemical conjugates are frequently very stable and potent, they are relatively large and often heterogeneous at their linkage sites, which may result in suboptimal activity.^{12,13} The requirements for making large quantities of IgG and chemical conjugation also put some limitations on the ability to manufacture the drug. Because the ability to penetrate tumors is inversely related to the size of the penetrating molecule, the large size of whole antibody-toxin conjugates may impair their ability to penetrate tumor masses such as those found in lymphomas.¹³

A number of antibody Fv fragments have recently been cloned and genetically fused to PE derivatives such as PE40, PE38, and PE35.¹⁴ The recombinant molecules produced from these constructs are one third the size of IgG-toxin chemical conjugates and are homogeneous in composition. A reduction in size is predicted to improve drug penetration in solid tumors, while elimination of the constant portion of the IgG molecule results in faster clearance from the circulation of experimental animals and patients. Together, these properties may lessen side effects by reducing the time in which the immunotoxin can interact with nontarget tissues and tissues that express very low levels of antigen. Finally homogeneous preparations of recombinant immunotoxins can easily be produced in large quantities.

To take advantage of the benefits of recombinant immunotoxin technology, we have cloned the variable light and heavy chains of RFB4 IgG and expressed them as a disulfide-linked (ds) Fv fusion with PE38. In disulfide-linked immunotoxins, cysteine replaces a single amino acid in each chain, whose location is chosen using predictions from structural models. Here we describe the cloning, mutagenesis, and expression of RFB4(dsFv)PE38, and characterize its antigen binding, cytotoxicity and antitumor activity properties.

MATERIALS AND METHODS

Cell lines. HUT102 cells were a gift from T. Waldmann (NCI) and CA46 and JD38 lines were from I. McGrath (NIH). Daudi, Raji, and Namalwa cells were purchased from ATCC, Rockville, MD.

Cloning. The RFB4 IgG-producing hybridoma was from the Royal Free Hospital School of Medicine, University of London.

From the Laboratory of Molecular Biology, DCBDC, National Cancer Institute, National Institutes of Health, Bethesda, MD; and the Department of Immunology, Royal Free Hospital, London, England.

Submitted December 23, 1996; accepted May 5, 1997.

Address reprint requests to David J. FitzGerald, PhD, Laboratory of Molecular Biology, DBS, National Cancer Institute, National Institutes of Health, 37/4E16, 37 Convent Dr, MSC 4255, Bethesda, MD 20892.

The publication costs of this article were defrayed in part by page charge payment. This article must therefore be hereby marked "advertisement" in accordance with 18 U.S.C. section 1734 solely to indicate this fact.

This is a US government work. There are no restrictions on its use. 0006-4971/97/9005-0026\$0.00/0

Table 1. PCR Primers

Heavy chain primers	
RFB4 VH5	GGACCTCATATGGAAGTGCAGCTGGTGGAGTCT
γ CH1	AGCAGATCCAGGGGCCAGTGGATA
RFB4 VH3	<u>AGATCCGCCACCAACCGGATCCGCTCCGCCTGCAGAGACAGTGACCAGATCC</u>
RFB4 VH3 dsFv	<u>CCGGAAGCTTTTCAGAGACAGTGACC</u>
RFB4 VH	
dsFv(cys)	GACCACTCCAGGCACTTCTCCGGAGTC
Light chain primers	
RFB4 VL5	<u>GGTGGCGGATCTGGAGGTGGCGGAAGCGATATCCAGATGACACAGACT</u>
C- κ	TGGTGGGAAGATGGATACAGTTGG
RFB4 VL3	<u>CCGGAAGCTTTGATTTCAGCTTGG</u>
RFB4 VL5 dsFv	GGACCTCATATGGATATCCAGATGACCC
RFB4 VL3 dsFv	<u>CCGGAATTCATTATTTGATTTCAGCTTGGTCCGCAACCGAACGTCC</u>

Primers are given 5' to 3'. Primers γ CH1 and C- κ were designed as described.¹⁵ RFB4 VH5 and RFB4 VL5 were designed according to the N-terminal protein sequences determined by Edman degradation. RFB4 VH5 encodes an *Nde* I site (bold) and an initiator Met (bold italicized). RFB4 VL3 encodes a *Hind*III site (italicized). Primers RFB4 VH3 and RFB4 VL3 were designed according to the nucleotide sequence determined from cDNA clones. Primers RFB4 VH3 and RFB4 VL5 include partial Gly₄Ser linker sequences which partially overlap (underlined italicized). Primer RFB4 VL3 dsFv mutates V_L Gly₁₀₀ residue to Cys (underlined), includes a terminator codon (bold) and an *Eco*RI site (italicized). Primer RFB4 VH dsFv(cys) mutates V_H Arg₄₄ to Cys (underlined). RFB4 VH3 dsFv includes an additional Lys codon and a *Hind*III site (italicized). RFB4 VL5 dsFv includes an *Nde* I (bold) and an initiator Met (bold italicized).

Purified RFB4 IgG was provided by E. Vitteta, UTSMC, Dallas, TX. RFB4 IgG was reduced with 10 mmol/L dithiothreitol (DTT) and light and heavy chains were separated on 4% to 20% sodium dodecyl sulfate-polyacrylamide gel electrophoresis (SDS-PAGE; Novex, San Diego, CA) and blotted onto a PVDF membrane. Light and heavy chain bands were cut from the membrane and subjected to N-terminal sequence analysis. DNA fragments encoding the light and heavy chains were prepared by polymerase chain reaction (PCR) amplification as described¹⁵ except using total RNA and RFB4-specific 5' primers RFB4 VH5 and RFB4 VL5, which were designed from N-terminal protein sequence data. The sequences of all primers used in cloning are listed in Table 1. PCR products were cloned into the PCR cloning vector (Invitrogen, San Diego, CA) and sequenced using Sequenase (US Biochemical Corp, Cleveland, OH) reagents and protocols. To make RFB4(dsFv)PE38, V_L was amplified using a 5' primer, RFB4 VL5 dsFv, introducing an *Nde* I site, and a 3' primer, RFB4 VL3 dsFv, introducing an *Eco*RI site and mutating glycine residue 100 to cysteine. V_H was amplified using RFB4 VH5 and RFB4 VH3 dsFv, which introduces a *Hind*III site and a lysine residue at the C-terminus of V_H. PCR products were digested with *Nde* I and either *Hind*III (V_H) or *Eco*RI (V_L) and were used to replace V_H-linker-V_L of pUL17 (V_H) or to replace the entire V_H-linker-V_L-PE38 (V_L). V_H-PE38 was mutagenized to change Arg₄₄ to Cys using the Muta-Gene site-directed mutagenesis kit and protocol (Bio-Rad, Hercules, CA) and a phosphorylated primer, VHdsFv(cys). Clones that had incorporated the Cys₄₄ mutation were identified by DNA sequencing.

Expression and purification of recombinant clones. Expression plasmids encoding RFB4 V_H-PE38 and RFB4 V_L were separately expressed in *Escherichia coli* BL21(ΔDE3).¹⁶ Disulfide-linked immunotoxins were produced by refolding of purified inclusion body protein generally as described.¹⁷ Briefly, inclusion bodies were prepared from cell paste by lysis and washing in nonionic detergent, then solubilized in 6 mol/L guanidine-HCl, 0.1 mol/L Tris, pH 8, 2 mmol/L EDTA. Solubilized protein at 10 mg/mL was reduced with 10 mg/mL dithioerythritol (DTT) (65 mmol/L), then rapidly diluted into 100 vol 0.1 mol/L Tris, 0.5 mol/L L-arginine, 0.9 mmol/L oxidized glutathione, 2 mmol/L EDTA at 10°C. Equal weight amounts of V_L and V_H-PE38 were used to refold RFB4(dsFv)PE38. Disulfide-linked immunotoxin was refolded in buffer adjusted to pH 9.5 (room temperature). Immunotoxin was allowed to refold for 48 hours, then was dialyzed against 100 mmol/L

L urea, 20 mmol/L Tris, pH 8 to a conductivity of less than 3.5 mMho. Properly refolded proteins were purified by sequential anion-exchange FPLC on Q-Sepharose and MonoQ (Pharmacia, Arlington Heights, IL) followed by gel filtration on 30 mL TSK G3000SW (TosoHaas, Montgomeryville, PA).

Binding. Relative binding affinities of recombinant immunotoxins was measured by competition against ¹²⁵I-labeled RFB4 IgG for binding to CA46 target cells at 4°C. CA46 cells grown to >10⁶/mL were washed twice in ice cold binding buffer (RPMI, 50 mmol/L BES, pH 6.8, 1% bovine serum albumin [BSA]), and plated at 10⁶ cells/150 μ L binding buffer/well in 96-well plates on ice. To the cells was added 0.35 ng ¹²⁵I-RFB4 (2.5 \times 10⁹ cpm/nmol) in binding buffer and varying concentrations of RFB4(dsFv)PE38. Cells were incubated for 3 hours on ice, washed twice in cold binding buffer, and solubilized in 200 μ L 0.5% SDS/TE. Bound ¹²⁵I-RFB4 was quantitated on a Wallac 1470 Wizard gamma counter (Turku, Finland). The means of duplicate samples were used for calculations.

Cytotoxicity assays. Cells were maintained in RPMI 1640 containing 20% (Daudi) or 10% fetal bovine serum (FBS) (all other lines), 50 U/mL penicillin, 50 μ g/mL streptomycin, 1 mmol/L sodium pyruvate, and an additional 2 mmol/L L-glutamine. For cytotoxicity assays, 4 \times 10⁴ cells/well in 200 μ L culture medium were plated in 96-well plates. Immunotoxins were serially diluted in phosphate-buffered saline (PBS)/0.2% human serum albumin (HSA) and 10 μ L added to cells. Plates were incubated for the indicated times at 37°C, then pulsed with 1 μ Ci/well ³H-leucine in 10 μ L PBS for 4 to 5 hours at 37°C. Radiolabeled material was captured on filters and counted in a Betaplate scintillation counter (Pharmacia, Gaithersburg, MD). Triplicate sample values were averaged and inhibition of protein synthesis determined by calculating percent incorporation compared with control wells without added toxin.

Toxicity in mice. Six- to eight-week-old Balb/C female mice were obtained from the National Cancer Institute, Frederick, MD. Multiple-dose intravenous (IV) LD₅₀ values were determined for a treatment schedule of dose \times 3 qod. Various amounts of immunotoxins were diluted to 200 μ L with PBS/0.2% HSA and injected into the tail veins every other day for three doses. Two mice were injected with each dose, and mice were monitored for weight loss and death for 14 days after last injection.

Inhibition of CA46 tumor establishment. Six- to eight-week-old female athymic nude mice were obtained from the National Cancer Institute, Frederick, MD. Mice were treated with 300 rad of gamma

RFB4 LIGHT CHAIN	
1	D I Q M T Q T T S S L S A S L G D R V T 60
1	gat atc cag atg acc cag act aca tcc tcc ctg tct gcc tct ctg gga gac aga gtc acc 20
21	I S C R A S Q D I S N Y L N W Y Q Q K P 40
61	att agt tgc agg gca agt cag gac att agc aat tat tta aac tgg tat cag cag aaa cca 120
41	D G T V K L L I Y Y T S I L H S G V P S 60
121	gat gga act gtt aaa ctc ctg atc tac tac aca tca ata tta cac tca gga gtc cca tca 180
61	R F S G S G S G T D Y S L T I S N L E Q 80
181	agg ttc agt ggc agt ggg tct gga aca gat tat tct ctc acc att agc aac ctg gag caa 240
81	E D F A T Y F C Q Q G N T L P W T F G G 100
241	gaa gat ttt gcc act tac ttt tgc caa cag ggt aat acg ctt ccg tgg acg ttc ggt gga 300
101	G T K L E I K 107
301	ggc acc aag ctg gaa atc aaa 121
RFB4 HEAVY CHAIN	
1	E V Q L V E S G G G L V K P G G S L K L 20
1	gaa gtg cag ctg gtg gag tct ggg gga ggc tta gtg aag cct gga ggg tcc ctg aaa ctc 60
21	S C A A S G F A F S I Y D M S W V R Q T 40
61	tcc tgt gca gcc tct gga ttc gct ttc agt atc tat gac atg tct tgg gtt cgc cag act 120
41	P E K R L E W V A Y I S S G G G T T Y Y 60
121	ccg gag aag agg ctg gag tgg gtc gca tac att agt agt ggt ggt ggt acc acc tac tat 180
61	P D T V K G R F T I S R D N A K N T L Y 80
181	cca gac act gtg aag ggc cga ttc acc atc tcc aga gac aat gcc aag aac acc ctg tac 240
81	L Q M S S L K S E D T A M Y Y C A R H S 100
241	ctg caa atg agc agt ctg aag tct gag gac aca gcc atg tat tac tgt gca aga cat agt 300
101	G Y G S S Y G V L F A Y W G Q G T L V T 120
301	ggc tac ggt agt agc tac ggg gtt ttg ttt gct tac tgg ggc caa ggg act ctg gtc act 360
121	T S A 123
361	gtc tct gca 369

Fig 1. Deduced amino acid sequence of the variable region of RFB4 light and heavy chains. Amino acids shown in bold were determined by N-terminal protein sequence analysis.

irradiation 3 or 4 days before injection of malignant cells. CA46 cells were seeded at 1.8×10^5 /mL 2 days before injection. On day 0, CA46 cells were washed in RPMI without serum and adjusted to either 10^5 cells/mL or 5×10^7 cells/mL in RPMI. Each mouse was given 100 μ L of the cell suspension by subcutaneous injection. Mice were treated by tail vein injection every day for 4 consecutive days with various amounts of immunotoxins or with control materials in 200 μ L volume. The appearance of tumors was monitored daily or every other day for 21 days following first treatment.

Cytotoxicity of RFB4(dsFv)PE38 after timed exposure to cells. RFB4(dsFv)PE38 dilutions were incubated with CA46 and JD38 cells for 2, 24, and 48 hours in standard cytotoxicity assays, except that for the 2-hour time point, immunotoxin was removed from the medium by washing with RPMI + 10% FCS, and replaced with standard medium for the remaining 22 hours of the assay. For 48-hour assays, the cells were incubated continuously for 48 instead of 24 hours.

RESULTS

Cloning of cDNAs encoding the heavy and light chain variable regions of RFB4 monoclonal antibody (MoAb).

N-terminal amino acid analysis yielded sequence data for both the light and heavy chains of the RFB4 MoAb, which is provided in Fig 1 (bold type). To obtain cDNAs encoding the heavy and light chain variable regions of RFB4, total RNA was prepared from RFB4 hybridoma cells and reverse transcribed to yield first strand cDNA. Subsequently PCR was performed to amplify the heavy and the light chains. Heavy and light chain specific primers were synthesized based on the N-terminal amino acid data, and amplification was performed using these primers together with primers from the constant regions CH1 (heavy) and C- κ (light). This resulted in the amplification of the variable portion of the heavy chain plus part of CH1 and amplification of the variable region of the light chain plus part of C- κ . These products were cloned and sequenced as described in Materials and Methods. There was complete agreement between the amino acid sequence data from the Edman degradations and the deduced sequence from our antibody clones. The nucleotide and deduced amino acid sequences of V_H and V_L are shown in Fig 1.

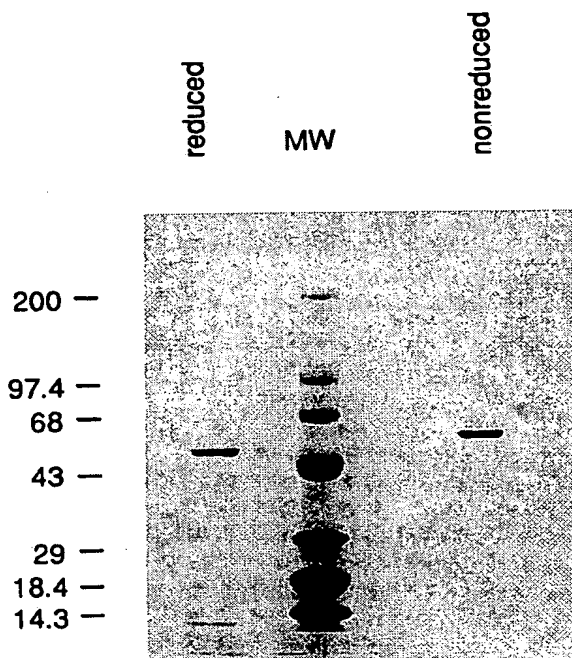


Fig 2. SDS-PAGE analysis of purified RFB4(dsFv)PE38. A total of 2 μ g of immunotoxin were loaded in each lane. Reduced: RFB4(dsFv)PE38 was reduced with 10 mmol/L DTT. The variable portion of the heavy chain fused with PE38 migrated with an apparent molecular mass of 48 kD. The light chain migrated faster than the 14.3 kD standard. MW, molecular mass standards. Nonreduced: non-reduced RFB4(dsFv)PE38 migrated with an apparent molecular mass of 58 kD.

Construction of RFB4(dsFv)PE38. The binding portion of disulfide-linked immunotoxins consists of V_H and V_L chains that are covalently linked through a single key residue in each chain that has been mutated to cysteine. Based on predictions using molecular models and empirical evidence with recombinant PE-containing immunotoxins, several different amino acids in the heavy and light chains can be mutated to cysteine to create a stable disulfide linkage between the chains.¹⁸⁻²¹ Using this data, we chose one amino acid in each chain (Gly₁₀₀ of the light chain and Arg₄₄ of the heavy chain) to mutate to cysteine to create a new disulfide linkage between heavy and light chains that would retain the binding affinity of the whole antibody. To construct the disulfide-linked immunotoxin (dsFv), RFB4 V_H and V_L clones were reamplified using primers VH5 and VH3-dsFv, and VL5-dsFv and VL3-dsFv, respectively. RFB4 VL3-dsFv, in addition to introducing a termination codon and an *Eco*RI site, mutates the naturally occurring Gly₁₀₀ of V_L to Cys. The amplified products were used to replace Fv and Fv-PE38 sequences of the plasmid pULI7. The cloned product pEM16 (encoding RFB4 V_L -cys₁₀₀) was sequenced and shown to have incorporated the Gly to Cys mutation. RFB4 V_H -PE38 was mutated using site-directed mutagenesis on single-stranded DNA with primer RFB4 VH dsFv(cys), which replaces V_H Arg₄₄ with a cysteine. The resulting mu-

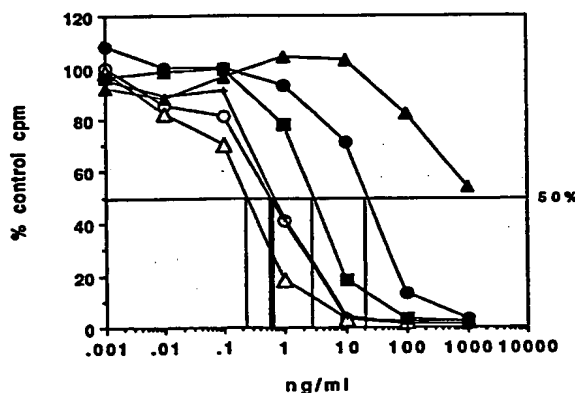


Fig 3. Cytotoxicity of RFB4(dsFv)PE38 for various cell lines after a 24-hour incubation. [³H]leucine incorporation is expressed as a percentage of cpm incorporated by control cells incubated without immunotoxin. (○), CA46; (Δ), JD38; (■), Raji; (●), Namalwa; (▲), Daudi; (◆), HUT102. Data are representative of at least three trials for each cell line.

tated construct, pEM15, was sequenced and shown to have incorporated the Arg to Cys mutation.

Expression and purification of RFB4(dsFv)PE38. Plasmids pEM15 and pEM16 were used to transform BL21(λDE3). Cultures of transformed bacteria were induced with IPTG (isopropyl-β-D-thiogalactopyranoside) for high level expression, with the protein products accumulating in inclusion bodies. Inclusion bodies were isolated and the proteins solubilized, reduced, and refolded as described in Materials and Methods. Properly refolded immunotoxins were purified to near-homogeneity by ion exchange and gel filtration column chromatography. SDS-PAGE analysis of the purified immunotoxin, run under reduced and nonreduced conditions, is shown in Fig 2. Purified immunotoxins were stored at -80°C.

Cytotoxicity of RFB4(dsFv)PE38. RFB4(dsFv)PE38 (Fig 3) was tested on five Burkitt's lymphoma cell lines (CA46, Daudi, JD38, Namalwa, and Raji) and HUT 102, a T-cell line that is CD22-negative. Of the B-cell lines tested, there were variations in sensitivity to RFB4(dsFv)PE38, which had IC₅₀ values ranging from 0.25 to 0.6 ng/mL on CA46, JD38 and Raji, 1.5 ng/mL on Namalwa and 20 ng/mL on Daudi (Table 2). Subsequent studies have shown that Daudi

Table 2. Cytotoxicity of RFB4(dsFv)PE38 Toward Various Cell Lines

Cell line*	Source	IC ₅₀ (ng/mL)† of RFB4(dsFv)PE38
CA46	Burkitt's lymphoma	0.6
Daudi		20
JD38		0.3
Namalwa		1.5
Raji		0.4
HUT102	T-cell leukemia	>1,000

* All the cell lines are of human origin.

† Cytotoxicity data are given as IC₅₀s, which are the concentrations of immunotoxin that cause a 50% reduction in protein synthesis compared with controls after incubation with cells for 24 hours.

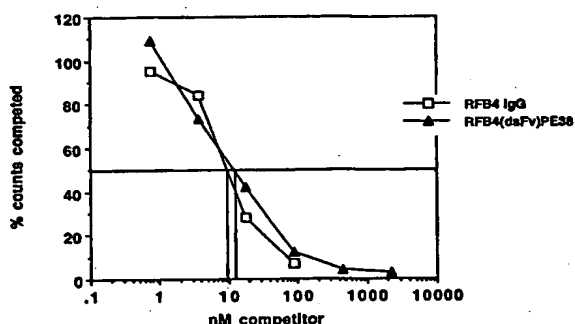


Fig 4. The relative binding activity of RFB4(dsFv)PE38 compared with native antibody on CA46 cells. Whole antibody and recombinant immunotoxin were used to compete for binding of trace amounts of 125 I-labeled RFB4 IgG. Counts competed are expressed as a percentage of counts from cells that were incubated without any competitor. (□), RFB4 IgG; (Δ), RFB4(dsFv)PE38.

cells cannot efficiently proteolytically process PE38 (*Biochemical Soc Transactions*, 1997, in press).

Antigen binding of RFB4(dsFv)PE38. The ability of the recombinant RFB4 immunotoxin to bind to antigen-positive cells was analyzed using competition assays in which increasing concentrations of immunotoxin were used to compete the binding of a fixed concentration of 125 I-labeled RFB4 IgG at 4°C. As shown in Fig 4, binding to CA46 cells was reduced by 50% at 10 nmol/L RFB4(dsFv)PE38. Native RFB4 IgG reduced the binding of labelled RFB4 IgG to CA46 cells by 50% at 8.5 nmol/L (Fig 4).

Stability of recombinant RFB4 immunotoxin at 37°C. The stability of RFB4(dsFv)PE38 was investigated by incubation of the immunotoxin for extended periods at 37°C. Stability of PE-based recombinant immunotoxins has been correlated with their activity in vitro.¹⁵ Accordingly, RFB4(dsFv)PE38 was incubated in PBS at 37°C for 1 to 7 days and its cytotoxic activity after incubation was compared with samples which were kept at -80°C. In keeping with the previous finding of high stability of dsFv immunotoxins at 37°C, RFB4(dsFv)PE38 was also very stable over the entire 7 days, as judged by maintenance of full cytotoxic activity toward CA46 cells in a 24-hour assay (Fig 5).

Temporal measurement of cytotoxic activity of RFB4(dsFv)PE38. The time required for cells to internalize and process immunotoxin is of therapeutic interest because blood levels of immunotoxin in patients must remain above a cytotoxic threshold for long enough to intoxicate the malignant cells. Therefore, we evaluated the consequences of varying exposure time of cells to immunotoxin. RFB4(dsFv)PE38 was added to cells and incubated at 37°C for 2, 24, or 48 hours. The 2-hour exposure was followed by 22 additional hours of incubation in immunotoxin-free medium to allow time for the intracellular trafficking that is required for intoxication. For both CA46 and JD38 cells, increasing the exposure time to immunotoxin from 2 to 24 hours decreased the IC₅₀ by fivefold to 10-fold. Incubation of cells for 48 hours continuously with RFB4(dsFv)PE38 resulted in little, if any, additional effect on cytotoxicity over that observed after 24 hours of incubation. Therefore, we conclude that the cell

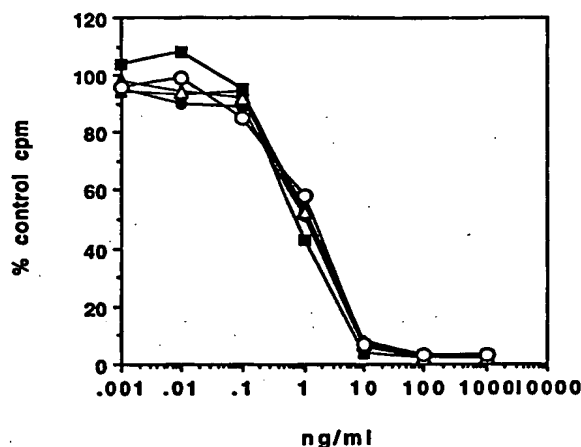


Fig 5. Stability of RFB4(dsFv)PE38. RFB4(dsFv)PE38 was incubated at 37°C for the number of days indicated and cytotoxicity on CA46 cells was compared with a sample that was stored at -80°C. (○), 7 days; (Δ), 5 days; (●), 3 days; (▲), 1 day; (■), 0 days.

lines used require greater than 2 hours of exposure to bind and internalize maximal amounts of immunotoxin and are intoxicated to nearly the fullest extent possible by 24 hours. Increasing exposure to times greater than 24 hours does not provide any advantage in vitro.

Toxicity of RFB4(dsFv)PE38. An evaluation of RFB4(dsFv)PE38 toxicity was performed to select appropriate doses of immunotoxin for antitumor experiments. A maximum tolerated dose (MTD) value was determined by multiple-dose IV injection of RFB4(dsFv)PE38 in varying amounts (Table 3). Two mice were injected for each dose level. At a dose of $3 \times 10 \mu\text{g}$ or $3 \times 8 \mu\text{g}$, no mice survived. At $3 \times 7 \mu\text{g}$ or less, all mice survived.

Antitumor activity of RFB4(dsFv)PE38 against CA46 cells in nude mice. The excellent cytotoxicity and stability of RFB4(dsFv)PE38 in vitro predicted that this molecule would have antitumor activity in an animal model of lymphoma. We evaluated the ability of RFB4(dsFv)PE38 to inhibit tumor development in a subcutaneous solid tumor model using CA46 Burkitt's lymphoma cells injected into nude mice. Two protocols were used. In the first, female athymic nude mice were irradiated on day -3 and then injected subcutaneously with 10^7 CA46 cells on day 0, while in the second, mice were irradiated on day -4 and injected with 5×10^6

Table 3. LD₅₀ of RFB4(dsFv)PE38

Dose (μg) [*]	Deaths/Total†
10	2/2
8	0/2
7	0/2
6	0/2
5	0/2
3	0/2

^{*} Doses were given IV every other day for three doses.

[†] Mice were observed for 7 days following last dose.

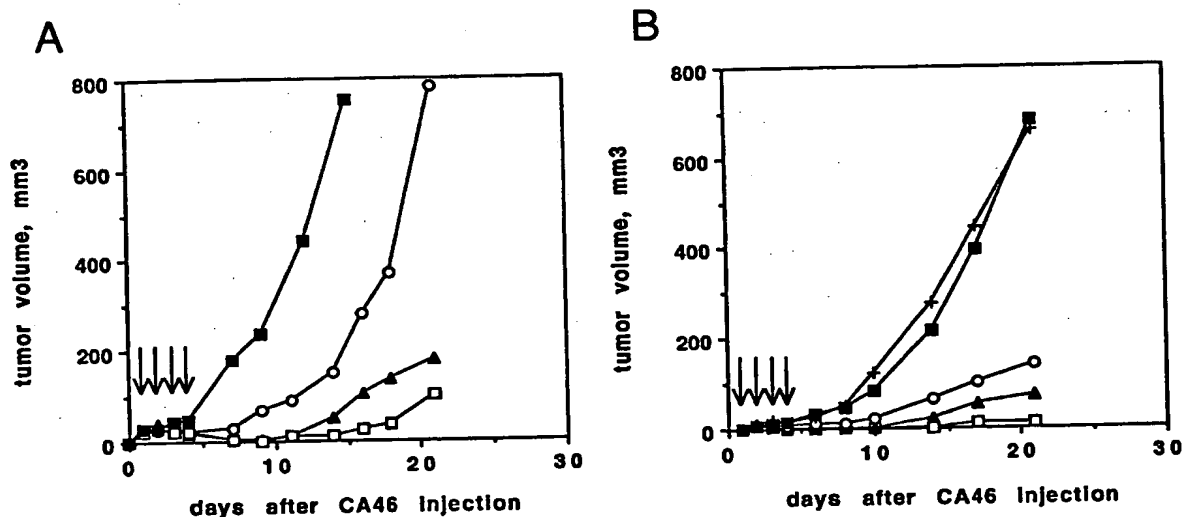


Fig 6. (A) Antitumor activity of RFB4(dsFv)PE38. Athymic nude mice irradiated on day -3 were inoculated with 10^7 CA46 cells on day 0. Beginning on day 1, injections of 5, 2, or 1 μ g RFB4(dsFv)PE38 or PBS/0.2% BSA were given every day for four doses. Tumor growth was monitored by measuring tumor volume and is expressed as the average tumor volume of each group. Control mice were killed before the end of the 21-day observation period because their tumor volumes would have exceeded humane limits. (□), 5 μ g; (Δ), 2 μ g; (○), 1 μ g; (■), PBS/0.2% BSA diluent control. Data are from one of two experiments that gave similar results. (B) Antitumor activity of RFB4(dsFv)PE38. Athymic nude mice irradiated on day -4 were inoculated with 5×10^6 CA46 cells on day 0. Beginning on day 1, injections of 5, 3, or 1 μ g RFB4(dsFv)PE38, 5 μ g nonrelevant control dsFv-PE38 immunotoxin, or PBS/0.2% BSA diluent were given every day for four doses. Tumor growth was monitored by measuring tumor volume and is expressed as the average tumor volume of each group. (□), 5 μ g; (Δ), 3 μ g; (○), 1 μ g; (+), 5 μ g nonrelevant control dsFv-PE38 immunotoxin; (■), PBS/0.2% BSA diluent control. Data are from one of two experiments that gave similar results.

CA46 cells. Mice were divided into groups of five and treated beginning 24 hours after injection of CA46 cells for 4 consecutive days (days 1 to 4) with various amounts of immunotoxin, in addition to diluent control (Fig 6). Tumor volumes were recorded for 21 days. Mice inoculated using the first protocol and treated with either 5 or 2 μ g of immunotoxin developed small tumor cell nodules that regressed on treatment and then slowly regrew (Fig 6A). Treatment with 1 μ g of immunotoxin delayed tumor development compared with controls, but tumors grew rapidly thereafter.

Mice inoculated using the second protocol and treated with 5 or 3 μ g of RFB4(dsFv)PE38 developed very small tumor nodules that completely regressed on treatment in 9 of 10 mice at the 5 μ g dose level and in 7 of 10 mice at the 3 μ g dose level (Fig 6B). No mice achieving complete regression at the 5 μ g \times 4 dose regrew tumors after extended observation (up to 90 days), while 4 of 7 mice receiving 3 μ g \times 4, and showing a complete regression, regrew tumors (within 90 days). Treatment with 1 μ g of immunotoxin delayed tumor development significantly throughout the observation period, but produced complete regressions in only 2 of 10 mice. Mice that were treated with 5 μ g of a nonrelevant dsFv-PE38 immunotoxin that is nonbinding for CA46 cells developed tumors that grew at the same rate as those in the diluent-treated control group, demonstrating specificity of the RFB4(dsFv)PE38 immunotoxin (Fig 6B).

DISCUSSION

The variable portions of the heavy and light chains of the MoAb RFB4 were cloned and sequenced. This antibody

recognizes the CD22 antigen, which is present exclusively on B cells and is found on many B-cell malignancies. RFB4 has already been extensively tested for its ability to direct deglycosylated ricin A chain to antigen-positive cells. Recently, it has also been used to make chemical conjugates with PE35, a truncated form of PE. As a way to prepare a wholly recombinant immunotoxin, a disulfide-linked Fv was constructed and then was fused with PE38.

Analysis of the recombinant immunotoxin showed that RFB4(dsFv)PE38 is stable at 37°C for extended incubation times. Cytotoxicity profiles on several antigen-positive and antigen-negative cell lines showed that the recombinant immunotoxin was highly and selectively toxic towards CD22-bearing cells and was nontoxic toward CD22⁻ lines. The duration of incubation required for maximum intoxication of cells was determined to be greater than 2 hours, but little additional benefit was noted at incubation times greater than 24 hours. The stability of RFB4(dsFv)PE38 is therefore compatible with the time required for efficient intoxication.

Binding of RFB4(dsFv)PE38 to CD22 antigen on CA46 cells was nearly identical to that of whole RFB4 IgG, although the recombinant molecule is monovalent. Previously, it was shown that a chemically conjugated immunotoxin, RFB4-PE35, bound with identical affinity to RFB4 IgG on Daudi cells.¹¹ It is, therefore, clear that RFB4(dsFv)PE38 and a chemically conjugated RFB4-PE35 are also very similar in ability to bind antigen. RFB4(dsFv)PE38 has slightly improved cytotoxicity towards CA46 cells compared with RFB4-PE35 (0.6 ng/mL v 1 ng/mL) and is equally stable over 24 hours at 37°C, demonstrating that the recombinant

RFB4(dsFv)PE38 has all of the advantages of the chemical conjugate in vitro, with the additional benefit that it can be easily prepared in large homogeneous batches.

Because the disulfide-linked immunotoxin was quite stable, had binding properties similar to the whole antibody, and superior cytotoxic effects, it was chosen for further evaluation in animal models. We evaluated its antitumor activity by assessing its ability to prevent formation of tumors after injection of CA46 cells into irradiated nude mice. We chose this model, which has been used previously in testing anti-CD22 immunotoxins, for several reasons. First, the subcutaneous tumors formed by CA46 cells are structurally very similar to human soft tissue lymphomas (unpublished observation, August 1994). This model then may more accurately represent this type of disease than do disseminated models, which are more similar to leukemic phase lymphomas usually associated with advanced disease and a high tumor burden. Secondly, we would predict that RFB4(dsFv)PE38 would not be effective in the widely-used Daudi/SCID model because Daudi cells are unique in their relative inability to process PE to an active form (*Biochemical Soc Transactions*, 1997, in press). Finally, this model produces quantitative, rapid, and reproducible results in terms of tumor reduction rather than relying on development of terminal disease for antitumor activity measurement. Using the CA46/nude mouse model, we showed that RFB4(dsFv)PE38 could eradicate tumor cells when immunotoxin administration began 24 hours after tumor implantation, in contrast to mice that were treated with diluent or a nonrelevant dsFv-PE38 immunotoxin.

Based on the data presented here, it would appear that RFB4(dsFv)PE38 merits further preclinical development as a possible treatment for B-cell lymphoma.

REFERENCES

1. Amlot P, Stone MJ, Cunningham D, Fay J, Newman J, Collins R, May R, McCarthy M, Richardson J, Ghetie V, Ramilo O, Thorpe PE, Uhr JW, Vitetta ES: A phase I study of anti-CD22 deglycosylated ricin A chain immunotoxin in the treatment of B cell lymphomas resistant to conventional therapy. *Blood* 82:2624, 1993
2. Sausville EA, Headlee D, Stetler-Stevenson M, Jaffe ES, Solomon D, Figg WD, Herdt J, Kopp WC, Rager H, Steinberg SM, Ghetie V, Schindler J, Uhr J, Wittes RE, Vitetta ES: Continuous infusion of the anti-CD22 immunotoxin IgG-RFB4-SMPT-dgA in patients with B-cell lymphoma: A phase I study. *Blood* 85:3457, 1995
3. Grossbard ML, Gribben JG, Freedman AS, Lambert JM, Kinsella J, Rabinowe SN, Eliseo L, Taylor JA, Blattler WA, Epstein CL, Nadler LM: Adjuvant immunotoxin therapy with anti-B4-blocked ricin after autologous bone marrow transplantation for patients with B-cell non-Hodgkin's lymphoma. *Blood* 81:2263, 1993
4. Grossbard ML, Lambert JM, Goldmacher VS, Spector NL, Kinsella J, Eliseo L, Coral F, Taylor JA, Blattler WA, Epstein CL, Nadler L: Anti-B4-blocked ricin: A phase I trial of 7-day continuous infusion in patients with B-cell neoplasms. *J Clin Oncol* 11:726, 1993
5. Uckun FM, Manivel C, Arthur D, Chelstrom LM, Finnegan D, Tuel-Ahlgren L, Irvin JD, Myers DE, Gunther R: In vivo efficacy of B43 (anti-CD19)-pokeweed antiviral protein immunotoxin against human pre-B cell acute lymphoblastic leukemia in mice with severe combined immunodeficiency. *Blood* 79:2201, 1992
6. Ghetie M-A, Richardson J, Tucker T, Jones D, Uhr JW, Vitetta ES: Antitumor activity of Fab' and IgG-anti-CD22 immunotoxins in disseminated human B lymphoma grown in mice with severe combined immunodeficiency disease: Effect on tumor cells in extranodal sites. *Cancer Res* 51:5876, 1991
7. Francisco JA, Gilliland LK, Stebbins MR, Norris NA, Ledbetter JA, Siegall CB: Activity of a single-chain immunotoxin that selectively kills lymphoma and other B-lineage cells expressing the CD40 antigen. *Cancer Res* 55:3099, 1995
8. Vaickus L, Ball ED, Foon KA: Immune markers in hematologic malignancies. *Crit Rev Oncol Hematol* 11:267, 1991
9. Li J-L, Shen G-L, Ghetie M-A, May RD, Till M, Ghetie V, Uhr JW, Janossy G, Thorpe PE, Amlot P, Vitetta ES: The epitope specificity and tissue reactivity of four murine monoclonal anti-CD22 antibodies. *Cell Immunol* 118:85, 1989
10. Ghetie M-A, May RD, Till M, Uhr JW, Ghetie V, Knowles PP, Relf M, Brown A, Wallace PM, Janossy G, Amlot P, Vitetta ES, Thorpe PE: Evaluation of ricin A chain-containing immunotoxins directed against CD19 and CD22 antigens on normal and malignant human B-cells as potential reagents for *in vivo* therapy. *Cancer Res* 48:2610, 1988
11. Mansfield E, Pastan I, FitzGerald DJ: Characterization of RFB4-PE immunotoxins targeted to CD22 on B-cell malignancies. *Bioconjug Chem* 7:557, 1996
12. Debinski W, Pastan I: Monovalent immunotoxin containing truncated form of *Pseudomonas* exotoxin as potent antitumor agent. *Cancer Res* 52:5379, 1992
13. Brinkmann U, Pastan I: Recombinant immunotoxins: From basic research to cancer therapy. *Methods* 8:143, 1995
14. Reiter Y, Brinkmann U, Lee B-K, Pastan I: Engineering antibody fragments for cancer detection and therapy: Disulfide-stabilized Fv fragments. *Nat Biotechnol* 14:1239, 1996
15. Benhar I, Pastan I: Cloning, expression and characterization of the Fv fragments of the anti-carbohydrate mAbs B1 and B5 as single-chain immunotoxins. *Protein Eng* 7:1509, 1994
16. Studier FW, Moffatt BA: Use of bacteriophage T7 polymerase to direct selective expression of cloned genes. *J Mol Biol* 189:113, 1986
17. Buchner J, Pastan I, Brinkmann U: A method for increasing the yield of properly folded recombinant fusion proteins: Single-chain immunotoxins from renaturation of bacterial inclusion bodies. *Anal Biochem* 205:263, 1992
18. Jung S-H, Pastan I, Lee B: Design of interchain disulfide bonds in the framework region of the Fv of the monoclonal antibody B3. *Proteins: Structure, Function and Genetics*. 19:35, 1994
19. Reiter Y, Brinkmann U, Webber K, Jung S-H, Lee B, Pastan I: Engineering interchain disulfide bonds into conserved framework regions of Fv fragments: Improved biochemical characteristics of recombinant immunotoxins containing disulfide-stabilized Fv. *Protein Eng* 7:697, 1994
20. Reiter Y, Brinkmann U, Kreitman RJ, Jung SH, Lee B, Pastan I: Stabilization of the Fv fragments in recombinant immunotoxins by disulfide bonds engineered into conserved framework regions. *Biochemistry* 33:5451, 1994
21. Reiter Y, Brinkmann U, Jung SH, Lee B, Kasprzyk PG, King CR, Pastan I: Improved binding and antitumor activity of a recombinant anti-erbB2 immunotoxin by disulfide stabilization of the Fv fragment. *J Biol Chem* 269:18327, 1994

Cytotoxic activity of a recombinant fusion protein between interleukin 4 and *Pseudomonas* exotoxin

(lymphokine/growth factor/immunology/bone marrow)

MASATO OGATA, VIJAY K. CHAUDHARY, DAVID J. FITZGERALD, AND IRA PASTAN

Laboratory of Molecular Biology, National Cancer Institute, National Institutes of Health, 37/4E16, 9000 Rockville Pike, Bethesda, MD 20892

Contributed by Ira Pastan, February 27, 1989

ABSTRACT A recombinant chimeric toxin in which the cell binding domain of *Pseudomonas* exotoxin (PE) was replaced by murine interleukin 4 (IL-4) was produced in *Escherichia coli*. This chimeric protein, IL-4-PE40, was cytotoxic to murine IL-4 receptor-bearing cell lines but had little effect on human cell lines lacking receptors capable of binding murine IL-4. A mutant form of IL-4-PE40 (termed IL-4-PE40 asp⁵⁵³) with very low ADP-ribosylating activity displayed mitogenic activity similar to that of IL-4 rather than cytotoxic activity. Because the cytotoxic effects of IL-4-PE40 were blocked by excess IL-4 or by neutralizing antibody to IL-4 (11B11), we conclude that the cytotoxic effect of IL-4-PE40 is specifically mediated through IL-4 receptors. IL-4-PE40 could be a useful reagent for specific elimination of cells bearing IL-4 receptors.

Bacterial and plant toxins have been attached to growth factors (1-5) and antibodies (6, 7) to make cytotoxic reagents specific for certain types of eukaryotic cells. Our laboratory has used *Pseudomonas* exotoxin (PE) for these studies. PE is composed of three structural domains (8): domain Ia for cell recognition, domain II for translocation across membranes, and domain III for ADP-ribosylation of elongation factor 2, the step actually responsible for cell death (9). We have produced a noncytotoxic mutant form of PE, termed PE40, which lacks domain Ia (the cell binding domain) but retains translocation and ADP-ribosylating activity (9). By fusing the gene encoding PE40 to genes encoding transforming growth factor α (1), interleukin 2 (IL-2) (2), interleukin 6 (4), and CD4 (10), we have developed chimeric proteins specifically toxic to cells expressing receptors or binding proteins for these.

Interleukin 4 (IL-4, also called BSF-1) is a 20,000-Da protein produced by activated T lymphocytes and was first described as a growth factor for B lymphocytes (11). IL-4 also increases the expression of class II major histocompatibility complex (MHC) molecules (12, 13) and enhances the production of IgG1 and IgE (14-17). Moreover, IL-4 has been shown to act on certain non-B cells; IL-4 enhances the growth and/or differentiation of T cells (18-21), activates macrophages (22, 23), and increases the growth of granulocytes, mast cell, and erythrocyte colonies (23-25). IL-4 seems to have a wide range of biological activities, including the proliferation and differentiation of lymphocytes and hemopoietic cells. Though the cells of various lineages have been reported to have IL-4 receptors, activated T and B lymphocytes and certain tumor cell lines derived from B lymphomas, T leukemias, and mastocytomas (26-28) have relatively high numbers of IL-4 receptors. Depletion of cells bearing high numbers of IL-4 receptors by the chimeric protein IL-4-PE40 may have some value in studying the

biological function of the IL-4/IL-4 receptor system and also in treating some immunological disorders or tumors.

In this report, we describe the construction of a chimeric gene in which the gene encoding PE40 was fused to a cDNA encoding murine IL-4. The fusion gene product, IL-4-PE40, was found to be highly toxic to a murine T-cell line (CT.4R) bearing about 15,000 IL-4 receptors (29) but to have no effect on human cell lines lacking receptors for murine IL-4. In addition, a chimeric protein composed of a mutant form of PE40 that had very low ADP-ribosylating activity (PE40 asp⁵⁵³) was also prepared. IL-4-PE40 asp⁵⁵³ displayed mitogenic activity similar to that of IL-4 rather than cytotoxic activity, showing that ADP-ribosylating activity was essential for cytotoxicity and that IL-4-PE40 asp⁵⁵³ bound specifically to the IL-4 receptor. Because the cytotoxic effects of IL-4-PE40 were blocked by excess IL-4 or by a neutralizing monoclonal antibody to IL-4 (11B11), we conclude that the cytotoxic effect of IL-4-PE40 is specifically mediated through IL-4 receptors.

MATERIALS AND METHODS

Reagents. Chemicals and enzymes were described previously (2). For polymerase chain reaction (PCR), we used a DNA amplification reagent kit (no. N801-0043) from Perkin-Elmer/Cetus. Anti-IL-4 monoclonal antibody, 11B11 (30), was purchased from Tex Star Monoclonals (Dallas). Recombinant murine IL-4 was a gift from W. E. Paul (National Institutes of Health).

Plasmids, Bacterial Strains, and Cell Lines. Plasmid pVC8(+)/T, which carries domains II and III of the PE gene (PE40) from pVC8 (1), a T7 transcription terminator at the end of PE40 gene, and a f1 origin of replication, was constructed in this laboratory (V.K.C., unpublished). The plasmid carrying murine IL-4 cDNA was a gift from S. Gillis (Immunex, Seattle). Plasmid pVC45M, which carries a gene for PE with an asp⁵⁵³ mutation (ADP-ribosylating mutant), was described previously (31, 32). CT.4R is an IL-4-dependent murine T-cell line expressing about 15,000 IL-4 receptors (29). HUT 102 is a human T-cell leukemia and a gift from T. A. Waldmann (National Cancer Institute). CTLL is an IL-2-dependent murine T-cell line. P815 is a murine mastocytoma cell line. P3X63-Ag8.653 is a clone derived from murine plasmacytoma, MOPC-21, and obtained from the American Type Culture Collection. NIH 3T3, Swiss 3T3, and L929 are murine fibroblast cell lines. A431 and KB are human epidermoid carcinoma cell lines.

Plasmid Construction. Plasmid DNA was prepared and oligonucleotides were synthesized as described (2). The chimeric gene encoding IL-4-PE40 under the control of the T7 promoter was constructed as summarized in Fig. 1. First, we created an *Nde* I site at the 5' and 3' ends of the IL-4

The publication costs of this article were defrayed in part by page charge payment. This article must therefore be hereby marked "advertisement" in accordance with 18 U.S.C. §1734 solely to indicate this fact.

Abbreviations: IL-4, interleukin 4; IL-2, interleukin 2; PE, *Pseudomonas* exotoxin; MHC, major histocompatibility complex; PCR, polymerase chain reaction.

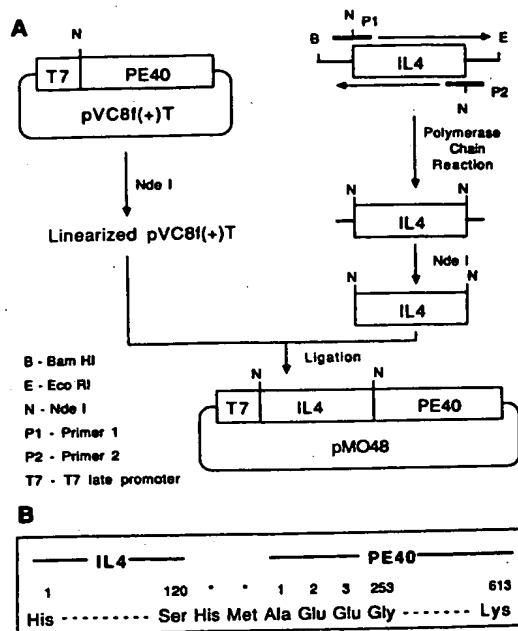


FIG. 1. Scheme for construction of expression plasmid pMO48, encoding IL-4-PE40.

(A) Scheme for construction of pMO48: Primer 1, 5'-CTTTCTCGAATGTACCCATATG
CATATCCACGGATGCGACAAAATC-3'; Primer 2, 5'-GTTAAAGCATGGTGGCTCACAT
ATCGAGTAATCCATTGTCATG-3'

The bases underlined were changed from that of IL-4 to create an *Nde* I site. (B) Abbreviated amino acid sequence of IL-4-PE40. Two amino acids (*) were added between IL-4 and PE40 to create an *Nde* I site.

coding sequence by PCR (33, 34) using primers with recognition sites for *Nde* I. As shown in the legend of Fig. 1, we synthesized two oligonucleotide primers: primer 1 is complementary to the 3' region of antisense strand of IL-4 cDNA and primer 2 is complementary to the 3' region of sense strand. In both primers, five bases were changed to create an *Nde* I site. After 25 cycles of PCR using primer 1 and primer 2 (1 μ M) and a 0.55-kilobase (kb) *Bam*HI-*Eco*RI DNA fragment (0.1 ng per reaction) that contained the IL-4 coding sequence as the template, a 0.406-kb DNA fragment was amplified. After separation on a low-melting-point agarose gel, the 0.406-kb DNA was eluted and cut with *Nde* I, and then a 0.366-kb fragment was separated. The 0.366-kb *Nde* I fragment was subcloned into the *Nde* I site of pVC8f(+)-T. The resulting plasmid had a 0.366-kb IL-4 coding gene in two orientations at the 5' end of the PE40 gene. After restriction analysis, a plasmid with IL-4 in the proper orientation with respect to the PE40 gene was identified (pMO48). Plasmid pMO48M (IL-4-PE40 *asp*⁵³³) was constructed by cleaving pMO48 with *Bam*HI and *Eco*RI and replacing the 0.46-kb fragment with a similar *Bam*HI-*Eco*RI fragment from pVC45M (30).

Expression and Localization of IL-4-PE40. *Escherichia coli* BL21 (ADE3) cells were transformed with the plasmid pMO48, cultured in 1 liter of LB broth with ampicillin (100 μ g/ml) up to OD₆₅₀ = 0.5, and induced with 1 mM isopropyl β -D-thiogalactoside for 90 min. The separation of different compartments of cells was described previously (4).

Gel Electrophoresis and Immunoblotting. SDS/PAGE on 10% gels was performed as described by Laemmli (35). The

gels were stained with Coomassie blue. For immunoblotting, electrophoresed samples were transferred to nitrocellulose paper and processed by using rabbit anti-PE antiserum as described (9).

Purification of IL-4-PE40. The purification protocol for IL-4-PE40 was essentially the same as described (4). Briefly, the pellet containing inclusion bodies was prepared by centrifuging the sonicated spheroplasts. This pellet, containing IL-4-PE40, was denatured in extraction buffer (7 M guanidine hydrochloride/100 mM Tris-HCl, pH 8.0/5 mM EDTA). After centrifugation at 40,000 rpm for 15 min, the supernatant containing denatured protein was rapidly diluted in 80 vol of buffer (150 mM NaCl/10 mM sodium phosphate, pH 7.4) and allowed to sit for 16 hr at 4°C for renaturation. After dialyzing against 20 mM Tris (pH 8.0), the samples were applied onto a Mono Q column (10 \times 100 mm) and eluted with a 200-ml linear gradient of NaCl (0-500 mM in 20 mM Tris, pH 8.0); 4-ml fractions were collected and the absorbance at 280 nm was monitored. The fraction containing the peak cytotoxic activity (fraction 33) was applied onto a TSK G3000 (7.8 \times 300 mm) gel filtration column and eluted with 0.2 M sodium phosphate (pH 7.0) containing 1 mM EDTA. The chimeric mutant protein, IL-4-PE40 *asp*⁵³³, was expressed and purified in the same way as IL-4-PE40. It also was shown to have the same molecular mass as determined by SDS/PAGE (data not shown).

Protein Synthesis Inhibition Assays. The cytotoxic activity of IL-4-PE40 was tested on CT.4R cells. CT.4R cells were maintained in the RPMI 1640 medium containing 5% fetal calf serum, 50 μ M 2-mercaptoethanol, 1 mM sodium pyruvate, 50 units of penicillin per ml, 50 μ g of streptomycin per ml, 50 μ g of gentamycin per ml, and 500 units of murine IL-4 per ml. For assay, cells were washed to remove IL-4 and plated in 96-well tissue culture plates at 8 \times 10³ cells in 100 μ l, and various concentrations of IL-4-PE40 were added. Five hundred units of IL-2 per ml was also added to keep the cells growing during the assay period. For blocking or neutralizing experiments, IL-4-PE40 was premixed with competitors or neutralizing antibodies and then added to the cells. After a 2-day incubation at 37°C, cells were cultured with 2 μ Ci (1 Ci = 37 GBq) of [³H]leucine for 4 hr, and the radioactivity incorporated into cells was measured as described (36). When IL-4-PE40 was tested on CTLL cells, the same protocol was used. For other cell lines, we used culture medium without IL-2 and different numbers of cells (HUT 102, and P3X63-Ag8.653, 1 \times 10⁴ cells per well; NIH 3T3, Swiss 3T3, L929, A431, and KB, 1.6 \times 10⁴ cells per well; P815, 8 \times 10³ cells per well).

Mitogenic Assay. CT.4R cells (5 \times 10³ cells in 200 μ l) were cultured in the absence or presence of various amounts of recombinant IL-4 or IL-4-PE40 *asp*⁵³³. After a 40-hr incubation, cells were incubated with [³H]thymidine (0.5 μ Ci) for 6 hr, and then the radioactivity incorporated into the cells was measured.

RESULTS

Construction of Expression Plasmid Encoding IL-4-PE40. A DNA fragment encoding murine IL-4 was subcloned into the *Nde* I site of pVC8f(+)-T (Fig. 1A). To do this, we first created *Nde* I sites at the 5' and 3' ends of the IL-4 coding sequence by PCR using primers with recognition sites for *Nde* I. After 25 cycles of PCR with these primers and a DNA template that contained the IL-4 coding sequence, the amplified DNA fragment acquired *Nde* I sites at both ends.

The resulting plasmid, pMO48, was expressed under the control of bacteriophage T7 late promoter. The chimeric protein, IL-4-PE40, is composed of 486 amino acids, in which a native IL-4 sequence of 120 amino acids is followed

by amino acids histidine, methionine, and 1-3 and 253-613 of PE (Fig. 1B).

Expression of IL-4-PE40. To express IL-4-PE40, *E. coli* BL21 (ADE3) cells were transformed with plasmid pMO48. After induction with isopropyl β -D-thiogalactoside, the cells were collected and processed as described in *Materials and Methods*. The new protein, migrating at 53 kDa, was readily detectable on SDS/PAGE of the total cell pellet (Fig. 2A, lane 2). The size of this protein corresponds to the expected size for IL-4-PE40, and immunoblotting analysis showed this protein reacted with anti-PE antibody (Fig. 2B, lane 2). The culture supernatant or the periplasm had negligible amounts of this protein. Separation of sonicated spheroplasts into cytoplasm and a pellet that contained inclusion bodies showed that the 53-kDa protein was mostly retained in the pellet (Fig. 2A and B, lanes 4).

Purification of IL-4-PE40. Because a 53-kDa protein of the size expected for IL-4-PE40 was produced and because this protein reacted with antibodies to PE, we tentatively concluded that the 53-kDa protein was IL-4-PE40 and purified this protein. To do this, the inclusion bodies were denatured in 7 M guanidine and then renatured as described in *Materials and Methods*. The renatured protein was applied to a Mono Q ion-exchange column (Fig. 3A). Fraction 33 from the Mono Q column showed high cytotoxic activity on IL-4 receptor-bearing cells and was applied to a TSK G3000 gel filtration column (Fig. 3B). Most of the cytotoxic activity came in fractions 19 and 20 (Fig. 3B). As shown in Fig. 3C, fraction 19 of the TSK G3000 column contained a 53-kDa protein that was about 90% pure and this protein reacted with anti-PE antibody (Fig. 3D). This protein also had almost the same ADP-ribosyltransferase activity as an equal amount of PE40 (data not shown).

Protein Synthesis Inhibition by IL-4-PE40. To test the cytotoxic activity of IL-4-PE40, we used a murine T-cell line, CT.4R, that expresses around 15,000 IL-4 receptors. This cell line can grow in the presence of either IL-4 or IL-2 and was maintained in culture medium containing recombinant murine IL-4.

CT.4R cells were treated with various amounts of IL-4-PE40. IL-2 (500 units/ml) was added to the culture to keep CT.4R cells growing during the assay period. After 2 days, the level of protein synthesis was determined. As shown in Fig. 4A, IL-4-PE40 inhibited protein synthesis in CT.4R cells in a concentration-dependent manner. The concentration of IL-4-PE40 giving a 50% reduction of protein synthesis (ID_{50})

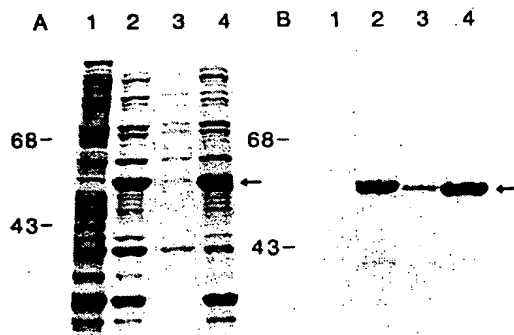


FIG. 2. Localization of IL-4-PE40 in *E. coli* BL21 (ADE3). *E. coli* BL21 (ADE3) cells were transformed by plasmid pMO48 and were processed as described in the text. (A) Coomassie blue-stained gel. (B) Immunoblotting with rabbit anti-PE antibody. Lanes 1, total cell pellet (nontransformed cells); lanes 2, total cell pellet (transformed cells); lanes 3, cytoplasm; lanes 4, $100,000 \times g$ pellet of sonicated spheroplasts. Molecular masses are indicated in kDa. The arrow shows the new protein migrating at 53 kDa.

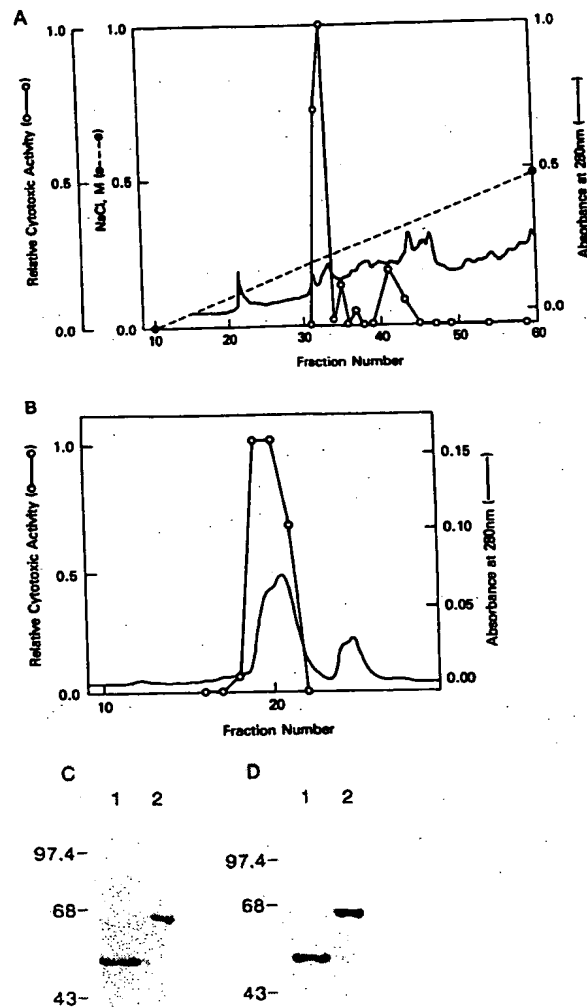


FIG. 3. Purification of IL-4-PE40. (A) Mono Q ion-exchange chromatography of IL-4-PE40; material from a 750-ml culture of *E. coli* BL21 (ADE3) was applied to a Mono Q column. (B) TSK G3000 gel filtration chromatography; fraction 33 of the Mono Q column (220 μ g of protein) was applied to a TSK G3000 column. In A and B, cytotoxic activity is expressed as the relative ratio of peak activities from protein synthesis inhibition assays using CT.4R cells. Absorbance at 280 nm was measured. (C and D) SDS/PAGE of purified IL-4-PE40. (C) Coomassie blue-stained gel. (D) Immunoblotting with rabbit anti-PE antibody. Lanes 1, fraction 19 of TSK G3000 column; lanes 2, PE. Molecular masses are indicated in kDa.

was 17 ng/ml. Conversely, the nonchimeric protein, PE40, which cannot bind to the IL-4 receptor, had little or no effect on protein synthesis ($ID_{50} > 1000$ ng/ml).

ADP-Ribosylation Activity Is Essential for the Cytotoxic Effect of IL-4-PE40. The nature of the cytotoxic effect of IL-4-PE40 was further investigated by determining the cytotoxicity of IL-4-PE40 asp^{553} , a mutant form of this chimeric protein that has very low ADP-ribosylation activity (data not shown). As shown in Fig. 4B, IL-4-PE40 asp^{553} was found not to have any cytotoxic effect up to a concentration of 1000 ng/ml. Rather than inhibiting the synthesis of protein by CT.4R cells, IL-4-PE40 asp^{553} displayed a mitogenic activity similar to that of IL-4 (Fig. 5). Although the mitogenic

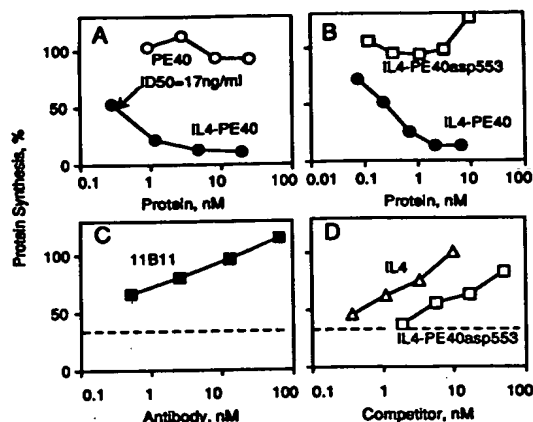


FIG. 4. Protein synthesis inhibition by IL-4-PE40. CT.4R cells (8×10^3 in 200 μ l) were incubated in the culture medium containing IL-2 (50 units/ml). (A and B) Various amounts of IL-4-PE40, PE40, or IL-4-PE40 asp⁵⁵³ were added to the culture. (C and D) IL-4-PE40 (1.9 nM) and various amounts of anti-IL-4 antibody (11B11), IL-4, or IL-4-PE40 asp⁵⁵³ were added to the culture. After a 20-hr (C and D) or 40-hr (A and B) incubation, protein synthesis was measured. Results are expressed as the % of the value of cells incubated without toxin. The dotted line (C and D) shows the protein synthesis level without antibody or competitor (36%).

activity of IL-4-PE40 asp⁵⁵³ was less than that of IL-4 by a factor of ≈ 10 , this result clearly showed that the IL-4 toxin retained substantial binding activity toward IL-4 receptors.

IL-4 Receptor-Mediated Cytotoxicity by IL-4-PE40. To demonstrate further that the cytotoxic activity of IL-4-PE40 was mediated by the IL-4 receptor, we used two other approaches. First, we examined the neutralizing effect of anti-IL-4 antibody, 11B11, on IL-4-PE40. 11B11 is a monoclonal antibody that can bind to IL-4 and inhibit IL-4 binding to the IL-4 receptor (26). As shown in Fig. 4C, 11B11 neutralized the cytotoxic effect of IL-4-PE40.

The second approach involved competition of the cytotoxic activity of IL-4-PE40 by either IL-4 or IL-4-PE40 asp⁵⁵³. Both IL-4 and IL-4-PE40 asp⁵⁵³ blocked the cytotoxic effect of IL-4-PE40 (Fig. 4D). IL-4 was about 10-fold more effective in blocking the cytotoxic effect of IL-4-PE40 than IL-4-PE40 asp⁵⁵³. These results clearly showed that the binding of IL-4-PE40 to IL-4 receptors is essential for its cytotoxic effect.

Cytotoxic Effect of IL-4-PE40 on Various Cell Lines. The effect of IL-4-PE40 on cell lines lacking receptors for murine IL-4 was examined to demonstrate further the specificity of the cytotoxic effect. HUT 102 is a human T-cell leukemia cell line. It is well known that murine IL-4 does not bind to human

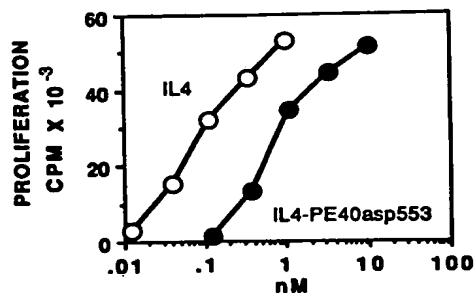


FIG. 5. Mitogenic effect of IL-4-PE40 asp⁵⁵³ on CT.4R cells. CT.4R cells (5×10^3 cells in 200 μ l) were incubated in the presence of various amounts of recombinant IL-4 or IL-4-PE40 asp⁵⁵³. After a 40-hr incubation, [³H]thymidine incorporation was measured.

Table 1. Cytotoxic activity of IL-4-PE40

Cell line	ID ₅₀ , ng/ml		
	IL-4-PE40	IL-4-PE40 asp ⁵⁵³	PE40
CT.4R	17	>1000	>1000
CTLL	250	>1000	1000
P3X63-Ag8.653	12	>1000	>1000
P815	20	>1000	>1000
NIH 3T3	>1000	>1000	>1000
Swiss 3T3	420	>1000	>1000
L929	350	>1000	>1000
HUT 102	>1000	ND	ND
A431	>1000	ND	ND
KB	>1000	ND	ND

Protein synthesis level was measured after 2 days of incubation with toxin. ID₅₀ is the protein concentration required to inhibit protein synthesis by 50%. ND, not done.

cells (26, 27). We first tested this cell line because it had been shown previously to be sensitive to another chimeric toxin, IL-2-PE40 (2). As shown in Table 1, IL-4-PE40 had very little or no cytotoxic effect on HUT 102 cells (ID₅₀ > 1000 ng/ml). We also tested two other human cell lines, A431 and KB, and IL-4-PE40 was not cytotoxic to them. On the contrary, IL-4-PE40 was cytotoxic to murine cell lines, CTLL (a T-cell line) and P815 (a mastocytoma cell line), that had been reported to possess IL-4 receptors (26, 27). IL-4-PE40 was also cytotoxic to a murine myeloma cell line, P3X63-Ag8.653. IL-4-PE40 had weak cytotoxic effects on two murine fibroblast cell lines, Swiss 3T3 and L929, but had little or no effect on NIH 3T3. The cytotoxic activity of IL-4-PE40 to CTLL, P815, Swiss 3T3, and L929 was neutralized by anti-IL-4 antibodies (11B11) (data not shown). IL-4-PE40 asp⁵⁵³ or PE40 lacking ADP-ribosylating activity or cell binding domain, respectively, had very low effects on all cell lines listed in Table 1. These results confirm the specific cytotoxicity of IL-4-PE40.

DISCUSSION

We have produced a chimeric protein IL-4-PE40, by fusing a gene encoding murine IL-4 to a gene encoding domains II and III of PE. IL-4-PE40 was highly cytotoxic to the murine T-cell clone CT.4R, bearing about 15,000 IL-4 receptors, and was nontoxic to human cell lines lacking receptors for murine IL-4. The cytotoxic effect of IL-4-PE40 on CT.4R was mediated by IL-4 receptor because PE40, a nonchimeric protein that cannot bind to the IL-4 receptor, showed no cytotoxicity and because an excess amount of IL-4 or a neutralizing monoclonal antibody (11B11) to IL-4 blocked the cytotoxicity of IL-4-PE40. We also investigated the cytotoxicity of a chimeric protein, IL-4-PE40 asp⁵⁵³, in which glutamic acid at position 553 was changed to aspartic acid. This change causes a large reduction of ADP-ribosylating activity to <1% of that of IL-4-PE40 (data not shown). IL-4-PE40 asp⁵⁵³ was not cytotoxic to CT.4R cells up to a concentration of 1000 ng/ml. This indicates that the ADP-ribosylating activity is essential for the cytotoxicity of IL-4-PE40. Moreover, IL-4-PE40 asp⁵⁵³ displayed mitogenic activity similar to that of IL-4, although IL-4-PE40 asp⁵⁵³ was less active than IL-4 by a factor of ≈ 10 . IL-4-PE40 asp⁵⁵³ was also less active than IL-4 by a factor of ≈ 10 in blocking the cytotoxicity of IL-4-PE40. All together these results showed that the chimeric protein between IL-4 and PE40 possessed a reasonably high affinity for the IL-4 receptor and had biological activity similar to that of IL-4.

Various lineages of cells including lymphocytes and hemopoietic cells at various differentiation stages have been reported to express IL-4 receptors (26–28). However, little is known about the biological role of the cells bearing high

number of IL-4 receptors. To investigate such questions, IL-4-PE40 could be useful by depleting cells with high numbers of IL-4 receptors. Another possible use of IL-4-PE40 may be suppressing immune responses. It has been reported that activation of B and T cells with mitogen or anti-IgM antibody produces a 5- to 10-fold increase in IL-4 receptor number (26-28). IL-4-PE40 could be immunosuppressive by depleting these activated lymphocytes. It may also be possible to use IL-4-PE40 for the treatment of certain tumors because it has been reported that certain tumor cell lines derived from B lymphomas, T leukemias, and mastocytomas have relatively high number of IL-4 receptors (26-28). For these purposes, it will be important to determine how many receptors on a cell are necessary for killing by IL-4-PE40 because the sensitivity of cells to growth factor-toxin fusion proteins seems to be largely dependent on the number of receptors on a cell (36).

We thank Dr. S. Gillis for the IL-4 cDNA, Dr. W. E. Paul for the CT.4R cell line and for his advice, Dr. C. B. Siegfal for helpful discussions, and A. Gaddis for preparing the manuscript.

- Chaudhary, V. K., FitzGerald, D. J., Adhya, S. & Pastan, I. (1987) *Proc. Natl. Acad. Sci. USA* 84, 4538-4542.
- Lorberboum-Galski, H., FitzGerald, D. J. P., Chaudhary, V., Adhya, S. & Pastan, I. (1988) *Proc. Natl. Acad. Sci. USA* 85, 1922-1926.
- Williams, D. P., Parker, K., Bacha, P., Bishai, W., Borowski, M., Genbauffe, F., Strom, T. B. & Murphy, J. R. (1987) *Protein Eng.* 1, 493-498.
- Siegall, C. B., Chaudhary, V. K., FitzGerald, D. J. & Pastan, I. (1988) *Proc. Natl. Acad. Sci. USA* 85, 9738-9742.
- Shimizu, N., Miskimins, W. K. & Shimizu, Y. (1980) *FEBS Lett.* 118, 274-278.
- Vitetta, E. S., Krolick, K. A., Miyama-Inaba, M., Cushley, W. & Uhr, J. W. (1983) *Science* 219, 644-650.
- Pastan, I., Willingham, M. C. & FitzGerald, D. J. (1986) *Cell* 47, 641-648.
- Allured, V., Collier, R. J., Carroll, S. F. & McKay, D. B. (1986) *Proc. Natl. Acad. Sci. USA* 83, 1320-1324.
- Hwang, J., FitzGerald, D. J. P., Adhya, S. & Pastan, I. (1987) *Cell* 48, 129-136.
- Chaudhary, V. K., Mizukami, T., Fuerst, T. R., FitzGerald, D. J., Moss, B., Pastan, I. & Berger, E. A. (1988) *Nature (London)* 335, 369-372.
- Howard, M., Farrar, J., Hilfiker, M., Johnson, B., Takatsu, K., Hamaoka, T. & Paul, W. E. (1982) *J. Exp. Med.* 155, 914-923.
- Noelle, R., Krammer, P. H., Ohara, J., Uhr, J. W. & Vitetta, E. S. (1984) *Proc. Natl. Acad. Sci. USA* 81, 6149-6153.
- Roehm, N. W., Liebson, J., Zlotnick, A., Kappler, J., Marack, P. & Cambier, J. C. (1984) *J. Exp. Med.* 160, 679-694.
- Vitetta, E. S., Brooks, K., Chen, Y. W., Isakson, P., Jones, S., Layton, J., Mishra, G. C., Pure, E., Weiss, E., Word, C., Yuan, D., Tucker, P., Uhr, J. W. & Krammer, P. H. (1984) *Immunol. Rev.* 78, 137-158.
- Sideras, P., Bergstedt-Lindqvist, S., MacDonald, H. R. & Severinson, E. (1985) *Eur. J. Immunol.* 15, 586-593.
- Vitetta, E. S., Ohara, J., Myers, C., Layton, J., Krammer, P. H. & Paul, W. E. (1985) *J. Exp. Med.* 162, 1726-1731.
- Coffman, R. L., Ohara, J., Bond, M. W., Carty, J., Zlotnick, E. & Paul, W. E. (1986) *J. Immunol.* 136, 4538-4541.
- Hu-Li, J., Shevach, E. M., Mizuguchi, J., Ohara, J., Mosmann, T. & Paul, W. E. (1987) *J. Exp. Med.* 165, 157-172.
- Mosmann, T. R., Bond, M. W., Coffman, R. L., Ohara, J. & Paul, W. E. (1986) *Proc. Natl. Acad. Sci. USA* 83, 5654-5658.
- Fernandez-Botran, R., Krammer, P. H., Diamenstein, T., Uhr, J. W. & Vitetta, E. S. (1986) *J. Exp. Med.* 164, 580-594.
- Palacios, R., Sideras, P. & von Boehmer, H. (1987) *EMBO J.* 6, 91-95.
- Crawford, R. M., Finbloom, D. S., Ohara, J., Paul, W. E. & Meltzer, M. S. (1987) *J. Immunol.* 139, 135-141.
- Rennick, D., Yang, G., Muller-Sieburg, C., Smith, C., Arai, N., Takabe, Y. & Gemmell, L. (1987) *Proc. Natl. Acad. Sci. USA* 84, 6889-6893.
- Peschel, C., Paul, W. E., Ohara, J. & Green, I. (1987) *Blood* 70, 254-263.
- Hamaguchi, Y., Hanakura, Y., Fugita, J., Takeda, S., Nakano, T., Tarui, S., Honjo, T. & Kitamura, Y. (1987) *J. Exp. Med.* 165, 268-274.
- Ohara, J. & Paul, W. E. (1987) *Nature (London)* 325, 537-540.
- Park, L. S., Friend, D., Grabstein, K. & Urdal, D. L. (1987) *Proc. Natl. Acad. Sci. USA* 84, 1669-1673.
- Park, L. S., Friend, D., Sassenfeld, H. M. & Urdal, D. L. (1987) *J. Exp. Med.* 166, 476-488.
- Hu-Li, J., Ohara, J., Watson, C., Tsang, W. & Paul, W. E. (1989) *J. Immunol.* 142, 800-807.
- Ohara, J. & Paul, W. E. (1985) *Nature (London)* 315, 333-336.
- Jinno, Y., Chaudhary, V. K., Kondo, T., Adhya, S., FitzGerald, D. J. & Pastan, I. (1988) *J. Biol. Chem.* 263, 13203-13209.
- Douglas, C. M. & Collier, R. J. (1987) *J. Bacteriol.* 169, 4967-4971.
- Saiki, R. K., Scharf, S., Faloona, F., Mullis, K. B., Horn, G. T., Erlich, H. A. & Arnheim, N. (1985) *Science* 230, 1350-1354.
- Scharf, S. J., Horn, G. T. & Erlich, H. A. (1986) *Science* 233, 1076-1078.
- Laemmli, U. K. (1970) *Nature (London)* 227, 680-685.
- Ogata, M., Lorberboum-Galski, H., FitzGerald, D. J. & Pastan, I. (1988) *J. Immunol.* 141, 4224-4228.
- Lorberboum-Galski, H., Kozak, R. W., Waldman, T. A., Bailon, P., FitzGerald, D. J. & Pastan, I. (1988) *J. Biol. Chem.* 263, 18650-18656.

Renal dysfunction accounts for the dose limiting toxicity of DT₃₉₀anti-CD3sFv, a potential new recombinant anti-GVHD immunotoxin

Daniel A. Vallera^{1,3}, Angela Panoskaltis-Mortari² and Bruce R. Blazar²

University of Minnesota Cancer Center, Departments of ¹Therapeutic Radiology, Section on Experimental Cancer Immunology and ²Pediatrics, Division of Bone Marrow Transplantation, Minneapolis, MN 55455, USA

³To whom correspondence should be addressed

The toxicity of a highly selective, recombinant fusion immunotoxin, DT₃₉₀anti-CD3sFv, was examined in mice. The protein was expressed from a hybrid gene in which the single chain Fv of the anti-murine CD3 epsilon antibody cDNA was spliced to truncated diphtheria toxin cDNA. DT₃₉₀anti-CD3sFv, previously shown to have significant anti-GVHD effects when administered to mice given transplants of allogeneic MHC-disparate donor T cells (Vallera *et al.*, *Blood* 88, 2342-2353, 1996), preferentially localized to kidney and had profound renal toxicity as assessed by histology and serum levels of blood urea nitrogen (BUN), and creatinine. Kidney effects were more severe than liver effects at the maximum tolerated dose (MTD) of 10 µg/day BID given over a six day interval. Toxic injury was attributed in part to the toxin moiety since DT₃₉₀ administered alone was more toxic than equivalent doses of DT₃₉₀ given in the context of DT₃₉₀anti-CD3sFv fusion protein. The presence of anti-CD3sFv ligand reduced toxicity since DT₃₉₀anti-CD3sFv was twice as toxic to severe combined immunodeficiency disease (scid) mice which do not have CD3epsilon expressing T cells as compared to their normal counterparts. Together, these findings further our understanding of the toxicities limiting the *in vivo* administration of DT fusion immunotoxins in mice and provide a foundation for future genetic modifications which should be directed at reducing these effects.

Keywords: fusion protein/immunotoxin/diphtheria toxin/graft-versus-host-disease/toxicity

Introduction

Immunotoxins (IT) may be important agents for controlling graft-versus-host disease (GVHD), a major problem in bone marrow (BM) transplantation since (i) successful therapy of ongoing GVHD will require a highly potent and selective killing signal to eliminate the expanding allogeneic donor T cells that attack MHC-disparate BM recipients (reviewed in Vallera, 1996), (ii) IT are made by linking monoclonal antibodies to catalytic toxins such as diphtheria toxin (DT) (reviewed in Murphy and Vanderspek, 1995) which have first order kinetics and a single molecule in the cytosol is sufficient for killing (Yamaizumi *et al.*, 1978), and (iii) unlike immunoconjugates made with radionuclides or most drugs, IT killing is directed at the cellular protein synthesis machinery and thus will kill dividing and non-dividing cells.

There has been considerable success in the past decade in synthesizing high affinity recombinant IT that even in nano-

gram quantities can selectively destroy target cells *in vitro* and can even demonstrate curative potential in difficult *in vivo* models (reviewed in Frankel, 1992). Numerous laboratories are exploring the potential of this new class of recombinant agent. It is now important to extend our knowledge of genetically engineered IT since they have the advantage of (i) increased homogeneity, since they can be produced as single chain proteins, (ii) stability, since they require no chemical linking agents, and (iii) small size, since they require only the single chain Fv, the smallest unit (about 20 kDa) of antibody that will still recognize antigen consisting of a single variable heavy (V_H) and variable light (V_L) domain. Thus, we made DT₃₉₀anti-CD3sFv by splicing the cDNA encoding the sFv region of anti-mouse CD3epsilon from the hamster hybridoma 145-C211 (Vallera *et al.*, 1996) to cDNA of truncated diphtheria toxin (DT₃₉₀). Our previous studies indicated that anti-CD3 IT was an excellent choice for an anti-GVHD IT protecting recipients long-term from GVHD (Vallera *et al.*, 1995). DT was chosen because it lends itself well to rational drug design, expression and clinical use (Frankel, 1992; Vallera *et al.*, 1995). DT was preferred over ricin toxin A chain for these studies because in our hands it has proven more suitable for genetic manipulation studies.

Intact DT contains two fragments, A and B. The A fragment catalyzes the ADP-ribosylation of elongation factor 2 (EF-2) leading to protein synthesis inhibition and cell death (Collier, 1975; Honjo *et al.*, 1968). Although a single molecule of DTA in the cytosol can be fatal to a cell, fragment A alone applied extracellularly theoretically is not highly toxic because the binding domain is located in fragment B. The rationale design of DT₃₉₀anti-CD3sFv was intended to reduce nonspecific toxic effects *in vivo* since the domain capable of binding the ubiquitous cell surface DT receptor was deleted and replaced with the anti-CD3sFv binding moiety. DT₃₉₀anti-CD3sFv fusion toxin showed potential as an anti-GVHD agent (Vallera *et al.*, 1995). However despite our genetic alterations, the administration of DT₃₉₀anti-CD3sFv and every other reported DT fusion toxin (including those used clinically) has been limited by toxicity. Since little is known regarding their toxicity and no single organ has been identified in limiting the dose of DT IT, we chose to study DT₃₉₀anti-CD3sFv as a paradigm for this class of agents to establish a clearer understanding of its toxicity and therapeutic window in an *in vivo* model. We found that renal toxicity is the dose limiting toxicity for DT₃₉₀anti-CD3sFv in mice.

Materials and methods

Recombinant DT₃₉₀anti-CD3sFv

Recombinant DT₃₉₀anti-CD3sFv was synthesized as previously described (Vallera *et al.*, 1996). Briefly, the hybrid gene encoding the DT₃₉₀-sFv145-2C11 was constructed by the method of gene splicing by overlap extension (SOE). The gene was digested with restriction enzymes and ligated into cloning sites in the pDT390 plasmid. Restriction endonuclease digestion

Table I. Determining the maximal tolerated dose of DT₃₉₀anti-CD3sFv in normal C57BL/6 mice

	Daily dosage (μg)				
	0	5	10	20	40
Experiment 1	ND	4/4	4/4	0/4	ND
Experiment 2	6/6	6/6	5/6	0/6	0/6
Experiment 3	5/5	5/5	5/5	0/5	ND
Pooled Data	11/11	15/15	14/15	0/15*	0/6*

C57BL/6 mice were randomly divided into groups and injected with varying concentrations of DT₃₉₀anti-CD3sFv given BID on days 0–5. Data are expressed as number survivors/number of mice treated on day 10 post-treatment. Mice were observed for at least an additional 40 days with no change in survival.

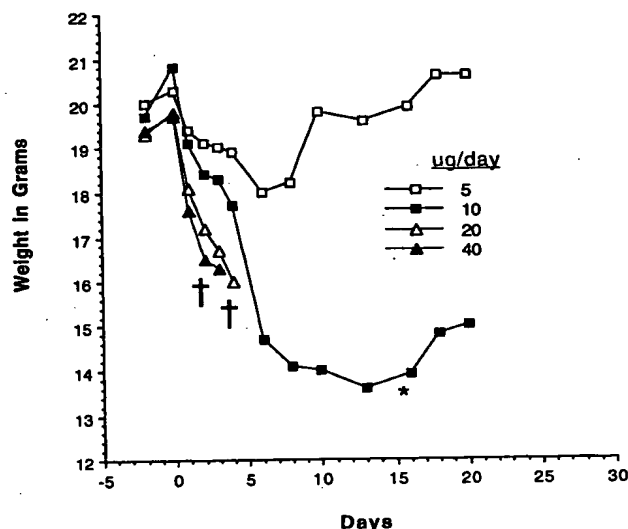


Fig. 1. C57BL/6 mice were divided into groups ($n = 6/\text{group}$) and then injected with varying concentrations of DT₃₉₀anti-CD3sFv given BID on days 0–5. Data are expressed as mean weight (y-axis) calculated at each daily point (x-axis). * $P < 0.001$ for mean animal weights in the 10 μg/day group as compared with the 5 μg/day group on days 10–20. †Mice died in the 20 and 40 μg/day groups.

and DNA sequencing analysis (University of Minnesota Microchemical Facility) were used to verify that DT₃₉₀anti-CD3sFv hybrid gene had been cloned in frame. Plasmid pDTCD3sFv was transformed into the *Escherichia coli* strain BL21(DE3) (Novagen, Madison, WI) and protein expressed. Expressed protein was isolated from inclusion bodies. Solubilization and reduction of the fusion protein was achieved in a buffer containing 7 M guanidine. To ensure proper tertiary structure, renaturation was initiated by a rapid 100-fold dilution of the denatured and reduced protein into refolding buffer. The refolded protein was diluted 10-fold and loaded on a Q-Sepharose (Sigma, St Louis, MO) column and subsequently applied to a Resource Q column (Pharmacia, Uppsala, Sweden). Purity was determined by SDS polyacrylamide gel electrophoresis and HPLC analysis. The integrity of the binding moiety and the toxin moiety was determined in PHA bioassay and ADP ribosylation assays, respectively, which have both been previously reported (Vallera *et al.*, 1996). For these experiments DT₃₉₀anti-CD3sFv met a minimal standard in bioassay which was an IC₅₀ (dose inhibiting 50% of PHA-

activated lymphocytes) of 1–5 nM/l. Uncoupled anti-CD3 mAb blocked activity. Also, cell free ADP ribosylation assays were performed and DT₃₉₀anti-CD3sFv was at least as toxic as native DT. Purity by SDS-PAGE was 95%.

A DT₃₉₀ gene was also constructed with the aim of producing a control fusion toxin which did not bind the T cell receptor. Protein was expressed, refolded and purified as described above.

Mice

C57BL/6 and C57BL/6-scid/scid (both H2b) mice were purchased from the National Institutes of Health (Bethesda, MD). Mice were 8–10 weeks of age.

Fusion toxin administration

Fusion toxin was given intraperitoneally (ip) in a 0.2 ml volume in the morning and then again 6–8 h later. Doses are total daily doses administered twice daily (BID) for six consecutive days.

Pathologic examination of tissues

Mice were sacrificed, autopsied and tissues were taken for histopathologic analysis as described (Vallera *et al.*, 1996). All samples were imbedded in OCT compound (Miles, Elkhart, IN), snap frozen in liquid nitrogen and stored at -80°C until sectioned. Serial 4 μm sections were cut, thaw mounted onto glass slides and fixed for 5 min in acetone. Slides were stained with hematoxylin and eosin (H & E) for histopathologic assessment. Organs were scored positive for GVHD if there was single cell necrosis with mononuclear cell infiltrate (skin, colon), crypt dropout (colon), peri-portal infiltrate with acute necrosis (liver) or endothelialitis with a lymphocytic infiltrate (lung).

Immunohistochemistry

Frozen tissues (kidney and liver) were stained for cell surface antigen determinants. After blocking with normal horse serum, sections were incubated with biotinylated mAbs specific for (i) Mac-1, recognizing macrophages and neutrophils from clone M1/70 (PharMingen, San Diego, CA), (ii) Gr-1 recognizing mostly granulocytes from clone RB6-8C5 (PharMingen), and (iii) F4/80 recognizing macrophages (generously provided by Dr Siamon Gordon, University of Oxford, Oxford, UK). Detection with peroxidase-conjugated avidin-biotin complex and DAB as chromogen was performed essentially as described (Blazar *et al.*, 1995) with reagents purchased from Vector Laboratories, Inc. (Burlingame, CA).

Blood urea nitrogen (BUN), creatinine and alanine transferase (ALT) assays

All three assays were performed on Kodak EKTACHEM clinical chemistry slides on a Kodak ETACHEM 950 by the Fairview University Medical Center-University Campus (Minneapolis, MN). Mice were sacrificed, individual serum samples collected and analysis was performed blindly on the undiluted samples. Minimum specimen volume was 11 μl for each assay. The BUN assay is read spectrophotometrically at 670 nm. The creatinine assay is read at 670 nm. In the ALT assay, the oxidation of NADH is used to measure ALT activity at 340 nm.

Statistical analyses

Groupwise comparisons of continuous data were made by Student's *t*-test. Survival data were analyzed by Mantel-Peto-Cox summary of chi square (Mantel, 1966). Probability (*P*) values less than 0.05 were considered significant.

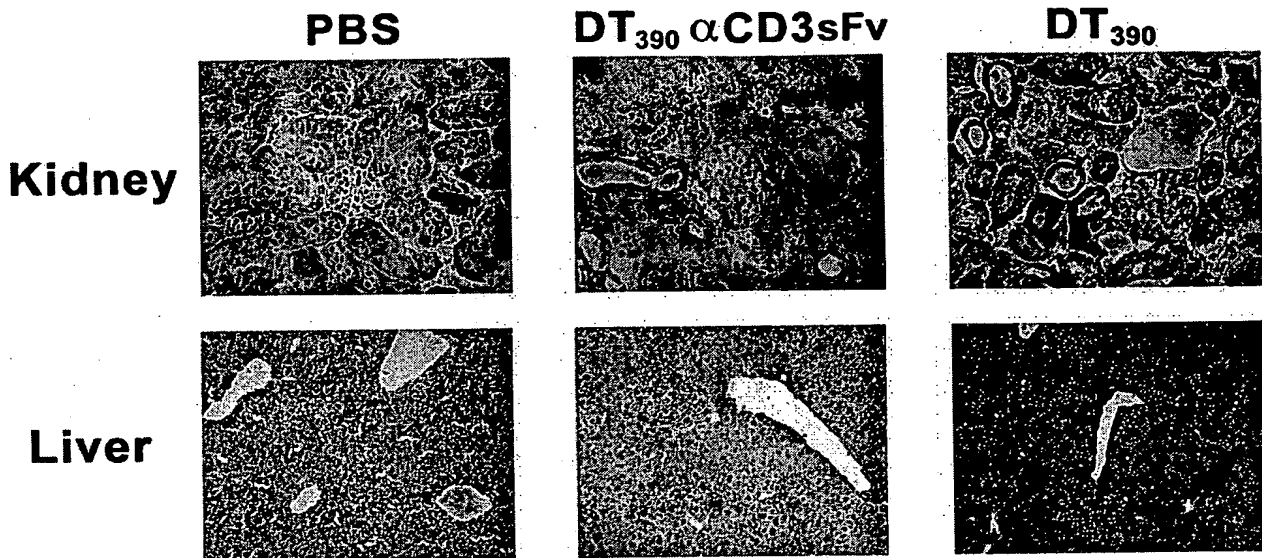


Fig. 2. C57BL/6 were randomly grouped and injected with DT₃₉₀anti-CD3sFv, DT₃₉₀, or PBS. BID over a course of 4 days. Kidney and liver were removed, sectioned and stained with H & E to visualize organ damage. Two animals/group were examined with identical results.

Results

Determination of the maximum tolerated dose (MTD) of DT₃₉₀anti-CD3sFv

To determine the MTD, DT₃₉₀anti-CD3sFv was injected into mice over a 6 day course BID. A dose of 2 µg/day BID over a 6 day interval was previously shown to induce a significant anti-GVHD effect (Vallera *et al.*, 1996). In three replicate experiments, the MTD was reproducibly found to be 10 µg/day (Table I). Pooled data showed that only 1 of 15 mice died at this dosage. In all three experiments, survivors were monitored for an additional 40 days with no signs of delayed toxic effects. In contrast, when the dose was increased to 20 or 40 µg/day all mice died in each of the three independent experiments. There was a significant ($P < 0.001$) difference between groups given 0–10 µg/day and 20–40 µg/day. These data show that 10 µg/day DT₃₉₀anti-CD3sFv BID over six days is the MTD as determined by survival, but that some toxicity reflected in weight loss is experienced at this dose.

Although survival was not significantly diminished at the 10 µg/day dose, a significant drop in mean body weight (Figure 1) was observed on days 3 through 22 (comparing post-injection weight values to pre-injection weight values). These differences were no longer significant after day 24 and mice entirely recovered to their pre-injection weight by day 40. Mice given 5 µg/day fusion toxin lost 2 grams over the course of injection, but regained it all by day 11. These losses were not statistically significant.

Organ toxicity

To determine the toxicity of DT₃₉₀anti-CD3sFv to liver and kidney, fusion protein was injected into mice. Mice were sacrificed and visually examined for tissue effects and functional assays in the form of sera analyses were performed. Figure 2 shows H & E stained sections from mice given 10 µg/day and then sacrificed on day 5 after the course was completed. Effects included partial, but not complete destruction of the glomeruli. Proximal tubular vacuolization and mononuclear cell and neutrophil infiltration in the distal tubular areas and

in the areas surrounding the glomeruli were observed. The level of damage in the kidney exceeded the level of damage in the liver at this dose level since the only hepatic pathologic changes observed were minimal endothelialitis. Higher doses resulted in even greater damage in the kidney including tubular rhexis and extensive neutrophil infiltration. Still, there was only minor fatty degeneration in the liver. The observed damage was not attributed to anti-CD3sFv since damage was also observed in mice given DT₃₉₀ alone. In mice given DT₃₉₀anti-CD3sFv, other tissues were examined at the MTD with no histological evidence or minimal evidence of damage. Brain and heart tissue were unaffected. There was some minimal mononuclear cell infiltration in pancreas, lung and small intestine. As would be expected, thymus (analyzed as a control) was mostly leukopenic with indications of apoptotic and dying cells. The T cell zones in the white pulp of the spleen were depleted with expansion of the red pulp.

To determine whether histologic observation had functional significance, a separate group of mice were treated identically to those in Figure 2 and serum was analyzed for levels of creatine and BUN as indicators of renal function and ALT activity as an indicator of hepatic function. Figure 3 shows that when groups of mice were treated with increasing concentrations of fusion protein, a significant ($P < 0.04$) increase in BUN and creatinine was observed at the 10 µg/day MTD as compared with groups given 0 or 1 µg/day dosages. This was not the case when hepatic activity was monitored with ALT. Together, both histologic and functional data indicate that toxic damage by DT₃₉₀anti-CD3sFv is most pronounced in the kidneys.

These findings were also supported by biodistribution studies in which normal C57BL/6 mice were injected i.v. with 10 µCi ¹²⁵I-labeled DT₃₉₀anti-CD3sFv using a previously described procedure (Vallera *et al.*, 1996). After 23 h, the highest percentage (percent injected dose/gram tissue = 0.93) was measured in kidney. In other organs, 0.37, 0.13 and 0.14% injected dose/gram tissue was distributed to blood, lung and liver, respectively.

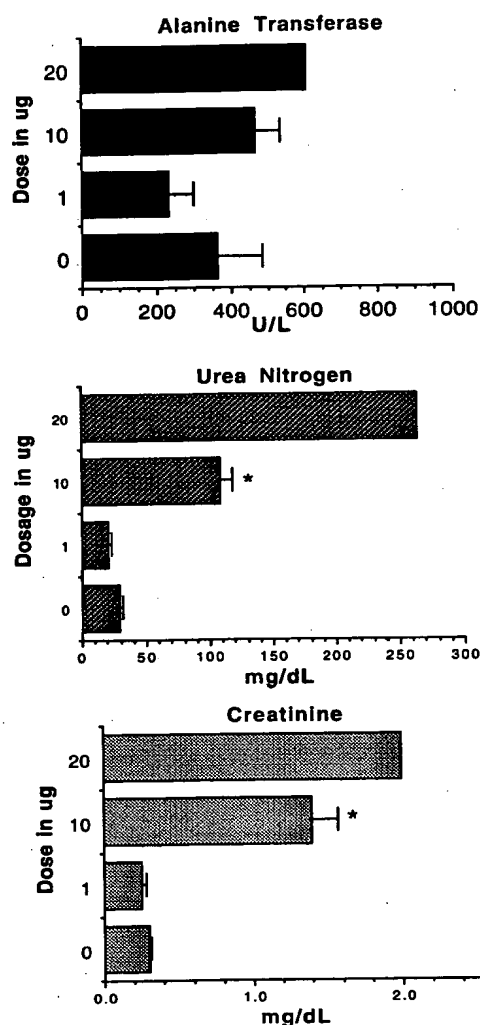


Fig. 3. C57BL/6 mice were randomly grouped ($n = 5$) and injected with differing concentrations of DT₃₉₀anti-CD3sFv BID on days 0–4. On day 5 mice were bled and individual serum samples were studied for creatinine, BUN and ALT levels. Data was averaged. Only one mouse survived for analysis in 20 µg/day group (probably because the dose was in excess of the MTD) so statistics were not performed on that group. * $P < 0.001$ when compared with the untreated control group.

The role of the anti-CD3sFv moiety in fusion toxin toxicity

Figure 2 indicated that kidney toxicity occurred when mice were given DT₃₉₀anti-CD3sFv or DT₃₉₀. To study the role of the anti-CD3sFv moiety, mice in the same experiment were given either DT₃₉₀anti-CD3sFv or DT₃₉₀ and survival was measured. Table II shows data presented to reflect the amount of DT₃₉₀ given to mice receiving DT₃₉₀anti-CD3sFv or DT₃₉₀. Fourteen µg/day of DT₃₉₀ in the form of DT₃₉₀anti-CD3sFv was the minimal uniformly lethal dose. Thus, DT₃₉₀anti-CD3sFv was at least fourfold less toxic than DT₃₉₀ which killed all mice at 3.5 µg/day. Additional studies suggested that anti-CD3sFv played a role in reducing the toxicity of DT₃₉₀anti-CD3sFv. Groups of C57BL/6 scid mice ($n = 5$ /group) which do not have CD3 expressing T cells and normal C57BL/6 mice which do were given identical treatments of 5, 10 or 20 µg/day BID DT₃₉₀anti-CD3sFv and survival was compared.

Table II. Comparative effects of DT₃₉₀anti-CD3sFv and DT₃₉₀ on the mortality of C57BL/6 mice

Group	Agent	Daily dose of DT ₃₉₀ anti-CD3sFv or DT ₃₉₀	Total DT in dose	Mortality
1	DT ₃₉₀ anti-CD3sFv	20	14	100
2	DT ₃₉₀ anti-CD3sFv	10	7	0*
3	DT ₃₉₀ anti-CD3sFv	5	3.5	0*
4	DT ₃₉₀	14	14	100
5	DT ₃₉₀	7	7	100
6	DT ₃₉₀	3.5	3.5	100

C57BL/6 mice were randomly divided into groups ($n = 4$, mean weight about 23–25 g) and injected with varying concentrations of DT₃₉₀anti-CD3 or DT₃₉₀ given BID on days 0–5. Percent mortality is reported on day 10. Mice were also observed for an additional 45 days with no change in survival.

* $P < 0.001$ as compared with relevant DT₃₉₀ control by Student *t*-test.

The MTD in scid mice was 5 µg/day, half the MTD measured in normal mice. This difference was not likely due to a variance in the susceptibility of normal and scid C57BL/6 mice to DT₃₉₀. We tested groups ($n = 4$ /group) of normal and scid mice (size and age-matched) by administering a 5 day BID course of 1 µg/day, 0.2 µg/day or 0.1 µg/day DT₃₉₀. There were no significant differences in weight loss or survival in normal compared with scid mice. Together, these data suggest that the anti-CD3sFv moiety reduces the toxicity of DT₃₉₀.

DT₃₉₀anti-CD3sFv administration enhances macrophage levels

Neutrophils play a major role as scavenger cells and might be elevated by toxin-related trauma. Based on a previous observation that Mac-1⁺ cells are elevated in DT₃₉₀anti-CD3sFv-treated mice (Vallera *et al.*, 1996), we examined liver for the presence of these cell populations (Figure 4). Mice were given increasing doses of DT₃₉₀anti-CD3sFv and since MAC-1 stains both macrophages and neutrophils, we used more discriminating immunohistochemical staining for Gr-1 (predominantly a neutrophil stain) and F4/80 (predominantly a macrophage stain). Our data indicate that both macrophages and neutrophils were elevated in mice given a course of 5, 10 (MTD) or 20 µg/day in a dose dependent manner. Similar effects were observed in sectioned and stained kidney samples.

Discussion

In this report, we analyzed the toxicity of a fusion protein, DT₃₉₀anti-CD3sFv that was previously shown to have significant anti-GVHD effects in mice *in vivo*, even in animals receiving bone marrow transplants across the full MHC barrier. The major contribution was the finding that the major rate limiting toxicity of DT₃₉₀anti-CD3sFv in mice was renal. Three sets of data support this observation including histologic detection of severe renal damage, biodistribution data indicating localization of DT₃₉₀anti-CD3sFv to the kidney, and creatine and BUN levels indicating a high level of dysfunction.

Our findings are in agreement with the limited toxicity information that has been reported in the literature. In earlier studies, Kirkman and co-workers (Kirkman *et al.*, 1989) evaluated an IL-2 fusion toxin missing the DT binding domain (consisting of IL-2 and DT486) and reported that toxicity was largely limited to the renal system. In mice treated *i.v.* for 5 days, the MTD was 42 µg/day (1.7 mg/kg). Mild renal tubule

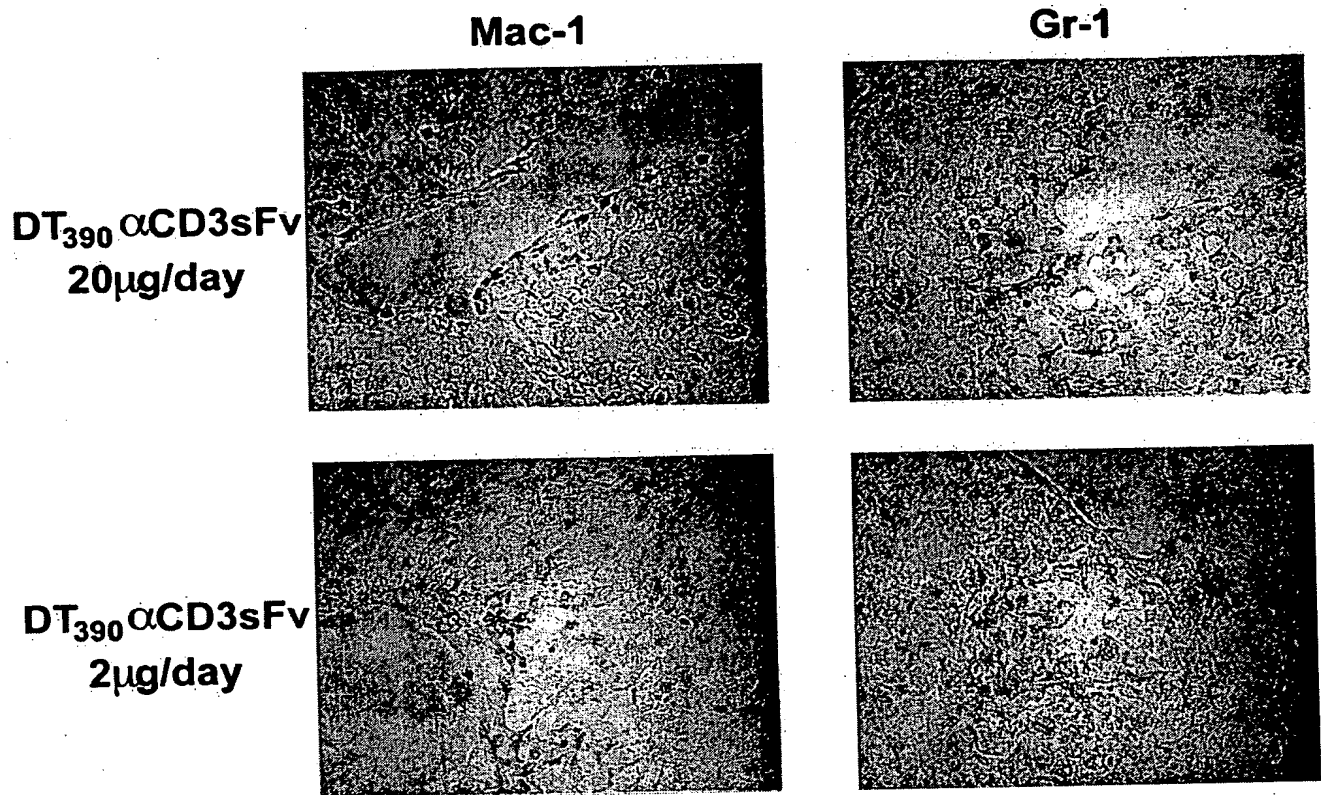


Fig. 4. Sections of liver (objective lens 40×) from a mouse receiving DT₃₉₀anti-CD3sFv. Cryosections were stained by immunoperoxidase using biotinylated monoclonal antibodies for Mac-1 or Gr-1.

epithelial damage associated with significant elevations in BUN and serum creatinine occurred at the next highest dose escalation 3.4 mg/kg at which death occurred in some mice. In a different study (Lakkis *et al.*, 1991), an IL-4 fusion IT consisting of IL-4 and DT389 (similar to our DT₃₉₀) given to mice subcutaneously at a dose of 2, 5 or 10 µg/day for 10 days has a similar MTD to DT₃₉₀anti-CD3sFv (10 µg/day). In mice given 20 µg/day, 2 of 3 mice died and serum chemistry revealed markedly elevated BUN and creatinine. Histopathologic examination of these mice revealed extensive necrosis of proximal renal tubular cells. As in our studies, hepatocytes had vacuolated cytoplasm but very little cellular necrosis was noted. Together with our studies, a pattern of toxicity emerges and at least some conclusions can be drawn. (i) In mice, the limiting toxicity is renal. (ii) Similar non-specific renal effects are observed despite targeting the CD3, IL-2 or IL-4 receptors. (iii) Renal toxicity was rate limiting regardless of whether the construct consisted of DT₃₈₉, DT₃₉₀ or a longer portion of the DT B fragment (DT486). (iv) The therapeutic window of our agent defined by dividing the MTD by the dose which gave an optimal anti-GVHD effect is quite narrow. Our previous study indicated that a dose of 2 µg/day DT₃₉₀anti-CD3sFv achieved efficacy, while the MTD was 10 µg/day.

A unique point of our studies is that the presence of anti-CD3sFv does reduce toxicity. Toxicity was enhanced when the CD3 component of the T cell receptor was absent from our studies using scid hosts. Scids reduced the MTD from 10 to 5 µg/day. These mice, due to deficiency of the enzyme recombinase which is required for T cell receptor gene

rearrangement, are genetically incapable of producing mature T cells (Bosma *et al.*, 1983). Thus, one interpretation of our data is that absence of CD3⁺ T cells permits more DT₃₉₀anti-CD3sFv to localize to the kidney. In these studies, 10 µg/day dosage produced more severe hepatic damage in scids than it did in normal mice. This was not likely due to a difference in susceptibility since our studies showed that normal or scid C57BL/6 mice were similarly effected by the administration of DT₃₉₀ alone. The localization theory is supported by the fact that when administered alone, DT₃₉₀ was at least fourfold more toxic to mice than an identical dose of DT₃₉₀ complexed with anti-CD3sFv in the form of DT₃₉₀anti-CD3sFv.

The toxic effects observed in our studies are also related to DT₃₉₀. In past studies we have shown that CD3 targeting with a divalent antibody containing an Fc region triggers the TCR resulting in life-threatening side effects (Blazar *et al.*, 1991). Activation does not occur with DT₃₉₀anti-CD3sFv since it is not divalent and does not contain an Fc region (Vallera *et al.*, 1996). Thus, there is no contribution of the binding moiety to T cell activation-related toxicity. Fusion toxin treatment resulted in enhanced levels of macrophages and neutrophils. This might be explained by neutrophil presence related to trauma or perhaps elevation of inflammatory cytokines.

The renal toxicity observed in our studies may relate to the filtration of the small 58 kDa DT₃₉₀anti-CD3sFv into the kidney. The kidney plays the major homeostatic role of maintaining the volume and composition of the body fluids largely through glomerular filtration and tubular reabsorption and secretion and small proteins readily enter the kidney.

Also, the renal toxicity observed may be species specific. When the pharmacokinetics of DAB486IL-2 were measured in rats, the primary site of distribution outside of the vasculature was the liver (Bacha *et al.*, 1990). Studies with DT and its various mutants have also indicated that untargeted DT has different effects in different species (Pappenheimer *et al.*, 1982). It has been known since the time of Loeffler (Loeffler, 1884) and Roux and Tersin (Roux and Yersin, 1888) that mice and rats are more resistant to the lethal action of diphtheria toxin than most other species when administered by ordinary routes of injection.

We do have some knowledge related to the mechanism of the non-specific toxicity of truncated DT. There are four hydrophobic domains (residues 269–289, 301–321, 338–358 and 418–439) in the B fragment which are likely to interact with the eukaryotic membrane (Eisenberg *et al.*, 1984). CRM45, a DT mutant (Uchida *et al.*, 1971) lacking 149 carboxy terminal amino acids and the fourth of the four hydrophobic domains, is a protein that is nearly identical to DT₃₉₀. Removal of the 149 amino acids enhances the reactivity of the remaining hydrophobic regions with membranes so that CRM45 (and DT₃₉₀ by analogy) forms channels in artificial lipid bilayers (Kagan *et al.*, 1981) and is readily inserted into membranes (Boquet *et al.*, 1976). It is possible that when a sufficient number of DT₃₉₀ molecules are filtered into the kidney, the toxin becomes concentrated enough to gain cytosol entry, even without the use of the specific DT cell surface receptor. Perhaps these hydrophobic regions should be targets of future mutagenesis studies.

In conclusion, the toxicity that we have observed for DT₃₉₀anti-CD3sFv is mostly renal, but the increased understanding of this toxicity may help in designing future fusion ITs.

Acknowledgements

This work was supported in part by US Public Health Service Grants RO1-CA36725, PO1-CA21737, RO1-AI34495 and PO1-AI35296 awarded by the NCI and the NIAID, DHHS. We wish to thank Dr David Segal and Dr Carolina Jost for providing plasmid containing the cDNA of sFv145-2C11.

References

- Bacha, P. and Reichlin, S. (1986) *Proc. Soc. Exp. Med.*, **18**, 131–138.
- Bacha, P., Forte, S., Kassam, N., Thomas, J., Akiyoshi, D., Waters, C., Nichols, J. and Rosenblum, M. (1990) *Cancer Chemother. Pharmacol.*, **26**, 409–414.
- Blazar, B.R., Hirsch, R., Gress, R.E., Carroll, S.F. and Vallera, D.A. (1991) *J. Immunol.*, **147**, 1492–1503.
- Blazar, B.R., Taylor, P.A., Panoskalsis-Mortari, A., Gray, G.S. and Vallera, D.A. (1995) *Blood*, **85**, 2607–2618.
- Boquet, P., Silverman, M.S., Pappenheimer, A.M., Jr. and Vernon, W.B. (1976) *Proc. Natl Acad. Sci. USA*, **73**, 4449–4453.
- Bosma, G.C., Custer, R.P. and Bosma, M.J. (1983) *Nature*, **301**, 527–530.
- Collier, R.J. (1975) *Bact. Rev.*, **39**, 54–85.
- Eisenberg, D., Schwarz, E., Komaromy, M. and Wall, R. (1984) *Mol. Biol.*, **179**, 125–142.
- Frankel, A. (ed.) (1992) *Genetically Engineered Toxins*. Marcel Dekker, Inc., p. 342.
- Honjo, J., Nishizuka, Y., Hataishi, O. and Kato, I. (1968) *J. Biol. Chem.*, **243**, 245–250.
- Kagan, B.L., Finkelstein, A. and Colombini, M. (1981) *Proc. Natl Acad. Sci. USA*, **78**, 4950–4954.
- Kirkman, R.L., Bacha, P., Barrett, L.V., Forte, S., Murphy, J.R. and Strom, T.B. (1989) *Transplantation*, **47**, 327–330.
- Lakkis, F., Steele, A., Pacheco-Silva, A., Rubin-Kelley, V., Strom, T.B. and Murphy, J.R. (1991) *Eur. J. Immunol.*, **21**, 2253–2258.
- Loeffler, F. (1884) *Mitteilung Gesundheitsamte*, **2**, 421–499.
- Mantel, N. (1966) *Cancer Chemother.*, **50**, 163–170.
- Murphy, J.R. and Vanderspek, J.C. (1995) *Cancer Biol.*, **6**, 259–267.
- Pappenheimer, A.M., Harper, A.A., Moynihan, M. and Brookes, J. (1982) *J. Infect. Dis.*, **145**, 94–102.
- Roux, E. and Yersin, D. (1888) *Annales l'Institut Pasteur*, **2**, 629–661.
- Uchida, T., Gill, D.M. and Pappenheimer, A.M., Jr. (1971) *Nature*, **233**, 8–11.
- Vallera, D.A., Taylor, P.A., Panoskalsis-Mortari, A. and Blazar, B.R. (1995) *Blood*, **86**, 4367–4375.
- Vallera, D.A. (1996) *Cancer Biol.*, **7**, 57–64.
- Vallera, D.A., Panoskalsis-Mortari, A., Yost, C., Ramakrishnan, S., Eide, C.R., Kreitman, R., Nicholls, P.J., Pennell, C. and Blazar, B.R. (1996) *Blood*, **88**, 2342–2353.
- Yamaizumi, M., Mekada, M., Uchida, T. and Okada, Y. (1978) *Cell*, **15**, 245–250.

Received March 11, 1997; revised June 30, 1997; accepted July 7, 1997

Advances in Brief

Human Glioma Cells Overexpress Receptors for Interleukin 13 and Are Extremely Sensitive to a Novel Chimeric Protein Composed of Interleukin 13 and *Pseudomonas* Exotoxin¹

Waldemar Debinski,² Nicholas I. Obiri,
Stephen K. Powers, Ira Pastan,
and Raj K. Puri

The Milton S. Hershey Medical Center, The Pennsylvania State University College of Medicine, Department of Surgery, Division of Neurosurgery, Hershey, Pennsylvania 17033 [W. D., S. K. P.]; Laboratory of Molecular Tumor Biology, Division of Cellular and Gene Therapies, Center for Biologics Evaluation and Research, FDA, Bethesda, Maryland 20895 [N. I. O., R. K. P.]; and Laboratory of Molecular Biology, Division of Cancer Biology Diagnosis and Centers, National Cancer Institute, NIH, Bethesda, Maryland 20892-4255 [I. P.]

Abstract

Recently, we have demonstrated that a spectrum of human adenocarcinoma cell lines express binding sites for interleukin 13 (IL-13). These cells are killed by a chimeric protein composed of human (h) IL-13 and a derivative of *Pseudomonas* exotoxin, PE38QQR (Debinski *et al.*, *J. Biol. Chem.*, 270: 16775-16780, 1995). The cell killing was hIL-13- and hIL-4-specific, indicating that a common binding site for the two cytokines is present in several solid tumor cell lines. Herein, we report that an array of established glioma cell lines is killed by very low concentrations of hIL-13-PE38QQR, often reaching <1 ng/ml (<20 pM). Glioma cells express up to 30,000 molecules of IL-13 receptor/cell which has intermediate affinity toward hIL-13. hIL-13-PE38QQR is more active (up to 3 logs difference in cytotoxic activities) than are the corresponding chimeric toxins containing hIL-4 or hIL-6. The cytotoxic action of hIL-13-PE38QQR is blocked by an excess of hIL-13 on all cell lines studied, and it is not neutralized by hIL-4 on some of these cells. Our results show that human brain cancers richly express receptors for IL-13. Furthermore, the interaction detected previously between receptors for IL-13 and IL-4 on solid tumors cell lines is of a qualitatively different character in U-251 MG and U-373 MG glioma cells. The receptor for IL-13 may represent a new marker of brain cancers and an attractive target for anticancer therapies.

Introduction

The outcome for patients with malignant brain tumors is bleak even when the best available radiation therapy, surgery, and chemotherapy are used (1). An extensive effort to implement specific and effective modalities of treatment includes the search for brain tumor-specific or brain tumor-associated targets. Such targets could be used in designing nonchemotherapeutic cancer treatment strategies. Chimeric toxins represent a promising approach in the treatment of brain tumors (2-4).

Chimeric toxins are composed of a targeting ligand, such as a growth factor, and a genetically engineered bacterial toxin moiety, such as the PE³ molecule (2). PE is a three-domain protein (2, 5, 6; Fig. 1A). Domain Ia of PE binds to α_2 -macroglobulin receptor (7), domain II is cleaved by furin (8, 9) and then catalyzes the translocation of the toxin into the cytosol, and domain III contains the ADP-ribosylation activity that inactivates elongation factor 2 and leads to cell death (10). To kill a cell, PE must be proteolyzed by furin to produce a *M*_r 37,000 COOH-terminal fragment composed of all of domain III and portion of domain II (2). This *M*_r 37,000 fragment penetrates the cytosol (11). On the basis of the known structure-function relationship of PE, several mutated versions of the toxin have been used to make chimeric toxins (2). One of these is PE38QQR, which is deprived of domain Ia and a portion of domain Ib and does not have a single lysine residue in its entire sequence (12).

To date, receptors for several growth factors have been identified to be distinctively overexpressed on brain tumors versus normal brain tissue. For example, EGFRs are detected in a relatively large number of human brain cancers (13-17). The ligands to this receptor, in the form of a mAb or a naturally occurring transforming growth factor α , have been used to target brain tumors with toxins or isotopes. Both preclinical and clinical studies have provided promising results (3, 4, 18, 19). The IGFs and FGFRs are also present on brain tumors (20-22). However, as judged by the limited responsiveness of brain malignant cells to a chimeric toxin containing either IGF or FGF and PE, the numbers of IGFs and FGFRs are low, or they do not internalize well on brain tumor cells (3). This may render IGFs and FGFRs more suitable for differentiation-oriented therapies than for targeting toxins, drugs, or isotopes to them.

Recently, we have demonstrated that a fusion protein composed of hIL-13 and a derivative of PE, PE38QQR, is cytotoxic to a spectrum of human adenocarcinoma cell lines (23). The

Received 7/13/95; revised 8/31/95; accepted 9/1/95.

¹ This work was supported in part by a grant from Children's Miracle Network to W. D. Presented in part at the International Conference on Gene Therapy for CNS Disorders, Philadelphia, PA, June 8-10, 1995.

² To whom requests for reprints should be addressed, at Milton S. Hershey Medical Center, Pennsylvania State University College of Medicine, Department of Surgery, Division of Neurosurgery, BRB-C3844, Hershey, PA 17033. Phone: (717) 531-4541; Fax: (717) 531-3858. E-mail: debinski@debin.nsr.hmc.psu.edu

³ The abbreviations used are: PE, *Pseudomonas* exotoxin; aa, amino acid; CT, chimeric toxin; EGF, epidermal growth factor; FGF, fibroblast growth factor; h, human; r, recombinant; R, receptor; IL, interleukin; IC₅₀, 50% inhibitory concentration; IGF, insulin-like growth factor; TGF, transforming growth factor; mAb, monoclonal antibody.

cytotoxic effect of hIL-13-PE38QQR is hIL-13- and hIL-4-specific because of the many similarities between the two cytokines (23, 24). Furthermore, brain tumors have been shown previously to express hIL-4-binding sites and to be sensitive to the cytotoxic action of an hIL-4-based chimeric fusion protein, hIL-4-PE4E (25, 26). For these reasons, it was of interest to test the cytotoxic activity of hIL-13-PE38QQR on human brain tumor cell lines.

Materials and Methods

Materials. Restriction endonucleases and DNA ligase were obtained from New England Biolabs (Beverly, MA), BRL (Gaithersburg, MD), and Boehringer Mannheim (Indianapolis, IN). [^3H]leucine and [^{125}I] were purchased from Amersham Corp. (Arlington Heights, IL). Fast protein liquid chromatography columns and media were purchased from Pharmacia (Piscataway, NJ). Oligonucleotide primers were synthesized at Pharmacia's Gene Assembler (Research Centre, Hotel-Dieu Hospital, Montreal, Quebec, Canada). The PCR kit was from Perkin Elmer/Cetus (Norwalk, CT). hIL-4 and hIL-13 were made by W. D. (23).

Plasmids, Bacterial Strains, and Cell Lines. Plasmid huIL-13-Tx, which encodes hIL-13-PE38QQR (23), and plasmid pWDMH4-38QQR (27), which encodes hIL-4-PE38QQR recombinant protein, both carry a T7 bacteriophage late promoter, a T7 transcription terminator at the end of the open-reading frame of the protein, an f1 origin of replication, and a gene for ampicillin resistance (28, 29).

Recombinant proteins were expressed in *Escherichia coli* BL21 (ΔDE3) under the control of the T7 late promoter (28). Plasmids were amplified in *E. coli* (HB101 or DH5- α high-efficiency transformation; BRL), and DNA was extracted by using Qiagen kits (Chatsworth, CA).

Construction of a Plasmid Encoding hIL-13-PE38QQR. The chimeric gene encoding hIL-13 fused to PE38QQR (plasmid huIL-13-Tx) was constructed by amplifying hIL-13 using the PCR protocol, as described previously (23). Several plasmids used in this study were sequenced by using the dideoxynucleosides termination method with the United States Biochemical (Cleveland, OH) Sequenase Ver. 2.0 kit.

Expression and Purification of Recombinant Proteins. *E. coli* BL21 (ΔDE3) cells were transformed with plasmids of interest, cultured in 1.0 liter of super broth with 100 μg ampicillin, 4 g glucose, and 0.4 g MgSO_4 /1.0 liter culture. The cells were grown up to $A_{600} = 1.0$ –2.5 and induced with isopropyl- β -D-thiogalactoside for 90 min. The separation of different cellular fractions was performed as described previously (23, 25, 30), and hIL-13-PE38QQR and hIL-4-PE38QQR, as well as hIL-4 and hIL-13, were localized to the inclusion bodies. The procedure for isolation of the chimeric proteins from the inclusion bodies also was described previously (25). The proteins were dissolved in 6 M guanidine solution, and renaturation was carried out in a dithioerythritol and oxidized glutathione reduction-oxidation mixture. After dialysis against 20 mM Tris-HCl (pH 7.4)-5 mM EDTA, the monomer of hIL-13-PE38QQR was first purified by chromatography on a Q-Sepharose Fast Flow column (HR 16/10). The renatured protein was eluted from Q-Sepharose with NaCl, and early fractions contained a pre-

dominantly monomeric form of the chimeric proteins. Additional purification was carried out on a size-exclusion chromatography column (Sephacryl S-200, HR 16/50).

Protein Synthesis Inhibition Assay. The cytotoxic activity of CTs was tested on brain tumor cell lines. This group of cells is represented by human gliomas and includes U-373 MG, DBTRG-05 MG, A-172, Hs 683, U-251 MG, T-98G, SNB-19, and SW-1088, as well as one human neuroblastoma SK-N-MC cell line. Most cell lines were obtained from American Type Culture Collection (Rockville, MD), and they were maintained under conditions recommended by the supplier. The SNB-19 cell line was obtained from the National Cancer Institute/Fredrick Cancer Research Facility, Division of Cancer Treatment tumor repository. The SW-1088 cell line was a gift from Dr. J. Connor (Pennsylvania State University College of Medicine, Hershey, PA). Both SNB-19 and SW-1088 cell lines are of neuroglial origins.

Usually, 1×10^4 cells/well were plated in a 24-well tissue culture plate in 1 ml of medium, and various concentrations of CTs were diluted in 0.1% BSA-PBS, and 25 μl of each dilution was added to 1 ml of cell culture medium. After 20-h incubation with CTs, [^3H]leucine was added to the cells for 3–5 h, and the cell-associated radioactivity was measured using a beta counter. For blocking studies, (a) rhIL-13 or (b) rhIL-4 was added to cells for 20 to 30 min before the addition of CTs. Data were obtained from the average of duplicates, and the assays were repeated several times.

Competitive Binding Assay. The rhIL-13 was labeled with [^{125}I] (Amersham) by using the IODO-GEN reagent (Pierce Chemical Co., Rockford, IL) according to the manufacturer's instructions, as described previously (24). The specific activity of the radiolabeled cytokines was estimated to range from 20 to 100 $\mu\text{Ci}/\mu\text{g}$ protein.

For binding experiments, typically 1×10^6 tumor cells were incubated at 4°C for 2 h with [^{125}I]-labeled hIL-13 (100 pM) with or without increasing concentrations (up to 500 nM) of unlabeled cytokine. The data were analyzed with the LIGAND program (31) to determine receptor number and binding affinity.

Results

To construct the CT, the coding region of the hIL-13 gene was fused to a gene encoding a mutated form of PE, PE38QQR (Fig. 1A; Ref. 23). hIL-13-PE38QQR is composed of 474 aa, 360 of which are from PE. The sequence from PE represents aa 253–613 of PE, with the deletion of aa 365–380 and mutations at positions 590, 606, and 613 to two glutamines and arginine (QQR; Ref. 12). The chimeric gene is in a bacterial vector under the control of a bacteriophage T7 late promoter; the protein was expressed in *E. coli* BL21 (ΔDE3), as described previously (23, 25). The final step of hIL-13-PE38QQR purification was carried out on a Sephacryl S-200 HR Pharmacia column. hIL-13-PE38QQR appeared as a single entity, thereby, demonstrating the very high purity of the recombinant protein (23).

hIL-13-PE38QQR Is Very Cytotoxic to Many Human Glioma Cell Lines. Although hIL-13-PE38QQR has been shown to cause cell death in various tumors (23), the sensitivity of brain tumors to this CT has not been examined. Therefore, we tested nine established human brain cancer cell lines to determine whether hIL-13-PE38QQR is cytotoxic to them. These cell

lines were available to us immediately for experimentation. We first examined cancers derived from glial cells. The cancer cells were sensitive to hIL-13-PE38QQR; CT concentrations that caused 50% inhibition in tritiated leucine incorporation (IC_{50}) ranged from <0.1 ng/ml to >300 ng/ml (2 pM–6.0 nM). Three groups of cell lines emerged, according to their responsiveness to the CT. The first group comprised the largest number of cell lines and was killed by hIL-13-PE38QQR at the lowest concentrations; IC_{50} ranging from <0.1 to 0.5 ng/ml (2–10 pM) were recorded (Fig. 1B). U-373 MG, U-251 MG (Figs. 1B, 2, and 3), SNB-19 (IC_{50} = 0.05 ng/ml), and A-172 (IC_{50} = 0.05 ng/ml) glioma cells were killed with these low concentrations of hIL-13 toxin. The second group of glioma cell lines, composed of DBTRG MG and Hs-683 cells, also responded very well to the hIL-13 toxin, and the IC_{50} ranged from 1 to 10 ng/ml (20–200 pM; Fig. 1B). The third group of glioma cell lines, composed of T-98G and SW 1088, had poorer responses; IC_{50} were 300 and >1000 ng/ml, respectively. The only human cancer cell line of neural origin tested, the SK-N-MC neuroblastoma cell line, responded relatively poor to the chimeric toxin.⁴ The cytotoxic action of hIL-13-PE38QQR was specific because it was blocked by a 10- or 100-fold excess of hIL-13 on the studied cells (Fig. 2). These data indicate that most of the human glioma cancer cells examined possess hIL-13-binding sites, and such cells are extremely sensitive to hIL-13-PE38QQR.

Cytotoxic Activities of Other Cytokine-based Chimeric Proteins in Glioma Cells. Next, we compared the cytotoxic action of hIL-13-PE38QQR with that of the CTs containing other ILs, such as hIL-4 or hIL-6. It has been shown previously that some glioma cell lines can be killed by hIL-4-PE4E (26); IC_{50} s exceeded 10 ng/ml. As seen in Fig. 3, hIL-13-PE38QQR was cytotoxic to U-251 MG, U-373 MG, and DBTRG MG cell lines; IC_{50} s were much less than 10 ng/ml. In addition, we tested hIL-4-PE38QQR, a hIL-4-based CT resembling hIL-13-PE38QQR, and found that it killed glioma cell lines, but that it did at concentrations of 1 to almost 3 logs higher than that of the hIL-13-based toxin (Fig. 3). The IC_{50} for hIL-4-PE38QQR were higher than the IC_{50} seen with the hIL-4-PE4E variant of the CT⁴ (25, 26), which is consistent with observations made with other growth factor-based chimeric proteins (32). It is of interest that hIL-6-PE40 also was active on some human glioma cells (shown in Fig. 3), and its activity was similar to or higher than that of the hIL-4 toxin; still, it was less active than was the hIL-13-based chimeric protein. These results clearly show that most of the studied human glioma cell lines are extremely sensitive to hIL-13-PE38QQR. The cytotoxic activity of this chimeric protein is considerably better than that of other IL-based CTs.

rhIL-4 Does Not Neutralize the Cytotoxicity of hIL-13-PE38QQR on Glioma Cells. We have demonstrated previously that the action of hIL-13-PE38QQR on several solid tumor cell lines is hIL-13- and hIL-4-specific (*i.e.*, it can be blocked by these two cytokines but not by IL-2; Ref. 23). However, we also have observed that hIL-4 cannot compete for hIL-13-binding sites (24), and it cannot block the cytotoxic

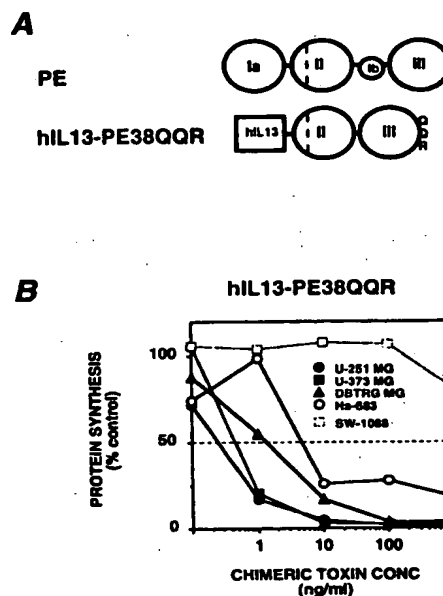


Fig. 1 A, schematic drawing of multidomain proteins: PE and hIL-13-PE38QQR. Circles correspond to the structural domains of PE: domain Ia (aa 1–252) is a binding domain, domain II (aa 253–364) is a place of the proteolytic cleavage by furin (interrupted line), domain Ib has no known function (aa 365–404), and domain III (aa 405–613) is the ADP-ribosylating domain. For PE38QQR: domain Ia and aa 365–380 in Ib are deleted, and the three lysine residues in domain III at positions 590, 606, and 613 are changed to two glutamines and arginine (QQR, Ref. 12). Rectangle, IL-13. B, cytotoxicity of hIL-13-PE38QQR on human glioma cells. Dashed lines, 50% of [3 H]leucine incorporation. CONC, concentration.

action of the hIL-13-based chimeric protein on some other cancer cell lines.⁵ For these reasons, we added hIL-4 to glioma cells and then treated them with hIL-13-PE38QQR. We found that hIL-4 was ineffective in preventing the cytotoxicity of hIL-13-PE38QQR on both U-251 MG and U-373 MG cell lines (Fig. 4). Conversely, hIL-13 did not significantly prevent the cytotoxic activity of hIL-4-PE38QQR.⁴ Therefore, the cytotoxicity of hIL-13-PE38QQR is blocked by an excess of hIL-13 but not hIL-4, and the cytotoxic action of hIL-4-PE38QQR is not blocked by hIL-13.

Human Glioma Cell Lines Express a Number of Receptors for IL-13. It was important to determine whether the human glioma cell lines express detectable binding sites for hIL-13. This supports the notion that the cytotoxic activity of hIL-13-PE38QQR is specific and mediated by hIL-13Rs. To investigate this, we performed competitive binding assays. The iodination of hIL-13 and the binding experiments were carried out as described in "Materials and Methods." Unlabeled hIL-13 competed for the binding of [125 I]-hIL-13 to U-373 MG cells

⁴ W. Debinski, unpublished observations.

⁵ R. K. Puri, unpublished observations.

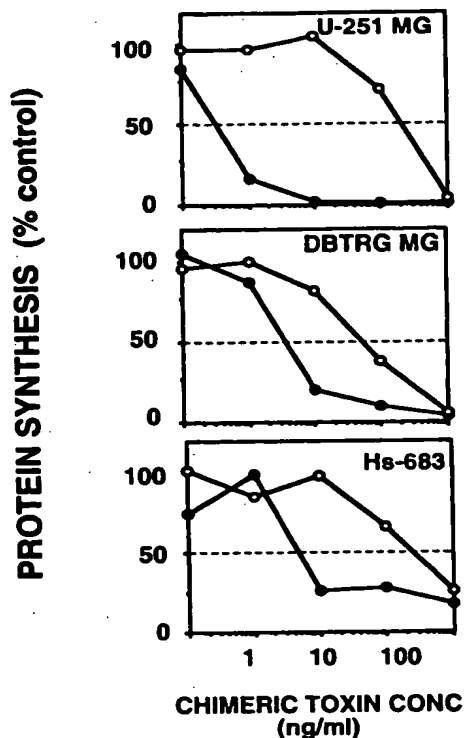


Fig. 2 Inhibition of the cytotoxicity of hIL-13-PE38QQR on glioma cell lines by rhIL-13. rhIL-13 was added at a concentration of 1 μ g/ml. Dashed lines, 50% of [3 H]leucine incorporation. ●, hIL-13-PE38QQR; ○, hIL-13-PE38QQR + rhIL-13.

efficiently (Fig. 5). The Scatchard plot analyses of displacement experiments revealed one single binding site for hIL-13 of intermediate affinity ($K_d = 1.8$ nM; Fig. 5, *inset*). There are approximately 16,000 binding sites for hIL-13 on the U-373 MG cell line. In addition, we evaluated the presence of hIL-13R in other human glioma cell lines (Table 1). As seen in Table 1, the glioma cells had hIL-13Rs ranging from 500 to 30,000 molecules/cell. The hIL-13Rs expressed in human glioma cells are of intermediate affinity; K_d ranged from 1 to 2 nM. It is noteworthy that four of five cell lines studied had very high numbers of hIL-13R (*i.e.*, above 15,000 molecules/cell). The very same cell lines also were the most responsive to the action of hIL-13-PE38QQR (Table 1). The T-98G cell line was poorly responsive to the hIL-13 toxin⁵ and was found to have only approximately 500 hIL-13-binding sites/cell (Table 1). Therefore, specific hIL-13Rs are expressed in glioma cell lines, and they mediate the cytotoxicity of hIL-13-PE38QQR.

Discussion

This study shows, for the first time, that human glioma cell lines express large numbers of the receptor for the newly discovered cytokine IL-13. Furthermore, it is possible to target hIL-13R with a CT composed of IL and a derivative of PE,

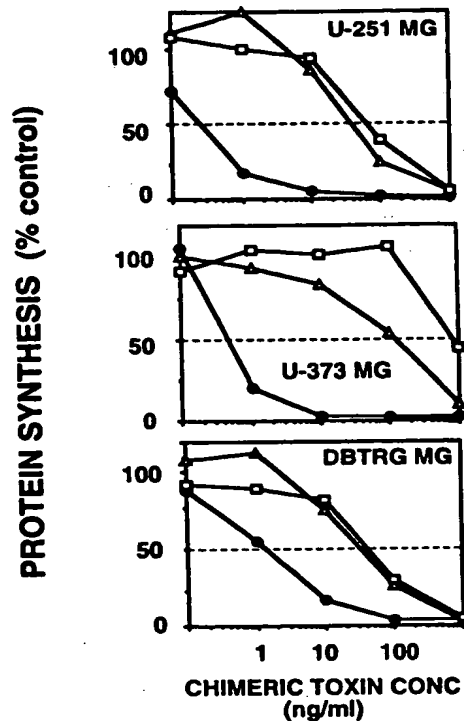


Fig. 3 Inhibition of protein synthesis in different glioma cell lines by hIL-13-PE38QQR (●), hIL-4-PE38QQR (□), and hIL-6-PE40 (Δ). Dashed lines, 50% of [3 H]leucine incorporation.

PE38QQR. The hIL-13-PE38QQR is extremely active on several glioma cell lines, and most of these cell lines are killed by the CT at the concentrations <1 ng/ml (<20 pM). These low concentrations can only be compared with the activity of another chimeric protein, transforming growth factor α -PE, which targets the EGFRs on cancer cells (2, 3).⁴ These findings may have identified a new widely spread marker/target of brain cancers.

The action of hIL-13-PE38QQR on glioma cells is hIL-13 specific because (a) hIL-13 by itself blocks the cytotoxicity of the CT on all of the studied cell lines; and (b) rhIL-4 does not prevent the cytotoxic action of hIL-13-PE38QQR on U-251 MG and U-373 MG glioma cells. The latter observation differs from the one made on adenocarcinomas of the skin, stomach, and colon origins (23). The action of hIL-13-PE38QQR was blocked efficiently by rhIL-4 on these adenocarcinoma cell lines. As documented in our previous reports (23, 24) and suggested by others (33), receptors for IL-4 and IL-13 are complex, and they have some common features detected in various systems, such as normal or malignant human cells. However, the U-251 MG cell line does not bind rhIL-4 in a standard binding assay at 4°C (26), whereas the number of hIL-13-binding sites is high on these cells. This phenomenon most likely explains why rhIL-4 does not block the action of hIL-13-PE38QQR on these cells.

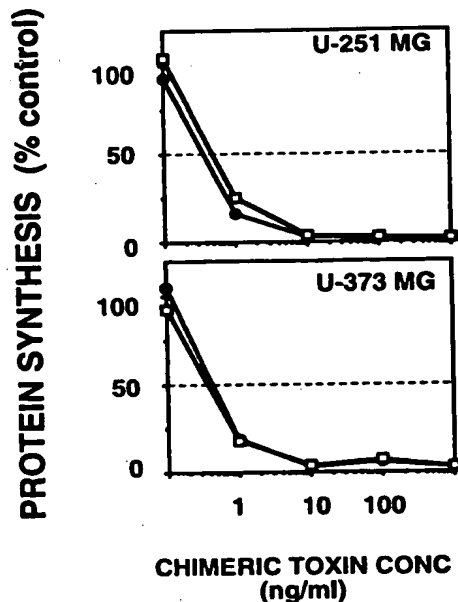


Fig. 4 Blocking the cytotoxicity of hIL-13-PE38QQR by hIL-4. rhIL-4 was added at a concentration of 1.0 μ g/ml. Dashed lines, 50% of [3 H]leucine incorporation. ●, hIL-13-PE38QQR; □, hIL-13-PE38QQR + hIL-4.

Therefore, the hIL-13R and hIL-4R in some glioma cells are different from those found in several solid tumor cell lines. The molecular basis for this observation is under additional investigation. It is important that similar findings were made on some renal cell carcinomas.⁵

hIL-13-PE38QQR is considerably more active on glioma cell lines than is the CT based on hIL-4. The most plausible reason for this difference is the difference in numbers of IL-13 and IL-4 molecules that can be bound by glioma cells. Many human glioma cells bind >15,000 and up to 30,000 molecules of IL-13/cell, whereas these cells bind from <3,000 to very few molecules of IL-4/cell (26). It is of interest that some human glioma cells also can be killed by a CT containing hIL-6 (32). However, the potency of hIL-6-PE40 chimeric protein is lower from that of hIL-13-PE38QQR.

Additional studies are underway to show the potential of hIL-13-based CT for its *in vivo* antitumor effect. Pilot experiments suggest a potent antitumor activity of the chimeric protein.⁴ We already have produced two other forms of a hIL-13-toxin that are almost ten times more cytotoxic than hIL-13-PE38QQR.⁴ These CTs will be used in animal models of human gliomas. We also have begun to screen primary cultures of human gliomas for their expression of IL-13R and responsiveness to the hIL-13-toxins.

In summary, many human glioma cell lines contain large number of IL-13R. The high levels of expression of this receptor make human glioma cells extremely susceptible to the cytotoxicity of hIL-13-PE38QQR chimeric fusion protein. Additional

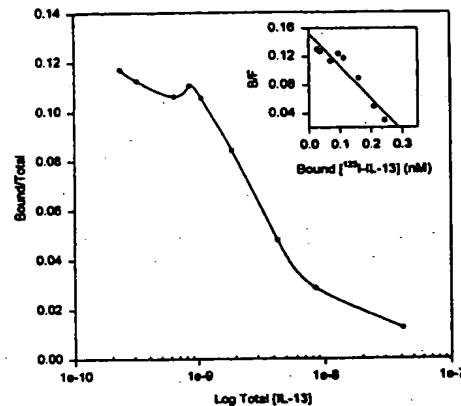


Fig. 5 Competitive binding assay on U-373 MG glioblastoma cells. Data are a percentage of total [125 I]-labeled-hIL-13 binding to cells. Points, mean of two determinations. Similar data were obtained on three other glioma cell lines. B/F, bound-free ratio.

Table 1 hIL13 binding to human glioma cells

Cell line	Binding sites ^a molecules/cell	K_d (nM)	hIL13-PE38QQR IC ₅₀ (ng/ml)
A172	22,600 (15)	1.6	<1
U-251 MG	28,000 (12)	2.1	<1
SNB-19	17,580 (19)	1.4	<1
T-98G	549 (37)	1.0	200
U-373 MG	16,400 (14)	1.8	<1

^a Cells (1×10^6) were incubated with [125 I]-labeled-hIL-13 (100 pM) with or without increasing concentrations (up to 500 nM) of unlabeled hIL-13. Displacement curves and Scatchard analyses were generated from the binding data using the LIGAND program (31). Numbers in parentheses, % coefficient of variation.

studies are underway to evaluate hIL-13R as a possible marker of and therapeutic target for human brain cancers.

Acknowledgments

We thank Robyn Miner and Tony Brown for excellent technical assistance and Pamela Leland for performing binding studies.

References

- Levin, V. A., Sheline, G. H., and Gutin, P. H. Neoplasms of the central nervous system. In: V. T. DeVita, S. A. Rosenberg, and S. Hellman (eds.), *Cancer: Principles and Practice of Oncology*, Ed. 3, pp. 1557-1611. Philadelphia: J. B. Lippincott Co., 1989.
- Pastan, I., Chaudhary, V., and Fitzgerald, D. Recombinant toxins as novel therapeutic agents. *Annu. Rev. Biochem.*, 61: 331-354, 1992.
- Kunwar, S., Pai, L. H., and Pastan, I. Cytotoxicity and antitumor effects of growth factor-toxin fusion proteins on human glioblastoma multiforme cells. *J. Neurosurg.*, 79: 569-576, 1993.
- Phillips, P. C., Levow, C., Catterall, M., Colvin, O. M., Pastan, I., and Brem, H. Transforming growth factor- α -*Pseudomonas* exotoxin fusion protein (TGF- α -PE38) treatment of subcutaneous and intracranial human glioma and medulloblastoma xenografts in athymic mice. *Cancer Res.*, 54: 1008-1015, 1994.

5. Gray, B. L., Smith, D. H., Baldridge, J. S., Harkins, R. N., Vasil, M. L., Chen, E. Y., and Heyneker, H. L. Cloning, nucleotide sequence and expression in *Escherichia coli* of the exotoxin A structural gene of *Pseudomonas aeruginosa*. *Proc. Natl. Acad. Sci. USA*, **81**: 2645-2649, 1984.
6. Allured, V. S., Collier, R. J., Carroll, S. F., and McKay, D. B. Structure of exotoxin A of *Pseudomonas aeruginosa* at 3.0-Ångstrom resolution. *Proc. Natl. Acad. Sci. USA*, **83**: 1320-1324, 1986.
7. Kounnas, M. Z., Morris, R. E., Thompson, M. R., FitzGerald, D. J., Strickland, D. K., and Saelinger, C. B. The α 2-macroglobulin receptor/low density lipoprotein receptor-related protein binds and internalizes *Pseudomonas* exotoxin A. *J. Biol. Chem.*, **267**: 12420-12423, 1992.
8. Moehring, J. M., Inocencio, N. M., Robertson, B. J., and Moehring, T. J. Expression of mouse furin in a Chinese hamster cell resistant to *Pseudomonas* exotoxin A and viruses complements the genetic lesion. *J. Biol. Chem.*, **268**: 2590-2594, 1993.
9. Inocencio, N. M., Moehring, J. M., and Moehring, T. J. Furin activates *Pseudomonas* exotoxin A by specific cleavage *in vivo* and *in vitro*. *J. Biol. Chem.*, **269**: 31831-31835, 1994.
10. Iglewski, B. H., and Kabat, D. NAD-dependent inhibition of protein synthesis by *Pseudomonas aeruginosa* toxin. *Proc. Natl. Acad. Sci. USA*, **72**: 2284-2288, 1975.
11. Ogata, M., Chaudhary, V. K., Pastan, I., and FitzGerald, D. J. Processing of *Pseudomonas* exotoxin by a cellular protease results in the generation of a 37,000-Da toxin fragment that is translocated to the cytosol. *J. Biol. Chem.*, **265**: 20678-20685, 1990.
12. Debinski, W., and Pastan, I. An immunotoxin with increased activity and homogeneity produced by reducing the number of lysine residues in recombinant *Pseudomonas* exotoxin. *Bioconj. Chem.*, **5**: 40-46, 1994.
13. Libermann, T. A., Razon, N., Bartal, A. D., Yarden, Y., Schlessinger, J., and Soreq, H. Expression of epidermal growth factor receptors in human brain tumors. *Cancer Res.*, **44**: 753-760, 1984.
14. Wong, A., Bigner, S. H., Bigner, D. D., Kinzler, K. W., Hamilton, S. R., and Vogelstein, B. Increased expression of the epidermal growth factor receptor gene in malignant gliomas is invariably associated with gene amplification. *Proc. Natl. Acad. Sci. USA*, **84**: 6899-6903, 1987.
15. Harsh, G. R., IV, Rosenblum, M. L., and Williams, L. T. Oncogene-related growth factors and growth factor receptors in human malignant glioma-derived cell lines. *J. Neurooncol.*, **7**: 47-56, 1989.
16. Hall, W. A., Merrill, M. J., Walbridge, S., and Youle, R. J. Epidermal growth factor receptors on ependymomas and other brain tumors. *J. Neurosurg.*, **72**: 641-646, 1990.
17. Mendelsohn, J. The epidermal growth factor receptor as a target for therapy with antireceptor monoclonal antibodies. *Semin. Cancer Biol.*, **1**: 339-344, 1990.
18. Brady, L. W., Miyamoto, C., Woo, D. V., Rackover, M., Emrich, J., Bender, H., Dadgar, S., Stepkowski, Z., Koprowski, H., Black, P., Lazzaro, B., Nair, S., McCormack, T., Nieves, J., Morabito, M., and Eshleman, J. Malignant astrocytomas treated with iodine-125 labeled monoclonal antibody 425 against epidermal growth factor receptor: a phase II trial. *Int. J. Radiat. Oncol. Biol. Phys.*, **22**: 225-230, 1991.
19. Bender, H., Takahashi, H., Adachi, K., Belser, P., Liang, S., Prewett, M., Schrappe, M., Sutter, A., Rodeck, U., and Herlyn, D. Immunotherapy of human glioma xenografts with unlabeled ^{131}I - or ^{125}I -labeled monoclonal antibody 425 to epidermal growth factor receptor. *Cancer Res.*, **52**: 121-126, 1992.
20. Gammeltoft, S., Ballotti, R., Kowalski, A., Westermark, B., and Van Obberghen, E. Expression of two types of receptor for insulin-like growth factors in human malignant glioma. *Cancer Res.*, **48**: 1233-1237, 1988.
21. Morrison, R. S., Gross, J. L., Herblin, W. F., Reilly, T. M., LaSala, P. A., Alterman, R. L., Moskal, J. R., Kornblith, P. L., and Dexter, D. L. Basic fibroblast growth factor-like activity and receptors are expressed in a human glioma cell line. *Cancer Res.*, **50**: 2524-2529, 1990.
22. Morrison, R. S., Yamaguchi, F., Bruner, J. M., Tang, M., McKeehan, W., and Berger, M. S. Fibroblast growth factor receptor gene expression and immunoreactivity are elevated in human glioblastoma multiforme. *Cancer Res.*, **54**: 2794-2799, 1994.
23. Debinski, W., Obiri, N. I., Pastan, I., and Puri, R. K. A novel chimeric protein composed of IL13 and *Pseudomonas* exotoxin is highly cytotoxic to human carcinoma cells expressing receptors for IL13 and IL4. *J. Biol. Chem.*, **270**: 16775-16780, 1995.
24. Obiri, N. I., Debinski, W., Leonard, W. J., and Puri, R. K. Receptor for interleukin 13: Interaction with interleukin 4 by mechanism that does not involve the common γ chain shared by receptors for interleukins 2, 4, 7, 9, and 15. *J. Biol. Chem.*, **270**: 8797-8804, 1995.
25. Debinski, W., Puri, R. K., Kreitman, R. J., and Pastan, I. A wide range of human cancers interleukin 4 (IL4) receptors that can be targeted with chimeric toxin composed of IL4 and *Pseudomonas* exotoxin. *J. Biol. Chem.*, **268**: 14065-14070, 1993.
26. Puri, R. K., Leland, P., Kreitman, R. J., and Pastan, I. Human neurological cancer cells express interleukin-4 (IL-4) receptors which are targets for the toxic effects of IL4-*Pseudomonas* exotoxin chimeric protein. *Int. J. Cancer*, **58**: 574-581, 1994.
27. Debinski, W., Puri, R. K., and Pastan, I. Interleukin-4 receptors expressed on tumors may serve as a target for anticancer therapy using chimeric *Pseudomonas* exotoxin. *Int. J. Cancer*, **58**: 744-748, 1994.
28. Studier, F. W., and Moffat, B. A. Use of bacteriophage T7 RNA polymerase to direct selective high-level expression of cloned genes. *J. Mol. Biol.*, **189**: 113-130, 1986.
29. Debinski, W., Karlsson, B., Lindholm, L., Siegall, C. B., Willingham, M. C., FitzGerald, D., and Pastan, I. Monoclonal antibody C242-*Pseudomonas* exotoxin A: a specific and potent immunotoxin with antitumor activity on a human colon cancer xenograft in nude mice. *J. Clin. Invest.*, **90**: 405-411, 1992.
30. Buchner, B., Pastan, I., and Brinkmann, U. A method for increasing the yield of properly folded recombinant fusion proteins: single-chain immunotoxins from renaturation of bacterial inclusion bodies. *Anal. Biochem.*, **205**: 263-270, 1992.
31. Munson, P. J., and Rodbard, D. LIGAND: a versatile computerized approach for characterization of ligand-binding systems. *Anal. Biochem.*, **107**: 220-239, 1980.
32. Siegall, C. B., Kreitman, R. J., FitzGerald, D. J., and Pastan, I. Antitumor effects of interleukin 6-*Pseudomonas* exotoxin chimeric molecules against the human hepatocellular carcinoma, PLC/PRF/5 in mice. *Cancer Res.*, **51**: 2831-2836, 1991.
33. Zurawski, S. M., Vega, F. J., Huyghe, B., and Zurawski, G. Receptors for interleukin-13 and interleukin-4 are complex and share a novel component that functions in signal transduction. *EMBO J.*, **12**: 2663-2670, 1993.

Characterization of a ricin fusion toxin targeted to the interleukin-2 receptor

Arthur E. Frankel,^{1,4} Chris Burbage,¹ Tao Fu,¹
Edward Tagge,² John Chandler² and Mark Willingham³

Departments of ¹Medicine, ²Surgery and ³Pathology, Medical University of South Carolina, Charleston, SC 29425, USA

⁴To whom correspondence should be addressed

Fusion toxins are hybrid proteins consisting of peptide ligands linked through amide bonds to polypeptide toxins. The ligand directs the molecule to the surface of target cells and the toxin enters the cytosol and induces cell death. Ricin is an excellent candidate for use in fusion toxins because of its extreme potency, the extensive knowledge of its atomic structure and the lack of prior immunological exposure in patients. We synthesized a baculovirus transfer vector with the polyhedrin promoter followed sequentially from the 5' end with DNA encoding the gp67A leader sequence, the tripeptide ADP, IL-2 (interleukin-2), another ADP tripeptide and RTB (ricin toxin B chain) with lectin-site mutations W37S and Y248H. Recombinant baculovirus was generated in Sf9 insect cells and used to infect Sf9 cells. Recombinant IL-2-RTB[W37S/Y248H] protein (fusion protein of IL-2 with modifications W37S and Y248H) was recovered at high yields from day 6 insect cell supernatants, partially purified by affinity chromatography and reassociated with RTA (ricin toxin A chain). The fusion toxin was soluble, immunoreactive with antibodies to RTB, IL-2 and RTA and had a molecular weight of 80 kDa by SDS-PAGE. The molecule reacted poorly with asialofetuin, but bound strongly to IL-2 receptor based on selective cytotoxicity to IL-2 receptor bearing cells. The specific cytotoxicity could be blocked with IL-2 but not lactose. Thus, we report a novel targeted fusion toxin protein with full biological activity.

Keywords: IL-2 fusion toxin/ricin

Introduction

Ricin toxin, the heterodimeric 65 kDa glycoprotein produced in the seeds of *Ricinus communis* plants, is composed of a 33 kDa lectin B chain [ricin toxin B chain (RTB)] disulfide linked to a 32 kDa RNA *N*-glycosidase A chain [ricin toxin A chain (RTA)] (Olsnes *et al.*, 1974). The toxin acts sequentially to bind β -galactosyl pyranoside moieties on cell surface glycoproteins (Baenziger and Fiete, 1979), internalizes by receptor-mediated endocytosis into endosomes (Sandvig and Olsnes, 1982) and undergoes sorting in the Golgi (Youle and Colombatti, 1987) followed by transport to a distal intracellular compartment which may be the endoplasmic reticulum (Wales *et al.*, 1993). Interchain disulfide reduction (Masuho *et al.*, 1982) and unfolding of RTA (Argent *et al.*, 1994) lead to translocation across the membrane bilayer and release of RTA into the cytosol. Once in the cytosol, RTA catalytically depurinates a critical adenine base from 28S ribosomal RNA causing loss of elongation factor binding

to the ribosome and irreversible inactivation of protein synthesis (Endo and Tsurugi, 1987).

Targeted toxins employing ricin have been synthesized and used in clinical trials of lymphoma with moderate clinical activity (Grossbard *et al.*, 1993; Sausville *et al.*, 1995). The normal tissue binding sites on RTB have been removed by either deletion of the entire RTB subunit (Vitetta *et al.*, 1982) or chemically blocking the lectin sites on RTB with an affinity cross-linker (Lambert *et al.*, 1991). The toxic moieties were then chemically conjugated to anti-lymphoma murine monoclonal antibodies. The limited clinical efficacy observed may in part have been due to the large size of the conjugates (200 kDa) reducing capillary permeability, the heterogeneity of the hybrid proteins (the *N*-succinimidyl coupling agent reacts with any lysine on the antibody ligand) and the loss of the intoxication enhancement functions of RTB.

One approach to improving the pharmacologic properties of targeted ricin molecules is to genetically engineer the toxin and ligand into a single small well defined molecule. O'Hare expressed an RTA-diphtheria toxin loop-Staphylococcal protein A chimera in *Escherichia coli* (O'Hare *et al.*, 1990). The protein was enzymatically cleaved with trypsin, mixed with antibody and tested for cytotoxicity to antigen-positive cells. The immunoconjugate was cytotoxic, but the disulfide loop was exposed on the surface of the conjugate and readily reduced. The molecule was large (>200 kDa) and heterogeneous due to varying sites of protein A-immunoglobulin binding. Cook reported the expression of IL-2-diphtheria toxin loop-RTA and IL-2-factor Xa recognition sequence-RTA fusions (Cook *et al.*, 1993). In both cases, the disulfide loop failed to form and proteolysis with trypsin or factor Xa released free ligand and toxin. Uncleaved chimeras showed no toxicity to IL-2 receptor bearing cells. Westby expressed preproricin containing a factor Xa-specific site in the linker sequence in *Xenopus* oocytes (Westby *et al.*, 1992). The product was produced at very low levels and had minimal protease sensitivity and no IL-2 binding specificity.

We have chosen an alternative approach for genetic engineering of ricin. We attached the ligand, IL-2, to the N-terminus of RTB and expressed the protein with a GP67A leader peptide in insect cells (Frankel *et al.*, 1995). Recombinant protein was purified from insect cell supernatants by affinity chromatography and reassociated with RTA. The fusion toxin was obtained in milligram yields and showed selective toxicity to IL-2 receptor bearing cells in the presence of lactose. We have subsequently produced recombinant RTB molecules with deficient lectin-site function (Frankel *et al.*, 1996a,b). Based on this work, we have chosen to link IL-2 to the RTB double lectin-site mutant W37S/Y248H and reassociate the product with RTA. In this paper, we report the expression, purification and characterization of a plant fusion toxin suitable for preclinical and clinical development.

Materials and methods

Materials

Restriction endonucleases, T4 ligase and Wizard DNA purification matrix were obtained from Promega (Madison, WI). [³²P]dCTP, [³⁵S]dATP and [³H]leucine were obtained from Amersham (Arlington Heights, IL). Rabbit anti-ricin antibody, alkaline phosphatase conjugated goat anti-(rabbit IgG), alkaline phosphatase conjugated goat anti-(mouse IgG), asialofetuin, α -lactose and other chemicals were purchased from Sigma (St Louis, MO). EX-CELL400 medium was obtained from JRH Scientific (Lexena, KS). Sf9 insect cells, TMNFH medium, BaculoGold DNA and pAcGP67A transfer vector were supplied by PharMingen (San Diego, CA). Low molecular weight prestained protein standards, nitrocellulose paper and other reagents for protein analysis were obtained from Bio-Rad (Hercules, CA). The Sequenase kit for dideoxy sequencing was obtained from USB (Cleveland, OH). The Random Primer labeling kit was provided by Stratagene (La Jolla, CA). Purified P2, P8 and P10 murine monoclonal antibodies to RTB and purified α BR12 murine monoclonal antibody to RTA were gifts from Dr Walter Blattler (ImmunoGen, Cambridge, MA). Mouse monoclonal antibody and rabbit polyclonal antibody to IL-2 were purchased from Genzyme (Cambridge, MA). RPMI1640 medium, leucine-free RPMI1640, penicillin, streptomycin, Dulbecco's phosphate-buffered saline (PBS), fetal bovine serum and dialyzed fetal bovine serum were obtained from GIBCO BRL (Grand Island, NY). The alkaline phosphatase Vectastain kit for Western blots was obtained from Vector Laboratories (Burlingame, CA). EIA plates, round-bottomed and flat-bottomed 96-well plates were purchased from Costar (Cambridge, MA). Plant RTB, ricin and RTA were obtained from Inland Laboratories (Austin, TX). Human recombinant IL-2 was a gift from Dr Kirsten Kothe (Chiron, Emeryville, CA). HUT102 human leukemia cell line, CEM human leukemia cell line and KB human epidermoid carcinoma cell lines were obtained from the American Type Culture Collection (Rockville, MD). INV α F' *E. coli* cells were obtained from Invitrogen (San Diego, CA). Calf intestinal phosphatase was obtained from Boehringer-Mannheim (Indianapolis, IN).

Construction of plasmid

pAcGP67A-ADP-RTB[W37S/Y248H] plasmid containing a *Bam*HI-*Eco*RI DNA fragment coding for ADP-RTB[W37S/Y248H] as described previously (Frankel *et al.*, 1996) was restricted with *Bam*HI, bound and eluted from a silica matrix, digested with calf intestinal phosphatase, heat inactivated and repurified on a silica matrix. The *Bam*HI fragment encoding IL-2 prepared by PCR of pDW27 plasmid DNA as described previously (Frankel *et al.*, 1995) was isolated from pUC119-IL-2 by digestion of cesium chloride density gradient purified plasmid with *Bam*HI, agarose electrophoresis and binding and elution from a silica matrix. The 406 bp fragment was subcloned into pAcGP67A-ADP-RTB[W37S/Y248H]. The expression vector was maintained in INV α F' *E. coli* using 100 μ g/ml ampicillin. Plasmid isolated by alkaline lysis followed by cesium chloride density gradient centrifugation was double-stranded dideoxy sequenced by the Sanger method (Sanger *et al.*, 1977).

Expression of fusion toxin

Sf9 *Spodoptera frugiperda* ovarian cells (2×10^6) maintained in TMNFH medium supplemented with 10% fetal calf serum and 50 μ g/ml gentamicin sulfate were co-transfected

with pAcGP67A-ADP-IL-2-ADP-RTB[W37S/Y248H] DNA (4 μ g) and 0.5 μ g of BaculoGold AcNPV DNA following the recommendations of the supplier. At 6 days post-transfection, the medium was centrifuged and the supernatant tested in a limiting dilution assay with Sf9 cells and dot blots with random primer [³²P]dCTP-labeled RTB DNA as described previously (Frankel *et al.*, 1994). Positive wells were identified and supernatants reassayed by limiting dilution until all wells up to 10^{-8} dilution were positive. Two rounds of selection were required. Recombinant virus in the supernatant was then amplified by infecting Sf9 cells at a multiplicity of infection (m.o.i.) of 0.1, followed by collection of day 7 supernatants. Recombinant baculovirus was then used to infect 2×10^8 Sf9 cells at an m.o.i. of 5–10 in 150 ml of EX-CELL400 medium with 25 mM α -lactose in spinner flasks. Media supernatants containing ADP-IL-2-ADP-RTB[W37S/Y248H] were collected at day 6 post-infection.

Protein purification

Media supernatants were adjusted to 0.01% sodium azide and maintained through all purification steps at 4°C. The supernatants were concentrated 15-fold by vacuum dialysis, centrifuged at 3000 g for 10 min to remove precipitate, dialyzed against 50 mM NaCl, 25 mM Tris (pH 8), 1 mM EDTA, 0.01% sodium azide and 25 mM α -lactose (NTEAL), ultracentrifuged at 100 000 g for 1 h and bound and eluted from a P2 monoclonal antibody-acrylamide matrix as described previously (Frankel *et al.*, 1994). P2 is an anti-RTB monoclonal antibody. The affinity matrix was prepared using Ultralink azlactone functionality bisacrylamide following the recommendations of the manufacturer. Recombinant protein was absorbed on the column in NTEAL, washed with 50 mM NaCl, 25 mM Tris (pH 8), 1 mM EDTA, 0.1% Tween 20, 0.01% sodium azide, 25 mM α -lactose and eluted with 0.1 M triethylamine hydrochloride (pH 11). The eluate was neutralized with 1/10 volume of 1 M sodium phosphate (pH 4.25) and stored at -20°C until assayed. Four preparations were made.

Characterization of recombinant protein

The total protein concentration of the affinity column eluate was determined by measuring the absorbance at 280 nm. Since the optical densities of a 1 mg/ml solution of RTB and IL-2 were 1.4 and 0.7, respectively, a 1 mg/ml solution of fusion protein should have a mass-average optical density of 1.16. Protein was also quantitated by Bio-Rad protein assay according to the recommendations of the supplier. Aliquots of ADP-IL-2-ADP-RTB[W37S/Y248H], plant RTB and prestained low molecular weight standards were subjected to a reducing 15% SDS-PAGE, stained with Coomassie Blue R-250 and scanned on an IBAS automatic image analysis system (Kontron, Germany).

Immunological analysis was performed using both an ELISA and immunoblot format. Costar EIA microtiter wells were coated with 100 μ l of 5 μ g/ml of monoclonal antibody P2, P8 or P10 reactive with RTB or monoclonal antibody to IL-2, washed with PBS plus 0.1% Tween 20, blocked with 3% BSA, rewashed and incubated with samples of ADP-IL-2-ADP-RTB[W37S/Y248H], human IL-2 or plant RTB, rewashed, reacted with 1:400 rabbit antibody to ricin or 1:500 rabbit antibody to IL-2, washed again, incubated with 1:5000 alkaline phosphatase conjugated goat anti-(rabbit IgG), rewashed, developed with 1 mg/ml *p*-nitrophenylphosphate in diethanolamine buffer (pH 9.6) and read on a Bio-Rad 450 microplate reader at 405 nm.

Aliquots of ADP-IL-2-ADP-RTB[W37S/Y248H], bacterial IL-2, recombinant RTB, plant RTB and prestained low molecular weight protein standards were subjected to a reducing 15% SDS-PAGE, transferred to nitrocellulose, blocked with 10% Carnation non-fat dry milk-0.1% bovine serum albumin (BSA)-0.1% Tween 20, washed with PBS plus 0.05% Tween 20, reacted with either 1:400 rabbit antibody to ricin or 1:100 mouse monoclonal antibody to IL-2 (5 µg/ml), rewashed, incubated with alkaline phosphatase conjugated goat anti-(rabbit IgG) or anti-(mouse IgG), washed again and developed with the Vectastain alkaline phosphatase kit.

Reassociation with RTA

An 18 µg amount of ADP-IL-2-ADP-RTB[W37S/Y248H] was mixed with 54 µg of plant RTA in a total volume of 0.5 ml of 0.1 M triethylamine-0.1 M sodium phosphate (pH 7), shaking overnight at room temperature. The reaction mixture was then analyzed by a modified ricin ELISA described previously (Frankel *et al.*, 1996). Reassociated mixtures were also analyzed by non-reducing SDS-PAGE followed by immunoblots with P2 and P10 anti-RTB monoclonal antibodies (10 µg/ml each), monoclonal antibody to IL-2 (5 µg/ml) or monoclonal antibody αBR12 to RTA (10 µg/ml). Densitometric scanning with the automatic image analysis system was done to quantify the shift of immunoreactive material from 50 to 80 kDa.

Lectin activity of heterodimer

Asialofetuin (1 µg/ml) was bound to Costar EIA plate wells and an ELISA was performed as detailed previously with samples of ADP-IL-2-ADP-RTB[W37S/Y248H]-RTA and castor bean ricin (Frankel *et al.*, 1996). Briefly, the asialofetuin coated wells were washed with PBS plus 0.1% Tween 20, blocked with 3% BSA, rewashed and incubated with 12 different concentrations of samples in EX-CELL400, rewashed and reacted with 100 µl of biotinylated αBR12 monoclonal anti-RTA antibody, rewashed and incubated with streptavidin-alkaline phosphatase, washed again and developed with *p*-nitrophenyl phosphate in 50 mM diethanolamine (pH 9.6). The absorbance of the wells was measured at 405 nm on a microtiter plate reader. The concentration of protein giving half-maximum binding was calculated.

IL-2 receptor binding specificity

HUT102 human T leukemia cells bearing the high-affinity IL-2 receptor, CEM human leukemia cells bearing the intermediate affinity IL-2 receptor and KB human epidermoid carcinoma cells lacking the IL-2 receptor were washed with PBS and attached to polylysine-coated tissue culture dishes and centrifuged at 2000 g for 10 min. The cells were then incubated live at 4°C. The cells were washed with 2 mg/ml BSA in PBS and incubated in PBS plus BSA with 1 µg/ml castor bean ricin or IL-2-lectin-deficient ricin. The incubation was done at 4°C. The cells were then washed with PBS and incubated with αBR12 mouse monoclonal antibody to RTA (5 µg/ml) plus BSA for 30 min at 4°C. The cells were then washed with PBS and reacted with goat anti-(mouse Ig) conjugated to rhodamine (Jackson ImmunoResearch, West Grove, PA) at 25 µg/ml for 30 min at 4°C. The cells were washed again in PBS and fixed in 3.7% formaldehyde in PBS, mounted under a No. 1 coverslip in glycerol-PBS (90:10) and examined using a Zeiss Axioplan epifluorescence microscope.

Cytotoxicity to mammalian cells

Measurement of protein synthesis inhibition by ricin and ADP-IL-2-ADP-RTB[W37S/Y248H]-RTA in cultured cells was

done as described previously using HUT102, CEM and KB cells (Frankel *et al.*, 1995). All assays were performed in triplicate. Twelve different concentrations of toxins were used. The ID_{50} was the concentration of protein which inhibited protein synthesis by 50% compared with control wells without toxin. There was no purification step after heterodimer reassociation. The free RTA concentration at the highest concentration of heterodimer in the assay (5×10^{-7} M) was 10^{-7} M. On all three cell lines, the ID_{50} for free RTA was $2-3 \times 10^{-6}$ M (Tagge *et al.*, 1995). Thus, in the range of heterodimer ID_{50} s (10^{-10} – 10^{-12} M), the free RTA concentration (2×10^{-11} – 2×10^{-13} M) should not produce cytotoxicity.

Blocking of cytotoxicity with IL-2 or lactose

HUT102 cells (1.5×10^4) were placed in sterile Eppendorf tubes at 4°C in 100 µl leucine-poor RPMI1640 + 10% dialyzed fetal calf serum with or without 20 µg/ml IL-2 or 60 mM α-lactose. Dilutions of IL-2-lectin-site modified ricin and ricin at varying concentrations were added in identical medium with or without IL-2 or lactose and incubated at 4°C for 30 min. Cells were pelleted at 2000 g for 5 min, washed once with leucine-poor RPMI1640 + 10% dialyzed fetal calf serum, resuspended in 150 µl of the same medium and incubated at 37°C in 5% CO₂ for 24 h. [³H]Leucine was added as above and, 4 h later, cells were harvested with the PhD Cell Harvester and incorporated [³H]leucine was measured in a liquid scintillation counter. Blocking of selective cytotoxicity was estimated by comparing the ID_{50} of toxins in the presence or absence of IL-2 or lactose.

Results

Yield and purity of ADP-IL-2-ADP-RTB[W37S/Y248H]

Five individual preparations from 100 ml of cell supernatants were partially purified. Peak eluate fractions contained 172, 107, 86, 175 and 100 µg of protein based on the absorbance at 280 nm. The Bio-Rad protein assay gave values of 80, 64, 80 and 84 µg of protein, respectively for preparations 1, 3, 4 and 5, using BSA standard. Densitometry of Coomassie-stained gels showed only a single detectable band at 50 kDa in each preparation (Figure 1). However, P2 antibody ELISA showed the concentration of anti-RTB immunoreactive protein was 38, 50, 18, 28 and 30 µg, respectively. Thus, the purity was between 16 and 47% based on absorbance, Bio-Rad protein assay and densitometry of Coomassie-stained gels.

Immunologic cross-reactivity of ADP-IL-2-ADP-RTB[W37S/Y248H]

Different monoclonal antibodies to RTB (P2, P8 and P10) and an antibody to IL-2 reacted similarly with the fusion molecule based on antibody capture ELISA. The concentration of the fusion molecule was based on a comparison of P2 antibody binding with plant RTB, so that its relative binding is taken as 100%. Antibody P8 bound 140% as well with the fusion molecule as with plant RTB. Antibody P10 bound 150% as well with IL-2-lectin-deficient RTB as with plant RTB. Antibody to IL-2 bound the hybrid molecule 65% as well as with recombinant human IL-2 on a molar basis.

Immunoblots demonstrated reactivity with the same 52 kDa band using anti-RTB or anti-IL-2 antibodies (Figure 2A and B). No weaker bands at lower molecular weight were observed with either set of antibodies, suggesting the partial proteolysis found with IL-2-'wild-type' RTB was not present with the lectin-deficient chimera.

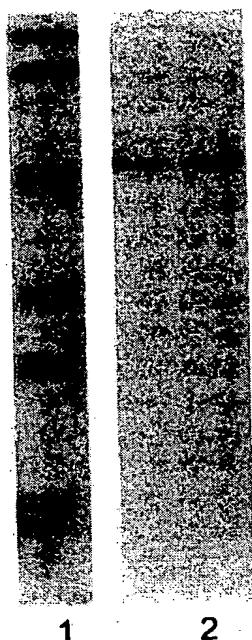


Fig. 1. Coomassie-stained 15% reducing SDS-PAGE of IL-2-mutant RTB fusion. Lane 1, low molecular weight prestained Bio-Rad protein standard; lane 2, ADP-IL-2-ADP-RTB[W37S/Y248H].

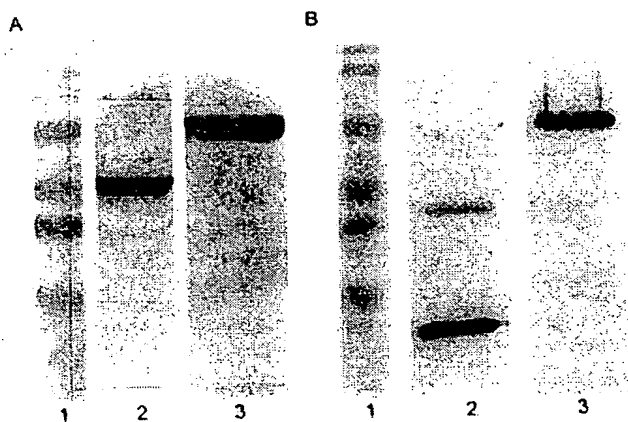


Fig. 2. Immunoblots of IL-2-mutant RTB fusion and plant RTB. (A) P2 and P10 mouse monoclonal antibodies to RTB; (B) mouse monoclonal antibody to human IL-2. Lane 1, low molecular weight prestained Bio-Rad protein standards; lane 2, plant RTB in (A) and human IL-2 in (B); lane 3, ADP-IL-2-ADP-RTB[W37S/Y248H].

Reassociation with RTA

Two preparations of fusion toxin heterodimer were made. Under the reaction conditions [10^{-6} M of IL-2-lectin-deficient RTB and 3×10^{-6} M of plant RTA, 0.1 M triethylamine–0.1 M sodium phosphate (pH 7), room temperature, room air], 50% reassociation was observed in one reaction and 60% reassociation in the other. The results from the sandwich ricin ELISA were confirmed by immunoblots with antibodies to RTB, RTA and IL-2 (Figure 3A–C).

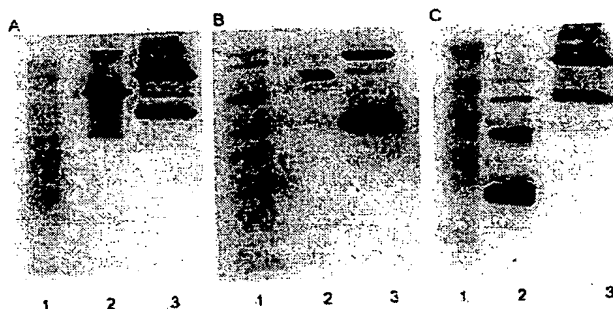


Fig. 3. Immunoblots of IL-2-mutant RTB-RTA heterodimers and plant ricin. (A) P2 and P10 mouse monoclonal antibodies to RTB; (B) αBR12 mouse monoclonal antibody to RTA; (C) mouse monoclonal antibody to human IL-2. Lane 1, low molecular weight prestained Bio-Rad protein standards; lane 2, plant ricin in (A) and (B) and human IL-2 in (C); lane 3, ADP-IL-2-ADP-RTB[W37S/Y248H]-RTA.

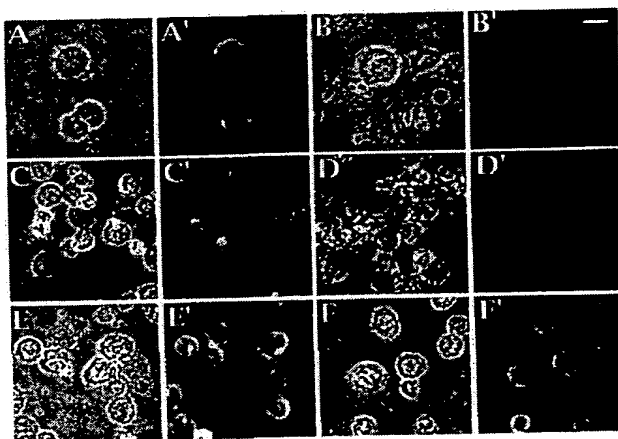


Fig. 4. Binding of IL-2-lectin-deficient ricin and ricin to mammalian cells. Cells were attached to polylysine-coated tissue culture dishes and all incubations were done at 4°C . The cells were washed with 2 mg/ml BSA in PBS and the PBS plus BSA plus $1 \mu\text{g/ml}$ of plant ricin or insect ADP-IL-2-ADP-RTB[W37S/Y248H]-RTA, rewashed, incubated with 1:100 αBR12 mouse monoclonal antibody to RTA in PBS plus BSA, rewashed, incubated with affinity-purified goat anti-(mouse IgG) coupled to rhodamine at $25 \mu\text{g/ml}$, washed again and fixed in 3.7% formaldehyde in PBS. Magnification = $\times 330$; bar = $20 \mu\text{m}$. (A–F) Phase contrast; (A'–F') surface fluorescence; (A, C, E) plant ricin; (B, D, F) ADP-IL-2-ADP-RTB[W37S/Y248H]-RTA. (A, B) KB cells; (C, D) CEM cells; (E, F) HUT102 cells.

Lectin activity and IL-2 receptor binding of the heterodimer

ADP-IL-2-ADP-RTB[W37S/Y248H]-RTA bound 1% as well as plant ricin to immobilized asialofetuin. Specificity for the high-affinity IL-2 receptor was demonstrated on a live cell immunofluorescence assay (Figure 4). The IL-2 fusion toxin bound to HUT102 cells, but bound minimally or not at all to CEM cells and KB cells.

Cell cytotoxicity

Cytotoxicities of fusion heterodimer and plant ricin for different cell lines are shown in Table 1. Ricin was uniformly toxic to all three cell lines tested with ID_{50} s of 5×10^{-12} , 3×10^{-12} and 1×10^{-11} M for HUT102, CEM and KB cells, respectively. Similarly, IL-2-wild-type RTB-RTA was also toxic to all three cell lines in the absence of lactose with ID_{50} s of 4×10^{-12} M on HUT102, CEM and KB cells as described previously (Frankel *et al.*, 1995). In contrast, the fusion toxin displayed

Table 1. Sensitivity of various cell lines to toxins

Protein	ID_{50} (M)		
	HUT102	CEM	KB
Ricin	5×10^{-12}	3×10^{-12}	1×10^{-11}
IL-2-wild-type ricin	4×10^{-12}	4×10^{-12}	4×10^{-12}
IL-2-lectin-deficient ricin	5×10^{-12}	2×10^{-10}	1×10^{-9}
DAB ₃₈₉ IL-2	2×10^{-12}	5×10^{-9}	ND

2×10^4 cells in 150 ml of leucine-free RPMI1640 were combined with dilutions of toxins for 24 h at $37^\circ\text{C}/5\% \text{CO}_2$ and $1 \mu\text{Ci}/\text{well}$ of $[^3\text{H}]\text{leucine}$ in 50 μl of the same medium was added for 4 h at $37^\circ\text{C}/5\% \text{CO}_2$. Cells were harvested with a PhD cell harvester on glass fiber mats, dried and counted in Econofluor in an LKB liquid scintillation counter. ID_{50} was the concentration of toxin reducing protein synthesis by 50%. Each assay was performed three times. Mean values are shown. HUT102 cells have the high-affinity IL-2 receptor, CEM cells have the intermediate-affinity IL-2 receptor and KB cells do not have the IL-2 receptor. The ID_{50} to IL-2-RTB[W37S/Y248H] alone was $>10^{-8}$ M. The experiments with IL-2-wild-type ricin were performed as described previously (Frankel *et al.*, 1995).

significant cytotoxicity only towards the high-affinity IL-2 receptor bearing HUT102 cells ($ID_{50} = 5 \times 10^{-12}$ M) (Figure 5A). The ID_{50} s of fusion toxin on the other cell lines were two orders of magnitude higher ($ID_{50} = 2 \times 10^{-10}$ and 1×10^{-9} M on CEM and KB cells, respectively) (Figure 5B and C). Thus, the *in vitro* therapeutic window was 200-fold. The ID_{50} to the ADP-IL-2-ADP-RTB[W37S/Y248H] protein alone was $>10^{-8}$ M.

IL-2 receptor-mediated cell toxicity was tested by blocking experiments with excess IL-2 or α -lactose (Figure 6). Excess IL-2 reduced IL-2-lectin-deficient-RTB-RTA toxicity towards HUT102 cells by 44-fold (the ID_{50} was 4×10^{-11} M with IL-2 and 9×10^{-13} M without IL-2). In contrast, excess IL-2 had no effect on ricin toxicity ($ID_{50} = 4 \times 10^{-13}$ M with and without IL-2). Lactose competition reduced ricin toxicity 100-fold (the ID_{50} with lactose was 4×10^{-10} M and without lactose 4×10^{-12} M). Again, IL-2-lectin-deficient ricin behaved uniquely. The ID_{50} with lactose was 1.5×10^{-12} M and without lactose 4.5×10^{-12} M. Thus, lactose had negligible or enhancing effects on cytotoxicity of the fusion toxin.

Discussion

The first step in the synthesis of targeted toxins is removal or modification of the normal tissue binding sites on the toxin. Ricin binds to cells via lectin sites on RTB (Olsnes *et al.*, 1974). Studies with synthetic methyl α -lactoside analogs showed that hydroxyl groups at positions 3, 4 and 6 of the α -D-galactopyranose moiety were required for ricin binding (Rivera-Sagredo *et al.*, 1991). Equilibrium dialysis measurements with ricin showed low-affinity ($K_s = 10^{-4} \text{ M}^{-1}$) binding of galactose and lactose (Zentz *et al.*, 1978) and high affinity ($K_s = 10^{-7}$ – 10^{-8} M^{-1}) binding to complex oligosaccharides and cell surfaces (Sandvig *et al.*, 1976; Baenziger and Fiete, 1979). These results suggested that multiple low-affinity sugar binding sites on ricin interacted with complex oligosaccharides and cells to yield high-affinity binding. The X-ray diffraction analysis of ricin crystals provided a structural basis for multiple binding functions. RTB has two domains each with three subdomains (Rutenber and Robertus, 1991). The six subdomains have similar folding and primary amino acid sequence and resemble the primitive galactose binding fold in discoidin I from the slime mold *Dictyostelium discoideum*. In each

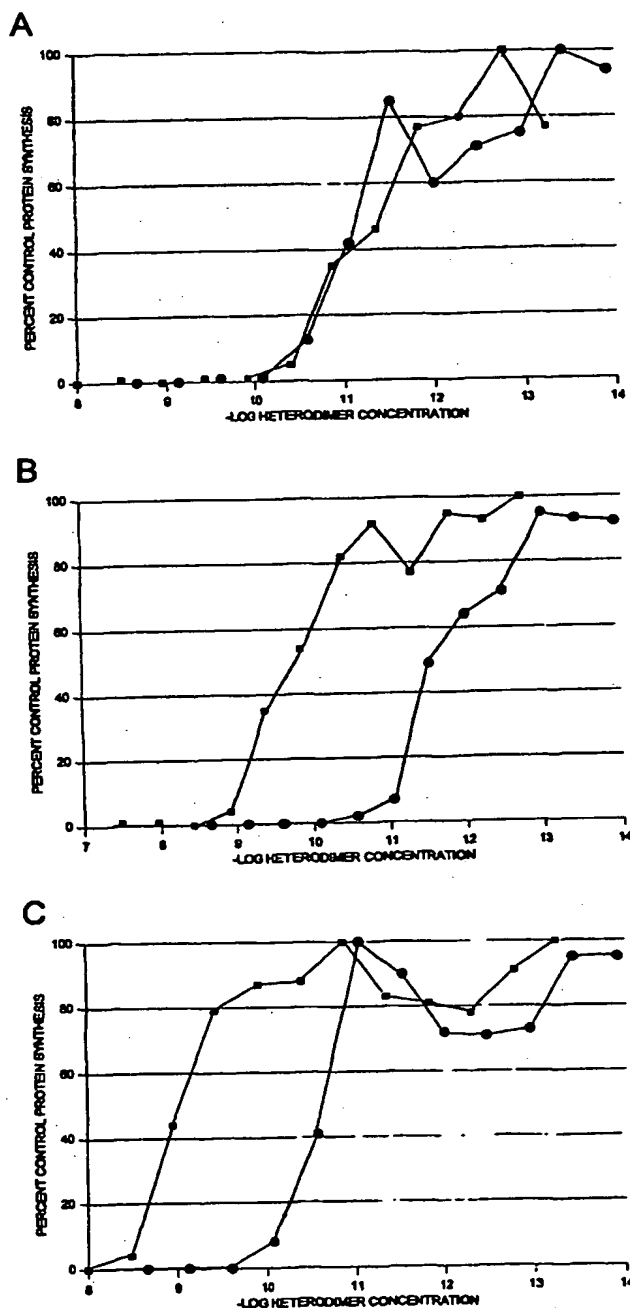


Fig. 5. Cell cytotoxicity of IL-2-lectin-deficient ricin and ricin proteins. (A) HUT102 cells; (B) CEM cells; (C) KB cells. In each case, (○) plant ricin; (■) ADP-IL-2-ADP-RTB[W37S/Y248H]-RTA. Cells were exposed at the dilutions indicated for 24 h at $37^\circ\text{C}/5\% \text{CO}_2$. Incorporation of $[^3\text{H}]\text{leucine}$ was assayed after a 4 h incubation and compared against untreated cell incorporation.

subdomain, the α -carbon chain forms a loop followed by a twist and a hook. X-ray diffraction analysis of ricin co-crystallized with lactose showed two lactose molecules bound to tripeptide kinks in the loops from subdomains 1 α and 2 γ .

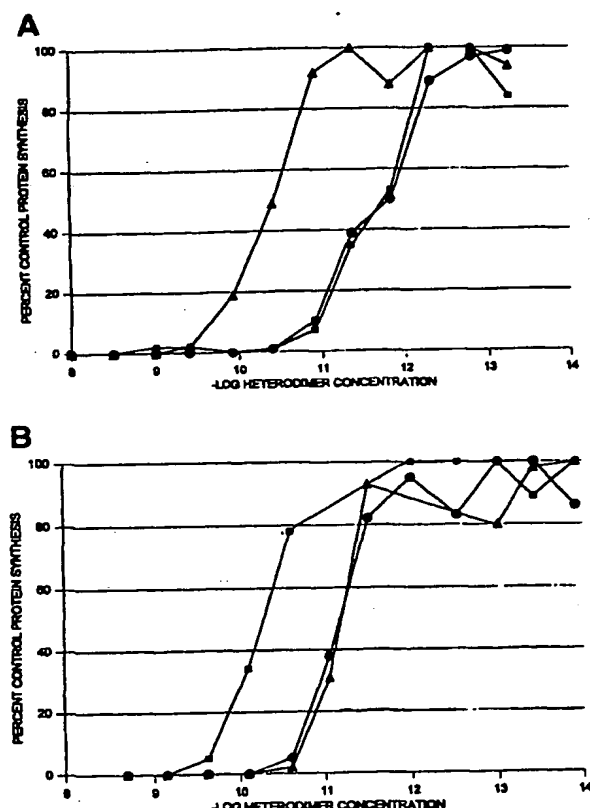


Fig. 6. Blocking experiments of IL-2-lectin-deficient ricin and ricin cytotoxicity to HUT102 cells by IL-2 and α -lactose. (A) Plant ricin; (B) ADP-IL-2-ADP-RTB[W37S/Y248H]-RTA. In each case, (○) media alone; (■) 100 mM α -lactose added; (▲) 20 μ g/ml human IL-2 added. Cells were exposed at the dilutions indicated for 30 min at 4°C, washed and incubated in media alone for 24 h at 37°C/5% CO₂. Incorporation of [³H]-leucine was assayed after a 4 h incubation and compared against untreated cell incorporation.

Bidentate hydrogen bonds were observed between D22 and D234 and the C3,C4 hydroxyls of the galactosyl moiety. Q35, N46 and N255 contributed additional hydrogen bonds to C6 and C3 hydroxyls, respectively. The aromatic rings of W37 and Y248 provide hydrophobic interactions with the non-polar C4-C6 atoms of the galactose ring. Biochemical modification studies confirmed participation of amino acid residues in subdomains 1 α and 2 γ in sugar binding. *N*-Bromosuccinimide modification of W37 reduced sugar binding (Hatakeyama *et al.*, 1986) and *N*-acetylimidazole *O*-acetylation of Y248 altered lactose affinity (Youle *et al.*, 1981).

This structural information was used to design recombinant ricin molecules with lectin sites modified by site-specific mutagenesis. While some of these mutants displayed decreased lectin site function, yields of recombinant product were very low. Cos cell RTB N255A was barely detectable in cell supernatants (Vitetta and Yen, 1990). *Xenopus laevis* oocyte expressed subdomain 1 α and 2 γ RTB mutants were recovered at nanogram levels (Wales *et al.*, 1991), and RTB mutants produced as bacteriophage gene III protein fusions were measured bound on phage particles (Lehar *et al.*, 1994). We recently reported a baculovirus-insect cell expression system

which permits production of milligram quantities of wild-type and mutant RTBs (Frankel *et al.*, 1994, 1995, 1996). Modification of single lectin sites produced less than a 10-fold reduction in sugar-binding affinity, and modifications of two lectin sites yielded 25–100-fold decreases in sugar binding. There were variable yields. The double-site mutant with changes in charged residues, D22E/D234E, was produced at low levels (0.02 mg/l). In contrast, the mutant with alterations in the aromatic residues, W37S/Y248H, was recovered in amounts 10% of wild-type at 0.27 mg/l. The better recovery of the latter mutant may be due to improved folding and solubility. This mutant was selected for generation of fusion toxins.

The next step in generating fusion toxins is coupling a cell-selective ligand. We initially chose to study IL-2 receptor targeting, because of the specificity of this target antigen to normal and malignant hematopoietic cells and the prior experience of other laboratories in producing targeted toxins to this antigen (Williams *et al.*, 1990; Engert *et al.*, 1991; Kreitman and Pastan, 1994). Attachment of IL-2 to the N-terminus of wild-type RTB did not previously alter immunologic reactivity, lectin activity, IL-2 receptor binding activity or yield (Frankel *et al.*, 1995). IL-2-wild-type RTB was produced at 1 mg/l versus 3 mg/l for RTB alone. The yields of ADP-IL-2-ADP-RTB[W37S/Y248H] were 0.34 mg/l insect cell culture, similar to the yields of the parent double-site mutant. The IL-2-lectin-deficient RTB fusion molecule showed immunoreactivity with antibodies to IL-2 and RTB by both ELISA and Western blots. These results are evidence of proper folding of both the IL-2 and RTB domains.

The third requirement for fusion toxins is the presence of an active toxophore domain. We chose to use RTA as the toxic polypeptide. RTB has an extensive surface region and free thiol group for coupling to RTA (Rutenber and Robertus, 1991). The K_d of RTB-RTA association is 10^{-6} M⁻¹, hence even at low subunit concentrations heterodimer formation is favored (Lewis and Youle, 1986). Our experiments employed concentrations of about 10^{-6} M, so we expected ~50% of IL-2-lectin-deficient RTB to reassociate with RTA. Our observation of 50–60% heterodimer formation suggests an excellent efficiency of reassociation. The RTB amino acid residues which interact with RTA include A1, D2, C4, F140, V141, F218, N220, P260 and F262, which are remote from the N-terminus or lectin sites. The recombinant fusion toxin was stable at high dilutions, suggesting disulfide bond formation between RTA C259 and the free thiol of RTB C4 of IL-2-lectin-deficient RTB.

The final IL-2-lectin-deficient ricin fusion toxin was characterized by ELISAs, immunoblots, cell binding assay and cell cytotoxicity assay. The sandwich ELISA demonstrated the presence of both RTA and RTB epitopes on the heterodimer. The immunoblots from non-reducing gels demonstrated the predicted molecular weight of 80 kDa composed of a 33 kDa RTB, a 16 kDa IL-2 and a 31 kDa RTA. Further, the Western blots confirmed the presence of RTA, RTB and IL-2 epitopes on the same molecule. The poor binding to immobilized asialofetuin (1% relative to plant RTB) and lack of binding to IL-2 receptor negative KB cells was consistent with the double lectin site mutation. Finally, the potent cytotoxicity of the IL-2 fusion toxin to IL-2 receptor positive HUT102 cells demonstrated that all of the intoxication functions of ricin and binding functions of IL-2 were present. The level of cytotoxicity was similar to DAB₃₈₉ IL-2, a diphtheria toxin-IL-2 fusion,

RFT5-dgA, an anti-CD25 monoclonal antibody-RTA conjugate, both currently in clinical trials (Engert *et al.*, 1994; Strom *et al.*, 1994) and IL-2-wild-type RTB-RTA (Frankel *et al.*, 1995). Unlike the IL-2-wild-type ricin, IL-2-lectin-deficient ricin displayed selective cytotoxicity to IL-2 receptor bearing cells in the absence of lactose.

Competition experiments with excess ligand has been a frequently used method for confirming specificity of ligand toxins (Bacha *et al.*, 1991; Kreitman and Pastan, 1994). We were able to demonstrate that IL-2, but not lactose, inhibited the cytotoxicity of IL-2-lectin-deficient-RTB-RTA hybrid molecules. Thus, the fusion toxin needed IL-2 receptor binding for cell intoxication. These results were different from those with IL-2-wild-type ricin where IL-2 alone was unable to block intoxication. Both IL-2 plus lactose at 4°C were required to block intoxication because of the residual lectin sites on the fusion molecule (Frankel *et al.*, 1995).

The potent cytotoxicity of the IL-2-lectin-deficient ricin suggests that either intracellular galactose binding is not required for intoxication in this molecule or the small residual galactose binding is adequate for intracellular routing.

This work opens up two new areas of investigation. The IL-2-ricin fusion protein may be tested in animal models of leukemia, lymphoma and autoimmune disease and compared with other IL-2 receptor-directed targeted therapeutics. Separately, this study provides a blueprint for the construction of other plant toxin fusions with other hormones and single-chain antibodies that may permit eventual therapy of a number of malignancies and autoimmune disorders.

Acknowledgements

We are grateful to Joseph Vesely and Billie Harris for expert technical assistance. This work was supported in part by ACS grant 93-80 (EPT).

References

- Argent, R., Roberts, L., Wales, R., Robertus, J. and Lord, J. (1994) *J. Biol. Chem.*, **269**, 26705–26710.
- Bacha, P., Forte, S., McCarthy, D., Estis, L., Yamada, G. and Nichols, J. (1991) *Int. J. Cancer*, **49**, 96–101.
- Baenziger, J. and Fiete, D. (1979) *J. Biol. Chem.*, **254**, 9795–9799.
- Cook, J., Savage, P., Lord, J. and Roberts, L. (1993) *Bioconj. Chem.*, **4**, 440–447.
- Endo, Y. and Tsurugi, K. (1987) *J. Biol. Chem.*, **262**, 8128–8130.
- Engert, A., Marin, G., Amlot, P., Wijdenes, J., Diehl, V. and Thorpe, P. (1991) *Int. J. Cancer*, **47**, 450–456.
- Engert, A., Gottstein, C., Winkler, U., Amlot, P., Pileri, S., Diehl, V. and Thorpe, P. (1994) *Leuk. Lymph.*, **13**, 441–448.
- Frankel, A., Roberts, H., Gulick, H., Afrin, L., Vesely, J. and Willingham, M. (1994) *Biochem. J.*, **303**, 787–794.
- Frankel, A., Tagge, E., Chandler, J., Burbage, C., Hancock, G., Vesely, J. and Willingham, M. (1995) *Bioconj. Chem.*, **6**, 666–672.
- Frankel, A., Tagge, E., Chandler, J., Burbage, C., Hancock, G., Vesely, J. and Willingham, M. (1996a) *Bioconj. Chem.*, **7**, 30–37.
- Frankel, A., Tagge, E., Chandler, J., Burbage, C. and Willingham, M. (1996b) *Protein Engng*, **9**, 371–379.
- Grossbard, M. *et al.* (1993) *Blood*, **81**, 2263–2271.
- Hatakeyama, T., Yamasaki, N. and Funatsu, G. (1986) *J. Biochem.*, **100**, 781–788.
- Kreitman, R. and Pastan, I. (1994) *Adv. Pharmacol.*, **28**, 193–219.
- Lambert, J., McIntyre, G., Gauthier, M., Zullo, D., Rao, V., Steeves, R., Goldmacher, V. and Blattler, W. (1991) *Biochemistry*, **30**, 3234–3247.
- Lehar, S., Pedersen, J., Kanath, R., Swimmer, C., Goldmacher, V., Lambert, J., Blattler, W. and Guild, B. (1994) *Protein Engng*, **7**, 1261–1266.
- Lewis, M. and Youle, R. (1986) *J. Biol. Chem.*, **261**, 11571–11577.
- Masuko, Y., Kishida, K., Saito, M., Umemoto, N. and Hara, T. (1982) *J. Biochem.*, **91**, 1583–1591.
- O'Hare, M., Brown, A., Hussain, K., Gebhardt, A., Watson, G., Roberts, L., Vitetta, E., Thorpe, P. and Lord, J. (1990) *FEBS Lett.*, **273**, 200–204.
- Olsnes, S., Refsnes, K. and Pihl, A. (1974) *Nature*, **249**, 627–631.
- Rivera-Segredo, A., Solis, D., Diaz-Maurino, T., Jimenez-Barbero, J. and Martin-Lomas, M. (1991) *Eur. J. Biochem.*, **197**, 217–228.
- Rutenber, E. and Robertus, J. (1991) *Proteins*, **10**, 260–269.
- Sandvig, K., Olsnes, S. and Pihl, A. (1976) *J. Biol. Chem.*, **251**, 3977–3984.
- Sandvig, K. and Olsnes, S. (1982) *J. Biol. Chem.*, **257**, 7504–7513.
- Sanger, F., Nicklen, S. and Coulson, A. (1977) *Proc. Natl Acad. Sci. USA*, **74**, 5463–5467.
- Sausville, E. *et al.* (1995) *Blood*, **85**, 3457–3465.
- Strom, T., Kelley, V., Murphy, J., Nichols, J. and Woodworth, T. (1994) *Adv. Nephrol.*, **23**, 347–356.
- Tagge, E., Chandler, J., Tang, B., Hong, W., Willingham, M. and Frankel, A. (1995) *J. Histochem. Cytochem.*, **44**, 159–165.
- Vitetta, E., Krolick, K., Miyama-Inaba, M., Cushley, W. and Uhr, J. (1983) *Science*, **219**, 644–650.
- Vitetta, E. and Yen, N. (1990) *Biochim. Biophys. Acta*, **1049**, 151–157.
- Wales, R., Richardson, P., Roberts, L., Woodland, H. and Lord, J. (1991) *J. Biol. Chem.*, **266**, 19172–19179.
- Wales, R., Roberts, L. and Lord, J. (1993) *J. Biol. Chem.*, **268**, 23986–23990.
- Westby, M., Argent, R., Petcher, C., Lord, J. and Roberts, L. (1992) *Bioconj. Chem.*, **3**, 375–381.
- Williams, D., Snider, C., Strom, T. and Murphy, J. (1990) *J. Biol. Chem.*, **265**, 11885–11889.
- Youle, R., Murray, J. and Neville, D. (1981) *Cell*, **23**, 551–559.
- Youle, R. and Colombatti, M. (1987) *J. Biol. Chem.*, **262**, 4676–4682.
- Zentz, C., Frenoy, J. and Bourmilion, R. (1978) *Biochim. Biophys. Acta*, **536**, 18–26.

Received April 14, 1996; revised May 20, 1996; accepted May 27, 1996

Reactivity of Murine Cytokine Fusion Toxin, Diphtheria Toxin₃₉₀-Murine Interleukin-3 (DT₃₉₀-mIL-3), With Bone Marrow Progenitor Cells

By Chung-Huang Chan, Bruce R. Blazar, Lawrence Greenfield, Robert J. Kreitman, and Daniel A. Vallera

Myeloid leukemias can express interleukin-3 receptors (IL-3R). Therefore, as an antileukemia drug, a fusion immunotoxin was synthesized consisting of the murine IL-3 (mIL-3) gene spliced to a truncated form of the diphtheria toxin (DT₃₉₀) gene coding for a molecule that retained full enzymatic activity, but excluded the native binding domain. The DT₃₉₀-mIL-3 hybrid gene was cloned into a vector under the control of an inducible promoter. The fusion protein was expressed in *Escherichia coli* and then purified from inclusion bodies. The fusion toxin was potent because it inhibited FDC-P1, an IL-3R-expressing murine myelomonocytic tumor line (IC₅₀ = 0.025 nmol/L or 1.5 ng/mL). Kinetics were rapid and cell-free studies showed that DT₃₉₀-mIL-3 was as toxic as native DT. DT₃₉₀-mIL-3 was selective because anti-mIL-3 monoclonal antibody, but not irrelevant antibody, inhibited its ability to kill. Cell lines not expressing IL-3R were not inhibited by the fusion protein. Because the use of DT₃₉₀-mIL-3 as an antileukemia agent could be restricted by its reactivity with committed and/or primitive progenitor cells, bone marrow (BM) progenitor assays were performed. DT₃₉₀-mIL-3 selectively inhibited committed BM progenitor cells

as measured by in vitro colony-forming unit-granulocyte-macrophage and in vivo colony-forming unit-spleen colony assays. To determine if this fusion protein was reactive against BM progenitor cells required to rescue lethally irradiated recipients, adoptive transfer experiments were performed. Eight million DT₃₉₀-mIL-3-treated C57BL/6 Ly5.2 BM cells, but not 4 million, were able to rescue lethally irradiated congenic C57BL/6 Ly5.1 recipients, suggesting that progenitor cells might be heterogeneous in their expression of IL-3R. This idea was supported in competitive repopulation experiments in which DT₃₉₀-mIL-3-treated C57BL/6 Ly5.2 BM cells were mixed with nontreated C57BL/6 Ly5.1 BM cells and used to reconstitute C57BL/6 Ly5.1 mice. A significant reduction, but not elimination, of Ly5.2-expressing cells 95 days post-BM transplantation and secondary transfer experiments indicated that IL-3R is not uniformly expressed on all primitive progenitor cells. The fact that some early progenitor cells survived DT₃₉₀-mIL-3 treatment indicates that this fusion toxin may be useful in the treatment of myeloid leukemias that express the IL-3R.

© 1996 by The American Society of Hematology.

INTERLEUKIN-3 (IL-3) is generally considered a cytokine with a broad spectrum of activities on different hematopoietic cells at various stages of development.^{1,2} This hematopoietic cytokine is also associated with leukemia. Murine and human myeloid and lymphoid leukemic cells display receptors for IL-3, and many have been shown to be responsive to exogenous IL-3 in vitro.^{3,4} Production of IL-3 has been shown in some transformed myeloid cells, raising the possibility that autocrine production of IL-3 may contribute to their transformed phenotype.^{5,6} In fact, neutralizing anti-IL-3 and anti-IL-3 receptor (anti-IL-3R) antibodies inhibit the growth of IL-3-producing transformed cell lines.^{7,8}

In normal hematopoiesis, it is controversial as to whether there are IL-3R expressed on primitive progenitor cells.⁹⁻¹¹ It is known that IL-3 supports the proliferation and terminal differentiation of multipotential and committed myeloid progenitors¹² and the activation of a variety of mature myeloid cells.¹³⁻¹⁵ IL-3 also has proliferative effects on CD10⁺ progenitor B cells, mature tonsillar B cells, plasma-cell precursors, and CD4⁺8⁺αβ⁺ T cells.¹⁶⁻¹⁹

To study the expression of IL-3R on primitive progenitor cells and perhaps devise a new antileukemia agent, we synthesized an IL-3 fusion toxin protein. The murine IL-3 (mIL-3) gene has been cloned and genetically mapped to chromosome 11.^{20,21} It consists of 5 exons and encodes a secretory peptide with 140 residues.²² Receptor expression is a prerequisite for response to a cytokine. The high-affinity IL-3R is composed of α and β subunits.²³ The binding of IL-3 to its receptor causes rapid internalization of the ligand-receptor complex.²⁴ Because of the internalization of IL-3, we reasoned that IL-3 could serve as a ligand for delivering a toxic molecule such as diphtheria toxin (DT) to the cells bearing the IL-3R.

DT is a well-studied glycoprotein with a molecular weight

of 58 kD. DT has potent cell killing ability through ADP-ribosylation of elongation factor-2, resulting in inhibition of cellular protein synthesis and death of the cell. Delivering a single DT molecule into the cytoplasm is sufficient to kill a cell.²⁵ Native DT contains three domains: the cell binding domain, the translocation domain, and the enzymatic cytotoxic domain.^{26,27} The cell-binding domain of the DT gene can be replaced by a growth factor gene, resulting in a toxin-growth factor hybrid gene, whose protein product is targeted to a specific growth factor receptor.²⁸⁻³³

The goal of these studies was to determine whether DT₃₉₀-mIL-3 could be used as an antileukemia agent and whether

From the Department of Therapeutic Radiology, Section on Experimental Cancer Immunology, the Department of Laboratory Medicine and Pathology, the Department of Pediatrics, Division of Bone Marrow Transplantation, University of Minnesota Hospital and Clinics, Minneapolis, MN; Roche Molecular Systems, Alameda, CA; and The National Cancer Institute, Bethesda, MD.

Submitted October 30, 1995; accepted April 11, 1996.

Supported in part by US Public Health Service Grants No. RO1-CA36725 and RO1-CA31618 awarded by the National Cancer Institute and the National Institutes for Allergy and Infectious Diseases, Department of Health and Human Services, and by Department of Energy Grant No. DE-FG05-93ER61573. B.R.B. is a recipient of the Edward Mallinckrodt Jr. Foundation Scholar Award.

This work is in partial fulfillment of doctoral requirements for C.-H.C.

Address reprint requests to Daniel A. Vallera, PhD, Box 367 UMHC, Harvard Street at East River Road, Minneapolis, MN 55455.

The publication costs of this article were defrayed in part by page charge payment. This article must therefore be hereby marked "advertisement" in accordance with 18 U.S.C. section 1734 solely to indicate this fact.

© 1996 by The American Society of Hematology.

0006-4971/96/8804-0003\$3.00/0

Table 1. Primers Used in These Studies

(a)	5'AGATATACCATGGCGCTGATGATGTTGAT3'
	Nco I-----DT-----
(b)	5'CCGGCCACTGATTGAAGC AAATGGTTCGTTT3'
	-----IL-3-----DT-----
(c)	5'AAAACGCAACCATTT GCTTCAATCAGTGGCGG3'
	-----DT-----IL-3-----
(d)	5'TGCCTTGATCATTAAATGATGATGATGATG ACATCCACGGTCCACG3'
	-Bcl I- -----His.Tag-----IL-3-----

its use would be restricted. Specifically, it was important to determine whether it would entirely eliminate committed and primitive progenitor cells and subsequently prevent bone marrow (BM) recovery in adoptive BM transfer and competitive repopulation experiments. This would provide further insight as to the expression of IL-3R on progenitor cells and indicate further potential of DT₃₉₀-mIL-3 as an antileukemia agent.

MATERIALS AND METHODS

Construction of hybrid gene and plasmid. The hybrid gene encoding DT₃₉₀-mIL-3 was constructed by the method of gene splicing by overlap extension (SOE), as described.³⁴ Oligonucleotide primers were synthesized using cyanomethyl phosphoramidite chemistry on an Applied Biosystems model 380 A DNA synthesizer and purified by chromatography on Oligonucleotide Purification Cartridges (Applied Biosystems Inc, Foster City, CA) as recommended by the manufacturer. Purified oligonucleotides were resuspended in TE buffer (10 mmol/L Tris base, 1 mmol/L EDTA, pH 8.0). The primers used in these studies are given in Table 1.

Briefly, a DT gene fragment was generated in the first polymerase chain reaction (PCR) by using 5.5 ng plasmid containing the cDNA of DT mutant cross-reacting material (CRM107) as a template with primers a and b. Primer a created an *Nco* I restriction site, an ATG initiation codon, and the coding sequence of the first 7 amino acids of the DT molecule. Primer b introduced a coding sequence of amino acids 385 to 389 of the mature DT and that of amino acids 27 to 32 of the murine IL-3 molecule. A murine IL-3 gene fragment was generated in the second PCR by using 2.74 ng plasmid containing the cDNA of murine IL-3 as a template with primers c and d. Primer c created sequence homology with the 3' end of the DT fragment generated in the first PCR. This region of homology was placed 5' to the sequence encoding amino acids 27 to 32 of the IL-3 molecule. Primer d introduced a *Bcl* I restriction site and a TAA stop codon at the end of the IL-3 molecule. The two fragments generated in the PCRs described above were then purified and used as templates in an SOE reaction using primers a and d. This SOE formed the full-length DT₃₉₀-mIL-3 hybrid gene that was digested with restriction enzymes *Nco* I and *Bcl* I (GIBCO BRL, Gaithersburg, MD) and ligated into the *Nco* I and *Bam*HI cloning sites in the pET11d plasmid (Novagen, Madison, WI). The assembly of plasmid pDT-IL-3 is shown in Fig 1.

DT₃₉₀-mIL-4 and DT₃₉₀-hIL-2 were made from hybrid genes by gene splicing by SOE, as described.³³ The plasmids were assembled with the same orientation as the DT₃₉₀-mIL-3 plasmid. For DT₃₉₀-mIL-4, the final protein contained amino acids 25 through 144 of the mature IL-4 molecule. For DT₃₉₀-mIL-2, the final protein contained amino acids 3 through 135 of the mature IL-2 molecule.

Expression and localization of fusion proteins. Plasmid, pDT-IL-3 was transformed into the *Escherichia coli* strain BL21(DE3) (Novagen) and protein expression was evaluated. Briefly, recombinant bacteria were grown in superbroth (32 g/L bacto-tryptone, 20 g/L bacto-yeast extract [Difco, Detroit, MI], and 5 g/L NaCl, pH

7.5) supplemented with 0.5% glucose, 1.6 mmol/L MgSO₄, and 100 µg/mL carbenicillin (Sigma, St Louis, MO) at 37°C. When the absorbency (A₆₀₀) of the culture reached 1.0, expression of the hybrid gene was induced by the addition of isopropyl-β-D-thiogalactopyranoside (IPTG; GIBCO BRL). Ninety minutes after induction, the bacteria were harvested by centrifugation at 5,000g for 10 minutes. To determine the localization of expressed protein, an aliquot of bacterial pellet was resuspended in 30 mmol/L Tris, pH 7.5, 20% sucrose, 1 mmol/L EDTA and osmotically shocked by placing in ice-cold 5 mmol/L MgSO₄. The periplasmic fraction (supernatant) was obtained by centrifugation at 8,000g for 10 minutes. Another aliquot of bacterial pellet was resuspended in sonication buffer (50 mmol/L sodium phosphate, pH 7.8, 300 mmol/L NaCl). After incubation at -20°C for 16 hours, the resuspended sample was sonicated for 5 minutes. The spheroplast fraction (pellet) and cytosolic fraction (supernatant) were collected separately by centrifugation at 10,000g for 20 minutes.

Sodium dodecyl sulfate-polyacrylamide gel electrophoresis (SDS-PAGE) and immunoblotting. Crude, as well as purified fusion proteins were analyzed on SDS-PAGE. SDS-PAGE was performed using 4% to 20% gradient gels (Bio-Rad, Richmond, CA) and a Mini-Protein II gel apparatus (Bio-Rad). Proteins were stained with Coomassie brilliant blue. For immunoblotting, electrophoresed proteins were transferred to nitrocellulose membranes. Membranes were blocked with 3% gelatin-containing TBS (20 mmol/L Tris, 500 mmol/L NaCl, pH 7.5) and washed with TTBS (TBS, 0.05% Tween-20, pH 7.5). Horse anti-DT sera (Connaught Lab, Switwater, PA) and anti-mIL-3 monoclonal antibody (MoAb; rat IgG₁; Genzyme, Cambridge, MA) were used as a source of primary antibodies. The blots were processed using horseradish peroxidase-conjugated protein-G (Protein G-HRP) and developed using HRP color reagents (Bio-Rad).

Isolation of inclusion bodies and renaturation and purification of the fusion proteins. The method of isolating the inclusion bodies

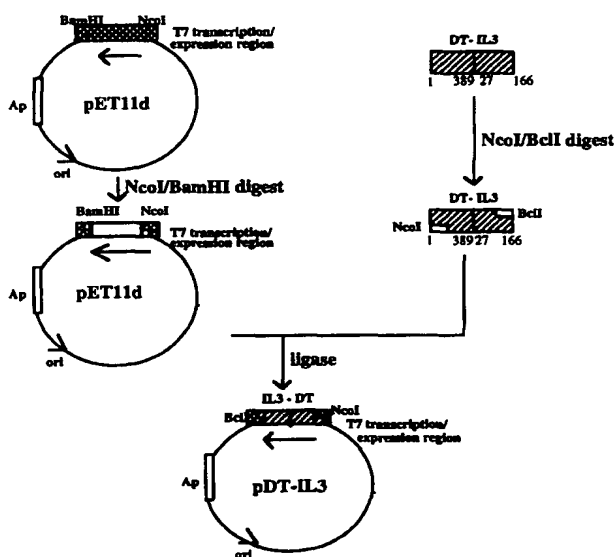


Fig 1. Assembly of the DT₃₉₀-mIL-3 gene in the pET11d vector. The hybrid gene encoding DT₃₉₀-mIL-3 was constructed by the method of gene splicing by overlap extension. The DT₃₉₀-mIL-3 hybrid gene was digested with restriction enzyme *Nco* I and *Bcl* I and ligated into the *Nco* I and *Bam*HI compatible cloning sites of a pET11d plasmid under the control of a T7 promoter.

was previously described.³³ In brief, bacterial pellets were resuspended in TE buffer (50 mmol/L Tris, pH 8.0, 20 mmol/L EDTA, 100 mmol/L NaCl) and treated with 0.02% lysozyme for 30 minutes. The pellet was then incubated in Triton X-100 buffer (11% vol/vol Triton X-100, 89% vol/vol TE) for 30 minutes at room temperature after briefly homogenizing with a tissuemizer (Thomas Scientifics, Germany). The pellets were washed 3 times with Triton X-100 buffer and 4 times with TE buffer by briefly homogenizing with a tissuemizer and incubating for 5 to 10 minutes. Inclusion bodies were collected by centrifugation at 24,000g for 50 minutes. Solubilization of the inclusion body pellet was achieved by sonicating in denaturant buffer consisting of 7 mol/L guanidine, 0.1 mol/L Tris, pH 8.0, and 2 mmol/L EDTA. Protein concentrations were determined by the Bradford method³⁵ and adjusted to 10 mg/mL with solubilization buffer. The solution was incubated at room temperature for 16 hours in the presence of 65 mmol/L dithioerythritol (DTE).

To remove insoluble material, the solution was centrifuged at 40,000g for 10 minutes and the supernatant was collected. Renaturation was initiated by a rapid 100-fold dilution of the denatured and reduced protein into chilled refolding buffer consisting of 0.1 mol/L Tris, pH 8.0, 0.5 mol/L L-arginine, 0.9 mmol/L oxidized glutathione (GSSG), and 2 mmol/L EDTA. The samples were incubated at 10°C for 48 hours. The refolded protein was diafiltered and ultrafiltered against 20 mmol/L Tris, pH 7.8, using a spiral membrane ultrafiltration cartridge on Amicon's CH2 system (Amicon, Beverly, MA). Samples were loaded on a Q-Sepharose (Sigma) column and eluted with 0.3 mol/L NaCl in 20 mmol/L Tris, pH 7.8. The protein was diluted fivefold and subsequently applied to a Resource Q column (Pharmacia, Uppsala, Sweden) and eluted with a linear salt gradient from 0 to 0.4 mol/L NaCl in 20 mmol/L Tris, pH 7.8. The main peak from the Resource Q column was purified by size-exclusion chromatography on a TSK 250 column (TosoHass, Philadelphia, PA).

ADP ribosylation assay. Duplicate samples of nicked DT and DT₃₉₀-mIL-3 were examined for their ADP ribosyl transferase activity, as previously described.^{33,36} The toxin was nicked by treating 15 µg of DT₃₉₀-mIL-3 with 0.04 µg of trypsin for 15 minutes at 37°C and the reaction was stopped with soybean trypsin inhibitor (Sigma). Briefly, ADP-ribosylation was performed in 80-µL reaction mixtures containing 40 µL of 0.01 mol/L Tris-HCl buffer with 1.0 mmol/L dithiothreitol, pH 8.0, 10 µL of rabbit reticulocyte lysate (containing elongation factor-2 [EF-2]), 10 µL 0.1% bovine serum albumin (BSA), and 10 µL of toxin sample. The reaction was initiated by the addition of 10 µL of 0.57 mmol/L [³²P] nicotinamide adenine dinucleotide (ICN Biomedicals, Irvine, CA). Reaction mixtures were incubated at room temperature for 1 hour and the reaction was stopped by the addition of 1 mL 10% trichloroacetic acid (TCA). The precipitate was collected by centrifugation and washed with 1 mL 10% TCA. The radioactivity was counted by standard scintillation techniques.

Cytotoxicity assay. To characterize the cytotoxic activity of DT₃₉₀-mIL-3, we used the murine myelomonocytic cell line FDC-P1³⁷ (provided by Immunex, Inc, Seattle, WA), which is dependent on mIL-3 for proliferation. Cultured FDC-P1 cells were maintained in complete culture media consisting of RPMI-1640 supplemented with 10% fetal bovine serum, 1% sodium pyruvate, 1% L-glutamine, 1% penicillin/streptomycin, and 10% WEHI-3B conditioned media.³⁸ We assayed the cytotoxic activity by measuring the ability of DT₃₉₀-mIL-3 to inhibit the proliferation of FDC-P1 cells. Cells were initially washed three times with nonsupplemented RPMI-1640 to remove any exogenous cytokine, followed by 1 hour of incubation at 37°C. Cells were seeded at 9×10^4 cells/tube in complete culture media and treated with one of the following toxins at concentrations ranging from 1×10^{-13} mol/L to 1×10^{-8} mol/L: DT₃₉₀-mIL-3,

DT₃₉₀-hIL-2, DT₃₉₀-mIL-4, and native DT. The cells were treated for 4 hours at 37°C in a 5% CO₂ atmosphere.

After incubation, the cells were washed three times and then seeded at 3×10^4 cells/well in 96-well flat-bottomed plates in a volume of 200 µL. [³H]-thymidine (1 µCi) and exogenous mIL-3 at a final concentration of 5 ng/mL were added into each well. After 24 hours, the cells were harvested on glass fiber filters and counted according to standard methods. Cells cultured with media alone served as the control. All assays were performed in triplicate. For kinetic analysis, cells were treated with DT₃₉₀-mIL-3, as described above, except that the designated toxin treatment intervals varied from 30 minutes to 8 hours. Three additional murine cell lines were used that did not respond to mIL-3: FDCP2.1d (a myelomonocytic cell line derived from FDCP2),³³ EL4 (a T-cell leukemia/lymphoma), and C1498 (a myeloid leukemia; American Type Culture Collection, Rockville, MD).

Granulocyte-macrophage colony-forming assay (CFU-GM). DT₃₉₀-mIL-3, DT₃₉₀-hIL2, or native DT was examined for its effects on committed BM progenitor cells in a CFU-GM assay, which was performed by culture of treated murine BM cells in complete methylcellulose medium (30% fetal calf serum, 1% pokeweed mitogen [PWM]-stimulated murine spleen cell-conditioned medium, 1% BSA, 0.9% methylcellulose, 10^{-4} mol/L 2-mercaptoethanol, and 3 U/mL erythropoietin; StemCell Technologies, Vancouver, British Columbia, Canada). Our CFU-GM-assay was previously described.³³ Briefly, BM cells were collected by flushing the shafts of femora and tibiae of C57BL/6 mice. Cells were resuspended at 5×10^4 cells/mL in complete methylcellulose medium and were plated in culture dishes for 14 days. Under an inverted microscope, colonies of greater than 50 cells were scored as CFU-GM according to their morphology.

During the kinetic studies, BM cells prepared as mentioned above were cultured with DT₃₉₀-mIL-3 at a final fusion toxin concentration of 10 nmol/L. After 4, 8, 12, or 16 hours, the treated cells were recovered by centrifugation for 10 minutes at 300g and the supernatant was decanted. The cells were washed with medium three times, resuspended at 5×10^4 cells/mL in complete methylcellulose medium, and scored as mentioned above.

Splenic colony-forming assay (CFU-S). Our CFU-S assay was previously described.³⁹ C57BL/6 BM cells were isolated and treated as described above. Treated BM cells (10^5) were injected into the lateral tail vein of sublethally irradiated (7.5 Gy Cesium at a dose rate of 57.72 rads/min; JL Shepherd and Associates, Glendale, CA) syngeneic mice. Eight or 13 days later, the spleens were removed and fixed with Bouin's solution. Visible surface colonies were counted and scored as CFU-S. Control mice that received irradiation but no BM showed no macroscopic spleen colonies on day 8 or 13. Mice were housed in our AAALAC-accredited facility under specific pathogen-free (SPF) conditions in microbarrier cages.

Adoptive transfer studies. An adoptive transfer assay to rescue irradiated mice was modified from a previously described assay.⁴⁰ C57BL/6 Ly5.1 (10 mice/group) recipients were irradiated with lethal total body irradiation (9 Gy x-ray at a dose rate of 39.30 rads/min; Phillips Medical System, Brookfield, WI) 18 hours before intravenous injection with varying cell doses of DT₃₉₀-mIL-3-treated donor BM. Donor BM from C57BL/6 Ly5.2 congenic mice was treated with fusion toxin for 8 hours and then infused. Ly5.2 is an allelic form of the Ly5.1 antigen expressed on all hematopoietic cells. These markers are typable by flow cytometry with fluorescein isothiocyanate [FITC]-anti-Ly5.2 for donor cells and phycoerythrin [PE]-anti-Ly5.1 for host cells.⁴¹ Recipient survival was monitored daily. The irradiated mice were confirmed as rescued by donor-derived cells if they survived for 30 days. Animals died on days 5 through 10 in these radiation protection studies. It is possible

that these deaths were related to the presence of bacteria in our SPF colony requiring larger doses of BM to effect radioprotection. However, attempts to isolate *Proteus vulgaris*, *Pseudomonas* species, or *Klebsiella* species from the colon, oropharynx, or ileum of sentinel mice were unsuccessful.

Competitive repopulation studies. The competitive repopulation assay was performed as previously described, with some modification.⁴² C57BL/6 Ly5.1 recipient mice (10 mice/group) were lethally irradiated (9 Gy). Eighteen hours later, mice received a mixture of C57BL/6 Ly5.1 and congenic C57BL/6 Ly5.2 BM cells. The C57BL/6 Ly5.2 BM cells were preincubated with either DT₃₉₀-mIL-3 or medium alone and the C57BL/6 Ly5.1 BM cells were preincubated with medium. After 8 hours of treatment, BM cells were thoroughly washed with media 3 times to remove the fusion toxin. Equal numbers of Ly5.1 (2.5×10^6) and Ly5.2 (2.5×10^6) cells were mixed together and injected intravenously into irradiated Ly5.1 mice. The percentage of Ly5.2 and Ly5.1 cells in the peripheral blood, bone marrow, spleen, and thymus were determined by flow cytometry by staining with FITC-anti-Ly5.2 and PE-anti-Ly5.1 MoAb as described above.

Statistical analysis. Group comparisons of data in Tables 2 through 4 were made using the Student's *t*-test. *P* values $\leq .05$ were considered significant.

RESULTS

Genetic construction of DT₃₉₀-mIL-3. The DNA fragments encoding the structural gene for DT₃₉₀ and mIL-3 were obtained by separate PCRs with the sizes of 1,197 bp and 467 bp, respectively. After the third PCR, the resulting SOE product, DT₃₉₀-mIL-3 hybrid gene, was generated with a 1,631-bp size. The DT₃₉₀-mIL-3 hybrid gene encodes an *Nco*I restriction site, an ATG initiation codon, the first 389 amino acids of the DT, the mature murine IL-3 polypeptide, six histidine tag, a TAA stop codon, and a *Bcl*I compatible restriction site. After digestion, the DT₃₉₀-mIL-3 hybrid gene was cloned into the pET11d plasmid under the control of the IPTG inducible T7 promoter to create a 7,255-bp pDT-IL-3 plasmid (Fig 1). Restriction endonuclease digestion verified that the DT₃₉₀-mIL-3 hybrid gene sequence had been cloned in frame. DNA sequencing analysis was performed by the University of Minnesota Microchemical Facilities (University of Minnesota, Minneapolis, MN) and no mutations were detected.

Expression and purification of DT₃₉₀-mIL-3 fusion protein. Expression of the fusion protein in *E coli* was induced with IPTG at either 30°C or 37°C with the same efficiency (data not shown). Coomassie brilliant blue-stained SDS-polyacrylamide gel of whole bacterial lysate after IPTG induction showed a novel expressed protein migrating at 58 kD, which corresponds to the expected size for DT₃₉₀-mIL-3 protein (Fig 2, lane 3). The localization study of the expressed fusion protein showed that DT₃₉₀-mIL-3 was retained in the inclusion bodies (Fig 2, lanes 4 through 6). To extract the DT₃₉₀-mIL-3 protein, the inclusion bodies were isolated and denatured, and the protein was refolded as described in the Materials and Methods. After the renaturation procedure, the crude DT₃₉₀-mIL-3 was purified by sequential chromatography. The elution from the anion-exchange Q-sepharose and resource Q columns showed an enrichment of a protein with an electrophoretic mobility corresponding to an apparent molecular mass of 58 kD (Fig 2, lane 7). To further purify

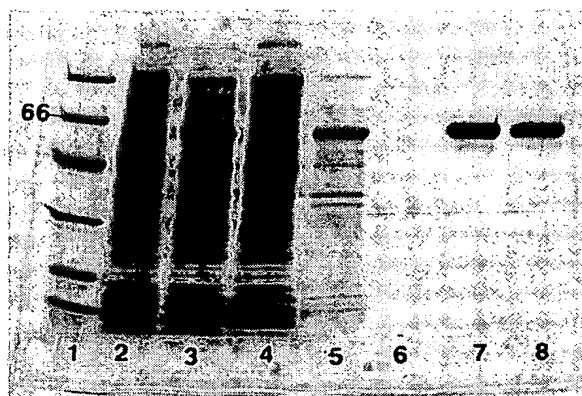


Fig 2. SDS-PAGE of the purified DT₃₉₀-mIL-3 protein stained with Coomassie blue. Lane 1, molecular weight standard; lane 2, uninduced total bacteria lysate; lane 3, IPTG-induced total bacteria lysate; lane 4, fraction of soluble protein in cytoplasm; lane 5, fraction of insoluble protein in inclusion body; lane 6, soluble protein in periplasmic space; lane 7, major eluate from anion-exchange column; and lane 8, major peak from HPLC sizing column. The molecular weight standards are at 97, 66, 45, 31, 22, and 14 kD.

this fusion protein, pooled peak fractions from the anion-exchange columns were subjected to high-performance liquid chromatography (HPLC) using a TSK-250 sizing column. The final product was greater than 95% pure (Fig 2, lane 8). The endotoxin level of the purified DT₃₉₀-mIL-3 was less than 2 EU/mg protein as detected by limulus amoebocyte lysate (LAL) assay. Additional analysis of this DT₃₉₀-mIL-3 protein by immunoblotting was performed. Anti-DT sera and anti-mIL-3 MoAbs were able to recognize the renatured and purified DT₃₉₀-mIL-3. The control native DT and DT₃₉₀-hIL-2 were immunoblotted with the anti-DT sera but not the anti-mIL-3 MoAb.

Enzymatic activity and in vitro cytotoxicity. Protein synthesis inhibition by DT is due to fragment A-catalyzed ADP-ribosylation of cytoplasmic EF-2. To determine whether the DT₃₉₀-mIL-3 protein also displays such enzymatic activity, a cell-free assay system was used in which rabbit reticulocyte lysate, a source of EF-2, was exposed to either native DT or DT₃₉₀-mIL-3 in the presence of [³²P]-NAD. Incubation with either native DT or DT₃₉₀-mIL-3 toxin showed a similar dose-dependent increase in [³²P] incorporation into the TCA-precipitable fraction of rabbit reticulocyte lysate (EF-2). In contrast, the negative control of BSA did not show such an ADP-ribosylation activity. This result confirmed that DT₃₉₀-mIL-3 possessed ADP-ribosyl transferase activity.

To characterize the cytotoxic activity of DT₃₉₀-mIL-3, a bioassay was devised using the mIL-3-dependent myelomonocytic leukemia cell line FDC-P1 that expresses IL-3R and is readily stimulated by IL-3. In our hands, IL-3-induced stimulation of FDC-P1 cells was dose-dependent and 16 ng/mL IL-3 resulted in a curve plateau with 350,000 cpm in a thymidine uptake assay representing a 100-fold increase compared with background. The cytotoxicity was evaluated by measuring the inhibition of cellular proliferation. The ability of various concentrations of DT₃₉₀-mIL-3 to inhibit

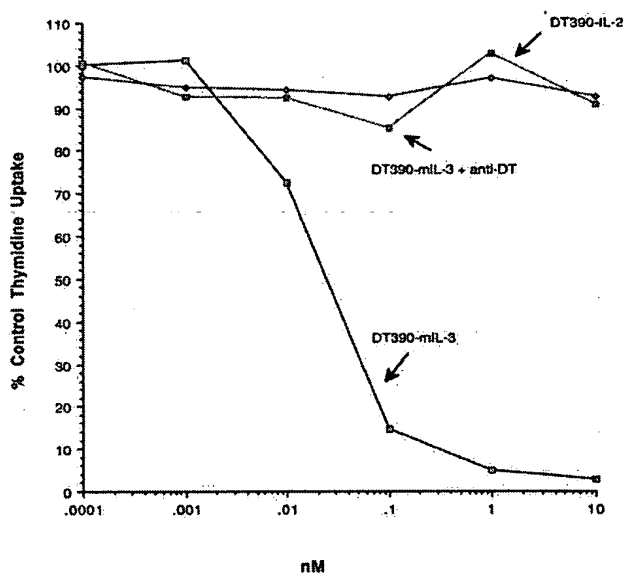


Fig 3. Cytotoxic activity of fusion toxins on FDC-P1 cells. Various amounts of DT₃₉₀-mIL-3 or DT₃₉₀-hIL-2 were added to FDC-P1 cells for 4 hours. After washing, the percentage of incorporation of [³H] thymidine relative to controls not treated with fusion toxin was determined. Neutralization of DT₃₉₀-mIL-3 was studied by adding 0.1% anti-DT antiserum during the 4 hours of incubation.

the proliferation on FDC-P1 cells was examined. FDC-P1 cells were inhibited by DT₃₉₀-mIL-3 in a dose-dependent manner with an IC₅₀ of 0.025 nmol/L (or 1.5 ng/mL; Fig 3). To determine if the cytotoxic activity of DT₃₉₀-mIL-3 on FDC-P1 cells was mediated by the binding of the mIL-3 moiety, FDC-P1 cells were cultured with DT₃₉₀-hIL-2, an irrelevant fusion toxin control. IL-2 did not stimulate the growth of this cell line; thus, the IL-2R is not expressed on FDC-P1 cells (data not shown). In contrast to DT₃₉₀-mIL-3, FDC-P1 cells were resistant to as much as 10 nmol/L DT₃₉₀-hIL-2. The cytotoxic effect of DT₃₉₀-mIL-3 was fully neutralized by 0.1% anti-DT sera (Fig 3), which suggested that the cytotoxicity of DT₃₉₀-mIL-3 was mediated by the enzymatic activity of DT₃₉₀ fragment. Furthermore, anti-mIL-3 antibodies blocked the cytotoxic effect of DT₃₉₀-mIL-3 (Fig 4). The addition of 10 nmol/L anti-mIL-3 antibodies fully neutralized the cytotoxic effect of 0.01 nmol/L or 0.1 nmol/L DT₃₉₀-mIL-3 and neutralized the cytotoxic effect of 1 nmol/L DT₃₉₀-mIL-3 up to 80%. However, 10 nmol/L of anti-mIL-3 antibodies did not block the cytotoxic effect of 10 nmol/L DT₃₉₀-mIL-3. The irrelevant anti-Thy1.2 antibodies did not block the activity of DT₃₉₀-mIL-3. IL-3 was not used to block the cytotoxic activity of DT₃₉₀-mIL-3 in this study because IL-3 itself was used to stimulate the proliferation of FDC-P1 cells.

The effect of DT₃₉₀-mIL-3 on kinetics of proliferative inhibition to FDC-P1 cells was plotted as a percentage of the control level versus a function of time (Fig 5). As expected, the rate of inhibition was concentration-dependent, with higher concentrations giving faster rates. The kinetics were

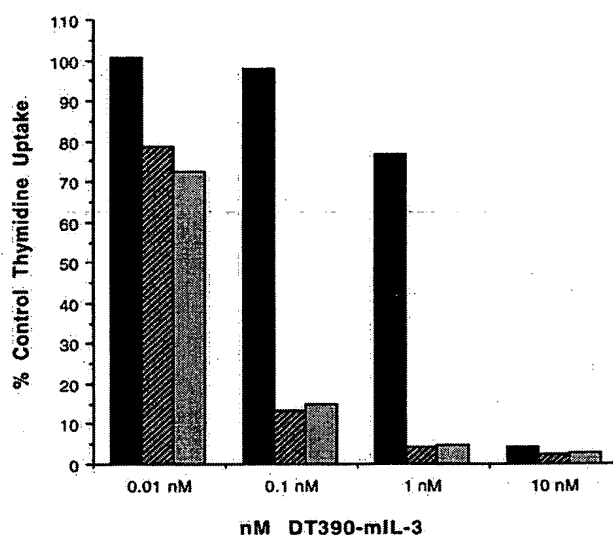


Fig 4. Neutralization of DT₃₉₀-mIL-3 by anti-mIL-3 and irrelevant antibody. Various concentrations of DT₃₉₀-mIL-3 were incubated with (■) 10 nmol/L of anti-mIL-3 antibody or (▨) irrelevant anti-Thy1.2 antibody and were added to FDC-P1 cells as described in Fig 3. (□) DT₃₉₀-mIL-3 alone. Results are expressed as the percentage of activity in control cultures not treated with fusion protein.

rapid because a treatment as short as 30 minutes resulted in 90% inhibition. After 8 hours, 98% inhibition was observed. Cellular proliferative inhibition increased linearly for those toxin concentrations of either 1 nmol/L or 0.1 nmol/L. These kinetics indicate a first-order single-hit process.

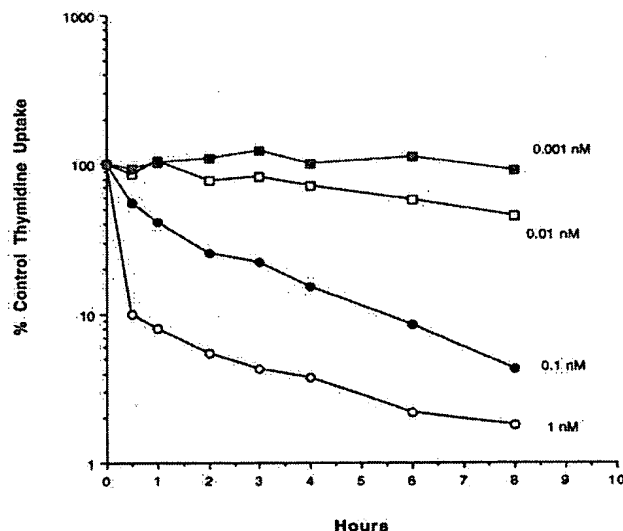


Fig 5. For kinetic analysis, FDC-P1 cells were treated with DT₃₉₀-mIL-3 as described in Fig 3, except that the designated toxin treatment intervals varied from 30 minutes to 8 hours. The effect of DT₃₉₀-mIL-3 on kinetics of proliferative inhibition to FDC-P1 cells was plotted as a percentage of the control level versus a function of time.

DT₃₉₀-mIL-3 had no effect on cell lines that did not express IL-3R. The FDC-P2.1d cell line, which was also derived from the FDC-P parental cell line, is murine granulocyte-macrophage colony-stimulating factor (mGM-CSF)-dependent and mIL-3 nonresponsive. It was not inhibited by DT₃₉₀-mIL-3 (data not shown). Furthermore, DT₃₉₀-mIL-3 showed a high IC₅₀ of greater than 2×10^{-8} mol/L on the T-cell line EL4 and the myelomonocytic leukemia cell line C1498 (data not shown). Together, these reduced effects on IL-3 nonresponsive lines indicate that DT₃₉₀-mIL-3 was specifically cytotoxic to cells via the IL-3 ligand-receptor complex.

The effect of DT₃₉₀-mIL-3 on hematopoietic progenitor cells. It has been well documented that IL-3 plays a role in the development of multiple lineages in hematopoiesis.^{1,2} It is of interest to know at which stages of development hematopoietic progenitor cells express the high-affinity IL-3R. To determine the effect of DT₃₉₀-mIL-3 on committed myeloid progenitor cells, we tested its ability to inhibit CFU-GM colonies. DT₃₉₀-mIL-3 inhibited colony formation 95% and 99% at toxin concentrations of 1 nmol/L or 10 nmol/L, respectively (Fig 6A). In contrast, DT₃₉₀-hIL-2, an irrelevant control fusion toxin, had little inhibitory effect. Native DT also had little effect. This is consistent with previous reports that mouse cells are more resistant to DT because they lack DT receptors.^{43,44} Kinetic studies (Fig 6B) showed a relationship between the increasing inhibition of CFU-GM and incubation time. Approximately 2 log inhibition was obtained after 8 hours. We chose this 8-hour incubation time for subsequent studies because untreated, cultured BM underwent a 40% reduction in CFU-GM colony number at longer incubation intervals. Under these culture conditions, 70% CFU-GM colonies were still preserved in untreated BM after 8 hours of culture. Concentrations of fusion toxin greater than 10 nmol/L resulted in nonspecific killing.

To test the effect of DT₃₉₀-mIL-3 on progenitor cells earlier than those giving rise to CFU-GM colonies, CFU-S assays were performed. CFU-S are heterogeneous with respect to their proliferative capacity, self-renewal ability, and cell cycle status.^{45,46} The progenitors that produce CFU-S colonies represent earlier committed progenitor cells, but not primitive progenitor cells. Day-8 CFU-S have little self-renewal potential and represent committed hematopoietic progenitors more closely related to erythroid progenitors (burst-forming unit-erythroid [BFU-E]) or granulocyte-macrophage progenitors (CFU-GM). Day-13 CFU-S contain cells with more than one lineage.^{47,48} However, recent evidence suggests that neither day-8 CFU-S nor day-13 CFU-S represent the pluripotent hematopoietic stem cells.⁴⁹⁻⁵¹ DT₃₉₀-mIL-3 was used at a dose of 10 nmol/L in an 8-hour preincubation because we knew that higher doses would result in nonspecific killing of CFU-S. At this dose, the DT₃₉₀-mIL-3 inhibited day-8 CFU-S about 80% and day-13 CFU-S about 50% (Fig 7). The inhibition of CFU-S colonies was specific and mediated by the DT portion of the molecule because the anti-DT sera was able to neutralize the CFU-S inhibition.

Together, the combined CFU-GM and CFU-S studies indicate that the high-affinity IL-3R are expressed on commit-

ted BM progenitor cells and that the progenitor cells of day-8 CFU-S are more sensitive to DT₃₉₀-mIL-3 treatment than those of day-13 CFU-S.

The ability of DT₃₉₀-mIL-3-treated cells to rescue lethally irradiated mice after adoptive transfer. To determine the effect of DT₃₉₀-mIL-3 on the progenitor cells capable of providing radiation protection, adoptive transfer assays were performed. C57BL/6 Ly5.2 BM cells were treated with 10 nmol/L DT₃₉₀-mIL-3. After washing, $1, 2, \text{ or } 4 \times 10^6$ treated cells were injected into lethally irradiated (9.0Gy) C57BL/6 Ly5.1 congenic recipients. The results showed that all of these recipients survived less than 19 days. When a higher dose (8×10^6) of DT₃₉₀-mIL-3 treated cells was injected, 60% of the recipients survived more than 30 days, indicating that recipients could be rescued with high BM doses despite

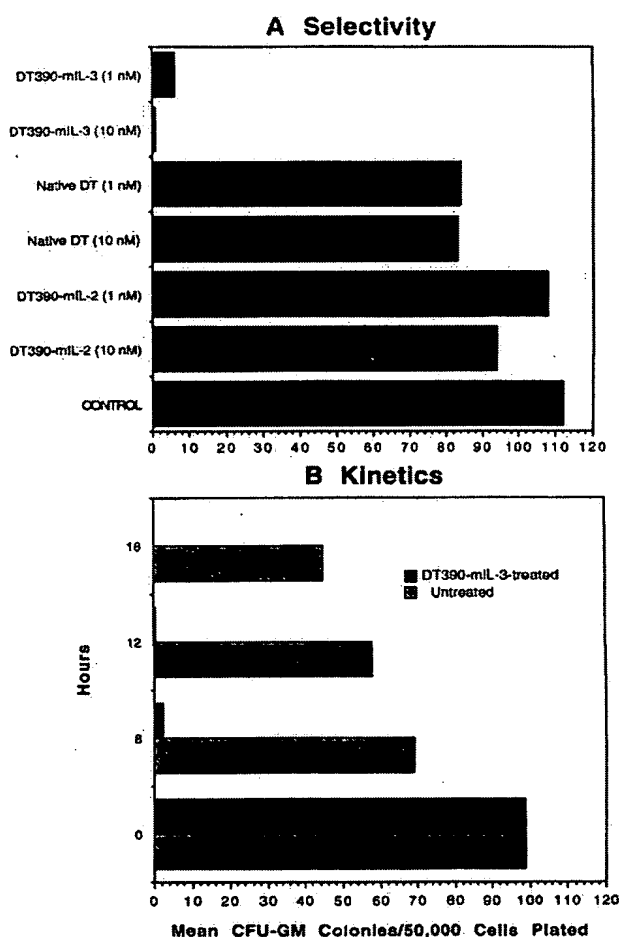


Fig 6. (A) Effect of DT₃₉₀-mIL-3 on the colony formation of CFU-GM myeloid progenitor cells. Mouse BM cells were incubated with either 1 nmol/L or 10 nmol/L fusion toxin for 8 hours. Toxin was removed by washing BM cells 3 times. Colony number was determined relative to 5×10^4 mononuclear BM cells plated on semisolid methylcellulose media in a 1-mL culture volume. (B) Mouse BM cells were treated with 10 nmol/L DT₃₉₀-mIL-3 or media alone for 8, 12, or 16 hours. After washing, the CFU-GM was assayed as in (A).

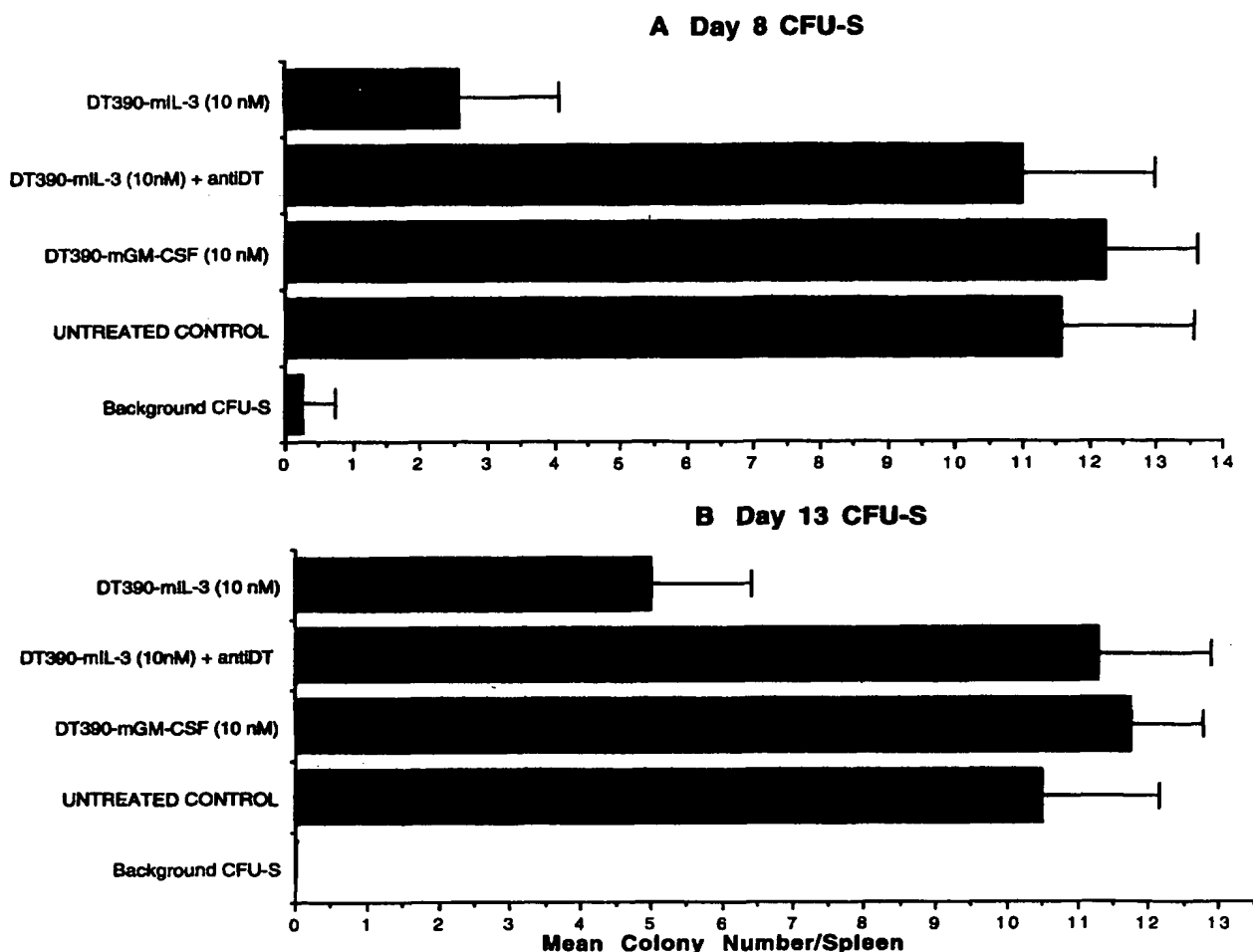


Fig 7. CFU-S activity on day 8 and day 13 of fusion toxin-treated BM cells. BM cells were incubated with toxin for 8 hours. After washing, BM cells (1×10^5) were injected into syngeneic irradiated (7.5 Gy Cs) recipients (C57BL/6). Mice were killed either 8 or 13 days later. The spleens were removed and fixed in Bouin's solution. Visible surface colonies were counted and scored ($n = 7$ to 8 mice/group).

treatment. Sixty percent of recipients survived when 1×10^6 nontreated cells were administered, indicating that DT₃₉₀-mIL-3 treatment removed about 87.5% of the progenitor cells capable of rescue. All recipients survived more than 30 days when the administered cell doses of nontreated cells were greater than 2×10^6 . Earlier published studies showed that DT₃₉₀-mGM-CSF killed committed myeloid progenitors³³ and Fig 8 showed that 2×10^6 DT₃₉₀-mGM-CSF-treated cells rescued 60% of the mice. A comparison of this curve to the curve in which mice received nontreated BM indicated that, with DT₃₉₀-mGM-CSF treatment, there was a removal of about 50% of the progenitor cells capable of rescue. All the recipients that survived for the first 30 days survived until the termination of the experiment on day 110.

On day 30, we typed donor peripheral blood leukocytes and confirmed that the survivors were indeed reconstituted with donor-type cells. The results given above suggested that DT₃₉₀-mIL-3 kills more progenitor cells capable of BM rescue than does DT₃₉₀-mGM-CSF.

The ability of DT₃₉₀-mIL-3-treated cells to competitively repopulate irradiated mice in BM mixing experiments. To determine whether DT₃₉₀-mIL-3 was acting on more primitive BM progenitor cells capable of long-term repopulation, competitive repopulation studies were performed. When differing proportions (percentages) of C57BL/6 and congenic C57BL/6 Ly5.2 BM cells totalling 10 million were mixed (100/0, 83/17, 50/50, 17/83, and 0/100) and transplanted into groups ($n = 5$ /group) of irradiated syngeneic recipients, similar proportions of reconstituting cells were measured in the peripheral blood by flow cytometry several weeks later (100/0, 84/16, 53/47, 13/87, and 6/94). This finding indicated that reconstituting cells correlated with the original proportion of BM progenitor cells and that a model was operational in which the effects of DT₃₉₀-mIL-3 could be determined.

In separate experiments, C57BL/6 Ly5.2 BM cells were treated with DT₃₉₀-mIL-3 and then mixed with an equal proportion of untreated C57BL/6 Ly5.1 BM cells. Mixed BM cells were injected into lethally irradiated (9.0 Gy) C57BL/

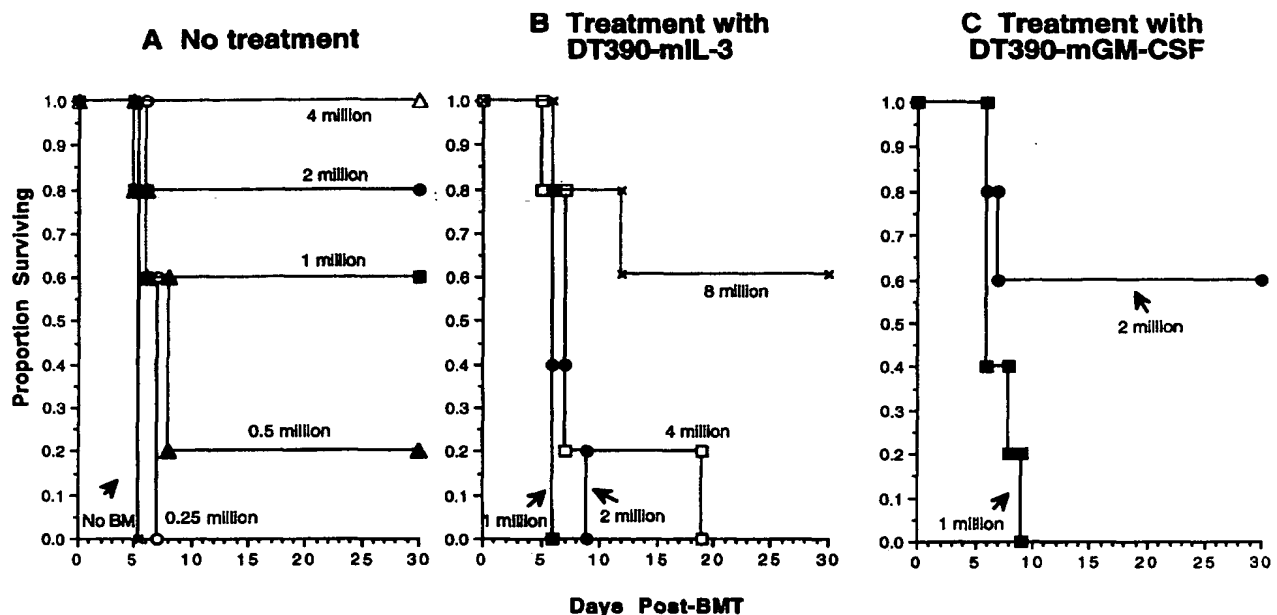


Fig 8. Adoptive transfer BM rescue experiments. C57BL/6 Ly5.2 congenic BM cells were incubated with or without DT₃₉₀-mIL-3 or DT₃₉₀-mGM-CSF for 8 hours. After washing, various doses of BM cells were injected into irradiated (9 Gy) C57BL/6 Ly5.1 recipients. Recipient survival was monitored daily.

6 Ly5.1 recipients. Peripheral blood cells of recipients were studied by flow cytometry for the presence of Ly5.1 and Ly5.2-expressing cells 28 to 31 days after transplantation. Table 2 shows that, in 2 experiments, the mice receiving the DT₃₉₀-mIL-3-treated Ly5.2 BM cells had less reconstitution of Ly5.2-expressing cells as compared with the mice receiving nontreated Ly5.2 BM cells. Long-term reconstitution was also affected. On day 95 post-BMT transplantation (BMT), various organs from animals from experiment 1 were typed. DT₃₉₀-mIL-3 inhibited reconstitution of Ly5.2 cells in blood, spleen, and thymus (Table 3). Interestingly, the inhibition of Ly5.2 cells was not complete. A failure of the fusion toxin to inhibit Ly5.2 BM cells in the treated culture is not a

likely explanation because CFU-GM measured in these same treated BM cells was inhibited 92% (data not shown). It is more likely that some primitive progenitors express enough high-affinity IL-3R to be intoxicated by DT₃₉₀-mIL-3, whereas others do not, or that there might be a difference in receptor number.

To prove that pluripotent hematopoietic stem cells were indeed present on day 95 post-BMT, BM cells from a group of these mice were adoptively transferred to irradiated recipients (Table 4). Upon secondary transfer, these mice reconstituted with both Ly5.1 and Ly5.2 BM cells. Levels of Ly5.2 BM cells were still significantly lower than levels of Ly5.1 BM cells in the mice that received cells from animals that had originally received DT₃₉₀-mIL-3-treated BM cells. Together, these findings indicate that DT₃₉₀-mIL-3 is reactive against some but not all of the primitive progenitor cells.

Table 2. Competitive Repopulation of the Blood With DT₃₉₀-mIL-3-Treated Ly5.2-Expressing Cells on Days 28 Through 31 Post-BMT

	Experiment 1		Experiment 2	
	Ly5.1	Ly5.2	Ly5.1	Ly5.2
Untreated	55 ± 5	46 ± 5	61 ± 8	39 ± 8
DT ₃₉₀ -mIL-3	62 ± 1*	38 ± 1*	81 ± 5*	19 ± 5*

C57BL/6 Ly5.2 BM cells were treated with 10⁻⁸ mol/L DT₃₉₀-mIL-3 for 8 hours. Treated cells were adjusted and mixed with C57BL/6 Ly5.1 congenic BM cells so that equal concentrations (2.5 × 10⁶ of Ly5.2 and 2.5 × 10⁶ of Ly5.1 BM cells) were administered to groups of lethally irradiated C57BL/6 Ly5.1 recipients. To determine competitive repopulation, 4 to 8 recipients were studied by flow cytometry on days 28 through 31 post-BMT for the presence of Ly5.1- or Ly5.2-expressing cells, as described. Data are expressed as a mean percentage of positive cells ± 1 standard error of the mean.

* *P* < .04 compared with untreated controls.

DISCUSSION

The unique contribution of this work is the construction and description of a fusion toxin, DT₃₉₀-mIL-3, by genetically splicing the DNA segment encoding the ADP-ribosyl transferase enzymatic and hydrophobic translocation enhancing region of DT, but not the native binding site, to the DNA segment encoding the amino acids of the mature mIL-3 molecule. The fusion toxin was potent and highly selective in its activity because we measured an IC₅₀ (concentration inhibiting 50% activity) of about 0.025 nmol/L (or 1.5 ng/mL) against the myelomonocytic cell line FDC-P1. Although amply equipped to kill leukemia cells, DT₃₉₀-mIL-3 might pose an equal threat to nonmalignant hematopoietic progenitor cells. The synthesis of the mouse reagent permitted the

Table 3. Long-Term Competitive Repopulation of the Various Tissues With DT₃₉₀-mIL-3-Treated Ly5.2-Expressing Cells on Day 95 Post-BMT

	Blood		BM		Spleen		Thymus	
	Ly5.1	Ly5.2	Ly5.1	Ly5.2	Ly5.1	Ly5.2	Ly5.1	Ly5.2
Untreated	39 ± 3	61 ± 3	52 ± 5	48 ± 5	36 ± 3	64 ± 3	39 ± 7	61 ± 7
DT ₃₉₀ -mIL-3	56 ± 5*	44 ± 5*	61 ± 6	39 ± 6	55 ± 5*	45 ± 5*	62 ± 13*	38 ± 13*

C57BL/6 Ly5.2 BM cells were treated with 10^{-8} mol/L DT₃₉₀-mIL-3 for 8 hours. Treated cells were adjusted and mixed with C57BL/6 Ly5.1 congenic BM cells so that equal concentrations (2.5×10^6 of Ly5.2 and 2.5×10^6 of Ly5.1 BM cells) were administered to groups of lethally irradiated C57BL/6 Ly5.1 recipients. To determine competitive repopulation, 4 recipients were studied by flow cytometry on day 95 post-BMT for the presence of Ly5.1- or Ly5.2-expressing cells as described. Data are expressed as a mean percentage of positive cells \pm 1 standard error of the mean. These same DT₃₉₀-mIL-3-treated C57BL/6 Ly5.2 BM cells were plated in *in vitro* colony assays and were found to have a 90% reduction in CFU-GM.

* $P < .04$ compared with untreated controls.

evaluation of its reactivity against primitive progenitor cells using adoptive transfer experiments and competitive repopulation experiments not possible in humans. These data indicate that IL-3R may not be expressed uniformly on primitive BM progenitor cells.

The expression of IL-3R on hematopoietic stem cells at early stages of development is still a highly controversial issue.⁹⁻¹¹ We approached this issue by testing the ability of a fusion toxin directed against the IL-3R to eliminate BM progenitor cells at various stages of commitment. The most committed progenitor cell that we evaluated was that which gave rise to CFU-GM colonies. First, a working treatment schedule was established based on thymidine incorporation and colony assays. DT₃₉₀-mIL-3 reproducibly inhibited about 99% CFU-GM colony growth, showing that IL-3R is expressed on most myeloid-committed cells. These findings agree with previous reports. For example, Ogata et al¹⁰ and Sugiura et al¹² reported that the hematopoietic progenitors can be separated into two populations by MoAbs against IL-3R-associated antigen(s) (IL-3RAA). Early differentiating progenitors (day-8 CFU-S and CFU-GM) were enriched in the IL-3RAA⁺ cell population, whereas more immature multipotential progenitors (day-12 to -14 CFU-S and CFU-GEMM) were contained in the IL-3RAA⁻ cell population. Therefore, IL-3RAA⁺ cells are more committed than IL-3RAA⁻ cells.

CFU-S colonies are considered to be derived from more primitive progenitor cells than CFU-GM. Most day-8 CFU-

S colonies are thought to be committed to the erythroid lineage and sensitive to 5-fluorouracil (5-FU), whereas day-12 to -14 CFU-S are thought to be more uncommitted with multilineage potential and be resistant to 5-FU.^{45,46} We found that the more committed day-8 CFU-S was more susceptible to the inhibitory effects of DT₃₉₀-mIL-3 (80%) than day-13 CFU-S (50%). These findings (1) provide further evidence that IL-3R is expressed on committed hematopoietic progenitor cells; (2) indicate that IL-3R is expressed on cells as primitive as day-12 to -14 CFU-S; and (3) suggest that more IL-3R are present on progenitor cells in the cycling phase than the Go phase. In other words, day-12 to -14 CFU-S are heterogeneous in their expression of IL-3R.

It is noteworthy that only high-affinity IL-3R are internalized when bound to their ligands. Although, theoretically, one DT molecule into the cytoplasm of the cell is required to produce cell death, the process of internalization and translocation into the cytoplasm is relatively inefficient, with only about 10% of the molecules that bind to the surface receptors entering the cytoplasm.^{33,34} Thus, it is reasonable to infer that a critical number of growth factor-toxin molecules must be able to bind to cell surface receptors to cause subsequent internalization and cell death and that the cells expressing larger numbers of receptors have a higher chance of being intoxicated by specific growth factor-toxin molecules. Thus, differential sensitivity to DT₃₉₀-mIL-3 treatment between fractions of progenitor cells may be derived from (1) different affinities of IL-3R (high-affinity v low-affinity); (2) different numbers of high-affinity IL-3R; and (3) heterogeneity in the expression of IL-3R (presence v absence of receptors on progenitors). In these studies, progenitor cell resistance to DT₃₉₀-mIL-3 treatment could be explained by the absence of high-affinity IL-3R or only a small number of high-affinity IL-3R.

The most primitive stem cells, termed pluripotent hematopoietic stem cells (PHSC), are defined operationally by their (1) ability to rescue animals from lethal irradiation, (2) capacity for self-renewal, and (3) potential to differentiate into all hematopoietic lineages.⁵⁵ In adoptive transfer BM rescue experiments designed to remove the more primitive BM progenitors, DT₃₉₀-mIL-3 treatment inhibited the ability of BM to rescue lethally irradiated recipients that died within the first 2 to 3 weeks, but the effect could be overcome by increasing the dose of treated BM cells. Others believe that

Table 4. BM From Competitively Repopulated Mice Can Be Adoptively Transferred to Secondary Recipients

	% Positive Cells	
	Ly5.1	Ly5.2
Nontreated	60 ± 1.7	40 ± 1.7
DT ₃₉₀ -mIL-3	67 ± 4.9*	33 ± 4.9*

BM cells (8×10^6) from the DT₃₉₀-mIL-3-treated mice in experiment 1 were transplanted into C57BL/6 lethally irradiated (9.0 Gy) secondary recipients ($n = 10$ /group) on day 110 post-BMT. Recipients were studied by flow cytometry on day 21 post-BMT for the presence of Ly5.1- or Ly5.2-expressing cells in the blood as described. Data are expressed as a mean percentage of positive cells \pm 1 standard error of the mean.

* $P < .001$ compared with untreated controls.

early engraftment of donor cells that provide a radioprotective ability is a function of primitive progenitor cells that are more differentiated than PHSC. Radioprotective cells were found in the same fraction as the CFU-S, suggesting that they could represent cells at comparable stages of development.³⁰ Ogata et al¹⁰ reported that the radioprotective ability of IL-3RAA⁻ cells was significantly higher than that of the IL-3RAA⁺ cell. Taken together with our results, these findings indicate that more primitive progenitor cells are heterogeneous in their expression of IL-3R numbers.

To test the effect of DT₃₉₀-mIL-3 on the PHSC, we further examined the long-term repopulating and self-renewal abilities of the treated BM cells using competitive repopulation assays. We used a 10 nmol/L DT₃₉₀-mIL-3 treatment for 8 hours because higher concentrations killed nonspecifically and longer incubations risked the survival of even nontreated cultured BM. Our competitive repopulation experiments showed that the percentage of long-term repopulating peripheral blood cells are proportional to the ratio of mixed congenic cells administered for BMT even though 10 million donor cells were injected. Even with the injection of such a high number of cells, the proportions of reconstituting progenitor cells correlated to the original proportion of donor BM cells, indicating that the relative effects of DT₃₉₀-mIL-3 on stem cells could be determined.

The studies in this report showed that congenic Ly5.2-marked stem cells were significantly inhibited, but not totally eliminated, by DT₃₉₀-mIL-3 treatment in either the primary recipients 95 days post-BMT or the secondary recipients 21 days postsecondary transfer. It is possible that the failure to eliminate all treated stem cells and entirely prevent long-term alloengraftment of Ly5.2 cells could be related to a failure of DT₃₉₀-mIL-3 to adequately kill these stem cells in the preincubation period. However, the treated Ly5.2 BM used in these experiments was simultaneously evaluated in colony assays and found to be inhibited by 95% for CFU-GM, indicating that DT₃₉₀-mIL-3 was indeed highly cytotoxic. A more likely explanation is that some but not all PHSC express IL-3R, perhaps related to differences in expression relative to the stages of differentiation. Perhaps IL-3R is upregulated on more highly differentiated cells, as illustrated by our *in vitro* colony data. Once committed to myeloid lineages, the IL-3R may be continuously present on these progenitor cells until the end stages of differentiation.

Will DT₃₉₀-mIL-3 be useful for leukemia treatment? Murine and human myeloid and lymphoid leukemic cells display receptors for growth factors including IL-3, and many have been shown to be responsive to exogenous IL-3 *in vitro*.^{3,4} The potency and specificity of DT₃₉₀-mIL-3 is high enough, with an IC₅₀ of 0.025 nmol/L as compared with other fusion toxins²⁹⁻³³ to render it an effective killing agent if it is not limited by its effects against progenitor cells. Our studies are encouraging in that, even when Ly5.2 stem cells were treated with DT₃₉₀-mIL-3, transplanted PHSC engrafted long-term and still had capacity for self-renewal when adoptively transferred into secondary recipients. One interpretation of these findings is that not all of the PHSC express IL-3R and that those that do not express the receptor escape killing. If this is the case, then DT₃₉₀-mIL-3 can be used for

leukemia treatment or as an agent for purging leukemia cells before autologous BM transplant as long as sufficient quantities of treated BM cells are administered for an effective BM rescue.

In conclusion, the primary purpose of these studies was to determine the reactivity of a novel fusion protein, DT₃₉₀-mIL-3, with BM progenitors. Our data show that the agent was more effective in killing committed BM progenitor cells than primitive progenitor cells, possibly related to higher levels of IL-3R expression on these cells. The fact that DT₃₉₀-mIL-3 was highly toxic to leukemia cells indicates that it has potential for purging cancer cells from myeloid BM leukemia grafts or even for *in vivo* conditioning to reduce minimal residual disease. However, future experiments must determine the differential sensitivity of BM progenitors as compared with leukemia progenitors. Future studies are warranted because alternative therapies are needed for acute nonlymphocytic leukemia, which still presents a serious clinical problem.

ACKNOWLEDGMENT

We thank Dr S. Ramakrishnan and Dr Richard J. Youle for helpful discussions regarding this project.

REFERENCES

1. Ihle JN: Interleukin-3 and hematopoiesis. *Chem Immunol* 51:65, 1992
2. Oster W, Schulz G: Interleukin 3: Biological and clinical effects. *Int J Cell Cloning* 9:5, 1991
3. Park LS, Waldron PE, Friend D, Sassenfeld HM, Price V, Anderson D, Cosman D, Andrews RG, Bernstein ID, Urdal DL: Interleukin-3, GM-CSF, and G-CSF receptor expression on cell lines and primary leukemia cells: Receptor heterogeneity and relationship to growth factor responsiveness. *Blood* 74:56, 1989
4. Miyauchi J, Kelleher CA, Wong GG, Yang CC, Clark SC, Minkin S, Minden MD, McCulloch EA: The effects of combinations of the recombinant growth factors GM-CSF, G-CSF, IL-3, and CSF-1 on leukemic blast cells in suspension culture. *Leukemia* 2:382, 1988
5. Stocking C, Loliger C, Kawai M, Suci S, Gough N, Ostertag W: Identification of genes involved in growth autonomy of hematopoietic cells by analysis of factor-independent mutants. *Cell* 53:869, 1988
6. Laker C, Kluge N, Stocking C, Just U, Franz MJ, Ostertag W, DeLamarter JF, Dexter M, Spooner E: Rates of mutation to growth factor autonomy and tumorigenicity differ in hematopoietic stem and precursor cells expressing the multilineage colony-stimulating factor gene. *Mol Cell Biol* 9:5746, 1989
7. Hapel AJ, Vande Woude G, Campbell HD, Young IG, Robins T: Generation of an autocrine leukemia using a retroviral expression vector carrying the interleukin-3 gene. *Lymphokine Res* 5:249, 1986
8. Twardy DJ, Morel PA, Herberman RB, Sakurai M: Inhibition of growth of mouse leukemic cell lines *in vitro* and *in vivo* by a monoclonal antibody that recognizes an interleukin 3 receptor-associated protein. *Cancer Res* 51:4355, 1991
9. Bernstein ID, Andrews RG, Zsebo KM: Recombinant human stem cell factor enhances the formation of colonies by CD34⁺ and CD34⁺lin⁻ cells, and the generation of colony-forming cell progeny from CD34⁺lin⁻ cells cultured with interleukin-3, granulocyte colony-stimulating factor, or granulocyte-macrophage colony-stimulating factor. *Blood* 77:2316, 1991
10. Ogata H, Taniguchi S, Inaba M, Sugawara M, Ohta Y, Inaba

K, Mori J, Ikehara S: Separation of hematopoietic stem cells into two populations and their characterization. *Blood* 80:91, 1992

11. Leary AG, Zeng HQ, Clark SC, Ogawa M: Growth factor requirements for survival in G₀ and entry into the cell cycle of primitive human hemopoietic progenitors. *Proc Natl Acad Sci USA* 89:4013, 1992

12. Suda T, Suda J, Ogawa M, Ihle JN: Permissive role of interleukin 3 (IL-3) in proliferation and differentiation of multipotential hemopoietic progenitors in culture. *J Cell Physiol* 124:182, 1985

13. Hapel AJ, Fung MC, Johnson RM, Young IG, Johnson G, Metcalf D: Biologic properties of molecularly cloned and expressed murine interleukin-3. *Blood* 65:1453, 1985

14. Rennick DM, Lee FD, Yokota T, Arai KI, Cantor H, Nabel GJ: A cloned M-CGF cDNA encodes a multilineage hematopoietic growth factor: Multiple activities of interleukin 3. *J Immunol* 134:910, 1985

15. Leary AG, Yang YC, Clark SC, Gasson JC, Golde DW, Ogawa M: Recombinant gibbon interleukin 3 supports formation of human multilineage colonies and blast cell colonies in culture: Comparison with recombinant human granulocyte-macrophage colony-stimulating factor. *Blood* 70:1343, 1987

16. Wormann B, Gesner TG, Mufson RA, LeBien TW: Proliferative effect of interleukin-3 on normal and leukemic human B cell precursors. *Leukemia* 3:399, 1989

17. Bergui L, Schena M, Gaidano G, Riva M, Caligaris-Cappio F: Interleukin 3 and interleukin 6 synergistically promote the proliferation and differentiation of malignant plasma cell precursors in multiple myeloma. *J Exp Med* 170:613, 1989

18. Xia X, Li L, Choi YS: Human recombinant IL-3 is a growth factor for normal B cells. *J Immunol* 148:491, 1992

19. Londei M, Verhoef A, De Berardinis P, Kissnerghis M, Grubeck-Loebenstein B, Feldmann M: Definition of a population of CD4⁺ T cells that express the alpha beta T-cell receptor and respond to interleukins 2, 3, and 4. *Proc Natl Acad Sci USA* 86:8502, 1989

20. Ihle JN, Silver J, Kozak C: Genetic mapping of the mouse interleukin 3 gene to chromosome 11. *J Immunol* 138:3051, 1987

21. Buchberg AM, Bedigian HG, Taylor BA, Brownell E, Ihle JN, Jenkins NA, Copeland NG: Localization of Evi-2 to chromosome 11: Linkage to other proto-oncogene and growth factor loci using interspecific backcross mice. *Oncogene Res* 2:149, 1988

22. Clark-Lewis I, Kent SB, Schrader JW: Purification to apparent homogeneity of a factor stimulating the growth of multiple lineages of hemopoietic cells. *J Biol Chem* 259:7488, 1984

23. Hara T, Miyajima A: Two distinct functional high affinity receptors for mouse interleukin-3 (IL-3). *EMBO J* 11:1875, 1992

24. Nicola NA, Peterson L, Hilton DJ, Metcalf D: Cellular processing of murine colony-stimulating factor (Multi-CSF, GM-CSF, G-CSF) receptors by normal hematopoietic cells and cell lines. *Growth Factors* 1:41, 1988

25. Yamaizumi M, Mekada E, Uchida T, Okada Y: One molecule of diphtheria toxin fragment A introduced into a cell can kill the cell. *Cell* 15:245, 1978

26. Middlebrook JL, Dorland RB, Leppla SH: Association of diphtheria toxin with Vero cells. *J Biol Chem* 253:7325, 1978

27. Lambert P, Falmagne P, Capiat C, Zanen J, Ruyschaert JM, Dirx J: Primary structure of diphtheria toxin fragment B: Structural similarities with lipid binding domains. *J Cell Biol* 87:837, 1980

28. Murphy JR, Bishai W, Borowski M, Miyanohara A, Boyd J, Nagle S: Genetic construction, expression, and melanoma-selective cytotoxicity of a diphtheria toxin-related alpha-melanocyte-stimulating hormone fusion protein. *Proc Natl Acad Sci USA* 83:8258, 1986

29. Williams DP, Parker K, Bacha P, Bishai W, Borowski M, Genbaffe F, Strom TB, Murphy JR: Diphtheria toxin receptor binding domain substitution with interleukin-2: Genetic construction and properties of a diphtheria toxin-related interleukin-2 fusion protein. *Protein Eng* 1:493, 1987

30. Lakkis F, Steele A, Pacheco-Silva A, Rubin-Kelley V, Strom TB, Murphy JR: Interleukin 4 receptor targeted cytotoxicity: Genetic construction and in vivo immunosuppressive activity of a diphtheria toxin-related murine interleukin 4 fusion protein. *Eur J Immunol* 21:2253, 1991

31. Jean LF, Murphy JR: Diphtheria toxin receptor-binding domain substitution with interleukin 6: Genetic construction and interleukin 6 receptor-specific action of a diphtheria toxin-related interleukin 6 fusion protein. *Protein Eng* 4:989, 1991

32. Chadwick DE, Williams DP, Niho Y, Murphy JR, Minden MD: Cytotoxicity of a recombinant diphtheria toxin-granulocyte colony-stimulating factor fusion protein on human leukemic blast cells. *Leuk Lymphoma* 11:249, 1993

33. Chan CH, Blazar BR, Eide CR, Kreitman RJ, Valleria DA: A murine cytokine toxin specifically targeting the murine granulocyte-macrophage colony-stimulating factor (GM-CSF) receptor on normal committed bone marrow progenitor cells and GM-CSF-dependent tumor cells. *Blood* 86:2732, 1995

34. Horton RM, Hunt HD, Ho SN, Pullen JK, Pease LR: Engineering hybrid genes without the use of restriction enzymes: Gene splicing by overlap extension. *Gene* 77:61, 1989

35. Bradford MM: A rapid and sensitive method for the quantitation of microgram quantities of protein utilizing the principle of protein-dye binding. *Anal Biochem* 72:248, 1976

36. Johnson VG, Wilson D, Greenfield L, Youle RJ: The role of the diphtheria toxin receptor in cytosol translocation. *J Biol Chem* 263:1295, 1988

37. Dexter DM, Garland JM, Scott D, Scolnick E, Metcalf D: Growth of factor-dependent hemopoietic precursor cell line. *J Exp Med* 152:1036, 1980

38. Brazill GW, Haynes M, Garland J, Dexter TM: Characterization and partial purification of a haemopoietic cell growth factor in WEHI-3 cell conditioned media. *Biochem J* 210:747, 1983

39. Valleria DA, Soderling CCB, Carlson GJ, Kersey JH: Bone marrow transplantation across major histocompatibility barrier in mice. *Transplantation* 31:218, 1981

40. Blazar BR, Taylor PA, Sehgal SN, Valleria DA: Rapamycin, a potent inhibitor of T-cell function, prevents graft rejection in murine recipients of allogeneic T-cell-depleted donor marrow. *Blood* 83:600, 1994

41. Valleria DA, Taylor PA, Sprent J, Blazar BR: The role of host T cell subsets in bone marrow rejection directed to isolated major histocompatibility complex class I versus class II differences of bm1 and bm12 mutant mice. *Transplantation* 57:249, 1994

42. Harrison DE: Competitive repopulation: A new assay for long-term stem cell functional capacity. *Blood* 55:77, 1980

43. Naglich JG, Metherall JE, Russell AW, Eidels L: Expression cloning of a diphtheria toxin receptor: Identity with a heparin-binding EGF-like growth factor precursor. *Cell* 69:1051, 1992

44. Stenmark H, Olsnes S, Sandvig K: Requirement of specific receptors for efficient translocation of diphtheria toxin A fragment across the plasma membrane. *J Biol Chem* 263:13449, 1988

45. Van Zant G: Studies of hematopoietic stem cells spared by 5-fluorouracil. *J Exp Med* 159:679, 1984

46. Inaba MM, Ogata H, Toki J, Kuma S, Sugiura S, Yasumizu R, Ikehara S: Isolation of murine pluripotent hematopoietic stem cells in the G₀ phase. *Biophys Res Commun* 147:687, 1987

47. Magli MC, Iscove NN, Odartchenko N: Transient nature of early haematopoietic spleen colonies. *Nature* 295:527, 1982

48. Baines P, Visser JW: Analysis and separation of murine bone

marrow stem cells by H33342 fluorescence-activated cell sorting. *Exp Hematol* 11:701, 1983

49. Ploemacher RE, Brons RHC: Separation of CFU-S from primitive cells responsible for reconstitution of the bone marrow hematopoietic stem cell compartment following irradiation: Evidence for a pre-CFU-S. *Exp Hematol* 17:263, 1989

50. Jones RJ, Wagner JE, Celano P, Zicha MS, Sharkis SJ: Separation of pluripotent haematopoietic stem cells from spleen colony-forming cells. *Nature* 347:188, 1990

51. Spangrude GJ, Johnson GR: Resting and activating subsets of mouse haematopoietic stem cells. *Proc Natl Acad Sci USA* 87:7433, 1990

52. Sugiura K, Ikehara S, Inaba M, Haraguchi S, Ogata H, Sardina EE, Sugawara M, Ohta Y, Good RA: Enrichment of murine bone

marrow natural suppressor activity in the fraction of hematopoietic progenitors with interleukin 3 receptor-associated antigen. *Exp Hematol* 20:256, 1992

53. Moynihan MR, Pappenheimer AM: Kinetics of adenosinophosphoribosylation of elongation factor 2 in cells exposed to diphtheria toxin. *Infect Immunity* 32:575, 1981

54. William DP, Wen Z, Watson RS, Boyd J, Storm TB, Murphy JR: Cellular processing of the interleukin-2 fusion toxin DAB486-IL-2 and efficient delivery of diphtheria fragment A to the cytosol of target cells requires Arg194. *J Biol Chem* 265:20673, 1990

55. Smith LG, Weissman IL, Heimfeld S: Clonal analysis of hematopoietic stem-cell differentiation in vivo. *Proc Natl Acad Sci USA* 88:2788, 1991

Anti-Tac(Fv)-PE40, a Single Chain Antibody *Pseudomonas* Fusion Protein Directed at Interleukin 2 Receptor Bearing Cells*

(Received for publication, April 23, 1990)

Janendra K. Batra, David FitzGerald, Maurice Gately†, Vijay K. Chaudhary, and Ira Pastan

From the Laboratory of Molecular Biology, Division of Cancer Biology and Diagnosis, National Cancer Institute, National Institutes of Health, Bethesda, Maryland 20892 and the †Department of Immunopharmacology, Roche Research Center, Hoffman-La Roche, Inc., Nutley, New Jersey 07110

Anti-Tac(Fv)-PE40 is a chimeric single chain immunotoxin in which anti-Tac variable heavy and light chains held together by a peptide linker are attached to PE40, a truncated form of *Pseudomonas* exotoxin. This molecule was shown to be extremely cytotoxic for interleukin 2 (IL2) receptor bearing cells in tissue culture (Chaudhary, V. K., Queen, C., Junghans, R. P., Waldmann, T. A., FitzGerald, D. J., and Pastan, I. (1989) *Nature* 339, 394-397). Here we describe various forms of anti-Tac(Fv)-PE40 protein in which the order of the variable domains of anti-Tac has been switched and also three different types of peptide linkers have been used. All these proteins were purified to near homogeneity and were found to have similar cytotoxic activities against various human cells expressing the p55 subunit of the IL2 receptor. Anti-Tac(Fv)-PE40 was also found to have a very potent suppressive activity against phytohemagglutinin-activated human lymphoblasts and in a human mixed lymphocyte reaction. Anti-Tac(Fv)-PE40 appeared in the blood rapidly in mice after intraperitoneal administration and could be detected in the blood for up to 8 h. Anti-Tac(Fv)-PE40 warrants evaluation as an anti-tumor and immunosuppressive agent in humans.

Immunotoxins are emerging as potential chemotherapeutic agents for the treatment of cancer, acquired immune deficiency syndrome, and immunological disorders (1, 2). Several different toxins have been employed to make immunotoxins. These include ricin, diphtheria toxin, *Pseudomonas* exotoxin, modecin, and saporin. We have been constructing immunotoxins using *Pseudomonas* exotoxin (PE).¹ PE is composed of three major structural domains each with a different function. Domain I is responsible for cell recognition, domain II for translocation across the cell membrane, and domain III for the ADP-ribosylation activity of the toxin, although recently the last five amino acids of the carboxyl end of domain III have also been shown to have a role in translocation (3-5). Immunotoxins are conventionally made by coupling monoclonal antibodies to toxins using chemical cross-linkers. Recently, it has been possible to produce immunotoxins in *Escherichia coli* by fusing DNA segments encoding the Fv

regions of antibodies to a truncated form of the toxin, thereby producing single chain antibody toxin fusion proteins (6, 7). We initially produced a molecule termed anti-Tac(Fv)-PE40 in which the variable region of the heavy chain of the anti-Tac antibody is attached through a peptide linker to the variable light chain which in turn is fused to PE40 (6). The latter is a truncated form of *Pseudomonas* exotoxin which lacks the binding domain of the toxin. Anti-Tac(Fv)-PE40 is cytotoxic to cells expressing the p55 subunit of the human IL2 receptor (6).

The affinity of anti-Tac(Fv)-PE40 for the p55 subunit of the IL2 receptor was found to be very close to that of native anti-Tac (6). To study the structural requirements for binding and to explore the possibility of creating a more active molecule, we have made several different anti-Tac(Fv)-PE40 constructions. In these, the order of the variable heavy and light chains has been switched and the role of the peptide linker joining the variable chains has been explored by using three different linkers. In addition, the activity of anti-Tac(Fv)-PE40 was assessed on various types of normal and malignant human T cells. The cytotoxicity was compared with that of two other chimeric toxins composed of IL2 linked to different mutant forms of PE. Anti-Tac(Fv)-PE40 was found to be more active than either IL2-PE40 or IL2-PE66^{CH1} (8, 9), two other chimeric toxins directed at IL2 receptor-bearing cells.

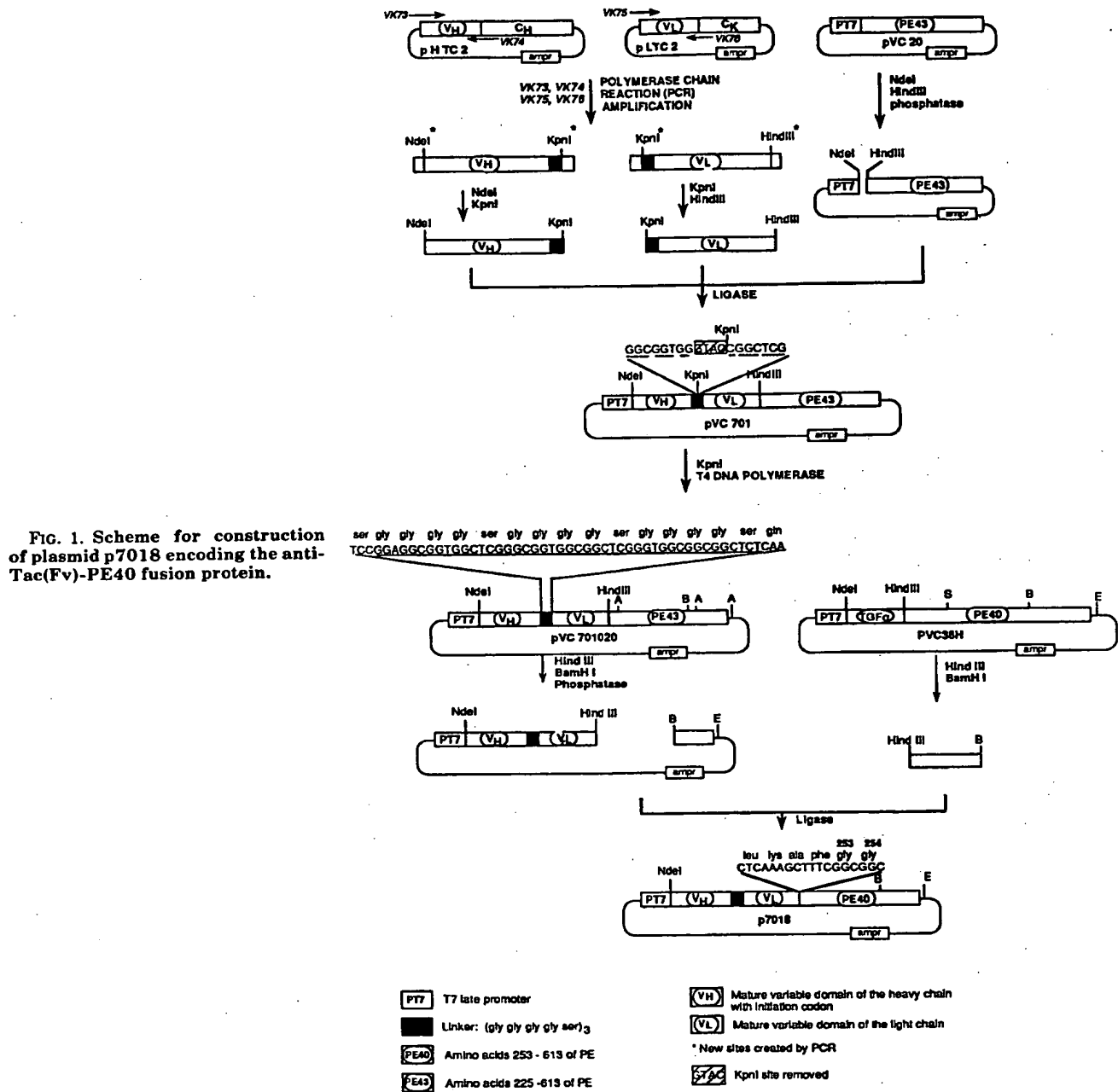
MATERIALS AND METHODS

Construction of Plasmids—Polymerase chain reaction-based methods were used to amplify, create cloning sites, and assemble the plasmids containing the variable domains of the light and the heavy chains of anti-Tac joined together by a peptide linker. These variable domains are fused to DNA sequences encoding PE40. These fusion genes are under the control of a T7 promoter and an appropriate ribosome binding site has been included.

p7018—Fig. 1 summarizes the cloning strategy employed for this construction. The starting template material was cDNA of the light and heavy chain of anti-Tac cloned as an *EcoRI* insert in pUC18. Oligonucleotides VK73 and VK74 were used to amplify the variable domain of the heavy chain (V_H) using anti-Tac heavy chain cDNA as template. VK75 and VK76 were used to amplify the variable domain of the light chain (V_L) using the anti-Tac light chain cDNA as template. The conditions of the polymerase chain reaction have been described previously (7). For VK73, 23 nucleotides at the 3'-end were the same as the 5'-sequence of the cDNA encoding the mature heavy chain of anti-Tac. VK73 also introduced an *NdeI* site and an initiation methionine at the 5'-end. The 3'-end of the oligonucleotide, VK74, was complementary to the 3'-end of the variable domain of the heavy chain. VK74 also encoded the first 8 anticodons of the peptide linker followed by a *KpnI* site, and the nucleotides at its 5'-end were complementary to the sequences in the CH1 domain. VK75 carried nucleotides for a *KpnI* site and for the last 8 codons of a peptide linker. The last 23 nucleotides of VK75, at the 3'-end, were the same as that of the 5'-end of the mature light chain. The 3'-end of oligonucleotide VK76 contained 24 nucleotides which were complementary to the 3'-end of the variable domain of the light chain,

* The costs of publication of this article were defrayed in part by the payment of page charges. This article must therefore be hereby marked "advertisement" in accordance with 18 U.S.C. Section 1734 solely to indicate this fact.

¹ The abbreviations used are: PE, *Pseudomonas* exotoxin; IL2, interleukin 2; anti-Tac, monoclonal antibody to p55 subunit of human IL2 receptor; V_H, heavy chain variable region; V_L, light chain variable region; kb, kilobase(s); SDS, sodium dodecyl sulfate; PAGE, polyacrylamide gel electrophoresis; PHA, phytohemagglutinin.



followed by nucleotides for a *HindIII* site. The 5'-end of VK76 was complementary to the constant domain of the κ light chain.

The amplified DNA containing *V_H* was digested with *NdeI* and *KpnI*, while that containing *V_L* was digested with *KpnI* and *HindIII*. The digested fragments were purified on 1.8% low melting point agarose (Sea Plaque GTG agarose, FMC). Separately, plasmid pVC20 was digested with *NdeI* and *HindIII* and dephosphorylated. pVC20 encodes a PE derivative of 43 kDa termed PE43 (10). A three fragment in-gel ligation was set up using two polymerase chain reaction-amplified, enzyme-digested fragments containing *V_H* and *V_L* with a 3.75-kb fragment of pVC20 carrying PE43 and promoter sequences. Correct clones were identified by restriction enzyme analysis. One of the right clones, pVC701, was digested with *KpnI* followed by T4 DNA polymerase to remove the 4-base overhang and ligated. The clones were screened for the loss of the *KpnI* site. These clones (pVC701020) produced a protein of approximately 66 kDa reacting with antibodies to PE. pVC701020 was digested with *HindIII* and

BamHI and dephosphorylated. Separately, pVC38H (7) was digested with *HindIII* and *BamHI* to isolate an 0.8-kb fragment which was ligated with the *HindIII*- and *BamHI*-restricted 2.9-kb fragment of pVC701020. The resulting clones contained *V_H*, linker L1, *V_L*, and DNA sequences for PE40 under the control of a T7 promoter (Fig. 2). The clones were checked by restriction enzyme digestions and, finally, by protein expression. One of the correct clones, p7018, which expressed a 63-kDa protein reactive with the antibodies to PE, was selected for large scale expression and purification of the protein.

p70528—This plasmid was constructed using a similar strategy as used for p7018, except that the oligonucleotide primers were different. In this plasmid, *V_L* is linked to the *V_H* through a 15-amino acid peptide linker L1, and *V_H* is linked to PE40 (Fig. 2). Accordingly, oligonucleotides VK77 and VK78 were used to amplify *V_L*. These oligonucleotides introduced an *NdeI* site, initiator methionine at the 5'-end, the first 7 codons of the peptide linker, and a *KpnI* site at 3'-end. VK79 and VK89 introduced a *KpnI* site, the last 8 codons of the

peptide linker at the 5'-end of V_H , and a *Hind*III site at the 3'-end of V_H . Other steps were the same as described above for the construction of p7018.

p70538—This plasmid is similar to p70528 but contains a 16-amino acid peptide linker termed L2 which has a different amino acid composition (Fig. 2). p70538 was derived from p70528 using two oligonucleotides, VK93 and VK89. The 5'-end of the VK93 is the same as the J region of V_L in p70538 followed by codons for the new peptide linker, and the 3'-end is the same as the 5'-end of the V_H . A polymerase chain reaction was set up with VK93 and VK89 using p70528 as template. The amplified product was digested with *Sst*I and *Hind*III and ligated with a 3.95-kb fragment of *Sst*I-*Hind*III-digested/dephosphorylated p70528. The correct clones were identified by restriction enzyme digestion followed by expression of protein in BL21 (Δ DE3).

p70548—This was created using a strategy identical with that described for p70538 except using oligo VK94 and VK89, which introduced a 14-amino acid linker L3 (Fig. 2).

The DNA sequences in the peptide linker region were confirmed by dideoxy sequencing.

Expression and Purification of Proteins—To express and localize anti-Tac(Fv)-PE40, *E. coli* BL21 (Δ DE3) cells were transformed with the appropriate plasmids and cultured at 37 °C in super broth supplemented with ampicillin (100 μ g/ml). At an OD₆₀₀ of 0.8, isopropyl-1-thio- β -D-galactopyranoside was added to a final concentration of 1 mM, and the culture was further incubated for 90 min. Cells were harvested and protein was localized as described previously (11). The fusion proteins were mostly contained in the inclusion bodies so these were used as the source for further purification. Proteins were denatured in 7 M guanidine hydrochloride and renatured by rapid dilution in phosphate-buffered saline (12). The renatured protein was applied onto a fast protein liquid chromatography Mono Q 10/10 column in 0.02 M Tris-HCl, pH 7.4, and eluted by a linear gradient of 0–0.5 M NaCl in the same buffer. Fractions containing the fusion protein were detected by SDS/PAGE and cytotoxic activity on HUT102 cells, pooled, and concentrated. For further purification, chimeric protein was applied to a TSK 250 gel filtration column and fractions corresponding to the monomeric form were pooled, quantitated, and used for further characterization.

Protein Synthesis Inhibition Assay—Cytotoxic activity of the fusion protein was determined by assaying the inhibition of protein synthesis on HUT102, Cr11.2, MT-1, ELT5, and EL4J3.4. Cells were washed twice with RPMI 1640, plated in 24-well plates, and incubated with several dilutions of the toxin for 16–20 h at 37 °C. Protein synthesis was assayed by labeling the cells with [³H]leucine for 90 min and counting the trichloroacetic acid-precipitable protein as described (6).

Determinations of Blood Level and Toxicity of Anti-Tac(Fv)-PE40 in Mice—Anti-Tac(Fv)-PE40 was injected intraperitoneally into five groups of female BALB/c mice in doses ranging from 5–100 μ g. Animals were observed for 72 h for signs of toxicity and death. LD₅₀ is the dose of toxin able to kill 50% of the animals in a group in 48 h. For blood level analysis, female BALB/c mice were injected intraperitoneally with 10 μ g of the fusion protein 7018. Blood was drawn from the orbital vein at different times after injection, and the level of anti-Tac(Fv)-PE40 was assayed by incubating the serum with HUT102 cells and measuring inhibition of protein synthesis. A standard curve made with pure anti-Tac(Fv)-PE40 on HUT102 cells was used to determine the concentration in the serum.

Effect of Anti-Tac(Fv)-PE40 on Human Lymphocytes—Peripheral blood mononuclear cells were prepared from the blood of normal volunteer donors using the Ficoll and sucrose density gradient centrifugation. For PHA stimulation, peripheral blood mononuclear cells were cultured at a density of 5×10^5 cells/ml at 37 °C in 0.1% phytohemagglutinin-P (PHA-P) for 3 days. The culture was diluted 1:1 with fresh medium, and human rIL2 was added to a concentration of 50 units/ml. The culture was further incubated for 1–2 days, cells were then harvested, washed, and resuspended at 8×10^5 cells/ml in assay medium consisting of leucine-free Eagle's minimal essential medium with 5% fetal bovine serum, 1 mM sodium pyruvate, 0.1 mM nonessential amino acids, 2 mM L-glutamine, 100 units/ml penicillin, 100 μ g/ml streptomycin, and 50 μ g/ml gentamycin. For two-way mixed lymphocyte reaction, 60 ml of heparinized blood was collected from two individuals and peripheral blood mononuclear cells were isolated. 5×10^6 cells from each individual were mixed in 10 ml of medium and incubated at 37 °C, rIL2 (50 units/ml) was added on day 3, and the culture was further incubated for 3 days. Cells were harvested and resuspended in the assay medium as described above.

To determine the effect of anti-Tac(Fv)-PE40, lymphoblasts were aliquoted into 96-well plates, and serial dilutions of the toxin were added along with rIL2 (10 units/ml). The culture was incubated for 2 days at 37 °C, pulsed for 6 h with [³H]leucine. Cells were harvested using a microplate harvester on glass fiber filters and counted.

Other Methods—Protein was measured by the method of Bradford using the Bio-Rad protein assay reagent. SDS/PAGE was done by using the method of Laemmli (13).

RESULTS

We have previously shown that a single chain anti-Tac(Fv)-PE40 molecule composed of the heavy and light chain variable regions of anti-Tac connected to PE40 makes a very active immunotoxin that inhibits protein synthesis in HUT102 cells with an ID₅₀ of ~0.15 ng/ml (6). To determine if the structure of the recombinant immunotoxin could be altered and its activity retained or improved, we made several new constructions in which the order of the V_L and V_H chains was reversed, or in which the amino acid sequence of the linking peptide was altered. The structures of these new constructions are illustrated in Fig. 2 and described under "Materials and Methods." All the chimeric proteins were expressed in *E. coli* using the T7 expression system, extracted from inclusion bodies by guanidine hydrochloride, and, after renaturation, purified to near homogeneity by successive ion exchange and size exclusion chromatography. In all cases, a highly purified chimeric toxin was obtained (Fig. 3), and the yields of toxin were approximately equal.

The purified toxins were tested on several different cell lines. These included HUT102 and CrIL2 which contain both

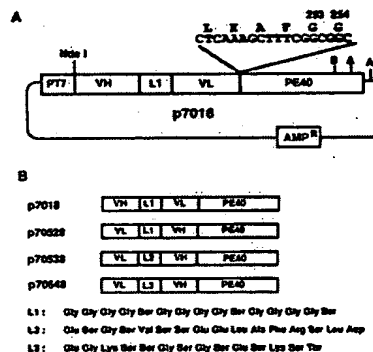


FIG. 2. Expression vector for various anti-Tac(Fv)-PE40 proteins. A, p7018 showing the basic plasmid used for expression of the chimeric proteins. B, order of variable domains in various constructions and linkers. V_H , variable heavy; V_L , variable light; L, linker; B, *Bam*HI; A, *Ava*I; Amp, β -lactamase gene.

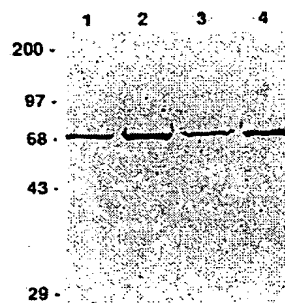


FIG. 3. SDS-PAGE of purified anti-Tac(Fv)-PE40 proteins. 10% SDS-polyacrylamide gels were run and stained with Coomassie Blue. Lane 1, 7018; lane 2, 70528; lane 3, 70538; lane 4, 70548. Molecular weight markers are shown $\times 10^{-3}$.

subunits of the human IL-2 receptor (p55 and p75), MT-1 which contains only human p55, ELT5 which has human p55 and mouse p75, and EL4J3.4 which has mouse p55 and p75. As shown in Fig. 4 and Table I, all four chimeric toxins were very active in inhibiting protein synthesis in HUT102 cells with ID_{50} values ranging from 0.10 to 0.15 ng/ml. The agents also had similar action against the other cell lines which contained the human p55 subunit (CrII.2, MT-1, and ELT5) but not on cells containing the mouse p55 subunit reflecting the species specificity of the anti-Tac antibody.

Effect of Anti-Tac(Fv)-PE40 on Human T Lymphoblast Proliferation—One possible use of anti-Tac(Fv)-PE40 is in the treatment of autoimmune diseases or allograft rejection. Therefore, we tested the activity of one of the recombinant immunotoxins on human lymphoblasts which were activated either by the mitogen, PHA, or in a mixed lymphocyte reaction. The stimulated lymphoblasts express functional IL2 receptor on their surface. For this purpose, we used the protein encoded by plasmid p7018 (Fig. 2). As shown in Table II, anti-Tac(Fv)-PE40 inhibited the protein synthesis of both PHA and mixed lymphocyte reaction-stimulated human lymphoblasts with ID_{50} values of 0.13 ng/ml and 0.05 ng/ml, respectively. As a control, we tested the toxin on K562 cells which do not express the IL2 receptors and found that high levels of the toxin were required to intoxicate these cells. The activity of anti-Tac(Fv)-PE40 on activated T lymphoblasts was compared with IL2-PE40 and IL2-PE66^{Glu}, chimeric toxins that also bind to the IL2 receptor. IL2-PE40, although previously shown to be very active against mouse splenocytes (14), had very little activity toward the human cells (Table II). IL2-PE66^{Glu}, a chimeric toxin in which the ability of domain I to bind to the *Pseudomonas* exotoxin receptor has been inactivated by mutations at positions 57, 246, 247, and

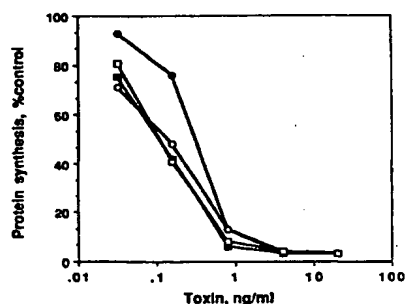


FIG. 4. Cytotoxicity of various fusion proteins on HUT102 cells. Cells were incubated with the respective toxin for 16–20 h and pulsed with [³H] leucine and protein synthesis is shown as percent of control where no toxin was added. ●, 7018; ■, 70528; ○, 70538; and □, 70548.

TABLE I
Cytotoxicity of anti-Tac(Fv)-PE40 proteins on various IL2-receptor-bearing cells

ID_{50} is the protein concentration required to inhibit protein synthesis by 50%. H, human; M, mouse. Other details are given under "Materials and Methods."

Cell line	Subunit present		ID_{50}			
	p55	p75	7018	70528	70538	70548
			ng/ml			
HUT102	H	H	0.15	0.11	0.13	0.10
CrII.2	H	H	1.7	1.1	1.8	1.6
MT-1	H	None	0.37	0.15	0.25	0.25
ELT5	H	M	0.56	0.32	0.54	0.45
EL4J3.4	M	M	>1,000	>1,000	>1,000	>1,000

TABLE II

Comparison of anti-Tac(Fv)-PE40, IL2-PE40, and IL2-PE66^{Glu} for inhibition of human lymphoblast protein synthesis

ID_{50} is the concentration of protein required to inhibit protein synthesis by 50%. K562 is an IL2 receptor-negative cell line.

	ID_{50}	
	Activated T lymphoblasts	K562
	ng/ml	
Experiment 1, PHA lymphoblasts		
Anti-Tac(Fv)-PE40	<0.16	93
IL2-PE40	380	345
IL2-PE66 ^{Glu}	15	910
Experiment 2, PHA lymphoblasts		
Anti-Tac(Fv)-PE40	0.13	91
IL2-PE40	>500	180
IL2-PE66 ^{Glu}	72	1145
Experiment 3, MLR lymphoblasts		
Anti-Tac(Fv)-PE40	0.05	
IL2-PE40	83	
IL2-PE66 ^{Glu}	12	

TABLE III

Toxicity of anti-Tac(Fv)-PE40 in mice

Female BALB/c mice were injected with a single indicated dose of the fusion protein. Number of deaths were recorded after 48 h of the toxin administration.

Amount injected	Number of deaths
μ g	
5	0/3
10	0/3
25	2/3
50	3/3
100	3/3

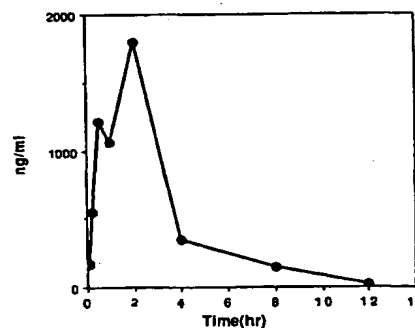


FIG. 5. Blood level of anti-Tac(Fv)-PE40. The experiment was performed as described under "Materials and Methods." Results are average of two experiments.

249, had more activity than IL2-PE40 against the activated human cells, but was nevertheless much less potent than anti-Tac(Fv)-PE40 (Table II). Clearly, anti-Tac(Fv)-PE40 was the most cytotoxic of the three molecules tested.

Blood Level and Toxicity of Anti-Tac(Fv)-PE40 in Mice—The extremely potent *in vitro* cytotoxicity of anti-Tac(Fv)-PE40 on IL2 receptor-bearing cells makes it a promising molecule for testing *in vivo* against IL2 receptor-bearing tumors or for immunosuppression. Accordingly, various amounts of anti-Tac(Fv)-PE40 were given intraperitoneally to mice to assess its toxicity. The LD_{50} of a single dose was found to be between 10 and 25 μ g (Table III). To determine the blood level of anti-Tac(Fv)-PE40, BALB/c female mice were injected intraperitoneally with 10 μ g of protein. Blood was drawn at various times after the injection and assayed on HUT102 cells for immunotoxin activity. A peak blood level

of 1.9 $\mu\text{g}/\text{ml}$ was obtained 2 h after the injections (Fig. 5). Detectable levels of toxin were present for up to 8 h, but by 12 h, toxin could no longer be found in the blood (Fig. 5).

DISCUSSION

We have shown that anti-Tac(Fv)-PE40, a single chain immunotoxin, is very active in killing cells bearing the human p55 subunit of the IL2 receptor. In this type of chimeric toxin, the variable regions of the heavy and light chain are held together by a linking peptide. We have utilized several different peptide linkers containing 14, 15, or 16 amino acids and found all of them to produce active immunotoxins with about the same activity. Furthermore, we have changed the order of the variable regions without affecting activity (Table I). Stimulated by the finding of Ward *et al.* (15) that a single variable region can bind antigen, we made a chimeric toxin composed of the V_H of anti-Tac fused to PE40, but found it to be inactive (data not shown). Apparently, V_H by itself does not have a high affinity for the p55 subunit. However, it may be possible to make active immunotoxins with single variable regions with selected antibodies.

Anti-Tac(Fv)-PE40 has much greater activity on human cells than IL2-PE40, a molecule which also binds to the IL2 receptor (Table II). There are several reasons that may account for this difference which are related to the number of p55 subunits on the target cells and the relative affinities of the two ligands for p55. Anti-Tac binds to p55 with a $K_d \sim 10^{-9}$ M, whereas the affinity of IL2 for p55 is $\sim 10^{-6}$ M (16). Only when p55 is associated with p75 is the affinity increased to $\sim 10^{-11}$ M. In MT-1 cells where there are 100,000 p55 subunits and no p75 subunits, the ID_{50} of anti-Tac(Fv)-PE40 is <1 ng/ml and the ID_{50} of IL2-PE40 is >100 ng/ml. This probably reflects the affinities of the two ligands. On HUT102 cells, where there are many p55 subunits and a moderate number of p75 subunits, IL2-PE40 and anti-Tac(Fv)-PE40 are about equally active. It has been shown previously that the high affinity IL2 receptor composed of p55 and p75 is rapidly internalized when occupied by IL2 (or anti-Tac), whereas the low affinity p55 receptor is internalized much more slowly (17). Nevertheless, it appears that this slow entry route is compensated for by the fact that there are many more p55 molecules than high affinity receptors on the surface of target cells and also because the binding of anti-Tac to these molecules is much stronger than the binding of IL2 to p55.

Anti-Tac(Fv)-PE40 is very active on HUT102 cells that express both the low and high affinity human IL2 receptor. Moreover, the fusion protein is also highly active on cells with moderate or low numbers of receptors (Table I). In a mixed lymphocyte (leukocyte) reaction, which is an *in vitro* model system for alloreactive responses, anti-Tac(Fv)-PE40 inhibited the protein synthesis of T-lymphoblasts very efficiently. It has been shown that IL2 receptor-bearing cells play a very crucial role in graft rejection and the administration of anti-IL2 receptor antibody prolongs allograft survival (18–20). We have earlier made a chimeric toxin containing IL2 and PE40, which is active on mouse IL2 receptor-bearing cells (8, 14) and has been shown to significantly prolong the survival of vascularized heart allografts in mice (21). However, IL2-PE40 has low activity on human activated T cells. Anti-Tac(Fv)-PE40, being enormously more active, might prove to be a potent immunosuppressive agent in humans.

Another objective of creating chimeric toxins is their potential use as anti-tumor agents. Since anti-Tac(Fv)-PE40 ap-

pears to be a very active protein *in vitro*, we performed several experiments to investigate its activity *in vivo*. The LD_{50} of anti-Tac(Fv)-PE40 in mice was determined to be between 10 and 25 μg . The protein appears to be slightly more toxic than some other chimeric toxins produced in our laboratory ($\text{LD}_{50} \sim 20\text{--}50$ μg). However, because of the extremely high activity of anti-Tac(Fv)-PE40, it may not be required to use very high doses *in vivo*. Anti-Tac(Fv)-PE40 when injected intraperitoneally in mice shows a peak of activity in the blood after 2 h and detectable levels are present up to 8 h.

In summary, anti-Tac(Fv)-PE40 is a chimeric toxin which has been shown to be extremely cytotoxic to IL2 receptor expressing cells in tissue culture and in mixed lymphocyte reaction. The agent warrants evaluation as an anti-tumor and immunosuppressive agent in humans.

Acknowledgments—We thank Dr. S. Seetharam for help with the DNA sequencing, Dr. M. Hatakeyama for ELT5 cells, and Jennie Evans for secretarial assistance.

REFERENCES

- Pastan, I., Willingham, M. C., and FitzGerald, D. J. P. (1986) *Cell* 47, 641–648.
- Vitetta, E. S., Fulton, R. J., May, R. D., Till, M., and Uhr, J. W. (1987) *Science* 238, 1098–1104.
- Allured, V., Collier, R. J., Carroll, S. F., and McKay, D. B. (1986) *Proc. Natl. Acad. Sci. U. S. A.* 83, 1320–1324.
- Hwang, J., FitzGerald, D. J. P., Adhya, S., and Pastan, I. (1987) *Cell* 48, 129–136.
- Chaudhary, V. K., Jinno, Y., FitzGerald, D., and Pastan, I. (1990) *Proc. Natl. Acad. Sci. U. S. A.* 87, 308–312.
- Chaudhary, V. K., Queen, C., Junghans, R. P., Waldmann, T. A., FitzGerald, D. J., and Pastan, I. (1989) *Nature* 339, 394–397.
- Chaudhary, V. K., Batra, J. K., Gallo, M. G., Willingham, M. C., FitzGerald, D. J., and Pastan, I. (1990) *Proc. Natl. Acad. Sci. U. S. A.* 87, 1066–1070.
- Lorberbom-Galski, H., FitzGerald, D., Chaudhary, V., Adhya, S., and Pastan, I. (1988) *Proc. Natl. Acad. Sci. U. S. A.* 85, 1922–1926.
- Lorberbom-Galski, H., Garsia, R. J., Gately, M., Brown, P. S., Clark, R. E., Waldmann, T. A., Chaudhary, V., FitzGerald, D. J. P., and Pastan, I. (1990) *J. Biol. Chem.* 265, in press.
- Chaudhary, V. K., Xu, Y.-H., FitzGerald, D. J. P., Adhya, S., and Pastan, I. (1988) *Proc. Natl. Acad. Sci. U. S. A.* 85, 2939–2943.
- Chaudhary, V. K., FitzGerald, D. J. P., Adhya, S., and Pastan, I. (1987) *Proc. Natl. Acad. Sci. U. S. A.* 84, 4538–4542.
- Chaudhary, V. K., Mizukami, T., Fuerst, T. R., FitzGerald, D. J., Moss, B., Pastan, I., and Berger, E. A. (1988) *Nature* 335, 369–372.
- Laemmli, U. K. (1970) *Nature* 227, 680–685.
- Ogata, M., Lorberbom-Galski, H., FitzGerald, D., and Pastan, I. (1988) *J. Immunol.* 141, 4224–4228.
- Ward, E. S., Gussow, D., Griffiths, A. D., Jones, P. T., and Winter, G. (1989) *Nature* 341, 544–546.
- Robb, R. J., Greene, W. C., and Rusk, C. M. (1984) *J. Exp. Med.* 160, 1126–1146.
- Lorberbom-Galski, H., Kozak, R. W., Waldmann, T. A., Bailon, P., FitzGerald, D. J. P., and Pastan, I. (1988) *J. Biol. Chem.* 263, 18650–18656.
- Kirkman, R. L., Barrett, L. V., Gaulton, G. N., Kelley, V. E., Ythier, A., and Strom, T. B. (1985) *J. Exp. Med.* 162, 358–362.
- Hahn, H. J., Kuttler, B., Dungar, A., Kloting, I., Lucke, S., Volk, H. D., vanBaehr, R., and Diamantstein, T. (1987) *Diabetologia* 30, 44–46.
- Reed, M. H., Shapiro, M. E., Strom, T. B., Milford, E. L., Carpenter, C. B., Weinberg, D., Reimann, K., Letvin, N. L., Waldmann, T. A., and Kirkman, R. L. (1989) *Transplantation* 47, 55–59.
- Lorberbom-Galski, H., Barrett, L. V., Kirkman, R. L., Ogata, M., Willingham, M. C., FitzGerald, D. J., and Pastan, I. (1989) *Proc. Natl. Acad. Sci. U. S. A.* 86, 1008–1012.

**This Page is Inserted by IFW Indexing and Scanning
Operations and is not part of the Official Record**

BEST AVAILABLE IMAGES

Defective images within this document are accurate representations of the original documents submitted by the applicant.

Defects in the images include but are not limited to the items checked:

☐ BLACK BORDERS

☐ IMAGE CUT OFF AT TOP, BOTTOM OR SIDES

☐ FADED TEXT OR DRAWING

☒ BLURRED OR ILLEGIBLE TEXT OR DRAWING

☐ SKEWED/SLANTED IMAGES

☒ COLOR OR BLACK AND WHITE PHOTOGRAPHS

☐ GRAY SCALE DOCUMENTS

☒ LINES OR MARKS ON ORIGINAL DOCUMENT

☐ REFERENCE(S) OR EXHIBIT(S) SUBMITTED ARE POOR QUALITY

☐ OTHER: _____

IMAGES ARE BEST AVAILABLE COPY.

As rescanning these documents will not correct the image problems checked, please do not report these problems to the IFW Image Problem Mailbox.